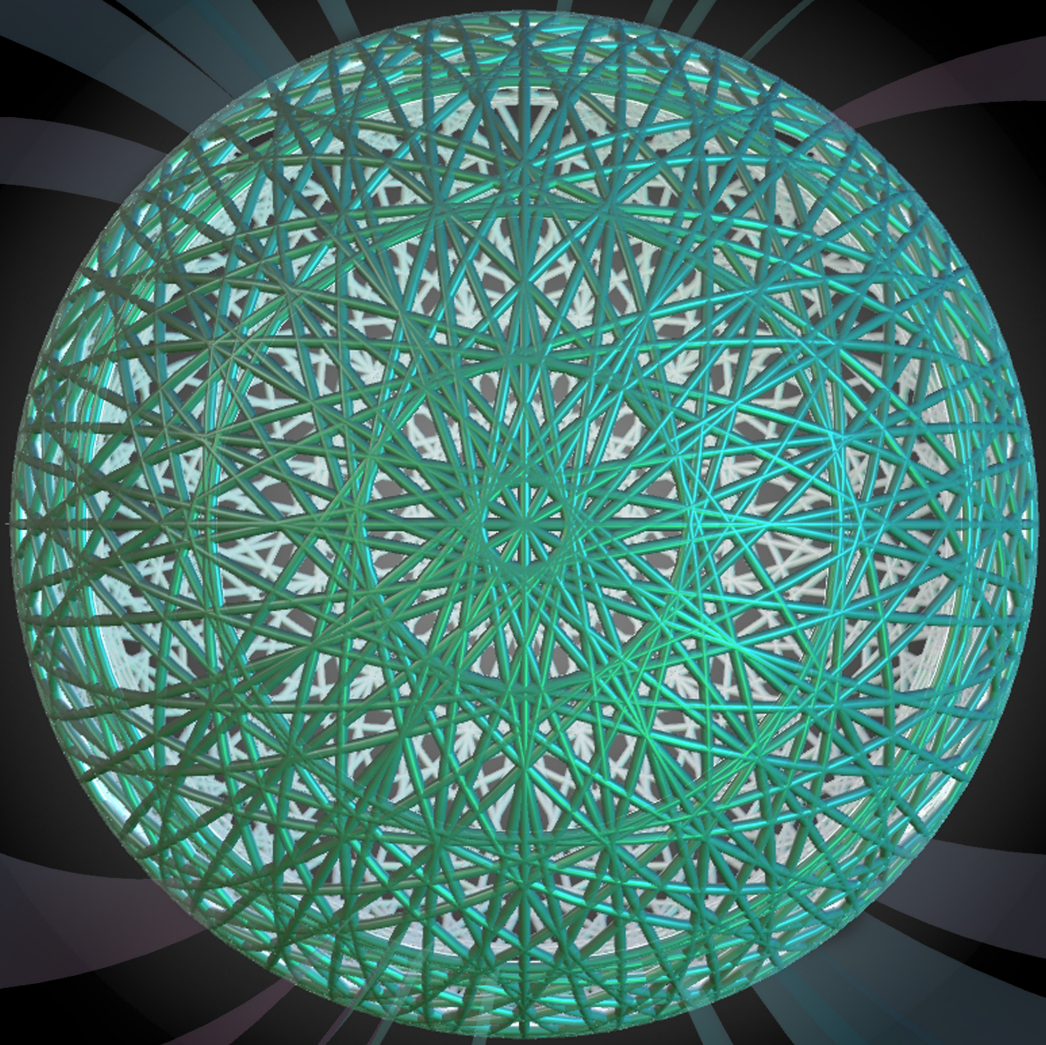
# The Grand Unified Theory of Classical Physics

Dr. Randell L. Mills



## Volume I: Atomic Physics

# *THE GRAND UNIFIED THEORY OF CLASSICAL PHYSICS*

*Volume 1 of 3*

# *THE GRAND UNIFIED THEORY OF CLASSICAL PHYSICS*

BY

**Dr. Randell L. Mills**

**July 2026 Edition**
**Volume 1 of 3**

Copyright © 2026 by Dr. Randell L. Mills

All rights reserved. No part of this work covered by copyright hereon may be reproduced or used in any form, or by any means-graphic, electronic, or mechanical, including photocopying, recording, taping, or information storage and retrieval systems-without written permission of Dr. Randell L. Mills. Manufactured in the United States of America.

ISBN #979-8-234-10247-8
Library of Congress Control Number 2026916690

*To Agueda, Aurora, and Randell Jr. Love you now. Will love you again in a trillion years.*

# TABLE OF CONTENTS

## VOLUME 1 ATOMIC PHYSICS

Preface ..... xxvii
References ..... xxviii

### INTRODUCTION

I.1 General Considerations ..... 1
I.2 CP Approach to the Solution of the Bound Electron ..... 3
I.2.1 Spin and Orbital Parameters Arise from First Principles Only in the Case of CP ..... 4
Box I.1 Misinterpretations of Observations as Weirdness of Quantum Mechanics is Revealed to be Due to Atomic-Scale Classical Physics ..... 5
References ..... 8
I.2.2 Three Atomic Theories ..... 9
I.2.3 Mathematical Relationship Between the Theories of Bohr and Schrödinger with Respect to Classical Atomic Theory ..... 11
I.2.4 Shortcomings of Quantum Theory and Reasons for a Complete Revision of Atomic Theory ..... 15
I.3 Classical Atomic Theory ..... 16
I.3.1 One-Electron Atoms ..... 17
I.3.1.1 Nonradiation Condition ..... 17
I.3.1.2 Electron Source Current ..... 17
I.3.1.3 Moment of Inertia and Spin and Rotational Energies ..... 20
I.4 Spin Function ..... 21
I.4.1 Generation of the BECVF ..... 22
I.4.2 Generation of the OCVF ..... 22
I.4.3 Generation of $Y_0^0(\theta,\phi)$ ..... 23
I.4.4 Force Balance Equation ..... 26
I.4.5 Energy Calculations ..... 26
I.5 The Nature of the Photon is the Basis of Quantization and Existence of Excited and Hydrino States of Atomic Hydrogen ..... 26
I.5.1 Excited States ..... 27
I.5.2 Instability of Excited States ..... 28
I.5.3 Hydrino States ..... 29
I.5.3.1 Extension of the Rydberg States to Lower Levels ..... 29
I.5.3.2 Photonic Equation ..... 32
I.5.3.3 Stability of the "Ground" and Hydrino States ..... 32
I.5.3.4 Catalytic Lower-Energy Hydrogen Electronic Transitions ..... 32
I.5.3.5 Catalyst Reaction Mechanism and Products ..... 33
I.5.3.6 Catalysts ..... 38
I.6 Outline of the Results of the Unified Theory Derived from First Principles ..... 40
I.6.1 Foundations ..... 40
I.6.2 Physical Concepts that Arise from CP Derivations on the Scale Range of 85 orders of Magnitude ..... 42
I.6.3 Summary of Foundations and Physical Phenomena Solved by Classical Physics ..... 45
References ..... 52
1. The One-Electron Atom ..... 57
1.1 Electron Source Current ..... 57
1.2 The Bound Electron "Atomic Orbital" ..... 60

1.2.1 Classical Physics of the de Broglie Relation ... 65
1.3 Rotational Parameters of the Electron (Angular Momentum, Rotational Energy, Moment of Inertia) ... 66
1.3.1 Electron Mechanics and the Corresponding Classical Wave Equation for the Derivation of the Rotational Parameters of the Electron ... 67
1.4 The Atomic Orbital Equation of Motion for $\ell = 0$ Based on the Current Vector Field (CVF) ... 70
1.4.1 Stern-Gerlach-Experiment Boundary Condition ... 70
1.5 Generation of the Atomic Orbital-CVFS ... 72
1.5.1 Generation of the BECVF ... 73
1.5.2 Generation of the OCVF ... 77
1.5.3 Generation of $Y_0^0(\theta,\phi)$ ... 80
1.5.4 Uniformity of $Y_0^0(\theta,\phi)$ ... 85
1.6 Spin Angular Momentum of the Atomic Orbital $Y_0^0\left(\theta,\phi\right)$ with $\ell = 0$ ... 90
1.7 Resonant Precession of the Spin-1/2-Current-Density Function Gives Rise to the Bohr Magneton ... 92
1.8 Magnetic Parameters of the Electron (Bohr Magneton) ... 96
1.8.1 The Magnetic Field of an Atomic Orbital from Spin ... 96
1.8.2 Derivation of the Magnetic Field ... 97
1.8.3 Derivation of the Energy ... 98
Box 1.1 Boundary Conditions of the Electron in a Magnetic Field are Met ... 99
References ... 102
1.9 Electron g Factor ... 103
1.9.1 Stored Magnetic Energy ... 103
1.9.2 Stored Electric Energy ... 104
1.9.3 Dissipated Energy ... 107
1.9.4 Total Energy of Spin-Flip Transition ... 108
1.10 Determination of Atomic Orbital Radii ... 111
1.11 Energy Calculations ... 114
1.12 Special Relativistic Effect on the Electron Radius and the Relativistic Ionization Energies ... 117
References ... 127
2. Excited States of the One-Electron Atom (Quantization) ... 129
2.1 Equation of the Electric Field inside the Atomic Orbital ... 129
2.2 Photon Absorption ... 133
2.3 Instability of Excited States ... 134
2.4 Source Current of Excited States ... 135
2.5 Selection Rules ... 137
2.6 Orbital and Spin Splitting ... 138
2.7 Stark Effect ... 140
2.8 State Lifetimes and Line Intensities ... 143
Box 2.1 Condensed Formula for the Excited-State Lifetimes and Line Intensities ... 153
2.9 Resonant Line Shape ... 155
2.10 Hydrogen Lamb Shift ... 156
2.10.1 Energy Calculations ... 157
2.11 Muonic Hydrogen Lamb Shift ... 159
2.11.1 Energy Calculations ... 160
2.12 Hydrogen Spin-Orbit Coupling (Fine Structure) ... 161
2.12.1 Energy Calculations ... 163
2.13 Hydrogen Knight Shift ... 164
2.14 Spin-Nuclear Coupling (Hyperfine Structure) ... 164

2.14.1 Energy Calculations ... 166
2.15 Muonium Hyperfine Structure Interval ... 167
2.15.1 Energy Calculations ... 168
References ... 170
3. Electron in Free Space ... 173
3.1 Charge-Density Function ... 173
3.2 Electric Field of a Free Electron ... 176
3.3 Current-Density Function ... 178
3.4 Force Balance Based on the Radiation-Reaction Force ... 181
3.5 Classical Physics of the de Broglie Relation ... 183
3.6 Stern-Gerlach Experiment ... 185
3.7 Free-Electron g Factor ... 192
3.7 Free-Electron Binding ... 193
References ... 197
4. Equation of the Photon ... 199
4.1 Right and Left Hand Circular and Elliptically Polarized Photons ... 199
4.2 Fields Based on Invariance Under Gauss' Integral Law ... 202
4.3 Linear Polarized Photons ... 204
4.4 Spherical Wave ... 204
4.5 Photon Torpedoes ... 205
4.6 Photoelectric Effect ... 205
4.7 Compton Effect ... 207
4.8 Transitions ... 208
4.9 Free Electron Photon Absorption ... 213
References ... 218
5. Hydrino Theory—BlackLight Process ... 219
5.1 BlackLight Process ... 219
5.2 Energy Transfer Mechanism ... 223
5.3 Energy Hole Concept ... 224
5.4 Catalysts ... 229
5.5 Energy Hole as a Multipole Expansion ... 232
5.6 Disproportionation of Energy States ... 232
5.7 Dipole-Dipole Coupling ... 238
5.8 Interstellar Disproportion Rate ... 240
5.9 Power Density of Gaseous Reactions ... 241
5.10 H Electronic Decay to Proton Decay Driving Subsequent Nuclear Reactions ... 242
5.11 Molecular BlackLight Process ... 249
5.11.1 Below "Ground" State Transitions of Hydrogen-Type Molecules and Molecular Ions ... 249
5.11.2 Energy Holes ... 249
5.11.3 Catalytic Energy Holes for Hydrogen-Type Molecules ... 252
References ... 253
6. Stability of Atoms and Hydrinos ... 257
6.1 Stability of "Ground" and Hydrino States ... 258
6.2 New "Ground" State ... 258
6.3 Spin-Nuclear and Orbital-Nuclear Coupling of Hydrinos ... 259
6.3.1 Energy Calculations ... 260
6.4 A Coefficient ... 261
6.5 Intensity of Spin-Nuclear and Orbital-Nuclear Coupling Transitions of Hydrinos ... 262
References ... 262
7. Two-Electron Atoms ... 265
7.1 Determination of Atomic Orbital Radii ... 265
7.2 Energy Calculations ... 273

7.2.1 Conservation of Energy ... 274
7.2.2 Ionization Energies ... 276
7.2.3 Dissipated Energy ... 277
7.3 Hydride Ion ... 279
7.3.1 Determination of the Atomic Orbital Radius, $r_n$ ... 280
7.3.2 Ionization Energy ... 280
7.4 Hydrino Hydride Ion ... 282
7.5 Hydrino Hydride Ion Nuclear Magnetic Resonance Shift ... 283
7.6 Hydrino Hydride Ion Hyperfine Lines ... 286
References ... 290
8. Classical Photon and Electron Scattering ... 291
8.1 Classical Scattering of Electromagnetic Radiation ... 291
8.1.1 Delta Function ... 291
8.1.2 The Array Theorem ... 292
8.1.3 Applications of the Array Theorem ... 292
8.1.3.1 Two-Slit Interference (Wave-Particle Duality) ... 292
8.2 Classical Wave Theory of Electron Scattering ... 295
8.2.1 Classical Wave Theory Applied to Scattering from Atoms and Molecules ... 298
8.3 Electron Scattering Equation for the Helium Atom Based on the Atomic Orbital Model ... 300
8.3.1 Results ... 302
8.4 Discussion ... 304
8.5 Physics of Classical Electron Diffraction Resolves the Wave-Particle Duality Mystery of Quantum Mechanics ... 305
8.6 Equations of Classical Diffraction ... 308
References ... 310
9. Excited States of Helium ... 311
9.1 Singlet Excited States with $\ell = 0$ $(1s^2 \rightarrow 1s^1(ns)^1)$ ... 313
9.2 Triplet Excited States with $\ell = 0$ $(1s^2 \rightarrow 1s^1(ns)^1)$ ... 315
9.3 Singlet Excited States with $\ell \neq 0$ ... 317
9.4 Triplet Excited States with $\ell \neq 0$ ... 320
9.5 All Excited He I States ... 323
9.6 Spin-Orbit Coupling of Excited States with $\ell \neq 0$ ... 327
References ... 328
10. Three- Through Twenty-Electron Atoms ... 329
10.1 Three-Electron Atoms ... 329
10.1.1 The Lithium Atom ... 329
10.1.2 The Radius of the Outer Electron of the Lithium Atom ... 333
10.1.3 The Ionization Energy of Lithium ... 333
10.1.4 Three Electron Atoms with a Nuclear Charge Z>3 ... 334
10.1.5 The Radius of the Outer Electron of Three-Electron Atoms with a Nuclear Charge Z>3 ... 336
10.1.6 The Ionization Energies of Three-Electron Atoms with a Nuclear Charge Z>3 ... 337
10.2 Four-Electron Atoms ... 339
10.2.1 Radii of the Outer Electrons of Four-Electron Atoms ... 339
10.2.2 Energies of the Beryllium Atom ... 340
10.2.3 The Ionization Energies of Four-Electron Atoms with a Nuclear Charge Z>4 ... 341
10.3 2P-Orbital Electrons Based on an Energy Minimum ... 343
10.4 Five-Electron Atoms ... 346
10.4.1 Radius and Ionization Energy of the Outer Electron of the Boron Atom ... 346
10.4.2 The Ionization Energies of Five-Electron Atoms with a Nuclear Charge Z>5 ... 347
10.5 Six-Electron Atoms ... 350

10.5.1 Radius and Ionization Energy of the Outer Electron of the Carbon Atom ..... 350
10.5.2 The Ionization Energies of Six-Electron Atoms with a Nuclear Charge Z>6 ..... 351
10.6 Seven-Electron Atoms ..... 353
10.6.1 Radius and Ionization Energy of the Outer Electron of the Nitrogen Atom ..... 353
10.6.2 The Ionization Energies of Seven-Electron Atoms with a Nuclear Charge Z>7 ..... 354
10.7 Eight-Electron Atoms ..... 357
10.7.1 Radius and Ionization Energy of the Outer Electron of the Oxygen Atom ..... 357
10.7.2 The Ionization Energies of Eight-Electron Atoms with a Nuclear Charge Z>8 ..... 358
10.8 Nine-Electron Atoms ..... 361
10.8.1 Radius and Ionization Energy of the Outer Electron of the Fluorine Atom ..... 361
10.8.2 The Ionization Energies of Nine-Electron Atoms with a Nuclear Charge Z>9 ..... 362
10.9 Ten-Electron Atoms ..... 365
10.9.1 Radius and Ionization Energy of the Outer Electron of the Neon Atom ..... 365
10.9.2 The Ionization Energies of Ten-Electron Atoms with a Nuclear Charge Z>10 ..... 366
10.10 General Equation for the Ionization Energies of Five Through Ten-Electron Atoms ..... 368
10.11 Eleven-Electron Atoms ..... 370
10.11.1 Radius and Ionization Energy of the Outer Electron of the Sodium Atom ..... 370
10.11.2 The Ionization Energies of Eleven-Electron Atoms with a Nuclear Charge Z>11 ..... 372
10.12 Twelve-Electron Atoms ..... 374
10.12.1 Radius and Ionization Energy of the Outer Electron of the Magnesium Atom ..... 374
10.12.2 The Ionization Energies of Twelve-Electron Atoms with a Nuclear Charge Z>12 ..... 376
10.13 3P-Orbital Electrons Based on an Energy Minimum ..... 378
10.14 Thirteen-Electron Atoms ..... 381
10.14.1 Radius and Ionization Energy of the Outer Electron of the Aluminum Atom ..... 381
10.14.2 The Ionization Energies of Thirteen-Electron Atoms with a Nuclear Charge Z>13 ..... 382
10.15 Fourteen-Electron Atoms ..... 385
10.15.1 Radius and Ionization Energy of the Outer Electron of the Silicon Atom ..... 385
10.15.2 The Ionization Energies of Fourteen-Electron Atoms with a Nuclear Charge Z>14 ..... 386
10.16 Fifteen-Electron Atoms ..... 388
10.16.1 Radius and Ionization Energy of the Outer Electron of the Phosphorous Atom ..... 388
10.16.2 The Ionization Energies of Fifteen-Electron Atoms with a Nuclear Charge Z>15 ..... 390
10.17 Sixteen-Electron Atoms ..... 392
10.17.1 Radius and Ionization Energy of the Outer Electron of the Sulfur Atom ..... 392
10.17.2 The Ionization Energies of Sixteen-Electron Atoms with a Nuclear Charge Z>16 ..... 393
10.18 Seventeen-Electron Atoms ..... 395
10.18.1 Radius and Ionization Energy of the Outer Electron of the Chlorine Atom ..... 395
10.18.2 The Ionization Energies of Seventeen-Electron Atoms with a Nuclear Charge Z>17 ..... 397
10.19 Eighteen-Electron Atoms ..... 399
10.19.1 Radius and Ionization Energy of the Outer Electron of the Argon Atom ..... 399
10.19.2 The Ionization Energies of Eighteen-Electron Atoms with a Nuclear Charge Z>18 ..... 401
10.20 General Equation for the Ionization Energies of Thirteen Through Eighteen-Electron Atoms ..... 403
10.21 Nineteen-Electron Atoms ..... 406
10.21.1 Radius and Ionization Energy of the Outer Electron of the Potassium Atom ..... 406
10.21.2 The Ionization Energies of Nineteen-Electron Atoms with a Nuclear Charge Z>19 ..... 407
10.22 Twenty-Electron Atoms ..... 409
10.22.1 Radius and Ionization Energy of the Outer Electron of the Calcium Atom ..... 409
10.22.2 The Ionization Energies of Twenty-Electron Atoms with a Nuclear Charge Z>20 ..... 411
10.23 General Equation for the Ionization Energies of Atoms Having an Outer S-Shell ..... 413
10.24 The Electron Configuration of Atoms ..... 416
References ..... 416

# SYMBOLS

| | |
|---|---|
| $\mu_0$ | permeability of free-space |
| $\varepsilon_0$ | permittivity or capacitivity of free-space |
| $\eta = \sqrt{\frac{\mu_0}{\varepsilon_0}}$ | intrinsic impedance of free-space |
| $c = \sqrt{\frac{1}{\mu_0 \varepsilon_0}}$ | speed of light |
| $\alpha = \frac{\mu_0 e^2 c}{2h}$ | fine structure constant |
| $g$ | electron g factor |
| $h$ | Planck constant |
| $\hbar$ | Planck constant bar |
| $e$ | fundamental charge |
| $m_e$ | mass of the electron |
| $\mu_e = \frac{m_e m_P}{m_e + m_P}$ | reduced mass of the electron |
| $a_0 = \frac{4\pi\varepsilon_0\hbar^2}{e^2 m_e} = \frac{\alpha}{4\pi R_\infty}$ | Bohr radius |
| $a_H = \frac{4\pi\varepsilon_0\hbar^2}{e^2 \mu_e} = \frac{\alpha}{4\pi R}$ | radius of the hydrogen atom |
| $R_\infty$ | Rydberg constant with $m_e$ |
| $R$ | Rydberg constant with $\mu_e$ |
| $\mu_B = \frac{e\hbar}{2m_e}$ | Bohr magneton |
| $\Phi_0 = \frac{h}{2e}$ | magnetic flux quantum |
| $\mu_N = \frac{e\hbar}{2m_P}$ | nuclear magneton |
| $\lambda\!\!\!^{-}_C = \frac{\lambda_C}{2\pi} = \frac{\hbar}{mc}$ | Compton wavelength bar |
| $\lambda\!\!\!^{-}_{Ce} = \frac{\lambda_{Ce}}{2\pi} = \alpha a_0 = \frac{\hbar}{m_e c} = \frac{\alpha^2}{4\pi R_\infty}$ | electron Compton wavelength bar |
| $G$ | Newtonian gravitational constant |
| $m_\mu$ | rest mass of the muon |
| $m_\tau$ | rest mass of the tau |
| $m_N$ | rest mass of the neutron |
| $m_P$ | rest mass of the proton |

Apparently there is color, apparently sweetness, apparently bitterness; actually there are only atoms and the void.

Democritus 420 BC

And God said, “Let there be light”; and there was light. And God saw that the light was good; and God separated the light from the darkness.

Genesis 1:3

All truth goes through three steps. First, it is ridiculed. Second, it is violently opposed, and finally it is accepted as self-evident.

Arthur Schopenhauer
German philosopher

We must be grateful to God that He created the world in such a way that everything simple is true and everything complicated is untrue.

Gregory Skovoroda
18th-century Ukrainian philosopher

One of the principal objects of theoretical research in any department of knowledge is to find the point of view from which the subject appears in its greatest simplicity.

Josiah Willard Gibbs

# PREFACE

Typically freshman students are introduced to classical laws that they apply to physical problems that can be understood intuitively and solved in closed form. As they advance to the second year, they are introduced to a contradictory view—that the atomic-scale world is nonphysical, counterintuitive, and incapable of being understood in physical, intuitive terms. In addition, they are asked to take for granted many fantastical concepts such as electrons being probability waves having an infinite number of energies and positions simultaneously, until measured, spooky actions at a distance, and virtual particles which occupy every point in space but can not be detected. With the introduction of quantum mechanics, which is not a theory of physical reality, students are taught to abandon all that they initially learned for laboratory scale systems and to accept that these laws do not apply to atomic systems; even though, they learned by direct experimental observation that these laws worked perfectly well and that laboratory scale objects are made up of atoms.

This non-physical treatment of atomic electrons is propagated into molecular theory. Repulsion between juxtaposed like charges is an undeniable reality; yet quantum theoreticians teach the opposite: chemical bonding is due to negative charges overlapping wherein the more negative charges occupying the same space, the stronger the bond; except that the electrons are also simultaneously repulsive requiring the addition of quantum mechanical wave function electron-electron repulsion terms. Even regions of empty space devoid of nuclei and electrons together with many other ad hoc, inconsistent, often nonphysical, and non-unique terms further comprise the quantum mechanical treatment of the nature of the chemical bond.

Many paradoxes and internal inconsistencies arise in quantum mechanics such as the requirement that two or more contradictory results exist simultaneously, the existence of infinities, non-locality, and violation of causality, to mention a few. Unlike the solutions learned in the freshman year, none of the solutions are unique—algorithms to remove infinities and to add fantastical corrections are totally discretionary [1-17]. One exception is the one-electron atom, but the Schrödinger equation is not a directly experimentally testable relationship. Rather, it is postulated. The solutions make no physical sense. Electron spin is missed completely. And, in many cases, the solutions contradict experimental observations [1-17].

To add to this confusion, Newton's Laws of mechanics are presented as invalid. With the assumption of Galilean transformations, they fail to remain invariant at high speed. Special relativity is introduced as an independent mechanics theory based on the constant maximum of the speed of light, which was demonstrated by the Michelson-Morley experiment. But, this experiment addressed light propagation and not mechanics, except for disproving the ether and a universal reference frame in the sense of the speed of light. Maxwell's equations, which govern light propagation, remain since they are consistent with special relativity and predict $c$ based on universal properties of spacetime. No connection to mass or mechanics is given despite the result of the equivalence of mass and electromagnetic energy from special relativity. There is no connection to particle masses and atomic theory. And, the infinite sea of virtual particles of atomic theory is paradoxically an ether which was abandoned with special relativity.

Furthermore, it is taught that the validity of Maxwell's equations is restricted only to the macro-scale and that they do not apply to the atomic scale. This is inconsistent with the application of special relativity to the mechanics of atomic particles at high speed and the radiation of accelerating atomic particles wherein, paradoxically, Maxwell's equations give the electromagnetic wave equation that governs the emitted radiation. Yet, when the particle motion is thought of as a current, Maxwell's equations predict the radiation of atomic particles as well. Then, contradictory, postulated quantum mechanical rules apply to the radiation or stability of electrons in atoms, which should be treated electrodynamically. Neither a special relativistic or Maxwellian approach to the radiation is deemed to apply even though the Maxwellian Coulomb potential and special relativistic corrections to the electron mass are invoked. Even more disconcerting is that supposedly special relativity is the basis of electron spin in the Dirac equation. But, the solution requires an infinite sea of virtual particles that is equivalent to the ether. This constitutes a glaring internal inconsistency because the absence of both an ether and an absolute frame is the basis of special relativity in the first place. In addition, considering the simplest atom, hydrogen, no physical mechanism for the existence of

discrete radiative energy levels or the stability of the $n = 1$ state exists—only circular reasoning between the empirical data and a postulated wave equation with an infinite number of solutions that was parameterized to match the Rydberg lines [1-17].

Furthermore, the elimination of absolute frame by special relativity results in the elimination of inertial mass and Newton's Second law, foundations of mechanics, and gives rise to the twin paradox and an infinite number of energy inventories of the universe based on the completely arbitrary definition of the observer's frame of reference. Newton's Law of gravitation is also to be unlearned. It is replaced by a postulated tensor relationship that only applies to massive gravitating objects. The replacement theory is explained in terms of warping of spacetime without any connection to the physical laws learned as a freshman or any connection to atoms that make up the massive gravitating bodies. General relativity predicts singularities and a deceleration cosmology—the opposite of that which is observed [18-19]. It is to be accepted with quantum mechanics as the correct atomic theory even though these theories are mutually incompatible. It is further disconcerting that the Uncertainty Principle of quantum mechanics—one of its fundamental tenets—predicts a continuum of particle masses and gives no mechanism for the existence of atomic particles of precise inertial and gravitational mass in the first place. And, the infinite sea of virtual particles and vacuum energy fluctuations throughout the entire universe requires an infinite cosmological constant that is obviously not observed [20].

This confused approach to physics is not due to nature, and it can be avoided. Physics can become transparent and intuitive on all scales and understood conceptually at all levels of specialization. The same is true for chemistry wherein the multitudes of ad hoc, nonphysical, inconsistent, nonunique, adjustable atomic and molecular modeling algorithms of quantum theory are replaced by exact physical solutions comprising fundamental constants only [3-7]. The fundamental laws of physics and chemistry of Maxwell's equations and Newton's Laws of mechanics and gravitation were developed after direct experimental observation of phenomena such as electricity and magnetism, mechanics, and gravity. Electricity and magnetism were unified with the prediction and later confirmation of electromagnetic waves. These laws, developed in the mid 1800's, with the extension to the atomic scale and taking into account the appropriate spacetime metric are sufficient for describing all phenomena in the universe. For objects moving with speeds approaching the speed of light, Newton's Laws must include the limiting maximum speed that is inherent in Maxwell's equations and determined by the permeability and permittivity of spacetime. In mechanics, the metric is Minkowskian wherein the speed relative to light speed must be invoked and Galilean transformations become Lorentzian. Similarly, when a photon transforms to a particle, any signal capable of transporting energy with a limiting velocity must propagate as a light wave front, and the limiting velocity is the speed of light. Thus, for particle production, the electromagnetic front of the photon and the gravitational front due to the particle must have a limiting speed $c$, the speed of light. As a consequence, the metric is required to be the Schwarzschild metric rather than Minkowskian. Specifically, fundamental particle production occurs when the energy of the particle given by the Planck equation, Maxwell's Equations, and Special Relativity is equal to $mc^2$, and the proper time is equal to the coordinate time according to Schwarzschild metric. The gravitational equations with the equivalence of the particle production energies permit the equivalence of mass-energy and the absolute spacetime wherein a *"clock" is defined which measures "clicks" on an observable in one aspect, and in another, it is the ruler of spacetime of the universe with the implicit dependence of spacetime on matter-energy conversion*. The masses of the leptons, the bosons, the quarks, and nucleons are derived from this metric of spacetime. Then, the gravitational equations with the equivalence of the particle production energies require the conservation relationship of mass-energy, $E = mc^2$, and spacetime, $\frac{c^3}{4\pi G} = 3.22\ X\ 10^{34}\ \frac{kg}{\sec}$. Consequently, the Universe is oscillatory in matter, energy, and spacetime. Spacetime expands as matter converts to energy, and spacetime contracts during particle production. An H atom decay and production cycle of the universe drives its corresponding spacetime expansion-contraction cycle. Specifically, the electrons of H atoms undergo electronic transitions to lower energy levels to form so called "hydrino atoms" which comprise the dark matter of the universe. Hydrino atoms of very low energy states cause proton decay with electron annihilation to gamma rays. Energy to matter conversion occurs by hydrogen atom production during gamma ray bursts triggered when the mass density of a black hole exceeds that of the Planck mass density wherein matter converts into energy, space time expands, and a gamma ray burst occurs with the conservation of the mass-energy in the production of protons and electrons emitted into interstellar medium. Production and annihilation of matter occur simultaneously with annihilation dominating during the expansion phase and production dominating during the contraction phase of the oscillatory cycle.

The relationship between matter, energy and spacetime further provides the basis of absolute space and the atomic, thermodynamic, and cosmological arrows of time. The observations of the acceleration of the cosmic expansion, the existence of stars, galaxies, and large-scale galactic structures which are older than the elapsed time of the present expansion as stellar and galactic evolution occurred during the contraction phase, the absence of the signatures of a Big Bang origin of the universe, the absence of time dilation due to relative local motion in redshifted quasars, near-light-speed ejection of electron jets from blackholes, gamma ray bursts from massive blackholes, and the observation of reactionless acceleration of free electrons by absorption of microwave photons ("space drive") confirm the absolute nature of spacetime.

With the conditions of the metric being Minkowskian for Newtonian mechanics and the Schwarzschild metric for Newtonian gravity, all of the fundamental laws of nature are directly derived from experiments. The universe is not mathematical; it is physical. A separate theory for near light speed mechanics, special relativity as it now exists, is unnecessary and incomplete. For example, in addition to the problems raised previously, the famous equation $E = mc^2$ does not predict fundamental particle masses, inertial or gravitational or why they are equivalent. Furthermore, separate theories of atomic physics such as quantum mechanics and quantum electrodynamics, separate nuclear theories such as quantum chromodynamics,

a separate theory for particles such as the standard model, a separate theory for gravity, general relativity as it now exists, and separate theories for cosmology such as the Big Bang, inflation, and dark energy are artificial, internally inconsistent, incorrect, incomplete, and not based on physical laws. The correct basis of the spacetime relationships of special relativity and general relativity are inherent in the classical laws that further predict all natural phenomena of physics and chemistry and compositions of matter and energy of any complexity from the scale of quarks to the cosmos in terms of the fundamental constants of nature only.

## REFERENCES


1. R. L. Mills, "Classical Quantum Mechanics," Physics Essays, Vol. 16, No. 4, December, (2003), pp. 433-498.
2. R. L. Mills, "Physical Solutions of the Nature of the Atom, Photon, and Their Interactions to Form Excited and Predicted Hydrino States," Phys. Essays, Vol. 20, No. 3, (2007), pp.403-460.
3. R. L. Mills, "Exact Classical Quantum Mechanical Solutions for One- Through Twenty-Electron Atoms," Physics Essays, Vol. 18, (2005), pp. 321-361.
4. R. L. Mills, "The Nature of the Chemical Bond Revisited and an Alternative Maxwellian Approach," Physics Essays, Vol. 17, (2004), pp. 342-389.
5. W. Xie, R. L. Mills, W. Good, A. Makwana, B. Holverstott, N. Hogle, "Millsian 2.0: A Molecular Modeling Software for Structures, Charge Distributions and Energetics of Biomolecules," Physics Essays, Vol. 24, (2011) 200–212.
6. R. L. Mills, B. Holverstott, W. Good, A. Makwana, "Total Bond Energies of Exact Classical Solutions of Molecules Generated by Millsian 1.0 Compared to Those Computed Using Modern 3-21G and 6-31G* Basis Sets," Phys. Essays, Vol. 23, (2010), 153–199; doi: 10.4006/1.3310832.
7. https://millsian.com.
8. R. L. Mills, "Maxwell's Equations and QED: Which is Fact and Which is Fiction," Vol. 19, (2006), pp. 225-262.
9. R. L. Mills, "Exact Classical Quantum Mechanical Solution for Atomic Helium Which Predicts Conjugate Parameters from a Unique Solution for the First Time," Phys. Essays, Vol. 21, No. 2, pp. 103-141.
10. R. L. Mills, "The Fallacy of Feynman's Argument on the Stability of the Hydrogen Atom According to Quantum Mechanics," Annales de la Fondation Louis de Broglie, Vol. 30, No. 2, (2005), pp. 129-151.
11. R. Mills, "The Grand Unified Theory of Classical Quantum Mechanics," Int. J. Hydrogen Energy, Vol. 27, No. 5, (2002), pp. 565-590.
12. R. Mills, "The Nature of Free Electrons in Superfluid Helium—a Test of Quantum Mechanics and a Basis to Review its Foundations and Make a Comparison to Classical Theory," Int. J. Hydrogen Energy, Vol. 26, No. 10, (2001), pp. 1059-1096.
13. R. Mills, "The Hydrogen Atom Revisited," Int. J. of Hydrogen Energy, Vol. 25, Issue 12, December, (2000), pp. 1171-1183.
14. V. F. Weisskopf, Reviews of Modern Physics, Vol. 21, No. 2, (1949), pp. 305-315.
15. P. Pearle, Foundations of Physics, "Absence of radiationless motions of relativistically rigid classical electron," Vol. 7, Nos. 11/12, (1977), pp. 931-945.
16. A. Einstein, B. Podolsky, N. Rosen, Phys. Rev., Vol. 47, (1935), p. 777.
17. F. Laloë, "Do we really understand quantum mechanics? Strange correlations, paradoxes, and theorems," Am. J. Phys. 69 (6), June 2001, 655-701.
18. R. M. Wald, *General Relativity*, University of Chicago Press, Chicago, (1984), pp. 91-101.
19. N. A. Bahcall, J. P. Ostriker, S. Perlmutter, P. J. Steinhardt, Science, May 28, 1999, Vol. 284, pp. 1481-1488.
20. M. M. Waldrop, Science, Vol. 242, December 2, (1988), pp. 1248-1250.

# INTRODUCTION

## GENERAL CONSIDERATIONS

Toward the end of the 19th century, many physicists believed that all of the principles of physics had been discovered. The accepted principles, now called ***classical physics***, included laws relating to Newton's mechanics, Gibbs' thermodynamics, LaGrange's and Hamilton's elasticity and hydrodynamics, Maxwell-Boltzmann molecular statistics, and Maxwell's equations. However, the discovery that the intensity of blackbody radiation goes to zero, rather than infinity as predicted by the prevailing laws, provided an opportunity for new principles to be discovered. In 1900, Planck made the revolutionary assumption that energy levels were quantized, and that atoms of the blackbody could emit light energy only in amounts given by $h\nu$, where $\nu$ is the radiation's frequency and $h$ is a proportionality constant (now called Planck's constant). This assumption also led to our understanding of the photoelectric effect and ultimately to the concept of light as a particle called a photon. A similar course arose in the development of the model of the electron. In 1923, de Broglie suggested that the motion of an electron has a wave aspect where the wavelength, $\lambda$, is inversely proportional to the electron's momentum, $p$, as $\lambda = \frac{h}{p}$. This concept seemed unlikely according to the familiar properties of electrons such as charge, mass and adherence to the laws of particle mechanics. But the wave nature of the electron was confirmed by Davisson and Germer in 1927, by observing diffraction effects when electrons were reflected from metals.

Experiments by the early part of the 20th century had revealed that both light and electrons behave as waves in certain instances and as particles in others. This was unanticipated from preconceptions about the nature of light and the electron. Early 20th century theoreticians proclaimed that light and atomic particles have a "wave-particle duality" that was unlike anything in our common-day experience. The wave-particle duality is the central mystery of the presently accepted atomic model, ***quantum mechanics*** (QM), the one to which all other mysteries could ultimately be reduced. The central equation, the Schrödinger equation, and its associated postulates, are now the basis of quantum mechanics, and it is the basis for the world view that the atomic realm including the electron and photon cannot be described in terms of "pure" wave and "pure" particle but in terms of a wave-particle duality. The wave-particle duality based on the fundamental principle that physics on an atomic scale is very different from physics on a macroscopic scale is central to present day atomic theory [1]. Further founding assumptions maintained from the earlier theories of Bohr and Schrödinger to what is dubbed "modern quantum mechanics" are that phenomena such as stability, quantization, and spin are intrinsic aspects of matter at the atomic scale and the electron is a probability wave requiring that the electron have infinite numbers of positions and energies including negative and infinite energies simultaneously. It is inherent that physical laws such as Maxwell's equations, Newton's laws, conservation of energy and angular momentum are not exactly obeyed. The exactness and determinism of classical physics are replaced by the Heisenberg Uncertainty Principle, an inequality defining the limitations of the existence of physical reality that has recently been tested for the first time and experimentally disproved [2]. Recently a new measuring technique that exploits superposition (i.e. interference) of two short pulses of light with different wavelengths circumvented the limitation formulated by the father of quantum physics, Werner Heisenberg, in 1927. According to Heisenberg's uncertainty principle (HUP), it is not possible to determine the position and the speed of an electron at the same instant. However, Isinger et al. [3] have shown definitively that it can be done and thereby experimentally disproving the HUP. Since the HUP is an inherent consequence of the theory of quantum mechanics (QM), QM is proven wrong as well.

The Schrödinger equation was originally postulated in 1926 as having a solution of the one-electron atom. It gives the principal energy levels of the hydrogen atom as eigenvalues of eigenfunction solutions of the Laguerre differential equation. But, as the principal quantum number n>>1, the eigenfunctions become nonsensical. Despite its wide acceptance, on deeper

inspection, the Schrödinger solution is plagued with many failings as well as difficulties in terms of physical interpretations that have caused it to remain controversial since its inception. Only the one-electron atom may be solved without approximations, but it fails to predict electron spin, leads to models with nonsensical consequences such as negative energy states of the vacuum, infinities, and negative kinetic energy, and it fails to predict the stability of the atomic hydrogen $n=1$ state except for an arbitrary definition[1] [4-15]. In addition to many predictions that simply do not agree with observations even regarding the one-electron atom [4-20], the Schrödinger equation predicts noncausality, nonlocality, spooky actions at a distance or quantum telepathy, perpetual motion, and many internal inconsistencies where contradicting statements have to be taken true simultaneously. The behavior of free electrons in superfluid helium is but one example of a phenomenon that forces the issue of the meaning of the wavefunction. Electrons form bubbles in superfluid helium, which reveal that the electron is real and that a physical interpretation of the wavefunction is necessary. Furthermore, when irradiated with light of energy of about a 0.5 to several eV [21], the electrons carry current at different rates as if they exist with different sizes. It has been proposed that the behavior of free electrons in superfluid helium can be explained in terms of the electron breaking into pieces at superfluid helium temperatures [21]. Yet, the electron has proven to be indivisible even under particle accelerator collisions at 90 GeV (LEPII). The nature of the wavefunction must now be addressed. It is time for the physical rather than the mathematical nature of the wavefunction to be determined.

A new approach has been developed to explain the seemingly mysterious physics of the atomic scale. The theory of ***classical physics*** (CP) now applied correctly to solving the structure of the electron is based on the foundation that laws of physics valid in the macroworld *do hold true* in the microworld of the atom. In the present case, the predictions, which arise from the equations of light and atomic particles are completely consistent with observation, including the wave-particle duality of light and atomic particles. Furthermore, it is shown herein that the quantization of atomic energy levels arises classically without invoking new physics. Continuous motion such as electronic transitions between quantized states and translational motion restores continuity and causality with the continuous nature of spacetime itself restored consistent with first principles and observation. Using Maxwell's equations, *the structure of the electron is derived as a boundary-value problem wherein the electron comprises the source current of time-varying electromagnetic fields during transitions with the constraint that the bound* $n=1$ *state electron cannot radiate energy*. The postulates and mathematical constructs of quantum mechanics are erroneous. Physical laws are shown to apply to the atomic scale in refutation to QM. This issue of treating the wavefunction physically is even more imperative given that classical physics predicts hydrogen atomic transitions below the inalienable quantum "ground state" and these predictions are experimentally confirmed [22-42] with the further result that the corresponding fractional principal quantum states match the observations of free electrons in superfluid helium [14]. (See Free Electrons in Superfluid Helium are Real in the Absence of Measurement Requiring a Connection of $\psi$ to Physical Reality section.)

QM has never dealt with the nature of fundamental particles. Rather, it postulates the impossible situation that they occupy no volume; yet are everywhere at once. In contrast, CP solves the structure of the electron using the constraint of nonradiation based on Maxwell's equations. CP gives closed-form physical solutions for the electron in atoms, the free electron, and excited states that match the observations. With these solutions, conjugate parameters can be solved for the first time, and atomic theory is at last made predictive and intuitive. Application of Maxwell's equations precisely predicts hundreds of fundamental spectral observations and atomic and molecular solutions in exact equations with no adjustable parameters (fundamental constants only). Moreover, unification of atomic and large-scale physics, the ultimate objective of natural theory, is enabled. The result gives a natural relationship between Maxwell's equations, special relativity, and general relativity. CP holds over a scale of spacetime of 85 orders of magnitude—it correctly predicts the nature of the universe from the scale of the quarks to that of the cosmos.

The Maxwellian approach allows the solution of previously intractable problems such as the equations of the masses of fundamental particles. Exemplary relations between fundamental particles are shown in Table I.1.

[1] The Schrödinger equation can only yield integer eigenvalue solutions by selection or definition from an infinite number of possibilities since the solution is over all space with no boundary (i.e. 0 to $\infty$). In contrast, wave equation solutions with integers are common for boundary-constrained systems such as waveguides and resonators.

**Table I.1.** The relations between the lepton masses and neutron to electron mass ratio are given in terms of the dimensionless fine structure constant $\alpha$ only.

$$\frac{m_\mu}{m_e}=\left(\frac{\alpha^{-2}}{2\pi}\right)^{\frac{2}{3}}\frac{\left(1+2\pi\frac{\alpha^2}{2}\right)}{\left(1+\frac{\alpha}{2}\right)}=206.76828 \qquad (206.76827)^{a}$$

$$\frac{m_\tau}{m_\mu}=\left(\frac{\alpha^{-1}}{2}\right)^{\frac{2}{3}}\frac{\left(1+\frac{\alpha}{2}\right)}{\left(1-4\pi\alpha^2\right)}=16.817 \qquad (16.817)$$

$$\frac{m_\tau}{m_e}=\left(\frac{\alpha^{-3}}{4\pi}\right)^{\frac{2}{3}}\frac{\left(1+2\pi\frac{\alpha^2}{2}\right)}{\left(1-4\pi\alpha^2\right)}=3477.2 \qquad (3477.3)$$

$$\frac{m_N}{m_e}=\frac{12\pi^2}{1-\alpha}\sqrt{\frac{\sqrt{3}}{\alpha}}\frac{\left(1+2\pi\frac{\alpha^2}{2}\right)}{\left(1-2\pi\frac{\alpha^2}{2}\right)}=1838.67 \qquad (1838.68)$$

[a] Experimental according to the 1998 CODATA and the Particle Data Group [43-44].

CP successfully predicted the mass of the top quark before it was reported and correctly predicted the acceleration of the expansion of the universe before it was observed [45]. It correctly predicts the behavior of free electrons in superfluid helium and further predicts the existence of new states of hydrogen that are lower in energy than the $n=1$ state that represents a new energy source and a new field of chemistry that has far reaching technological implications in power generation, materials, lighting, and lasers. The existence of such states has been confirmed by the data presented in over 100 published journal articles and over 50 independent test reports and articles [22].

## CP APPROACH TO THE SOLUTION OF THE BOUND ELECTRON

CP solves the electron by a different approach than that used to solve the Schrödinger wave equation. Rather than using a postulated wave equation with time eliminated in terms of the energy of the electron in a Coulomb field and solving the charge wave (Schrödinger interpretation) or the probability wave (Born interpretation), the solution for the scalar (charge) and vector potential (current) functions of the electron are sought based on first principles. Since the hydrogen atom is stable and nonradiative, the electron has constant energy. Furthermore, it is time dynamic with a corresponding current that serves as a source of electromagnetic radiation during transitions. The wave equation solutions of the radiation fields permit the source currents to be determined as a boundary-value problem. These source currents match the field solutions of the wave equation for two dimensions plus time when the nonradiation condition is applied. Then, the mechanics of the electron can be solved from the two-dimensional wave equation plus time in the form of an energy equation wherein it provides for conservation of energy and angular momentum, as given in the Electron Mechanics and the Corresponding Classical Wave Equation for the Derivation of the Rotational Parameters of the Electron section.

Specifically, CP first assumes that the functions that physically describe the mass and charge of the electron in space and time comprise time-harmonic multipole source currents of time-varying electromagnetic fields between transitions. Rather than use the postulated Schrödinger boundary condition: "$\Psi\to 0$ as $r\to\infty$," which leads to a purely mathematical model of the electron, the constraint is based on the experimental observation that the moving charge must not radiate in the $n=1$ state of hydrogen. The condition for nonradiation based on Maxwell's equations after Haus [46] is that its spacetime Fourier transform does not possess components that are synchronous with waves traveling at the speed of light. Jackson [47] gives a generalized expansion in vector spherical waves that are convenient for electromagnetic boundary-value problems possessing spherical symmetry properties and for analyzing multipole radiation from a localized source distribution. The special case of nonradiation determines that the current functions are confined to two-spatial dimensions plus time and match the electromagnetic wave-equation solutions for these dimensions. The boundary-value solutions for the current-density functions comprise spherical harmonic functions and time harmonic functions confined to two dimensions ($\theta$ and $\phi$) plus time. In order for the current to be positive definite, a constant function corresponding to the electron spin function is added to each of the spherical harmonic functions corresponding to orbital angular momentum to give the charge (mass)-density functions of the bound electron as a

function of time called an electron atomic orbital. The integral of the constant function over the atomic orbital is the total charge (mass) of the electron. The integral of a spherical harmonic function over the atomic orbital is zero; thus, it modulates the spin function. These functions comprise the well-known s, p, d, f, etc. electrons or orbitals. In the case that such an electron state arises as an excited state by photon absorption, it is radiative due to a radial dipole term in its current-density function since it possesses spacetime Fourier components synchronous with waves traveling at the speed of light, as shown in the Instability of the Excited States section.

The excited states involving the corresponding multipole photon radiation are solved including the radii of the atomic orbitals using Maxwell's equations with the traditional source current boundary constraints at the electron. Quantization arises from the equation of the photon and the electron—not from the solution of the electron alone. After all, each solution models an excited state created by the absorption of a photon. The solutions are analogous to those of excited resonator modes except that the cavity is dynamic. The photon field is described by a Dirac delta function at the radius of the electron, $\delta(r-r_n)$, and due to relativistic effects the field is radially local at the electron. The field lines from the proton superimpose with those of the photon at the electron and end on the current-density function of the electron such that the electric field is zero for $r > r_n$, where $r_n$ is the radius of the electron. The trapped photons are solutions of Maxwell's equations. The electrodynamic field of the photon is a constant function plus a time and spherical harmonic function that is in phase with source currents at the electron, which is given by a constant plus a time and spherical harmonic function. Only particular solutions are possible as resonant photons of the electron, which is a dynamic resonator cavity. The results are in agreement with first principle physics and experimental observations of the hydrogen atom, excited states, free electron, and free space photon including the wave particle duality aspects.

## SPIN AND ORBITAL PARAMETERS ARISE FROM FIRST PRINCIPLES ONLY IN THE CASE OF CP

An electron is a two-dimensional spherical surface, called an *electron atomic orbital*, that can exist in a bound state only at specific radii $r_n$ from the nucleus. (See Figures I.1 and I.2 for a pictorial representation of an atomic orbital.) The result for the $n=1$ state of hydrogen is that the charge-density function remains constant with each point on the surface moving at the same angular and linear velocity. The constant function corresponds to the spin function that has a corresponding spin angular momentum that may be calculated from $\mathbf{r}\times\mathbf{p}$ applied directly to the current-density function that describes the electron. The radius of the nonradiative ($n=1$) state is solved using the electromagnetic force equations of Maxwell relating the charge and mass-density functions wherein the angular momentum of the electron is $\hbar$ (Eq. (1.253)). The reduced mass arises naturally from an electrodynamic interaction between the electron and the proton, rather than from a point mass revolving around a point nucleus in the case of Schrödinger wave equation solutions, which presents an internal inconsistency since the wave functions are spherically symmetrical.

CP gives closed form solutions for the resonant photons and excited state electron functions. The free space photon also comprises a radial Dirac delta function, and the angular momentum of the photon given by $\mathbf{m}=\int\frac{1}{8\pi c}\mathrm{Re}\left[\mathbf{r}\times(\mathbf{E}\times\mathbf{B}^*)\right]dx^4=\hbar$ in the Photon section is conserved for the solutions for the resonant photons and excited state electron functions. It can be demonstrated that the resonance condition between these frequencies is to be satisfied in order to have a net change of the energy field [48]. In the present case, the correspondence principle holds. That is the change in angular frequency of the electron is equal to the angular frequency of the resonant photon that excites the resonator cavity mode corresponding to the transition, and the energy is given by Planck's equation. The predicted energies, Lamb shift, fine structure splitting, hyperfine structure, resonant line shape, line width, selection rules, etc., are in agreement with observation.

The radii of excited states are solved using the electromagnetic force equations of Maxwell relating the field from the charge of the proton, the electric field of the photon, and charge and mass-density functions of the electron wherein the angular momentum of the electron is $\hbar$ (Eq. (1.253)).

For excited states of the hydrogen atom, the constant function corresponds to the spin function. Each spherical harmonic function modulates the constant spin function and corresponds to an orbital function of a specific excited state with a corresponding phase-matched trapped photon and orbital angular momentum. Thus, the spherical harmonic function behaves as a charge-density wave, which travels time harmonically on the surface of the atomic orbital about a specific axis. (See Figure 1.2 for a pictorial representation for several $\ell$ values.) The amplitude of the corresponding orbital energy may be calculated from Maxwell's equations. Since the constant function is modulated harmonically, the time average of the orbital energy is zero except in the presence of a magnetic field. Nondegeneracy of energy levels arises from spin, orbital, and spin-orbit coupling interactions with the applied field. The electrodynamic interaction with the magnetic field gives rise to the observed hyperfine splitting of the hydrogen spectrum.

Many inconsistencies arise in the case of the corresponding solutions of the Schrödinger wave equation. For example, where is the photon in excited states given by the Schrödinger equation? A paradox also arises for the change in angular momentum due to photon absorption. The Schrödinger equation solutions for the kinetic energy of rotation $K_{rot}$ is given by Eq. (10) of Ref. [14] and the value of the electron angular momentum $L$ for the state $Y_{lm}(\theta,\phi)$ is given by Eq. (11) of Ref. [14]. They predict that the excited state rotational energy levels are nondegenerate as a function of the $\ell$ quantum number even in the

absence of an applied magnetic field, and the predicted energy is over six orders of magnitude of the observed nondegenerate energy in the presence of a magnetic field. In the absence of a magnetic field, no preferred direction exists. In this case, the $\ell$ quantum number is a function of the orientation of the atom with respect to an arbitrary coordinate system. Therefore, the nondegeneracy is nonsensical and violates conservation of angular momentum of the photon.

In quantum mechanics, the spin angular momentum of the electron is called the "intrinsic angular momentum" since no physical interpretation exists. The Schrödinger equation is not Lorentz invariant in violation of special relativity. It fails to predict the results of the Stern-Gerlach experiment that indicates the need for an additional quantum number. Quantum Electrodynamics (QED) was proposed by Dirac in 1926 to provide a generalization of quantum mechanics for high energies in conformity with the theory of special relativity and to provide a consistent treatment of the interaction of matter with radiation. It is fatally flawed. From Weisskopf [16], "Dirac's quantum electrodynamics gave a more consistent derivation of the results of the correspondence principle, but it also brought about a number of new and serious difficulties." Quantum electrodynamics: (i) *does not explain nonradiation of bound electrons*; (ii) contains an internal inconsistency with special relativity regarding the classical electron radius—the electron mass corresponding to its electric energy is infinite (the Schrödinger equation fails to predict the classical electron radius); (iii) it admits solutions of negative rest mass and negative kinetic energy; (iv) the interaction of the electron with the predicted zero-point field fluctuations leads to infinite kinetic energy and infinite electron mass; (v) Dirac used the unacceptable states of negative mass for the description of the vacuum; yet, infinities still arise. Dirac's equation, which was postulated to explain spin, relies on the unfounded notions of negative energy states of the vacuum, virtual particles, and gamma factors. All of these features are untenable or are inconsistent with observation. These problems regarding spin and orbital angular momentum and energies and the classical electron radius are nonexistent with CP solutions.

From the time of its inception, quantum mechanics (QM) has been controversial because its foundations are in conflict with physical laws and are internally inconsistent. Interpretations of quantum mechanics such as hidden variables, multiple worlds, consistency rules, and spontaneous collapse have been put forward in an attempt to base the theory in reality. Unfortunately, many theoreticians ignore the requirement that the wave function must be real and physical in order for it to be considered a valid description of reality. These issues and other such flawed philosophies and interpretations of experiments that arise from quantum mechanics are discussed in the Retrospect section and Ref. [10, 12, 14]. Reanalysis of old experiments and many new experiments including electrons in superfluid helium and data confirming the existence of hydrinos challenge the Schrödinger equation predictions. Many noted physicists rejected quantum mechanics, even those whose work undermined classical laws. Feynman attempted to use first principles including Maxwell's Equations to discover new physics to replace quantum mechanics [49] and Einstein searched to the end. "Einstein [...] insisted [...] that a more detailed, wholly deterministic theory must underlie the vagaries of quantum mechanics [50]." He believed scientists were misinterpreting the data. Examples of quantum mechanical misinterpretations of experiments are given in Box I.1. (See the following sections: The One-Electron Atom, Electron in Free Space, Classical Photon and Electron Scattering, Three- Through Twenty-Electron Atoms, Superconductivity, Gravity, Wave-Particle Duality, and Refs. [9, 10, 12].)

## BOX I.1 MISINTERPRETATIONS OF OBSERVATIONS AS WEIRDNESS OF QUANTUM MECHANICS IS REVEALED TO BE DUE TO ATOMIC-SCALE CLASSICAL PHYSICS

***QM:*** The rise in current of free electrons in superfluid helium when irradiated with low-energy light and the formation of an unexpected plethora of exotic negative charge carriers in superfluid helium with mobilities greater than that of the normal electron are due to the electron breaking into fractional pieces.

**CP:** Fractional principal quantum energy states of the electron in liquid helium match the photoconductivity and mobility observations without requiring that the electron is divisible.

***QM:*** Virtual particles surround the electron, and as the electron's center is approached, they shield the electron's charge less effectively.

**CP:** The electron is an extended particle, rather than a point, and the charge density is greatest in the center.

***QM:*** Spooky actions at a distance are predicted.

**CP:** Photon momentum is conserved on a photon-by-photon basis rather than statistically as predicted by quantum mechanics which predicts photon coincidence counts at separated detectors (Aspect experiment).

***QM:*** The purely postulated Hund's Rule and the Pauli Exclusion Principle of the assignment of unique quantum numbers to all electrons are "weird spooky action" phenomena unique to quantum mechanics that require all electrons in the universe to have instantaneous communication and coordination with no basis in physical laws such as Maxwell's equations.

**CP:** The observations that all electrons have unique quantum numbers and that the electron configuration of atoms follows a pattern based on solutions of Laplace's equation are phenomenological consequences of physical laws such as Maxwell's equations.

***QM:*** Since fundamental particles are probability waves and their position and energy are uncertain according to the Uncertainty Principle, they can "magically" appear on the other side of a supposedly insurmountable energy barrier based on their energy on the initial side of the barrier; thus, they defy physical laws and tunnel through the barrier.

**CP:** Fundamental particles such as an electron are real, extended particles each of size equal to its de Broglie wavelength, rather than a point-particle-probability-wave. Potential energy is gained as the particle traverses the barrier that is cleared; even though its initial kinetic energy was less than the barrier height. Energy conservation is obeyed at all times. Tunneling arises from physical laws.

***QM:*** A $^{9}Be^{+}$ ion may be in two separate locations at once.

**CP:** The fluorescence emission spectrum of a Penning trapped $^{9}Be^{+}$ ion shows interference peaks due to coupling between oscillator modes and a Stern Gerlach transition.

***QM:*** Supercurrent may go in both directions at once.

**CP:** The energy difference of a superconducting loop observed by Friedman et al. [1] matches the energy corresponding to the flux linkage of the magnetic flux quantum by the ensemble of superconducting electrons in their entirety with a reversal of the corresponding macroscopic current.

***QM:*** O'Connell et al. [2] claimed to have achieved a quantum state of motion for a mechanical object by causing a Josephson junction qbit to be entangled with a macroscopic mechanical resonator and thereby extending, in their opinion, the weird rules of quantum mechanics such as zero-order vibration and entanglement to the macroworld.

**CP:** In reality, the device that O'Connell's team fabricated and tested is no more than a variant of a SQUID, a known classical (Chp. 42) macrodevice, except that it uniquely exploits piezoelectricity to form the weak link of a superconducting loop to enable the device. It demonstrates quantized excitation independently of the qbit and cannot exhibit zero-order vibration due to the nature of the SQUID; moreover, zero-order vibration is experimentally shown to be nonexistent in measurements with the qbit.

***QM:*** Perpetual motion is predicted.

**CP:** Perpetual motion is not permitted nor observed.

***QM:*** A weak force is observed between the two precision-machined plates with minuscule separation because the plates serve to limit the number of virtual particle modes between the plates, as opposed to those outside the plates, and the resulting imbalance in pressure between two infinite quantities gives rise to the feeble force known as the Casimir effect.

**CP:** The Casimir effect is predicted by Maxwell's equations wherein the attractive force is due only to the interactions of the material bodies themselves. Charge and current fluctuations in a material body with a general susceptibility serve as source terms for Maxwell's equations, i.e. classical fields, subject to the boundary conditions presented by the body surfaces. In the limiting case of rarefied media, the van der Waals force of interaction between individual atoms is obtained [3-4].

***QM:*** The *postulated* Quantum Electrodynamics (QED) theory of $\frac{g}{2}$ is based on the determination of the terms of a *postulated* power series in $\alpha/\pi$ where each *postulated* virtual particle is a source of *postulated* vacuum polarization that gives rise to a *postulated* term. The algorithm involves scores of *postulated* Feynman diagrams corresponding to thousands of matrices with thousands of integrations per matrix requiring decades to reach a consensus on the "appropriate" *postulated* algorithm to remove the intrinsic infinities.

**CP:** The remarkable agreement between Eqs. (1.236) and (1.237) of the Electron g Factor section demonstrates that $\frac{g}{2}$ may be derived in closed form from Maxwell's equations in a simple straight forward manner that yields a result with eleven-figure agreement with experiments—the limit of the experimental capability is the measurement of the fundamental constants that determine $\alpha$.

***QM:*** The muon $g$ factor $g_{\mu}$ is required to be different from the electron $g$ factor in the standard model due to the mass dependent interaction of each lepton with vacuum polarizations due to virtual particles. The BNL Muon (g-2)

Collaboration used a "magic" $\gamma = 29.3$ which satisfied the BMT equation identically for the theoretical value of $\frac{g_\mu}{2}$ with assumption that $\frac{g_\mu}{2} \neq \frac{g_e}{2}$ and obtained a measured result that was internally consistent.

**CP:** Rather than indicating an expanded plethora of postulated super-symmetry virtual particles, which make contributions such as smuon-neutralino and sneutrino-chargino loops, the muon, like the electron, is a lepton with $\hbar$ of angular momentum, and the muon and electron $g$ factors are predicted by classical physics to be identical. Using the experimental "magic" $\gamma = 29.3$ and $\frac{g_\mu}{2} = \frac{g_e}{2}$ in the BMT equation, the predicted measurement exactly matched $\frac{g_\mu}{2}$ measured by the BNL Muon (g-2) Collaboration proving that their assumption that the $\gamma = 29.3$ condition eliminated the effect of the electrostatic field on $\omega_a$ was flawed and showed the equivalence of the muon and electron $g$ factors.

***QM:*** The expansion of the universe is accelerating due to the presence of "dark energy" throughout all space.

**CP:** The constant maximum speed $c$ for the propagation of light and gravity results in the conservation relationship of mass-energy, $E = mc^2$ and spacetime, $\frac{c^3}{4\pi G} = 3.22\ X\ 10^{34}\ \frac{kg}{\text{sec}}$. Spacetime expands as mass is converted to energy, and the predictions match the observed Hubble constant and the acceleration of the expansion.

***QM:*** In the double-slit experiment, single electrons break into pieces, go through both slits at once, and interfere with themselves over all space.

**CP:** Electrons are not divisible and comprise an extended current distribution with $\hbar$ of angular momentum that is conserved with the electrodynamic interaction of the charged propagating electron with the conducting electrons of the material of the slits such that an angular momentum vector change corresponds to a translational displacement. In the far-field, the transverse momentum pattern is given by the Fourier transform of the slit aperture pattern, and the characteristic interference pattern is observed even with single electrons over time.

***QM:*** In photon diffraction through slits, light-wave crests and troughs superimpose to cancel to give dark spots; whereas, superposition of crest with crest and trough with trough reinforces the intensity and gives bright spots.

**CP:** Photons are not destroyed by other photons. They interact with the electrons of the slit material, and the electrodynamic currents reradiate the light to give the characteristic interference pattern as by the Fourier transform of the slit aperture pattern.

***QM:*** According to Nesvizhevsky et al. [5], a step in the transmission of falling neutrons through a variable-height channel comprising a mirror on the bottom and an absorber at the top occurred at a height of $13\ \mu m$ because neutrons fell in quantized jumps.

**CP:** The de Broglie wavelength in the vertical direction corresponding to the scattering of a falling neutron from the mirror to the absorber was given by $\lambda = z_1 = \frac{1}{2}\left(\frac{h}{m_n}\right)^{2/3} (g)^{-1/3} = 12.6\ \mu m$ where $h$ is Planck's constant, $m_n$ is the mass of the neutron, and $g$ is the acceleration due to gravity. For absorber heights greater than $13\ \mu m$, the height was greater than the de Broglie wavelength; thus, a step in the transmission of falling neutrons occurred at $13\ \mu m$. The observed transmission matched identically that predicted by Newton's Law of Gravitation; no quantum gravity effect was observed.

***QM:*** The nature of the chemical bond is based on a nonphysical "exchange integral," a "strictly quantum mechanical phenomena," that is a consequence of a postulated linear combination of product wavefunctions wherein it is implicit that each point electron with infinite self-electric-and-magnetic-field energies must exist as a "probability-wave cloud" and be in two places at the same time (i.e. centered on two nuclei simultaneously).

**CP:** The nature of the chemical bond solved using first principles including stability to radiation requires that the electron charge of the molecular orbital is a prolate spheroid, a solution of the Laplacian as an equipotential minimum energy surface in the natural ellipsoidal coordinates compared to spheroidal in the atomic case, and the current is time harmonic and obeys Newton's laws of mechanics in the central field of the nuclei at the foci of the spheroid.

***QM:*** The electron clouds mutually shield the nuclear charge to provide an adjustable parameter, "effective nuclear charge"; yet, neither has any self-shielding effect; even though the clouds are mutually indistinguishable and must classically result in a self-interaction force equivalent to 1/2 the central attractive force. Furthermore, the electron–electron

repulsion term in the Hamiltonian can be infinite in atoms and molecules; yet, electron overlap is the basis of bonding in molecules.

**CP:** Electrons are concentric spherical shells in atoms and two-dimensional prolate spheroids in molecules such that there is no electron-electron repulsion, and bonding is due to the attraction between the oppositely charged electrons and nuclei at the origin and foci of the spheroids, respectively.

***QM:*** The lowest energy vibrational state of any molecule is not zero rather, in violation of the second law of thermodynamics and experimental observation such as the formation of a Bose-Einstein condensate of molecules, it is the zero order vibration of $\frac{1}{2}h\nu = \frac{1}{2}\sqrt{\frac{k}{\mu}}$ that is equivalent to zero point energy. Moreover, the basis of zero order vibration, the Heisenberg Uncertainty Principle, has been experimentally disproved [6].

**CP:** The lowest energy vibrational state of any molecule is zero as its lowest vibrational and rotational energies, and the molecules can be solved using first principles in closed form equations in agreement with experimental observations including the difference in bond energies and vibrational energies with isotope substitution.

***QM:*** Since flux is linked by a superconducting loop with a weak link in quantized units of the magnetic flux quantum, $\Phi_0 = \frac{h}{2e}$, the basis of superconductivity is interpreted as arising from the formation of electron pairs corresponding to the $2e$ term in the denominator; the so-called Cooper pairs form even though electrons repel each other, the electron repulsion should increase the resistance to electron flow, and such pairs cannot form at the critical temperature of high $T_c$ superconductors.

**CP:** To conserve the electron's invariant angular momentum of $\hbar$, flux is linked by each electron in quantized units of the magnetic flux quantum, $\Phi_0 = \frac{h}{2e}$, and the basis of superconductivity is a correlated flow of an ensemble of individual electrons such that no energy is dissipated (i.e. superconductivity arises when the lattice is a band-pass for the magnetic field of an array of magnetic dipoles; therefore, no energy is dissipated with current flow).

***QM:*** In a realization of Wheeler's delayed-choice gedanken experiment, modulated output is observed at two orthogonal detectors that has a trigonometric dependence on the phase angle with a relative phase angle of $\pi$ between the outputs when an electro-optical modulator (EOM) is active because the absence of knowledge determines that each single photon must travel back in time, change history, travel along two paths simultaneously, and interfere with itself.

**CP:** An EOM is not a time machine. The interference results are predicted in terms of the classical nature of each linearly polarized single photon being comprised of two oppositely circular polarized components that conserve angular momentum when each interacts with the EOM at a tilt angle $\frac{\pi}{4}$ relative to the axis of linear polarization. The orthogonal circular polarizations input to the EOM each rotate in opposite directions by $\frac{\pi}{4}$, and the action of the EOM on the opposite circular polarized component vectors is antisymmetrical about the axes with the interchange of initial direction of the linear polarization from $E_y$ to $E_x$ to cause the appearance of interference at the outputs.

# REFERENCES


1. J. R. Friedman, V. Patella, W. Hen, S. K. Tolpygo, J. E. Lukens, "Quantum superposition of distinct macroscopic states," Nature, Vol. 406, July, 6, (2000), pp. 43-45.
2. A. D. O'Connell, M. Hofheinz, M. Ansmann, R. C. Bialczak, M. Lenander, E. Lucero, M. Neeley, D. Sank, H. Wang, M. Weides, J. Wenner, J. M. Martinis, A. N. Cleland, "Quantum ground state and single-phonon control of a mechanical resonator," Nature, Vol. 464, (2010), pp. 697-703.
3. A. W. Rodriguez, A. P. McCauley, J. D. Joannopoulos, S. G. Johnson,"Casimir forces in the time domain: Theory," Phys. Rev. A,Vol. 80, (2009), p. 012115.
4. E. M. Lifshitz and L. P. Pitaevskii, Statistical Physics: Part 2 (Pergamon, Oxford, 1980).
5. V. V. Nesvizhevsky, H. G. Borner, A. K. Petukhov, H. Abele, S. Baebler, F. J. Rueb, T. Stoferele, A. Westphal, A. M. Gagarski, G. A. Petrov, A. V. Strelkov, "Quantum states of neutrons in the Earth's gravitational field," Nature, Vol. 415, (2002), pp. 297-299.
6. L. A. Rozema, A. Darabi, D. H. Mahler, A. Hayat, Y. Soudagar, A. M. Steinberg, "Violation of Heisenberg's Measurement-Disturbance Relationship by Weak Measurements," Phys. Rev. Lett., 109 (2012), 100404.

## THREE ATOMIC THEORIES

It is possible to arrive at the Rydberg formula using the wrong physics. The statement "the results justify the means" is a fundamental argument for the validity of quantum mechanics no matter how strained the explanations or the consequences. Consider that in fact, the mathematics of the three theories of Bohr, Schrödinger, and presently CP converge to Eq. (I.1) as the principal energy levels of the hydrogen atom.

$$E_n = -\frac{e^2}{n^2 8\pi\varepsilon_0 a_H} = -\frac{13.598\ eV}{n^2} \tag{I.1}$$

$$n = 1, 2, 3, ... \tag{I.2}$$

where $a_H$ is the Bohr radius for the hydrogen atom (52.947 pm), $e$ is the magnitude of the charge of the electron, and $\varepsilon_o$ is the vacuum permittivity. The theories of Bohr and Schrödinger depend on specific postulates to yield Eq. (I.1). A mathematical relationship exists between the theories of Bohr and Schrödinger with respect to CP that involves these postulates. CP solves the source currents of spherical multipole radiation fields. The current-density functions are the same as the spherical-harmonic and time-harmonic functions of the spherical electromagnetic waves, but are confined to a two-dimensional sphere of fixed radius except between transitions involving emission or absorption of the corresponding multipole radiation. Then, the currents match the wave equation solutions for two dimensions, the angular and time-dependent solutions of the wave equation. The Fourier transform of the current-density function is a solution of the three-dimensional wave equation in frequency $(k, \omega)$ space. Whereas, the Schrödinger-equation solutions are three dimensional in spacetime. The energy is given by:

$$\int_{-\infty}^{\infty} \psi^* H \psi dv = E \int_{-\infty}^{\infty} \psi^2 dv; \tag{I.3}$$

$$\int_{-\infty}^{\infty} \psi^2 dv = 1 \tag{I.4}$$

Thus,

$$\int_{-\infty}^{\infty} \psi^* H \psi dv = E \tag{I.5}$$

In the case that the potential energy of the Hamiltonian, $H$, is a constant times the wavenumber, the Schrödinger equation becomes the well-known Bessel equation. Then, with one of the solutions for $\psi$, Eq. (I.5) is equivalent to an inverse Fourier transform. According to the duality and scale change properties of Fourier transforms, the energy equation of CP and that of quantum mechanics are identical, the energy of a radial Dirac delta function of radius equal to an integer multiple of the radius of the hydrogen atom (Eq. (I.1)). Bohr obtained the same energy formula by postulating nonradiative states with angular momentum

$$L_z = m\hbar \tag{I.6}$$

and solving the energy equation classically.

The mathematics of all three theories result in Eq. (I.1). However, the physics is quite different. CP is derived from first principles and holds over a scale of spacetime of 85 orders of magnitude—it correctly predicts the nature of the universe from the scale of quarks to that of the cosmos. The two other theories are more or less mathematical curve fits to the Rydberg formula with inherent physical and mathematical flaws.

Specifically, the Bohr theory has inherent physical shortcomings such as failing to predict the spectrum of hydrogen in a magnetic field and the inability to solve helium and other multi-electron atoms and the nature of the chemical bond as well as the prediction of infinite angular momentum according to Eq. (I.6). Its success can be attributed to the rigging of the angular momentum to give rise to the Rydberg formula with the dismissal of the radiative stability problem.

The electron in the Schrödinger model is a singularity that exists over all space simultaneously at each instantaneous time point that is physically impossible and violates all first principles including stability to radiation. It is not relativistically invariant and fails to predict electron spin, the electron's magnetic moment, the g factor, the Stern-Gerlach experimental results, the Lamb shift, the fine structure, and the hyperfine structure. Furthermore, the Schrödinger equation is mathematically inconsistent in the excited state quantum numbers and does not give the proper quantization of the one-electron atom energy states.

In contrast, the stable electron current at the $n = 1$ state and the quantized excited states and their lifetimes can be solved precisely in closed-form equations containing fundamental constants only using physical laws that do not miss the Lamb shift, fine structure, hyperfine structure, magnetic moment, Stern Gerlach experimental results, g factor, and relativistic invariance as the Schrödinger equation does. Eq. (I.100) is also the de Broglie matter wave condition used heuristically in the Bohr model to give the Rydberg formula, but in this case, the standing wave involves the photon. Furthermore, the quantization involves excitation of discrete resonator modes imposed by the spherical cavity. In quantum mechanics, quantization is purely mathematical, but similarly dependent on the integer spherical periodicity of the spherical harmonics, and the principal quantum is defined in a manner to give integer angular quantum numbers of complete harmonic wavelengths as well as fit the Rydberg formula. However, the result is not even mathematically consistent. The principal quantum number is defined as the integer radial quantum number minus the integer angular quantum number. But, experimentally the angular or orbital quantum number is multi-valued for any principal quantum number causing the internal inconsistency that the radial quantum number must be multi-valued for a given principal quantum number [51]. In contrast, as shown by Eq. (I.103), Eq. (I.100) gives the angular

harmonic solutions and the corresponding integer radial and angular quantum numbers for physical states.

Specifically, there is an inescapable inconsistency in the mathematics of quantum mechanics identified in Section 11.3 of Margenau and Murphy [51] regarding the definition of the quantum numbers in the solutions of the Schrödinger equation. With the mathematical constraints of normalization and power series termination, the hydrogen atomic energy levels given by Margenau and Murphy are:

$$W = \frac{1}{2}\frac{me^4}{\left(n^* - l\right)^2 \hbar^2} \tag{I.7}$$

wherein $n^*$ is the quantum number of the solution of separable radial function and $l$ is the independent quantum number of the solution of the separable angular function. The quantity $\left(n^* - l\right)$ is then denoted by $n$ and called the total quantum number such that the energy states of the hydrogen atom may be written as:

$$W = \frac{1}{2}\frac{me^4}{n^2\hbar^2} \tag{I.8}$$

Now, let's say that the hydrogen atom is in the $n = 5$ state. If the angular quantum number is $l = 0$, then the radial quantum number must be $n^* = 5$, but if the mathematically independent angular quantum number is $l = 1$, then the radial quantum number must be $n^* = 6$. Thus, an internal inconsistency arises due to the mathematics of the separable functions and independent quantum numbers of the corresponding solutions such as the requirement that the radial quantum number be both $n^* = 5$ and $n^* = 6$ for the state $n = 5$. Indeed as $n \to \infty$, each principal quantum state has the possibility of an infinite number of radial functions corresponding to the degenerate energy level of that state which is impossible. Specifically, it is impossible for the different radial wave functions having different expectation values for the radius of a given energy state to be both physical and energy degenerate for an electron in an inverse-squared Coulomb field.

Other problems exist with QM. QM makes inescapable predictions that do not match observations. For example, at page 365, Margenau and Murphy [51] state:

> *but with the term* $\frac{\ell(\ell+1)\hbar^2}{2mr^2}$ *added to the normal potential energy. What is the meaning of that term? In classical mechanics, the energy of a particle moving in three dimensions differs from that of a one-dimensional particle by the kinetic energy of rotation,* $\frac{1}{2}mr^2\omega^2$. *This is precisely the quantity* $\frac{\ell(\ell+1)\hbar^2}{2mr^2}$, *for we have seen that* $\ell(\ell+1)\hbar^2$ *is the certain value of the square of the angular momentum for the state* $Y_\ell$, *in classical language* $\left(mr^2\omega\right)^2$ *which is divided by* $2mr^2$, *gives exactly the kinetic energy of rotation.*

From these equations, zero rotational energy and zero angular momentum are predicted for the $n = 1$ state, but these conditions are impossible since the electron is bound in a Coulomb field and must have nonzero instantaneous motion. Thus, the Schrödinger equation solutions further predict that the ionized electron may have infinite angular momentum. The Schrödinger equation solutions also predict that the excited state rotational energy levels are nondegenerate as a function of the $\ell$ quantum number even in the absence of an applied magnetic field, and the predicted energy is over six orders of magnitude greater than the typically observed nondegenerate energy in the presence of a magnetic field. In the absence of a magnetic field, no preferred direction exists. In this case, the $\ell$ quantum number is a function of the orientation of the atom with respect to an arbitrary coordinate system. Therefore, the nondegeneracy is nonsensical and violates conservation of angular momentum of the photon. Furthermore, as the principal quantum number and therefore $\ell$ go to infinity, the rotational energy and angular momentum become infinite while the wavefunction becomes sinusoidal over all space and is not normalizable [51]. In the latter case, a strict mathematical constraint of the founding postulates is violated. Thus, the theory is not mathematically consistent besides being physically impossible. It does not properly give rise to the observed quantized states of the hydrogen atom.

Moreover, only CP predicts reciprocal integers as "allowed" in the Rydberg energy equation. Explicitly, CP gives Eq. (I.1) as the energy-level equation for atomic hydrogen, but the restriction on "$n$," Eq. (I.2), should be replaced by Eq. (I.9).

$$n = 1, 2, 3, ..., \text{ and, } n = \frac{1}{2}, \frac{1}{3}, \frac{1}{4}, ... \tag{I.9}$$

Experimental observations lead to the conclusion that atomic hydrogen can exist in fractional quantum states that are at lower energies than the traditional "ground" ($n = 1$) state [22-42], and the observation of 54.4 $eV$ and 122.4 $eV$ short-wavelength-cutoff continuum radiation from hydrogen alone [23-29, 31] confirms CP in the prediction of hydrinos and directly disproves atomic theories such as the Bohr theory and the Schrödinger and Dirac equations based on the definition of $n = 1$ as the ground state, the defined state below which it is impossible to go. Thus, postulates were established to give the correct formula for the principal energies of the excited states of atomic hydrogen, but being devoid of the correct physics, the resulting mathematical models failed to predict unanticipated results and are disproved experimentally.

## MATHEMATICAL RELATIONSHIP BETWEEN THE THEORIES OF BOHR AND SCHRÖDINGER WITH RESPECT TO CLASSICAL ATOMIC THEORY

The mathematical relationship whereby the Schrödinger equation may be transformed into a form consistent with first principles is shown *infra*. In the case that the potential energy of the Hamiltonian, $H$, is a constant times the wavenumber, the Schrödinger equation is the well-known Bessel equation. Then, one of the solutions for the wavefunction $\Psi$ (a current-density function rather than a probability wave) is equivalent to an inverse Fourier transform. According to the duality and scale change properties of Fourier transforms, the energy equation of CP and that of quantum mechanics are identical, the energy of a radial Dirac delta function of radius equal to an integer multiple of the radius of the hydrogen atom.

Historically, J. J. Balmer showed, in 1885, that the frequencies for some of the lines observed in the emission spectrum of atomic hydrogen could be expressed with a completely empirical relationship. This approach was later extended by J. R. Rydberg who showed that all of the spectral lines of atomic hydrogen were given by the equation:

$$\bar{\nu} = R\left(\frac{1}{n_f^2} - \frac{1}{n_i^2}\right) \tag{I.10}$$

where $R = 10,967,758\ m^{-1}$, $n_f = 1,2,3,...$, $n_i = 2,3,4,...$, and $n_i > n_f$. In 1911, Rutherford proposed a planetary model for the atom where the electrons revolve about the nucleus (which contained the protons) in various orbits. There was, however, a fundamental conflict with this model and the prevailing classical physics. According to classical electromagnetic theory, an accelerated particle radiates energy as electromagnetic waves. Thus, an electron in a Rutherford orbit, circulating at constant speed but with a continually changing direction of its velocity vector is being accelerated whereby the electron should constantly lose energy by radiating and spiral into the nucleus.

An explanation was provided by Bohr in 1913 when he assumed that the energy levels were quantized and the electron was constrained to move in only one of a number of allowed states. Niels Bohr's theory for atomic hydrogen was based on an unprecedented postulate of stable circular orbits that do not radiate. Although no explanation was offered for the existence of stability for these orbits, the results gave energy levels in agreement with Rydberg's equation. Bohr's theory was a straightforward application of Newton's laws of motion and Coulomb's law of electric force. According to Bohr's model, the point particle electron was held to a circular orbit around the relatively massive point particle nucleus by the balance between the Coulomb force of attraction between the proton and the electron and centrifugal force of the electron.

$$\frac{e^2}{4\pi\varepsilon_0 r^2} = \frac{m_e v^2}{r} \tag{I.11}$$

Bohr postulated the existence of stable orbits in defiance of classical physics (Maxwell's equations), but he applied classical physics according to Eq. (I.11). Bohr then realized that the energy formula Eq. (I.1) was given by postulating nonradiative states with angular momentum

$$L_z = m_e v r = n\hbar \qquad n = 1,2,3... \tag{I.12}$$

and by solving the energy equation classically. The Bohr radius is given by substituting the solution of Eq. (I.12) for $v$ into Eq. (I.11).

$$r = \frac{4\pi\varepsilon_0 \hbar^2 n^2}{m_e e^2} = n^2 a_0 \qquad n = 1,2,3... \tag{I.13}$$

The total energy is the sum of the potential energy and the kinetic energy. In the present case of an inverse squared central field, the total energy (which is the negative of the binding energy) is one half the potential energy [52]. The potential energy, $\phi(\mathbf{r})$, is given by Poisson's equation

$$\phi(\mathbf{r}) = -\int_{V'} \frac{\rho(\mathbf{r}')\,dv'}{4\pi\varepsilon_0 |\mathbf{r} - \mathbf{r}'|} \tag{I.14}$$

For a point charge at a distance $r$ from the nucleus the potential is:

$$\phi(r) = -\frac{e^2}{4\pi\varepsilon_0 r} \tag{I.15}$$

Thus, the total energy is given by:

$$E = -\frac{Z^2 e^2}{8\pi\varepsilon_0 r} \tag{I.16}$$

Substitution of Eq. (I.13) into Eq. (I.16) with the replacement of the electron mass by the reduced electron mass gives Eq. (I.1).

Bohr's model was in agreement with the observed hydrogen spectrum, but it failed with the helium spectrum, and it could not account for chemical bonds in molecules. The prevailing wisdom was that the Bohr model failed because it was based on the application of Newtonian mechanics for discrete particles. Its limited applicability was attributed to the unwarranted assumption that the energy levels are quantized.

In 1923, de Broglie suggested that the motion of an electron has a wave aspect— $\lambda = \frac{h}{p}$. This was confirmed by Davisson and Germer in 1927 by observing diffraction effects when electrons were reflected from metals. Schrödinger reasoned

that if electrons have wave properties, there must be a wave equation that governs their motion. In 1926, he proposed the Schrödinger equation

$$H\Psi = E\Psi \tag{I.17}$$

where $\Psi$ is the wave function, $H$ is the wave operator, and $E$ is the energy of the wave. To give the sought three quantum numbers, the Schrödinger equation solutions are three-dimensional in space and four-dimensional in spacetime.

$$\left[\nabla^2 - \frac{1}{v^2}\frac{\partial^2}{\partial t^2}\right]\Psi(r,\theta,\phi,t) = 0 \tag{I.18}$$

where $\Psi(r,\theta,\phi,t)$ according to quantum theory is the probability-density function of the electron, as described below. When the time harmonic function is eliminated [53-54], the result is

$$-\frac{\hbar^2}{2\mu}\left[\frac{1}{r^2}\frac{\partial}{\partial r}\left(r^2\frac{\partial\Psi}{\partial r}\right)+\frac{1}{r^2\sin\theta}\frac{\partial}{\partial\theta}\left(\sin\theta\frac{\partial\Psi}{\partial\theta}\right)_{r,\phi}+\frac{1}{r^2\sin^2\theta}\left(\frac{\partial^2\Psi}{\partial\phi^2}\right)_{r,\theta}\right]+U(r)\Psi(r,\theta,\phi)=E\Psi(r,\theta,\phi) \tag{I.19}$$

where $U(r)$ is the classical Coulomb potential energy which in MKS units is:

$$U(r) = -\frac{e^2}{4\pi\varepsilon_0 r} \tag{I.20}$$

The Schrödinger equation (Eq. (I.19)) can be transformed into a sum comprising a part that depends only on the radius and a part that is a function of angle only obtained by separation of variables and linear superposition in spherical coordinates. The general form of the solutions for $\psi(r,\theta,\phi)$ is:

$$\psi(r,\theta,\phi) = \sum_{l,m} f_{lm}(r)Y_{lm}(\theta,\phi) \tag{I.21}$$

where $l$ and $m$ are separation constants. The solutions for the full angular part of Eq. (I.19), $Y_{lm}(\theta,\phi)$, are the spherical harmonics.

$$Y_{lm}(\theta,\phi) = \sqrt{\frac{(2l+1)(l-m)!}{4\pi(l+m)!}}P_l^m(\cos\theta)e^{im\phi} \tag{I.22}$$

In general, the Schrödinger equation has an infinite number of solutions. To arrive at the solution, which represents the electron, a suitable boundary condition must be imposed. Schrödinger postulated the boundary condition: "$\Psi \to 0$ as $r \to \infty$," which leads to a purely mathematical model of the electron. In addition, to arrive at the Rydberg series for the principal energy levels, further definitions of constants in the corresponding Laguerre differential equation are required [14-15]. The historical solution [54] may be approached differently to arrive at a solution that is based in physics. The angular part of Eq. (I.19) is the generalized Legendre equation which is derived from the Laplace equation by Jackson ([55] at Eq. (3.9)). For the case that the potential energy is a constant times the wavenumber of the electron, $k$ (a constant times the inverse of the de Broglie wavelength of the electron—$k = \frac{2\pi}{\lambda};\ \lambda = \frac{h}{p}$), the radial part of Eq. (I.19) is just the Bessel equation, Eq. (3.75) of Jackson [55] with $\upsilon = l + \frac{1}{2}$. (In the present case of an inverse squared central field, the magnitude of each of the binding energy and the kinetic energy is one half the potential energy [52], and the de Broglie wavelength requires that the kinetic energy, $\frac{p^2}{2m_e}$, is a constant times the wavenumber squared.) Thus, the solution for $f_{lm}(r)$ is:

$$f_{lm}(r) = \frac{A_{lm}}{r^{1/2}}J_{l+1/2}(kr)+\frac{B_{lm}}{r^{1/2}}N_{l+1/2}(kr) \tag{I.23}$$

It is customary to define the spherical Bessel, Neumann, and Hankel functions, denoted by $j_l(x)$, $n_l(x)$, $h_l^{(1,2)}(x)$, as follows:

$$\begin{aligned} j_l(x) &= \left(\frac{\pi}{2x}\right)^{1/2}J_{l+1/2}(x) \\ n_l(x) &= \left(\frac{\pi}{2x}\right)^{1/2}N_{l+1/2}(x) \\ h_l^{(1,2)}(x) &= \left(\frac{\pi}{2x}\right)^{1/2}\left[J_{l+1/2}(x) \pm iN_{l+1/2}(x)\right] \end{aligned} \tag{I.24}$$

For $l = 0$ the explicit forms are:

$$j_0(x)=\frac{\sin x}{x}$$
$$n_0(x)=-\frac{\cos x}{x} \tag{I.25}$$
$$h_0^{(1)}(x)=\frac{e^{ix}}{ix}$$

Eq. (I.19) has the general form:

$$H\psi = E\psi \tag{I.26}$$

The energy is given by:

$$\int_{-\infty}^{\infty} \psi H\psi dv = E\int_{-\infty}^{\infty} \psi^2 dv\,; \tag{I.27}$$

Typically, the solutions are normalized.

$$\int_{-\infty}^{\infty} \psi^2 dv = 1 \tag{I.28}$$

thus,

$$\int_{-\infty}^{\infty} \psi H\psi dv = E \tag{I.29}$$

A physical interpretation of Eq. (I.26) is sought. Schrödinger interpreted $e\Psi^*(x)\Psi(x)$ as the charge density or the amount of charge between $x$ and $x+dx$ ($\Psi^*$ is the complex conjugate of $\Psi$). Presumably, then, he pictured the electron to be spread over large regions of space. Three years after Schrödinger's interpretation, Max Born, who was working with scattering theory, found that this interpretation led to logical difficulties, and he replaced the Schrödinger interpretation with the probability of finding the electron between $x$ and $x+dx$ as:

$$\int \Psi(x)\Psi^*(x)dx \tag{I.30}$$

Born's interpretation is generally accepted. Nonetheless, interpretation of the wave function is a never-ending source of confusion and conflict. Many scientists have solved this problem by conveniently adopting the Schrödinger interpretation for some problems and the Born interpretation for others. This duality allows the electron to be everywhere at one time—yet to have no volume. Alternatively, the electron can be viewed as a discrete particle that moves here and there (from $r=0$ to $r=\infty$), and $\Psi\Psi^*$ gives the time average of this motion. According to the Copenhagen interpretation, every observable exists in a state of superposition of possible states, and observation or the potential for knowledge causes the wavefunction corresponding to the possibilities to collapse into a definite state. The postulate of quantum measurement asserts that the process of measuring an observable forces the state vector of the system into an eigenvector of that observable, and the value measured will be the eigenvalue of that eigenvector. Thus, Eq. (I.26) corresponds to collapsing the wave function, and $E$ is the eigenvalue of the eigenvector.

However, an alternative interpretation of Eq. (I.26) and the corresponding solutions for $\psi$ exists. In this case, $\psi$ is a function given by Eqs. (I.23-I.25), and Eq. (I.19) is equivalent to an inverse Fourier transform. The spacetime inverse Fourier transform in three dimensions in spherical coordinates is given [56-57], as follows:

$$M(s,\Theta,\Phi)=\int_0^{\infty}\int_0^{\pi}\int_0^{2\pi} \rho(r,\theta,\phi)\exp(-i2\pi sr[\cos\Theta\cos\theta+\sin\Theta\sin\theta\cos(\phi-\Phi)])r^2\sin\theta dr d\theta d\phi \tag{I.31}$$

With circular symmetry [56]:

$$M(s,\Theta)=2\pi\int_0^{\infty}\int_0^{\pi} \rho(r,\theta)J_o\left(2\pi sr\sin\Theta\sin\theta\right)\exp\left(-i2\pi sr\cos\Theta\cos\theta\right)r^2\sin\theta dr d\theta \tag{I.32}$$

With spherical symmetry [56],

$$M(s)=4\pi\int_0^{\infty}\rho(r)\mathrm{sinc}\left(2sr\right)r^2dr=4\pi\int_0^{\infty}\rho(r)\frac{\sin 2sr}{2sr}r^2dr \tag{I.33}$$

By substitution of the eigenvalues corresponding to the angular part [54] of Eq. (I.21), the Schrödinger equation becomes the radial equation, $R(r)$, given by:

$$-\frac{\hbar^2}{2\mu r^2}\frac{d}{dr}\left(r^2\frac{dR}{dr}\right)+\left[\frac{\hbar^2 l(l+1)}{2\mu r^2}+U(r)\right]R(r)=ER(r) \tag{I.34}$$

Consider the case that $\ell = 0$, that the potential energy is a constant times the wavenumber, and that the radial function is a spherical Bessel function as given by Eqs. (I.23-I.25). In this case, multiplication of both sides of Eq. (I.34) by $4\pi\left(\frac{\sin 2sr}{2sr}\right)^2$ followed by integration with respect to the radius over its limits (0 to $\infty$) gives

$$4\pi\int_0^\infty \frac{\sin 2sr}{2sr}\left[-\frac{\hbar^2}{2\mu r^2}\frac{d}{dr}\left(r^2\frac{d}{dr}\right)+U(r)\right]\frac{\sin 2sr}{2sr}r^2dr = E4\pi\int_0^\infty \frac{\sin 2sr}{2sr}\frac{\sin 2sr}{2sr}r^2dr \tag{I.35}$$

Eq. (I.33) is the Fourier transform integral in spherical coordinates with spherical symmetry. The left hand side (LHS) of Eq. (I.35) is equivalent to the LHS of Eq. (I.29) wherein $\psi$ is given by Eq. (I.25). Then the LHS of Eq. (I.35) is the Fourier transform integral of $H\psi$ wherein the kernel is $r^2\frac{\sin 2sr}{2sr}$. The integral of Eq. (I.29) gives $E$ which is a constant. The energy $E$ of Eq. (I.26) is a constant such as $b$. Thus, $H\psi$ according to Eq. (I.26) is a constant times $\psi$.

$$H\psi = b\psi \tag{I.36}$$

Since $b$ is an *arbitrary* constant, consider the following case wherein $b$ is the Rydberg quantized energy formula:

$$b = -\frac{Z^2e^2}{8\pi\varepsilon_0 n^2 a_H} \tag{I.37}$$

Then the energy of Eq. (I.29) is that given by Eq. (I.1). However, the Schrödinger equation can be solved to give the energy corresponding to the radial function given by Eq. (I.59) of CP. The radial function used to calculate the energy is a delta function that corresponds to an inverse Fourier transform of the solution for $\psi$.

$$\Psi(s) = \delta(s - s_n) \tag{I.38}$$

With a change of variable, Eq. (I.38) becomes Eq. (I.59). Eq. (I.35) can be expressed, as follows:

$$4\pi\int_0^\infty \frac{\sin 2sr}{2sr}\left[-\frac{\hbar^2}{2\mu r^2}\frac{d}{dr}\left(r^2\frac{d}{dr}\right)+U(r)\right]\frac{\sin s_n r}{s_n r}r^2dr = E4\pi\int_0^\infty \frac{\sin 2sr}{2sr}\frac{\sin 2s_n r}{2s_n r}r^2dr \tag{I.39}$$

It follows from Eq. (I.33) that the right side integral is the Fourier transform of a radial Dirac delta function:

$$4\pi E\int_0^\infty \frac{\sin 2s_n r}{2s_n r}\frac{\sin 2sr}{2sr}r^2dr = E\frac{\delta(s - s_n)}{4\pi s_n^2} \tag{I.40}$$

Substitution of Eq. (I.36) into Eq. (I.39) gives:

$$4\pi b\int_0^\infty \frac{\sin 2s_n r}{2s_n r}\frac{\sin 2sr}{2sr}r^2dr = b\frac{\delta(s - s_n)}{4\pi s_n^2} \tag{I.41}$$

Substitution of Eq. (I.40) and Eq. (I.41) into Eq. (I.39) gives:

$$b\delta(s - s_n) = E\delta(s - s_n) \tag{I.42}$$

Consider the case where $b$ is given by:

$$b = -\frac{\hbar^2}{2m_e n\frac{a_0}{Z^2}s} = -\frac{\frac{1}{n}Z^2e^2}{8\pi\varepsilon_0 s} \tag{I.43}$$

and $s_n$ is given by:

$$s_n = na_H \tag{I.44}$$

where $r_n = na_H$. According to the duality and change of scale properties of Fourier transforms [58], ***the energy equation of CP and that of QM are identical***, the energy of a radial Dirac delta function of a radius that's equal to an integer multiple of the radius of the hydrogen atom. The total energy of the electron is given by Gauss' law for the potential and the relationship that the total energy is one half the potential energy in the case of an inverse squared central force [52]:

$$E = \int_{-\infty}^{\infty} E\delta(r - r_n)dr = -\int_{-\infty}^{\infty} \delta(r - r_n)\frac{\frac{1}{n}Z^2e^2}{8\pi\varepsilon_0 r}dr = -\frac{\frac{1}{n}Z^2e^2}{8\pi\varepsilon_0 r_n} = -\frac{Z^2e^2}{8\pi\varepsilon_0 n^2 a_H} \tag{I.45}$$

Thus, the mathematical relationship of CP and QM is based on the Fourier transform of the radial function. CP requires that the electron is real and physically confined to a two-dimensional surface comprising source currents that match the wave equation solutions for spherical waves in two dimensions (angular) and time. The corresponding Fourier transform is a wave over all space that is a solution of the three-dimensional wave equation (e.g. the Schrödinger equation). In essence, QM may be considered as a theory dealing with the Fourier transform of an electron, rather than the physical electron. By Parseval's theorem, the energies may be equivalent, but the quantum mechanical case is nonphysical—only mathematical. It may mathematically produce numbers that agree with experimental energies as eigenvalues, but the mechanisms lack internal consistency and conformity with physical laws. If these are the criteria for a valid solution of physical problems, then QM has never successfully solved any problem. The theory of Bohr similarly failed.

## SHORTCOMINGS OF QUANTUM THEORY AND REASONS FOR A COMPLETE REVISION OF ATOMIC THEORY

In general, QM has proved to be a deadend towards unification of the fundamental forces including gravity and further failed to give the basis of the inertial and gravitational masses, the equivalence of these masses, predicting the masses of fundamental particles, and the acceleration behavior of the cosmos. Fundamentally, quantum mechanics based on the Schrödinger equation and modifications of the Schrödinger equation has encountered several obstacles that have proved insurmountable even from the beginning with the hydrogen atom, as was the case with the Bohr theory (See the Retrospect section, and Mills' publications [4-15]). The Schrödinger equation mathematically gives the Rydberg equation as a set eigenvalues. On this basis alone, it is justified despite its inconsistency with physical laws and numerous experimental observations such as:

- The appropriate eigenvalue must be postulated and the variables of the Laguerre differential equation must be defined as integers in order to obtain the Rydberg formula.
- The Schrödinger equation is not Lorentz invariant.
- The Schrödinger equation violates first principles, including special relativity and Maxwell's equations [4-20, 59].
- The Schrödinger equation gives no basis why excited states are radiative and the 13.6 eV state is stable. Mathematics does not determine physics; it only models physics.
- The Schrödinger equation solutions, Eq. (36) and Eq. (37) of Ref. [15], predict that the ground state electron has zero angular energy and zero angular momentum, respectively.
- The Schrödinger equation solution, Eq. (37) of Ref. [15], predicts that the ionized electron may have infinite angular momentum.
- The Schrödinger equation solutions, Eq. (36) and Eq. (37) of Ref. [15], predict that the excited state rotational energy levels are nondegenerate as a function of the $\ell$ quantum number even in the absence of an applied magnetic field, and the predicted energy is over six orders of magnitude of the observed nondegenerate energy in the presence of a magnetic field. In the absence of a magnetic field, no preferred direction exists. In this case, the $\ell$ quantum number is a function of the orientation of the atom with respect to an arbitrary coordinate system. Therefore, the nondegeneracy is nonsensical and violates conservation of angular momentum of the photon.
- The Schrödinger equation predicts that each of the functions that corresponds to a highly excited state electron is not integrable and cannot be normalized; thus, each is infinite.
- The Schrödinger equation predicts that the ionized electron is sinusoidal over all space and cannot be normalized; thus, it is infinite.
- The Heisenberg Uncertainty Principle arises as the standard deviation in the electron probability wave, but experimentally it is not the basis of wave-particle duality [12, 60].
- The correspondence principle does not hold experimentally.
- The Schrödinger equation does not predict the electron magnetic moment and misses the spin quantum number altogether.
- The Schrödinger equation provides no rational basis for the phenomenon of spin, the Pauli exclusion principle, or Hund's rules. Instantaneous exchange of information between particles is required, which violates special relativity.
- The Schrödinger equation is not a wave equation since it gives the velocity squared proportional to the frequency.
- The Schrödinger equation is not consistent with conservation of energy in an inverse potential field wherein the binding energy is equal to the kinetic energy and the sum of the binding energy and the kinetic energy is equal to the potential energy.
- The Schrödinger equation permits the electron to exist in the nucleus, a state that is physically nonsensical with infinite potential energy and infinite negative kinetic energy.
- The Schrödinger equation interpreted as a probability wave of a point particle cannot explain neutral scattering of electrons from hydrogen.

- The Schrödinger equation interpreted as a probability wave of a point particle gives rise to infinite magnetic and electric energy in the corresponding fields of the electron. For example, the electron must spin in one dimension and give rise to a Bohr magneton; yet, classically the energy of a magnetic moment is $\frac{\mu^2}{r^3}$ which in the present case is infinity (by substitution of $r = 0$ for the model that the electron is a point particle), not the required $mc^2$. This interpretation is in violation of Special Relativity [61].

- A modification of the Schrödinger equation was developed by Dirac to explain spin.[2] The *postulated* QED theory of $\frac{g}{2}$ is based on the determination of the terms of a *postulated* power series in $\alpha/\pi$ where each *postulated* virtual particle is a source of *postulated* vacuum polarization that gives rise to a *postulated* term. The algorithm involves scores of *postulated* Feynman diagrams corresponding to thousands of matrices with thousands of integrations per matrix requiring decades to reach a consensus on the "appropriate" *postulated* algorithm to remove the intrinsic infinities.[3]

These failures of QM are attributed to the unwarranted assumption that atomic-size particles obey different physical laws than macroscopic objects. Specifically, QM is incorrect in its basis that first principles such as Maxwell's Equations do not apply to the electron and the notion that the electron is described by a probability distribution function of a point particle. Quantum mechanics is based on engendering the electron with a wave nature, as suggested by the Davisson-Germer experiment and fabricating a set of associated postulates and mathematical rules for wave operators. QM is in violation of Maxwell's equations, as shown through application of the Haus condition to the Schrödinger wave functions (See Schrödinger Wavefunction in Violation of Maxwell's Equation section). Nonradiation based on Maxwell's equations is a necessary boundary constraint, since nonradiation is observed experimentally. The shortcomings of QM regarding violation of Maxwell's equations and other first principles are further discussed in the Retrospect section and Mills' publications [4-15]. These issues indicate that QM atomic theory requires revision.

## CLASSICAL ATOMIC THEORY

The physics of numerous phenomena in electricity and magnetism, optics, celestial and orbital mechanics, heat, hydrodynamics, aerodynamics, elasticity, and others obey equations containing the Laplacian:

$$\nabla^2\phi = 0 \qquad \text{is Laplace's equation} \tag{I.46}$$

$$\nabla^2\phi = \frac{1}{a^2}\frac{\partial^2\phi}{\partial t^2} \qquad \text{is the wave equation} \tag{I.47}$$

$$\nabla^2\phi = \frac{1}{a^2}\frac{\partial\phi}{\partial t} \qquad \text{is the diffusion or heat-conduction equation} \tag{I.48}$$

The wave equation is useful to describe electric and magnetic fields and orbiting bodies, as well as in the form of an energy equation wherein it can provide for conservation of energy and angular momentum. Thus, it is the logical choice to solve for the nature of the bound electron as a boundary-value problem. In contrast, the time-dependent Schrödinger equation has the form of Eq. (I.48) and is not a true wave equation. The current QM theory based on the time dependent and time independent Schrödinger equation has many problems, is not based on physical laws, and is not predictive, as discussed previously [4-20]. QM has never dealt with the nature or structure of fundamental particles. They are treated as zero-dimensional points that occupy no volume and are everywhere at once. This view is impossible since occupying no volume would preclude their existence; the inherent infinities are not observed nor are they possible, and the possibility of a particle being everywhere at once violates all physical laws including conservation of energy and causality. Now, a physical approach is followed based on the classical wave equation and the condition for nonradiation from Maxwell's equations.

---

[2] In the old quantum theory the spin angular momentum of the electron is called the "intrinsic angular momentum." This term arises because it is difficult to provide a physical interpretation for the electron's spin angular momentum. Dirac's Quantum Electrodynamics (QED) attempts a physical interpretation by proposing that the "vacuum" contains fluctuating electric and magnetic fields called "zero point energy," negative energy states of the vacuum, virtual particles and their corresponding "polarization" of vacuum space, and arbitrarily disregarding infinities that even Dirac opposed. These aspects render QED fatally flawed in terms of predicting a corresponding inescapable infinite cosmological constant and the unobserved requirement of particle emission by blackholes called Hawking radiation. (See the Wave-Particle Duality section and prior publications [4-15], especially Ref. [10].)

[3] In the Electron g Factor section and Ref. [10], the closed-form Maxwellian result (eleven figure agreement with experiment—the limit of the experimental capability of the measurement of the fundamental constants that determine $\alpha$) is contrasted with the QED algorithm of invoking virtual particles, zero point fluctuations of the vacuum, and negative energy states of the vacuum.

# ONE-ELECTRON ATOMS

## NONRADIATION CONDITION

One-electron atoms include the hydrogen atom, $He^{+}$, $Li^{2+}$, $Be^{3+}$, and so on. In each case, the nucleus contains $Z$ protons and the atom has a net positive charge of $(Z-1)e$. To arrive at the solution that represents the electron, a suitable boundary condition must be imposed. It is well known from experiments that the single atomic electron of hydrogen radiates to the same stable state. Thus, CP uses the physical boundary condition of nonradiation of the bound electron to be imposed on the solution for the charge- and current-density functions of the electron. The condition for radiation by a moving point charge given by Haus [46] is that its spacetime Fourier transform possesses components that are synchronous with waves traveling at the speed of light. Conversely, it is proposed that the condition for nonradiation by an ensemble of moving charge that comprises a current-density function is

*For non-radiative states, the current-density function must not possess spacetime Fourier components that are synchronous with waves traveling at the speed of light.*

The Haus derivation and the condition for nonradiation are given in Appendix I: Nonradiation Condition wherein the nonradiative condition is also derived directly by the determination of the electrodynamic fields with the electron current-density function as the source current. Given the infinite number of possible current-density functions, it is fortuitous that the spherical radiation corresponding to the symmetry and the conditions for emission and absorption of such radiation provide the additional boundary conditions to determine the current-density functions.

## ELECTRON SOURCE CURRENT

Since the hydrogen atom is stable and nonradiative, the electron has constant energy. Furthermore, it is time dynamic with a corresponding current that serves as a source of electromagnetic radiation during transitions. The wave equation solutions of the radiation fields permit the source currents to be determined as a boundary-value problem. These source currents match the field solutions of the wave equation for two dimensions plus time and the nonradiative `n = 1` state when the nonradiation condition is applied. Then, the mechanics of the electron can be solved from the two-dimensional wave equation plus time in the form of an energy equation wherein it provides for conservation of energy and angular momentum, as given in the Electron Mechanics and the Corresponding Classical Wave Equation for the Derivation of the Rotational Parameters of the Electron section. Once the nature of the electron is solved, all problems involving electrons can be solved in principle. Thus, in the case of one-electron atoms, the electron radius, binding energy, and other parameters are solved after solving for the nature of the bound electron.

As shown in Appendix I, for time-varying spherical electromagnetic fields, Jackson [47] gives a generalized expansion in vector spherical waves that are convenient for electromagnetic boundary-value problems possessing spherical symmetry properties and for analyzing multipole radiation from a localized source distribution. The Green function $G(\mathbf{x}',\mathbf{x})$ which is appropriate to the inhomogeneous Helmholtz equation

$$\left(\nabla^2+k^2\right)G(\mathbf{x}',\mathbf{x})=-\delta(\mathbf{x}'-\mathbf{x}) \tag{I.49}$$

in the infinite domain with the spherical wave expansion for the outgoing wave Green function is:

$$G(\mathbf{x}',\mathbf{x})=\frac{e^{-ik|\mathbf{x}-\mathbf{x}'|}}{4\pi|\mathbf{x}-\mathbf{x}'|}=ik\sum_{\ell=0}^{\infty}j_\ell(kr_<)h_\ell^{(1)}(kr_>)\sum_{m=-\ell}^{\ell}Y_{\ell,m}^{*}(\theta',\phi')Y_{\ell,m}(\theta,\phi) \tag{I.50}$$

Jackson [47] further gives the general multipole field solution to Maxwell's equations in a source-free region of empty space with the assumption of a time dependence $e^{i\omega t}$:

$$\begin{aligned}\mathbf{B}&=\sum_{\ell,m}\left[a_E(\ell,m)f_\ell(kr)\mathbf{X}_{\ell,m}-\frac{i}{k}a_M(\ell,m)\nabla\times g_\ell(kr)\mathbf{X}_{\ell,m}\right]\\ \mathbf{E}&=\sum_{\ell,m}\left[\frac{i}{k}a_E(\ell,m)\nabla\times f_\ell(kr)\mathbf{X}_{\ell,m}+a_M(\ell,m)g_\ell(kr)\mathbf{X}_{\ell,m}\right]\end{aligned} \tag{I.51}$$

where the cgs units used by Jackson are retained in this section. The radial functions $f_\ell(kr)$ and $g_\ell(kr)$ are of the form:

$$g_\ell(kr)=A_\ell^{(1)}h_\ell^{(1)}+A_\ell^{(2)}h_\ell^{(2)} \tag{I.52}$$

$\mathbf{X}_{\ell,m}$ is the vector spherical harmonic defined by:

$$\mathbf{X}_{\ell,m}(\theta,\phi)=\frac{1}{\sqrt{\ell(\ell+1)}}\mathbf{L}Y_{\ell,m}(\theta,\phi) \tag{I.53}$$

where

$$\mathbf{L}=\frac{1}{i}(\mathbf{r}\times\nabla) \tag{I.54}$$

The coefficients $a_E(\ell,m)$ and $a_M(\ell,m)$ of Eq. (I.51) specify the amounts of electric $(\ell,m)$ multipole and magnetic $(\ell,m)$ multipole fields, and are determined by sources and boundary conditions as are the relative proportions in Eq. (I.52). Jackson gives the result of the electric and magnetic coefficients from the sources as

$$a_E(\ell,m)=\frac{4\pi k^2}{i\sqrt{\ell(\ell+1)}}\int Y_\ell^{m*}\left\{\rho\frac{\partial}{\partial r}\left[rj_\ell(kr)\right]+\frac{ik}{c}(\mathbf{r}\cdot\mathbf{J})\,j_\ell(kr)-ik\nabla\cdot(r\times\boldsymbol{M})\,j_\ell(kr)\right\}d^3x \tag{I.55}$$

and

$$a_M(\ell,m)=\frac{-4\pi k^2}{\sqrt{\ell(\ell+1)}}\int j_\ell(kr)Y_\ell^{m*}\mathbf{L}\cdot\left(\frac{\mathbf{J}}{c}+\nabla\times\boldsymbol{M}\right)d^3x \tag{I.56}$$

respectively, where the distribution of charge $\rho(\mathbf{x},t)$, current $\mathbf{J}(\mathbf{x},t)$, and intrinsic magnetization $\boldsymbol{M}(\mathbf{x},t)$ are harmonically varying sources: $\rho(\mathbf{x})e^{-i\omega t}$, $\mathbf{J}(\mathbf{x})e^{-i\omega t}$, and $\boldsymbol{M}(\mathbf{x})e^{-i\omega t}$.

The electron current-density function can be solved as a boundary value problem regarding the time varying corresponding source current $\mathbf{J}(\mathbf{x})e^{-i\omega t}$ that gives rise to the time-varying spherical electromagnetic fields during transitions between states with the further constraint that the electron is nonradiative in a state defined as the $n=1$ state. The potential energy, $V(\mathbf{r})$, is an inverse-radius-squared relationship given by Gauss' law, which for a point charge or a two-dimensional spherical shell at a distance $r$ from the nucleus the potential is:

$$V(r)=-\frac{e^2}{4\pi\varepsilon_0 r} \tag{I.57}$$

Thus, consideration of conservation of energy would require that the electron radius must be fixed. Additional constraints requiring a two-dimensional source current of fixed radius are matching the delta function of Eq. (I.49) with no singularity, no time dependence and consequently no radiation, absence of self-interaction (See Appendix II: Stability and Absence of Self Interaction and Self Energy), and exact electroneutrality of the hydrogen atom wherein the electric field is given by

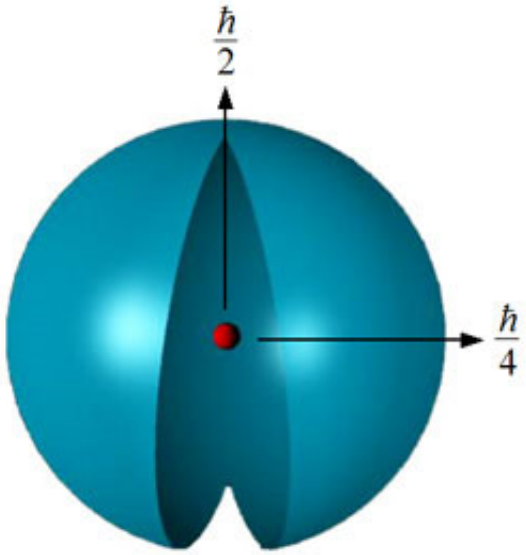
$$\mathbf{n}\bullet(\mathbf{E}_1-\mathbf{E}_2)=\frac{\sigma_s}{\varepsilon_0} \tag{I.58}$$

where $\mathbf{n}$ is the normal unit vector, $\mathbf{E}_1$ and $\mathbf{E}_2$ are the electric field vectors that are discontinuous at the opposite surfaces, $\sigma_s$ is the discontinuous two-dimensional surface charge density, and $\mathbf{E}_2=0$. Then, the solution for the radial electron function that satisfies the boundary conditions is a delta function in spherical coordinates—a spherical shell [62]:

$$f(r)=\frac{1}{r^2}\delta(r-r_n) \tag{I.59}$$

where $r_n$ is an allowed radius. This function defines the charge density on a spherical shell of a fixed radius (See Figure I.1), not yet determined, with the charge motion confined to the two-dimensional spherical surface. The integer subscript $n$ here and in Eqs. (I.60-I.62) is *determined during photon absorption* as given in the Excited States of the One-Electron Atom (Quantization) section. It is shown in this section that the force balance between the electric fields of the electron and proton plus any resonantly absorbed photons gives the result that $r_n=nr_1$ wherein $n$ is an integer in an excited state. In general, leptons such as the electron are indivisible, perfectly conducting, and possess an inalienable $\hbar$ of intrinsic angular momentum such that any inelastic perturbation involves the entire particle wherein the intrinsic angular momentum remains unchanged. Bound state transitions are allowed involving the exchange of photons between states, each having $\hbar$ of angular momentum in their fields.

**Figure I.1.** A bound electron is a constant two-dimensional spherical surface of charge (zero thickness, total charge of $-e$, and total mass of $m_e$), called *an electron atomic orbital.* The corresponding uniform current-density function having intrinsic angular momentum components of $\mathbf{L}_{xy} = \frac{\hbar}{4}$ and $\mathbf{L}_z = \frac{\hbar}{2}$ following Larmor excitation in a magnetic field give rise to the phenomenon of electron spin.




Given time harmonic motion and a radial delta function, the relationship between an allowed radius and the electron wavelength is given by:

$$2\pi r_n = \lambda_n \tag{I.60}$$

Based on conservation of the electron's angular momentum of $\hbar$, the magnitude of the velocity and the angular frequency for *every* point on the surface of the bound electron are:

$$v_n = \frac{h}{m_e \lambda_n} = \frac{h}{m_e 2\pi r_n} = \frac{\hbar}{m_e r_n} \tag{I.61}$$

$$\omega_n = \frac{\hbar}{m_e r_n^2} \tag{I.62}$$

To further match the required multipole electromagnetic fields between transitions of states, the trial nonradiative source current functions are time and spherical harmonics, each having an exact radius and an exact energy. Then, each allowed electron charge-density (mass-density) function is the product of a radial delta function $(f(r) = \frac{1}{r^2}\delta(r - r_n))$, two angular functions (spherical harmonic functions $Y_\ell^m(\theta,\phi) = P_\ell^m(\cos\theta)e^{im\phi}$), and a time-harmonic function $e^{im\omega_n t}$. The spherical harmonic $Y_0^0(\theta,\phi) = 1$ is also an allowed solution that is in fact required in order for the electron charge and mass densities to be positive definite and to give rise to the phenomena of electron spin. The real parts of the spherical harmonics vary between $-1$ and 1. However, the mass of the electron cannot be negative; and the charge cannot be positive. Thus, to insure that the function is positive definite, the form of the angular solution must be a superposition:

$$Y_0^0(\theta,\phi) + Y_\ell^m(\theta,\phi) \tag{I.63}$$

The current is constant at every point on the surface for the s orbital corresponding to $Y_0^0(\theta,\phi)$. The quantum numbers of the spherical harmonic currents can be related to the observed electron orbital angular momentum states. The currents corresponding to s, p, d, f, etc. orbitals are:

$\ell = 0$

$$\rho(r,\theta,\phi,t) = \frac{e}{8\pi r^2}[\delta(r - r_n)]\left[Y_0^0(\theta,\phi) + Y_\ell^m(\theta,\phi)\right] \tag{I.64}$$

$\ell \neq 0$

$$\rho(r,\theta,\phi,t) = \frac{e}{4\pi r^2}[\delta(r - r_n)]\left[Y_0^0(\theta,\phi) + \mathrm{Re}\left\{Y_\ell^m(\theta,\phi)e^{im\omega_n t}\right\}\right] \tag{I.65}$$

where $Y_\ell^m(\theta,\phi)$ are the spherical harmonic functions that spin about the z-axis with angular frequency $\omega_n$ with $Y_0^0(\theta,\phi)$ the

constant function. $\mathrm{Re}\left\{Y_\ell^m(\theta,\phi)e^{i\omega_n t}\right\} = P_\ell^m(\cos\theta)\cos(m\phi + m\omega_n t)$ to keep the form of the spherical harmonic of quantum number $m$ as a traveling wave about the z-axis at angular frequency $\omega_n$.

The Fourier transform of the electron charge-density function is a solution of the four-dimensional wave equation in frequency space (**k**, $\omega$-space). Then, the corresponding Fourier transform of the current-density function $K_\ell^{m_\ell}(s,\Theta,\Phi,\omega)$ is given by multiplying it by the constant angular frequency $\omega_n$ given by Eq. (1.36) corresponding to a potentially emitted photon.

$$K_\ell^{m_\ell}(s,\Theta,\Phi,\omega) = 4\pi\omega_n \frac{\sin(2sr_n)}{2sr_n} \otimes G_\ell^{m_\ell}(s,\Theta) \otimes H_\ell^{m_\ell}(s,\Theta,\Phi) \otimes \frac{1}{4\pi}[\delta(\omega-\omega_n)+\delta(\omega+\omega_n)] \tag{I.66}$$

wherein $G_\ell^{m_\ell}(s,\Theta)$ and $H_\ell^{m_\ell}(s,\Theta,\Phi)$ are the spherical-coordinate Fourier transforms of $N_{\ell,m}P_\ell^m(\cos\theta)$ and $e^{im\phi}$, respectively. The motion on the atomic orbital is angular; however, a radial correction exists due to Special Relativistic effects. Consider the wave vector of the sinc function. When the velocity is $c$ corresponding to a potentially emitted photon.

$$\mathbf{s}_n \bullet \mathbf{v}_n = \mathbf{s}_n \bullet \mathbf{c} = \omega_n \tag{I.67}$$

the relativistically corrected wavelength given by Eq. (1.279) is:

$$r_n = \lambda_n \tag{I.68}$$

Substitution of Eq. (I.68) into the sinc function results in the vanishing of the entire Fourier transform of the current-density function. Thus, spacetime harmonics of $\frac{\omega_n}{c} = k$ or $\frac{\omega_n}{c}\sqrt{\frac{\varepsilon}{\varepsilon_0}} = k$, for which the Fourier transform of the current-density function is nonzero, do not exist. Radiation due to charge motion does not occur in any medium when this boundary condition is met. There is acceleration without radiation. (Also see Abbott and Griffiths and Goedecke [63-64]). Nonradiation is also shown directly using Maxwell's equations in Appendix I: Nonradiation Based on the Electromagnetic Fields and the Poynting Power Vector. However, in the case that such a state arises as an excited state by photon absorption, it is radiative due to a radial dipole term in its current-density function since it possesses spacetime Fourier transform components synchronous with waves traveling at the speed of light, as shown in the Instability of Excited States section. The *radiation emitted or absorbed during electron transitions is the multipole radiation given by Eq. (I.50)* as given in the Excited States of the One-Electron Atom (Quantization) section and the Equation of the Photon section wherein Eqs. (4.18-4.23) give a macro-spherical wave in the far-field.

Thus, a bound electron is a constant two-dimensional spherical surface of charge (zero thickness and total charge of $-e$) called an electron atomic orbital that can exist in a bound state at only specified distances from the nucleus determined by an energy minimum for the $n = 1$ state and integer multiples of this radius due to the action of resonant photons as shown in the Determination of Atomic Orbital Radii section and Excited States of the One-Electron Atom (Quantization) section, respectively. The bound electron is not a point, but it is point-like (behaves like a point at the origin). The free electron is continuous with the bound electron as it is ionized and is also point-like, as shown in the Electron in Free Space section. The total function that describes the spinning motion of each electron atomic orbital is composed of two functions. One function, the spin function (see Figure I.1 for the charge function and Figure I.2 for the current function), is spatially uniform over the atomic orbital, where each point moves on the surface with the same quantized angular and linear velocity, and gives rise to spin angular momentum. It corresponds to the nonradiative $n = 1$, $\ell = 0$ state of atomic hydrogen, which is well known as an s state or orbital. The other function, the modulation function, can be spatially uniform—in which case there is no orbital angular momentum and the magnetic moment of the electron atomic orbital is one Bohr magneton—or not spatially uniform—in which case there is orbital angular momentum. The modulation function rotates with a quantized angular velocity about a specific (by convention) z-axis. The constant spin function that is modulated by a time and spherical harmonic function as given by Eq. (I.65) is shown in Figure 1.2 for several $\ell$ values. The modulation or traveling charge-density wave that corresponds to an orbital angular momentum in addition to a spin angular momentum are typically referred to as p, d, f, etc. orbitals and correspond to an $\ell$ quantum number not equal to zero.

## MOMENT OF INERTIA AND SPIN AND ROTATIONAL ENERGIES

In the derivation of the rotational energy and related parameters, first consider that the electron atomic orbital experiences a constant potential energy because it is fixed at $r = r_n$. The boundary condition is that the modulation of the charge density by a traveling wave is not dissipative corresponding to absence of radiation and further has a time average of zero kinetic energy. The mechanics of motion is such that there is a time and spatially harmonic redistribution of matter and kinetic energy that flows on the surface such that the total of either is unchanged. Wave motion has such behavior and the corresponding equation is a wave equation that is solved with energy degeneracy and a time average of zero for the charge and energy flow as the boundary constraints. In this case, the energy degeneracy is only lifted due to the electrodynamic interaction with an applied field consistent with experimental observations, as given in the Orbital and Spin Splitting section.

The moments of inertia and the rotational energies as a function of the $\ell$ quantum number for the solutions of the time-dependent electron charge-density functions (Eqs. (I.64-I.65)) are solved using the classical wave equation. With rotation about the designated z-axis, the velocity of the spherical shell depends on the angular position on the surface and consequently is a

function of $Y_0^0(\theta,\phi)$. By expressing the wave equation in the energy form, the angular dependent velocity may be eliminated, and this equation can be solved using the boundary constraints. The corresponding equation is the well known rigid rotor equation [65]:

$$-\frac{\hbar^2}{2I}\left[\frac{1}{\sin\theta}\frac{\partial}{\partial\theta}\left(\sin\theta\frac{\partial}{\partial\theta}\right)_{r,\phi}+\frac{1}{\sin^2\theta}\left(\frac{\partial^2}{\partial\phi^2}\right)_{r,\theta}\right]Y(\theta,\phi)=E_{rot}Y(\theta,\phi) \tag{I.69}$$

The resulting parameters for the spin and orbital angular momentum given in the Rotational Parameters of the Electron (Angular Momentum, Rotational Energy, Moment of Inertia) section are:

$\ell=0$

$$I_z=I_{spin}=\frac{m_e{r_n}^2}{2} \tag{I.70}$$

$$L_z=I\omega\mathbf{i}_z=\pm\frac{\hbar}{2} \tag{I.71}$$

$$E_{rotational}=E_{rotational,\,spin}=\frac{1}{2}\left[I_{spin}\left(\frac{\hbar}{m_e{r_n}^2}\right)^2\right]=\frac{1}{2}\left[\frac{m_e{r_n}^2}{2}\left(\frac{\hbar}{m_e{r_n}^2}\right)^2\right]=\frac{1}{4}\left[\frac{\hbar^2}{2I_{spin}}\right] \tag{I.72}$$

$$T=\frac{\hbar^2}{2m_e r_n^2} \tag{I.73}$$

$\ell\neq 0$

$$I_{orbital}=m_e{r_n}^2\sqrt{\frac{\ell(\ell+1)}{\ell^2+2\ell+1}}=m_e{r_n}^2\sqrt{\frac{\ell}{\ell+1}} \tag{I.74}$$

$$\mathbf{L}_{orbital}=I\omega\mathbf{i}_z=I_{orbital}\omega\mathbf{i}_z=m_e{r_n}^2\sqrt{\frac{\ell(\ell+1)}{\ell^2+2\ell+1}}\omega\mathbf{i}_z=m_e{r_n}^2\frac{\hbar}{m_e{r_n}^2}\sqrt{\frac{\ell}{\ell+1}}\mathbf{i}_z=\hbar\sqrt{\frac{\ell}{\ell+1}}\mathbf{i}_z \tag{I.75}$$

$$E_{rotational\ orbital}=\frac{\hbar^2}{2I}\frac{\ell(\ell+1)}{\ell^2+2\ell+1}=\frac{\hbar^2}{2I}\frac{\ell}{\ell+1}=\frac{\hbar^2}{2m_e{r_n}^2}\frac{\ell}{\ell+1}\qquad \ell=1,2,3,..., \tag{I.76}$$

$$L_{z\ total}=L_{z\ spin}+L_{z\ orbital} \tag{I.77}$$

$$\langle L_{z\ orbital}\rangle=0 \tag{I.78}$$

$$\langle E_{rotational\ orbital}\rangle=0 \tag{I.79}$$

The orbital rotational energy arises from a spin function (spin angular momentum) modulated by a spherical harmonic angular function (orbital angular momentum). The time-averaged mechanical angular momentum and rotational energy associated with the wave-equation solution comprising a traveling charge-density wave on the atomic orbital is zero as given in Eqs. (I.78) and (I.79), respectively. Thus, the principal levels are degenerate except when a magnetic field is applied. In the case of an excited state, the angular momentum of $\hbar$ is carried by the fields of the trapped photon. The amplitudes that couple to external magnetic and electromagnetic fields are given by Eq. (I.76) and (I.77), respectively. The rotational energy due to spin is given by Eq. (I.72), and the total kinetic energy is given by Eq. (I.73).

## SPIN FUNCTION

It is known from the Stern-Gerlach experiment that a beam of silver atoms is split into two components when passed through an inhomogeneous magnetic field. This implies that the electron is a spin 1/2 particle or fermion with an intrinsic angular momentum of $\pm\frac{\hbar}{2}$ that can only exist parallel or antiparallel to the direction of the applied field (spin axis), and the magnitude of the angular momentum vector, which precesses about the spin axis is $\sqrt{\frac{3}{4}}\hbar$. Furthermore, the magnitude of the splitting implies a magnetic moment of $\mu_B$, a full Bohr magneton, given by Eq. (1.131) corresponding to $\hbar$ of total angular momentum on the axis of the applied field, implying an impossibility of being classically reconciled with the $\pm\frac{\hbar}{2}$ electron angular momentum. Yet, the extraordinary aspects of the magnetic properties and behavior of the electron are the basis to solve its structure that gives rise to these observations. In general, the Maxwell's-equations solution for the source of any magnetic field is unique. Thus, the electron field requires a corresponding unique current according to Maxwell's equations that matches the boundary condition

imposed by the results of the Stern-Gerlach experiment. The solution is given in the Atomic Orbital Equation of Motion For $\ell$ = 0 Based on the Current Vector Field (CVF) section.

The current density function $Y_0^0(\theta,\phi)$ (Eqs. (I.64-I.65)) that gives rise to the magnetostatic spin of the electron comprises a constant charge (current) density function with moving charge confined to a two-dimensional spherical shell and comprises a uniform complete coverage. It is generated as a continuum of correlated orthogonal great-circle current loops wherein each point charge(current)-density element moves time harmonically with constant angular velocity, $\omega_n$, given by Eq. (I.62) and velocity, $v_n$, in the direction of the current given by Eq. (I.61). O*rthogonal great-circle current-density elements (one dimensional "current loops")* serve as basis elements to form two distributions of an infinite number of great circles wherein each covers one-half of a two-dimensional spherical shell and is defined as a basis element current vector field ("BECVF") and an atomic orbital current-vector field ("OCVF"). Then, the *continuous* uniform electron current density function $Y_0^0(\theta,\phi)$ (part of Eqs. (I.64-I.65)) that covers the entire spherical surface as a distribution of an infinite number of great circles is generated using the CVFs.

First, the generation of the BECVF is achieved by rotation of two great circle basis elements, one in the x'z'-plane and the other in the y'z'-plane, about the $\left(-\mathbf{i}_x,\mathbf{i}_y,0\mathbf{i}_z\right)$ axis by an infinite set of infinitesimal increments of the rotational angle over a span of $\pi$ wherein the current direction is such that the resultant angular momentum vector of the basis elements of $\frac{\hbar}{2\sqrt{2}}$ is stationary on this axis.

## GENERATION OF THE BECVF

Consider two infinitesimal charge(mass)-density elements at two separate positions or points, one and two, of the first pair of orthogonal great-circle current loops that serve as the basis set for generation of the BECVF as shown in Figure 1.4. The rotating Cartesian coordinates, x',y',z', in which the basis element great circles are fixed is designated the basis-set reference frame. In this frame at time zero, element one is at $x'=0$, $y'=r_n$, and $z'=0$, and element two is at $x'=r_n$, $y'=0$, and $z'=0$. Let element one move on a great circle clockwise toward the -z'-axis, and let element two move counter clockwise on a great circle toward the -z'-axis, as shown in Figure 1.4. . The equations of motion, in the basis-set reference frame with $t=0$ defined at the points (0,1,0) and (1,0,0), respectively, are given by

point one:

$$x_1' = 0 \qquad y_1' = r_n\cos(\omega_n t) \qquad z_1' = -r_n\sin(\omega_n t) \tag{I.80}$$

point two:

$$x_2' = r_n\cos(\omega_n t) \qquad y_2' = 0 \qquad z_2' = -r_n\sin(\omega_n t) \tag{I.81}$$

The great circle basis elements and rotational matrix of the BECVF are given by:

### BECVF MATRICES ($R_{\left(-\mathbf{i}_x,\mathbf{i}_y,0\mathbf{i}_z\right)}(\theta)$)

$$\begin{bmatrix} x' \\ y' \\ z' \end{bmatrix} = \begin{bmatrix} \frac{1}{2}+\frac{\cos\theta}{2} & -\frac{1}{2}+\frac{\cos\theta}{2} & -\frac{\sin\theta}{\sqrt{2}} \\ -\frac{1}{2}+\frac{\cos\theta}{2} & \frac{1}{2}+\frac{\cos\theta}{2} & -\frac{\sin\theta}{\sqrt{2}} \\ \frac{\sin\theta}{\sqrt{2}} & \frac{\sin\theta}{\sqrt{2}} & \cos\theta \end{bmatrix} \bullet \left( \begin{bmatrix} 0 \\ r_n\cos\phi \\ -r_n\sin\phi \end{bmatrix} + \begin{bmatrix} r_n\cos\phi \\ 0 \\ -r_n\sin\phi \end{bmatrix} \right) \tag{I.82}$$

## GENERATION OF THE OCVF

The generation of the OCVF is achieved by rotation of two great circle basis elements, one in the x'y'-plane and the other in the plane that bisects the x'y'-quadrant and is parallel to the z'-axis, about the $\left(-\frac{1}{\sqrt{2}}\mathbf{i}_x,\frac{1}{\sqrt{2}}\mathbf{i}_y,\mathbf{i}_z\right)$-axis by an infinite set of infinitesimal increments of the rotational angle over a span of $\pi$ wherein the current direction is such that the resultant angular momentum vector of the basis elements of $\frac{\hbar}{2}$ having components of $\mathbf{L}_{xy}=\frac{\hbar}{2\sqrt{2}}$ and $\mathbf{L}_z=\frac{\hbar}{2\sqrt{2}}$ is stationary on this axis. For the generation of the OCVF, consider two charge(mass)-density elements, point one and two, in the basis-set reference frame at

time zero. Element one is at $x'=\frac{r_n}{\sqrt{2}}$, $y'=\frac{r_n}{\sqrt{2}}$, and $z'=0$, and element two is at $x'=r_n$, $y'=0$, and $z'=0$. Let element one move clockwise on a great circle toward the -z'-axis, and let element two move counter clockwise on a great circle toward the y'-axis as shown in Figure 1.8. The equations of motion, in the basis-set reference frame are given by:

point one:

$$x_1'=r_n\sin\left(\frac{\pi}{4}\right)\cos(\omega_n t) \qquad y_1'=r_n\cos\left(\frac{\pi}{4}\right)\cos(\omega_n t) \qquad z_1'=-r_n\sin(\omega_n t) \tag{I.83}$$

point two:

$$x_2'=r_n\cos(\omega_n t) \qquad y_2'=r_n\sin(\omega_n t) \qquad z_2'=0 \tag{I.84}$$

The great circle basis elements and rotational matrix of the OCVF are given by:

**OCVF Matrices ($R_{\left(-\frac{1}{\sqrt{2}}\mathbf{i}_x,\frac{1}{\sqrt{2}}\mathbf{i}_y,\mathbf{i}_z\right)}(\theta)$)**

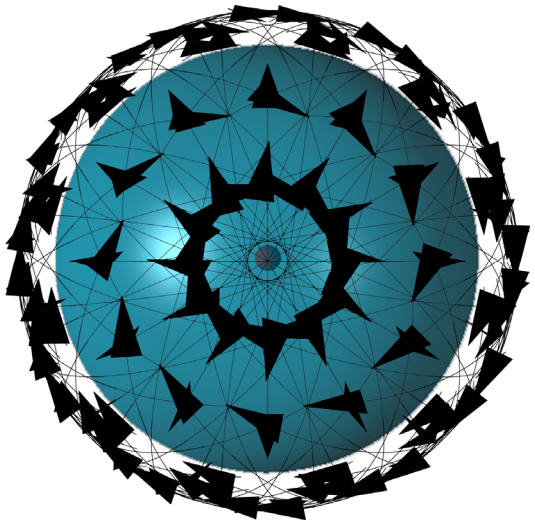
$$\begin{bmatrix}x'\\y'\\z'\end{bmatrix}=\begin{bmatrix}\frac{1}{4}\left(1+3\cos\theta\right) & \frac{1}{4}\left(-1+\cos\theta+2\sqrt{2}\sin\theta\right) & \frac{1}{4}\left(-\sqrt{2}+\sqrt{2}\cos\theta-2\sin\theta\right)\\ \frac{1}{4}\left(-1+\cos\theta-2\sqrt{2}\sin\theta\right) & \frac{1}{4}\left(1+3\cos\theta\right) & \frac{1}{4}\left(\sqrt{2}-\sqrt{2}\cos\theta-2\sin\theta\right)\\ \frac{1}{2}\left(\frac{-1+\cos\theta}{\sqrt{2}}+\sin\theta\right) & \frac{1}{4}\left(\sqrt{2}-\sqrt{2}\cos\theta+2\sin\theta\right) & \cos^2\frac{\theta}{2}\end{bmatrix}\bullet\left(\begin{bmatrix}\frac{r_n\cos\phi}{\sqrt{2}}\\ \frac{r_n\cos\phi}{\sqrt{2}}\\ -r_n\sin\phi\end{bmatrix}+\begin{bmatrix}r_n\cos\phi\\ r_n\sin\phi\\ 0\end{bmatrix}\right) \tag{I.85}$$

## GENERATION OF $Y_0^0(\theta,\phi)$

Then, the uniform great-circle distribution $Y_0^0(\theta,\phi)$ is exactly generated from the CVFs. The BECVF is convolved with the OCVF over a $2\pi$ span that results in the placement of a BECVF at each great circle of the OCVF. Since the angular momentum vector of the BECVF is matched to twice that of one of the OCVF great circle basis elements and the span is over a $2\pi$, the resultant angular momentum of the distribution is the same as that of the OCVF, except that coverage of the spherical surface is complete. This current vector distribution is normalized by scaling the constant current of each great circle element resulting in the exact uniformity of the distribution independent of time since $\nabla\cdot K=0$ along each great circle. There is no alteration of the angular momentum with normalization since it only affects the density parallel to the angular momentum axis of the distribution, the $\left(-\frac{1}{\sqrt{2}}\mathbf{i}_x,\frac{1}{\sqrt{2}}\mathbf{i}_y,\mathbf{i}_z\right)$-axis. Then, the boundary conditions of $Y_0^0(\theta,\phi)$ having the desired angular momentum components, coverage, element motion, and uniformity are shown to have been achieved by designating the $\left(-\frac{1}{\sqrt{2}}\mathbf{i}_x,\frac{1}{\sqrt{2}}\mathbf{i}_y,\mathbf{i}_z\right)$-axis as the z-axis. Specifically, this uniform spherical shell of current (Figure I.2) meets the boundary conditions of having an angular velocity magnitude at each point on the surface given by Eq. (I.62), and angular momentum projections of $\mathbf{L}_{xy}=+/-\frac{\hbar}{4}$ and $\mathbf{L}_z=\frac{\hbar}{2}$ (Eqs. (1.127-1.128) and Figure 1.23)[4] that give rise to the Stern Gerlach experiment and the phenomenon corresponding to the spin quantum number as shown in the Magnetic Parameters of the Electron (Bohr Magneton) section, and in the Electron g Factor section.

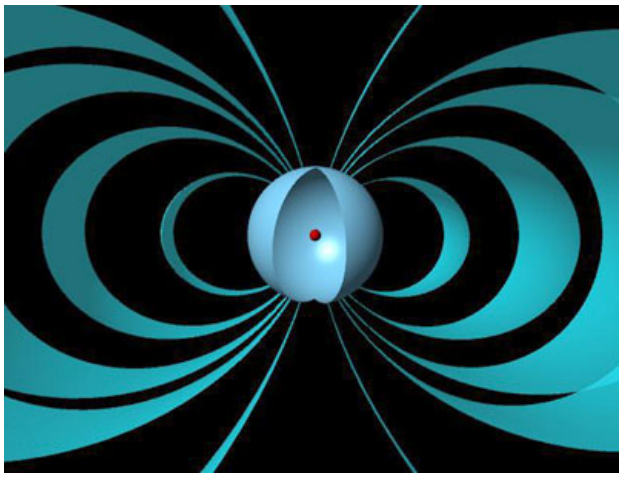
[4] $+/-$ designates both the positive and negative vector directions along an axis in the xy-plane.

**Figure I.2.** The bound electron exists as a spherical two-dimensional supercurrent (electron *atomic orbital*), an extended distribution of charge and current completely surrounding the nucleus. Unlike a spinning sphere, there is a complex pattern of motion on its surface (indicated by vectors) that generates two orthogonal components of angular momentum (Figure I.1) that give rise to the phenomenon of electron spin. A representation of the $\left(-\frac{1}{\sqrt{2}}\mathbf{i}_x, \frac{1}{\sqrt{2}}\mathbf{i}_y, \mathbf{i}_z\right)$-axis view of the total uniform supercurrent-density pattern of the $Y_0^0(\phi,\theta)$ atomic orbital with 144 vectors overlaid on the continuous bound-electron current density giving the direction of the current of each great circle element (nucleus not to scale) is shown.



As shown in the Atomic Orbital Equation of Motion for $\ell = 0$ Based on the Current Vector Field (CVF) section, the application of a magnetic field to the atomic orbital gives rise to a precessing angular momentum vector $\mathbf{S}$ directed from the origin of the atomic orbital at an angle of $\theta = \frac{\pi}{3}$ relative to the applied magnetic field. The precession of $\mathbf{S}$ with an angular momentum of $\hbar$ forms a cone in the nonrotating laboratory frame to give a perpendicular projection of $\mathbf{S}_\perp = \pm\sqrt{\frac{3}{4}}\hbar$ (Eq. (1.129)) and a projection onto the axis of the applied magnetic field of $\mathbf{S}_\parallel = \pm\frac{\hbar}{2}$ (Eq. (1.130)). The superposition of the $\frac{\hbar}{2}$ z-axis component of the atomic orbital angular momentum and the $\frac{\hbar}{2}$ z-axis component of $\mathbf{S}$ gives $\hbar$ corresponding to the observed magnetostatic electron magnetic moment of a Bohr magneton. The $\hbar$ of angular momentum along $\mathbf{S}$ has a corresponding precessing magnetic moment of 1 Bohr magneton. The magnetostatic dipole magnetic field corresponding to $\mu_B$ is shown in Figure I.3.

**Figure I.3.** The three-dimensional cut-away representation of the magnetic field of an electron atomic orbital showing the nucleus (not to scale). The field is a dipole outside the atomic orbital.



In contrast to the QM and QED cases (See Ref [10]), the fourth quantum number arises naturally in CP as derived in the Electron g Factor section. The Stern-Gerlach experiment implies a magnetic moment of one Bohr magneton and an associated angular momentum quantum number of 1/2. Historically, this quantum number is called the spin quantum number, s ($s=\frac{1}{2};\ m_s=\pm\frac{1}{2}$). Conservation of angular momentum of the atomic orbital permits a discrete change of its "kinetic angular momentum" ($\mathbf{r}\times m\mathbf{v}$) with respect to the field of $\frac{\hbar}{2}$, and concomitantly the "potential angular momentum" ($\mathbf{r}\times e\mathbf{A}$) must change by $-\frac{\hbar}{2}$. The flux change, $\phi$, of the atomic orbital for $r<r_n$ is determined as follows:

$$\Delta\mathbf{L}=\frac{\hbar}{2}-\mathbf{r}\times e\mathbf{A} \tag{I.86}$$

$$=\left[\frac{\hbar}{2}-\frac{e2\pi rA}{2\pi}\right]\hat{z} \tag{I.87}$$

$$=\left[\frac{\hbar}{2}-\frac{e\phi}{2\pi}\right]\hat{z} \tag{I.88}$$

In order that the change of angular momentum, $\Delta\mathbf{L}$, equals zero, $\phi$ must be $\Phi_0=\frac{h}{2e}$, the magnetic flux quantum. Thus, to conserve angular momentum in the presence of an applied magnetic field, the atomic orbital magnetic moment can be parallel or antiparallel to an applied field as observed with the Stern-Gerlach experiment, and the flip between orientations is accompanied by the "capture" of the magnetic flux quantum by the atomic orbital. During the spin-flip transition, power must be conserved. Power flow is governed by the Poynting power theorem,

$$\nabla\bullet(\mathbf{E}\times\mathbf{H})=-\frac{\partial}{\partial t}\left[\frac{1}{2}\mu_0\mathbf{H}\bullet\mathbf{H}\right]-\frac{\partial}{\partial t}\left[\frac{1}{2}\varepsilon_0\mathbf{E}\bullet\mathbf{E}\right]-\mathbf{J}\bullet\mathbf{E} \tag{I.89}$$

Eq. (I.90) derived in the Electron g Factor section gives the total energy of the flip transition, which is the sum of the energy of reorientation of the magnetic moment (1st term), the magnetic energy (2nd term), the electric energy (3rd term), and the dissipated energy of a fluxon treading the atomic orbital (4th term), respectively.

$$\Delta E_{mag}^{spin}=2\left(1+\frac{\alpha}{2\pi}+\frac{2}{3}\alpha^2\left(\frac{\alpha}{2\pi}\right)-\frac{4}{3}\left(\frac{\alpha}{2\pi}\right)^2\right)\mu_B B \tag{I.90}$$

$$\Delta E_{mag}^{spin}=g\mu_B B \tag{I.91}$$

The spin-flip transition can be considered as involving a magnetic moment of $g$ times that of a Bohr magneton. The $g$ factor is now designated the fluxon $g$ factor as opposed to the unwarranted historical anomalous $g$ factor. The calculated value of $\frac{g}{2}$ is $1.001\ 159\ 652\ 137$. The experimental value [66] of $\frac{g}{2}$ is $1.001\ 159\ 652\ 188(4)$.

## FORCE BALANCE EQUATION

The radius of the nonradiative ($n=1$) state is solved using the electromagnetic force equations of Maxwell relating the charge and mass density functions wherein the angular momentum of the electron is given by $\hbar$. The reduced mass arises naturally from an electrodynamic interaction between the electron and the proton of mass $m_p$.

$$\frac{m_e}{4\pi r_1^2}\frac{v_1^2}{r_1} = \frac{e}{4\pi r_1^2}\frac{Ze}{4\pi\varepsilon_0 r_1^2} - \frac{1}{4\pi r_1^2}\frac{\hbar^2}{m_p r_n^3} \tag{I.92}$$

$$r_1 = \frac{a_H}{Z} \tag{I.93}$$

where $a_H$ is the radius of the hydrogen atom and the electron velocity is given by Eq. (I.61).

## ENERGY CALCULATIONS

From Maxwell's equations, the potential energy $V$, kinetic energy $T$, electric energy or binding energy $E_{ele}$ are:

$$V = \frac{-Ze^2}{4\pi\varepsilon_0 r_1} = \frac{-Z^2e^2}{4\pi\varepsilon_0 a_H} = -Z^2\ X\ 4.3675\ X\ 10^{-18}\ J = -Z^2\ X\ 27.2\ eV \tag{I.94}$$

$$T = \frac{Z^2e^2}{8\pi\varepsilon_0 a_H} = Z^2\ X\ 13.59\ eV \tag{I.95}$$

$$T = E_{ele} = -\frac{1}{2}\varepsilon_0\int_{\infty}^{r_1}\mathbf{E}^2 dv \quad \text{where } \mathbf{E} = -\frac{Ze}{4\pi\varepsilon_0 r^2} \tag{I.96}$$

$$E_{ele} = -\frac{Ze^2}{8\pi\varepsilon_0 r_1} = -\frac{Z^2e^2}{8\pi\varepsilon_0 a_H} = -Z^2\ X\ 2.1786\ X\ 10^{-18}\ J = -Z^2\ X\ 13.598\ eV \tag{I.97}$$

The calculated Rydberg constant is $10{,}967{,}758\ m^{-1}$, and the experimental Rydberg constant is $10{,}967{,}758\ m^{-1}$. For increasing $Z$, the velocity becomes a significant fraction of the speed of light; thus, special relativistic corrections were included in the calculation of the ionization energies of one-electron atoms that are given by

$$E_B = m_{e0}c^2\left(1-\sqrt{1-(\alpha Z)^2}\right) \tag{I.98}$$

## THE NATURE OF THE PHOTON IS THE BASIS OF QUANTIZATION AND EXISTENCE OF EXCITED AND HYDRINO STATES OF ATOMIC HYDROGEN

It is well known that resonator cavities can trap electromagnetic radiation of discrete resonant frequencies. The atomic orbital is a resonator cavity that traps photons of discrete frequencies. The radius of an atomic orbital increases with the absorption of electromagnetic energy. The solutions to Maxwell's equations for modes that can be excited in the atomic orbital resonator cavity give rise to four quantum numbers, and the energies of the modes are the experimentally known hydrogen spectrum including the Lamb shift, fine structure, and hyperfine structure.

The excited states involving the corresponding multipole photon radiation are solved including the radii of the atomic orbitals using Maxwell's equations with the traditional source current boundary constraints at the electron. The "trapped photon" is a "standing electromagnetic wave" which actually is a circulating wave that propagates along the current density of the atomic orbital. The time-function factor, $k(t)$, for the "standing wave" is identical to the time-function factor of the atomic orbital in order to satisfy the boundary (phase) condition at the atomic orbital surface. Thus, the angular frequency of the "trapped photon" has to be identical to the angular frequency of the electron atomic orbital, $\omega_n$. Furthermore, the phase condition requires that the angular functions of the "trapped photon" have to be identical to the spherical harmonic angular functions of the electron atomic orbital. Combining $k(t)$ with the $\phi$-function factor of the spherical harmonic gives $e^{i(m\phi-m\omega_n t)}$ for both the electron and the "trapped photon" functions. The photon can be considered a solution of Laplace's equation in spherical coordinates that is "glued" to the inner atomic orbital surface corresponding to a radial Dirac delta function at the electron radius, $\delta(r-r_n)$, and due to relativistic effects the field is radially local at the electron. The field lines from the proton superimpose with those of the photon at the electron and end on the current-density function of the electron such that the electric field is zero for $r > r_n$, where $r_n$ is the radius of the electron. The corresponding photon source current given by Gauss' law in

two dimensions determines the stability condition.

The instability of excited states, as well as the stability of the $n=1$ state arises naturally in CP. The central field of the proton corresponds to an integer charge of one. Excited states comprise an electron with a trapped photon. In all energy states of hydrogen, the photon has an electric field that superposes with the field of the proton. In the $n=1$ state, the sum is one, and the sum is zero in the ionized state. In an excited state, the sum is a fraction of one (i.e. between zero and one), specifically, $\frac{1}{\text{integer}}$. The relationship between the electric field function and the "trapped photon" source charge-density function is given by Gauss' law in two dimensions, Eq. (I.102) where $\mathbf{n}$ is the radial normal unit vector, $\mathbf{E}_1 = 0$ ($\mathbf{E}_1$ is the electric field outside of the atomic orbital), $\mathbf{E}_2$ is given by the total electric field at $r_n = na_H$, and $\sigma_s$ is the equivalent surface charge density. The electric field of an excited state is fractional; therefore, the source charge function is fractional corresponding to a radiative current-density function. Thus, an excited electron is unstable and decays to the first nonradiative state corresponding to an integer field, $n=1$ (i.e. a field of integer one times the central field of the proton).

Equally valid from first principles are electronic states where the magnitude of the sum of the electric field of the photon and the proton central field are an integer times the central field of the proton. These states are nonradiative. A catalyst can effect a transition between these states via a nonradiative energy transfer to form *hydrinos*, stable hydrogen atoms having energy levels below the ground state and corresponding to principal quantum numbers $n = 1, \frac{1}{2}, \frac{1}{3}, \frac{1}{4}, ..., \frac{1}{p}$; $p \le 137$ replaces the well known parameter $n = \text{integer}$ in the Rydberg equation for hydrogen excited states. *Hydrinos* and the corresponding *hydrino hydride ions* and *molecular hydrinos* have been confirmed experimentally as shown in the Data section. Until now, this predicted discovery was missed entirely due to the erroneous concept of the hydrogen atom "ground state" based on its definition regarding the Schrödinger equation since the Schrödinger equation does not physically explain the observation that spontaneous emission of radiation does not occur for the state having a binding energy of 13.6 eV. Nor, does the Schrödinger equation provide a physical basis for the existence of the $n = \text{integer}$ excited states or absorption or emission of radiation. (See Schrödinger Wavefunction in Violation of Maxwell's Equation section, the Retrospect section, and papers by Mills' [4-15]).

## EXCITED STATES

CP gives closed form solutions for the resonant photons and excited state electron functions. The angular momentum of the photon given by

$$\mathbf{m} = \int \frac{1}{8\pi c} \mathrm{Re}\left[\mathbf{r} \times (\mathbf{E} \times \mathbf{B}^*)\right] dx^4 = \hbar \tag{I.99}$$

is conserved [67]. The change in angular velocity of the electron is equal to the angular frequency of the resonant photon. The energy is given by Planck's equation. The predicted energies, Lamb shift, hyperfine structure, resonant line shape, line width, selection rules, etc. are in agreement with observation.

The discretization of the angular momentum of the electron and the photon gives rise to quantized electron radii and energy levels. Transitions occur in integer units of the electron's inalienable intrinsic angular momentum of $\hbar$ (Appendix II) such that the exciting photons carry an integer multiple of $\hbar$. Thus, for $\mathbf{r} \times m_e \mathbf{v}_e = \mathbf{p}$ to be constant, the radius increases by a factor of the integer and the electron velocity decreases by the factor of the integer. This quantization condition is equivalent to that of Bohr except that the electron angular momentum is $\hbar$, the angular momentum of one or more photons that give rise to an excited state is $n\hbar$, and the photon field changes the central force balance. Also, the standing wave regards the photon field and not the electron that comprises an extended current and is not a wave function. Thus, the quantization condition can also be considered as arising from the discretization of the photon standing wave including the integer spherical periodicity of the spherical harmonics of the excited state of the bound electron as a spherical cavity.

The atomic orbital is a dynamic spherical resonator cavity which traps photons of discrete frequencies. The relationship between an allowed radius and the "photon standing wave" wavelength is

$$2\pi r = n\lambda \tag{I.100}$$

where $n$ is an integer. The relationship between an allowed radius and the electron wavelength is:

$$2\pi(nr_1) = 2\pi r_n = n\lambda_1 = \lambda_n \tag{I.101}$$

where $n = 1, 2, 3, 4, \ldots$. The radius of an atomic orbital increases with the absorption of electromagnetic energy due to a corresponding decrease in the central field. *The radii of excited states are solved using the electromagnetic force equations of Maxwell relating the field from the charge of the proton, the electric field of the photon, and charge and mass density functions of the electron wherein the angular momentum of the electron is given by $\hbar$ (Eq. (1.37))*. The solutions to Maxwell's equations for modes that can be excited in the atomic orbital resonator cavity give rise to four quantum numbers, and the energies of the modes are the experimentally known hydrogen spectrum. The relationship between the electric field equation and the "trapped photon" source charge-density function is given by Maxwell's equation in two dimensions.

$$\mathbf{n} \bullet \left(\mathbf{E}_1 - \mathbf{E}_2\right) = \frac{\sigma}{\varepsilon_0} \tag{I.102}$$

The photon standing electromagnetic wave is phase matched with the electron

$$\mathbf{E}_{r\,photon\;\;n,l,m_\ell} = \frac{e\left(na_H\right)^\ell}{4\pi\varepsilon_0}\frac{1}{r^{(\ell+2)}}\left[-Y_0^0\left(\theta,\phi\right)+\frac{1}{n}\left[Y_0^0\left(\theta,\phi\right)+\mathrm{Re}\left\{Y_\ell^m\left(\theta,\phi\right)e^{im\omega_n t}\right\}\right]\right]\delta\left(r-r_n\right)\mathbf{i}_r$$
$$\ell = 0,1,2,...,n-1 \tag{I.103}$$
$$m_\ell = -\ell,-\ell+1,...,0,....+\ell$$

$$\mathbf{E}_{r\,total} = \frac{e}{4\pi\varepsilon_0 r^2}+\frac{e\left(na_H\right)^\ell}{4\pi\varepsilon_0}\frac{1}{r^{(\ell+2)}}\left[-Y_0^0\left(\theta,\phi\right)+\frac{1}{n}\left[Y_0^0\left(\theta,\phi\right)+\mathrm{Re}\left\{Y_\ell^m\left(\theta,\phi\right)e^{im\omega_n t}\right\}\right]\right]\delta\left(r-r_n\right)\mathbf{i}_r \tag{I.104}$$

For $r = na_H$ and $m = 0$, the total radial electric field is:

$$\mathbf{E}_{r\,total} = \frac{1}{n}\frac{e}{4\pi\varepsilon_0\left(na_H\right)^2}\mathbf{i}_r \tag{I.105}$$

When an electron in the $n=1$ state absorbs a photon of energy sufficient to take it to a new resonant state, $n = 2,3,4,...,$ force balance must be maintained with the reduction of the central field caused by the superposition of the electric field of the proton and the photon trapped in the atomic orbital, a spherical resonator cavity. According to Eq. (I.105), the central field is equivalent to that of a central charge of $\frac{e}{n}$, and the excited-state force balance equation is

$$\frac{m_e v_n^2}{r_n} = \frac{\hbar^2}{m_e r_n^3} = \frac{1}{n}\frac{e^2}{4\pi\varepsilon_0 r_n^2} \tag{I.106}$$

where $r_1$ is the $n=1$ state radius of the electron, $r_n$ is the nth excited state radius of the electron, and the electron velocity is given by Eq. (I.61). The radius of the nth excited state given by Eq. (I.106) is

$$r_n = na_H \tag{I.107}$$

The energy of the photon that excites a mode in the electron spherical resonator cavity from radius $a_H$ to radius $na_H$ is

$$E_{photon} = \frac{e^2}{8\pi\varepsilon_0 a_H}\left[1-\frac{1}{n^2}\right] = h\nu = \hbar\omega \tag{I.108}$$

The change in angular velocity of the atomic orbital for an excitation from $n=1$ to $n=n$ is:

$$\Delta\omega = \frac{\hbar}{m_e\left(a_H\right)^2}-\frac{\hbar}{m_e\left(na_H\right)^2} = \frac{\hbar}{m_e\left(a_H\right)^2}\left[1-\frac{1}{n^2}\right] \tag{I.109}$$

The kinetic energy change of the transition is

$$\frac{1}{2}m_e(\Delta v)^2 = \frac{e^2}{8\pi\varepsilon_0 a_H}\left[1-\frac{1}{n^2}\right] = \hbar\omega \tag{I.110}$$

The change in angular velocity of the electron atomic orbital is identical to the angular velocity of the photon necessary for the excitation, $\omega_{photon}$. The *correspondence principle holds*. It can be demonstrated that the resonance condition between these frequencies is to be satisfied in order to have a net change of the energy field [48].

## INSTABILITY OF EXCITED STATES

For the excited energy states of the hydrogen atom, $\sigma_{photon}$, the two-dimensional surface charge due to the "trapped photons" at the electron atomic orbital, given by Eq. (I.102) and Eq. (I.103) is:

$$\sigma_{photon} = \frac{e}{4\pi(r_n)^2}\left[Y_0^0\left(\theta,\phi\right)-\frac{1}{n}\left[Y_0^0\left(\theta,\phi\right)+\mathrm{Re}\left\{Y_\ell^m\left(\theta,\phi\right)e^{im\omega_n t}\right\}\right]\right]\delta(r-r_n) \tag{I.111}$$

where $n = 2,3,4,...,$. Whereas, $\sigma_{electron}$, the two dimensional surface charge of the electron atomic orbital given by Eq. (I.65) is

$$\sigma_{electron} = \frac{-e}{4\pi(r_n)^2}\left[Y_0^0\left(\theta,\phi\right)+\mathrm{Re}\left\{Y_\ell^m\left(\theta,\phi\right)e^{im\omega_n t}\right\}\right]\delta(r-r_n) \tag{I.112}$$

The superposition of $\sigma_{photon}$ (Eq. (I.111)) and $\sigma_{electron}$ (Eq. (I.112)) is equivalent to the sum of a radial electric dipole represented by a doublet function and a radial electric monopole represented by a delta function:

$$\sigma_{photon}+\sigma_{electron} =$$
$$\frac{e}{4\pi(r_n)^2}\left[Y_0^0\left(\theta,\phi\right)\dot{\delta}(r-r_n)-\frac{1}{n}Y_0^0\left(\theta,\phi\right)\delta(r-r_n)-\left(1+\frac{1}{n}\right)\left[\mathrm{Re}\left\{Y_\ell^m\left(\theta,\phi\right)e^{im\omega_n t}\right\}\right]\delta(r-r_n)\right] \tag{I.113}$$

where $n = 2,3,4,...,$. Due to the radial doublet, excited states are radiative since spacetime harmonics of $\frac{\omega_n}{c} = k$ or $\frac{\omega_n}{c}\sqrt{\frac{\varepsilon}{\varepsilon_0}} = k$ do exist for which the spacetime Fourier transform of the current density function is nonzero. An excited state is meta-stable because it is the sum of nonradiative (stable) and radiative (unstable) components and de-excites with a transition probability given by the ratio of the power to the energy of the transition [68]. There is motion in the radial direction only when the energy of the system is changing, and the *radiation emitted or absorbed during electron transitions is the multipole radiation given by Eq. (I.50)* as given in the Excited States of the One-Electron Atom (Quantization) section and the Equation of the Photon section. The discontinuous harmonic radial current in Eq. (I.55) that connects the initial and final states of the transition is:

$$\mathbf{r}\cdot\mathbf{J} = \frac{er}{4\pi r^2}\tau^{-1}\sin\frac{\pi t'}{\tau}\left(u(t') - u(t'-\tau)\right) \tag{I.114}$$

where $\tau$ is the lifetime of the transition given by Eq. (2.107) and $t'$ is time during the transition as given in the Excited States of the One-Electron Atom (Quantization) section. The vector potential of the current that connects the initial and final states of a transition, each having currents of the form given by Eq. (1.12), is:

$$\mathbf{A}(r) = \frac{\mu_0}{2\pi}\frac{e\hbar}{m_e}\frac{1}{r_{n_i} - r_{n_f}}\frac{e^{-ik_r r}}{4\pi r}\mathbf{i}_z \tag{I.115}$$

The magnetic and electric fields are derived from the vector potential and are used in the Poynting power vector to give the power. The transition probability or Einstein coefficient $A_{ki}$ for initial state $n_i$ and final state $n_f$ of atomic hydrogen given by the power divided by the energy of the transition is:

$$\frac{1}{\tau} = \frac{1}{m_e c^2}\frac{\eta}{24\pi}\left(\frac{e\hbar}{m_e a_0^2}\right)^2\frac{1}{\left(n_f n_i\right)^2} = 2.678\ X\ 10^9\frac{1}{\left(n_f n_i\right)^2}\ s^{-1} \tag{I.116}$$

which matches the NIST values for all transitions extremely well as shown in Excited States of the One-Electron Atom (Quantization) section.

# HYDRINO STATES

## EXTENSION OF THE RYDBERG STATES TO LOWER LEVELS

For a spherical resonator cavity, the nonradiative boundary condition and the relationship between the electron and the photon give the hydrogen energy states that are quantized as a function of the parameter $n$. That is the nonradiative boundary condition and the relationship between an allowed radius and the photon standing wave wavelength (Eq. (I.100)) gives rise to Eq. (I.101), the boundary condition for allowed radii and allowed electron wavelengths as a function of the parameter $n$. Each value of $n$ corresponds to an allowed transition effected by a resonant photon that excites the transition in the atomic orbital resonator cavity. In addition to the traditional integer values (1, 2, 3,...,) of $n$, values of $\frac{1}{\text{integer}}$ are allowed by Eq. (I.101) which correspond to transitions with an increase in the central field and decrease in the radius of the atomic orbital. This occurs, for example, when the electron couples to another electronic transition or electron transfer reaction that can absorb energy—an energy sink. This ***transition reaction*** of the electron of hydrogen to a lower energy state occurs by the ***absorption of an energy hole by the hydrogen atom***. The absorption of an energy hole destroys the balance between the centrifugal force and the resulting increased central electric force. Consequently, the electron undergoes a transition to a lower energy nonradiative state.

From energy conservation, the energy hole of a hydrogen atom that excites resonator modes of radial dimensions $\frac{a_H}{m+1}$ is

$$m\cdot 27.2\ eV, \tag{I.117}$$

where $m$ is an integer. After resonant absorption of the energy hole, the radius of the atomic orbital, $a_H$, shrinks to $\frac{a_H}{m+1}$ and after $t$ cycles of transition, the radius is $\frac{a_H}{mt+1}$. In other words, the radial ground state field can be considered as the superposition of Fourier components. The removal of negative Fourier components of energy $m\cdot 27.2\ eV$, where $m$ is an integer increases the positive electric field inside the spherical shell by $m$ times the charge of a proton. The resultant electric field is a time harmonic solution of Laplace's Equations in spherical coordinates. In this case, the radius at which force balance and nonradiation are achieved is $\frac{a_H}{m+1}$ where $m$ is an integer. In decaying to this radius from the $n=1$ state, a total energy of $[(m+1)^2 - 1^2]\cdot 13.6\ eV$ is released. The process involving the transition reaction is hereafter referred to as the **BlackLight Process**. The source of energy holes may not be consumed in the transition reaction; therefore they serve as a hydrogen catalyst.

The increased-binding-energy hydrogen atom is called a *hydrino atom* having a binding energy of:

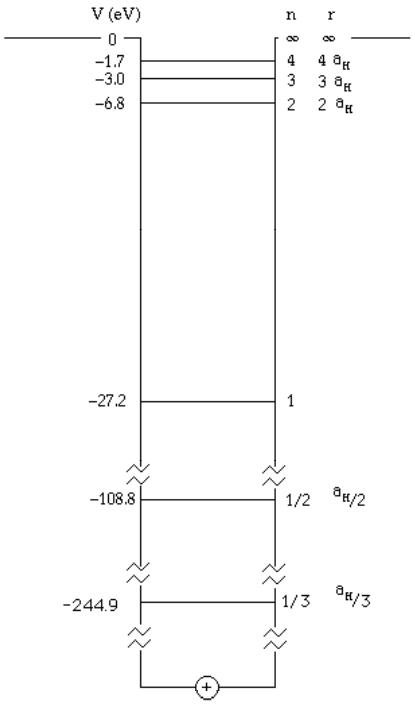
$$Binding\ Energy = \frac{13.6\ eV}{n^2} \tag{I.118}$$

where

$$n = \frac{1}{2}, \frac{1}{3}, \frac{1}{4}, ..., \frac{1}{p} \tag{I.119}$$

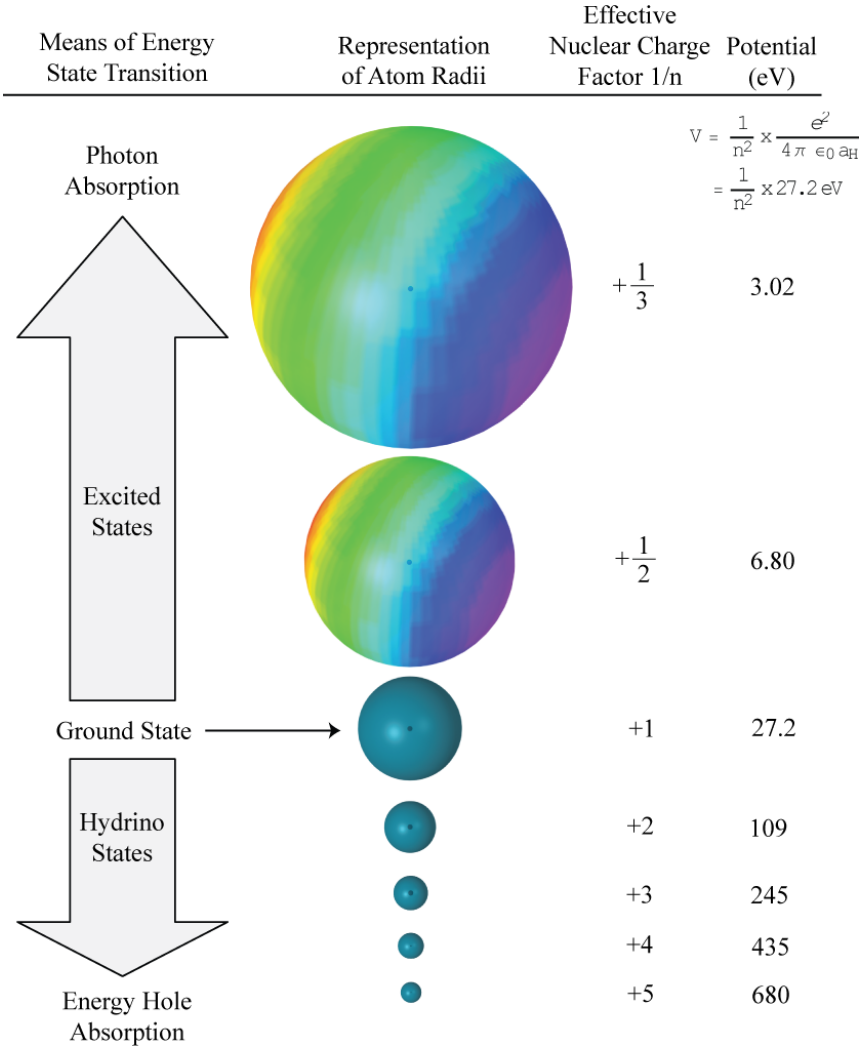
and $p$ is an integer greater than 1. Hydrino atoms designated as $H(1/p)$ have a radius of $a_H / p$, the hydrogen atom divided by an integer. The potential energy diagram of the hydrogen atom is extended to lower Rydberg states, as given in Figure I.4.

**Figure I.4.** Potential energy well of a hydrogen atom.




The size of the electron atomic orbital as a function of potential energy is given in Figure I.5.

**Figure I.5.** Quantized sizes of hydrogen atoms where $n$ is an integer for excited states and $n = 1/p$ for hydrino states where $p$ is an integer.



## PHOTONIC EQUATION

As shown previously, the hydrino photonic equation must be a solution of Laplace's equation in spherical coordinates. The "trapped photon" field comprises an electric field that provides force balance and a nonradiative state. Following the Maxwellian approach given for excited states in the Excited States section (Eq. (I.103)), the solution to this boundary value problem of the radial photon electric field is:

$$\mathbf{E}_{r\ photon\ n,l,m} = \frac{e(na_H)^{\ell}}{4\pi\varepsilon_0}\frac{1}{r^{(\ell+2)}}\left[-Y_0^0(\theta,\phi)+\frac{1}{n}\left[Y_0^0(\theta,\phi)+\mathrm{Re}\left\{Y_\ell^m(\theta,\phi)e^{im\omega_n t}\right\}\right]\right]\delta(r-r_n)$$

$$n=\frac{1}{p}$$

$$p=2,3,4,... \tag{I.120}$$

$$\ell=0,1,2,...,n-1$$

$$m_\ell=-\ell,-\ell+1,...,0,....+\ell$$

The quantum numbers of the electron are $p$, $\ell$, $m_\ell$, and $m_s$ as given in the Electron Source Current section and the Excited States section wherein the principal quantum number of excited states is replaced by $n=1/p$. (Also, see Hydrino Theory—BlackLight Process section.)

## STABILITY OF THE "GROUND" AND HYDRINO STATES

For the below "ground" (fractional quantum number) energy states of the hydrogen atom, $\sigma_{photon}$, the two-dimensional surface charge due to the "trapped photon" at the electron atomic orbital, is given by Eqs. (I.120) and (I.102).

$$\sigma_{photon}=\frac{e}{4\pi(r_n)^2}\left[Y_0^0(\theta,\phi)-\frac{1}{n}\left[Y_0^0(\theta,\phi)+\mathrm{Re}\left\{Y_\ell^m(\theta,\phi)e^{im\omega_n t}\right\}\right]\right]\delta(r-r_n)\quad n=1,\frac{1}{2},\frac{1}{3},\frac{1}{4},..., \tag{I.121}$$

And, $\sigma_{electron}$, the two-dimensional surface charge of the electron atomic orbital is:

$$\sigma_{electron}=\frac{-e}{4\pi(r_n)^2}\left[Y_0^0(\theta,\phi)+\mathrm{Re}\left\{Y_\ell^m(\theta,\phi)e^{im\omega_n t}\right\}\right]\delta(r-r_n) \tag{I.122}$$

The superposition of $\sigma_{photon}$ (Eq. (I.121)) and $\sigma_{electron}$, (Eq. (I.122)) where the spherical harmonic functions satisfy the conditions given in the Electron Source Current section is a radial electric monopole represented by a delta function.

$$\sigma_{photon}+\sigma_{electron}=\frac{-e}{4\pi(r_n)^2}\left[\frac{1}{n}Y_0^0(\theta,\phi)+\left(1+\frac{1}{n}\right)\mathrm{Re}\left\{Y_\ell^m(\theta,\phi)e^{im\omega_n t}\right\}\right]\delta(r-r_n)\quad n=1,\frac{1}{2},\frac{1}{3},\frac{1}{4},..., \tag{I.123}$$

As given in the Spacetime Fourier Transform of the Electron Function section, the radial delta function does not possess spacetime Fourier components synchronous with waves traveling at the speed of light (Eqs. (I.66-I.68)). Thus, the below "ground" (fractional quantum) energy states of the hydrogen atom are stable. The "ground" ($n=1$ quantum) energy state is just the first of the nonradiative states of the hydrogen atom; thus, it is the state to which excited states decay.

## CATALYTIC LOWER-ENERGY HYDROGEN ELECTRONIC TRANSITIONS

Classical physics gives closed-form solutions of the hydrogen atom, the hydride ion, the hydrogen molecular ion, and the hydrogen molecule and predicts corresponding species having fractional principal quantum numbers. The nonradiative state of atomic hydrogen, which is historically called the "ground state" forms the basis of the boundary condition of CP to solve the bound electron. The solutions for electron states having principal energy levels with quantum numbers that are integers and those where $n=\frac{1}{\text{integer}}$ each reveal the corresponding mechanism of the transitions. In the case of excited states, the superposition given by Eq. (I.113) involves the sum of a delta function with a fractional charge (radial monopole term) and two delta functions of charge plus one and minus one that is a doublet function (radial dipole term). The radial dipole is radiative. Whereas, in the case of lower-energy states, the superposition given by Eq. (I.123) involves integer charge (equivalent) only. As given in Appendix I these states having a radial delta function are nonradiative since spacetime harmonics of $\frac{\omega_n}{c}=k$ or $\frac{\omega_n}{c}\sqrt{\frac{\varepsilon}{\varepsilon_0}}=k$ for which the Fourier transform of the current-density function is nonzero do not exist.

Therefore, for the excited-energy states of atomic hydrogen given by Eq. (I.1) with $n>1$, the $n=1$ state is the "ground" state for spontaneous pure photon transitions, and conversely, the $n=1$ state can absorb a photon and go to an excited electronic state. However, the $n=1$ state cannot directly release a photon and go to a lower-energy electronic state. An electron transition from the $n=1$ state to a lower-energy state is only possible by a nonradiative energy transfer such as multipole coupling or a resonant collision mechanism to form the lower-energy states have fractional quantum numbers, $n=\frac{1}{\text{integer}}$.

Processes such as the transition reaction that occur without photons and that require collisions or nonradiative energy transfer are common. For example, the exothermic chemical reaction of $H+H$ to form $H_2$ does not occur with the emission of a photon. Rather, the reaction requires a collision with a third body, $M$, to remove the bond energy- $H+H+M \rightarrow H_2+M^*$ [69]. The third body distributes the energy from the exothermic reaction, and the end result is the $H_2$ molecule and an increase in the temperature of the system. Some commercial phosphors are based on nonradiative energy transfer involving multipole coupling. For example, the strong absorption strength of $Sb^{3+}$ ions along with the efficient nonradiative transfer of excitation from $Sb^{3+}$ to $Mn^{2+}$, are responsible for the strong manganese luminescence from phosphors containing these ions [70].

Thus, it is well known that the electric field of an absorbed photon superimposes that of the proton such that the electron of $H$ moves to a higher-energy excited state at a radius that is greater than that of the $n=1$ state. Similarly, in order to conserve energy, a resonant nonradiative energy transfer from $H$ to a catalyst (source of an energy hole) of $m \cdot 27.2\ eV$ results in an increased interaction between the electron and the central field that is equivalent to $m+1$ times that of a proton. The increased interaction then causes the radius to decrease with the further release of energy such that a total energy of $[(m+1)^2-1^2] \cdot 13.6\ eV$ is released.

## CATALYST REACTION MECHANISM AND PRODUCTS

Classical physics (CP) gives closed-form solutions of the hydrogen atom, the hydride ion, the hydrogen molecular ion, and the hydrogen molecule and predicts corresponding species having fractional principal quantum numbers. The nonradiative state of atomic hydrogen, which is historically called the "ground state" forms the basis of the boundary condition of CP to solve the bound electron. CP predicts a reaction involving a resonant, nonradiative energy transfer from otherwise stable atomic hydrogen to a catalyst capable of accepting the energy to form hydrogen in lower-energy states than previously thought possible called a ***hydrino atom*** designated as $H\left[\frac{a_H}{p}\right]$ where $a_H$ is the radius of the hydrogen atom. Specifically, CP predicts that atomic hydrogen may undergo a catalytic reaction with certain atoms, excimers, ions, and diatomic hydrides which provide a reaction with a net enthalpy of an integer multiple of the potential energy of atomic hydrogen, $E_h = 27.2\ eV$ where $E_h$ is one Hartree. Specific species (e.g. $He^+$, $Ar^+$, $Sr^+$, $K$, $Li$, $HCl$, $NaH$, and $H_2O$) identifiable on the basis of their known electron energy levels are required to be present with atomic hydrogen to catalyze the process. The reaction involves a nonradiative energy transfer of an integer multiple of $27.2\ eV$ from atomic hydrogen to the catalyst followed by $q \cdot 13.6\ eV$ continuum emission or $q \cdot 13.6\ eV$ transfer to another $H$ to form extraordinarily hot, excited-state $H$ and a hydrogen atom that is lower in energy than unreacted atomic hydrogen that corresponds to a fractional principal quantum number. That is, in the formula for the principal energy levels of the hydrogen atom:

$$E_n = -\frac{e^2}{n^2 8\pi\varepsilon_o a_H} = -\frac{13.598\ eV}{n^2} \tag{I.124}$$

$$n = 1, 2, 3, \ldots \tag{I.125}$$

where $a_H$ is the Bohr radius for the hydrogen atom (52.947 pm), $e$ is the magnitude of the charge of the electron, and $\varepsilon_o$ is the vacuum permittivity, fractional quantum numbers:

$$n = 1, \frac{1}{2}, \frac{1}{3}, \frac{1}{4}, \ldots, \frac{1}{p}; \quad p \le 137 \text{ is an integer} \tag{I.126}$$

replace the well known parameter $n = \text{integer}$ in the Rydberg equation for hydrogen excited states. Then, similar to an excited state having the analytical solution of Maxwell's equations given by Eq. (2.15), a hydrino atom also comprises an electron, a proton, and a photon as given by Eq. (5.27). However, the electric field of the latter increases the binding corresponding to desorption of energy rather than decreasing the central field with the absorption of energy as in an excited state, and the resultant photon-electron interaction of the hydrino is stable rather than radiative.

The $n=1$ state of hydrogen and the $n = \frac{1}{\text{integer}}$ states of hydrogen are nonradiative, but a transition between two nonradiative states, say $n=1$ to $n=1/2$, is possible via a nonradiative energy transfer. Hydrogen is a special case of the stable states given by Eqs. (I.124) and (I.126) wherein the corresponding radius of the hydrogen or hydrino atom is given by:

$$r = \frac{a_H}{p}, \tag{I.127}$$

where $p = 1, 2, 3, \ldots$. In order to conserve energy, energy must be transferred from the hydrogen atom to the catalyst in units of

$$m \cdot 27.2\ eV,\ m = 1, 2, 3, 4, \ldots. \tag{I.128}$$

and the radius transitions to $\frac{a_H}{m+p}$. The catalyst reactions involve two steps of energy release: a nonradiative energy transfer to the catalyst followed by additional energy release as the radius decreases to the corresponding stable final state. Thus, the general reaction is given by:

$$m \cdot 27.2\ eV + Cat^{q+} + H\left[\frac{a_H}{p}\right] \rightarrow Cat^{(q+r)+} + re^- + H*\left[\frac{a_H}{(m+p)}\right] + m \cdot 27.2\ eV \quad \text{(I.129)}$$

$$H*\left[\frac{a_H}{(m+p)}\right] \rightarrow H\left[\frac{a_H}{(m+p)}\right] + [(p+m)^2 - p^2] \cdot 13.6\ eV - m \cdot 27.2\ eV \quad \text{(I.130)}$$

$$Cat^{(q+r)+} + re^- \rightarrow Cat^{q+} + m \cdot 27.2\ eV \quad \text{(I.131)}$$

And, the overall reaction is:

$$H\left[\frac{a_H}{p}\right] \rightarrow H\left[\frac{a_H}{(m+p)}\right] + [(p+m)^2 - p^2] \cdot 13.6\ eV \quad \text{(I.132)}$$

$q$, $r$, $m$, and $p$ are integers. $H*\left[\frac{a_H}{(m+p)}\right]$ has the radius of the hydrogen atom (corresponding to 1 in the denominator) and a central field equivalent to $(m+p)$ times that of a proton, and $H\left[\frac{a_H}{(m+p)}\right]$ is the corresponding stable state with the radius of $\frac{1}{(m+p)}$ that of $H$. As the electron undergoes radial acceleration from the radius of the hydrogen atom to a radius of $\frac{1}{(m+p)}$ this distance, energy is released as characteristic light emission or as third-body kinetic energy. The emission may be in the form of an extreme-ultraviolet continuum radiation having an edge at $[(p+m)^2 - p^2 - 2m] \cdot 13.6\ eV$ or $\frac{91.2}{[(p+m)^2 - p^2 - 2m]}\ nm$ and extending to longer wavelengths. In addition to radiation, a resonant kinetic energy transfer to form fast $H$ may occur (See the Dipole-Dipole Coupling section). Subsequent excitation of these fast $H(n=1)$ atoms by collisions with the background $H_2$ followed by emission of the corresponding $H(n=3)$ fast atoms gives rise to broadened Balmer $\alpha$ emission. Alternatively, fast H is a direct product of H or hydrino serving as the catalyst or source of energy holes as given by Eqs. (5.60), (5.65), (5.70), and (5.83) wherein the acceptance of the resonant energy transfer regards the potential energy rather than the ionization energy. Conservation of energy gives a proton of the kinetic energy corresponding to one half the potential energy in the former case and a catalyst ion at essentially rest in the latter case. The H recombination radiation of the fast protons gives rise to broadened Balmer $\alpha$ emission that is disproportionate to the inventory of hot hydrogen consistent with the excess power balance [22-42].

As given in Disproportionation of Energy States section, hydrogen atoms $H(1/p)$ $p = 1, 2, 3, ...137$ can undergo further transitions to lower-energy states given by Eqs. (I.124) and (I.126) wherein the transition of one atom is catalyzed by a second that resonantly and nonradiatively accepts $m \cdot 27.2\ eV$ with a concomitant opposite change in its potential energy. The overall general equation for the transition of $H(1/p)$ to $H(1/(p+m))$ induced by a resonance transfer of $m \cdot 27.2\ eV$ to $H(1/p')$ given by Eq. (5.87) is represented by:

$$H(1/p') + H(1/p) \rightarrow H + H(1/(p+m)) + \left[2pm + m^2 - p'^2 + 1\right] \cdot 13.6\ eV \quad \text{(I.133)}$$

Hydrogen atoms may serve as a catalyst wherein $m = 1$, $m = 2$, and $m = 3$ for one, two, and three atoms, respectively, acting as a catalyst for another. The rate for the two-atom-catalyst, $2H$, may be high when extraordinarily fast H as reported previously [22-42] collides with a molecule to form the $2H$ wherein two atoms resonantly and nonradiatively accept $54.4\ eV$ from a third hydrogen atom of the collision partners. By the same mechanism, the collision of two hot $H_2$ provide $3\,H$ to serve as a catalyst of $3 \cdot 27.2\ eV$ for the fourth. The EUV continua at 22.8 nm and 10.1 nm and extraordinary (>100 eV) Balmer $\alpha$ line broadening are observed consistent with predictions [22-42].

The catalyst product, $H(1/p)$, may also react with an electron to form a hydrino hydride ion $H^-(1/p)$, or two $H(1/p)$ may react to form the corresponding molecular hydrino $H_2(1/p)$. Specifically, the catalyst product, $H(1/p)$, may also react with an electron to form a novel hydride ion $H^-(1/p)$ with a binding energy $E_B$ (Eq. (7.74)) derived in the Hydrino Hydride Ion section:

$$E_B = \frac{\hbar^2\sqrt{s(s+1)}}{8\mu_e a_0^2\left[\frac{1+\sqrt{s(s+1)}}{p}\right]^2} - \frac{\pi\mu_0 e^2\hbar^2}{m_e^2}\left(\frac{1}{a_H^3} + \frac{2^2}{a_0^3\left[\frac{1+\sqrt{s(s+1)}}{p}\right]^3}\right) \tag{I.134}$$

where $p = \text{integer} > 1$, $s = 1/2$, $\hbar$ is Planck's constant bar, $\mu_o$ is the permeability of vacuum, $m_e$ is the mass of the electron, $\mu_e$ is the reduced electron mass given by $\mu_e = \frac{m_e m_p}{\frac{m_e}{\sqrt{\frac{3}{4}}} + m_p}$ where $m_p$ is the mass of the proton, $a_o$ is the Bohr radius, and the ionic radius is $r_1 = \frac{a_0}{p}\left(1+\sqrt{s(s+1)}\right)$ (Eq. (7.73)). From Eq. (I.134), the calculated ionization energy of the hydride ion is $0.75418\ eV$, and the experimental value given by Lykke [71] is $6082.99 \pm 0.15\ cm^{-1}$ (0.75418 eV).

Upfield-shifted NMR peaks are direct evidence of the existence of lower-energy state hydrogen with a reduced radius relative to ordinary hydride ion and having an increase in diamagnetic shielding of the proton. The shift is given by the sum of the contributions of the diamagnetism of the two electrons and the trapped photon field of magnitude $p$ (Eq. (7.87)):

$$\frac{\Delta B_T}{B} = -\mu_0\frac{pe^2}{12m_e a_0\left(1+\sqrt{s(s+1)}\right)}\left(1+p\alpha^2\right) = -\left(p29.9 + p^2 1.59\ X\ 10^{-3}\right)ppm \tag{I.135}$$

where the first term applies to $H^-$ with $p = 1$ and $p = \text{integer} > 1$ for $H^-(1/p)$ and $\alpha$ is the fine structure constant.

$H(1/p)$ may react with a proton and two $H(1/p)$ may react to form $H_2(1/p)^+$ and $H_2(1/p)$, respectively. The hydrogen molecular ion and molecular charge and current density functions, bond distances, and energies were solved in the Nature of the Chemical Bond of Hydrogen-Type Molecules and Molecular Ions section from the Laplacian in ellipsoidal coordinates with the constraint of nonradiation.

$$(\eta-\zeta)R_\xi\frac{\partial}{\partial\xi}(R_\xi\frac{\partial\phi}{\partial\xi}) + (\zeta-\xi)R_\eta\frac{\partial}{\partial\eta}(R_\eta\frac{\partial\phi}{\partial\eta}) + (\xi-\eta)R_\zeta\frac{\partial}{\partial\zeta}(R_\zeta\frac{\partial\phi}{\partial\zeta}) = 0 \tag{I.136}$$

The total energy $E_T$ of the hydrogen molecular ion having a central field of $+pe$ at each focus of the prolate spheroid molecular orbital is (Eqs. (11.192-11.193))

$$E_T = -p^2\left\{\begin{array}{l}\frac{e^2}{8\pi\varepsilon_o a_H}(4\ln 3 - 1 - 2\ln 3)\left[1+\sqrt{\frac{2\hbar\sqrt{\frac{2e^2}{4\pi\varepsilon_o(2a_H)^3}}}{m_e c^2}}\right] \\ -\frac{1}{2}\hbar\sqrt{\frac{\frac{pe^2}{4\pi\varepsilon_o\left(\frac{2a_H}{p}\right)^3} - \frac{pe^2}{8\pi\varepsilon_o\left(\frac{3a_H}{p}\right)^3}}{\mu}}\end{array}\right\} = -p^2 16.2526\ eV \tag{I.137}$$

where $p$ is an integer, $c$ is the speed of light in vacuum, and $\mu$ is the reduced nuclear mass. The total energy of the hydrogen molecule having a central field of $+pe$ at each focus of the prolate spheroid molecular orbital is (Eqs. (11.240-11.241)).

$$E_T = -p^2 \left\{ \begin{array}{l} \frac{e^2}{8\pi\varepsilon_o a_0}\left[\left(2\sqrt{2}-\sqrt{2}+\frac{\sqrt{2}}{2}\right)\ln\frac{\sqrt{2}+1}{\sqrt{2}-1}-\sqrt{2}\right]\left[1+\sqrt{\frac{2\hbar\sqrt{\frac{e^2}{4\pi\varepsilon_o a_0^3 m_e}}}{m_e c^2}}\right] \\ -\frac{1}{2}\hbar\sqrt{\frac{\frac{pe^2}{8\pi\varepsilon_o\left(\frac{a_0}{p}\right)^3}-\frac{pe^2}{8\pi\varepsilon_o\left(\frac{\left(1+\frac{1}{\sqrt{2}}\right)a_0}{p}\right)^3}}{\mu}} \end{array} \right\} \quad \text{(I.138)}$$

$$= -p^2 31.677\ eV$$

The bond dissociation energy, $E_D$, of the hydrogen molecule $H_2(1/p)$ is the difference between the total energy of the corresponding hydrogen atoms and $E_T$

$$E_D = E(2H(1/p)) - E_T \quad \text{(I.139)}$$

where [72]

$$E(2H(1/p)) = -p^2 27.20\ eV \quad \text{(I.140)}$$

$E_D$ is given by Eqs. (I.139-I.140) and (I.138):

$$\begin{aligned} E_D &= -p^2 27.20\ eV - E_T \\ &= -p^2 27.20\ eV - \left(-p^2 31.677\ eV\right) \\ &= p^2 4.478\ eV \end{aligned} \quad \text{(I.141)}$$

The NMR of catalysis-product gas provides a definitive test of the theoretically predicted chemical shift of $H_2(1/p)$. In general, the $^1H$ NMR resonance of $H_2(1/p)$ is predicted to be upfield from that of $H_2$ due to the fractional radius in elliptic coordinates wherein the electrons are significantly closer to the nuclei. The predicted shift, $\frac{\Delta B_T}{B}$, for $H_2(1/p)$ is given by the sum of the contributions of the diamagnetism of the two electrons and the trapped photon field of magnitude $p$ (Eqs. (11.415-11.416)).

$$\frac{\Delta B_T}{B} = -\mu_0\left(4-\sqrt{2}\ln\frac{\sqrt{2}+1}{\sqrt{2}-1}\right)\frac{pe^2}{36a_0 m_e}\left(1+p\alpha^2\right) \quad \text{(I.142)}$$

$$\frac{\Delta B_T}{B} = -\left(p28.01 + p^2 1.49\ X\ 10^{-3}\right) ppm \quad \text{(I.143)}$$

where the first term applies to $H_2$ with $p=1$ and $p=\text{integer}>1$ for $H_2(1/p)$. The experimental absolute $H_2$ gas-phase resonance shift of -28.0 ppm [73-76] is in excellent agreement with the predicted absolute gas-phase shift of -28.01 ppm (Eq. (I.143)).

The vibrational energies, $E_{vib}$, for the $\upsilon=0$ to $\upsilon=1$ transition of hydrogen-type molecules $H_2(1/p)$ are (Eq. (11.223))

$$E_{vib} = p^2 0.515902\ eV \quad \text{(I.144)}$$

where $p$ is an integer and the experimental vibrational energy for the $\upsilon=0$ to $\upsilon=1$ transition of $H_2$, $E_{H_2(\upsilon=0\to\upsilon=1)}$, is given by Beutler [77] and Herzberg [78].

The rotational energies, $E_{rot}$, for the $J$ to $J+1$ transition of hydrogen-type molecules $H_2(1/p)$ are (Eq. (12.74)).

$$E_{rot} = E_{J+1} - E_J = \frac{\hbar^2}{I}\left[J+1\right] = p^2\left(J+1\right)0.01509\ eV \quad \text{(I.145)}$$

where $p$ is an integer, $I$ is the moment of inertia, and the experimental rotational energy for the $J=0$ to $J=1$ transition of $H_2$ is given by Atkins [79]. Ro-vibrational emission of $H_2(1/4)$ was observed on e-beam excited molecules in gases and trapped in solid matrix [31, 35] and by Raman spectroscopy [23, 31-35].

The $p^2$ dependence of the rotational energies results from an inverse $p$ dependence of the internuclear distance and the corresponding impact on the moment of inertia $I$. The predicted internuclear distance $2c'$ for $H_2(1/p)$ is:

$$2c' = \frac{a_o\sqrt{2}}{p} \tag{I.146}$$

The calculated and experimental parameters of $H_2$, $D_2$, $H_2^+$, and $D_2^+$ from the Chemical Bond of Hydrogen-Type Molecules section are given in Table I.2.

**Table I.2.** The Maxwellian closed form calculated and experimental parameters of $H_2$, $D_2$, $H_2^+$ and $D_2^+$.

| Parameter | Calculated | Experimental | Eqs. | Ref. for Exp. |
|---|---|---|---|---|
| $H_2$ Bond Energy | 4.478 $eV$ | 4.478 $eV$ | 11.300 | 24 |
| $D_2$ Bond Energy | 4.556 $eV$ | 4.556 $eV$ | 11.302 | 24 |
| $H_2^+$ Bond Energy | 2.654 $eV$ | 2.651 $eV$ | 11.269 | 24 |
| $D_2^+$ Bond Energy | 2.696 $eV$ | 2.691 $eV$ | 11.271 | 25 |
| $H_2$ Total Energy | 31.677 $eV$ | 31.675 $eV$ | 11.296 | 24, 30, 19[a] |
| $D_2$ Total Energy | 31.760 $eV$ | 31.760 $eV$ | 11.297 | 20, 25[b] |
| $H_2$ Ionization Energy | 15.425 $eV$ | 15.426 $eV$ | 11.298 | 30 |
| $D_2$ Ionization Energy | 15.463 $eV$ | 15.466 $eV$ | 11.299 | 25 |
| $H_2^+$ Ionization Energy | 16.253 $eV$ | 16.250 $eV$ | 11.267 | 24, 19[c] |
| $D_2^+$ Ionization Energy | 16.299 $eV$ | 16.294 $eV$ | 11.268 | 20, 25[d] |
| $H_2^+$ Spin Magnetic Moment | $0.5\mu_B$ | $0.5\mu_B$ | 12.24 | 31 |
| Absolute $H_2$ Gas-Phase NMR Shift | -28.0 ppm | -28.0 ppm | 11.416 | 32-33 |
| $H_2$ Quadrupole Moment | 0.4764 X $10^{-16}$ $cm^2$ | 0.38 0.15 X $10^{-16}$ $cm^2$ | 11.430-11.431 | 46 |
| $H_2$ Internuclear Distance | 0.7411 Å | 0.741 Å | 12.75 | 34 |
| $D_2$ Internuclear Distance | 0.7411 Å | 0.741 Å | 12.75 | 34 |
| $H_2^+$ Internuclear Distance | 1.0577 Å | 1.06 Å | 12.81 | 24 |
| $D_2^+$ Internuclear Distance | 1.0577 Å | 1.0559 Å | 12.81 | 25 |
| $H_2$ Vibrational Energy | 0.517 $eV$ | 0.516 $eV$ | 11.308 | 27, 28 |
| $D_2$ Vibrational Energy | 0.371 $eV$ | 0.371 $eV$ | 11.313 | 14, 20 |
| $H_2$ $\omega_e x_e$ | 120.4 $cm^{-1}$ | 121.33 $cm^{-1}$ | 11.310 | 25 |
| $D_2$ $\omega_e x_e$ | 60.93 $cm^{-1}$ | 61.82 $cm^{-1}$ | 11.314 | 20 |
| $H_2^+$ Vibrational Energy | 0.270 $eV$ | 0.271 $eV$ | 11.277 | 14, 20 |
| $D_2^+$ Vibrational Energy | 0.193 $eV$ | 0.196 $eV$ | 11.281 | 20 |
| $H_2$ J=1 to J=0 Rotational Energy | 0.01511 $eV$ | 0.01509 $eV$ | 12.77 | 24 |
| $D_2$ J=1 to J=0 Rotational Energy | 0.007557 $eV$ | 0.00755 $eV$ | 12.78 | 24 |
| $H_2^+$ J=1 to J=0 Rotational Energy | 0.00742 $eV$ | 0.00739 $eV$ | 12.83 | 24 |
| $D_2^+$ J=1 to J=0 Rotational Energy | 0.0037095 $eV$ | 0.003723 $eV$ | 12.84 | 25 |

## CATALYSTS

$He^+$, $Ar^+$, $Sr^+$, $Li$, $K$, $NaH$, and $H_2O$ are predicted to serve as catalysts since they meet the catalyst criterion—a chemical or physical process with an enthalpy change equal to an integer multiple of the potential energy of atomic hydrogen, $27.2\ eV$, or have a potential energy of $m \cdot 27.2\ eV$. Specifically, an exemplary catalytic system is provided by the ionization of $t$ electrons from an atom each to a continuum energy level such that the sum of the ionization energies of the $t$ electrons is approximately $m \cdot 27.2\ eV$ where $m$ is an integer. One such catalytic system involves lithium atoms. The first and second ionization energies of lithium are $5.39172\ eV$ and $75.64018\ eV$, respectively [72]. The double ionization ($t = 2$) reaction of $Li$ to $Li^{2+}$ then, has a net enthalpy of reaction of $81.0319\ eV$, which is equivalent to $3 \cdot 27.2\ eV$.

$$81.0319\ eV + Li(m) + H\left[\frac{a_H}{p}\right] \rightarrow Li^{2+} + 2e^- + H\left[\frac{a_H}{(p+3)}\right] + [(p+3)^2 - p^2] \cdot 13.6\ eV \tag{I.147}$$

$$Li^{2+} + 2e^- \rightarrow Li(m) + 81.0319\ eV \tag{I.148}$$

And, the overall reaction is:

$$H\left[\frac{a_H}{p}\right] \rightarrow H\left[\frac{a_H}{(p+3)}\right] + [(p+3)^2 - p^2] \cdot 13.6\ eV \tag{I.149}$$

where $m = 3$ in Eq. (I.128). The energy given off during catalysis is much greater than the energy lost to the catalyst. The energy released is large compared to conventional chemical reactions. For example, when hydrogen and oxygen gases undergo combustion to form water ($H_2\ (g) + \frac{1}{2} O_2\ (g) \rightarrow H_2O\ (l)$) the known enthalpy of formation of water is $\Delta H_f = -286\ kJ / mole$ or $1.48$ eV per hydrogen atom. By contrast, each ($n = 1$) ordinary hydrogen atom undergoing a catalysis step to $n = \frac{1}{2}$ releases a net of $40.8\ eV$. Moreover, further catalytic transitions may occur: $n = \frac{1}{2} \rightarrow \frac{1}{3}$, $\frac{1}{3} \rightarrow \frac{1}{4}$, $\frac{1}{4} \rightarrow \frac{1}{5}$, and so on. Once catalysis begins, hydrinos autocatalyze further in a process called disproportionation discussed in the Disproportionation of Energy States section.

Certain molecules may also serve to affect transitions of H to form hydrinos. In general, a compound comprising hydrogen such as $MH$, where M is an element other than hydrogen, serves as a source of hydrogen and a source of catalyst. A catalytic reaction is provided by the breakage of the $M-H$ bond plus the ionization of $t$ electrons from the atom $M$ each to a continuum energy level such that the sum of the bond energy and ionization energies of the $t$ electrons is approximately $m \cdot 27.2\ eV$, where $m$ is an integer. One such catalytic system involves sodium hydride. The bond energy of $NaH$ is $1.9245\ eV$ [80], and the first and second ionization energies of $Na$ are $5.13908\ eV$ and $47.2864\ eV$, respectively [72]. Based on these energies $NaH$ molecule can serve as a catalyst and $H$ source, since the bond energy of $NaH$ plus the double ionization ($t = 2$) of $Na$ to $Na^{2+}$ is $54.35\ eV$ ($2 \cdot 27.2\ eV$). The concerted catalyst reactions are given by

$$54.35\ eV + NaH \rightarrow Na^{2+} + 2e^- + H\left[\frac{a_H}{3}\right] + [3^2 - 1^2] \cdot 13.6\ eV \tag{I.150}$$

$$Na^{2+} + 2e^- + H \rightarrow NaH + 54.35\ eV \tag{I.151}$$

And, the overall reaction is:

$$H \rightarrow H\left[\frac{a_H}{3}\right] + [3^2 - 1^2] \cdot 13.6\ eV \tag{I.152}$$

With $m = 2$, the product of catalyst NaH is $H(1/3)$ that may further rapidly react to form $H(1/4)$, then molecular hydrino, $H_2(1/4)$. Specifically, in the case of a high hydrogen atom concentration, the further transition given by Eq. (I.133) of $H(1/3)$ ($p = 3$) to $H(1/4)$ ($p + m = 4$) with $H$ as the catalyst ($p' = 1$; $m = 1$) can be fast:

$$H(1/3) \xrightarrow{H} H(1/4) + 95.2\ eV \tag{I.153}$$

A molecule that accepts $m \cdot 27.2\ eV$ from atomic H with a decrease in the magnitude of the potential energy of the molecule by the same energy may serve as a catalyst. For example, the potential energy of $H_2O$ given by Eq. (13.201) is

$$V_e = \left(\frac{3}{2}\right) \frac{-2e^2}{8\pi\varepsilon_0 \sqrt{a^2 - b^2}} \ln \frac{a + \sqrt{a^2 - b^2}}{a - \sqrt{a^2 - b^2}} = -81.8715\ eV \tag{I.154}$$

The catalysis reaction $(m = 3)$ is:

$$81.6\ eV + H_2O + H\left[a_H\right] \rightarrow 2H^+ + O^+ + 3e^- + H*\left[\frac{a_H}{4}\right] + 81.6\ eV \quad \text{(I.155)}$$

$$H*\left[\frac{a_H}{4}\right] \rightarrow H\left[\frac{a_H}{4}\right] + 122.4\ eV \quad \text{(I.156)}$$

$$2H^+ + O^+ + 3e^- \rightarrow H_2O + 81.6\ eV \quad \text{(I.157)}$$

And, the overall reaction is:

$$H\left[a_H\right] \rightarrow H\left[\frac{a_H}{4}\right] + 81.6\ eV + 122.4\ eV \quad \text{(I.158)}$$

wherein $H*\left[\frac{a_H}{4}\right]$ has the radius of the hydrogen atom and a central field equivalent to 4 times that of a proton and $H\left[\frac{a_H}{4}\right]$ is the corresponding stable state with the radius of 1/4 that of H.

Hydrogen and hydrinos may serves as catalysts. As given in the Disproportionation of Energy States section hydrogen atoms $H\left(1/p\right)$ $p = 1, 2, 3, ...137$ can undergo transitions to lower-energy states given by Eqs. (I.124) and (I.126) wherein the transition of one atom is catalyzed by a second that resonantly and nonradiatively accepts $m \cdot 27.2\ eV$ with a concomitant opposite change in its potential energy. The overall general equation for the transition of $H\left(1/p\right)$ to $H\left(1/\left(m+p\right)\right)$ induced by a resonance transfer of $m \cdot 27.2\ eV$ to $H\left(1/p'\right)$ is represented by Eq. (I.133). Thus, hydrogen atoms may serve as a catalyst wherein $m = 1$, $m = 2$, and $m = 3$ for one, two, and three atoms, respectively, acting as a catalyst for another. The rate for the two- or three-atom-catalyst case would be appreciable only when the $H$ density is high. But, high H densities are not uncommon. A high hydrogen atom concentration permissive of 2H or 3H serving as the energy acceptor for a third or fourth may be achieved under several circumstances such as on the surface of the Sun and stars due to the temperature and gravity driven density, on metal surfaces that support multiple monolayers, and in highly dissociated plasmas, especially pinch hydrogen plasmas. Additionally, a three-body H interaction is easily achieved when two $H$ atoms arise with the collision of a hot $H$ with $H_2$. This event can commonly occur in plasmas having a large population of extraordinarily fast H as reported previously [36-42]. This is evidenced by the unusual intensity of atomic H emission. In such cases, energy transfer can occur from a hydrogen atom to two others within sufficient proximity, being typically a few angstroms as given in the Dipole-Dipole Coupling section. Then, the reaction between three hydrogen atoms whereby two atoms resonantly and nonradiatively accept $54.4\ eV$ from the third hydrogen atom such that $2H$ serves as the catalyst is given by:

$$54.4\ eV + 2H + H \rightarrow 2H^+_{fast} + 2e^- + H*\left[\frac{a_H}{3}\right] + 54.4\ eV \quad \text{(I.159)}$$

$$H*\left[\frac{a_H}{3}\right] \rightarrow H\left[\frac{a_H}{3}\right] + 54.4\ eV \quad \text{(I.160)}$$

$$2H^+_{fast} + 2e^- \rightarrow 2H + 54.4\ eV \quad \text{(I.161)}$$

And, the overall reaction is:

$$H \rightarrow H\left[\frac{a_H}{3}\right] + \left[3^2 - 1^2\right] \cdot 13.6\ eV \quad \text{(I.162)}$$

Characteristic continuum emission starting at 22.8 nm ($54.4\ eV$) and continuing to longer wavelengths was observed as predicted for this transition reaction as the energetic hydrino intermediate $H*\left[\frac{a_H}{3}\right]$ decays [23-29, 31]. Alternatively, fast H is producted by the mechanism of Eq. (I.161) or a resonant kinetic energy transfer to form fast $H$ may occur consistent with the observation of extraordinary Balmer $\alpha$ line broadening corresponding to high-kinetic energy H [31, 36-42].

In another $H$-atom catalyst reaction involving a direct transition to $\left[\frac{a_H}{4}\right]$ state, two hot $H_2$ molecules collide and dissociate such that three $H$ atoms serve as a catalyst of $3 \cdot 27.2\ eV$ for the fourth. Then, the reaction between four hydrogen atoms whereby three atoms resonantly and nonradiatively accept $81.6\ eV$ from the fourth hydrogen atom such that $3H$ serves as the catalyst is given by:

$$81.6\ eV + 3H + H \rightarrow 3H^+_{fast} + 3e^- + H*\left[\frac{a_H}{4}\right] + 81.6\ eV \quad \text{(I.163)}$$

$$H*\left[\frac{a_H}{4}\right]\rightarrow H\left[\frac{a_H}{4}\right]+122.4\ eV \tag{I.164}$$

$$3H^+_{fast}+3e^-\rightarrow 3H+81.6\ eV \tag{I.165}$$

And, the overall reaction is:

$$H\rightarrow H\left[\frac{a_H}{4}\right]+[4^2-1^2]\cdot 13.6\ eV \tag{I.166}$$

The extreme-ultraviolet continuum radiation band due to the $H*\left[\frac{a_H}{4}\right]$ intermediate of Eq. (I.163) is predicted to have short wavelength cutoff at $122.4\ eV$ (10.1 nm) and extend to longer wavelengths. This continuum band was confirmed experimentally [23-29, 31]. In general, the transition of $H$ to $H\left[\frac{a_H}{p=m+1}\right]$ due by the acceptance of $m\cdot 27.2\ eV$ gives a continuum band with a short wavelength cutoff and energy $E_{\left(H\rightarrow H\left[\frac{a_H}{p=m+1}\right]\right)}$ given by:

$$E_{\left(H\rightarrow H\left[\frac{a_H}{p=m+1}\right]\right)}=m^2\cdot 13.6\ eV \tag{I.167}$$

$$\lambda_{\left(H\rightarrow H\left[\frac{a_H}{p=m+1}\right]\right)}=\frac{91.2}{m^2}\ nm \tag{I.168}$$

and extending to longer wavelengths than the corresponding cutoff. Considering the 91.2 nm continuum shown in Figures 17 and 31 of Ref. [81] and the results shown in Figures 3-8 of Ref. [26], hydrogen may emit the series of 10.1 nm, 22.8 nm, and 91.2 nm continua.

# OUTLINE OF THE RESULTS OF THE UNIFIED THEORY DERIVED FROM FIRST PRINCIPLES

To overcome the limitations of quantum mechanics (QM), physical laws that are exact on all scales are sought. Rather than engendering the electron with a wave nature, as suggested by the Davisson-Germer experiment and fabricating a set of associated postulates and mathematical rules for wave operators, a new theory is derived from first principles.

## FOUNDATIONS

- Start with first principles
  - Conservation of mass-energy
  - Conservation of linear and angular momentum
  - Maxwell's Equations
  - Newton's Laws
  - Lorentz transforms of Special Relativity

- Highly predictive– application of Maxwell's equations precisely predicts hundreds of fundamental spectral observations in exact equations with no adjustable parameters (fundamental constants only).

- In addition to first principles, the only assumptions needed to predict the Universe over 85 orders of magnitude of scale (Quarks to Cosmos):
  - Four-dimensional spacetime
  - The fundamental constants that comprise the fine structure constant
  - Fundamental particles including the photon have $\hbar$ of angular momentum
  - The Newtonian gravitational constant G
  - The spin of the electron neutrino

Classical Physics (CP) now comprises the unified Maxwell's Equations, Newton's Laws, and General and Special Relativity. The closed form calculations of a broad spectrum of fundamental phenomena containing fundamental constants only are given in subsequent sections. CP gives closed form solutions for the atom that give four quantum numbers, the Rydberg constant, the stability of the $n=1$ state and the instability of the excited states, relativistic invariance of the wave equation, the equations of the photon and electron in excited states, the equations of the free electron, and photon which predict the wave particle duality behavior of particles and light. The current and charge-density functions of the electron may be directly physically interpreted. For example, spin angular momentum results from the motion of negatively charged mass moving systematically, and the equation for angular momentum, $\mathbf{r}\times\mathbf{p}=\hbar$, can be applied directly to the wave function (a current-density

function) that describes the electron. The following observables are derived in closed-form equations based on Maxwell's equations: the magnetic moment of a Bohr magneton, Stern Gerlach experiment, electron and muon g factors, fine structure splitting, Lamb shift, hyperfine structure, muonium hyperfine structure interval, resonant line width and shape, selection rules, correspondence principle, wave particle duality, excited states, reduced mass, rotational energies and momenta, spin-orbit coupling, Knight shift and spin-nuclear coupling, closed form solutions for multielectron atoms, excited states of the helium atom, elastic electron scattering from helium atoms, proton scattering from atomic hydrogen, the nature of the chemical bond, bond energies, vibrational energies, rotational energies, and bond distances of hydrogen-type molecules and molecular ions, the solutions for all major functional groups that give the exact solutions of an infinite number of molecules, solutions to the bonding in the major classes of materials, Davisson Germer experiment, Aspect experiment, Durr experiment on the Heisenberg Uncertainty Principle, Penning trap experiments on single ions, hyperfine structure interval of positronium, magnetic moments of the nucleons, beta decay energy of the neutron, the binding energy of deuterium, and alpha decay. The theory of collective phenomena including statistical mechanics, superconductivity and Josephson junction experiments, integral and fractional quantum Hall effects, and the Aharonov-Bohm effect, is given. The calculations agree with experimental observations.

From the closed form solution of the helium atom, the predicted electron scattering intensity is derived. The closed form scattering equation matches the experimental data; whereas, calculations based on the Born model of the atom utterly fail at small scattering angles. The implications for the invalidity of the Schrödinger and Born models of the atom and the dependent Heisenberg Uncertainty Principle are discussed.

For any kind of wave advancing with limiting velocity and capable of transmitting signals, the equation of front propagation is the same as the equation for the front of a light wave. By applying this condition to electromagnetic and gravitational fields at particle production, the Schwarzschild metric (SM) is derived from the classical wave equation, which modifies general relativity to include conservation of spacetime, in addition to momentum and matter/energy and identifies absolute space. The result gives a natural relationship between Maxwell's equations, special relativity, and general relativity. It gives gravitation from the atom to the cosmos. The gravitational equations with the equivalence of the particle production energies permit the equivalence of mass-energy and the spacetime that determine the nature of absolute space wherein a *"clock" is defined that measures "clicks" on an observable in one aspect, and in another, it is the ruler of spacetime of the universe with the implicit dependence of spacetime on matter-energy conversion*. The masses of the leptons, the quarks, and nucleons are derived from this metric of spacetime that gives the equivalence of the gravitational and inertial masses. The universe is time harmonically oscillatory in matter, energy, and spacetime expansion and contraction with a minimum radius that is the gravitational radius. In closed form equations with fundamental constants only, CP gives the basis of the atomic, thermodynamic, and cosmological arrows of time, the deflection of light by stars, the precession of the perihelion of Mercury, the Hubble constant, the age of the universe, the observed acceleration of the expansion, the power of the universe, the power spectrum of the universe, the microwave background temperature, the primary uniformity of the microwave background radiation, the polarization and microkelvin temperature spatial variation of the microwave background radiation, the observed violation of the GZK cutoff, the mass density of the universe, the large scale structure of the universe, and the identity of dark matter which matches the criteria for the structure of galaxies and emission from interstellar medium and the Sun which have been observed in the laboratory [23-29, 31]. In a special case wherein the gravitational potential energy density of a blackhole equals that of the Planck mass, matter converts to energy and spacetime expands with the release of a gamma ray burst. The singularity in the SM is eliminated. The basis of the antigravitational force is presented with supporting experimental evidence.

In addition to the above known phenomena and characteristics of fundamental particles and forces, the theory predicts the existence of a previously unknown form of matter—hydrogen atoms and molecules having electrons of lower energy than the conventional "ground" state called ***hydrinos*** and ***molecular hydrinos***, respectively, where each energy level corresponds to a fractional quantum number. The existence of hydrinos has been confirmed experimentally proving GUT-CP, and this identity additionally resolves many celestial mysteries [23-29, 31]. It provides resolution to many otherwise inexplicable celestial observations with (a) the identity of dark matter being hydrinos, (b) the hydrino-transition radiation being the radiation source heating the warm-hot interstellar medium (WHIM) and behind the observation that diffuse H$\alpha$ emission is ubiquitous throughout the Galaxy requiring widespread sources of flux shortward of 912 $\mathring{A}$, and (c) the energy and radiation from the hydrino transitions being the source of extraordinary temperatures and power regarding the solar corona problem, the cause of sunspots and other solar activity, and why the Sun emits X-rays [23-29, 31].

## PHYSICAL CONCEPTS THAT ARISE FROM CP DERIVATIONS ON THE SCALE RANGE OF 85 ORDERS OF MAGNITUDE

Starting from the simple observation that the bound electron of the hydrogen atom is experimentally observed to be stable to radiation, the classical electromagnetic wave equation is used to solve the electron source current by matching it to emitted electromagnetic waves with the constraint that a bound electron in the $n=1$ state cannot radiate energy. The solution is based on Maxwell's equations and other experimentally confirmed physical laws. The resulting CP gives predictions that are unprecedented in success, achieving highly accurate agreement with observations over 85 orders of magnitude from the scale of fundamental particles to that of the cosmos. A summary of some of the salient features of the theory derived in subsequent sections follows:

- Bound electrons are described by a charge-density (mass-density) function which is the product of a radial delta function ( $f(r)=\delta(r-r_n)$ ), angular functions, and a time function. The latter comprise a constant angular function, a time and spherically harmonic function, and linear combinations of these functions. Thus, a bound electron is a constant two-dimensional spherical surface of charge (zero thickness and total charge of $-e$ ), called an electron atomic orbital that can exist in a bound state at only specified distances from the nucleus determined by the force balance between the electric fields of the electron and proton plus any resonantly absorbed photons.

- The uniform current density function $Y_0^0(\theta,\phi)$ (Eqs. (I.63-I.65)) that gives rise to the spin of the electron is generated from two current-vector fields (CVFs). Each CVF comprises a continuum of correlated *orthogonal great circle current-density elements (one dimensional "current loops")*. The current pattern comprising each CVF is generated over a half-sphere surface by a set of rotations of two orthogonal great circle current loops that serve as basis elements about each of the $\left(-\mathbf{i}_x,\mathbf{i}_y,0\mathbf{i}_z\right)$ and $\left(-\frac{1}{\sqrt{2}}\mathbf{i}_x,\frac{1}{\sqrt{2}}\mathbf{i}_y,\mathbf{i}_z\right)$-axis; the span being $\pi$ radians. Then, the two CVFs are convoluted, and the result is normalized to exactly generate the *continuous* uniform electron current density function $Y_0^0(\theta,\phi)$ covering a spherical shell and having the three angular momentum components of $\mathbf{L}_{xy}=+/-\frac{\hbar}{4}$ and $\mathbf{L}_z=\frac{\hbar}{2}$.

- Then, the total function that describes the spinning motion of each electron atomic orbital is composed of two functions. One function, the spin function, is spatially uniform over the atomic orbital, where each point moves on the surface with the same quantized angular and linear velocity, and gives rise to spin angular momentum. The other function, the modulation function, can be spatially uniform—in which case there is no orbital angular momentum and the magnetic moment of the electron atomic orbital is one Bohr magneton—or not spatially uniform—in which case there is orbital angular momentum. The modulation function moves harmonically on the surface as a charge-density wave with a quantized angular velocity about a specific (by convention) z-axis. Numerical values for the angular velocity, radii of allowed atomic orbitals, energies, and associated quantities are calculated.

- Atomic orbital radii are calculated by setting the centripetal force equal to the electric and magnetic forces.

- The atomic orbital is a resonator cavity which traps photons of discrete frequencies. The radius of an atomic orbital increases with the absorption of electromagnetic energy. The solutions to Maxwell's equations for modes that can be excited in the atomic orbital resonator cavity give rise to four quantum numbers, and the energies of the modes are the experimentally known hydrogen spectrum. The spectrum of helium is the solution of Maxwell's equations for the energies of modes of this resonator cavity with a contribution from electron-electron spin and orbital interactions.

- Excited states are unstable because the charge-density function of the electron plus photon have a radial doublet function component which corresponds to an electric dipole. The doublet possesses spacetime Fourier components synchronous with waves traveling at the speed of light; thus it is radiative. The charge-density function of the electron plus photon for the $n=1$ principal quantum state of the hydrogen atom as well as for each of the $n=\frac{1}{\text{integer}}$ states mathematically is purely a radial delta function. The delta function does not possess spacetime Fourier components synchronous with waves traveling at the speed of light; thus, each is nonradiative.

- The spectroscopic line-width arises from the classical rise-time band-width relationship, and the Lamb Shift is due to conservation of energy and linear momentum and arises from the radiation reaction force between the electron and the photon.

- The photon is an atomic orbital with electric and magnetic field lines along orthogonal great circles.

- Upon ionization, the atomic orbital radius goes to infinity and the electron becomes a plane wave (consistent with double-slit experiments) with the de Broglie wavelength, $\lambda=h/p$.

- The energy of atoms is stored in their electric and magnetic fields. Chemical bonding occurs when the total energy of

the participant atoms can be lowered with the formation of two-dimensional equipotential energy surfaces (molecular orbitals (MO)) where the current motion in the case of $H_2$ is along orbits, each comprising an elliptic plane cross section of a spheroidal MO through the foci, and a general form of the nonradiative boundary condition is met.

- Certain atoms and ions serve as catalysts to release energy from hydrogen to produce an increased binding energy hydrogen atom having a binding energy of $\frac{13.6\ eV}{\left(\frac{1}{p}\right)^2}$ where $p$ is an integer greater than 1, designated as $H\left[\frac{a_H}{p}\right]$ where $a_H$ is the radius of the hydrogen atom. Increased binding energy hydrogen atoms called hydrinos are predicted to form by reacting an ordinary hydrogen atom with a catalyst having a net enthalpy of reaction of about the potential energy of hydrogen in its first nonradiative state, $m \cdot 27.2\ eV$, where $m$ is an integer, or have a potential energy of $m \cdot 27.2\ eV$. This catalysis releases energy from the hydrogen atom with a commensurate decrease in size of the hydrogen atom, $r_n = na_H$. For example, the catalysis of $H(n=1)$ to $H(n=1/2)$ releases $40.8\ eV$, and the hydrogen radius decreases from $a_H$ to $\frac{1}{2}a_H$. One such atomic catalytic system involves H itself. The potential energy of H is $27.2\ eV$; thus, one or more $(m)$ H atoms may accept an integer $m$ times $27.2\ eV$ from another that undergoes a transition to a corresponding hydrino state $H\left(1/\left(m+1\right)\right)$. The process is hereafter referred to as the **BlackLight Process**.
- The existence of hydrinos as the product of the BlackLight Process—a new energy source—has been confirmed experimentally.
- For any kind of wave advancing with limiting velocity and capable of transmitting signals, the equation of front propagation is the same as the equation for the front of a light wave. By applying the condition to electromagnetic and gravitational fields at particle production, the Schwarzschild metric (SM) is derived from the classical wave equation, which modifies general relativity to include conservation of spacetime, in addition to momentum and matter/energy. The result gives a natural relationship between Maxwell's equations, special relativity, and general relativity, and defines absolute space that rescues Newton's Second law, resolves the twin paradox, and preserves the energy inventory of the universe. It gives gravitation from the atom to the cosmos.
- The Schwarzschild metric gives the relationship whereby matter causes relativistic corrections to spacetime that determines the curvature of spacetime and is the origin of gravity. The correction is based on the boundary conditions that no signal can travel faster than the speed of light including the gravitational field that propagates following particle production from a photon wherein the particle has a finite gravitational velocity given by Newton's Law of Gravitation.
- The limiting velocity $c$ results in the contraction of spacetime due to particle production. The contraction is given by $2\pi r_g$ where $r_g$ is the gravitational radius of the particle. This has implications for the expansion of spacetime when matter converts to energy.
- The spacetime contraction during particle production is analogous to Lorentz length contraction and time dilation of an object in one inertial frame relative to another moving at constant relative velocity. In the former case, the corresponding correction is a function of the square of the ratio of the gravitational velocity to the speed of light. In the latter case, the corresponding correction is a function of the square of the ratio of the relative velocity of two inertial frames to the speed of light.
- Fundamental particle production occurs when the energy of the particle given by the Planck equation, Maxwell's Equations, and Special Relativity is equal to $mc^2$, and the proper time is equal to the coordinate time according to the Schwarzschild metric. The gravitational equations with the equivalence of the particle production energies permit the equivalence of mass-energy and the absolute spacetime wherein a *"clock" is defined which measures "clicks" on an observable in one aspect, and in another, it is the ruler of spacetime of the universe with the implicit dependence of spacetime on matter-energy conversion*. The masses of the leptons, the quarks, and nucleons are derived from this metric of spacetime.
- The gravitational equations with the equivalence of the particle production energies require the conservation relationship of mass-energy, $E = mc^2$, and spacetime, $\frac{c^3}{4\pi G} = 3.22\ X\ 10^{34}\ \frac{kg}{\sec}$. Spacetime expands as mass is released as energy which provides the basis of absolute space and the atomic, thermodynamic, and cosmological arrows of time. Entropy and the expansion of the universe are large scale consequences. The universe is closed independently of the total mass of the universe, and different regions of space are isothermal even though they are separated by greater

distances than that over which light could travel during the time of the expansion of the universe. The universe is oscillatory in matter/energy and spacetime with a finite minimum radius, the gravitational radius; thus, the gravitational force causes celestial structures to evolve on a time scale corresponding to the period of oscillation. The equation of the radius of the universe, $\aleph$, is $\aleph = \left( \frac{2Gm_U}{c^2} + \frac{cm_U}{\frac{c^3}{4\pi G}} \right) - \frac{cm_U}{\frac{c^3}{4\pi G}} \cos\left( \frac{2\pi t}{\frac{2\pi G m_U}{c^3}} \right)$ which predicts the observed acceleration of the expansion. The calculated Hubble constant is $H_0 = 78.5 \frac{km}{\sec \cdot Mpc}$. Presently, stars and large-scale structures exist that are older than the elapsed time of the present expansion, as stellar and celestial evolution occurred during the contraction phase. The maximum energy release of the universe that occurs at the beginning of the expansion phase is: $P_U = \frac{c^5}{4\pi G} = 2.88\ X\ 10^{51}\ W$.

- H is the "phoenix particle" of the universe. The recycling of matter and energy in the universe occurs in an oscillatory cycle wherein matter converts to energy primarily by hydrogen atom decay via a hydrino pathway, and energy to matter conversion occurs by hydrogen atom production during gamma ray bursts. The matter-energy cycle drives a dependent space-time expansion contraction cycle. The decaying dark matter signatures of power and 511 keV gamma, neutral pion, neutron capture, and ratio of muon to electron neutrino emission match those of hydrogen atom decay from the high-p-state hydrino inventory comprising the dark matter. The characteristics, composition, and high energetics of cosmic rays in the absence of neutrino emission overturn long-held theory but match the signatures of H atom production. The rates of production and annihilation of matter and energy match those required to the complete the cycle over the period of oscillation of the universe (1T years). Hydrogen atom decay also matches a broad range of laboratory experiments such as transmutation, and neutron and energetic particle emission. H(1/p) decay releases energy of magnitude 1000 times that of atomic and thermonuclear energy, equivalent to that of matter antimatter annihilation.

- The relationship between inertial and gravitational mass is based on the result that only fundamental particles having an equivalence of the inertial and gravitational masses at particle production are permitted to exist since only in these cases are Maxwell's equations and the conditions inherent in the Schwarzschild metric of spacetime satisfied simultaneously wherein space must be absolute. The equivalence is maintained for any velocity thereafter due to the absolute nature of space and the absolute speed of light. The invariant speed, $c$, is set by the permittivity and permeability of absolute space, which determines the relativity principle based on propagation of fields and signals as light-wave fronts.

- In addition to the propagation velocity, the intrinsic velocity of the particle and the geometry of this 2-dimensional velocity surface with respect to the limiting speed of light determine that the particle such as an electron may have gravitational mass different from its inertial mass. A constant velocity confined to a spherical surface corresponds to a positive gravitational mass equal to the inertial mass (e.g. particle production or a bound electron). A constant angular velocity function confined to a flat surface corresponds to a gravitational mass less than the inertial mass, which is zero in the limit of an absolutely unbound particle (e.g. absolutely free electron). A pseudoelectron formed in a massive gravitational field comprising a two-dimensional surface of constant negative curvature has a negative gravitational mass.

- Free electrons with a velocity in a vector direction will absorb microwave photons to be selectively accelerated in the vector direction of propagation. ½ of the energy of an absorbed photon given by $\hbar\omega$ wherein $\hbar$ is Planck's constant bar and $\omega$ is the photon angular frequency is conserved as increased electron kinetic energy and ½ is conserved as an increased rotational kinetic energy that manifests as the invariant electron angular momentum of $\hbar$ and corresponding Bohr magneton of magnetic moment at a reduced de Broglie wavelength. The classical theory regarding the nature of the photon and free electron that give rise to the reactionless force exploited as the mechanism a novel means of propulsion called "space drive".

- Superconductivity arises when electron plane waves extend throughout the lattice, and the lattice is a band-pass for the magnetic field of an array of magnetic dipoles; so, no energy is dissipated with current flow.

- The Quantum Hall Effect arises when the forces of crossed electric and magnetic fields balance, and the lattice is a band-pass for the magnetic field of an array of magnetic dipoles.

- The vector potential component of the electron's angular momentum gives rise to the Aharonov-Bohm Effect.

- Alpha decay occurs as a transmission of a plane wave through a potential barrier.

- The proton and neutron functions each comprise a linear combination of a constant function and three orthogonal

spherical harmonic functions resulting in three quark/gluon functions per nucleon. The nucleons are locally two-dimensional.

## SUMMARY OF FOUNDATIONS AND PHYSICAL PHENOMENA SOLVED BY CLASSICAL PHYSICS

The electron current-density functions are solved to match time-harmonic multipole source currents of time-varying electromagnetic fields during transitions with the constraint that a bound electron in the $n=1$ state cannot radiate energy. The mathematical formulation for zero radiation based on Maxwell's equations follows from a derivation by Haus [46]. The function that describes the motion of the electron corresponding to a potentially emitted photon must not possess spacetime Fourier components that are synchronous with waves traveling at the speed of light. Classical physics gives closed form solutions for the atom including the stability of the $n=1$ state and the instability of the excited states, relativistic invariance of the wave equation, the equations of the photon and electron in excited states, and the equations of the free electron and photon which also predict the wave-particle duality behavior of particles and light. The current and charge-density functions of the electron may be directly physically interpreted. For example, spin angular momentum results from the motion of negatively charged mass moving systematically, and the equation for angular momentum, $\mathbf{r}\times\mathbf{p}=\hbar$, can be applied directly to the wave function (a current-density function) that describes the electron. A partial listing of well-known and documented phenomena, which are derivable in closed form from classical physics, especially Maxwell's equations are given in Table I.3. The calculations agree with experimental observations.

**Table I.3.** Partial List of Physical Phenomena Solved by Classical Physics.

- Stability of the atom to radiation
- Magnetic moment of a Bohr magneton and relativistic invariance of each of $\frac{e}{m_e}$ of the electron, the electron angular momentum of $\hbar$, and the electron magnetic moment of $\mu_B$ from the spin angular momentum
- De Broglie relationship
- Stern Gerlach experiment
- Electron and muon g factors
- Rotational energies and momenta
- Reduced electron mass
- Ionization energies of multi-electron atoms
- Special relativistic effects
- Excited states
- Resonant line width and shape
- Selection rules
- State Lifetimes and line intensities
- Correspondence principle
- Orbital and spin splitting
- Stark effect
- Lamb Shift
- Knight shift
- Spin-orbit coupling (fine structure)
- Spin-nuclear coupling (hyperfine structure)
- Hyperfine structure interval of muonium
- Nature of the free electron
- Nature of the photon
- Photoelectric effect
- Compton effect
- Wave-particle duality
- Double-slit experiment for photons and electrons
- Davisson Germer experiment
- Elastic electron scattering from helium atoms
- Ionization energies of multielectron atoms
- Hydride ion binding energy and absolute NMR shift
- Hydride lattice parameters and energies
- Excited states of the helium atom with singlet and triplet vector diagrams
- Proton scattering from atomic hydrogen
- Nature of the chemical bond
- Bond energies, vibrational energies, rotational energies, bond distances, magnetic moment and fields of hydrogen-type molecules and molecular ions, absolute NMR shift of $H_2$
- Molecular Ion and Molecular Excited States
- Parameters of polyatomic molecules
- Superconductivity and Josephson junction experiments
- Integral and fractional quantum Hall effects
- Aharonov-Bohm effect
- Aspect experiment
- Durr experiment on the Heisenberg Uncertainty Principle
- Penning trap experiments on single ions
- Mobility of free electrons in superfluid helium
- Gravitational behavior of neutrons
- Hyperfine structure interval of positronium
- Structure of nucleons
- Magnetic moments of the nucleons
- Beta decay energy of the neutron
- Binding energy of deuterium
- Alpha decay
- Nature of neutrinos
- Proton radius puzzle

For the first time in history, the key building blocks of organic chemistry have been solved from two basic equations. Now, the true physical structure and parameters of an infinite number of organic molecules up to infinite length and complexity can be obtained to permit the engineering of new pharmaceuticals and materials at the molecular level. The solutions of the basic functional groups of organic chemistry were obtained by using generalized forms of a geometrical and an energy equation for the nature of the H-H bond. The geometrical parameters and total bond energies of about 800 exemplary organic molecules were calculated using the functional group composition [4]. The results obtained essentially instantaneously match the experimental values typically to the limit of measurement. The solved functional groups are given in Table I.4.

**Table I.4.** Partial List of Organic Functional Groups Solved by Classical Physics.

| | | |
|---|---|---|
| Continuous-Chain Alkanes | N,N-dialkyl Amides | Aniline |
| Branched Alkanes | Urea | Aryl Nitro Compounds |
| Alkenes | Carboxylic Acid Halides | Benzoic Acid Compounds |
| Branched Alkenes | Carboxylic Acid Anhydrides | Anisole |
| Alkynes | Nitriles | Pyrrole |
| Alkyl Fluorides | Thiols | Furan |
| Alkyl Chlorides | Sulfides | Thiophene |
| Alkyl Bromides | Disulfides | Imidizole |
| Alkyl Iodides | Sulfoxides | Pyridine |
| Alkenyl Halides | Sulfones | Pyrimidine |
| Aryl Halides | Sulfites | Pyrazine |
| Alcohols | Sulfates | Quinoline |
| Ethers | Nitroalkanes | Isoquinoline |
| Primary Amines | Alkyl Nitrates | Indole |
| Secondary Amines | Alkyl Nitrites | Adenine |
| Tertiary Amines | Conjugated Alkenes | Fullerene ($C_{60}$) |
| Aldehydes | Conjugated Polyenes | Graphite |
| Ketones | Aromatics | Phosphines |
| Carboxylic Acids | Naphthalene | Phosphine Oxides |
| Carboxylic Acid Esters | Toluene | Phosphites |
| Amides | Chlorobenzene | Phosphates |
| N-alkyl Amides | Phenol | |

The two basic equations, one for geometrical parameters and the other for energy parameters that solves organic molecules were applied to bulk forms of matter containing trillions of trillions of electrons. For example, using the same alkane- and alkene-bond solutions as elements in an infinite network, the nature of the solid molecular bond for all known allotropes of carbon (graphite, diamond, $C_{60}$, and their combinations) were solved. By further extension of this modular approach, the solid molecular bond of silicon and the nature of the semiconductor bond were solved. The nature of other fundamental forms of matter such as the nature of the ionic bond, the metallic bond, and additional major fields of chemistry such as that of silicon, organometallics, and boron were solved exactly such that the position and energy of each and every electron is precisely specified. These results agree with observations to the limit of measurement. The implication of these results is that it is possible using physical laws to solve the structure of all types of matter. Some of the solved forms of matter of infinite extent, as well as additional major fields of chemistry, are given in Table I.5.

**Table I.5.** Partial List of Additional Molecules and Compositions of Matter Solved by Classical Physics.

- Solid Molecular Bond of the Three Allotropes of Carbon
  - Diamond
  - Graphite
  - Fullerene ($C_{60}$)
- Dipole-Dipole Bonding
  - Hydrogen Bonding
  - Van der Waals Bonding
- Solid Ionic Bond of Alkali-Hydrides
  - Alkali-Hydride Crystal Structures
    - Lithium Hydride
    - Sodium Hydride
    - Potassium Hydride
    - Rubidium & Cesium Hydride
    - Potassium Hydrino Hydride
- Solid Metallic Bond of Alkali Metals
  - Alkali Metal Crystal Structures
    - Lithium Metal
    - Sodium Metal
    - Potassium Metal
    - Rubidium & Cesium Metals
- Alkyl Aluminum Hydrides
- Silicon Groups and Molecules
  - Silanes
  - Alkyl Silanes and Disilanes
- Solid Semiconductor Bond of Silicon
  - Insulator-Type Semiconductor Bond
  - Conductor-Type Semiconductor Bond
- Boron Molecules
  - Boranes
    - Bridging Bonds of Boranes
  - Alkoxy Boranes
- Alkyl Boranes
  - Alkyl Borinic Acids
  - Tertiary Aminoboranes
  - Quaternary Aminoboranes
  - Borane Amines
  - Halido Boranes
- Organometallic Molecular Functional Groups and Molecules
  - Alkyl Aluminum Hydrides
    - Bridging Bonds of Organoaluminum Hydrides
  - Organogermanium and Digermanium
  - Organolead
  - Organoarsenic
  - Organoantimony
  - Organobismuth
- Organic Ions
  - 1° Amino
  - 2° Amino
  - Carboxylate
  - Phosphate
  - Nitrate
  - Sulfate
  - Silicate
- Proteins
  - Amino Acids
  - Peptide Bonds
- DNA
  - Bases
  - 2-deoxyribose
  - Ribose
  - Phosphate Backbone
- Water
- Condensed Noble Gases

For any kind of wave advancing with limiting velocity and capable of transmitting signals, the equation of front propagation is the same as the equation for the front of a light wave. By applying this condition to electromagnetic and gravitational fields at particle production, the Schwarzschild metric (SM) is derived from the classical wave equation, which modifies general relativity to include conservation of spacetime in addition to momentum and mass-energy. The result gives a natural relationship between Maxwell's equations, special relativity, and general relativity and identifies absolute space to give the basis and the equivalence of the inertial and gravitational masses. It gives gravitation from the atom to the cosmos. The universe is time harmonically oscillatory in matter, energy, and spacetime expansion and contraction with a minimum radius that is the gravitational radius. A partial listing of the particle and cosmological phenomena derivable from classical physics in closed form equations with fundamental constants only is given in Table I.6.

**Table I.6.** Partial List of Particle and Cosmological Phenomena Solved by Classical Physics.

- Equivalence of the inertial and gravitational masses
- Newton's second law
- Deflection of light by stars
- Precession of the perihelion of Mercury
- Lepton masses
- Quark masses
- Boson masses
- Hubble constant
- Age of the universe
- Observed acceleration of the expansion
- Absence of antimatter
- Absence of a Big Bang origin of the Universe
- Identity of dark matter
- Identity of UV crisis/Cosmic EUV continuum emission
- Identity of the Diffuse Interstellar Bands (DIBs)
- Origin of hot interstellar medium
- Solar corona temperature problem
- Power of the universe
- Power spectrum of the universe
- Microwave background temperature
- Uniformity of the microwave background radiation
- Microkelvin spatial variation of the cosmic microwave background radiation (CMBR)
- Polarization of the CMBR data
- Observed violation of the GZK cutoff
- Mass density of the universe
- Web-like, large scale structure of the universe
- Source of 511 keV emission
- Source of $\pi^0$ decay emission
- Source of solar and interstellar neutrons, isotope shifts and transmutation
- Power source of flares
- Photoneutron production and neutron capture as the mechanism to form deuterium rather than p-p chain
- Solar photoneutron production as the source of 2/3 muon and 1/3 electron solar neutrinos to resolve the Solar Neutrino Paradox
- Mechanism of H decay to recycle H of the universe
- Gamma ray bursts as the source of proton and electron production to recycle H of the universe at the required rate
- Observed H decay and production rates match those required for the oscillatory cycle of matter-energy interconversion and corresponding spacetime expansion-contraction

Classical physics further gives the identity of dark matter, which matches the criteria for the structure of galaxies and spectral emission from interstellar medium and the Sun that have been observed in the laboratory [23-29, 31]. In a special case wherein the gravitational potential energy density of a blackhole equals that of the Planck mass, matter converts to energy and spacetime expands with the release of a gamma ray burst. The singularity in the SM is eliminated. The predictions of classical physics are unprecedented in that agreement with observations is achieved over 85 orders of magnitude from the scale of fundamental particles to that of the cosmos.

From the success at predicting the vast scope of known phenomena, it can be appreciated that CP is anticipated to predict new, previously unknown phenomena, as well as now solve previously unsolvable mysteries for which old theories were incapable. In this book, the structure of the bound electron is solved using classical laws and from there a unification theory is developed based on those laws called the Grand Unified Theory of Classical Physics (GUTCP) with results that match observations for the basic phenomena of physics and chemistry from the scale of the quarks to the cosmos. In addition to the observables on the hydrogen atom that are known, it further predicts that atomic hydrogen may undergo a catalytic reaction with certain atomized elements and ions which singly or multiply ionize at integer multiples of the potential energy of atomic hydrogen, $m \cdot 27.2\,eV$ wherein $m$ is an integer or have a potential energy of $m \cdot 27.2\,eV$. Recently, there has been the announcement of some unexpected astrophysical results that support the existence of hydrinos. In the 1995 Edition of the GUTCP, the prediction [45] that the expansion of the universe was accelerating was made from the same equations that correctly predicted the mass of the top quark before it was measured. To the astonishment of cosmologists, this was confirmed by 2000. Another prediction about the nature of dark matter based on GUTCP may be close to being confirmed. Based on recent evidence, Bournaud et al. [82-83] suggest that dark matter is hydrogen in dense molecular form that somehow behaves differently in terms of being unobservable except by its gravitational effects. Theoretical models predict that dwarfs formed from collisional debris of massive galaxies should be free of nonbaryonic dark matter. So, their gravity should tally with the stars and gas within them. By analyzing the observed gas kinematics of such recycled galaxies, Bournaud et al. [82-83] have measured the gravitational masses of a series of dwarf galaxies lying in a ring around a massive galaxy that has recently

experienced a collision. Contrary to the predictions of Cold-Dark-Matter (CDM) theories, their results demonstrate that they contain a massive dark component amounting to about twice the visible matter. This baryonic dark matter is argued to be cold molecular hydrogen, but it is distinguished from ordinary molecular hydrogen in that it is not traced at all by traditional methods, such as emission of CO lines. These results match the predictions of the dark matter being molecular hydrino. Additionally, astronomers Jee at al. [84] using data from NASA's Hubble Telescope have mapped the distribution of dark matter, galaxies, and hot gas in the core of the merging galaxy cluster Abell 520 formed from a violent collision of massive galaxy clusters and have determined that the dark matter had collected in a dark core containing far fewer galaxies than would be expected if dark matter was collisionless with dark matter and galaxies anchored together. The collisional debris left behind by the galaxies departing the impact zone behaved as hydrogen did, another indication that the identity of dark matter is molecular hydrino.

The best evidence yet for the existence of dark matter is its direct observation as a source of massive gravitational mass evidenced by gravitational lensing of background galaxies that does not emit or absorb light as shown in Figure I.6 [85]. Hydrogen transitions to hydrinos that comprise the dark matter can be observed celestially and in the laboratory. Characteristic EUV continua of hydrino transitions following radiationless energy transfer with cutoffs at $\lambda_{\left(H\to H\left[\frac{a_H}{p=m+1}\right]\right)}=\frac{91.2}{m^2}\ nm$ are observed from hydrogen plasmas in the laboratory that match significant celestial observations and further confirm hydrino as the identity of dark matter [23-29, 31]. Hydrinos have been isolated in the laboratory and confirmed by 23 analytical techniques [22-42]. Addition laboratory and astrophysical signatures of hydrino as the dark matter of the universe is given in the Dark Matter section.

The continua spectra directly and indirectly match significant celestial observations. Hydrogen self-catalysis and disproportionation may be reactions occurring ubiquitously in celestial objects and interstellar medium comprising atomic hydrogen. Stars are sources of atomic hydrogen and hydrinos as stellar wind for interstellar reactions wherein very dense stellar atomic hydrogen and singly ionized helium, $He^+$, serve as catalysts in stars. Hydrogen continua from transitions to form hydrinos matches the emission from white dwarfs, provides a possible mechanism of linking the temperature and density conditions of the different discrete layers of the coronal/chromospheric sources, and provides a source of the diffuse ubiquitous EUV cosmic background with a 10.1 nm continuum matching the observed intense 11.0-16.0 nm band in addition to resolving the identity of the radiation source behind the observation that diffuse H$\alpha$ emission is ubiquitous throughout the Galaxy and widespread sources of flux shortward of 912 $\AA$ are required. Moreover, the product hydrinos provides resolution to the identity of dark matter [23-29, 31].

**Figure I.6.** Dark matter ring in galaxy cluster. This Hubble Space Telescope composite image shows a ghostly "ring" of dark matter in the galaxy cluster Cl 0024+17. The ring is one of the strongest pieces of evidence to date for the existence of dark matter, a prior unknown substance that pervades the universe. Courtesy of NASA/ESA, M.J. Jee and H. Ford (Johns Hopkins University), Nov. 2004.



The recent experimental confirmation of the predictions for transitions of atomic hydrogen to form hydrinos, such as power production and characterization of hydrino reaction products [22-42], as well as pumped catalyst states, fast H, characteristic continuum radiation, and the hydrino product have profound implications theoretically, scientifically, and technologically in that they (1) confirm GUTCP in the prediction of hydrinos, (2) directly disprove atomic theories such as the Schrödinger and Dirac equation theories based on the definition of $n = 1$ as the ground state, the defined state below which it is impossible to go, as expected based on many physical failings and preexisting mathematical inconsistencies [4-20], (3) offer resolution to many otherwise inexplicable celestial observations with (a) the identity of dark matter being hydrinos, (b) the hydrino-transition radiation being the radiation source heating the WHIM and behind the observation that diffuse H emission is ubiquitous throughout the Galaxy requiring widespread sources of flux shortward of $912\ \mathring{A}$, and (c) the energy and radiation from the hydrino transitions being the source of extraordinary temperatures and power regarding the solar corona problem, the cause of sunspots and other solar activity, and why the Sun emits X-rays [23-29, 31], and (4) directly demonstrate a new field of hydrogen chemistry and a powerful new energy source.

An H atom decay and production cycle drives the spacetime expansion-contraction cycle of the universe wherein the recycling of matter and energy in the universe occurs during the oscillatory cycle wherein matter converts to energy primarily by hydrogen atom decay wherein the proton and electron are annihilated to gamma rays via a hydrino pathway, and energy to matter conversion occurs by hydrogen atom production during gamma ray bursts (See H Electronic Decay to Proton Decay Driving Subsequent Nuclear Reactions section and the H Atom Decay and Production Cycle Drive the Spacetime Expansion-Contraction Cycle of the Universe section). The emission of high energy gamma rays in the presence of hydrogen results in photoneutron production which may undergo neutron capture and beta decay of the resulting nucleus. The predicted decaying dark matter signatures of power and 511 keV gamma [86-91], neutral pion [92-93], and neutron capture emission [92, 94] match those of hydrogen atom decay from the high-p-state hydrino inventory comprising the dark matter. The characteristics, composition, and high energetics of cosmic rays in the absence of neutrino emission overturn long-held theory but match the signatures of H atom production [95]. The rates of production and annihilation of matter and energy match those required to

complete the cycle over the period of oscillation of the universe [96-97]. Furthermore, the recent unanticipated Webb telescope images confirm additional GUTCP predictions of fully formed galaxies and old galaxies at the beginning of the expansion of the universe that disprove the long held metaphysical Big Bang and related theories of cosmology and confirm the oscillatory evolutionary cycle of the universe wherein stellar and galactic evolution occurred during the contraction phase.

The purpose of a physical theory is to not only explain observations but predict novel ones such as the acceleration of the expansion of the universe, the absence of a Big Bang origin of the Universe, and the mass of the top quark [45]. Our entire modern technological society was created and depends on engineering using classical physical laws. For example, electromagnetic waves were predicted by Maxwell's equations before they were discovered as a transformational technology. A partial listing of new disruptive technologies invented using classical physics is given in Table I.7.

**Table I.7.** Partial List of New Disruptive Technologies Invented Using Classical Physics.

| |
|---|
| • Hydrino power |
| • Energetic materials for propellants and explosives |
| • Super magnets |
| • Conversion of common salts into hydrogen storage materials |
| • Photonic computer |
| • Single-molecule super conducting quantum interference devices (SQUIDs) |
| • Molecular SQUID magnetometer, detectors, switches, gates, logic elements |
| • X-ray molecular laser and molecular lasers over other sought wavelength ranges |
| • Hydrino hydride battery and energetic materials |
| • Molecular hydrino cryogen, coolant, and buoyancy gas |
| • Sequence of Hydrino induced proton decay-photoneutron production- neutron capture for tritium production |
| •Hydrino induced proton decay for power and military applications |
| • Photon torpedoes |
| • Space drive |
| • Neutrino telecommunications system |
| • Neutrino imaging system |
| • Laser wavelength doubler |
| • High temperature superconductors |
| • Millsian molecular modeling |
| • Alternative intelligence |

# REFERENCES


1. A. Beiser, *Concepts of Modern Physics*, Fourth Edition, McGraw-Hill, New York, (1987), pp. 87-117.
2. L. A. Rozema, A. Darabi, D. H. Mahler, A. Hayat, Y. Soudagar, A. M. Steinberg, "Violation of Heisenberg's Measurement-Disturbance Relationship by Weak Measurements," Phys. Rev. Lett., 109 (2012), 100404.
3. M. Isinger, R. J. Squibb, D. Busto, S. Zhong, A. Harth, D. Kroon, S. Nandi, C. L. Arnold, M. Miranda, J. M. Dahlström, E. Lindroth, R. Feifel, M. Gisselbrecht, A. L'Huillier, "Photoionization in the time and frequency domain," Science, (2017), eaao7043 DOI: 10.1126/science.aao7043MLA.
4. R. L. Mills, B. Holverstott, B. Good, N. Hogle, A. Makwana, J. Paulus, "Total Bond Energies of Exact Classical Solutions of Molecules Generated by Millsian 1.0 Compared to Those Computed Using Modern 3-21G and 6-31G* Basis Sets," Phys. Essays **23**, 153 (2010); doi: 10.4006/1.3310832.
5. W. Xie, R.L. Mills, W. Good, A. Makwana, B. Holverstott, N. Hogle, "Millsian 2.0: A Molecular Modeling Software for Structures, Charge Distributions and Energetics of Biomolecules," Physics Essays, 24 (2011) 200-212.
6. R. L. Mills, "Classical Quantum Mechanics," Physics Essays, Vol. 16, No. 4, December, (2003), pp. 433-498.
7. R. L. Mills, "Physical Solutions of the Nature of the Atom, Photon, and Their Interactions to Form Excited and Predicted Hydrino States," Phys. Essays, Vol. 20, No. 3, (2007), pp. 403-460.
8. R. L. Mills, "Exact Classical Quantum Mechanical Solutions for One- Through Twenty-Electron Atoms," Physics Essays, Vol. 18, (2005), pp. 321-361.
9. R. L. Mills, "The Nature of the Chemical Bond Revisited and an Alternative Maxwellian Approach," Physics Essays, Vol. 17, (2004), pp. 342-389.
10. R. L. Mills, "Maxwell's Equations and QED: Which is Fact and Which is Fiction," Physics Essays, Vol. 19, (2006), pp. 225-262.
11. R. L. Mills, "Exact Classical Quantum Mechanical Solution for Atomic Helium Which Predicts Conjugate Parameters from a Unique Solution for the First Time," Phys. Essays, Vol. 21, No. 2, (2008), pp. 103-141.
12. R. L. Mills, "The Fallacy of Feynman's Argument on the Stability of the Hydrogen Atom According to Quantum Mechanics," Annales de la Fondation Louis de Broglie, Vol. 30, No. 2, (2005), pp. 129-151.
13. R. Mills, "The Grand Unified Theory of Classical Quantum Mechanics," Int. J. Hydrogen Energy, Vol. 27, No. 5, (2002), pp. 565-590.

14. R. Mills, The Nature of Free Electrons in Superfluid Helium—a Test of Quantum Mechanics and a Basis to Review its Foundations and Make a Comparison to Classical Theory, Int. J. Hydrogen Energy, Vol. 26, No. 10, (2001), pp. 1059-1096.
15. R. Mills, "The Hydrogen Atom Revisited," Int. J. of Hydrogen Energy, Vol. 25, Issue 12, December, (2000), pp. 1171-1183.
16. V. F. Weisskopf, Reviews of Modern Physics, Vol. 21, No. 2, (1949), pp. 305-315.
17. P. Pearle, Foundations of Physics, "Absence of radiationless motions of relativistically rigid classical electron," Vol. 7, Nos. 11/12, (1977), pp. 931-945.
18. A. Einstein, B. Podolsky, N. Rosen, Phys. Rev., Vol. 47, (1935), p. 777.
19. F. Laloë, "Do we really understand quantum mechanics? Strange correlations, paradoxes, and theorems," Am. J. Phys. 69 (6), June 2001, pp. 655-701.
20. Z. Merali, "What is really real? A wave of experiments is probing the root of quantum weirdness," Nature, Vol. 521, (2015), pp. 278-280.
21. H. J. Maris, Journal of Low Temperature Physics, Vol. 120, (2000), p. 173.
22. http://www.brilliantlightpower.com/
23. R. Mills, Y. Lu, R. Frazer, "Power Determination and Hydrino Product Characterization of Ultra-low Field Ignition of Hydrated Silver Shots", Chinese Journal of Physics, Vol. 56, (2018), pp. 1667-1717.
24. R. Mills, J. Lotoski, Y. Lu, "Mechanism of soft X-ray continuum radiation from low-energy pinch discharges of hydrogen and ultra-low field ignition of solid fuels", Plasma Science and Technology, Vol. 19, (2017), pp. 1-28.
25. R. L. Mills, R. Booker, Y. Lu, "Soft X-ray Continuum Radiation from Low-Energy Pinch Discharges of Hydrogen," J. Plasma Physics, Vol. 79, (2013), pp 489-507; doi:10.1017/S0022377812001109.
26. R. L. Mills, Y. Lu, "Time-resolved hydrino continuum transitions with cutoffs at 22.8 nm and 10.1 nm," Eur. Phys. J. D, Vol. 64, (2011), pp. 65, DOI: 10.1140/epjd/e2011-20246-5.
27. R. L. Mills, Y. Lu, "Hydrino continuum transitions with cutoffs at 22.8 nm and 10.1 nm," Int. J. Hydrogen Energy, 35 (2010), pp. 8446-8456, doi: 10.1016/j.ijhydene.2010.05.098.
28. R. L. Mills, Y. Lu, K. Akhtar, "Spectroscopic observation of helium-ion- and hydrogen-catalyzed hydrino transitions," Cent. Eur. J. Phys., 8 (2010), pp. 318-339, doi: 10.2478/s11534-009-0106-9.
29. A. Bykanov, "Validation of the observation of soft X-ray continuum radiation from low energy pinch discharges in the presence of molecular hydrogen," http://www.blacklightpower.com/wp-content/uploads/pdf/GEN3_Harvard.pdf.
30. W. R. Hagen, R. L. Mills, "Electron Paramagnetic Resonance Proof for the Existence of Molecular Hydrino", Int. J. Hydrogen Energy, Vol. 47, No. 56, (2022), pp. 23751-23761; https://www.sciencedirect.com/science/article/pii/S0360319922022406.
31. R. Mills, "Hydrino States of Hydrogen", https://brilliantlightpower.com/pdf/Hydrino_States_of_Hydrogen_Paper.pdf, submitted for publication.
32. R. Mills J. Lotoski, "$H_2O$-based solid fuel power source based on the catalysis of H by HOH catalyst", Int'l J. Hydrogen Energy, Vol. 40, (2015), 25-37.
33. R. Mills, J. Lotoski, W. Good, J. He, "Solid Fuels that Form HOH Catalyst," Int'l J. Hydrogen Energy, Vol. 39 (2014), pp. 11930–11944 DOI: 10.1016/j.ijhydene.2014.05.170.
34. R. Mills, J. Lotoski, J. Kong, G. Chu, J. He, J. Trevey, "High-Power-Density Catalyst Induced Hydrino Transition (CIHT) Electrochemical Cell." Int. J. Hydrogen Energy, 39 (2014), pp. 14512–14530 DOI: 10.1016/j.ijhydene.2014.06.153.
35. R. Mills, X Yu, Y. Lu, G Chu, J. He, J. Lotoski, "Catalyst induced hydrino transition (CIHT) electrochemical cell," (2012), Int. J. Energy Res., (2013), DOI: 10.1002/er.3142.
36. R. L. Mills, K. Akhtar, "Fast H in Hydrogen Mixed Gas Microwave Plasmas when an Atomic Hydrogen Supporting Surface Was Present," Int. J. Hydrogen Energy, Vol. 35, (2010), pp. 2546–2555, doi: 10.1016/j.ijhydene.2009.12.148.
37. K. Akhtar, J. Scharer, R. L. Mills, "Substantial Doppler Broadening of Atomic Hydrogen Lines in DC and Capactively Coupled RF Plasmas," J. Phys. D: Appl. Phys., Vol. 42, Issue 13 (2009), pp. 135207-135219, doi:10.1088/0022-3727/42/13/135207 42 135207.
38. R. L. Mills, K. Akhtar, "Tests of Features of Field-Acceleration Models for the Extraordinary Selective H Balmer α Broadening in Certain Hydrogen Mixed Plasmas," Int. J. Hydrogen Energy, Vol. 34, (2009), 6465–6477.
39. R. L. Mills, B. Dhandapani, K. Akhtar, "Excessive Balmer $\alpha$ Line Broadening of Water-Vapor Capacitively-Coupled RF Discharge Plasmas," Int. J. Hydrogen Energy, Vol. 33, (2008), 802–815.
40. R. L. Mills, P. Ray, B. Dhandapani, Evidence of an energy transfer reaction between atomic hydrogen and argon II or helium II as the source of excessively hot H atoms in radio-frequency plasmas, J. Plasma Physics, Vol. 72, No. 4, (2006), 469–484.
41. J. Phillips, C. K. Chen, K. Akhtar, B. Dhandapani, R. L. Mills, "Evidence of Catalytic Production of Hot Hydrogen in RF-Generated Hydrogen/Argon Plasmas," Int. J. Hydrogen Energy, Vol. 32(14), (2007), 3010–3025.
42. R. L. Mills, P. C. Ray, R. M. Mayo, M. Nansteel, B. Dhandapani, J. Phillips, "Spectroscopic Study of Unique Line Broadening and Inversion in Low Pressure Microwave Generated Water Plasmas," J. Plasma Physics, Vol. 71, No 6, (2005), 877–888.
43. K. Hagiwara et al., Phys. Rev. D 66, 010001 (2002); http://pdg.lbl.gov/2002/s035.pdf.
44. P. J. Mohr and B. N. Taylor, "CODATA recommended values of the fundamental physical constants: 1998," Reviews of Modern Physics, Vol. 72, No. 2, April, (2000), pp. 351-495.
45. R. L. Mills, *The Grand Unified Theory of Classical Quantum Mechanics*, November 1995 Edition, HydroCatalysis Power Corp., Malvern, PA, Library of Congress Catalog Number 94-077780, ISBN 0-9635171-1-2, Chp. 22.

46. H. A.Haus, "On the radiation from point charges," American Journal of Physics, 54, (1986), pp. 1126-1129.
47. J. D. Jackson, *Classical Electrodynamics*, Second Edition, John Wiley & Sons, New York, (1975), pp. 739-779.
48. M. Mizushima, *Quantum Mechanics of Atomic Spectra and Atomic Structure*, W.A. Benjamin, Inc., New York, (1970), p.17.
49. F. Dyson, "Feynman's proof of Maxwell equations," Am. J. Phys., Vol. 58, (1990), pp. 209-211.
50. J. Horgan, "Quantum Philosophy," Scientific American, July, (1992), p. 96.
51. H. Margenau, G. M. Murphy, *The Mathematics of Chemistry and Physics*, D. Van Nostrand Company, Inc., New York, (1956), Second Edition, pp. 77, 363-367.
52. G. R. Fowles, *Analytical Mechanics*, Third Edition, Holt, Rinehart, and Winston, New York, (1977), pp. 154-156.
53. D. A. McQuarrie, *Quantum Chemistry*, University Science Books, Mill Valley, CA, (1983), pp. 78-79.
54. D. A. McQuarrie, *Quantum Chemistry*, University Science Books, Mill Valley, CA, (1983), pp. 221-225.
55. J. D. Jackson, *Classical Electrodynamics*, Second Edition, John Wiley & Sons, New York, (1975), pp. 84-108.
56. R. N. Bracewell, *The Fourier Transform and Its Applications*, McGraw-Hill Book Company, New York, (1978), pp. 252-253.
57. W. McC. Siebert, *Circuits, Signals, and Systems*, The MIT Press, Cambridge, Massachusetts, (1986), p. 415.
58. W. McC. Siebert, *Circuits, Signals, and Systems*, The MIT Press, Cambridge, Massachusetts, (1986), p. 416.
59. C. A. Fuchs, A. Peres, "Quantum theory needs no 'interpretation,'" Phys. Today, Vol. 53, March, (2000), No. 3, pp. 70-71.
60. S. Durr, T. Nonn, G. Rempe, Nature, September 3, (1998), Vol. 395, pp. 33-37.
61. A. Pais, "George Uhlenbeck and the discovery of electron spin," Physics Today, 42, Dec., (1989), pp. 34-40.
62. J. D. Jackson, *Classical Electrodynamics*, Second Edition, John Wiley & Sons, New York, (1975), p. 111.
63. T. A. Abbott, D. J. Griffiths, Am. J. Phys., Vol. 153, No. 12, (1985), pp. 1203-1211.
64. G. Goedecke, Phys. Rev 135B, (1964), p. 281.
65. D. A. McQuarrie, *Quantum Chemistry*, University Science Books, Mill Valley, CA, (1983), pp. 206-225.
66. R. S. Van Dyck, Jr., P. Schwinberg, H. Dehmelt, "New high precision comparison of electron and positron g factors," Phys. Rev. Lett., Vol. 59, (1987), p. 26-29.
67. J. D. Jackson, *Classical Electrodynamics*, Second Edition, John Wiley & Sons, New York, (1975), pp. 739-779.
68. J. D. Jackson, *Classical Electrodynamics*, Second Edition, John Wiley & Sons, New York, (1975), pp. 758-763.
69. N. V. Sidgwick, *The Chemical Elements and Their Compounds*, Volume I, Oxford, Clarendon Press, (1950), p.17.
70. M. D. Lamb, *Luminescence Spectroscopy*, Academic Press, London, (1978), p. 68.
71. K. R. Lykke, K. K. Murray, W. C. Lineberger, "Threshold photodetachment of $H^-$," Phys. Rev. A, Vol. 43, No. 11, (1991), pp. 6104-6107.
72. D. R. Lide, *CRC Handbook of Chemistry and Physics*, 86th Edition, CRC Press, Taylor & Francis, Boca Raton, (2005-6), pp. 10-202 to 10-204.
73. K. K. Baldridge, J. S. Siegel, "Correlation of empirical $\delta$(TMS) and absolute NMR chemical shifts predicted by ab initio computations," J. Phys. Chem. A, Vol. 103, (1999), pp. 4038-4042.
74. J. Mason, Editor, *Multinuclear NMR*, Plenum Press, New York, (1987), Chp. 3.
75. C. Suarez, E. J. Nicholas, M. R. Bowman, "Gas-phase dynamic NMR study of the internal rotation in N-trifluoroacetlypyrrolidine," J. Phys. Chem. A, Vol. 107, (2003), pp. 3024-3029.
76. C. Suarez, "Gas-phase NMR spectroscopy," The Chemical Educator, Vol. 3, No. 2, (1998).
77. H. Beutler, Z. Physical Chem., "Die dissoziationswarme des wasserstoffmolekuls $H_2$, aus einem neuen ultravioletten resonanzbandenzug bestimmt," Vol. 27B, (1934), pp. 287-302.
78. G. Herzberg, L. L. Howe, "The Lyman bands of molecular hydrogen," Can. J. Phys., Vol. 37, (1959), pp. 636-659.
79. P. W. Atkins, *Physical Chemistry*, Second Edition, W. H. Freeman, San Francisco, (1982), p. 589.
80. D. R. Lide, *CRC Handbook of Chemistry and Physics*, 86th Edition, CRC Press, Taylor & Francis, Boca Raton, (2005-6), pp. 9-54 to 9-59.
81. R. Mills, "Spectroscopic Identification of a Novel Catalytic Reaction of Atomic Hydrogen and the Hydride Ion Product," Int. J. Hydrogen Energy, Vol. 26, No. 10, (2001), pp. 1041-1058.
82. F. Bournaud, P. A. Duc, E. Brinks, M. Boquien, P. Amram, U. Lisenfeld, B. Koribalski, F. Walter, V. Charmandaris, "Missing mass in collisional debris from galaxies," Science, Vol. 316, (2007), pp. 1166–1169.
83. B. G. Elmegreen, "Dark matter in galactic collisional debris," Science, Vol. 316, (2007), pp. 32-33.
84. M. J. Jee, A. Mahdavi, H. Hoekstra, A. Babul, J. J. Dalcanton, P. Carroll, P. Capak, "A study of the dark core in A520 with the Hubble Space Telescope: The mystery deepens," Astrophys. J., Vol. 747, No.96, (2012), pp. 96-103.
85. M. J. Jee, et al., "Discovery of a ringlike dark matter structure in the core of the galaxy cluster C1 0024+17," Astrophysical Journal, Vol. 661, (2007), pp. 728-749.
86. A. C. Vincent, P. Martin, J. M. Cline, "Interacting dark matter contribution to the Galactic 511 keV gamma ray emission: constraining the morphology with INTEGRAL/SPI observations", https://arxiv.org/pdf/1201.0997.
87. G. De Cesare, "Searching for the 511 keV annihilation line from galactic compact objects with the IBIS gamma ray telescope", A&A 531, A56 (2011) DOI: 10.1051/0004-6361/201116516, https://www.aanda.org/articles/aa/pdf/2011/07/aa16516-11.pdf.
88. J. Knodlseder, et al., "The all-sky distribution of 511 keV electron-positron annihilation emission", Astronomy & Astrophysics manuscript no. 2063, November 7, 2018, https://arxiv.org/pdf/astro-ph/0506026.

89. J. Knodlseder, et al., "The all-sky distribution of 511 keV electron-positron annihilation emission", astro-ph/0506026, Masaki Mori, ICRR Group Internal Seminar, June 20, 2005,https://www.icrr.u-tokyo.ac.jp/~morim/Presentations/INTEGRAL511keV.pdf.
90. N. Prantzos, C. Boehm, A. M. Bykov, et al., "The 511 keV emission from positron annihilation in the Galaxy", (2010), https://arxiv.org/abs/1009.4620.
91. N. Prantzos, C. Boehm, A. M. Bykov, et al., "The 511 keV emission from positron annihilation in the Galaxy", Reviews of Modern Physics, Vol. 83, July (2011), pp. 1001–1056.
92. R. Yang, E. Kafexhiu1, F. Aharonian, "Exploring the shape of the γ-ray spectrum around the "$\pi^0$-bump", A&A, Volume 615, July (2018), A108, https://doi.org/10.1051/0004-6361/201730908, https://www.aanda.org/articles/aa/pdf/2018/07/aa30908-17.pdf.
93. National Aeronautics and Space Administration, Goddard Space Flight Center, Fermi Gamma-ray Space Telescope, "Overview of GRB spectral analysis", https://fermi.gsfc.nasa.gov/ssc/data/analysis/documentation/Cicerone/Cicerone_GRBs/Overview_GRB_Spec_Anal.html.
94. R. Ramaty, R. J. Murphy, C. D. Dermer, "On the origin of the pion-decay radiation in the 1982 June 3 solar flare", The Astrophysical Journal, 316:L41-L44,1987 May 1. https://articles.adsabs.harvard.edu/cgi-bin/nph-iarticle_query?1987ApJ...316L..41R&defaultprint=YES&filetype=.pdf.
95. IceCube Collaboration. "An absence of neutrinos associated with cosmic-ray acceleration in γ-ray bursts", Nature. Vol. 484, (2012), pp. 351–354, https://doi.org/10.1038/nature11068.
96. G. Ghisellini, G. Ghirlanda, "Proton–synchrotron as the radiation mechanism of the prompt emission of gamma-ray bursts?", A&A, Vol. 636, April (2020), A82, https://doi.org/10.1051/0004-6361/201937244, https://www.aanda.org/articles/aa/full_html/2020/04/aa37244-19/aa37244-19.html.
97. D. Kazanas, D. C. Ellison, "Proton acceleration in γ-ray bursts", Advances in Space Research, Vol. 6, Issue 4, (1986), pp. 81-84, ISSN 0273-1177, https://doi.org/10.1016/0273-1177(86)90243-7, https://www.sciencedirect.com/science/article/abs/pii/0273117786902437.

# Chapter 1

## THE ONE-ELECTRON ATOM

One-electron atoms include the hydrogen atom, $He^{+}$, $Li^{2+}$, $Be^{3+}$, and so on. In each case, the nucleus contains $Z$ protons and the atom has a net positive charge of $(Z-1)e$. The mass-energy and angular momentum of the electron are constant and the flow of current must be conservative and without radiation. A point charge undergoing periodic motion accelerates and as a consequence radiates power according to the Larmor formula. The condition for radiation by a moving point charge derived from Maxwell's equations by Haus [1] is that its spacetime Fourier transform does possess components that are synchronous with waves traveling at the speed of light. The Haus derivation applies to a moving charge-density function as well because charge obeys superposition. Thus, the general condition extended beyond one-dimension is that to radiate, the spacetime Fourier transform of the current-density function must possess components synchronous with waves traveling at the speed of light [1]. Although an accelerated *point* particle radiates, an *extended distribution* modeled as a continuous superposition of accelerating charges does not have to radiate [1-2]. Then, conversely, the nonradiative condition is

*For non-radiative states, the current-density function must not possess spacetime Fourier components that are synchronous with waves traveling at the speed of light.*

The Haus derivation and the condition for nonradiation are given in Appendix I: Nonradiation Condition wherein the nonradiative condition is also derived directly by the determination of the electrodynamic fields with the electron current-density function as the source current during electron transitions. Given the infinite number of possible current-density functions, it is fortuitous that the spherical radiation corresponding to the symmetry and the conditions for emission and absorption of such radiation provide the additional boundary conditions to determine the current-density functions.

### ELECTRON SOURCE CURRENT

Leptons such as the electron (Leptons section) are indivisible, perfectly conducting, and possess an inalienable $\hbar$ of intrinsic angular momentum such that any inelastic perturbation involves the entire particle wherein the intrinsic angular momentum remains unchanged. Bound state transitions are allowed involving the exchange of photons between states, each having $\hbar$ of angular momentum in their fields (Appendix II: Stability and Absence of Self Interaction and Self Energy). A physical approach to solving the structure of the bound electron is followed based on the principles of radiation and the corresponding electron energy state change:

*Using Maxwell's equations, the structure of the electron is derived as a boundary-value problem wherein the electron comprises the source current of time-varying electromagnetic fields during transitions with the constraint that the bound $n=1$ state electron cannot radiate energy.*

Since the hydrogen atom is stable and nonradiative, the electron has constant energy. Furthermore, it is time dynamic with a corresponding current that serves as a source of electromagnetic radiation during transitions. The wave equation solutions of the radiation fields permit the source currents to be determined as a boundary-value problem. These source currents match the field solutions of the wave equation for two dimensions plus time and the nonradiative $n = 1$ state when the nonradiation condition is applied. Then, the mechanics of the electron can be solved from the two-dimensional wave equation plus time in the form of an energy equation, wherein it provides for conservation of energy and angular momentum as given in the Electron Mechanics and the Corresponding Classical Wave Equation for the Derivation of the Rotational Parameters of the Electron section. Once

the nature of the electron is solved, all problems involving electrons can be solved in principle. Thus, in the case of one-electron atoms, the electron radius, binding energy, and other parameters are solved after solving for the nature of the bound electron.

As shown in Appendix I: Nonradiation Condition, for time-varying spherical electromagnetic fields, Jackson [3] gives a generalized expansion in vector spherical waves that are convenient for electromagnetic boundary-value problems possessing spherical symmetry properties and for analyzing multipole radiation from a localized source distribution. The Green function $G(\mathbf{x}',\mathbf{x})$ that is appropriate to the inhomogenous Helmholtz equation

$$\left(\nabla^2 + k^2\right) G(\mathbf{x}',\mathbf{x}) = -\delta(\mathbf{x}'-\mathbf{x}) \tag{1.1}$$

in the infinite domain with the spherical wave expansion for the outgoing wave Green function is:

$$G(\mathbf{x}',\mathbf{x}) = \frac{e^{-ik|\mathbf{x}-\mathbf{x}'|}}{4\pi|\mathbf{x}-\mathbf{x}'|} = ik\sum_{\ell=0}^{\infty} j_\ell(kr_<)\, h_\ell^{(1)}(kr_>) \sum_{m=-\ell}^{\ell} Y_{\ell,m}^*(\theta',\phi') Y_{\ell,m}(\theta,\phi) \tag{1.2}$$

Jackson [3] further gives the general multipole field solution to Maxwell's equations in a source-free region of empty space with the assumption of time dependence $e^{i\omega t}$:

$$\begin{aligned} \mathbf{B} &= \sum_{\ell,m}\left[ a_E(\ell,m) f_\ell(kr)\mathbf{X}_{\ell,m} - \frac{i}{k} a_M(\ell,m)\nabla\times g_\ell(kr)\mathbf{X}_{\ell,m}\right] \\ \mathbf{E} &= \sum_{\ell,m}\left[ \frac{i}{k} a_E(\ell,m)\nabla\times f_\ell(kr)\mathbf{X}_{\ell,m} + a_M(\ell,m) g_\ell(kr)\mathbf{X}_{\ell,m}\right] \end{aligned} \tag{1.3}$$

where the cgs units used by Jackson are retained in this section. The radial functions $f_\ell(kr)$ and $g_\ell(kr)$ are of the form:

$$g_\ell(kr) = A_\ell^{(1)} h_\ell^{(1)} + A_\ell^{(2)} h_\ell^{(2)} \tag{1.4}$$

$\mathbf{X}_{\ell,m}$ is the vector spherical harmonic defined by:

$$\mathbf{X}_{\ell,m}(\theta,\phi) = \frac{1}{\sqrt{\ell(\ell+1)}}\mathbf{L}Y_{\ell,m}(\theta,\phi) \tag{1.5}$$

where

$$\mathbf{L} = \frac{1}{i}(\mathbf{r}\times\nabla) \tag{1.6}$$

The coefficients $a_E(\ell,m)$ and $a_M(\ell,m)$ of Eq. (1.3) specify the amounts of electric $(\ell,m)$ multipole and magnetic $(\ell,m)$ multipole fields, and are determined by sources and boundary conditions as are the relative proportions in Eq. (1.4). Jackson gives the result of the electric and magnetic coefficients from the sources as

$$a_E(\ell,m) = \frac{4\pi k^2}{i\sqrt{\ell(\ell+1)}}\int Y_\ell^{m*}\left\{\rho\frac{\partial}{\partial r}\left[rj_\ell(kr)\right] + \frac{ik}{c}(\mathbf{r}\cdot\mathbf{J})\, j_\ell(kr) - ik\nabla\cdot(r\times\boldsymbol{M})\, j_\ell(kr)\right\} d^3x \tag{1.7}$$

and

$$a_M(\ell,m) = \frac{-4\pi k^2}{\sqrt{\ell(\ell+1)}}\int j_\ell(kr) Y_\ell^{m*}\mathbf{L}\cdot\left(\frac{\mathbf{J}}{c} + \nabla\times\boldsymbol{M}\right) d^3x \tag{1.8}$$

respectively, where the distribution of charge $\rho(\mathbf{x},t)$, current $\mathbf{J}(\mathbf{x},t)$, and intrinsic magnetization $\boldsymbol{M}(\mathbf{x},t)$ are harmonically varying sources: $\rho(\mathbf{x})e^{-i\omega t}$, $\mathbf{J}(\mathbf{x})e^{-i\omega t}$, and $\boldsymbol{M}(\mathbf{x})e^{-i\omega t}$.

The electron current-density function can be solved as a boundary value problem regarding the time varying corresponding source current $\mathbf{J}(\mathbf{x})e^{-i\omega t}$ that gives rise to the time-varying spherical electromagnetic fields during transitions between states with the further constraint that the electron is nonradiative in a state defined as the $n=1$ state. The potential energy, $V(\mathbf{r})$, is an inverse-radius-squared relationship given by Gauss' law, which for a point charge or a two-dimensional spherical shell at a distance $r$ from the nucleus, the potential is:

$$V(r) = -\frac{e^2}{4\pi\varepsilon_0 r} \tag{1.9}$$

Thus, consideration of conservation of energy would require that the electron radius must be fixed. Additional constraints requiring a two-dimensional source current of fixed radius are matching the delta function of Eq. (1.1) with no singularity, no

time dependence and consequently no radiation, absence of self-interaction (See Appendix II: Stability and Absence of Self Interaction and Self Energy), and exact electroneutrality of the hydrogen atom wherein the electric field is given by:

$$\mathbf{n} \bullet \left( \mathbf{E}_1 - \mathbf{E}_2 \right) = \frac{\sigma_s}{\varepsilon_0} \tag{1.10}$$

where $\mathbf{n}$ is the normal unit vector, $\mathbf{E}_1$ and $\mathbf{E}_2$ are the electric field vectors that are discontinuous at the opposite surfaces, $\sigma_s$ is the discontinuous two-dimensional surface charge density, and $\mathbf{E}_2 = 0$. Then, the solution for the radial electron function, which satisfies the boundary conditions, is a delta function in spherical coordinates—a perfect spherical shell [4]

$$f(r) = \frac{1}{r^2} \delta(r - r_n) \tag{1.11}$$

where $r_n$ is an allowed radius. The perfect spherical nature of a bound electron has been confirmed experimentally by a zero electric dipole moment $d_e$ to an upper limit of $\left| d_e \right| < 10.5X10^{-30} e\ m$ [5]. The function of Eq. (1.11) defines the charge density on a spherical shell of a fixed radius, not yet determined where the integer subscript $n$ is *determined during photon absorption,* as given in the Excited States of the One-Electron Atom (Quantization) section. It is shown in this section that the force balance between the electric fields of the electron and proton plus any resonantly absorbed photons gives the result that $r_n = nr_1$ wherein $n$ is an integer in an excited state. To further match the required multipole electromagnetic fields between transitions of states, the trial nonradiative source current functions are time and spherical harmonics, each having an exact radius and an exact energy. Then, each allowed electron charge-density (mass-density) function is the product of a radial delta function $\left( f(r) = \frac{1}{r^2} \delta(r - r_n) \right)$, two angular functions (spherical harmonic functions), and a time-harmonic function. The corresponding currents $\mathbf{J}$ are

$$\begin{aligned} \mathbf{J} &= \frac{m\omega_n}{2\pi} \frac{e}{4\pi r_n^2} N[\delta(r - r_n)] \mathrm{Re}\left\{ Y_\ell^m(\theta, \phi) \right\} \left[ \mathbf{u}(t) \times \mathbf{r} \right] \\ &= \frac{m\omega_n}{2\pi} \frac{e}{4\pi r_n^2} N'[\delta(r - r_n)] \left( P_\ell^m(\cos\theta) \cos\left( m\phi + m\omega_n t \right) \right) \left[ \mathbf{u} \times \mathbf{r} \right] \\ &= \frac{m\omega_n}{2\pi} \frac{e}{4\pi r_n^2} N'[\delta(r - r_n)] \left( P_\ell^m(\cos\theta) \cos\left( m\phi + m\omega_n t \right) \right) \sin\theta \hat{\phi} \end{aligned} \tag{1.12}$$

where $N$ and $N'$ are normalization constants. The vectors are defined as:

$$\hat{\phi} = \frac{\hat{u} \times \hat{r}}{\left| \hat{u} \times \hat{r} \right|} = \frac{\hat{u} \times \hat{r}}{\sin\theta}; \qquad \hat{u} = \hat{z} = orbital\ axis \tag{1.13}$$

$$\hat{\theta} = \hat{\phi} \times \hat{r} \tag{1.14}$$

"^" denotes the unit vectors $\hat{u} \equiv \frac{\mathbf{u}}{|\mathbf{u}|}$, non-unit vectors are designated in bold, and the current function is normalized.

The Fourier transform of the radial Dirac delta function is a sinc function as shown in Appendix I. Given time harmonic motion with angular velocity $\omega_n$ corresponding to a potentially emitted photon, and a radial delta function, the relationship between an allowed radius and the electron wavelength is given by

$$2\pi r_n = \lambda_n \tag{1.15}$$

Consider the sinc function when the velocity is $c$ corresponding to a potentially emitted photon where Eq. (1.15) applies. In this case, the relativistically corrected wavelength (Eq. (1.279)) is

$$\lambda_n = r_n \tag{1.16}$$

Substitution of Eq. (1.16) into the sinc function results in the vanishing of the entire Fourier transform of the current-density function. Thus, spacetime harmonics of $\frac{\omega_n}{c} = k$ or $\frac{\omega_n}{c} \sqrt{\frac{\varepsilon}{\varepsilon_0}} = k$ do not exist for which the Fourier transform of the current-density function is nonzero. Radiation due to charge motion does not occur in any medium when this boundary condition is met. (Note that in contrast the purely mathematical boundary condition for the solution of the radial function of the hydrogen atom with the Schrödinger equation is $\Psi \to 0$ as $r \to \infty$ wherein the electron exists everywhere at once and has the maximum of the squared wavefunction at the origin inside of the nucleus.)

In addition to satisfaction of the Haus' condition given, the electron currents given by Eq. (1.12) are shown to be nonradiative with the same condition as that of Eq. (1.16) applied to the vector potential based on the electromagnetic fields and the Poynting power vector as shown in Appendix I: Nonradiation Condition. From Eq. (1.12), the charge and intrinsic

magnetization terms are zero. Also, the current $\mathbf{J}(\mathbf{x},t)$ is in the $\hat{\phi}$ direction; thus, the $a_E(\ell,m)$ coefficient given by Eq. (1.7) is zero since $\mathbf{r}\cdot\mathbf{J}=0$. Substitution of Eq. (1.12) into Eq. (1.8) gives the magnetic multipole coefficient $a_M(\ell,m)$:

$$a_M(\ell,m)=\frac{-ek^2}{c\sqrt{\ell(\ell+1)}}\frac{\omega_n}{2\pi}Nj_\ell(kr_n)\Theta\sin(ks) \tag{1.17}$$

For the electron source current given by Eq. (1.12), each comprising a multipole of order $(\ell,m)$ with a time dependence $e^{i\omega t}$, the far-field solutions to Maxwell's equations given by Eq. (1.3) are:

$$\begin{aligned}\mathbf{B}&=-\frac{i}{k}a_M(\ell,m)\nabla\times g_\ell(kr)\mathbf{X}_{\ell,m}\\ \mathbf{E}&=a_M(\ell,m)g_\ell(kr)\mathbf{X}_{\ell,m}\end{aligned} \tag{1.18}$$

and the time-averaged power radiated per solid angle $\frac{dP(\ell,m)}{d\Omega}$ is:

$$\frac{dP(\ell,m)}{d\Omega}=\frac{c}{8\pi k^2}\left|a_M(\ell,m)\right|^2\left|\mathbf{X}_{\ell,m}\right|^2 \tag{1.19}$$

where $a_M(\ell,m)$ is given by Eq. (1.17). In the case that $k$ is the lightlike $k^0$, then $k=\omega_n/c$ regarding an emitted photon, in Eq. (1.17), and Eqs. (1.18-1.19) vanishes for:

$$s=vT_n=R=r_n=\lambda_n \tag{1.20}$$

*There is no radiation*.

There is no radiation due to the azimuthal charge density wave even in an excited state. However, for excited states there exists a radial dipole that is unstable to radiation as shown in the Instability of Excited States section, and this instability gives rise to a radial electric dipole current. In a nonradiative state, there is no emission or absorption of radiation corresponding to the absence of radial motion wherein Eq. (1.7) is zero since $\mathbf{r}\cdot\mathbf{J}=0$. Conversely, there is motion in the radial direction only when the energy of the system is changing, and the *radiation emitted or absorbed during electron transitions is the multipole radiation given by Eq. (1.2)* as given in the Excited States of the One-Electron Atom (Quantization) section and the Equation of the Photon section wherein Eqs. (4.18-4.23) give a macro-spherical wave in the far-field. Thus, radial motion corresponds to the emission or absorption of photons. The form of the radial solution during a transition is then the corresponding electron source current comprising a time-dependent radial Dirac delta function that connects the initial and final states as boundary conditions. The photon carries fields and corresponding angular momentum. The physical characteristics of the photon and the electron are the basis of physically solving for excited states according to Maxwell's equations. The discontinuous harmonic radial current in Eq. (1.7) that connects the initial and final states of the transition is:

$$\mathbf{r}\cdot\mathbf{J}=\frac{er}{4\pi r^2}\tau^{-1}\sin\frac{\pi t'}{\tau}\left(u(t')-u(t'-\tau)\right) \tag{1.21}$$

where $\tau$ is the lifetime of the transition given by Eq. (2.107) and $t'$ is time during the transition as given in the Excited States of the One-Electron Atom (Quantization) section. The vector potential of the current that connects the initial and final states of a transition, each having currents of the form given by Eq. (1.12), is:

$$\mathbf{A}(r)=\frac{\mu_0}{2\pi}\frac{e\hbar}{m_e}\frac{1}{r_{n_i}-r_{n_f}}\frac{e^{-ik_r r}}{4\pi r}\mathbf{i}_z \tag{1.22}$$

The magnetic and electric fields are derived from the vector potential and are used in the Poynting power vector to give the power. The transition probability or Einstein coefficient $A_{ki}$ for initial state $n_i$ and final state $n_f$ of atomic hydrogen given by the power divided by the energy of the transition is:

$$\frac{1}{\tau}=\frac{1}{m_e c^2}\frac{\eta}{24\pi}\left(\frac{e\hbar}{m_e a_0^2}\right)^2\frac{1}{\left(n_f n_i\right)^2}=2.678\ X\ 10^9\frac{1}{\left(n_f n_i\right)^2}\ s^{-1} \tag{1.23}$$

which matches the NIST values for all transitions extremely well as shown in Excited States of the One-Electron Atom (Quantization) section.

## THE BOUND ELECTRON "ATOMIC ORBITAL"

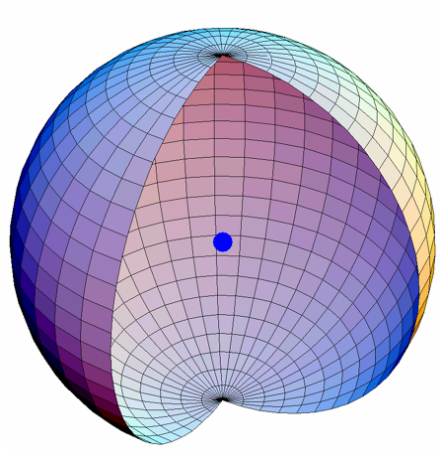
From Eqs. (1.27-1.29), the electron angular functions are the spherical harmonics, $Y_\ell^m(\theta,\phi)=P_\ell^m(\cos\theta)e^{im\phi}$. The spherical harmonic $Y_0^0(\theta,\phi)=1$ is also an allowed solution that is in fact required in order for the electron charge and mass densities to be

positive definite and to give rise to the phenomena of electron spin. The real parts of the spherical harmonics vary between $-1$ and 1. But, the mass of the electron cannot be negative, and the charge cannot be positive. Thus, to insure that the function is positive definite, the form of the angular solution must be a superposition:

$$Y_0^0(\theta,\phi)+Y_\ell^m(\theta,\phi) \tag{1.24}$$

(Note that $Y_\ell^m(\theta,\phi)=P_\ell^m(\cos\theta)e^{im\phi}$ are not normalized here as given by Eq. (3.53) of Jackson [6]; however, it is implicit that the magnitude is made to satisfy the boundary condition that the function is positive definite and Eq. (1.26) is satisfied.) $Y_0^0(\theta,\phi)$ is called the angular spin function corresponding to the quantum numbers $\mathrm{s}=\frac{1}{2};\ \mathrm{m_s}=\pm\frac{1}{2}$ as given in the Atomic Orbital Equation of Motion For $\ell = 0$ Based on the Current Vector Field (CVF) section. Thus, bound electrons are described by a charge-density (mass-density) function that is the product of a radial delta function, Eq. (1.11), two angular functions (spherical harmonic functions), and a time harmonic function. This radial function implies that allowed states are two-dimensional spherical shells (zero thickness [1]) of charge density (and mass density) at specific radii $r_n$. Thus, a bound electron is a constant two-dimensional spherical surface of charge (zero thickness, total charge of $-e$, and total mass of $m_e$), called *an electron atomic orbital shown in Figure 1.1, that can exist in a bound state at only specified distances from the nucleus determined by an energy minimum for the n=1 state and integer multiples of this radius due to the action of resonant photons as shown in the Determination of Atomic Orbital Radii section and the Equation of the Electric Field Inside the Atomic Orbital section, respectively.*

**Figure 1.1.** A bound electron is a constant two-dimensional spherical surface of charge (zero thickness, total charge of $-e$, and total mass of $m_e$), called *an electron atomic orbital.* For the $n=1$ state of the hydrogen atom, the atomic orbital has the Bohr radius of the hydrogen atom, $r=a_H$. It is a nonradiative, minimum-energy surface, that is absolutely stable except for quantized state changes with the corresponding balanced forces in the $n=1$ state providing a pressure equivalent of twenty million atmospheres.



The equipotential, uniform or constant charge-density function (Eq. (1.27)) further comprises a current pattern given in the Atomic Orbital Equation of Motion For $\ell = 0$ Based on the Current Vector Field (CVF) section and corresponds to the spin function of the electron. It also corresponds to the nonradiative $n=1$, $\ell = 0$ state of atomic hydrogen. The uniform current density function $Y_0^0(\theta,\phi)$ (Eqs. (1.27-1.29)) that gives rise to the spin of the electron is generated from two current-vector fields (CVFs). Each CVF comprises a continuum of correlated *orthogonal great circle current-density elements (one dimensional "current loops").* The current pattern comprising each CVF is generated over a half-sphere surface by a set of rotations of two

[1] The atomic orbital has zero thickness, but in order that the speed of light is a constant maximum in any frame including that of the gravitational field that propagates out as a light-wave front at particle production, it gives rise to a spacetime dilation equal to $2\pi$ times the Newtonian gravitational or Schwarzschild radius $r_g=\frac{2Gm_e}{c^2}=1.3525\ X\ 10^{-57}\ m$ according to Eqs. (32.36) and (32.140b) and the discussion at the footnote after Eq. (32.40). This corresponds to a spacetime dilation of $8.4980\ X\ 10^{-57}\ m$ or $2.8346\ X\ 10^{-65}\ s$. Although the atomic orbital does not occupy space in the third spatial dimension, its mass discontinuity effectively "displaces" spacetime wherein the spacetime dilation can be considered a "thickness" associated with its gravitational field. The inertial frame of the orbital motion of the bound electron and the atom in motion is with respect to absolute space of the electron and proton as given in the Equivalence of Inertial and Gravitational Masses due Absolute Space and Absolute Light Velocity.

orthogonal great circle current loops that serve as basis elements about each of the $\left(-\mathbf{i}_x, \mathbf{i}_y, 0\mathbf{i}_z\right)$ and $\left(-\frac{1}{\sqrt{2}}\mathbf{i}_x, \frac{1}{\sqrt{2}}\mathbf{i}_y, \mathbf{i}_z\right)$-axis; the span being $\pi$ radians. Then, the two CVFs are convoluted, and the result is normalized to exactly generate the *continuous* uniform electron current density function $Y_0^0(\theta,\phi)$ covering a spherical shell and having the three angular momentum components of $\mathbf{L}_{xy} = +/-\frac{\hbar}{4}$ and $\mathbf{L}_z = \frac{\hbar}{2}$ (Figure 1.23)[2]. There is acceleration without radiation, in this case, centripetal acceleration. A static charge distribution exists even though there is acceleration along a great circle at each point on the surface. Haus' condition predicts no radiation for the entire ensemble.

In cases of orbitals of heavier elements and excited states of one-electron atoms and atoms or ions of heavier elements which are not constant as given by Eq. (1.29), the constant spin function is modulated by a time and spherical harmonic function. The modulation or traveling charge-density wave corresponds to an orbital angular momentum, in addition to a spin angular momentum. These states are typically referred to as p, d, f, etc. orbitals and correspond to an $\hbar$ quantum number not equal to zero. Haus' condition also predicts nonradiation for a constant spin function modulated by a time and spherically harmonic orbital function. However, in the case that such a state arises as an excited state by photon absorption, it is radiative due to a radial dipole term in its current-density function since it possesses spacetime Fourier transform components synchronous with waves traveling at the speed of light, as given in the Instability of Excited States section.

In the case of an excited state, the charge-density function of the electron atomic orbital can be modulated by the corresponding "trapped" photon to give rise to orbital angular momentum about the z-axis. The "trapped photon" is a "standing electromagnetic wave" which actually is a circulating wave that propagates around the z-axis. Its source current superimposes with the current-density of the atomic orbital at its radius corresponding to a radial Dirac delta function at the electron radius, $\delta\left(r - r_n\right)$, and due to relativistic effects the field is radially local at the electron. In order to satisfy the boundary (phase) condition at the atomic orbital surface, the angular and time functions of the photon must match those of its source current which modulates the atomic orbital charge-density function as given in the Equation of the Electric Field Inside the Atomic Orbital section. The time-function factor, *k(t)*, for the photon "standing wave" is identical to the time-function factor of the atomic orbital. Thus, the angular frequency of the "trapped photon" has to be identical to the angular frequency of the electron atomic orbital, $\omega_n$ given by Eq. (1.36). However, the linear velocity of the multipole modulation component is not given by Eq. (1.35)—the orbital angular frequency is with respect to the z-axis; thus, the distance from the z-axis, $\rho = r_n \sin\theta$, must be substituted for the atomic orbital radius of Eq. (1.35).

$Y_\ell^m(\theta,\phi)$ is called the angular orbital function corresponding to the quantum numbers $\ell = 0, 1, 2, 3, 4,...;\ \mathrm{m}_\ell = -\ell, -\ell + 1, ..., 0, ..., +\ell$. $Y_\ell^m(\theta,\phi)$ can be thought of as a modulation function. The charge density of the entire atomic orbital is the total charge divided by the total area, $\frac{-e}{4\pi r_n^2}$. The fraction of the charge of an electron in any area element is given by:

$$N\left[Y_0^0(\theta,\phi) + Y_\ell^m(\theta,\phi)\right] r_n^2 \sin\theta d\theta d\phi, \tag{1.25}$$

where $N$ is the normalization constant. Therefore, the normalization constant is given by:

$$-e = N r_n^2 \int_0^{\pi}\int_0^{2\pi} \left[Y_0^0(\theta,\phi) + Y_\ell^m(\theta,\phi)\right] \sin\theta d\theta d\phi \tag{1.26}$$

For $\ell = 0$, $N = \frac{-e}{8\pi r_n^2}$. For $\ell \neq 0$, $N = \frac{-e}{4\pi r_n^2}$. The quantum numbers of the spherical harmonic currents can be related to the observed electron orbital angular momentum states. The current is constant at every point on the surface for the s orbital corresponding to $Y_0^0(\theta,\phi)$. The charge-density functions including the time-function factor corresponding to s, p, d, f, etc. orbitals are

$\ell = \mathbf{0}$

$$\rho(r,\theta,\phi,t) = \frac{e}{8\pi r_n^2}[\delta(r - r_n)]\left[Y_0^0(\theta,\phi) + Y_\ell^m(\theta,\phi)\right] \tag{1.27}$$

$\ell \neq \mathbf{0}$

[2] $+/-$ designates both the positive and negative vector directions along an axis in the xy-plane.

$$\rho(r,\theta,\phi,t)=\frac{e}{4\pi r_n^2}[\delta(r-r_n)]\left[Y_0^0(\theta,\phi)+\mathrm{Re}\left\{\pi\left(R_z(\omega_n t)\right)Y_\ell^m(\theta,\phi)\right\}\right] \tag{1.28}$$

$$\rho(r,\theta,\phi,t)=\frac{e}{4\pi r_n^2}[\delta(r-r_n)]\left[Y_0^0(\theta,\phi)+\mathrm{Re}\left\{Y_\ell^m(\theta,\phi)e^{im\omega_n t}\right\}\right] \tag{1.29}$$

where to keep the form of the spherical harmonic as a traveling wave about the z-axis $\pi(R_z)$ is the representation of the rotational matrix about the z-axis $R_z$ (Eq. (1.82)) in the space of functions $\pi\left(R_z(\omega_n t)\right)Y_\ell^m(\theta,\phi)=Y_\ell^m(\theta,\phi+m\omega_n t)$ and $\mathrm{Re}\left\{Y_\ell^m(\theta,\phi)e^{im\omega_n t}\right\}=P_\ell^m(\cos\theta)\cos(m\phi+m\omega_n t)$[3]. Each of the Eqs. (1.28-1.29) represents a traveling charge-density wave that moves on the surface of the atomic orbital about the z-axis with frequency $\omega_n$ and modulates the atomic orbital corresponding to $\ell=0$. The latter gives rise to spin angular momentum as given in the Spin Angular Momentum of the Atomic Orbital $Y_0^0(\theta,\phi)$ with $\ell = 0$ section. The spin and orbital angular momentum may couple as given in the Orbital and Spin Splitting section. In the cases that $\ell\neq 0$ and $m=0$, the charge is moving or rotating about the z-axis with frequency $\omega_n$, but the charge density is not time dependent. The photon equations that correspond to the atomic orbital states, Eqs. (1.27-1.29), are given in the Excited States of the One-Electron Atom (Quantization) section. It is shown in Appendix I: Nonradiation Condition that in addition to Haus' condition, the atomic orbital states given by Eqs. (1.27-1.29) are nonradiative with the same relationships given by Eqs. (1.15-1.16) applied to the vector potential.

For $n$ = 1, and $\ell$ = 0, $m$ = 0, and $s$ = 1/2, the charge (and mass) distribution is spherically symmetric and $M_{1,0,0,1/2}=-4.553\ Cm^{-2}$ everywhere on the atomic orbital. Similarly, for $n=2$, $\ell$ = 0, $m=0$, and $s=1/2$, the charge distribution everywhere on the sphere is $M_{2,0,0,1/2}=-1.138\ Cm^{-2}$. For $n$ = 2, $\ell$ = 1, $m$ = 0, and $s$ = 1/2, the charge distribution varies with $\theta$. $Y_1^0(\phi,\theta)$ is a maximum at $\theta=0°$ and the charge density is also a maximum at this point, $M_{2,1,0,1/2}(\theta=0°)=-2.276\ Cm^{-2}$. The charge density decreases as $\theta$ increases; a minimum in the charge density is reached at $\theta=180°$, $M_{2,1,0,1/2}(\theta=180°)=0\ Cm^{-2}$.

For $\ell$ = 1 and $m=\pm1$, the spherical harmonics are complex, and the angular functions comprise linear combinations of

$$Y_{1,x}=\sin\theta\cos\phi \tag{1.30}$$

$$Y_{1,y}=\sin\theta\sin\phi \tag{1.31}$$

Each of $Y_{1,x}$ and $Y_{1,y}$ is the component factor part of a phasor. They are not components of a vector; however, the $x$ and $y$ designation corresponds, respectively, to the historical $p_x$ and $p_y$ probability-density functions of quantum mechanics. $Y_{1,x}$ is a maximum at $\theta=90°$ and $\phi=0°$; $M_{2,1,x,1/2}(90°,0°)=-1.138\ Cm^{-2}$. Figure 1.2 gives pictorial representations of how the modulation function changes the electron density on the atomic orbital for several $\ell$ values[4]. Figure 1.3 gives a pictorial representation of the charge-density wave of a p orbital that modulates the constant spin function and rotates around the z-axis. A single time point is shown for $\ell$ = 1 and $m=\pm1$ in Eqs. (1.28-1.29).

---

[3] In Eq. (1.28), $Y_0^0(\theta,\phi)$, a constant function, is added to a spherical harmonic function wherein each term $\mathrm{Re}\left\{\pi\left(R_z(\omega_n t)\right)Y_\ell^m(\theta,\phi)\right\}$ and $\mathrm{Re}\left\{Y_\ell^m(\theta,\phi)e^{im\omega_n t}\right\}$ represents a modulation function rotated in time. The latter is defined as a phasor corresponding to the modulation function spinning about the z-axis. This is equivalent to the constant function (first term) modulated by the spherical harmonic function (second term) that spins around the z-axis and comprises a traveling modulation wave. One rotation of the spherical harmonic function occurs in one period.

[4] When the electron charge appears throughout this text in a function involving a linear combination of the spin and orbital functions, it is implicit that the charge is normalized. The integral of the constant mass-density function corresponding to spin over the atomic orbital is the mass of the electron. The integral of any spherical harmonic modulation function corresponding to orbital angular momentum over the atomic orbital is zero. The modulated mass-density function has a lower limit of zero due to the trapped photon that is phase-locked to the modulation function. And, the mass density cannot be negative. Thus, the maximum magnitude of the unnormalized spherical harmonic function over all angles must be one. The summation of the constant function and the orbital function is normalized.

**Figure 1.2.** The orbital function modulates the constant (spin) function, (shown for t = 0; three-dimensional view).

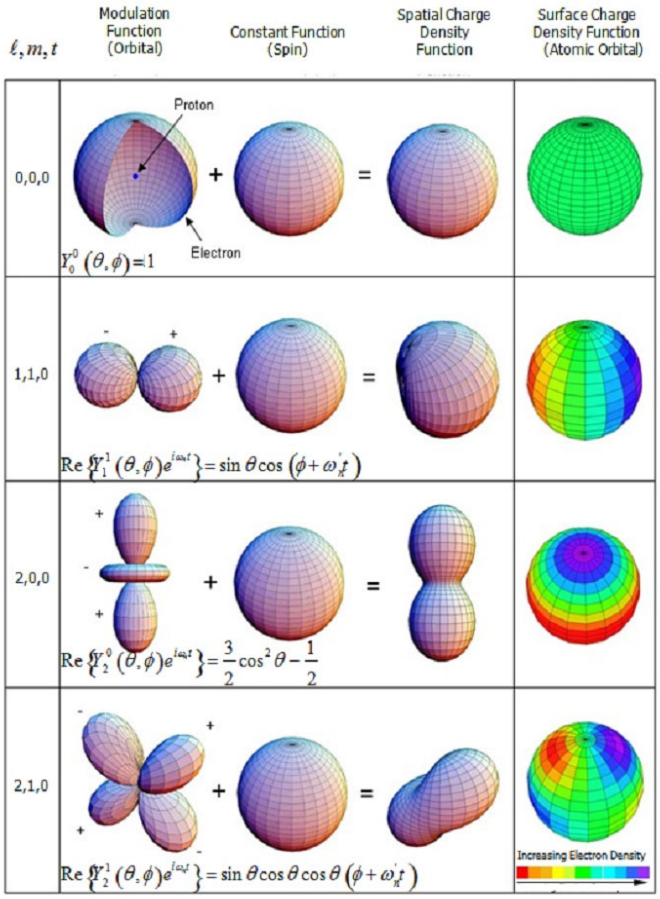
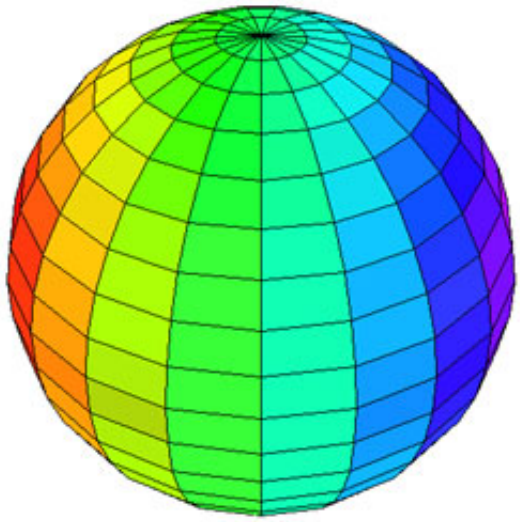



**Figure 1.3.** A pictorial representation of the charge-density wave of a p orbital that modulates the constant spin function and travels on the surface of the atomic orbital around the z-axis. A single time point is shown for $\ell = 1$ and $m = \pm 1$ in Eq. (1.36). The charge density increases from red to violet. The z-axis is the vertical axis.



## CLASSICAL PHYSICS OF THE DE BROGLIE RELATION

Consider the constant function $Y_0^0(\theta,\phi)$ of Eqs. (1.27-1.29). The angular velocity must be constant (at a given $n$) because $r$ is constant and the energy and angular momentum are constant. Given time-harmonic motion and a radial delta function, the relationship between an allowed radius and the electron wavelength is given by Eq. (1.15). The allowed angular frequencies are related to the allowed frequencies by:

$$\omega_n = 2\pi\nu_n \tag{1.32}$$

The allowed velocities are related to allowed frequencies and wavelengths by:

$$v_n = \nu_n\lambda_n \tag{1.33}$$

The allowed velocities and angular frequencies are related to $r_n$ by:

$$v_n = 2\pi r_n\nu_n = r_n\omega_n \tag{1.34}$$

such that magnitude of the velocity and the angular frequency for *every* point on the surface of the bound electron and their relationships with the wavelengths and $r_n$ are:

$$v_n = \frac{\hbar}{m_e r_n} = \frac{h}{m_e\lambda_n} = \frac{h}{m_e 2\pi r_n} = \frac{\hbar}{m_e r_n} \tag{1.35}$$

$$\omega_n = \frac{\hbar}{m_e r_n^2} \tag{1.36}$$

where the velocity (Eq. (1.35)) and angular frequency (Eq. (1.36)) are determined by the boundary conditions that the angular momentum density at each point on the surface is constant and the magnitude of the total angular momentum of the atomic orbital $\mathbf{L}$ must also be constant. The constant total is $\hbar$ given by the integral:

$$\begin{aligned}\mathbf{m} &= \int \frac{1}{4\pi r^2}\left|\mathbf{r}\times m_e\mathbf{v}\right|\delta\left(r-r_n\right)dx^3 \\ &= m_e r_n\frac{\hbar}{m_e r_n} = \hbar\end{aligned} \tag{1.37}$$

Special relativity requires that the mathematical equations expressing the laws of nature must be covariant, invariant in form, under the transformations of the Lorentz group [7]. The integral of the magnitude of the angular momentum of the electron is always $\hbar$ for any state and is ***relativistically invariant*** since as shown by Eq. (1.37) the angular momentum is invariant of radius or velocity. It is a Lorentz scalar $\mathbf{L} = \hbar$ with respect to the radius of the state. The vector projections of the atomic orbital spin angular momentum relative to the Cartesian coordinates arrived at by summation of the contributions from the electron current elements are given in the Spin Angular Momentum of the Atomic Orbital $Y_0^0(\theta,\phi)$ with $\ell = 0$ section. The same relationship applies to the photon as well as given by Eq. (4.1). Eq. (1.35) also gives the de Broglie relationship:

$$\lambda_n = \frac{h}{p_n} = \frac{h}{m_e v_n} \tag{1.38}$$

The free electron is equivalent to a continuum-excited state with conservation of the parameters of the bound electron. Thus, the de Broglie relationship applied to the free electron is again due to conservation of the electron's angular momentum of $\hbar$. Specifically, it is shown in the Free Electron section that the free electron is a two-dimension lamina of charge with an azimuthal current with a corresponding angular momentum of $\hbar$. The linear velocity of the free electron can be considered to be due to absorption of photons that excite surface currents corresponding to a decreased electron de Broglie wavelength:

$$\lambda_o = \frac{h}{m_e v_z} = 2\pi\rho_0 \tag{1.39}$$

The relationship between the electron wavelength, its radius, $\rho_0$, and its linear velocity is:

$$\frac{\lambda}{2\pi} = \rho_0 = \frac{\hbar}{m_e v_z} = k^{-1} = \frac{v_z}{\omega_z} \tag{1.40}$$

In this case, the angular frequency $\omega_z$ is given by:

$$\omega_z = \frac{\hbar}{m_e\rho_0^2} \tag{1.41}$$

which conserves the photon's angular momentum of $\hbar$ with that of the electron.

It is further shown (Eq. (3.51)) that the total energy $E_T$, is given by the sum of the change in the free-electron translational kinetic energy, $T$, the rotational energy of the azimuthal current, $E_{rot}$, and the corresponding magnetic potential energy, $E_{mag}$:

$$\begin{aligned} E_T &= T + E_{rot} + E_{mag} \\ &= \frac{1}{2}\frac{\hbar^2}{m_e\rho_0^2} + \frac{5}{4}\frac{\hbar^2}{m_e\rho_0^2} - \frac{5}{4}\frac{\hbar^2}{m_e\rho_0^2} = \frac{1}{2}\frac{\hbar^2}{m_e\rho_0^2} \end{aligned} \tag{1.42}$$

Thus, the total energy, $E_T$, of the excitation of a free-electron transitional state by a photon having $\hbar$ of angular momentum and an energy given by Planck's equation of $\hbar\omega$ is:

$$E_T = T = \frac{1}{2}m_e v_z^2 = \frac{1}{2}\frac{h^2}{m_e\lambda^2} = \frac{1}{2}\hbar\omega_z \tag{1.43}$$

where $\lambda$ is the de Broglie wavelength. The angular momentum of the free electron of $\hbar$ is unchanged. The energies in the currents in the plane lamina are balanced so that the total energy is unchanged. The radius $\rho_0$ decreases to match the de Broglie wavelength and frequency at an increased velocity. At this velocity, the kinetic energy matches the energy provided by the photon wherein the de Broglie frequency matches the photon frequency and both the electron-kinetic energy and the photon energy are given by Planck's equation.

The correspondence principle is the basis of the de Broglie wavelength relationship. The de Broglie relationship is not an independent fundamental property of matter in conflict with physical laws as formalized in the wave-particle-duality-related postulates of quantum mechanics and the corresponding Schrödinger wave equation. The Stern-Gerlach experimental results and the double-slit interference pattern of electrons are also predicted classically as given in the Physics of Classical Electron Diffraction Resolves the Wave-Particle Duality Mystery of Quantum Mechanics section.

## ROTATIONAL PARAMETERS OF THE ELECTRON (ANGULAR MOMENTUM, ROTATIONAL ENERGY, AND MOMENT OF INERTIA)

The spin function corresponds to $\ell = 0$. The electron atomic orbital experiences a constant potential energy because it is fixed at $r = r_n$. In general, the kinetic energy for an inverse squared electric force is half the potential energy. It is the rotation of the atomic orbital, projections of the uniform current density, that causes spin angular momentum. The rotational energy of a rotating body, $E_{rot}$, is

$$E_{rot} = \frac{1}{2}I\omega^2 = \frac{1}{2}I\left(\frac{v}{r}\right)^2 \tag{1.44}$$

where $I$ is the moment of inertia and $\omega$ is the angular velocity. The angular momentum is given by:

$$\mathbf{L} = I\omega\mathbf{i}_z \tag{1.45}$$

The angular velocity must be constant (at a given $n$) because $r$ is constant and the energy and angular momentum are constant. The total kinetic energy, $T$, of the atomic orbital spin function $Y_0^0(\phi,\theta)$ is:

$$T = \frac{1}{2}m_e v_n^2 \tag{1.46}$$

Substitution of Eq. (1.35) gives:

$$T = \frac{\hbar^2}{2m_e r_n^2} \tag{1.47}$$

One result of the correlated motion along great circles is that some of the kinetic energy is not counted in the rotational energy (i.e. for any spin axis, there will be an infinite number of great circles with planes passing through that axis with $\theta$ angles other than $90°$). All points on any one of these great circles will be moving, but not all of that motion will be part of the rotational energy; only that motion perpendicular to the spin axis will be part of the rotational energy. Thus, the rotational kinetic energy will always be less than the total kinetic energy. Furthermore, the following relationships must hold.

$$E_{rotational} = \frac{1}{2}I\omega^2 \le T = \frac{1}{2}m_e v^2 \tag{1.48}$$

$$I\omega \le L = \hbar \tag{1.49}$$

$$I \le m_e r^2 \tag{1.50}$$

Additionally, it is known from the Stern-Gerlach experiment that a beam of silver atoms splits into two components when passed through an inhomogeneous magnetic field. This experiment implies a magnetic moment of one Bohr magneton and an associated angular momentum quantum number of 1/2. Historically, this quantum number is called the spin quantum number, and that designation will be retained. The angular momentum can be thought of as arising from a spin component or equivalently from an orbital component of the spin. The z-axis projection of the spin angular momentum was derived in the Atomic Orbital Equation of Motion For $\ell = 0$ Based on the Current Vector Field (CVF) section and is:

$$\mathbf{L}_z = I\omega \mathbf{i}_z = \pm\frac{\hbar}{2} \tag{1.51}$$

where $\omega$ is given by Eq. (1.36); so, for $\ell = 0$

$$\mathbf{L}_z = I\frac{\hbar}{m_e r^2}\mathbf{i}_z = \frac{\hbar}{2}\mathbf{i}_z \tag{1.52}$$

Thus,

$$I_z = I_{spin} = \frac{m_e r_n^{\,2}}{2} \tag{1.53}$$

From Eq. (1.44),

$$E_{rotational\ \ spin} = \frac{1}{2}\left[I_{spin}\omega^2\right] \tag{1.54}$$

From Eqs. (1.36) and (1.53),

$$E_{rotational} = E_{rotational\ \ spin} = \frac{1}{2}\left[I_{spin}\left(\frac{\hbar}{m_e r_n^{\,2}}\right)^2\right] = \frac{1}{2}\left[\frac{m_e r_n^{\,2}}{2}\left(\frac{\hbar}{m_e r_n^{\,2}}\right)^2\right] = \frac{1}{4}\left[\frac{\hbar^2}{2I_{spin}}\right] \tag{1.55}$$

## ELECTRON MECHANICS AND THE CORRESPONDING CLASSICAL WAVE EQUATION FOR THE DERIVATION OF THE ROTATIONAL PARAMETERS OF THE ELECTRON

When $\ell \neq 0$, the spherical harmonic is not a constant and the charge-density function is not uniform over the atomic orbital. Thus, the angular momentum can be thought of arising from a spin component and an orbital component. The charge, mass, energy, and angular momentum of the electron are constant, and the flow of current must be conservative and without radiation. The corresponding dynamic charge and mass-density functions are time and spherically harmonic and are interchangeable by the conversion factor of the corresponding ratio $m_e / e$. In order to match the source current condition of Maxwell's equations, the multipole of the current density must be constant. Then, the spatial and time motion obeys a classical wave equation. The boundary conditions on conservation of kinetic energy and angular momentum, for azimuthal current flow about a defined axis at the angular frequency $\omega_n$ given by Eq. (1.36), require classical wave behavior, as well, and the corresponding rotational energy equation is given by the rigid rotor equation [8].

In the derivation of the rotational energy and related parameters, first consider that the electron atomic orbital experiences a constant potential energy because it is fixed at $r = r_n$. The boundary condition is that the modulation of the charge density by a traveling wave is not dissipative corresponding to absence of radiation and further has a time average of zero kinetic energy. The mechanics of motion is such that there is a time and spatially harmonic redistribution of matter and kinetic energy that flows on the surface such that the total of either is unchanged. Wave motion has such behavior and the corresponding equation is a wave equation that is solved with energy degeneracy and a time average of zero for the charge and energy flow as the boundary constraints. In this case, the energy degeneracy is only lifted due to the electrodynamic interaction with an applied field consistent with experiential observations, as given in the Orbital and Spin Splitting section.

The general form of the classical wave equation[5] applies to the mechanics of the bound electron

$$\left[\nabla^2 - \frac{1}{v^2}\frac{\partial^2}{\partial t^2}\right]\rho(r,\theta,\phi,t) = 0 \tag{1.56}$$

where $\rho(r,\theta,\phi,t)$ is the function of the electron in time and space. Here, the current densities of $\rho(r,\theta,\phi,t)$ comprise time

[5] This is not to be confused with the Schrödinger equation that is not a proper wave equation; rather, it is a diffusion equation.

harmonics and the spherical harmonics on a two-dimensional spherical surface (Eqs. (1.28-1.29)) for the temporal and spatial functions. Thus, the mechanics equation is given by

$$\left[\nabla^2_{\theta,\phi}-\frac{1}{v^2}\frac{\partial^2}{\partial t^2}\right]\frac{e}{4\pi r^2}[\delta(r-r_n)]\left[Y_0^0(\theta,\phi)+\mathrm{Re}\left\{Y_\ell^m(\theta,\phi)e^{im\omega_n t}\right\}\right]=0 \tag{1.57}$$

Since the rotation is defined to be about the z-axis, the velocity $v$ in Eq. (1.57) is *not constant*, but has the same angular dependence as the corresponding spherical harmonic $Y_\ell^m(\theta,\phi)$ where the motion is azimuthal to the radius. In general, the spherical harmonic charge density functions satisfy the equation [3]:

$$-\left[\frac{1}{\sin\theta}\frac{\partial}{\partial\theta}\left(\sin\theta\frac{\partial}{\partial\theta}\right)_{r,\phi}+\frac{1}{\sin^2\theta}\left(\frac{\partial^2}{\partial\phi^2}\right)_{r,\theta}\right]Y_{\ell,m_\ell}(\theta,\phi)=\ell(\ell+1)Y_{\ell,m_\ell}(\theta,\phi) \tag{1.58}$$

which may be written in the form:

$$L^2Y_{\ell,m_\ell}(\theta,\phi)=\ell(\ell+1)Y_{\ell,m_\ell}(\theta,\phi) \tag{1.59}$$

The charge/mass flow corresponding to Eq. (1.12) and Eqs. (1.28-1.29) time averages to zero and corresponds to modulation of the constant spin function. Similarly, the current densities are eigenfunctions such that kinetic energy flow time averages to zero and corresponds to the modulation of the constant kinetic energy of the spin function. The amplitude of the orbital rotational energy can be solved from the mechanics equation (Eq. (1.57)) operating on $\mathrm{Re}\left\{Y_\ell^m(\theta,\phi)e^{im\omega_n t}\right\}$. Since the motion of the atomic orbital is transverse to the radius, the motion constitutes an inertial frame that is ***relativistically invariant***, as given in the Special Relativistic Effect on the Electron Radius and the Relativistic Ionization Energies section. The total spin angular momentum of the electron is an invariant Lorentz scalar $\mathbf{L}=\hbar$ [7], as given in the Atomic Orbital Equation of Motion For $\ell=0$ Based on the Current Vector Field (CVF) section, and the time-averaged orbital angular momentum is zero that is also a Lorentz scalar $\mathbf{L}=0$. By expressing the wave equation in the energy form, the angular dependent velocity may be eliminated, and this equation can be solved using the boundary constraints. The time and angular functions are separable.

$$\left[\frac{1}{r_n^2\sin\theta}\frac{\partial}{\partial\theta}\left(\sin\theta\frac{\partial}{\partial\theta}\right)_{r,\phi}+\frac{1}{r_n^2\sin^2\theta}\left(\frac{\partial^2}{\partial\phi^2}\right)_{r,\theta}-\frac{1}{v^2}\frac{\partial^2}{\partial t^2}\right]A(\theta,\phi,t)=0 \tag{1.60}$$

where $\rho(r,\theta,\phi,t)=f(r)A(\theta,\phi,t)=\frac{1}{r^2}\delta(r-r_n)A(\theta,\phi,t)$ *and* $A(\theta,\phi,t)=Y(\theta,\phi)k(t)$. The mass of an electron is superimposable with its charge. That is, the angular mass-density function, $A(\theta,\phi,t)$, is also the angular charge-density function. Elimination of the separable time function of Eq. (1.60) gives:

$$\left[\nabla^2+\frac{\omega^2}{v^2}\right]Y_\ell^m(\theta,\phi)=0 \tag{1.61}$$

Eq. (1.61) can be expressed in terms of the wavenumber and wavelength:

$$\left[\nabla^2+k^2\right]Y_\ell^m(\theta,\phi)=0 \tag{1.62}$$

$$\left[\nabla^2+\left(\frac{2\pi}{\lambda}\right)^2\right]Y_\ell^m(\theta,\phi)=0 \tag{1.63}$$

Using Eq. (1.44) and the de Broglie relationship (Eq. (1.38)) based on conservation of angular momentum gives the relationships:

$$\frac{(2\pi r)^2}{\lambda^2}=\frac{2m_e r_n^2E_{rot}}{\hbar^2}=\frac{2IE_{rot}}{\hbar^2} \tag{1.64}$$

Substitution of Eq. (1.64) into Eq. (1.63) gives the well-known rigid rotor equation [8]:

$$-\frac{\hbar^2}{2I}\left[\frac{1}{\sin\theta}\frac{\partial}{\partial\theta}\left(\sin\theta\frac{\partial}{\partial\theta}\right)_{r,\phi}+\frac{1}{\sin^2\theta}\left(\frac{\partial^2}{\partial\phi^2}\right)_{r,\theta}\right]Y(\theta,\phi)=E_{rot}Y(\theta,\phi) \tag{1.65}$$

The energies corresponding to Eq. (1.65) are given by [8]:

$$E_{rot}=\frac{\hbar^2\ell(\ell+1)}{2I}=\frac{\hbar^2\ell(\ell+1)}{2m_e r_n^2}\quad \ell=1,2,3,..., \tag{1.66}$$

and the solution of Eq. (1.65) for $\mathbf{L}$, the orbital angular momentum defined to be about the z-axis, is

$$\mathbf{L} = \hbar\sqrt{\ell(\ell+1)}\mathbf{i}_z \tag{1.67}$$

where the moment of inertia, $I$, assumed by McQuarrie [8] is that of a point particle, $mr_n^2$. It is demonstrated by Eq. (1.37) that the total integrated magnitude of the angular momentum density over the surface of the electron atomic orbital is $\hbar$; therefore, the magnitude of the angular momentum of an electron atomic orbital about the z-axis must be less than $\hbar$, and the corresponding moment of inertia must be less than that given by $m_e r_n^2$. For example, the moment of inertia of the uniform spherical shell, $I_{RS}$,
is [9]:

$$I_{RS} = \frac{2}{3}mr_n^2 \tag{1.68}$$

The current density of the electron is a two-dimensional shell with a constant or a constant plus a spherical harmonic angular dependence. In this case, the relationships given by Eqs. (1.48-1.50) must hold. Eq. (1.65) can be expressed in terms of the variable $x$ that is substituted for $\cos\theta$. The resulting function $P(x)$ is called Legendre's equation and is a well-known equation in classical physics. It occurs in a variety of problems that are formulated in spherical coordinates. When the power series method of solution is applied to $P(x)$, the series must be truncated in order that the solutions be finite at $x = \pm 1$. The solution to Legendre's equation given by Eq. (1.66) is the maximum term of a series of solutions corresponding to the $m_\ell$ and $\ell$ values [8, 10]. The rotational energy must be normalized by the total number of states—each corresponding to a set of quantum numbers of the power series solution. As demonstrated in the Excited States of the One-Electron Atom (Quantization) section, the quantum numbers of the excited states are:

$$\begin{aligned} &n = 2,3,4,... \\ &\ell = 1,2,...,n-1 \\ &m_\ell = -\ell,-\ell+1,...,0,...,+\ell \end{aligned} \tag{1.69}$$

In the case of an atomic orbital excited state, each rotational state solution of Eq. (1.65) (Legendre's equation) corresponds to a multipole moment of the charge-density function (Eqs. (1.28-1.29)). The orbital rotational energy $E_{rotational\ orbital}$ is given by normalizing $E_{rot}$ (Eq. (1.66)) using $N_{\ell,s}$, the total number of multipole moments where each corresponds to an $\ell$ and $m_\ell$ quantum number of an energy level corresponding to a principal quantum number of $n$:

$$N_{\ell,s} = \sum_{\ell=0}^{n-1}\sum_{m_\ell=-\ell}^{+\ell} 1 = \sum_{\ell=0}^{n-1} 2\ell+1 = n^2 = (\ell+1)^2 = \ell^2+2\ell+1 \tag{1.70}$$

Multiplication of Eq. (1.66) by the normalization factor $N_{\ell,s}^{-1}$ given by Eq. (1.70) and substitution of the angular velocity given by Eq. (1.36) results in:

$$E_{rotational\ orbital} = \frac{\hbar^2}{2I}\frac{\ell(\ell+1)}{\ell^2+2\ell+1} = \frac{\hbar^2}{2I}\frac{\ell}{\ell+1} = \frac{\hbar^2}{2m_e r_n^{\,2}}\frac{\ell}{\ell+1} \qquad \ell = 1,2,3,..., \tag{1.71}$$

Multiplication of Eq. (1.67) by the normalization factor $N_{\ell,s}^{-1}$ given by Eq. (1.70) and using Eq. (1.36) gives the corresponding orbital angular momentum, $L_{orbital}$, and moment of inertia , $I_{orbital}$, of the atomic orbital where $\ell \neq 0$:

$$\mathbf{L}_{orbital} = I\omega\mathbf{i}_z = I_{orbital}\omega\mathbf{i}_z = m_e r_n^{\,2}\sqrt{\frac{\ell(\ell+1)}{\ell^2+2\ell+1}}\omega\mathbf{i}_z = m_e r_n^{\,2}\frac{\hbar}{m_e r_n^{\,2}}\sqrt{\frac{\ell}{\ell+1}}\mathbf{i}_z = \hbar\sqrt{\frac{\ell}{\ell+1}}\mathbf{i}_z \tag{1.72}$$

$$I_{orbital} = m_e r_n^{\,2}\sqrt{\frac{\ell(\ell+1)}{\ell^2+2\ell+1}} = m_e r_n^{\,2}\sqrt{\frac{\ell}{\ell+1}} \tag{1.73}$$

where

$$\sqrt{\frac{\ell}{\ell+1}} < 1 \tag{1.74}$$

consistent with Eq. (1.50).

In the case of the excited states with $\ell \neq 0$, the atomic orbital charge-density functions are given by Eqs. (1.28-1.29), and the total angular momentum is the sum of two functions of equal magnitude. $\mathbf{L}_{ztotal}$ is given by the sum of the spin and orbital angular momentum. The principal energy levels of the excited states are split when a magnetic field is applied. The energy shifts due to spin and orbital angular momentum are given in the Orbital and Spin Splitting section.

$$L_{z\ total} = L_{z\ spin} + L_{z\ orbital} \tag{1.75}$$

Similarly, the orbital rotational energy arises from a spin function (spin angular momentum) modulated by a spherical harmonic angular function (orbital angular momentum). The time-averaged mechanical angular momentum and rotational energy associated with the traveling charge-density wave on the atomic orbital is zero:

$$\langle L_{z\ orbital}\rangle = 0 \tag{1.76}$$

$$\langle E_{rotational\ orbital} \rangle = 0 \tag{1.77}$$

In the case of an excited state, the angular momentum comprising a Lorentz scalar $\mathbf{L} = \hbar$ is carried by the fields of the trapped photon. The energy and angular momentum amplitudes that couple to external magnetic and electromagnetic fields are given by Eq. (1.71) and (1.72), respectively. The rotational energy due to spin is given by Eq. (1.55), and the total kinetic energy is given by Eq. (1.47).

# THE ATOMIC ORBITAL EQUATION OF MOTION FOR $\ell$ = 0 BASED ON THE CURRENT VECTOR FIELD (CVF)

## STERN-GERLACH-EXPERIMENT BOUNDARY CONDITIONS

It is known from the Stern-Gerlach experiment that a beam of silver atoms is split into two components when passed through an inhomogeneous magnetic field. This implies that the electron is a spin 1/2 particle or fermion with an intrinsic angular momentum of $\pm\frac{\hbar}{2}$ that can only exist parallel or antiparallel to the direction of the applied field (spin axis), and the magnitude of the angular momentum vector, which precesses about the spin axis, is $\sqrt{\frac{3}{4}}\hbar$. Furthermore, the magnitude of the splitting implies a magnetic moment of $\mu_B$, a full Bohr magneton, given by Eq. (1.131) corresponding to $\hbar$ of total angular momentum on the axis, implying an impossibility of being classically reconciled with the $\pm\frac{\hbar}{2}$ electron angular momentum. Yet, the extraordinary aspects of the magnetic properties and behavior of the electron are the basis to solve its structure that gives rise to these observations.

Experimentally, the electron has a measured magnetic field and corresponding magnetic moment of a Bohr magneton that can only exist parallel or antiparallel to the direction of the applied magnetic field and behaves as if it possesses only $\frac{\hbar}{2}$ of intrinsic angular momentum. For any magnetic field, the Maxwell's-equations solution for the corresponding source current is unique. Thus, the electron field requires a corresponding unique current according to Maxwell's equations. Several boundary conditions must be satisfied, and the atomic orbital equation of motion for $\ell$ = 0 is solved as a boundary value problem. The boundary conditions are:

(1) to maintain electroneutrality, force balance, absence of a magnetic or electric multipole, and give the proper Lorentz invariant angular momentum, each point position on the atomic orbital surface designates a charge(mass)-density element, and each point element must have the same magnitude of linear and angular velocity given by Eqs. (1.35) and (1.36), respectively;

(2) according to condition 1, every such infinitesimal point element must move along a great circle and the current-density distribution must be uniform;

(3) the electron magnetic moment must align completely parallel or antiparallel with an applied magnetic field in agreement with the Stern-Gerlach experiment;

(4) it is shown *infra* that according to condition #3, the projection of the intrinsic angular momentum of the atomic orbital onto the z-axis must be $\pm\frac{\hbar}{2}$, and the projection into the transverse plane must be $\pm\frac{\hbar}{4}$ to achieve the spin 1/2 aspect;

(5) it is further shown that the Larmor excitation of the electron in the applied magnetic field must give rise to a component of electron spin angular momentum that precesses about the applied magnetic field such that the contribution along the z-axis is $\pm\frac{\hbar}{2}$ and the projection onto the orthogonal axis which precesses about the z-axis must be $\pm\sqrt{\frac{3}{4}}\hbar$;

(6) due to conditions #4 and #5, the angular momentum components corresponding to the current of the atomic orbital and that due to the Larmor precession give rise to a total angular momentum on the applied-field axis of $\pm\hbar$;

(7) due to condition #6, the precessing electron has a magnetic moment of a Bohr magneton, and

(8) the energy of the transition of the alignment of the magnetic moment with an applied magnetic field must be given by Eqs. (1.226-1.227) wherein the g factor and Bohr magneton factors are due to the extended-nature of the electron such that it links flux in units of the magnetic flux quantum and has a total angular momentum on the applied-field axis of $\pm\hbar$.

The algorithm to generate the spin function designated as $Y_0^0(\theta,\phi)$ (part of Eqs. (1.27-1.29)) and called the electron atomic orbital is developed in this section. It was shown in the Classical Physics of the De Broglie Relationship section that the integral of the magnitude of the angular momentum over the atomic orbital must be constant. The constant is $\hbar$ as given by Eq. (1.37). It is shown in this section that the projection of the intrinsic atomic orbital angular momentum onto the spin axis is $\pm\frac{\hbar}{2}$, and the projection onto **S**, the axis that precesses about the spin axis, is $\hbar$ with a precessing component in the perpendicular plane of $\sqrt{\frac{3}{4}}\hbar$ and a component on the spin axis of $\pm\frac{\hbar}{2}$. Thus, the mystery of an intrinsic angular momentum of $\pm\frac{\hbar}{2}$ and a total angular momentum in a resonant RF experiment of $\mathbf{L}_z = \hbar$ is resolved since the sum of the intrinsic component and the spin-axis projection of the precessing component is $\hbar$. The Stern-Gerlach experiment implies a magnetic moment of one Bohr magneton and an associated angular momentum quantum number of 1/2. Historically, this quantum number is called the spin quantum number, s ($s = \frac{1}{2};\ m_s = \pm\frac{1}{2}$), and that designation is maintained.

Consider the derivation of Eq. (1.65). The moment of inertia of a point particle orbiting an axis is $mr^2$, and that of a globe spinning about some axis is $I = \frac{2}{3}mr^2$. For $\ell = 0$, the electron mass and charge are uniformly distributed over the atomic orbital, a two-dimensional spherical shell, but the atomic orbital is *not* analogous to a globe. The velocity of a point mass on a spinning globe is a function of $\theta$, but the magnitude of the velocity at each point of the atomic orbital is not a function of $\theta$. To picture the distinction, it is a useful concept to consider that the continuous current density of the atomic orbital is comprised of an infinite number of point elements that move on the spherical surface. Then, each point on the sphere with mass $m_i$ has the same angular velocity, $\omega_n$, the same magnitude of linear velocity, $v_n$, and the same moment of inertia, $m_i r_n^2$. The motion at each point of the atomic orbital is along a great circle, and the motion along each great circle is correlated with the motion on all other great circles such that the sum of all the contributions of the corresponding angular momentum is different from that of an orbiting point or a globe spinning about an axis. The atomic orbital angular momentum is directed along two orthogonal axes having three angular momentum components of $\mathbf{L}_{xy} = +/-\frac{\hbar}{4}$ and $\mathbf{L}_z = \frac{\hbar}{2}$.

The atomic orbital spin function comprises a constant uniform charge (current) density with moving charge confined to a two-dimensional spherical shell. The current-density is *continuous*, but it may be modeled as a current pattern comprising a superposition of an infinite series of correlated orthogonal great-circle current loops. The equation of motion for each charge-density element (and correspondingly for each mass-density element) corresponds to that of a current on a one-dimensional great circle wherein each point charge(current)-density element moves time harmonically with constant angular velocity, $\omega_n$, given by Eq. (1.36) and has the corresponding velocity, $v_n$, on the surface in the direction of the current given by Eq. (1.35). The distribution of the great circles is such that all of the boundary conditions are satisfied.

The uniform, equipotential charge-density function of the atomic orbital having only a radial discontinuous field at the surface according to Eq. (1.10) is constant in time due to the motion of the current along great circles. The current flowing into any given point of the atomic orbital equals the current flowing out to satisfy the current continuity condition, $\nabla \cdot J = 0$ as in the case of any macrocurrent carried by an ensemble of electrons. There are many crossings amongst great circle elements at single, zero-dimensional points on the two-dimensional surface of the electron embedded in a three-dimensional space. Thus, the velocity direction is multivalued at each point. But, there is nothing in Maxwell's equations in two dimensions that precludes this result, since these laws only regard fields external to the two-dimensional charge density and current density sources. As in the macro-case, the continuous two-dimensional atomic orbital current density distribution constitutes a uniform, constant two-dimensional *supercurrent* (See Figure 1.22 for the vector supercurrent pattern) wherein the crossings have no effect on the current pattern. Each one-dimensional element is independent of the others, and its contribution to the angular momentum and magnetic field independently superimposes with that of the others.

The aspect of no interaction at local zero-dimensional crossings of a two-dimensional fundamental particle has the same properties as the superposition properties of the electric and magnetic fields of a photon from which the electron forms. Field lines of photons traveling at the speed of light also superimpose with the field- and velocity-direction vectors multivalued at each point that they cross. Indeed, the photon field pattern of a single photon shown in the Equation of the Photon section is very similar to the great-circle pattern of the atomic orbital shown *infra*. As shown in the Excited States of the One-Electron Atom (Quantization), the Creation of Matter from Energy, Pair Production, and the Leptons sections, the angular momentum in the

electric and magnetic fields is conserved in excited states and in the creation of an electron from a photon in agreement with Maxwell's equations. Thus, it is useful to regard an electron as a special-state photon.

Thus, the electron as an indivisible fundamental particle is related to the concepts of current and momentum elements, but the great-circle-current-loop basis elements used to generate and represent the bound electron current corresponding to spin should be considered more fundamentally in terms of sources of electric and magnetic field and sources of momentum that in aggregate gives the corresponding properties of the electron as a whole. In fact, as shown in the Gravity section, all physical observables including the laws of nature and the fundamental constants can ultimately only be related to others and have no independent meaning. Then, the basis elements of an electron are understood in terms of what they do when added in aggregate to constitute an electron. The nomenclature used to describe the elements reflects the analogous macroscopic sources and is adopted for convenience.

## GENERATION OF THE ATOMIC ORBITAL CVFS

The atomic orbital spin function comprises a constant charge(current)-density function with moving charge confined to a two-dimensional spherical shell and comprises a uniform complete coverage. The uniform magnetostatic current-density function $Y_0^0(\theta,\phi)$ of the atomic orbital spin function comprises a continuum of correlated orthogonal great-circle current loops wherein each point charge(current)-density element moves time harmonically with constant angular velocity, $\omega_n$, given by Eq. (1.36) and velocity, $v_n$, in the direction of the current given by Eq. (1.35). The current-density function of the atomic orbital is generated from *orthogonal great-circle current-density elements (one dimensional "current loops")* that serve as basis elements to form two distributions of an infinite number of great circles wherein each covers one-half of a two-dimensional spherical shell and is defined as a basis element current vector field ("BECVF") and an atomic orbital current-vector field ("OCVF"). Then, the *continuous* uniform electron current density function $Y_0^0(\theta,\phi)$ (part of Eqs. (1.27-1.29)) that covers the entire spherical surface as a distribution of an infinite number of great circles is generated using the CVFs.

First, the generation of the BECVF is achieved by rotation of two great circle basis elements, one in the x'z'-plane and the other in the y'z'-plane, about the $\left(-\mathbf{i}_x,\mathbf{i}_y,0\mathbf{i}_z\right)$ axis by an infinite set of infinitesimal increments of the rotational angle wherein the current direction is such that the resultant angular momentum vector of the basis elements of $\frac{\hbar}{2\sqrt{2}}$ is stationary on this axis. The generation of the OCVF is achieved by rotation of two great circle basis elements, one in the x'y'-plane and the other in the plane that bisects the x'y'-quadrant and is parallel to the z'-axis, about the $\left(-\frac{1}{\sqrt{2}}\mathbf{i}_x,\frac{1}{\sqrt{2}}\mathbf{i}_y,\mathbf{i}_z\right)$ axis by an infinite set of infinitesimal increments of the rotational angle wherein the current direction is such that the resultant angular momentum vector of the basis elements of $\frac{\hbar}{2}$ having components of $\mathbf{L}_{xy}=\frac{\hbar}{2\sqrt{2}}$ and $\mathbf{L}_z=\frac{\hbar}{2\sqrt{2}}$ is stationary on this axis. The operator to form each CVF comprises a convolution of the rotational matrix of great circles basis elements with an infinite series of delta functions of argument of the infinitesimal angular increment. Then, the uniform great-circle distribution $Y_0^0(\theta,\phi)$ is exactly generated from the CVFs. The BECVF is convolved with the OCVF over a $2\pi$ span that results in the placement of a BECVF at each great circle of the OCVF. Since the angular momentum vector of the BECVF is matched to twice that of one of the OCVF great circle basis elements and the span is over $2\pi$, the resultant angular momentum of the distribution is the same as that of the OCVF, except that coverage of the spherical surface is complete. This current vector distribution is normalized by scaling the constant current of each great circle element resulting in the exact uniformity of the distribution independent of time since $\nabla\cdot K=0$ along each great circle. There is no alteration of the angular momentum by normalization since it only affects the density parallel to the angular momentum axis of the distribution, the $\left(-\frac{1}{\sqrt{2}}\mathbf{i}_x,\frac{1}{\sqrt{2}}\mathbf{i}_y,\mathbf{i}_z\right)$-axis. Then, the boundary conditions of $Y_0^0(\theta,\phi)$ having the desired angular momentum components, coverage, element motion, and uniformity are shown to have been achieved by designating the $\left(-\frac{1}{\sqrt{2}}\mathbf{i}_x,\frac{1}{\sqrt{2}}\mathbf{i}_y,\mathbf{i}_z\right)$-axis as the z-axis. The resulting exact uniform current distribution (Figure 1.22) has the angular momentum components of $\mathbf{L}_{xy}=+/-\frac{\hbar}{4}$ and $\mathbf{L}_z=\frac{\hbar}{2}$ (Eqs. (1.127-1.128) and Figure 1.23).

The z-projection of the angular momentum of a photon given by its orthogonal electric and magnetic fields is $\mathbf{m}=\int\frac{1}{8\pi c}\mathrm{Re}\left[\mathbf{r}\times(\mathbf{E}\times\mathbf{B}^*)\right]dx^4=\hbar$ (Eq. (4.1)). When an electron is formed from a photon as given in the Leptons section, the angular momentum is conserved in the projections of the orthogonal great circle current loops that serve as the basis elements of the atomic orbital. Special relativity requires that the mathematical equations expressing the laws of nature must be covariant, that is, invariant in form, under the transformations of the Lorentz group. As shown by Eq. (1.37) the angular momentum is invariant of radius or velocity. It is a Lorentz scalar $\mathbf{L}=\hbar$ [7] with respect to the radius of the state. The vector projections of

the atomic orbital spin angular momentum relative to the Cartesian coordinates arrived at by summation of the contributions from the electron current elements of the current distribution are given in the Spin Angular Momentum of the Atomic Orbital $Y_0^0(\theta,\phi)$ with $\ell = 0$ section. The *time-independent* current pattern is obtained by defining a basis set for generating the current distribution over the surface of a spherical shell of zero thickness.

As such a basis set, consider that the electron current is distributed within the basis elements and then distributed evenly amongst all great circles such that the final distribution $Y_0^0(\theta,\phi)$ possesses $\hbar$ of angular momentum before and after normalization. First, the basis element BECVF is generated from two orthogonally linked great-circle current loops having $\frac{\hbar}{4}$ apiece and a resultant angular momentum of $\frac{\hbar}{2\sqrt{2}}$. The OCVF is generated from two orthogonally linked great-circle current loops having an angular momentum of $\frac{\hbar}{2\sqrt{2}}$ apiece and a resultant angular momentum of $\frac{\hbar}{2}$. The current pattern of each CVF is generated over the surface by a corresponding infinite set of infinitesimal rotations of the two orthogonal great-circle current loops that serve as basis elements by $\pi$ radians about the $\left(-\mathbf{i}_x, \mathbf{i}_y, 0\mathbf{i}_z\right)$-axis for the BECVF and $\left(-\frac{1}{\sqrt{2}}\mathbf{i}_x, \frac{1}{\sqrt{2}}\mathbf{i}_y, \mathbf{i}_z\right)$-axis for the OCVF. The BECVF is convolved with the OCVF resulting in the BECVF of matched angular momentum substituting for the great circle basis elements of the OCVF over its great-circle distribution, and the resulting current vector pattern is normalized numerically by individually scaling the current density of each great circle element as given in the Uniformity of $Y_0^0(\theta,\phi)$ section. In the generation of $Y_0^0(\theta,\phi)$, the rotations of the basis elements comprising the convolutions are about the resultant angular momentum axis of the basis elements that leaves the resultant vector unchanged, and the angular momentum is unaffected by normalization. Then, after reorienting the resultant angular momentum vector from along the $\left(-\frac{1}{\sqrt{2}}\mathbf{i}_x, \frac{1}{\sqrt{2}}\mathbf{i}_y, \mathbf{i}_z\right)$-axis to along the z-axis, it is trivial to confirm that the boundary-condition components of having components of $\mathbf{L}_{xy} = +/-\frac{\hbar}{4}$ and $\mathbf{L}_z = \frac{\hbar}{4}$ is met while further achieving the condition that the magnitude of the velocity at any point on the surface is given by Eq. (1.35). Since the final distribution is uniform, the electron charge, current, mass, and angular momentum density can be obtained by equating the surface area integral to $-e$, $-e\omega_n$, $m_e$, and $\hbar$, respectively. Then, the physical properties are derived in the Spin Angular Momentum of the Atomic Orbital $Y_0^0(\theta,\phi)$ with $\ell = 0$ section and are shown to match the boundary conditions. The derivation of the matrix mechanics to generate the electron spin current distribution called the electron atomic orbital $Y_0^0(\theta,\phi)$ and its uniform charge and current resulting from normalization are considered first and then utilized herein.

## GENERATION OF THE BECVF

Next, consider two infinitesimal charge(mass)-density elements at two separate positions or points, one and two, of the first pair of orthogonal great-circle current loops that serve as the basis set for generation of the BECVF as shown in Figure 1.4. The rotating Cartesian coordinates, x',y',z', in which the basis element great circles are fixed is designated the basis-set reference frame. In this frame at time zero, element one is at $x' = 0$, $y' = r_n$, and $z' = 0$, and element two is at $x' = r_n$, $y' = 0$, and $z' = 0$. Let element one move on a great circle clockwise toward the -z'-axis, and let element two move counter clockwise on a great circle toward the -z'-axis, as shown in Figure 1.4. The equations of motion, in the basis-set reference frame with $t = 0$ defined at the points (0,1,0) and (1,0,0), respectively, are given by:

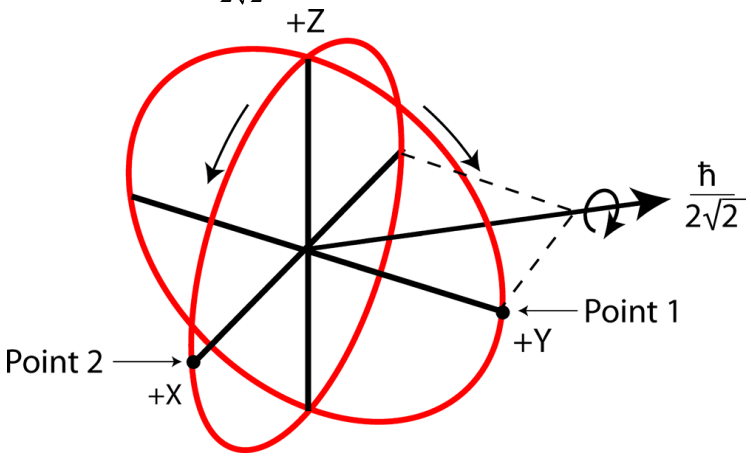
point one:

$$x_1' = 0 \qquad y_1' = r_n \cos(\omega_n t) \qquad z_1' = -r_n \sin(\omega_n t) \tag{1.78}$$

point two:

$$x_2' = r_n \cos(\omega_n t) \qquad y_2' = 0 \qquad z_2' = -r_n \sin(\omega_n t) \tag{1.79}$$

**Figure 1.4.** The BECVF is generated from two orthogonal great-circle current loops that serve as basis elements. The current on the great circle in the y'z'-plane moves clockwise and the current on the great circle in the x'z'-plane moves counter clockwise as indicated by arrows. Each point or coordinate position on the continuous two-dimensional BECVF defines an infinitesimal charge (mass)-density element, which moves along a geodesic orbit comprising a great circle. Two such infinitesimal charges (masses) are shown at point one, moving clockwise on the great circle in the y'z'-plane, and at point two moving counter clockwise on the great circle in the x'z'-plane. The xyz-system is the laboratory frame, and the orthogonal-current-loop basis set is rigid with respect to the x'y'z'-system that rotates about the $\left(-\mathbf{i}_x, \mathbf{i}_y, 0\mathbf{i}_z\right)$-axis by $\pi$ radians to generate the elements of the BECVF. The resultant angular momentum vector of the orthogonal great-circle current loops that is stationary in the xy-plane that is evenly distributed over the half-surface is $\frac{\hbar}{2\sqrt{2}}$ in the direction of $\left(-\mathbf{i}_x, \mathbf{i}_y, 0\mathbf{i}_z\right)$.




The orthogonal great circle basis set to generate the BECVF is shown in Figure 1.4. It is generated by the rotation of the two orthogonal great circles about the $\left(-\mathbf{i}_x, \mathbf{i}_y, 0\mathbf{i}_z\right)$-axis by an infinite set of infinitesimal increments of the rotational angle totaling a span of $\pi$. As shown in Figure 1.4, the current direction is such that the resultant angular momentum vector of the basis elements of magnitude $\frac{\hbar}{2\sqrt{2}}$ is stationary on this axis wherein one basis-element great circle is initially in the yz-plane having angular momentum $\mathbf{L}_x = -\frac{\hbar}{4}$ and the other is initially in the xz-plane having angular momentum $\mathbf{L}_y = \frac{\hbar}{4}$. The operator to form the BECVF comprises a convolution [11] of the rotational matrix of great circles basis elements with an infinite series of delta functions of argument of the infinitesimal angular increment.

The principal rotations in Cartesian coordinates are around each of the orthogonal axes, x, y, and z. Rotations about other axes can be obtained as a noncommutative combination of rotations that rotates one of the principal axes to align on the desired rotational axis relative to the Cartesian coordinates, the principal-axis rotation is applied, and then the matrices to rotate the principal axis to its Cartesian original coordinates are applied. A nonprincipal axis of rotation can be further rotated to a desired position. This can be achieved by rotating the axis about a principal axis relative to the Cartesian coordinates that is unchanged in the process. Principal rotational matrices with a clockwise rotation defined as a positive angle are given in Fowles [12]. The rotational matrix about the x-axis by $\theta$, $R_x(\theta)$, is given by:

$$R_x(\theta) = \begin{bmatrix} 1 & 0 & 0 \\ 0 & \cos(\theta) & \sin(\theta) \\ 0 & -\sin(\theta) & \cos(\theta) \end{bmatrix} \tag{1.80}$$

The rotational matrix about the y-axis by $\theta$, $R_y(\theta)$, is given by:

$$R_y(\theta) = \begin{bmatrix} \cos(\theta) & 0 & -\sin(\theta) \\ 0 & 1 & 0 \\ \sin(\theta) & 0 & \cos(\theta) \end{bmatrix} \tag{1.81}$$

The rotational matrix about the z-axis by $\theta$, $R_z(\theta)$, is given by:

$$R_z(\theta) = \begin{bmatrix} \cos(\theta) & \sin(\theta) & 0 \\ -\sin(\theta) & \cos(\theta) & 0 \\ 0 & 0 & 1 \end{bmatrix} \tag{1.82}$$

The rotational matrix about the $(-\mathbf{i}_x, \mathbf{i}_y, 0\mathbf{i}_z)$-axis by $\theta$, $R_{(-\mathbf{i}_x,\mathbf{i}_y,0\mathbf{i}_z)}(\theta)$, is given by:

$$R_{(-\mathbf{i}_x,\mathbf{i}_y,0\mathbf{i}_z)}(\theta) = R_z\left(\frac{\pi}{4}\right) R_x(-\theta) R_z\left(\frac{-\pi}{4}\right) \tag{1.83}$$

Then, using Eqs. (1.78-1.80, 1.82-1.83), the great circle basis elements and rotational matrix are given by:

**BECVF MATRICES ($R_{(-\mathbf{i}_x,\mathbf{i}_y,0\mathbf{i}_z)}(\theta)$)**

$$\begin{bmatrix} x' \\ y' \\ z' \end{bmatrix} = \begin{bmatrix} \frac{1}{2}+\frac{\cos\theta}{2} & -\frac{1}{2}+\frac{\cos\theta}{2} & -\frac{\sin\theta}{\sqrt{2}} \\ -\frac{1}{2}+\frac{\cos\theta}{2} & \frac{1}{2}+\frac{\cos\theta}{2} & -\frac{\sin\theta}{\sqrt{2}} \\ \frac{\sin\theta}{\sqrt{2}} & \frac{\sin\theta}{\sqrt{2}} & \cos\theta \end{bmatrix} \bullet \left( \begin{bmatrix} 0 \\ r_n\cos\phi \\ -r_n\sin\phi \end{bmatrix} + \begin{bmatrix} r_n\cos\phi \\ 0 \\ -r_n\sin\phi \end{bmatrix} \right) \tag{1.84}$$

Using Eq. (1.84), the BECVF matrix representation of the convolution is given by:

$$BECVF = \lim_{\Delta\theta\to 0} \sum_{m=1}^{m=\frac{\pi}{|\Delta\theta|}} \left[ \left( R_{(-\mathbf{i}_x,\mathbf{i}_y,0\mathbf{i}_z)}(\theta) \bullet \left( GC^{basis}_{(0\mathbf{i}_x,\mathbf{i}_y,\mathbf{i}_z)} + GC^{basis}_{(\mathbf{i}_x,0\mathbf{i}_y,\mathbf{i}_z)} \right) \right) \otimes \delta(\theta - m\Delta\theta_M) \right] \tag{1.85}$$

wherein $R_{(-\mathbf{i}_x,\mathbf{i}_y,0\mathbf{i}_z)}(\theta)$ is the rotational matrix about the $(-\mathbf{i}_x, \mathbf{i}_y, 0\mathbf{i}_z)$-axis, $GC^{basis}_{(0\mathbf{i}_x,\mathbf{i}_y,\mathbf{i}_z)}$ and $GC^{basis}_{(\mathbf{i}_x,0\mathbf{i}_y,\mathbf{i}_z)}$ are the great circle basis elements initially in the yz and xz planes, respectively, and $\otimes$ designates the convolution with the delta function of the infinitesimal incremental angle $m\Delta\theta_M$. The integral form of the convolution is

$$BECVF = \int_0^{\pi} \left( R_{(-\mathbf{i}_x,\mathbf{i}_y,0\mathbf{i}_z)}(\theta) \bullet \left( GC^{basis}_{(0\mathbf{i}_x,\mathbf{i}_y,\mathbf{i}_z)} + GC^{basis}_{(\mathbf{i}_x,0\mathbf{i}_y,\mathbf{i}_z)} \right) \right) \lim_{\Delta\theta\to 0} \sum_{m=1}^{m=\frac{\pi}{|\Delta\theta|}} \delta(\theta - m\Delta\theta_M) d\theta \tag{1.86}$$

The integration gives the infinite sum of great circles that constitute the BECVF:

$$BECVF = \lim_{\Delta\theta\to 0} \sum_{m=1}^{m=\frac{\pi}{|\Delta\theta|}} \left[ \left( R_{(-\mathbf{i}_x,\mathbf{i}_y,0\mathbf{i}_z)}(m\Delta\theta_M) \bullet \left( GC^{basis}_{(0\mathbf{i}_x,\mathbf{i}_y,\mathbf{i}_z)} + GC^{basis}_{(\mathbf{i}_x,0\mathbf{i}_y,\mathbf{i}_z)} \right) \right) \right] \tag{1.87}$$

The BECVF given by Eqs. (1.84-1.87) can also be generated by each of rotating a great circle basis element initially in the yz or the xz-planes about the $(-\mathbf{i}_x, \mathbf{i}_y, 0\mathbf{i}_z)$-axis over the range of 0 to $2\pi$ as shown in Figures 1.5 and 1.6, respectively. The BECVF of Figure 1.6 with vectors overlaid giving the direction of the current of each great circle element is shown in Figure 1.7. The current pattern of the BECVF generated by the rotations of the orthogonal great-circle current loops is a continuous half coverage of the spherical surface, but it is shown as visual representations using 6 degree increments of $\theta$ for Eqs. (1.84) and (1.87) in Figures 1.5-1.7 wherein the incremental angle becomes discrete rather than the actual continuous distribution in the limit that the incremental angle approaches zero. The same applies to the case of the representations of the OCVF and $Y_0^0(\theta,\phi)$ given *infra*.

**Figure 1.5.** The current pattern of the BECVF given by Eqs. (1.84) and (1.87) shown with 6 degree increments of $\theta$ from the perspective of looking along the z-axis. The yz-plane great circle current loop that served as a basis element that was initially in the yz-plane is shown as red.

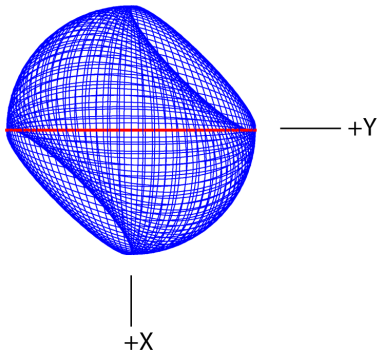



**Figure 1.6.** The current pattern of the BECVF shown with 6 degree increments of $\theta$ from the perspective of looking along the z-axis. The great-circle current loop that served as a basis element that was initially in the xz-plane is shown as red.

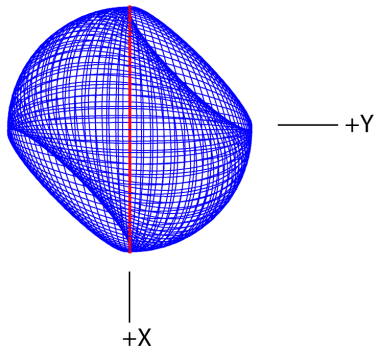
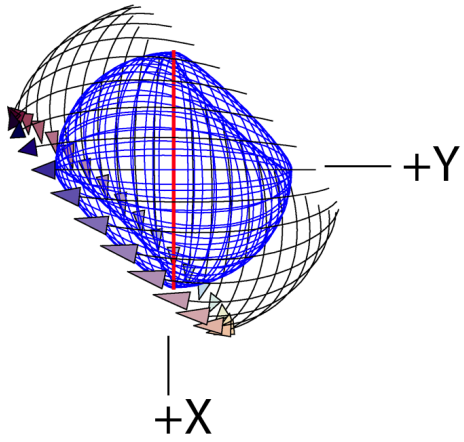



**Figure 1.7.** A representation of the z-axis perspective view of the BECVF shown in Figure 1.6 with 30 vectors overlaid giving the direction of the current of each great circle element.



## GENERATION OF THE OCVF

For the generation of the OCVF, consider two charge(mass)-density elements, point one and two, in the basis-set reference frame at time zero. Element one is at $x'=\frac{r_n}{\sqrt{2}}$, $y'=\frac{r_n}{\sqrt{2}}$, and $z'=0$, and element two is at $x'=r_n$, $y'=0$, and $z'=0$. Let element one move clockwise on a great circle toward the -z'-axis, and let element two move counter clockwise on a great circle toward the y'-axis as shown in Figure 1.8. The equations of motion, in the basis-set reference frame are given by

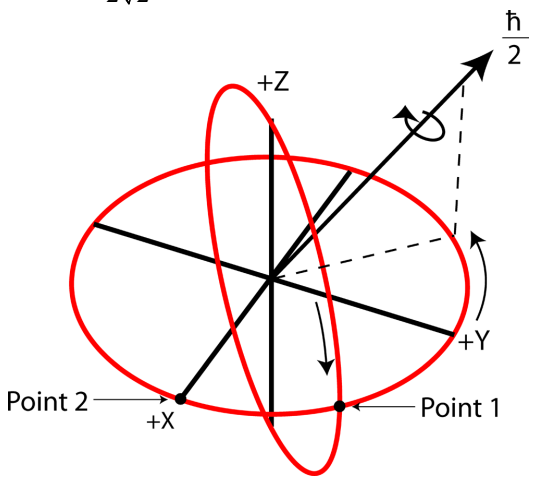
point one:

$$x_1'=r_n\sin\left(\frac{\pi}{4}\right)\cos(\omega_n t) \qquad y_1'=r_n\cos\left(\frac{\pi}{4}\right)\cos(\omega_n t) \qquad z_1'=-r_n\sin(\omega_n t) \tag{1.88}$$

point two:

$$x_2'=r_n\cos(\omega_n t) \qquad y_2'=r_n\sin(\omega_n t) \qquad z_2'=0 \tag{1.89}$$

**Figure 1.8.** In the generation of the OCVF, the current on the great circle in the plane that bisects the x'y'-quadrant and is parallel to the z'-axis moves clockwise, and the current on the great circle in the x'y'-plane moves counter clockwise. Rotation of the great circles about the $\left(-\frac{1}{\sqrt{2}}\mathbf{i}_x,\frac{1}{\sqrt{2}}\mathbf{i}_y,\mathbf{i}_z\right)$-axis by $\pi$ radians generates the elements of the OCVF. The stationary resultant angular momentum vector of the orthogonal great-circle current loops along the $\left(-\frac{1}{\sqrt{2}}\mathbf{i}_x,\frac{1}{\sqrt{2}}\mathbf{i}_y,\mathbf{i}_z\right)$-axis is $\frac{\hbar}{2}$ corresponding to each of the z and -xy-components of magnitude $\frac{\hbar}{2\sqrt{2}}$.




The orthogonal great-circle basis set for the OCVF is shown in Figure 1.8. It is generated by the rotation of the two orthogonal basis-element great circles about the $\left(-\frac{1}{\sqrt{2}}\mathbf{i}_x,\frac{1}{\sqrt{2}}\mathbf{i}_y,\mathbf{i}_z\right)$-axis by an infinite set of infinitesimal increments of the rotational angle totaling a span of $\pi$. As shown in Figure 1.8, the current direction is such that the resultant angular momentum vector of the basis elements of magnitude $\frac{\hbar}{2}$ is stationary on this axis wherein one basis-element great circle is initially in the plane that bisects the xy-quadrant and is parallel to the z-axis having angular momentum in the xy plane of $\mathbf{L}_{xy}=\frac{\hbar}{2\sqrt{2}}$ and the other is initially in the xy-plane having angular momentum $\mathbf{L}_z=\frac{\hbar}{2\sqrt{2}}$. The operator to form the OCVF comprises a convolution [11] of the rotational matrix of great circles basis elements with an infinite series of delta functions of argument of the infinitesimal angular increment.

An equivalent distribution to that of the OCVF may be generated by the rotation of a great circle in the yz-plane about the $\left(-\mathbf{i}_x,0\mathbf{i}_y,\mathbf{i}_z\right)$-axis by $2\pi$ followed by a rotation about the z-axis by $\frac{\pi}{4}$. The coordinates of the great circle in the yz-plane are given by the matrix:

$$\left[x',y',z'\right]^{\mathrm{T}}=\left[0,r_n\cos\phi,-r_n\sin\phi\right]^{\mathrm{T}} \tag{1.90}$$

The rotational matrix about the $\left(-\mathbf{i}_{\mathbf{x}},0\mathbf{i}_{\mathbf{y}},\mathbf{i}_{\mathbf{z}}\right)$-axis by $\theta$, $R_{\left(-\mathbf{i}_{\mathbf{x}},0\mathbf{i}_{\mathbf{y}},\mathbf{i}_{\mathbf{z}}\right)}\left(\theta\right)$, followed by a rotation about the z-axis by $\frac{\pi}{4}$, $R_z\left(\theta\right)$, is given by:

$$R_z\left(\frac{\pi}{4}\right)R_{\left(-\mathbf{i}_{\mathbf{x}},0\mathbf{i}_{\mathbf{y}},\mathbf{i}_{\mathbf{z}}\right)}\left(\theta\right)=R_z\left(\frac{\pi}{4}\right)R_y\left(\frac{\pi}{4}\right)R_z\left(\theta\right)R_y\left(\frac{-\pi}{4}\right) \tag{1.91}$$

In this case, the angular momentum vector of the great circle basis element over a $2\pi$ span is not equivalent to a stationary vector on the $\left(-\frac{1}{\sqrt{2}}\mathbf{i}_{\mathbf{x}},\frac{1}{\sqrt{2}}\mathbf{i}_{\mathbf{y}},\mathbf{i}_{\mathbf{z}}\right)$-axis. In order to achieve this result, the OCVF is generated by a $R_{\left(-\frac{1}{\sqrt{2}}\mathbf{i}_{\mathbf{x}},\frac{1}{\sqrt{2}}\mathbf{i}_{\mathbf{y}},\mathbf{i}_{\mathbf{z}}\right)}\left(\theta\right)$ rotation of the great circle basis-element that bisects the xy-quadrant and is parallel to the z-axis over a $2\pi$ span. The coordinates of the great circle are given by the matrix that rotates a great circle in the yz-plane about the z-axis by $\frac{\pi}{4}$:

$$\left[x',y',z'\right]^{\mathrm{T}}=\left[\frac{r_n\cos\phi}{\sqrt{2}},\frac{r_n\cos\phi}{\sqrt{2}},-r_n\sin\phi\right]^{\mathrm{T}}=R_z\left(\frac{\pi}{4}\right)\bullet\left[0,r_n\cos\phi,-r_n\sin\phi\right]^{\mathrm{T}} \tag{1.92}$$

Since the OCVF is given by the $2\pi$, $R_z\left(\frac{\pi}{4}\right)R_{\left(-\mathbf{i}_{\mathbf{x}},0\mathbf{i}_{\mathbf{y}},\mathbf{i}_{\mathbf{z}}\right)}\left(\theta\right)$ rotation of the yz-plane basis-element great circle (Eqs. (1.90-1.91)), the equivalent result may be obtained by first rotating the great circle given by Eq. (1.90) about the z-axis by $-\frac{\pi}{4}$, $R_z\left(-\frac{\pi}{4}\right)$, then applying Eq. (1.91). This combination is equivalent to a rotation about the $\left(-\frac{1}{\sqrt{2}}\mathbf{i}_{\mathbf{x}},\frac{1}{\sqrt{2}}\mathbf{i}_{\mathbf{y}},\mathbf{i}_{\mathbf{z}}\right)$-axis by $\theta$, $R_{\left(-\frac{1}{\sqrt{2}}\mathbf{i}_{\mathbf{x}},\frac{1}{\sqrt{2}}\mathbf{i}_{\mathbf{y}},\mathbf{i}_{\mathbf{z}}\right)}\left(\theta\right)$, and is given by:

$$R_{\left(-\frac{1}{\sqrt{2}}\mathbf{i}_{\mathbf{x}},\frac{1}{\sqrt{2}}\mathbf{i}_{\mathbf{y}},\mathbf{i}_{\mathbf{z}}\right)}\left(\theta\right)=R_z\left(\frac{\pi}{4}\right)R_y\left(\frac{\pi}{4}\right)R_z\left(\theta\right)R_y\left(\frac{-\pi}{4}\right)R_z\left(-\frac{\pi}{4}\right)=R_z\left(\frac{\pi}{4}\right)R_{\left(-\mathbf{i}_{\mathbf{x}},0\mathbf{i}_{\mathbf{y}},\mathbf{i}_{\mathbf{z}}\right)}\left(\theta\right)R_z\left(-\frac{\pi}{4}\right) \tag{1.93}$$

Then, the great circle basis-element that bisects the xy-quadrant and is parallel to the z-axis given by Eq. (1.92) is input to the rotational matrix given by Eq. (1.93) to give the desired stationary rotation about the great circle angular momentum axis, the $\left(-\frac{1}{\sqrt{2}}\mathbf{i}_{\mathbf{x}},\frac{1}{\sqrt{2}}\mathbf{i}_{\mathbf{y}},\mathbf{i}_{\mathbf{z}}\right)$-axis. The equivalent OCVF is also generated by the rotation of a great circle in the xy-plane about the $\left(-\frac{1}{\sqrt{2}}\mathbf{i}_{\mathbf{x}},\frac{1}{\sqrt{2}}\mathbf{i}_{\mathbf{y}},\mathbf{i}_{\mathbf{z}}\right)$-axis by $2\pi$ wherein the great circle is given by:

$$\left[x',y',z'\right]^{\mathrm{T}}=\left[r_n\cos\phi,r_n\sin\phi,0\right]^{\mathrm{T}} \tag{1.94}$$

Then, using Eqs. (1.92-1.94) and Eqs. (1.81-1.82), the great circle basis elements and rotational matrix are given by:

**OCVF MATRICES ($R_{\left(-\frac{1}{\sqrt{2}}\mathbf{i}_{\mathbf{x}},\frac{1}{\sqrt{2}}\mathbf{i}_{\mathbf{y}},\mathbf{i}_{\mathbf{z}}\right)}\left(\theta\right)$)**

$$\begin{bmatrix}x'\\y'\\z'\end{bmatrix}=\begin{bmatrix}\frac{1}{4}\left(1+3\cos\theta\right) & \frac{1}{4}\left(-1+\cos\theta+2\sqrt{2}\sin\theta\right) & \frac{1}{4}\left(-\sqrt{2}+\sqrt{2}\cos\theta-2\sin\theta\right)\\ \frac{1}{4}\left(-1+\cos\theta-2\sqrt{2}\sin\theta\right) & \frac{1}{4}\left(1+3\cos\theta\right) & \frac{1}{4}\left(\sqrt{2}-\sqrt{2}\cos\theta-2\sin\theta\right)\\ \frac{1}{2}\left(\frac{-1+\cos\theta}{\sqrt{2}}+\sin\theta\right) & \frac{1}{4}\left(\sqrt{2}-\sqrt{2}\cos\theta+2\sin\theta\right) & \cos^2\frac{\theta}{2}\end{bmatrix}\bullet\left(\begin{bmatrix}\frac{r_n\cos\phi}{\sqrt{2}}\\ \frac{r_n\cos\phi}{\sqrt{2}}\\ -r_n\sin\phi\end{bmatrix}+\begin{bmatrix}r_n\cos\phi\\ r_n\sin\phi\\ 0\end{bmatrix}\right) \tag{1.95}$$

Using Eq. (1.95), the OCVF matrix representation of the convolution is given by:

$$OCVF=\lim_{\Delta\theta\to 0}\sum_{m=1}^{m=\frac{\pi}{|\Delta\theta|}}\left[\left(R_{\left(-\frac{1}{\sqrt{2}}\mathbf{i}_{\mathbf{x}},\frac{1}{\sqrt{2}}\mathbf{i}_{\mathbf{y}},\mathbf{i}_{\mathbf{z}}\right)}\left(\theta\right)\bullet\left(GC^{basis}_{\left(\frac{1}{\sqrt{2}}\mathbf{i}_{\mathbf{x}},\frac{1}{\sqrt{2}}\mathbf{i}_{\mathbf{y}},\mathbf{i}_{\mathbf{z}}\right)}+GC^{basis}_{\left(\mathbf{i}_{\mathbf{x}},\mathbf{i}_{\mathbf{y}},0\mathbf{i}_{\mathbf{z}}\right)}\right)\right)\otimes\ \delta\left(\theta-m\Delta\theta_M\right)\right] \tag{1.96}$$

wherein $R_{\left(-\frac{1}{\sqrt{2}}\mathbf{i}_{\mathbf{x}},\frac{1}{\sqrt{2}}\mathbf{i}_{\mathbf{y}},\mathbf{i}_{\mathbf{z}}\right)}\left(\theta\right)$ is the rotational matrix about the $\left(-\frac{1}{\sqrt{2}}\mathbf{i}_{\mathbf{x}},\frac{1}{\sqrt{2}}\mathbf{i}_{\mathbf{y}},\mathbf{i}_{\mathbf{z}}\right)$-axis, $GC^{basis}_{\left(\frac{1}{\sqrt{2}}\mathbf{i}_{\mathbf{x}},\frac{1}{\sqrt{2}}\mathbf{i}_{\mathbf{y}},\mathbf{i}_{\mathbf{z}}\right)}$ and $GC^{basis}_{\left(\mathbf{i}_{\mathbf{x}},\mathbf{i}_{\mathbf{y}},0\mathbf{i}_{\mathbf{z}}\right)}$ are the great circle basis elements initially in the plane that bisects the xy-quadrant and is parallel to the z-axis and xy-plane, respectively, and $\otimes$ designates the convolution with the delta function of the infinitesimal incremental angle $m\Delta\theta_M$. The integral form of the convolution is:

$$OCVF = \int_0^{\pi}\left( R_{\left(-\frac{1}{\sqrt{2}}\mathbf{i}_x,\frac{1}{\sqrt{2}}\mathbf{i}_y,\mathbf{i}_z\right)}(\theta)\bullet\left( GC^{basis}_{\left(\frac{1}{\sqrt{2}}\mathbf{i}_x,\frac{1}{\sqrt{2}}\mathbf{i}_y,\mathbf{i}_z\right)} + GC^{basis}_{(\mathbf{i}_x,\mathbf{i}_y,0\mathbf{i}_z)}\right)\right)\lim_{\Delta\theta\to 0}\sum_{m=1}^{m=\frac{\pi}{|\Delta\theta|}}\delta(\theta - m\Delta\theta_M)d\theta \tag{1.97}$$

The integration gives the infinite sum of great circles that constitute the OCVF:

$$OCVF = \lim_{\Delta\theta\to 0}\sum_{m=1}^{m=\frac{\pi}{|\Delta\theta|}}\left[\left( R_{\left(-\frac{1}{\sqrt{2}}\mathbf{i}_x,\frac{1}{\sqrt{2}}\mathbf{i}_y,\mathbf{i}_z\right)}(m\Delta\theta_M)\bullet\left( GC^{basis}_{\left(\frac{1}{\sqrt{2}}\mathbf{i}_x,\frac{1}{\sqrt{2}}\mathbf{i}_y,\mathbf{i}_z\right)} + GC^{basis}_{(\mathbf{i}_x,\mathbf{i}_y,0\mathbf{i}_z)}\right)\right)\right] \tag{1.98}$$

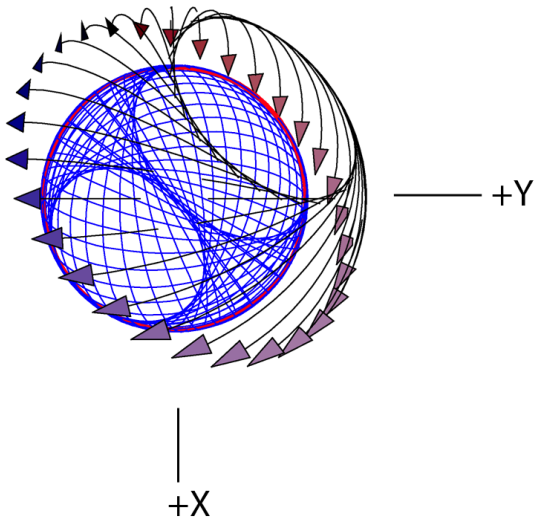
The OCVF given by Eq. (1.95) can also be generated by each of rotating a great circle basis element initially in the plane that bisects the xy-quadrant and is parallel to the z-axis or in the xy-plane about the $\left(-\frac{1}{\sqrt{2}}\mathbf{i}_x,\frac{1}{\sqrt{2}}\mathbf{i}_y,\mathbf{i}_z\right)$-axis over the range of 0 to $2\pi$ as shown in Figures 1.9 and 1.10, respectively. The OCVF of Figure 1.10 with vectors overlaid giving the direction of the current of each great circle element is shown in Figure 1.11.

**Figure 1.9.** The current pattern of the OCVF given by Eqs. (1.95) and (1.98) shown with 6 degree increments of $\theta$ from the perspective of looking along the z-axis. The great-circle current loop that served as a basis element that was initially in the plane that bisects the xy-quadrant and was parallel to the z-axis is shown as red.

**Figure 1.10.** The current pattern of the OCVF shown with 6 degree increments of $\theta$ from the perspective of looking along the z-axis. The great-circle current loop that served as a basis element that was initially in the xy-plane is shown as red.




**Figure 1.11.** A representation of the z-axis perspective view of the OCVF shown in Figure 1.10 with 30 vectors overlaid giving the direction of the current of each great circle element.




The CVFs, BECVF and OCVF, are used to generate $Y_0^0(\theta,\phi)$. Each CVF involves a unique combination of the initial and final directions of the primed coordinates and orientations of the angular momentum vectors due to the rotation of the basis-element great circles as summarized in Table 1.1. The angular momentum vector of the BECVF is stationary along its rotational

axis, the $\left(-\mathbf{i}_x,\mathbf{i}_y,0\mathbf{i}_z\right)$-axis, and the angular momentum vector of the OCVF is stationary along its rotational axis, the $\left(-\frac{1}{\sqrt{2}}\mathbf{i}_x,\frac{1}{\sqrt{2}}\mathbf{i}_y,\mathbf{i}_z\right)$-axis.

**Table 1.1.** Summary of the results of the matrix rotations of the two sets of two orthogonal current loops to generate the CVFs.

| CVF | Initial Direction of Angular Momentum Components $(\hat{r}\times\hat{K})$[a] | Final Direction of Angular Momentum Components $(\hat{r}\times\hat{K})$[a] | Initial to Final Axis Transformation | $\mathbf{L}_{xy}$ | $\mathbf{L}_z$ |
|---|---|---|---|---|---|
| BECVF | $\left(-\frac{1}{\sqrt{2}}\mathbf{i}_x,\frac{1}{\sqrt{2}}\mathbf{i}_y,0\mathbf{i}_z\right)$ | $\left(-\frac{1}{\sqrt{2}}\mathbf{i}_x,\frac{1}{\sqrt{2}}\mathbf{i}_y,0\mathbf{i}_z\right)$ | $x'\to -y$<br>$y'\to -x$<br>$z'\to -z$ | $\frac{\hbar}{2\sqrt{2}}$ | 0 |
| OCVF | $\left(-\frac{1}{\sqrt{2}}\mathbf{i}_x,\frac{1}{\sqrt{2}}\mathbf{i}_y,\mathbf{i}_z\right)$ | $\left(-\frac{1}{\sqrt{2}}\mathbf{i}_x,\frac{1}{\sqrt{2}}\mathbf{i}_y,\mathbf{i}_z\right)$ | $x'\to\left(-\frac{1}{2},-\frac{1}{2},-\frac{1}{\sqrt{2}}\right)$<br>$y'\to\left(-\frac{1}{2},-\frac{1}{2},\frac{1}{\sqrt{2}}\right)$<br>$z'\to\left(-\frac{1}{\sqrt{2}},\frac{1}{\sqrt{2}},0\right)$ | $\frac{\hbar}{2\sqrt{2}}$ | $\frac{\hbar}{2\sqrt{2}}$ |

[a] **K** is the current density, **r** is the polar vector of the great circle, and "^" denotes the unit vectors $\hat{u}\equiv\frac{\mathbf{u}}{|\mathbf{u}|}$.

## GENERATION OF $Y_0^0(\theta,\phi)$

The further constraint that the current density is uniform such that the charge density is uniform, corresponding to an equipotential, minimum energy surface is satisfied by using the CVFs to generate the uniform great-circle distribution $Y_0^0(\theta,\phi)$ by the convolution of the BECVF with the OCVF followed by normalization. Consider that the BECVF (Eq. (1.84)) for the OCVF convolution can also be generated by rotating a great circle basis element initially in the yz-plane about the $\left(-\mathbf{i}_x,\mathbf{i}_y,0\mathbf{i}_z\right)$-axis by $2\pi$ radians as shown in Figure 1.5. Similarly, the OCVF (Eq. (1.95)) can also be generated by rotating a great circle basis element initially in the plane that bisects the xy-quadrant and is parallel to the z-axis about the $\left(-\frac{1}{\sqrt{2}}\mathbf{i}_x,\frac{1}{\sqrt{2}}\mathbf{i}_y,\mathbf{i}_z\right)$-axis over the range of 0 to $2\pi$ as shown in Figure 1.9. The convolution operator treats each CVF independently and results in the placement of a BECVF at each great circle of the OCVF such that the resultant angular momentum of the distribution is the same as that of the OCVF. This is achieved by rotating the orientation, phase[6], and vector-matched basis-element, the BECVF, about the same axis as that which generated the OCVF. Thus, the BECVF replaces one great circle basis element, in this case, the one initially in the plane that bisects the xy-quadrant and is parallel to the z-axis. To match to the resultant angular momentum of both great circle basis elements, the angular momentum of the BECVF is $\mathbf{L}_{xy}=\frac{\hbar}{\sqrt{2}}$ (Figure 1.8) along the $\left(-\mathbf{i}_x,\mathbf{i}_y,0\mathbf{i}_z\right)$-axis. Then, $Y_0^0(\theta,\phi)$ is generated by rotation of the BECVF, about the $\left(-\frac{1}{\sqrt{2}}\mathbf{i}_x,\frac{1}{\sqrt{2}}\mathbf{i}_y,\mathbf{i}_z\right)$-axis by an infinite set of infinitesimal increments of the rotational angle. The current direction is such that the resultant angular momentum vector of the BECVF basis element rotated over the $2\pi$ span is equivalent to that of both of the OCVF great circle basis elements, $\frac{\hbar}{2}$ having components of

[6] The resultant angular momentum vector, $\mathbf{L}_\mathbf{R}$, is along $\left(-\mathbf{i}_x,\mathbf{i}_y,0\mathbf{i}_z\right)$; thus, the angular momentum is constant for any rotation about this axis which establishes it as a $C_\infty$-axis relative to the angular momentum. However, rotation about this axis does change the phase (coordinate position relative to the starting position) of the BECVF. For example, a rotation by $|\theta|=\pi$ about the $\left(-\mathbf{i}_x,\mathbf{i}_y,0\mathbf{i}_z\right)$-axis using Eqs. (1.83) and (1.84) causes the BECVF basis-element great circle to rotate by $\frac{\pi}{2}$ about the z-axis such that its position changes between the xz and yz-planes.

$\mathbf{L}_{xy} = \frac{\hbar}{2\sqrt{2}}$ and $\mathbf{L}_z = \frac{\hbar}{2\sqrt{2}}$ that is stationary on the $\left(-\frac{1}{\sqrt{2}}\mathbf{i}_\mathbf{x}, \frac{1}{\sqrt{2}}\mathbf{i}_\mathbf{y}, \mathbf{i}_\mathbf{z}\right)$-axis. Since the resultant angular momentum vector of the BECVF over the $2\pi$ span matches that of the replaced great circle basis elements and is stationary on the rotational axis as in the case of the OCVF, the resultant angular momentum of the distribution is the same as that of the OCVF, except that coverage of the spherical surface is complete. The resulting uniformity of the distribution is achieved by normalization as shown in the Uniformity of $Y_0^0(\theta,\phi)$ section.

The operator to form $Y_0^0(\theta,\phi)$ comprises the BECVF convolution [11] of the rotational matrix of great circles basis element about the $\left(-\mathbf{i}_\mathbf{x}, \mathbf{i}_\mathbf{y}, 0\mathbf{i}_\mathbf{z}\right)$-axis with an infinite series of delta functions of argument of the infinitesimal angular increment that is further convolved with the OCVF convolution of the rotational matrix of great circles basis element about the $\left(-\frac{1}{\sqrt{2}}\mathbf{i}_\mathbf{x}, \frac{1}{\sqrt{2}}\mathbf{i}_\mathbf{y}, \mathbf{i}_\mathbf{z}\right)$-axis with an infinite series of delta functions of argument of the infinitesimal angular increment. Using the BECVF matrix representation of its convolution operation (Eq. (1.85)) and the OCVF matrix representation of its convolution operation (Eq. (1.96)), the $Y_0^0(\theta,\phi)$ matrix representation of the convolution is given by:

$$Y_0^0(\theta,\phi) = OCVF \otimes BECVF = \left\{ \begin{array}{l} \left( \lim\limits_{\Delta\theta\to 0} \sum\limits_{m=1}^{m=\frac{2\pi}{|\Delta\theta|}} \left[ \left( R_{\left(-\frac{1}{\sqrt{2}}\mathbf{i}_\mathbf{x}, \frac{1}{\sqrt{2}}\mathbf{i}_\mathbf{y}, \mathbf{i}_\mathbf{z}\right)}(\theta) \bullet GC^{basis}_{\left(\frac{1}{\sqrt{2}}\mathbf{i}_\mathbf{x}, \frac{1}{\sqrt{2}}\mathbf{i}_\mathbf{y}, \mathbf{i}_\mathbf{z}\right)} \right) \otimes \delta\left(\theta - m\Delta\theta_M\right) \right] \right) \\ \otimes \left( \lim\limits_{\Delta\theta\to 0} \sum\limits_{n=1}^{n=\frac{2\pi}{|\Delta\theta|}} \left[ \left( R_{\left(-\mathbf{i}_\mathbf{x}, \mathbf{i}_\mathbf{y}, 0\mathbf{i}_\mathbf{z}\right)}(\theta) \bullet GC^{basis}_{\left(0\mathbf{i}_\mathbf{x}, \mathbf{i}_\mathbf{y}, \mathbf{i}_\mathbf{z}\right)} \right) \otimes \delta\left(\theta - n\Delta\theta_N\right) \right] \right) \end{array} \right\} \tag{1.99}$$

where the commutative property of convolutions [11] allows for the interchange of the order of CVFs, but the rotational matrices are noncommutative [12]. The integral form of the convolution is

$$Y_0^0(\theta,\phi) = \left\{ \begin{array}{l} \left[ \int_0^{2\pi} \left( R_{\left(-\frac{1}{\sqrt{2}}\mathbf{i}_\mathbf{x}, \frac{1}{\sqrt{2}}\mathbf{i}_\mathbf{y}, \mathbf{i}_\mathbf{z}\right)}(\theta) \bullet GC^{basis}_{\left(\frac{1}{\sqrt{2}}\mathbf{i}_\mathbf{x}, \frac{1}{\sqrt{2}}\mathbf{i}_\mathbf{y}, \mathbf{i}_\mathbf{z}\right)} \right) \lim\limits_{\Delta\theta\to 0} \sum\limits_{m=1}^{m=\frac{2\pi}{|\Delta\theta|}} \delta\left(\theta - m\Delta\theta_M^{OCVF}\right) d\theta \right] \\ \otimes \left[ \int_0^{2\pi} \left( R_{\left(-\mathbf{i}_\mathbf{x}, \mathbf{i}_\mathbf{y}, 0\mathbf{i}_\mathbf{z}\right)}(\theta) \bullet GC^{basis}_{\left(0\mathbf{i}_\mathbf{x}, \mathbf{i}_\mathbf{y}, \mathbf{i}_\mathbf{z}\right)} \right) \left( \lim\limits_{\Delta\theta\to 0} \sum\limits_{n=1}^{n=\frac{2\pi}{|\Delta\theta|}} \delta\left(\theta - n\Delta\theta_N^{BECVF}\right) \right) d\theta \right] \end{array} \right\} \tag{1.100}$$

$$Y_0^0(\theta,\phi) = \lim_{\Delta\theta\to 0} \sum_{m=1}^{m=\frac{2\pi}{|\Delta\theta|}} \lim_{\Delta\theta\to 0} \sum_{n=1}^{n=\frac{2\pi}{|\Delta\theta|}} \int_0^{2\pi} d\theta_1 \int_0^{2\pi} d\theta_2 R_{\left(-\frac{1}{\sqrt{2}}\mathbf{i}_\mathbf{x}, \frac{1}{\sqrt{2}}\mathbf{i}_\mathbf{y}, \mathbf{i}_\mathbf{z}\right)}(\theta_1) \bullet R_{\left(-\mathbf{i}_\mathbf{x}, \mathbf{i}_\mathbf{y}, 0\mathbf{i}_\mathbf{z}\right)}(\theta_2) \bullet GC^{basis}_{\left(0\mathbf{i}_\mathbf{x}, \mathbf{i}_\mathbf{y}, \mathbf{i}_\mathbf{z}\right)} \delta\left(\theta_1 - m\Delta\theta_M^{OCVF}\right) \delta\left(\theta_2 - n\Delta\theta_N^{BECVF}\right) \tag{1.101}$$

The integration gives the infinite double sum of great circles that constitute $Y_0^0(\theta,\phi)$:

$$Y_0^0(\theta,\phi) = \lim_{\Delta\theta\to 0} \sum_{m=1}^{m=\frac{2\pi}{|\Delta\theta|}} \left[ R_{\left(-\frac{1}{\sqrt{2}}\mathbf{i}_\mathbf{x}, \frac{1}{\sqrt{2}}\mathbf{i}_\mathbf{y}, \mathbf{i}_\mathbf{z}\right)}\left(m\Delta\theta_M^{OCVF}\right) \bullet \lim_{\Delta\theta\to 0} \sum_{n=1}^{n=\frac{2\pi}{|\Delta\theta|}} \left[ R_{\left(-\mathbf{i}_\mathbf{x}, \mathbf{i}_\mathbf{y}, 0\mathbf{i}_\mathbf{z}\right)}\left(n\Delta\theta_N^{BECVF}\right) \bullet GC^{basis}_{\left(0\mathbf{i}_\mathbf{x}, \mathbf{i}_\mathbf{y}, \mathbf{i}_\mathbf{z}\right)} \right] \right] \tag{1.102}$$

Using Eq. (1.102), a discrete representation of the current distribution $Y_0^0(\theta,\phi)$ that shows a finite number of current elements can be generated by showing the BECVF as a finite sum of the convolved great circle elements using Eqs. (1.84) and (1.87) and by showing the continuous convolution of the BECVF with the OCVF as a superposition of discrete incremental rotations of the position of the BECVF rotated according to Eqs. (1.95) and (1.98) corresponding to the matrix which generated the OCVF. In the case that the discrete representation of the BECVF comprises $N$ great circles and the number of convolved BECVF elements is $M$, the representation of the current density function showing current loops is given by Eq. (1.103) and shown in Figure 1.12. The $\left(\frac{1}{\sqrt{2}}\mathbf{i}_\mathbf{x}, -\frac{1}{\sqrt{2}}\mathbf{i}_\mathbf{y}, \mathbf{i}_\mathbf{z}\right)$-axis view of this representation with 144 vectors overlaid giving the direction of the current of each great circle element is shown in Figure 1.13. The corresponding mass(momentum) density is also represented by Figures 1.12 and 1.13 wherein the charge and mass are interchangeable by the conversion factor $m_e / e$.

$$\begin{bmatrix} x' \\ y' \\ z' \end{bmatrix} = \sum_{m=1}^{m=M} \begin{bmatrix} \frac{1}{4}\left(1+3\cos\left(\frac{m2\pi}{M}\right)\right) & \frac{1}{4}\left(-1+\cos\left(\frac{m2\pi}{M}\right)+2\sqrt{2}\sin\left(\frac{m2\pi}{M}\right)\right) & \frac{1}{4}\left(-\sqrt{2}+\sqrt{2}\cos\left(\frac{m2\pi}{M}\right)-2\sin\left(\frac{m2\pi}{M}\right)\right) \\ \frac{1}{4}\left(-1+\cos\left(\frac{m2\pi}{M}\right)-2\sqrt{2}\sin\left(\frac{m2\pi}{M}\right)\right) & \frac{1}{4}\left(1+3\cos\left(\frac{m2\pi}{M}\right)\right) & \frac{1}{4}\left(\sqrt{2}-\sqrt{2}\cos\left(\frac{m2\pi}{M}\right)-2\sin\left(\frac{m2\pi}{M}\right)\right) \\ \frac{1}{2}\left(\frac{-1+\cos\left(\frac{m2\pi}{M}\right)}{\sqrt{2}}+\sin\left(\frac{m2\pi}{M}\right)\right) & \frac{1}{4}\left(\sqrt{2}-\sqrt{2}\cos\left(\frac{m2\pi}{M}\right)+2\sin\left(\frac{m2\pi}{M}\right)\right) & \cos^2\frac{\left(\frac{m2\pi}{M}\right)}{2} \end{bmatrix}$$

$$\bullet \sum_{n=1}^{n=N} \begin{bmatrix} \frac{1}{2}+\frac{\cos\left(\frac{n2\pi}{N}\right)}{2} & -\frac{1}{2}+\frac{\cos\left(\frac{n2\pi}{N}\right)}{2} & -\frac{\sin\left(\frac{n2\pi}{N}\right)}{\sqrt{2}} \\ -\frac{1}{2}+\frac{\cos\left(\frac{n2\pi}{N}\right)}{2} & \frac{1}{2}+\frac{\cos\left(\frac{n2\pi}{N}\right)}{2} & -\frac{\sin\left(\frac{n2\pi}{N}\right)}{\sqrt{2}} \\ \frac{\sin\left(\frac{n2\pi}{N}\right)}{\sqrt{2}} & \frac{\sin\left(\frac{n2\pi}{N}\right)}{\sqrt{2}} & \cos\left(\frac{n2\pi}{N}\right) \end{bmatrix} \begin{bmatrix} 0 \\ r_n\cos\phi \\ -r_n\sin\phi \end{bmatrix} \tag{1.103}$$

**Figure 1.12.** A representation of the z-axis view of the current pattern of $Y_0^0(\theta,\phi)$ shown with 30 degree increments ($N=M=12$ in Eq. (1.103)) of the angle to generate the BECVF corresponding to Eqs. (1.84) and (1.87) and 30 degree increments of the rotation of this basis element about the $\left(-\frac{1}{\sqrt{2}}\mathbf{i}_x,\frac{1}{\sqrt{2}}\mathbf{i}_y,\mathbf{i}_z\right)$-axis corresponding to Eqs. (1.95) and (1.98).

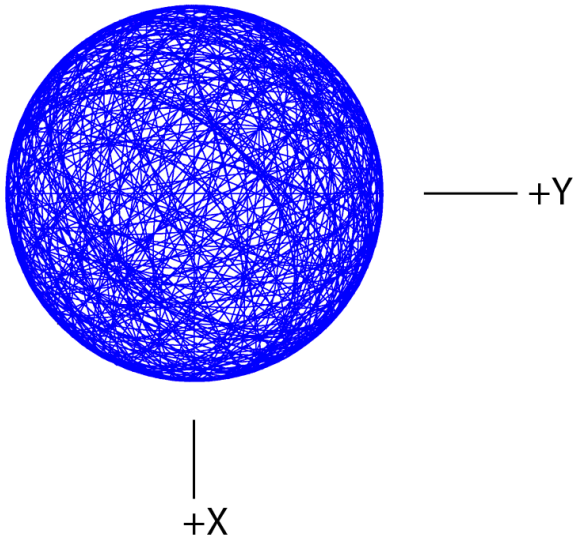
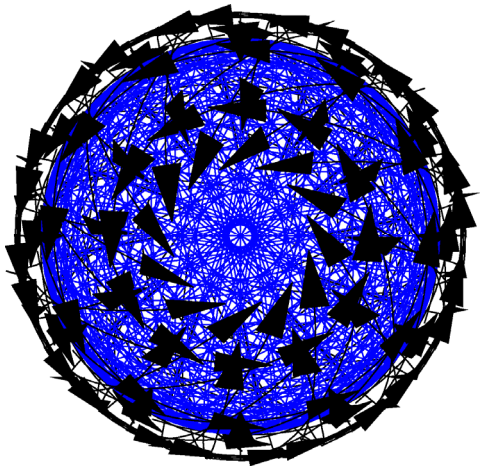



**Figure 1.13.** A representation of the $\left(\frac{1}{\sqrt{2}}\mathbf{i}_x,-\frac{1}{\sqrt{2}}\mathbf{i}_y,\mathbf{i}_z\right)$-axis view of $Y_0^0(\theta,\phi)$ shown in Figure 1.12 with 144 vectors overlaid giving the direction of the current of each great circle element.



A BECVF can also be generated to replace the great circle basis element of the OCVF that lies in the xy-plane. In the case that the current is counter clockwise with the angular momentum in the direction of the z-axis, the equivalent rotational transformations that maintain the resultant angular momentum stationary on the z-axis over a $2\pi$ rotation is the combination of a $-\frac{\pi}{4}$ rotation about the y-axis followed by a $2\pi$ rotation of the tilted great circle about the z-axis. The angular-momentum-and-orientation-matched distribution shown in Figure 1.14 is generated by:

$$[x', y', z']^{\mathrm{T}} = R_z(\theta) R_y\left(\frac{-\pi}{4}\right) \bullet [r_n \cos\phi, r_n \sin\phi, 0]^{\mathrm{T}} \tag{1.104}$$

In order to match phase with the OCVF rotational axis, $\left(-\frac{1}{\sqrt{2}}\mathbf{i}_x, \frac{1}{\sqrt{2}}\mathbf{i}_y, \mathbf{i}_z\right)$-axis, Eq. (1.104) must be rotated about the z-axis by $\frac{\pi}{4}$ using $R_z\left(\frac{\pi}{4}\right)$ using Eq. (1.82). In this case, the BECVF is aligned on the xy-plane and the resultant angular momentum vector, $\mathbf{L}_\mathbf{R}$, is also along the z-axis. The final phase-matched distribution shown in Figure 1.15 is given by:

$$[x', y', z']^{\mathrm{T}} = R_z\left(\frac{\pi}{4}\right) R_z(\theta) R_y\left(\frac{-\pi}{4}\right) \bullet [r_n \cos\phi, r_n \sin\phi, 0]^{\mathrm{T}} \tag{1.105}$$

**Figure 1.14.** The current pattern given by Eq. (1.104) shown with 6 degree increments of $\theta$ from the perspective of looking along the z-axis. The great circle current loop that served as a basis element that was initially in the xy-plane is shown as red.

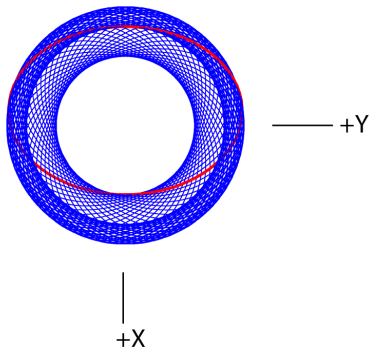
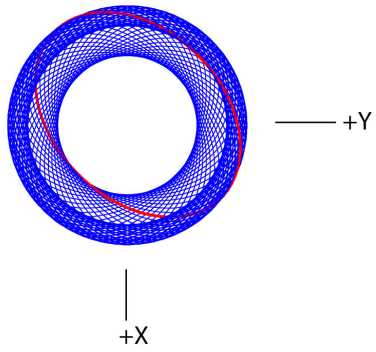



**Figure 1.15.** The current pattern given by Eq. (1.105) shown with 6 degree increments of $\theta$ from the perspective of looking along the z-axis. The great circle current loop that served as a basis element that was initially in the xy-plane is shown as red.




Then, using Eq. (1.105) and Eqs. (1.81-1.82), the great circle basis elements and rotational matrix are given by:

**BECVF MATRICES** ($R_z\left(\frac{\pi}{4}\right) R_z(\theta) R_y\left(\frac{-\pi}{4}\right)$)

$$\begin{bmatrix} x' \\ y' \\ z' \end{bmatrix} = \begin{bmatrix} \frac{\cos\theta}{2} - \frac{\sin\theta}{2} & \frac{\sin\theta}{\sqrt{2}} + \frac{\cos\theta}{\sqrt{2}} & \frac{\cos\theta}{2} - \frac{\sin\theta}{2} \\ -\frac{\cos\theta}{2} - \frac{\sin\theta}{2} & -\frac{\sin\theta}{\sqrt{2}} + \frac{\cos\theta}{\sqrt{2}} & -\frac{\cos\theta}{2} - \frac{\sin\theta}{2} \\ -\frac{1}{\sqrt{2}} & 0 & \frac{1}{\sqrt{2}} \end{bmatrix} \begin{bmatrix} r_n \cos\phi \\ r_n \sin\phi \\ 0 \end{bmatrix} \tag{1.106}$$

Using the procedure of Eqs. (1.85-1.87) on Eq. (1.106), the infinite sum of great circles that constitute the BECVF is:

$$BECVF = \lim_{\Delta\theta \to 0} \sum_{m=1}^{m=\frac{2\pi}{|\Delta\theta|}} \left[ \left( R_z\left(\frac{\pi}{4}\right) R_z(\theta) R_y\left(\frac{-\pi}{4}\right) (m\Delta\theta_M) \bullet GC^{basis}_{(\mathbf{i}_x, \mathbf{i}_y, 0\mathbf{i}_z)} \right) \right] \tag{1.107}$$

Using Eqs. (1.99-1.102), and (1.107), the corresponding infinite double sum of great circles that constitute $Y_0^0(\theta, \phi)$ is given by:

$$Y_0^{\,0}(\theta,\phi) = \lim_{\Delta\theta\to 0}\sum_{m=1}^{m=\frac{2\pi}{|\Delta\theta|}}\left[R_{\left(-\frac{1}{\sqrt{2}}\mathbf{i}_x,\frac{1}{\sqrt{2}}\mathbf{i}_y,\mathbf{i}_z\right)}\left(m\Delta\theta_M^{OCVF}\right)\bullet\lim_{\Delta\theta\to 0}\sum_{n=1}^{n=\frac{2\pi}{|\Delta\theta|}}\left[R_z\left(\frac{\pi}{4}\right)R_z(\theta)R_y\left(\frac{-\pi}{4}\right)\left(n\Delta\theta_N^{BECVF}\right)\bullet GC^{basis}_{\left(0\mathbf{i}_x,\mathbf{i}_y,\mathbf{i}_z\right)}\right]\right] \tag{1.108}$$

Using Eq. (1.108), a discrete representation of the current distribution $Y_0^{\,0}(\theta,\phi)$ that shows a finite number of current elements can be generated by showing the BECVF as a finite sum of the convolved great circle elements using Eqs. (1.106-1.107) and by showing the continuous convolution of the BECVF with the OCVF as a superposition of discrete incremental rotations of the position of the BECVF rotated according to Eqs. (1.95) and (1.98) corresponding to the matrix which generated the OCVF. In the case that the discrete representation of the BECVF comprises $N$ great circles and the number of convolved BECVF elements is $M$, the representation of the current density function showing current loops is given by Eq. (1.109) and shown in Figure 1.16. The $\left(\frac{1}{\sqrt{2}}\mathbf{i}_x,-\frac{1}{\sqrt{2}}\mathbf{i}_y,\mathbf{i}_z\right)$-axis view of this representation with 144 vectors overlaid giving the direction of the current of each great circle element is shown in Figure 1.17. The corresponding mass(momentum) density is also represented by Figures 1.16 and 1.17 wherein the charge and mass are interchangeable by the conversion factor $m_e/e$.

$$\begin{bmatrix}x'\\y'\\z'\end{bmatrix} = \sum_{m=1}^{m=M}\begin{bmatrix}\frac{1}{4}\left(1+3\cos\left(\frac{m2\pi}{M}\right)\right) & \frac{1}{4}\left(-1+\cos\left(\frac{m2\pi}{M}\right)+2\sqrt{2}\sin\left(\frac{m2\pi}{M}\right)\right) & \frac{1}{4}\left(-\sqrt{2}+\sqrt{2}\cos\left(\frac{m2\pi}{M}\right)-2\sin\left(\frac{m2\pi}{M}\right)\right)\\ \frac{1}{4}\left(-1+\cos\left(\frac{m2\pi}{M}\right)-2\sqrt{2}\sin\left(\frac{m2\pi}{M}\right)\right) & \frac{1}{4}\left(1+3\cos\left(\frac{m2\pi}{M}\right)\right) & \frac{1}{4}\left(\sqrt{2}-\sqrt{2}\cos\left(\frac{m2\pi}{M}\right)-2\sin\left(\frac{m2\pi}{M}\right)\right)\\ \frac{1}{2}\left(\frac{-1+\cos\left(\frac{m2\pi}{M}\right)}{\sqrt{2}}+\sin\left(\frac{m2\pi}{M}\right)\right) & \frac{1}{4}\left(\sqrt{2}-\sqrt{2}\cos\left(\frac{m2\pi}{M}\right)+2\sin\left(\frac{m2\pi}{M}\right)\right) & \cos^2\frac{\left(\frac{m2\pi}{M}\right)}{2}\end{bmatrix}$$

$$\bullet\sum_{n=1}^{n=N}\begin{bmatrix}\frac{\cos\left(\frac{n2\pi}{N}\right)}{2}-\frac{\sin\left(\frac{n2\pi}{N}\right)}{2} & \frac{\sin\left(\frac{n2\pi}{N}\right)}{\sqrt{2}}+\frac{\cos\left(\frac{n2\pi}{N}\right)}{\sqrt{2}} & \frac{\cos\left(\frac{n2\pi}{N}\right)}{2}-\frac{\sin\left(\frac{n2\pi}{N}\right)}{2}\\ -\frac{\cos\left(\frac{n2\pi}{N}\right)}{2}-\frac{\sin\left(\frac{n2\pi}{N}\right)}{2} & -\frac{\sin\left(\frac{n2\pi}{N}\right)}{\sqrt{2}}+\frac{\cos\left(\frac{n2\pi}{N}\right)}{\sqrt{2}} & -\frac{\cos\left(\frac{n2\pi}{N}\right)}{2}-\frac{\sin\left(\frac{n2\pi}{N}\right)}{2}\\ -\frac{1}{\sqrt{2}} & 0 & \frac{1}{\sqrt{2}}\end{bmatrix}\begin{bmatrix}r_n\cos\phi\\ r_n\sin\phi\\ 0\end{bmatrix} \tag{1.109}$$

**Figure 1.16.** A representation of the z-axis view of the current pattern of the $Y_0^0(\theta,\phi)$ shown with 30 degree increments ($N=M=12$ in Eq. (1.109)) of the angle to generate the BECVF corresponding to Eqs. (1.106) and (1.107) and 30 degree increments of the rotation of this basis element about the $\left(-\frac{1}{\sqrt{2}}\mathbf{i}_x,\frac{1}{\sqrt{2}}\mathbf{i}_y,\mathbf{i}_z\right)$-axis corresponding to Eqs. (1.95) and (1.98). The great circle current loop that served as a basis element of the BECVF is shown as red.

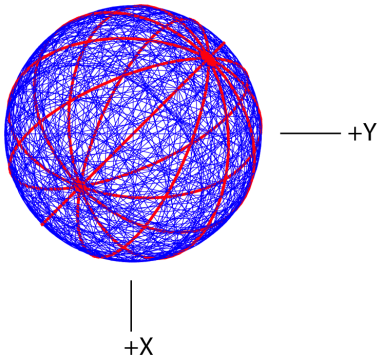
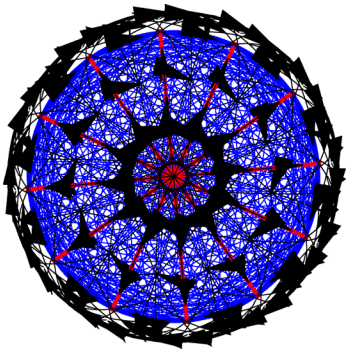



**Figure 1.17.** A representation of the $\left(\frac{1}{\sqrt{2}}\mathbf{i}_x,-\frac{1}{\sqrt{2}}\mathbf{i}_y,\mathbf{i}_z\right)$-axis view of $Y_0^0(\theta,\phi)$ shown in Figure 1.16 with 144 vectors overlaid giving the direction of the current of each great circle element.



## UNIFORMITY OF $Y_0^0(\theta,\phi)$

By using the rotational matrices to generate $Y_0^0(\theta,\phi)$, it is shown to be uniform about the angular momentum axis that is permissive of normalization such that the spherical uniformity and angular momentum boundary conditions are met. Consider the $Y_0^0(\theta,\phi)$ convolution in summation form given by Eqs. (1.99) and (1.102). The BECVF is periodic in $\theta$ with a period of $\pi$ wherein the basis elements interchange. Thus, only one basis need be considered with the range increased to $2\pi$:

$$\begin{bmatrix} x' \\ y' \\ z' \end{bmatrix} = \left( \lim_{\Delta\theta\to 0} \sum_{m=1}^{m=\frac{2\pi}{|\Delta\theta|}} \left[ \left( R_{\left(-\frac{1}{\sqrt{2}}\mathbf{i}_x,\frac{1}{\sqrt{2}}\mathbf{i}_y,\mathbf{i}_z\right)}\left(m\Delta\theta_M^{OCVF}\right) \bullet BECVF^{basis}_{\left(\frac{1}{\sqrt{2}}\mathbf{i}_x,\frac{1}{\sqrt{2}}\mathbf{i}_y,\mathbf{i}_z\right)} \right) \right] \right) \tag{1.110}$$

wherein $BECVF^{basis}_{\left(\frac{1}{\sqrt{2}}\mathbf{i}_x,\frac{1}{\sqrt{2}}\mathbf{i}_y,\mathbf{i}_z\right)}$ is the distribution that replaced the great circle basis element of the OCVF distribution in the convolution given by Eqs. (1.87), (1.92), (1.98), and (1.99), respectively. Consider the rotation of both sides of Eq. (1.110) about the $\left(\mathbf{i}_x,\mathbf{i}_y,0\mathbf{i}_z\right)$-axis, the orthogonal axis to that which generated the BECVF, by $\frac{\pi}{4}$:

$$R_{(\mathbf{i}_x,\mathbf{i}_y,0\mathbf{i}_z)}\left(\frac{\pi}{4}\right)\begin{bmatrix} x' \\ y' \\ z' \end{bmatrix} = \left( R_{(\mathbf{i}_x,\mathbf{i}_y,0\mathbf{i}_z)}\left(\frac{\pi}{4}\right) \lim_{\Delta\theta\to 0} \sum_{m=1}^{m=\frac{2\pi}{|\Delta\theta|}} \left[ \left( R_{\left(-\frac{1}{\sqrt{2}}\mathbf{i}_x,\frac{1}{\sqrt{2}}\mathbf{i}_y,\mathbf{i}_z\right)}\left(m\Delta\theta_M^{OCVF}\right) \bullet BECVF^{basis}_{\left(\frac{1}{\sqrt{2}}\mathbf{i}_x,\frac{1}{\sqrt{2}}\mathbf{i}_y,\mathbf{i}_z\right)} \right) \right] \right) \tag{1.111}$$

The rotation of a sum is the same as the sum of the rotations

$$R_{(\mathbf{i}_x,\mathbf{i}_y,0\mathbf{i}_z)}\left(\frac{\pi}{4}\right)\begin{bmatrix} x' \\ y' \\ z' \end{bmatrix} = \left( \lim_{\Delta\theta\to 0} \sum_{m=1}^{m=\frac{2\pi}{|\Delta\theta|}} \left[ \left( R_{(\mathbf{i}_x,\mathbf{i}_y,0\mathbf{i}_z)}\left(\frac{\pi}{4}\right) \bullet R_{\left(-\frac{1}{\sqrt{2}}\mathbf{i}_x,\frac{1}{\sqrt{2}}\mathbf{i}_y,\mathbf{i}_z\right)}\left(m\Delta\theta_M^{OCVF}\right) \bullet BECVF^{basis}_{\left(\frac{1}{\sqrt{2}}\mathbf{i}_x,\frac{1}{\sqrt{2}}\mathbf{i}_y,\mathbf{i}_z\right)} \right) \right] \right) \tag{1.112}$$

When the distribution given by Eq. (1.98) having its $C_\infty$-axis along the $\left(-\frac{1}{\sqrt{2}}\mathbf{i}_x,\frac{1}{\sqrt{2}}\mathbf{i}_y,\mathbf{i}_z\right)$-axis is rotated about the $\left(\mathbf{i}_x,\mathbf{i}_y,0\mathbf{i}_z\right)$-axis by $\frac{\pi}{4}$, the resulting distribution having the $C_\infty$-axis along the $\left(-\mathbf{i}_x,\mathbf{i}_y,0\mathbf{i}_z\right)$-axis is equivalent to the distribution given by Eq. (1.87) of matching $C_\infty$-axis. Substitution of Eq. (1.87) into Eq. (1.112) gives:

$$R_{\left(\mathbf{i}_x,\mathbf{i}_y,0\mathbf{i}_z\right)}\left(\frac{\pi}{4}\right)\begin{bmatrix}x'\\y'\\z'\end{bmatrix}=\left(\lim_{\Delta\theta\to 0}\sum_{m=1}^{m=\frac{2\pi}{|\Delta\theta|}}\left[\left(R_{\left(-\mathbf{i}_x,\mathbf{i}_y,0\mathbf{i}_z\right)}\left(m\Delta\theta_M^{OCVF}\right)\bullet BECVF^{basis}_{\left(\frac{1}{\sqrt{2}}\mathbf{i}_x,\frac{1}{\sqrt{2}}\mathbf{i}_y,\mathbf{i}_z\right)}\right)\right]\right) \tag{1.113}$$

Substitution of Eq. (1.87) for BECVF and using the $\pi$ periodicity property of the great circle basis elements gives:

$$R_{\left(\mathbf{i}_x,\mathbf{i}_y,0\mathbf{i}_z\right)}\left(\frac{\pi}{4}\right)\begin{bmatrix}x'\\y'\\z'\end{bmatrix}=\left(\lim_{\Delta\theta\to 0}\sum_{m=1}^{m=\frac{2\pi}{|\Delta\theta|}}\left[\left(R_{\left(-\mathbf{i}_x,\mathbf{i}_y,0\mathbf{i}_z\right)}\left(m\Delta\theta_M\right)\bullet\lim_{\Delta\theta\to 0}\sum_{n=1}^{n=\frac{2\pi}{|\Delta\theta|}}\left[\left(R_{\left(-\mathbf{i}_x,\mathbf{i}_y,0\mathbf{i}_z\right)}\left(n\Delta\theta_N\right)\bullet GC^{basis}_{\left(0\mathbf{i}_x,\mathbf{i}_y,\mathbf{i}_z\right)}\right)\right]\right)\right]\right) \tag{1.114}$$

Using the distributive property of the double sum gives:

$$R_{\left(\mathbf{i}_x,\mathbf{i}_y,0\mathbf{i}_z\right)}\left(\frac{\pi}{4}\right)\begin{bmatrix}x'\\y'\\z'\end{bmatrix}=\lim_{\Delta\theta\to 0}\sum_{m=1}^{m=\frac{2\pi}{|\Delta\theta|}}\lim_{\Delta\theta\to 0}\sum_{n=1}^{n=\frac{2\pi}{|\Delta\theta|}}R_{\left(-\mathbf{i}_x,\mathbf{i}_y,0\mathbf{i}_z\right)}\left(m\Delta\theta_M\right)\bullet R_{\left(-\mathbf{i}_x,\mathbf{i}_y,0\mathbf{i}_z\right)}\left(n\Delta\theta_N\right)\bullet GC^{basis}_{\left(0\mathbf{i}_x,\mathbf{i}_y,\mathbf{i}_z\right)} \tag{1.115}$$

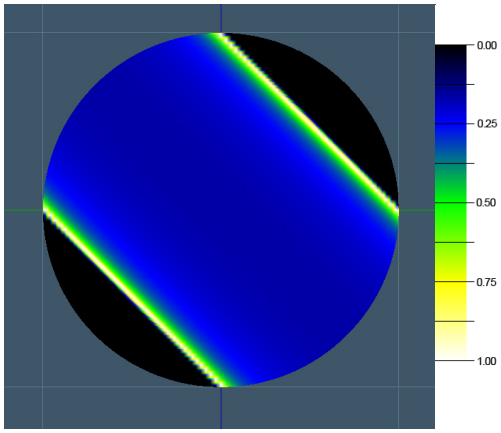
Rotation of the BECVF about its $C_\infty$-axis, the $\left(\mathbf{i}_x,\mathbf{i}_y,0\mathbf{i}_z\right)$-axis, leaves the BECVF distribution unchanged.

$$R_{\left(\mathbf{i}_x,\mathbf{i}_y,0\mathbf{i}_z\right)}\left(\frac{\pi}{4}\right)\begin{bmatrix}x'\\y'\\z'\end{bmatrix}=BECVF^{basis}_{\left(\frac{1}{\sqrt{2}}\mathbf{i}_x,\frac{1}{\sqrt{2}}\mathbf{i}_y,\mathbf{i}_z\right)} \tag{1.116}$$

Eq. (1.116) represents the properties of the distribution perpendicular to the $\left(-\frac{1}{\sqrt{2}}\mathbf{i}_x,\frac{1}{\sqrt{2}}\mathbf{i}_y,\mathbf{i}_z\right)$-axis since the distribution was rotated about the $\left(\mathbf{i}_x,\mathbf{i}_y,0\mathbf{i}_z\right)$-axis to align the $\left(-\frac{1}{\sqrt{2}}\mathbf{i}_x,\frac{1}{\sqrt{2}}\mathbf{i}_y,\mathbf{i}_z\right)$-axis with the $\left(-\mathbf{i}_x,\mathbf{i}_y,0\mathbf{i}_z\right)$-axis. This result confirms that the distribution is uniform about the $\left(-\frac{1}{\sqrt{2}}\mathbf{i}_x,\frac{1}{\sqrt{2}}\mathbf{i}_y,\mathbf{i}_z\right)$-axis since the $BECVF^{basis}_{\left(\frac{1}{\sqrt{2}}\mathbf{i}_x,\frac{1}{\sqrt{2}}\mathbf{i}_y,\mathbf{i}_z\right)}$ that served to generate the distribution of $Y_0^0(\theta,\phi)$ is azimuthally uniform. This is an important result since the spherically uniform distribution can be obtained by normalizing the distribution given by Eq. (1.102). Since any density normalization is along the $\left(-\frac{1}{\sqrt{2}}\mathbf{i}_x,\frac{1}{\sqrt{2}}\mathbf{i}_y,\mathbf{i}_z\right)$-axis, there is no change in the angular momentum since the distribution was formed by rotation of the basis elements about the angular momentum axis, the $\left(-\frac{1}{\sqrt{2}}\mathbf{i}_x,\frac{1}{\sqrt{2}}\mathbf{i}_y,\mathbf{i}_z\right)$-axis. Furthermore, the motion on the great circles maintains the uniform distribution since the normalization only scales the constant current on each to achieve uniformity.

Consider the color-scale rendering of the BECVF current density distribution shown in Figure 1.18. It was determined using a computer algorithm [13] that assigns a given number of points to a great circle basis element of Eqs. (1.84) and (1.87), generates the BECVF distribution of points along the great circles using a designated number of rotations about the $\left(-\mathbf{i}_x,\mathbf{i}_y,0\mathbf{i}_z\right)$-axis over a span of $2\pi$ radians, and for each point on the half-sphere, it calculates the number of points in a unit circular region in the neighborhood of each point. The radius of each point's neighborhood was taken to be 100 times smaller than the radius of the half-spherical distribution.

**Figure 1.18.** The numerically determined current density of the BECVF given by Eqs. (1.84) and (1.87) shown with 500 points on the great circle basis element and 0.72 degree increments of $\theta$ from the perspective of looking along the z-axis.




As shown in Figures 1.5 and 1.18 the great circle number of the BECVF is conserved, and the perimeter on the half sphere through which each great circle traverses can be defined by a bisecting plane that is parallel to the $\sigma_v$ plane and $C_2$ axis. At the center of the distribution, the circles traverse a perimeter having a circumference of $2\pi r_n$. The corresponding circumference at an angle $\theta_{sc}$ from the center of the distribution is $2\pi r_n \cos\theta_{sc}$ wherein $\theta_{sc}$ is the spherical coordinate and not the rotational angle $\theta$ of the CVFs. This gives rise to a $\cos\theta_{sc}$ dependency of the loop density for $0 \le \theta_{sc} \le \frac{\pi}{4}$. In addition, the great circles converge as the perimeter becomes smaller. Since the distribution of $Y_0^0(\theta,\phi)$ is given by the superposition of the current density of the BECVF as a function of the rotation of the BECVF about the $\left(-\frac{1}{\sqrt{2}}\mathbf{i}_x, \frac{1}{\sqrt{2}}\mathbf{i}_y, \mathbf{i}_z\right)$-axis, the $Y_0^0(\theta,\phi)$ current density is given by the azimuthal integral of the current density of the BECVF. This superposition is difficult to integrate, but a convenient method of determining the density is by numerical integration. The unnormalized $Y_0^0(\theta,\phi)$ current density was determined using the computer algorithm that assigns a given number of points to each great circle basis element, generates the distribution given by Eq. (1.103), and calculates the number of points in a unit circular neighborhood of each point on the surface. The numerically determined density is shown in color scale on the sphere in Figure 1.19. The density distribution is displayed as a distance and a color scale in Figure 1.20.

**Figure 1.19.** The z-axis view of the numerically determined unnormalized current density of $Y_0^0(\theta,\phi)$ shown with 100 points per great circle basis element, 3.6 degree increments ($N = M = 100$ in Eq. (1.103)) of the angle to generate the BECVF corresponding to Eqs. (1.84) and (1.87), and 3.6 degree increments of the rotation of this basis element about the $\left(-\frac{1}{\sqrt{2}}\mathbf{i}_x, \frac{1}{\sqrt{2}}\mathbf{i}_y, \mathbf{i}_z\right)$-axis corresponding to Eqs. (1.95) and (1.98).

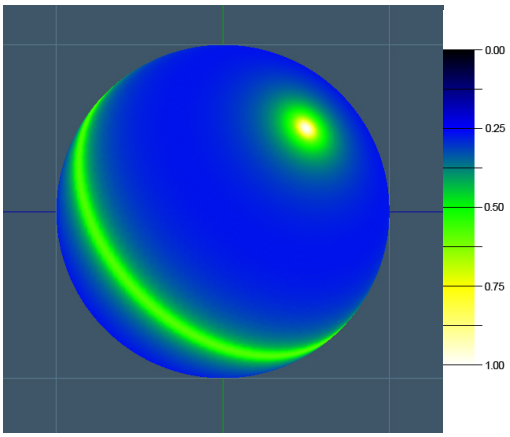
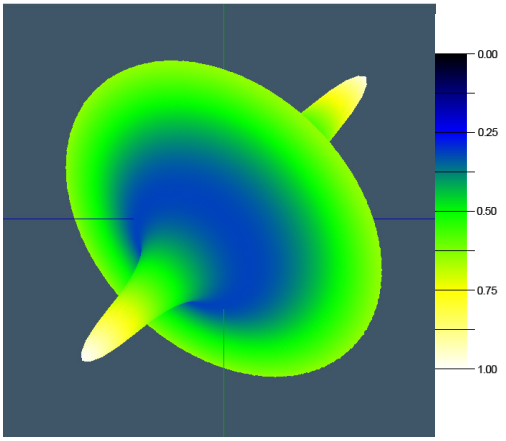



**Figure 1.20.** The z-axis view of the numerically determined unnormalized current density of $Y_0^0(\theta,\phi)$ wherein the density distribution is displayed as a distance and a color scale, and the view is rotated by 180° relative to Figure 1.19.



The normalization of the $Y_0^0(\theta,\phi)$ current pattern given by Eqs. (1.102) and (1.103) was performed using the numerical procedure developed by Bujnak and Hlucha [13]. It is based on forming a uniform great-circle normal-vector distribution. This is equivalent to a uniform great-circle current distribution due to the one-to-one map on the sphere between the former and latter. For a total of $N_{GC}$ great circles distributed over the sphere, the algorithm treats the normal vector of each great circle as coincident with the corresponding angular momentum axis as given by the right hand rule and assigns a dot of integer index $i$ to the intersection of this vector and the spherical shell. For each dot $i$, the number of other dots $D_i$ within a local neighborhood of dot $i$ are counted, and the corresponding normalization factor $N_i^{factor}$ is given by

$$N_i^{factor} = D_i^{-1} \tag{1.117}$$

Then, the linear current density on the great circle $GC_i$ corresponding to the dot of index $i$ is normalized by $N_i^{factor}$. The program treats the linear current density as a series of evenly spaced mass(current)-density elements ("points") with the initial condition that the total number of points on each great circle is the constant $P_{\text{initial}}$. Thus, the normalization scales the linear density, and in the discrete case, this is achieved by scaling the mass of each of the points on the great circle by the factor given by Eq. (1.117). This is repeated over all great circles. Since $Y_0^0(\theta,\phi)$ is given by the superposition of all points, using Eq. (1.117), the final total effective or weighted number of points on the surface $P_{\text{final}}^{Y_0^0(\theta,\phi)}$ is given by the normalized sum:

$$P_{\text{final}}^{Y_0^0(\theta,\phi)} = \sum_{i=1}^{N_{GC}} N_i^{factor} P_{\text{initial}} \tag{1.118}$$

Eq. (1.118) is representative of the total mass and current on the surface. The normalization is confirmed by determining the existence of a constant current density at multiple random positions on the sphere. Here, for any point that defines a position on the sphere of integer index $k$, the factor $N_j^{factor}$ of the other points of integer index $j$ within a local neighborhood of fixed area of position $k$ are counted, and uniformity is confirmed when the following condition is met over many cases:

$$\sum_j N_j^{factor} = \text{constant} \tag{1.119}$$

where $j$ runs through the points in the small circular neighborhood.

The angular momentum components corresponding to the unnormalized and normalized distributions were calculated numerically. According to the numerical algorithm, the total magnitude of the angular momentum over all of the great circles is set equal to $\hbar$ with the initial direction due to the great circle basis element in the y'z'-plane along the $(-1,0,0)$-axis. Then, in the unnormalized case, the magnitude of the contribution from each great circle is given by:

$$|L_i| = \frac{\hbar}{\sum_{j=1}^{N_{GC}} 1} = \frac{\hbar}{N_{GC}} \tag{1.120}$$

Since the direction of the angular momentum of the other great circles of the distribution are given by $R\left(\theta_i^{BECVF}, \theta_i^{OCVF}\right)$, the rotation by the two angles $\theta_i^{BECVF}, \theta_i^{OCVF}$ corresponding to the convolution of the respective CVFs, the total angular momentum $L_{Total}$ is given by:

$$L_{Total} = \sum_i^{N_{GC}} L_i = \sum_i^{N_{GC}} \frac{\hbar}{N_{GC}} R\left(\theta_i^{BECVF}, \theta_i^{OCVF}\right) \cdot (-1,0,0) \tag{1.121}$$

In the normalized case, the magnitude of the contribution from each great circle is given by:

$$|L_i| = \frac{N_i^{factor}\hbar}{\sum_{j=1}^{N_{GC}} N_j^{factor}} \tag{1.122}$$

Then, the total angular momentum $L_{Total}$ is given by:

$$L_{Total} = \sum_i^{N_{GC}} L_i = \sum_i^{N_{GC}} \frac{N_i^{factor}\hbar}{\sum_{j=1}^{N_{GC}} N_j^{factor}} R\left(\theta_i^{BECVF}, \theta_i^{OCVF}\right) \cdot (-1,0,0) \tag{1.123}$$

In both cases, the calculated results are given as follows:

$$\begin{aligned} L_x^{total} &\sim -0.248\hbar \sim -\frac{\hbar}{4} \\ L_y^{total} &\sim 0.248\hbar \sim \frac{\hbar}{4} \\ L_z^{total} &\sim 0.35\hbar \sim \frac{\hbar}{2\sqrt{2}} \end{aligned} \tag{1.124}$$

$$|L_{xyTotal}| = \sqrt{\left(L_x^{total}\right)^2 + \left(L_y^{total}\right)^2} \sim 0.35\hbar \sim \frac{\hbar}{2\sqrt{2}} \tag{1.125}$$

$$\left|L_{Total}\right| = \sqrt{\left(L_x^{total}\right)^2 + \left(L_y^{total}\right)^2 + \left(L_z^{total}\right)^2} \sim 0.495\hbar \sim \frac{\hbar}{2} \tag{1.126}$$

These results confirm that the normalization does not affect the angular momentum. The numerically normalized $Y_0^0(\theta,\phi)$ (Figure 1.21) gives the desired spherical uniformity and is permissive of demonstrating the motion of the current in time over the entire surface according to the great circle pattern having constant current per loop each weighted by the normalization algorithm. An ideal representation overlaid with the great-circle pattern showing the vector direction of the current is shown in Figure 1.22.

**Figure 1.21.** The z-axis view of the numerically normalized current density of $Y_0^0(\theta,\phi)$ shown with 100 points per great circle basis element, 3.6 degree increments ($N = M = 100$ in Eq. (1.103)) of the angle to generate the BECVF corresponding to Eqs. (1.84) and (1.87), and 3.6 degree increments of the rotation of this basis element about the $\left(-\frac{1}{\sqrt{2}}\mathbf{i}_x, \frac{1}{\sqrt{2}}\mathbf{i}_y, \mathbf{i}_z\right)$-axis corresponding to Eqs. (1.95) and (1.98). As the number of points increased and the size of the local neighborhood decreased, the exact uniformity was numerically approached.

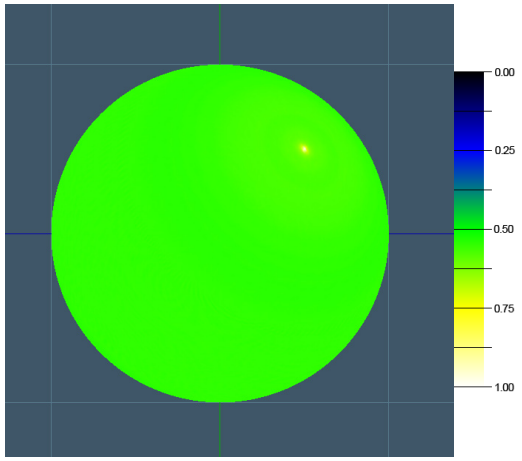
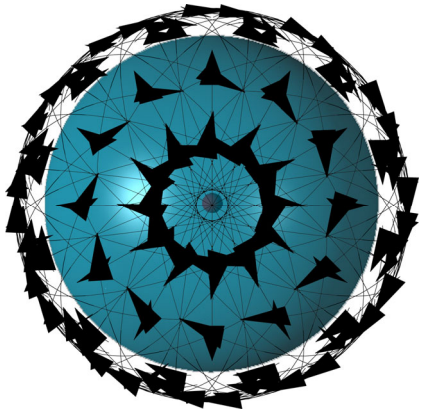



**Figure 1.22.** An ideal representation of the uniform current pattern of $Y_0^0(\theta,\phi)$ comprising the superposition of an infinite number of great circle elements generated by normalizing the distribution of Eqs. (1.102) and (1.103). The constant uniform current density is overlaid with 144 vectors giving the direction of the current of each great circle element for 30 degree increments ($N = M = 12$ in Eq. (1.103)) of the angle to generate the BECVF corresponding to Eqs. (1.84) and (1.87) and 30 degree increments of the rotation of this basis element about the $\left(-\frac{1}{\sqrt{2}}\mathbf{i}_x, \frac{1}{\sqrt{2}}\mathbf{i}_y, \mathbf{i}_z\right)$-axis corresponding to Eqs. (1.95) and (1.98). The perspective is along the $\left(-\frac{1}{\sqrt{2}}\mathbf{i}_x, \frac{1}{\sqrt{2}}\mathbf{i}_y, \mathbf{i}_z\right)$-axis.



The electron current shown in Figure 1.22 is consistent with Maxwell's equations, other first principles, and the boundary conditions implied by the Stern Gerlach experiment. The crossings reveal an intrinsic property regarding self-interactions of fundamental particles having angular momentum, mass, and an extended nature. Extrinsic fundamental particle scattering interactions depend on the cross section for momentum or energy transfer. These cross sections can vary over an enormous range. Neutrinos and neutrons, for example, have negligible cross sections with condensed matter compared to charged particles. The cross section for interaction amongst photons or field lines within a single photon is zero. The electron is an indivisible special state of a 510 keV photon, and the cross section for momentum transfer amongst current elements of the electron is likewise experimentally zero. This is consistent with the original boundary condition that momentum transfer among fundamental particles having $\hbar$ of angular momentum occurs in quantized units of $\hbar$ requiring that electron momentum transfer must involve its intrinsic angular momentum in its entirety as discussed in Appendix II[7]. Computer modeling of the analytical equations to generate the atomic orbital current vector field and the uniform current (charge) density function $Y_0^0(\theta,\phi)$ is available on the web [13-14]. Also, the precession motion of the free electron over time in the presence of an applied magnetic field generates the equivalent current pattern and the angular momentum of $Y_0^0(\theta,\phi)$ of the bound electron as shown in the Electron in Free Space section and Appendix IV. Given the angular momentum projections of the bound electron shown in Figure 1.23 and that the free electron has $\hbar$ of angular momentum on the z-axis due to in-plane current loops, the free-electron

[7] The angular momentum of neutrinos are $\frac{\hbar}{2}$ which accounts for their negligible interaction cross section as discussed in the Neutrinos section.

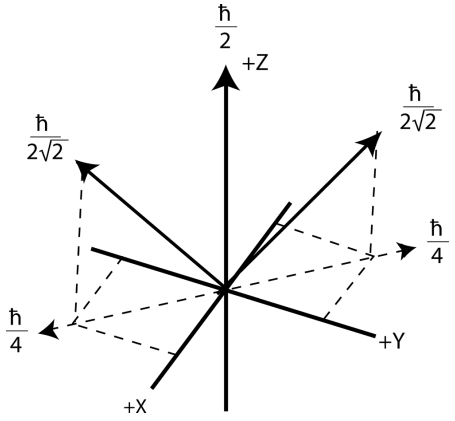
angular momentum can be considered to partition into two orthogonal, equal magnitude components of $\frac{\hbar}{2\sqrt{2}}$ and the current, carried on great circle elements, to rescale to form a uniform density due to binding to the central field.

## SPIN ANGULAR MOMENTUM OF THE ATOMIC ORBITAL $Y_0^0(\theta,\phi)$ WITH $\ell$ = 0

Consider the vector current directions shown in Figure 1.8. The orthogonal great-circle basis set is rotated about the $\left(-\frac{1}{\sqrt{2}}\mathbf{i}_x,\frac{1}{\sqrt{2}}\mathbf{i}_y,\mathbf{i}_z\right)$-axis. The resultant angular momentum vector is along this axis. Thus, the resultant angular momentum vector of magnitude $\frac{\hbar}{2}$ is stationary throughout the rotations that transform the axes as given in Table 1.1. The convolution operation of the BECVF with the OCVF is also about the resultant angular momentum axis, the $\left(-\frac{1}{\sqrt{2}}\mathbf{i}_x,\frac{1}{\sqrt{2}}\mathbf{i}_y,\mathbf{i}_z\right)$-axis. Here, the resultant angular momentum vector of the one BECVF of $\frac{\hbar}{\sqrt{2}}$ in the direction of the $\left(-\mathbf{i}_x,\mathbf{i}_y,0\mathbf{i}_z\right)$-axis over a $2\pi$ span is matched to and replaces that of the basis element great circles. Thus, the resultant angular momentum of $\frac{\hbar}{2}$ having components of $\mathbf{L}_{xy}=\frac{\hbar}{2\sqrt{2}}$ and $\mathbf{L}_z=\frac{\hbar}{2\sqrt{2}}$ is stationary on this axis for all rotations. There is no alteration of the angular momentum with normalization since it only affects the density parallel to the angular momentum axis of the distribution, the $\left(-\frac{1}{\sqrt{2}}\mathbf{i}_x,\frac{1}{\sqrt{2}}\mathbf{i}_y,\mathbf{i}_z\right)$-axis. This was proven by numerical integration of the normalized distribution.

Next, it is shown that the properties of $Y_0^0(\theta,\phi)$ match the boundary conditions of having the desired angular momentum components, coverage, element motion, and uniformity by designating the $\left(-\frac{1}{\sqrt{2}}\mathbf{i}_x,\frac{1}{\sqrt{2}}\mathbf{i}_y,\mathbf{i}_z\right)$-axis as the z-axis. The resulting reoriented initial angular momentum component vectors and their new projections relative to the laboratory Cartesian coordinates are shown in Figure 1.23.

**Figure 1.23.** With the application of a magnetic field the magnetic moment corresponding to the intrinsic angular momentum of the electron of $\frac{\hbar}{2}$ aligns with the applied field direction designated the z-axis. Thus, the resultant angular momentum initially along the $\left(-\frac{1}{\sqrt{2}}\mathbf{i}_x,\frac{1}{\sqrt{2}}\mathbf{i}_y,\mathbf{i}_z\right)$-axis aligns with the z-axis. The new projections relative to the Cartesian coordinates are shown.



Referring to the new coordinates, the new angular momentum components are $\frac{\hbar}{2}$ along the z-axis, $\frac{\hbar}{2\sqrt{2}}$ along the $\left(\frac{1}{\sqrt{2}}\mathbf{i}_x,-\frac{1}{\sqrt{2}}\mathbf{i}_y,\mathbf{i}_z\right)$ and $\left(-\frac{1}{\sqrt{2}}\mathbf{i}_x,\frac{1}{\sqrt{2}}\mathbf{i}_y,\mathbf{i}_z\right)$-axes, and the xy-plane projections of the latter of $+/-\frac{\hbar}{4}$ along the $\left(\mathbf{i}_x,-\mathbf{i}_y,0\mathbf{i}_z\right)$-axis. (Note that the crossed vectors in Figure 1.22 are the source of the orthogonal components of $\frac{\hbar}{2\sqrt{2}}$.) Then, the Zeeman-splitting-active vector projections of the angular momentum that give rise to the Stern Gerlach phenomenon and other aspects of spin are those components that are onto the xy-plane and the z-axis.

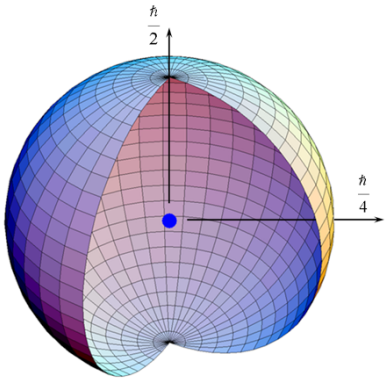
### Zeeman L Components

$$\mathbf{L}_{xy}=+/-\frac{\hbar}{4} \tag{1.127}$$

$$\mathbf{L}_{z}=\frac{\hbar}{2} \tag{1.128}$$

where $+/-$ designates both the positive and negative vector directions along an axis in the xy-plane such as the $\left(\mathbf{i}_x,-\mathbf{i}_y,0\mathbf{i}_z\right)$-axis. Consider the behavior of the electron in the presence of an applied magnetic field wherein the Zeeman-active angular momentum of $Y_0^0(\theta,\phi)$ (Figure 1.24) for a right-handed circularly polarized photon is $\mathbf{L}_{xy}=\frac{\hbar}{4}$ and $\mathbf{L}_{z}=\frac{\hbar}{2}$ (Eqs. (1.127-1.128)). As shown in the Resonant Precession of the Spin-1/2-Current-Density Function Gives Rise to the Bohr Magneton section, the electron undergoes resonant Larmor-precession excitation. The angular momentum of the photon of the Larmor excited state electrodynamically interacts with one component of $\mathbf{L}_{xy}$ depending on its handedness to establish a torque balance that results in the orientation of the $\hbar$ of angular momentum of the photon such that its vector projections are $\mathbf{L}_{xy}=\sqrt{\frac{3}{4}}\hbar$ in a Larmor rotating frame and $\mathbf{L}_{z}=\frac{\hbar}{2}$ such that the total angular momentum onto the z-axis, sum of the photon and electron contributions, is $\hbar$. These results meet the boundary condition for the unique current having an angular velocity magnitude at each point on the surface given by Eq. (1.36) and give rise to the result of the Stern Gerlach experiment as shown *infra*, in the Magnetic Parameters of the Electron (Bohr Magneton) section, and in the Electron g Factor section.

**Figure 1.24.** The atomic orbital is a two dimensional spherical shell of zero thickness with the Bohr radius of the hydrogen atom, $r=a_H$, having intrinsic angular momentum components of $\mathbf{L}_{xy}=\frac{\hbar}{4}$ and $\mathbf{L}_{z}=\frac{\hbar}{2}$ following Larmor excitation in a magnetic field.



## RESONANT PRECESSION OF THE SPIN-1/2-CURRENT-DENSITY FUNCTION GIVES RISE TO THE BOHR MAGNETON

The Stern Gerlach experiment described below demonstrates that the magnetic moment of the electron can only be parallel or antiparallel to an applied magnetic field. In spherical coordinates, this implies a spin quantum number of 1/2 corresponding to an angular momentum on the z-axis of $\frac{\hbar}{2}$. However, the Zeeman splitting energy corresponds to a magnetic moment of $\mu_B$ and implies an electron angular momentum on the z-axis of $\hbar$—twice that given by Eq. (1.128). Consider the case of a magnetic field applied to the atomic orbital. As shown in Figure 1.23, the atomic orbital comprises an angular momentum component of $\frac{\hbar}{2}$ along the z-axis and two $\frac{\hbar}{4}$ angular momentum components in opposite directions in the xy-plane. The magnetic moment corresponding to the angular momentum along the z-axis results in the alignment of the z-axis of the atomic orbital with the magnetic field while one of the $\frac{\hbar}{4}$ vectors in the xy-plane causes precession about the applied field. The precession arises from a Larmor excitation by a corresponding resonant photon that couples to one of the $\frac{\hbar}{4}$ angular momentum components to conserve the angular momentum of the photon such that the precession direction matches the handedness of the Larmor photon. An example given in Figure 1.25 regards a right-hand polarized photon that excites the right-handed Larmor precession by coupling to the corresponding $\frac{\hbar}{4}$ angular momentum component as shown. The precession frequency is the Larmor frequency given by the product of the gyromagnetic ratio of the electron, $\frac{e}{2m}$, and the magnetic flux $\mathbf{B}$ [15]. The energy of the precessing electron corresponds to Zeeman splitting—energy levels corresponding to the parallel or antiparallel alignment of the electron magnetic moment with the magnetic field and the excitation of transitions between these states by flipping the orientation along the field by a further resonant photon of the Larmor frequency. Thus, the energy of the transition between these states is that of the resonant photon. The angular momentum of the precessing atomic orbital comprises the initial $\frac{\hbar}{2}$ projection on the z-axis and the initial $\frac{\hbar}{4}$ vector component in the xy-plane that then precesses about the z-axis with the Larmor photon. As shown in the Excited States of the One-Electron Atom (Quantization) section, conservation of the angular momentum of the photon of $\hbar$ gives rise to $\hbar$ of electron angular momentum that gives rise to a $\frac{\hbar}{2}$ contribution to the angular momentum along the magnetic-field or z-axis. The parameters of the photon standing wave for the Zeeman effect are given in the Magnetic Parameters of the Electron (Bohr Magneton) section and Box 1.1.

The angular momentum of the atomic orbital in a magnetic field comprises the static $\frac{\hbar}{2}$ projection on the z-axis (Eq. (1.128)) and the $\frac{\hbar}{4}$ vector component in the xy-plane (Eq. (1.127)) that precesses about the z-axis at the Larmor frequency. The precession at the Larmor frequency as well as the excitation of a spin-flip transition is equivalent to the excitation of an excited state as given in the Excited States of the One-Electron Atom (Quantization) section. Consider the first resonant process. A resonant excitation of the Larmor precession frequency gives rise to a trapped photon with $\hbar$ of angular momentum along a precessing $\mathbf{S}$-axis. In the coordinate system rotating at the Larmor frequency (denoted by the axes labeled $X_R$, $Y_R$, and $Z_R$ in Figure 1.25), the $X_R$-component of magnitude $\frac{\hbar}{4}$ and $\mathbf{S}$ of magnitude $\hbar$ are stationary. The $\frac{\hbar}{4}$ angular momentum along $X_R$ with a corresponding magnetic moment of $\frac{\mu_B}{4}$ (Eq. (28) of Box 1.1) causes $\mathbf{S}$ to rotate in the $Y_R\,Z_R$-plane to an angle of $\theta = \frac{\pi}{3}$ such that the torques due to the $Z_R$-component of $\frac{\hbar}{2}$ and the orthogonal $X_R$-component of $\frac{\hbar}{4}$ are balanced. Then the $Z_R$-component due to $\mathbf{S}$ is $\pm\hbar\cos\frac{\pi}{3} = \pm\frac{\hbar}{2}$. The reduction of the magnitude of $\mathbf{S}$ along $Z_R$ from $\hbar$ to $\frac{\hbar}{2}$ corresponds to the ratio of

the $X_R$-component and the static $Z_R$-component of $\frac{\frac{\hbar}{4}}{\frac{\hbar}{2}}=\frac{1}{2}$[8]. Since the $X_R$-component is $\frac{\hbar}{4}$, the $Z_R$-component of **S** is $\frac{\hbar}{2}$ which adds to the initial $\frac{\hbar}{2}$ component to give a total $Z_R$-component of $\hbar$.

[8] The torque balance can be appreciated by considering that **S** is aligned with $Z_R$ if the $X_R$-component is zero, and the three vectors are mutually orthogonal if the $X_R$-component is $\frac{\hbar}{2}$. The balance can be shown by considering the magnetic energies resulting from the corresponding torques when they are balanced. Using Eqs. (23) and (25) of Box 1.1, the potential energy $E_V$ due to the projection of **S**'s angular momentum of $\hbar$ along $Z_R$ having $\frac{\hbar}{2}$ of angular momentum is

$$E_V = \mu_B B\cos\theta = \mu_B \frac{1}{2} B_{\mu_B}\cos\theta = \frac{1}{2}\hbar\omega_{\mu_B}\cos\theta \tag{1}$$

where $B_{\mu_B}$ is the flux due to a magnetic moment of a Bohr magneton and $\omega_{\mu_B}$ is the corresponding gyromagnetic frequency. The application of a magnetic moment along the $X_R$-axis causes **S** to precess about the $Z_R$ and $X_R$-axes. In the $X_R\,Y_R\,Z_R$-frame rotating at $\omega_{\mu_B}$, **S** precesses about the $X_R$-axis. The corresponding precession energy $E_{X_R}$ of **S** about the $X_R$-component of $\frac{\hbar}{4}$ is the corresponding Larmor energy

$$E_{X_R} = -\frac{1}{4}\hbar\omega_{\mu_B} \tag{2}$$

The energy $E_{Z_R}$ of the magnetic moment corresponding to **S** rotating about $Z_R$ having $\frac{\hbar}{2}$ of angular momentum is the corresponding Larmor energy:

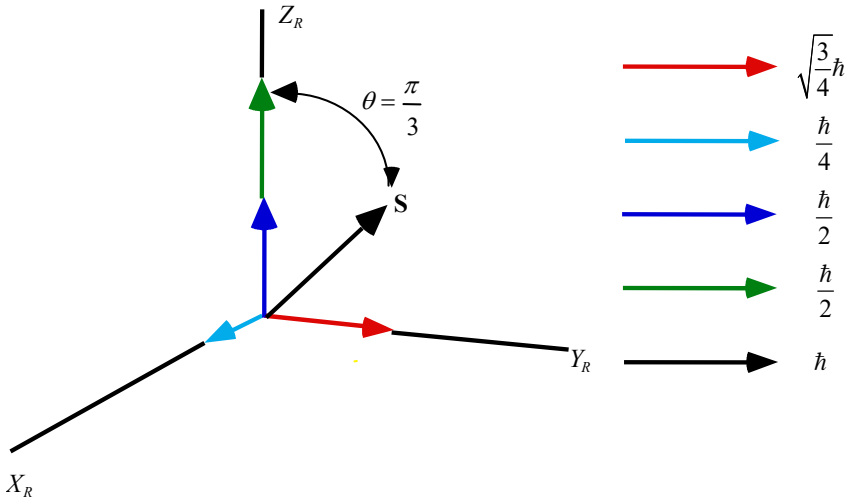
$$E_{Z_R} = \frac{1}{2}\hbar\omega_{\mu_B} \tag{3}$$

At torque balance, the potential energy is equal to the sum of the Larmor energies:

$$E_{Z_R} + E_{X_R} = \hbar\left(\frac{1}{2}-\frac{1}{4}\right)\omega_{\mu_B} = \frac{\hbar}{2}\left(1-\frac{\frac{1}{4}}{\frac{1}{2}}\right)\omega_{\mu_B} = \frac{1}{2}\hbar\omega_{\mu_B}\cos\theta \tag{4}$$

Balance occurs when $\theta=\frac{\pi}{3}$. Thus, the intrinsic torques are balanced. Furthermore, energy is conserved relative to the external field as well as to the intrinsic, $Z_R$ and $X_R$-components of the atomic orbital, and the Larmor relationships for both the gyromagnetic ratio and the potential energy of the resultant magnetic moment are satisfied as shown in Box 1.1.

**Figure 1.25.** The angular momentum components of the atomic orbital and **S** in the rotating coordinate system $X_R$, $Y_R$, and $Z_R$ that precesses at the Larmor frequency about $Z_R$ such that the vectors are stationary.




In summary, since the vector **S** that precesses about the z-axis is at an angle of $\theta = \frac{\pi}{3}$ with respect to this axis, has an $X_R\,Y_R$-plane projection at an angle of $\phi = \frac{\pi}{2}$ with respect to $\mathbf{L}_{xy}$ given by Eq. (1.127), and has a magnitude of $\hbar$, the **S** projections in the $X_R\,Y_R$-plane and along the $Z_R$-axis are:

$$\mathbf{S}_{\perp} = \pm\hbar \sin\frac{\pi}{3} = \pm\sqrt{\frac{3}{4}}\hbar\,\mathbf{i}_{Y_R} \tag{1.129}$$

$$\mathbf{S}_{\parallel} = \pm\hbar \cos\frac{\pi}{3} = \pm\frac{\hbar}{2}\,\mathbf{i}_{Z_R} \tag{1.130}$$

The plus or minus sign of Eqs. (1.129) and (1.130) corresponds to the two possible vector orientations which are observed with the Stern-Gerlach experiment described below. The sum of the torques in the external magnetic field is balanced unless an RF field is applied to cause a Stern-Gerlach transition as discussed in Box 1.1.

**Figure 1.26.** The angular momentum components of the atomic orbital and **S** in the stationary coordinate system. **S** and the components in the xy-plane precess at the Larmor frequency about the z-axis.

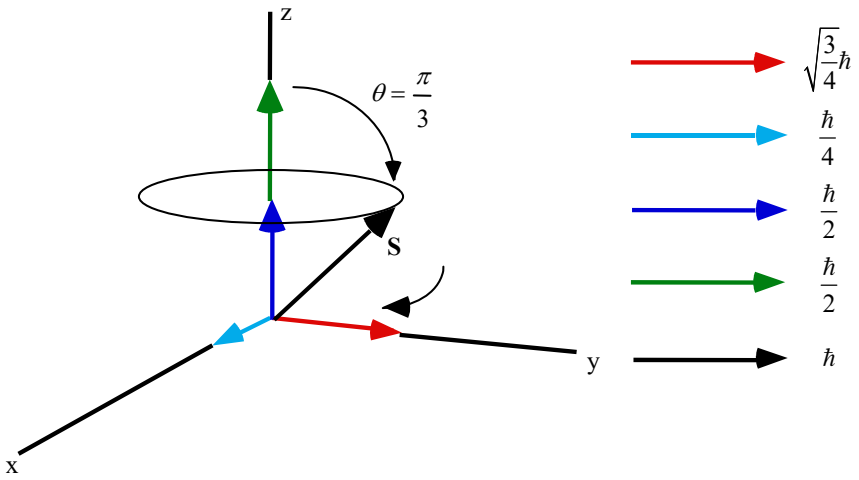
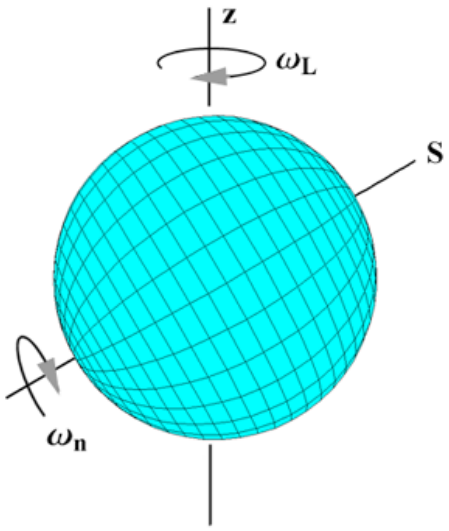


**Figure 1.27.** The orientation of the atomic orbital and **S** that has the angular momentum components shown in Figure 1.26. The applied magnetic field is in the z-axis direction. The dipole-current spins about the **S**-axis at angular velocity $\omega_n$ given by Eq. (1.36) and the atomic orbital and **S** precess at the Larmor frequency about the z-axis.




As shown in Figures 1.26 and 1.27, **S** forms a cone in time in the nonrotating laboratory frame with an angular momentum of $\hbar$ that is the source of the known magnetic moment of a Bohr magneton (Eq. (28) of 1.1) as shown in the Magnetic Parameters of the Electron (Bohr Magneton) section. The projection of this angular momentum onto the z-axis of $\frac{\hbar}{2}$ adds to the z-axis component before the magnetic field was applied to give a total of $\hbar$. Thus, in the absence of a resonant precession, the z-component of the angular momentum is $\frac{\hbar}{2}$, but the excitation of the precessing **S** component gives $\hbar$—twice the angular momentum on the z-axis. In addition, rather than a continuum of orientations with corresponding energies, the orientation of the magnetic moment must be only parallel or antiparallel to the magnetic field. This arises from conservation of angular momentum between the "static" and "dynamic" z-axis projections of the angular momentum with the additional constraint that the angular momentum has a "kinetic" as well as a "potential" or vector potential component. To conserve angular momentum, flux linkage by the electron is quantized in units of the magnetic flux quantum, $\Phi_0 = \frac{h}{2e}$, as shown in Box 1.1 and in the Electron g Factor section. Thus, the spin quantum number is $s = \frac{1}{2}$; $m_s = \pm\frac{1}{2}$, but the observed Zeeman splitting corresponds to a full Bohr magneton due to $\hbar$ of angular momentum. This aspect was historically felt to be inexplicable in terms of classical physics and merely postulated in the past.

The demonstration that the boundary conditions of the electron in a magnetic field are met appears in Box 1.1. The observed electron parameters are explained physically. Classical laws give (1) a gyromagnetic ratio of $\frac{e}{2m}$, (2) a Larmor precession frequency of $\frac{e\mathbf{B}}{2m}$, (3) the Stern-Gerlach experimental result of quantization of the angular momentum that implies a spin quantum number of 1/2 corresponding to an angular momentum of $\frac{\hbar}{2}$ on the z-axis, and (4) the observed Zeeman splitting due to a magnetic moment of a Bohr magneton $\mu_B = \frac{e\hbar}{2m_e}$ corresponding to an angular momentum of $\hbar$ on the z-axis. Furthermore, the solution is relativistically invariant as shown in the Special Relativistic Effect on the Electron Radius and the Relativistic Ionization Energies section. Dirac originally attempted to solve the bound electron physically with stability with respect to radiation according to Maxwell's equations with the further constraints that it was relativistically invariant and thus gave rise to electron spin [16]. He was unsuccessful and resorted to the current mathematical probability-wave model that has many problems as discussed in Refs. [17-18].

# MAGNETIC PARAMETERS OF THE ELECTRON (BOHR MAGNETON)

## THE MAGNETIC FIELD OF AN ATOMIC ORBITAL FROM SPIN

The atomic orbital with $\ell = 0$ is a shell of negative charge current comprising correlated charge motion along great circles. The superposition of the vector projection of the atomic orbital angular momentum on the z-axis is $\frac{\hbar}{2}$ with an orthogonal component of $\frac{\hbar}{4}$. As shown in the Atomic Orbital Equation of Motion For $\ell = 0$ Based on the Current Vector Field (CVF) section, the application of a magnetic field to the atomic orbital gives rise to a precessing angular momentum vector $\mathbf{S}$ directed from the origin of the atomic orbital at an angle of $\theta = \frac{\pi}{3}$ relative to the applied magnetic field. The precession of $\mathbf{S}$ with an angular momentum of $\hbar$ forms a cone in the nonrotating laboratory frame to give a perpendicular projection of $\mathbf{S}_{\perp} = \pm\sqrt{\frac{3}{4}}\hbar$ (Eq. (1.129)) and a projection onto the axis of the applied magnetic field of $\mathbf{S}_{\parallel} = \pm\frac{\hbar}{2}$ (Eq. (1.130)). The superposition of the $\frac{\hbar}{2}$ z-axis component of the atomic orbital angular momentum and the $\frac{\hbar}{2}$ z-axis component of $\mathbf{S}$ gives $\hbar$ corresponding to the observed magnetostatic electron magnetic moment of one Bohr magneton. The $\hbar$ of angular momentum along $\mathbf{S}$ has a corresponding precessing magnetic moment of 1 Bohr magneton [19]:

$$\mu_B = \frac{e\hbar}{2m_e} = 9.274\ X\ 10^{-24}\ JT^{-1} \tag{1.131}$$

The rotating magnetic field of $\mathbf{S}$ is discussed in Box 1.1. The magnetostatic magnetic field corresponding to $\mu_B$ derived below is given by

$$\mathbf{H} = \frac{e\hbar}{m_e r_n^3}(\mathbf{i}_r \cos\theta - \mathbf{i}_\theta \sin\theta) \qquad \text{for } r < r_n \tag{1.132}$$

$$\mathbf{H} = \frac{e\hbar}{2m_e r^3}(\mathbf{i}_r 2\cos\theta + \mathbf{i}_\theta \sin\theta) \qquad \text{for } r > r_n \tag{1.133}$$

It follows from Eq. (1.131), the relationship for the Bohr magneton, and relationship between the magnetic dipole field and the magnetic moment $\mathbf{m}$ [20] that Eqs. (1.132) and (1.133) are the equations for the magnetic field due to a magnetic moment of a Bohr magneton, $\mathbf{m} = \mu_B \mathbf{i}_\mathbf{z}$ where $\mathbf{i}_\mathbf{z} = \mathbf{i}_\mathbf{r}\cos\theta - \mathbf{i}_\theta \sin\theta$. Note that the magnetic field is a constant for $r < r_n$. See Figures 1.28 and 1.29. It is shown in the Magnetic Parameters of the Electron (Bohr Magneton) section that the energy stored in the magnetic field of the electron atomic orbital is

$$E_{mag,total} = \frac{\pi\mu_0 e^2\hbar^2}{m_e^2 r_1^3} \tag{1.134}$$

**Figure 1.28.** The two-dimensional cut-away representation of the magnetic field of an electron atomic orbital. The field is a dipole outside the atomic orbital and uniform inside the atomic orbital.

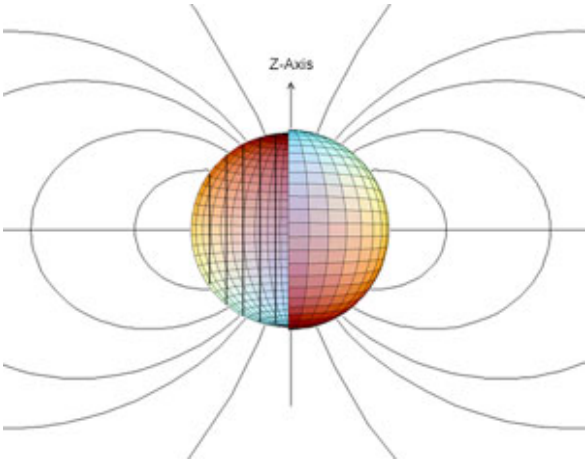
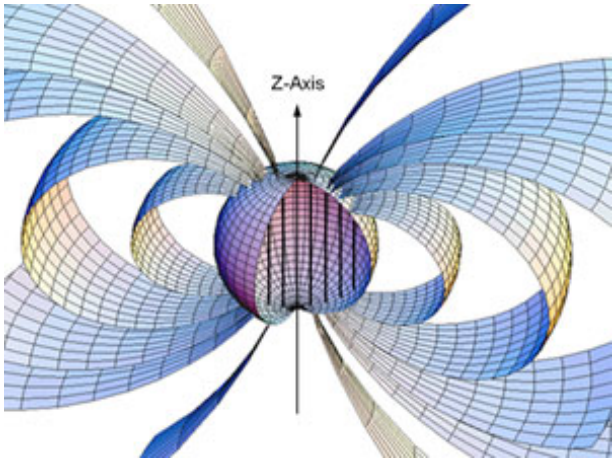



**Figure 1.29.** The three-dimensional cut-away representation of the magnetic field of an electron atomic orbital. The field is a dipole outside the atomic orbital and uniform inside the atomic orbital.



## DERIVATION OF THE MAGNETIC FIELD

For convenience the angular momentum vector with a magnitude in the stationary frame of $\hbar$ will be defined as the z-axis as shown in Figures 1.28 and 1.29[9] . The magnetic field must satisfy the following relationships:

$$\nabla \cdot \mathrm{H} = 0 \text{ } \textit{in free space} \tag{1.135}$$

$$\mathbf{n}\ X\ (\mathbf{H}_a - \mathbf{H}_b) = \mathbf{K} \tag{1.136}$$

$$\mathbf{n} \cdot (\mathbf{H}_a - \mathbf{H}_b) = 0 \tag{1.137}$$

$$\mathbf{H} = -\nabla \psi \tag{1.138}$$

Since the field is magnetostatic, the current is equivalent to that of current loops extending along the z-axis with the current direction perpendicular to the z-axis. Then, the component of the current about the z-axis, $\mathbf{i}_\phi$, for a current loop of total charge, $e$, oriented at an angle $\theta$ with respect to the z-axis, is given by the product of the charge, the angular velocity given by Eq. (1.36), and $\sin\theta$ since the projection of the current of the atomic orbital perpendicular to the z-axis which carries the incremental current, $\mathbf{i}_\phi$, is a function of $\sin\theta$.

$$\mathbf{i}_\phi = \frac{e\hbar}{m_e {r_n}^2} \sin\theta \hat{i}_\phi \tag{1.139}$$

where $\hat{i}_\phi$ is the unit vector. The angular function of the current density of the atomic orbital is normalized by the geometrical factor $N$ [9] given by:

$$N = \frac{4\pi r_n^3}{2\pi \int_{-r_n}^{r_n} \left(r_n^2 - z^2\right) dz} = \frac{3}{2} \tag{1.140}$$

corresponding to the angular momentum of $\hbar$. (Eq. (1.140) can also be expressed in spherical coordinates for the density of a uniform shell divided by the integral in $\theta$ and $\phi$ of that of a spherical dipole squared [8]. The integration gives $\frac{8\pi}{3}$ which normalized by the uniform mass-density factor of $4\pi$ gives the geometrical factor of $\left(\frac{2}{3}\right)^{-1}$.) The current density $\mathbf{K}\hat{i}_\phi$ along the z-axis having a vector orientation perpendicular to the angular momentum vector is given by dividing the magnitude of $\mathbf{i}_\phi$ (Eq. (1.139)) by the length $r_n$. The current density of the atomic orbital in the incremental length $dz$ is:

$$\mathbf{K}(\rho, \phi, z)\hat{i}_\phi = \hat{i}_\phi N \frac{e\hbar}{m_e {r_n}^3} = \hat{i}_\phi \frac{3}{2} \frac{e\hbar}{m_e {r_n}^3} \tag{1.141}$$

Because

$$z = r\cos\theta \tag{1.142}$$

the differential length is given by:

$$dz = -\sin\theta r_n d\theta \tag{1.143}$$

and so the current density in the differential length $r_n d\theta$ as measured along the periphery of the atomic orbital is a function of $\sin\theta$ as given in Eq. (1.139). From Eq. (1.141), the surface current-density function of the atomic orbital about the z-axis (**S**-axis) is given by:

$$\mathbf{K}(r, \theta, \varphi)\hat{i}_\phi = \hat{i}_\phi \frac{3}{2} \frac{e\hbar}{m_e {r_n}^3} \sin\theta \tag{1.144}$$

Substitution of Eq. (1.144) into Eq. (1.136) gives:

$$H_\theta^a - H_\theta^b = \frac{3}{2} \frac{e\hbar}{m_e {r_n}^3} \sin\theta \tag{1.145}$$

---

[9] As shown in Box 1.1, the angular momentum of $\hbar$ on the **S**-axis is due to a photon standing wave that is phase-matched to a spherical harmonic source current, a spherical harmonic dipole $Y_1^m(\theta, \phi) = \sin\theta$ with respect to the **S**-axis. The dipole spins about the **S**-axis at the angular velocity given by Eq. (1.36). Since the field is magnetostatic in the RF rotating frame, the current is equivalent to current loops along the **S**-axis. Thus, the derivation of the corresponding magnetic field is the same as that of the stationary field given in this section.

To obtain $H_\theta$, the derivative of $\psi$ with respect to $\theta$ must be taken, and this suggests that the $\theta$ dependence of $\psi$ be taken as $\cos\theta$. The field is finite at the origin and is zero at infinity; so, solutions of Laplace's equation in spherical coordinates are selected because they are consistent with these conditions [21].

$$\Psi = C\left[\frac{r}{r_n}\right]\cos\theta \ ; \qquad r < r_n \tag{1.146}$$

$$\Psi = A\left[\frac{r_n}{r}\right]^2\cos\theta \ ; \qquad r > r_n \tag{1.147}$$

The negative gradients of these potentials are

$$\mathbf{H} = \frac{-C}{r_n}(\mathbf{i}_r\cos\theta - \mathbf{i}_\theta\sin\theta) \quad \text{for } r < r_n \tag{1.148}$$

$$\mathbf{H} = \frac{A}{r_n}\left[\frac{r_n}{r}\right]^3(\mathbf{i}_r 2\cos\theta + \mathbf{i}_\theta\sin\theta) \quad \text{for } r > r_n \tag{1.149}$$

where $\mathbf{i}_r$ and $\mathbf{i}_\theta$ are unit vectors. The continuity conditions of Eqs. (1.136), (1.137), (1.144), and (1.145) are applied to obtain the following relationships among the variables:

$$\frac{-C}{r_n} = \frac{2A}{r_n} \tag{1.150}$$

$$\frac{A}{r_n} - \frac{C}{r_n} = \frac{3}{2}\frac{e\hbar}{m_e r_n^3} \tag{1.151}$$

Solving the variables algebraically gives the magnetic fields of an electron:

$$\mathbf{H} = \frac{e\hbar}{m_e r_n^3}(\mathbf{i}_r\cos\theta - \mathbf{i}_\theta\sin\theta) \qquad \text{for } r < r_n \tag{1.152}$$

$$\mathbf{H} = \frac{e\hbar}{2m_e r^3}(\mathbf{i}_r 2\cos\theta + \mathbf{i}_\theta\sin\theta) \quad \text{for } r > r_n \tag{1.153}$$

The field is that of a Bohr magneton which matches the observed boundary conditions given in the Atomic Orbital Equation of Motion For $\ell$ = 0 Based on the Current Vector Field (CVF) section including the required spherical symmetry. The demonstration that the boundary conditions of the electron in a magnetic field are met appears in Box 1.1.

## DERIVATION OF THE ENERGY

The energy stored in the magnetic field of the electron is:

$$E_{mag} = \frac{1}{2}\mu_0\int_0^{2\pi}\int_0^{\pi}\int_0^{\infty} H^2 r^2\sin\theta dr d\theta d\Phi \tag{1.154}$$

$$E_{mag\ \text{total}} = E_{mag\ \text{external}} + E_{mag\ \text{internal}} \tag{1.155}$$

$$E_{mag\ \text{internal}} = \frac{1}{2}\mu_0\int_0^{2\pi}\int_0^{\pi}\int_0^{r_1}\left[\frac{e\hbar}{m_e r_1^3}\right]^2\left(\cos^2\theta + \sin^2\theta\right)r^2\sin\theta dr d\theta d\Phi \tag{1.156}$$

$$E_{mag\ \text{internal}} = \frac{2\pi\mu_0 e^2\hbar^2}{3m_e^2 r_1^3} \tag{1.157}$$

$$E_{mag\ \text{external}} = \frac{1}{2}\mu_0\int_0^{2\pi}\int_0^{\pi}\int_{r_1}^{\infty}\left[\frac{e\hbar}{2m_e r_1^3}\right]^2\left(4\cos^2\theta + \sin^2\theta\right)r^2\sin\theta dr d\theta d\Phi \tag{1.158}$$

$$E_{mag\ \text{external}} = \frac{\pi\mu_0 e^2\hbar^2}{3m_e^2 r_1^3} \tag{1.159}$$

$$E_{mag\ \text{total}} = \frac{2\pi\mu_0 e^2\hbar^2}{3m_e^2 r_1^3} + \frac{\pi\mu_0 e^2\hbar^2}{3m_e^2 r_1^3} \tag{1.160}$$

$$E_{mag\ \text{total}} = \frac{\pi \mu_0 e^2 \hbar^2}{m_e^2 r_1^3} \tag{1.161}$$

$$E_{mag\ \text{total}} = \frac{4\pi \mu_0 \mu_B^2}{r_1^3} \tag{1.162}$$

## BOX 1.1 BOUNDARY CONDITIONS OF THE ELECTRON IN A MAGNETIC FIELD ARE MET

As shown in the Electron g Factor section, when a magnetic field with flux **B** is applied to an electron in a central field which comprises current loops, the orbital radius of each does not change due to the Lorentz force provided by **B**, but the velocity changes as follows [1]:

$$\Delta v = \frac{erB}{2m_e} \tag{1}$$

corresponding to a precession frequency of

$$\omega = \frac{\Delta v}{r} = \frac{eB}{2m_e} = \gamma_e B \tag{2}$$

where $\gamma_e$ is the electron gyromagnetic ratio and $\omega$ is the Larmor frequency. Eq. (1) applies to the current perpendicular to the magnetic flux. Since the atomic orbital is a uniformly-charged spherical shell, the magnetically induced current according to Lenz' law gives rise to a corresponding moment of inertia $I$ [2], due to circulation about the z-axis of:

$$I = \frac{2}{3} m_e r_1^2 \tag{3}$$

From Eqs. (2) and (3), the corresponding angular momentum $L$ and rotational energy $E_{rot}$ are:

$$L = I\omega = \frac{2}{3} m_e r_1^2 \gamma_e B \tag{4}$$

and

$$E_{rot} = \frac{1}{2} I \omega^2 = \frac{1}{3} m_e r_1^2 \left(\gamma_e B\right)^2 \tag{5}$$

respectively. The change in the magnetic moment corresponding to Eq. (1) is [1]:

$$\Delta \mathbf{m} = -\frac{e^2 r_1^2}{4m_e} \mathbf{B} \tag{6}$$

Using Eqs. (2-6), in the case of a very strong magnetic flux of 10 T applied to atomic hydrogen:

$$\omega = 8.794\ X\ 10^{11}\ rad \cdot \sec^{-1} \tag{7}$$

$$I = 1.701\ X\ 10^{-51}\ kg \cdot m^2 \tag{8}$$

$$L = 1.496\ X\ 10^{-39}\ J \cdot s \tag{9}$$

$$E_{rot} = 6.576\ X\ 10^{-28} J = 4.104\ X\ 10^{-9}\ eV \tag{10}$$

and

$$\Delta m = 1.315\ X\ 10^{-28} J \cdot T^{-1} \tag{11}$$

where the radius is given by Eq. (1.260) and $2/3$, the geometrical factor of a uniformly charged spherical shell [2], was used in the case of Eq. (11). Thus, these effects of the magnetic field are very small when they are compared to the intrinsic angular momentum of the electron of

$$L = \hbar = 1.055\ X\ 10^{-34}\ J \cdot s \tag{12}$$

The electronic angular frequency of hydrogen given by Eqs. (1.36) and (1.260)

$$\omega_1 = \frac{\hbar}{m_e r_1^2} = 4.134\ X\ 10^{16}\ rad \cdot \sec^{-1} \tag{13}$$

the total kinetic energy given by Eq. (1.262)

$$T = 13.606\ eV \tag{14}$$

and the magnetic moment of a Bohr magneton given by Eq. (1.131)

$$\mu_B = \frac{e\hbar}{2m_e} = 9.274\ X\ 10^{-24}\ JT^{-1} \tag{15}$$

$E_{rot}$ is the energy that arises due to the application of the external flux **B**. Thus, the external work required to apply the field is also given by Eq. (10). Since the atomic orbital is uniformly charged and is superconducting, this energy is conserved when the field is removed. It is also independent of the direction of the magnetic moment due to the intrinsic angular momentum of the atomic orbital of $\hbar$. The corresponding magnetic moment given by Eq. (6) does not change when the intrinsic magnetic moment

of the electron changes orientation. Thus, it does not contribute to the energy of a spin-flip transition observed by the Stern Gerlach experiment. It always opposes the applied field and gives rise to the phenomenon of the diamagnetic susceptibility of materials which Eq. (6) predicts with very good agreement with observations [1]. Eq. (6) also predicts the absolute chemical shifts of hydride ions that match experimental observations as shown in the Hydrino Hydride Ion Nuclear Magnetic Resonance Shift section.

As shown in the Spin Angular Momentum of the Atomic Orbital $Y_0^0(\theta,\phi)$ with $\ell = 0$ section, the angular momentum of the atomic orbital in a magnetic field comprises the initial $\frac{\hbar}{2}$ projection on the z-axis and the initial $\frac{\hbar}{4}$ vector component in the xy-plane that precesses about the z-axis. A resonant excitation of the Larmor precession frequency gives rise to an additional component of angular momentum, which is consistent with Maxwell's equations. As shown in the Excited States of the One-Electron Atom (Quantization) section, conservation of the $\hbar$ of angular momentum of a trapped photon can give rise to $\hbar$ of electron angular momentum along the **S**-axis. The photon standing waves of excited states are spherical harmonic functions which satisfy Laplace's equation in spherical coordinates and provide the force balance for the corresponding charge (mass)-density waves. Consider the photon in the case of the precessing electron with a Bohr magneton of magnetic moment along the **S**-axis. The radius of the atomic orbital is unchanged, and the photon gives rise to current on the surface that satisfies the condition

$$\nabla \cdot J = 0 \tag{16}$$

corresponding to a rotating spherical harmonic dipole [3] that phase-matches the current (mass) density of Eq. (1.144). Thus, the electrostatic energy is constant, and only the magnetic energy need be considered as given by Eqs. (23-25). The corresponding central field at the atomic orbital surface given by the superposition of the central field of the proton and that of the photon follows from Eqs. (2.10-2.17):

$$\mathbf{E} = \frac{e}{4\pi\varepsilon_0 r^2}\left[ Y_0^0(\theta,\phi)\mathbf{i}_r + \mathrm{Re}\left\{ Y_\ell^m(\theta,\phi) e^{im\omega_n t} \right\} \mathbf{i}_y \delta(r - r_1) \right] \tag{17}$$

where the spherical harmonic dipole $Y_\ell^m(\theta,\phi) = \sin\theta$ is with respect to the **S**-axis. Force balance according to Eq. (1.253) is maintained by the equivalence of the harmonic modulation of the charge and the mass where $e/m_e$ is invariant as given in the Special Relativistic Effect on the Electron Radius and the Relativistic Ionization Energies section. The dipole spins about the **S**-axis at the angular velocity given by Eq. (1.36). In the frame rotating about the **S**-axis, the electric field of the dipole is

$$\mathbf{E} = \frac{e}{4\pi\varepsilon_0 r^2} \sin\theta \sin\varphi \delta(r - r_1)\mathbf{i}_y \tag{18}$$

$$\mathbf{E} = \frac{e}{4\pi\varepsilon_0 r^2}\left( \sin\theta\sin\phi\mathbf{i}_r + \cos\theta\sin\phi\mathbf{i}_\theta + \sin\theta\cos\phi\mathbf{i}_\phi \right)\delta(r - r_1) \tag{19}$$

The resulting current is nonradiative as shown in Appendix I: Nonradiation Condition. Thus, the field in the RF rotating frame is magnetostatic as shown in Figures 1.28 and 1.29 but directed along the **S**-axis. The time-averaged angular momentum and rotational energy due to the charge density wave are zero as given by Eqs. (1.76) and (1.77). However, the corresponding time-dependent surface charge density $\langle\sigma\rangle$ that gives rise to the dipole current of Eq. (1.144) as shown by Haus [4] is equivalent to the current due to a uniformly charged sphere rotating about the **S**-axis at the constant angular velocity given by Eq. (1.36). The charge density is given by Gauss' law at the two-dimensional surface:

$$\sigma = -\varepsilon_0 \mathbf{n} \cdot \nabla\Phi|_{r=r_1} = -\varepsilon_0 \mathbf{n} \cdot \mathbf{E}|_{r=r_1} \tag{20}$$

From Eq. (19), $\langle\sigma\rangle$ is

$$\langle\sigma\rangle = \frac{e}{4\pi r_1^2}\frac{3}{2}\sin\theta \tag{21}$$

and the current (Eq. (1.144)) is given by the product of Eq. (21) and the constant angular frequency (Eq. (1.36)). The precession of the magnetostatic dipole results in magnetic dipole radiation or absorption during a Stern-Gerlach transition. The application of a magnetic field causes alignment of the intrinsic electron magnetic moment of atoms of a material such that the population of electrons parallel versus antiparallel is a Boltzmann distribution, which depends on the temperature of the material. Following the removal of the field, the original random-orientation distribution is restored as is the original temperature. The distribution may be altered by the application of an RF pulse at the Larmor frequency.

The application of a magnetic field with a resonant Larmor excitation gives rise to a precessing angular momentum vector **S** of magnitude $\hbar$ directed from the origin of the atomic orbital at an angle of $\theta = \frac{\pi}{3}$ relative to the applied magnetic field. **S** rotates about the axis of the applied field at the Larmor frequency. The magnitude of the components of **S** that are parallel and orthogonal to the applied field (Eqs. (1.129-1.130)) are $\frac{\hbar}{2}$ and $\sqrt{\frac{3}{4}}\hbar$, respectively. Since both the RF field and the orthogonal components shown in Figure 1.25 rotate at the Larmor frequency, the RF field that causes a Stern Gerlach transition produces a stationary magnetic field with respect to these components as described by Patz [5].

The component of Eq. (1.130) adds to the initial $\frac{\hbar}{2}$ parallel component to give a total of $\hbar$ in the stationary frame corresponding to a Bohr magneton, $\mu_B$, of magnetic moment. Eqs. (2) and (6) also hold in the case of the Stern Gerlach experiment. Superposition holds for Maxwell's equations, and only the angular momentum given by Eqs. (1.127-1.128) and the source current corresponding to Eq. (17) need be considered. Since it does not change, the diamagnetic component given from Eq. (1) does not contribute to the spin-flip transition as discussed *supra*. The potential energy of a magnetic moment **m** in the presence of flux **B** [6] is:

$$E = \mathbf{m} \cdot \mathbf{B} \tag{22}$$

The angular momentum of the electron gives rise to a magnetic moment of $\mu_B$. Thus, the energy $\Delta E_{mag}^{spin}$ to switch from parallel to antiparallel to the field is given by Eq. (1.168)

$$\Delta E_{mag}^{spin} = 2\mu_{\mathbf{B}}\, \mathbf{i_z} \cdot \mathbf{B} = 2\mu_B B \cos\theta = 2\mu_B B \tag{23}$$

In the case of an applied flux of 10 T, Eq. (23) gives:

$$\Delta E_{mag}^{spin} = 1.855\ X\ 10^{-22} J = 1.158 X\ 10^{-3} eV \tag{24}$$

$\Delta E_{mag}^{spin}$ is also given by Planck's equation. It can be shown from conservation of angular momentum considerations (Eqs. (26-32)) that the Zeeman splitting is given by Planck's equation and the Larmor frequency based on the gyromagnetic ratio (Eq. (2)). The electron's magnetic moment may only be parallel or antiparallel to the magnetic field rather than at a continuum of angles including perpendicular according to Eq. (22). No continuum of energies predicted by Eq. (22) for a pure magnetic dipole are possible. The energy difference for the magnetic moment to flip from parallel to antiparallel to the applied field is:

$$\Delta E_{mag}^{spin} = 2\hbar\omega = 1.855\ X\ 10^{-22} J = 1.158 X\ 10^{-3} eV \tag{25}$$

corresponding to magnetic dipole radiation.

As demonstrated in the Atomic Orbital Equation of Motion For $\ell$ = 0 Based on the Current Vector Field (CVF) section, $\frac{\hbar}{2}$ of the atomic orbital angular momentum designated the static component is initially parallel to the field. An additional $\frac{\hbar}{2}$ parallel component designated the dynamic component comes from the $\hbar$ of angular momentum along **S**. The angular momentum in the presence of an applied magnetic field is [7]

$$\mathbf{L} = \mathbf{r} \times (m_e \mathbf{v} + e\mathbf{A}) \tag{26}$$

where **A** is the vector potential evaluated at the location of the atomic orbital. The circular integral of **A** is the flux linked by the electron. During a Stern-Gerlach transition a resonant RF photon is absorbed or emitted, and the $\hbar$ component along **S** reverses direction. It is shown by Eqs. (29-32) that the dynamic parallel component of angular momentum corresponding to the vector potential due to the lightlike transition is equal to the "kinetic angular momentum" $(\mathbf{r} \times m\mathbf{v})$ of $\frac{\hbar}{2}$. Conservation of angular momentum of the atomic orbital requires that the static angular momentum component concomitantly flips. The static component of angular momentum undergoes a spin flip, and concomitantly the "potential angular momentum" $(\mathbf{r} \times e\mathbf{A})$ of the dynamic component must change by $-\frac{\hbar}{2}$ due to the linkage of flux by the electron such that the total angular momentum is conserved.

In spherical coordinates, the relationship between the vector potential **A** and the flux **B** is

$$2\pi r A = \pi r^2 B \tag{27}$$

Eq. (27) can be substituted into Eq. (26) since the magnetic moment $m$ is given [6] as:

$$m = \frac{\text{charge} \cdot \text{angular momentum}}{2 \cdot \text{mass}} \tag{28}$$

and the corresponding energy is consistent with Eqs. (23) and (25) in this case as follows:

$$\Delta \mathbf{m} = -\frac{e(\mathbf{r} \times e\mathbf{A})}{2m_e} = \frac{e\frac{\hbar}{2}}{2m_e} = \frac{\mu_B}{2}\mathbf{i}_z \tag{29}$$

The boundary condition that the angular momentum is conserved is shown by Eqs. (1.165-1.167). It can be shown that Eq. (29) is also consistent with the vector potential along the axis of the applied field [8] given by:

$$\mathbf{A} = \cos\frac{\pi}{3}\mu_0 \frac{e\hbar}{2m_e r^2}\sin\theta \mathbf{i}_\phi = \mu_0 \frac{1}{2}\frac{e\hbar}{2m_e r^2}\sin\theta \mathbf{i}_\phi \tag{30}$$

Substitution of Eq. (30) into Eq. (29) gives:

$$\Delta \mathbf{m} = -\frac{e(\mathbf{r} \times e\mu_0 \frac{1}{2}\frac{e\hbar}{2m_e r^2}\sin\theta \mathbf{i}_\phi)}{2m_e}\mathbf{i}_z = -\frac{1}{2}\left[\frac{\mu_0 e^2}{2m_e r}\right]\frac{e\hbar}{2m_e}\mathbf{i}_z \tag{31}$$

with the geometrical factor of $2/3$ [2] and the current given by Eq. (1.144). Since $k$ is the lightlike $k^0$, then $k = \omega_n / c$ corresponding to the RF photon field. The relativistic corrections of Eq. (31) are given by Eqs. (1.250) and (1.251) and the relativistic radius $r = \lambda\!\!\!^{-}_c$ given by Eq. (1.249). The relativistically corrected Eq. (31) is:

$$\Delta\mathbf{m} = -\frac{1}{2}(2\pi\alpha)^{-1}\left[\frac{\mu_0 e^2}{2m_e\alpha a_0}\right]\frac{e\hbar}{2m_e} = \frac{\mu_B}{2}\mathbf{i}_z \tag{32}$$

The magnetic flux of the electron is given by:

$$\nabla \times \mathbf{A} = \mathbf{B} \tag{33}$$

Substitution of Eq. (30) into Eq. (33) gives 1/2 the flux of Eq. (1.153).

From Eq. (28), the $\frac{\hbar}{2}$ of angular momentum before and after the field is applied corresponds to an initial magnetic moment on the applied-field-axis of $\frac{\mu_B}{2}$. After the field is applied, the contribution of $\frac{\mu_B}{2}$ from Eq. (29) with Eq. (27) gives a total magnetic moment along the applied-field-axis of $\mu_B$, a Bohr magneton, wherein the additional contribution (Eq. (28)) arises from the angular momentum of $\hbar$ on the $\mathbf{S}$-axis. Thus, even though the magnitude of the vector projection of the angular momentum of the electron in the direction of the magnetic field is $\frac{\hbar}{2}$, the magnetic moment corresponds to $\hbar$ due to the $\frac{\hbar}{2}$ contribution from the dynamic component, and the quantized transition is due to the requirement of angular momentum conservation as given by Eq. (28).

Eq. (22) implies a continuum of energies; whereas, Eq. (29) shows that the static-kinetic and dynamic vector potential components of the angular momentum are quantized at $\frac{\hbar}{2}$. Consequently, as shown in the Electron g Factor section, the flux linked during a spin transition is quantized as the magnetic flux quantum:

$$\Phi_0 = \frac{h}{2e} \tag{34}$$

Only the states corresponding to:

$$m_s = \pm\frac{1}{2} \tag{35}$$

are possible due to conservation of angular momentum. It is further shown using the Poynting power vector with the requirement that flux is linked in units of the magnetic flux quantum, that the factor 2 of Eqs. (23) and (25) is replaced by the electron g factor.

Thus, in terms of flux linkage, the electron behaves as a superconductor with a weak link [9] as described in the Josephson Junction, Weak Link section and the Superconducting Quantum Interference Device (SQUID) section. Consider the case of a current loop with a weak link comprising a large number of superconducting electrons (e.g. $10^{10}$). As the applied field increases, the Meissner current increases. In equilibrium, a dissipationless supercurrent can flow around the loop driven by the difference between the flux $\Phi$ that threads the loop and the external flux $\Phi_x$ applied to the loop. Based on the physics of the electrons carrying the supercurrent, when the current reaches the critical current, the kinetic angular momentum change of $\frac{\hbar}{2}$ equals the magnitude of the potential angular momentum change corresponding to the vector potential according to Eqs. (26) and (31). As a consequence, the flux is linked in units of the magnetic flux quantum as shown in the Electron g Factor section.

## REFERENCES


1. E. M. Purcell, *Electricity and Magnetism*, McGraw-Hill, New York, (1965), pp. 370-379.
2. G. R. Fowles, *Analytical Mechanics*, Third Edition, Holt, Rinehart, and Winston, New York, (1977), p. 196.
3. J. D. Jackson, *Classical Electrodynamics*, Second Edition, John Wiley & Sons, New York, (1975), pp. 84-102; 752-763.
4. H. A. Haus, J. R. Melcher, "Electromagnetic Fields and Energy," Department of Electrical Engineering and Computer Science, Massachusetts Institute of Technology, (1985), Sec. 8.6.
5. S. Patz, Cardiovasc. Interven. Radiol., (1986), 8:25, pp. 225-237.
6. D. A. McQuarrie, *Quantum Chemistry*, University Science Books, Mill Valley, CA, (1983), pp. 238-241.
7. E. M. Purcell, *Electricity and Magnetism*, McGraw-Hill, New York, (1965), p. 447.
8. E. M. Purcell, *Electricity and Magnetism*, McGraw-Hill, New York, (1965), pp. 361-367.
9. C. E. Gough, M. S. Colclough, E. M. Forgan, R. G. Jordan, M. Keene, C. M. Muirhead, A. I. M. Rae, N. Thomas, J. S. Abell, S. Sutton, Nature, Vol. 326, (1987), P. 855.

## ELECTRON G FACTOR

As demonstrated by Purcell [15], when a magnetic field is applied to an electron in a central field which comprises a current loop, the orbital radius does not change, but the velocity changes as follows:

$$\Delta v = \frac{erB}{2m_e} \tag{1.163}$$

This corresponds to diamagnetism and gives rise to precession with a corresponding resonance as shown in Box 1.1. The angular momentum in the presence of an applied magnetic field is [15]:

$$\mathbf{L} = \mathbf{r} \times (m_e \mathbf{v} + e\mathbf{A}) \tag{1.164}$$

where $\mathbf{A}$ is the vector potential evaluated at the location of the atomic orbital. Conservation of angular momentum of the atomic orbital permits a discrete change of its "kinetic angular momentum" $(\mathbf{r} \times m\mathbf{v})$ with respect to the field of $\frac{\hbar}{2}$, and concomitantly the "potential angular momentum" $(\mathbf{r} \times e\mathbf{A})$ must change by $-\frac{\hbar}{2}$. The flux change, $\phi$, of the atomic orbital for $r < r_n$ is determined as follows [15]:

$$\Delta \mathbf{L} = \frac{\hbar}{2} - \mathbf{r} \times e\mathbf{A} \tag{1.165}$$

$$= \left[ \frac{\hbar}{2} - \frac{e 2\pi r A}{2\pi} \right] \hat{z} \tag{1.166}$$

$$= \left[ \frac{\hbar}{2} - \frac{e\phi}{2\pi} \right] \hat{z} \tag{1.167}$$

In order that the change in angular momentum, $\Delta \mathbf{L}$, equals zero, $\phi$ must be $\Phi_0 = \frac{h}{2e}$, the magnetic flux quantum. Thus, to conserve angular momentum in the presence of an applied magnetic field, the atomic orbital magnetic moment can be parallel or antiparallel to an applied field as observed with the Stern-Gerlach experiment, and the flip between orientations is accompanied by the "capture" of the magnetic flux quantum by the atomic orbital "coils" comprising infinitesimal loops of charge moving along geodesics (great circles). A superconducting loop with a weak link also demonstrates this effect [22].

The energy to flip the orientation of the atomic orbital due to its magnetic moment of a Bohr magneton, $\mu_B$, is:

$$\Delta E_{mag}^{spin\ moment} = 2\mu_B B \tag{1.168}$$

where

$$\mu_B = \frac{e\hbar}{2m_e} \tag{1.169}$$

During the spin-flip transition, power must be conserved. Power flow is governed by the Poynting power theorem,

$$\nabla \bullet (\mathbf{E} \times \mathbf{H}) = -\frac{\partial}{\partial t}\left[ \frac{1}{2}\mu_0 \mathbf{H} \bullet \mathbf{H} \right] - \frac{\partial}{\partial t}\left[ \frac{1}{2}\varepsilon_0 \mathbf{E} \bullet \mathbf{E} \right] - \mathbf{J} \bullet \mathbf{E} \tag{1.170}$$

## STORED MAGNETIC ENERGY

Energy superimposes; thus, the calculation of the spin-flip energy is determined as a sum of contributions. The energy change corresponding to the "capture" of the magnetic flux quantum is derived below. From Eq. (1.161) for one electron,

$$\int_{vol} \frac{1}{2}\mu_0 \mathbf{H} \bullet \mathbf{H} dv = E_{mag}^{fluxon} = \frac{\pi \mu_0 e^2 \hbar^2}{(m_e)^2 r_n^3} \tag{1.171}$$

is the energy stored in the magnetic field of the electron. The atomic orbital is equivalent to a Josephson junction which can trap integer numbers of fluxons where the quantum of magnetic flux is $\Phi_0 = \frac{h}{2e}$. Consider Eq. (1.171). During the flip transition a fluxon treads the atomic orbital at the speed of light; therefore, the radius of the atomic orbital in the lab frame is $2\pi$ times the relativistic radius in the fluxon frame as shown in the Special Relativistic Effect on the Electron Radius and the Relativistic Ionization Energies section. Thus, the energy of the transition corresponding to the "capture" of a fluxon by the atomic orbital, $E_{mag}^{fluxon}$, is:

$$E_{mag}^{fluxon} = \frac{\pi \mu_0 e^2 \hbar^2}{(m_e)^2 (2\pi r_n)^3} \tag{1.172}$$

$$= \frac{\mu_0 e^2}{4\pi^2 m_e r_n} \left( \frac{e\hbar}{2m_e} \right) \left( \frac{h}{2e\pi {r_n}^2} \right) \tag{1.173}$$

$$= \frac{\mu_0 e^2}{4\pi^2 m_e r_n} \mu_B \left( \frac{\Phi_0}{A} \right) \tag{1.174}$$

where $A$ is the area and $\Phi_0$ is the magnetic flux quantum.

$$E_{mag}^{fluxon} = 2\left[ \frac{e^2 \mu_0}{2 m_e r_n} \right] \frac{1}{4\pi^2} \mu_B B \tag{1.175}$$

where the nth fluxon treading through the area of the atomic orbital is equivalent to the applied magnetic flux. Furthermore, the term in brackets can be expressed in terms of the fine structure constant, $\alpha$, as follows:

$$\frac{e^2 \mu_0}{2 m_e r_n} = \frac{e^2 \mu_0 c v}{2 m_e v r_n c} \tag{1.176}$$

Substitution of Eq. (1.35) gives:

$$\frac{e^2 \mu_0}{2 m_e r_n} = \frac{e^2 \mu_0 c v}{2 \hbar c} \tag{1.177}$$

Substitution of

$$c = \sqrt{\frac{1}{\varepsilon_0 \mu_0}} \tag{1.178}$$

and

$$\alpha = \frac{\mu_0 e^2 c}{2h} \tag{1.179}$$

gives

$$\frac{e^2 \mu_0 c v}{2 \hbar c} = 2\pi\alpha \frac{v}{c} \tag{1.180}$$

The fluxon treads the atomic orbital at $v = c$ ($k$ is the lightlike $k^0$, then $k = \omega_n / c$). Thus,

$$E_{mag}^{fluxon} = 2 \frac{\alpha}{2\pi} \mu_B B \tag{1.181}$$

## STORED ELECTRIC ENERGY

The superposition of the vector projection of the atomic orbital angular momentum on the z-axis is $\frac{\hbar}{2}$ with an orthogonal component of $\frac{\hbar}{4}$. Excitation of a resonant Larmor precession gives rise to $\hbar$ on an axis **S** that precesses about the spin axis at an angle of $\theta = \frac{\pi}{3}$. **S** rotates about the z-axis at the Larmor frequency. $\mathbf{S}_\perp$, the transverse projection, is $\pm\sqrt{\frac{3}{4}}\hbar$ (Eq. (1.129)), and $\mathbf{S}_\parallel$, the projection onto the axis of the applied magnetic field, is $\pm\frac{\hbar}{2}$ (Eq. (1.130)). As shown in the Spin Angular Momentum of the Atomic Orbital $Y_0^0(\theta,\phi)$ with $\ell = 0$ section, the superposition of the $\frac{\hbar}{2}$ z-axis component of the atomic orbital angular momentum and the $\frac{\hbar}{2}$ z-axis component of **S** gives $\hbar$ corresponding to the observed electron magnetic moment of a Bohr magneton, $\mu_B$. The reorientation of **S** and the atomic orbital angular momentum from parallel to antiparallel due to the magnetic field applied along the z-axis gives rise to a current. The current is acted on by the flux corresponding to $\Phi_0$, the magnetic flux quantum, linked by the electron during the transition which gives rise to a Hall voltage. The electric field corresponding to the Hall voltage corresponds to the electric power term, $\frac{\partial}{\partial t}\left[\frac{1}{2}\varepsilon_0 \mathbf{E} \bullet \mathbf{E}\right]$, of the Poynting power theorem (Eq. (1.170)).

Consider a conductor in a uniform magnetic field and assume that it carries a current driven by an electric field perpendicular to the magnetic field. The current in this case is not parallel to the electric field, but is deflected at an angle to it by the magnetic field. This is the Hall Effect, and it occurs in most conductors. A spin-flip transition is analogous to the Quantum Hall Effect given in the corresponding section wherein the applied magnetic field quantizes the Hall conductance. The current is then precisely perpendicular to the magnetic field, so that no dissipation (that is, no ohmic loss) occurs. This is seen in two-dimensional systems, at cryogenic temperatures, in quite high magnetic fields. Furthermore, the ratio of the total electric potential drop to the total current, the Hall resistance, $R_H$, is precisely equal to:

$$R_H = \frac{h}{ne^2} \tag{1.182}$$

The factor $n$ is an integer in the case of the Integral Quantum Hall Effect, and $n$ is a small rational fraction in the case of the Fractional Quantum Hall Effect. In an experimental plot [23] as the function of the magnetic field, the Hall resistance exhibits flat steps precisely at these quantized resistance values; whereas, the regular resistance vanishes (or is very small) at these Hall steps. Thus, the quantized Hall resistance steps occur for a transverse superconducting state.

Consider the case that an external magnetic field is applied along the x-axis to a two dimensional superconductor in the yz-plane which exhibits the Integral Quantum Hall Effect. (See Figure 1.30.) Conduction electrons align with the applied field in the x direction as the field permeates the material. The normal current carrying electrons experience a Lorentz force, $\mathbf{F}_L$, due to the magnetic flux. The y-directed Lorentz force on an electron having a velocity $\mathbf{v}$ in the z direction by an x-directed applied flux, **B**, is:

$$\mathbf{F}_L = e\mathbf{v}\times\mathbf{B} \tag{1.183}$$

The electron motion is a cycloid where the center of mass experiences an $\mathbf{E}\times\mathbf{B}$ drift [24]. Consequently, the normal Hall Effect occurs. Conduction electron energy states are altered by the applied field and by the electric field corresponding to the Hall Effect. The electric force, $\mathbf{F}_H$, due to the Hall electric field, $\mathbf{E}_y$, is:

$$\mathbf{F}_H = e\mathbf{E}_y \tag{1.184}$$

When these two forces are equal and opposite, conduction electrons propagate in the z direction alone. For this special case, it is demonstrated in Jackson [24] that the ratio of the corresponding Hall electric field $E_H$ and the applied magnetic flux is:

$$E_H/B = v \tag{1.185}$$

where $v$ is the electron velocity. And, it is demonstrated in the Integral Quantum Hall Effect section that the Hall resistance, $R_H$, in the superconducting state is given by:

$$R_H = \frac{h}{ne^2} \tag{1.186}$$

where $n$ is an integer.

**Figure 1.30.** Coordinate system of crossed electric field, $\mathbf{E}_y$, corresponding to the Hall voltage, magnetic flux, $\mathbf{B}_x$, due to applied field, and superconducting current $\mathbf{i}_z$.

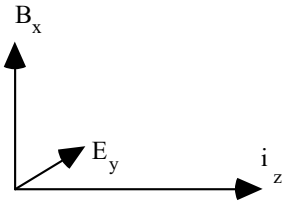
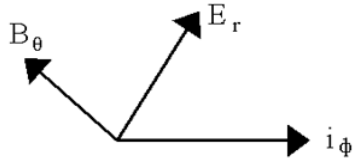



**Figure 1.31.** Coordinate system of crossed electric field, $\mathbf{E}_r$, corresponding to the Hall voltage, magnetic flux, $\mathbf{B}_\theta$, due to applied field, and superconducting current $\mathbf{i}_\phi$.




Consider the case of the spin-flip transition of the electron. In the case of an exact balance between the Lorentz force (Eq. (1.183)) and the electric force corresponding to the Hall voltage (Eq. (1.184)), each superconducting point mass-density element of the electron propagates along a great circle where

$$E/B = v \tag{1.187}$$

where $v$ is given by Eq. (1.35). Substitution of Eq. (1.35) into Eq. (1.187) gives:

$$E/B = \frac{\hbar}{m_e r} \tag{1.188}$$

Eq. (1.185) is the condition for superconductivity in the presence of crossed electric and magnetic fields. The electric field corresponding to the Hall voltage corresponds to the electric energy term, $E_{ele}$, of the Poynting power theorem (Eq. (1.170)).

$$E_{ele} = \frac{1}{2}\int_0^{2\pi}\int_0^{\pi}\int_0^{r_1}\varepsilon_0\mathbf{E}\bullet\mathbf{E}r^2\sin\theta dr d\theta d\phi \tag{1.189}$$

The electric term for this superconducting state is derived as follows using the coordinate system shown in Figure 1.31.

The current is perpendicular to $\mathbf{E}_r$, thus there is no dissipation. This occurs when:

$$e\mathbf{E} = e\mathbf{v}\times\mathbf{B} \tag{1.190}$$

or

$$E/B = v \tag{1.191}$$

The electric field corresponding to the Hall voltage is:

$$\mathbf{E} = \mathbf{v}\times\mathbf{B} \tag{1.192}$$

Substitution of Eq. (1.192) into Eq. (1.189) gives:

$$E_{ele} = \frac{1}{2}\varepsilon_o \int_0^{2\pi}\int_0^{\pi}\int_0^{r_1} (vB)^2 r^2 \sin\theta dr d\theta d\phi \tag{1.193}$$

The spin flip transition may be induced by the absorption of a resonant photon. The velocity is determined from the distance traversed by each point element and the time of the transition due to capture of a photon resonant with the spin-flip transition energy. The current $\mathbf{i}_\phi$ corresponding to the Hall voltage and $\mathbf{E}_r$ is given by the product of the electron charge and the frequency $f$ of the photon where the correspondence principle holds as given in the Photon Absorption section.

$$i = ef \tag{1.194}$$

The resistance of free space for the propagation of a photon is the radiation resistance of free space, $\eta$.

$$\eta = \sqrt{\frac{\mu_0}{\varepsilon_0}} \tag{1.195}$$

The power $P_r$ of the electron current induced by the photon as it transitions from free space to being captured by the electron is given by the product of the corresponding current and the resistance $R$ which is given by Eq. (1.195).

$$P_r = i^2 R \tag{1.196}$$

Substitution of Eq. (1.194) and Eq. (1.195) gives

$$P_r = e^2 f^2 \sqrt{\frac{\mu_0}{\varepsilon_0}} \tag{1.197}$$

It follows from the Poynting power theorem (Eq. (1.170)) with spherical radiation that the transition time $\tau$ is given by the ratio of the energy and the power of the transition [25].

$$\tau = \frac{energy}{power} \tag{1.198}$$

The energy of the transition, which is equal to the energy of the resonant photon, is given by Planck's equation.

$$E = \hbar\omega = hf \tag{1.199}$$

Substitution of Eq. (1.197) and Eq. (1.199) into Eq. (1.198) gives:

$$\tau = \frac{hf}{e^2 f^2 \sqrt{\frac{\mu_0}{\varepsilon_0}}} \tag{1.200}$$

The distance $\ell$ traversed by the electron with a kinetic angular momentum change of $\frac{\hbar}{2}$ is:

$$\ell = \frac{2\pi r}{2} = \frac{\lambda}{2} \tag{1.201}$$

where the wavelength is given by Eq. (1.15). The velocity is given by the distance traversed divided by the transition time. Eq. (1.200) and Eq. (1.201) gives:

$$v = \frac{\lambda/2}{\tau} = \frac{\lambda/2}{\frac{hf}{e^2 f^2 \sqrt{\frac{\mu_0}{\varepsilon_0}}}} = \frac{\sqrt{\frac{\mu_0}{\varepsilon_0}} e^2}{2h} \lambda f \tag{1.202}$$

The relationship for a photon in free space is:

$$c = \lambda f \tag{1.203}$$

As shown in the Unification of Spacetime, the Forces, Matter, and Energy section, the fine structure constant given by Eq. (1.179) is the dimensionless factor that corresponds to the relativistic invariance of charge.

$$\alpha = \frac{1}{4\pi}\sqrt{\frac{\mu_0}{\varepsilon_0}}\frac{e^2}{\hbar} = \frac{1}{2}\frac{\sqrt{\frac{\mu_0}{\varepsilon_0}}}{\frac{h}{e^2}} = \frac{\mu_0 e^2 c}{2h} \tag{1.204}$$

It is equivalent to one half the ratio of the radiation resistance of free space, $\sqrt{\frac{\mu_0}{\varepsilon_0}}$, and the Hall resistance, $\frac{h}{e^2}$. The radiation resistance of free space is equal to the ratio of the electric field and the magnetic field of the photon (Eq. (4.10)). Substitution of Eq. (1.203) and Eq. (1.204) into Eq. (1.202) gives:

$$v = \alpha c \tag{1.205}$$

Substitution of Eq. (1.205) into Eq. (1.193) gives:

$$E_{ele} = \frac{1}{2}\varepsilon_0 \int_0^{2\pi}\int_0^{\pi}\int_0^{r_1} \left(\alpha c \mu_0 H\right)^2 r^2 \sin\theta dr d\theta d\phi \tag{1.206}$$

where

$$B = \mu_0 H \tag{1.207}$$

The relationship between the speed of light, $c$, and the permittivity of free space, $\varepsilon_0$, and the permeability of free space, $\mu_0$, is

$$c = \frac{1}{\sqrt{\mu_0 \varepsilon_0}} \tag{1.208}$$

Thus, Eq. (1.206) may be written as:

$$E_{ele} = \frac{1}{2}\alpha^2 \int_0^{2\pi}\int_0^{\pi}\int_0^{r_1} \mu_0 H^2 r^2 \sin\theta dr d\theta d\phi \tag{1.209}$$

Substitution of Eq. (1.157) gives

$$E_{ele} = \alpha^2 \frac{2\pi\mu_0 e^2 \hbar^2}{3 m_e^2 r_1^3} \tag{1.210}$$

The magnetic flux, $\mathbf{B}$, is quantized in terms of the Bohr magneton because the electron links flux in units of the magnetic flux quantum,

$$\Phi_0 = \frac{h}{2e} \tag{1.211}$$

Substitution of Eqs. (1.171-1.181) gives:

$$E_{ele} = 2\left(\frac{2}{3}\alpha^2 \frac{\alpha}{2\pi}\mu_B B\right) \tag{1.212}$$

## DISSIPATED ENERGY

The $\mathbf{J} \bullet \mathbf{E}$ energy over time is derived from the electron current corresponding to the Larmor excitation and the electric field given by Faraday's law due to the linkage of the magnetic flux of the fluxon during the spin-flip. Consider the electron current due to the external field. The application of a magnetic field with a resonant Larmor excitation gives rise to a precessing angular momentum vector **S** of magnitude $\hbar$ directed from the origin of the atomic orbital at an angle of $\theta = \frac{\pi}{3}$ relative to the applied magnetic field. As given in the Spin Angular Momentum of the Atomic Orbital $Y_0^0(\theta,\phi)$ with $\ell = 0$ section, **S** rotates about the axis of the applied field at the Larmor frequency. The magnitude of the components of **S** that are parallel and orthogonal to the applied field (Eqs (1.129-1.130)) are $\frac{\hbar}{2}$ and $\sqrt{\frac{3}{4}}\hbar$, respectively. Since both the RF field and the orthogonal components shown in Figure 1.25 rotate at the Larmor frequency, the RF field that causes a Stern Gerlach transition produces a stationary magnetic field with respect to these components as described in Box 1.1. The corresponding central field at the atomic orbital surface given by the superposition of the central field of the proton and that of the photon follows from Eqs. (2.10-2.17) and Eq. (17) of Box 1.1:

$$\mathbf{E} = \frac{e}{4\pi\varepsilon_o r^2}\left[Y_0^0(\theta,\phi)\mathbf{i}_\mathbf{r} + \mathrm{Re}\left\{Y_\ell^m(\theta,\phi)e^{im\omega_n t}\right\}\mathbf{i}_\mathbf{y}\delta(r - r_1)\right] \tag{1.213}$$

where the spherical harmonic dipole $Y_\ell^m(\theta,\phi) = \sin\theta$ is with respect to the **S**-axis. The dipole spins about the **S**-axis at the angular velocity given by Eq. (1.36). The resulting current is nonradiative as shown in Appendix I: Nonradiation Condition. Thus, the field in the RF rotating frame is magnetostatic as shown in Figures 1.28 and 1.29 but directed along the **S**-axis. Thus, the corresponding current given by Eq. (1.144) is

$$\mathbf{K}(\rho,\phi,z) = \frac{3}{2}\frac{e\hbar}{m_e r_n^3}\sin\theta \mathbf{i}_\phi \tag{1.214}$$

Next consider Faraday's equation for the electric field

$$\oint_C \mathbf{E} \bullet d\mathbf{s} = -\frac{d}{dt}\int_S \mu_0 \mathbf{H} \bullet d\mathbf{a} \tag{1.215}$$

As demonstrated by Purcell [15], the velocity of the electron changes according to Lenz's law, but the change in centrifugal force is balanced by the change in the central field due to the applied field. The magnetic flux of the electron given by Eq. (1.152) is

$$\mathbf{B} = \mu_0 \mathbf{H} = \frac{\mu_0 e\hbar}{m_e r_1^3}(\mathbf{i}_r \cos\theta - \mathbf{i}_\theta \sin\theta) \qquad \text{for } r < r_n \tag{1.216}$$

From Eq. (1.181), the magnetic flux $B_{\mathbf{J}\bullet\mathbf{E}}$ of the fluxon is:

$$\mathbf{B}_{\mathbf{J}\bullet\mathbf{E}} = \frac{\alpha}{2\pi}\frac{\mu_0 e\hbar}{m_e r_1^3}(\mathbf{i}_r \cos\theta - \mathbf{i}_\theta \sin\theta) = \frac{\alpha}{2\pi}\frac{\mu_0 e\hbar}{m_e r_1^3}\mathbf{i}_z \tag{1.217}$$

The electric field $\mathbf{E}$ is constant about the line integral of the atomic orbital. Using Eq. (1.215) with the change in flux in units of fluxons along the z-axis given by Eq. (1.217) gives:

$$\int_{-r_1}^{+r_1}\oint_C \mathbf{E}\bullet d\mathbf{s}dz = \int_{-r_1}^{+r_1} -\pi r^2 \frac{dB}{dt}dz\mathbf{i}_\phi \tag{1.218}$$

$$2\pi\ \mathbf{E}\int_0^\pi r_1 \sin^2\theta \mathrm{d}\theta\ = -\pi\frac{\Delta B}{\Delta t}r_1^2 \sin^3\theta \mathrm{d}\theta \mathbf{i}_\phi = -\pi r_1^2 \frac{2\Delta B}{3\Delta t}\mathbf{i}_\phi \tag{1.219}$$

Substitution of Eq. (1.217) into Eq. (1.219) gives:

$$\pi r_1\ \mathbf{E} = -\pi r_1^2 \frac{2}{3}\frac{\alpha}{2\pi}\frac{\mu_0 e\hbar}{m_e r_1^3 \Delta t}\mathbf{i}_\phi \tag{1.220}$$

$$\pi r_1\ \mathbf{E} = -\pi \frac{2}{3}\frac{\alpha}{2\pi}\frac{\mu_0 e\hbar}{m_e r_1 \Delta t}\mathbf{i}_\phi \tag{1.221}$$

Thus,

$$\mathbf{E} = -\frac{2}{3}\frac{\alpha}{2\pi}\frac{\mu_0 e\hbar}{m_e r_1^2 \Delta t}\mathbf{i}_\phi \tag{1.222}$$

The dissipative power density $\mathbf{E}\bullet\mathbf{J}$ can be expressed in terms of the surface current density $\mathbf{K}$ as:

$$\int_V (\mathbf{E}\bullet\mathbf{J})\Delta t dv = \int_S (\mathbf{E}\bullet\mathbf{K})\Delta t da \tag{1.223}$$

Using the electric field from Eq. (1.222) and the current density from Eq. (1.214) gives:

$$\int_V (\mathbf{E}\bullet\mathbf{J})\Delta t dv = \int_0^{2\pi}\int_0^{\pi}\left(\frac{2}{3}\frac{\alpha}{2\pi}\frac{\mu_0 e\hbar}{m_e r_1^2 \Delta t}\frac{3}{2}\frac{e\hbar}{m_e r_1^3}\sin^2\theta\right)\Delta t r_1^2 \sin\theta d\theta d\varphi = \frac{4}{3}\frac{\alpha}{2\pi}\frac{\pi\mu_0 e^2\hbar^2}{m_e^2 r_1^3} \tag{1.224}$$

Substitution of Eqs. (1.171-1.181) into Eq. (1.224) gives:

$$\int_V (\mathbf{E}\bullet\mathbf{J})\Delta t dv = 2\left(\frac{4}{3}\right)\left(\frac{\alpha}{2\pi}\right)^2 \mu_B B \tag{1.225}$$

## TOTAL ENERGY OF SPIN-FLIP TRANSITION

The principal energy of the transition corresponding to a reorientation of the atomic orbital is given by Eq. (1.168). And, the total energy of the flip transition is the sum of Eq. (1.168), and Eqs. (1.181), (1.212), and (1.225) corresponding to the magnetic energy, the electric energy, and the dissipated energy of a fluxon treading the atomic orbital, respectively.

$$\Delta E_{mag}^{spin} = 2\left(1 + \frac{\alpha}{2\pi} + \frac{2}{3}\alpha^2\left(\frac{\alpha}{2\pi}\right) - \frac{4}{3}\left(\frac{\alpha}{2\pi}\right)^2\right)\mu_B B \tag{1.226}$$

$$\Delta E_{mag}^{spin} = g\mu_B B \tag{1.227}$$

where the stored magnetic energy corresponding to the $\frac{\partial}{\partial t}\left[\frac{1}{2}\mu_0 \mathbf{H}\bullet\mathbf{H}\right]$ term increases, the stored electric energy corresponding to the $\frac{\partial}{\partial t}\left[\frac{1}{2}\varepsilon_0 \mathbf{E}\bullet\mathbf{E}\right]$ term increases, and the $\mathbf{J}\bullet\mathbf{E}$ term is dissipative. The magnetic moment of Eq. (1.168) is twice that from the gyromagnetic ratio as given by Eq. (28) of Box 1.1. The magnetic moment of the electron is the sum of the component

corresponding to the kinetic angular momentum, $\frac{\hbar}{2}$, and the component corresponding to the vector potential angular momentum, $\frac{\hbar}{2}$, (Eq. (1.164)). The spin-flip transition can be considered as involving a magnetic moment of $g$ times that of a Bohr magneton. The $g$ factor is redesignated the fluxon $g$ factor as opposed to the anomalous $g$ factor, and it is given by Eq. (1.226).

$$\frac{g}{2}=1+\frac{\alpha}{2\pi}+\frac{2}{3}\alpha^2\left(\frac{\alpha}{2\pi}\right)-\frac{4}{3}\left(\frac{\alpha}{2\pi}\right)^2 \tag{1.228}$$

For $\alpha^{-1}=137.03604(11)$ [26]

$$\frac{g}{2}=1.001\ 159\ 652\ 120 \tag{1.229}$$

The experimental value [27] is:

$$\frac{g}{2}=1.001\ 159\ 652\ 188(4) \tag{1.230}$$

The calculated and experimental values are within the propagated error of the fine structure constant. Different values of the fine structure constant have been recorded from different experimental techniques, and $\alpha^{-1}$ depends on a circular argument between theory and experiment [28]. One measurement of the fine structure constant based on the electron $g$ factor is $\alpha_{g_e}^{-1}=137.036006(20)$ [29]. This value can be contrasted with equally precise measurements employing solid state techniques such as those based on the Josephson effect [30] ($\alpha_J^{-1}=137.035963(15)$) or the quantized Hall effect [31] ($\alpha_H^{-1}=137.035300(400)$). A method of the determination of $\alpha^{-1}$ that depends on the circular methodology between theory and experiment to a lesser extent is the substitution of the independently measured fundamental constants $\mu_0$, $e$, $c$, and $h$ into Eq. (1.204). The following values of the fundamental constants are given by Weast [26]:

$$\mu_0=4\pi\ X\ 10^{-7}\ Hm^{-1} \tag{1.231}$$

$$e=1.6021892(46)\ X\ 10^{-19}\ C \tag{1.232}$$

$$c=2.99792458(12)\ X\ 10^{8}\ ms^{-1} \tag{1.233}$$

$$h=6.626176(36)\ X\ 10^{-34}\ JHz^{-1} \tag{1.234}$$

For these constants,

$$\alpha^{-1}=137.03603(82) \tag{1.235}$$

Substitution of the $\alpha^{-1}$ from Eq. (1.235) into Eq. (1.228) gives

$$\frac{g}{2}=1.001\ 159\ 652\ 137 \tag{1.236}$$

The experimental value [27] is

$$\frac{g}{2}=1.001\ 159\ 652\ 188(4) \tag{1.237}$$

Conversely, the fine structure calculated for the experimental $\frac{g}{2}$ and Eq. (1.228) is $\alpha^{-1}=137.036\ 032\ 081$.

The *postulated* QED theory of $\frac{g}{2}$ is based on the determination of the terms of a *postulated* power series in $\alpha/\pi$ where each *postulated* virtual particle is a source of *postulated* vacuum polarization that gives rise to a *postulated* term. The algorithm involves scores of *postulated* Feynman diagrams corresponding to thousands of matrices with thousands of integrations per matrix requiring decades to reach a consensus on the "appropriate" *postulated* algorithm to remove the intrinsic infinities. The solution so obtained using the perturbation series further requires a *postulated* truncation since the series **diverges**. The remarkable agreement between Eqs. (1.236) and (1.237) demonstrates that $\frac{g}{2}$ may be derived in closed form from Maxwell's equations in a simple straightforward manner that yields a result with eleven figure agreement with experiment—the limit of the experimental capability of the measurement of the fundamental constants that determine $\alpha$. In Ref. [17], the Maxwellian result

is contrasted with the QED algorithm of invoking virtual particles, zero point fluctuations of the vacuum, and negative energy states of the vacuum. Rather than an infinity of radically different QED models, an essential feature is that *Maxwellian solutions are unique*.

The muon, like the electron, is a lepton with $\hbar$ of angular momentum. The magnetic moment of the muon is given by Eq. (1.169) with the electron mass replaced by the muon mass. It is twice that predicted using the gyromagnetic ratio (given in Eq. (2) of Box 1.1) in Eq. (2.65) of the Orbital and Spin Splitting section wherein the intrinsic angular momentum for the spin 1/2 fermion is $\frac{\hbar}{2}$. As is the case with the electron, the magnetic moment of the muon is the sum of the component corresponding to the kinetic angular momentum, $\frac{\hbar}{2}$, and the component corresponding to the vector potential angular momentum, $\frac{\hbar}{2}$, (Eq. (1.164)). The spin-flip transition can be considered as involving a magnetic moment of *g* times that of a Bohr magneton of the muon. The *g* factor is equivalent to that of the electron given by Eq. (1.228).

The muon anomalous magnetic moment has been measured in a new experiment at Brookhaven National Laboratory (BNL) [32]. Polarized muons were stored in a superferric ring, and the angular frequency difference $\omega_a$ between the spin precession and orbital frequencies was determined by measuring the time distribution of high-energy decay positrons. The dependence of $\omega_a$ on the magnetic and electric fields is given by the BMT equation which is the relativistic equation of motion for spin in uniform or slowly varying external fields [33]. The dependence on the electric field is eliminated by storing muons with the "magic" $\gamma = 29.3$, which corresponds to a muon momentum $p = 3.09\ GeV/c$. Hence measurement of $\omega_a$ and of *B* determines the anomalous magnetic moment.

The "magic" $\gamma$ wherein the contribution to the change of the longitudinal polarization by the electric quadrupole focusing fields are eliminated occurs when

$$\frac{g_\mu \beta}{2} - \frac{1}{\beta} = 0 \tag{1.238}$$

where $g_\mu$ is the muon *g* factor which is required to be different from the electron $g$ factor in the standard model due to the dependence of the mass dependent interaction of each lepton with vacuum polarizations due to virtual particles. For example, the muon is much heavier than the electron, and so high energy (short distance) effects due to strong and weak interactions are more important here [29]. The BNL Muon (g-2) Collaboration [32] used a "magic" $\gamma = 29.3$ which satisfied Eq. (1.238) identically for $\frac{g_\mu}{2}$; however, their assumption that this condition eliminated the effect of the electrostatic field on $\omega_a$ is flawed as shown in Appendix III: Muon g Factor. Internal consistency was achieved during the determination of $\frac{g_\mu}{2}$ using the BMT equation with the flawed assumption that $\frac{g_\mu}{2} \neq \frac{g_e}{2}$. The parameter measured by Carey et al. [32] corresponding to $\frac{g_\mu}{2}$ was the sum of a finite electric term as well as a magnetic term. The calculated result based on the equivalence of the muon and electron *g* factors:

$$\frac{g_\mu}{2} = 1.001\ \ 165\ \ 923 \tag{1.239}$$

is in agreement with the result of Carey et al. [32]:

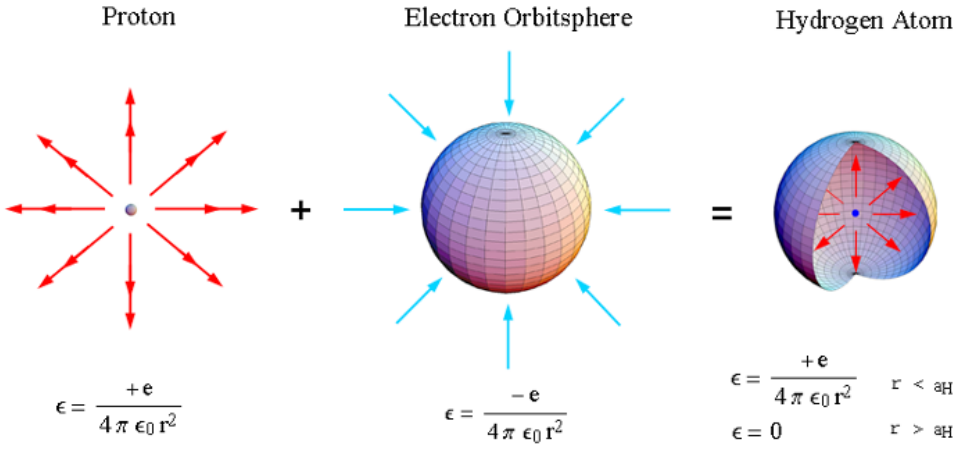
$$\frac{g_\mu}{2} = 1.001\ \ 165\ \ 925\ \ (15) \tag{1.240}$$

Rather than indicating an expanded plethora of postulated super-symmetry virtual particles which make contributions such as smuon-neutralino and sneutrino-chargino loops as suggested by Brown et al. [34], the deviation of the experimental value of $\frac{g_\mu}{2}$ from that of the standard model prediction simply indicates that the muon *g* factor is equivalent to the electron *g* factor.

## DETERMINATION OF ATOMIC ORBITAL RADII

The one-electron atomic orbital is a spherical shell of negative charge (total charge = $-e$) of zero thickness at a distance $r_n$ from the nucleus of charge $+Ze$. It is well known that the field of a spherical shell of charge is zero inside the shell and that of a point charge at the origin outside the shell [35]. See Figure 1.32.

**Figure 1.32.** The point-like electric fields of a proton, a bound electron, and their superposition as the hydrogen atom corresponding to a minimum energy and no electron self interaction. The electron's field is normal and finite only radially distant from its surface, being zero inside of the electron shell according to Gauss' and Faraday's laws which is also consistent with experiments showing zero self field inside of a charged perfect conductor. Thus, only the proton's central field at the electron determines the force balance which causes the flat 2-D geometry of a free electron to transition to the 2-D bubble-like geometry of the atomic orbital.




Thus, for a nucleus of charge $Z$, the force balance equation for the electron atomic orbital is obtained by equating the forces on the mass and charge densities. For the ground state, $n = 1$, the centrifugal force of the electron is given by:

$$\mathbf{F}_{centrifugal} = \frac{m_e}{4\pi r_1^2}\frac{\mathbf{v}_1^2}{r_1} \tag{1.241}$$

where $\frac{m_e}{4\pi r_1^2}$ is the mass density of the atomic orbital. The centripetal force is the electric force, $\mathbf{F}_{ele}$, between the electron and the nucleus.

$$\mathbf{F}_{ele} = \frac{e}{4\pi r_1^2}\frac{Ze}{4\pi\varepsilon_0 r_1^2} \tag{1.242}$$

where $\varepsilon_0$ is the permittivity of free-space.

The second centripetal force is an electrodynamic force or radiation reaction force, a force dependent on the second derivative of charge position, with respect to time, which arises between the electron and the nucleus. This force given in Sections 6.6, 12.10, and 17.3 of Jackson [36] achieves the condition that the sum of the mechanical momentum and electromagnetic momentum is conserved. The motion of each point in the magnetic field of the nucleus will cause a relativistic central force, $\mathbf{F}_{mag}$, which acts on each point mass. The magnetic central force is derived as follows from the Lorentz force, which is relativistically corrected. Each infinitesimal point of the atomic orbital moves on a great circle, and the charge density at each point is $\frac{e}{4\pi r_n^2}$. As given in the Proton and Neutron section, the proton is comprised of a linear combination of three constant functions and three orthogonal spherical harmonic quark/gluon functions. The magnetic field front due to the motion of the electron propagates at the speed of light. From the photon inertial reference frame at the radius of each infinitesimal point of the electron atomic orbital, the proton charge distribution is given as the product of the quark and gluon functions, which gives rise to a uniform distribution. The magnetic flux of the proton in the $v = c$ inertial frame at the electron radius follows from McQuarrie [19]:

$$\mathbf{B} = \frac{\mu_0 e\hbar}{2m_p r_n^3} \tag{1.243}$$

And, the magnetic flux due to a nucleus of charge $Z$ and mass $m$ is:

$$\mathbf{B} = \frac{\mu_0 Ze\hbar}{2mr_n^3} \tag{1.244}$$

The motion of each point will cause a relativistic central force, $\mathbf{F}_{i\,mag}$, which acts on each point mass. The magnetic central force is derived as follows from the Lorentz force which is relativistically corrected. The Lorentz force density on each point moving at velocity $\mathbf{v}$ is:

$$\mathbf{F}_{mag} = \frac{e}{4\pi r_n^2}\mathbf{v}\times\mathbf{B} \tag{1.245}$$

For the hydrogen atom with $Z=1$ and $m=m_p$, substitution of Eq. (1.35) for $\mathbf{v}$ and Eq. (1.244) for $\mathbf{B}$ gives:

$$\mathbf{F}_{mag} = \frac{1}{4\pi r_1^2}\left[\frac{e^2\mu_0}{2m_e r_n}\right]\frac{\hbar^2}{mr_n^3}\hat{r} \tag{1.246}$$

The term in brackets can be expressed in terms the fine structure constant $\alpha$ wherein the radius of the electron relative to the $v=c$ frame ($k$ is the lightlike $k^0$, then $k=\omega_n/c$ regarding a potentially emitted photon), $r_\alpha^*$, is the corresponding relativistic radius. From Eq. (1.15), the relationship between the radius and the electron wavelength is:

$$2\pi r = \lambda \tag{1.247}$$

Using the de Broglie Eq. (1.38) with $v=c$

$$\lambda = \frac{h}{mv} = \frac{h}{mc} \tag{1.248}$$

With substitution of Eq. (1.248) into Eq. (1.247)

$$r_\alpha^* = \frac{\hbar}{mc} = \lambda\!\!\!^{-}_c = \alpha a_0 \tag{1.249}$$

The radius of the electron atomic orbital in the $v=c$ frame is $\lambda\!\!\!^{-}_C$, where $v=c$ corresponds to the magnetic field front propagation velocity which is the same in all inertial frames, independent of the electron velocity as shown by the velocity addition formula of special relativity [37]. From Eqs. (1.179) and (1.249),

$$\frac{e^2\mu_0}{2m_e r_n} = 2\pi\alpha \tag{1.250}$$

where $\lambda\!\!\!^{-}_C$ is the Compton wavelength bar substituted for $r_n$, and $a_o$ is the Bohr radius.

From Lorentz transformations with the electron's invariant angular momentum of $\hbar$ (Eq. (1.37)), it can be shown that the relativistic correction to Eq. (1.246) is the reciprocal of Eq. (1.250). Consider an inertial frame following a great circle of radius $r_n$ with $v=c$ (Here, constant angular velocity as well as constant velocity constitutes an inertial frame for relativistic effects in a general sense, as shown in Chp. 34). The motion is tangential to the radius; thus, $r_n$ is Lorentz invariant. But, as shown in the Special Relativistic Correction to the Ionization Energies section, the tangential distance along a great circle is $2\pi r_n$ in the laboratory frame and $r_n$ in the $v=c$ frame ($k$ is the lightlike $k^0$, then $k=\omega_n/c$). In addition, the corresponding radius is reduced by $\alpha$ for the light speed radial field. Thus, the term in brackets in Eq. (1.246) is the inverse of the relativistic correction $\gamma'$ for the electrodynamic central force.

The electron's magnetic moment of a Bohr magneton $\mu_B$ given by Eq. (1.131) is also invariant as well as its angular momentum of $\hbar$. The electron is nonradiative due to its angular motion as shown in Appendix I: Nonradiation Condition and the Stability of Atoms and Hydrinos section. Furthermore, the angular momentum of the photon given in the Equation of the Photon section is $\mathbf{m} = \int \frac{1}{8\pi c}\mathrm{Re}\left[\mathbf{r}\times(\mathbf{E}\times\mathbf{B}^*)\right]dx^4 = \hbar$. It is conserved for the solutions for the resonant photons and excited state electron functions given in the Excited States of the One-Electron Atom (Quantization) section and the Equation of the Photon section. Thus, the electrodynamic angular momentum and the inertial angular momentum are matched such that the correspondence principle holds. It follows from the principle of conservation of angular momentum that $\frac{e}{m_e}$ of Eq. (1.131) is invariant. The same applies for the intrinsic magnetic moment $\mu_B$ and angular momentum $\hbar$ of the free electron since it is given by the projection of the bound electron into a plane as shown in the Electron in Free Space section. However, special relativity must be applied to physics relative to the electron's center of mass due to the invariance of charge and the invariant

four momentum as given by Purcell [37].

The correction to the term in brackets of Eq. (1.246) also follows from the Lorentz transformation of the electron's invariant magnetic moment as well as its invariant angular momentum of $\hbar$. Consider a great circle of the electron atomic orbital. As shown in the Special Relativistic Effect on the Electron Radius and the Relativistic Ionization Energies section, the tangential distance along a great circle is $2\pi r_n$ in the laboratory frame and $r_n$ in the $v = c$ frame. The corresponding relativistic electron mass density regarding the invariant angular momentum increases by a factor of $2\pi$ (Eq. (1.281)). Furthermore, due to invariance of charge under Gauss' Integral Law, with the radius given by (1.209), the charge corresponding to the source current of the magnetic field must be corrected by $\alpha^{-1}$. Thus, from the perspective of the invariance of $\mu_B$, the term in brackets in Eq. (1.246) is the inverse of the relativistic correction for the electrodynamic central force.

$$\frac{\alpha^{-1}e^2\mu_0}{2(2\pi m_e)r_n} = \frac{\alpha^{-1}e^2\mu_0}{2(2\pi m_e)\lambda\!\!\!^{-}} = \frac{2\pi\alpha^{-1}e^2\mu_0}{2(2\pi m_e)\dfrac{h}{m_e c}} = 1 \tag{1.251}$$

Therefore, the force is given by:

$$\mathbf{F}_{mag} = -\frac{1}{4\pi r_1^2}\frac{\hbar^2}{mr_1^3}\hat{r} \tag{1.252}$$

The force balance equation is given by equating the centrifugal and centripetal force densities:

$$\frac{m_e}{4\pi r_1^2}\frac{v_1^2}{r_1} = \frac{1}{4\pi r_1^2}\frac{\hbar^2}{m_e r_1^3} = \frac{e}{4\pi r_1^2}\frac{Ze}{4\pi\varepsilon_0 r_1^2} - \frac{1}{4\pi r_1^2}\frac{\hbar^2}{mr_1^3} \tag{1.253}$$

where $Z = 1$ and $m = m_p$ for the hydrogen atom and the velocity is given by Eq. (1.35). (Since the surface-area factor cancels in all cases, this factor will be left out in subsequent force calculations throughout this book). From the force balance equation:

$$r_1 = \frac{4\pi\varepsilon_o\hbar^2}{Ze^2\mu_e} \tag{1.254}$$

where the reduced electron mass, $\mu_e$, is:

$$\mu_e = \frac{m_e m}{m_e + m} \tag{1.255}$$

The Bohr radius is:

$$a_0 = \frac{4\pi\varepsilon_0\hbar^2}{e^2 m_e} \tag{1.256}$$

And, the radius given by force balance between the centrifugal force and central electrostatic force alone is:

$$r_1 = \frac{4\pi\varepsilon_o\hbar^2}{Ze^2 m_e} = \frac{a_0}{Z} \tag{1.257}$$

And, for hydrogen, $m$ of Eq. (1.255) is:

$$m = m_p \tag{1.258}$$

Substitution of the reduced electron mass for the electron mass gives, $a_H$, the Bohr radius of the hydrogen atom.

$$a_H = \frac{4\pi\varepsilon_0\hbar^2}{e^2\mu_e} \tag{1.259}$$

Thus, Eq. (1.254) becomes

$$r_1 = \frac{a_H}{Z} \tag{1.260}$$

where $Z = 1$ for the hydrogen atom. The results can also be arrived at by the familiar minimization of the energy.

## ENERGY CALCULATIONS

The potential energy $V$ between the electron and the nucleus separated by the radial distance radius $r_1$ considering the force balance between the centrifugal force and central electrostatic force alone is

$$V = \frac{-Ze^2}{4\pi\varepsilon_0 r_1} = \frac{-Z^2e^2}{4\pi\varepsilon_0 a_0} = -Z^2 \cdot 4.3598\ X\ 10^{-18}\ J = -Z^2 \cdot 27.212\ eV \tag{1.261}$$

Because this is a central force problem, the kinetic energy, $T$, is $-\frac{1}{2}V$.

$$T = \frac{Z^2e^2}{8\pi\varepsilon_0 a_0} = Z^2 \cdot 13.606\ eV \tag{1.262}$$

The same result can be obtained from $T = \frac{1}{2}m_e v_1^2$ and Eq. (1.35). Alternatively, the kinetic energy $T$ and the binding energy $E_B$, which are each equal to the change in stored electric energy, $\Delta E_{ele}$, can be calculated from

$$T = \Delta E_{ele} = -\frac{1}{2}\varepsilon_0 Z \int_{\infty}^{r_1} \mathbf{E}^2 dv \text{ where } \mathbf{E} = -\frac{e}{4\pi\varepsilon_0 r^2}\mathbf{i_r} \tag{1.263}$$

Thus, as the atomic orbital shrinks from $\infty$ *to* $r_1$,

$$E_B = -\frac{Ze^2}{8\pi\varepsilon_0 r_1} = -\frac{Z^2e^2}{8\pi\varepsilon_0 a_0} = -Z^2 \cdot 2.1799\ X\ 10^{-18}\ J = -Z^2 \cdot 13.606\ eV \tag{1.264}$$

The calculated Rydberg constant $R$ using Eq. (1.259) in Eqs. (1.261-1.264) which includes the relativistic correction corresponding to the magnetic force given by Eq. (1.252) is $10,967,758\ m^{-1}$. The experimental Rydberg constant is $10,967,758\ m^{-1}$. Furthermore, a host of parameters can be calculated for the hydrogen atom, as shown in Table 1.2.

**Table 1.2.** Some calculated parameters for the hydrogen atom ( $n = 1$ ).

| | | |
|---|---|---|
| radius | $r_1 = a_H$ | 5.294654 $X$ $10^{-11}$ $m$ |
| potential energy | $V = \frac{-e^2}{4\pi\varepsilon_0 a_H}$ | –27.196 $eV$ |
| kinetic energy | $T = \frac{e^2}{8\pi\varepsilon_0 a_H}$ | 13.598 $eV$ |
| angular velocity (spin) | $\omega_1 = \frac{\hbar}{m_e r_1^2}$ | 4.1296 $X$ $10^{16}$ $rad\ s^{-1}$ |
| linear velocity | $v_1 = r_1\omega_1$ | 2.1865 $X$ $10^{6}$ $ms^{-1}$ |
| wavelength | $\lambda_1 = 2\pi r_1$ | 3.325 $X$ $10^{-10}$ $m$ |
| spin quantum number | $s = \frac{1}{2}$ | $\frac{1}{2}$ |
| moment of Inertia | $I = \frac{m_e r_1^2}{2}$ | 1.277 $X$ $10^{-51}$ $kgm^2$ |
| angular kinetic energy | $E_{angular} = \frac{1}{2} I\omega_1^2$ | 6.795 $eV$ |
| magnitude of the angular momentum | $\hbar$ | 1.0545 $X$ $10^{-34}$ $Js$ |
| projection of the angular momentum onto the transverse-axis | $\frac{\hbar}{4}$ | 2.636 $X$ $10^{-35}$ $Js$ |
| projection of the angular momentum onto the z-axis | $S_z = \frac{\hbar}{2}$ | 5.273 $X$ $10^{-35}$ $Js$ |
| mass density | $\frac{m_e}{4\pi r_1^2}$ | 2.589 $X$ $10^{-11}$ $kgm^{-2}$ |
| charge density | $\frac{e}{4\pi r_1^2}$ | 4.553 $Cm^{-2}$ |

Table 1.3 gives the radii and energies for some one-electron atoms. In addition to the energies, the wavelength, angular frequency, and the linear velocity can be calculated for any one-electron atom from Eqs. (1.38), (1.36), and (1.35). Values are given in Table 1.4.

**Table 1.3.** Calculated energies (non-relativistic) and calculated ionization energies for some one-electron atoms.

| Atom | Calculated $r_1$ [a] ($a_0$) | Calculated Kinetic Energy[b] (eV) | Calculated Potential Energy[c] (eV) | Calculated Ionization Energy[d] (eV) | Experimental Ionization Energy[e] (eV) |
|---|---|---|---|---|---|
| $H$ | 1.000 | 13.61 | –27.21 | 13.61 | 13.59 |
| $He^{+}$ | 0.500 | 54.42 | –108.85 | 54.42 | 54.42 |
| $Li^{2+}$ | 0.333 | 122.45 | –244.90 | 122.45 | 122.45 |
| $Be^{3+}$ | 0.250 | 217.69 | –435.39 | 217.69 | 217.71 |
| $B^{4+}$ | 0.200 | 340.15 | –680.29 | 340.14 | 340.22 |
| $C^{5+}$ | 0.167 | 489.81 | –979.62 | 489.81 | 489.98 |
| $N^{6+}$ | 0.143 | 666.68 | –1333.37 | 666.68 | 667.03 |
| $O^{7+}$ | 0.125 | 870.77 | –1741.54 | 870.77 | 871.39 |

[a] from Equation (1.257)
[b] from Equation (1.262)
[c] from Equation (1.261)
[d] from Equation (1.264)
[e] experimental

It is noteworthy that the potential energy is a constant (at a given $n$) because the electron is at a fixed distance, $r_n$, from the nucleus. And, the kinetic energy and velocity squared are constant because the atom does not radiate at $r_n$ and the potential energy is constant.

**Table 1.4.** Calculated radii, angular frequencies, linear velocities, and wavelengths for the $n$=1 state of some one-electron atoms (non-relativistic).

| Atom | $r_1$ [a] ($a_0$) | angular[b] velocity ($10^{17}\,rad\,s^{-1}$) | linear[c] velocity ($10^{6}\,ms^{-1}$) | wavelength[d] ($10^{-10}\,m$) |
|---|---|---|---|---|
| $H$ | 1.000 | 0.413 | 2.19 | 3.325 |
| $He^{+}$ | 0.500 | 1.65 | 4.38 | 1.663 |
| $Li^{2+}$ | 0.333 | 3.72 | 6.56 | 1.108 |
| $Be^{3+}$ | 0.250 | 6.61 | 8.75 | 0.831 |
| $B^{4+}$ | 0.200 | 10.3 | 10.9 | 0.665 |
| $C^{5+}$ | 0.167 | 14.9 | 13.1 | 0.554 |
| $N^{6+}$ | 0.143 | 20.3 | 15.3 | 0.475 |
| $O^{7+}$ | 0.125 | 26.5 | 17.5 | 0.416 |

[a] from Equation (1.257)
[b] from Equation (1.36)
[c] from Equation (1.35)
[d] from Equation (1.38)

It should be noted that the linear velocity is an appreciable percentage of the velocity of light for some of the atoms in Table 1.4—5.9% for $O^{7+}$ for example. Relativistic corrections must be applied before a comparison between the total energy and ionization energy (Table 1.3) is made.

## SPECIAL RELATIVISTIC EFFECT ON THE ELECTRON RADIUS AND THE RELATIVISTIC IONIZATION ENERGIES

The electron current constitutes an orbit relative to the laboratory frame. Muons and electrons are both leptons. The increase in the lifetime of muonic decay due to relativistic motion in a cyclotron orbit relative to a stationary laboratory frame provides strong confirmation of time dilation and confirms that the electron's frame is an inertial frame [38]. $\frac{eB}{m_e}$ bunching of electrons in a gyrotron [39] occurs because the cyclotron frequency is inversely proportional to the relativistic electron mass. This further demonstrates that the electron frame is an inertial frame and that relativistic electron mass increase and time dilation occur relative to the laboratory frame. The special relativistic relationship in polar coordinates is derived. The result of the treatment of the electron motion relative to the laboratory frame is in excellent agreement with numerous experimental observables such as the electron g factor, the invariance of the electron magnetic moment of $\mu_B$ and angular momentum of $\hbar$, the fine structure of the hydrogen atom, and the relativistic ionization energies of one and two electron atoms found *infra* and in the Excited States of the One-Electron Atom (Quantization) and the Two-Electron Atoms sections.

Following the same derivation as given by Beiser [40], it can be shown that the consequences of maintaining a constant maximum speed of light with preservation of physical laws independent of inertial frames of reference for the bound electron requires that the coordinate transformations are Lorentzian. First, the consequences for the electron in its frame are considered. The motion at each infinitesimal point of the atomic orbital is on a great circle as shown in the Atomic Orbital Equation of Motion For $\ell = 0$ Based on the Current Vector Field (CVF) section. The electron motion is tangential to the radius; thus, $r_n$ for the electron-frame is Lorentz invariant. A further consequence of the electron's motion always being perpendicular to its radius is that the electron's angular momentum of $\hbar$ is invariant as shown by Eq. (1.37). The electron's magnetic moment of a Bohr magneton $\mu_B$ given by Eq. (1.131) is also invariant as well as its angular momentum of $\hbar$.

Further using the required Lorentz transforms, the special relativistic effects for the laboratory frame are determined on the bound electron by considering lightlike events where there is a decrease in the electron wavelength and period due to relativistic length contraction and time dilation of the electron motion in the laboratory inertial frame relative to the lightlike

frame as shown *infra*[10]. A lightlight event regards the nature of an electron, excited state since only excited states of the bound electron can emit radiation. The nature of excited states depends on the properties of photons as well as the bound electron. The angular momentum of the electric and magnetic fields of the photon given in the Equation of the Photon section is $\hbar$. It is conserved for the solutions for the resonant photons and excited state electron functions given in the Excited States of the One-Electron Atom (Quantization) section and the Equation of the Photon section. The photons emitted during the formation of each one-electron atom are its excited state photons. Thus, the electrodynamic angular momentum and the inertial angular momentum are matched such that the correspondence principle holds. It follows from the principle of conservation of angular momentum of $\hbar$ that $\frac{e}{m_e}$ of Eq. (1.131) is invariant (See the Determination of Atomic Orbital Radii section). Since charge is invariant according to special relativity, the electron mass of the atomic orbital must also be invariant. But, as shown *infra*, the electron radius in the laboratory frame goes to a factor of $\frac{1}{2\pi}$ of that in the lightlike ($v = c$) frame. Thus, the effect of special relativity is to increase the mass and charge densities identically such that $\frac{e}{m_e}$ is a constant invariant. In the present case, the electron mass density increases by factor of $2\pi$ relative to that in the lightlike frame. The remarkable agreement between the calculated and observed value of the fine structure of the hydrogen atom which depends on the conditions of the invariance of the electron's charge and charge-to-mass ratio $\frac{e}{m_e}$ as given in the Spin-Orbit Coupling section further confirms the validity of this result. A further consequence of the decrease of the radius of the atomic orbital by a factor of $2\pi$ relative to that in the lightlike frame is that the bound electron is nonradiative due to its angular motion even in the case that $\ell \neq 0$. This is shown by using the relativistic wavelength to radius relationship given by Eq. (1.279) in Appendix I: Nonradiation Condition and in the Stability of Atoms and Hydrinos section. The radiative instability of excited states is due to a radial dipole term in the function representative of the excited state due to the interaction of the photon and the excited state electron as shown in the Instability of Excited States section.

Specifically, to derive the relativistic relationships consider that the electron is in constant angular velocity and is an inertial frame of reference relative to absolute space as given in the Equivalence of Inertial and Gravitational Masses Due to Absolute Space and Absolute Light Velocity section. This can be defined as the laboratory frame of the electron's motion upon which the spatial and temporal Lorentzian transforms may be applied. The motion of a possible photon is also relative to absolute space. The nature of an exited state as shown in the Excited States of the One-Electron Atom (Quantization) section is a superposition of an electron and a photon comprising two-dimensional shells of current and field lines, respectively, at the same radius defined by $\delta(r - r_n)$. Due to the further nature of the photon possessing light-speed angular motion, the electron motion and corresponding spatial and temporal parameters may be considered relative to light speed for the laboratory frame of the electron's constant angular velocity. The derivation of Eqs. (1.279) and (1.280) regards the use of Lorentz spatial and temporal transforms for the case of constant angular velocity along a path on a great-circle element. Such transforms are unconventional from the standard transforms on rectilinear motion, but they are perfectly physical as shown in the Newton's Absolute Space Was Abandoned by Special Relativity Because Its Nature Was Unknown section.

The equation of a photon is given in the Equation of the Photon section. An emitted free-space photon comprises a field-line pattern called a photon electric and magnetic vector field (e&mvf) similar to the atomic orbital wherein the former is generated from two orthogonal great circle field lines rather than two great circle current loops as in the case of the electron spin function. The motion along each field line is at light speed. The angular momentum, **m**, of the electric and magnetic fields of the emitted photon given by Eq. (4.1) is $\mathbf{m} = \int \frac{1}{8\pi c} \mathrm{Re}\left[\mathbf{r} \times (\mathbf{E} \times \mathbf{B}^*)\right] dx^4 = \hbar$. The equation of the photon of an exited state is given by Eq. (2.15). The absorption or emission of a photon regards an excited state given in the Excited States of the One-Electron Atom (Quantization) section. The excited state comprises a two-dimension field surface of great-circle field lines at the inner surface of the electron atomic orbital that has a slow component of motion phase-locked with and propagating the electron modulation wave ($\ell \neq 0$) that travels about the z-axis with angular frequency $\omega_n$. The corresponding change in electron angular frequency between states matches the frequency of the photon that excited the transition, and the angular momentum of the fields (Eq. (4.1)) is conserved in the excited state. In addition, the motion along each great-circle field line is at velocity $c$; so, the

[10] Many problems arise in the case of applying special relativity to standard quantum mechanical solutions for one-electron atoms as discussed in the Quantum Theory Past and Future section, the Shortcomings of Quantum Theory section, and Refs. [16-17]. Spin was missed entirely by the Schrödinger equation, and it was forced by spin matrices in the Dirac equation. It does not arise from first principles, and it results in nonsensical consequences such as infinities and "a sea of virtual particles." These are not consistent with observation and paradoxically the virtual particles constitute an ether, the elimination of which was the basis of special relativity and is the supposed basis of the Dirac equation. In addition, the electron motion in the Schrödinger and Dirac equations is in all directions; consequently, the relativistic increase in electron mass results in an instability since the electron radius is inversely proportional to the electron mass. Since the electron mass in special relativity is not invariant, but the charge is, the electron magnetic moment of a Bohr magneton $\mu_B$ as well as its angular momentum of $\hbar$ cannot be invariant in contradiction with experimental observations known to 14-figure accuracy [26].

relative electron to absorbed-photon velocity is $c$. This is also the velocity that must be considered for the emission of a photon by the bound electron since this state must form in order for emission to occur. The corresponding source current follows from $\mathbf{n} \bullet \left(\mathbf{E}_1 - \mathbf{E}_2\right) = \frac{\sigma}{\varepsilon_0}$ (Eq. (2.11)), and the relativistically corrected wavelength given by Eq. (1.279) is $\lambda_n = r_n$. This is Eq. (41) of the Appendix I that determines the nonradiative property of the atomic orbital and its time and spherically harmonic angular functions as given by Eqs. (38) and (70) and (73) of Appendix I[9]. Emission or absorption corresponds to an energy-state transition. The corresponding change in electron radius with emission or absorption of a photon is the source current for a free-space photon as given in the State Lifetimes and Line Intensities section.

Consider that the motion at each infinitesimal point on the atomic orbital is on a great circle, and that each point-charge element has the charge density $\frac{e}{4\pi r_n^2}$ and mass density $\frac{m_e}{4\pi r_n^2}$ as shown in the Atomic Orbital Equation of Motion For $\ell = 0$ Based on the Current Vector Field (CVF) section. Next, consider a charge-density element (and correspondingly a mass-density element) of a great-circle current loop of the electron atomic orbital in the y'z'-plane as shown in Figure 1.4. The distance on a great circle is given by:

$$\int_0^{2\pi} r_n d\theta = r_n \theta \Big|_0^{2\pi} = 2\pi r_n \tag{1.265}$$

Due to relative motion, the distance along the great circle must contract and the time must dilate due to special relativity. The special relativistic length contraction relationship observed for a laboratory frame relative to an inertial frame moving at constant velocity $v$ is:

$$l = l_o \sqrt{1 - \left(\frac{v}{c}\right)^2} \tag{1.266}$$

Consider a point initially at (0,0,1) moving clockwise on a great circle in the Cartesian y'z'-plane. The relationship between polar and Cartesian coordinates used for special relativity[11] is given by:

$$x_1' = 0 \qquad y_1' = r_n \sin(\omega_n t) \qquad z_1' = r_n \cos(\omega_n t) \tag{1.267}$$

where $\omega_n$ is given by Eq. (1.36), $r_n$ is from Eq. (1.257), and

$$\phi = \omega_n t \tag{1.268}$$

Due to relativity, a contracted wavelength arises. The distance on the great circle undergoes length contraction only in the $\hat{\phi}$ direction as $v \to c$. Thus, as $v \to c$ the distance on a great circle approaches its radius which is the relativistically contracted electron wavelength since the relationship between the radius and the wavelength given by Eq. (1.15) is

$$2\pi r_n = \lambda_n \tag{1.269}$$

With $v = c$,

$$r^* = \lambda \tag{1.270}$$

where * indicates the relativistically corrected parameter. Thus,

$$r^* = \frac{r_n}{2\pi} \tag{1.271}$$

The relativistically corrected mass $m^*$ follows from Eq. (1.271) with maintenance of the invariance of the electron angular momentum of $\hbar$ given by Eqs. (1.35) and (1.37).

$$m\mathbf{r} \times \mathbf{v} = m_e r \frac{\hbar}{m_e r} \tag{1.272}$$

[11] The Cartesian coordinate system as compared to general coordinates is special with regard to a fundamental aspect of Lorentz transforms on Cartesian coordinates discussed in the Relativity section.

With Eq. (1.271), the relativistically corrected mass $m*$ corresponding to an increase in its density only is[12]

$$m* = 2\pi m_e \tag{1.273}$$

The effect of the relativistic contraction of the distance along a great circle loop is to change the angle of constant motion in Eq. (1.267) with a corresponding decrease in the electron wavelength. For the point initially at (0,0,1) moving clockwise on a great circle in the Cartesian y'z'-plane as shown in Figure 1.4, the relativistically corrected wavelength that follows from Eqs. (1.265-1.269) is given by the sum of the relativistic electron motion along the great circle (y' direction) and that projected along the radial axis (z' direction):

$$\lambda_n = r^*_{n,y'} \sin\phi^* \int_0^{2\pi} d\phi + \cos\phi^* \int_0^{r^*_{n,z'}} dr \tag{1.274}$$

where the * indices correspond to the relativistically corrected parameters in the y' and z' directions. The length contraction is only in the direction of motion that is orthogonal to the radius and constant as a function of angle. Thus, Eq. (1.268) is given by

$$\lambda_n = 2\pi r'_n \sqrt{1-\left(\frac{v}{c}\right)^2} \sin\phi^* + r'_n \cos\phi^* \tag{1.275}$$

The projection of the angular motion onto the radial axis is determined by determining the relativistic angle $\phi^*$ corresponding to a decrease in the electron wavelength and period due to relativistic length contraction and time dilation of the electron motion in the laboratory inertial frame. Substitution of Eq. (1.36) into Eq. (1.268) gives:

$$\phi = \omega_n t = \frac{\hbar}{m_e r_n^2} t \tag{1.276}$$

The correction for the time dilation and length contraction due to electron motion gives the relativistic angle $\phi^*$ as:

$$\phi^* = \omega_n t = \frac{\hbar}{m_e \left(\frac{r_n}{\sqrt{1-\left(\frac{v}{c}\right)^2}}\right)^2} t\sqrt{1-\left(\frac{v}{c}\right)^2} = \frac{\hbar}{m_e r_n^2} t\left(1-\left(\frac{v}{c}\right)^2\right)^{3/2} \tag{1.277}$$

---

[12] The magnitude of the total angular momentum of the atomic orbital $\mathbf{L}$ must be constant. The constant total is $\hbar$ given by the integral

$$\mathbf{m} = \int \frac{1}{4\pi r^2} |\mathbf{r} \times m_e \mathbf{v}| \delta(r - r_n) dx^4 = m_e r_n \frac{\hbar}{m_e r_n} = \hbar \tag{1}$$

where the corresponding velocity is given by Eq. (1.35). The integral of the magnitude of the angular momentum of the electron is $\hbar$ in any inertial frame and is *relativistically invariant*.

According to special relativity, the electron's relative motion with respect to the laboratory frame causes the distance along the great circle to contract and the time to dilate such that a contracted radius arises as given by Eq. (1.280). As $v \to c$ the relativistically corrected radius in the laboratory frame $r*$ is given by

$$r* = \frac{r_n}{2\pi} \tag{2}$$

where $r_n$ is the radius in the electron frame. Eq. (1.271) applies for both the mass and charge densities that are interchangeable by the ratio $\frac{e}{m_e}$. Thus, the ratio is invariant.

However, a relativistically corrected mass $m*$ can be defined from Eq. (1.271) with maintenance of the invariance of the electron angular momentum of $\hbar$ given by Eqs. (1.35) and (1.37). Due to spherical symmetry, the correction is the same along each great circle of the atomic orbital. Thus, the motion of the mass density of the electron along a great circle may be considered. Then,

$$m\mathbf{r} \times \mathbf{v} = m_e r \frac{\hbar}{m_e r} \tag{3}$$

With Eq. (1.271), the relativistically corrected mass $m*$ corresponding to an increase in its density only is

$$m* = 2\pi m_e \tag{4}$$

In other words, the correction of the radius gives an effective relativistic mass as follows:

$$m\mathbf{r} \times \mathbf{v} = m_e \frac{r}{2\pi} \frac{\hbar}{m_e \frac{r}{2\pi}} = 2\pi m_e \frac{r}{2\pi} \frac{\hbar}{m_e r} = m^* \frac{r}{2\pi} \frac{\hbar}{m_e r} = m^* r^* v = \hbar \tag{5}$$

where $v$ is the electron velocity in its frame given by Eq. (1.35).

The period for a wavelength due to electron motion is:

$$T = \frac{2\pi}{\omega} = \frac{\lambda}{v} \tag{1.278}$$

Only the elements of the second y'z'-quadrant need be considered due to symmetry and continuity of the motion. Thus, using Eqs. (1.276-1.277) for a quarter period of time, Eq. (1.275) becomes:

$$\lambda_n = 2\pi r_n' \sqrt{1-\left(\frac{v}{c}\right)^2}\ \sin\left[\frac{\pi}{2}\left(1-\left(\frac{v}{c}\right)^2\right)^{3/2}\right] + r_n' \cos\left[\frac{\pi}{2}\left(1-\left(\frac{v}{c}\right)^2\right)^{3/2}\right] \tag{1.279}$$

Using a phase matching condition, the wavelengths of the electron (Eq. (1.269)) and laboratory (Eq. (1.279)) inertial frames are equated, and the corrected radius is given by:

$$r_n = r_n' \left[\sqrt{1-\left(\frac{v}{c}\right)^2}\ \sin\left[\frac{\pi}{2}\left(1-\left(\frac{v}{c}\right)^2\right)^{3/2}\right] + \frac{1}{2\pi}\cos\left[\frac{\pi}{2}\left(1-\left(\frac{v}{c}\right)^2\right)^{3/2}\right]\right] \tag{1.280}$$

which gives a relativistic factor $\gamma^*$ of:

$$\gamma^* = \frac{2\pi}{2\pi\sqrt{1-\left(\frac{v}{c}\right)^2}\ \sin\left[\frac{\pi}{2}\left(1-\left(\frac{v}{c}\right)^2\right)^{3/2}\right] + \cos\left[\frac{\pi}{2}\left(1-\left(\frac{v}{c}\right)^2\right)^{3/2}\right]} \tag{1.281}$$

where the velocity is given by Eq. (1.35) with the radius given by Eq. (1.254). Plots of ratio of the radii from Eq. (1.280) and $\gamma^*$ (Eq. (1.281)) as a function of the electron velocity $v$ relative to the speed of light $c$ are given in Figures 1.33 and 1.34, respectively.

As the electron velocity goes to the speed of light ($v \to c$) corresponding to any real or potentially emitted phase-locked photon, the electron radius in the laboratory frame goes to a factor of $\frac{1}{2\pi}$ of that in the lightlike electron frame ($\frac{r_n}{r_n'} = \frac{1}{2\pi}$). Thus, with $v = c$, due to symmetry the electron motion corresponds to an atomic orbital of radius $\frac{1}{2\pi}$ that of the radius in the lightlike frame. In the case where the velocity is the speed of light, the relativistic behavior predicts that the production masses of leptons are each the rest mass times the speed of light squared calculated from each of the Planck-equation, electric, and magnetic energies in the Leptons section. The radius correction given by Eq. (1.280) and shown in Figure 1.33 also correctly predicts the nonradiation condition, the force corresponding to the reduced electron mass in the radius of the hydrogen atom, spin-orbit coupling, the electron pairing force, and other relativistic observables given in this and subsequent chapters.

**Figure 1.33.** The normalized radius as a function of $v/c$ due to relativistic contraction.

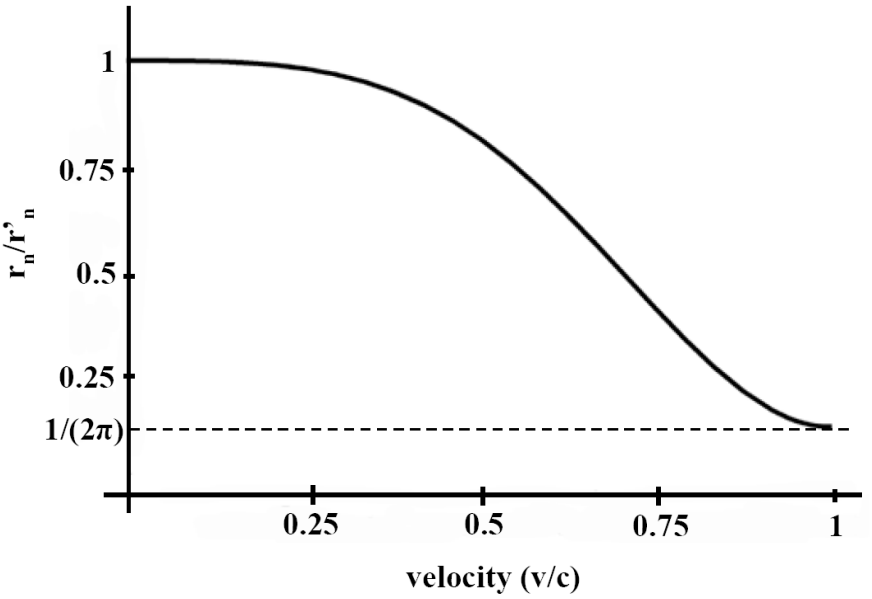
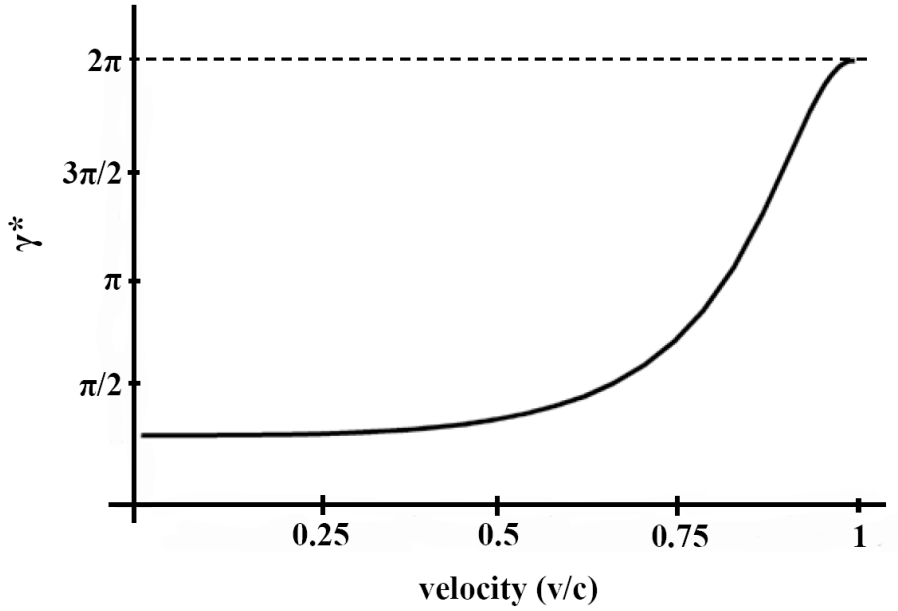



**Figure 1.34.** The relativistic factor $\gamma^*$ as a function of $v/c$.




Next, a convenient way to determine the relativistic ionization energies is to use the relativistic total energy equation [41]. Consider the motion of the electron in its frame of reference. Since its motion is perpendicular to the radius, the radius (Eq. (1.260)) is invariant to length contraction, the charge is invariant, and only the dependency of the radius on the relativistic mass needs to be considered. The force balance equation (Eq. (1.253)) given by equating the centrifugal and centripetal force densities applies in the relativistic case as well where $m_e = m_e(v)$ is the relativistic electron mass, $Z$ is the nuclear charge, $m = Am_p$ is the nuclear mass with $A$ being the atomic mass number, and the velocity given by Eq. (1.35) is due to conservation of angular momentum which must be obeyed in the relativistic case as well as the nonrelativistic one. From the force balance equation:

$$r = \frac{4\pi\varepsilon_o\hbar^2}{Ze^2 m_{e0}}\left(\frac{m_{e0}}{m_e} + \frac{m_{e0}}{m_p A}\right) = \frac{a_0}{Z}\frac{m_{e0}}{m_e}\left(1 + \frac{m_e}{m_p A}\right) \tag{1.282}$$

Using the relativistic velocity (Eq. (1.35) with $m_e = m_e(v)$) and the radius from the force balance equation, the relativistic parameter $\beta$ is:

$$\beta = \frac{v}{c} = \frac{\hbar}{m_e c r} = \frac{\hbar}{m_e c \frac{a_0}{Z}\frac{m_{e0}}{m_e}\left(1+\frac{m_e}{m_p A}\right)} = \frac{\hbar}{m_{e0} c \frac{a_0}{Z}\left(1+\frac{m_e}{m_p A}\right)} \tag{1.283}$$

Eqs. (1.178) and (1.179) give a relationship between the fine structure constant and the constants of Eq. (1.283):

$$\alpha = \frac{\mu_0 e^2 c}{4\pi\hbar} = \frac{e^2}{4\pi\varepsilon_0 \hbar c}\frac{a_0}{a_0} = \frac{e^2}{4\pi\varepsilon_0 \hbar c a_0}\frac{4\pi\varepsilon_0\hbar^2}{e^2 m_{e0}} = \frac{\hbar}{m_{e0} c a_0} \tag{1.284}$$

Then, from Eqs. (1.283) and (1.284), the relativistic parameter $\beta$ simplifies to:

$$\beta = \frac{v}{c} = \frac{\alpha Z}{\left(1+\frac{m_e}{m_p A}\right)} \tag{1.285}$$

The relativistic mass is given by the Lorentz transformation:

$$m_e(v) = m_e = \frac{m_{e0}}{\sqrt{1-\beta^2}} = \frac{m_{e0}}{\sqrt{1-\frac{v^2}{c^2}}} \tag{1.286}$$

Next, a relationship for the velocity in the relativistic correction for the electron mass is determined from the boundary constraints. In the nonrelativistic limit, Eq. (1.282) reduces to Eq. (1.259) even in the case that Eq. (1.286) is substituted into Eq. (1.285); however, at any finite velocity the spin-nuclear interaction becomes velocity dependent according to Eqs. (1.285-1.286). Since the interaction arises from the invariant magnetic moments corresponding to the invariant angular momentum of the electron and proton, the $m_e = m_e(v)$ parameter in Eq. (1.285) must be the fixed constant of $m_{e0}$. The corresponding relativistic invariant magnetic moment of the nucleus is the nuclear magneton $\mu_N$ given by

$$\mu_N = \frac{e\hbar}{2m_p} \tag{1.287}$$

such that the relativistic mass ratio for the spin-nuclear interaction is $\frac{m_{e0}}{2m_p}$. Thus, Eq. (1.285) is given by:

$$\beta = \frac{v}{c} = \frac{\alpha Z}{\left(1+\frac{m_{e0}}{2m_p A}\right)} \tag{1.288}$$

Thus, from Eqs. (1.282), (1.286), and (1.288), the relativistic radius of the bound electron is given by:

$$r = \frac{a_0}{Z}\left(\sqrt{1-\frac{v^2}{c^2}}+\frac{m_{e0}}{m_p A}\right) = \frac{a_0}{Z}\left(\sqrt{1-\left(\frac{\alpha Z}{\left(1+\frac{m_{e0}}{2m_p A}\right)}\right)^2}+\frac{m_{e0}}{m_p A}\right) \tag{1.289}$$

The ionization energy or ionization potential $IP$ is given by the negative of the sum of the potential $V$ and kinetic energies $T$:

$$IP = -(V+T) \tag{1.290}$$

The potential energy is given by Eq. (1.261), and the relativistic kinetic energy from Eq. (34.17) is [41]:

$$T = m_{e0}c^2\left(\frac{1}{\sqrt{1-\left(\frac{v}{c}\right)^2}}-1\right) \tag{1.291}$$

Thus, $IP$ is given by:

$$IP = \frac{Ze^2}{4\pi\varepsilon_0 r} - m_{e0}c^2\left(\frac{1}{\sqrt{1-\left(\frac{v}{c}\right)^2}} - 1\right) \tag{1.292}$$

Substitution of Eqs. (1.288-1.289) into Eq. (1.292) gives:

$$\begin{aligned} IP &= \frac{Ze^2}{4\pi\varepsilon_0 \frac{a_0}{Z}\left(\sqrt{1-\left(\frac{\alpha Z}{\left(1+\frac{m_{e0}}{2m_pA}\right)}\right)^2} + \frac{m_{e0}}{m_pA}\right)} - m_{e0}c^2\left(\frac{1}{\sqrt{1-\left(\frac{\alpha Z}{\left(1+\frac{m_{e0}}{2m_pA}\right)}\right)^2}} - 1\right) \\ &= \frac{(\alpha Z)^2 m_{e0}c^2}{\left(\sqrt{1-\left(\frac{\alpha Z}{\left(1+\frac{m_{e0}}{2m_pA}\right)}\right)^2} + \frac{m_{e0}}{m_pA}\right)} - m_{e0}c^2\left(\frac{1}{\sqrt{1-\left(\frac{\alpha Z}{\left(1+\frac{m_{e0}}{2m_pA}\right)}\right)^2}} - 1\right) \end{aligned} \tag{1.293}$$

where Eqs. (28.8-28.9) were used. In the case that the electron spin-nuclear interaction is negligible, Eq. (1.293) reduces to:

$$IP = m_{e0}c^2\left(1-\sqrt{1-(\alpha Z)^2}\right) \tag{1.294}$$

In the special case where the velocity is the speed of light and $Z = \alpha^{-1}$, the relativistic behavior predicts that the production masses of fundamental particles are the same in both the particle and laboratory frames as given in the Leptons and Quarks sections. The energies given by Eq. (1.293) are plotted in Figure 1.35 and are given in Table 1.5. The agreement between the experimental and calculated values is excellent. The small deviation is anticipated to be due to the Lamb shift [42] and experimental error.

**Figure 1.35.** The relativistic one-electron-atom ionization energies as a function of the nuclear charge Z.

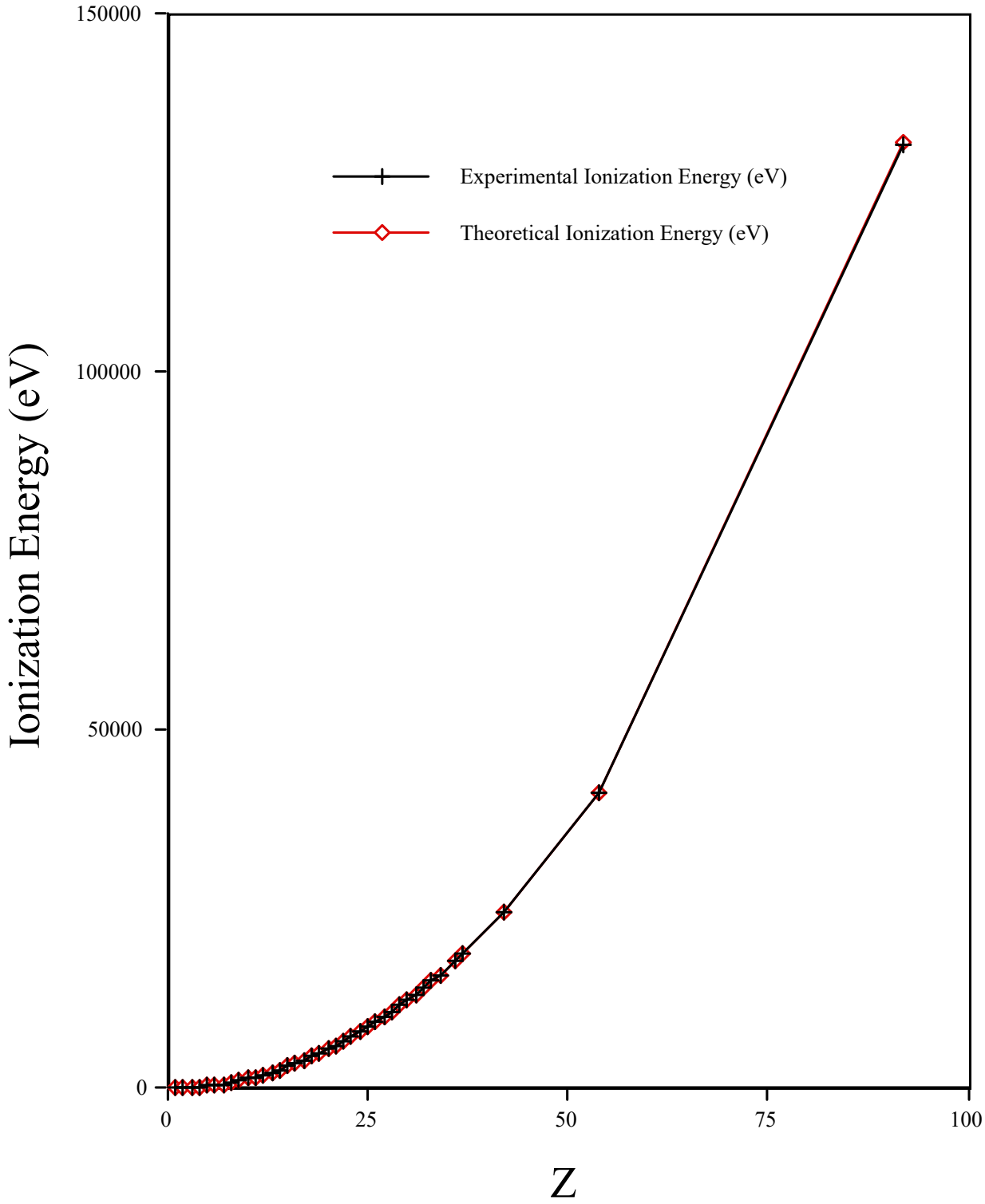


**Table 1.5.** Relativistic ionization energies for some one-electron atoms.

| One e Atom | Z | $\beta$ (Eq. (1.288)) | Theoretical Ionization Energies (eV) (Eq. (1.293)) | Experimental Ionization Energies (eV) [a] | Relative Difference between Experimental and Calculated [b] |
|---|---|---|---|---|---|
| $H$ | 1 | 0.00730 | 13.59847 | 13.59844 | -0.000002 |
| $He^{+}$ | 2 | 0.01459 | 54.41826 | 54.41778 | -0.000009 |
| $Li^{2+}$ | 3 | 0.02189 | 122.45637 | 122.45429 | -0.000017 |
| $Be^{3+}$ | 4 | 0.02919 | 217.72427 | 217.71865 | -0.000026 |
| $B^{4+}$ | 5 | 0.03649 | 340.23871 | 340.2258 | -0.000038 |
| $C^{5+}$ | 6 | 0.04378 | 490.01759 | 489.99334 | -0.000049 |
| $N^{6+}$ | 7 | 0.05108 | 667.08834 | 667.046 | -0.000063 |
| $O^{7+}$ | 8 | 0.05838 | 871.47768 | 871.4101 | -0.000078 |
| $F^{8+}$ | 9 | 0.06568 | 1103.220 | 1103.1176 | -0.000093 |
| $Ne^{9+}$ | 10 | 0.07297 | 1362.348 | 1362.1995 | -0.000109 |
| $Na^{10+}$ | 11 | 0.08027 | 1648.910 | 1648.702 | -0.000126 |
| $Mg^{11+}$ | 12 | 0.08757 | 1962.945 | 1962.665 | -0.000143 |
| $Al^{12+}$ | 13 | 0.09486 | 2304.512 | 2304.141 | -0.000161 |
| $Si^{13+}$ | 14 | 0.10216 | 2673.658 | 2673.182 | -0.000178 |
| $P^{14+}$ | 15 | 0.10946 | 3070.451 | 3069.842 | -0.000198 |
| $S^{15+}$ | 16 | 0.11676 | 3494.949 | 3494.1892 | -0.000217 |
| $Cl^{16+}$ | 17 | 0.12405 | 3947.228 | 3946.296 | -0.000236 |
| $Ar^{17+}$ | 18 | 0.13135 | 4427.363 | 4426.2296 | -0.000256 |
| $K^{18+}$ | 19 | 0.13865 | 4935.419 | 4934.046 | -0.000278 |
| $Ca^{19+}$ | 20 | 0.14595 | 5471.494 | 5469.864 | -0.000298 |
| $Sc^{20+}$ | 21 | 0.15324 | 6035.681 | 6033.712 | -0.000326 |
| $Ti^{21+}$ | 22 | 0.16054 | 6628.064 | 6625.82 | -0.000339 |
| $V^{22+}$ | 23 | 0.16784 | 7248.745 | 7246.12 | -0.000362 |
| $Cr^{23+}$ | 24 | 0.17514 | 7897.827 | 7894.81 | -0.000382 |
| $Mn^{24+}$ | 25 | 0.18243 | 8575.426 | 8571.94 | -0.000407 |
| $Fe^{25+}$ | 26 | 0.18973 | 9281.650 | 9277.69 | -0.000427 |
| $Co^{26+}$ | 27 | 0.19703 | 10016.63 | 10012.12 | -0.000450 |
| $Ni^{27+}$ | 28 | 0.20432 | 10780.48 | 10775.4 | -0.000471 |
| $Cu^{28+}$ | 29 | 0.21162 | 11573.34 | 11567.617 | -0.000495 |
| $Zn^{29+}$ | 30 | 0.21892 | 12395.35 | 12388.93 | -0.000518 |
| $Ga^{30+}$ | 31 | 0.22622 | 13246.66 | 13239.49 | -0.000542 |
| $Ge^{31+}$ | 32 | 0.23351 | 14127.41 | 14119.43 | -0.000565 |
| $As^{32+}$ | 33 | 0.24081 | 15037.75 | 15028.62 | -0.000608 |
| $Se^{33+}$ | 34 | 0.24811 | 15977.86 | 15967.68 | -0.000638 |
| $Kr^{35+}$ | 36 | 0.26270 | 17948.05 | 17936.21 | -0.000660 |
| $Rb^{36+}$ | 37 | 0.27000 | 18978.49 | 18964.99 | -0.000712 |
| $Mo^{41+}$ | 42 | 0.30649 | 24592.04 | 24572.22 | -0.000807 |
| $Xe^{53+}$ | 54 | 0.39406 | 41346.76 | 41299.7 | -0.001140 |
| $U^{91+}$ | 92 | 0.67136 | 132279.32 | 131848.5 | -0.003268 |

[a] From theoretical calculations, interpolation of H isoelectronic and Rydberg series, and experimental data [42-45].
[b] (Experimental-theoretical)/experimental.

The physical basis of electron spin is experimentally proven by observation of gyroscopic coupling in a non-spinning levitated ferromagnet demonstrating that quantum spin corresponds to a genuine form of mechanical angular momentum according to Maxwell's equations rather than "bookkeeping" of non-physical spin quantum numbers as postulated according to quantum mechanics [46]. The electron possesses an invariant angular momentum and magnetic moment of $\hbar$ and a Bohr magneton, respectively. *This invariance feature provides for the stability of multielectron atoms and the existence of excited states wherein electrons magnetically interact* as shown in the Two-Electron Atoms section, the Three- Through Twenty-Electron Atoms section, and the Excited States of Helium section. The electron's motion corresponds to a current which gives rise to a magnetic field with a field strength that is inversely proportional to its radius cubed wherein the magnetic field is a relativistic effect of the electric field as shown by Jackson [47]. As there is *no electrostatic self-energy* as shown in the Determination of Atomic Orbital Radii section and Appendix II, there is also *no magnetic self-energy* for the bound electron since the magnetic moment is invariant for all states and the surface current is the source of the discontinuous field that does not exist inside of the electron as given by Eq. (1.136), $\mathbf{n}\ X\ (\mathbf{H}_a - \mathbf{H}_b) = \mathbf{K}$. No energy term is associated with the magnetic field unless another source of magnetic field is present. In general, the corresponding relativistic correction can be calculated from the effect of the electron's magnetic field on the force balance and energies of other electrons and the nucleus, which also produce magnetic fields. In the case of one-electron atoms, the nuclear-electron magnetic interaction is the only factor. Thus, for example, the effect of the proton was included in the derivation of Eq. (1.260) for the hydrogen atom.

# REFERENCES


1. H. A. Haus, "On the radiation from point charges," American Journal of Physics, 54, (1986), pp. 1126-1129.
2. T. A. Abbott, D. J. Griffiths, Am. J. Phys., Vol. 53, No. 12, (1985), pp. 1203-1211.
3. J. D. Jackson, *Classical Electrodynamics*, Second Edition, John Wiley & Sons, New York, (1975), pp. 739-779.
4. J. D. Jackson, *Classical Electrodynamics*, Second Edition, John Wiley & Sons, New York, (1975), p. 111.
5. J. J. Hudson et al., "Improved measurement of the shape of the electron," Nature, Vol. 473, (2011), pp. 493-496.
6. J. D. Jackson, *Classical Electrodynamics*, Second Edition, John Wiley & Sons, New York, (1975), p. 99.
7. J. D. Jackson, *Classical Electrodynamics*, Second Edition, John Wiley & Sons, New York, (1975), p. 532.
8. D. A. McQuarrie, *Quantum Chemistry*, University Science Books, Mill Valley, CA, (1983), pp. 206-225.
9. G. R. Fowles, *Analytical Mechanics*, Third Edition, Holt, Rinehart, and Winston, New York, (1977), p. 196.
10. L. Pauling, E. B. Wilson, *Introduction to Quantum Mechanics with Applications to Chemistry*, McGraw-Hill Book Company, New York, (1935), pp. 118-121.
11. W. McC. Siebert, *Circuits, Signals, and Systems*, The MIT Press, Cambridge, Massachusetts, (1986), pp. 261, 272, 286, 287, 290, 410, 569, 599.
12. G. R. Fowles, *Analytical Mechanics,* Third Edition, Holt, Rinehart, and Winston, New York, (1977), pp. 17-20.
13. T. Bujnak, H. Hlucha personal communication June 2009, http://brilliantlightpower.com/y00-visualization/density_normalization_angular_momentum_Y00.html.
14. Mathematica modeling of R. Mills' theory by B. Holverstott in "Modeling the Analytical Equations to Generate the Atomic Orbital Current Vector Field and the Uniform Current (Charge) Density Function $Y_0^0(\theta,\phi)$," posted at http://brilliantlightpower.com/atomic-theory/.
15. E. M. Purcell, *Electricity and Magnetism*, McGraw-Hill, New York, (1965), pp. 370-375, 447.
16. P. Pearle, Foundations of Physics, "Absence of radiationless motions of relativistically rigid classical electron," Vol. 7, Nos. 11/12, (1977), pp. 931-945.
17. R. L. Mills, "Maxwell's Equations and QED: Which is Fact and Which is Fiction," Physics Essays, Vol. 19, (2006), pp. 225-262.
18. R. L. Mills, "The Fallacy of Feynman's Argument on the Stability of the Hydrogen Atom According to Quantum Mechanics," Annales de la Fondation Louis de Broglie, Vol. 30, No. 2, (2005), pp. 129-151.
19. D. A. McQuarrie, *Quantum Chemistry*, University Science Books, Mill Valley, CA, (1983), pp. 238-241.
20. J. D. Jackson, *Classical Electrodynamics*, Second Edition, John Wiley & Sons, New York, (1975), p. 178.
21. J. D. Jackson, *Classical Electrodynamics*, Second Edition, John Wiley & Sons, New York, (1975), pp. 194-197.
22. C. E. Gough et al., Nature, Vol. 326, (1987), p. 855.
23. S. Das Sarma, R. E. Prange, Science, Vol. 256, (1992), pp. 1284-1285.
24. J. D. Jackson, *Classical Electrodynamics*, Second Edition, John Wiley & Sons, New York, (1975), pp. 582-584.
25. J. D. Jackson, *Classical Electrodynamics*, Second Edition, John Wiley & Sons, New York, (1975), pp. 758-763.
26. R. C. Weast, *CRC Handbook of Chemistry and Physics*, 68th Edition, CRC Press, Boca Raton, Florida, (1987-88), p. F-186 to p. F-187.
27. R. S. Van Dyck, Jr., P. Schwinberg, H. Dehmelt, "New high precision comparison of electron and positron g factors," Phys. Rev. Lett., Vol. 59, (1987), p. 26-29.
28. P. J. Mohr, B. N. Taylor, "CODATA recommended values of the fundamental physical constants: 1998," Reviews of Modern Physics, Vol. 72, No. 2, April, (2000), pp. 351-495.
29. G. P. Lepage, "Theoretical advances in quantum electrodynamics, International Conference on Atomic Physics, Atomic Physics; Proceedings, Singapore, World Scientific, Vol. 7, (1981), pp. 297-311.

30. E. R. Williams and P. T. Olsen, Phys. Rev. Lett. Vol. 42, (1979), p. 1575.
31. K. V. Klitzing et al., Phys. Rev. Lett. Vol. 45, (1980), p. 494.
32. R. M. Carey et al., Muon (g-2) Collaboration, "New measurement of the anomalous magnetic moment of the positive muon," Phys. Rev. Lett., Vol. 82, (1999), pp. 1632-1635.
33. J. D. Jackson, *Classical Electrodynamics*, Second Edition, John Wiley & Sons, New York, (1975), pp. 556-560.
34. H. N. Brown et al., Muon (g-2) Collaboration, "Precise measurement of the positive muon anomalous magnetic moment," Phys. Rev. D62, 091101 (2000).
35. F. Bueche, *Introduction to Physics for Scientists and Engineers*, McGraw-Hill, (1975), pp. 352-353.
36. J. D. Jackson, *Classical Electrodynamics*, Second Edition, John Wiley & Sons, New York, (1975), pp. 236-240, 601-608, 786-790.
37. E. M. Purcell, *Electricity and Magnetism*, McGraw-Hill, New York, (1985), Second Edition, pp. 451-458.
38. J. Bailey et al., "Final report on the CERN muon storage ring including the anomalous magnetic moment and the electric dipole moment of the muon," and a direct test of relativistic time dilation, Nuclear Physics B150, (1979), pp. 1-75.
39. P. Sprangle, A. T. Drobot, "The linear and self-consistent nonlinear theory of the electron cyclotron maser instability," IEEE Transactions on Microwave Theory and Techniques, Vol. MTT-25, No. 6, June, (1977), pp. 528-544.
40. A. Beiser, *Concepts of Modern Physics*, Fourth Edition, McGraw-Hill, New York, (1987), pp. 1-40.
41. Personal communication, Dr.-Ing. Günther Landvogt, Hamburg, Germany, March, (2004).
42. A. Gemberidze, Th. Stöhlker, D. Banas, K. Beckert, P. Beller, H. F. Beyer, F. Bosch, S. Hafmann, C. Kozhuharov, D. Liesen, F. Nolden, X. Ma, P. H. Mokler, M. Steck, D. Sierpowski, and S. Tashenov, "Quantum electrodynamics in strong electric fields: The ground-state Lamb shift in hydrogenlike uranium," Phys. Rev. Letts., Vol. 94, 223001 (2005).
43. C. E. Moore, "Ionization Potentials and Ionization Limits Derived from the Analyses of Optical Spectra," Nat. Stand. Ref. Data Ser.-Nat. Bur. Stand. (U.S.), No. 34, 1970.
44. D. R. Lide, *CRC Handbook of Chemistry and Physics*, 79th Edition, CRC Press, Boca Raton, Florida, (1998-9), p. 10-175 to p. 10-177.
45. http://physics.nist.gov/PhysRefData/ASD/levels_form.html.
46. F. Ahrens, A. Vinante, "Observation of gyroscopic coupling in a nonspinning levitated ferromagnet", Phys. Rev. Lett., Vol. 136, 10 April, (2026), p. 146703; DOI: https://doi.org/10.1103/hdh6-r1gy.
47. J. D. Jackson, *Classical Electrodynamics*, Second Edition, John Wiley & Sons, New York, (1975), pp. 503-561.

# Chapter 2

# EXCITED STATES OF THE ONE-ELECTRON ATOM (QUANTIZATION)

## EQUATION OF THE ELECTRIC FIELD INSIDE THE ATOMIC ORBITAL

It is well known that resonator cavities can trap electromagnetic radiation of discrete resonant frequencies. The atomic orbital is a resonator cavity that traps single photons of discrete frequencies. Thus, photon absorption occurs as an excitation of a resonator mode. The "trapped photon" is a "standing electromagnetic wave" which actually is a circulating wave that propagates around the z-axis, and its source current superimposes with each great circle current loop of the atomic orbital. The time-function factor, $k(t)$, for the "standing wave" is identical to the time-function factor of the atomic orbital in order to satisfy the boundary (phase) condition at the atomic orbital surface. Thus, the angular frequency of the "trapped photon" has to be identical to the angular frequency of the electron atomic orbital, $\omega_n$, given by Eq. (1.36). Furthermore, the phase condition requires that the angular functions of the "trapped photon" have to be identical to the spherical harmonic angular functions of the electron atomic orbital. Combining $k(t)$ with the $\phi$-function factor of the spherical harmonic gives $e^{i(m\phi - m\omega_n t)}$ for both the electron and the "trapped photon" function.

Consider the hydrogen atom. The atom and the "trapped photon" caused by a transition to a resonant state other than the $n = 1$ state have neutral charge. As shown *infra*, the photon's electric field superposes that of the proton such that the radial electric field has a magnitude proportional to $Z/n$ at the electron where $n = 1, 2, 3, ...$ for excited states and $n = \frac{1}{2}, \frac{1}{3}, \frac{1}{4}, ..., \frac{1}{137}$ for lower energy states given in the Hydrino Theory—BlackLight Process section. This causes the charge density of the electron to correspondingly decrease and the radius to increase for states higher than 13.6 eV and the charge density of the electron to correspondingly increase and the radius to decrease for states lower than 13.6 eV as shown in Figure 5.2. Thus, the field lines of the proton always end on the electron. A way to conceptualize the effect of the photon "standing wave" in an electronic state other than $n = 1$ is to consider a solution of Laplace's equation in spherical coordinates with source currents "glued" to the electron and to the nucleus and phase-locked to the rotating electron current density with a radial electric field that only exists at the electron. Or, alternatively to a source current at the nucleus, a Poisson equation solution may comprise a delta function inhomogeneity at the origin [1]. Thus, the "trapped photon" is analogous to a gluon described in the Proton and Neutron section and a photon in free space as described in the Equation of the Photon section. However, the true nature of the photon field does not change the nature of the electrostatic field of the nucleus or its energy except at the position of the electron. The photon "standing wave" function further comprises a radial Dirac delta function that "samples" the Laplacian equation solution only at the position infinitesimally inside of the electron current-density function and superimposes with the proton field to give a field of radial magnitude proportional to $Z/n$, and the Fourier transform of the photon "standing wave" of the electronic states other than the $n = 1$ state is continuous over all frequencies in $s_r$-space and is given by $\frac{\sin s_r r}{s_r r}$. The free space photon also comprises a radial Dirac delta function, and the angular momentum of the photon given by $\mathbf{m} = \int \frac{1}{8\pi c} \mathrm{Re}\left[\mathbf{r} \times (\mathbf{E} \times \mathbf{B}^*)\right] dx^4 = \hbar$ in the Photon section is conserved [2] for the solutions for the resonant photons and excited state electron functions given *infra*. It can be demonstrated that the resonance condition between these frequencies is to be satisfied in order to have a net change of the electromagnetic energy field [3]. In the present case, the correspondence principle holds. That is the change in angular frequency of the electron is equal to the angular frequency of the resonant photon that excites the resonator cavity mode corresponding to the transition, and the energy is given by Planck's equation. The predicted energies, Lamb shift, fine structure, hyperfine structure, resonant line shape, line width, selection rules, etc. are in agreement with observation as shown *infra*.

The discretization of the angular momentum of the electron and the photon gives rise to quantized electron radii and energy levels. Transitions occur in integer units of the electron's inalienable intrinsic angular momentum of $\hbar$ (Appendix II) wherein the exciting photons carry an integer multiple of $\hbar$. Thus, for $\mathbf{r}\times m_e\mathbf{v}_e=\mathbf{p}$ to be constant, the velocity of the electron source current decreases by a factor of the integer, and the radius increases by the factor of the integer. Concomitantly, the photon field superimposes that of the proton causing a resultant central field of a reciprocal integer that establishes the force balance at the excited state radius. This quantization condition is equivalent to that of Bohr except that the electron angular momentum is $\hbar$, the angular momentum of one or more photons that give to an excited state is $n\hbar$, and the photon field changes the central force balance. Also, the standing wave regards the photon field and not the electron that comprises an extended current and is not a wave function. Thus, the quantization condition can also be considered as arising from the discretization of the photon standing wave including the integer spherical periodicity of the spherical harmonics of the excited state of the bound electron as a spherical cavity.

For a spherical resonator cavity, the relationship between an allowed radius and the "photon standing wave" wavelength is

$$2\pi r_n = n\lambda \tag{2.1}$$

where $n$ is an integer. Now, the question arises: given that this is a resonator cavity, which resonant states are possible where the transition is effected by a "trapped photon?" For the electron atomic orbital, a spherical resonator cavity, the relationship between an allowed radius and the electron wavelength is:

$$2\pi(nr_1) = 2\pi r_n = n\lambda_1 = \lambda_n \tag{2.2}$$

where

$n = 1, 2, 3, 4, \ldots$, and

$$n = \frac{1}{2}, \frac{1}{3}, \frac{1}{4}, \ldots$$

$\lambda_1$ is the allowed wavelength for $n=1$

$r_1$ is the allowed radius for $n=1$

(The mechanism for transitions to the reciprocal integer states involves coupling with another resonator called a catalyst as given in the Hydrino Theory—BlackLight Process section.) An electron in the ground state, $n=1$, is in force balance including the electrodynamic force which is included by using the reduced electron mass as given by Eqs. (1.254), (1.259), and (1.260).

$$\frac{m_e v_1^2}{r_1} = \frac{Ze^2}{4\pi\varepsilon_0 r_1^2} \tag{2.3}$$

When an electron in the ground state absorbs a photon of sufficient energy to take it to a new resonant state, $n = 2, 3, 4, \ldots$, force balance must be maintained. This is possible only if the central field is equivalent to that of a central charge of $\frac{Ze}{n}$, and the excited state force balance equation is:

$$\frac{m_e v_n^2}{r_n} = \frac{1}{n}\frac{Ze^2}{4\pi\varepsilon_0 r_n^2} \tag{2.4}$$

where $r_1$ is the "ground" state radius of the electron, and $r_n$ is the nth excited state radius of the electron. The radius of the nth excited state follows from Eq. (1.260) and Eq. (2.4).

$$r_n = na_H \tag{2.5}$$

The reduction of the effective charge from $Ze$ to $\frac{Ze}{n}$ is caused by trapping a photon in the atomic orbital, a spherical resonator cavity. (This condition for excited states is also determined by considering the boundary condition for the multipole expansion of the excited states as solutions of Maxwell's equations wherein the angular momentum and energy of each resonant photon are quantized as $\hbar$ and $\hbar\omega$, respectively, as given in the Excited States of Helium section.) The photon's electric field creates a "standing wave" in the cavity with an effective charge of $\left[-1+\frac{1}{n}\right]Ze$ $(at\ r_n)$. The total charge experienced by the electron is the sum of the proton and "trapped photon" charge components. The equation for these "trapped photons" can be solved as a boundary value problem of Laplace's equation. For the hydrogen atom, the boundary conditions are that the electric field is in phase with the atomic orbital and that the radial function for the electric field of the "trapped photon" at $r_n$ is:

$$\mathbf{E}_{r\,photon} = \left[-1+\frac{1}{n}\right]\frac{e}{4\pi\varepsilon_0\left(r_n\right)^2} \qquad n = 2, 3, 4, \ldots, \tag{2.6}$$

The general form of the solution to Laplace's equation in spherical coordinates is:

$$\Phi(r,\theta,\phi)=\sum_{\ell=0}^{\infty}\sum_{m=-\ell}^{\ell}\left[A_{\ell,m}r^{\ell}+B_{\ell,m}r^{-(\ell+1)}\right]\left[Y_0^0(\theta,\phi)+Y_\ell^m(\theta,\phi)\right] \tag{2.7}$$

All $A_{\ell,m}$ are zero because the electric field given by the potential must be inversely proportional to the radius to obtain force balance. The electric field is the gradient of the potential:

$$\mathbf{E}=-\nabla\Phi \tag{2.8}$$

$$\begin{aligned}\mathbf{E}_r&=-\frac{\partial\Phi}{\partial r}\,\hat{i}_r\\ \mathbf{E}_\theta&=-\frac{1}{r}\frac{\partial\Phi}{\partial\theta}\,\hat{i}_\theta\\ \mathbf{E}_\phi&=-\frac{1}{r\sin\theta}\frac{\partial\Phi}{\partial\phi}\,\hat{i}_\phi\end{aligned} \tag{2.9}$$

Thus,

$$\mathbf{E}_r=\sum_{\ell=0}^{\infty}\sum_{m=-\ell}^{\ell}B_{\ell,m}(\ell+1)r^{-(\ell+2)}\left[Y_0^0(\theta,\phi)+Y_\ell^m(\theta,\phi)\right] \tag{2.10}$$

Given that $\mathbf{E}_{proton}=\frac{+e}{4\pi\varepsilon_0 r_n^2}$, and that the electric fields of the proton and "trapped photon" must superimpose to yield a field equivalent to a central point charge of $\frac{+Ze}{n}$, the "trapped photon" electric field for each mode is determined as follows. The time-function factor and the angular-function factor of the charge-density function of the atomic orbital (Eqs. (1.27) and (1.28-1.29)) at force balance must be in phase with the electric field of the "trapped photon." The relationship between the electric field equation and the "trapped photon" source charge-density function is given by Maxwell's equation in two dimensions.

$$\mathbf{n}\bullet(\mathbf{E}_1-\mathbf{E}_2)=\frac{\sigma}{\varepsilon_0} \tag{2.11}$$

where $\mathbf{n}$ is the radial normal unit vector, $\mathbf{E}_1=0$ ($\mathbf{E}_1$ is the electric field outside of the atomic orbital), $\mathbf{E}_2$ is given by the total electric field at $r_n=na_H$, and $\sigma$ is the surface charge-density. Thus,

$$\mathbf{E}_{r\,photon\;\;n,l,m|_{r_n=na_H}}=\frac{e}{4\pi\varepsilon_0(na_H)^2}\left[-1+\frac{1}{n}\left[Y_0^0(\theta,\phi)+\mathrm{Re}\left\{Y_\ell^m(\theta,\phi)e^{im\omega_n t}\right\}\right]\right]\delta(r-r_n) \tag{2.12}$$

$$=\sum_{\ell=0}^{\infty}\sum_{m=-\ell}^{\ell}-B_{\ell,m}(\ell+1)(na_H)^{-(\ell+2)}\left[Y_0^0(\theta,\phi)+\mathrm{Re}\left\{Y_\ell^m(\theta,\phi)e^{im\omega_n t}\right\}\right]\delta(r-r_n) \tag{2.13}$$

Therefore,

$$\sum_{\ell=0}^{\infty}\sum_{m=-\ell}^{\ell}-B_{\ell,m}=\frac{e(na_H)^{\ell}}{4\pi\varepsilon_0(\ell+1)}\left[-1+\frac{1}{n}\right],\text{ and} \tag{2.14}$$

$$\mathbf{E}_{r\,photon\;\;n,l,m}=\frac{e(na_H)^{\ell}}{4\pi\varepsilon_0}\frac{1}{r^{(\ell+2)}}\left[-Y_0^0(\theta,\phi)+\frac{1}{n}\left[Y_0^0(\theta,\phi)+\mathrm{Re}\left\{Y_\ell^m(\theta,\phi)e^{im\omega_n t}\right\}\right]\right]\delta(r-r_n) \tag{2.15}$$

$n=1,2,3,4,...$
$\ell=0,1,2,...,n-1$
$m=-\ell,-\ell+1,...,0,...,+\ell$

$\mathbf{E}_{rtotal}$ is the sum of the "trapped photon" and proton electric fields,

$$\mathbf{E}_{rtotal}=\frac{e}{4\pi\varepsilon_0 r^2}+\frac{e(na_H)^{\ell}}{4\pi\varepsilon_0}\frac{1}{r^{(\ell+2)}}\left[-Y_0^0(\theta,\phi)+\frac{1}{n}\left[Y_0^0(\theta,\phi)+\mathrm{Re}\left\{Y_\ell^m(\theta,\phi)e^{im\omega_n t}\right\}\right]\right]\delta(r-r_n) \tag{2.16}$$

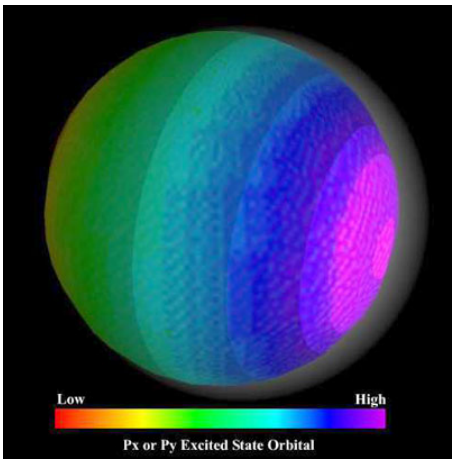
For $r=na_H$ and $m=0$, the total radial electric field is:

$$\mathbf{E}_{rtotal}=\frac{1}{n}\frac{e}{4\pi\varepsilon_0(na_H)^2} \tag{2.17}$$

Photons carry electric field, and the direction of field lines change with relative motion as required by special relativity. They increase in the direction perpendicular to the propagation direction. As shown by Eq. (4.9), the linear velocity of each point along a great circle of the photon atomic orbital is $c$. And, as shown in the Special Relativistic Correction to the Ionization Energies section and by Eq. (1.280), when the velocity along a great circle is light speed, the motion relative to the non-light speed frame is purely radial. In the case of the electric field lines of a trapped resonant photon of an excited state, the relativistic electric field is radial[1]. It is given by Eq. (2.15), and it exists only at $\delta\left(r-r_n\right)$. Thus, the photon only changes the radius and energy of the electron directly. Since the electric field of the photon at the electron superimposes that of the nucleus, the excited-state-energy levels are given by Eq. (2.18), and the hydrogen atom, for example, remains neutral.

The spherical harmonic function has a velocity less than light speed given by Eq. (1.35) and is phase-matched with the electron such that angular momentum is conserved during the excited state transition. This radial field can be considered a corresponding surface charge density as given in the Instability of Excited States section and the Stability of Atoms and Hydrinos section. All boundary conditions are met for the electric fields and the wavelengths of the "trapped photon" and the electron. Thus, Eq. (2.16) is the solution for the excited modes of the atomic orbital, a spherical resonator cavity. And, the quantum numbers of the electron are $n$, $\ell$, $m_\ell$, and $m_s$ (Described in the Stern-Gerlach Experiment section). A $p_x$ or $p_y$ atomic-hydrogen excited state is shown in Figure 2.1.

**Figure 2.1.** The electron atomic orbital is a resonator cavity wherein the radii of the excited states are related by integers. The electronic charge-density function of a $p_x$ or $p_y$ atomic-hydrogen excited state is shown with positive and negative charge-density proportional to red intensity and blue intensity, respectively. The function corresponds to a charge density wave on the two-dimensional spherical surface of radius $na_0$ that travels time harmonically about the z-axis at the angular frequency given by Eq. (1.36). It is comprised of a linear combination of a constant function modulated by time and spherically harmonic functions. The centrifugal force is balanced by the electric field of its photon that is phase-locked to the spinning electron. The brightness corresponds to the intensity of the two-dimensional radial photon field.




In the limit, the electric field of a photon cancels that of the proton ($n \to \infty$ in Eq. (2.17)), and the electron ionizes. The radius of the spherical shell (electron atomic orbital) goes to infinity as in the case of a spherical wavefront of light emitted from a symmetrical source, but it does not achieve an infinite radius. Rather it becomes ionized as shown in Figure 2.2 with the free electron propagating as a plane wave with linear velocity, $v_z$, and the size of the electron is the de Broglie wavelength, $\lambda = h/p$, as given in the Electron in Free Space section.

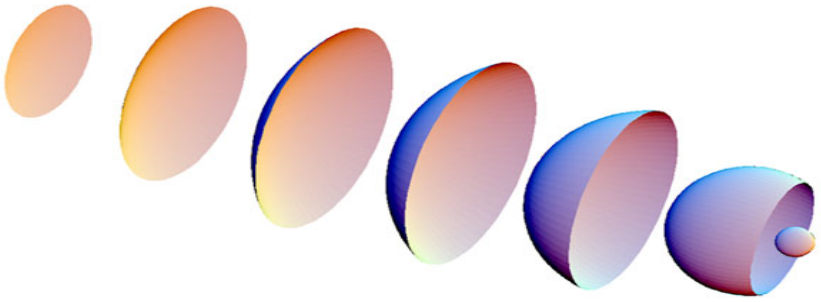
In general, the mechanism of photon absorption to form an excited state is given in the Transitions section wherein ionization is a special case. The extrema excited state photon is annihilated as the electron is ionized. The ionized electron gains kinetic energy with free electron radiation reaction field cancellation of the remnant extrema photon field. Specifically, as the electron radius goes to infinity, the photon field intensity goes to zero, but an infinite radius electron is not physical without interaction. So, the extrema comprising the $n = \infty$ state is a limiting state that cannot be achieved. Instead, the electron is ionized with finite kinetic energy whereby there is a radiation reaction during the corresponding electron acceleration to gain the kinetic energy, and the remnant extrema photon field is annihilated. The field equations follow the superposition of excited states into free states.

---

[1] A positive electric field is given by a trapped photon of an excited state if the velocity of the field lines is in the direction of the field line, and a negative central field is given if they are in opposite directions. The "trapped" photon can be considered the superposition of two free space photons given in the Photon section generated according to Eqs. (4.4-4.7) with the magnetic and electric fields interchanged such that when the two are superposed the great circle electric field lines add and the great circle magnetic field lines cancel.

Photons can transition into particles at rest through a transition state. A transition state atomic orbital of particle production is very similar to a trapped photon of an excited state as given in the Particle Production section, the Lepton section, and the Quarks section.

**Figure 2.2.** Time-lapsed image of electron ionization. With the absorption of a photon of energy in excess of the binding energy, the bound electron's radius increases and the electron ionizes as a plane-wave with the de Broglie wavelength. Similar to the mechanism of the propagation of a current in a classical conductor, ionization of an inner shell electron proceeds by successive displacement of contiguous outer shell electrons until the most outer shell electron ionizes.



## PHOTON ABSORPTION

The energy of the photon, which excites a mode in a stationary spherical resonator cavity from radius $a_H$ to radius $na_H$ is

$$E_{photon} = \frac{e^2}{4\pi\varepsilon_0 a_H}\left[1-\frac{1}{n^2}\right] = h\nu = \hbar\omega \tag{2.18}$$

After multiplying Eq. (2.18) by $\frac{a_H}{a_H} = \frac{4\pi\varepsilon_0\hbar^2}{e^2\mu_e a_H}$, where $a_H$ is given by Eq. (1.259), $\omega_{photon}$ is:

$$\omega_{photon} = \frac{\hbar}{m_e a_H^2}\left[1-\frac{1}{n^2}\right] \tag{2.19}$$

In the case of an electron atomic orbital, the resonator possesses kinetic energy before and after the excitation. The kinetic energy is always one-half of the potential energy because the centripetal force is an inverse squared central force. As a result, the energy and angular frequency to excite an electron atomic orbital are only one-half of the values above, Eqs. (2.18) and (2.19). From Eq. (1.36), the angular velocity of an electron atomic orbital of radius $na_H$ is

$$\omega_n = \frac{\hbar}{m_e\left(na_H\right)^2} \tag{2.20}$$

The change in angular velocity of the atomic orbital for an excitation from $n=1$ to $n>1$ is:

$$\Delta\omega = \frac{\hbar}{m_e\left(a_H\right)^2} - \frac{\hbar}{m_e\left(na_H\right)^2} = \frac{\hbar}{m_e\left(a_H\right)^2}\left[1-\frac{1}{n^2}\right] \tag{2.21}$$

The kinetic energy change of the transition is

$$E = \frac{1}{2}m_e(\Delta v)^2 = \frac{1}{2}\frac{e^2}{4\pi\varepsilon_0 a_H}\left[1-\frac{1}{n^2}\right] = \frac{e^2}{8\pi\varepsilon_0 a_H}\left[1-\frac{1}{n^2}\right] = \frac{1}{2}\hbar\omega \tag{2.22}$$

wherein Eq. (2.22) is also the equation for the ionization energy. The change in angular velocity of the electron atomic orbital, Eq. (2.21), is identical to the angular velocity of the photon necessary for the excitation, $\omega_{photon}$ (Eq. (2.19)). The energy of the photon necessary to excite the equivalent transition in an electron atomic orbital is one-half of the excitation energy of the stationary cavity because the change in kinetic energy of the electron atomic orbital supplies one-half of the necessary energy. The change in the angular frequency of the atomic orbital during a transition and the angular frequency of the photon corresponding to the superposition of the free space photon and the photon corresponding to the kinetic energy change of the atomic orbital during a transition are equivalent. The correspondence principle holds. It can be demonstrated that the resonance condition between these frequencies is to be satisfied in order to have a net change of the energy field [3]. Similarly photons are emitted when an electron is bound. Relations between the free space photon wavelength, radius, and velocity to the corresponding parameters of a free electron as it is bound are given in the Equation of the Photon section.

The excited states of hydrogen are given in Table 2.1.

**Table 2.1.** Calculated energies (non-relativistic; no spin-orbit interaction; no electronic spin/nuclear spin interaction) and ionization energies for the hydrogen atom in the ground state and some excited states.

| $n$ | $Z$ | Calculated $r_n$ [a] ($a_H$) | Calculated Kinetic Energy [b] (eV) | Calculated Potential Energy [c] (eV) | Calculated Ionization Energy [d] (eV) | Experimental Ionization Energy [e] (eV) |
|---|---|---|---|---|---|---|
| 1 | 1 | 1.000 | 13.598 | -27.196 | 13.598 | 13.595 |
| 2 | $\frac{1}{2}$ | 2.000 | 3.400 | -6.799 | 3.400 | 3.393 |
| 3 | $\frac{1}{3}$ | 3.000 | 1.511 | -3.022 | 1.511 | 1.511 |
| 5 | $\frac{1}{5}$ | 5.000 | 0.544 | -1.088 | 0.544 | 0.544 |
| 10 | $\frac{1}{10}$ | 10.000 | 0.136 | -0.272 | 0.136 | 0.136 |

[a] from Eq. (2.5)

[b] from $T = -\frac{1}{2}V$

[c] from Eq. (1.261)

[d] from Eq. (2.22)

[e] experimental

## INSTABILITY OF EXCITED STATES

Satisfaction of the Haus condition [4] of the presence of spacetime Fourier components of the current density synchronous with those traveling at the speed of light, $k = \frac{\omega}{c}$, gives rise to radiation. For the excited (integer quantum number) energy states of the hydrogen atom, $\sigma_{photon}$, the two-dimensional surface charge due to the "trapped photons" at the atomic orbital, is given by Eqs. (2.6) and (2.11).

$$\sigma_{photon} = \frac{e}{4\pi(r_n)^2}\left[Y_0^0(\theta,\phi) - \frac{1}{n}\left[Y_0^0(\theta,\phi) + \mathrm{Re}\left\{Y_\ell^m(\theta,\phi)e^{im\omega_n t}\right\}\right]\right]\delta(r-r_n) \quad n = 2,3,4,..., \tag{2.23}$$

Whereas, $\sigma_{electron}$, the two-dimensional surface charge of the electron atomic orbital is

$$\sigma_{electron} = \frac{-e}{4\pi(r_n)^2}\left[Y_0^0(\theta,\phi) + \mathrm{Re}\left\{Y_\ell^m(\theta,\phi)e^{im\omega_n t}\right\}\right]\delta(r-r_n) \tag{2.24}$$

The superposition of $\sigma_{photon}$ (Eq. (2.23)) and $\sigma_{electron}$ (Eq. (2.24)) where the spherical harmonic functions satisfy the conditions given in the Bound Electron "Atomic Orbital" section is equivalent to the sum of a radial electric dipole represented by a doublet function and an radial electric monopole represented by a delta function.

$$\sigma_{photon} + \sigma_{electron} = \frac{e}{4\pi(r_n)^2}\left[Y_0^0(\theta,\phi)\dot{\delta}(r-r_n) - \frac{1}{n}Y_0^0(\theta,\phi)\delta(r-r_n) - \left(1+\frac{1}{n}\right)\left[\mathrm{Re}\left\{Y_\ell^m(\theta,\phi)e^{im\omega_n t}\right\}\right]\delta(r-r_n)\right] \tag{2.25}$$
$$n = 2,3,4,...,$$

where

$$\left[+\delta(r-r_n) - \delta(r-r_n)\right] = \dot{\delta}(r-r_n) \tag{2.26}$$

is the Dirac doublet function [5] which is defined by the property

$$\begin{aligned} &x(t)\otimes\dot{\delta}(t) = \dot{x}(t) \\ &\int_{-\infty}^{\infty} x(\tau)\dot{\delta}(t-\tau)\,d\tau = \dot{x}(t) \end{aligned} \tag{2.27}$$

or equivalently by the property

$$\int_{-\infty}^{\infty} x(t)\dot{\delta}(t)\,dt = -\dot{x}(0) \tag{2.28}$$

The Dirac doublet is the impulse response of an ideal differentiator and corresponds to the radial electrostatic dipole.

The symbol $\dot{\delta}(t)$ is appropriate since operationally the doublet is the derivative of the impulse.

The doublet does possess spacetime Fourier components synchronous with waves traveling at the speed of light. Whereas, the radial delta function does not. The Spacetime Fourier Transform of the atomic orbital comprising a radial Dirac delta function is given in Appendix I: Nonradiation Condition:

$$M_\ell^{m_\ell}(s,\Theta,\Phi,\omega) = 4\pi \mathrm{sinc}(2sr_n) \otimes G_\ell^{m_\ell}(s,\Theta) \otimes H_\ell^{m_\ell}(s,\Theta,\Phi) \otimes \frac{1}{4\pi}[\delta(\omega-\omega_n)+\delta(\omega+\omega_n)] \tag{2.29}$$

wherein $G_\ell^{m_\ell}(s,\Theta)$ and $H_\ell^{m_\ell}(s,\Theta,\Phi)$ are the spherical-coordinate Fourier transforms of $N_{\ell,m}P_\ell^m(\cos\theta)$ and $e^{im\phi}$, respectively. The radial doublet function is the derivative of the radial Dirac delta function; thus, the Fourier transform of the doublet function can be obtained from the Fourier transform of the Dirac delta function, Eq. (2.29), and the differentiation property of Fourier transforms [6].

$$\begin{array}{lll} x(t) = \int_{-\infty}^{\infty} X(f) e^{j2\pi ft} df & & X(t) = \int_{-\infty}^{\infty} x(t) e^{-j2\pi ft} dt \\ \hline \textit{Differentiation} \quad \dfrac{dx(t)}{dt} & \Leftrightarrow & j2\pi f X(f) \end{array} \tag{2. 30}$$

From Eq. (2.29) and Eq. (2.30), the spacetime Fourier transform of Eq. (2.25), the superposition of $\sigma_{photon}$ (Eq. (2.23)) and $\sigma_{electron}$ (Eq. (2.24)) is

$$M_\ell^{m_\ell}(s,\Theta,\Phi,\omega) = 4\pi s_n e^{j\frac{\pi}{2}} \frac{\sin(2s_n r_n)}{2s_n r_n} \otimes G_\ell^{m_\ell}(s,\Theta) \otimes H_\ell^{m_\ell}(s,\Theta,\Phi) \otimes \frac{1}{4\pi}[\delta(\omega-\omega_n)+\delta(\omega+\omega_n)] \tag{2.31}$$

$$M_\ell^{m_\ell}(s,\Theta,\Phi,\omega) = 4\pi s_n \frac{\cos(2s_n r_n)}{2s_n r_n} \otimes G_\ell^{m_\ell}(s,\Theta) \otimes H_\ell^{m_\ell}(s,\Theta,\Phi) \otimes \frac{1}{4\pi}[\delta(\omega-\omega_n)+\delta(\omega+\omega_n)] \tag{2.32}$$

In the case of time harmonic motion, the current-density function is given by the time derivative of the charge-density function. Thus, the current-density function is given by the product of the constant angular velocity and the charge-density function. The Fourier transform of the current-density function of the excited-state atomic orbital is given by the product of the constant angular velocity and Eq. (2.32):

$$K_\ell^{m_\ell}(s,\Theta,\Phi,\omega) = 4\pi s_n \omega_n \frac{\cos(2s_n r_n)}{2s_n r_n} \otimes G_\ell^{m_\ell}(s,\Theta) \otimes H_\ell^{m_\ell}(s,\Theta,\Phi) \otimes \frac{1}{4\pi}[\delta(\omega-\omega_n)+\delta(\omega+\omega_n)] \tag{2.33}$$

Consider the wave vector of the cosine function of Eq. (2.33). When the velocity is $c$ corresponding to a potentially emitted photon

$$\mathbf{s}_n \bullet \mathbf{v}_n = \mathbf{s}_n \bullet \mathbf{c} = \omega_n \tag{2.34}$$

the relativistically corrected wavelength (Eq. (1.280)) is:

$$\mathbf{r}_n = \lambda_n \tag{2.35}$$

Substitution of Eq. (2.35) into the cosine function does not result in the vanishing of the Fourier transform of the current-density function. Thus, spacetime harmonics of $\frac{\omega_n}{c} = k$ or $\frac{\omega_n}{c}\sqrt{\frac{\varepsilon}{\varepsilon_0}} = k$ do exist for which the Fourier transform of the current-density function is nonzero. An excited state is metastable because it is the sum of nonradiative (stable) and radiative (unstable) components and de-excites with a transition probability given by the ratio of the power to the energy of the transition [7]. Alternatively, the radiative fields may be considered directly. In the case of the nonradiative currents of nonexcited states, the corresponding far fields have a vanishing Poynting power vector as shown in Appendix I. In contrast, regarding the dipole, the vector -/+ can flip to +/- and radiate the well known current dipole radiation having a finite Poynting power vector in the far field [8].

## SOURCE CURRENT OF EXCITED STATES

As shown in Appendix I, for time-varying electromagnetic fields, Jackson [2] gives a generalized expansion in vector spherical waves that are convenient for electromagnetic boundary-value problems possessing spherical symmetry properties and for analyzing multipole radiation from a localized source distribution. The Green function $G(\mathbf{x}',\mathbf{x})$ which is appropriate to the equation:

$$\left(\nabla^2 + k^2\right) G(\mathbf{x}',\mathbf{x}) = -\delta(\mathbf{x}'-\mathbf{x}) \tag{2.36}$$

in the infinite domain with the spherical wave expansion for the outgoing wave Green function is:

$$G(\mathbf{x}',\mathbf{x}) = \frac{e^{-ik|\mathbf{x}-\mathbf{x}'|}}{4\pi|\mathbf{x}-\mathbf{x}'|} = ik\sum_{\ell=0}^{\infty} j_\ell(kr_<) h_\ell^{(1)}(kr_>) \sum_{m=-\ell}^{\ell} Y_{\ell,m}^*(\theta',\phi') Y_{\ell,m}(\theta,\phi) \tag{2.37}$$

Jackson [2] further gives the general multipole field solution to Maxwell's equations in a source-free region of empty space with the assumption of a time dependence $e^{i\omega_n t}$:

$$\mathbf{B}=\sum_{\ell,m}\left[a_E(\ell,m)f_\ell(kr)\mathbf{X}_{\ell,m}-\frac{i}{k}a_M(\ell,m)\nabla\times g_\ell(kr)\mathbf{X}_{\ell,m}\right]$$
$$\mathbf{E}=\sum_{\ell,m}\left[\frac{i}{k}a_E(\ell,m)\nabla\times f_\ell(kr)\mathbf{X}_{\ell,m}+a_M(\ell,m)g_\ell(kr)\mathbf{X}_{\ell,m}\right] \tag{2.38}$$

where the cgs units used by Jackson are retained in this section. The radial functions $f_\ell(kr)$ and $g_\ell(kr)$ are of the form:

$$g_\ell(kr)=A_\ell^{(1)}h_\ell^{(1)}+A_\ell^{(2)}h_\ell^{(2)} \tag{2.39}$$

$\mathbf{X}_{\ell,m}$ is the vector spherical harmonic defined by:

$$\mathbf{X}_{\ell,m}(\theta,\phi)=\frac{1}{\sqrt{\ell(\ell+1)}}\mathbf{L}Y_{\ell,m}(\theta,\phi) \tag{2.40}$$

where

$$\mathbf{L}=\frac{1}{i}(\mathbf{r}\times\nabla) \tag{2.41}$$

The coefficients $a_E(\ell,m)$ and $a_M(\ell,m)$ of Eq. (2.38) specify the amounts of electric $(\ell,m)$ multipole and magnetic $(\ell,m)$ multipole fields, and are determined by sources and boundary conditions as are the relative proportions in Eq. (2.39). Jackson gives the result of the electric and magnetic coefficients from the sources as:

$$a_E(\ell,m)=\frac{4\pi k^2}{i\sqrt{\ell(\ell+1)}}\int Y_\ell^{m*}\left\{\rho\frac{\partial}{\partial r}\left[rj_\ell(kr)\right]+\frac{ik}{c}(\mathbf{r}\cdot\mathbf{J})j_\ell(kr)-ik\nabla\cdot(r\times\boldsymbol{M})j_\ell(kr)\right\}d^3x \tag{2.42}$$

and

$$a_M(\ell,m)=\frac{-4\pi k^2}{\sqrt{\ell(\ell+1)}}\int j_\ell(kr)Y_\ell^{m*}\mathbf{L}\cdot\left(\frac{\mathbf{J}}{c}+\nabla\times\boldsymbol{M}\right)d^3x \tag{2.43}$$

respectively, where the distribution of charge $\rho(\mathbf{x},t)$, current $\mathbf{J}(\mathbf{x},t)$, and intrinsic magnetization $\boldsymbol{M}(\mathbf{x},t)$ are harmonically varying sources: $\rho(\mathbf{x})e^{-i\omega t}$, $\mathbf{J}(\mathbf{x})e^{-i\omega t}$, and $\boldsymbol{M}(\mathbf{x})e^{-i\omega t}$. The currents corresponding to Eq. (1.27) and the first term of Eqs. (1.28-1.29) are static. Thus, they are trivially nonradiative. The current due to the time dependent term of Eq. (1.29) corresponding to p, d, f, etc. orbitals is:

$$\begin{aligned}\mathbf{J}&=\frac{m\omega_n}{2\pi}\frac{e}{4\pi r_n^2}N[\delta(r-r_n)]\,\mathrm{Re}\left\{Y_\ell^m(\theta,\phi)\right\}\left[\mathbf{u}(t)\times\mathbf{r}\right]\\&=\frac{m\omega_n}{2\pi}\frac{e}{4\pi r_n^2}N'[\delta(r-r_n)]\left(P_\ell^m(\cos\theta)\cos(m\phi+m\omega_n t)\right)\left[\mathbf{u}\times\mathbf{r}\right]\\&=\frac{m\omega_n}{2\pi}\frac{e}{4\pi r_n^2}N'[\delta(r-r_n)]\left(P_\ell^m(\cos\theta)\cos(m\phi+m\omega_n t)\right)\sin\theta\hat{\phi}\end{aligned} \tag{2.44}$$

where $N$ and $N'$ are normalization constants. $\mathbf{J}$ corresponds to a spherical harmonic traveling charge-density wave of quantum number $m$ that moves on the surface of the atomic orbital, spins about the z-axis at angular frequency $\omega_n$, and modulates the constant atomic orbital at frequency $m\omega_n$. The vectors are defined as:

$$\hat{\phi}=\frac{\hat{u}\times\hat{r}}{|\hat{u}\times\hat{r}|}=\frac{\hat{u}\times\hat{r}}{\sin\theta};\qquad \hat{u}=\hat{z}=orbital\ axis \tag{2.45}$$

$$\hat{\theta}=\hat{\phi}\times\hat{r} \tag{2.46}$$

"^" denotes the unit vectors $\hat{u}\equiv\frac{\mathbf{u}}{|\mathbf{u}|}$, non-unit vectors are designed in bold, and the current function is normalized. From Eq. (2.44), the charge and intrinsic magnetization terms are zero. Also, the current $\mathbf{J}(\mathbf{x},t)$ is in the $\hat{\phi}$ direction; thus, the $a_E(\ell,m)$ coefficient given by Eq. (2.42) is zero since $\mathbf{r}\cdot\mathbf{J}=0$. Substitution of Eq. (2.44) into Eq. (2.43) gives the magnetic multipole coefficient $a_M(\ell,m)$:

$$a_M(\ell,m)=\frac{-ek^2}{c\sqrt{\ell(\ell+1)}}\frac{\omega_n}{2\pi}Nj_\ell(kr_n)\Theta\sin(ks) \tag{2.47}$$

For the electron source current given by Eq. (2.44), each comprising a multipole of order $(\ell,m)$ with a time dependence $e^{i\omega t}$, the far-field solutions to Maxwell's equations given by Eq. (2.38) are:

$$\begin{aligned}\mathbf{B} &= -\frac{i}{k}a_M(\ell,m)\nabla\times g_\ell(kr)\mathbf{X}_{\ell,m}\\ \mathbf{E} &= a_M(\ell,m)\,g_\ell(kr)\mathbf{X}_{\ell,m}\end{aligned} \tag{2.48}$$

and the time-averaged power radiated per solid angle $\frac{dP(\ell,m)}{d\Omega}$ is:

$$\frac{dP(\ell,m)}{d\Omega} = \frac{c}{8\pi k^2}\left|a_M(\ell,m)\right|^2\left|\mathbf{X}_{\ell,m}\right|^2 \tag{2.49}$$

where $a_M(\ell,m)$ is given by Eq. (2.47). In the case that $k$ is the lightlike $k^0$, then $k=\omega_n/c$ regarding a potentially emitted photon, in Eq. (2.47), and Eqs. (2.48-2.49) vanishes for:

$$s = vT_n = R = r_n = \lambda_n \tag{2.50}$$

*There is no radiation*. Thus, there is no radiation due to the azimuthal charge density wave even in an excited state. However, for excited states there exists a radial dipole that is unstable to radiation as shown in the Instability of Excited States section. This instability gives rise to a radial electric dipole current considered next.

In a nonradiative state, there is no emission or absorption of radiation corresponding to the absence of radial motion wherein Eq. (2.42) is zero since $\mathbf{r}\cdot\mathbf{J}=0$; conversely, there is motion in the radial direction only when the energy of the system is changing. The same physical consequence can also be easily shown with a matter-wave dispersion relationship. Thus, radial motion corresponds to the emission or absorption of photons. The form of the radial solution during a transition is then the corresponding electron source current comprising a time-dependent radial Dirac delta function that connects the initial and final states as boundary conditions. The photon carries fields and corresponding angular momentum. This aspect is ignored in standard quantum mechanics as shown in the Schrödinger Wavefunction in Violation of Maxwell's Equations section and Refs. [9-17] where the radii of excited states are purely mathematical probability-wave eigenfunctions and are not square integrable, but are infinite in highly-excited states and have many discrepancies with observations as discussed previously [18]. In contrast, the physical characteristics of the photon and the electron are the basis of physically solving for excited states according to Maxwell's equations. The discontinuous harmonic radial current in Eq. (2.42) that connects the initial and final states of the transition is:

$$\mathbf{r}\cdot\mathbf{J} = \frac{er}{4\pi r^2}\tau^{-1}\sin\frac{\pi t'}{\tau}\left(u(t')-u(t'-\tau)\right) \tag{2.51}$$

Where $\tau$ is the lifetime of the transition given by Eq. (2.107) and $t'$ is time during the transition.

## SELECTION RULES

The multipole fields of a radiating source can be used to calculate the energy and angular momentum carried off by the radiation [19]. For definiteness we consider a linear superposition of electric ($\ell$, $m$) multipoles with different m values, but all having the same $\ell$, and following Eq. (16.46) of Jackson [19], write the fields as:

$$\begin{aligned}\mathbf{B}_\ell &= \sum_m a_E(\ell,m)\mathbf{X}_{\ell m}h_\ell^{(1)}(kr)e^{i\omega t}\\ \mathbf{E}_\ell &= \frac{i}{k}\nabla\times\mathbf{B}_\ell\end{aligned} \tag{2.52}$$

For harmonically varying fields, the time-averaged energy density is:

$$u = \frac{1}{16\pi}\left(\mathbf{E}\bullet\mathbf{E}^* + \mathbf{B}\bullet\mathbf{B}^*\right) \tag{2.53}$$

In the radiation zone, the two terms are equal. Consequently, the energy in a spherical shell between $r$ and $(r+dr)$ $(for\ kr>>1)$ is:

$$dU = \frac{dr}{8\pi k^2}\sum_{m,m'} a_E^*(\ell,m')\,a_E(\ell,m)\int\mathbf{X}_{\ell m'}^*\bullet\mathbf{X}_{\ell m}d\Omega \tag{2.54}$$

where the asymptotic form (Eq. (16.13) of Jackson [19]) of the spherical Hankel function has been used. With the orthogonality integral (Eq. (16.44) of Jackson [19]) this becomes:

$$\frac{dU}{dr} = \frac{1}{8\pi k^2}\sum_m\left|a_E(\ell,m)\right|^2 \tag{2.55}$$

independent of the radius. For a general superposition of electric and magnetic multipoles, the sum over m becomes a sum over $\ell$ and m and $|a_E|^2$ becomes $|a_E|^2+|a_M|^2$. The total energy in a spherical shell in the radiation zone is thus an *incoherent sum*

over all multipoles.

The time-averaged angular-momentum density is:

$$m = \frac{1}{8\pi c}\mathrm{Re}\left[\mathbf{r}\times\left(\mathbf{E}\times\mathbf{B}^*\right)\right] \tag{2.56}$$

The triple cross product can be expanded, and the electric field substituted to yield, for a superposition of electric multipoles,

$$m = \frac{1}{8\pi\omega}\mathrm{Re}\left[\mathbf{B}^*\left(\mathbf{L}\bullet\mathbf{B}\right)\right] \tag{2.57}$$

Then the angular momentum in a spherical shell between $r$ and $(r+dr)$ in the radiation zone is:

$$dM = \frac{dr}{8\pi\omega k^2}\mathrm{Re}\sum_{m,m'} a_E^*\left(\ell,m'\right)a_E\left(\ell,m\right)\int\left(\mathbf{L}\bullet\mathbf{X}_{\ell m'}\right)^*\mathbf{X}_{\ell m}d\Omega \tag{2.58}$$

With the explicit form (Eq. (16.43) of Jackson [19]) for $X_{lm}$, Eq. (2.58) can be written

$$\frac{dM}{dr} = \frac{1}{8\pi\omega k^2}\mathrm{Re}\sum_{m,m'} a_E^*\left(\ell,m'\right)a_E\left(\ell,m\right)\int Y_{\ell m'}^*\mathbf{L}Y_{\ell m}d\Omega \tag{2.59}$$

From the properties of $LY_{\ell m}$ listed in Eq. (16.28) of Jackson [19] and the orthogonality of the spherical harmonics, we obtain the following expressions for the Cartesian components of $\frac{dM}{dr}$

$$\frac{dM_x}{dr} = \frac{1}{16\pi\omega k^2}\mathrm{Re}\left[\sqrt{\left(\ell-m\right)\left(\ell+m+1\right)}a_E^*\left(\ell,m+1\right)+\sqrt{\left(\ell+m\right)\left(\ell-m+1\right)}a_E^*\left(\ell,m-1\right)\right]a_E\left(\ell,m\right) \tag{2.60}$$

$$\frac{dM_y}{dr} = \frac{1}{16\pi\omega k^2}\mathrm{Im}\left[\sqrt{\left(\ell-m\right)\left(\ell+m+1\right)}a_E^*\left(\ell,m+1\right)-\sqrt{\left(\ell+m\right)\left(\ell-m+1\right)}a_E^*\left(\ell,m-1\right)\right]a_E\left(\ell,m\right) \tag{2.61}$$

$$\frac{dM_z}{dr} = \frac{1}{8\pi\omega k^2}\sum_m m\left|a_E\left(\ell,m\right)\right|^2 \tag{2.62}$$

These equations show that for a general $\ell$th order electric multipole that consists of a superposition of different m values, only the z component of the angular momentum is relatively simple.

For a multipole with a single m value, $M_x$ and $M_y$ vanish, while a comparison of Eq. (2.62) and Eq. (2.55) shows that

$$\frac{dM_z}{dr} = \frac{m}{\omega}\frac{dU}{dr} \tag{2.63}$$

Independent of $r$ [19]. Experimentally, the photon can carry $\hbar$ units of angular momentum. Thus, during excitation the spin, orbital, or total angular momentum of the atomic orbital can change by zero or $\pm\hbar$. The electron transition rules arise from conservation of angular momentum. The selection rules for multipole transitions between quantum states arise from conservation of total angular momentum and component angular momentum where the photon carries $\hbar$ of angular momentum.

## ORBITAL AND SPIN SPLITTING

The ratio of the square of the angular momentum, $M^2$, to the square of the energy, $U^2$, for a pure ($\ell$,m) multipole follows from Eqs. (2.54-2.55) and Eqs. (2.60-2.62) [19]

$$\frac{M^2}{U^2} = \frac{m^2}{\omega^2} \tag{2.64}$$

The magnetic moment is defined [20] as:

$$\mu = \frac{\text{charge x angular momentum}}{\text{2 x mass}} \tag{2.65}$$

The radiation of a multipole of order ($\ell$, m) carries m$\hbar$ units of the z component of angular momentum comprised of $\hbar$ per photon of energy $\hbar\omega$. Thus, the z component of the angular momentum of the corresponding excited state electron atomic orbital is:

$$L_z = m\hbar \tag{2.66}$$

Therefore,

$$\mu_z = \frac{em\hbar}{2m_e} = m\mu_B \tag{2.67}$$

where $\mu_B$ is the Bohr magneton. The presence of a magnetic field causes the principal excited state energy levels of the hydrogen atom (Eq. (2.22)) to split by the energy $E_{mag}^{orb}$ corresponding to the interaction of the magnetic flux with the magnetic

moment given by Eq. (2.67). This energy is called orbital splitting.

$$E_{mag}^{orb} = m\mu_B B \tag{2.68}$$

As is the case with spin splitting given by one half the energy of Eq. (1.227) which corresponds to the transition between spin states, the energy of the electron is increased in the case that the magnetic flux is antiparallel to the magnetic moment, or the energy of the electron is decreased in the case that the magnetic flux is parallel to the magnetic moment. The spin and orbital splitting energies superimpose; thus, the principal excited state energy levels of the hydrogen atom (Eq. (2.22)) are split by the energy $E_{mag}^{spin/orb}$

$$E_{mag}^{spin/orb} = m_\ell \frac{e\hbar}{2m_e} B + m_s g \frac{e\hbar}{2m_e} B \tag{2.69}$$

where it follows from Eq. (2.15) that

$$\begin{aligned} &n = 1, 2, 3, 4, ... \\ &\ell = 0, 1, 2, ..., n-1 \\ &m_\ell = -\ell, -\ell+1, ..., 0, ..., +\ell \\ &m_s = \pm 1/2 \end{aligned} \tag{2.70}$$

Based on the vector multipolarity of the corresponding source currents and the quantization of the angular momentum of photons in terms of $\hbar$, the selection rules for the electric dipole transition after Jackson [19] are:

$$\begin{aligned} &\Delta\ell = \pm 1 \\ &\Delta m_\ell = 0, \pm 1 \\ &\Delta m_s = 0 \end{aligned} \tag{2.71}$$

Splitting of the energy levels in addition to that given by Eq. (2.69) occurs due to a relativistic effect described in the Spin-Orbit Coupling (Fine Structure) section. Also, a very small shift that is observable by radio-frequency spectroscopy is due to the radiation reaction force between the electron and the photon and conservation of energy and linear momentum involving recoil during emission. This so-called Lamb shift is described in the Resonant Line Shape, and Hydrogen and Muonic Hydrogen Lamb Shift sections.

Decaying spherical harmonic currents on the surface of the atomic orbital give rise to spherical harmonic radiation fields during emission; conversely, absorbed spherical harmonic radiation fields produce spherical harmonic currents on the surface of the atomic orbital to effect a transition. Excited states are radiative according to Maxwell's equations as given in the Instability of Excited States section, and the transition probabilities or $A$ coefficients are shown to be a function of the initial and final radii in the State Lifetime and Line Intensities section. The distribution of multipole radiation and the multipole moments of the atomic orbital for absorption and emission are derived by Jackson [7]. Some of the simpler angular distributions are listed in Table 2.2.

**Table 2.2.** Some of the simpler angular distributions of multipole radiation and the multipole moments of the atomic orbital for absorption and emission.

| | $\left\|\mathbf{X}_{l,m}(\theta,\phi)\right\|^2$ | | |
|---|---|---|---|
| $\ell$ | $m$ | | |
| | 0 | $\pm 1$ | $\pm 2$ |
| 1<br>Dipole | $\frac{3}{8\pi}\sin^2\theta$ | $\frac{3}{16\pi}\left(1+\cos^2\theta\right)$ | |
| 2<br>Quadrupole | $\frac{15}{8\pi}\sin^2\theta\cos^2\theta$ | $\frac{5}{16\pi}\left(1-3\cos^2\theta+4\cos^4\theta\right)$ | $\frac{5}{16\pi}\left(1-\cos^4\theta\right)$ |

## STARK EFFECT

Similarly to the splitting of the energy levels due to an external applied magnetic field, an applied electric field lifts the degeneracy of the principal energy levels of the one-electron atom to give rise to a splitting called the Stark Effect. Since the magnetic field is a relativistic effect of the electric field as shown by Jackson [21] and the electron's charge, $e$, charge-to-mass ratio, $\frac{e}{m_e}$, angular momentum of $\hbar$, and the magnetic moment of $\mu_B$ are relativistically invariant, it is not surprising as shown in this section that the energy, $E_{Stark}$, of a one-electron atom in an electric field follows from Eqs. (2.68-2.69) with the magnetic dipole moment replaced by the electric dipole moment and the magnetic flux replaced by the electric field $\mathbf{E}_{applied}$. Considering only an electric dipole $\mathbf{p_z}$ and the direct influence of the external field, the energy is:

$$E_{Stark} = \mathbf{p_z} \cdot \mathbf{E}_{applied} \tag{2.72}$$

The bound electron has a field equivalent to that of a point charge at the origin for a radius greater than that of the atomic orbital as given in the Determination of Atomic Orbital Radii section. The electric field of the nucleus is also equivalent to that of a point particle at the origin. This condition also holds for the spherically and time harmonic excited-state charge-density waves on the surface of the atomic orbital given in the Excited States of the One-Electron Atom (Quantization) section. In these cases, the dipole moment over the angular integrals is zero, but excited-state Stark splittings with the equivalent of the corresponding electric dipole moments given by Eq. (2.72) exist due to the interaction of the applied electric field and the angular momentum of the excited-state photon field.

As further shown in the Excited States of the One-Electron Atom (Quantization) section, quantization is trivial given that the bound electron forms a cavity and the photon has quantized energy and angular momentum corresponding to the multipolarity of the excited-state photon. According to Eq. (2.64), the angular momentum of the excited-state-photon field of energy $\hbar\omega$ carries $m_\ell\hbar$ units of angular momentum to excite the orbital having the quantum number $m_\ell$. Then, the transition with $\Delta m_\ell = \pm 1$ of Eq. (2.71) gives the result of Eq. (4.1), and the superposition principle of photons gives the general case corresponding to Eq. (2.64).

The photon-field is phase-locked to the electron charge-density wave of matching multipole moment, and both rotate about the z-axis at the angular velocity given by Eq. (2.20). The rotation is without dissipation; thus, it is a supercurrent. It can be shown that the maintenance of the supercurrent condition and the quantization of the photon-field in terms of $m_\ell\hbar$ quantizes the electric dipole moment of Eq. (2.72) in terms of the quantum number $m_\ell$. According to Eq. (2.69), the energy of the excited state due to the orbital angular momentum caused by the excited-state photon in the presence of a magnetic flux $B$ is:

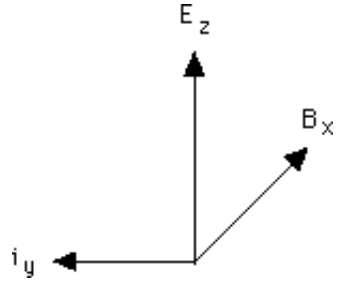
$$E_{mag}^{orb} = m_\ell \frac{e\hbar}{2m_e} B = \frac{m_\ell e}{2} \frac{na_0}{Z} \frac{\hbar}{m_e \frac{na_0}{Z}} B = \frac{3}{2} \frac{m_\ell e}{2} \frac{na_0}{Z} v_n B \sin\theta \tag{2.73}$$

where the velocity, $v_n$, is given by Eq. (1.35), the geometric factor of $\frac{3}{2}\sin\theta$ is given by Eq. (1.144), and the radii of the excited states are given by Eq. (2.5).

It is shown in the Stored Electric Energy section that during a Stern-Gerlach transition, the applied flux gives rise to a Lorentz force on the atomic orbital current resulting in a crossed electric field corresponding to a Hall voltage. With an exact balance between the Lorentz force (Eq. (1.183)) and the electric force corresponding to the Hall voltage (Eq. (1.184)), each superconducting charge-density element of the electron propagates along a great circle according to Eq. (1.187) which is the condition for superconductivity in the presence of crossed electric and magnetic fields. Consider the case of a Stark-split transition of the electron wherein the applied electric field causes a current that gives rise to a magnetic flux $\mathbf{B}_x$. In this case, the superconductor condition for the vectors shown in Figure 2.3 is

$$E / B = v_n \sin\theta \tag{2.74}$$

**Figure 2.3.** Coordinate system of crossed electric field, $\mathbf{E}_z$, corresponding to the applied field, magnetic flux, $\mathbf{B}_x$, due to photon field, and superconducting current $\mathbf{i}_y$.




The magnetic field $\mathbf{B}_x$ that is crossed with the applied electric field arises when the electron flips by 180° which doubles the energy of Eq. (2.73). Then, the energies due to an applied electric field are given by the substitution of Eq. (2.74) into Eq. (2.73)

and the multiplication of the result by 2:

$$E_{Stark} = m_\ell \frac{3}{2}\frac{ena_0}{Z} E_{applied} \tag{2.75}$$

From Eqs. (2.72) and (2.75), the eccentric dipole $\mathbf{p}_z$ is:

$$\mathbf{p}_z = m_\ell \frac{3}{2}\frac{ena_0}{Z}\mathbf{i}_z \tag{2.76}$$

wherein $m_\ell$ is given by Eq. (2.70).

There is no Stark effect unless the charge density is time-dependent modulated by the photon-field. Since the degeneracy is lifted by the external electric field by the induction of an effective electric dipole moment in the atom, transitions between all $m_\ell$ levels are allowed corresponding to the maximum value of the quantum number $\ell$ of each level. In this case, the superconductor condition is met since the amplitude of the rotational energy of the charge-density wave given by Eq. (1.71):

$$E_{rotational\ orbital} = \frac{\hbar^2}{2I}\left[\frac{\ell(\ell+1)}{\ell^2+2\ell+1}\right] = \frac{\hbar^2}{2m_e r_n^{\,2}}\left[\frac{\ell}{\ell+1}\right] = \frac{\hbar^2}{2m_e r_n^{\,2}}\left[\frac{n-1}{(n-1)+1}\right] = \frac{\hbar^2}{2m_e r_n^{\,2}}\left[1-\frac{1}{n}\right] = \frac{1}{2}h\nu_n\left[1-\frac{1}{n}\right] \tag{2.77}$$

is that corresponding to the photon as given by Eqs. (2.16) and (2.23), and the corresponding supercurrent component of the photon is given by the frequency (Eqs. (1.32) and (1.36)) times the charge $e$. Thus, the allowed quantum numbers for the state with principal quantum number $n$ having an effective electric dipole that is a function of principal quantum number $n$ are:

$$\begin{aligned} &n = 1, 2, 3, 4, ... \\ &\ell = n-1 \\ &m_\ell = -\ell, -\ell+1, ..., 0, ..., +\ell \\ &m_s = \pm\frac{1}{2} \end{aligned} \tag{2.78}$$

The splitting of the energy level with principal quantum number $n$ into $(2n-1)$ equidistant sub-levels determined by the quantum number $m_\ell$ for the $n=1$ to $n=6$ levels is given in Table 2.3. The predictions given by Eq. (2.75) for hydrogen match those given in Ryde [22][2].

---

[2] The theory of the Stark Effect according to quantum mechanics does not arise naturally, rather it must be forced by simultaneously using internally inconsistent spherical and parabolic quantum numbers. The theory also requires the "mutual perturbation" of orbitals involving a single electron in the absence of a transition which is nonphysical [22-23]. Hund's-Rule and Pauli-Exclusion-Principle-type violations are encountered by this "mutual perturbation" as well as by the existence of more than one set of quantum numbers for the same state. Moreover, lines corresponding to the redundant, nonunique quantum numbers are predicted that are not observed.

The agreement between the predictions of Eq. (2.75) and observations also confirms that the radius of the atomic-hydrogen-excited states is given by $na_0$ rather than $n^2 a_0$ as incorrectly given by the Bohr, Schrödinger, and Dirac equations. These theories are further internally inconsistent because the one-electron-atom wave functions cannot give rise to the electric dipole moments given by Eq. (2.76). In fact, except for the directional orbitals such as $np_z$, there are no electric dipole moments possible, and the requirement of the localization of the entire charge of the electron along the z-axis violates the Uncertainty Principle as well as all physical laws for a charge bound in a Coulombic central field. Furthermore, mixing of orbitals to give an electric dipole of $nea_0$ requires the hydrogen atom to have positive and negative poles separated by $na_0$ in contradiction to the experimental observation that its symmetric neutrality does not change in an electric field.

The argument that such an enormous electric dipole of $nea_0$ exists only in an excited state does not save the quantum-mechanical basis of the Stark effect. The dielectric susceptibility of any atom is a function of any induced electric dipole moment. Hydrogen has a dielectric constant different from vacuum in the ground state. The physics for the dipole moment of any excited state must also apply to the ground state. Since the experimentally observed susceptibility and thus the induced moment is many orders of magnitude less than that predicted for hydrogen, the quantum mechanical basis for the Stark Effect of electric polarization is disproved. The need to reject the quantum mechanical premise is further easily appreciated by considering the enormous predicted, but unobserved, change in reactivity of hydrogen due to the application of even a very weak electric field.

**Table 2.3.** The splitting of the energy level with principal quantum number $n$ into $(2n-1)$ equidistant sub-levels determined by the quantum number $m_\ell$ for the $n=1$ to $n=6$ levels.

| $n$ | $\ell$ | $m_\ell$ | $\Delta E$ [a] |
|---|---|---|---|
| 1 | 0 | 0 | 0 |
| 2 | 1 | 1 | 2a |
| | | 0 | 0 |
| | | -1 | -2a |
| 3 | 2 | 2 | 6a |
| | | 1 | 3a |
| | | 0 | 0 |
| | | -1 | -3a |
| | | -2 | -6a |
| 4 | 3 | 3 | 12a |
| | | 2 | 8a |
| | | 1 | 4a |
| | | 0 | 0 |
| | | -1 | -4a |
| | | -2 | -8a |
| | | -3 | -12a |
| 5 | 4 | 4 | 20a |
| | | 3 | 15a |
| | | 2 | 10a |
| | | 1 | 5a |
| | | 0 | 0 |
| | | -1 | -5a |
| | | -2 | -10a |
| | | -3 | -15a |
| | | -4 | -20a |
| 6 | 5 | 5 | 30a |
| | | 4 | 24a |
| | | 3 | 18a |
| | | 2 | 12a |
| | | 1 | 6a |
| | | 0 | 0 |
| | | -1 | -6a |
| | | -2 | -12a |
| | | -3 | -18a |
| | | -4 | -24a |
| | | -5 | -30a |

[a] Eq. (2.75) with $\frac{3}{2}ea_0E_{applied}$ defined as a.

Here, as shown in the Instability of Excited States section, the excited states are radiative due to a radial electric dipole term. The spectral line emitted as a transition between energy levels $n_i$ and $n_f$ of the hydrogen atom consists of numerous components. The selection rules for electric dipole transitions in the presence of an applied electric field are given by:

$$\begin{aligned}\Delta\ell &= \ell_f - \ell_i = (n_f - 1) - (n_i - 1) = n_f - n_i \\ \Delta m_\ell &= m_{\ell f} - m_{\ell i} = \pm\left(0,1,2....(n_f - 1) + (n_i - 1)\right) == \pm\left(0,1,2....(n_f + n_i - 2)\right)\end{aligned} \tag{2.79}$$

where the subscripts $i$ and $f$ denote the initial and final states, respectively. Due to the vector multipolarity of the corresponding source currents and the quantization of the angular momentum of photons in terms of $\hbar$, these components are either linearly polarized parallel to the vector of the external field, **E**, or circularly polarized in the plane perpendicular to **E**. The polarization is determined by the parity of the sum of the change in the $\ell$ and $m_\ell$ quantum numbers after Jackson [19]; so, that

$$\begin{aligned}\Delta\ell + \Delta m_\ell &= \text{even integers} \;\rightarrow\; (\pi\text{-components}) \\ \Delta\ell + \Delta m_\ell &= \text{odd integers} \;\rightarrow\; (\sigma\text{-components})\end{aligned} \tag{2.80}$$

The zero components are forbidden except for the $\sigma$-component when $\Delta\ell$ is odd such that the state change conserves the angular momentum of the photon. The intensities of the lines are determined by Eq. (2.107) where the multipolarity of the photon is a z-oriented dipole.

From Table 2.3 and Eq. (2.80), $L_\alpha$ ($\lambda$ =1215 Å) is split into a triplet comprising a central $\Delta E = 0$, $\sigma$-component and

two external $\Delta E = \pm 2a$, $\pi$-components. $L_\beta$ ($\lambda$ =1025 Å) is split up into two inner $\Delta E = \pm 3a$, $\sigma$-components and two $\Delta E = \pm 6a$, $\pi$-components having twice the displacement. $L_\gamma$ ($\lambda$ =972 Å) comprises 4 $\pi$- and three $\sigma$-components. The middle undisplaced line being a $\sigma$-component and the other alternating $\pi$- and $\sigma$-components. In general, the number of Lyman lines is equal to the number of sublevels of the initial emitting state $(2n-1)$. The lines comprise $n$ $\pi$-components and $n-1$ $\sigma$-components except that the zero component is absent when it is a $\pi$-component. In this case, $2n-2$ lines are observed comprising each of $n-1$ $\pi$- and $\sigma$-components. The predicted splitting of the Lyman lines and their corresponding polarizations and energies match those observed experimentally [22].

The three sublevels of $L_\alpha$ form the final states in the emission of Balmer lines. Theoretically, the number of components into which the Balmer lines are split is $3n-1$ $\pi$-components and $3n-2$ $\sigma$-components except that the zero component is absent when it is a $\pi$-component. For $H_\alpha$ ($\lambda$ =6562 Å), there are eight $\pi$-components with $\Delta E = \pm 2a$, $\pm 3a$, $\pm 4a$, and $\pm 8a$, and seven $\sigma$-components with $\Delta E = 0$, $\pm 1a$, $\pm 5a$, and $\pm 6a$. Again, the predictions match the experimental data [22].

For $H_\beta$ ($\lambda$ =4861Å), ten $\pi$-components with $\Delta E = \pm 2a$, $\pm 6a$, $\pm 8a$, $\pm 10a$, and $\pm 14a$, and ten $\sigma$-components with $\Delta E = \pm 2a$, $\pm 4a$, $\pm 6a$, $\pm 10a$, and $\pm 12a$ are predicted. All of these lines have been recorded except the faintest ones, the outermost $\pi$-components with $\Delta E = \pm 14a$ [22]. For $H_\gamma$ ($\lambda$ =4340 Å), the energy shifts of the predicted $\pi$- and $\sigma$-components are $\Delta E = \pm 2a$, $\pm 5a$, $\pm 8a$, $\pm 12a$, $\pm 15a$, $\pm 18a$, and $\pm 22a$ and $\Delta E = 0$, $\pm 3a$, $\pm 7a$, $\pm 10a$, $\pm 13a$, $\pm 17a$, and $\pm 20a$, respectively. For $H_\delta$ ($\lambda$ =4101 Å), the energy shifts of the predicted $\pi$- and $\sigma$-components are $\Delta E = \pm 4a$, $\pm 8a$, $\pm 12a$, $\pm 16a$, $\pm 20a$, $\pm 24a$, $\pm 28a$, and $\pm 32a$ and $\Delta E = \pm 2a$, $\pm 6a$, $\pm 10a$, $\pm 14a$, $\pm 18a$, $\pm 22a$, $\pm 26a$, and $\pm 30a$, respectively. All of the theoretically predicted $H_\gamma$ and $H_\delta$ lines have been observed by Stark and others [22-24]. For Balmer lines having odd $n$, no $\pi$- and $\sigma$-components coincide, but this does not apply for some components of lines with even $n$. Such components are consequently partially polarized. Furthermore, zero components only appear in $\sigma$-polarization when $n$ is odd (i.e. for $H_\alpha$, $H_\gamma$, $H_\varepsilon$...) corresponding to the case where $\Delta\ell$ is odd. This confirms the basis of the selection and polarization rules as the conservation of angular momentum between the initial and final states and the emitted multipole radiation.

## STATE LIFETIMES AND LINE INTENSITIES

The power radiated from an excited state can be calculated from the oscillating current corresponding to the motion of the electron from the initial to the final radius. It is evident from Maxwell's equations that oscillating currents are required in order to generate electromagnetic radiation:

$$\nabla X\mathbf{E} = -i\omega\mu\mathbf{H} \tag{2.81}$$

$$\nabla X\mathbf{H} = \mathbf{J} + i\omega\varepsilon\mathbf{E} \tag{2.82}$$

From the electron-transition current **J**, the electric and magnetic fields can be solved through an auxiliary function to Eqs. (2.81-2.82) called the vector potential **A**:

$$\mathbf{B} = \nabla X\mathbf{A} \tag{2.83}$$

Using Eqs. (2.81-2.83) the inhomogeneous wave equation is derived [25]:

$$\nabla^2\mathbf{A} + \omega^2\mu\varepsilon\mathbf{A} = -\mu\mathbf{J} \tag{2.84}$$

which has the solution

$$\mathbf{A}(r) = \frac{\mu}{4\pi}\int\int\int_V dV'\frac{\mathbf{J}(r')e^{-ik|\mathbf{r}-\mathbf{r}'|}}{|\mathbf{r}-\mathbf{r}'|} \tag{2.85}$$

where $k = \omega\sqrt{\mu\varepsilon}$, $\mathbf{r}$ is the vector-potential position, **r'** is the position vector of the sources, and $|\mathbf{r}-\mathbf{r}'|$ is the distance between the observation point **r** and the source point **r'**.

The radial current for an electric dipole transition is only finite during the movement of the electron from a state with quantum numbers $n_i, \ell, m_s, m_\ell$ and radius $r_{n_i}$ to another state with quantum numbers $n_f, \ell \pm 1, m_s, m_\ell$ and radius $r_{n_f}$. As shown by Eq. (2.66), the photon carries quantized units of $m\hbar$ of angular momentum along the z-axis. Consequently, for an electric dipole transition, the selection rule on the $\ell$ quantum number that conserves the angular momentum of the electron and emitted photon given by Eq. (2.71) is

$$\Delta\ell = \pm 1 \tag{2.86}$$

In this case, the multipolarity of the radiation and that of the source current correspond to spherical harmonics that are related by Eq. (2.42). The radial and azimuthal transition currents over the transition lifetime $\tau$ are:

$$\mathbf{J}_r = \frac{e}{4\pi r^2}\tau^{-1}\sin\frac{\pi t'}{\tau}\left(u(t') - u(t'-\tau)\right)\mathbf{i}_r \tag{2.87}$$

and

$$\mathbf{J}_\phi = \left(\frac{\omega_n + \Delta\omega_n \sin\frac{\pi t'}{2\tau}}{2\pi}\right)\frac{e}{4\pi r^2}N'\delta\left(r-\left(r_n+\Delta r_n \sin\frac{\pi t'}{2\tau}\right)\right)$$
$$\left(\begin{array}{l}\left(\begin{array}{l}Y_0^0(\theta,\phi)+\\ P_\ell^m(\cos\theta)\cos\left(m\phi+m\omega_n t+\Delta m\omega_n t\sin\frac{\pi t'}{2\tau}\right)\end{array}\right)\cos\frac{\pi t'}{2\tau}\\ +\left(\begin{array}{l}Y_0^0(\theta,\phi)+\\ P_{\ell\pm1}^m(\cos\theta)\cos\left(m\phi+m\omega_n t+\Delta m\omega_n t\sin\frac{\pi t'}{2\tau}\right)\end{array}\right)\sin\frac{\pi t'}{2\tau}\end{array}\right)\left(u(t')-u(t'-\tau)\right)\mathbf{i}_\phi \tag{2.88}$$

respectively, where the lifetime $\tau$ of the transition is given by Eq. (2.107), $\Delta\omega = \omega_f - \omega_i$ is the final angular frequency minus the initial, $\Delta r_n = r_f - r_i$ is the final discrete radius minus the initial, $t'$ is time during the transition, and $t$ is the continuous time variable independent of the transition.

As shown in the Photon section, the photon-field equation gives rise to a Green function given by Eqs. (4.18-4.23) with the superposition of many photons. The spherical-wave radiation that propagates in the radial direction has the same form as the source radial current. Due to the spherical symmetry and the time harmonic nature of the electron transition current, the vector potential corresponds to a current dipole at the origin and is a solution of Eq. (2.84). The Green function solution (Eq. (2.85)) matches a spherical radiation wave comprised of photons (Eq. (4.23)) wherein the quantized electron transition current and photon field are basis elements for the macroscopic (continuous) Maxwellian solutions for source current and the corresponding radiation fields.

The vector potential and power can be solved using the constraints of conservation of power and linear and angular momentum between the outgoing discrete (quantized) photon field with the change of the current densities between the initial and final discrete (quantized) states for an electric dipole transition. The electric dipole selection rule is given by Eq. (2.86). In order to conserve the photon's quantized angular momentum along the z-axis, the $\ell$ quantum number corresponding to the angular momentum of the excited electronic state must change by $\pm1$ corresponding to the transition from initial quantum states $n_i, \ell, m_s, m_\ell$ and radius $r_{n_i}$ to the final state with quantum numbers $n_f, \ell\pm1, m_s, m_\ell$ and radius $r_{n_f}$. The angular dependence of the current which connects the initial and final states is conserved in the photon field. Since there is no special preparation of the states, the radiation pattern is isotropic, and the power and concomitantly, the intensity of each electric dipole transition connecting states with the same initial and final principal quantum numbers are the same. However, the multiplicity of a given $\ell$ state does change the relative intensities based on statistical population distributions as discussed *infra*.

During an electronic transition, the current-density comprises a radially propagating constant spherical shell of current that is modulated by a traveling charge density wave. The angular integral of the vector potential is given by

$$\begin{aligned}\mathbf{A}(r) &= \frac{\mu_0}{4\pi}\frac{1}{4\pi}\int_0^{2\pi}\int_0^{\pi}\left(Y_0^0(\theta,\phi)+\frac{1}{2}Y_\ell^m(\theta,\phi)+\frac{1}{2}Y_{\ell\pm1}^m(\theta,\phi)\right)\sin\theta d\theta d\phi\int_{r_n}^{r_{n_f}}\mathbf{J}(r')\frac{e^{-ik_r|\mathbf{r}-\mathbf{r}'|}}{|\mathbf{r}-\mathbf{r}'|}dr'\\ &= \frac{\mu_0}{4\pi}\int_{r_n}^{r_{n_f}}\mathbf{J}(r')\frac{e^{-ik_r|\mathbf{r}-\mathbf{r}'|}}{|\mathbf{r}-\mathbf{r}'|}dr'\end{aligned} \tag{2.89}$$

The radial electric dipole current for the selection-rule condition of Eq. (2.86) is:

$$\frac{\mathbf{r}}{|\mathbf{r}|}\cdot\mathbf{J} = J\mathbf{i}_z \tag{2.90}$$

In order to achieve conservation of energy and power flow as well as angular momentum:

$$J = \frac{e}{4\pi r^2}\frac{\omega}{2\pi} = \frac{e}{4\pi r^2}\frac{\hbar}{2\pi m_e r^2} = \frac{e}{2\pi 4\pi r^2}\frac{v}{r} \tag{2.91}$$

where Eqs. (1.36) and (1.35) were used for the angular and linear velocity, respectively. The current that gives rise to quantized radiation comprises two terms. One corresponds to the quantized angular frequency change that matches the angular frequency of the corresponding emitted photon, and the other corresponds to the quantized wavenumber change with the transition from the initial to final radius. Using Eq. (1.280), the relationship between the electron radius and wavelength in the lightlike frame is given by Eq. (1.16). The radial current from the initial to final radius must be one wavelength in order to be phase-matched with the photon wavelength. Thus, the electron wavenumber corresponding to the propagating photon traveling at $v = c$ is given by the difference in the lightlike electron wavelength in going from the initial to final radius:

$$k_r = k_{r_f} - k_{r_i} = \frac{2\pi}{\lambda_f} - \frac{2\pi}{\lambda_i} = \frac{2\pi}{r_f} - \frac{2\pi}{r_i} \tag{2.92}$$

From Eqs. (2.89-2.92), the quantized current changes in the radial integral of the vector potential are:

$$\mathbf{A}(r) = \frac{\mu_0}{4\pi}\frac{e\hbar}{m_e}\int_{r_{n_i}-r_{n_f}}^{\infty}\frac{1}{2\pi r'^4}\frac{e^{-ik_r|\mathbf{r}-\mathbf{r}'|}}{|\mathbf{r}-\mathbf{r}'|}r'^2\,dr'\mathbf{i}_z \tag{2.93}$$

where the current is a function of $r_{n_i} - r_{n_f}$ in order to conserve the electron and photon angular momentum as in the case of Eq. (1.37). Due to spherical symmetry, the electric dipole current is equivalent to that of a dipole at the origin. With $r' = 0$ in the Green function, $\mathbf{A}(r)$ is:

$$\mathbf{A}(r) = \frac{\mu_0}{2\pi}\frac{e\hbar}{m_e}\int_{r_{n_i}-r_{n_f}}^{\infty}\frac{1}{r'^4}\frac{e^{-ik_r r}}{4\pi r}r'^2\,dr'\mathbf{i}_z = \frac{\mu_0}{2\pi}\frac{e\hbar}{m_e}\frac{1}{r_{n_i}-r_{n_f}}\frac{e^{-ik_r r}}{4\pi r}\mathbf{i}_z \tag{2.94}$$

Applying Eq. (2.83) to $\mathbf{A}(r)$ given by Eq. (2.94) gives the magnetic field **H**:

$$\mathbf{H} = \frac{1}{\mu}\nabla X\mathbf{A} = \frac{e\hbar}{m_e}\frac{1}{r_{n_i}-r_{n_f}}\frac{jk_r}{2\pi}\frac{e^{-ik_r r}}{4\pi r}\left(1+\frac{1}{jk_r r}\right)\sin\theta\mathbf{i}_\phi \tag{2.95}$$

where

$$\mathbf{i}_z = \cos\theta\mathbf{i}_r - \sin\theta\mathbf{i}_\theta \tag{2.96}$$

Outside the dipole source, the corresponding electric field **E** of the radiation with angular frequency $\omega$ is given by Ampere's law:

$$\mathbf{E} = \frac{1}{i\omega\varepsilon_0}\nabla X\mathbf{H} = \sqrt{\frac{\mu_0}{\varepsilon_0}}\frac{e\hbar}{m_e}\frac{1}{r_{n_i}-r_{n_f}}\frac{ik_r}{2\pi}\frac{e^{-ik_r r}}{4\pi r}\left\{\begin{array}{l}\left(\frac{1}{ik_r r}+\frac{1}{(ik_r r)^2}\right)2\cos\theta\mathbf{i}_r + \\ \left(1+\frac{1}{ik_r r}+\frac{1}{(ik_r r)^2}\right)\sin\theta\mathbf{i}_\theta\end{array}\right\} \tag{2.97}$$

wherein a further phase match between the electron and photon wavelengths gives the replacement of $\omega$ by $k_r c$ corresponding to the Haus condition [4] $k = \frac{\omega}{c}$ given in the Instability of Excited States section. The photon and the electron wave relationships are given in the Equation of the Photon section. For the initial conditions of an unbound electron at rest, the ratio of the linear velocity of the subsequently bound electron to the emitted free-space photon given by (Eq. (4.5)) is:

$$\frac{v_n}{c_{photon}} = \frac{\lambda_n\frac{\omega_n}{2\pi}}{\lambda_{photon}\frac{\omega_{photon}}{2\pi}} = \frac{\lambda_n}{\lambda_{photon}} = \frac{\pi r_n}{r_{photon}} \tag{2.98}$$

where the $n$ subscripts refer to atomic orbital. The relations between the free space photon wavelength, radius, and velocity and the corresponding parameters of a free electron as it is bound are:

(1) $r_{n,photon}$, the radius of the photon electric and magnetic vector field (photon-e&mvf), is equal to $r_n\pi\frac{c}{v_n} = na_H\pi\frac{c}{v_n}$, the electron atomic orbital radius given by Eqs. (2.2) and (2.5) times the product of $\pi$ and the ratio of the speed of light $c$ and $v_n$, the velocity of the atomic orbital given by Eq. (1.35):

$$r_{n,photon} = r_n\frac{c}{v_n} = na_H\frac{c}{v_n} \tag{2.99}$$

(2) $\lambda_{photon}$, the photon wavelength, is equal to $\lambda_n\frac{c}{v_n}$, where $\lambda_n$ is the atomic orbital de Broglie wavelength:

$$\lambda_{photon} = \lambda_n\frac{c}{v_n} \tag{2.100}$$

(3) $\omega_{photon} = \frac{2\pi c}{\lambda}$, the photon angular velocity, is equal to $\omega_n$, the atomic orbital angular velocity given by Eq. (1.36):

$$\omega_{photon} = \frac{2\pi c}{\lambda} = \omega_n \tag{2.101}$$

In the far field, the photon radiation is that of a spherical wave as given in the Equation of the Photon section. In this case $k_r r >> 1$, and the terms having powers of $(k_r r)^{-1}$ vanish. The corresponding radiation fields are:

$$\mathbf{H} = \frac{e\hbar}{m_e}\frac{1}{r_{n_i}-r_{n_f}}\frac{ik_r}{2\pi}\frac{e^{-ik_r r}}{4\pi r}\sin\theta\mathbf{i}_\phi \tag{2.102}$$

$$\mathbf{E} = \sqrt{\frac{\mu_0}{\varepsilon_0}}\frac{e\hbar}{m_e}\frac{1}{r_{n_i}-r_{n_f}}\frac{ik_r}{2\pi}\frac{e^{-ik_r r}}{4\pi r}\sin\theta\mathbf{i}_\theta \tag{2.103}$$

The time-averaged power density in the radiation zone is given by

$$\langle \mathbf{S} \rangle = \frac{1}{2}\mathrm{Re}\left[\mathbf{E}\times\mathbf{H}^*\right] = \frac{1}{2}\sqrt{\frac{\mu_0}{\varepsilon_0}}\left|H_\phi\right|^2 = \frac{\eta}{2}\left(\frac{e\hbar}{m_e}\left|\frac{1}{r_{n_i}-r_{n_f}}\right|\frac{k_r}{2\pi}\frac{1}{4\pi r}\right)^2 \sin^2\theta\,\mathbf{i}_r \tag{2.104}$$

The total radiated power $P$ is given by integrating the Poynting power density (Eq. (2.104)) over the surface of a sphere at radius $r$:

$$P = \int_0^{2\pi}\int_0^{\pi}\langle \mathbf{S} \rangle r^2 \sin\theta d\theta d\phi = \frac{2\pi\eta}{2}\left(\frac{k_r}{2\pi}\frac{e\hbar}{4\pi m_e}\left|\frac{1}{r_{n_i}-r_{n_f}}\right|\right)^2 \int_0^{\pi}\sin^3\theta d\theta = \frac{4\pi}{3}\eta\left|\frac{k_r}{2\pi}\frac{e\hbar}{4\pi m_e}\left(\frac{1}{r_{n_i}-r_{n_f}}\right)\right|^2 \tag{2.105}$$

Eq. (2.105) is the form of the Maxwellian result for continuous fields and the corresponding source current. As shown in the Equation of the Photon section, atomic transitions are quantized and the continuous-field result of Eq. (2.105) is given by the superposition of many photons as the number goes to infinity.

The discrete or quantized power must further include the conservation of linear momentum of the radiating electron with that of the photon. Since power is the energy divided by the lifetime, the correction to the power is the same as that of the energy. The application of the correction for linear momentum conservation given by Eq. (2.153) gives the power of the quantized transition of energy $\hbar\omega$ as:

$$P = \frac{\hbar\omega}{2m_ec^2}\frac{4\pi}{3}\eta\left|\frac{k_r}{2\pi}\frac{e\hbar}{4\pi m_e}\left(\frac{1}{r_{n_i}-r_{n_f}}\right)\right|^2 \tag{2.106}$$

The transition probability $\frac{1}{\tau}$ or $A_{ki}$ coefficient is given by Jackson [7]:

$$\frac{1}{\tau} = A_{ki} = \frac{power}{energy} \tag{2.107}$$

Substitution of Eqs. (2.106) and (2.148) into Eq. (2.107) gives the electric dipole electronic transition probability from initial quantum states $n_i,\ell,m_s,m_\ell$ and radius $r_{n_i}$ to the final state with quantum numbers $n_f,\ell\pm1,m_s,m_\ell$ and radius $r_{n_f}$:

$$\frac{1}{\tau} = \frac{\frac{\hbar\omega}{2m_ec^2}\frac{4\pi}{3}\eta\left|\frac{2\pi\left(\frac{1}{r_{n_f}}-\frac{1}{r_{n_i}}\right)}{2\pi}\frac{e\hbar}{4\pi m_e}\frac{1}{r_{n_i}-r_{n_f}}\right|^2}{\hbar\omega} = \frac{1}{m_ec^2}\frac{\eta}{24\pi}\left(\frac{e\hbar}{m_ea_0^2}\right)^2\left|\frac{1}{n_i-n_f}\left(\frac{1}{n_f}-\frac{1}{n_i}\right)\right|^2 = 2.678\ X\ 10^9\,\Re\ s^{-1} \tag{2.108}$$

where Eq. (2.5) was used for the radii and $\Re$ is defined as

$$\Re = \left|\frac{1}{n_i-n_f}\left(\frac{1}{n_f}-\frac{1}{n_i}\right)\right|^2 = \left|\frac{1}{n_i-n_f}\left(\frac{n_i-n_f}{n_fn_i}\right)\right|^2 = \frac{1}{\left(n_fn_i\right)^2} \tag{2.109}$$

The reciprocal of Eq. (2.108) gives the mean state lifetime[3]:

$$\tau = 2m_ec^2\frac{3}{4\pi\eta}\left|\frac{2\pi\left(\frac{1}{r_{n_f}}-\frac{1}{r_{n_i}}\right)}{2\pi}\frac{e\hbar}{4\pi m_e}\frac{1}{r_{n_i}-r_{n_f}}\right|^{-2} = m_ec^2\frac{24\pi}{\eta}\left(\frac{e\hbar}{m_ea_0^2}\right)^{-2}\left|\frac{1}{n_i-n_f}\left(\frac{1}{n_f}-\frac{1}{n_i}\right)\right|^{-2} = 3.735\ X\ 10^{-10}\,\Re^{-1}\ s \tag{2.110}$$

where Eq. (2.5) was used for the radii. Using Eqs. (2.108-2.2110), the parameters of representative hydrogen emission series of lines are given in Tables 2.4-2.16.

Since there is no special preparation of the states, the radiation pattern is isotropic, and the power and concomitantly the intensity of each electric dipole transition connecting states with the same initial and final principal quantum numbers are the same. However, the multiplicity of a given $\ell$ state does change the relative intensities based on the statistical population of states of the same principal quantum number $n$, but different $\ell$ quantum numbers. As given in Jackson, the "sum rule" for the squares of the $Y_{\ell,m}$'s is

$$\sum_{m=-\ell}^{\ell}\left|Y_{\ell,m}(\theta,\phi)\right|^2 = \frac{2\ell+1}{4\pi} \tag{2.111}$$

Furthermore, the total number of states $N$ for a given principal quantum number $n$ is given by (Eq. (1.70)):

$$N = \sum_{\ell=0}^{n-1}\sum_{m_\ell=-\ell}^{+\ell}1 = \sum_{\ell=0}^{n-1}2\ell+1 = n^2 \tag{2.112}$$

[3] A mean lifetime arises due to the superposition of transitions over an ensemble of individual atoms. Each atom has an exact lifetime due to an exact transition involving specific initial, final, and any intermediate $\ell$, $m$ states and the corresponding exact photon in space relative to the states. The mean lifetime arises from the mean current given by Eq. (2.87) and the spherical radiation field due to the superposition of emitted photons. Similarly, Maxwell's equations apply to macroscopic fields that are in actuality the superposition of quantized photons. Thus, deterministic physics arises as the aggregate behavior of entities that also in turn obey deterministic physics.

where each state corresponds to an $\ell$ and $m_\ell$ quantum number of an energy level corresponding to the principal quantum number $n$. Consequently, a source comprised of a set of multipoles of order $\ell$, independent of $m_\ell$ gives rise to an isotropic radiation distribution when the multipoles superimpose incoherently. This is the typical case in atomic and nuclear radiative transitions unless the initial state has been prepared in a special way. In the case that the $\ell$ states can be distinguished, the relative intensities are given statistically by the ratios of the multiplicity of each state divided by the total number of states. Thus, the relative intensity of state $\ell$ is given by

$$\frac{2\ell+1}{n^2} \tag{2.113}$$

Using Eq. (2.113), the relative line intensities for the transitions ${}^2P^0_{3/2} \rightarrow {}^2S_{1/2}$ and ${}^2D_{5/2} \rightarrow {}^2P^0_{3/2}$ wherein are $\ell = 1$ and $\ell = 2$ are 3:5 which closely matches the NIST observed relative intensities of 120:180 [26].

**Table 2.4.** The parameters of the Lyman series of emission lines.

| $n_i$ | $n_f$ | $\Re$ [a] | $\Re_{n_i \rightarrow 1} / \Re_{2 \rightarrow 1}$ | $1/\tau$ [b] | $\tau$ [c] |
|---|---|---|---|---|---|
| 2 | 1 | 2.50E-01 | 1.00 | 6.70E+08 | 1.49E-09 |
| 3 | 1 | 1.11E-01 | 0.44 | 2.98E+08 | 3.36E-09 |
| 4 | 1 | 6.25E-02 | 0.25 | 1.67E+08 | 5.97E-09 |
| 5 | 1 | 4.00E-02 | 0.16 | 1.07E+08 | 9.34E-09 |
| 6 | 1 | 2.78E-02 | 0.11 | 7.44E+07 | 1.34E-08 |
| 7 | 1 | 2.04E-02 | 0.08 | 5.47E+07 | 1.83E-08 |
| 8 | 1 | 1.56E-02 | 0.06 | 4.18E+07 | 2.39E-08 |
| 9 | 1 | 1.23E-02 | 0.05 | 3.31E+07 | 3.02E-08 |
| 10 | 1 | 1.00E-02 | 0.04 | 2.68E+07 | 3.73E-08 |
| 11 | 1 | 8.26E-03 | 0.03 | 2.21E+07 | 4.52E-08 |
| 12 | 1 | 6.94E-03 | 0.03 | 1.86E+07 | 5.38E-08 |
| 13 | 1 | 5.92E-03 | 0.02 | 1.58E+07 | 6.31E-08 |
| 14 | 1 | 5.10E-03 | 0.02 | 1.37E+07 | 7.32E-08 |
| 15 | 1 | 4.44E-03 | 0.02 | 1.19E+07 | 8.40E-08 |
| 16 | 1 | 3.91E-03 | 0.02 | 1.05E+07 | 9.56E-08 |
| 17 | 1 | 3.46E-03 | 0.01 | 9.27E+06 | 1.08E-07 |
| 18 | 1 | 3.09E-03 | 0.01 | 8.27E+06 | 1.21E-07 |
| 19 | 1 | 2.77E-03 | 0.01 | 7.42E+06 | 1.35E-07 |
| 20 | 1 | 2.50E-03 | 0.01 | 6.70E+06 | 1.49E-07 |

[a] Eq. (2.109).
[b] Eq. (2.108).
[c] Eq. (2.110).

**Table 2.5.** The parameters of the Balmer series of emission lines.

| $n_i$ | $n_f$ | $\Re$ [a] | $\Re_{n_i \to 2} / \Re_{3 \to 2}$ | $1/\tau$ [b] | $\tau$ [c] |
|---|---|---|---|---|---|
| 3 | 2 | 2.78E-02 | 1.00 | 7.44E+07 | 1.34E-08 |
| 4 | 2 | 1.56E-02 | 0.56 | 4.18E+07 | 2.39E-08 |
| 5 | 2 | 1.00E-02 | 0.36 | 2.68E+07 | 3.73E-08 |
| 6 | 2 | 6.94E-03 | 0.25 | 1.86E+07 | 5.38E-08 |
| 7 | 2 | 5.10E-03 | 0.18 | 1.37E+07 | 7.32E-08 |
| 8 | 2 | 3.91E-03 | 0.14 | 1.05E+07 | 9.56E-08 |
| 9 | 2 | 3.09E-03 | 0.11 | 8.27E+06 | 1.21E-07 |
| 10 | 2 | 2.50E-03 | 0.09 | 6.70E+06 | 1.49E-07 |
| 11 | 2 | 2.07E-03 | 0.07 | 5.53E+06 | 1.81E-07 |
| 12 | 2 | 1.74E-03 | 0.06 | 4.65E+06 | 2.15E-07 |
| 13 | 2 | 1.48E-03 | 0.05 | 3.96E+06 | 2.52E-07 |
| 14 | 2 | 1.28E-03 | 0.05 | 3.42E+06 | 2.93E-07 |
| 15 | 2 | 1.11E-03 | 0.04 | 2.98E+06 | 3.36E-07 |
| 16 | 2 | 9.77E-04 | 0.04 | 2.62E+06 | 3.82E-07 |
| 17 | 2 | 8.65E-04 | 0.03 | 2.32E+06 | 4.32E-07 |
| 18 | 2 | 7.72E-04 | 0.03 | 2.07E+06 | 4.84E-07 |
| 19 | 2 | 6.93E-04 | 0.02 | 1.85E+06 | 5.39E-07 |
| 20 | 2 | 6.25E-04 | 0.02 | 1.67E+06 | 5.97E-07 |

[a] Eq. (2.109).
[b] Eq. (2.108).
[c] Eq. (2.110).

**Table 2.6.** The parameters of the Paschen series of emission lines.

| $n_i$ | $n_f$ | $\Re$ [a] | $\Re_{n_i \to 3} / \Re_{4 \to 3}$ | $1/\tau$ [b] | $\tau$ [c] |
|---|---|---|---|---|---|
| 4 | 3 | 6.94E-03 | 1.00 | 1.86E+07 | 5.38E-08 |
| 5 | 3 | 4.44E-03 | 0.64 | 1.19E+07 | 8.40E-08 |
| 6 | 3 | 3.09E-03 | 0.44 | 8.27E+06 | 1.21E-07 |
| 7 | 3 | 2.27E-03 | 0.33 | 6.07E+06 | 1.65E-07 |
| 8 | 3 | 1.74E-03 | 0.25 | 4.65E+06 | 2.15E-07 |
| 9 | 3 | 1.37E-03 | 0.20 | 3.67E+06 | 2.72E-07 |
| 10 | 3 | 1.11E-03 | 0.16 | 2.98E+06 | 3.36E-07 |
| 11 | 3 | 9.18E-04 | 0.13 | 2.46E+06 | 4.07E-07 |
| 12 | 3 | 7.72E-04 | 0.11 | 2.07E+06 | 4.84E-07 |
| 13 | 3 | 6.57E-04 | 0.09 | 1.76E+06 | 5.68E-07 |
| 14 | 3 | 5.67E-04 | 0.08 | 1.52E+06 | 6.59E-07 |
| 15 | 3 | 4.94E-04 | 0.07 | 1.32E+06 | 7.56E-07 |
| 16 | 3 | 4.34E-04 | 0.06 | 1.16E+06 | 8.60E-07 |
| 17 | 3 | 3.84E-04 | 0.06 | 1.03E+06 | 9.71E-07 |
| 18 | 3 | 3.43E-04 | 0.05 | 9.18E+05 | 1.09E-06 |
| 19 | 3 | 3.08E-04 | 0.04 | 8.24E+05 | 1.21E-06 |
| 20 | 3 | 2.78E-04 | 0.04 | 7.44E+05 | 1.34E-06 |

[a] Eq. (2.109).
[b] Eq. (2.108).
[c] Eq. (2.110).

**Table 2.7.** The parameters of the Brackett series of emission lines.

| $n_i$ | $n_f$ | $\Re$ [a] | $\Re_{n_i\to 4} / \Re_{5\to 4}$ | $1/\tau$ [b] | $\tau$ [c] |
|---|---|---|---|---|---|
| 5 | 4 | 2.50E-03 | 1.00 | 6.70E+06 | 1.49E-07 |
| 6 | 4 | 1.74E-03 | 0.69 | 4.65E+06 | 2.15E-07 |
| 7 | 4 | 1.28E-03 | 0.51 | 3.42E+06 | 2.93E-07 |
| 8 | 4 | 9.77E-04 | 0.39 | 2.62E+06 | 3.82E-07 |
| 9 | 4 | 7.72E-04 | 0.31 | 2.07E+06 | 4.84E-07 |
| 10 | 4 | 6.25E-04 | 0.25 | 1.67E+06 | 5.97E-07 |
| 11 | 4 | 5.17E-04 | 0.21 | 1.38E+06 | 7.23E-07 |
| 12 | 4 | 4.34E-04 | 0.17 | 1.16E+06 | 8.60E-07 |
| 13 | 4 | 3.70E-04 | 0.15 | 9.90E+05 | 1.01E-06 |
| 14 | 4 | 3.19E-04 | 0.13 | 8.54E+05 | 1.17E-06 |
| 15 | 4 | 2.78E-04 | 0.11 | 7.44E+05 | 1.34E-06 |
| 16 | 4 | 2.44E-04 | 0.10 | 6.54E+05 | 1.53E-06 |
| 17 | 4 | 2.16E-04 | 0.09 | 5.79E+05 | 1.73E-06 |
| 18 | 4 | 1.93E-04 | 0.08 | 5.17E+05 | 1.94E-06 |
| 19 | 4 | 1.73E-04 | 0.07 | 4.64E+05 | 2.16E-06 |
| 20 | 4 | 1.56E-04 | 0.06 | 4.18E+05 | 2.39E-06 |

[a] Eq. (2.109).
[b] Eq. (2.108).
[c] Eq. (2.110).

**Table 2.8.** The parameters of the Pfund series of emission lines.

| $n_i$ | $n_f$ | $\Re$ [a] | $\Re_{n_i\to 5} / \Re_{6\to 5}$ | $1/\tau$ [b] | $\tau$ [c] |
|---|---|---|---|---|---|
| 6 | 5 | 1.11E-03 | 1.00 | 2.98E+06 | 3.36E-07 |
| 7 | 5 | 8.16E-04 | 0.73 | 2.19E+06 | 4.57E-07 |
| 8 | 5 | 6.25E-04 | 0.56 | 1.67E+06 | 5.97E-07 |
| 9 | 5 | 4.94E-04 | 0.44 | 1.32E+06 | 7.56E-07 |
| 10 | 5 | 4.00E-04 | 0.36 | 1.07E+06 | 9.34E-07 |
| 11 | 5 | 3.31E-04 | 0.30 | 8.85E+05 | 1.13E-06 |
| 12 | 5 | 2.78E-04 | 0.25 | 7.44E+05 | 1.34E-06 |
| 13 | 5 | 2.37E-04 | 0.21 | 6.34E+05 | 1.58E-06 |
| 14 | 5 | 2.04E-04 | 0.18 | 5.47E+05 | 1.83E-06 |
| 15 | 5 | 1.78E-04 | 0.16 | 4.76E+05 | 2.10E-06 |
| 16 | 5 | 1.56E-04 | 0.14 | 4.18E+05 | 2.39E-06 |
| 17 | 5 | 1.38E-04 | 0.12 | 3.71E+05 | 2.70E-06 |
| 18 | 5 | 1.23E-04 | 0.11 | 3.31E+05 | 3.02E-06 |
| 19 | 5 | 1.11E-04 | 0.10 | 2.97E+05 | 3.37E-06 |
| 20 | 5 | 1.00E-04 | 0.09 | 2.68E+05 | 3.73E-06 |

[a] Eq. (2.109).
[b] Eq. (2.108).
[c] Eq. (2.110).

**Table 2.9.** The parameters of the $n_i > 6$ to $n_f = 6$ series of emission lines.

| $n_i$ | $n_f$ | $\Re$ [a] | $\Re_{n_i \to 6} / \Re_{7 \to 6}$ | $1/\tau$ [b] | $\tau$ [c] |
|---|---|---|---|---|---|
| 7 | 6 | 5.67E-04 | 1.00 | 1.52E+06 | 6.59E-07 |
| 8 | 6 | 4.34E-04 | 0.77 | 1.16E+06 | 8.60E-07 |
| 9 | 6 | 3.43E-04 | 0.60 | 9.18E+05 | 1.09E-06 |
| 10 | 6 | 2.78E-04 | 0.49 | 7.44E+05 | 1.34E-06 |
| 11 | 6 | 2.30E-04 | 0.40 | 6.15E+05 | 1.63E-06 |
| 12 | 6 | 1.93E-04 | 0.34 | 5.17E+05 | 1.94E-06 |
| 13 | 6 | 1.64E-04 | 0.29 | 4.40E+05 | 2.27E-06 |
| 14 | 6 | 1.42E-04 | 0.25 | 3.80E+05 | 2.63E-06 |
| 15 | 6 | 1.23E-04 | 0.22 | 3.31E+05 | 3.02E-06 |
| 16 | 6 | 1.09E-04 | 0.19 | 2.91E+05 | 3.44E-06 |
| 17 | 6 | 9.61E-05 | 0.17 | 2.57E+05 | 3.88E-06 |
| 18 | 6 | 8.57E-05 | 0.15 | 2.30E+05 | 4.36E-06 |
| 19 | 6 | 7.69E-05 | 0.14 | 2.06E+05 | 4.85E-06 |
| 20 | 6 | 6.94E-05 | 0.12 | 1.86E+05 | 5.38E-06 |

[a] Eq. (2.109).
[b] Eq. (2.108).
[c] Eq. (2.110).

**Table 2.10.** The parameters of the $n_i > 7$ to $n_f = 7$ series of emission lines.

| $n_i$ | $n_f$ | $\Re$ [a] | $\Re_{n_i \to 7} / \Re_{8 \to 7}$ | $1/\tau$ [b] | $\tau$ [c] |
|---|---|---|---|---|---|
| 8 | 7 | 3.19E-04 | 1.00 | 8.54E+05 | 1.17E-06 |
| 9 | 7 | 2.52E-04 | 0.79 | 6.75E+05 | 1.48E-06 |
| 10 | 7 | 2.04E-04 | 0.64 | 5.47E+05 | 1.83E-06 |
| 11 | 7 | 1.69E-04 | 0.53 | 4.52E+05 | 2.21E-06 |
| 12 | 7 | 1.42E-04 | 0.44 | 3.80E+05 | 2.63E-06 |
| 13 | 7 | 1.21E-04 | 0.38 | 3.23E+05 | 3.09E-06 |
| 14 | 7 | 1.04E-04 | 0.33 | 2.79E+05 | 3.59E-06 |
| 15 | 7 | 9.07E-05 | 0.28 | 2.43E+05 | 4.12E-06 |
| 16 | 7 | 7.97E-05 | 0.25 | 2.13E+05 | 4.68E-06 |
| 17 | 7 | 7.06E-05 | 0.22 | 1.89E+05 | 5.29E-06 |
| 18 | 7 | 6.30E-05 | 0.20 | 1.69E+05 | 5.93E-06 |
| 19 | 7 | 5.65E-05 | 0.18 | 1.51E+05 | 6.61E-06 |
| 20 | 7 | 5.10E-05 | 0.16 | 1.37E+05 | 7.32E-06 |

[a] Eq. (2.109).
[b] Eq. (2.108).
[c] Eq. (2.110).

**Table 2.11.** The parameters of the $n_i > 8$ to $n_f = 8$ series of emission lines.

| $n_i$ | $n_f$ | $\Re$ [a] | $\Re_{n_i \to 8} / \Re_{9 \to 8}$ | $1/\tau$ [b] | $\tau$ [c] |
|---|---|---|---|---|---|
| 9 | 8 | 1.93E-04 | 1.00 | 5.17E+05 | 1.94E-06 |
| 10 | 8 | 1.56E-04 | 0.81 | 4.18E+05 | 2.39E-06 |
| 11 | 8 | 1.29E-04 | 0.67 | 3.46E+05 | 2.89E-06 |
| 12 | 8 | 1.09E-04 | 0.56 | 2.91E+05 | 3.44E-06 |
| 13 | 8 | 9.25E-05 | 0.48 | 2.48E+05 | 4.04E-06 |
| 14 | 8 | 7.97E-05 | 0.41 | 2.13E+05 | 4.68E-06 |
| 15 | 8 | 6.94E-05 | 0.36 | 1.86E+05 | 5.38E-06 |
| 16 | 8 | 6.10E-05 | 0.32 | 1.63E+05 | 6.12E-06 |
| 17 | 8 | 5.41E-05 | 0.28 | 1.45E+05 | 6.91E-06 |
| 18 | 8 | 4.82E-05 | 0.25 | 1.29E+05 | 7.74E-06 |
| 19 | 8 | 4.33E-05 | 0.22 | 1.16E+05 | 8.63E-06 |
| 20 | 8 | 3.91E-05 | 0.20 | 1.05E+05 | 9.56E-06 |

[a] Eq. (2.109).
[b] Eq. (2.108).
[c] Eq. (2.110).

**Table 2.12.** The parameters of the $n_i > 100$ to $n_f = 1$ series of emission lines.

| $n_i$ | $n_f$ | $\Re$ [a] | $\Re_{n_i \to 1} / \Re_{101 \to 1}$ | $1/\tau$ [b] | $\tau$ [c] |
|---|---|---|---|---|---|
| 101 | 1 | 9.80E-05 | 1.00 | 2.63E+05 | 3.81E-06 |
| 102 | 1 | 9.61E-05 | 0.98 | 2.57E+05 | 3.88E-06 |
| 103 | 1 | 9.43E-05 | 0.96 | 2.52E+05 | 3.96E-06 |
| 104 | 1 | 9.25E-05 | 0.94 | 2.48E+05 | 4.04E-06 |
| 105 | 1 | 9.07E-05 | 0.93 | 2.43E+05 | 4.12E-06 |
| 106 | 1 | 8.90E-05 | 0.91 | 2.38E+05 | 4.20E-06 |
| 107 | 1 | 8.73E-05 | 0.89 | 2.34E+05 | 4.28E-06 |
| 108 | 1 | 8.57E-05 | 0.87 | 2.30E+05 | 4.36E-06 |
| 109 | 1 | 8.42E-05 | 0.86 | 2.25E+05 | 4.44E-06 |
| 110 | 1 | 8.26E-05 | 0.84 | 2.21E+05 | 4.52E-06 |

[a] Eq. (2.109).
[b] Eq. (2.108).
[c] Eq. (2.110).

**Table 2.13.** The parameters of the $n_i > 100$ to $n_f = 100$ series of emission lines.

| $n_i$ | $n_f$ | $\Re$ [a] | $\Re_{n_i \to 100} / \Re_{101 \to 100}$ | $1/\tau$ [b] | $\tau$ [c] |
|---|---|---|---|---|---|
| 101 | 100 | 9.80E-09 | 1.00 | 2.63E+01 | 3.81E-02 |
| 102 | 100 | 9.61E-09 | 0.98 | 2.57E+01 | 3.88E-02 |
| 103 | 100 | 9.43E-09 | 0.96 | 2.52E+01 | 3.96E-02 |
| 104 | 100 | 9.25E-09 | 0.94 | 2.48E+01 | 4.04E-02 |
| 105 | 100 | 9.07E-09 | 0.93 | 2.43E+01 | 4.12E-02 |
| 106 | 100 | 8.90E-09 | 0.91 | 2.38E+01 | 4.20E-02 |
| 107 | 100 | 8.73E-09 | 0.89 | 2.34E+01 | 4.28E-02 |
| 108 | 100 | 8.57E-09 | 0.87 | 2.30E+01 | 4.36E-02 |
| 109 | 100 | 8.42E-09 | 0.86 | 2.25E+01 | 4.44E-02 |
| 110 | 100 | 8.26E-09 | 0.84 | 2.21E+01 | 4.52E-02 |

[a] Eq. (2.109).
[b] Eq. (2.108).
[c] Eq. (2.110).

**Table 2.14.** The parameters of the $n_i > 500$ to $n_f = 1$ series of emission lines.

| $n_i$ | $n_f$ | $\Re$ [a] | $\Re_{n_i \to 1} / \Re_{501 \to 1}$ | $1/\tau$ [b] | $\tau$ [c] |
|---|---|---|---|---|---|
| 501 | 1 | 3.98E-06 | 1.00 | 1.07E+04 | 9.37E-05 |
| 502 | 1 | 3.97E-06 | 1.00 | 1.06E+04 | 9.41E-05 |
| 503 | 1 | 3.95E-06 | 0.99 | 1.06E+04 | 9.45E-05 |
| 504 | 1 | 3.94E-06 | 0.99 | 1.05E+04 | 9.49E-05 |
| 505 | 1 | 3.92E-06 | 0.98 | 1.05E+04 | 9.52E-05 |
| 506 | 1 | 3.91E-06 | 0.98 | 1.05E+04 | 9.56E-05 |
| 507 | 1 | 3.89E-06 | 0.98 | 1.04E+04 | 9.60E-05 |
| 508 | 1 | 3.88E-06 | 0.97 | 1.04E+04 | 9.64E-05 |
| 509 | 1 | 3.86E-06 | 0.97 | 1.03E+04 | 9.67E-05 |
| 510 | 1 | 3.84E-06 | 0.97 | 1.03E+04 | 9.71E-05 |

[a] Eq. (2.109).
[b] Eq. (2.108).
[c] Eq. (2.110).

**Table 2.15.** The parameters of the $n_i > 500$ to $n_f = 100$ series of emission lines.

| $n_i$ | $n_f$ | $\Re$ [a] | $\Re_{n_i \to 100} / \Re_{501 \to 100}$ | $1/\tau$ [b] | $\tau$ [c] |
|---|---|---|---|---|---|
| 501 | 100 | 3.98E-10 | 1.00 | 1.07E-00 | 9.37E-01 |
| 502 | 100 | 3.97E-10 | 1.00 | 1.06E-00 | 9.41E-01 |
| 503 | 100 | 3.95E-10 | 0.99 | 1.06E-00 | 9.45E-01 |
| 504 | 100 | 3.94E-10 | 0.99 | 1.05E-00 | 9.49E-01 |
| 505 | 100 | 3.92E-10 | 0.98 | 1.05E-00 | 9.52E-01 |
| 506 | 100 | 3.91E-10 | 0.98 | 1.05E-00 | 9.56E-01 |
| 507 | 100 | 3.89E-10 | 0.98 | 1.04E-00 | 9.60E-01 |
| 508 | 100 | 3.88E-10 | 0.97 | 1.04E-00 | 9.64E-01 |
| 509 | 100 | 3.86E-10 | 0.97 | 1.03E-00 | 9.67E-01 |
| 510 | 100 | 3.84E-10 | 0.97 | 1.03E-00 | 9.71E-01 |

[a] Eq. (2.109).
[b] Eq. (2.108).
[c] Eq. (2.110).

**Table 2.16.** The parameters of the $n_i > 500$ to $n_f = 500$ series of emission lines.

| $n_i$ | $n_f$ | $\Re$ [a] | $\Re_{n_i \to 500} / \Re_{501 \to 500}$ | $1/\tau$ [b] | $\tau$ [c] |
|---|---|---|---|---|---|
| 501 | 500 | 1.59E-11 | 1.00 | 4.27E-02 | 2.34E+01 |
| 502 | 500 | 1.59E-11 | 1.00 | 4.25E-02 | 2.35E+01 |
| 503 | 500 | 1.58E-11 | 0.99 | 4.23E-02 | 2.36E+01 |
| 504 | 500 | 1.57E-11 | 0.99 | 4.22E-02 | 2.37E+01 |
| 505 | 500 | 1.57E-11 | 0.98 | 4.20E-02 | 2.38E+01 |
| 506 | 500 | 1.56E-11 | 0.98 | 4.18E-02 | 2.39E+01 |
| 507 | 500 | 1.56E-11 | 0.98 | 4.17E-02 | 2.40E+01 |
| 508 | 500 | 1.55E-11 | 0.97 | 4.15E-02 | 2.41E+01 |
| 509 | 500 | 1.54E-11 | 0.97 | 4.13E-02 | 2.42E+01 |
| 510 | 500 | 1.54E-11 | 0.97 | 4.12E-02 | 2.43E+01 |

[a] Eq. (2.109).
[b] Eq. (2.108).
[c] Eq. (2.110).

The lifetime of the Balmer $\alpha$ transition of $1.34X\ 10^{-8}\ s$ given in Table 2.5 is in good agreement with the experimental upper limit of $1.5X\ 10^{-8}\ s$ [26-27]. The relative line intensities are dependent on the electron temperature which causes a Boltzmann-distribution skewing [28] of the predominantly lifetime-determined state populations.. However, states that are close in energy are expected to be close to the theoretical limit with greater deviations as the energy differences become larger. The experimental Balmer-series line intensities are given with the calculated intensities in Table 2.17. As expected the predicted and experimental intensities match well for the lowest levels and deviate at the higher levels.

**Table 2.17.** The parameters of the Balmer series of emission lines.

| $n_i$ | $n_f$ | $\Re$ [a] | $\Re_{n_i \to 2} / \Re_{3 \to 2}$ | $\Re_{n_i \to 2} / \Re_{3 \to 2}$ X 300 | NIST [26] Balmer Line Intensities |
|---|---|---|---|---|---|
| 3 | 2 | 2.78E-02 | 1.00 | 300 | 300 |
| 4 | 2 | 1.56E-02 | 0.56 | 169 | 160 |
| 5 | 2 | 1.00E-02 | 0.36 | 108 | 60 |
| 6 | 2 | 6.94E-03 | 0.25 | 75 | 30 |
| 7 | 2 | 5.10E-03 | 0.18 | 55 | 8 |
| 8 | 2 | 3.91E-03 | 0.14 | 42 | 6 |
| 9 | 2 | 3.09E-03 | 0.11 | 33 | 5 |

[a] Eq. (2.109).

Ornstein and Burger [29-30] studied the relative emission intensities of Balmer and Paschen lines having the same initial states in order to eliminate the uncertainty of the number of atoms in each initial state. The results of the relative intensities from each state having the same initial number of atoms is given in Table 2.18. The calculated and experimental results agree very well. In contrast, standard quantum mechanics has many shortcomings in this result as well as in general[4].

**Table 2.18.** The parameter $\Re$ and the calculated and experimental intensity ratios of selected Balmer and Paschen emission lines.

| $n_i$ | $n_f$ | $\Re$ [a] | $\Re_{Paschen,n_i} / \Re_{Balmer,n_i}$ | | Experimental Intensity Ratio [29-30] $\frac{Paschen,n_i}{Balmer,n_i}$ |
|---|---|---|---|---|---|
| 4 | 2 | 1.56E-02 | $H_\beta / P_\alpha (4\to2) : (4\to3)$ | **2.25** | **2.6** |
| 4 | 3 | 6.94E-03 | | | |
| 5 | 2 | 1.00E-02 | $H_\gamma / P_\beta (5\to2) : (5\to3)$ | **2.25** | **2.5** |
| 5 | 3 | 4.44E-03 | | | |
| 6 | 2 | 6.94E-03 | $H_\delta / P_\gamma (6\to2) : (6\to3)$ | **2.25** | **2** |
| 6 | 3 | 3.09E-03 | | | |

[a] Eq. (2.109).

The radii of all one-electron atoms are given by Eq. (1.260). For $He^+$,

[4] The quantum mechanical calculation of the line intensities is also based on classical electrodynamics [32], but there are many internally inconsistent features that arise due to the intrinsic nonphysical aspects peculiar to quantum mechanics. The possibility that $\Delta l = +1$ is not treated. The A coefficients are not symmetrical with respect to excitation and de-excitation as they must be. The $-\sin\theta \mathbf{i}_\theta$ dependence of the current dipole is ignored. The calculation of the current multipole based on integration of the products of wavefunctions over all space is not physical. The electron can not be "everywhere at once," and even the frequency times the average radial displacement during a transition results in an electron velocity that exceeds the speed of light. The calculations are extraordinarily complicated involving hypergeometric series, and the results contain products of terms raised to enormously high and low powers (e.g. power of $\sim \pm 20$ for even the Balmer lines). The results do not match the experimental results by significant factors.

$$r_1 = \frac{a_0}{2} \tag{2.114}$$

Substitution of Eq. (2.114) into Eqs. (2.108) and (2.110) gives the electric dipole electronic transition probability from initial quantum states $n_i, \ell, m_s, m_\ell$ and radius $r_{n_i}$ to the final state with quantum numbers $n_f, \ell \pm 1, m_s, m_\ell$ and radius $r_{n_f}$ and the corresponding state lifetime, respectively:

$$\begin{aligned}\frac{1}{\tau} &= \frac{\dfrac{\hbar\omega}{2m_e c^2}\dfrac{4\pi}{3}\eta\left|\dfrac{2\pi\left(\dfrac{1}{r_{n_f}}-\dfrac{1}{r_{n_i}}\right)}{2\pi}\dfrac{e\hbar}{4\pi m_e}\dfrac{1}{r_{n_i}-r_{n_f}}\right|^2}{\hbar\omega} \\ &= \frac{1}{m_e c^2}\frac{\eta}{24\pi}\left(\frac{e\hbar}{m_e\left(\dfrac{a_0}{2}\right)^2}\right)^2\left|\frac{1}{n_i-n_f}\left(\frac{1}{n_f}-\frac{1}{n_i}\right)\right|^2 \\ &= 4.284\ X\ 10^{10}\Re\ s^{-1}\end{aligned} \tag{2.115}$$

$$\begin{aligned}\tau &= 2m_e c^2\frac{3}{4\pi\eta}\left|\frac{2\pi\left(\dfrac{1}{r_{n_f}}-\dfrac{1}{r_{n_i}}\right)}{2\pi}\frac{e\hbar}{4\pi m_e}\frac{1}{r_{n_i}-r_{n_f}}\right|^{-2} \\ &= m_e c^2\frac{24\pi}{\eta}\left(\frac{e\hbar}{m_e\left(\dfrac{a_0}{2}\right)^2}\right)^{-2}\left|\frac{1}{n_i-n_f}\left(\frac{1}{n_f}-\frac{1}{n_i}\right)\right|^{-2} \\ &= 2.334\ X\ 10^{-11}\Re^{-1}\ s\end{aligned} \tag{2.116}$$

where $\Re$ is given by Eq. (2.109). The predicted lifetimes for $He^+$ are 1/16 those of atomic hydrogen. The equations for the excited-state lifetimes and line intensities can be condensed as given in Box 2.1.

## BOX 2.1 CONDENSED FORMULA FOR THE EXCITED-STATE LIFETIMES AND LINE INTENSITIES

Using

$$\alpha = \frac{e^2}{4\pi\varepsilon_0\hbar c} \tag{1}$$

Allows the substitutions

$$a_0 = \frac{4\pi\varepsilon_0\hbar^2}{e^2 m_e} = \frac{\hbar}{\alpha m_e c} \tag{2}$$

and

$$e^2 = 4\pi\varepsilon_0\alpha\hbar c \tag{3}$$

such that the equations for the excited-state lifetimes and line intensities can be condensed [31]. Eq. (2.108) can be written as

$$\frac{1}{\tau} = \frac{1}{2m_e c^2}\cdot\frac{4\pi}{3}\cdot\left(\frac{e\hbar}{4\pi m_e}\right)^2\cdot\frac{1}{\left(r_{nf}r_{ni}\right)^2} \qquad \text{as} \qquad r_{nf} \neq r_{ni} \tag{4}$$

This can be transformed to

$$\begin{aligned}\frac{1}{\tau} &= \frac{1}{6m_e c^2}\sqrt{\frac{\mu_0}{\varepsilon_0}}\frac{e^2\hbar^2}{4\pi m_e^2}\frac{a_0^4}{\left(r_{nf}r_{ni}\right)^2}\left(\frac{e^2 m_e}{4\pi\varepsilon_0\hbar^2}\right)^4 \\ &= \frac{1}{6m_e c^2}\sqrt{\frac{\mu_0}{\varepsilon_0}}\frac{4\pi\varepsilon_0\alpha\hbar c\hbar^2}{4\pi m_e^2}\frac{a_0^4}{\left(r_{nf}r_{ni}\right)^2}\left(\frac{4\pi\varepsilon_0\alpha\hbar c m_e}{4\pi\varepsilon_0\hbar^2}\right)^4 \\ &= \frac{1}{6m_e c^2}\frac{\alpha\hbar^3}{m_e^2}\frac{a_0^4}{\left(r_{nf}r_{ni}\right)^2}\left(\frac{\alpha c m_e}{\hbar}\right)^4 = \frac{1}{6}\alpha^5\frac{m_e c^2}{\hbar}\left(\frac{a_0^2}{r_{nf}r_{ni}}\right)^2\end{aligned} \tag{5}$$

and the corresponding Eq. (2.110) becomes:

$$\tau = 6\alpha^{-5}\frac{\hbar}{m_e c^2}\left(\frac{r_{nf}r_{ni}}{a_0^2}\right)^2 \qquad \text{as} \qquad r_{nf} \neq r_{ni} \tag{6}$$

The result confirms that:

$$\frac{r_{nf}r_{ni}}{a_0^2} = n_f n_i \tag{7}$$

Alternatively, Eq. (2.110) in condensed form is:

$$\tau = 6\alpha^{-5}\cdot\frac{\hbar}{m_e c^2}\cdot\left(n_f n_i\right)^2 = 3.734826\times10^{-10}\,s\cdot\left(n_f n_i\right)^2 \tag{8}$$

And, Eq. (2.116) becomes

$$\tau = \frac{6}{16}\alpha^{-5}\cdot\frac{\hbar}{m_e c^2}\cdot\left(n_f n_i\right)^2 = 2.334266\times10^{-11}\,s\cdot\left(n_f n_i\right)^2 \tag{9}$$

---

Maxwell made an absolute measurement of the lifetime of excited states of $He^+$ formed by narrow-beam, electron-impact excitation [30, 33]. The excited $He^+$ ions were spread by a transverse electric field which did not appreciably affect the ionizing electron beam because a controlling longitudinal magnetic field was applied. The time-of-flight to radiating was recorded as the distance-of-flight and gave the probability distribution of the lifetimes of the excited states. By studying the spatial distribution of the light intensity, Maxwell inferred the mean lifetimes of the excited-state ions. For the $n = 6$ states of $He^+$, an average lifetime of $\left(1.1 \pm 0.2\right)\ X\ 10^{-8}\ s$ was observed. From Tables 2.4-2.8, the average life time of the $n = 6$ state of $H$ is $1.48\ X\ 10^{-7}\ s$, and from Eq. (2.116), the corresponding average lifetime of $He^+$ is $9.3X\ 10^{-9}\ s$. The lifetimes of states of $He^+$ were found to be 1/16 those of $H$. The agreement between the experimental and calculated results is excellent.

In addition to the electron electric dipole transitions, Eq. (2.107) can be applied to transitions with a multipole distribution in the radial direction such as in the case of nuclear decay given in the Nuclear and X-ray Multipole Radiation section. The transition probability in the case of the electric multipole moment given by Jackson [7] as:

$$Q_{\ell m} = \frac{3}{\ell+3}e\left(na_0\right)^{\ell} \tag{2.117}$$

is [7]:

$$\begin{aligned}
\frac{1}{\tau} &= \frac{power}{energy} \\
\frac{1}{\tau} &= \frac{\left[\dfrac{2\pi c}{\left[(2\ell+1)!!\right]^2}\left(\dfrac{\ell+1}{\ell}\right)k^{2\ell+1}\left|Q_{\ell m}+Q'_{\ell m}\right|^2\right]}{\left[\hbar\omega\right]} \\
&= 2\pi\left(\frac{e^2}{h}\right)\sqrt{\frac{\mu_0}{\varepsilon_0}}\frac{2\pi}{\left[(2\ell+1)!!\right]^2}\left(\frac{\ell+1}{\ell}\right)\left(\frac{3}{\ell+3}\right)^2\left(kna_0\right)^{2\ell}\omega
\end{aligned} \tag{2.118}$$

Eq. (2.118) gives very predictive results as shown by Jackson [7].

## RESONANT LINE SHAPE

The spectroscopic linewidth arises from the classical rise-time band-width relationship, and the Lamb shift is due to the radiation reaction force between the electron and the photon and conservation of energy and linear momentum involving recoil during emission. It follows from the Poynting Power Theorem (Eq. (7.43)) with spherical radiation that the transition probabilities are given by the ratio of power and the energy of the transition [7]. The lifetime $\tau$ for an electric dipole transition is derived in the State Lifetime and Line Intensities section. This rise-time gives rise to $\Gamma$, the spectroscopic line-width. The relationship between the rise-time and the band-width is given by Siebert [34].

$$\tau^2 = 4\left[\frac{\int_{-\infty}^{\infty} t^2 h^2(t)dt}{\int_{-\infty}^{\infty} h^2(t)dt} - \left(\frac{\int_{-\infty}^{\infty} th^2(t)dt}{\int_{-\infty}^{\infty} h^2(t)dt}\right)^2\right] \tag{2.119}$$

$$\Gamma^2 = 4\frac{\int_{-\infty}^{\infty} f^2 \left|H(f)\right|^2 df}{\int_{-\infty}^{\infty} \left|H(f)\right|^2 df} \tag{2.120}$$

By application of the Schwartz inequality, the relationship between the rise-time and the band-width is[5]:

$$\tau\Gamma \geq \frac{1}{\pi} \tag{2.121}$$

From Eq. (2.118), the line-width is proportional to the ratio of the Quantum Hall resistance, $\frac{h}{e^2}$, and, $\eta$, the radiation resistance of free space.

$$\eta = \sqrt{\frac{\mu_0}{\varepsilon_0}} \tag{2.122}$$

And, the Quantum Hall resistance given in the Quantum Hall Effect section was derived using the Poynting Power Theorem. Also, from Eq. (2.118), the line-width is proportional to the fine structure constant, $\alpha$,

$$\alpha = \frac{1}{4\pi}\sqrt{\frac{\mu_0}{\varepsilon_0}}\frac{e^2}{\hbar} \tag{2.123}$$

During a transition, the total energy of the system decays exponentially. Applying Eqs. (2.119) and (2.120) to the case of exponential decay,

$$h(t) = e^{-\alpha t}u(t) = e^{-\frac{2\pi}{T}t}u(t) \tag{2.124}$$

$$\left|H(f)\right| = \frac{1}{\sqrt{\left(\frac{1}{T}\right)^2 + (2\pi f)^2}} \tag{2.125}$$

where the rise-time, $\tau$, is the time required for $h(t)$ of Eq. (2.124) to decay to $1/e$ of its initial value and where the band-width, $\Gamma$, is the half-power bandwidth, the distance between points at which:

$$\left|H(f)\right| = \frac{\left|H(0)\right|}{\sqrt{2}} \tag{2.126}$$

From Eq. (2.119) [34],

$$\tau = T \tag{2.127}$$

From Eq. (2.120) [34],

$$\Gamma = \frac{1}{\pi T} \tag{2.128}$$

---

[5] Eq. (2.121) is erroneously interpreted as a physical law of the indeterminate nature of conjugate parameters of atomic particles, such as position and momentum or energy and time. This so called Heisenberg Uncertainty Principle is not a physical law; rather it is a misinterpretation of applying the Schwartz Inequality to a probability-wave model of a particle [35]. The mathematical consequence is that a particle, such as an electron, can have a continuum of momenta and positions with a continuum of energies simultaneously, which cannot be physical. This result is independent of error or limitations introduced by measurement. Jean B. Fourier was the first to discover the relationship between time and frequency compositions of physical measurables. Eq. (2.121) expresses the limitation of measuring these quantities since an impulse contains an infinity of frequencies, and no instrument has such bandwidth. Similarly, an exact frequency requires an infinite measurement time, and all measurements must be finite in length. Thus, Eq. (2.121) is a statement about the limitations of measurement in time and frequency. It is further a conservation statement of energy of a signal in the time and frequency domains. Werner Heisenberg's substitution of momentum and position for a single particle, probability-wave into this relationship says nothing about conjugate parameters of a particle in the absence of their measurement or the validity of the probability-wave model. In fact, this approach was shown to be flawed experimentally (See Wave-Particle Duality section and Refs. [8-11]).

From Eq. (2.127) and Eq. (2.128), the relationship between the rise-time and the band-width for exponential decay is:

$$\tau\Gamma = \frac{1}{\pi} \tag{2.129}$$

Bosons obey Bose-Einstein statistics as given in the Statistical Mechanics section. The emitted radiation, the summation of an ensemble of emitted photons each of an exact frequency and energy given by Eq. (4.8), appears as a wave train with effective length $c/\Gamma$. Such a finite pulse of radiation is not exactly monochromatic but has a frequency spectrum covering an interval of the order $\Gamma$. The exact shape of the frequency spectrum is given by the square of the Fourier transform of the electric field. Thus, the amplitude spectrum is proportional to

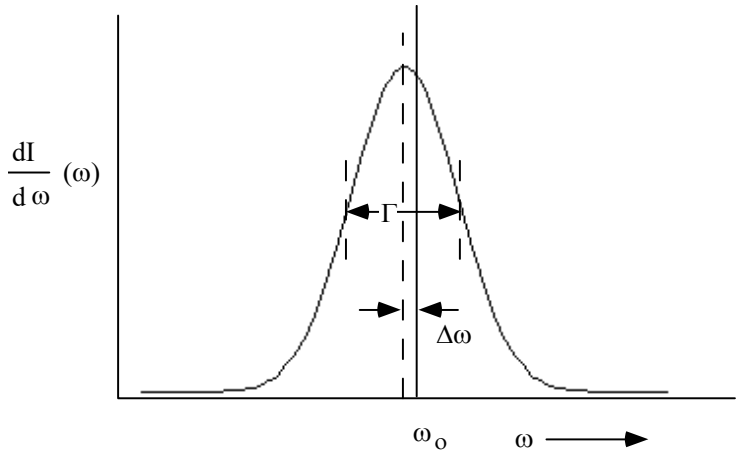
$$\mathbf{E}(\omega) \propto \int_0^\infty e^{-\alpha_t t} e^{-i\omega t}\, dt = \frac{1}{\alpha_t - i\omega} \tag{2.130}$$

The coefficient $\alpha_t$ corresponds to the spectroscopic linewidth and also to a shift in frequency that arises from the radiation reaction force between the electron and the photon. The energy radiated per unit frequency interval is therefore:

$$\frac{dI(\omega)}{d\omega} = I_0 \frac{\Gamma}{2\pi} \frac{1}{(\omega - \omega_0 - \Delta\omega)^2 + (\Gamma/2)^2} \tag{2.131}$$

where $I_0$ is the total energy radiated. The spectral distribution is called a resonant line shape. The width of the distribution at half-maximum intensity is called the half-width or line-breadth and is equal to $\Gamma$. Shown in Figure 2.4 is such a spectral line. Because of the reactive effects of radiation the line is shifted in frequency. The small radiative shift of the energy levels of atoms was first observed by Lamb in 1947 [36] and is called the Lamb shift in his honor.

**Figure 2.4.** Broadening of the spectral line due to the rise-time and shifting of the spectral line due to the radiative reaction. The resonant line shape has width $\Gamma$. The level shift is $\Delta\omega$.




## HYDROGEN LAMB SHIFT

The Lamb shift corresponding to the transition energy from the $^2P_{1/2}$ state to the $^2S_{1/2}$ state of the hydrogen atom having the quantum numbers $n = 2,\ \ell = 1,\ m_\ell = 0$ and $n = 2,\ \ell = 0,\ m_\ell = 0$, respectively, is calculated from the radiation reaction force and the atom recoil energy due to photon emission. For a transition between initial and final states having quantum numbers $n_i$ and $n_f$, respectively, the time-averaged power density in the radiation zone is given by Eq. (2.104). The total radiated power $P$ given by integrating the Poynting power density (Eq. (2.104)) over the surface of a sphere at radius $r$ is given by Eq. (2.105). The corresponding radiation reaction force is derived from the relativistically corrected fields of the radiated power. Consider that the power is proportional to $\mathbf{E}\times\mathbf{H}$ and then $|H_\phi|^2$ (Eq. (2.104)). A radiation reaction force due to current flow to form the trigonometric current distribution of the $2P_{1/2}$ state from the uniform $2S_{1/2}$ state given in Sections 6.6, 12.10, and 17.3 of Jackson [37] achieves the condition that the sum of the mechanical momentum and electromagnetic momentum is conserved. Since the change in angular momentum between the initial and final atomic states is conserved by the photon's angular momentum, the angular momentum, **m**, of the emitted photon follows from the time-averaged angular-momentum density given by Eq. (24.61) of Jackson [2] in cgs units:

$$\mathbf{m} = \int \frac{1}{8\pi c} \mathrm{Re}\left[\mathbf{r}\times(\mathbf{E}\times\mathbf{B}^*)\right] dx^4 = \hbar \tag{2.132}$$

The corresponding energy, *E*, is given from the Poynting power density [38]:

$$E = \int \frac{c}{4\pi} \mathrm{Re}(\mathbf{E} \times \mathbf{H}^*) dx^4 = \hbar\omega \tag{2.133}$$

As shown by Eqs. (1.280-1.281) and Eq. (29.9), each of the magnetic and electric field is corrected by the product of the factors $2\pi$ and $\alpha$, respectively. Also, the field in excited states scales as $1/n$ due to the corresponding central field from the superposition of the excited-state photon's and proton's fields (Eqs. (2.17)). Thus, using each relativistic and central field correction given by $2\pi\alpha$ and $1/2$, respectively, and using the limit of $r = r_{n_i} - r_{n_f}$ with the radiation reaction perturbation with respect to $r$, the radiation reaction power $P_{RR}$ given by Eq. (2.105) is

$$P_{RR} = (2\pi\alpha)^2 \left(\frac{1}{2}\right)^2 \frac{\eta}{12\pi} \left(\frac{e\hbar}{m_e r^2}\right)^2 \tag{2.134}$$

The radiation reaction force $F_{RR}$ is given by the power (Eq. (2.108)) divided by the electron velocity $v$ (Eq. (1.35)):

$$\begin{aligned} F_{RR} &= \frac{P_{RR}}{v} \\ &= (2\pi\alpha)^2 \frac{\frac{\eta}{48\pi}\left(\frac{e\hbar}{m_e r^2}\right)^2}{\frac{\hbar}{m_e r}} \\ &= (2\pi\alpha)^2 \frac{\eta}{48\pi} \frac{e^2\hbar}{m_e r^3} \end{aligned} \tag{2.135}$$

The radius of the hydrogen atom given by Eqs. (2.4-2.5) and Eq. (1.253), with $n = 2$, is $r = 2a_H$. The radiation reaction force perturbs the force balance and consequently the radius between the electron and proton relative to the condition in its absence. The outward centrifugal force on the electron is balanced by the electric force and the magnetic force (Eqs. (1.253) and (2.4)), and the radiation reaction force (Eq. (2.135)) corresponding to the current flow to achieve the current distribution of the $2P_{1/2}$ state:

$$\frac{m_e v^2}{r} = \frac{\hbar^2}{m_e r^3} = \frac{0.5e^2}{4\pi\varepsilon_0 r^2} - \frac{\hbar^2}{m_P r^3} + (2\pi\alpha)^2 \frac{\eta}{48\pi} \frac{e^2\hbar}{m_e r^3} \tag{2.136}$$

$$r = 2a_H - (2\pi\alpha)^2 \frac{\hbar}{6m_e c} \tag{2.137}$$

$$r = 1.99999744 a_H \tag{2.138}$$

where Eq. (1.35) was used for the velocity and $a_H$ is the radius of the hydrogen atom given by Eq. (1.259).

## ENERGY CALCULATIONS

The change in the electric energy of the electron $\Delta E_{ele}^{H\ Lamb}$ due to the slight shift of the radius of the atom is given by the difference between the electric energies associated with the unperturbed and radiation-reaction-force-perturbed radius. Each electric energy is given by the substitution of the corresponding radius given by Eq. (2.138) into Eqs. (1.264) and (2.4):

$$\Delta E_{ele}^{H\ Lamb} = \frac{-0.5e^2}{8\pi\varepsilon_0}\left[\frac{1}{r_0} - \frac{1}{r_-}\right] = 6.95953\ X\ 10^{-25}\ J \tag{2.139}$$

wherein the unperturbed radius given by Eq. (2.5) is $r_0 = 2a_H$.

In addition, the change in the magnetic energy $\Delta E_{mag}^{H\ Lamb}$ of the electron is given by Eqs. (1.161-1.162) with the substitution of the corresponding radii:

$$\begin{aligned} \Delta E_{mag}^{H\ Lamb} &= \frac{\pi\mu_0 e^2\hbar^2}{m_e^{\ 2}}\left(\frac{1}{r_0^3} - \frac{1}{r_-^3}\right) \\ &= 4\pi\mu_0\mu_B^2\left(\frac{1}{r_0^3} - \frac{1}{r_-^3}\right) \\ &= -4.38449\ X\ 10^{-27}\ J \end{aligned} \tag{2.140}$$

where $\mu_B$ is the Bohr magneton.

The $n = 2$ state comprises an electron, a photon, and a proton having the analytical solution of Maxwell's equations given by Eq. (2.15). The recoil energy of this photon gives rise to an energy contribution to the Lamb shift that is calculated by applying conservation of energy and linear momentum to the emitted photon and atom. The photon emitted by an excited state atom carries away energy, linear momentum, and angular momentum. The initial and final values of the energies and

momentum must be conserved between the atom, the electron, and the photon[6]. Consider an isolated atom of mass $M$ having an electron in an excited state level at an energy $E$. The atom is moving with velocity $\mathbf{V}$ along the direction in which the excited-state photon is to be emitted (the components of motion perpendicular to this direction remain unaffected by the emission and may be ignored). The energy above the "ground" state at rest is

$$\left(E+\frac{1}{2}M\mathbf{V}^2\right) \tag{2.141}$$

When a photon of energy $E_{h\upsilon}$ is emitted, the atom and/or electron recoils and has a new velocity

$$\mathbf{V}+\mathbf{v} \tag{2.142}$$

(which is a vector sum in that $\mathbf{V}$ and $\mathbf{v}$ may be opposed), and a total energy of:

$$\frac{1}{2}M\left(\mathbf{V}+\mathbf{v}\right)^2 \tag{2.143}$$

By conservation of energy,

$$E+\frac{1}{2}M\mathbf{V}^2=E_{h\upsilon}+\frac{1}{2}M\left(\mathbf{V}+\mathbf{v}\right)^2 \tag{2.144}$$

so, that the actual energy of the photon emitted is given by:

$$E_{h\upsilon}=E-\frac{1}{2}M\mathbf{v}^2-M\mathbf{v}\mathbf{V} \tag{2.145}$$

$$E_{h\upsilon}=E-E_R-E_D$$

The photon is thus deficient in energy by a recoil kinetic energy

$$E_R=\frac{1}{2}M\mathbf{v}^2 \tag{2.146}$$

which is independent of the initial velocity $\mathbf{V}$, and by a thermal or Doppler energy

$$E_D=M\mathbf{v}\mathbf{V} \tag{2.147}$$

which depends on $\mathbf{V}$; therefore, it can be positive or negative.

Momentum must also be conserved in the emission process. The energy, $E$, of the photon is given by Eq. (4.8)

$$E=\hbar\omega=h\frac{\omega}{2\pi}=h\nu=hf=h\frac{c}{\lambda} \tag{2.148}$$

From special relativity,

$$E=\hbar\omega=mc^2 \tag{2.149}$$

Thus, $\mathbf{p}$, the momentum of the photon is:

$$\mathbf{p}=mc=\frac{E_{h\nu}}{c} \tag{2.150}$$

where $c$ is the velocity of light, so that:

$$M\mathbf{V}=M\left(\mathbf{V}+\mathbf{v}\right)+\frac{E_{h\nu}}{c} \tag{2.151}$$

And, the recoil momentum is:

$$M\mathbf{v}=-\frac{E_{h\nu}}{c} \tag{2.152}$$

Thus, the recoil energy is given by:

$$E_R=\frac{E_{h\nu}^2}{2Mc^2} \tag{2.153}$$

and depends on the mass of the atom and the energy of the photon. The Doppler energy, $E_D$, is dependent on the thermal motion of the atom, and will have a distribution of values which is temperature dependent. A mean value, $E_D$, can be defined which is related to $\bar{E}_K$, the mean kinetic energy per translational degree of freedom [39-40]:

$$\bar{E}_D\cong\frac{1}{2}kT \tag{2.154}$$

by

$$\bar{E}_D\cong 2\sqrt{E_K E_R}=E_{h\nu}\sqrt{\frac{2\bar{E}_K}{Mc^2}} \tag{2.155}$$

where $k$ is Boltzmann's constant and $T$ is the absolute temperature[7]. As a result, the statistical distribution in energy of the emitted photons is displaced from the true excited-state energy by $-E_R$ and broadened by $E_D$ into a Gaussian distribution of width $2\bar{E}_D$. The distribution for absorption has the same shape but is displaced by $+E_R$.

[6] Conservation of angular momentum is used to derive the photon's equation in the Equation of the Photon section.

[7] This relationship may also apply to an electron undergoing bonding as given in the Doppler Energy Term of Hydrogen-Type Molecular Ions section.

For the photon of the hydrogen atom, the linear momentum of the emitted photon is balanced by the recoil momentum of the entire atom of mass $m_H$, and the corresponding recoil energy adds to the energy due to the radiation reaction force. The recoil energy $E_{recoil}^{H\ Lamb}$ for the electron in the $n=2$ and the corresponding frequency shift $\Delta f_{recoil}^{H\ Lamb}$ of the hydrogen atom is given by Eq. (2.153):

$$E_{recoil}^{H\ Lamb} = \frac{\left(E_{h\upsilon}\right)^2}{2m_H c^2} = 8.87591\ X\ 10^{-27}\ J \tag{2.156}$$

$$\Delta f_{recoil}^{H\ Lamb} = \frac{\Delta\omega}{2\pi} = \frac{\left(E_{h\upsilon}\right)^2}{2hm_H c^2} = 13.40\ MHz \tag{2.157}$$

where $E_{h\upsilon}$ corresponds to the recoil energy (Eqs. (2.153) and (2.22)) is

$$E_{h\upsilon} = -13.5983\ eV\left(1-\frac{1}{n^2}\right) \tag{2.158}$$

wherein $n=2$ [8].

Then, the total energy of the hydrogen Lamb shift is given by the sum of Eqs. (2.139-2.140) and (2.156):

$$\begin{aligned}\Delta E_{total}^{H\ Lamb} &= \Delta E_{ele}^{H\ Lamb} + \Delta E_{mag}^{H\ Lamb} + E_{recoil}^{H\ Lamb} \\ &= 6.95953\ X\ 10^{-25}\ J - 4.38449\ X\ 10^{-27}\ J + 8.87591\ X\ 10^{-27}\ J \\ &= 7.00445\ X\ 10^{-25}\ J\end{aligned} \tag{2.159}$$

The Planck relationship (Eq. (2.148)) gives $\Delta f_{total}^{H\ Lamb}$, the Lamb shift energy expressed in terms of frequency:

$$\Delta f_{total}^{H\ Lamb} = \frac{\left|\Delta E_{total}^{H\ Lamb}\right|}{h} = 1057.09\ MHz \tag{2.160}$$

The experimental Lamb shift is [42]

$$\Delta f_{total}^{H\ Lamb}\left(\text{experimental}\right) = 1057.845\ MHz \tag{2.161}$$

There is good agreement between the theoretical and experimental values given the 100 MHz natural linewidth of the $2P$ state. The 0.07% relative difference is within the propagated errors in the fundamental constants of the equations. In addition to the Lamb shift, the spectral lines of hydrogen are Zeeman split by spin-orbit coupling and electron-nuclear magnetic interactions given in the Fine Structure and Hyperfine Structure sections, respectively.

## MUONIC HYDROGEN LAMB SHIFT

The Lamb shift corresponding to the transition energy from the ${}^2P_{1/2}$ state to the ${}^2S_{1/2}$ state of the muonic hydrogen atom having the quantum numbers $n=2,\ \ell=1,\ m_\ell=0$ and $n=2,\ \ell=0,\ m_\ell=0$, respectively, is also calculated from the radiation reaction force and the atom recoil energy due to photon emission. The radiation reaction force $F_{RR}$ of muonic hydrogen comprises three terms that follow from Eq. (2.135) and arise from lepton-photon-momentum transfer during the ${}^2P_{1/2} \rightarrow {}^2S_{1/2}$ transition wherein the photon couples with the three possible states of the electron mass corresponding to the three possible leptons. The electron, muon, and tau masses are based on the relativistic corrections of the Planck, electric, and magnetic energies, respectively, as given in Eq. (32.48). The masses of the heavier leptons, the muon and tau are dependent on the first lepton's mass, the electron mass, and each can be considered a relativistic effect of the electron mass. Specifically, the muon is a resonant state of an electron given by a relativistic effect of the electron mass as given by Eqs. (36.5-36.6), wherein the muon decays to the electron:

$$2\pi\frac{\hbar}{m_\mu c^2} = 2\pi\sec\sqrt{\frac{2Gm_e\alpha^2 m_\mu}{c\hbar}} \tag{2.162}$$

$$m_\mu = \frac{\hbar}{c}\left(\frac{1}{2Gm_e\left(\alpha\sec\right)^2}\right)^{\frac{1}{3}} = 1.8874\ X\ 10^{-28}\ kg \tag{2.163}$$

Likewise, the tau mass having a dependency on the electron mass is given by Eqs. (36.7-36.8):

$$2\pi\frac{\hbar}{m_\tau c^2} = 2\sec\sqrt{\frac{2Gm_e(2\pi)^2\alpha^4 m_\tau}{c\hbar}} \tag{2.164}$$

$$m_\tau = \frac{\hbar}{c}\left(\frac{1}{2Gm_e}\right)^{\frac{1}{3}}\left(\frac{1}{2\sec\alpha^2}\right)^{\frac{2}{3}} = 3.1604\ X\ 10^{-27}\ kg \tag{2.165}$$

[8] As a further example, conservation of linear momentum of the photon is central to the Mössbauer phenomenon. See Mills patent [41].

Thus, the radiation reaction force of relativistic origin is determined by the action on the electron mass with each mass hierarchy requiring an additional relativistic correction factor of $2\pi\alpha$. Then, using Eqs. (2.135) and (32.48), the first radiation reaction term $(2\pi\alpha)^2$ regards the photon coupling to the electron whose mass is based on the Planck equation. The second term $(2\pi\alpha)^3$ regards the relativistically corrected electric energy whereby the photon couples to the electron via the muon, and the third term $(2\pi\alpha)^4$ regards the magnetic energy which is a relativistic correction to the electric energy whereby the photon couples to the electron via a possible tau state. The first and second radiation reaction terms are negative since the mass-energy of the electron and muon are less than or equal to the mass-energy of the bound particle in muonic H with the lower energy state being relative to the energy of the state involving an electron. The third term is positive since it is a loss term for a possible, but not obtained mass-energy state. The second and third terms involve lepton couplings between two and three leptons, respectively.

Since the magnetic force between the muon and proton magnetic moment given by Eqs. (1.243-1.252) is also a relativistic electrodynamic force involving the lepton mass, it must be corrected by the ratio of the electron to muon mass. The radiation reaction force in the muonic hydrogen atom also perturbs the force balance between the muon and proton relative to the condition in its absence. The outward centrifugal force on the muon is balanced by the electric force and the mass-ratio-corrected magnetic force (Eqs. (1.253) and (2.4)), and the three-term-expanded radiation reaction force (Eq. (2.135)) corresponding to the current flow to achieve the current distribution of the $2S_{1/2}$ from the $2P_{1/2}$ state:

$$\frac{m_\mu v^2}{r} = \frac{\hbar^2}{m_\mu r^3} = \frac{0.5e^2}{4\pi\varepsilon_0 r^2} - \frac{m_e}{m_\mu}\frac{\hbar^2}{m_P r^3} - \left[(2\pi\alpha)^2 + 2(2\pi\alpha)^3 - 3(2\pi\alpha)^4\right]\frac{\eta}{48\pi}\frac{e^2\hbar}{m_e r^3} \tag{2.166}$$

$$r = \frac{4\pi\varepsilon_0}{0.5e^2}\left[\frac{m_e}{m_\mu}\left(\frac{\hbar^2}{m_e} + \frac{\hbar^2}{m_P}\right) + \left[(2\pi\alpha)^2 + 2(2\pi\alpha)^3 - 3(2\pi\alpha)^4\right]\frac{\eta}{48\pi}\frac{e^2\hbar}{m_e}\right] \tag{2.167}$$

$$r = 2a_H\frac{m_e}{m_\mu} + \left[(2\pi\alpha)^2 + 2(2\pi\alpha)^3 - 3(2\pi\alpha)^4\right]\frac{\hbar}{6m_e c} \tag{2.168}$$

$$r = 2.0005735a_{\mu p} = 9.6755983\ X\ 10^{-3}a_H \tag{2.169}$$

where Eq. (1.35) was used for the velocity, $a_H$ is the radius of the hydrogen atom given by Eq. (1.259), and $a_{\mu p}$ is defined as $a_H\frac{m_e}{m_\mu}$. The radius in the absence of the radiation reaction force is $r_0 = 2a_{\mu p} = 9.6728246\ X\ 10^{-3}a_H$.

## ENERGY CALCULATIONS

The change in the electric energy of the muon $\Delta E_{ele}^{\mu p\ Lamb}$ due to the slight shift of the radius of the atom is given by the difference between the electric energies associated with the unperturbed and radiation-reaction-force-perturbed radius. Each electric energy is given by the substitution of the corresponding radius given by Eq. (2.167) into Eqs. (1.264) and (2.4):

$$\Delta E_{ele}^{\mu p\ Lamb} = \frac{-0.5e^2}{8\pi\varepsilon_0}\left[\frac{1}{r_0} - \frac{1}{r_+}\right] = -3.22846\ X\ 10^{-20}\ J \tag{2.170}$$

wherein the unperturbed radius given by Eq. (2.5) and Eqs. (1.253-1.259) is $r_0 = 2a_{\mu p}$.

In addition, the change in the magnetic energy $\Delta E_{mag}^{\mu p\ Lamb}$ of the muon is given by Eqs. (1.161-1.162) with the substitution of the corresponding radii

$$\begin{aligned}\Delta E_{mag}^{\mu p\ Lamb} &= \frac{\pi\mu_0 e^2\hbar^2}{m_\mu^{\ 2}}\left(\frac{1}{r_0^3} - \frac{1}{r_+^3}\right)\\ &= 4\pi\mu_0\mu_{B_\mu}^2\left(\frac{1}{r_0^3} - \frac{1}{r_+^3}\right)\\ &= 2.03334\ X\ 10^{-22}\ J\end{aligned} \tag{2.171}$$

where $\mu_{B_\mu}$ is the muon Bohr magneton.

For the photon of the muonic hydrogen atom, the linear momentum of the emitted photon is balanced by the recoil momentum of the entire atom of mass $m_{\mu p}$, and the corresponding recoil energy adds to the energy due to the radiation reaction force. The recoil energy $E_{recoil}^{\mu p\ Lamb}$ for the muon in the $n = 2$ state and the corresponding frequency shift $\Delta f_{recoil}^{\mu p\ Lamb}$ of the muonic hydrogen atom is given by Eqs. (2.153):

$$E_{recoil}^{\mu p\ Lamb} = -\frac{(E_{h\upsilon})^2}{2m_{\mu p}c^2} = -3.41241\ X\ 10^{-22}\ J \tag{2.172}$$

$$\Delta f_{recoil}^{\mu p\ Lamb} = \frac{\Delta\omega}{2\pi} = \frac{\left(E_{h\upsilon}\right)^2}{\left|2hm_{\mu p}c^2\right|} = 514.99\ GHz \tag{2.173}$$

where $E_{h\upsilon}$ corresponds to the recoil energy (Eqs. (2.153) and (2.22)) for muonic H is:

$$E_{h\upsilon} = -13.5983\frac{m_\mu}{m_e}\ eV\left(1-\frac{1}{n^2}\right) = -2811.67\ eV\left(1-\frac{1}{n^2}\right) \tag{2.174}$$

wherein $n = 2$.

Then, the total energy of the muonic hydrogen Lamb shift corresponding to the transition ${}^2P_{1/2} \rightarrow {}^2S_{1/2}$ is given by the sum of Eqs. (2.170-2.172):

$$\begin{aligned}\Delta E_{total}^{\mu p\ Lamb} &= \Delta E_{ele}^{\mu p\ Lamb} + \Delta E_{mag}^{\mu p\ Lamb} + E_{recoil}^{\mu p\ Lamb} \\ &= -3.22846\ X\ 10^{-20}\ J + 2.03334\ X\ 10^{-22}\ J - 3.41241\ X\ 10^{-22}\ J \\ &= -3.24225\ X\ 10^{-20}\ J\end{aligned} \tag{2.175}$$

The Planck relationship (Eq. (2.148)) gives $\Delta f_{total}^{\mu p\ Lamb}$, the magnitude of the muonic hydrogen Lamb shift energy corresponding to the transition ${}^2P_{1/2} \rightarrow {}^2S_{1/2}$ expressed in terms of frequency:

$$\Delta f_{total}^{\mu p\ Lamb} = \frac{\left|\Delta E_{total}^{\mu p\ Lamb}\right|}{h} = 48{,}931.0\ GHz \tag{2.176}$$

The literature energies for $E_{2P_{3/2}^{F=2}\rightarrow 2P_{1/2}}$, the ${}^2P_{3/2}^{F=2}$ level shift with respect to the unperturbed ${}^2P_{1/2}$ level, and, $E_{2S_{1/2}^{F=1}}$, the ${}^2S_{1/2}^{F=1}$ level shift with respect to the unperturbed ${}^2S_{1/2}$ level, are [43]:

$$E_{2P_{3/2}^{F=2}\rightarrow 2P_{1/2}} = 9.6243\ meV = 1.54199\ X\ 10^{-21}\ J \tag{2.177}$$

$$E_{2S_{1/2}^{F=1}} = 5.7037\ meV = 9.13841\ X\ 10^{-22}\ J \tag{2.178}$$

Then, using Eqs. (2.175) and (2.177-2.178), the total energy of the muonic hydrogen Lamb shift corresponding to the transition ${}^2P_{3/2}\ F=2 \rightarrow {}^2S_{1/2}\ F=1$ is:

$$\begin{aligned}\Delta E_{total}^{\mu p\ Lamb\ {}^2P_{3/2}\ F=2\rightarrow {}^2S_{1/2}\ F=1} &= \Delta E_{total}^{\mu p\ Lamb} - E_{2P_{3/2}^{F=2}\rightarrow 2P_{1/2}} + E_{2S_{1/2}^{F=1}} \\ &= -3.24225\ X\ 10^{-20}\ J - 1.54199\ X\ 10^{-21}\ J + 9.13841\ X\ 10^{-22}\ J \\ &= -3.30507\ X\ 10^{-20}\ J\end{aligned} \tag{2.179}$$

The Planck relationship (Eq. (2.148)) gives $\Delta f_{total}^{\mu p\ Lamb\ {}^2P_{3/2}\ F=2\rightarrow {}^2S_{1/2}\ F=1}$, the magnitude of the muonic hydrogen Lamb shift energy expressed in terms of frequency:

$$\Delta f_{total}^{\mu p\ Lamb\ {}^2P_{3/2}\ F=2\rightarrow {}^2S_{1/2}\ F=1} = \frac{\left|\Delta E_{total}^{\mu p\ Lamb\ {}^2P_{3/2}\ F=2\rightarrow {}^2S_{1/2}\ F=1}\right|}{h} = 49{,}879.0\ GHz \tag{2.180}$$

The magnitude of the experimental muonic hydrogen Lamb shift matching the ${}^2S_{1/2}$ state lower than the ${}^2P_{1/2}$ and states ${}^2P_{3/2}$ is [43]:

$$\Delta f_{total}^{\mu p\ Lamb\ {}^2P_{3/2}\ F=2\rightarrow {}^2S_{1/2}\ F=1}\left(\text{experimental}\right) = 49{,}881.88\ GHz \tag{2.181}$$

There is good agreement between the theoretical and experimental values given the 18.6 GHz natural linewidth of the $2P$ state. The 0.0058% relative difference is within the measurement error and propagated errors in the fundamental constants of the equations. For example, the relative difference is 0.0025% using the 2002 CODATA constants [44]. These results solve the proton radius puzzle wherein QED erroneously invokes the proton radius in computation of the muonic hydrogen Lamb shift.

## HYDROGEN SPIN-ORBIT COUPLING (FINE STRUCTURE)

For the $2P$ level, the possible quantum numbers are $n = 2,\ \ell = 1,\ m_\ell = 0$ and $n = 2,\ \ell = 1,\ m_\ell = \pm 1$ corresponding to the states ${}^2P_{1/2}$ and ${}^2P_{3/2}$, respectively. Thus, for $\ell = 1$, the electron may or may not possess orbital angular momentum in addition to spin angular momentum corresponding to $m_\ell = \pm 1$ and $m_\ell = 0$, respectively. As a consequence, the energy of the $2P$ level is split by a relativistic interaction between the spin and orbital angular momentum as well as the corresponding radiation reaction force. The corresponding energy for the transition ${}^2P_{1/2} \rightarrow {}^2P_{3/2}$ is known as the hydrogen fine structure.

The electron's motion in the hydrogen atom is always perpendicular to its radius; consequently, as shown by Eq. (1.37), the electron's angular momentum of $\hbar$ is invariant. Furthermore, the electron is nonradiative due to its angular motion as shown in Appendix I and the Stability of Atoms and Hydrinos section. The radiative instability of excited states is due to a radial dipole term in the function representative of the excited state due to the interaction of the photon and the excited-state electron as shown in the Instability of Excited States section. The angular momentum of the photon given in the Equation of the Photon section is given by Eqs. (2.132) and (4.1). It is conserved for the solutions for the resonant photons and excited-state electron functions

given in the Excited States of the One-Electron Atom (Quantization) section and the Equation of the Photon section. Thus, the electrodynamic angular momentum and the inertial angular momentum are matched such that the correspondence principle holds. It follows from the principle of conservation of angular momentum that $\frac{e}{m_e}$ of Eq. (1.131) is invariant (See the Determination of Atomic Orbital Radii section).

A magnetic field is a relativistic effect of the electrical field as shown by Jackson [21]. No energy term is associated with the magnetic field of the electron of the hydrogen atom unless another source of magnetic field is present. In the case of spin-orbit coupling, the invariant $\hbar$ of spin angular momentum and orbital angular momentum each give rise to a corresponding invariant magnetic moment of a Bohr magneton, and their corresponding energies superimpose as given in the Orbital and Spin Splitting section. The interaction of the two magnetic moments gives rise to a relativistic spin-orbit coupling energy. The vector orientations of the momentum must be considered as well as the condition that flux must be linked by the electron in units of the magnetic flux quantum in order to conserve the invariant electron angular momentum of $\hbar$. The energy may be calculated with the additional conditions of the invariance of the electron's charge and charge-to-mass ratio $\frac{e}{m_e}$.

As shown in the Electron g Factor section (Eq. (1.181)), flux must be linked by the electron atomic orbital in units of the magnetic flux quantum that treads the atomic orbital at $v = c$ with a corresponding energy of:

$$E_{mag}^{fluxon} = 2\frac{\alpha}{2\pi}\mu_B B \tag{2.182}$$

As shown in the Atomic Orbital Equation of Motion for $\ell = 0$ Based on the Current Vector Field (CVF) section, the Two-Electron Atoms section, and Appendix VI, the maximum projection of the rotating spin angular momentum of the electron onto an axis is $\sqrt{\frac{3}{4}}\hbar$. From Eq. (2.65), the magnetic flux due to the spin angular momentum of the electron is [20]:

$$\mathbf{B} = \frac{\mu_0 \mu}{r^3} = \frac{\mu_0 e\hbar}{2m_e r_2^3}\sqrt{\frac{3}{4}} \tag{2.183}$$

where $\mu$ is the magnetic moment. The maximum projection of the orbital angular momentum onto an axis is $\hbar$ as shown in the Orbital and Spin Splitting section with a corresponding magnetic moment of a Bohr magneton $\mu_B$. Substitution of the magnetic moment of $\mu_B$ corresponding to the orbital angular momentum and Eq. (2.183) for the magnetic flux corresponding to the spin angular momentum into Eq. (2.182) gives the spin-orbit coupling energy $E_{s/o}$.

$$E_{s/o} = 2\frac{\alpha}{2\pi}\mu_B B = 2\frac{\alpha}{2\pi}\left(\frac{e\hbar}{2m_e}\right)\frac{\mu_0 e\hbar}{2m_e r^3}\sqrt{\frac{3}{4}} \tag{2.184}$$

The Bohr magneton corresponding to the orbital angular momentum is invariant and the corresponding invariant electron charge $e$ is common with that which gives rise to the magnetic field due to the spin angular momentum. The condition that the magnetic flux quantum treads the atomic orbital at $v = c$ with the maintenance of the invariance of the electron's charge-to-mass ratio $\frac{e}{m_e}$ and electron angular momentum of $\hbar$ requires that the radius and the electron mass of the magnetic field term of Eq. (2.184) be relativistically corrected. As shown by Eq. (1.280) and in Appendix I and the Determination of Atomic Orbital Radii sections, the relativistically corrected radius $r^*$ follows from the relationship between the electron wavelength and the radius.

$$2\pi r = \lambda \tag{2.185}$$

The phase matching condition requires that the electron wavelength be the same for orbital and spin angular momentum. Using Eq. (1.280) with $v = c$:

$$r^* = \lambda \tag{2.186}$$

Thus,

$$r^* = \frac{r}{2\pi} \tag{2.187}$$

The relativistically corrected mass $m^*$ follows from Eq. (2.187) with maintenance of the invariance of the electron angular momentum of $\hbar$ given by Eqs. (1.35) and (1.37).

$$m\mathbf{r} \times \mathbf{v} = m_e r \frac{\hbar}{m_e r} \tag{2.188}$$

With Eq. (2.187), the relativistically corrected mass $m^*$ is:

$$m^* = 2\pi m_e \tag{2.189}$$

With the substitution of Eq. (2.187) and Eq. (2.189) into Eq. (2.184), the spin-orbit coupling energy $E_{s/o}$ is given by

$$E_{s/o} = 2\frac{\alpha}{2\pi}\left(\frac{e\hbar}{2m_e}\right)\frac{\mu_0 e\hbar}{2\left(2\pi m_e\right)\left(\frac{r}{2\pi}\right)^3}\sqrt{\frac{3}{4}} = \frac{\alpha\pi\mu_0 e^2\hbar^2}{m_e^2 r^3}\sqrt{\frac{3}{4}} \tag{2.190}$$

(The magnetic field in this case is equivalent to that of a point electron at the origin with $\sqrt{\frac{3}{4}}\hbar$ of angular momentum.)

In the case that $n=2$, the radius given by Eq. (2.5) is $r=2a_0$. The predicted energy difference between the $^2P_{1/2}$ and $^2P_{3/2}$ levels of the hydrogen atom, $E_{s/o}$, given by Eq. (2.190) is:

$$E_{s/o}=\frac{\alpha\pi\mu_0 e^2\hbar^2}{8m_e^2{a_0}^3}\sqrt{\frac{3}{4}} \tag{2.191}$$

wherein $\ell=1$ and both levels are equivalently Lamb shifted.

$E_{s/o}$ may be expressed in terms of the mass energy of the electron. The energy stored in the magnetic field of the electron atomic orbital (Eq. (1.183)) is:

$$E_{mag}=\frac{\pi\mu_0 e^2\hbar^2}{(m_e)^2 r_n^3} \tag{2.192}$$

As shown in the Pair Production section with the $v=c$ condition, the result of the substitution of $\alpha a_o=\lambda\!\!\!^{-}_C$ for $r_n$, the relativistic mass, $2\pi m_e$, for $m_e$, and multiplication by the relativistic correction, $\alpha^{-1}$, which arises from Gauss' law surface integral and the relativistic invariance of charge is:

$$E_{mag}=m_e c^2 \tag{2.193}$$

Thus, Eq. (2.191) can be expressed as:

$$E_{s/o}=\frac{\alpha^5(2\pi)^2}{8}m_e c^2\sqrt{\frac{3}{4}}=7.24043\ X\ 10^{-24}\ J \tag{2.194}$$

Using the Planck equation, the corresponding frequency, $\Delta f_{s/o}$, is:

$$\Delta f_{s/o}=10{,}927.02\ MHz \tag{2.195}$$

As in the case of the $^2P_{1/2}\rightarrow{}^2S_{1/2}$ transition, an additional term arises in the fine structure interval from the radiation reaction force involving electron-photon-momentum transfer during the $^2P_{1/2}\rightarrow{}^2P_{3/2}$ transition corresponding to the rotating orbital dipole that couples with the spin angular momentum. The radiation reaction force $F_{RR}$ is given by Eq. (2.135) having the additional relativistic correction factor of $2\pi\alpha$ with an additional geometrical correction factor of $\sqrt{\frac{3}{4}}$ matching the rotating projection of the spin angular momentum:

$$F_{RR}=(2\pi\alpha)^3\frac{\eta}{48\pi}\frac{e^2\hbar}{m_e r^3}\sqrt{\frac{3}{4}} \tag{2.196}$$

The outward centrifugal force on the electron is balanced by the electric force and the magnetic force (Eqs. (1.253) and (2.4)), and the radiation reaction force (Eq. (2.196)):

$$\frac{m_e v^2}{r}=\frac{\hbar^2}{m_e r^3}=\frac{0.5e^2}{4\pi\varepsilon_0 r^2}-\frac{\hbar^2}{m_P r^3}+(2\pi\alpha)^3\frac{\eta}{48\pi}\frac{e^2\hbar}{m_e r^3}\sqrt{\frac{3}{4}} \tag{2.197}$$

$$r=2a_H-(2\pi\alpha)^3\frac{\hbar}{6m_e c}\sqrt{\frac{3}{4}} \tag{2.198}$$

$$r=1.99999990a_H \tag{2.199}$$

where Eq. (1.35) was used for the velocity and $a_H$ is the radius of the hydrogen atom given by Eq. (1.259).

## ENERGY CALCULATIONS

The change in the electric energy of the electron $\Delta E_{ele}^{H\ FS}$ due to the slight shift of the radius of the atom is given by the difference between the electric energies associated with the unperturbed and radiation-reaction-force-perturbed radius. Each electric energy is given by the substitution of the corresponding radius given by Eq. (2.199) into Eqs. (1.264) and (2.4):

$$\Delta E_{ele}^{H\ FS}=\frac{-0.5e^2}{8\pi\varepsilon_0}\left[\frac{1}{r_0}-\frac{1}{r_-}\right]=2.76347\ X\ 10^{-26}\ J \tag{2.200}$$

wherein the unperturbed radius given by Eq. (2.5) is $r_0=2a_H$.

In addition, the change in the magnetic energy $\Delta E_{mag}^{H\ FS}$ of the electron is given by Eqs. (1.161-1.162) with the substitution of the corresponding radii:

$$\Delta E_{mag}^{H\ FS} = \frac{\pi\mu_0 e^2\hbar^2}{m_e^{\ 2}}\left(\frac{1}{r_0^3}-\frac{1}{r_-^3}\right)$$
$$= 4\pi\mu_0\mu_B^2\left(\frac{1}{r_0^3}-\frac{1}{r_-^3}\right) \tag{2.201}$$
$$= -1.74098\ X\ 10^{-28}\ J$$

where $\mu_B$ is the Bohr magneton.

Then, the total radiation reaction energy of the hydrogen fine structure $\Delta E_{RRtotal}^{H\ FS}$ is given by the sum of Eqs. (2.200-2.201):

$$\Delta E_{RRtotal}^{H\ FS} = \Delta E_{ele}^{H\ FS} + \Delta E_{mag}^{H\ FS}$$
$$= 2.76347\ X\ 10^{-26}\ J - 1.74098\ X\ 10^{-28}\ J \tag{2.202}$$
$$= 2.74606\ X\ 10^{-26}\ J$$

The Planck relationship (Eq. (2.148)) gives $\Delta f_{RRtotal}^{H\ FS}$, the radiation reaction energy contribution expressed in terms of frequency:

$$\Delta f_{RRtotal}^{H\ FS} = \frac{\left|\Delta E_{RRtotal}^{H\ FS}\right|}{h} = 41.44\ MHz \tag{2.203}$$

Then, the total energy of the hydrogen fine structure $\Delta E_{total}^{H\ FS}$ is given by the sum of Eqs. (2.194) and (2.202):

$$\Delta E_{total}^{H\ FS} = E_{s/o} + \Delta E_{RRtotal}^{H\ FS}$$
$$= 7.24043\ X\ 10^{-24}\ J + 2.74606\ X\ 10^{-26}\ J \tag{2.204}$$
$$= 7.26789\ X\ 10^{-24}\ J$$

The Planck relationship (Eq. (2.148)) gives $\Delta f_{total}^{H\ FS}$, the fine structure energy expressed in terms of frequency:

$$\Delta f_{total}^{H\ FS} = \frac{\left|\Delta E_{total}^{H\ FS}\right|}{h} = 10,968.46\ MHz \tag{2.205}$$

The experimental hydrogen fine structure is [42]

$$\Delta f_{total}^{H\ FS}\left(\text{experimental}\right) = 10,969.05\ MHz \tag{2.206}$$

The large natural widths of the hydrogen $2P$ levels limits the experimental accuracy [45]; yet, given this limitation, the agreement between the theoretical and experimental fine structure (0.005% relative difference) is excellent and within the cited and propagated errors.

## HYDROGEN KNIGHT SHIFT

In an external magnetic field, the unpaired electron of the hydrogen atom gives rise to a uniform magnetic field contribution at the nucleus which is given by Eq. (1.152).

$$\mathbf{H} = \frac{e\hbar}{m_e r_n^3}(\mathbf{i}_r\cos\theta - \mathbf{i}_\theta\sin\theta) \qquad r < r_n \tag{2.207}$$

Multiplication of Eq. (2.207) by the permeability of free space, $\mu_0$, and substitution of the Bohr radius of the hydrogen atom, $a_H$, given by Eq. (1.259) for $r_n$ of Eq. (2.207) gives the magnetic flux, $\mathbf{B_s}$, at the nucleus due to electron spin.

$$\mathbf{B_s} = \frac{\mu_0 e\hbar}{m_e a_H^3}\mathbf{i}_z = 157.29\ T \tag{2.208}$$

The shift of the NMR frequency of a nucleus by an unpaired electron is called the Knight Shift. The Knight Shift of the hydrogen atom is given by the magnetic flux (Eq. (2.208)) times the proton gyromagnetic ratio of $42.5775\ MHzT^{-1}$. The experimental value is unknown; however, magnetic hyperfine structure shifts of Mössbauer spectra corresponding to magnetic fluxes of 100 $T$ or more due to unpaired electrons are common.

## SPIN - NUCLEAR COUPLING (HYPERFINE STRUCTURE)

The radius of the hydrogen atom is increased or decreased very slightly due to the Lorentz force on the electron due to the magnetic field of the proton and its orientation relative to the electron's angular momentum vector. The additional small centripetal magnetic force is the relativistic corrected Lorentz force, $\mathbf{F}_{mag}$, as also given in the Two-Electron Atoms section and the Three- Through Twenty-Electron Atoms section.

The atomic orbital with $\ell = 0$ is a shell of negative charge current comprising correlated charge motion along great circles. The superposition of the vector projection of the atomic orbital angular momentum on the z-axis is $\mathbf{L}_z = \frac{\hbar}{2}$ (Eq. (1.128))

with an orthogonal component of $\mathbf{L}_{xy} = \frac{\hbar}{4}$ (Eq. (1.127)). The magnetic field of the electron at the nucleus due to $\mathbf{L}_z$ after McQuarrie [20] is

$$\mathbf{B} = \frac{\mu_0 e\hbar}{2m_e r^3} \tag{2.209}$$

where $\mu_0$ is the permeability of free-space ($4\pi\ X\ 10^{-7}\ N/A^2$). An electrodynamic force or radiation reaction force, a force dependent on the second derivative of the charge's position with respect to time, arises between the electron and the proton. This force given in Sections 6.6, 12.10, and 17.3 of Jackson [37] achieves the condition that the sum of the mechanical momentum and electromagnetic momentum is conserved.

The magnetic moment of the proton, $\mu_P$, aligns in the direction of $\mathbf{L}_z$, but experiences a torque due to the orthogonal component $\mathbf{L}_{xy}$. As shown in the Atomic Orbital Equation of Motion for $\ell = 0$ Based on the Current Vector Field (CVF) section, the magnetic field of the atomic orbital gives rise to the precession of the magnetic moment vector of the proton directed from the origin of the atomic orbital at an angle of $\theta = \frac{\pi}{3}$ relative to the z-axis. The precession of $\mu_P$ forms a cone in the nonrotating laboratory frame to give a perpendicular projection of:

$$\mu_{P\perp} = \pm\sqrt{\frac{3}{4}}\mu_P \tag{2.210}$$

after Eq. (1.129) and a projection onto the z-axis of:

$$\mu_{P\parallel} = \pm\frac{\mu_P}{2} \tag{2.211}$$

after Eq. (1.130). At torque balance, $\mathbf{L}_{xy}$ also precesses about the z-axis at 90° with respect to $\mu_{P\parallel}$. Using Eq. (2.209), the magnitude of the force $F_{mag}$ between the antiparallel field of the electron and $\mu_P$ is:

$$F_{mag} = \left|\frac{\mu_P \times \mathbf{B}}{r}\right| = \mu_P \frac{\mu_0 e\hbar}{2m_e r^4} \tag{2.212}$$

The radiation reaction force corresponding to photon emission or absorption is radial as given in the Equation of the Electric Field inside the Atomic Orbital section. The reaction force on the electron due to the force of the electron's field on the magnetic moment of the proton is the corresponding relativistic central force, $\mathbf{F}_{mag}$, which acts uniformly on each charge (mass)-density element of the electron. The magnetic central force is derived as follows from the Lorentz force which is relativistically corrected. The Lorentz force at each point of the electron moving at velocity $\mathbf{v}$ due to a magnetic flux $\mathbf{B}$ is:

$$\mathbf{F}_{mag} = e\mathbf{v} \times \mathbf{B} \tag{2.213}$$

Eqs. (2.212) and (2.213) may be expressed in terms of the electron velocity given by Eq. (1.35):

$$F_{mag} = \frac{\hbar}{m_e r}\frac{e\mu_0\mu_P}{2r^3} = \frac{e}{2}|\mathbf{v} \times \mathbf{B}| \tag{2.214}$$

where $\mathbf{B}$ is the magnetic flux of the proton at the electron. (The magnetic moment $\mathbf{m}$ of the proton is given by Eq. (37.29), and the magnetic field of the proton follows from the relationship between the magnetic dipole field and the magnetic moment $\mathbf{m}$ as given by Jackson [46] where $\mathbf{m} = \mu_P \mathbf{i}_z$.) In the lightlike frame, the velocity $\mathbf{v}$ is the speed of light, and $\mathbf{B}$ corresponds to the time-dependent component of the proton magnetic moment given by Eq. (2.210). Thus, the central force is:

$$\mathbf{F}_{mag} = \pm\frac{e\alpha c}{2}\frac{\mu_0}{r^3}\ \mu_P\sqrt{\frac{3}{4}} \tag{2.215}$$

where the relativistic factor from Eq. (1.249) is $\alpha$ (Eq. (1.205) also gives the velocity as $\alpha c$), the plus sign corresponds to antiparallel alignment of the magnetic moments of the electron and proton, and the minus sign corresponds to parallel alignment. The outward centrifugal force (Eq. (1.241)) on the electron is balanced by the electric force (Eq. (1.242)) and the magnetic forces given by Eqs. (1.252) and (2.215):

$$\frac{m_e v^2}{r} = \frac{e^2}{4\pi\varepsilon_0 r^2} - \frac{\hbar^2}{mr^3} \pm \frac{e\alpha c}{2}\frac{\mu_0}{r^3}\ \mu_P\sqrt{\frac{3}{4}} \tag{2.216}$$

Using Eq. (1.35),

$$\frac{\hbar^2}{m_e r^3} = \frac{e^2}{4\pi\varepsilon_0 r^2} - \frac{\hbar^2}{mr^3} \pm \frac{e\alpha c}{2}\frac{\mu_0}{r^3}\ \mu_P\sqrt{\frac{3}{4}} \tag{2.217}$$

$$\frac{\hbar^2}{m_e r^3} + \frac{\hbar^2}{mr^3} = \frac{e^2}{4\pi\varepsilon_0 r^2} \pm \frac{e\alpha c}{2}\frac{\mu_0}{r^3}\ \mu_P\sqrt{\frac{3}{4}} \tag{2.218}$$

$$\frac{\hbar^2}{\mu_e} \pm \frac{e\alpha c\mu_0\ \mu_P}{2}\sqrt{\frac{3}{4}} = \frac{e^2}{4\pi\varepsilon_0} r \tag{2.219}$$

$$r = a_H \pm \frac{4\pi\varepsilon_0}{2e^2} e\alpha c\mu_0 \ \mu_P \sqrt{\frac{3}{4}} \tag{2.220}$$

$$r = a_H \pm \frac{2\pi\alpha \ \mu_P}{ec} \sqrt{\frac{3}{4}} \tag{2.221}$$

where $\mu_e$ is the reduced electron mass given by Eq. (1.255), $a_H$ is the Bohr radius of the hydrogen atom given by Eq. (1.259), the plus sign corresponds to parallel alignment of the magnetic moments of the electron and proton, and the minus sign corresponds to antiparallel alignment.

## ENERGY CALCULATIONS

The magnetic energy to flip the orientation of the proton's magnetic moment, $\mu_P$, from antiparallel to parallel to the direction of the magnetic flux $\mathbf{B}_s$ of the electron (180° rotation of the magnetic moment vector) given by Eqs. (1.168), (2.209), and (2.210) is:

$$\Delta E_{mag}^{\text{proton spin}} = -\frac{\mu_0 e\hbar}{2m_e} \mu_P \sqrt{\frac{3}{4}} \left( \frac{1}{r_+^3} + \frac{1}{r_-^3} \right) = -\mu_0 \mu_B \mu_P \sqrt{\frac{3}{4}} \left( \frac{1}{r_+^3} + \frac{1}{r_-^3} \right) = -1.918365 \ X \ 10^{-24} \ J \tag{2.222}$$

where the Bohr magneton, $\mu_B$, is given by Eq. (1.131).

The change in the electric energy of the electron due to the slight shift of the radius of the electron is given by the difference between the electric energies associated with the two possible orientations of the magnetic moment of the electron with respect to the magnetic moment of the proton, parallel versus antiparallel. Each electric energy is given by the substitution of the corresponding radius given by Eq. (2.221) into Eq. (1.264). The change in electric energy for the flip from antiparallel to parallel alignment, $\Delta E_{ele}^{S/N}$, is:

$$\Delta E_{ele}^{S/N} = \frac{-e^2}{8\pi\varepsilon_0} \left[ \frac{1}{r_+} - \frac{1}{r_-} \right] = 9.597048 \ X \ 10^{-25} \ J \tag{2.223}$$

In addition, the interaction of the magnetic moments of the electron and proton increases the magnetic energy, $E_{mag}$, of the electron given by Eqs. (1.161-1.162). The term of $E_{mag}$ for the hyperfine structure of the hydrogen atom is similar to that of muonium given by Eq. (2.244) in the Muonium Hyperfine Structure Interval section:

$$\begin{aligned} E_{mag} &= -\left( 1 + \left( \frac{2}{3} \right)^2 + \alpha \left( \cos\frac{\pi}{3} \right)^2 \right) \frac{\pi\mu_0 e^2\hbar^2}{m_e^{\ 2}} \left( \frac{1}{r_+^3} - \frac{1}{r_-^3} \right) \\ &= -\left( 1 + \left( \frac{2}{3} \right)^2 + \frac{\alpha}{4} \right) 4\pi\mu_0 \mu_B^2 \left( \frac{1}{r_+^3} - \frac{1}{r_-^3} \right) \\ &= 1.748861 \ X \ 10^{-26} \ J \end{aligned} \tag{2.224}$$

where the contribution corresponding to electron spin gives the first term, 1, and the second term, $\left( \frac{2}{3} \right)^2$, corresponds to the rotation of the electron about the z-axis corresponding to the precession of $\mathbf{L}_{xy}$. The geometrical factor of $\frac{2}{3}$ for the rotation is given in the Derivation of the Magnetic Field section in Chapter One (Eq. (1.140)) and by Eq. (11.391), and the energy is proportional to the magnetic field strength squared according to Eq. (1.154). The relativistic factor from Eq. (1.249) and Eqs. (1.161) and (2.190) is $\alpha$ times $\left( \cos\frac{\pi}{3} \right)^2$ where the latter term is due to the nuclear magnetic moment oriented $\theta = \frac{\pi}{3}$ relative to the z-axis. The energy is proportional to the magnetic field strength squared according to Eq. (1.154).

The total energy of the transition from antiparallel to parallel alignment, $\Delta E_{total}^{S/N}$, is given as the sum of Eqs. (2.222-2.224):

$$\begin{aligned} \Delta E_{total}^{S/N} &= \Delta E_{mag}^{\text{proton spin}} + \Delta E_{ele}^{S/N} + E_{mag} \\ &= -1.918365 \ X \ 10^{-24} \ J + 9.597048 \ X \ 10^{-25} \ J + 1.748861 \ X \ 10^{-26} \ J \\ &= -9.411714 \ X \ 10^{-25} \ J \end{aligned} \tag{2.225}$$

The energy is expressed in terms of wavelength using the Planck relationship, Eq. (2.148):

$$\lambda_{total}^{S/N} = \frac{hc}{\Delta E_{total}^{S/N}} = 21.10610\ cm \tag{2.226}$$

The experimental value from the hydrogen maser is [47]:

$$\lambda_{total}^{S/N} = 21.10611\ cm \tag{2.227}$$

The 21 cm line is important in astronomy for the determination of the presence of hydrogen. There is remarkable agreement between the calculated and experimental values of the hyperfine structure that is only limited by the accuracy of the fundamental constants in Eqs. (2.221-2.224).

## MUONIUM HYPERFINE STRUCTURE INTERVAL

Muonium ( $\mu^+e^-$, $M$ ) is the hydrogenlike bound state of a positive muon and an electron. The solution of the ground state ($1^2S_{1/2}$) hyperfine structure interval of muonium, $\Delta\nu_{Mu}$, is similar to that of the hydrogen atom. The electron binds to the muon as both form concentric atomic orbitals with a minimization of energy. The outward centrifugal force (Eq. (1.241)) on the outer electron is balanced by the electric force (Eq. (1.242)) and the magnetic forces due to the inner positive muon given by Eqs. (1.252) and (2.215). The resulting force balance equation is the same as that for the hydrogen atom given by Eq. (2.216) with the muon mass, $m_\mu$, replacing the proton mass, $m$, and the muon magnetic moment, $\mu_\mu$, replacing the proton magnetic moment, $\mu_P$. The radius of the electron, $r_2$, is given by:

$$\frac{m_e v^2}{r_2} = \frac{e^2}{4\pi\varepsilon_0 r_2^2} - \frac{\hbar^2}{m_\mu r_2^3} \pm \frac{e\alpha c}{2}\frac{\mu_0}{r_2^3}\ \mu_\mu\sqrt{\frac{3}{4}} \tag{2.228}$$

Using Eq. (1.35),

$$\frac{\hbar^2}{m_e r_2^3} = \frac{e^2}{4\pi\varepsilon_0 r_2^2} - \frac{\hbar^2}{m_\mu r_2^3} \pm \frac{e\alpha c}{2}\frac{\mu_0}{r_2^3}\ \mu_\mu\sqrt{\frac{3}{4}} \tag{2.229}$$

$$\frac{\hbar^2}{\mu_{e,\mu}} \pm \frac{e\alpha c\mu_0\ \mu_\mu}{2}\sqrt{\frac{3}{4}} = \frac{e^2}{4\pi\varepsilon_0} r_2 \tag{2.230}$$

$$r_2 = a_\mu \pm \frac{2\pi\alpha\ \mu_\mu}{ec}\sqrt{\frac{3}{4}} \tag{2.231}$$

$$r_{2+} = a_\mu + \frac{2\pi\alpha\ \mu_\mu}{ec}\sqrt{\frac{3}{4}} = 5.31736859\ X\ 10^{-11}\ m \tag{2.232}$$

$$r_{2-} = a_\mu - \frac{2\pi\alpha\ \mu_\mu}{ec}\sqrt{\frac{3}{4}} = 5.31736116\ X\ 10^{-11}\ m \tag{2.233}$$

where $\mu_{e,\mu}$ is the reduced muonium-electron mass given by Eq. (1.255) with the mass of the proton replaced by the mass of the muon, $a_\mu$ is the Bohr radius of the muonium atom given by Eq. (1.259) with the reduced electron mass, $\mu_e$ (Eq. (1.255)), replaced by $\mu_{e,\mu}$. The plus sign corresponds to parallel alignment of the magnetic moments of the electron and muon, and the minus sign corresponds to antiparallel alignment.

The radii of the muon, $r_1$, in different spin states can be determined from $r_2$, the radii of the electron (Eqs. (2.232-2.233)), and the opposing forces on the muon due to the bound electron. The outward centrifugal force (Eq. (1.241)) on the muon is balanced by the reaction forces given by Eq. (2.228):

$$\frac{m_\mu v^2}{r_1} = \frac{\hbar^2}{m_e r_2^3} \pm \frac{e\alpha c}{2}\frac{\mu_0}{r_2^3}\ \mu_\mu\sqrt{\frac{3}{4}} \tag{2.234}$$

Using Eq. (1.35),

$$\frac{\hbar^2}{m_\mu r_1^3} = \frac{\hbar^2}{m_e r_2^3} \pm \frac{e\alpha c}{2}\frac{\mu_0}{r_2^3}\ \mu_\mu\sqrt{\frac{3}{4}} \tag{2.235}$$

$$r_2^3 = \left(\frac{m_\mu}{m_e} \pm \frac{m_\mu e\alpha c}{2\hbar^2}\mu_0\ \mu_\mu\sqrt{\frac{3}{4}}\right) r_1^3 \tag{2.236}$$

$$r_1 = \frac{r_2}{\left(\frac{m_\mu}{m_e} \pm \frac{m_\mu e\alpha c}{2\hbar^2}\mu_0\ \mu_\mu\sqrt{\frac{3}{4}}\right)^{1/3}} \tag{2.237}$$

Using Eqs. (2.232-2.233) for $r_2$,

$$r_1 = \frac{a_\mu \pm \frac{2\pi\alpha\ \mu_\mu}{ec}\sqrt{\frac{3}{4}}}{\left(\frac{m_\mu}{m_e} \pm \frac{m_\mu e\alpha c}{2\hbar^2}\mu_0\ \mu_\mu\sqrt{\frac{3}{4}}\right)^{1/3}} \tag{2.238}$$

$$r_{1+} = \frac{a_\mu + \frac{2\pi\alpha\ \mu_\mu}{ec}\sqrt{\frac{3}{4}}}{\left(\frac{m_\mu}{m_e} + \frac{m_\mu e\alpha c}{2\hbar^2}\mu_0\ \mu_\mu\sqrt{\frac{3}{4}}\right)^{1/3}} = 8.9922565\ X\ 10^{-12}\ m \tag{2.239}$$

$$r_{1-} = \frac{a_\mu - \frac{2\pi\alpha\ \mu_\mu}{ec}\sqrt{\frac{3}{4}}}{\left(\frac{m_\mu}{m_e} - \frac{m_\mu e\alpha c}{2\hbar^2}\mu_0\ \mu_\mu\sqrt{\frac{3}{4}}\right)^{1/3}} = 8.99224822\ X\ 10^{-12}\ m \tag{2.240}$$

where the plus sign corresponds to parallel alignment of the magnetic moments of the electron and muon and the minus sign corresponds to antiparallel alignment.

## ENERGY CALCULATIONS

The magnetic energy, $\Delta E_{mag}^{spin}\left(\Delta\nu_{Mu}\right)$, to flip the orientation of the muon's magnetic moment, $\mu_\mu$, from antiparallel to parallel to the direction of the magnetic flux $\mathbf{B}_s$ of the electron (180° rotation of the magnetic moment vector) given by Eq. (2.222) is:

$$\Delta E_{mag}^{spin}\left(\Delta\nu_{Mu}\right) = -\frac{\mu_0 e\hbar}{2m_e}\mu_\mu\sqrt{\frac{3}{4}}\left(\frac{1}{r_{2+}^3} + \frac{1}{r_{2-}^3}\right) = -\mu_0\mu_B\mu_\mu\sqrt{\frac{3}{4}}\left(\frac{1}{r_{2+}^3} + \frac{1}{r_{2-}^3}\right) = -6.02890320\ X\ 10^{-24}\ J \tag{2.241}$$

wherein the muon magnetic moment replaces the proton magnetic moment and the electron Bohr magneton, $\mu_B$, is given by Eq. (1.131).

An electric field equivalent to that of a point charge of magnitude $+e$ at the origin only exists for $r_1 < r \le r_2$. Thus, the change in the electric energy of the electron due to the slight shift of the radius of the electron is given by the difference between the electric energies associated with the two possible orientations of the magnetic moment of the electron with respect to the magnetic moment of the muon, parallel versus antiparallel. Each electric energy is given by the substitution of the corresponding radius given by Eq. (2.231) into Eq. (1.264) or Eq. (2.223). The change in electric energy for the flip from antiparallel to parallel alignment, $\Delta E_{ele}\left(\Delta\nu_{Mu}\right)$, is:

$$\Delta E_{ele}\left(\Delta\nu_{Mu}\right) = \frac{-e^2}{8\pi\varepsilon_0}\left[\frac{1}{r_{2+}} - \frac{1}{r_{2-}}\right] = 3.02903048\ X\ 10^{-24}\ J \tag{2.242}$$

For each lepton, the application of a magnetic field with a resonant Larmor excitation gives rise to a precessing angular momentum vector **S** of magnitude $\hbar$ directed from the origin of the atomic orbital at an angle of $\theta = \frac{\pi}{3}$ relative to the applied magnetic field. As given in the Spin Angular Momentum of the Atomic Orbital $Y_0^0(\theta,\phi)$ with $\ell = 0$ section, **S** rotates about the axis of the applied field at the Larmor frequency. The magnitude of the components of **S** that are parallel and orthogonal to the applied field (Eqs. (1.129-1.130)) are $\frac{\hbar}{2}$ and $\sqrt{\frac{3}{4}}\hbar$, respectively. Since both the RF field and the orthogonal components shown in Figure 1.25 rotate at the Larmor frequency, the RF field that causes a Stern Gerlach transition produces a stationary magnetic field with respect to these components as described by Patz [48]. The corresponding central field at the atomic orbital surface given by the superposition of the central field of the lepton and that of the photon follows from Eqs. (2.10-2.17) and Eq. (17) of Box 1.1:

$$\mathbf{E} = \frac{e}{4\pi\varepsilon_0 r^2}\left[Y_0^0(\theta,\phi)\mathbf{i}_\mathbf{r} + \mathrm{Re}\left\{Y_\ell^m(\theta,\phi)e^{im\omega_n t}\right\}\mathbf{i}_\mathbf{y}\delta\left(r - r_1\right)\right] \tag{2.243}$$

where the spherical harmonic dipole $Y_\ell^m(\theta,\phi)=\sin\theta$ is with respect to the **S**-axis. The dipole spins about the **S**-axis at the angular velocity given by Eq. (1.36). The resulting current is nonradiative as shown in Appendix I: Nonradiation Condition. Thus, the field in the RF rotating frame is magnetostatic as shown in Figures 1.28 and 1.29 but directed along the **S**-axis.

The interaction of the magnetic moments of the leptons increases their magnetic energies given by Eqs. (1.161-1.162) with the mass of the corresponding lepton:

$$\begin{aligned} E_{mag,e}^{stored}(\Delta\nu_{Mu}) &= -\left(1+\left(\frac{2}{3}\cos\frac{\pi}{3}\right)^2+\alpha\right)\frac{\pi\mu_0 e^2\hbar^2}{m_e{}^2}\left(\frac{1}{r_{2+}^3}-\frac{1}{r_{2-}^3}\right) \\ &= -\left(1+\left(\frac{2}{3}\cos\frac{\pi}{3}\right)^2+\alpha\right)4\pi\mu_0\mu_B^2\left(\frac{1}{r_{2+}^3}-\frac{1}{r_{2-}^3}\right) \\ &= 4.23209178\ X\ 10^{-26}\ J \end{aligned} \tag{2.244}$$

$$\begin{aligned} E_{mag,\mu}^{stored}(\Delta\nu_{Mu}) &= -\left(1+\left(\frac{2}{3}\cos\frac{\pi}{3}\right)^2+\alpha\right)\frac{\pi\mu_0 e^2\hbar^2}{m_\mu{}^2}\left(\frac{1}{r_{1+}^3}-\frac{1}{r_{1-}^3}\right) \\ &= -\left(1+\left(\frac{2}{3}\cos\frac{\pi}{3}\right)^2+\alpha\right)4\pi\mu_0\mu_{B,\mu}^2\left(\frac{1}{r_{1+}^3}-\frac{1}{r_{1-}^3}\right) \\ &= 1.36122030\ X\ 10^{-28}\ J \end{aligned} \tag{2.245}$$

where (1) the radii of the electron and muon are given by Eq. (2.232-2.233) and Eqs. (2.239-2.240)), respectively, (2) $\mu_{B,\mu}$ is the muon Bohr magneton given by Eq. (1.131) with the electron mass replaced by the muon mass, (3) the first term is due to lepton spin, (4) the second term, $\left(\frac{2}{3}\cos\frac{\pi}{3}\right)^2$ is due to **S**, oriented $\theta=\frac{\pi}{3}$ relative to the z-axis, wherein the geometrical factor of $\frac{2}{3}$ corresponds to the source current of the dipole field (Eq. (2.243)) given in the Derivation of the Magnetic Field section (Eq. (1.140)) and by Eq. (11.391), and the energy is proportional to the magnetic field strength squared according to Eq. (1.154), and (5) the relativistic factor from Eq. (1.249) and Eqs. (1.161) and (2.190) is $\alpha$.

The energy of the ground state ($1^2S_{1/2}$) hyperfine structure interval of muonium, $\Delta E(\Delta\nu_{Mu})$, is given by the sum of Eqs. (2.241-2.242) and (2.244-2.245):

$$\begin{aligned} \Delta E(\Delta\nu_{Mu}) &= \Delta E_{mag}^{spin}(\Delta\nu_{Mu})+\Delta E_{ele}(\Delta\nu_{Mu})+E_{mag,e}^{stored}(\Delta\nu_{Mu})+E_{mag,\mu}^{stored}(\Delta\nu_{Mu}) \\ &= -6.02890320\ X\ 10^{-24}\ J+3.02903048\ X\ 10^{-24}\ J+4.23209178\ X\ 10^{-26}\ J+1.36122030\ X\ 10^{-28}\ J \\ &= -2.95741568\ X\ 10^{-24}\ J \end{aligned} \tag{2.246}$$

Using Planck's equation (Eq. (2.148)), the interval frequency, $\Delta\nu_{Mu}$, and wavelength, $\Delta\lambda_{Mu}$, are:

$$\Delta\nu_{Mu} = 4.46330328\ GHz \tag{2.247}$$

$$\Delta\lambda_{Mu} = 6.71682919\ \text{cm} \tag{2.248}$$

The experimental hyperfine structure interval of muonium [49] is:

$$\begin{aligned} &\Delta E(\Delta\nu_{Mu}) = -2.957415336\ X\ 10^{-24}\ J \\ &\Delta\nu_{Mu} = 4.463302765(53)\ GHz\ \ (12\,ppm) \\ &\Delta\lambda_{Mu} = 6.71682998\ \text{cm} \end{aligned} \tag{2.249}$$

There is remarkable (7 to 8 significant figure-) agreement between the calculated and experimental values of $\Delta\nu_{Mu}$ that is only limited by the accuracy of the fundamental constants in Eqs. (2.239-2.240), (2.241-2.242), and (2.244-2.245) as shown by using different CODATA values [50-51].

## REFERENCES


1. J. D. Jackson, *Classical Electrodynamics*, Second Edition, John Wiley & Sons, New York, (1975), pp. 110-113.
2. J. D. Jackson, *Classical Electrodynamics*, Second Edition, John Wiley & Sons, New York, (1975), pp. 739-779.
3. M. Mizushima, *Quantum Mechanics of Atomic Spectra and Atomic Structure*, W.A. Benjamin, Inc., New York, (1970), p.17.
4. H. A. Haus, "On the radiation from point charges," American Journal of Physics, 54, (1986), pp. 1126-1129.
5. W. McC. Siebert, *Circuits, Signals, and Systems*, The MIT Press, Cambridge, Massachusetts, (1986), pp. 338-339.
6. W. McC. Siebert, *Circuits, Signals, and Systems*, The MIT Press, Cambridge, Massachusetts, (1986), p. 416.
7. J. D. Jackson, *Classical Electrodynamics*, Second Edition, John Wiley & Sons, New York, (1975), pp. 758-763.
8. J. D. Jackson, *Classical Electrodynamics*, Second Edition, John Wiley & Sons, New York, (1975), pp. 394-397.
9. R. L. Mills, "Maxwell's Equations and QED: Which is Fact and Which is Fiction," *Physics Essays*, Vol. 19, No. 2, (2006), 225-262. Posted with spreadsheets at http://www.blacklightpower.com/techpapers.shtml.
10. R. L. Mills, "The Fallacy of Feynman's Argument on the Stability of the Hydrogen Atom According to Quantum Mechanics," Annales de la Fondation Louis de Broglie, Vol. 30, No. 2, (2005), pp.129-151; posted at www.blacklightpower.com/theory/theory.shtml.
11. R. Mills, "The Nature of Free Electrons in Superfluid Helium—a Test of Quantum Mechanics and a Basis to Review its Foundations and Make a Comparison to Classical Theory," Int. J. Hydrogen Energy, Vol. 26, No. 10, (2001), pp. 1059-1096.
12. R. Mills, "The Hydrogen Atom Revisited," Int. J. of Hydrogen Energy, Vol. 25, Issue 12, December, (2000), pp. 1171-1183.
13. J. Daboul and J. H. D. Jensen, Z. Physik, Vol. 265, (1973), pp. 455-478.
14. T. A. Abbott and D. J. Griffiths, Am. J. Phys., Vol. 53, No. 12, (1985), pp. 1203-1211.
15. G. Goedecke, Phys. Rev 135B, (1964), p. 281.
16. P. Pearle, Foundations of Physics, "Absence of radiationless motions of relativistically rigid classical electron," Vol. 7, Nos. 11/12, (1977), pp. 931-945.
17. V. F. Weisskopf, Reviews of Modern Physics, Vol. 21, No. 2, (1949), pp. 305-315.
18. H. Margenau, G. M. Murphy, *The Mathematics of Chemistry and Physics*, D. Van Nostrand Company, Inc., New York, (1956), Second Edition, pp. 363-367.
19. J. D. Jackson, *Classical Electrodynamics*, Second Edition, John Wiley & Sons, New York, (1975), pp. 739-752.
20. D. A. McQuarrie, *Quantum Chemistry*, University Science Books, Mill Valley, CA, (1983), pp. 238-241.
21. J. D. Jackson, *Classical Electrodynamics*, Second Edition, John Wiley & Sons, New York, (1975), pp. 503-561.
22. N. Ryde, *Atoms and Molecules in Electric Fields*, Almqvist & Wiksell International, Stockholm, Sweden, (1976), pp. 168-177.
23. N. Ryde, *Atoms and Molecules in Electric Fields*, Almqvist & Wiksell International, Stockholm, Sweden, (1976), pp. 44-74.
24. J. Stark, do. V. Feinzerlegung der Wasserstoffserie, Ann. d. Phys., Vol. 48, (1915), p. 193.
25. L. C. Shi, J. A. Kong, *Applied Electromagnetism*, Brooks/Cole Engineering Division, Monterey, CA, (1983), pp. 170-209.
26. NIST Atomic Spectra Database, http://physics.nist.gov/PhysRefData/ASD/index.html.
27. S. Djurovic, J. R. Roberts, "Hydrogen Balmer alpha line shapes for hydrogen-argon mixtures in a low-pressure rf discharge," J. Appl. Phys., Vol. 74, No. 11, (1993), pp. 6558-6565.
28. G. Sultan, G. Baravian, M. Gantois, G. Henrion, H. Michel, A. Ricard, "Doppler-broadened $H_\alpha$ line shapes in a dc low-pressure discharge for $TiN$ deposition," Chemical Physics, Vol. 123, (1988), pp. 423-429.
29. L. S. Ornstein, H. C. Burger, Zeits. für Phys., Intensitätsverhältnis von Balmer- und Paschenlinien," Vol. 62, (1930), pp. 636-639.
30. E. U. Condon, G. H. Shortley, *The Theory of Atomic Spectra*, Cambridge University Press, (1967), p. 141.
31. Personal communication, Dr.-Ing. Günther Landvogt, Hamburg, Germany, November, (2005).
32. E. U. Condon, G. H. Shortley, *The Theory of Atomic Spectra*, Cambridge University Press, (1967), Chp. 4 and Chp 5, sections 6 and 7.
33. L. R. Maxwell, "The average life of the ionized helium atom," Phys. Rev., Vol. 38, (1931), pp. 1664-1686.
34. W. McC. Siebert, *Circuits, Signals, and Systems*, The MIT Press, Cambridge, Massachusetts, (1986), pp. 488-502.
35. D. A. McQuarrie, *Quantum Chemistry*, University Science Books, Mill Valley, CA, (1983), pp. 135-140.
36. W. E. Lamb, R. C. Retherford, "Fine Structure of the Hydrogen Atom by a Microwave Method," R. C., Phys. Rev., Vol. 72, No. 3, August 1, (1947), pp. 241-243.
37. D. Jackson, *Classical Electrodynamics*, Second Edition, John Wiley & Sons, New York, (1975), pp. 236-240, 601-608, 786-790.
38. J. D. Jackson, *Classical Electrodynamics*, Second Edition, John Wiley & Sons, New York, (1975), pp. 236-240.
39. T. C. Gibb, *Principles of Mössbauer Spectroscopy*, Chapman and Hall: London (1977), Chp. 1.
40. U. Gonser, From a Strange Effect to Mössbauer Spectroscopy in *Mössbauer Spectroscopy*, U. Gonser, Ed. Springer-Verlag: New York (1975), pp. 1-51.
41. R. L. Mills, EPO Patent Number 86103694.5/0 198 257, Method and Apparatus for Selective Irradiation of Biological Materials, (1986).
42. P. J. Mohr, B. N. Taylor, D. B. Newell, "CODATA recommended values of the fundamental physical constants: 2006," Reviews of Modern Physics, Vol. 80, (2008), pp. 633-730.
43. R. Pohl, A. Antognini, F. N., F. D. Amaro, F. Biraben, J. M. R. Cardoso, D. S. Covita, A. Dax, S. Dhawan, L. M. P. Fernandes, A. Giesen, T. Graf, T. W. Hansch, P. Indelicato, L. Julien, C-Y. Kao, P. Knowles, E-O. Le Bigot, Y-W. Liu, J. A. M. Lopes, L. Ludhova, C. M. B. Monteiro, F. Mulhauser, T. Nebel, P. Rabinowitz, J. M. F. dos Santos, L. A. Schaller, K.

Schuhmann, C. Schwob, D. Taqqu, J. F. C. A. Veloso, F. Kottmann, "The size of the proton," Nature, Vol. 466, (2010), pp. 213-216, doi:10.1038/nature09250.

44. P. J. Mohr, B. N. Taylor, "CODATA recommended values of the fundamental physical constants: 2002," Rev. Mod. Phys. 77, (2005), pp. 1–107, http://dx.doi.org/10.1103/RevModPhys.77.1.
45. P. J. Mohr, B. N. Taylor, "CODATA recommended values of the fundamental physical constants: 1998," Reviews of Modern Physics, Vol. 72, No. 2, April, (2000), p. 418.
46. J. D. Jackson, *Classical Electrodynamics*, Second Edition, John Wiley & Sons, New York, (1975), p. 178.
47. P. J. Mohr, B. N. Taylor, "CODATA recommended values of the fundamental physical constants: 1998," Reviews of Modern Physics, Vol. 72, No. 2, April, (2000), pp. 418-419.
48. S. Patz, Cardiovasc Interven Radiol, (1986), 8:25, pp. 225-237.
49. W. Liu, M. G. Boshier, S. Dhawan, O. van Dyck, P. Egan, X. Fei, M. Grosse Perdekamp, V. W. Hughes, M. Janousch, K. Jungmann, D. Kawall, F. G. Mariam, C. Pillai, R. Prigl, G. zu Putlitz, I. Reinhard, W. Schwarz, P. A. Thompson, K. A. Woodle, "High Precision measurements of the ground state hyperfine structure interval of muonium and the muon magnetic moment," Phys. Rev. Letts., Vol. 82, No. 4, (1999), pp. 711-714.
50. P. J. Mohr, B. N. Taylor, "CODATA recommended values of the fundamental physical constants: 1998," Reviews of Modern Physics, Vol. 72, No. 2, April, (2000), pp. 448-453.
51. P. J. Mohr, B. N. Taylor, "CODATA recommended values of the fundamental physical constants: 2002," Reviews of Modern Physics, Vol. 77, No. 1, (2005), pp. 1-107.

# Chapter 3

# ELECTRON IN FREE SPACE

## CHARGE-DENSITY FUNCTION

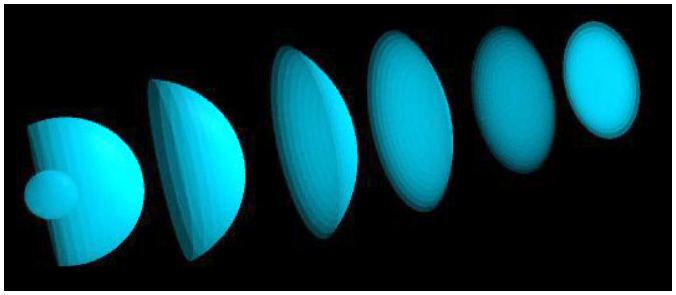
The radius of a spherical wavefront of light goes to infinity as it propagates from a spherically-symmetrical source such that its propagation in the far-field is given by the plane-wave equation:

$$\mathbf{E} = E_0 e^{-ik_z z} \tag{3.1}$$

Light and electrons display identical propagation and diffraction behavior. (This is expected because an electron is created from a photon as derived in the Pair Production section). Electrons behave as two-dimensional wavefronts with the de Broglie wavelength, $\lambda = h/p$, in double-slit experiments (Davisson-Germer experiment) [1]. The plane wave nature of free electrons is demonstrated in the Electron Scattering by Helium section[1]. The results of the double-slit experiment are derived classically in the Two-Slit Interference (Wave-Particle Duality) section. Analogous to the behavior of light, the radius of the spherically-symmetrical electron atomic orbital increases with the absorption of electromagnetic energy [2].

Consider an idealized hypothetical state. With the absorption of exactly the ionization energy, the atomic radius *r* goes to infinity, the electron momentum goes to zero, and the de Broglie relationship given by Eq. (1.15) predicts that the electron wavelength concomitantly goes to infinity corresponding to an infinitely large electron. The interaction radius of an infinitely large atom goes to infinity also. Such a state is not physical; so, let's consider the case observed. In order for the atom to become ionized to form a free electron, the atom must absorb energy greater than its ionization energy. The radius of the spherical shell (electron atomic orbital) goes to infinity as in the case of a spherical wavefront of light emitted from a symmetrical source, but it does not achieve an infinite radius. Rather it becomes ionized with the free electron propagating with linear velocity, $v_z$, and the de Broglie wavelength is finite as shown in Figure 3.1. The ionized electron is a plane wave that propagates as a wavefront with the de Broglie wavelength where the size of the electron is the de Broglie wavelength, $\lambda = h/p$, as shown below.

**Figure 3.1.** Time-lapsed image of spherical to plane-wave front continuity that determines the boundary conditions for atomic electron ionization. With the absorption of a photon of energy in excess of the binding energy, the bound electron's radius increases, and the electron ionizes as a plane-wave.



[1] Particles such as the proton and neutron also demonstrate interference patterns during diffraction. The observed far-field position distribution is a picture of the particles' transverse momentum distribution after the interaction. The momentum transfer is given by $\hbar k$ where $k = \frac{2\pi}{\lambda}$ is the wave number. The wavelength $\lambda$ is the de Broglie wavelength associated with the momentum of the particles which is transferred through interactions. An example is the interference pattern for rubidium atoms given in the Wave-Particle Duality is Not Due to the Uncertainty Principle Section.

The ionized electron traveling at constant velocity, $v_z$, is nonradiative and is a two-dimensional surface having a total charge of $e$ and a total mass of $m_e$. The spacetime charge-density function of the ionized electron is solved as a boundary value problem as described previously for the bound electron in the One Electron-Atom section. The de Broglie wavelength relationship given by Eq. (1.38) must hold independent of the radius of the electron. The relationship between the electron atomic orbital radius and its wavelength, is given by Eq. (1.15). The integral of the magnitude of the angular momentum density is $\hbar$ (Eq. (1.37)) independent of the electron radius; thus, for both the bound electron and the free electron, the total magnitude of the angular momentum is $\hbar$. The spacetime plane-wave charge-density function of the free electron is a solution of the classical wave equation (Eq. (1.56)). The current-density function possesses no spacetime Fourier components synchronous with waves traveling at the speed of light; thus it is nonradiative. As shown below, the solution of the boundary value problem of the free electron is given by the projection of the atomic orbital into a plane that linearly propagates along an axis perpendicular to the plane. The velocity of the plane and the atomic orbital is given by Eq. (1.35) where the radius of the atomic orbital in spherical coordinates is equal to the radius of the free electron in cylindrical coordinates.

Consider an electron atomic orbital of radius $r_0$. The boundary condition that the de Broglie wavelength holds and the angular momentum is conserved as shown *infra* for any electron radius requires that the ionized electron is the projection of the atomic orbital into $\pi(z)$, the Cartesian xy-plane that propagates linearly along the z-axis with the same linear velocity as the electron atomic orbital. The mass-density function, $\sigma_m(\rho,\phi,z)$, of the electron with linear velocity along the z-axis of $v_z$ ***in the inertial frame of the proton***[2] given by Eq. (1.35):

$$\mathbf{v}_z = \frac{\hbar}{m_e r_n} = \frac{\hbar}{m_e r_0} = \frac{\hbar}{m_e \rho_0} \tag{3.2}$$

is given by the projection into the xy-plane of the convolution, $\otimes$, of the xy-plane, $\pi(z)$, with an atomic orbital of radius $r_0$. The convolution is

$$\pi(z) \otimes \delta(r - r_0) = \sqrt{r_0^2 - z^2}\,\delta(r - \sqrt{r_0^2 - z^2}) \tag{3.3}$$

where the atomic orbital function is given in spherical coordinates. The equation of the free electron is given as the projection of Eq. (3.3) into the xy-plane which in cylindrical coordinates is:

$$\begin{aligned} &\sigma_m(\rho,\phi,z) = N\sqrt{\rho_0^2 - \rho^2}\,\delta(z) \quad for\ 0 \le \rho \le \rho_0 \\ &\sigma_m(\rho,\phi,z) = 0 \qquad\qquad\qquad for\ \rho_0 < \rho \end{aligned} \tag{3.4}$$

where $N$ is the normalization factor for the charge and mass plane-wave defined by $\pi\left(\frac{\rho}{2\rho_0}\right)$ which represents a two-dimensional disc or plane-lamina disc of radius $\rho_0$. In spherical coordinates, Eq. (3.4) is given by $\sin\theta$, the projection of the charge density of a spherical shell into a plane. The total mass is $m_e$. Thus, the normalization factor $N$ in Eq. (3.4) is given by:

$$m_e = N\int_0^{2\pi}\int_0^{\rho_0}\sqrt{\rho_0^2 - \rho^2}\,\rho\, d\rho\, d\phi \tag{3.5}$$

$$N = \frac{m_e}{\frac{2}{3}\pi\rho_0^3} \tag{3.6}$$

The mass-density function of a free electron is a two-dimensional disc (essentially zero thickness equal to its Schwarzschild radius $r_g = \frac{2Gm_e}{c^2} = 1.3525\ X\ 10^{-57}\ m$ according to Eqs. (32.36) and (32.140b)). The mass-density distribution, $\sigma_m(\rho,\phi,z)$, and charge-density distribution, $\sigma_e(\rho,\phi,z)$, in the xy-plane at $\delta(z)$ are:

---

[2] The universe is electrically neutral and contains no antimatter according to the particle production equation (Eq. (32.172)) of the contracting phase of the oscillatory universe. Particle production proceeds through a neutron pathway that gives the number of electrons of the universe equal to the number of protons. The wavelength and the radius of the electron must depend on the velocity relative to the proton's inertial frame in order that relativistic invariance of charge holds and the universe is electrically neutral. In the case of an observer in an inertial frame with constant relative motion with respect to the direction perpendicular to the two-dimensional plane containing the free-electron, the de Broglie wavelength of the electron in both the proton frame (the special frame of origin of the free electron) and the second inertial frame are the same. The radius of the electron is also the same in both frames and is given by

$$\rho_0 = \frac{\hbar}{\mathbf{p}_z} \tag{1}$$

where $\mathbf{p}_z$ is the electron momentum in the z-direction relative to the proton. There is no Lorentz contraction in the second frame since the electron is oriented perpendicular to the direction of relative motion. Eq. (1) further satisfies the conditions that the moving electron acquires velocity by acceleration with concomitant photon emission in quantized units of $\hbar$ and that the electric field of the moving electron is no longer that of the electron at rest. Conservation of angular momentum and energy gives rise to the de Broglie relationship as given in the Classical Physics of the de Broglie Relationship section.

$$\sigma_m(\rho,\phi,z) = \frac{m_e}{\frac{2}{3}\pi\rho_0^3}\sqrt{\rho_0^2-\rho^2} = \frac{3}{2}\frac{m_e}{\pi\rho_0^2}\sqrt{1-\left(\frac{\rho}{\rho_0}\right)^2}\,\delta(z) \quad for\ 0 \le \rho \le \rho_0$$
$$\sigma_m(\rho,\phi,z) = 0 \qquad for\ \rho_0 < \rho \tag{3.7}$$

and

$$\sigma_e(\rho,\phi,z) = \frac{e}{\frac{2}{3}\pi\rho_0^3}\sqrt{\rho_0^2-\rho^2} = \frac{3}{2}\frac{e}{\pi\rho_0^2}\sqrt{1-\left(\frac{\rho}{\rho_0}\right)^2}\,\delta(z) \quad for\ 0 \le \rho \le \rho_0$$
$$\sigma_e(\rho,\phi,z) = 0 \qquad for\ \rho_0 < \rho \tag{3.8}$$

respectively, where $\frac{m_e}{\pi\rho_0^2}$ is the average mass density and $\frac{e}{\pi\rho_0^2}$ is the average charge density of the free electron. The magnitude of each distribution is shown in Figure 3.2. ***The charge-density distribution of the free electron given by Eq. (3.8) and shown in Figure 3.2 has recently been confirmed experimentally*** [3,4]. Researchers working at the Japanese National Laboratory for High Energy Physics (KEK) demonstrated that the charge of the free electron increases toward the particle's core and is symmetrical as a function of $\phi$.

**Figure 3.2A.** The angular-momentum-axis view of the magnitude of the continuous mass(charge)-density function in the xy-plane of a polarized free electron propagating along the z-axis and the side view of this electron. For the polarized electron, the angular momentum axis is aligned along the direction of propagation, the z-axis.

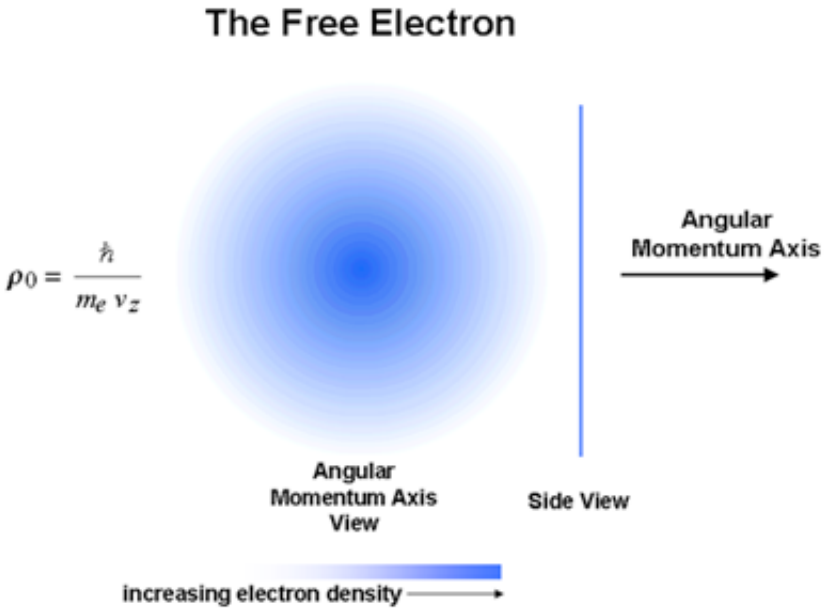
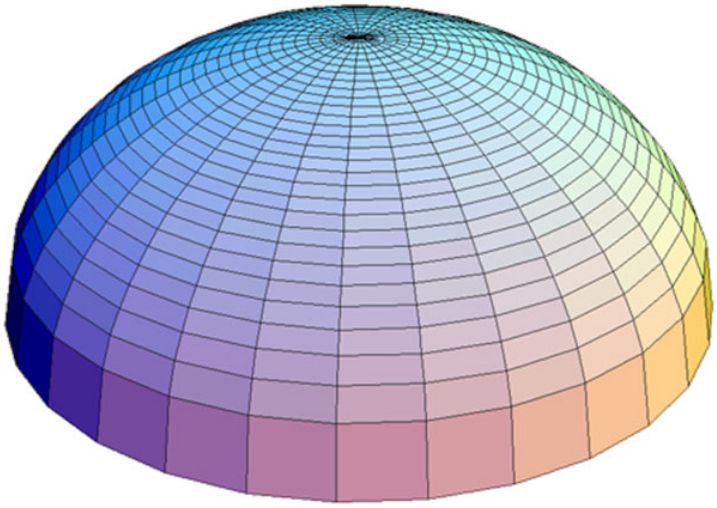


**Figure 3.2B.** The magnitude plotted along the z-axis of the mass(charge)-density function of the free electron traveling at $10^5\ m/s$ relative to the observer. From Eq. (3.29), the radius of the xy-plane-lamina disc is $1.16\ X\ 10^{-9}\ m$, and from Eqs. (3.7) and (3.8), the maximum mass density and charge density at $\rho = 0$ are $3.25\ X\ 10^{-13}\ kg/m^2$ and $0.0571\ \mathrm{C}/m^2$, respectively.



This surface has an electric field equivalent to a point charge at the origin along the z-axis as shown in the Electric Field of a Free Electron section.

## ELECTRIC FIELD OF A FREE ELECTRON

The electrical neutrality of the universe must be maintained. A free electron is a continuum excited state of a state bound in an inverse r-squared positive electric field as given in the Excited States of the One-Electron Atom (Quantization). A free electron is tethered to photon electromagnetic field that created the free electron state away from the proton field and changed its radius $\rho$ and velocity $v_z$ according to Eq. (3.45). Specifically, the photon that excites the state is glued to the linearly traveling electron and maintains its radius $\rho$, charge density function, angular momentum, and velocity as shown in the Force Balance Based on the Radiation-Reaction Force section and the Classical Physics of the de Broglie Relation section. (The only exception to this configuration is when all fields have been cancelled to form a free electron with no gravitational mass as given in the Positive, Zero, and Negative Gravitational Mass section.) As given in the Force Balance Based on the Radiation-Reaction Force section, the current density of the free electron can be modeled as a continuum of circular current elements having the same rotational frequency. The photon field lines propagate along these current elements. The photon field lines and the free electron charge density only exist at the position of the two-dimensional plane of the free electron and superimpose only at that plane. Considering electrodynamic interactions (Eqs. (3.30-3.52)), the charge and current densities are determined to be absent any in-plane forces; thus, the charge density comprises an equipotential such that the electric field lines at the surface of the free electron are normal to the surface. The relationship between the electric field and the source charge density is given by Gauss' law and Faraday's law equation in two dimensions [5-7]:

$$\mathbf{n} \bullet \left(\mathbf{E}_1 - \mathbf{E}_2\right) = \frac{\sigma}{\varepsilon_0} \tag{3.9}$$

where $\mathbf{n}$ is the radial normal unit vector, $\mathbf{E}_1$ is the electric field on one side of the free electron, $\mathbf{E}_2$ is the electric field on the other side of the free electron, and $\sigma$ is the surface charge density distribution of the free electron given by Eq. (3.8). Based on symmetry, the condition that the free electron comprises an equipotential surface requiring the absence of an in-plane electric field component at $\delta(z)$, and by using the substitution of $\rho = \rho_0 \sin\theta$ in Eqs. (3.8) and (3.9), the electric field at each surface is given by:

$$\begin{aligned} \mathbf{E}_{\pm z=0} &= \pm \frac{3e}{4\pi\varepsilon_0 \rho_0^2} \cos\theta \delta(z) \mathbf{i}_z \quad for\ 0 \le \rho \le \rho_0 \\ \mathbf{E}_{\pm z=0} &= 0 \qquad\qquad\qquad\qquad for\ \rho_0 < \rho \end{aligned} \tag{3.10}$$

The charge distribution and z-axis field is the spherical harmonic $Y_0^1(\theta,\phi)$, an allowed spherical harmonic solution of an excited state, which is required for the selection rules based on conservation of electron and photon angular momentum and continuity of excited states though the continuum series.

Since the photon field only exists in the two-dimensional plane, the electric potential of a free electron for $z \neq 0$ is given

by Poisson's Equation for a charge-density function, $\rho(x',y',z')$ given by Eq. (3.8):

$$\begin{aligned}\Phi(x,y,z) &= \iiint \frac{\rho(x',y',z')\,dv'}{4\pi\varepsilon_0\sqrt{(x-x')^2+(y-y')^2+(z-z')^2}} \\ &= -\frac{e}{\frac{2}{3}\pi\rho_0^3}\frac{1}{4\pi\varepsilon_0}\int_{-\infty}^{\infty}\int_{-\rho_0}^{\rho_0}\int_{-\sqrt{\rho_0^2-y'^2}}^{+\sqrt{\rho_0^2-y'^2}} \frac{\sqrt{\rho_0^2-x'^2-y'^2}\,\delta(z')\,dx'dy'dz'}{\sqrt{(x-x')^2+(y-y')^2+z^2}}\end{aligned} \tag{3.11}$$

For $r=\sqrt{x^2+y^2+z^2} >> \rho_0$, the magnitude of the integral over the charge density is $e$, and

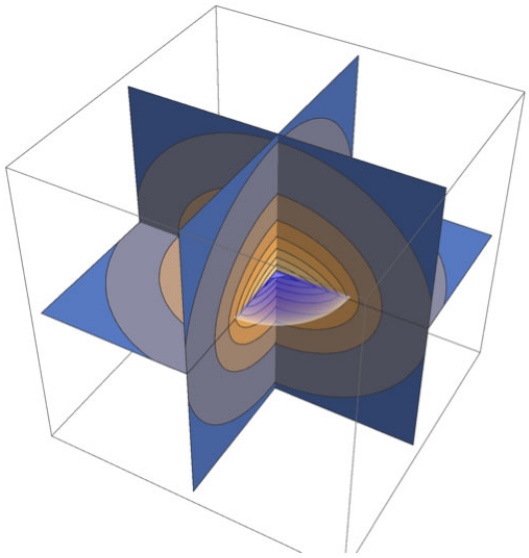
$$\Phi(r) = -\frac{e}{4\pi\varepsilon_0 r} \tag{3.12}$$

Eq. (3.12) is equivalent to the potential of a point charge at the origin. The electric field, $\mathbf{E}$, is the gradient of the electric potential given by Eqs. (3.11-3.12):

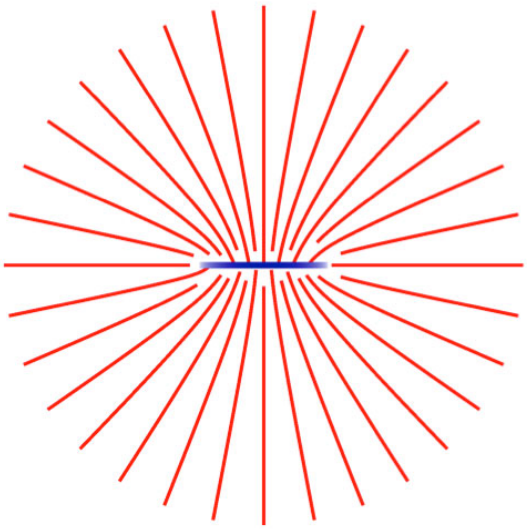
$$\mathbf{E} = -\nabla\Phi \tag{3.13}$$

A numerical plot of the electric field out of plane is shown in Figure 3.3 wherein the plot is discontinuous at the plane wherein the normal direct field at $\delta(z)$ is given by Eq. (3.10) corresponding to an equipotential membrane due to the superposition of the photon field with the electron charge only at the plane of the free electron.

**Figures 3.3A-B.** The electric potential and electric field of the free electron. A. Three-dimensional cutaway view of the electric potential of a free electron that approaches that of a point charge at the center-of-mass in the far field. B. The two-dimensional cross section of the electric field lines of a free electron. The electric field is symmetrical about the z-axis and approaches that of a point charge at the center-of-mass in the far-field.



**(A)**



**(B)**

## CURRENT-DENSITY FUNCTION

In general, the current-density function is the product of the charge-density function times the angular velocity function. If the intrinsic electron current was variable over time, then radiation would result, and the electron would be unstable. A current that changes over time is also inconsistent with the Lorentz invariant electron magnetic moment of one Bohr magneton. Thus, in order for the current to be stable over time, the current must be constant as a function of the radial distance and given by the product of $\rho$, the free-electron charge density (Eq. (3.8)) and a constant angular velocity. The magnitude of the angular velocity of the atomic orbital is given by Eq. (1.36):

$$\omega = \frac{\hbar}{m_e r^2} \tag{3.14}$$

Rather than being confined to a spherical shell, the free electron possesses time harmonic charge motion in the xy-plane at a constant angular frequency. That is, at each point on the free electron, the current moves along a flat current loop time harmonically. This holds for all points such that the current confined to a plane is constant. Since the charge density is determined, the boundary condition on the angular velocity is applied next to solve the current density function of the free electron. Consider the boundary condition that arises during the ionization of a bound electron to form a free electron. During ionization of the electron, the scalar sum of the magnitude of the angular momentum, $\hbar$, must be conserved. The current-density function of a free electron propagating with ***velocity*** $v_z$ ***along the z-axis in the inertial frame of the proton*** is given by the product of the charge density and the constant angular velocity. Since the mass to charge ratio of the electron is invariant, the corresponding boundary condition is that the angular momentum of $\hbar$ is conserved. The projection of the constant angular velocity of the atomic orbital into the plane of the free electron gives the angular velocity of the form

$$\omega = N_\omega \frac{\hbar}{m_e \rho_0^2} \tag{3.15}$$

where $N_\omega$ is the normalization constant that gives $\hbar$ of angular momentum. The angular momentum, $\mathbf{L}$, is given by:

$$\mathbf{Li}_z = m_e \rho^2 \omega \tag{3.16}$$

Consider the case that $N_\omega = \frac{5}{2}$ such that:

$$\omega = \frac{5}{2} \frac{\hbar}{m_e \rho_0^2} \tag{3.17}$$

Substitution of the mass density, $\sigma_m$, given by Eq. (3.7) and the angular frequency, $\omega$, given by Eq. (3.17) into Eq. (3.16) gives the angular momentum-density function $\mathbf{L}$ which is shown in Figures 3.4A and 3.4B.

$$\mathbf{Li}_z = \frac{m_e}{\frac{2}{3}\pi\rho_0^3} \sqrt{\rho_0^2 - \rho^2} \frac{5}{2} \frac{\hbar}{m_e \rho_0^2} \rho^2 \tag{3.18}$$

**Figure 3.4A.** The plot as a function of $\rho$ of the angular momentum density in the plane of a free electron having $\mathbf{v}_z == 100\ m/s$.

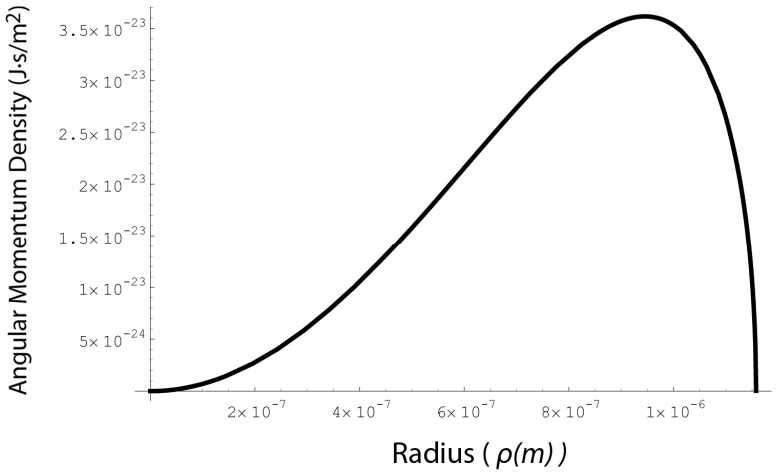
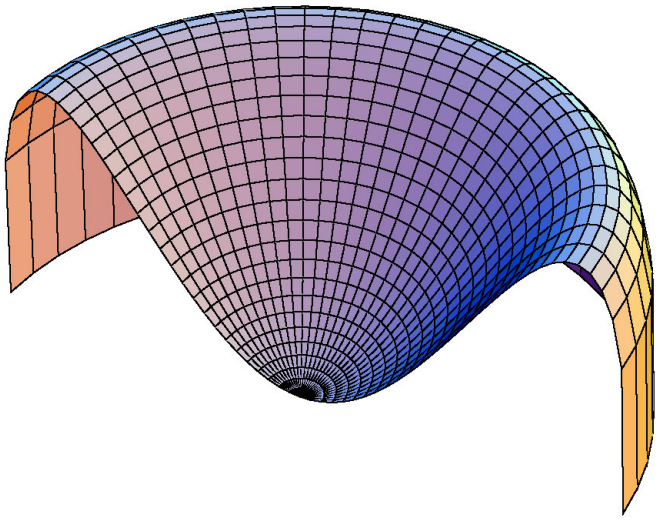



**Figure 3.4B.** The cut-away, relief view of the angular momentum density in the plane of a free electron having $\mathbf{v}_z == 100\ m/s$.



The total angular momentum of the free electron is given by integration over the two-dimensional disc having the angular-momentum density given by Eq. (3.18). Using integral #211 of Lide [8] gives:

$$\mathbf{Li}_z = \int_0^{2\pi}\int_0^{\rho_0} \frac{m_e}{\frac{2}{3}\pi\rho_0^3}\sqrt{\rho_0^2-\rho^2}\,\frac{5}{2}\frac{\hbar}{m_e\rho_0^2}\rho^2\rho d\rho d\phi$$

$$= 2\pi\frac{\hbar}{\frac{2}{3}\pi\rho_0^5}\frac{5}{2}\left(\left(-\frac{1}{5}\rho^2-\frac{2}{15}\rho_0^2\right)\left(\rho_0^2-\rho^2\right)^{3/2}\right)_0^{\rho_0} \tag{3.19}$$

$$= 2\pi\frac{\hbar}{\frac{2}{3}\pi\rho_0^5}\frac{5}{2}\frac{2}{15}\rho_0^5$$

$$\mathbf{Li}_z = \hbar \tag{3.20}$$

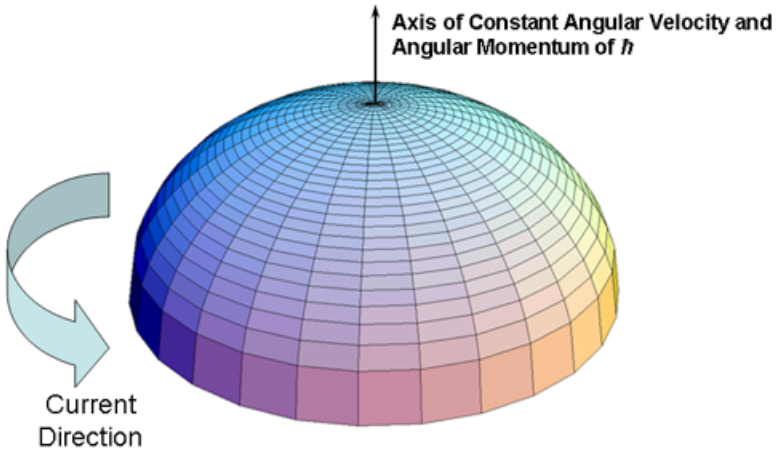
Thus, the constant angular velocity at each point on the two-dimensional lamina is given by Eq. (3.17).

The intrinsic current-density function of the free electron is given by the product of the angular velocity $\omega$ and the charge-density function given by Eqs. (3.17) and (3.8), respectively. The total current density $\mathbf{J}(\rho,\phi,z,t)$ additionally comprises the component due to translational motion. The total current-density function is given by:

$$\mathbf{J}(\rho,\phi,z,t)=\rho\left[\frac{e}{\frac{2}{3}\pi\rho_0^3}\sqrt{\rho_0^2-\rho^2}\,\frac{5}{2}\frac{\hbar}{m_e\rho_0^2}\,\mathbf{i}_\phi\right]\delta(z)+\frac{e\hbar}{m_e\rho_0}\delta(z-\frac{\hbar}{m_e\rho_0}t)\mathbf{i}_z \tag{3.21}$$

The intrinsic current is shown in Figure 3.5.

**Figure 3.5.** The magnitude plotted along the z-axis of the current-density function, $J$, of the free electron traveling at $10^5\ ms^{-1}$ relative to the observer. From Eq. (3.29), the radius of the xy-plane-lamina disc is $1.16X10^{-9}\ m$, and from Eq. (3.21), the maximum current density at $\rho=0$ is $1.23\ X\ 10^{13}\ Am^{-2}$.




The spacetime Fourier transform of Eq. (3.21) is [9,10]:

$$\frac{e}{\frac{4}{3}\pi\rho_0^3}\frac{\hbar}{m_e}\text{sinc}(s\rho_0)+2\pi e\frac{\hbar}{m_e\rho_0}\delta(\omega-\mathbf{k}_z\bullet\mathbf{v}_z) \tag{3.22}$$

where $s$ is the wavenumber $\frac{2\pi}{\rho_0}$. The condition for nonradiation of a moving charge-density function is that the spacetime Fourier transform of the current-density function must not possess components synchronous with waves traveling at the speed of light, that is synchronous with $\frac{\omega}{c}$ or synchronous with $\frac{\omega}{c}\sqrt{\frac{\varepsilon}{\varepsilon_0}}$ where $\varepsilon$ is the dielectric constant of the medium. The Fourier transform of the current-density function of the free electron is given by Eq. (3.22). Consider the radial part of, $J_\perp$, the Fourier transform of the current-density function where the z spatial dimensional transform is not zero:

$$J_\perp\propto\text{sinc}(s\rho_0)=\frac{\sin s\rho_0}{s\rho_0} \tag{3.23}$$

For time harmonic motion corresponding to the electron parameters $\omega_0$ and $s_0$, Eq. (1.15),

$$2\pi\rho_0=\lambda_0 \tag{3.24}$$

The charge motion of the free electron is angular, and consequently the radius undergoes Lorentz contraction as shown in the Special Relativistic Correction to the Ionization Energies section. Consider the wave vector of the sinc function. When the velocity is $c$ corresponding to a potentially emitted photon, $\mathbf{s}$ is the lightlike $\mathbf{s}^0$ wherein

$$\mathbf{s}\bullet\mathbf{v}=\mathbf{s}\bullet\mathbf{c}=\omega_0 \tag{3.25}$$

The relativistically corrected wavelength given by Eq. (1.280) is:

$$\rho_0=\lambda_0 \tag{3.26}$$

as also shown in Appendix I: Nonradiation Based on the Electromagnetic Fields and the Poynting Power Vector. Substitution of Eq. (3.26) into the sinc function results in the vanishing of the entire Fourier transform of the current-density function. Thus, spacetime harmonics of $\frac{\omega}{c}=k$ *or* $\frac{\omega}{c}\sqrt{\frac{\varepsilon}{\varepsilon_0}}=k$ do not exist. Radiation due to charge motion does not occur in any medium when

this boundary condition is met. Furthermore, consider the z spatial dimensional transform of, $J_\perp$, the Fourier transform of the current-density function:

$$J_\perp \propto 2\pi e \frac{\hbar}{m_e \rho_0} \delta(\omega - \mathbf{k}_z \bullet \mathbf{v}_z) \tag{3.27}$$

The only nonzero Fourier components are for:

$$k_z = \frac{\omega}{v_z \cos\theta} > \frac{\omega}{c} \tag{3.28}$$

where $\theta$ is the angle between $\mathbf{k}_z$ and $\mathbf{v}_z$. Thus, no Fourier components that are synchronous with light velocity with the propagation constant $|\mathbf{k}_z| = \frac{\omega}{c}$ exist. Radiation due to charge motion does not occur when this boundary condition is met. It follows from Eq. (3.2) and Eq. (3.24) that the wavelength of the free electron is:

$$\lambda_0 = \frac{h}{m_e v_z} = 2\pi\rho_0 \tag{3.29}$$

which is the de Broglie wavelength.

## FORCE BALANCE BASED ON THE RADIATION-REACTION FORCE

Consideration must be made of the free electron as a continuum excited electronic state caused by absorption of a photon. The physics of excited states is continuous with the free electron or continuum excited states. For excited states given in the Equation of the Electric Field inside the Atomic Orbital section, the vector direction of the photon electric field was determined directly by considering the relativistic effect of its motion relative to the electron. In the case of the free electron, the electrodynamic field may be treated as a magnetic field since a magnetic field is a relativistic effect of the corresponding electric field. The free electron is a two-dimensional disc with a charge distribution given by Eq. (3.8) having a radius $\rho_0$ given by Eq. (3.29) and an in-plane electric field given by Eqs. (3.8 and (3.9). This distribution is a minimum energy, two-dimensional surface[3]. An attractive magnetic force exists between current circles in the xy-plane, and the force balance equation is given by equating the centrifugal and the centripetal forces.

The centripetal force, $\mathbf{F}_{mag}$, between the current loops is the electrodynamic or radiation-reaction magnetic force as given in the One Electron Atom—Determination of Atomic Orbital Radii section and the Two-Electron Atoms section. Here, each infinitesimal point (mass or charge-density element) of the free electron moves azimuthally about the angular-momentum axis on a circle at the same angular velocity given by Eq. (3.17) at a radius $0 \le \rho \le \rho_0$, and each point has the mass density and charge density given by Eqs. (3.7) and (3.8), respectively. Due to the relative motion of the charge-density elements of each electron current loop, a radiation reaction force arises between each loop. This force given in Sections 6.6, 12.10, and 17.3 of Jackson [11] achieves the condition that the sum of the mechanical momentum and electromagnetic momentum is conserved. The magnetic central force is derived from the Lorentz force, which is relativistically corrected. The magnetic field at the

---

[3] This relation shows that only a 2-D geometry meets the criterion for a fundamental particle. This is the nonsingularity geometry that is no longer divisible. It is the dimension from which it is not possible to lower dimensionality. In this case, there is no electrostatic self-interaction since the corresponding potential is continuous across the surface according to Faraday's law in the electrostatic limit, and the field is discontinuous and normal to the charge according to Gauss' law [8-10]. Thus, only the continuous current density function need be considered.

It was shown in the Electron g Factor section that as a requirement of the conservation of angular momentum, the magnetic moment of the electron can only be parallel or antiparallel to an applied magnetic field. Similarly, in order to conserve angular momentum, any internal change in the bound-electron current distribution and its corresponding angular momentum requires emission of a photon that carries angular momentum in its electric and magnetic fields only in discrete units of $\hbar$ as given in the Equation of the Photon section. Conservation of angular momentum also requires that this condition be met for the free electron. Self interaction of the current of the free electron having the angular momentum distribution given in the Current-Density Function section and the Stern-Gerlach Experiment section requires the emission of a photon having an angular momentum that is a fraction of $\hbar$ which is not possible according to Maxwell's equations as given in the Excited States of the One-Electron Atom (Quantization) section. Thus, any self interaction is a radiation-reaction type wherein $k$ is also the lightlike $k^0$ such that $k = \omega_n / c$. Any such light-like interaction can only be central. Since the velocity of each point of the electron for a given $\rho$ is the same, the current of the atomic orbital is confined to a circle in the $v = c$ frame as well as the lab frame as given by Eq. (1.280). Since the current is orthogonal to the central vector at the same $\rho$ for each circular current-density element, there is no self interaction, but there is an interaction between circular current-density elements for different values of $\rho$ that balances the centrifugal force as given by Eq. (3.30) and Eqs. (3.37-3.38) to maintain the free electron as an equipotential 2-D surface..

As given by Eq. (3.15), the total angular momentum confined to the plane of the free electron is $\hbar$. The radiation reaction force requires conservation of the reaction photon's angular momentum of $\hbar$. Thus, this force is only present for the free electron as opposed to the bound electron since the radial direction in the bound case is perpendicular to the surface and a photon of $\hbar$ of angular momentum may only be emitted through a release of energy due to the central field.

Furthermore, since fundamental particles such as the electron are superconducting, nonresonant collisions cannot change the intrinsic angular momentum. Such collisions involve the entire particle. And, the intrinsic angular momentum remains unchanged, except when a resonant photon is emitted or absorbed according to the Maxwellian-based conservation rules given in the Excited States section and the Equation of the Photon section.

Similar to the case of the electric field, a discontinuity in surface mass density gives rise to a discontinuity in the curvature of spacetime originating at the two-dimensional surface. Thus, in addition to the absence of electric self-interaction (Appendix II), the Virial theorem does not apply regarding gravitational self-interaction. The derivation of the gravitational field is given in the Gravity section.

electron current loop at position $\rho < \rho_0$ due to the electron current loop at position $\rho_0$ follows from Eq. (1.130) after McQuarrie [12]:

$$\mathbf{B} = \frac{\mu_o e\hbar}{2m_e\rho_0^3} \tag{3.30}$$

wherein the intrinsic angular momentum during photon interaction is the same as that of a bound electron as shown in the Stern-Gerlach Experiment section and $\mu_0$ is the permeability of free-space ($4\pi\ X\ 10^{-7}\ N/A^2$). The motion at each position of the electron loop at radius $\rho < \rho_0$ in the presence of the magnetic field of the current loop at position $\rho_0$ gives rise to a central force which acts at each charge density element of the former. The Lorentz force at each element moving at velocity $\mathbf{v}$ is

$$\mathbf{F}_{mag} = e\mathbf{v}\times\mathbf{B} = e\rho\omega\times\mathbf{B} \tag{3.31}$$

Substitution of Eq. (3.17) for $\omega$ and Eq. (3.30) for $\mathbf{B}$ based on the angular momentum of the free electron of $\hbar$ gives:

$$\mathbf{F}_{mag} = \frac{5}{2}\left(\rho\frac{e\hbar}{m_e\rho_0^2}\right)\frac{\mu_0 e\hbar}{2m_e\rho_0^3} = \frac{5}{2}\left[\frac{e^2\mu_o}{2m_e\rho_0}\right]\frac{\hbar^2\rho}{m_e\rho_0^4} \tag{3.32}$$

Furthermore, the term in brackets can be expressed in terms of the fine structure constant $\alpha$. The radius of the electron loop in the light-like frame is $\lambda\!\!\!^{-}_C$. From Eq. (1.250)

$$\frac{e^2\mu_o}{2m_e\rho_0} = 2\pi\alpha \tag{3.33}$$

Based on the relativistic invariance of $\frac{e}{m_e}$ corresponding to the invariance of $\mu_B$ given by Eq. (1.131) as well as its invariant angular momentum of $\hbar$, it can be shown that the relativistic correction to Eq. (3.32) is the reciprocal of Eq. (3.33). Specifically, as shown previously in the One Electron Atom—Determination of Atomic Orbital Radii section and the Two-Electron Atoms section, the relativistic correction $\gamma'$ due to the light speed electrodynamic central force is:

$$\gamma' = (2\pi\alpha)^{-1} \tag{3.34}$$

Thus, Eq. (3.32) becomes:

$$\mathbf{F}_{mag} = \frac{5}{2}\frac{\hbar^2\rho}{m_e\rho_0^4} \tag{3.35}$$

Eq. (3.35) gives the force as a function of the radius $\rho$.

The centrifugal force due to each charge density element on each current loop about the angular-momentum axis is balanced by the centripetal force $\mathbf{F}_{mag}$. During the radiation reaction event, the centrifugal force, $\mathbf{F}_{i\ centrifugal}$, at each point of the free electron of mass $m_i$ is given by:

$$\mathbf{F}_{i\ centrifugal} = m_i\rho\omega^2\mathbf{i}_\rho = m_i\frac{v^2}{\rho}\mathbf{i}_\rho \tag{3.36}$$

(An equation for $\mathbf{F}_{mag}$ that is also proportional to the angular frequency squared that parallels that of Eq. (3.41) is given by expressing the magnetic flux in terms of the current given by the charge times the angular frequency [13].) The velocity $\mathbf{v}$ at each point follows from the angular velocity (Eq. (3.17)) and is given by:

$$\mathbf{v} = \rho\frac{5}{2}\frac{\hbar}{m_e\rho_0^2}\mathbf{i}_\phi \tag{3.37}$$

where $\rho$ is the radius of the point. Substitution of Eq. (3.37) into Eq. (3.36) gives:

$$\mathbf{F}_{i\ centrifugal} = -\frac{m_i}{\rho}\left(\rho\frac{5}{2}\frac{\hbar}{m_e\rho_0^2}\right)^2\mathbf{i}_\rho \tag{3.38}$$

The integral over the density gives the total force $\mathbf{F}_{centrifugal}$. As in the case of $\mathbf{F}_{mag}$, $\mathbf{F}_{centrifugal}$ for the radiation reaction event is linear in $\rho$ such that the force per unit area is equal over the two-dimensional lamina to maintain the constraints that the electron is an equipotential, minimum-energy surface and the corresponding energy is proportional to $\hbar\omega$ of a photon. Thus, $F_{centrifugal}$, the linear factor for $\mathbf{F}_{centrifugal}$ is given by multiplication of Eq. (3.38) by $\frac{\rho}{\rho_0}$, substitution of the mass density (Eq. (3.7)) for $m_i$, and integration over the plane lamina:

$$F_{centrifugal} = \frac{1}{\rho_0}\left(\frac{5}{2}\frac{\hbar}{m_e\rho_0^2}\right)^2 \int_0^{2\pi}\int_0^{\rho_0} \frac{m_e}{\frac{2}{3}\pi\rho_0^3}\sqrt{\rho_0^2-\rho^2}\,\rho^2\rho d\rho d\phi$$

$$= 2\pi\frac{m_e}{\frac{2}{3}\pi\rho_0^4}\frac{1}{\rho_0}\left(\frac{5}{2}\frac{\hbar}{m_e\rho_0^2}\right)^2\left(\left(-\frac{1}{5}\rho^2-\frac{2}{15}\rho_0^2\right)\left(\rho_0^2-\rho^2\right)^{3/2}\right)_0^{\rho_0} \tag{3.39}$$

$$= \frac{5}{2}2\pi\frac{\hbar^2}{\frac{2}{3}\pi m_e\rho_0^8}\frac{5}{2}\frac{2}{15}\rho_0^5 = \frac{5}{2}\frac{\hbar^2}{m_e\rho_0^3}$$

$F_{centrifugal}$ is also the magnitude of the total centrifugal force of the ensemble of current loops that is equally distributed throughout the plane lamina. It is also given by using Eq. (3.36) in another form:

$$\mathbf{F}_{i\ centrifugal} = m_i\rho^2\omega\frac{\omega}{\rho}\mathbf{i}_\rho \tag{3.40}$$

Substitution of the total angular momentum given by Eqs. (3.18-3.20), the angular velocity given by Eq. (3.17), and the total radius $\rho_0$ into Eq. (3.40) gives $F_{centrifugal}$:

$$F_{centrifugal} = \hbar\frac{\frac{5}{2}\frac{\hbar}{m_e\rho_0^2}}{\rho_0} = \frac{5}{2}\frac{\hbar^2}{m_e\rho_0^3} \tag{3.41}$$

Using Eq. (3.39) or Eq. (3.41), $\mathbf{F}_{centrifugal}$ is given by:

$$\mathbf{F}_{centrifugal} = \frac{\rho}{\rho_0}\frac{5}{2}\frac{\hbar^2}{m_e\rho_0^3}\mathbf{i}_\rho = \frac{5}{2}\frac{\hbar^2\rho}{m_e\rho_0^4}\mathbf{i}_\rho \tag{3.42}$$

$\mathbf{F}_{centrifugal}$ is further given by the derivative of $E_{rot}$:

$$F_{centrifugal} = -\frac{\rho}{\rho_0}\frac{\delta E_{rot}}{\delta\rho_0}\mathbf{i}_\rho = -\frac{\rho}{\rho_0}\frac{\delta}{\delta\rho_0}\left(\frac{5}{4}\frac{\hbar^2}{m_e\rho_0^2}\right)\mathbf{i}_\rho = \frac{5}{2}\frac{\hbar^2\rho}{m_e\rho_0^4}\mathbf{i}_\rho \tag{3.43}$$

where $E_{rot}$ is given by Eq. (3.50). From Eqs. (3.42-3.43) and (3.35), the outward centrifugal force, $\mathbf{F}_{centrifugal}$, due to each element on each current loop about the angular-momentum axis is balanced by the centripetal force $\mathbf{F}_{mag}$ due to the magnetic interactions between the current loops.

Furthermore, the free electron possesses a total charge $e$, a total mass $m_e$, and an angular momentum of $\hbar$. The magnetic moment is given by Eq. (2.65); thus,

$$\mu_B = \frac{e\hbar}{2m_e} = 9.274\ X\ 10^{-24}\ JT^{-1} \tag{3.44}$$

which is the Bohr magneton. Conservation of angular momentum with the linking of flux in discrete increments of the magnetic flux quantum gives rise to the spin quantum number, $m_s$, and the $g$ factor which is the same as given previously in the Electron g Factor section. The behavior of the free electron in a magnetic field is given in the Stern-Gerlach Experiment section. It is shown next that the intrinsic angular momentum of $\hbar$ is unchanged as the electron acquires linear velocity with a concomitant change in its de Broglie wavelength.

# CLASSICAL PHYSICS OF THE DE BROGLIE RELATIONSHIP

As shown in Appendix IV, the plane-lamina of the free electron generates a spherical current-density pattern over time during the interaction with photons designated $Y_0^0(\theta,\phi)$. The angular momentum of the photon given by $\mathbf{m} = \int\frac{1}{8\pi c}\mathrm{Re}\left[\mathbf{r}\times(\mathbf{E}\times\mathbf{B}^*)\right]dx^4 = \hbar$ in the Photon section is conserved [14] for the solutions for the resonant photons and excited state electron functions given in the Excited States of the One-Electron Atom (Quantization) section. It can be demonstrated that the resonance condition between these frequencies is to be satisfied in order to have a net change of the energy field [15]. In this case, the correspondence principle holds. That is the change in angular frequency of the electron is equal to the angular frequency of the resonant photon that excites the resonator cavity mode corresponding to the transition, and the energy is given by Planck's equation. The same conditions apply to the free electron, and the correspondence between the principles of the bound and free electrons further hold in the case of the Stern-Gerlach experiment as given in the Stern-Gerlach Experiment section.

The linear velocity of the free electron can be considered to be due to absorption of photons that excite surface currents corresponding to a decreased de Broglie wavelength where the free electron is equivalent to a continuum excited state with

conservation of the parameters of the bound electron discussed *supra*. The relationship between the electron wavelength and the linear velocity is

$$\frac{\lambda}{2\pi} = \rho_0 = \frac{\hbar}{m_e v_z} = k^{-1} = \frac{v_z}{\omega_z} \tag{3.45}$$

In this case, the angular frequency $\omega_z$ is given by:

$$\omega_z = \frac{\hbar}{m_e \rho^2{}_0} \tag{3.46}$$

which conserves the photon's angular momentum of $\hbar$ with that of the electron relative to its center of mass. The angular momentum conservation relationship of $\hbar$ is the same as that of the bound electron given by Eq. (1.37) where the velocity is $v_z$ given by Eq. (3.2) and the radius is $\rho_0$ given by Eq. (3.29). In addition, the electron kinetic energy $T$ is given by

$$T = \frac{1}{2} m_e v_z^2 = \frac{1}{2} \frac{\hbar^2}{m_e \rho_0^2} = \frac{1}{2} \hbar \omega_z \tag{3.47}$$

The potential energy, $E_{mag}$, corresponding to $\mathbf{F}_{mag}$ is given by the integral over the radius:

$$E_{mag} = \int_{\rho_0}^{0} \frac{5}{2} \frac{\hbar^2}{m_e \rho_0^4} \rho d\rho = \frac{5}{2} \frac{\hbar^2}{m_e \rho_0^4} \left( \frac{\rho^2}{2} \right)_{\rho_0}^{0} = -\frac{5}{4} \frac{\hbar^2}{m_e \rho_0^2} \tag{3.48}$$

The rotational kinetic energy, $E_{rot}$, of the free electron corresponding to the angular momentum given by Eqs. (3.18-3.20) is:

$$E_{rot} = \frac{1}{2} L\omega = \frac{1}{2} I\omega^2 = \frac{1}{2} m_e v^2 \tag{3.49}$$

Using Eqs. (3.17), (3.20), and (3.49) gives:

$$E_{rot} = \frac{1}{2} L\omega = \frac{1}{2} \hbar \frac{5}{2} \frac{\hbar}{m_e \rho_0^2} = \frac{5}{4} \frac{\hbar^2}{m_e \rho_0^2} \tag{3.50}$$

Similarly to Eq. (3.48), $E_{rot}$ is also given by the integral of the corresponding force, $\mathbf{F}_{centrifugal}$, given by Eq. (3.43).

The total energy, $E_T$, is given by the sum of the change in the free-electron translational kinetic energy, $T$, the rotational energy, $E_{rot}$, corresponding to the current of the loops, and the potential energy, $E_{mag}$, due to the radiation reaction force $\mathbf{F}_{mag}$, the magnetic attractive force between the current loops due to the relative rotational or current motion:

$$E_T = T + E_{rot} + E_{mag} = \frac{1}{2} \frac{\hbar^2}{m_e \rho_0^2} + \frac{5}{4} \frac{\hbar^2}{m_e \rho_0^2} - \frac{5}{4} \frac{\hbar^2}{m_e \rho_0^2} = \frac{1}{2} \frac{\hbar^2}{m_e \rho_0^2} \tag{3.51}$$

Thus, the total energy, $E_T$, of the excitation of a free-electron transitional state by a photon having $\hbar$ of angular momentum and an energy given by Planck's equation of $\hbar\omega$ is:

$$E_T = T = \frac{1}{2} m_e v_z^2 = \frac{1}{2} \frac{h^2}{m_e \lambda^2} = \frac{1}{2} \hbar \omega_z \tag{3.52}$$

where $\lambda$ is de Broglie wavelength. The angular momentum of the free electron of $\hbar$ is unchanged, the energies in the currents in the plane lamina are balanced so that the total energy is unchanged, and the radius $\rho_0$ changes to match the de Broglie wavelength and frequency at an increased velocity. At this velocity, the kinetic energy matches the energy provided by the photon wherein the de Broglie frequency matches the photon frequency and both the electron-kinetic energy and the photon energy are given by Planck's equation.

Eq. (3.52) is identical to Eq. (2.22) that gives the relationship between the energy and frequency of a photon that causes a bound excited state and the corresponding change in the electron's kinetic energy. A photon of the same energy as Eq. (3.52) is emitted due to acceleration of the free electron by an applied electric field to acquire the velocity $v_z$ in agreement with the Abraham-Lorentz equation of motion [16]. This relationship is identical to that of the binding energy and kinetic energy of the bound electron in the central field of the proton given in the Photon Absorption section. The exception is that the photon-bound-electron interaction results in a trapped photon with the electron in a different orbit with a maintained eccentricity of zero and a decreased angular and linear velocity; whereas, the eccentricity of the orbit for the photon-free-electron interaction goes to infinity corresponding to a hyperbolic orbit that approaches rectilinear motion with an increased linear velocity. The angular distribution of radiation emitted by an accelerated charge and the distribution in frequency and angle of energy radiated by accelerated charges is also given classically in Sections 14.3 and 14.5 of Jackson [17,18].

The correspondence principle is the basis of the de Broglie wavelength relationship. Stated in other words, the de Broglie relationship is not an independent fundamental property of matter in conflict with physical laws as formalized in the wave-particle-duality-related postulates of quantum mechanics and the corresponding Schrödinger wave equation. Nothing is waving including probability. The relationship arises from the correspondence principle that is based on Maxwell's equations and conservation of angular momentum and energy. The other fundamental misconceptions of quantum mechanics that serve as its foundations are the impossibility of explaining the Stern-Gerlach experimental results and the double-slit interference pattern

of electrons classically. In contradiction to widely accepted beliefs, these phenomena are also shown to be exactly predicted from first principles (Stern-Gerlach Experiment section and in the Two-Slit Interference (Wave-Particle Duality) section).

## STERN-GERLACH EXPERIMENT

The Stern Gerlach experiment demonstrates that the magnetic moment of the electron can only be parallel or antiparallel to an applied magnetic field. This implies a spin quantum number of 1/2 corresponding to an angular momentum on the z-axis of $\frac{\hbar}{2}$. However, the Zeeman splitting energy corresponds to a magnetic moment of a Bohr magneton $\mu_B$ and implies an electron angular momentum on the z-axis of $\hbar$—twice that expected. This in turn implies that the gyromagnetic ratio is twice that expected for a classical magnetic moment generated by a current loop. Historically, this dilemma was felt to be inexplicable and could only be resolved by purely mathematical approaches rather than physics. It is shown *infra* that this is not the case. The Stern-Gerlach results are completely predictable from first principles, and the results are intuitive.

The free electron arises during pair production and ionization. In both cases, the production photon or the ionizing photon carries $\hbar$ of angular momentum. The derivations of the parameters of the free electron given *supra* were made with the conservation of the photon angular momentum implicit. The vector and scalar parameters of the bound electron in a magnetic field given in the Atomic Orbital Equation of Motion for $\ell = 0$ Based on the Current Vector Field (CVF) section and the Magnetic Parameters of the Electron (Bohr Magneton) Stern-Gerlach Experiment section are also conserved in the case of a free electron in a magnetic field.

Consider the case of a magnetic field applied to the free electron. The direction of the electron's intrinsic angular momentum of $\hbar$ and the corresponding magnetic moment of $\mu_B$ can change orientation with the application of a magnetic field or an electric field. It is also reoriented by interaction with photons. Randomly-directed fields and random photon interactions give rise to random orientations. Thus, in the absence of an applied orienting field or a specific procedure to produce a polarized state, the free electron is unpolarized. The Bohr magneton of magnetic moment of the free electron corresponding to its $\hbar$ of angular momentum is initially in a random direction relative to the z-axis, the axis of an applied magnetic field. The center of mass of the electron propagates at the original constant velocity $v_z$ in Eq. (3.2).

Then, a small diamagnetic azimuthal current in the plane of the lamina opposes an applied field according to Lenz's law as given for the bound electron in Box 1.1. Furthermore, the application of the magnetic field causes a resonant excitation of the Larmor precession as in the case of the bound electron wherein the energy arises from that stored in the applied magnetic field. The excitation can be described in terms of photons in the same manner as in the case of photon emission or absorption due to an applied electric field that causes the free electron to accelerate. The Larmor precession frequency is given by the product of the gyromagnetic ratio of the electron, $\frac{e}{2m}$, and the magnetic flux **B** [19]. As in the case of the bound electron, the precessing free electron is a spin-1/2 particle ($L_z = \frac{\hbar}{2}$), but the stationary resultant angular momentum projection that is either parallel or antiparallel to the applied-field axis is $\hbar$ corresponding to a full Bohr magneton of magnetic moment. Here, each of the resonant photons which excites the Larmor precession and the intrinsic angular momentum of the free electron (Eq. (3.20)) contribute equally to the resultant z-axis projection. As shown in the Excited States of the One-Electron Atom (Quantization) section, conservation of the angular momentum of the photon of $\hbar$ gives rise to $\hbar$ of electron angular momentum in the excited state. The photon having the Larmor frequency corresponding to the energy given by Eq. (1.227) and $\hbar$ of angular momentum initially along an axis in the transverse (xy)-plane causes the electron and the photon to precess about both the z-axis and the transverse-axis. Then, as a time average the angular momentum of the precessing electron contributes one-half of its intrinsic angular momentum of $\hbar$ to the projection on the z-axis, and the photon angular momentum also contributes $\frac{\hbar}{2}$ to the z-projection.

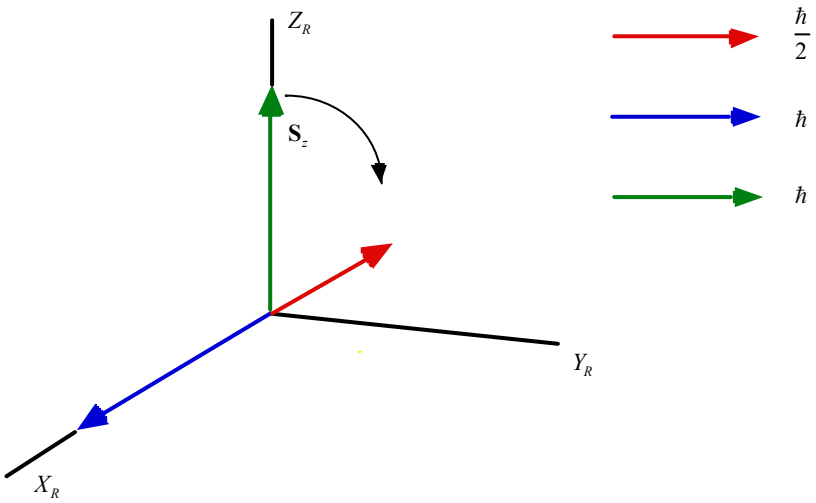
As shown in Appendix IV, with the electron current in the counter clockwise direction, the Larmor precession of the angular momentum vector of the free electron is about two axes simultaneously, the $\left(\mathbf{i}_x, 0\mathbf{i}_y, \mathbf{i}_z\right)$-axis and the laboratory-frame z-axis defined by the direction of the applied magnetic field. The precessions are about the opposite axes with the current in the opposite direction. The motion generates CVFs equivalent to those of the bound electron given in the Atomic Orbital Equation of Motion for $\ell = 0$ Based on the Current Vector Field (CVF) section. Over one time period, the first motion sweeps out the equivalent of a BECVF, and the rotation about the z-axis sweeps out the equivalent of an OCVF. The combined motions sweep out the equivalent of the convolution of the BECVF with the OCVF, an angular-momentum distribution equivalent to $Y_0^0(\theta,\phi)$ of the bound electron. The Larmor excited precessing electron can further interact with another resonant photon that gives rise to Zeeman splitting—energy levels corresponding to flipping of the parallel or antiparallel alignment of the electron magnetic moment of a Bohr magneton with the magnetic field.

The parameters of the photon standing wave for the Larmor precession and the Zeeman effect of the free electron follow from those of the bound electron given in the Magnetic Parameters of the Electron (Bohr Magneton) section and Box 1.1. To cause the Larmor excitation and the spin-flip transition, the corresponding photon gives rise to surface currents in the plane of the free electron that are equivalent to the projection of the time- and spherically-harmonic dipole Larmor currents of the bound

electron into the free-electron plane. The currents cause a precession of the disc to form a time-averaged bi-conical cavity that is azimuthally symmetrical about the $(\mathbf{i}_x, 0\mathbf{i}_y, \mathbf{i}_z)$-axis (Figure 3.8). The time-averaged angular momentum and rotational energy of the currents that are phase-locked to the photon field is zero as given by Eqs. (1.76-1.77), but the photon's angular momentum is $\hbar$ corresponding to a magnetic moment of one Bohr magneton $\mu_B$ as shown for the case of the Larmor resonant excitation of a bound electron in Box 1.1.

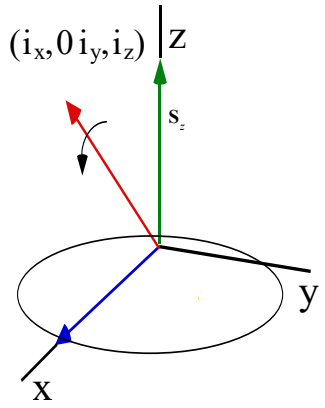
The $\hbar$ of angular momentum of the photon that excites the Larmor precession is initially along an axis in the transverse (xy)-plane. This causes a torque on the z-axis-directed $\hbar$ of angular momentum of the electron and causes it to rotate into the xy-plane. This in turn causes a torque on the angular momentum of the photon. As a result the electron and the photon undergo mutual precession about both the $(\mathbf{i}_x, 0\mathbf{i}_y, \mathbf{i}_z)$-axis and the z-axis. The motion is more easily analyzed by first considering a coordinate system that rotates about the z-axis. In the coordinate system rotating at the Larmor frequency (denoted by the axes labeled $X_R$, $Y_R$, and $Z_R$ in Figure 3.6), the positive $X_R$-component of magnitude $\hbar$ corresponding to the photon and a negative $X_R$-component of magnitude $\frac{\hbar}{2}$ (Eq. (3.65)), corresponding to the current generated by the rotation of the free electron about the $X_R$-axis, are stationary. The angular momentum vector of the free electron of magnitude $\hbar$ corresponding to a magnetic moment of one Bohr magneton $\mu_B$ is designated by $\mathbf{S}_z$. The photon's positive $\hbar$ of angular momentum along $X_R$ with a corresponding magnetic moment of $\mu_B$ (Eq. (28) of Box 1.1) causes the $\mathbf{S}_z$ to rotate about $X_R$. As the $Z_R$-axis precesses about the $X_R$-axis, it causes a reactive torque such that the $X_R$-axis also rotates about the $Z_R$-axis. Consequently, the two vectors shown in Figure 3.6 precess about both the $(\mathbf{i}_x, 0\mathbf{i}_y, \mathbf{i}_z)$-axis and the z-axis.

**Figure 3.6.** The initial angular momentum components of the free electron and positive and negative $X_R$ components in the rotating coordinate system ($X_R$, $Y_R$, $Z_R$) that precesses at the Larmor frequency about $Z_R$ such that the vectors are stationary. The electron is initially in the $X_R\,Y_R$-plane.




For further convenience, a second primed Cartesian coordinate system refers to the axes that rotate with the $(\mathbf{i}_x, 0\mathbf{i}_y, \mathbf{i}_z)$-axis about the z-axis at the Larmor frequency wherein the x'y'-plane of the plane-lamina disc of the free electron aligns with the xy-plane time harmonically at this frequency. Then, each of the $X_R$-, $Y_R$, and $Z_R$-axis is designated the x'-, y', and z'-axis, respectively. The initial corresponding precession of the plane lamina in the x'y'-plane about each of the z- and x-axes results in a precession about the $(\mathbf{i}_x, 0\mathbf{i}_y, \mathbf{i}_z)$-axis as shown in Figure 3.7. The electron precession motion about the $(\mathbf{i}_x, 0\mathbf{i}_y, \mathbf{i}_z)$-axis which is stationary in the rotating frame generates a BECVF as given in Appendix IV which is a solid version of the BECVF for the case of the bound electron. The rotation of the BECVF in the laboratory frame generates the $Y_0^0(\theta,\phi)$ distribution.

**Figure 3.7.** In the Larmor-frequency rotating ( $X_R$, $Y_R$, $Z_R$ ) frame, the plane-lamina disc of the free electron rotates about the $\left(\mathbf{i}_x, 0\mathbf{i}_y, \mathbf{i}_z\right)$-axis. The resultant angular momentum vector of $\sqrt{2}\hbar$ (red vector) having projections onto each of the $Z_R$-axis (green vector) and the $X_R$-axis (blue vector) of $\hbar$ is stationary on the rotating $\left(\mathbf{i}_x, 0\mathbf{i}_y, \mathbf{i}_z\right)$-axis. The electron precession motion about the $\left(\mathbf{i}_x, 0\mathbf{i}_y, \mathbf{i}_z\right)$-axis generates the free electron BECVF. The green and blue vectors can be assigned to the intrinsic electron and photon angular momentum at $t = 0$, respectively. These components rotate about the $\left(\mathbf{i}_x, 0\mathbf{i}_y, \mathbf{i}_z\right)$-axis and harmonically interchange at each one-half period of rotation. Thus, z-axis component of $\hbar$ comprises a time-averaged contribution of $\frac{\hbar}{2}$ from each of the electron and the photon.




The Larmor excitation comprises a double precession. The z-axis angular momentum projection before and after the excitation of the Larmor precession is $\hbar$, and the energy of the photon to cause the precession of the $\left(\mathbf{i}_x, 0\mathbf{i}_y, \mathbf{i}_z\right)$-axis about the z-axis at the Larmor frequency is given by Eq. (25) of Box 1.1. Therefore, only the torque balance of the precession of the electron about the $\left(\mathbf{i}_x, 0\mathbf{i}_y, \mathbf{i}_z\right)$-axis in the Larmor-frequency rotating ( $X_R$, $Y_R$, $Z_R$ ) frame (Figure 3.7) needs to be considered. The derivation of the corresponding current density about the x'-axis follows that for the bound electron given in the Magnetic Parameters of the Electron (Bohr Magneton) section. The magnetic moment (angular momentum) can be determined from the current (mass)-density function. The magnetic moment of a current loop of area $\pi y'^2$ due to a point charge element of charge $e_i$ that has an angular velocity of $\omega_{x'}\ \mathbf{i}_{x'}$ is given by

$$\mathbf{m}_{x'} = e_i y'^2 \frac{\omega_{x'}}{2}\ \mathbf{i}_{x'} \tag{3.53}$$

The angular momentum of a point mass element of mass $m_i$ at a distance $y'$ from the rotation axis with an angular velocity of $\omega_{x'}\ \mathbf{i}_{x'}$ is given by

$$\mathbf{L}_{x'} = m_i y'^2\ \omega_{x'}\ \mathbf{i}_{x'} = I_x \omega_{x'}\ \mathbf{i}_{x'} \tag{3.54}$$

where $I_x$ is the moment of inertia. If the free electron simply rotated as a rigid plane-lamina disc with the mass density maintained in the plane as given by Eq. (3.7) and as shown in Figure 3.2, then the moment of inertia $I_x$ corresponding to a rotation of the disc about the x'-axis would be given by

$$\begin{aligned} I_{x'} &= 2\frac{m_e}{\frac{2}{3}\pi\rho_0^3}\int_{-\rho_0}^{\rho_0}\int_{0}^{\sqrt{\rho_0^2 - x'^2}} \sqrt{\rho_0^2 - \left(x'^2 + y'^2\right)}\, y'^2\, dy'dx'\ \mathbf{i}_{x'} \\ &= \frac{3}{\pi}\frac{m_e}{\rho_0^3}\int_{-\rho_0}^{\rho_0}\int_{0}^{\sqrt{\rho_0^2 - x'^2}} y'^2 \sqrt{\left(\rho_0^2 - x'^2\right) - y'^2}\, dy'dx'\ \mathbf{i}_{x'} \end{aligned} \tag{3.55}$$

Using the integral with respect to $y'$ given by #210 of Lide [20], Eq. (3.55) becomes

$$I_{x'}=\frac{3}{\pi}\frac{m_e}{\rho_0^3}\int_{-\rho_0}^{\rho_0}\left(\begin{array}{l}-\dfrac{y'}{4}\sqrt{\left(\left(\rho_0^2-x'^2\right)-y'^2\right)^3}+\\ \dfrac{\rho_0^2-x'^2}{8}\left(y'\sqrt{\left(\rho_0^2-x'^2\right)-y'^2}+\left(\rho_0^2-x'^2\right)\arcsin\dfrac{y'}{\left|\sqrt{\rho_0^2-x'^2}\right|}\right)\end{array}\right|_0^{\sqrt{\rho_0^2-x'^2}}dx'\ \mathbf{i}_{x'} \tag{3.56}$$

Evaluation at the integration limits gives

$$I_{x'}=\frac{3}{16}\frac{m_e}{\rho_0^3}\int_{-\rho_0}^{\rho_0}\left(\rho_0^2-x'^2\right)^2dx'\ \mathbf{i}_{x'} \tag{3.57}$$

The multiplication and integration of each term followed by evaluation at the limits gives

$$\begin{aligned}I_{x'}&=\frac{3}{16}\frac{m_e}{\rho_0^3}\left(\rho_0^4x'-\frac{2\rho_0^2x'^3}{3}+\frac{x'^5}{5}\right)_{-\rho_0}^{\rho_0}\ \mathbf{i}_{x'}\\&=\frac{3}{16}\frac{m_e}{\rho_0^3}\left(2\rho_0^5-\frac{4\rho_0^5}{3}+\frac{2\rho_0^5}{5}\right)\ \mathbf{i}_{x'}=\frac{1}{5}m_e\rho_0^2\ \mathbf{i}_{x'}\end{aligned} \tag{3.58}$$

which is 1/2 the moment of inertia of a uniform disc as shown by Fowles [21].

The angular momentum $\mathbf{L}_{x'}$ follows from Eq. (3.54) as Eq. (3.58) times the constant angular velocity $\omega_{x'}\ \mathbf{i}_{x'}$. It is shown *infra* that the torque due to the photon's angular momentum of $\hbar$ initially along the x'-axis does cause $\mathbf{S}_z$ to rotate such that the mass-density function and the magnitude of the angular momentum-density function about the x'-axis are the same as those about the z-axis given by Eqs. (3.7) and (3.17), respectively.

By the perpendicular-axis theorem [21], the corresponding angular momentum about the x'-axis is 1/2 that about the z-axis. This is easily shown since Eq. (3.19) can be expanded as

$$\mathbf{L}\mathbf{i}_z=\int_0^{2\pi}\int_0^{\rho_0}\frac{m_e}{\frac{2}{3}\pi{\rho_0}^3}\sqrt{{\rho_0}^2-\rho^2}\,\frac{5}{2}\frac{\hbar}{m_e\rho_0^2}\left(x^2+y^2\right)\rho d\rho d\phi\ \mathbf{i}_z \tag{3.59}$$

Then the angular momentum about the x'-axis is

$$\mathbf{L}\mathbf{i}_{x'}=-\int_0^{2\pi}\int_0^{\rho_0}\frac{m_e}{\frac{2}{3}\pi{\rho_0}^3}\sqrt{{\rho_0}^2-\rho^2}\,\frac{5}{2}\frac{\hbar}{m_e\rho_0^2}\left(y'^2\right)\rho d\rho d\phi\ \mathbf{i}_z \tag{3.60}$$

which is 1/2 that of Eq. (3.59) since the number of symmetrical axes of integration was reduced to 1/2. This result can also be shown directly. Then, the angular momentum along the x'-axis corresponding to a rotation of the mass of the electron about this axis during a Larmor excitation is given by

$$\begin{aligned}\mathbf{L}\mathbf{i}_{x'}&=-\frac{m_e}{\frac{2}{3}\pi{\rho_0}^3}\frac{5}{2}\int_{-\rho_0}^{\rho_0}\int_{-\sqrt{\rho_0^2-x'^2}}^{\sqrt{\rho_0^2-x'^2}}\sqrt{\rho_0^2-\left(x'^2+y'^2\right)}\,\frac{\hbar}{m_e\rho_0^2}\,y'^2\,dy'dx'\ \mathbf{i}_{x'}\\&=-\frac{15\hbar}{4\pi{\rho_0}^5}\int_{-\rho_0}^{\rho_0}\int_{-\sqrt{\rho_0^2-x'^2}}^{\sqrt{\rho_0^2-x'^2}}\sqrt{\left(\rho_0^2-x'^2\right)-y'^2}\,y'^2\,dy'dx'\ \mathbf{i}_{x'}\end{aligned} \tag{3.61}$$

with the mass density and $\omega_{x'}$ equivalent to that of Eq. (3.19) but directed around the x'-axis and $\rho d\rho d\phi$ was replaced by $dy'dx'$. Using the integral with respect to $y'$ given by # 210 of Lide [20], Eq. (3.61) becomes

$$\mathbf{L}\mathbf{i}_{x'}=-\frac{15\hbar}{4\pi{\rho_0}^5}\int_{-\rho_0}^{\rho_0}\left(\begin{array}{l}-\dfrac{y'}{4}\sqrt{\left(\rho_0^2-x'^2-y'^2\right)^3}\\ +\dfrac{\rho_0^2-x'^2}{8}\left(y'\sqrt{\rho_0^2-x'^2-y'^2}+\left(\rho_0^2-x'^2\right)\sin^{-1}\dfrac{y'}{\left|\sqrt{\rho_0^2-x'^2}\right|}\right)\end{array}\right|_{-\sqrt{\rho_0^2-x'^2}}^{\sqrt{\rho_0^2-x'^2}}dx'\mathbf{i}_{x'} \tag{3.62}$$

$$\begin{aligned}\mathbf{L}\mathbf{i}_{x'}&=-\frac{15\hbar}{4\pi{\rho_0}^5}\frac{\pi}{8}\int_{-\rho_0}^{\rho_0}\left(\rho_0^2-x'^2\right)^2dx'\ \mathbf{i}_{x'}\\&=-\frac{15\hbar}{32{\rho_0}^5}\int_{-\rho_0}^{\rho_0}\left(\rho_0^4-2\rho_0^2x'^2+x'^4\right)dx'\ \mathbf{i}_{x'}\end{aligned} \tag{3.63}$$

The integration of each term with respect to $x'$ followed by evaluation at the limits gives:

$$\mathbf{L}\mathbf{i}_{x'} = -\frac{15\hbar}{32\rho_0^{\,5}}\left(\rho_0^4 x' - 2\frac{\rho_0^2 x'^3}{3} + \frac{x'^5}{5}\right)_{-\rho_0}^{\rho_0} \mathbf{i}_{x'} = -\frac{\hbar}{2}\,\mathbf{i}_{x'} \tag{3.64}$$

which is 1/2 the angular momentum of the free electron given by Eqs. (3.19-3.20).

The torque **N** in rotating coordinates is given by [22]

$$\mathbf{N} = \dot{\mathbf{L}} + \omega\mathbf{i}_{x'} \times \mathbf{L} \tag{3.65}$$

The electron's angular momentum of $\hbar$ is conserved. Thus, the torque $\mathbf{N}_\mathbf{p}$ on the electron's angular momentum of $\hbar$ due to the photon's angular momentum of $\hbar$ and corresponding magnetic moment of $\mu_B$ is

$$\mathbf{N}_\mathbf{p} = \omega\hbar\mathbf{i}_{x'} \tag{3.66}$$

The torque $\mathbf{N}_c$ corresponding to the centrifugal force $\mathbf{F}_\mathbf{c}$ for a rotating system is given by:

$$\mathbf{N}_\mathbf{c} = r \times \mathbf{F}_\mathbf{c} = -mr^2\omega^2\mathbf{i}_{x'} = -I_{x'}\omega^2\mathbf{i}_{x'} = -\mathbf{L}_{x'}\omega\mathbf{i}_{x'} \tag{3.67}$$

Substitution of Eq. (3.64) into Eq. (3.67) gives

$$\mathbf{N}_\mathbf{c} = -\frac{\hbar}{2}\omega\mathbf{i}_{x'} \tag{3.68}$$

The rotating mass/charge density gives rise to an angular momentum of $\frac{\hbar}{2}$ (Eq. (3.64)) and a corresponding magnetic moment of $\frac{\mu_B}{2}$ (Eq. (28) of Box 1.1) that opposes the magnetic moment of the photon. The corresponding torque is:

$$\mathbf{N}_{x'} = -\mathbf{L}_{x'}\omega\mathbf{i}_{x'} = -\frac{\hbar}{2}\omega\mathbf{i}_{x'} \tag{3.69}$$

The required torque balance is:

$$\mathbf{N}_\mathbf{p} + \mathbf{N}_c + \mathbf{N}_{x'} = \omega\mathbf{i}_{x'}\left(\hbar - \frac{\hbar}{2} - \frac{\hbar}{2}\right) = 0 \tag{3.70}$$

The result of Eq. (3.70) confirms the match of the mass-density function and magnitude of the angular frequency function of Eqs. (3.59-3.64) with those of Eq. (3.19).

Thus, the application of a magnetic field causes a resonant excitation of the Larmor precession. The $\hbar$ of angular momentum on the z'-axis and the $\hbar$ of angular momentum on the x'-axis gives a resultant stationary projection of $\sqrt{2}\hbar$ onto the $\left(\mathbf{i}_\mathbf{x}, 0\mathbf{i}_\mathbf{y}, \mathbf{i}_\mathbf{z}\right)$-axis. The static projection of the resultant onto the z-axis is $\hbar$. The precessing electron can further interact with a resonant photon directed along the x-axis that rotates the z-axis-directed static projection of the resultant of $\hbar$ such that it flips it to the opposite direction. Thus, absorption of an RF photon gives rise to a Zeeman transition corresponding to flipping of the parallel or antiparallel alignment of the electron magnetic moment of a Bohr magneton with respect to the magnetic field wherein the energy of the transition between Zeeman states is that of the resonant photon given by Eq. (1.227).

The parameters of the photon standing wave for the Zeeman effect of the free electron follow from those of the bound electron given in the Magnetic Parameters of the Electron (Bohr Magneton) section and Box 1.1. The charge density of the free electron is given by the projection of the atomic orbital into a plane as given in the Charge-Density Function section. To cause the Larmor excitation and the spin-flip transition, the corresponding photon gives rise to surface currents in the plane of the free electron that are also equivalent to the projection of the time- and spherically-harmonic dipole Larmor currents of the bound electron into the free-electron plane. Specifically, the photon gives rise to a current on the surface of the disc that corresponds to a rotating time- and polar-harmonic dipole that phase-matches the mass (charge) density of Eqs. (3.7-3.8).

The current of the free electron is initially azimuthally symmetrical about the z-axis. The resonant Larmor photon induces transient currents in the xy-plane to give rise to $\hbar$ of angular momentum initially along the x-axis. The corresponding torque causes the electron to precess about the x- and z-axes giving rise to Larmor precession about the $\left(\mathbf{i}_\mathbf{x}, 0\mathbf{i}_\mathbf{y}, \mathbf{i}_\mathbf{z}\right)$-axis and the z-axis at steady state depending on the initial direction of the free-electron magnetic moment relative to the applied magnetic-field direction. Thus, the currents cause a precession of the disc to form a time-averaged bi-conical cavity shown in Figure 3.8 that is azimuthally symmetrical about the $\left(\mathbf{i}_\mathbf{x}, 0\mathbf{i}_\mathbf{y}, \mathbf{i}_\mathbf{z}\right)$-axis, and this distribution further precesses about the z-axis to generate the $Y_0^{\,0}(\theta,\phi)$ distribution.

The photon-induced surface current satisfies the condition

$$\nabla \cdot J = 0 \tag{3.71}$$

And, the radius, $\rho_0$, of the free electron is unchanged. The time-averaged angular momentum and rotational energy of the currents that are phase-locked to the photon field are zero as given by Eqs. (1.76-1.77), but the photon's angular momentum is $\hbar$ corresponding to a magnetic moment of one Bohr magneton $\mu_B$ as shown for the case of the Larmor resonant excitation of a bound electron in Box 1.1. Thus, the electrostatic energy is constant, and only the magnetic energy need be considered as given by Eqs. (23-25) of Box 1.1.

The photon-field is central according to special relativity as given in the Equation of the Electric Field inside the Atomic Orbital section. The corresponding central field at the free-electron surface follows from Eq. (17) of Box 1.1 and the force balance condition between the centrifugal force and the electric-field force:

$$\mathbf{E} = \frac{3}{\varepsilon_0 2}\frac{e}{\pi\rho_0^3}\sqrt{\rho_0^2-\rho_n^2}\,\mathrm{Re}\left\{Y_\ell^m(\theta,\phi)e^{i\omega t}\right\}\mathbf{i}_\rho\delta(\rho-\rho_n)\delta(z') \tag{3.72}$$

where the spherical harmonic dipole $Y_\ell^m(\theta,\phi)=\sin\theta$ is with respect to the xy-plane of the free electron and gives the magnitude at position $\rho_n$ in the plane, the centrifugal force is given by Eq. (3.67), and $\omega$ is given by Eq. (3.17). The mass density given by Eq. (3.7) may be given in terms of spherical coordinates as follows:

Let

$$\rho = \rho_0\cos\theta \tag{3.73}$$

Then

$$\sigma_m(\rho,\phi,z) = \frac{3}{2}\frac{m_e}{\pi\rho_0^2}\sqrt{1-\left(\frac{\rho_0\cos\theta}{\rho_0}\right)^2} = \frac{3}{2}\frac{m_e}{\pi\rho_0^2}\sin\theta \tag{3.74}$$

Force balance is maintained by the equivalence of the harmonic modulation of the charge and the mass where $e/m_e$ is invariant.

The in-plane time- and polar-harmonic dipole further spins about the z-axis at the Larmor frequency, $\omega_L$. By considering the Larmor frequency component and the motion at the frequency given by Eq. (3.17), the free-electron motion in a magnetic field parallels that of the bound electron that also has two components of motion. The angular frequency about the rotation axis of the bound electron is given by Eq. (1.36), and the resulting dipole current rotates about the z-axis at the Larmor frequency. The parallels continue. In the free-electron frame rotating about the z-axis, the electric field of the dipole is

$$\mathbf{E} = \frac{3}{\varepsilon_0 2}\frac{e}{\pi\rho_0^3}\sqrt{\rho_0^2-\rho_n^2}\sin\theta\sin(\varphi-\omega t)\delta(\rho-\rho_n)\delta(z')\mathbf{i}_\rho \tag{3.75}$$

corresponding to Eq. (18) of Box 1.1. From Eqs. (20) and (21), the corresponding photon surface current is equivalent to the projection of the charge of a uniformly-charged spherical shell rotating at constant angular velocity of $\omega$ about the z-axis into the free-electron plane. Given that the charge moving azimuthally and time-harmonically at the constant frequency is equivalent to the planar projection of a spherical dipole, the resulting current is nonradiative as shown for this condition in Appendix I. The z-axis directed field in the laboratory frame and the field in frames rotating about the $(\mathbf{i}_x, 0\mathbf{i}_y, \mathbf{i}_z)$-axis are magnetostatic as shown in Figures 1.32 and 1.33 but directed along the respective axis. The precession of the magnetostatic dipole results in magnetic dipole radiation or absorption during a Stern-Gerlach transition.

Consider next the physics of the free-electron Zeeman splitting based on the electron structure and corresponding behavior in magnetic and photon fields based on Maxwell's equations. The free electron is a two-dimensional plane lamina comprised of a series of concentric circular current loops in the xy-plane ($\rho$-plane) that circulate about the z-axis as given in the Current-Density Function section. Each current loop can be considered a great-circle basis element analogous to those given in the Atomic Orbital Equation of Motion for $\ell$ = 0 Based on the Current Vector Field (CVF) section. The rotation of each such great circle about the $(\mathbf{i}_x, 0\mathbf{i}_y, \mathbf{i}_z)$- axis by $2\pi$ during a period generates the equivalent of the current pattern of a BECVF. Furthermore, the rotation of the free-electron disc having a continuous progression of larger current loops along $\rho$ forms two conical surfaces over a period that join at the origin and face in the opposite directions along the $(\mathbf{i}_x, 0\mathbf{i}_y, \mathbf{i}_z)$-axis, the axis of rotation, as shown in Figure 3.8. At each position of $0<\rho$, there exists a BECVF of that radius that is concentric to the one of infinitesimally larger radius to the limit at $\rho=\rho_0$. The BECVFs at each position $\rho$ generated over a period by the precession about the $(\mathbf{i}_x, 0\mathbf{i}_y, \mathbf{i}_z)$-axis by $2\pi$ is given in Appendix IV.

Over one time period, the first motion about the $(\mathbf{i}_x, 0\mathbf{i}_y, \mathbf{i}_z)$-axis by $2\pi$ sweeps out the equivalent of a BECVF, and the rotation about the z-axis sweeps out the equivalent of an OCVF. The combined motions sweep out the equivalent of the convolution of the BECVF with the OCVF, an angular-momentum distribution equivalent to $Y_0^0(\theta,\phi)$ of the bound electron. A discrete representation from Appendix IV as a series of great circle current loops is shown in Figure 3.9

**Figure 3.8.** A view of one of the two conical surfaces formed by rotation of the plane-lamina disc comprised of concentric great circles about the $(\mathbf{i}_x, 0\mathbf{i}_y, \mathbf{i}_z)$-axis that join at the origin and face in the opposite directions along the axis of rotation, the $(\mathbf{i}_x, 0\mathbf{i}_y, \mathbf{i}_z)$-axis.

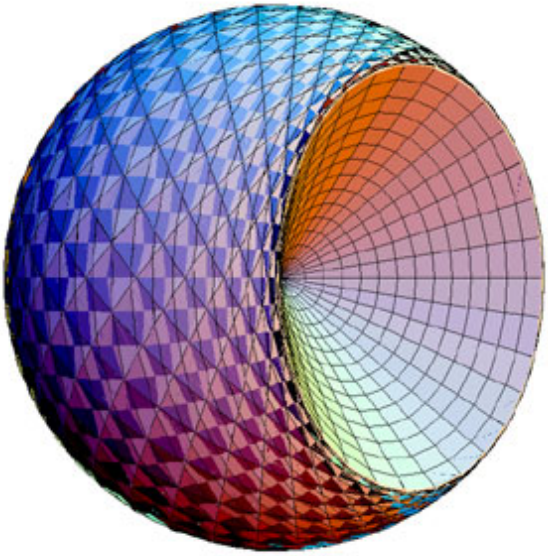
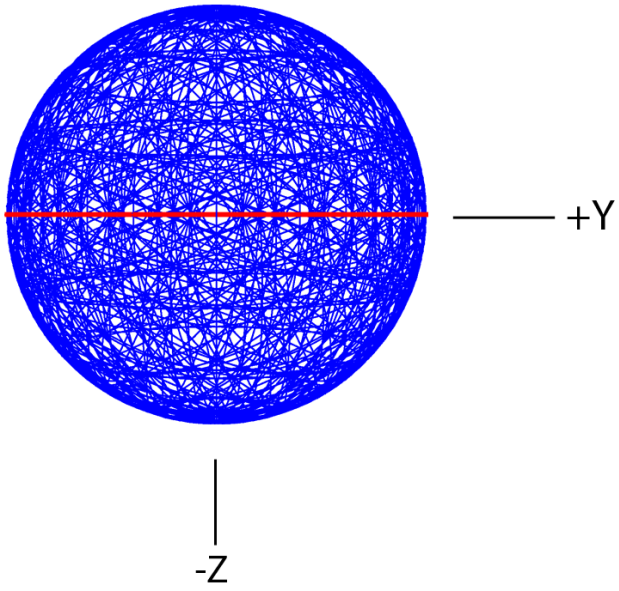


**Figure 3.9.** A representation of the uniform current pattern of the $Y_0^0(\theta,\phi)$ free electron motion over a period of both precessional motions shown with 30 degree increments of the angle to generate the free electron BECVF and 30 degree increments of the rotation of this basis element about the z-axis. The perspective is along the x-axis. The great circle current loop that served as a basis element that was initially in the xy-plane of each free electron BECVF is shown as red.




Now, consider the dynamics when the precessing electron further interacts with a resonant photon that gives rise to Zeeman splitting. As shown in Appendix IV, the combined rotations about the $(\mathbf{i}_x, 0\mathbf{i}_y, \mathbf{i}_z)$-axis and the z-axis generates a distribution over a period of motion that is equivalent to the current pattern and angular momentum of $Y_0^0(\theta,\phi)$ of the bound electron. The absorbed Larmor-frequency-resonant photon provides $\hbar$ of angular momentum along the x-axis that causes the $Y_0^0(\theta,\phi)$ distribution to rotate about the x-axis by $\pi$ to flip the magnetic moment in the opposite direction while maintaining the distribution with the currents reversed.

Since the Larmor precession sweeps out the form of the $Y_0^0(\theta,\phi)$ distribution for each position of $\rho$ and the current of each concentric shell along $\rho$ obeys superposition, the free electron in aggregate behaves as a shell of charge, current, and angular-momentum density of the free-electron radius $\rho_0$ having a total magnitude of angular momentum of $\hbar$ and the projection $\mathbf{L}_z = \frac{\hbar}{2}$. Then, the resulting time-averaged azimuthally uniform spherical momentum density interacts with the external applied magnetic field in a manner that is equivalent to that of the atomic orbital equation of motion, $Y_0^0(\theta,\phi)$, of the bound electron of radius $r_n = \rho_0$. Note the parallels between the bound and free electrons wherein the free electron angular momentum was considered as the plane projection of the constant angular momentum density of a bound electron confined to a spherical shell of radius $\rho_0$ having a total magnitude of angular momentum of $\hbar$ and the projection $\mathbf{L}_z = \frac{\hbar}{2}$ (Eqs. (3.2-3.4) and (3.19-3.20)).

## FREE-ELECTRON g FACTOR

Since the projection of the time-averaged intrinsic free electron angular momentum and that of the resonant photon that excites the Larmor precession onto the z-axis are both $\frac{\hbar}{2}$, and the angular motion distribution of the free electron is spherically symmetric, the Larmor-excited free electron behaves equivalently to the bound electron in a magnetic field during a spin flip transition. Flux must be linked in the same manner in units of the magnetic flux quantum, $\Phi_0 = \frac{h}{2e}$. Consequently, the g factor for the free electron is the same as that of the bound electron, and the energy of the transition between these states is that of the resonant photon given by Eq. (1.227).

Consider the bound electron. As demonstrated in the Atomic Orbital Equation of Motion for $\ell = 0$ Based on the Current Vector Field (CVF) section, $\frac{\hbar}{2}$ of the atomic orbital angular momentum designated the static component is initially parallel to the field. An additional $\frac{\hbar}{2}$ parallel component designated the dynamic component comes from the $\hbar$ of angular momentum along $\mathbf{S}$. The angular momentum in the presence of an applied magnetic field is [23]:

$$\mathbf{L} = \mathbf{r} \times (m_e \mathbf{v} + e\mathbf{A}) \tag{3.76}$$

where $\mathbf{A}$ is the vector potential evaluated at the location of the atomic orbital. The circular integral of $\mathbf{A}$ is the flux linked by the atomic orbital. During a Stern-Gerlach transition a resonant RF photon is absorbed or emitted, and the $\hbar$ component along $\mathbf{S}$ reverses direction. Referring to Box 1.1, it is shown by Eqs. (29-32) that the dynamic parallel component of angular momentum corresponding to the vector potential due to the lightlike transition is equal to the "kinetic angular momentum" $(\mathbf{r} \times m\mathbf{v})$ of $\frac{\hbar}{2}$. Conservation of angular momentum of the electron requires that the static angular momentum component concomitantly flips. The static component of angular momentum undergoes a spin flip, and concomitantly the "potential angular momentum" $(\mathbf{r} \times e\mathbf{A})$ of the dynamic component must change by $-\frac{\hbar}{2}$ due to the linkage of flux by the electron such that the total angular momentum is conserved.

In the case of the free electron, the application of a further $\hbar$ component along the x'-axis with the absorption of a resonant photon causes the $Y_0^0(\theta,\phi)$ distribution to flip about the x-axis to reverse the magnetic moment with respect to the applied magnetic field. The photon having $\hbar$ of angular momentum along the positive x'-axis of the free electron has an energy that is equivalent to that of the spin-flip transition given by Eq. (1.227). Here also, the dynamic parallel component of angular momentum corresponding to the vector potential due to the lightlike transition is equal to the "kinetic angular momentum" $(\mathbf{r} \times m\mathbf{v})$ of $\frac{\hbar}{2}$. Conservation of angular momentum of the $Y_0^0(\theta,\phi)$ distribution requires that the static angular momentum component concomitantly flips. The static component of angular momentum undergoes a spin flip, and concomitantly the "potential angular momentum" $(\mathbf{r} \times e\mathbf{A})$ of the dynamic component must change by $-\frac{\hbar}{2}$ due to the linkage of flux by the electron such that the total angular momentum is conserved.

From Eq. (28) of Box 1.1, the $\frac{\hbar}{2}$ of intrinsic angular momentum after the field is applied corresponds to a magnetic moment on the applied-field-axis of $\frac{\mu_B}{2}$ in the case of the free electron as well as the atomic orbital. The resonant Larmor-precession-angular-momentum contribution of $\frac{\hbar}{2}$ corresponds to another $\frac{\mu_B}{2}$ of magnetic moment that gives a total magnetic moment along the applied-field-axis of $\mu_B$, a Bohr magneton. The additional contribution (Eq. (28)) arises from the angular momentum of $\hbar$ on the $\mathbf{S}$-axis and the x'-axis for the atomic orbital and free electron, respectively. Thus, even though the magnitude of the vector projection of the angular momentum of the electron in the direction of the magnetic field is $\frac{\hbar}{2}$, the magnetic moment corresponds to $\hbar$ due to the $\frac{\hbar}{2}$ contribution from the dynamic component, and the quantized transition is due to the requirement of angular momentum conservation as given by Eq. (28) of Box 1.1.

Eq. (22) of Box 1.1 implies a continuum of energies; whereas, Eq. (29) of Box 1.1 shows that the static-kinetic and dynamic vector potential components of the angular momentum are quantized at $\frac{\hbar}{2}$. Consequently, as shown in the Electron g Factor section, the flux linked during a spin transition is quantized as the magnetic flux quantum:

$$\Phi_0 = \frac{h}{2e} \tag{3.77}$$

Only the states corresponding to:

$$m_s = \pm\frac{1}{2} \tag{3.78}$$

are possible due to conservation of angular momentum. It is further shown using the Poynting power vector with the requirement that flux is linked in units of the magnetic flux quantum, that the factor 2 of Eqs. (23) and (25) of Box 1.1 is replaced by the electron g factor.

In summary, since the corresponding properties of the free electron are equivalent to those of the bound electron, conservation of angular momentum of the electron permits a discrete change of its "kinetic angular momentum" $(\mathbf{r}\times m\mathbf{v})$ with respect to the field of $\frac{\hbar}{2}$, and concomitantly the "potential angular momentum" $(\mathbf{r}\times e\mathbf{A})$ must change by $-\frac{\hbar}{2}$ (Eqs. (1.171-1.174)). Consequently, flux linkage by the electron is quantized in units of the magnetic flux quantum, $\Phi_0 = \frac{h}{2e}$, and the electron magnetic moment can be parallel or antiparallel to an applied field as observed with the Stern-Gerlach experiment (See Box 1.1 and in the Electron g Factor section). Rather than a continuum of orientations with corresponding energies, the energy, $\Delta E_{mag}^{spin}$, of the spin flip transition corresponding to the $m_s = \pm\frac{1}{2}$ quantum number is given by Eq. (1.227):

$$\Delta E_{mag}^{spin} = g\mu_B B \tag{3.79}$$

The Stern-Gerlach experiment implies a magnetic moment of one Bohr magneton and an associated angular momentum quantum number of 1/2. Historically, this quantum number is called the spin quantum number, $m_s$, and that designation is maintained.

The Stern Gerlach experiment was historically felt to be inexplicable in terms of classical physics. Past explanations based on associated postulates were purely mathematical. However, the observed electron parameters are explained physically. Classical laws give (1) a gyromagnetic ratio of $\frac{e}{2m}$, (2) a Larmor precession frequency of $\frac{e\mathbf{B}}{2m}$, (3) the Stern-Gerlach experimental result of quantization of the angular momentum that implies a spin quantum number of 1/2 corresponding to an angular momentum of $\frac{\hbar}{2}$ on the z-axis, and (4) the observed Zeeman splitting due to a magnetic moment of a Bohr magneton $\mu_B = \frac{e\hbar}{2m_e}$ corresponding to an angular momentum of $\hbar$ on the z-axis. Furthermore, the solution is relativistically invariant as shown in the Special Relativistic Correction to the Ionization Energies section. Dirac originally attempted to solve the bound electron physically with stability with respect to radiation according to Maxwell's equations with the further constraints that it was relativistically invariant and gave rise to electron spin [24]. He was unsuccessful and resorted to the current mathematical-probability-wave model that has many problems as discussed in Refs. [25-26].

## FREE-ELECTRON BINDING

The free electron comprises a planar disc wherein the azimuthal charge density increases towards the origin of the disc according to Eq. (3.8). When an electron undergoes binding by a nucleus, the opposite of the reversible and time-symmetrical process of electron ionization, any linear kinetic energy is lost as radiation such that the initial de Broglie wavelength and radius $\rho_0$ are large according to Eq. (3.2). During binding in the nuclear central field, the electron current pattern over time is equivalent to the pattern traced out over time by the planar great circle of radius $\rho_0$ of a free electron undergoing a precession in a magnetic field during a spin flip transition. In the binding case, as the free electron undergoes a wobble rotational motion, the concentric planar great circles of current shown in Figure 3.2A flow from the disc origin to the perimeter edge at $\rho_0$ and successively spread the electron charge density over a BECVF such as that shown in Figures 1.5-1.7. Next, a wobble rotational motion of the BECVF spreads the charge over a spherical shell as a uniform density to comprise the bound electron atomic orbital $Y_0^0(\theta,\phi)$ of spherical radius $R$ as shown in Figures 1.12, 1.13, 1.16, 1.17, and 1.22.

Specifically, consider the rotation of the angular momentum vector of the free electron current about two axes, the $\left(\mathbf{i}_x, 0\mathbf{i}_y, \mathbf{i}_z\right)$-axis in a first step and the laboratory-frame z-axis in a second step as shown in Appendix IV. The corresponding motion of the perimeter great circle current loop at $\rho_0$ in the plane perpendicular to the angular momentum vector generates CVFs equivalent to those of the bound electron given in the Atomic Orbital Equation of Motion for $\ell = 0$ Based on the Current Vector Field (CVF) section. Specifically, the first rotation sweeps out the equivalent of a BECVF (Figure IV.1), wherein the concentric planar great circle current loops shown in Figure 3.2A flow from the disc origin to the perimeter edge at $\rho_0$ during the rotation to successively spread the charge density over the BECVF. The second rotation of the BECVF sweeps out the equivalent of the convolution of the BECVF with the OCVF given in Figure IV.5. The result is a charge and current density

distribution equivalent to $Y_0^0(\theta,\phi)$ of the bound electron wherein charge density of the bound electron has the same angular frequency and linear velocity everywhere on the surface. During binding, the radii of the great circles of the BECVF and $Y_0^0(\theta,\phi)$ may change with the emssion of the equivalent of at least one excited state photon. However, due to the indivisiblity of the electron and conservation of energy in an inverse squared Coulomb nuclear field, the time average radius of the BECVF or $Y_0^0(\theta,\phi)$ must change as an ensemble wherein the time average of the kinetic energy, $<T>$, for any circular or elliptical motion in an inverse-squared field is $1/2$ that of the time average of the magnitude of the potential energy, $|<V>|$. $<T>=1/2|<V>|$ [27]. The common radial current of a bound electon during an excited state transition and the corresponding lifetime is given in the State Lifetimes and Line Intensities section. The reversible and time-symetric mechanism of the emission or absorption of photons by the bound electron is given in the Transitions section. The uninform charge density is proportional to the spherical coordinate term $\rho_0 \sin\theta$ relative to the z-axis which follows from Eq. (3.8) with the substitution of $\rho = \rho_0 \cos\theta$ as given by Eq. (3.74). Additionally, the bound electron may comprise time and spherical harmonic modulation functions given by Eq. (1.28) depending on the electron configuration. The opposite process to binding described herein occurs during electron ionization.

Specifically, consider the free electron traveling along the z-axis with plane of the electron disc in the xz-plane as it approaches the proton at the origin. The bonding proceeds by the rotation of the angular momentum vector of the free electron current about two axes, the $(\mathbf{i}_x, 0\mathbf{i}_y, \mathbf{i}_z)$-axis in a first step and the laboratory-frame z-axis in a second step as shown in Appendix IV. The corresponding motion of the perimeter great circle current loop at $\rho_0$ in the plane perpendicular to the angular momentum vector generates CVFs equivalent to those of the bound electron given in the Atomic Orbital Equation of Motion for $\ell = 0$ Based on the Current Vector Field (CVF) section. Specifically, the first rotation sweeps out the equivalent of a BECVF (Figure IV.1), wherein the concentric planar great circle current loops shown in Figure 3.2A flow from the disc origin to the perimeter edge at $\rho_0$ during the rotation to successively spread the charge density over the BECVF as the disc converters into an annulus with the inner radius increasing to $\rho_0$ at the step completing the BECVF. The second rotation of the BECVF sweeps out the equivalent of the convolution of the BECVF with the OCVF given in Figure IV.5 to form the uniform charge, mass, current density, and momentum-density function $Y_0^0(\theta,\phi)$.

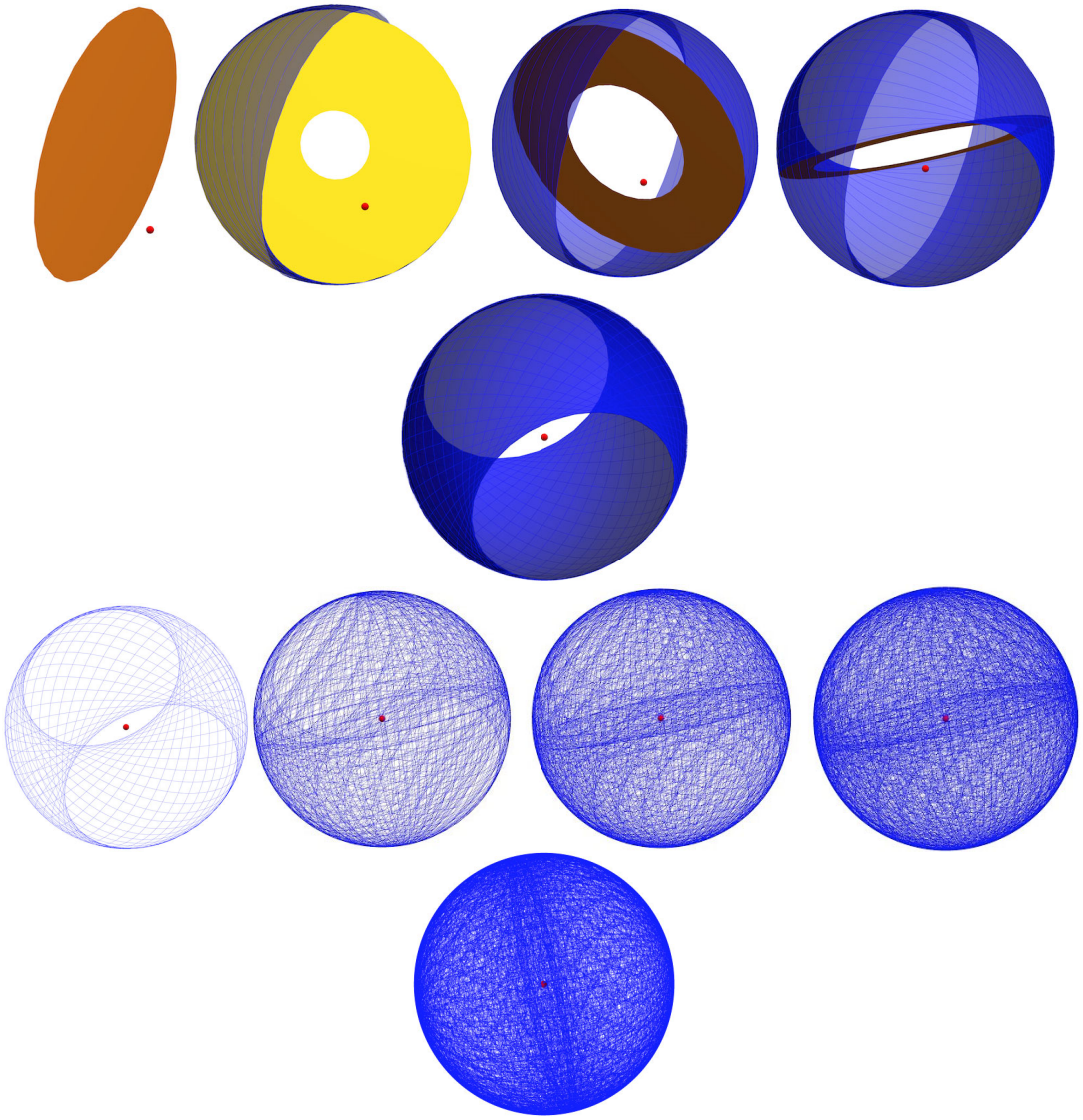
Electron binding is a continuous process with continuous current flow. An equation providing visualization in discrete steps that generates the angular momentum vectors of the bound electron follows from Eq. (18) of Appendix IV.

$$\begin{bmatrix} x' \\ y' \\ z' \end{bmatrix} = \sum_{m=1}^{m=M} \begin{bmatrix} \cos\left(\frac{m2\pi}{M}\right) & \sin\left(\frac{m2\pi}{M}\right) & 0 \\ -\sin\left(\frac{m2\pi}{M}\right) & \cos\left(\frac{m2\pi}{M}\right) & 0 \\ 0 & 0 & 1 \end{bmatrix} \bullet \delta\left(z-\rho_0\left(1-\frac{n}{N}\right)\right) \sum_{n=1}^{n=N} \begin{bmatrix} \frac{1}{2}+\frac{\cos\left(\frac{n2\pi}{N}\right)}{2} & \frac{\sin\left(\frac{n2\pi}{N}\right)}{\sqrt{2}} & \frac{1}{2}-\frac{\cos\left(\frac{n2\pi}{N}\right)}{2} \\ -\frac{\sin\left(\frac{n2\pi}{N}\right)}{\sqrt{2}} & \cos\left(\frac{n2\pi}{N}\right) & \frac{\sin\left(\frac{n2\pi}{N}\right)}{\sqrt{2}} \\ \frac{1}{2}-\frac{\cos\left(\frac{n2\pi}{N}\right)}{2} & -\frac{\sin\left(\frac{n2\pi}{N}\right)}{\sqrt{2}} & \frac{1}{2}+\frac{\cos\left(\frac{n2\pi}{N}\right)}{2} \end{bmatrix} \begin{bmatrix} \rho\cos\phi \\ \rho\sin\phi \\ 0 \end{bmatrix}_{\substack{\phi=0 \text{ to } 2\pi \\ \rho=\frac{n}{N}\rho_0 \text{ to } \rho_0}} \tag{3.80}$$

Consider that the free electron translates along the z-axis towards the proton at the origin. To maintain an equipotential, the N rotations of the free electron disc (Eq. (3.80)) commences at a distance from the proton equal to the outer radius of the disc $\rho_0$. The current within the disc flows towards the outer radius $\rho_0$ to form a set of time-delayed concentric great circles. At each step of the rotation to transfer a great circle current element from the free electron current density to that of the forming BECVF

according to Eq. (Eq. (3.80)), as a great circle of radius $\rho_0$ is transferred to the forming BECVF a next great circle replaces it such that the remaining electron disc current density forms an annulus with a constant outer radius $\rho = \rho_0$ and an increasing inner radius $\rho = \frac{n}{N}\rho_0$. The center of mass of the forming BECVF/annulus translates a distance of $\frac{\rho_0}{N}$ along the z-axis towards the proton for each $n$ rotation step such that the proton is in the coordinate origin of the BECVF at the end of the N rotations. Next, the M rotations of the BECVF form the spherical shell with the proton at the center. During the formation of the BECVF, each point of the forming BECVF surface and the disc are equipotential relative to the Coulomb field between the proton and electron. Computer modeling of the analytical equations to generate the free electron current vector field, the current vector fields during electron binding, and the azimuthally uniform momentum-density function $Y_0^0(\theta,\phi)$ is available on the web [28]. Excerpts of the animation of the continuous electron binding process are shown in Figure 3.10. The discrete representation of the current distribution $Y_0^0(\theta,\phi)$ that shows a finite number of current elements wherein the BECVF comprises $N$ great circles and the number of convolved BECVF elements is $M$ is shown in Figures 3.11 and 3.12.

**Figure 3.10.** Representations of stages of the bound electron current pattern of the $Y_0^0(\theta,\phi)$ formed by free electron binding to a proton (Eq. (3.80)) wherein the current density of the free electron disc is converted into great circles covering a two-dimensional spherical shell.



**Figures 3.11 and 3.12.** Representations of the current pattern of the $Y_0^0(\theta,\phi)$ formed by electron binding with 30 degree increments ( $N=M=12$ in Eq. (3.80)) of the angle to generate the free electron binding BECVF and 30 degree increments of the rotation of this BECVF about the z-axis to form the bound electron current vector field. The free electron disc that served as the source of great circle basis element current loops that was initially in the xy-plane is shown as red

**Figure 3.11.** The perspective is along the z-axis.

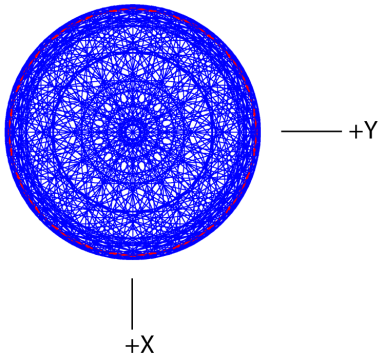
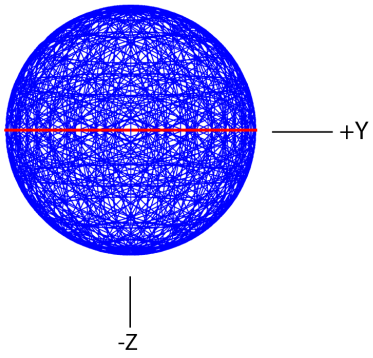
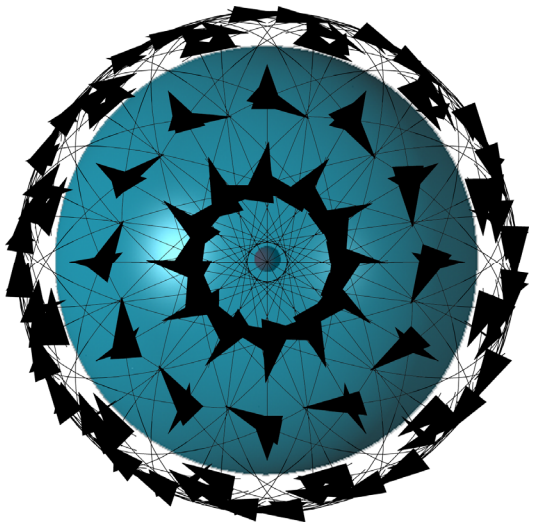



**Figure 3.12.** The perspective is along the x-axis.




The z-axis view of this representation with 144 vectors overlaid giving the direction of the current of each great circle element is shown in Figure 3.13. The corresponding mass (momentum) density is also represented by Figures 3.11 and 3.12 wherein the charge and mass are interchangeable by the conversion factor $m_e/e$.

**Figure 3.13.** An ideal representation of the uniform current pattern of $Y_0^0(\theta,\phi)$ comprising the superposition of an infinite number of great circle elements generated by normalizing the distribution of Eq. (3.80). The constant uniform current density is overlaid with 144 vectors giving the direction of the current of each great circle element for 30 degree increments ( $N=M=12$ in Eq. (3.80)) of the angle to generate the BECVF and 30 degree increments of the rotation of this basis element about the z-axis. The perspective is along the z-axis. The corresponding uniform current-density function having intrinsic angular momentum components of $\mathbf{L}_{xy}=\frac{\hbar}{4}$ and $\mathbf{L}_z=\frac{\hbar}{2}$ following Larmor excitation in a magnetic field give rise to the phenomenon of electron spin.



The result is a charge and current density distribution equivalent to $Y_0^0(\theta,\phi)$ of the bound electron wherein charge density of the bound electron has the same angular frequency and linear velocity everywhere on the surface. During binding, the radii of the great circles of the BECVF and $Y_0^0(\theta,\phi)$ may change with the emssion of the equivalent of at least one excited state photon. However, due to the indivisiblity of the electron and conservation of energy in an inverse squared Coulomb nuclear field, the time average radius of the BECVF or $Y_0^0(\theta,\phi)$ must change as an ensemble wherein the time average of the kinetic energy, $<T>$, for any circular or elliptical motion in an inverse-squared field is $1/2$ that of the time average of the magnitude of the potential energy, $|<V>|$. $<T>=1/2|<V>|$ [27]. The common radial current of a bound electon during an excited state

transition and the corresponding lifetime is given in the State Lifetimes and Line Intensities section. The reversible and time-symetric mechanism of the emission or absorption of photons by the bound electron is given in the Transitions section. The uninform charge density is proportional to the spherical coordinate term $\rho_0 \sin\theta$ relative to the z-axis which follows from Eq. (3.8) with the substitution of $\rho = \rho_0 \cos\theta$ as given by Eq. (3.74). Additionally, the bound electron may comprise time and spherical harmonic modulation functions given by Eq. (1.28) depending on the electron configuration. The opposite process to binding described herein occurs during electron ionization.

## REFERENCES


1. G. Matteucci, "Electron wavelike behavior: a historical and experimental introduction," Am. J. Phys., 58, No. 12, (1990), pp. 1143-1147.
2. D. Clark, "Very large hydrogen atoms in interstellar space," Journal of Chemical Education, 68, No. 6, (1991), pp. 454-455.
3. J. Gribbin, New Scientist, January, 25, (1997), p. 15.
4. I. Levine, et al., Physical Review Letters, Vol. 78, No. 3, (1997), pp. 424-427.
5. J. A. Stratton, *Electromagnetic Theory*, McGraw-Hill Book Company, (1941), p. 195.
6. J. D. Jackson, Classical Electrodynamics, Second Edition, John Wiley & Sons, New York, (1975), pp. 17-22
7. H. A. Haus, J. R. Melcher, "Electromagnetic Fields and Energy," Department of Electrical Engineering and Computer Science, Massachusetts Institute of Technology, (1985), Sec. 5.3.
8. D. R. Lide, *CRC Handbook of Chemistry and Physics*, 79th Edition, CRC Press, Boca Raton, Florida, (1998-9), pp. A-32 to A-33.
9. R. N. Bracewell, *The Fourier Transform and Its Applications*, McGraw-Hill Book Company, New York, (1978), pp. 248-249.
10. H. A. Haus, "On the radiation from point charges," American Journal of Physics, 54, (1986), pp. 1126-1129.
11. J. D. Jackson, *Classical Electrodynamics*, Second Edition, John Wiley & Sons, New York, (1975), pp. 236-240, 601-608, 786-790.
12. D. A. McQuarrie, *Quantum Chemistry*, University Science Books, Mill Valley, CA, (1983), pp. 238-241.
13. J. D. Jackson, *Classical Electrodynamics*, Second Edition, John Wiley & Sons, New York, (1975), pp. 168-173.
14. J. D. Jackson, *Classical Electrodynamics*, Second Edition, John Wiley & Sons, New York, (1975), pp. 739-779.
15. M. Mizushima, *Quantum Mechanics of Atomic Spectra and Atomic Structure*, W.A. Benjamin, Inc., New York, (1970), p.17.
16. J. D. Jackson, *Classical Electrodynamics*, Second Edition, John Wiley & Sons, New York, (1975), pp. 780-791.
17. J. D. Jackson, *Classical Electrodynamics*, Second Edition, John Wiley & Sons, New York, (1975), pp. 662-665.
18. J. D. Jackson, *Classical Electrodynamics*, Second Edition, John Wiley & Sons, New York, (1975), pp. 668-672.
19. E. M. Purcell, *Electricity and Magnetism*, McGraw-Hill, New York, (1965), pp. 370-375, 447.
20. D. R. Lide, *CRC Handbook of Chemistry and Physics*, 79th Edition, CRC Press, Boca Raton, Florida, (1998-9), p. A-33.
21. G. R. Fowles, *Analytical Mechanics*, Third Edition, Holt, Rinehart, and Winston, New York, (1977), pp. 193-199.
22. G. R. Fowles, *Analytical Mechanics*, Third Edition, Holt, Rinehart, and Winston, New York, (1977), pp. 243-247.
23. E. M. Purcell, *Electricity and Magnetism*, McGraw-Hill, New York, (1965), p. 447.
24. P. Pearle, "Absence of radiationless motions of relativistically rigid classical electron," Foundations of Physics, Vol. 7, Nos. 11/12, (1977), pp. 931-945.
25. R. L. Mills, "Maxwell's Equations and QED: Which is Fact and Which is Fiction," Physics Essays, Vol. 19, (2006), pp. 225-262.
26. R. L. Mills, "The Fallacy of Feynman's Argument on the Stability of the Hydrogen Atom According to Quantum Mechanics," Annales de la Fondation Louis de Broglie, Vol. 30, No. 2, (2005), pp. 129-151.
27. G. R. Fowles, *Analytical Mechanics*, Third Edition, Holt, Rinehart, and Winston, New York, (1977), pp. 145-158.
28. "Modeling of the Analytical Equations of the Binding of a Free Electron to form the Bound Electron Current Vector Field $Y_0^0(\theta,\phi)$ and Corresponding Ionization by Time Reversal" posted at www.brilliantlightpower.com.

# Chapter 4

# EQUATION OF THE PHOTON

## RIGHT AND LEFT HAND CIRCULAR AND ELLIPTICALLY POLARIZED PHOTONS

The equation of the photon in free space is derived as a boundary value problem involving the transition from the ground state to an excited state of the hydrogen atom. The "ground" state function of the hydrogen atom is an atomic orbital given in the Atomic Orbital Equation of Motion $\ell = 0$ Based on the Current Vector Field (CVF) section, and the excited-state function comprising the atomic orbital and a resonant trapped photon is given in the Excited States of the One-Electron Atom (Quantization) section. The atomic orbital CVF equations are given by Eqs. (1.78-1.98), and the CVFs are shown in Figures 1.4-1.11. The "trapped photon" of an excited state is given by Eq. (2.15). The latter gives rise to a corresponding phase-matched source current given by Eq. (2.11). During the transition from the excited state to the ground state, the excited-atomic-state angular momentum given by Eq. (2.66) and the emitted-photon angular momentum are quantized in unit of $\hbar$ such that Eq. (9.2) is obeyed. Since the change in angular momentum between the initial and final atomic states is conserved by the photon's angular momentum, the angular momentum, **m**, of the emitted photon follows from the time-averaged angular-momentum density given by Eq. (16.61) of Jackson [1]:

$$\mathbf{m} = \int \frac{1}{8\pi c} \mathrm{Re}\left[\mathbf{r} \times (\mathbf{E} \times \mathbf{B}^*)\right] dx^4 = \hbar \tag{4.1}$$

Thus, the photon equation is given by the superposition of two atomic orbital-type current-vector fields at the same radius—one with electric field lines, which follow great circles and one with magnetic field lines, which follow great circles. The magnetic current-vector field is rotated $\frac{\pi}{2}$ relative to the electric current-vector field; thus, the magnetic field lines are orthogonal to the electric field lines

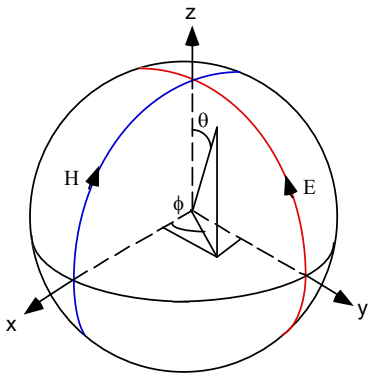
$$\nabla X \mathbf{E} = -\frac{\partial \mu_0 \mathbf{H}}{\partial t} \tag{4.2}$$

$$\nabla X \mathbf{H} = \frac{\partial \varepsilon_0 \mathbf{E}}{\partial t} \tag{4.3}$$

where the magnitude of the electric and magnetic fields are give by Eq. (4.1) with the boundary condition that photon angular momentum is $\hbar$.

A photon comprising a field-line pattern called a photon electric and magnetic vector field (e&mvf) similar to the atomic orbital is generated from two orthogonal great circle field lines shown in Figure 4.1 rather than two great circle current loops as in the case of the electron spin function. Consider the fields of the photon to be generated from two orthogonal great circles field lines, one for E and one for B. The Cartesian coordinate system wherein a first great circle magnetic field line lies in the x'z'-plane, and a second great circle electric field line lies in the y'z'-plane is designated the basis-set reference frame, and the xyz Cartesian-coordinate frame is the laboratory frame as given in the Atomic Orbital Equation of Motion $\ell = 0$ Based on the Current Vector Field (CVF) section.

**Figure 4.1.** The stationary Cartesian coordinate system xyz wherein the first great circle magnetic field line lies initially in the xz-plane, and the second great circle electric field line lies initially in the yz-plane. The rotated coordinates are primed.




Consider a point on each of the two orthogonal great-circle field lines, one and two, in the basis-set reference frame at time zero wherein initially the first loop lies in the xz-plane, and the second loop lies in the yz-plane. Point one is at $x'=r_n$, $y'=0$, and $z'=0$ and point two is at $x'=0$, $y'=0$, and $z'=r_n$. Let point one move clockwise on the great circle in the x'z'-plane toward the positive z'-axis, and let point two move counterclockwise on the great circle in the y'z'-plane toward the negative y'-axis, as shown in Figure 4.1. The equations of motion, in the sub-basis-set reference frame are given by:

point one (H FIELD):

$$x_2'=r_n\cos(\omega_n t) \qquad y_2'=0 \qquad z_2'=r_n\sin(\omega_n t) \tag{4.4}$$

point two (E FIELD):

$$x_1'=0 \qquad y_1'=-r_n\sin(\omega_n t) \qquad z_1'=r_n\cos(\omega_n t) \tag{4.5}$$

The right-handed-circularly-polarized photon electric and magnetic vector field (RHCP photon-e&mvf) and the left-handed-circularly-polarized photon electric and magnetic vector field (LHCP photon-e&mvf) are generated by rotating the great circles about the $(\mathbf{i}_x,\mathbf{i}_y,0\mathbf{i}_z)$-axis or the $(\mathbf{i}_x,-\mathbf{i}_y,0\mathbf{i}_z)$-axis by $\frac{\pi}{2}$, respectively. The corresponding primed Cartesian coordinate system refers to the axes that rotate with the great circles relative to the xyz-system and determines the basis-element reference frame. The fields are continuous on the spherical surface, but they can be visualized by a discrete-element representation wherein each element of the field-line density function is obtained with each incremental rotation of a series over the span of $\frac{\pi}{2}$. Thus, the two points, one and two, are on the first member pair of the orthogonal great circles of an infinite series that comprises a representation of a photon.

The right-handed-circularly-polarized photon electric and magnetic vector field (RHCP photon-e&mvf) shown in Figure 4.2 is generated by the rotation of the basis elements comprising the great circle magnetic field line in the xz-plane and the great circle electric field line in the yz-plane about the $(\mathbf{i}_x,\mathbf{i}_y,0\mathbf{i}_z)$-axis by $\frac{\pi}{2}$ corresponding to the output of the matrix given by Eq. (4.6).

**RHCP PHOTON E FIELD and H FIELD:**

$$\begin{bmatrix}x'\\y'\\z'\end{bmatrix}=\begin{bmatrix}\frac{1}{2}+\frac{\cos\theta}{2} & \frac{1}{2}-\frac{\cos\theta}{2} & -\frac{\sin\theta}{\sqrt{2}}\\ \frac{1}{2}-\frac{\cos\theta}{2} & \frac{1}{2}+\frac{\cos\theta}{2} & \frac{\sin\theta}{\sqrt{2}}\\ \frac{\sin\theta}{\sqrt{2}} & -\frac{\sin\theta}{\sqrt{2}} & \cos\theta\end{bmatrix}\bullet\left(\begin{bmatrix}0\\ r_n\cos\phi\\ r_n\sin\phi\end{bmatrix}_{\text{Red}}+\begin{bmatrix}r_n\cos\phi\\ 0\\ r_n\sin\phi\end{bmatrix}_{\text{Blue}}\right) \tag{4.6}$$

The left-handed-circularly-polarized photon electric and magnetic vector field (LHCP photon-e&mvf) is generated by the rotation of the basis elements comprising the great circle magnetic field line in the xz-plane and the great circle electric field line in the yz-plane about the $(\mathbf{i}_x,-\mathbf{i}_y,0\mathbf{i}_z)$-axis by $\frac{\pi}{2}$ corresponding to the output of the matrix given by Eq. (4.7). The mirror image of the RHCP photon-e&mvf, the left-handed circularly polarized photon-e&mvf, is shown with three orthogonal views in Figure 4.3.

**LHCP PHOTON E FIELD and H FIELD:**

$$\begin{bmatrix} x' \\ y' \\ z' \end{bmatrix} = \begin{bmatrix} \frac{1}{2}+\frac{\cos\theta}{2} & -\frac{1}{2}+\frac{\cos\theta}{2} & \frac{\sin\theta}{\sqrt{2}} \\ -\frac{1}{2}+\frac{\cos\theta}{2} & \frac{1}{2}+\frac{\cos\theta}{2} & \frac{\sin\theta}{\sqrt{2}} \\ -\frac{\sin\theta}{\sqrt{2}} & -\frac{\sin\theta}{\sqrt{2}} & \cos\theta \end{bmatrix} \bullet \left( \begin{bmatrix} 0 \\ r_n\cos\phi \\ r_n\sin\phi \end{bmatrix}_{\text{Red}} + \begin{bmatrix} r_n\cos\phi \\ 0 \\ r_n\sin\phi \end{bmatrix}_{\text{Blue}} \right) \tag{4.7}$$

**Figure 4.2.** The field-line pattern given by Eq. (4.6) from three orthogonal perspectives of a RHCP photon-e&mvf corresponding to the first great circle magnetic field line and the second great circle electric field line shown with 6 degree increments of the angle $\theta$. (Electric field lines red; Magnetic field lines blue).

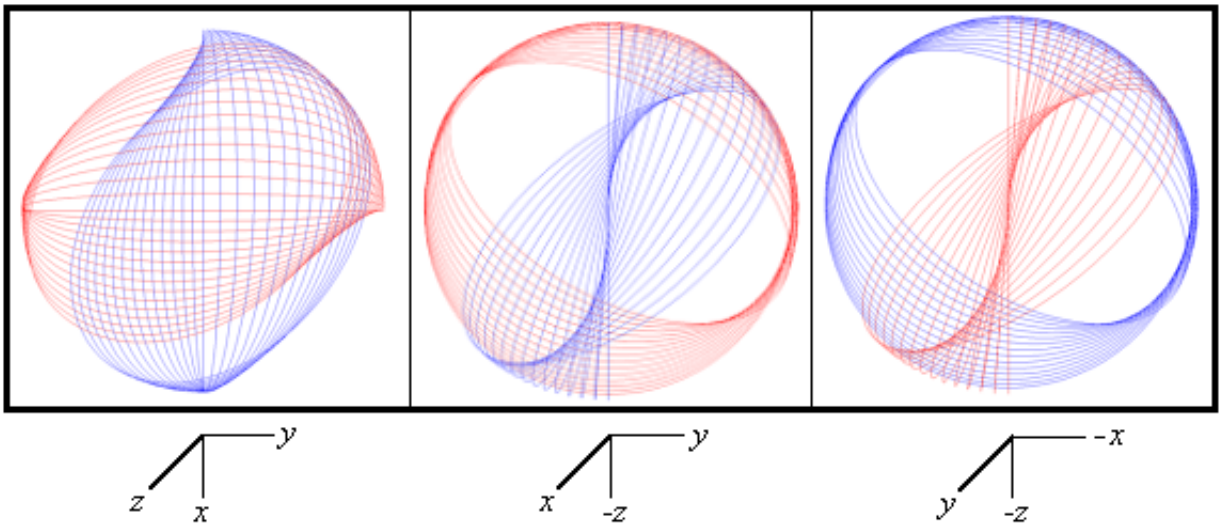
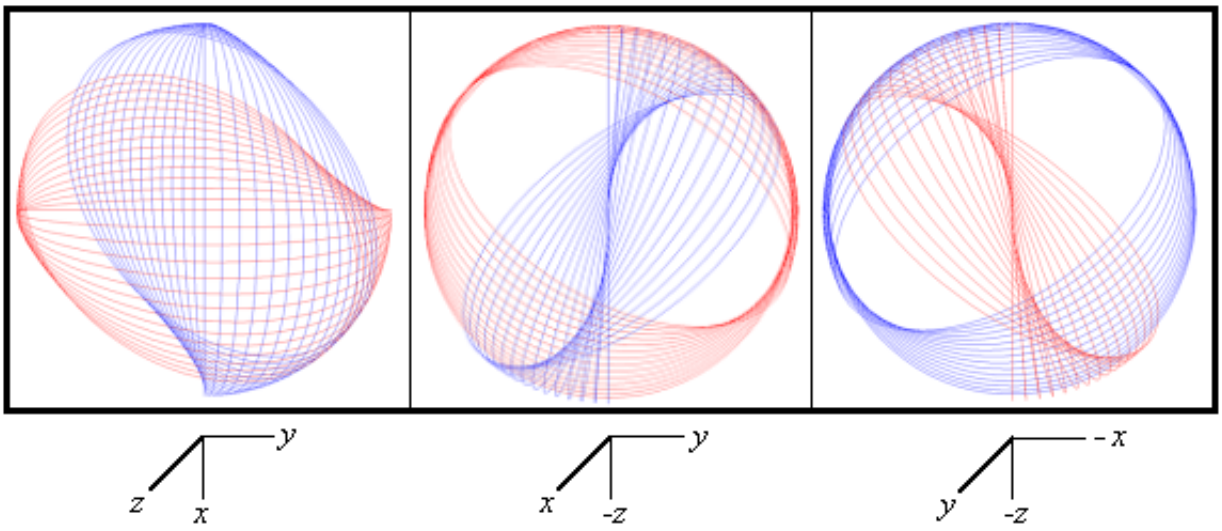



**Figure 4.3.** The field-line pattern given by Eq. (4.7) from three orthogonal perspectives of a left-handed circularly polarized photon-e&mvf corresponding to the first great circle magnetic field line, and the second great circle electric field line shown with 6 degree increments of the angle $\theta$. (Electric field lines red; Magnetic field lines blue).



## FIELDS BASED ON INVARIANCE UNDER GAUSS' INTEGRAL LAW

The angular velocity of the photon-e&mvf is equal to the change in angular velocity of the electron atomic orbital for a de-excitation from the energy level with principal quantum number $n = n_i$ to $n = n_f$, where $n_i > n_f$, given by Eq. (2.21) for $n_f = 1$. From Eq. (2.22), the photon is an electromagnetic wave that carries energy, $E$, given by:

$$E = \hbar\omega \tag{4.8}$$

Given the relationships, Eqs. (4.2) and (4.3) for the electric and magnetic fields, the solution of the classical wave equation Eq. (I.45) requires that the linear velocity at each point along a great circle of the photon-e&mvf is $c$,

$$c = \sqrt{\frac{1}{\varepsilon_0 \mu_0}} \tag{4.9}$$

and, that the velocity of the photon in the lab frame is $c$. Therefore, with the velocity addition property of special relativity, the velocity in all frames of reference is $c$ including the rest frame. Thus, the zero rest mass concept of the photon can be discarded. The "mass" of the photon in any frame is actually momentum contained in its electric and magnetic fields as given by Eqs. (2.150) and (4.1). An additional consequence of the light speed in all frames is that the radius of the photon is invariant. The field lines in the lab frame follow from the relativistic invariance of charge as given by Purcell [2]. The relationship between the relativistic velocity and the electric field of a moving charge is shown schematically in Figure 4.4A and 4.4B.

**Figure 4.4A.** The electric field of a moving point charge ($v = \frac{1}{3}c$).

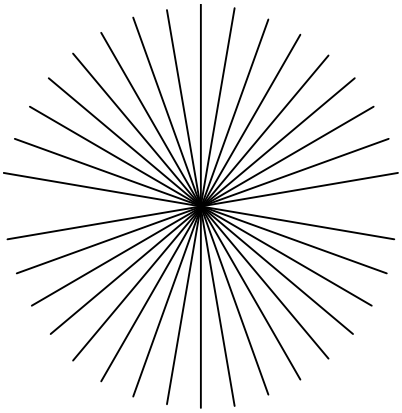
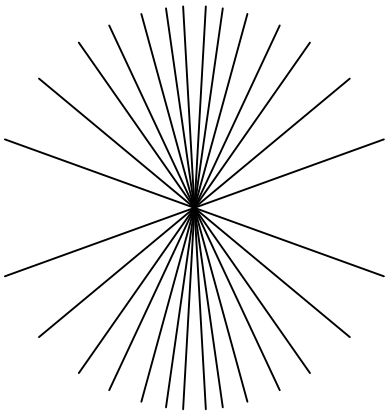


**Figure 4.4B.** The electric field of a moving point charge ($v = \frac{4}{5}c$).



The field invariance under Gauss' Integral Law also applies to the fields of the photon-e&mvf. From Eqs. (4.4-4.7) and as shown in Appendix V, the electric and magnetic fields are harmonic in space and time wherein $c = \lambda \frac{\omega}{2\pi}$ is satisfied which is a solution of the wave equation for an electromagnetic wave, and the fields are orthogonal such that Faraday's and Ampere's Laws are satisfied. The photon equation in the lab frame (shown in Figures 4.5 and 4.6) of a right-handed circularly polarized photon-e&mvf is:

$$\begin{aligned} \mathbf{E} &= \mathbf{E}_0 \left[\mathbf{x} + i\mathbf{y}\right] e^{-jk_z z} e^{-j\omega t} \\ \mathbf{H} &= \left(\frac{\mathbf{E}_0}{\eta}\right)\left[\mathbf{y} - i\mathbf{x}\right] e^{-jk_z z} e^{-j\omega t} = \mathbf{E}_0 \sqrt{\frac{\varepsilon}{\mu}}\left[\mathbf{y} - i\mathbf{x}\right] e^{-jk_z z} e^{-j\omega t} \end{aligned} \tag{4.10}$$

with a wavelength of:

$$\lambda = 2\pi \frac{c}{\omega} \tag{4.11}$$

The relationship between the photon-e&mvf radius and wavelength is:

$$2r_{photon} = \lambda \tag{4.12}$$

The wavelength (radius) changes for moving observers according to the Doppler formula of Lorentz transforms. In terms of Eqs. (4.4-4.7), $E_0$ of the photon is given by the boundary condition that the angular momentum given by Eq. (4.1) is $\hbar$; thus, the energy is given by Planck's equation (Eq. (2.18)) as shown by Eqs. (2.56-2.64). The relationship between Planck's equation and Maxwell's equations is also consistent with regard to the energies of excited states as given by Eqs. (2.18-2.22).

**Figure 4.5.** The direction of rotation of the electric field lines of a right-handed circularly polarized photon-e&mvf as seen along the axis of propagation in the lab inertial reference frame as it passes a fixed point.

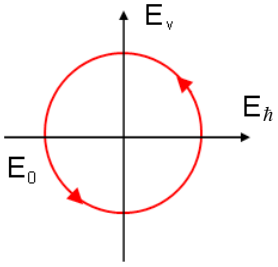
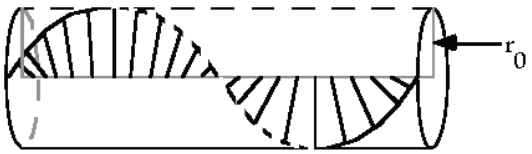



**Figure 4.6.** The electric field rotation as a function of z of a right-handed circularly polarized photon-e&mvf as seen transverse to the z-axis, axis of propagation, in the lab inertial reference frame at a fixed time wherein $2r_{photon} = \lambda$




The cross-sectional area, $\sigma$, transverse to the propagation direction of the photon is

$$\sigma = \pi\left[\frac{\lambda}{2}\right]^2 \tag{4.13}$$

The geometric cross section (Eq. (4.13)) is consistent with the Rayleigh scattering formula, which is derived from Maxwell's equations [3].

The photon-e&mvf may comprise basis element magnetic and electric field lines that are constant in magnitude as a function of angle over the surface, or the magnitude of the fields of the basis elements may vary as a function of angular position $(\theta,\phi)$ on the photon-e&mvf. The general photon equation for the electric field in its frame is:

$$\mathbf{E}_{\theta,\phi} = \frac{e}{4\pi\varepsilon_0 r_{photon}^2}\left(-1+\frac{1}{n}\left[Y_0^0(\theta,\phi)+\mathrm{Re}\left\{Y_\ell^m(\theta,\phi)e^{im\omega_n t}\right\}\right]\right)\delta\left(r-\frac{\lambda}{2\pi}\right) \tag{4.14}$$

where $r_{photon}$ is the radius of the photon-e&mvf and $\omega_n = \frac{2\pi c}{\lambda}$ is the photon angular velocity which is equal to $\Delta\omega$, the change in atomic orbital angular velocity given by Eq. (2.21) and the light speed changes the direction of the field lines to the transverse direction.

Similarly photons are emitted when an electron is bound. Using Eq. (1.34) for the photon and the electron wave relationships for the initial conditions of an unbound electron at rest, the ratio of the linear velocity of the subsequently bound electron to the emitted free-space photon is given by:

$$\frac{v_n}{c_{photon}} = \frac{\lambda_n\frac{\omega_n}{2\pi}}{\lambda_{photon}\frac{\omega_{photon}}{2\pi}} = \frac{\lambda_n}{\lambda_{photon}} = \frac{\pi r_n}{r_{photon}} \tag{4.15}$$

where the $n$ subscripts refer to atomic orbital quantities and the far-right-hand-side relationship follows from Eq. (2.2) and Eq. (4.12). From Eq. (4.15), the relations between the free space photon wavelength, radius, and velocity and the corresponding parameters of a free electron as it is bound are:

(1) $r_{photon}$, the radius of the photon-e&mvf, is equal to $r_n\pi\frac{c}{v_n} = na_H\pi\frac{c}{v_n}$, the electron atomic orbital radius given by Eqs. (2.2) and (2.5) times the product of $\pi$ and the ratio of the speed of light $c$ and $v_n$, the velocity of the atomic orbital given by Eq. (1.35),

(2) $\lambda_{photon}$, the photon wavelength, is equal to $\lambda_n\frac{c}{v_n}$, where $\lambda_n$ is the atomic orbital de Broglie wavelength, and

(3) $\omega_{photon} = \frac{2\pi c}{\lambda}$, the photon angular velocity, is equal to $\omega_n$, the atomic orbital angular velocity given by Eq. (1.36).

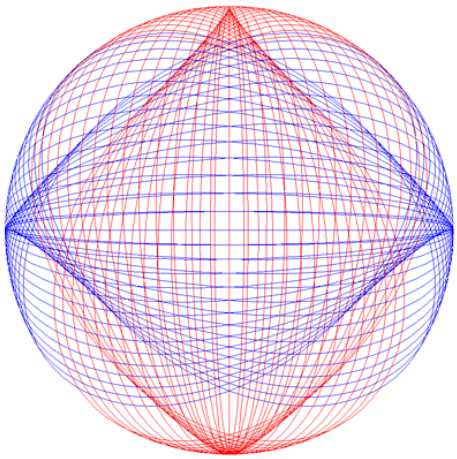
The magnetic field photon-e&mvf is given by Eqs. (4.14) and (4.2). In the case of $Y_\ell^m(\theta,\phi) = 0$ in Eq. (4.14), a right-handed and a left-handed circularly polarized photon-e&mvf are superimposed to comprise a linearly polarized photon-e&mvf. A right-handed or left-handed circularly polarized photon is obtained by attenuating the oppositely polarized component. For Eq. (4.14), the power density per unit area, **S**, is:

$$\mathbf{S} = \mathbf{E}\times\mathbf{B}^* \tag{4.16}$$

## LINEAR POLARIZED PHOTONS

The linearly polarized photon is given by the superposition of the right-handed circularly polarized photon-e&mvf shown in Figure 4.2 and its mirror image, the left-handed circularly polarized photon-e&mvf, shown in Figure 4.3. The field-line pattern of a linearly polarized (LP) photon-e&mvf shown from the perspective of looking along the z-axis is shown in Figure 4.7. Thus, the LP photon-e&mvf is obtained by rotation of the basis-element-great-circle electric and magnetic fields lines about each of the $(\mathbf{i}_x, \mathbf{i}_y, 0\mathbf{i}_z)$- and $(\mathbf{i}_x, -\mathbf{i}_y, 0\mathbf{i}_z)$-axes by $\frac{\pi}{2}$. The analytical functions and matrices to generate the RHCP, LHCP, and LP photon-e&mvfs are given in Appendix V, and the RHCP, LHCP, and LP photon-e&mvfs are visually demonstrated by computer simulations [4]. The conditions whereby a photon becomes an electron and a positron are given in the Pair Production and the Leptons sections.

**Figure 4.7.** The field-line pattern of a linearly polarized photon-e&mvf shown with 6 degree increments of the angle $\theta$ from the perspective of looking along the z-axis. (Electric field lines red; Magnetic field lines blue).



The linearly polarized photon-e&mvf equation in the lab frame is

$$\mathbf{E} = E_0 e^{-jk_z z} e^{-j\omega t} \tag{4.17}$$

In the case of $Y_\ell^m(\theta,\phi) \neq 0$ in Eq. (4.14), a right-handed and a left-handed elliptically polarized photon-e&mvf are superimposed to comprise a linearly polarized photon-e&mvf with the plane of polarization rotated relative to the case of $Y_\ell^m(\theta,\phi) = 0$. A right-handed or left-handed elliptically polarized photon is obtained by attenuating the oppositely polarized component.

## SPHERICAL WAVE

Photons superimpose and the amplitude due to $N$ photons is:

$$\mathbf{E}_{total} = \sum_{n=1}^{N} \frac{e^{-ik_r|\mathbf{r}-\mathbf{r}'|}}{4\pi\,|\,\mathbf{r}-\mathbf{r}'\,|} f(\theta,\phi) \tag{4.18}$$

When the observation point is very far from the source as shown in Figure 4.8, the distance in Eq. (4.18) becomes:

$$|\mathbf{r}-\mathbf{r}'| \approx r - \hat{\mathbf{r}} \bullet \mathbf{r}' \tag{4.19}$$

where $\hat{\mathbf{r}}$ is the radial unit vector. Substitution of Eq. (4.19) into Eq. (4.18) gives:

$$\mathbf{E}_{total} = \frac{e^{-ikr}}{r} \sum_{n=1}^{N} e^{-i\mathbf{k}\cdot\mathbf{r}'} f(\theta,\phi) \tag{4.20}$$

where we neglect $\hat{\mathbf{r}} \bullet \mathbf{r}'$ in the denominator, and

$$\mathbf{k} = \hat{\mathbf{r}} k \tag{4.21}$$

For an assembly of incoherent emitters

$$\sum_{n=1}^{N} e^{i\mathbf{k}\cdot\mathbf{r}'} f(\theta,\phi) = 1 \tag{4.22}$$

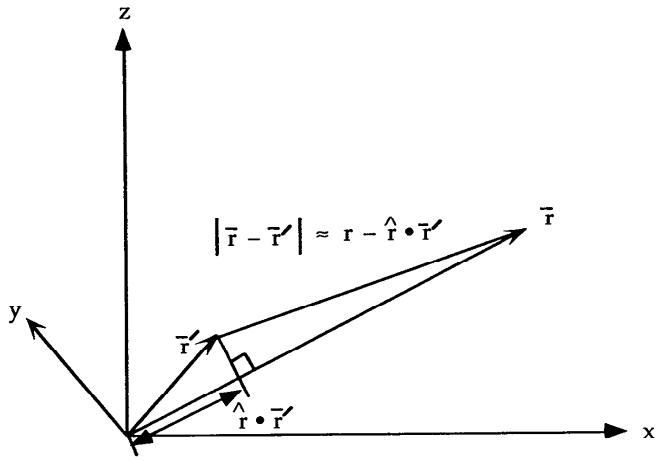
Thus, in the far field, the emitted wave is a spherical wave

$$\mathbf{E}_{total} = E_0 \frac{e^{-ikr}}{r} \tag{4.23}$$

which is shown by Bonham to be required in order to insure continuity of power flow for wavelets from a single source [5]. Also, as a conservation law at the photon level, the density of photons decreases as the number of photons divided by the area of the outgoing spherical wave front. The Green Function, (Eq. (6.62) of Jackson [1]) is given as the solution of the wave equation

(Eq. (6.58) of Jackson [1]). Thus, the superposition of photons gives the classical result. As $r$ goes to infinity, the spherical wave given by Eq. (4.23) becomes a plane wave. The double slit interference pattern is derived in Eqs. (8.15-8.23). From the equation of a photon (Eqs. (4.4-4.7), the wave-particle duality arises naturally. The energy is always given by Planck's equation; yet, an interference pattern is observed when photons add over time or space.

**Figure 4.8.** Far field approximation.




The photon spin angular momentum corresponding to the first term of Eq. (4.14) and the orbital angular momentum corresponding to the second term of Eq. (4.14) are conserved during electronic excitation as described in the Excited States of the One-Electron Atom (Quantization) section. And, the spin and orbital angular momentum of photons superimpose to give the classical result. For example, second harmonic generation has been obtained by Dholakia et al. [6] by use of Laguerre-Gaussian beams in a variety of mode orders. Each mode becomes doubled in frequency and transformed to a higher order, which is shown to be a consequence of the phase-matching conditions. The experiment is consistent with the interpretation that the orbital angular momentum of the Laguerre-Gaussian mode is directly proportional to the azimuthal mode index $\ell$ where each photon possesses orbital angular momentum of $\ell\hbar$ in addition to any spin angular momentum due to its state of polarization.

The macroscopic Maxwell's equations for reflection and refraction arise from the superposition of individual photon behavior at a bulk material surface. A totally internally reflected photon incident at an angle greater than the critical angle giving rise to a surface wave and an evanescent field arises from charge separation in the reflecting matter. Free or polarization current and charge produce the corresponding purely decaying electric and magnetic fields.

## PHOTON TORPEDOES

Recent evidence suggests that energy packets like photon torpedoes are creeping toward reality [7]. The possibility of solutions of the scalar wave equation and Maxwell's equations that describe localized, slowly decaying transmission of energy in spacetime has been suggested by several groups in recent years. These include exact pulse solutions such as focus wave modes [8-9], electromagnetic directed energy pulse trains [10], splash modes [11], transient beams [12], continuous-wave modes (Bessel beams) [13], and asymptotic fields (electromagnetic missiles [14], electromagnetic bullets [15], Gaussian wave packets [16]).

A macroscopic surface current having a distribution given as an atomic orbital transition comprises a means to emit electromagnetic energy having electric and magnetic field lines which comprise a photon-e&mvf. In this case, energy is not diminished in intensity as the electromagnetic wave propagates through space. Thus, "photon torpedoes" can be realized. High power densities can be achieved by increasing the magnitude of the electric and magnetic fields of the photon where the energy is given by Eq. (1.263) and Eq. (1.154). Also, neutrino-type photons described in the Weak Nuclear Force: Beta Decay of the Neutron section represent a means to transfer energy without scattering or attenuation between matched emitters and receivers. Applications in both cases include power transfer, communications, and weapons. An example of a device that produces photon torpedoes is a mode-locked femtosecond laser.

## PHOTOELECTRIC EFFECT

Electrons are ejected, and a photocurrent is observed when a clean surface of a metal such as sodium is irradiated with ultraviolet light in the wavelength range 2000–400 Å in an evacuated vessel. The photoelectric current, which is the amount of charge arriving at a collection plate per unit time, is proportional to the rate of liberation of electrons from the metal surface; that is, if $\Delta n_e$ is the number of free electrons produced in the time interval $\Delta t$ and $i$ is the current,

$$\frac{\Delta n_e}{\Delta t} = \frac{i}{e} \tag{4.24}$$

To determine the velocity with which the photoelectrons travel, a potential is applied to a grid mounted between the metal surface and the collection plate. The potential creates an electric field, which decelerates the photoelectrons. As the potential difference between the grid and the emitting metal is increased, a *stopping voltage* $V_s$ is observed, the value above which the electrons are stopped before they reach the plate and the current ceases to flow. At the stopping voltage, the initial kinetic energy of the photoelectrons liberated from the metal by the light has all been converted to potential energy; thus

$$\frac{1}{2}mv^2 = eV_s \tag{4.25}$$

The number of electrons produced per second and their maximum kinetic energy as functions of the intensity *I* and frequency $\nu$ of the incident light is determined by measuring *i* and $V_s$.

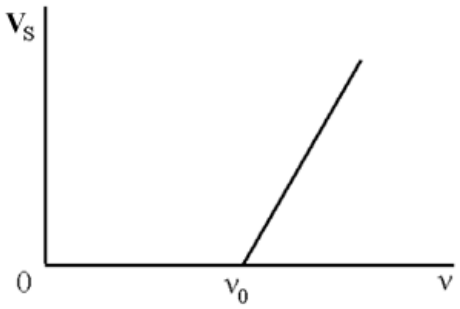
Physicists of the early 20th century had a misconception regarding classical wave theory and the photoelectric effect that has been promulgated to the present. They erroneously predicted that the energy of the radiation should be continuously absorbed by the electrons in the metal. After an electron has absorbed an amount of energy in excess of its binding energy $eV_0$, it may be ejected from the surface. The adjustable potential $V_s$ is used to stop electrons whose energy exceeds $eV_0$ by $eV_s$ or less. Since the intensity *I* of the light is the rate at which energy is propagated by the radiation waves, an increase in intensity should increase the average kinetic energy of ejected electrons which implies that the stopping voltage $V_s$ is proportional to *I*.

It is experimentally observed that $V_s$ is proportional to the *frequency* of the light and *independent of the intensity*. As shown in Figure 4.9, if the frequency $\nu$ is below a certain threshold value $\nu_0$, no photoelectric current is produced. At frequencies greater than $\nu_0$, the empirical equation for the stopping voltage is:

$$V_s = k(\nu - \nu_0) \tag{4.26}$$

where $k$ is a constant independent of the metal used, but $\nu_0$ varies from one metal to another. Although there is no relation between $V_s$ and the light intensity, it is found that the photoelectric current, and therefore the number of electrons liberated per second, is proportional to $I$.

**Figure 4.9.** The stopping voltage $V_s$ of photoelectrons as a function of the frequency $\nu$ of the incident light.




These results are *not* in disagreement with expectations from the classical wave theory based on the equations of a photon (Eqs. (4.4-4.7)). The electric and magnetic fields of a photon carry $\hbar$ of angular momentum as given by Eq. (4.1), and the corresponding energy is given by Planck's equation (Eq. (4.8)). As shown in the Excited States of the One-Electron Atom (Quantization) section, the angular momentum of the photon is conserved [1] for the solutions for the resonant photons and excited state electron functions. It can be demonstrated that the resonance condition between these corresponding frequencies is to be satisfied in order to have a net change of the energy field [17]. Thus, the correspondence principle holds. That is the change in angular frequency of the electron is equal to the angular frequency of the resonant photon that excites the resonator cavity mode corresponding to the transition, and the energy is given by Planck's equation. In the case of photoelectrons, the resonant transition is from a bound state in the metal to a continuum level. Thus, a photon of energy $h\nu$ strikes a bound electron, which may absorb the photon energy. If $h\nu$ is greater than the binding energy (or *work function*) $eV_0$, the electron is liberated. Thus, the threshold frequency $\nu_0$ is given by:

$$\nu_0 = \frac{eV_0}{h} \tag{4.27}$$

Since $V_0$ is a characteristic of the particular metal, which is used in the experiment, $\nu_0$ depends upon the metal, in accordance with the experimentally observed result.

For a photon of energy $h\nu$, the total energy of the excited electron is $h\nu$, with the excess over the potential energy $eV_0$ required to escape from the metal appearing as kinetic energy. Conservation of energy requires that the kinetic energy is the difference between the energy of the absorbed photon and the work function of the metal, which is the binding energy. The relationship is:

$$\frac{1}{2}mv^2 = h\nu - eV_0 = eV_s \tag{4.28}$$

which is identical to Eq. (4.26), with $k = h/e$. The photoelectric effect provides another means to determine Planck's constant $h$ originally used by Planck for blackbody radiation and by Bohr for the hydrogen spectrum.

Furthermore, since the energy of each photon is $h\nu$, the intensity of the radiation is not related to the energy of each photon, but instead determines the number of photons striking the metal surface per second. The rate of electron ejection is expected to be proportional to the rate at which the photons impinge upon the metal surface; thus, an increase in light intensity is predicted to increase the photoelectric current, as observed. Because the amount of energy absorbed by an electron is $h\nu$ regardless of the rate at which photons impinge on the surface, the kinetic energy of the ejected electrons should be independent of the intensity of the light. Thus, all of the predictions of the photon mechanism for the photoelectric effect are in agreement with the experimental results.

## COMPTON EFFECT

An experiment that is related to the photoelectric effect is the Compton effect. This experiment, which provides more detailed information about the interaction of radiation and matter was performed in the early 1920's and analyzed by Compton in 1923. The experiment comprises the irradiation of a sample of material such as a paraffin hydrocarbon with X-rays or $\gamma$-rays, high-frequency radiation. The photons are scattered from bound electrons, which are ionized. The wavelength of the scattered radiation and the energy of the emitted electron are determined as a function of angle, relative to the incident beam. It is found that the radiation scattered from the material contains not only wavelengths equal to that of the incident radiation $\lambda$, but also wavelengths of the order of a few hundredths of an Angstrom longer than $\lambda$. The dependence of the scattered wavelength $\lambda'$ upon the angle $\theta$ between the primary and scattered beams is found to be:

$$\lambda' = \lambda + k \sin^2\left(\frac{\theta}{2}\right) \tag{4.29}$$

where $k$ is a constant.

Physicists of the early 20th century had a misconception regarding classical wave theory and the Compton effect that has been promulgated to the present. They erroneously predicted that the wavelength of the radiation would increase based on the Doppler effect since an electron in the sample would be accelerated by the impinging radiation and would therefore emit waves with longer wavelengths. The Doppler effect does not correctly explain the observations, however, since (a) the Doppler shift is proportional to the wavelength of the primary radiation and (b) the Doppler shift increases with the electron velocity and therefore should increase with time, since the electrons are accelerated continuously while they absorb energy during the irradiation. Neither of these predictions is corroborated by the experimental results, not as a consequence of the failure of classical theory, but because of an erroneous misconception about the nature of the photon and its interaction with matter. As was the case for the photoelectric effect, the observations can be explained quantitatively by the photon theory of radiation given *supra* and the laws of conservation of energy and momentum for particles including photons and electrons.

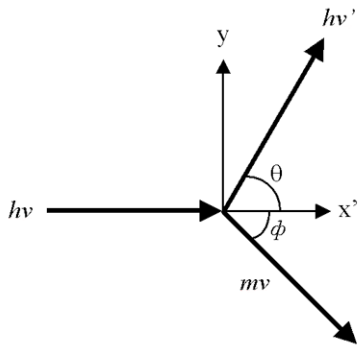
According to Eqs. (2.148-2.150), the incident photon with wavelength $\lambda$ and frequency $\nu = c/\lambda$ has a momentum $h\nu/c$. Correspondingly, the scattered photon, which has a longer wavelength $\lambda'$, and therefore a lower frequency $\nu' = c'/\lambda'$, has a lower momentum $h\nu'/c$. Since $\nu$ is in the X-ray region $(\lambda \sim 1\text{–}10\ \text{Å})$, the energy $(h\nu \sim 1000\ \text{eV})$ is so much greater than the binding energy of the electrons $(\approx 10\ \text{eV})$ that to a first approximation the latter be neglected. Thus, the electron is ejected in the direction $\phi$ with a momentum $mv$, which is calculable from an energy and momentum balance for the process as shown in Figure 4.10. The classical equations of conservation of energy and of the two components of the linear momentum are:

$$h\nu = h\nu' + \frac{1}{2}m_e v^2 \qquad \text{(energy)} \tag{4.30}$$

$$\frac{h\nu}{c} = \frac{h\nu'}{c}\cos\theta + m_e v \cos\phi \qquad (x \text{ component of momentum}) \tag{4.31}$$

$$0 = \frac{h\nu'}{c}\sin\theta - m_e v \sin\phi \qquad (y \text{ component of momentum}) \tag{4.32}$$

**Figure 4.10.** The Compton effect based on conservation of energy and momentum of a scattered photon and an electron.




Eliminating $\nu$ and $\phi$ from these equations, introducing $\lambda$ by the definition $\lambda = c/\nu$, and making the approximation that $\lambda\lambda' \approx \lambda^2$, gives:

$$\Delta\lambda = \lambda' - \lambda = 2\frac{h}{m_e c}\sin^2\left(\frac{\theta}{2}\right) \tag{4.33}$$

in agreement with Eq. (4.29). For $\lambda$ in Angstroms, Eq. (4.33) gives:

$$\Delta\lambda = 0.0485\ \sin^2\left(\frac{\theta}{2}\right) \tag{4.34}$$

If the ejected electron is treated relativistically with its total energy given by Eq. (34.17):

$$E = \left(m_e^2c^4 + p_e^2c^2\right)^{1/2} = m_e c^2\sqrt{1+\left(\frac{v_e}{c}\right)^2} \tag{4.35}$$

and the kinetic energy is obtained by subtracting the rest energy $m_e c^2$, Eq. (4.33) can be derived without using the approximation that $\lambda' \approx \lambda$. The maximum shift is seen to occur for $\theta = \pi$, where $\Delta\lambda = 0.0485$ Å.

The photon mechanism was tested by using $\gamma$-rays of energy $\approx 10^6$ eV, and the scattered photon and the Compton electron were recorded by means of scintillation counters. Cross and Ramsey [18] found that the angles $\phi$ and $\theta$ for an electron and a photon which were simultaneously detected were within $\pm 1^\circ$ of those required by the conservation laws (Eqs. 4.30-4.32)).

The analysis of the photoelectric and Compton effects shows that the particle viewpoint and Newtonian mechanics lead to a simple and quantitatively correct interpretation of these experiments, and that predictions based upon the classical wave theory are *not* wrong, but must be understood from the nature of the photon given by Eqs. (4.4-4.7). Individual photons behave as particles with energy given by Planck's equation (Eq. (4.8)). As shown by Eqs. (4.18-4.23), photons superimpose to give a spherical wave which gives rise to certain other phenomena such as diffraction and interference which are typically ascribed to wave theory with waves as an independent aspect of photons. The character exhibited by radiation, whether wave-like or particle-like, depends upon the type of experiment that is done. If the interaction of radiation with matter produces a measurable change in the matter, such as the ejection of an electron, the phenomenon appears to require the photon theory for its interpretation. If the interaction produces a measurable change in the spatial distribution of the radiation, such as diffraction at a slit, but produces no measurable change in the matter, invoking the wave theory seems appropriate as shown in the Classical Scattering of Electromagnetic Radiation section. Superficially, these results suggest that a synthesis of the two points of view is required which takes into account the nature of the experiment being analyzed; that is, the measuring process itself must be included in the theory. In actuality, both particle and wave aspects arise naturally from the particle-like photons which superimpose in time or space to form a wave which accounts precisely for the wave-particle duality of light.

## TRANSITIONS

Other interactions involving electromagnetic radiation and matter are given classically wherein the photon carries $\hbar$ of angular momentum in its electric and magnetic fields as given by Eq. (4.1) with a corresponding energy given by Planck's equation (Eq. (4.8)). Bremsstrahlung radiation is given classically as radiation due to acceleration of charged particles by Jackson [19]. *Cherenkov radiation* occurs when charges moving at constant velocity in a medium different from vacuum possess spacetime Fourier components of the current that are synchronous with a wave traveling at the speed of light as given by a radiative condition derived from Maxwell's equations by Haus [20]. That is spacetime harmonics of $\frac{\omega_n}{c}\sqrt{\frac{\varepsilon}{\varepsilon_0}} = k$ do exist for which the Fourier transform of the current-density function is nonzero [20].

Although Einstein did not anticipate the physics of the lifetimes of excited states as given in the State Lifetimes and Line Intensities section, lasing, or laser devices, the concept of stimulated emission originated in 1917, ten years before the Schrödinger equation was postulated, when Einstein proposed that Planck's formula for blackbody radiation could better curve fit the data if an ensemble of atoms with quantized energy levels underwent stimulated as well as spontaneous emission [21]. Stimulated emission can occur for an inverted population in a suitable resonator cavity to such an extent that amplification or lasing occurs. The *maser* and its extension to shorter wavelengths, the *laser*, are predicted by Maxwell's equations[1] as shown by Lamb [23] and Townes [24], respectively. From this approach, Townes invented first the maser, and he latter extended his work to optical wavelengths with the invention of the laser. The $B_{ki}$ coefficient for lasing can be calculated from the $A_{ki}$ coefficient using Eq. (6) of Carmichael [25]. The $A_{ki}$ coefficient given by Eq. (2.108) is calculated from the excited-state electron source current in the State Lifetimes and Line Intensities section.

Photons possess both wave and particle characteristics. The physical basis of the wave behavior is given in the Spherical Wave section, and particle behavior is observed during the photoelectron and Compton effects given in the corresponding sections. Another manifestation of particle behavior is the absorption and emission of indivisible photons each having an irreducible quantized angular momentum of $\hbar$ (Eq. (4.1)). Electrons and photons both have conserved angular momentum of $\hbar$ such that the inalienability of the quantization is intrinsic to the transition partners and the conservative physical laws. Except for the case of particle production, the radius of two-dimensional sphere of the photon comprising the photon-e&mvf and being proportional to the photon wavelength is typically orders of magnitude larger than the dimensions of the photon-absorbing electron (Eqs. (2.98-2.101)). The photon travels at light speed and a collision with an electron can only initially involve a small fraction of the photon-e&mvf; yet, the entire photon is either elastically scattered or entirely absorbed. Consider the relationship between the radius and wavelength of an electron and a photon of the resonant frequency that excites an electronic transition of the electron to form an electronic excited state given by Eq. (4.15) wherein the photon angular frequency and energy match the change in energy and angular frequency of the electron that is excited by the photon (Eqs. (2.18-2.22)). When the photon collides with the electron, the photon excites a resonator mode of the spherical superconducting electron resonator cavity such that the photon wavelength decreases to match the dimensions of the electron absorbing the photon akin to the process of total internal reflection wherein the two-dimensional ensemble of field lines propagates along the inner surface of the electron membrane. In the case of a macrocavity excitation, the field comprises the superposition of many photons with fields ending on time-dependent surface source charges and currents. In contrast, each electric field line of the quantum excitation by a single photon is closed onto itself. Moreover, uniquely the energy in the electric and magnetic fields of a free-space photon are equal, and the magnetic field is dependent on the electric field with both propagating at light speed. Consequently, as the photon initially traveling in free space at the speed of light is trapped by the atomic, ionic, or molecular electron undergoing excitation, the photon magnetic field lines transition to electric field lines. The result is a corresponding transition-state-evf (TS-evf) comprising only the electric field lines of the free space photon with the intensity increased by a factor or $\sqrt{2}$ corresponding an increase in the electric energy by a factor of 2 according to Eq. (1.189). For example, consider the left-handed-circularly-polarized photon electric and magnetic vector field (LHCP photon-e&mvf) given by the output of the matrix of Eq. (4.7) and shown in Figure 4.3. With the transition of the magnetic field to electric field according to Faraday's law (Eq. (4.2)), the corresponding left-handed-transition-state electric vector field (LHTS-evf) is generated by the rotation of a basis element comprising a great circle electric field line in the yz-plane about the $\left(\mathbf{i}_x,-\mathbf{i}_y,0\mathbf{i}_z\right)$-axis by $\frac{\pi}{2}$ wherein the radius $r_n$ is equal to the spherical radius of the excited state atomic or ionic electron or the ellipsoidal radius $\xi_n$ of the excited state molecular orbital, respectively.

[1] The development of the laser was impeded by quantum mechanics since its existence disproves the Heisenberg Uncertainty Principle as discussed by Carver Meade [22]:

> As late as 1956, Bohr and Von Neumann, the paragons of quantum theory, arrived at the Columbia laboratories of Charles Townes, who was in the process of describing his invention. With the transistor, the laser is one of the most important inventions of the twentieth century. Designed into every CD player and long-distance telephone connection, lasers today are manufactured by the billions. At the heart of laser action is perfect alignment of the crests and troughs of myriad waves of light. Their location and momentum must be theoretically knowable. But this violates the holiest canon of Copenhagen theory: Heisenberg Uncertainty. Bohr and Von Neumann proved to be true believers in Heisenberg's rule. Both denied that the laser was possible. When Townes showed them one in operation, they retreated artfully.

**LH TRANSITION STATE E FIELD:**

$$\begin{bmatrix} x' \\ y' \\ z' \end{bmatrix} = \sqrt{2}\begin{bmatrix} \frac{1}{2}+\frac{\cos\theta}{2} & -\frac{1}{2}+\frac{\cos\theta}{2} & \frac{\sin\theta}{\sqrt{2}} \\ -\frac{1}{2}+\frac{\cos\theta}{2} & \frac{1}{2}+\frac{\cos\theta}{2} & \frac{\sin\theta}{\sqrt{2}} \\ -\frac{\sin\theta}{\sqrt{2}} & -\frac{\sin\theta}{\sqrt{2}} & \cos\theta \end{bmatrix} \bullet \begin{bmatrix} 0 \\ r_n\cos\phi \\ r_n\sin\phi \end{bmatrix}_{\text{Red}} ;\ \theta \text{ to } \frac{\pi}{2} \tag{4.36}$$

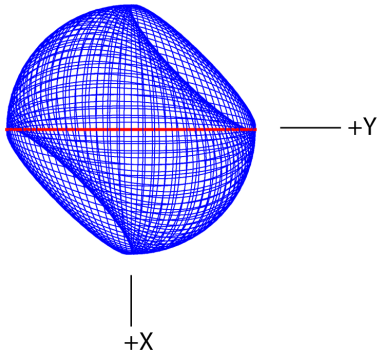
Free space photons, transition states, and excited state photons carry electric field as given by Eqs. (4.6), (4.7), (4.36), and (2.15). The directions of field lines change with relative motion as required by special relativity. They increase in the direction perpendicular to the propagation direction. As shown by Eq. (4.9), the linear velocity of each point along a great circle of the photon atomic orbital is $c$. The same applies to the transition state. And, as shown in the Special Relativistic Correction to the Ionization Energies section and by Eq. (1.280), when the velocity along a great circle is light speed, the motion relative to the non-light speed frame is purely radial. In the case of the electric field lines of a trapped resonant photon of an excited state, the relativistic electric field is radial. It is given by Eq. (2.15), and it exists only at $\delta(r-r_n)$ wherein $r_n$ is the radius of the excited electron.

The bound electron is an equipotential, equi-energy surface comprising the uniform current density function $Y_0^0(\theta,\phi)$. The radial field of the TS-evf only covers 1/4$^{\text{th}}$ of the inner surface of the electron membrane. Thus, the imbalance in central force on the spherical surface gives rise to a rotation over the range of $\frac{\pi}{2}$ to $2\pi$ about the axis that forms the TS-evf. In the case of excitation by a RHCP photon, the rotation is about the $(\mathbf{i}_x,\mathbf{i}_y,0\mathbf{i}_z)$-axis to form the corresponding right-handed transition state basis element electric vector field (RHTSBE-evf). In turn, the RHTSBE-evf undergoes a transition that distributes the field lines uniformly over the surface of a spherical electric field vector membrane corresponding to a convolution operator acting on the RHTSBE-evf about the $\left(\frac{1}{\sqrt{2}}\mathbf{i}_x,\frac{1}{\sqrt{2}}\mathbf{i}_y,\mathbf{i}_z\right)$ -axis. In the case of excitation by a LHCP photon the rotation is about the $(\mathbf{i}_x,-\mathbf{i}_y,0\mathbf{i}_z)$-axis to form the corresponding left-handed transition state basis element electric vector field (LHTSBE-evf). Likewise, the LHTSBE-evf is transitioned to the uniform field distribution by the convolution operator acting on the LHTSBE-evf about the $\left(\frac{1}{\sqrt{2}}\mathbf{i}_x,-\frac{1}{\sqrt{2}}\mathbf{i}_y,\mathbf{i}_z\right)$-axis. Both are convolved over the range $0$ to $2\pi$ to form the uniform excited state electric vector field (ES-evf) that matches the uniform current density distribution of the electron wherein each convolution is normalized to produce a central field given by Eq. (2.15).

The uniform distribution current density function $Y_0^0(\theta,\phi)$ corresponds to electron's spin that is matched by the ES-evf corresponds to electron spin (Eq. (1.27-1.28)). Consider the exemplary case to generate the ES-evf using the same the matrices as those used to generate the electron spin current density function given in the Generation of the Atomic Orbital CVFS section. Two current loops, one in the yz-plane and one in the xz-plane, serve as great circle basis elements for the electron current density pattern called the basis element current vector field (BECVF) that is formed by the rotation of the basis elements about the $(-\mathbf{i}_x,\mathbf{i}_y,0\mathbf{i}_z)$-axis as given by Eqs. (1.84) and (1.87). The LHCP photon and corresponding LHTS-evf and LHTSBE-evf may also be generated by rotation of the electric and magnetic field basis elements and the electric field basis element, respectively, about the $(-\mathbf{i}_x,\mathbf{i}_y,0\mathbf{i}_z)$-axis wherein the current loop in the yz-plane is replaced with an electric field great circle, the current loop in the xz-plane is replaced with a magnetic field great circle, and $\theta$ of the $(\mathbf{i}_x,-\mathbf{i}_y,0\mathbf{i}_z)$-axis rotation (Eqs. (1.84) and (1.87)) is replaced by $-\theta$. With $E_0$ given by Eq. (29) of Appendix V and $H_0=\frac{E_0}{\eta}$ according to Eq. (19) of Appendix V, the LHCP photon-e&mvf is given by Eq. (4.37) for $a_1=1;\ a_2=1,\ \theta=0$ to $\theta=-\frac{\pi}{2}$; the LHTS-evf given by Eq. (4.37) for $a_1=\sqrt{2};\ a_2=0$, $\theta=0$ to $\theta=-\frac{\pi}{2}$, and the LHTSBE-evf is given by Eq. (4.37) for $a_1=\sqrt{2};\ a_2=0,\ \theta=0$ to $\theta=-2\pi$. The LHTSBE-evf is shown in Figure 4.11.

$$\begin{bmatrix} x' \\ y' \\ z' \end{bmatrix} = a_1 E_0 \begin{bmatrix} \frac{1}{2}+\frac{\cos\theta}{2} & -\frac{1}{2}+\frac{\cos\theta}{2} & -\frac{\sin\theta}{\sqrt{2}} \\ -\frac{1}{2}+\frac{\cos\theta}{2} & \frac{1}{2}+\frac{\cos\theta}{2} & -\frac{\sin\theta}{\sqrt{2}} \\ \frac{\sin\theta}{\sqrt{2}} & \frac{\sin\theta}{\sqrt{2}} & \cos\theta \end{bmatrix} \bullet \begin{bmatrix} 0 \\ r_n\cos\phi \\ r_n\sin\phi \end{bmatrix}_{\text{Red}} + a_2 H_0 \begin{bmatrix} \frac{1}{2}+\frac{\cos\theta}{2} & -\frac{1}{2}+\frac{\cos\theta}{2} & -\frac{\sin\theta}{\sqrt{2}} \\ -\frac{1}{2}+\frac{\cos\theta}{2} & \frac{1}{2}+\frac{\cos\theta}{2} & -\frac{\sin\theta}{\sqrt{2}} \\ \frac{\sin\theta}{\sqrt{2}} & \frac{\sin\theta}{\sqrt{2}} & \cos\theta \end{bmatrix} \bullet \begin{bmatrix} r_n\cos\phi \\ 0 \\ r_n\sin\phi \end{bmatrix}_{\text{Blue}} \tag{4.37}$$

**Figure 4.11.** The photon electric field pattern of the LHTSBE-evf corresponding to the electron BECVF shown with 6-degree increments of $\theta$ from the perspective of looking along the z-axis. The yz-plane great circle electric field loop that served as a basis element that was initially in the yz-plane is shown as red.

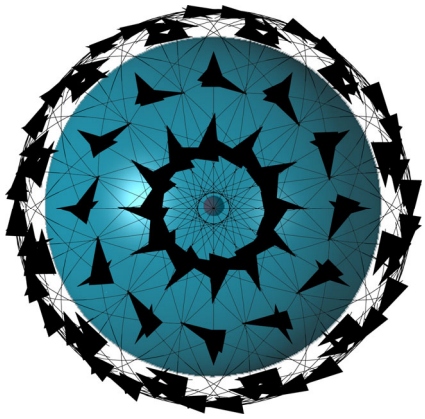



The exemplary transition of the LHTSBE-evf to the uniform distribution that matches the equipotential, equi-energy condition of the atomic orbital is given by the convolution of the output of Eq. (4.37) with the matrix given by Eq. (1.95) corresponding to a convolution about the $\left(-\frac{1}{\sqrt{2}}\mathbf{i}_x, \frac{1}{\sqrt{2}}\mathbf{i}_y, \mathbf{i}_z\right)$-axis wherein the output of the matrix of Eq. (1.95) called the orbital current vector field (OCVF) used to generate the uniform electron current distribution corresponding to electron spin. Due to symmetry over a range of $2\pi$, the LHTSBE-evf is also given for $\theta$ positive in Eq. (4.37). Using (1.103), a discrete representation of the electric field distribution $Y_0^0(\theta,\phi)$ is generated. The continuous convolution of the LHTSBE-evf about the $\left(-\frac{1}{\sqrt{2}}\mathbf{i}_x, \frac{1}{\sqrt{2}}\mathbf{i}_y, \mathbf{i}_z\right)$-axis to form the ES-evf is shown as a superposition of discrete incremental rotations of the position of the LHTSBE-evf rotated according to Eqs. (1.95) and (1.98) corresponding to the matrix which generated the OCVF of the electron spin current function. In the case that the discrete representation of the LHTSBE-evf comprises $N$ great circle electric field element and the number of convolved RHTSBE-evf elements is $M$, the representation of the ES-evf function showing electric field loops is given by Eq. (4.38) with $E_0$ given by Eq. (2.15), and the $\left(\frac{1}{\sqrt{2}}\mathbf{i}_x, -\frac{1}{\sqrt{2}}\mathbf{i}_y, \mathbf{i}_z\right)$-axis view with 144 vectors overlaid giving the initial free-photon-frame direction of each great circle electric field element is shown in Figure 4.12.

$$\begin{bmatrix} x' \\ y' \\ z' \end{bmatrix} = E_0 \sum_{m=1}^{m=M} \begin{bmatrix} \frac{1}{4}\left(1+3\cos\left(\frac{m2\pi}{M}\right)\right) & \frac{1}{4}\left(-1+\cos\left(\frac{m2\pi}{M}\right)+2\sqrt{2}\sin\left(\frac{m2\pi}{M}\right)\right) & \frac{1}{4}\left(-\sqrt{2}+\sqrt{2}\cos\left(\frac{m2\pi}{M}\right)-2\sin\left(\frac{m2\pi}{M}\right)\right) \\ \frac{1}{4}\left(-1+\cos\left(\frac{m2\pi}{M}\right)-2\sqrt{2}\sin\left(\frac{m2\pi}{M}\right)\right) & \frac{1}{4}\left(1+3\cos\left(\frac{m2\pi}{M}\right)\right) & \frac{1}{4}\left(\sqrt{2}-\sqrt{2}\cos\left(\frac{m2\pi}{M}\right)-2\sin\left(\frac{m2\pi}{M}\right)\right) \\ \frac{1}{2}\left(\frac{-1+\cos\left(\frac{m2\pi}{M}\right)}{\sqrt{2}}+\sin\left(\frac{m2\pi}{M}\right)\right) & \frac{1}{4}\left(\sqrt{2}-\sqrt{2}\cos\left(\frac{m2\pi}{M}\right)+2\sin\left(\frac{m2\pi}{M}\right)\right) & \cos^2\frac{\left(\frac{m2\pi}{M}\right)}{2} \end{bmatrix}$$

$$\bullet \sum_{n=1}^{n=N} \begin{bmatrix} \frac{1}{2}+\frac{\cos\left(\frac{n2\pi}{N}\right)}{2} & -\frac{1}{2}+\frac{\cos\left(\frac{n2\pi}{N}\right)}{2} & -\frac{\sin\left(\frac{n2\pi}{N}\right)}{\sqrt{2}} \\ -\frac{1}{2}+\frac{\cos\left(\frac{n2\pi}{N}\right)}{2} & \frac{1}{2}+\frac{\cos\left(\frac{n2\pi}{N}\right)}{2} & -\frac{\sin\left(\frac{n2\pi}{N}\right)}{\sqrt{2}} \\ \frac{\sin\left(\frac{n2\pi}{N}\right)}{\sqrt{2}} & \frac{\sin\left(\frac{n2\pi}{N}\right)}{\sqrt{2}} & \cos\left(\frac{n2\pi}{N}\right) \end{bmatrix} \begin{bmatrix} 0 \\ r_n \cos\phi \\ r_n \sin\phi \end{bmatrix} \tag{4.38}$$

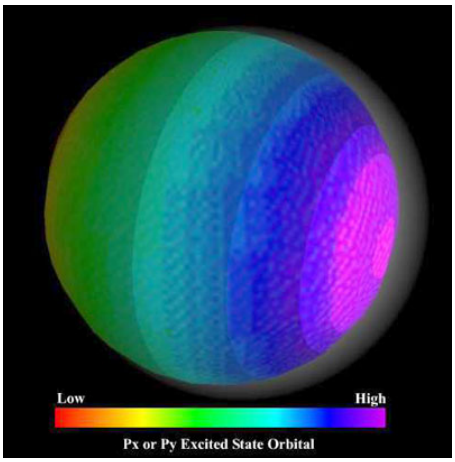
**Figure 4.12.** A representation of the $\left(\frac{1}{\sqrt{2}}\mathbf{i}_x,-\frac{1}{\sqrt{2}}\mathbf{i}_y,\mathbf{i}_z\right)$-axis view of ES-evf comprising the $Y_0^0(\theta,\phi)$ distribution matching the electron spin function shown with 144 vectors overlaid giving the initial free-photon-frame direction of the electric field of each great circle basis element.



As shown by Eq. (2.11) and (2.15) the ES-evf obeys some of the properties of electrostatic charge. In addition to matching the spin function of the excited electron, the $\hbar$ angular momentum in the electric and magnetic fields of the excitation photon given by Eq. (4.1) must be conserved as electron angular momentum. Thus, the ES-evf must possess a spherical harmonic modulation component that matches an allowed spherical harmonic electron current distribution given by Eqs. (1.27-1.29) wherein the ES-evf obeys the corresponding properties of rotating electrostatic charge. The spherical harmonic function has a velocity less than light speed given by Eq. (1.35) and is phase-matched with the electron such that angular momentum is conserved during the excited state transition. The multipole of the photon is conserved in the spherical harmonic of the excited state having the corresponding orbital angular momentum given by Eq. (1.72). Moreover, the radial field can be considered a corresponding surface charge density according to Eq. (2.11)). The effect of the nature of this photon charge-equivalent on the stability and lifetime of excited states is given in the Instability of Excited States section, the State Lifetimes and Line Intensities section, and the Stability of Atoms and Hydrinos section. All boundary conditions are met for the electric fields and the wavelengths of the "trapped photon" and the electron. Eq. (2.16) is the solution for the excited modes of the atomic orbital, a spherical resonator cavity. And, the quantum numbers of the electron are $n$, $\ell$, $m_\ell$, and $m_s$ (Described in the Stern-Gerlach

Experiment section). A $p_x$ or $p_y$ atomic-hydrogen excited state is shown in Figure 4.13.

**Figure 4.13.** The electron atomic orbital is a resonator cavity wherein the radii of the excited states are related by integers. The electronic charge-density function of a $p_x$ or $p_y$ atomic-hydrogen excited state is shown with positive and negative charge-density proportional to red intensity and blue intensity, respectively. The function corresponds to a charge density wave on the two-dimensional spherical surface of radius $na_0$ that travels time harmonically about the z-axis at the angular frequency given by Eq. (1.36). It is comprised of a linear combination of a constant function modulated by time and spherically harmonic functions. The centrifugal force is balanced by the electric field of its photon that is phase-locked to the rotating electron. The brightness corresponds to the intensity of the two-dimensional radial photon field.




Regarding the energy balance of the transition to an excited state, the effect of the deceleration of the electron during the transition and the consequence for the ES-evf must be considered. Upon collision of a photon with an electron, the photon electric fields induce a decelerating current component along impacted great circle basis elements of the current vector field (CVF) of the electron given in the Generation of $Y_0^0(\theta,\phi)$ section. Decelerating current results in radiation. Given the indivisibility of the electron, the deceleration current produces a field along every great circle current element of the electron. The photon scatters elastically except in the case that the correspondence principle holds whereby the frequency of the photon matches the allowed frequency change of the electron as given in the Photon Absorption section. In the latter resonance case, the photon e&mvfs transition to the ES-evf, and the superposition of the field energy of the photon and the equivalent radiation field energy from the decrease in kinetic energy due to resonant electron current deceleration gives rise to the central photonic field along every great circle. The lifetime $\tau$ of this process is very small based on the time for a resonant photon to transverse the dimensions of a bound electron at lightspeed (e.g. $3\,X\,10^{-19}\,s$ for a 1 Å diameter electron). In superposition, the photon field reduces central nuclear field at the position of the electron only. In case of the hydrogen atom, the excitation photon decreases the central spherical field to that of a reciprocal integer of the fundamental charge at the central nucleus, wherein ½ of the excitation energy is contributed by the resonant photon and ½ of the energy is contributed by the decrease in kinetic energy due to electron deceleration during the transition as shown by Eqs. (2.18-2.22). Consequently, the radius of the electron increases to give rise to a radial current. The energy and angular momentum of the photon given by Eqs. (4.1) and (4.8), respectively, are conserved in the corresponding excited electronic state. The multipole of the photon is conserved in the spherical harmonic of the excited state having the corresponding orbital angular momentum given by Eq. (1.72). The transition probability and state lifetime are given by the ratio of the power and energy of the transition determined by the radial and angular source currents of photon absorption and emission events as given in the State Lifetimes and Line Intensities section. Absorption and emission of a photon are reversible, time-symmetrical processes wherein the opposite process to a that described herein occurs during photon emission. Computer modeling of the analytical equations of the mechanism of photon absorption and corresponding emission by time reversal is available on the web [26].

## FREE ELECTRON PHOTON ABSORPTION

Consider next the physics of the free-electron photon absorption based on the free electron structure and corresponding behavior in the electric and magnetic photon fields based on Maxwell's equations. The free electron is a two-dimensional plane lamina comprised of a series of concentric circular current loops in the xy-plane ($\rho$-plane) that circulate about the z-axis as given in the Current-Density Function section. The circulation corresponds to rotational kinetic energy, and additionally the free electron center of mass may undergo linear translation corresponding to linear kinetic energy wherein the sum of these two components comprises the total energy of the free electron. With conservation of photon energy, the rotational and linear kinetic energies of a free electron can be arbitrarily large starting from a bound electron by absorption of a single high energy photon or starting from a bound electron that is ionized to form a low-energy free electron that then absorbs a series of photons. In either

case, the ionization of a bound electron to produce a free electron of any final total energy may proceed through a series of excited state levels each having a principal, orbital, and spin quantum number wherein the orbital quantum number $\ell$ may comprise a superposition of $\ell$ quantum numbers. The superposition may comprise a Fourier series of corresponding spherical harmonics wherein the orbital quantum number $\ell$ may approach infinity as the principal quantum number approaches infinity. In general, the physics of photon emission and absorption obeys time-reversal symmetry and superposition of states akin to Hess's law on a macroscopic scale. Consider the physics of the bound-electron absorption of a photon having energy excess of the ionization energy to form a free electron. The energy excess of the ionization energy is conserved in the free electron rotational energy, corresponding to the plane-lamina circular current with $\hbar$ of angular momentum, and the linear kinetic energy, corresponding to a linear velocity that derive from Eqs. (3.29) and (3.52). From a bound electronic state, free electron total energies each comprising a given set of rotational and linear kinetic energy states of arbitrary high energies can be achieved by absorption of a photon equal to the sum of the bound electron ionization energy and the total energy of the free electron. Alternatively, a free electron may absorb a plurality of photons with a concomitant increase in its rotational and linear kinetic energies to any final total energy that may be achieved starting from a bound state wherein the summation of the photon energies is conserved.

As shown by Eqs. (3.29) and (3.52), the radius $\rho_0$ decreases and the linear velocity increases to match the conservation condition that the change in the disc radius $\Delta\rho_0$ is given by Eq. (3.29), and the velocity increase corresponds to a kinetic energy increase that is exactly ½ the energy of the photon (Eq. (3.52)). The resulting energy balance is given by Eqs. (3.51) and (3.52). Specifically, using Eqs. (3.29) and (3.52), the absorption of a photon of frequency $\omega_{photon}$ by a free electron with an initial velocity along the z-axis of $v_z$ gives rise to the radius decrease $\Delta\rho_0$ and the linear velocity increase $\Delta v_z$ of

$$\Delta\rho_0 = \frac{\hbar}{m_e}\left(\frac{1}{v_z + \Delta v_z} - \frac{1}{v_z}\right) \tag{4.39}$$

wherein based on the kinetic energy increase (Eq. 3.52)) for velocities $v_z << c$:

$$\Delta v_z = \sqrt{\frac{\hbar\omega_{photon}}{m_e}} \tag{4.40}$$

Substitution of Eq. (4.40) into Eq. (4.39) gives

$$\Delta\rho_0 = \frac{\hbar}{m_e}\left(\frac{1}{v_z + \sqrt{\frac{\hbar\omega_{photon}}{m_e}}} - \frac{1}{v_z}\right) \tag{4.41}$$

To obey time time-reversal symmetry and superposition of states, the mechanism of absorption or emission of a photon by a free electron with a change in the free electron rotational and linear kinetic energies involves the formation of a transient, free-electron excited state. The spherically symmetric electronic state comprises a photon that provides the binding radial electric field force; whereafter the state decays as the photon applies equal average magnitude radial and linear forces on the excited state electron. The electric field of an exited state photon given in the Equation of the Electric Field inside the Atomic Orbital section comprises electric field great circles that are matched to each great circle of the bound electron and further circulate at light speed along each electron great circle wherein additionally the photon field intensity is modulated by time and spherical harmonics that are phase matched to any modulation of the electron current. Consequentially, the relativistic direction of the photon electric field lines is radial. To match the boundary conditions on nature of electron excited states and the required direction of the photon-electric-field-sourced radial and linear electronic forces, the excited electronic state electron comprises a charge and current density distribution equivalent to $Y_0^0(\theta,\phi)$ of the bound electron that is modulated by a Fourier series of time and spherically harmonic functions. The $Y_0^0(\theta,\phi)$ current density of the bound electron has the same angular frequency and linear velocity everywhere on the surface corresponding to electron spin, and the time and spherically harmonic modulation current densities correspond to orbital angular momentum. The photon modulated current density function that provides the required forces can be determined by considering the corresponding modulation of each great circle current of the free electron excited state. The modulated current density that matches the boundary conditions of the resultant photon force fields can be generated from an initial free electron great circle basis element with cylindrical radius $\rho = \rho_0$ comprising a constant function modulated by a time-constant trigonometric function that undergoes the series of BECVF and OCVF rotations to generate the free electron excited state. With the conversion of energy of the photon field to angular and linear kinetic energies as the electron ionizes to a new free state, each electron great circle transitions to a smaller radius, and the free electron is linearly accelerated in the direction perpendicular to the plane of the initial free electron basis element reference frame.

Specifically, consider the incidence of a linearly polarized photon having $\hbar$ of angular momentum aligned on the x-axis and propagating along the x-axis with a free electron in the xy-plane having $\hbar$ of angular momentum aligned on the z-axis and propagating along the z-axis. The photon angular momentum of the free electron creates a torque to cause the rotation of the angular momentum vector of the free electron current about two axes, the $\left(\mathbf{i}_x, 0\mathbf{i}_y, \mathbf{i}_z\right)$-axis in a first step and the laboratory-frame z-axis in a second step. The corresponding motion of the perimeter great circle current loop at $\rho_0$ in the plane perpendicular to

the angular momentum vector generates CVFs equivalent to those of the bound electron given in the Atomic Orbital Equation of Motion for $\ell = 0$ Based on the Current Vector Field (CVF) section. Specifically, as given by Eq. (3.80) and shown in Figure 3.10 the first rotation sweeps out the equivalent of a BECVF, wherein the concentric planar great circle current loops shown in Figure 3.2A flow from the disc origin to the perimeter edge at $\rho_0$. The remaining electron disc current density at each rotational angle forms an annulus with a constant outer radius $\rho = \rho_0$ and an increasing inner radius during the rotation to successively spread the charge density over the BECVF. The second rotation of the BECVF sweeps out the equivalent of the convolution of the BECVF with the OCVF. The result is a charge and current density distribution equivalent to $Y_0^0(\theta,\phi)$ of the bound electron wherein charge density of the bound electron has the same angular frequency and linear velocity everywhere on the surface.

The field of a bound photon replaces the proton as the source of central field to create equivalent event as the binding of the electron to a proton as given Eq. (3.80) and shown in Figure 3.10 wherein the equations of a free linearly polarized and bound photon are given by Eqs. (4.6-4.7) and (4.38), and Figures 4.7 and 4.12, respectively. In the absence of the central field of a nucleus, the trapped photon field from Eq. (2.16) has the form:

$$\mathbf{E}_r = \mathrm{Re}\left\{Y_0^0(\theta,\phi) + Y_\ell^m(\theta,\phi)e^{im\omega_n t}\right\}\delta(r - r_n) \tag{4.42}$$

except that the trapped photon of a free electron comprises a Fourier series of spherical harmonics that result in a central force and a linear force along the z-axis wherein the orthogonal components are equal on average. The photon field of the free electron excited state comprises a Fourier series of time harmonic and spherically harmonic functions that can be constructed from a great circle electric field basis element having a time-constant trigonometrically modulated photon intensity along the great circle current basis element. The corresponding time-constant, relativistic radial electrical field of the photon field basis element that is phase matched to the great circle current basis element is given by:

$$\mathbf{E}_\rho = (1 - \cos\theta)\delta(\rho - \rho_0) \tag{4.43}$$

wherein for when $\theta = \pi$, the vector $\mathbf{i}_\rho$ is in the direction of the positive x-axis of the original free electron reference frame before excitation by the incident photon. The electron great circle current density is spatially modulated in phase with the electric field modulation wherein the spatial modulation is constant in time. Electron ionization of the free electron excited state is a continuous process with continuous current flow. An equation providing visualization in discrete steps that generates the angular momentum vectors of the bound electron is given by Eq. (3.80), but time reversed with the spherical and cylindrical radii scaled sequentially according to the average of the forces acting of the electron current during each step of the event. The visualization of the ionization event is given by the reverse sequence shown in Figure 3.10 with the excited state photon substituting for the proton and with a scaling factor applied. The scaling factor $S$ of the spatial dimensions that multiples the output of the reverse sequence of Eq. (3.80) corresponding the indices in the direction m = M to m = 1 and n= N to n = 1 is given by

$$S = \left(1 - \left(1 - \frac{n-1}{N}\right)\frac{\Delta\rho_0}{\rho_0}\right) \tag{4.44}$$

Considering the translational acceleration over the ionization event, the linear velocity concomitantly incrementally increases by the factor $S'$:

$$S' = \left(1 + \frac{n-1}{N}\frac{\Delta v_z}{v_z}\right) \tag{4.45}$$

The absorbed photon must form a spherical bound state in the moving reference frame of the free electron to result in an inelastic event. Time reversal symmetry resulting in ionization favors the photon kinetic energy contribution to add positively to the initial velocity of the free electron. Additionally, conservation of energy for a single absorption event favors the absorbed photon contributing the positive addition to the initial velocity. Consider the magnitude of the increase in electron linear momentum due to photon absorption compared to the linear momentum of the absorbed photon of angular frequency $\omega$ given by

$$p = \frac{\hbar\omega}{c} \tag{4.46}$$

The relativistic three vector momentum for rectilinear motion along the z-axis (Eq. (34.12)) is

$$p = \frac{m_{e0}}{\sqrt{1 - \left(\frac{v}{c}\right)^2}}v \tag{4.47}$$

wherein $v$ is the three velocities. Considering that ½ of the energy of an absorbed photon is converted to electron linear kinetic energy, the increase in electron linear kinetic energy $T$ corresponding to an increase in linear velocity $v$ from rest in the electron's absolute frame given by Eqs. (1.291) and (3.52) is

$$T = \frac{\hbar\omega}{2} = m_{e0}c^2\left(\frac{1}{\sqrt{1-\left(\frac{v}{c}\right)^2}} - 1\right) \tag{4.48}$$

Using Eq. (4.48), the increase in linear velocity is given by

$$v = c\sqrt{1-\left(\frac{m_{e0}}{\left(\frac{\hbar\omega}{2c^2} + m_{e0}\right)}\right)^2} \tag{4.49}$$

Using Eq. (4.47), the relativistic three vector momentum for rectilinear motion along the z-axis is

$$p = \left(\frac{\hbar\omega}{2c^2} + m_{e0}\right)c\sqrt{1-\left(\frac{m_{e0}}{\left(\frac{\hbar\omega}{2c^2} + m_{e0}\right)}\right)^2} \tag{4.50}$$

Consider the case of a microwave photon of frequency $f$ of 5 GHz ($3.3\,X\,10^{-24}J$). The corresponding photon linear momentum (Eq. (4.50)) is $1.1\,X\,10^{-32}kgms^{-1}$ and the corresponding increase in electron linear momentum is $1.73\,X\,10^{-27}kgms^{-1}$ which is five orders of magnitude greater.

A free space photon having $\hbar$ in its electric and magnetic fields is not divisible, and the electric field of a photon cannot be translated by an external action due to the properties of spacetime. Photon propagation in free space at an exact velocity of $c = \frac{1}{\sqrt{\mu_0\varepsilon_0}}$ is based on the permittivity $\varepsilon_0$ and permeability $\mu_0$ of free space. The relationship between the energies of a photon as it converts to mass due to angular frequency, electric field, magnetic field, gravitational energy, and space time contraction are given by Eqs. (32.48a-32.48b) wherein the relationship between spacetime contraction and expansion due to energy to matter conversion and vice versa is given by Eqs. (32.140a-32.140b). Kinetic energy contributes to the inertial mass of an electron according to Eq. (1.291). Photons and free electrons each have zero gravitational mass; consequently, there is no violation of particle production laws by the absorption of a photon by an electron to increase its kinetic mass/energy.

In effect spacetime of the photon field-free electron interaction serves as the body that conserves momentum from the free-electron photon absorption event wherein the photon angular momentum is partially converted to linear momentum. This phenomenon is enabling of a novel propulsion device that drives against spacetime called space drive [27-31].

The mechanisms of technologies almost without exception are also observed in Nature. This is also the case with space-drive phenomenon as the mechanism of the formation of ***sprites*** formed during lightning storms. Specifically, electrons are accelerated to relativistic energies in the direction away from the Earth during atmospheric discharges called red sprites and blue jets (Figure 4.14). These comprise large-scale vertically ascending pillars of emission from electrons accelerated from the tops of thunderclouds out into space that are associated with gamma ray bursts during lightning events. The Italian Space Agency's AGILE observatory found that the energy spectrum of terrestrial gamma-ray flashes extends up to 100 MeV. These otherwise inexplicable observations can be resolved as being due to the space drive mechanism. The high voltage within clouds or between clouds and Earth directionally accelerates electrons during a lightening discharge. The high current of lightning causes a strong vector magnetic field. The directional relativistic electron flow directly and the flow in the presence of the directional magnetic field results in the emission of microwaves that are absorbed by an upward (downward) flow of plasma causing the electrons to accelerate selectively in the upward (downward) direction by the space-drive effect. Ions such as $H_3^+$ are dragged by the directionally accelerated electrons. Predominantly collisional air molecular excitation as well as recombination of upward ion and electron flow in the high-altitude atmosphere emit the high-altitude light emission of a sprite. In addition to the traditional colliding counter flowing ice particles mechanism, the upward space drive current may serve to further positively charge clouds to achieve run-away relativistic electron energies of greater than 100 MeV to give rise to the extraordinarily 100 MeV gamma ray flashes.

**Figure 4.14.** Upward jet of electrons accelerated away from the Earth at near light speed associated with gamma ray bursts during lightning events.




The same mechanism may be the source of the gamma rays of extraordinary energies of over 1 TeV emitted by the Sun [32], beyond those anticipated from magnetic field acceleration of electrons [33].

## REFERENCES


1. J. D. Jackson, *Classical Electrodynamics*, Second Edition, John Wiley & Sons, New York, (1975), pp. 739-779.
2. E. Purcell, *Electricity and Magnetism*, McGraw-Hill, New York, (1965), pp. 156-167.
3. L. C. Shi, J. A. Kong, *Applied Electromagnetism*, Brooks/Cole Engineering Division, Monterey, CA, (1983), pp. 210-215.
4. Mathematica modeling of R. Mills' theory by B. Holverstott in "Analytical-Equation Derivation of the Photon Electric and Magnetic Fields," posted at http://www.blacklightpower.com.
5. R. A. Bonham, M. Fink, *High Energy Electron Scattering*, ACS Monograph, Van Nostrand Reinhold Company, New York, (1974), pp. 1-3.
6. K. Dholakia, N. B. Simpson, M. J. Padgett, L. Allen, Physical Review A, Volume 54, Number 5, (1996), pp. R3742-R3745.
7. R. W. Ziolkowski, K. D. Lewis, Phys. Rev. Letts., Vol. 62, No. 2, (1989), pp. 147-150.
8. J. B. Brittingham, J. Appl. Phys., Vol. 54, (1983), p. 1179.
9. R. W. Ziolkowski, J. Math. Phys., Vol. 26, (1985), p. 861.
10. R. W. Ziolkowski, *Microwave and Particle Beam Sources and Propagation*, edited by N. Rostoker, SPIE Conference Proceedings, No. 873, (SPIE, Bellingham, WA, 1988).
11. P. Hillion, J. Appl. Phys., Vol. 60, (1986), p. 2981; P. Hillion, J. Math. Phys., Vol. 28, (1987), p. 1743.
12. E. Heyman, L. B. Felsen, IEEE Trans. Antennas Propag., Vol. 34, (1986), p. 1062; E. Heyman, B. Z. Steinberg, J. Opt. Soc. Am. A, Vol. 4, (1987), p. 473; E. Heyman, B. Z. Steinberg, L. P. Felsen, J. Opt. Soc. Am. A, Vol. 4, (1987), p. 2081.
13. J. Durnin, Opt. Soc. Am. A, Vol. 4, (1987), p. 651; J. Durnin, J. Miceli, J. H. Eberly, Phys. Rev. Lett., Vol. 58, (1987), p. 1499.
14. T. T. Wu, J. Appl. Phys., Vol. 57, (1985), p. 2370; T. T. Wu, R. W. P. King, H. Shen, J. Appl. Phys., Vol. 62, (1987), p. 4036; H. Shen, *Microwave and Particle Beam Sources and Propagation*, edited by N. Rostoker, SPIE Conference Proceedings, No. 873, (SPIE, Bellingham, WA, 1988).
15. H. E. Moses, J. Math. Phys., Vol. 25, (1984), p. 1905; H. E. Moses, R. T. Prosser, IEEE Trans. Antennas Propag., Vol. 34, (1986), p. 188.
16. A. N. Norris, B. White, S. Schrieffer, Proc. Roy. Soc. London A, Vol. 412, (1987), p. 93.
17. M. Mizushima, *Quantum Mechanics of Atomic Spectra and Atomic Structure*, W.A. Benjamin, Inc., New York, (1970), p.17.
18. W. G. Cross, N. F. Ramsey, Phys. Rev., Vol. 80, (1950), p. 929.
19. J. D. Jackson, *Classical Electrodynamics*, Second Edition, John Wiley & Sons, New York, (1975), Chp. 15.
20. H. A. Haus, "On the radiation from point charges," Am. J. Phys., 54, (1986), pp. 1126-1129.
21. A. Einstein, Phys. Z, Vol. 18, (1917), 121.
22. "The Interview Carver Meade," The American Spectator, September/October, (2001).
23. W. E. Lamb, "Theory of an optical maser," Phys. Rev., Vol. 134, No. 6A, (1964), pp. A1429-1450.
24. A. L. Schawlow, C. H. Townes, "Infrared and optical masers," Phys. Rev., Vol. 112, (1958), pp. 1940-1949.
25. H. J. Carmichael, "Quantum theory of the laser," Proc. of the International School on Lasers and Quantum Optics, Laser and Quantum Optics, L. M. Narducci, E. J. Quell, J. R. Tredicce, Editors, CIF Series Vol. 13, Mar del Plata, Argentina, 22-31 Aug., (1988), pp. 52-85.
26. "Modeling of the Analytical Equations of the Mechanism of Photon Absorption and Corresponding Emission by Time Reversal" posted at www.brilliantlightpower.com.
27. R. Mills, "System and method for increasing the kinetic energy of a directional plasma flow with reflection arresting," PCT Application No. PCT/US2026/033184, filed 061726.
28. R. Mills, D. Hsieh, K. Sadman, "Reactionless propulsion", (2025), submitted for publication, https://brilliantlightpower.com/pdf/Space-Drive-Paper-wfigures.pdf.
29. R. Mills, "System and method for increasing the kinetic energy of a directional plasma flow with magnetohydrodynamic reflection arresting", PCT Application No. PCT/US2023/084769, December 19, 2023; https://tinyurl.com/7hmsyrh.
30. R. Mills, "System and method for increasing the kinetic energy of a directional plasma flow", U.S. App. No. No. 63/512304, filed December 22, 2022; https://tinyurl.com/mpv4buwd.
31. R. Mills, "Free electron absorption mechanism", https://brilliantlightpower.com/free-electron-photon-absorption-mechanism/.
32. Ravisetti, "Sun blasts out highest-energy radiation ever recorded, raising questions for solar physics"SPACE.com, August 6, 2023, https://www.space.com/sun-blasts-highest-energy-radiation-ever-recorded-raising-questions-solar-physics.
33. J. A. Miller, R. Reuven, "Relativistic Electron Transport and Bremsstrahlung Production in Solar Flares", Astrophysical Journal, Vol. 344, (1989), p. 973.

# Chapter 5

# HYDRINO THEORY – BLACKLIGHT PROCESS

## BLACKLIGHT PROCESS

Classical physics (CP) gives closed-form solutions of the hydrogen atom, the hydride ion, the hydrogen molecular ion, and the hydrogen molecule and predicts corresponding species having fractional principal quantum numbers. The nonradiative state of atomic hydrogen, which is historically called the "ground state" forms the basis of the boundary condition of CP to solve the bound electron. CP predicts a reaction involving a resonant, nonradiative energy transfer from otherwise stable atomic hydrogen to a catalyst capable of accepting the energy to form hydrogen in lower-energy states than previously thought possible called a ***hydrino atom*** designated as $H\left[\frac{a_H}{p}\right]$ where $a_H$ is the radius of the hydrogen atom. Specifically, CP predicts that atomic hydrogen may undergo a catalytic reaction with certain atoms, excimers, ions, and diatomic hydrides which provide a reaction with a net enthalpy of an integer multiple of the potential energy of atomic hydrogen, $E_h = 27.2\ eV$ where $E_h$ is one Hartree. Specific species (e.g. $He^+$, $Ar^+$, $Sr^+$, $K$, $Li$, $HCl$, $NaH$, and $H_2O$) identifiable on the basis of their known electron energy levels are required to be present with atomic hydrogen to catalyze the process. The reaction involves a nonradiative energy transfer of an integer multiple of $27.2\ eV$ from atomic hydrogen to the catalyst followed by $q \cdot 13.6\ eV$ continuum emission or $q \cdot 13.6\ eV$ transfer to another $H$ to form extraordinarily hot, excited-state $H$ and a hydrogen atom that is lower in energy than unreacted atomic hydrogen that corresponds to a fractional principal quantum number. That is, in the formula for the principal energy levels of the hydrogen atom:

$$E_n = -\frac{e^2}{n^2 8\pi\varepsilon_o a_H} = -\frac{13.598\ eV}{n^2} \tag{5.1}$$

$$n = 1, 2, 3, ... \tag{5.2}$$

where $a_H$ is the Bohr radius for the hydrogen atom (52.947 pm), $e$ is the magnitude of the charge of the electron, and $\varepsilon_o$ is the vacuum permittivity, fractional quantum numbers:

$$n = 1, \frac{1}{2}, \frac{1}{3}, \frac{1}{4}, ..., \frac{1}{p};\quad p \le 137 \text{ is an integer} \tag{5.3}$$

replace the well known parameter $n = \text{integer}$ in the Rydberg equation for hydrogen excited states. Then, similar to an excited state having the analytical solution of Maxwell's equations given by Eq. (2.15), a hydrino atom also comprises an electron, a proton, and a photon as given by Eq. (5.27). However, the electric field of the latter increases the binding corresponding to desorption of energy rather than decreasing the central field with the absorption of energy as in an excited state, and the resultant photon-electron interaction of the hydrino is stable rather than radiative.

The $n = 1$ state of hydrogen and the $n = \frac{1}{\text{integer}}$ states of hydrogen are nonradiative, but a transition between two nonradiative states, say $n = 1$ to $n = 1/2$, is possible via a nonradiative energy transfer. Hydrogen is a special case of the stable states given by Eqs. (5.1) and (5.3) wherein the corresponding radius of the hydrogen or hydrino atom is given by:

$$r = \frac{a_H}{p}, \tag{5.4}$$

where $p = 1, 2, 3, \ldots$. In order to conserve energy, energy must be transferred from the hydrogen atom to the catalyst in units of

$$m \cdot 27.2\ eV,\ m = 1, 2, 3, 4, \ldots. \tag{5.5}$$

and the radius transitions to $\frac{a_H}{m+p}$. The catalyst reactions involve two steps of energy release: a nonradiative energy transfer to the catalyst followed by additional energy release as the radius decreases to the corresponding stable final state. Thus, the general reaction is given by:

$$m \cdot 27.2\ eV + Cat^{q+} + H\left[\frac{a_H}{p}\right] \rightarrow Cat_{fast}^{(q+r)+} + re^- + H^*\left[\frac{a_H}{(m+p)}\right] + m \cdot 27.2\ eV \tag{5.6}$$

$$H^*\left[\frac{a_H}{(m+p)}\right] \rightarrow H\left[\frac{a_H}{(m+p)}\right] + [(p+m)^2 - p^2] \cdot 13.6\ eV - m \cdot 27.2\ eV \tag{5.7}$$

$$Cat_{fast}^{(q+r)+} + re^- \rightarrow Cat^{q+} + m \cdot 27.2\ eV \tag{5.8}$$

And, the overall reaction is:

$$H\left[\frac{a_H}{p}\right] \rightarrow H\left[\frac{a_H}{(m+p)}\right] + [(p+m)^2 - p^2] \cdot 13.6\ eV \tag{5.9}$$

$q$, $r$, $m$, and $p$ are integers. $H^*\left[\frac{a_H}{(m+p)}\right]$ has the radius of the hydrogen atom (corresponding to $p = 1$) and a central field equivalent to $(m+p)$ times that of a proton, and $H\left[\frac{a_H}{(m+p)}\right]$ is the corresponding stable state with the radius of $\frac{1}{(m+p)}$ that of $H$. As the electron undergoes radial acceleration from the radius of the hydrogen atom to a radius of $\frac{1}{(m+p)}$ this distance, energy is released as characteristic light emission or as third-body kinetic energy. The emission may be in the form of an extreme-ultraviolet continuum radiation having an edge at $[(p+m)^2 - p^2 - 2m] \cdot 13.6\ eV$ or $\frac{91.2}{[(p+m)^2 - p^2 - 2m]}\ nm$ and extending to longer wavelengths. In addition to radiation, a resonant kinetic energy transfer to form fast $H$ may occur. Subsequent excitation of these fast $H(n=1)$ atoms by collisions with the background $H_2$ followed by emission of the corresponding $H(n=3)$ fast atoms gives rise to broadened Balmer $\alpha$ emission.

As given in Disproportionation of Energy States section, hydrogen atoms $H(1/p)$ $p = 1, 2, 3, \ldots 137$ can undergo further transitions to lower-energy states given by Eqs. (5.1) and (5.3) wherein the transition of one atom is catalyzed by a second that resonantly and nonradiatively accepts $m \cdot 27.2\ eV$ with a concomitant opposite change in its potential energy. The overall general equation for the transition of $H(1/p)$ to $H(1/(p+m))$ induced by a resonance transfer of $m \cdot 27.2\ eV$ to $H(1/p')$ given by Eq. (5.75) is represented by:

$$H(1/p') + H(1/p) \rightarrow H + H(1/(p+m)) + \left[2pm + m^2 - p'^2 + 1\right] \cdot 13.6\ eV \tag{5.10}$$

Hydrogen atoms may serve as a catalyst wherein $m = 1$, $m = 2$, and $m = 3$ for one, two, and three atoms, respectively, acting as a catalyst for another. The rate for the two-atom-catalyst, $2H$, may be high when extraordinarily fast H as reported previously [1-7] collides with a molecule to form the $2H$ wherein two atoms resonantly and nonradiatively accept $54.4\ eV$ from a third hydrogen atom of the collision partners. By the same mechanism, the collision of two hot $H_2$ provide $3\,H$ to serve as a catalyst of $3 \cdot 27.2\ eV$ for the fourth. The EUV continua at 22.8 nm and 10.1 nm and extraordinary (>100 eV) Balmer $\alpha$ line broadening are observed consistent with predictions [1-9].

The catalyst product, $H(1/p)$, may also react with an electron to form a hydrino hydride ion $H^-(1/p)$, or two $H(1/p)$ may react to form the corresponding molecular hydrino $H_2(1/p)$. Specifically, the catalyst product, $H(1/p)$, may also react with an electron to form a novel hydride ion $H^-(1/p)$ with a binding energy $E_B$ (Eq. (7.74)) derived in the Hydrino Hydride Ion section:

$$E_B = \frac{\hbar^2\sqrt{s(s+1)}}{8\mu_e a_0^2\left[\frac{1+\sqrt{s(s+1)}}{p}\right]^2} - \frac{\pi\mu_0 e^2\hbar^2}{m_e^2}\left(\frac{1}{a_H^3} + \frac{2^2}{a_0^3\left[\frac{1+\sqrt{s(s+1)}}{p}\right]^3}\right) \tag{5.11}$$

where $p = \text{integer} > 1$, $s = 1/2$, $\hbar$ is Planck's constant bar, $\mu_o$ is the permeability of vacuum, $m_e$ is the mass of the electron, $\mu_e$ is the reduced electron mass given by $\mu_e = \frac{m_e m_p}{\frac{m_e}{\sqrt{\frac{3}{4}}} + m_p}$ where $m_p$ is the mass of the proton, $a_o$ is the Bohr radius, and the ionic radius is $r_1 = \frac{a_0}{p}\left(1+\sqrt{s(s+1)}\right)$ (Eq. (7.73)). From Eq. (5.11), the calculated ionization energy of the hydride ion is $0.75418\ eV$, and the experimental value given by Lykke [10] is $6082.99 \pm 0.15\ cm^{-1}$ (0.75418 eV).

Upfield-shifted NMR peaks are direct evidence of the existence of lower-energy state hydrogen with a reduced radius relative to ordinary hydride ion and having an increase in diamagnetic shielding of the proton. The shift is given by the sum of the contributions of the diamagnetism of the two electrons and the trapped photon field of magnitude $p$ (Eq. (7.87)):

$$\frac{\Delta B_T}{B} = -\mu_0 \frac{pe^2}{12 m_e a_0\left(1+\sqrt{s(s+1)}\right)}\left(1 + p\alpha^2\right) = -\left(p29.9 + p^2 1.59\ X\ 10^{-3}\right) ppm \tag{5.12}$$

where the first term applies to $H^-$ with $p = 1$ and $p = \text{integer} > 1$ for $H^-(1/p)$ and $\alpha$ is the fine structure constant.

$H(1/p)$ may react with a proton and two $H(1/p)$ may react to form $H_2(1/p)^+$ and $H_2(1/p)$, respectively. The hydrogen molecular ion and molecular charge and current density functions, bond distances, and energies were solved in the Nature of the Chemical Bond of Hydrogen-Type Molecules and Molecular Ions section from the Laplacian in ellipsoidal coordinates with the constraint of nonradiation.

$$(\eta-\zeta)R_\xi \frac{\partial}{\partial\xi}(R_\xi \frac{\partial\phi}{\partial\xi}) + (\zeta-\xi)R_\eta \frac{\partial}{\partial\eta}(R_\eta \frac{\partial\phi}{\partial\eta}) + (\xi-\eta)R_\zeta \frac{\partial}{\partial\zeta}(R_\zeta \frac{\partial\phi}{\partial\zeta}) = 0 \tag{5.13}$$

The total energy $E_T$ of the hydrogen molecular ion having a central field of $+pe$ at each focus of the prolate spheroid molecular orbital is (Eqs. (11.192-11.193))

$$\begin{aligned} E_T &= -p^2\left\{\frac{e^2}{8\pi\varepsilon_o a_H}(4\ln 3 - 1 - 2\ln 3)\left[1+\sqrt{\frac{2\hbar\sqrt{\frac{2e^2}{4\pi\varepsilon_o(2a_H)^3}}}{m_e c^2}}\right]\right. \\ &\left. -\frac{1}{2}\hbar\sqrt{\frac{\frac{pe^2}{4\pi\varepsilon_o\left(\frac{2a_H}{p}\right)^3} - \frac{pe^2}{8\pi\varepsilon_o\left(\frac{3a_H}{p}\right)^3}}{\mu}}\right\} \\ &= -p^2 16.2526\ eV \end{aligned} \tag{5.14}$$

where $p$ is an integer, $c$ is the speed of light in vacuum, and $\mu$ is the reduced nuclear mass. The total energy of the hydrogen molecule having a central field of $+pe$ at each focus of the prolate spheroid molecular orbital is (Eqs. (11.240-11.241))

$$E_T = -p^2\left\{\begin{array}{l}\dfrac{e^2}{8\pi\varepsilon_o a_0}\left[\left(2\sqrt{2}-\sqrt{2}+\dfrac{\sqrt{2}}{2}\right)\ln\dfrac{\sqrt{2}+1}{\sqrt{2}-1}-\sqrt{2}\right]\left[1+\sqrt{\dfrac{2\hbar\sqrt{\dfrac{e^2}{4\pi\varepsilon_o a_0^3}}}{m_e c^2}}\right] \\ -\dfrac{1}{2}\hbar\sqrt{\dfrac{\dfrac{pe^2}{8\pi\varepsilon_o\left(\dfrac{a_0}{p}\right)^3}-\dfrac{pe^2}{8\pi\varepsilon_o\left(\dfrac{\left(1+\frac{1}{\sqrt{2}}\right)a_0}{p}\right)^3}}{\mu}}\end{array}\right\} \tag{5.15}$$

$$= -p^2 31.677\ eV$$

The bond dissociation energy, $E_D$, of the hydrogen molecule $H_2(1/p)$ is the difference between the total energy of the corresponding hydrogen atoms and $E_T$

$$E_D = E(2H(1/p)) - E_T \tag{5.16}$$

where [11]

$$E(2H(1/p)) = -p^2 27.20\ eV \tag{5.17}$$

$E_D$ is given by Eqs. (5.16-5.17) and (5.15):

$$\begin{aligned} E_D &= -p^2 27.20\ eV - E_T \\ &= -p^2 27.20\ eV - \left(-p^2 31.677\ eV\right) \\ &= p^2 4.478\ eV \end{aligned} \tag{5.18}$$

The calculated and experimental parameters of $H_2$, $D_2$, $H_2^+$, and $D_2^+$ are given in Table 11.1.

The NMR of catalysis-product gas provides a definitive test of the theoretically predicted chemical shift of $H_2(1/p)$. In general, the $^1H$ NMR resonance of $H_2(1/p)$ is predicted to be upfield from that of $H_2$ due to the fractional radius in elliptic coordinates wherein the electrons are significantly closer to the nuclei. The predicted shift, $\frac{\Delta B_T}{B}$, for $H_2(1/p)$ is given by the sum of the contributions of the diamagnetism of the two electrons and the trapped photon field of magnitude $p$ (Eqs. (11.415-11.416)):

$$\frac{\Delta B_T}{B} = -\mu_0\left(4-\sqrt{2}\ln\frac{\sqrt{2}+1}{\sqrt{2}-1}\right)\frac{pe^2}{36a_0 m_e}\left(1+p\alpha^2\right) \tag{5.19}$$

$$\frac{\Delta B_T}{B} = -\left(p28.01 + p^2 1.49\ X\ 10^{-3}\right)ppm \tag{5.20}$$

where the first term applies to $H_2$ with $p=1$ and $p=\text{integer}>1$ for $H_2(1/p)$. The experimental absolute $H_2$ gas-phase resonance shift of -28.0 ppm [12-15] is in excellent agreement with the predicted absolute gas-phase shift of -28.01 ppm (Eq. (5.20)).

The vibrational energies, $E_{vib}$, for the $\upsilon=0$ to $\upsilon=1$ transition of hydrogen-type molecules $H_2(1/p)$ are (Eq. (11.223))

$$E_{vib} = p^2 0.515902\ eV \tag{5.21}$$

where $p$ is an integer and the experimental vibrational energy for the $\upsilon=0$ to $\upsilon=1$ transition of $H_2$, $E_{H_2(\upsilon=0\to\upsilon=1)}$, is given by Beutler [16] and Herzberg [17].

The rotational energies, $E_{rot}$, for the $J$ to $J+1$ transition of hydrogen-type molecules $H_2(1/p)$ are (Eq. (12.74))

$$E_{rot} = E_{J+1} - E_J = \frac{\hbar^2}{I}\left[J+1\right] = p^2\left(J+1\right)0.01509\ eV \tag{5.22}$$

where $p$ is an integer, $I$ is the moment of inertia, and the experimental rotational energy for the $J=0$ to $J=1$ transition of $H_2$ is given by Atkins [18].

The $p^2$ dependence of the rotational energies results from an inverse $p$ dependence of the internuclear distance and the corresponding impact on the moment of inertia $I$. The predicted internuclear distance $2c'$ for $H_2(1/p)$ is:

$$2c' = \frac{a_o\sqrt{2}}{p} \tag{5.23}$$

The data from a broad spectrum of investigational techniques strongly and consistently indicates that hydrogen can exist in lower-energy states than previously thought possible and support the existence of these states called hydrino, for "small hydrogen", and the corresponding hydride ions and molecular hydrino. Some of these prior related studies supporting the possibility of a novel reaction of atomic hydrogen, which produces hydrogen in fractional quantum states that are at lower energies than the traditional "ground" ($n=1$) state, include extreme ultraviolet (EUV) spectroscopy, characteristic emission from catalysts and the hydride ion products, lower-energy hydrogen emission, chemically-formed plasmas, Balmer $\alpha$ line broadening, population inversion of $H$ lines, elevated electron temperature, anomalous plasma afterglow duration, power generation, and analysis of novel chemical compounds.

## ENERGY TRANSFER MECHANISM

Consider the excited energy states of ***atomic*** hydrogen given by Eq. (5.1) with $n=2,3,4,...$ (Eq. (5.2)). The $n=1$ state is the "ground" state for "pure" photon transitions (the $n=1$ state can absorb a photon and go to an excited electronic state, but it cannot release a photon and go to a lower-energy electronic state). However, an electron transition from the $n=1$ state to a lower-energy state hydrino state is possible by a nonradiative energy transfer such as multipole coupling or a resonant collision mechanism. Processes that occur without photons and that require collisions are common. For example, the exothermic chemical reaction of $H+H$ to form $H_2$ does not occur with the emission of a photon. Rather, the reaction requires a collision with a third body, $M$, to remove the bond energy: $H+H+M \rightarrow H_2+M^*$ [19]. The third body distributes the energy from the exothermic reaction, and the end result is the $H_2$ molecule and an increase in the temperature of the system. Further exemplary of an inelastic collision with resonant energy transfer is the Franck-Hertz experiment wherein an excited state atom [20] is formed. Additionally, some commercial phosphors are based on nonradiative energy transfer involving multipole coupling. For example, the strong absorption strength of $Sb^{3+}$ ions along with the efficient nonradiative transfer of excitation from $Sb^{3+}$ to $Mn^{2+}$ are responsible for the strong manganese luminescence from phosphors containing these ions [21][1]. Another example of resonant, nonradiative energy transfer involves atomic hydrogen wherein resonant energy transfer from excited $Ne_2^*$ excimer formed in high pressure microhollow cathode discharges to hydrogen atoms in the ground state occurs with high efficiency to give predominantly Lyman $\alpha$ and Lyman $\beta$ emission [22-24] in the absence of excimer emission observed with pure neon plasmas. Thus, the normal emission is consequently quenched as H emits.

Similarly, the $n=1$ state of hydrogen and the $n=\frac{1}{\text{integer}}$ states of hydrogen are nonradiative, but a transition between two nonradiative states is possible via a nonradiative energy transfer, say $n=1$ to $n=1/4$. In these cases, during the transition the H electron couples to another electron transition, electron transfer reaction, or inelastic scattering reaction that can absorb the

---

[1] An example of *nonradiative energy transfer* is the basis of commercial fluorescent lamps. Consider $Mn^{2+}$ which when excited sometimes emits yellow luminescence. The absorption transitions of $Mn^{2+}$ are spin-forbidden. Thus, the absorption bands are weak, and the $Mn^{2+}$ ions cannot be efficiently raised to excited states by direct optical pumping. Nevertheless, $Mn^{2+}$ is one of the most important luminescence centers in commercial phosphors. For example, the double-doped phosphor $Ca_5\left(PO_4\right)_3F:Sb^{3+},Mn^{2+}$ is used in commercial fluorescent lamps where it converts mainly ultraviolet light from a mercury discharge into visible radiation. When 2536 Å mercury radiation falls on this material, the radiation is absorbed by the $Sb^{3+}$ ions rather than the $Mn^{2+}$ ions. Some excited $Sb^{3+}$ ions emit their characteristic blue luminescence, while other excited $Sb^{3+}$ ions transfer their energy to $Mn^{2+}$ ions. These excited $Mn^{2+}$ ions emit their characteristic yellow luminescence. The efficiency of transfer of ultraviolet photons through the $Sb^{3+}$ ions to the $Mn^{2+}$ ions can be as high as 80%. The strong absorption strength of $Sb^{3+}$ ions along with the efficient transfer of excitation from $Sb^{3+}$ to $Mn^{2+}$ are responsible for the strong manganese luminescence from this material.

This type of *nonradiative energy transfer* is common. The ion which emits the light and which is the active element in the material is called the *activator*; and the ion that helps to excite the activator and makes the material more sensitive to pumping light is called the *sensitizer*. Thus, the sensitizer ion absorbs the radiation and becomes excited. Because of a coupling between sensitizer and activator ions, the sensitizer transmits its excitation to the activator, which becomes excited, and the activator may release the energy as its own characteristic radiation. The sensitizer to activator transfer is *not* a radiative emission and absorption process, rather a *nonradiative transfer*. The nonradiative transfer may be by electric or magnetic multipole interactions. In the transfer of energy between dissimilar ions, the levels will, in general, not be in resonance, and some of the energy is released as a phonon or phonons. In the case of similar ions the levels should be in resonance, and phonons are not needed to conserve energy.

Sometimes the host material itself may absorb (usually in the ultraviolet) and the energy can be transferred nonradiatively to dopant ions. For example, in $YVO_4:Eu^{3+}$, the vanadate group of the host material absorbs ultraviolet light, then transfers its energy to the $Eu^{3+}$ ions which emit characteristic $Eu^{3+}$ luminescence.

exact amount of energy that must be removed from the hydrogen atom to initiate the transition. These reactions comprise a resonant energy sink generally referred to as an ***energy hole***. Thus, a ***catalyst*** is a source of an energy hole because it provides a net positive enthalpy of reaction of $m \cdot 27.2\ eV$ (i.e. it absorbs or provides an energy sink of $m \cdot 27.2\ eV$). The reaction of hydrogen-type atoms to lower-energy states may also be referred to as a ***transition reaction***. The certain atoms or ions that serve as transition reaction catalysts resonantly accept energy from hydrogen atoms and release the energy to the surroundings to effect electronic transitions to hydrino states comprising energy levels corresponding to fractional quantum numbers in the Rydberg formula. The catalysis of hydrogen involves the nonradiative transfer of energy from atomic hydrogen to a catalyst to form an intermediate (Eq. (5.7)) that may then release the additional energy by radiative and nonradiative mechanisms. Thus, as a consequence of the nonradiative energy transfer, the hydrogen atom becomes unstable and emits further energy until it achieves a lower-energy nonradiative state having a principal energy level given by Eqs. (5.1) and (5.3). Characteristic continuum radiation and extraordinary (>100 eV) Balmer $\alpha$ line broadening corresponding to fast H observed from mixed hydrogen plasmas containing a hydrino catalyst [1-9] are signatures of the reaction to form hydrinos. The latter release may occur via a collisional or nonradiative energy transfer from the corresponding formed metastable intermediate to yield the fast $H\left(n=1\right)$. The mechanism of energy release may be akin to a quenching reaction [25-26] that is selection rule dependent.

## ENERGY HOLE CONCEPT

For a spherical resonator cavity, the nonradiative boundary condition and the relationship between the electron and the photon give the "allowed" hydrogen energy states that are quantized as a function of the parameter $n$. That is, the nonradiative boundary condition and the relationship between an allowed radius and the photon standing wave wavelength (Eq. (2.1)) give rise to Eq. (2.2), the boundary condition for allowed radii and allowed electron wavelengths as a function of the parameter $n$. Each value of $n$ corresponds to an allowed transition caused by a resonant photon, which excites the transition in the atomic orbital resonator cavity from the initial to the final state. In addition to the traditional integer values (1, 2, 3,...) of $n$, fractional values are allowed by Eq. (2.2) which correspond to transitions between energy states with an increase in the central field (effective charge) and decrease in the radius of the atomic orbital. This occurs, for example, when the atomic orbital couples to another resonator cavity, which can absorb energy. This is the ***absorption of an energy hole by the hydrogen-type atom***. The absorption of an energy hole destroys the balance between the centrifugal force and the increased central electric force. Consequently, the electron undergoes a transition to a stable lower energy state. Thus, the corresponding reaction from an initial energy state to a lower energy state requiring an energy hole is called a ***transition reaction*** and the resonant energy acceptor including a catalyst that is unchanged in the over all reaction to form hydrinos can generally be considered a ***source of energy holes***.

From energy conservation, the energy hole of a hydrogen atom, which excites resonator modes of radial dimensions $\frac{a_H}{m+1}$ is:

$$m \cdot 27.2\ eV, \quad \text{where } m = 1, 2, 3, 4, .... \tag{5.24}$$

After resonant absorption of the energy hole, the radius of the atomic orbital, $a_H$, shrinks to $\frac{a_H}{m+1}$ and after $t$ cycles of transition, the radius is $\frac{a_H}{mt+1}$. In other words, the radial ground state field can be considered as the superposition of Fourier components. The removal of negative Fourier components of energy $m \cdot 27.2\ eV$, where $m$ is an integer, increases the positive electric field inside the spherical shell by $m$ times that of a proton charge. The resultant electric field is a time harmonic solution of Laplace's Equations in spherical coordinates. In this case, the radius at which force balance and nonradiation are achieved is $\frac{a_H}{m+1}$ where $m$ is an integer. In decaying to this radius from the "ground" state, a total energy of $[(m+1)^2 - 1^2] \cdot 13.6\ eV$ is released. The process is called the **Atomic BlackLight Process.**

For the hydrogen atom, the radius of the ground state atomic orbital is $a_H$. This atomic orbital contains no photonic waves and the centrifugal force and the electric force balance including the electrodynamic force, which is included by using the reduced electron mass as given by Eqs. (1.254), (1.259), and (1.260) is:

$$\frac{m_e v_1^2}{a_H} = \frac{e^2}{4\pi\varepsilon_0 a_H^2} \tag{5.25}$$

where $v_1$ is the velocity in the "ground" state. It was shown in the Excited States of the One-Electron Atom (Quantization) section that the electron atomic orbital is a resonator cavity, which can trap electromagnetic radiation of discrete frequencies. The photon electric field functions are solutions of Laplace's equation. The "trapped photons" decrease the effective nuclear charge or nuclear charge factor $Z_{eff}$ to $1/n$ and increase the radius of the atomic orbital to $na_H$. The new configuration is also in force balance.

$$\frac{\hbar^2}{m_e r_n^3} = \frac{Z_{eff} e^2}{4\pi\varepsilon_0 r_n^2} \tag{5.26}$$

Similarly a transition to a hydrino state occurs because the effective nuclear charge increases by an integer, $m$, when Eqs. (5.26-5.28) are satisfied by the introduction of an energy hole. The source of energy holes may not be consumed in the transition reaction; therefore it serves as a catalyst. The catalyst provides energy holes and causes the transition from the initial radius $\frac{a_H}{p}$ and an effective nuclear charge of $p$ to the second radius $\frac{a_H}{p+m}$ and an effective nuclear charge of $p+m$. Energy conservation and the boundary condition that "trapped photons" must be a solution to Laplace's equation determine that the energy hole to cause a transition is given by Eq. (5.24). As a result of coupling, the hydrogen atom nonradiatively transfers $m \cdot 27.2\ eV$ to the catalyst.

Stated another way, the hydrogen atom absorbs an energy hole of $m \cdot 27.2\ eV$. The energy hole absorption causes a standing electromagnetic wave ("photon") to be trapped in the hydrogen atom electron atomic orbital having the same form of Maxwellian solution of electromagnetic radiation of discrete energy trapped in a resonator cavity as for excited states given in the Excited States of the One-Electron Atom (Quantization) section. As shown previously, the photonic equation must be a solution of Laplace's equation in spherical coordinates. The "trapped photon" field comprises an electric field, which provides force balance and a nonradiative electron current. Following that given for excited states (Eq. (2.15)), the solution to this boundary value problem of the radial photon electric field is given by:

$$\mathbf{E}_{r\,photon\,n,l,m} = \frac{e(na_H)^{\ell}}{4\pi\varepsilon_0} \frac{1}{r^{(\ell+2)}} \left[ -Y_0^0(\theta,\phi) + \frac{1}{n}\left[ Y_0^0(\theta,\phi) + \mathrm{Re}\left\{ Y_\ell^m(\theta,\phi) e^{im\omega_n t} \right\} \right] \right] \delta(r - r_n) \tag{5.27}$$

$$n = \frac{1}{p}$$

$$2 \le p \le 137$$

$$\ell = 0, 1, 2, ..., p-1$$

$$m_\ell = -\ell, -\ell + 1, ..., 0, ..., +\ell$$

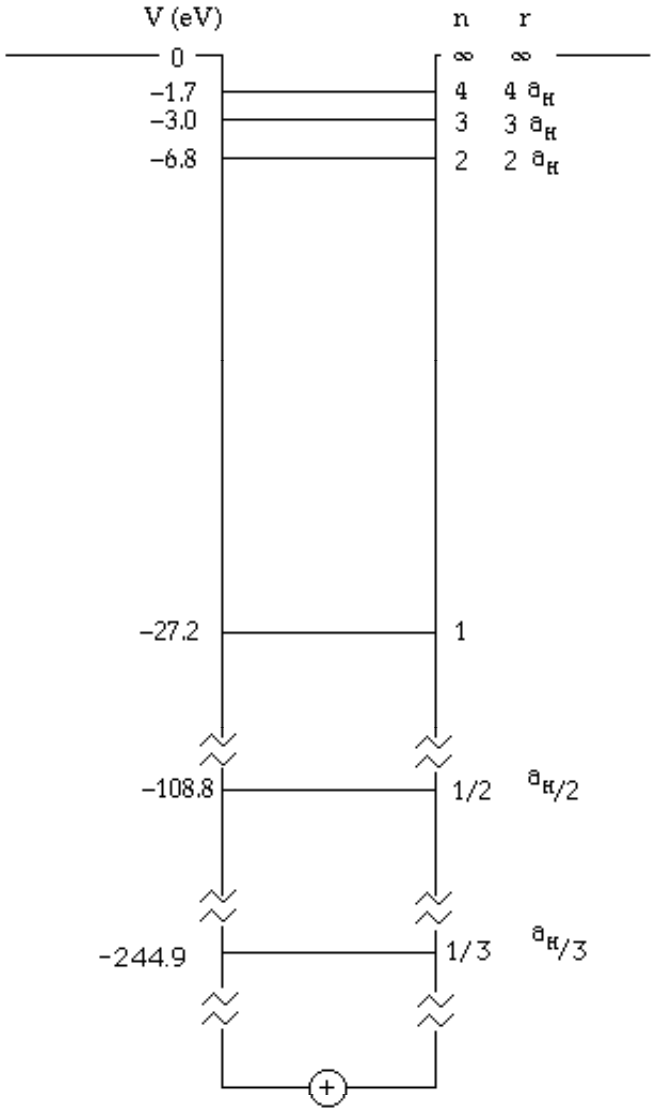
$$m_s = \pm\frac{1}{2}$$

The quantum numbers of the electron are $p$, $\ell$, $m_\ell$, and $m_s$ as described in the Excited States of the One-Electron Atom (Quantization) section wherein the principal quantum number of excited states is replaced by $n = \frac{1}{p}$. It is apparent from this equation that given an initial radius of $\frac{a_H}{p}$ and a final radius of $\frac{a_H}{p+m}$, the central field is increased by $m$ with the absorption of an energy hole of $m \cdot 27.2\ eV$. The potential energy decreases by this energy; thus, energy is conserved. However, the force balance equation is not initially satisfied as the effective nuclear charge increases by $m$. Further energy is emitted as force balance is achieved at the final radius. By replacing the initial radius with the final radius, and by increasing the charge by $m$ in Eq. (5.26).

$$[p+m]^3 \frac{\hbar^2}{m_e a_H^3} = [p+m]^2 \frac{((p+m)e)e}{4\pi\varepsilon_0 a_H^2} \tag{5.28}$$

Force balance is achieved and the electron is non-radiative. The energy balance for $m = 1$ is as follows. An initial energy of $27.2\ eV$ is transferred as the energy hole absorption event. This increases the nuclear charge (effective nuclear charge factor) by one elementary charge unit and decreases the potential by $27.2\ eV$. More energy is emitted until the total energy released is $[(p+1)^2 - p^2] \cdot 13.6\ eV$. The potential energy diagram of the electron is given in Figure 5.1.

**Figure 5.1.** Potential Energy well of a Hydrogen Atom.



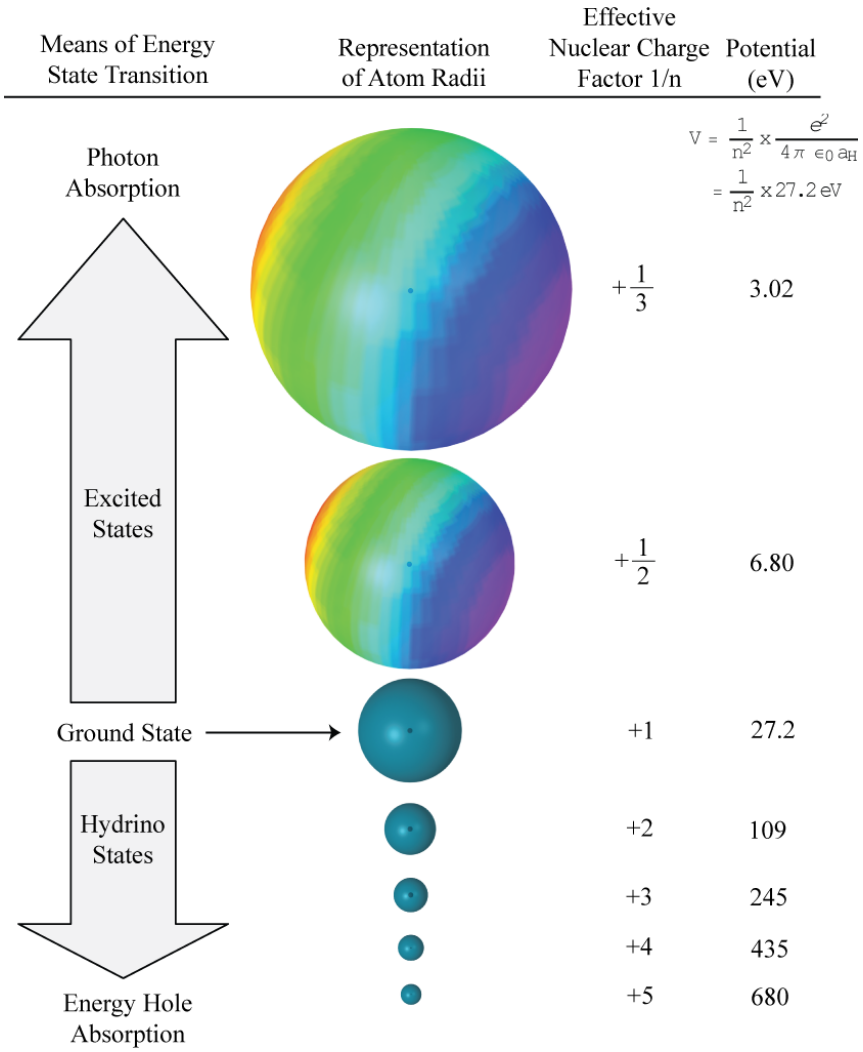

The energy hole ( $m \cdot 27.2\ eV$ ) required to cause a hydrogen atom to undergo a transition reaction to form a given hydrino atom ( $H\left(\frac{a_H}{m+1}\right)$ ) as well as the corresponding radius ( $\frac{a_H}{(m+1)}$ ), effective nuclear charge factor ( $Z_{eff} = m+1$ ) and energy parameters of several states of atomic hydrogen are given in Table 5.1.

**Table 5.1.** Principal quantum number, radius, potential energy, kinetic energy, effective nuclear charge factor, energy hole required to form the hydrino from atomic hydrogen (n=1), and hydrino binding energy, respectively, for several states of hydrogen.

| $H(n)$ | $R$ | $V$ (eV) | $T$ (eV) | $Z_{eff}$ | Energy Hole (eV) | Binding Energy (eV) |
|---|---|---|---|---|---|---|
| 1 | $a_H$ | -27.2 | 13.6 | 1 | 0 | 13.6 |
| $\frac{1}{2}$ | $\frac{a_H}{2}$ | -108.8 | 54.4 | 2 | 27.2 | 54.4 |
| $\frac{1}{3}$ | $\frac{a_H}{3}$ | -244.9 | 122.4 | 3 | 54.4 | 122.4 |
| $\frac{1}{4}$ | $\frac{a_H}{4}$ | -435.4 | 217.7 | 4 | 81.6 | 217.7 |
| $\frac{1}{5}$ | $\frac{a_H}{5}$ | -680.2 | 340.1 | 5 | 108.8 | 340.1 |
| $\frac{1}{6}$ | $\frac{a_H}{6}$ | -979.6 | 489.6 | 6 | 136.1 | 489.6 |
| $\frac{1}{7}$ | $\frac{a_H}{7}$ | -1333.3 | 666.4 | 7 | 163.3 | 666.4 |
| $\frac{1}{8}$ | $\frac{a_H}{8}$ | -1741.4 | 870.4 | 8 | 190.5 | 870.4 |
| $\frac{1}{9}$ | $\frac{a_H}{9}$ | -2204.0 | 1101.6 | 9 | 217.7 | 1101.6 |
| $\frac{1}{10}$ | $\frac{a_H}{10}$ | -2721.0 | 1360.5 | 10 | 244.9 | 1360.5 |

The size of the electron atomic orbital as a function of potential energy is given in Figure 5.2.

**Figure 5.2.** Quantized sizes of hydrogen atoms where $n$ is an integer for excited states and $n = 1/p$. for hydrino states where $p$ is an integer.



## CATALYSTS

A source of energy holes that is not consumed in the reaction serves as a catalyst that provides a net positive enthalpy of reaction of $m \cdot 27.2\ eV$ (i.e. it resonantly accepts the nonradiative energy transfer from hydrogen atoms and releases the energy to the surroundings to affect electronic transitions to fractional quantum energy levels). $K$, $He^+$, $Ar^+$, $Sr^+$, $Li$, $K$, $NaH$, and $H_2O$, for example, are predicted to serve as catalysts since they meet the catalyst criterion—a chemical or physical process with an enthalpy change equal to an integer multiple of the potential energy of atomic hydrogen, $27.2\ eV$, or have a potential energy of $m \cdot 27.2\ eV$. Specifically, an exemplary catalytic system is provided by the ionization of $t$ electrons from an atom each to a continuum energy level such that the sum of the ionization energies of the $t$ electrons is approximately $m \cdot 27.2\ eV$ where $m$ is an integer. One such catalytic system involves potassium atoms. $K$ can serve as a catalyst since the ionization of $K$ to $K^{3+}$ is about $81.6\ eV$ ($3 \cdot 27.2\ eV$). As a consequence of the nonradiative energy transfer, the hydrogen atom becomes unstable and emits further energy until it achieves a lower-energy nonradiative state having a principal energy level given by Eqs. (5.1) and (5.3). Thus, the catalysis releases energy from the hydrogen atom with a commensurate decrease in size of the hydrogen atom, $r_n = na_H$ where $n$ is given by Eq. (5.3). For example, the catalysis of $H(n=1)$ to $H(n=1/4)$ releases $204\ eV$, and the hydrogen radius decreases from $a_H$ to $\frac{1}{4}a_H$. Specifically, the first, second, and third ionization energies of potassium are $4.34066\ eV$, $31.63\ eV$, $45.806\ eV$, respectively [11]. The triple ionization ($t=3$) reaction of $K$ to $K^{3+}$, then, has a net enthalpy of reaction of $81.7767\ eV$, which is equivalent to $m=3$ in Eq. (5.24).

$$81.7767\ eV + K(m) + H\left[\frac{a_H}{p}\right] \rightarrow K^{3+} + 3e^- + H\left[\frac{a_H}{(p+3)}\right] + [(p+3)^2 - p^2] \cdot 13.6\ eV \tag{5.29}$$

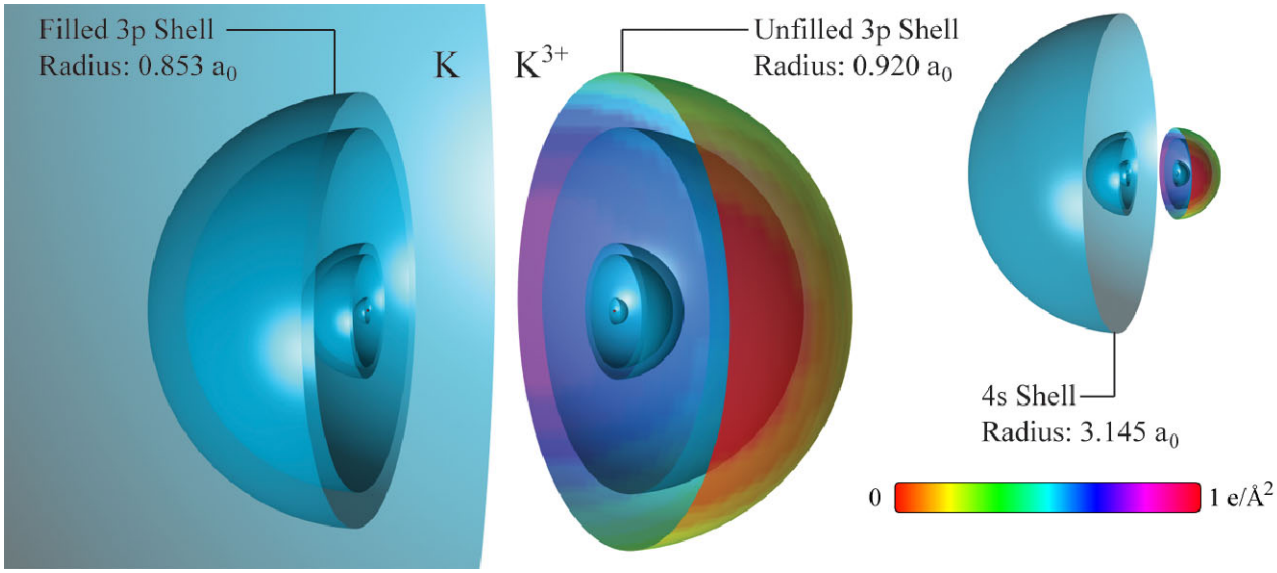
$$K^{3+} + 3e^- \rightarrow K(m) + 81.7767\ eV \tag{5.30}$$

And, the overall reaction is

$$H\left[\frac{a_H}{p}\right] \rightarrow H\left[\frac{a_H}{(p+3)}\right] + [(p+3)^2 - p^2] \cdot 13.6\ eV \tag{5.31}$$

The potassium-atom catalyst ($K$) and the $3+$ ion ($K^{3+}$) that arises from the resonant energy transfer are solved in the Three-Through Twenty-Electron Atoms section and are shown in Figure 5.3.

**Figure 5.3.** Cross Section of Charge-Density Functions of $K$ and $K^{3+}$ Shown in Color Scale. The electrons of multielectron atoms exist as concentric atomic orbitals ("bubble-like" charge-density functions) of discrete radii, which are given by $r_n$ of the radial Dirac delta function, $\delta(r-r_n)$ and serve as resonator cavities during the resonant nonradiative energy transfer that gives rise to ionization. Each s orbital is a constant current-density function which gives rise to spin, and the charge-density of each p orbital is a superposition of a constant and a spherical and time harmonic function. The corresponding charge-density wave on the surface gives rise to electron orbital angular momentum that superimposes the spin angular momentum. The insert on the right shows the atom and ions at a lower magnification to view the outer 4s electron of $K$.




The energy given off during catalysis is much greater than the energy lost to the catalyst. The energy released is large as compared to conventional chemical reactions. For example, when hydrogen and oxygen gases undergo combustion to form water $\left(H_2\,(g)+\frac{1}{2}O_2\,(g)\rightarrow H_2O\,(l)\right)$ the known enthalpy of formation of water is $\Delta H_f=-286\ kJ/mole$ or 1.48 eV per hydrogen atom. By contrast, each $(n=1)$ ordinary hydrogen atom undergoing a catalysis step to $n=\frac{1}{2}$ releases a net of $40.8\ eV$. Moreover, further catalytic transitions may occur: $n=\frac{1}{2}\rightarrow\frac{1}{3}$, $\frac{1}{3}\rightarrow\frac{1}{4}$, $\frac{1}{4}\rightarrow\frac{1}{5}$, and so on. Once catalysis begins, hydrinos autocatalyze further in a process called disproportionation discussed in the Disproportionation of Energy States section.

Helium ions can serve as a catalyst because the second ionization energy of helium is $54.417\ eV$, which is equivalent to $2\cdot 27.2\ eV$. In this case, $54.417\ eV$ is transferred nonradiatively from atomic hydrogen to $He^+$ which is resonantly ionized. The electron decays to the $n=1/3$ state with the further release of $54.417\ eV$ as given in Eq. (5.7). The full catalysis reaction invoving an energetic intermediate formed by the energy transfer to the catalyst is:

$$54.417\ eV+He^++H\left[a_H\right]\rightarrow He^{2+}+e^-+H^*\left[\frac{a_H}{3}\right]+54.4\ eV \tag{5.32}$$

$$H^*\left[\frac{a_H}{3}\right]\rightarrow H\left[\frac{a_H}{3}\right]+54.4\ eV \tag{5.33}$$

$$He^{2+}+e^-\rightarrow He^++54.417\ eV \tag{5.34}$$

And, the overall reaction is:

$$H\left[a_H\right]\rightarrow H\left[\frac{a_H}{3}\right]+54.4\ eV+54.4\ eV \tag{5.35}$$

wherein $H^*\left[\frac{a_H}{3}\right]$ has the radius of the hydrogen atom and a central field equivalent to 3 times that of a proton and $H\left[\frac{a_H}{3}\right]$ is the corresponding stable state with the radius of 1/3 that of H. As the electron undergoes radial acceleration from the radius of the hydrogen atom to a radius of 1/3 this distance, energy is released as characteristic light emission or as third-body kinetic energy.

Hydrogen catalysts capable of providing a net enthalpy of reaction of approximately $m\cdot 27.2\ eV$ where $m$ is an integer to produce a hydrino (whereby $t$ electrons are ionized from an atom or ion) are given in Table 5.2. The atoms or ions given in

the first column are ionized to provide the net enthalpy of reaction of $m \cdot 27.2\ eV$ given in the tenth column where $m$ is given in the eleventh column. The electrons that participate in ionization are given with the ionization potential (also called ionization energy or binding energy). The ionization potential of the $n$ th electron of the atom or ion is designated by $IP_n$ and is given by the CRC [11]. That is for example, $Li + 5.39172\ eV \rightarrow Li^+ + e^-$ and $Li^+ + 75.6402\ eV \rightarrow Li^{2+} + e^-$. The first ionization potential, $IP_1 = 5.39172\ eV$, and the second ionization potential, $IP_2 = 75.6402\ eV$, are given in the second and third columns, respectively. The net enthalpy of reaction for the double ionization of $Li$ is $81.0319\ eV$ as given in the tenth column, and $m = 3$ in Eq. (5.24) as given in the eleventh column.

**Table 5.2.** Hydrogen Catalysts.

| Catalyst | IP1 | IP2 | IP3 | IP4 | IP5 | IP6 | IP7 | IP8 | Enthalpy | m |
|---|---|---|---|---|---|---|---|---|---|---|
| Li | 5.39172 | 75.6402 | | | | | | | 81.032 | 3 |
| Be | 9.32263 | 18.2112 | | | | | | | 27.534 | 1 |
| K | 4.34066 | 31.63 | 45.806 | | | | | | 81.777 | 3 |
| Ca | 6.11316 | 11.8717 | 50.9131 | 67.27 | | | | | 136.17 | 5 |
| Ti | 6.8282 | 13.5755 | 27.4917 | 43.267 | 99.3 | | | | 190.46 | 7 |
| V | 6.7463 | 14.66 | 29.311 | 46.709 | 65.2817 | | | | 162.71 | 6 |
| Cr | 6.76664 | 16.4857 | 30.96 | | | | | | 54.212 | 2 |
| Mn | 7.43402 | 15.64 | 33.668 | 51.2 | | | | | 107.94 | 4 |
| Fe | 7.9024 | 16.1878 | 30.652 | | | | | | 54.742 | 2 |
| Fe | 7.9024 | 16.1878 | 30.652 | 54.8 | | | | | 109.54 | 4 |
| Co | 7.881 | 17.083 | 33.5 | 51.3 | | | | | 109.76 | 4 |
| Co | 7.881 | 17.083 | 33.5 | 51.3 | 79.5 | | | | 189.26 | 7 |
| Ni | 7.6398 | 18.1688 | 35.19 | 54.9 | 76.06 | | | | 191.96 | 7 |
| Ni | 7.6398 | 18.1688 | 35.19 | 54.9 | 76.06 | 108 | | | 299.96 | 11 |
| Cu | 7.72638 | 20.2924 | | | | | | | 28.019 | 1 |
| Zn | 9.39405 | 17.9644 | | | | | | | 27.358 | 1 |
| Zn | 9.39405 | 17.9644 | 39.723 | 59.4 | 82.6 | 108 | 134 | 174 | 625.08 | 23 |
| As | 9.8152 | 18.633 | 28.351 | 50.13 | 62.63 | 127.6 | | | 297.16 | 11 |
| Se | 9.75238 | 21.19 | 30.8204 | 42.945 | 68.3 | 81.7 | 155.4 | | 410.11 | 15 |
| Kr | 13.9996 | 24.3599 | 36.95 | 52.5 | 64.7 | 78.5 | | | 271.01 | 10 |
| Kr | 13.9996 | 24.3599 | 36.95 | 52.5 | 64.7 | 78.5 | 111 | | 382.01 | 14 |
| Rb | 4.17713 | 27.285 | 40 | 52.6 | 71 | 84.4 | 99.2 | | 378.66 | 14 |
| Rb | 4.17713 | 27.285 | 40 | 52.6 | 71 | 84.4 | 99.2 | 136 | 514.66 | 19 |
| Sr | 5.69484 | 11.0301 | 42.89 | 57 | 71.6 | | | | 188.21 | 7 |
| Nb | 6.75885 | 14.32 | 25.04 | 38.3 | 50.55 | | | | 134.97 | 5 |
| Mo | 7.09243 | 16.16 | 27.13 | 46.4 | 54.49 | 68.8276 | | | 220.10 | 8 |
| Mo | 7.09243 | 16.16 | 27.13 | 46.4 | 54.49 | 68.8276 | 125.664 | 143.6 | 489.36 | 18 |
| Pd | 8.3369 | 19.43 | | | | | | | 27.767 | 1 |
| Sn | 7.34381 | 14.6323 | 30.5026 | 40.735 | 72.28 | | | | 165.49 | 6 |
| Te | 9.0096 | 18.6 | | | | | | | 27.61 | 1 |
| Te | 9.0096 | 18.6 | 27.96 | | | | | | 55.57 | 2 |
| Cs | 3.8939 | 23.1575 | | | | | | | 27.051 | 1 |
| Ce | 5.5387 | 10.85 | 20.198 | 36.758 | 65.55 | | | | 138.89 | 5 |
| Ce | 5.5387 | 10.85 | 20.198 | 36.758 | 65.55 | 77.6 | | | 216.49 | 8 |
| Pr | 5.464 | 10.55 | 21.624 | 38.98 | 57.53 | | | | 134.15 | 5 |
| Sm | 5.6437 | 11.07 | 23.4 | 41.4 | | | | | 81.514 | 3 |
| Gd | 6.15 | 12.09 | 20.63 | 44 | | | | | 82.87 | 3 |
| Dy | 5.9389 | 11.67 | 22.8 | 41.47 | | | | | 81.879 | 3 |
| Pb | 7.41666 | 15.0322 | 31.9373 | | | | | | 54.386 | 2 |
| Pt | 8.9587 | 18.563 | | | | | | | 27.522 | 1 |
| $He^+$ | | 54.4178 | | | | | | | 54.418 | 2 |
| $Na^+$ | | 47.2864 | 71.6200 | 98.91 | | | | | 217.816 | 8 |
| $Rb^+$ | | 27.285 | | | | | | | 27.285 | 1 |
| $Fe^{3+}$ | | | | 54.8 | | | | | 54.8 | 2 |
| $Mo^{2+}$ | | | 27.13 | | | | | | 27.13 | 1 |
| $Mo^{4+}$ | | | | | 54.49 | | | | 54.49 | 2 |
| $In^{3+}$ | | | | 54 | | | | | 54 | 2 |
| $Ar^+$ | | 27.62 | | | | | | | 27.62 | 1 |
| $Sr^+$ | | 11.03 | 42.89 | | | | | | 53.92 | 2 |
| $2K^+$ to K and $K^{2+}$ | 4.34 | 31.63 | | | | | | | 27.28 | 1 |
| $2Ba^{2+}$ to $Ba^+$ and $Ba^{3+}$ | 5.21 | 10 | 37.3 | | | | | | 27.3 | 1 |

Certain molecules may also serve to affect transitions of H to form hydrinos. In general, a compound comprising hydrogen such as $MH$, where M is an element other than hydrogen, serves as a source of hydrogen and a source of catalyst. A catalytic reaction is provided by the breakage of the $M-H$ bond plus the ionization of $t$ electrons from the atom $M$ each to a continuum energy level such that the sum of the bond energy and ionization energies of the $t$ electrons is approximately

$m \cdot 27.2\ eV$, where $m$ is an integer. One such catalytic system involves sodium hydride. The bond energy of $NaH$ is $1.9245\ eV$ [27], and the first and second ionization energies of $Na$ are $5.13908\ eV$ and $47.2864\ eV$, respectively [11]. Based on these energies $NaH$ molecule can serve as a catalyst and $H$ source, since the bond energy of $NaH$ plus the double ionization ($t = 2$) of $Na$ to $Na^{2+}$ is $54.35\ eV$ ($2 \cdot 27.2\ eV$). The concerted catalyst reactions are given by:

$$54.35\ eV + NaH \rightarrow Na^{2+} + 2e^- + H\left[\frac{a_H}{3}\right] + [3^2 - 1^2] \cdot 13.6\ eV \tag{5.36}$$

$$Na^{2+} + 2e^- + H \rightarrow NaH + 54.35\ eV \tag{5.37}$$

And, the overall reaction is:

$$H \rightarrow H\left[\frac{a_H}{3}\right] + [3^2 - 1^2] \cdot 13.6\ eV \tag{5.38}$$

A molecule that accepts $m \cdot 27.2\ eV$ from atomic H with a decrease in the magnitude of the potential energy of the molecule by the same energy may serve as a catalyst. For example, the potential energy of $H_2O$ given by Eq. (13.201) is:

$$V_e = \left(\frac{3}{2}\right)\frac{-2e^2}{8\pi\varepsilon_0\sqrt{a^2 - b^2}} \ln\frac{a + \sqrt{a^2 - b^2}}{a - \sqrt{a^2 - b^2}} = -81.8715\ eV \tag{5.39}$$

The full catalysis reaction $(m = 3)$ is:

$$81.6\ eV + H_2O + H[a_H] \rightarrow 2H^+_{fast} + O^+ + 3e^- + H*\left[\frac{a_H}{4}\right] + 81.6\ eV \tag{5.40}$$

$$H*\left[\frac{a_H}{4}\right] \rightarrow H\left[\frac{a_H}{4}\right] + 122.4\ eV \tag{5.41}$$

$$2H^+_{fast} + O^+ + 3e^- \rightarrow H_2O + 81.6\ eV \tag{5.42}$$

And, the overall reaction is:

$$H[a_H] \rightarrow H\left[\frac{a_H}{4}\right] + 81.6\ eV + 122.4\ eV \tag{5.43}$$

wherein $H*\left[\frac{a_H}{4}\right]$ has the radius of the hydrogen atom and a central field equivalent to 4 times that of a proton and $H\left[\frac{a_H}{4}\right]$ is the corresponding stable state with the radius of 1/4 that of H.

## ENERGY HOLE AS A MULTIPOLE EXPANSION

The potential energy (Eq. (1.261)) of the hydrino states of radius $\frac{a_H}{p}$ having a central field of magnitude $p$ is:

$$-p^2 \cdot 27.2\ eV \tag{5.44}$$

where $p$ is an integer. The potential energy is given as the superposition of $\ell$ energy-degenerate quantum states corresponding to a multipole expansion of the central electromagnetic field. Based on the selection rules given in the Excited States of the One-Electron Atom (Quantization) section that are enabled by multipole coupling, one multipole moment of all those possible, need be excited to stimulate the below "ground" state transition. The total number, $N$, of multipole moments where each corresponds to an $\ell$ and $m_\ell$ quantum number of an energy level corresponding to a principal quantum number of $p$ is:

$$N = \sum_{\ell=0}^{p-1} \sum_{m_\ell=-\ell}^{+\ell} 1 = \sum_{\ell=0}^{n-1} 2\ell + 1 = p^2 \tag{5.45}$$

Thus, the energy hole to stimulate a transition of a hydrogen atom from radius $\frac{a_H}{p}$ to radius $\frac{a_H}{p+1}$ with an increase in the central field from $p$ to $p+1$ where $p$ is an integer is:

$$(p+1)^2 \cdot 27.2 \cdot \frac{1}{(p+1)^2} = 27.2\ eV \tag{5.46}$$

Eq. (5.46) obeys superposition such that the energy hole for the excitation of $m$ multipoles is $m \cdot 27.2\ eV$. Energy conservation occurs during the absorption of an energy hole. For a hydrogen atom with a principal quantum number of $p$ having a radius of $\frac{a_H}{p}$, the absorption of an energy hole of $m \cdot 27.2\ eV$ instantaneously decreases the potential energy by $m \cdot 27.2\ eV$. The calculation of the instantaneous electric field of the photon standing wave corresponding to the absorbed energy hole is determined by the conservation of the potential energy change due to the absorption of the energy hole of equal but opposite

energy. It is given by the summation over all possible multipoles of the integral of the product of the electric field of the photon standing wave and the multipoles of the electron charge-density function. The multipole of the photon standing wave and each multipole of the electron charge-density function correspond to an $\ell$ and $m_\ell$ quantum number.

## DISPROPORTIONATION OF ENERGY STATES

Hydrogen and hydrinos may serves as catalysts. As given *infra* hydrogen atoms $H\left(1/p\right)$ $p=1,2,3,...137$ can undergo transitions to lower-energy states given by Eqs. (5.1) and (5.3) wherein the transition of one atom is catalyzed by a second that resonantly and nonradiatively accepts $m\cdot 27.2\ eV$ with a concomitant opposite change in its potential energy. The overall general equation for the transition of $H\left(1/p\right)$ to $H\left(1/\left(m+p\right)\right)$ induced by a resonance transfer of $m\cdot 27.2\ eV$ to $H\left(1/p'\right)$ is represented by (Eq. (5.75))

$$H\left(1/p'\right)+H\left(1/p\right)\rightarrow H+H\left(1/(m+p)\right)+\left[2pm+m^2-p'^2+1\right]\cdot 13.6\ eV \tag{5.47}$$

Thus, hydrogen atoms may serve as a catalyst wherein $m=1$, $m=2$, and $m=3$ for one, two, and three atoms, respectively, acting as a catalyst for another. The rate for the two- or three-atom-catalyst case would be appreciable only when the $H$ density is high. But, high H densities are not uncommon. A high hydrogen atom concentration permissive of 2H or 3H serving as the energy acceptor for a third may be achieved under several circumstances such as on the surface of the Sun and stars due to the temperature and gravity driven density, on metal surfaces that support multiple monolayers, and in highly dissociated plasmas, especially pinched hydrogen plasmas. Additionally, a three-body H interaction is easily achieved when two $H$ atoms arise with the collision of a hot $H$ with $H_2$. This event can commonly occur in plasmas having a large population of extraordinarily fast H as reported previously [1-7]. This is evidenced by the unusual intensity of atomic H emission. In such cases, energy transfer can occur from a hydrogen atom to two others within sufficient proximity, being typically a few angstroms as given in the Dipole-Dipole Coupling section. Then, the reaction between three hydrogen atoms whereby two atoms resonantly and nonradiatively accept $54.4\ eV$ from the third hydrogen atom such that $2H$ serves as the catalyst is given by:

$$54.4\ eV+2H+H\rightarrow 2H^+_{fast}+2e^-+H*\left[\frac{a_H}{3}\right]+54.4\ eV \tag{5.48}$$

$$H*\left[\frac{a_H}{3}\right]\rightarrow H\left[\frac{a_H}{3}\right]+54.4\ eV \tag{5.49}$$

$$2H^+_{fast}+2e^-\rightarrow 2H+54.4\ eV \tag{5.50}$$

And, the overall reaction is:

$$H\rightarrow H\left[\frac{a_H}{3}\right]+[3^2-1^2]\cdot 13.6\ eV \tag{5.51}$$

$H*\left[\frac{a_H}{2+1}\right]$ has the radius of the hydrogen atom (corresponding to the 1 in the denominator) and a central field equivalent to 3 times that of a proton, and $H\left[\frac{a_H}{3}\right]$ is the corresponding stable state with the radius of 1/3 that of H. As the electron undergoes radial acceleration from the radius of the hydrogen atom to a radius of 1/3 this distance, energy is released as characteristic light emission or as third-body kinetic energy. The emission may be in the form of an extreme-ultraviolet continuum radiation having an edge at $54.4\ eV$ (22.8 nm) and extending to longer wavelengths. Alternatively, H is the lightest atom; thus, it is the most probable fast species in collisional energy exchange from the H intermediate (e.g. $H*\left[\frac{a_H}{2+1}\right]$). Additionally, H is unique with regard to the energetic transition state intermediate (generally represented by $H*\left[\frac{a_H}{m+p}\right]$) in that all these species are energy states of hydrogen with corresponding harmonic frequencies. Thus, the cross section for H excitation by a nonradiative energy transfer to form fast H is predicted to be large since it is a resonant process. Efficient energy transfer can occur by common through-space mechanisms such as dipole-dipole interactions as described by Förster's theory *infra*. Consequently, in addition to radiation, a resonant kinetic energy transfer to form fast H may occur. Alternatively, fast H is a direct product of H or hydrino serving as the catalyst or source of energy holes as given by Eqs. (5.48), (5.53), (5.58), and (5.71) wherein the acceptance of the resonant energy transfer regards the potential energy rather than the ionization energy. Conservation of energy gives a proton of

the kinetic energy corresponding to one half the potential energy in the former case and a catalyst ion at essentially rest in the latter case. The H recombination radiation of the fast protons gives rise to broadened Balmer $\alpha$ emission that is disproportionate to the inventory of hot hydrogen consistent with the excess power balance. Conservation of momentum in the formation of fast protons also gives rise to hot hydrinos that heat H. Subsequent excitation of these fast $H(n=1)$ atoms by collisions with the background $H_2$ followed by emission of the corresponding $H(n=3)$ fast atoms gives rise to broadened Balmer $\alpha$ emission but of less intensity than directly formed hot protons that emit by recombination. With increasingly lower-energy states formed over time as the reaction progresses, very large kinetic energies are predicted throughout the cell. Only isotropic non-directional broadening of hydrogen atomic lines is predicted with an increase in fast H with time. These features have been confirmed experimentally [1-7], especially regarding closed hydrogen plasmas or water vapor plasmas that become predominantly H plasmas in time [1-3]. Overall, the EUV continuum radiation and fast H were observed with hydrogen plasmas wherein 2H served as the catalyst [8-9]. Astrophysical soft X-ray continuum radiation bands are observed at 10.1 nm, 22.8 nm, and 91.2 nm as predicted for $mH$ catalyst, $m=1$, $m=2$, and $m=3$, respectively [8]. Soft X-ray continuum radiation having a 10.1 nm cutoff was also observed in the laboratory as predicted for $H_2O$ catalyst [8]. Thus, the predictions corresponding to transitions of atomic hydrogen to form hydrinos were experimentally confirmed.

The predicted product of 2H (Eqs. (5.48-5.51)) catalyst reaction is $H(1/3)$. In the case of a high hydrogen atom concentration, the further transition given by Eq. (5.47) of $H(1/3)$ ($p=3$) to $H(1/4)$ ($m+p=4$) with $H$ as the catalyst ($p'=1$; $m=1$) can be fast:

$$H(1/3) \xrightarrow{H} H(1/4) + 95.2\ eV \tag{5.52}$$

In another $H$-atom catalyst reaction involving a direct transition to $\left[\frac{a_H}{4}\right]$ state, two hot $H_2$ molecules collide and dissociate such that three $H$ atoms serve as a catalyst of $3 \cdot 27.2\ eV$ for the fourth. Then, the reaction between four hydrogen atoms whereby three atoms resonantly and nonradiatively accept $81.6\ eV$ from the fourth hydrogen atom such that $3H$ serves as the catalyst is given by:

$$81.6\ eV + 3H + H \rightarrow 3H^+_{fast} + 3e^- + H*\left[\frac{a_H}{4}\right] + 81.6\ eV \tag{5.53}$$

$$H*\left[\frac{a_H}{4}\right] \rightarrow H\left[\frac{a_H}{4}\right] + 122.4\ eV \tag{5.54}$$

$$3H^+_{fast} + 3e^- \rightarrow 3H + 81.6\ eV \tag{5.55}$$

And, the overall reaction is

$$H \rightarrow H\left[\frac{a_H}{4}\right] + [4^2 - 1^2] \cdot 13.6\ eV \tag{5.56}$$

The extreme-ultraviolet continuum radiation band due to the $H*\left[\frac{a_H}{3+1}\right]$ intermediate of Eq. (5.53) is predicted to have short wavelength cutoff at $122.4\ eV$ (10.1 nm) and extend to longer wavelengths. This continuum band also formed by $H_2O$ catalyst was confirmed experimentally [8]. In general, the transition of $H$ to $H\left[\frac{a_H}{p=m+1}\right]$ due by the acceptance of $m \cdot 27.2\ eV$ gives a continuum band with a short wavelength cutoff and energy $E_{\left(H \rightarrow H\left[\frac{a_H}{p=m+1}\right]\right)}$ given by:

$$\begin{aligned} E_{\left(H \rightarrow H\left[\frac{a_H}{p=m+1}\right]\right)} &= m^2 \cdot 13.6\ eV \\ \lambda_{\left(H \rightarrow H\left[\frac{a_H}{p=m+1}\right]\right)} &= \frac{91.2}{m^2}\ nm \end{aligned} \tag{5.57}$$

and extending to longer wavelengths than the corresponding cutoff. The radiation band is in the region from zero to the cutoff wavelength with a Bremsstrahlung profile that is predominantly in the high-energy region.

Consistent with Eq. (5.57) with $m=1$, a 91.2 nm continuum in argon plasma with trace hydrogen was observed where the catalyst reaction $Ar^+$ to $Ar^{2+}$ has a net enthalpy of reaction of $27.63\ eV$ [28]. Two hydrogen atoms may react to give the

same continuum band by a reaction similar to those given by Eqs. (5.48-5.51). The reaction whereby one H resonantly and nonradiatively accepts $27.2\ eV$ from the other hydrogen atom such that it serves as the catalyst is given by:

$$27.2\ eV + H + H \rightarrow H^{+}_{fast} + e^{-} + H*\left[\frac{a_H}{2}\right] + 27.2\ eV \tag{5.58}$$

$$H*\left[\frac{a_H}{2}\right] \rightarrow H\left[\frac{a_H}{2}\right] + 13.6\ eV \tag{5.59}$$

$$H^{+}_{fast} + e^{-} \rightarrow H + 27.2\ eV \tag{5.60}$$

And, the overall reaction is:

$$H \rightarrow H\left[\frac{a_H}{2}\right] + [2^2 - 1^2]\cdot 13.6\ eV \tag{5.61}$$

The emission from Eq. (5.59) may be in the form of an extreme-ultraviolet continuum radiation having an edge at $13.6\ eV$ (91.2 nm) and extending to longer wavelengths. This band was also observed in pulsed pure hydrogen plasmas using the normal incidence spectrometer, but temporal studies are required in order to eliminate the background hydrogen molecular band. These bands were eliminated previously in the argon plasma with trace hydrogen [28] wherein H is highly dissociated. Hydrogen may emit the series of 10.1 nm, 22.8 nm, and 91.2 nm continua as shown in Ref. [8].

Since the products of the catalysis reactions (e.g. Eqs. (5.48-5.51)) have binding energies of $m\cdot 27.2\ eV$, they may further serve as catalysts. Thus, further catalytic transitions may occur: $n=\frac{1}{3}\rightarrow\frac{1}{4}$, $\frac{1}{4}\rightarrow\frac{1}{5}$, and so on. Thus, lower-energy hydrogen atoms, *hydrinos*, can act as catalysts by resonantly and nonradiatively accepting energy of $m\cdot 27.2\ eV$ from another H or hydrino atom (Eq. (5.24)). The process can occur by several mechanisms: metastable excitation, resonance excitation, and ionization energy of a hydrino atom is $m\cdot 27.2\ eV$ (Eq. (5.24)). The transition reaction mechanism of a first hydrino atom affected by a second hydrino atom involves the resonant coupling between the atoms of $m$ degenerate multipoles each having $27.2\ eV$ of potential energy. (See the Energy Hole as a Multipole Expansion section).

The energy transfer of $m\cdot 27.2\ eV$ from the first hydrino atom to the second hydrino atom causes the central field of the first to increase by $m$ and the electron of the first to drop $m$ levels lower from a radius of $\frac{a_H}{p}$ to a radius of $\frac{a_H}{p+m}$. The second lower-energy hydrogen is excited to a metastable state, excited to a resonance state, or ionized by the resonant energy transfer. The resonant transfer may occur in multiple stages. For example, a nonradiative transfer by multipole coupling may occur wherein the central field of the first increases by $m$, then the electron of the first drops $m$ levels lower from a radius of $\frac{a_H}{p}$ to a radius of $\frac{a_H}{p+m}$ with further resonant energy transfer. The energy transferred by multipole coupling may occur by a mechanism that is analogous to photon absorption involving an excitation to a virtual level. Or, the energy transferred by multipole coupling during the electron transition of the first hydrino atom may occur by a mechanism that is analogous to two-photon absorption involving a first excitation to a virtual level and a second excitation to a resonant or continuum level [29-31]. Similarly to the case with H as the catalyst, the transition energy greater than the energy transferred to the second hydrino atom may appear as a characteristic light emission in a vacuum medium or extraordinary fast H.

The transition of the hydrino intermediate from its radius to the corresponding hydrino radius gives rise to continuum radiation. By time reversal symmetry, the hydrino can serve as a catalyst to accept the energy difference between its state and a corresponding intermediate state at the radius of the intermediate wherein the decay to the hydrino radius releases the transferred energy. The release may be as continuum radiation or fast H.

For example, $H\left[\frac{a_H}{p'}\right]$ may serve as a source of energy holes for $H\left[\frac{a_H}{p}\right]$. In general, the transition of $H\left[\frac{a_H}{p}\right]$ to $H\left[\frac{a_H}{p+m}\right]$ induced by a resonance transfer of $m\cdot 27.2\ eV$ (Eq. (5.24)) with a metastable state excited in $H\left[\frac{a_H}{p'}\right]$ is represented by:

$$m\cdot 27.2\ eV + H\left[\frac{a_H}{p'}\right] + H\left[\frac{a_H}{p}\right] \rightarrow H*\left[\frac{a_H}{p'}\right] + H*\left[\frac{a_H}{p+m}\right] + m\cdot 27.2\ eV \tag{5.62}$$

$$H*\left[\frac{a_H}{p'}\right] \rightarrow H\left[\frac{a_H}{p'}\right] + m\cdot 27.2\ eV \tag{5.63}$$

$$H*\left[\frac{a_H}{p+m}\right] \rightarrow H\left[\frac{a_H}{p+m}\right] + \left[(p+m)^2 - p^2\right]\cdot 13.6\ eV - m\cdot 27.2\ eV \tag{5.64}$$

where $p$, $p'$, and $m$ are integers and the asterisk represents an excited metastable state. And, the overall reaction is:

$$H\left[\frac{a_H}{p}\right] \rightarrow H\left[\frac{a_H}{p+m}\right] + [(p+m)^2 - p^2] \cdot 13.6\ eV \tag{5.65}$$

The short-wavelength cutoff energy of the continuum radiation given by Eq. (5.57) is the maximum energy release of the hydrino intermediate as it decays. For example, both the reaction of H with $H\left[\frac{a_H}{p'}\right]$ as the source of an energy hole of $3 \cdot 27.2\ eV$ to form $H\left[\frac{a_H}{4}\right]$ and the reaction of $H\left[\frac{a_H}{5}\right]$ with $H\left[\frac{a_H}{p'}\right]$ as the source of an energy hole of $27.2\ eV$ to form $H\left[\frac{a_H}{6}\right]$ gives rise to a cutoff of 10.1 nm (122.4 $eV$) wherein the magnitude of the potential energy of $H\left[\frac{a_H}{p'}\right]$ is greater than $m \cdot 27.2\ eV$ for each case.

In another mechanism, the transition of $H\left[\frac{a_H}{p}\right]$ to $H\left[\frac{a_H}{p+m}\right]$ induced by a multipole resonance transfer of $m \cdot 27.2\ eV$ (Eq. (5.24)) and a transfer of $[(p')^2 - (p'-m')^2] \cdot 13.6\ eV - m \cdot 27.2\ eV$ with a resonance state of $H\left[\frac{a_H}{p'-m'}\right]$ excited in $H\left[\frac{a_H}{p'}\right]$ is represented by:

$$H\left[\frac{a_H}{p'}\right] + H\left[\frac{a_H}{p}\right] \rightarrow H\left[\frac{a_H}{p'-m'}\right] + H\left[\frac{a_H}{p+m}\right] + [\left((p+m)^2 - p^2\right) - \left(p'^2 - (p'-m')^2\right)] \cdot 13.6\ eV \tag{5.66}$$

where $p$, $p'$, $m$, and $m'$ are integers.

In two other mechanisms, the hydrino atom that serves as the source of the energy hole may be ionized by the resonant energy transfer. Consider the transition cascade for the pth cycle of the hydrogen-type atom, $H\left[\frac{a_H}{p}\right]$, with the hydrogen-type atom, $H\left[\frac{a_H}{p'}\right]$, that is ionized as the source of energy holes that causes the transition. The equation for the absorption of an energy hole of $m \cdot 27.2\ eV$ (Eq. (5.24)) equivalent to the binding energy of $H\left[\frac{a_H}{p'}\right]$, is represented by:

$$m \cdot 27.2\ eV + H\left[\frac{a_H}{p'}\right] + H\left[\frac{a_H}{p}\right] \rightarrow H^+ + e^- + H^*\left[\frac{a_H}{p+m}\right] + m \cdot 27.2\ eV \tag{5.67}$$

$$H^*\left[\frac{a_H}{p+m}\right] \rightarrow H\left[\frac{a_H}{p+m}\right] + \left[(p+m)^2 - p^2\right] \cdot 13.6\ eV - m \cdot 27.2\ eV \tag{5.68}$$

$$H^+ + e^- \rightarrow + H\left[\frac{a_H}{1}\right] + 13.6\ eV \tag{5.69}$$

And, the overall reaction is:

$$H\left[\frac{a_H}{p'}\right] + H\left[\frac{a_H}{p}\right] \rightarrow H\left[\frac{a_H}{1}\right] + H\left[\frac{a_H}{(p+m)}\right] + \left[2pm + m^2 - p'^2 + 1\right] \cdot 13.6\ eV \tag{5.70}$$

wherein $m \cdot 27.2\ eV = p'^2 \cdot 13.6\ eV$.

Alternatively, the energy transfer may affect the potential energy of the acceptor rather than the total energy. The energy transfer from a first hydrogen-type atom $H\left[\frac{a_H}{p}\right]$ to a second acceptor hydrogen-type atom $H\left[\frac{a_H}{p'}\right]$ serving as a catalyst causes the electric potential energy of the acceptor hydrogen-type atom to become zero, and the energy conservation gives rise to a hot proton with the ionization of the energy acceptor hydrogen-type atom. The transition reaction equation for the pth cycle transition cascade of the hydrogen-type atom, $H\left[\frac{a_H}{p}\right]$, with the hydrogen-type atom, $H\left[\frac{a_H}{p'}\right]$, that is ionized with the absorption of an energy hole of $m \cdot 27.2\ eV$ (Eq. (5.24)) equivalent to its potential energy, is represented by:

$$m\cdot 27.2\ eV + H\left[\frac{a_H}{p'}\right] + H\left[\frac{a_H}{p}\right] \rightarrow H^+_{fast} + e^- + H^*\left[\frac{a_H}{p+m}\right] + m\cdot 27.2\ eV \tag{5.71}$$

$$H^*\left[\frac{a_H}{p+m}\right] \rightarrow H\left[\frac{a_H}{p+m}\right] + \left[(p+m)^2 - p^2\right]\cdot 13.6\ eV - m\cdot 27.2\ eV \tag{5.72}$$

$$H^+_{fast} + e^- \rightarrow H\left[\frac{a_H}{1}\right] + (m+1)\cdot 13.6\ eV \tag{5.73}$$

And, the overall reaction is:

$$H\left[\frac{a_H}{p'}\right] + H\left[\frac{a_H}{p}\right] \rightarrow H\left[\frac{a_H}{1}\right] + H\left[\frac{a_H}{(p+m)}\right] + \left[2pm + m^2 - m + 1\right]\cdot 13.6\ eV \tag{5.74}$$

wherein $m\cdot 27.2\ eV = p'^2\cdot 27.2\ eV$. Consider all stable states of hydrogen and their ability to serve as a source of energy holes regarding a general reaction involving a transition of hydrogen to a lower-energy state caused by another hydrogen or hydrino. In the case that H is the source of energy hole involving either mechanism (Eq (5.70) or Eq. (5.74)), the reaction is given by

$$H(1/p') + H(1/p) \rightarrow H + H(1/(m+p)) + \left[2pm + m^2 - p'^2 + 1\right]\cdot 13.6\ eV \tag{5.75}$$

where $p$, $p'$, and $m$ are integers with $m = p' = 1$.

The laboratory results of the formation of hydrinos with emission of continuum radiation has celestial implications. Hydrogen self-catalysis and disproportionation may be reactions occurring ubiquitously in celestial objects and interstellar medium comprising atomic hydrogen. Stars are sources of atomic hydrogen and hydrinos as stellar wind for interstellar reactions wherein very dense stellar atomic hydrogen and singly ionized helium, $He^+$, serve as catalysts in stars. $H_2O$ catalyst may also be active in interstellar medium. Hydrogen continua from transitions to form hydrinos matches the emission from white dwarfs, provides a possible mechanism of linking the temperature and density conditions of the different discrete layers of the coronal/chromospheric sources, and provides a source of the diffuse ubiquitous EUV cosmic background with a 10.1 nm continuum matching the observed intense 11.0-16.0 nm band in addition to resolving the identity of the radiation source behind the observation that diffuse $H_\alpha$ emission is ubiquitous throughout the Galaxy and widespread sources of flux shortward of 912Å are required. Moreover, the product hydrinos provides resolution to the identity of dark matter [8-9].

Disproportionation reactions of hydrinos are predicted to given rise to features in the X-ray region. As shown by Eqs. (5.40-5.43) the reaction product of HOH catalyst is $H\left[\frac{a_H}{4}\right]$. Consider a likely transition reaction in hydrogen clouds containing $H_2O$ gas wherein the first hydrogen-type atom $H\left[\frac{a_H}{p}\right]$ is an H atom and the second acceptor hydrogen-type atom $H\left[\frac{a_H}{p'}\right]$ serving as a catalyst is $H\left[\frac{a_H}{4}\right]$. Since the potential energy of $H\left[\frac{a_H}{4}\right]$ is $4^2\cdot 27.2\ eV = 16\cdot 27.2\ eV = 435.2\ eV$, the transition reaction is represented by:

$$16\cdot 27.2\ eV + H\left[\frac{a_H}{4}\right] + H\left[\frac{a_H}{1}\right] \rightarrow H^+_{fast} + e^- + H^*\left[\frac{a_H}{17}\right] + 16\cdot 27.2\ eV \tag{5.76}$$

$$H^*\left[\frac{a_H}{17}\right] \rightarrow H\left[\frac{a_H}{17}\right] + 3481.6\ eV \tag{5.77}$$

$$H^+_{fast} + e^- \rightarrow H\left[\frac{a_H}{1}\right] + 231.2\ eV \tag{5.78}$$

And, the overall reaction is:

$$H\left[\frac{a_H}{4}\right] + H\left[\frac{a_H}{1}\right] \rightarrow H\left[\frac{a_H}{1}\right] + H\left[\frac{a_H}{17}\right] + 3712.8\ eV \tag{5.79}$$

The extreme-ultraviolet continuum radiation band due to the $H^*\left[\frac{a_H}{p+m}\right]$ intermediate (e.g. Eq. (5.72) and Eq. (5.7) is predicted to have a short wavelength cutoff and energy $E_{\left(H\rightarrow H\left[\frac{a_H}{p+m}\right]\right)}$ given by:

$$E_{\left(H\rightarrow H\left[\frac{a_H}{p+m}\right]\right)} = \left[\left(p+m\right)^2 - p^2\right]\cdot 13.6\ eV - m\cdot 27.2\ eV$$
$$\lambda_{\left(H\rightarrow H\left[\frac{a_H}{p+m}\right]\right)} = \frac{91.2}{\left[\left(p+m\right)^2 - p^2\right] - 2m}\ nm \tag{5.80}$$

and extending to longer wavelengths than the corresponding cutoff. Here the extreme-ultraviolet continuum radiation band due to the decay of the $H*\left[\frac{a_H}{17}\right]$ intermediate is predicted to have a short wavelength cutoff at $E = 3481.6\ eV$; $0.35625\ nm$ and extending to longer wavelengths. A broad X-ray peak with a 3.48 keV cutoff was recently observed in the Perseus Cluster by NASA's Chandra X-ray Observatory and by the XMM-Newton [32-34] that has no match to any known atomic transition. The 3.48 keV feature assigned to dark matter of unknown identity by BulBul et al. [32, 34] matches the $H\left[\frac{a_H}{4}\right] + H\left[\frac{a_H}{1}\right] \rightarrow H\left[\frac{a_H}{17}\right]$ transition and further confirms hydrinos as the identity of dark matter.

## DIPOLE-DIPOLE COUPLING

The process referred to as the Atomic BlackLight Process described in the Hydrino Theory—BlackLight Process section comprises the transition of ordinarily stable hydrogen atoms with $n = 1$ in Eq. (5.1) to lower-energy stable states via an initial resonant nonradiative energy transfer to an acceptor comprising a source of an energy hole. Comparing the implications of the source-current-to-stability relationship (Eqs. (2.23-2.25) and (6.7-6.9)) of Rydberg transitions to excited $n = 1, 2, 3, ...$ states as opposed to the transitions to hydrino states having $n = 1, \frac{1}{2}, \frac{1}{3}, \frac{1}{4}, ..., \frac{1}{p}$, it can be appreciated that the former transitions directly involve photons; whereas, the latter do not. Transitions are symmetric with respect to time. Current-density functions, which give rise to photons are created by photons by the reverse process. Excited energy states correspond to this case. And, current-density functions, which do not directly give rise to photons are not created by photons by the reverse process. Hydrino energy states correspond to this case. But, radiationless processes generally classified as atomic collisions involving an energy hole can cause a stable H state to undergo a transition to a lower-energy stable state. Examples of radiationless energy transfer mechanisms are given in the Energy Transfer Mechanism section.

Since the initial state in each case is not a radiative multipole as described in the Excited States of the One-Electron Atom (Quantization) section, the transitions to lower energy states of hydrogen are forbidden. However, forbidden transitions can become allowed by coupling. For example, forbidden electronic transitions in transition metal complexes couple to vibrational transitions with a dramatic increase in the absorption cross section that results in absorption. This is well known as vibronic coupling [35]. In addition to direct physical collision, several interactions can be generally classified as "collisions" that perturb the current density function of a hydrogen atom. Catalyst ions can electrostatically polarize the current density of the hydrogen atom. Similarly induced polarization may occur by the same mechanism that gives rise to van der Waals forces. In addition, all hydrogen atoms and hydrinos have a single unpaired electron that can interact through a magnetic dipole interaction. Once the current density function is altered energy transfer may occur between the hydrogen atom or hydrino and the catalyst.

In an otherwise radiative system containing two fluorescent species such that the emission spectrum of one (the "donor") overlaps the absorption spectrum of the other (the "acceptor"), the excitation energy of the donor atoms may be transferred by a resonance Coulombic electromagnetic interaction mechanism over relatively large distances to the acceptor species (energy hole) rather than the donors radiating into free space. The total Coulombic interaction may be taken as the sum of terms including dipole-dipole, dipole-quadrupole, and terms involving higher order multipoles. Multipole-multipole resonance such as dipole-dipole resonance initially occurs in the electro and magnetostatic limit rather than involving transverse fields as in the case of pure radiation coupling. The Förster theory [36-40] is general to dipole-dipole energy transfer, which is often predominant. A modification of Förster theory applies to the case of transitions to or between hydrino states. The mechanism for the coupling between the $n = 1/p$ ($p = 1, 2, 3, ...$)-state electron of the hydrogen atom and the catalyst may involve direct coupling between existing multipoles, or the catalyst may induce a multipole in the reactant H or hydrino atom. Mechanisms for the catalyst to induce a multipole in the electron current include collisional perturbations and polarizations by electric or magnetic field interactions.

The hydrogen-type electron atomic orbital is a spherical shell of negative charge (total charge = $-e$) of zero thickness at a distance $r_n$ from the nucleus (charge = $+Ze$). It is well known that the field of a spherical shell of charge is zero inside the shell and that of a point charge at the origin outside the shell [41]. The electric field of the proton is that of a point charge at the origin. And, the superposition, $\mathbf{E}$, of the electric fields of the electron and the proton is that of a point charge inside the shell and zero outside.

$$\mathbf{E} = \frac{e}{4\pi\varepsilon_0 r^2} \qquad \text{for } r < r_n \tag{5.81}$$

$$\mathbf{E} = 0 \qquad \text{for } r > r_n \tag{5.82}$$

The magnetic field of the electron, $\mathbf{H}$, is derived in the Derivation of the Magnetic Field section:

$$\mathbf{H} = \frac{e\hbar}{m_e r_n^3}(\mathbf{i}_r \cos\theta - \mathbf{i}_\theta \sin\theta) \qquad \text{for } r < r_n \tag{5.83}$$

$$\mathbf{H} = \frac{e\hbar}{2m_e r^3}(\mathbf{i}_r 2\cos\theta - \mathbf{i}_\theta \sin\theta) \qquad \text{for } r > r_n \tag{5.84}$$

Power flow is governed by the Poynting power theorem,

$$\nabla \bullet (\mathbf{E} \times \mathbf{H}) = -\frac{\partial}{\partial t}\left[\frac{1}{2}\mu_0 \mathbf{H} \bullet \mathbf{H}\right] - \frac{\partial}{\partial t}\left[\frac{1}{2}\varepsilon_0 \mathbf{E} \bullet \mathbf{E}\right] - \mathbf{J} \bullet \mathbf{E} \tag{5.85}$$

It follows from Eqs. (5.81-5.85) that $\nabla \bullet (\mathbf{E} \times \mathbf{H})$ is zero until an interaction occurs between a hydrogen-type atom and a catalyst. Here, a nonradiative transition can couple to one that is radiative. As given in Jackson [42], each current distribution can be written as a multipole expansion. A catalytic interaction or collision gives rise to radiative terms including a dipole term. (There is at least current in the radial direction until force balance is achieved again at the next nonradiative level). Förster's theory [36] gives the following equation for $n(R)$, the nonradiative transfer rate constant:

$$n(R) = \frac{9000(\ln 10)\kappa^2 \Phi_D}{128\pi^5 n^4 N_A \tau_D R^6} \int_0^\infty f_D(\bar{\nu}) \varepsilon_A(\bar{\nu}) \frac{d\bar{\nu}}{\bar{\nu}^4} \tag{5.86}$$

where $\varepsilon_A(\bar{\nu})$ is the molar decadic extinction coefficient of the acceptor (at wave-number $\bar{\nu}$), $f_D(\bar{\nu})$ is the spectral distribution of the fluorescence of the donor (measured in quanta and normalized to unity on a wave-number scale), $N_A$ is Avogadro's number, $\tau_D$ is the mean lifetime of the excited state, $\Phi_D$ is the quantum yield of the fluorescence of the donor, $n$ is the refractive index , $R$ is the distance between the donor and acceptor, and $\kappa$ is an orientation factor which for a random distribution equals $\left(\frac{2}{3}\right)^{\frac{1}{2}}$.

Adaptation of Förster's theory gives the transfer rate constant. In this case, the form of the equation is the same except that $\varepsilon_A(\bar{\nu})$ is the molar decadic energy acceptor cross section (at wave-number $\bar{\nu}$), $f_D(\bar{\nu})$ is the spectral distribution of the transferred energy of the donor (measured in quanta and normalized to unity on a wave-number scale), $\tau_D$ is the mean lifetime of the transition, and $\kappa$ is a factor dependent on the mutual orientation of the donor and acceptor transition moments which for a random distribution equals $\left(\frac{2}{3}\right)^{\frac{1}{2}}$. $\Phi_D$ is the transition probability of the donor that is dependent on establishing a radiative state in both the acceptor and donor via the nonradiative resonant energy transfer. $\Phi_D$ is analogous to the excitation probability to a doubly excited state.

The collision of two hydrino atoms will result in an elastic collision, an inelastic collision with a hydrogen-type molecular reaction, or an inelastic collision with a disproportionation reaction as described in the Disproportionation of Energy States section**.** An estimate of the transition probability for electric multipoles is given by Eq. (16.104) of Jackson [43]. For an electric dipole $\ell = 1$, and Eq. (16.104) of Jackson is:

$$\frac{1}{\tau_E} \cong \left(\frac{e^2}{\hbar c}\right)\frac{\pi}{16}(ka)^2 \omega \tag{5.87}$$

where $a$ is the radius of the hydrogen-type atom, and $k$ is the wave-number of the transition. Substitution of:

$$k = \frac{\omega}{c} \tag{5.88}$$

into Eq. (5.87) gives:

$$\frac{1}{\tau_E} \cong \left(\frac{e^2}{\hbar c}\right)\frac{\pi}{16}\left(\frac{a}{c}\right)^2 \omega^3 \tag{5.89}$$

From Eq. (5.89), the transition probability is proportional to the frequency cubed. Thus, the disproportionation reaction of hydrinos is favored over molecular bond formation because it is the most energetic transition for the donor hydrino atom, and bond formation further requires a third body to remove the bond energy.

In one example wherein nonradiative energy transfer occurs between two hydrino atoms, the mean lifetime of the transition of Eq. (5.86), $\tau_D$, is taken as the vibrational period of the corresponding dihydrino molecule that serves as a model of the transition state. The lifetime follows from Eq. (11.223) and Planck's Equation (Eq. (2.148)). The distance between the donor and acceptor, $R$, is given by the internuclear distance which is twice $c'$ of Eq. (11.203), and the orientation factor, $\kappa$,

equals one because of the spherical symmetry of the hydrino atoms. Electronic transitions of hydrino atoms occur only by an initial nonradiative energy transfer, and the transition probability based on a physical collision approaches one in the limit. Thus, $\Phi_D$, is set equal to one. Ideally, in free space, the overlap integral between the frequency-dependent energy acceptor cross-section and the transferred energy of the donor (energy of $m \cdot 27.2\ eV$ given by Eq. (5.24)) is also one.

Consider the following disproportionate reaction where the additional energy release for the transition given by $m=1$, $m'=2$ and $p=2$ in Eqs. (5.67-5.70) involving the absorption of an energy hole of $27.21\ eV$, $m=1$ in Eq. (5.24), is $13.6\ eV$.

$$H\left[\frac{a_H}{2}\right] \xrightarrow{H\left[\frac{a_H}{2}\right]} H\left[\frac{a_H}{3}\right] \tag{5.90}$$

The transfer rate constant, $n(R)$, for Eq. (5.90) using Eq. (5.86) is:

$$n(R)=\frac{9000(\ln 10)(1)^2 1}{128\pi^5(1)^4\left(6.02\ X\ 10^{23}\right)\left(1.77\ X\ 10^{-15}\right)\left(3.73\ X\ 10^{-11}\right)^6\left(6.91\ X\ 10^{7}\right)^4}=8\ X\ 10^{21}\ \text{sec}^{-1} \tag{5.91}$$

According to the adaptation of Förster's theory [40], the efficiency $E$ of such nonradiative energy transfer given by the product of the transfer rate constant and the mean lifetime of the transition may be expressed by:

$$E=\frac{1}{1+\left[\frac{r}{R_0}\right]^6} \tag{5.92}$$

$$R_0^6=\left(8.8\ X\ 10^{-25}\right)J\eta^{-4}\phi_D\kappa^2$$

where $r$ is the distance between the donor and the acceptor, $J$ is the overlap integral between the frequency-dependent energy acceptor cross section and the transferred energy of the donor, and $\eta$ is the dielectric constant. In the case that the radius of Eq. (5.91) is a fraction of the Bohr radius, the efficiency of energy transfer may be high and approaches one in the limit.

The reaction rate of oxygen with carbon and hydrocarbons is very low at room temperature; however, once the material is ignited, the oxidation reaction can be very fast. This is due to the formation of free radicals that cause a chain reaction known as pyrolysis, which dominates the reaction rate. The formation of hydrinos by a first catalyst such as $He^+$, $Li$, $K$, $nH$, or $H_2O$ gives rise to subsequent disproportionation reactions to additional lower energy states. Analogously, the latter reactions may dominate the power released if a substantial concentration of hydrinos may be maintained as shown in the Power Density of Gaseous Reactions section.

## INTERSTELLAR DISPROPORTIONATION RATE

Disproportionation may be the predominant mechanism of hydrogen electronic transitions to lower energy levels of interstellar hydrogen and hydrinos. The reaction rate is dependent on the collision rate between the reactants and the coupling factor for resonant energy transfer. The collision rate can be calculated by determining the collision frequency. The collision frequency, $f$, and the mean free path, $\ell$, for a gas containing $n_u$ spherical particles per unit volume, each with radius $r$ and velocity $v$ is given by Bueche [44].

$$f=4\pi\sqrt{2}n_u r^2 v \tag{5.93}$$

$$\ell=\frac{1}{4\pi\sqrt{2}n_u r^2} \tag{5.94}$$

The average velocity, $v_{avg}$, can be calculated from the temperature, $T$, [44].

$$\frac{1}{2}m_H v_{avg}^2=\frac{3}{2}kT \tag{5.95}$$

where $k$ is Boltzmann's constant. Substitution of Eq. (5.95) into Eq. (5.93) gives the collision rate, $f_{H\left[\frac{a_H}{p}\right]}$, in terms of the temperature, $T$, the number of hydrogen or hydrino atoms per unit volume, $n_H$, and the radius of each hydrogen atom or hydrino, $\frac{a_H}{p}$.

$$f_{H\left[\frac{a_H}{p}\right]}=4\pi\sqrt{2}n_H\left(\frac{a_H}{p}\right)^2\sqrt{\frac{3kT}{m_H}} \tag{5.96}$$

The rate constant of the disproportionation reaction, $k_{m,m',p}$, to the transition reaction, Eqs. (5.67-5.70), is given by the product of the collision rate per atom, Eq. (5.96), and the coupling factor for resonant energy transfer, $g_{m,m',p}$.

$$k_{m,m',p} = g_{m,p} 4\pi\sqrt{2} n_H \left(\frac{a_H}{p}\right)^2 \sqrt{\frac{3kT}{m_H}} \tag{5.97}$$

Using an upper limit of the coupling factor $g_{m,m',p}$ for resonant energy transfer consistent with the efficiencies of dipole-dipole resonant energy transfers [36-40], an estimate of the rate constant of the disproportionation reaction, $k_{m,m',p}$, to cause the transition reaction, Eqs. (5.67-5.70), is given by substitution of $g_{m,m',p} = 1$ into Eq. (5.97).

$$k_{m,m',p} = 4\pi\sqrt{2} n_H \left(\frac{a_H}{p}\right)^2 \sqrt{\frac{3kT}{m_H}} \ \text{sec}^{-1} \tag{5.98}$$

The rate of the disproportionation reaction, $r_{m,m',p}$, to cause the transition reaction, Eqs. (5.67-5.70), is given by the product of the rate constant, $k_{m,m',p}$ given by Eq. (5.98), and the total number of hydrogen or hydrino atoms, $N_H$.

$$r_{m,m',p} = N_H 4\pi \frac{1}{2}\sqrt{2} n_H \left(\frac{a_H}{p}\right)^2 \sqrt{\frac{3kT}{m_H}} \ \frac{transitions}{\text{sec}} \tag{5.99}$$

The factor of one half in Eq. (5.99) corrects for double counting of collisions [45]. The power, $P_{m,m',p}$, is given by the product of the rate of the transition, Eq. (5.99), and the energy of the transition, Eq. (5.70).

$$P_{m,m',p} = \frac{N_H^2}{V} \frac{4\pi}{\sqrt{2}} \left(\frac{a_H}{p}\right)^2 \sqrt{\frac{3kT}{m_H}} \left[2mp + m^2 - p'^2 + 1\right] X 2.2X10^{-18} \ W \tag{5.100}$$

where $V$ is the volume.

## POWER DENSITY OF GASEOUS REACTIONS

The reaction of atomic hydrogen or hydrinos to lower-energy states releases energy intermediate that of typical chemical reactions and nuclear reactions. However, in order to be consequential as a power source celestially in processes such as heating the corona of the Sun [9] or terrestrially as an alternative to conventional sources such as combustion or nuclear power, the rate of the reaction must be nontrivial. A hydrino is formed by reaction of atomic hydrogen with a source of energy holes, and hydrinos may subsequently undergo transitions to successively lower states in reactions involving the initial source of energy holes or by disproportionation. Once it starts, the latter process has the potential to be a predominant source of power depending on the maintenance of a substantial concentration of hydrinos in steady state. The power contribution can be conservatively calculated considering only a single relative low-energy transition.

The disproportionation reaction rate, $r_{m,m',p}$, Eqs. (5.67-5.70), is dependent on the collision rate between the reactants and the efficiency of resonant energy transfer. It is given by the product of the rate constant, $k_{m,m',p}$,(Eq. (5.98)), the total number of hydrogen or hydrino atoms, $N_H$, and the efficiency, $E$, of the transfer of the energy from the donor hydrino atom to the energy hole provided by the acceptor hydrino atom given by Eq. (5.93). Thus, the rate of the disproportionation reaction, $r_{m,m',p}$, to cause a transition reaction is

$$r_{m,m',p} = E\ N_H 4\pi \frac{1}{2}\sqrt{2} n_H \left(\frac{a_H}{p}\right)^2 \sqrt{\frac{3kT}{m_H}} \tag{5.101}$$

The factor of one half in Eq. (5.101) corrects for double counting of collisions [45]. The power, $P_{m,m',p}$, is given by the product of the rate of the transition, Eq. (5.101), and the energy of the disproportionation reaction (Eq. (5.70)).

$$P_{m,m',p} = E\ \frac{N_H^2}{V} 4\pi \frac{1}{\sqrt{2}} \left(\frac{a_H}{p}\right)^2 \sqrt{\frac{3kT}{m_H}} \left[2pm + m^2 - p'^2 + 1\right] \cdot 2.2X10^{-18} \ W \tag{5.102}$$

where $V$ is the volume. For a disproportionation reaction in the gas phase with $\Phi_D$ and the overlap integral both equal to one, the energy transfer efficiency is one as given by Eq. (5.92). The power given by substitution of

$$E = 1,\ p = 2,\ m = 1,\ p' = 2,\ V = 1\ m^3,\ N = 3\ X\ 10^{19},\ T = 675\ K \tag{5.103}$$

into Eq. (5.102) is:

$$P_{m,m',p} = 100\ kW \tag{5.104}$$

corresponding to $100\ mW / cm^3$.

Next, the power due to a reaction involving a catalyst such as an atom to form hydrinos is considered. In the case that the reaction of hydrogen to lower-energy states occurs by the reaction of a catalytic source of energy holes with hydrogen or hydrino atoms, the reaction rate is dependent on the collision rate between the reactants and the efficiency of resonant energy transfer.

The hydrogen-or-hydrino-atom/catalyst-atom collision rate per unit volume, $Z_{H\left[\frac{a_H}{p}\right]\text{ Catalyst}}$, for a gas containing $n_H$ hydrogen or hydrino atoms per unit volume, each with radius $\frac{a_H}{p}$ and velocity $v_H$ and $n_C$ catalyst atoms per unit volume, each with radius $r_{\text{Catalyst}}$ and velocity $v_C$ is given by the general equation of Levine [45] for the collision rate per unit volume between atoms of two dissimilar gases.

$$Z_{H\left[\frac{a_H}{p}\right]\text{ Catalyst}} = \pi\left(\frac{a_H}{p} + r_{\text{Catalyst}}\right)^2 \left[\langle v_H \rangle^2 + \langle v_C \rangle^2\right]^{1/2} n_H n_C \tag{5.105}$$

The average velocity, $v_{avg}$, can be calculated from the temperature, $T$, [46].

$$\frac{1}{2} m_H v_{avg}^2 = \frac{3}{2} kT \tag{5.106}$$

where $k$ is Boltzmann's constant. Substitution of Eq. (5.106) into Eq. (5.105) gives the collision rate per unit volume, $Z_{H\left[\frac{a_H}{p}\right]\text{ Catalyst}}$, in terms of the temperature, $T$.

$$Z_{H\left[\frac{a_H}{p}\right]\text{ Catalyst}} = \pi\left(\frac{a_H}{p} + r_{\text{Catalyst}}\right)^2 \left[3kT\left(\frac{1}{m_H} + \frac{1}{m_C}\right)\right]^{1/2} n_H n_C \tag{5.107}$$

The rate of the catalytic reaction, $r_{m,p}$, to cause a transition reaction is given by the product of the collision rate per unit volume, $Z_{H\left[\frac{a_H}{p}\right]\text{ Catalyst}}$, the volume, $V$, and the efficiency, $E$, of resonant energy transfer given by Eq. (5.92).

$$r_{m,p} = E\ \pi\left(\frac{a_H}{p} + r_{\text{Catalyst}}\right)^2 \left[3kT\left(\frac{1}{m_H} + \frac{1}{m_C}\right)\right]^{1/2} \frac{N_H N_C}{V} \tag{5.108}$$

The power, $P_{m,p}$, is given by the product of the rate of the transition, Eq. (5.108), and the energy of the transition, Eq. (5.9).

$$P_{m,p} = E\pi\left(\frac{a_H}{p} + r_{\text{Catalyst}}\right)^2 \left[3kT\left(\frac{1}{m_H} + \frac{1}{m_C}\right)\right]^{1/2} \frac{N_H N_C}{V}\left[2mp + m^2\right] \cdot 2.2X10^{-18}\ W \tag{5.109}$$

In the exemplary case that the efficiency is $E = 10^{-4}$, the power for the $Li$ catalyst reaction given by Eqs. (5.32-5.34) with the substitution of

$$\begin{aligned} &E = 10^{-4},\ p = 1,\ m = 3,\ V = 1\ m^3,\ N_H = 3\ X\ 10^{21},\ N_C = 3\ X\ 10^{19}, \\ &m_C = 1.15\ X\ 10^{-26}\ \text{kg},\ r_C = 1.35\ X\ 10^{-10}\ \text{m},\ T = 675\ K \end{aligned} \tag{5.110}$$

into Eq. (5.109) is:

$$P_{m,p} = 144\ kW \tag{5.111}$$

corresponding to 144 $mW / cm^3$.

# H ELECTRONIC DECAY TO PROTON DECAY DRIVING SUBSEQUENT NUCLEAR REACTIONS

It is shown *infra.* that in the limit of H electronic decay corresponding to hydrino transitions to higher p quantum numbers and lower energy states causes the corresponding proton to decay to gamma rays and the ~1GeV energy released drives subsequent nuclear reactions such as photoneutron production, fission, spallation, neutron capture and neutron capture/beta decay. H electronic decay may also drive a fusion reaction by a similar mechanism as muonic catalyzed fusion. Ordinarily, fusion reaction rates are extraordinarily small [47]. In fact, fusion is virtually impossible in the laboratory. A high relative kinetic energy corresponding to extraordinary temperatures of the participating nuclei must be sufficient to overcome their repulsive potential energy. The recent NIF experimental results confirm that so called "ignition" requires 250,000,000°C and a deuterium-

tritium density of ten times that of lead to achieve about 0.2% fusion power over that input to the NIF lasers. In this case, the lasers consumed 500 trillion watts of power, 33 times the peak power of the entire world![1]

Cold fusion regarding hydrogen loading, excess hydrogen absorbed in a metal lattice to form relatively chemically unstable compound palladium hydride (deuteride), to force nuclei together is not possible since the Coulombic energy barrier for deuterium is 0.1 MeV [47], whereas the vibrational energies within crystals are much less, about 0.01 eV. Palladium hydride (deuteride) decomposes if thermal energies exceed 0.05 eV. Coulombic screening is also not plausible based on the known crystalline structure of metal hydrides. Given the relationship between temperature and energy, 11,600 K/eV, the disparity in temperature in both cases is 1.16 X $10^7$ versus 116 K, a factor of one hundred thousand. Moreover, proton-proton fusion is not possible under any condition as shown by 13 TeV proton-proton collisions at CERN wherein fusion have never been observed.

Albeit that muonic catalyzed fusion (MCF) is high-energy physics involving colliders, MCF may propagate at a high rate at more conventional plasma temperatures. Rather than directly using high temperature and density conditions, fusion occurs by a muonic catalyzed mechanism involving forming muons in a high-energy accelerator that transiently replace electrons in atoms and molecules (time scale of the muon half-life of 2.2 $\mu s$). In muon catalyzed fusion [48-49], the internuclear separation of muonic $H_2$ is reduced by a factor of 207 that of electron $H_2$ (the muon to electron mass ratio), and the fusion rate increases by about 80 orders of magnitude. A few hundred fusion events can occur per muon (vanishingly small compared to Avogadro's number of $6.022X10^{23}$). To be permissive of even this miniscule rate of fusion, the muonic molecules provide the same conditions as those at high energies. Correspondingly, the vibrational energies regarding the movement of the nuclei towards each other in an oscillating linear manner can be very large in the muonic hydrogen case, $E_{vib} \approx \nu 207X\ 0.517\ eV = \nu 107\ eV$ wherein $\nu$ is the vibrational quantum number. During the close approach of the vibrational compression phase, the nuclei can assume an orientation that allows the mutual electric fields to induce multipoles in the quarks and gluons to trigger a transition to a fusion product. The highest vibrational energy states such as the state $\nu = 9$ with $E_{vib} \approx \nu 107\ eV = 9X107\ eV = 963\ eV$ are at the bond dissociation limit. Given the extraordinary confinement time in a bound state, these muonic molecules have sufficiently large kinetic energy to overcome the Coulombic barrier for fusion of the heavy hydrogen isotopes of tritium with deuterium at just detectable rates.

Fusion in the Sun occurs due to extreme gravitational compression and thermal temperatures that provide sufficient confinement time, enormous reactant densities, and incredible energies. But even here, the Sun considered as a fusion machine of $1.412\ X10^{30}\ liter$ outputting $3.846\ X10^{26}\ W$ corresponds to a feeble $272\ \mu W / liter$. Fusion bombs (e.g. Tsar Bomba) require ignition by a fission bomb that produces power density on the order of $\frac{240X10^{15}\ J}{\left(10^{-3}\ s\right)\left(2.7X10^{7}\ liters\right)} = 8.8X10^{12}\ W / liter$, $3.2X10^{16}$ times the average power density of the Sun.[2]

Next, consider the feasibility of hydrino catalyzed fusion (HCF) based on a similar mechanism to that of muonic catalyzed fusion. Once a deuterium or tritium hydrino atom is formed by a catalyst, further catalytic transitions $n = \frac{1}{2} \to \frac{1}{3}$, $\frac{1}{3} \to \frac{1}{4}$, $\frac{1}{4} \to \frac{1}{5}$, and so on may occur to a limited extent in competition with molecular hydrino formation that terminates this cascade. The hydrino atom radius can be reduced to $1/p$ that of the $n = 1$ state atom. Analogous to muonic catalyzed fusion, the internuclear separation in the corresponding hydrino molecules is $1/p$ that of ordinary molecular hydrogen as given in the Nature of the Chemical Bond of Hydrogen-Type Molecules and Molecular Ions section (Eq. (11.204)). As the internuclear separation decreases due to high p states, fusion becomes more probable. As p becomes large, relativistic effects (e.g. relativistic electron mass and kinetic energy) become appreciable for the energy transferred from a hydrino atom and accepted by the catalyst that provides the corresponding energy hole. As in the nonrelativistic case, the energy transferred is the potential energy of the hydrogen-type atom H(1/p) that transitions to a lower energy state, divided by $p^2$, the total number of multipole modes of the state according to Eq. (5.45). Due to similar relativistic effects in hydrino atoms of similar p states, hydrino atoms may serve as the catalyst by disproportionation reactions such as ones given by Eqs. (5.62-5.80). Disproportionation reactions may propagate or cascade to very low hydrino energy states of corresponding very high p values. The corresponding hydrino molecules have vastly shorter internuclear distances (Eq. (11.204)) such that finite rates of nuclear reactions may occur in the case of heavy hydrogen isotopes, deuterium and tritium.

In the case that the electron spin-nuclear interaction is negligible, using Eq. (1.292), the relativistic potential energy of a hydrino atom $H\left(1/p\right)$ of a given state p is

[1] It is also remarkable that the NIF device cost $3.5B, and the fusion pellet cost $1M for a single shot that requires months to repeat. The product was less than one cent worth of radioactive thermal as an explosive shock wave.

[2] Arc current detonation of hydrated silver shots and other conductive solid fuels comprising a source of hydrogen and a source of HOH catalyst yielded power densities comparable to those of nuclear weapons [50-54].

$$V = \frac{Ze^2}{4\pi\varepsilon_0 r} = \frac{Z^2 e^2}{4\pi\varepsilon_0 a_0 \sqrt{1-(\alpha Z)^2}} = \frac{(\alpha p)^2 m_{e0} c^2}{\sqrt{1-(\alpha p)^2}} \tag{5.112}$$

wherein the radius given by Eq. (1.289) is

$$r = \frac{a_0}{p}\sqrt{1-(\alpha p)^2} \tag{5.113}$$

and Eqs. (28.8-28.9) were used. Thus, the energy hole according to Eqs. (5.112), (5.5), and (5.45) is

$$m = \frac{\alpha^2 m_{e0} c^2}{\sqrt{1-(\alpha p)^2}} \tag{5.114}$$

which in the low-speed limit is $m \cdot 27.2\ eV$ given by Eq. (5.5). Using Eq. (1.294) and Eqs. (5.6-5.9), the energy released from a hydrino state p during the transition involving an energy hole of quanta $m$ is given by the difference in ionization energies between the initial and final energy states wherein the final $p_f$ state is $p_f = p + m$:

$$\Delta E = m_{e0} c^2 \left( \sqrt{1-(\alpha p)^2} - \sqrt{1-(\alpha(p+m))^2} \right) \tag{5.115}$$

In the low-speed-limit the energy released is given by Eq. (5.9).

Consider the hydrino photon electric field given by Eq. (5.27) that superimposes and adds to the proton field at the position of the electron and the mechanism of its creation given in the Energy Hole Concept section. For sufficient energy available in the central electric field of the binding positive center, the highest p quantum number possible is p=137 due to the limiting speed of light for the bound electron. Otherwise, the p quantum number may be lower. In the case of a proton as the binding center, all the energy in the electric field of the proton is converted to relativistic kinetic energy and binding energy before the p =137 state can be reached. For H(1/p), the minimum radius corresponds to the energy level at which the total energy in electric field of the nucleus has been released as ionization energy and relativistic kinetic energy, the sum of which is given by Eq. (5.112). This total energy is the potential energy of the electric field of a proton given by Eqs. (1.261) and (5.112) wherein the radius is the radius of the proton given by Eq. (37.1):

$$V = \frac{e^2}{4\pi\varepsilon_0 r} = \frac{e^2}{4\pi\varepsilon_0 1.30\ X\ 10^{-15} m} = 1.77\ X\ 10^{-13} J\ =\ 1.11 X 10^6 eV \tag{5.116}$$

Then, the minimum radius and the maximum value of p is determined by equating Eq. (5.112) to Eq. (5.116):

$$\frac{(\alpha p)^2 m_{e0} c^2}{\sqrt{1-(\alpha p)^2}} = 1.77\ X\ 10^{-13} J\ =\ 1.11 X 10^6 eV \tag{5.117}$$

The reiterative solution of Eq. (5.116) is p = 126 corresponding to a minimum radius of $1.651\text{X}10^{-13}$ m. Using Eq. (5.115), the energy for the cascade of a hydrogen atom to the final state of H(1/126) results in an energy release of $2\times10^5$ eV. This energy release process is the basis of a clean, non-nuclear power source that is autonomous of the grid and fuels infrastructure with a projected on-site electricity generation cost of $0.001/kWh, a factor of about 200 times less expensive than other power sources [59].

Next consider the consequences of producing a hydrogen atom with the minimum radius of $1.651\text{X}10^{-13}$ m by driving the cascade of hydrino transition reactions to this state. The radius of a muonic hydrogen is given by the Bohr radius (Eq. (1.256)) with the mass of the electron replaced by the mass of the muon, $1.883\text{X}10^{-28}$ kg resulting in a radius of $2.560\ \text{X}10^{-13}$ m. Comparing the muon radius to the minimum hydrino radius demonstrates that in the limit, the hydrino atom H(1/126) is 2/3 the size of the muonic hydrogen atom such that the fusion rates should be comparable. Unlike inertial confinement fusion and confined plasma fusion that require temperatures on the order of $10^8$ K, muonic catalyzed fusion may occur at close to room temperature, so it was dubbed "cold fusion". However, muonic catalyzed fusion is not cold in the sense that long confinement times at very high vibrational energies are required to cause the close approach of the fusing nuclei against the nuclear coulombic repulsion [60]. The non-relativistic vibrational energies for molecular hydrino are given by Eq. (11.223) as $E_{vib} = p^2 0.517\ eV$, and the relativistic atomic radii are given by Eq. (5.113). A sufficiently high $p$ can provide vibrational energies and close approach of nuclei of corresponding molecules sufficient for fusion to ensue. Considering the $p^2$ dependency of the vibrational energies of $H_2(1/p)$, and excitation of highest vibrational energy state at the bond dissociation limit (e.g. $v = 9$), the state $p = 15$ can achieve comparable vibrational energies as muonic molecules, yet the $p = 15$ hydrino atomic radius (Eq. (5.113)) and corresponding molecular hydrino internuclear distance are about 14 times greater than those of the muonic species. The $p$ state that achieves comparable dimensions to those of muonic atoms and molecules is $p = 115$ (Eq. (5.113)) which has a corresponding nonrelativistic vibrational energy of 6840 eV. Only the lowest energy vibrational state would likely be populated with the energy from bond formation $p^2 4.478 eV$ (Eq. (11.252)) since the temperature required to excite 7 keV vibrational modes is on the order of $10^8$ K, compared to an ordinary plasma temperature of about 1000 K. Considering that the muon catalysis event occurs on the time scale of $0.5\times10^{-12}$ [61], and the internuclear distance of hydrogen-isotopic molecular hydrino such as $^2H_2(1/p)$ and $^3H_2(1/p)$ may be shorter than the corresponding muonic molecules, very high

fusion rates may be achieved with a large population of high-p-state molecular hydrinos.

Hydrino Catalyzed Fusion (HCF) has utility to produce (i) neutrons (D + T and D + D fusion), and (ii) $^3$He, tritium, and high energy protons (D + D fusion) which have industrial applications. Using heavy hydrogen, trace production of tritium by HCF may be competitive with atomic accelerators and hot fusion reactors. According to a study by Kovari [62], D-D tritium breeding might cost $2 billion per kilogram tritium produced. Tritium stockpiles are projected to be depleted near term wherein Savannah River's tritium facilities are the United States' only source of tritium, an essential component in nuclear weapons.

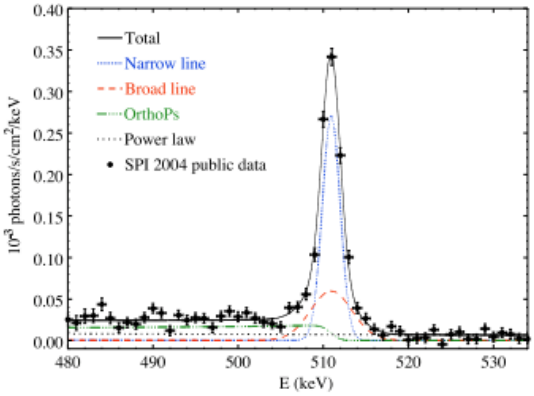
Consider the consequence of the formation of the state wherein p =127. In this case the central photon field may be increased without sufficient energy to increase the relativistic kinetic energy of the electron required to maintain a stable non-radiative orbit. Specifically, the increased electric field due to the photon results in the corresponding central electric field force exceeding the centrifugal force. In this case, the electron may collapse onto the proton, and the proton may decay. The products of the widely believed pathway for proton decay are a positron and a neutral pion that further decays into two gamma rays. In the hydrino decay pathway, the hydrino electron annihilates the positron and emits two 511 keV photons. The ***total energy release of 930.8 MeV*** is that of the annihilation of H(1/126) which is the sum of the mass energy of the proton (931 MeV) and the electron (511 keV) minus the binding energy of H(1/126) (200.9 keV) given by Eq. (5.115). The reaction is given by:

$$\begin{array}{lccc} H(1/p)\rightarrow & e^+ + e^- + & \pi^0 & \\ & \downarrow & \downarrow & \\ & 2\gamma & 2\gamma & \end{array} \tag{5.118}$$

wherein $e^+$ is the positron, $e^-$ is the electron, $\pi^0$ is the neutral pion, and $\gamma$ is a gamma ray.

Collision of the positron with the electron produces the characteristic 511 keV annihilation energy emission. 511 keV radiation is observed as a distinct peak in the cosmic gamma ray spectrum (Figure 5.4) wherein the origin is yet unknown [63-68].

**Figure 5.4.** Fit of the spectrum of the positron annihilation emission measured by SPI with narrow and broad Gaussian lines and an ortho-positronium continuum (Prantzos et al., 2010, ref. [67]).




A forerunner explanation of the diffuse 511keV positron annihilation emission [63-68] with no point source [64] and a narrow line-width [67-68] is decaying dark matter [63-68] that is consistent with the ***hydrino as the identity of dark matter*** as given in the Composition of the Universe section and Refs.[9, 58] with ***H(1/p) decay (Eq. (5.118)) as the 511 keV source***. Further support of this assignment is that the neutral pion decay energy is also observed as a maximum intensity broad peak in the cosmic gamma ray spectrum [69].

***Specifically, the 511 keV gamma ray line intensity observed by the INTEGRAL/SPI experiment is consistent with the galactic bulge annihilation rate of ~ (1.5±0.1)×10$^{43}$ low-energy positrons per second within ~ 1 kpc (3.26×10$^3$ light years) of the galactic center [63-64]***. The prior inexplicable source of low-energy positrons from the Milky Way bulge is assigned to hydrino decay wherein hydrino is the identity of dark matter in agreement with many analyses indicating that dark matter decay is the most plausible assignment [63-68]. Consider the magnitude of mass of H atoms that undergo decay over the oscillatory cycle of the universe at the bulge rate corrected for the size of the galactic dark matter halo. The Milky Way is a barred spiral galaxy that is roughly 100,000 light years across and 1,000 light years thick. The Milky Ways dark matter halo is estimated to extend roughly 1,000,000 light-years in radius, meaning it is significantly larger than the visible bulge of the galaxy, which is around 5,000 light-years in radius [70]. The halo is thought to contain most of the galaxy mass and is dominated by dark matter. The H(1/p) decay rate corrected for the volume of the halo relative to the sampled volume of the bulge is about 1.5×10$^{50}$. ***Multiplying dark matter-halo-corrected decay rate of 1.5×10$^{50}$/s times the oscillatory period of the universe of 9.83×10$^{11}$ years (Eq. (32.149)) gives total mass of decayed hydrino atoms and corresponding protons of the Milky Way of 6.2×10$^{42}$ kg compared to the total mass of the Milky Way galaxy of about 6×10$^{42}$ kg [70].*** This estimate demonstrates that H(1/p) decay is a very prominent process in the evolution of the cosmos. The decay rate decreases with time in the expansion phase of the expansion-contraction cycle of the universe, but the measured rate is low since it assumes that the positron travels great distances

before encountering an electron and annihilating whereas the positron annihilates with the electron of H(1/p) and does not travel. Further decay of proton mass/energy occurs through the mechanism of matter to energy conversion during fusion and other nuclear reactions culminating in the formation of black holes. Subsequently, when the mass density of a black hole reaches the threshold of the Planck mass density, a gamma ray burst occurs contributing to the energy portion of the pathway of recycling of protons as given in Composition of the Universe section. Concerted H(1/p) decay may also give rise to gamma ray bursts consistent with the gamma ray spectrum recorded on a burst [71] showing a characteristic "$\pi^0$-decay bump" [69]. These are likely the long duration, lower energy type gamma ray bursts.

***In addition to 511 keV gamma ray emission, neutral pion $\pi^0$, gamma and X-ray, and neutron emission are observed from a broad array of astrophysical environments such as interstellar medium, supernova remnants (SNRs), molecular clouds, galaxy clusters, and other sources [69] as well as solar flares [72] and thunderstorms [73]***. Regarding supernova remnants (SNRs), old stars may comprise an abundance of high p-state hydrinos that may facilitate proton decay and neutron production with enormous energy release, high-atomic-number nucleogenesis of elements beyond iron by neutron capture and beta decay, and neutron star formation. Rather than the implausible mechanism of the low power release of gravitational collapse due to a stellar pressure drop occurring over billions of years, supernova explosions are likely due to a catastrophic positive-feedback proton decay event of the extremely unstable state of a high composition of high p state hydrinos wherein the massive energy release of a perturbed population of high p-state hydrinos creates a shock wave that causes a propagating wave of proton decay throughout the star. Regarding thunderstorms, the Italian Space Agency's AGILE observatory found that the energy spectrum of terrestrial gamma-ray flashes extends up to 100 MeV [74], and 100 MeV gamma, 511 keV, as well as neutral pion decay radiation and neutrons were recorded on solar flare emission [72] wherein neutron emission was observed via observation of characteristic 2.223 MeV emission from the neutron capture reaction with protons to form deuterium. Shane et al. [75] report on data from Fermi LAT of solar flare spectra showing the characteristic "$\pi^0$-decay bump" [69] and a cutoff of about 1 GeV. A proposed source of the Sun's gamma rays is decaying dark matter [76]. These signatures are characteristic of decay of hydrino atoms H(1/p) each comprising a proton and an electron in a high p state. The neutral pion $\pi^0$ emission has a distinct bell-type feature ("$\pi^0$-decay bump") between 100 MeV and a few GeV [69]. The energy of the mass to energy conversion of the proton's mass of 938.27 MeV and the electron's mass of 511 keV of a first hydrino may be transferred as kinetic energy or as a gamma ray to a proton such as that of a second hydrino in proximity, or alternatively to a proton of a hydrogen atom. The gamma ray incident a proton may give rise to neutron production. The neutron production reaction of the gamma energy from hydrino decay is given by the photoneutron production reaction in hydrogen [77]:

$$\begin{array}{l} \gamma + p^+ \rightarrow n \; + \; \pi^+ \; + \quad \pi^0 \\ \qquad\qquad\quad \downarrow \qquad\quad \downarrow \\ \qquad\qquad\quad \mu^+ + \nu_\mu \qquad 2\gamma \\ \qquad\qquad\quad \downarrow \\ \qquad\quad e^+ + \; \nu_e \; + \; \bar{\nu}_\mu \\ \qquad\quad \downarrow e^- \\ \qquad\quad 2\gamma \end{array} \tag{5.119}$$

where $p^+$ is the proton, $n$ is the neutron, $\pi^+$ is the positive pion, $\mu^+$ is the positive muon, $\nu_e$ is the electron neutrino, $\nu_\mu$ is the muon neutrino, and $\bar{\nu}_\mu$ is the muon antineutrino. The neutral pion decays to two gamma rays. The positive pion decays to a positive muon and a muon neutrino. The positive muon decays to a positron, an electron neutrino, and a muon antineutrino. The positron annihilates with an electron to produce two 511 keV gamma photons. Overall, photoneutron production from a proton additionally produces four gamma rays and three neutrinos, one of electron flavor and two of muon flavor. Another possible reaction is that the gamma ray energy of the decay of a first hydrino atom causes the production of an energetic neutron and an electron neutrino from a second hydrino atom:

$$\gamma \; + \; H\left(1/p\right) \; \rightarrow \; n \; + \; \nu_e \tag{5.120}$$

The pathway of Eq. (5.119) predicts 2 muon neutrinos to 1 electron neutrino which matches the results of solar neutrino experiments. Specifically, photoneutron production ***(Eq. (5.119)) predicts the relative number of electron to muon neutrinos being 1/3 and 2/3 of the total, respectively. The predicted electron and muon neutrino ratios match solar neutron observations by detectors such as the Homestake Solar Neutrino Experiment, GALLEX, SAGE, Sudbury Solar Neutrino Observatory, and Kamiokande and Super-Kamiokande detectors [78]. The results do not match the Standard Solar Model prediction of an electron neutrino intensity 3 times higher than observations with no muon neutrinos observed***. The only direct evidence that fusion occurs in the Sun and stars is the solar neutrino data. However, the solar neutrino data indicate that the source of sunlight from the Sun is not only the p-p chain to form helium nuclei from protons by fusion. Rather the hydrino-decay-driven chain:

$$hydrino\ decay \; - \; neutron\ production \; - \; neutron\ capture \; - \; beta\ decay \tag{5.121}$$

contributes significantly wherein the density of H(1/p) increases with increasing p state which favors gravitational concentration

of high-p-state H(1/p) in the core of the Sun. Proton-proton fusion has not been measured in the laboratory under any condition and may not occur in the Sun. The p-p chain may be initiated by protons undergoing neutron capture to form deuterium. Additionally, the neutron capture and beta decay reaction may repeat to higher atomic number elements as known in the formation of heavier nuclei than iron during supernova. The possibility that the p-p chain was not the only source of solar power was considered by Bahcall [78]. According to Bahcall, [78] the possibility of a revolutionary discovery of a new source of energy in the Sun based on a prior undiscovered process is an open question.

This neutron production reaction is more favorable for high-p-state H(1/p), and this reaction suppresses gamma emission from the primary hydrino decay reaction. The production of neutrons can be observed by the subsequent signature of neutron capture reactions. Neutron capture by protons to form deuterium produces a characteristic 2.223 MeV peak that is observed in cosmic gamma ray spectra [79-81] and spectra of solar flares [72] wherein the energy to drive the neutron-production reactions is assigned to proton decay of high-p-state hydrino atoms and molecules. Other nuclei of interstellar medium are capable of undergoing neutron capture resulting in isotope shifts and atomic number shifts. Abundances and depletions of other neutron-capture elements in addition to proton and deuterium nuclei have been observed in the interstellar medium consistent with a high neutron flux wherein the source of the neutrons is assigned to hydrino decay (Eq. (5.118)) [82-83].

The power from hydrino decay may be very high wherein the energy yield is equivalent to matter-antimatter annihilation. For example, the power of a solar flare can exceed that of one billion hydrogen bombs. Consider that the solar flare event is powered by the hydrino transition and decay reactions. These reactions are capable of positive feedback wherein the rates increase as the plasma temperature rises from reaction heating. Consider the limit of the highest $p$ value for a hydrino state H(1/p). The energy release per hydrino atom decay in a so called "dark matter device" given by Eq. (5.118) is 930.8 MeV ($1.49\times10^{-10}$ J) corresponding to 89.8 TJ/mol, or 89,806 TJ/kg with no radioactive fuel or products involved and absent the requirement of a critical mass. As an atomic bomb comparison, the fission of one atom of uranium-235 locally releases 202.5 MeV ($3.24\times10^{-11}$ J) corresponding to 19.54 TJ/mol, or 83.14 TJ/kg with another 8.8 MeV that is lost as anti-neutrinos. As a chemical comparison, the energy released by detonation of 1 kg of TNT is 4.184 MJ. The hydrino decay reaction is thermonuclear in nature such that the reaction can go to completion. Any size material may be made to detonate by means such as the creation of an electrical arc or a shock wave in a material comprising at least one of high-p-state H(1/p) and $H_2$(1/p) initiated by a detonation of conventical explosive, explosive wire detonation, blasting caps, or use of other conventional detonators to create an arc, shock wave, and/or high thermal event. Given that the ***energy production of hydrino decay is 1080 times nuclear and $2.15\times10^{10}$ times TNT, detonation of an exemplary energetic hydrino material comprising a 1g hydrino (H(1/p), p>>4) (less than the size of a sugar cube) can release 25 kilotons of explosive energy equivalent to twice that of early atomic bombs***. Serving as a fuel, 1 g of hydrino (H(1/p), p>>4) can provide enough energy to power over one million homes for a year. Additionally, hydrino decay can serve as a source of neutrons that can propagate transmutation by fission reactions such as fission of $^{235}$U, $^{239}$Pu, $^{7}$Li, and $^{6}$Li to form desired products such as energy, tritium, and neutrons. The fission energy release may further serve to drive thermonuclear fusion reactions for important applications such as radionuclide and isotope production or radioactive waste remediation, weapons, and power.

In the case of extraordinarily high p states approaching p = 126, bonding with inner shell electrons may result in fusion of higher atomic number elements than hydrogen. Such states wherein a high-p-state hydrino atom served as a "fat neutron" is supported by such a species formed by muonic atoms [84].

Another more favorable transmutation reaction pathway especially for heavy elements is by neutron capture. Specifically, a further application of neutron production by hydrino decay is transmutation by neutron capture followed by beta decay. In general, isotope transmutation occurs when nuclei absorb neutrons. This process may occur until an unstable isotope is formed and subsequently undergoes beta decay with an increase in atomic number, balance of proton to neutron ratio, and stability. Hydrino decay may serve as a neutron source. Transmutation by neutron capture or fission is valuable for several industrial applications such as production of elements and isotopes of elements with industrial applications such as radioisotopes for medical and labeling purposes and as nuclear fuel. Transmutation may also be useful for remediation of radioactive waste.

In addition to photoneutron production from high-energy gamma photons reacting with protons, high-energy gamma rays incident deuterium may cause photoneutron production [85] with a threshold of 2.223 MeV by the reaction:

$$\gamma + d^+ \rightarrow n + p^+ \tag{5.122}$$

where $d^+$ is the deuterium nucleus, $p^+$ is the proton, and $n$ is the neutron. Several research laboratories report results consistent with the production of neutrons and neutron capture as well as transmutation reactions that are caused by neutron capture followed by beta decay from H and D reactants. The experiments like those reported by Mills et al. [86] involve creation of atomic hydrogen by aqueous electrolysis on a cathode comprising at least one of a metal and a co-deposited metal such as Ni, Pd, or Pt that is favorable to dissociate and absorb hydrogen wherein hydrino reactants comprising a source of H(D) and HOH(DOD) catalyst are generated. Jones for example reports anomalous neutron emission from cathodes during aqueous electrolysis [87], and Smith et al. [88] report neutron emission from co-deposition cathodes during aqueous electrolysis. Palladium and platinum are examples of candidate elements wherein hydrino decay followed by neutron capture by the nucleus of a heavy element creates isotope ratios different from those of natural abundance wherein the product may decay by beta emission to form the element with the next higher atomic number. Palladium and platinum are known to undergo neutron capture followed by beta emission with silver [89-90] and gold [91] as the products, respectively. Gadly et al. [92] also report the emission of fast neutrons from Pd cathodes undergoing aqueous electrolysis recorded with a diamond detector, gas filled $^{3}$He detectors after thermalization with high density polythene, as well as novel epoxy resin, and CR-39 detectors. Gadly et al. [92]

further report observations of transmutation of the Pd to Ag consistent with the anticipated neutron capture-beta decay reaction. Consistent with neutron capture and neutron capture with beta decay Pala et al. [93] report the observation of Pt and Pd isotope shifts as well as transmutation of Pd to Ag and Pt to Au from isotope and elemental analysis (EDX, WDS, ICPMS, and ToF-SIMS) of a Pt cathode onto which Pd is co-deposited during aqueous electrolysis. High energy tracks in CR-39 detectors consistent with several neutron-induced carbon-12 nuclear splitting reactions were also reported indicating that the neutron energy was greater than the threshold of these reaction of 100 MeV [94]. Energetic neutron, particle, and gamma ray production recorded by CR-39 detectors on the co-deposition experiment were reported earlier by a group at SPAWAR [95-97] as well as other researchers [98].

Carbon does not readily undergo fission; it is considered too small and stable to split apart in a fission reaction, making it much more likely to participate in fusion instead, especially when considering its most abundant isotope, carbon-12. However, products of the over 1 GeV hydrino decay event are energetic neutrons. When high-energy neutrons collide with heavy nuclei, a reaction called spallation occurs, where the heavy nucleus is violently broken apart, emitting multiple smaller particles like protons, neutrons, alpha particles, and other lighter nuclei, effectively "spalling" or chipping away at the heavy nucleus; this process is often used to produce secondary beams of particles in particle accelerators. Spallation may also occur after a neutron is captured wherein the nucleus fragments into several parts. The process is important only at energies more than 100 MeV for the incident neutron, and the cross sections increase to energies as high as 400–500 MeV. Several neutrons may serve to carry increased energy to the spallation reaction whereby de-excitation gamma rays may be emitted [99]. Kumar et al. [100] also report spallation products in addition to isotope shifts and transmutation products during aqueous electrolysis.

H(1/p) of high p state may be produced by successive transitions of H(1/p) to lower-energy, higher p states catalyzed by other hydrino states once formed by HOH catalyst. This reaction requires long H(1/p) containment times, a source of activation energy, and a source of H(1/p) to serve as reactants and catalyst. Metal can serve as matrix as demonstrated by electrolysis at metal cathodes and by co-deposited metals on base metal cathodes [93, 95-98] wherein the HOH (DOD) catalyst and H (D) to form H(1/4) (D(1/4) are produced by aqueous electrolysis, and the applied electrical power may serve as the source of activation energy. In the case that the cathode comprises a water-reactive metal that reacts with the electrolyte to form atomic H on the cathode surface, the hydrino reaction may be enhanced by the production of H. For example, Kumar et al. [100] report superior transmutation results with a Kanthal cathode and a basic electrolyte wherein aluminum reacts with water in basic solution to evolve atomic H. The hydrino reaction may be promoted using hydrogen storage and dissociating materials, such as nickel, palladium, and platinum. Moreover, the hydrino reaction may be made more efficient by intermittent application of electrolysis current wherein hydrogen is created on the metal cathode surface. The metal further serves to dissociate hydrogen as the metal releases absorbed hydrogen during the off phase of the intermittent cycle as shown by Mills et al. [86]. Gas chromatography of gas collected from the SunCell, a plasma based hydrino reaction system comping two molten tin injectors to maintain two intersecting molten metal streams, demonstrated the formation of high-p state H(1/p) [58] wherein supplied $H_2$ and trace $O_2$ supply the H and HOH catalyst, and at least one of the high temperature plasma, and a low voltage high current applied through the molten metal streams provided the activation energy. The high kinetic impact of ball milling also propagates chemical reactions [101]. Electron paramagnetic spectroscopy (EPR) recorded on ball milled salts that provide a source of H and HOH catalyst as well as a matrix to trap hydrino demonstrated that high p states can be formed in this system as well [102]. A light source (e.g. high powered laser), a particle beam, or a high- or low-voltage high-current low-impedance electricity source may provide at least one of high power density irradiation, activation, arc plasma formation, and heating of solid (e.g. solid fuels reported by Mills et al. [8-12]), liquid (e.g. aqueous), or gaseous hydrino reactants each comprising a source of H and a source of HOH to provide high reaction kinetics to form high-p-state H(/p) wherein at least one of the laser, particle beam, and high- or low-voltage high-current low-impedance electricity source provides the activation energy.

Molecular hydrino such as $H_2(1/p)$ comprises a paired and an unpaired electron in a single molecular orbital (MO) with a current density function given by ½ (↑↑ + ↓↑) wherein the current density function of $H_2(1/p)$ is given graphically by the sum of current density of Figure 11.2 plus ½ times the current of Figure 11.2 superimposed on its mirror image as given in the Parameters and Magnetic Energies Due to the Spin Magnetic Moment of $H_2(1/4)$ section. Since H(1/p) comprises an unpaired electron, it is magnetic. The unpaired MO electron gives rise to spin flip transitions observed by electron paramagnetic spectroscopy (EPR) and well as magnetism observed by magnetic susceptibility measurements [58, 103]. EPR was reported on a matrix material Ga(O)OH that had the rare ability to trap individual $H_2(1/4)$ molecules in a gas-like state that allowed for the study of theoretically predicted fine structure in the EPR hydrino signature. Specifically, Hagen and Mills [102] reported the theoretically predicted g factor for the spin flip transition with the predicted extraordinary features of a series of multiplets due to fluxon linkage within a series of multiplets due to spin-orbital splitting between the diamagnetic paired and paramagnetic unpaired electron of the MO during the EPR transition.

As a sequel to the 2022 paper, Hagen and Mills [103] report a large down-field singlet signature and temperature dependencies recorded by EPR that confirm the theoretical prediction of the formation of molecular hydrino dimers $[H_2(1/p)]_2$ as an extension of ordinary hydrogen chemistry. $H_2$ is known to form dimers $[H_2]_2$ only at cryogenic temperatures whereas $[H_2(1/p)]_2$ was shown to be stable at elevated temperatures. Moreover, at low temperatures, it was observed that $[H_2(1/4)]_2$ dimers form tetramers that were not EPR active by anti-pairing side by side. As the temperature was raised the EPR singlet for the dimer reappeared at the predicted temperature. The results further show the production of $H_2(1/8)$ and $[H_2(1/8)]_2$ dimers indicating greater release of energy than production of $H_2(1/4)$.

The observation of the formation of a dimer between molecular hydrino $H_2(1/4)$ and $H_2$ ($[H_2\text{-}H_2(1/4)]$) and the temperature dependence of hydrogen release explains the massive amounts of hydrogen observed from salts containing

molecular hydrino reported previously [58, 103]. These salts are not known to absorb any hydrogen and indicate a new very significant technology comprising the conversion of common salts to hydrogen storage materials which are of great industrial value. These results further indicate the entrapment of hydrino promotes the further entrapment by a magnetic attraction. Very high magnetic fields are possible as shown by Hagen and Mills [103]. The use of ferromagnetic material such as Ni electrolysis cathodes or the use of FeOOH in the case of ball milling [58] with the further application of an external magnetic field would further boost the entrapment of hydrino and promote the formation of high-p-state H(1/p). A further implication of the formation of H(1/p), $H_2(1/p)$, $[H_2(1/p)]_2$, $[H_2(1/p)]_4$ ,…, $[H_2(1/p)]_n$ and corresponding D and T species is that multiple neutrons may be formed via decay of H(1/p) or D(1/p) due to the increased favorability of hydrino species to undergo these reactions. Dineutrons [104] and possibly tetraneutrons [105] are known to exist.

Fusion is another possible reaction for hydrogen isotope nuclei that have acquired high kinetic energy from hydrino decay. This reaction is limited to light nuclei wherein the exemplary Coulombic barrier for proton-proton fusion is 1 MeV [106]. Miles et al. [107] report the production of helium-4 by nuclear fusion of deuterium during aqueous electrolysis. In this case, room temperature or so called "cold fusion" is possible via hydrino decay in addition to a hydrino-muonic mechanism, but as in the case of room temperature muonic catalyzed fusion the reaction mechanism is not cold.

Helium-4 can also be formed by hydrino-decay-produced neutrons causing fission of the LiOH electrolyte used [108]. Specifically, $^6$Li or $^7$Li may undergo fission to $^4$He and $^3$H with additionally a neutron product in the case of $^7$Li. Both fusion and hydrino decay are favorable for high-p-state H(1/p). Fusion and hydrino decay require a hydrino transition reaction cascade such as one propagated by disproportionation reactions to hydrino states of high p. The cascade is favored by (i) massive kinetics, (ii) hydrino and plasma confinement, and (iii) increasing duration of the hydrino reaction. One exemplary system to cause massive kinetics and hydrino and plasma confinement is detonation of hydrino reactant solid fuels under arc current conditions [54-58]. Hydrino confinement is achieved by using as a component of the reactor comprising at least one of (i) a source of an applied magnetic field and (ii) a cryogenic system, or a hydrino reactant mixture comprising at least one of (i) a solid material to absorb hydrino atoms such as a metal surface or bulk metal such as one that also absorbs H atoms (e.g. Ni, Ti, Pd, Pt, Nb, or Ta) [58], (ii) a magnetic material such as FeOOH or $Fe_2O_3$, that favors magnetic bonding of hydrinos [58], and (iii) an oxide such as a metal oxide such as GaOOH or $Ga_2O_3$ that binds hydrinos [58,102]. Mosier-Boss et al. [96] report a summary of the ***nuclear signatures of hydrino decay observed ubiquitously from astrophysical and terrestrial sources are also observed from aqueous electrolysis experiments at hydrogen absorbing cathodes. Specifically, the nuclear signatures of energy, neutrons, helium-4, tritium, gamma rays, X-rays, energetic particles, spallation products, isotope shifts, and transmutation of heavy elements were observed.*** The evidence for fusion [107] has an alternative fission explanation, and the fusion assignment is discounted due to the observation of the absence of the known branching ratios for helium and tritium products of the D-D fusion reaction [108], and tritium is also a separate product of photoneutron capture by deuterium.

# MOLECULAR BLACKLIGHT PROCESS

## BELOW "GROUND" STATE TRANSITIONS OF HYDROGEN-TYPE MOLECULES AND MOLECULAR IONS

As is the case with the hydrogen atom, higher and lower molecular energy states are equally valid wherein the central field of molecular hydrogen ions and molecules can also be a reciprocal integer or an integer value of that of the ordinary states corresponding to molecular excited states and molecular hydrino states as given in the Diatomic Molecular Energy States section and the Nature of the Chemical Bond of Hydrogen-Type Molecules and Molecular Ions section, respectively. The photon changes the effective charge at the MO surface where the central field is ellipsoidal and arises from the protons at the foci and the "trapped photon" as effectively at the foci of the MO. Force balance is achieved at a series of two-dimensional ellipsoidal equipotential surfaces. The "trapped photons" are solutions of the Laplacian in ellipsoidal coordinates, Eq. (11.27). Thus, each molecular state comprises two electrons, two protons, and a photon, but the excited states are radiative; whereas, the hydrino states are stable. Excited and hydrino electronic states are created when photons of discrete frequencies are trapped in the ellipsoidal resonator cavity of the MO by resonant photon absorption and resonant nonradiative energy transfer, respectively.

## ENERGY HOLES

From Eqs. (11.207) and (11.208), the magnitude of the elliptic field corresponding to a below "ground state" transition of the hydrogen molecule is an integer. The potential energy equations of hydrogen-type molecules are:

$$V_e = \frac{-p2e^2}{8\pi\varepsilon_0\sqrt{a^2-b^2}}\ln\frac{a+\sqrt{a^2-b^2}}{a-\sqrt{a^2-b^2}} \tag{5.123}$$

$$V_p = \frac{pe^2}{8\pi\varepsilon_0\sqrt{a^2-b^2}} \tag{5.124}$$

where

$$a = \frac{a_0}{p} \tag{5.125}$$

$$b = \frac{1}{p\sqrt{2}} a_0 \tag{5.126}$$

$$c' = \sqrt{a^2 - b^2} = \frac{\sqrt{2} a_0}{2p} \tag{5.127}$$

and where $p$ is an integer. The quantum number $p$ is a scaling parameter of the molecular dimensions and energies. In the latter case it corresponds to the effective nuclear charge factor. Using the convention defined in the Energy Hole Concept section, this factor $Z_{effective}$ is given by $Z_{effective} = 1/n = p$ where the principal quantum number $n = 1/p$. From energy conservation, the resonance energy hole of a hydrogen-type molecule which causes the transition

$$H_2\left[2c' = \frac{\sqrt{2} a_0}{p}\right] \rightarrow H_2\left[2c' = \frac{\sqrt{2} a_0}{p+m}\right] \tag{5.128}$$

is

$$mp^2 \, X \; 48.6 \; eV \tag{5.129}$$

where $m$ and $p$ are integers. During the transition, the elliptic field is increased from magnitude $p$ to magnitude $p+m$. The corresponding potential energy change equals the energy absorbed by the energy hole.

$$Energy \; hole = -V_e - V_p = mp^2 \, X \; 48.6 \; eV \tag{5.130}$$

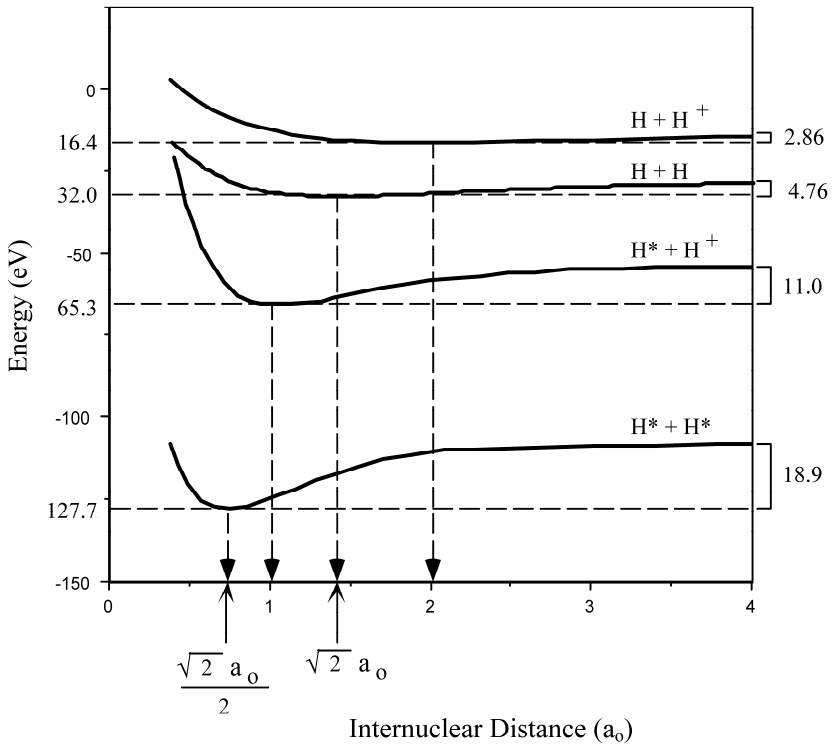
Further energy is released by the hydrogen-type molecule as the internuclear distance "shrinks." The total energy, $E_T$, released during the transition is:

$$E_T = -13.6 \; eV\left[\left(2(m+p)^2\sqrt{2} - (m+p)^2\sqrt{2} + \frac{(m+p)^2\sqrt{2}}{2}\right)\ln\frac{\sqrt{2}+1}{\sqrt{2}-1} - (m+p)^2\sqrt{2}\right] \tag{5.131}$$

$$+13.6 \; eV\left[\left(2p^2\sqrt{2} - p^2\sqrt{2} + \frac{p^2\sqrt{2}}{2}\right)\ln\frac{\sqrt{2}+1}{\sqrt{2}-1} - p^2\sqrt{2}\right]$$

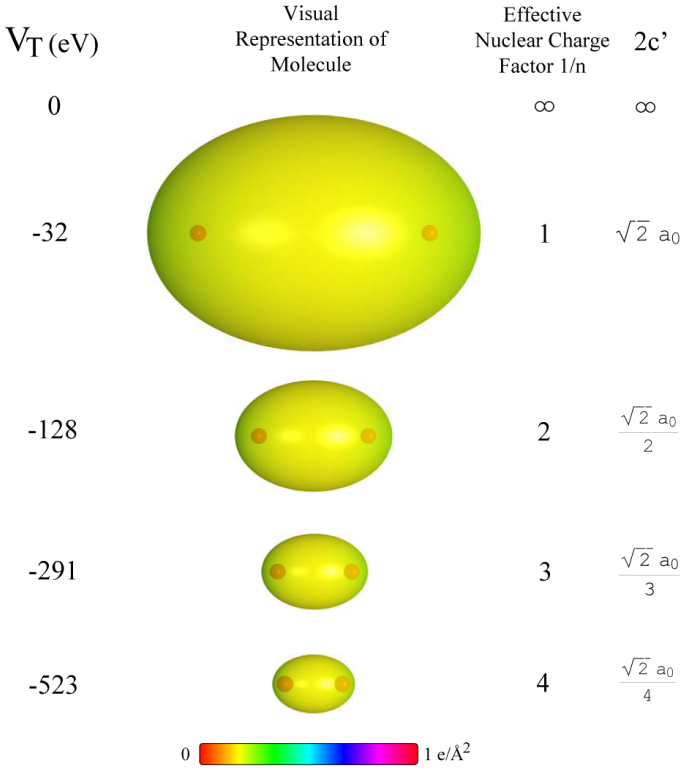
A schematic drawing of the total energy well of hydrogen-type molecules and molecular ions is given in Figure 5.5. The exothermic reaction involving transitions from one potential energy level to a lower level is also hereafter referred to as the Molecular BlackLight Process.

**Figure 5.5.** The total energy well of hydrogen-type molecules and molecular ions.



A hydrogen-type molecule with its electrons in a lower than "ground state" energy level corresponding to a fractional quantum number is hereafter referred to as a dihydrino molecule. The designation for a dihydrino molecule of internuclear distance, $2c' = \frac{\sqrt{2}a_0}{p}$, where $p$ is an integer, is $H_2\left[2c' = \frac{\sqrt{2}a_0}{p}\right]$. A schematic drawing of the size of hydrogen-type molecules as a function of total energy is given in Figure 5.6.

**Figure 5.6.** The size of hydrogen-type molecules as a function of total energy where $n = 1/p$ for dihydrino states, $p$ is an integer, and 2c' is the internuclear distance.




The magnitude of the elliptic field corresponding to the first below "ground state" transition of the hydrogen molecule is $2$ times the magnitude of a reference field defined by two elementary charges $e$ at a distance of $2c'$ from each other. From energy conservation, the resonance energy hole of a hydrogen molecule, which excites the transition of the hydrogen molecule with internuclear distance $2c' = \sqrt{2}a_o$ to the first below "ground state" with internuclear distance $2c' = \frac{1}{\sqrt{2}}a_0$ is given by Eqs. (5.123-5.127) where the elliptic field is increased from magnitude one to magnitude two:

$$V_e = \frac{-2e^2}{8\pi\varepsilon_0\sqrt{a^2-b^2}}\ln\frac{a+\sqrt{a^2-b^2}}{a-\sqrt{a^2-b^2}} = -67.836\ eV \tag{5.132}$$

$$V_p = \frac{e^2}{8\pi\varepsilon_0\sqrt{a^2-b^2}} = 19.24\ eV \tag{5.133}$$

$$Energy\ hole = -V_e - V_p = 48.6\ eV \tag{5.134}$$

In other words, the elliptic "ground state" field of the hydrogen molecule can be considered as the superposition of Fourier components. The removal of negative Fourier components of energy

$$m\ X\ 48.6\ eV \tag{5.135}$$

where $m$ is an integer, increases the positive electric field inside the ellipsoidal shell by $m$ times the charge of a proton at each focus. The resultant electric field is a time harmonic solution of the Laplacian in ellipsoidal coordinates. The corresponding potential energy change equals the energy absorbed by the energy hole.

$$Energy\ hole = -V_e - V_p = m\ X\ 48.6\ eV \tag{5.136}$$

Further energy is released by the hydrogen molecule as the internuclear distance "shrinks." The hydrogen molecule with

internuclear distance $2c' = \sqrt{2}a_o$ is caused to undergo a transition to the below "ground state" level, and the internuclear distance for which force balance and nonradiation are achieved is $2c' = \frac{\sqrt{2}a_0}{1+m}$. In decaying to this internuclear distance from the "ground state," a total energy of:

$$-13.6\ eV\left[\left(2(1+m)^2\sqrt{2}-(1+m)^2\sqrt{2}+\frac{(1+m)^2\sqrt{2}}{2}\right)\ln\frac{\sqrt{2}+1}{\sqrt{2}-1}-(1+m)^2\sqrt{2}\right]$$
$$+13.6\ eV\left[\left(2\sqrt{2}-\sqrt{2}+\frac{\sqrt{2}}{2}\right)\ln\frac{\sqrt{2}+1}{\sqrt{2}-1}-\sqrt{2}\right] \quad (5.137)$$

is released.

## CATALYTIC ENERGY HOLES FOR HYDROGEN-TYPE MOLECULES

An efficient catalytic system that hinges on the coupling of three resonator cavities involves iron and lithium. For example, the fourth ionization energy of iron is $54.8\ eV$. This energy hole is obviously too high for resonant absorption. However, $Li^+$ releases $5.392\ eV$ when it is reduced to $Li$. The combination of $Fe^{3+}$ to $Fe^{4+}$ and $Li^+$ to $Li$, then, has a net energy change of $49.4\ eV$.

$$49.4\ eV + Fe^{3+} + Li^+ + H_2\left[2c' = \sqrt{2}a_0\right] \rightarrow Fe^{4+} + Li + H_2\left[2c' = \frac{\sqrt{2}a_0}{2}\right] + 94.9\ eV \quad (5.138)$$

$$Li + Fe^{4+} \rightarrow Li^+ + Fe^{3+} + 49.4\ eV \quad (5.139)$$

And, the overall reaction is:

$$H_2\left[2c' = \sqrt{2}a_0\right] \rightarrow H_2\left[2c' = \frac{\sqrt{2}a_0}{2}\right] + 94.9\ eV \quad (5.140)$$

Note that the energy given off as the molecule shrinks is much greater than the energy lost to the energy hole. And, the energy released is large compared to conventional chemical reactions.

An efficient catalytic system that hinges on the coupling of three resonator cavities involves scandium. For example, the fourth ionization energy of scandium is $73.47\ eV$. This energy hole is obviously too high for resonant absorption. However, $Sc^{3+}$ releases $24.76\ eV$ when it is reduced to $Sc^{2+}$. The combination of $Sc^{3+}$ to $Sc^{4+}$ and $Sc^{3+}$ to $Sc^{2+}$, then, has a net energy change of $48.7\ eV$.

$$48.7\ eV + Sc^{3+} + Sc^{3+} + H_2\left[2c' = \sqrt{2}a_0\right] \rightarrow Sc^{4+} + Sc^{2+} + H_2\left[2c' = \frac{\sqrt{2}a_0}{2}\right] + 94.9\ eV \quad (5.141)$$

$$Sc^{2+} + Sc^{4+} \rightarrow Sc^{3+} + Sc^{3+} + 48.7\ eV \quad (5.142)$$

And, the overall reaction is:

$$H_2\left[2c' = \sqrt{2}a_0\right] \rightarrow H_2\left[2c' = \frac{\sqrt{2}a_0}{2}\right] + 94.9\ eV \quad (5.143)$$

An efficient catalytic system that hinges on the coupling of three resonator cavities involves gallium and lead. For example, the fourth ionization energy of gallium is $64.00\ eV$. This energy hole is obviously too high for resonant absorption. However, $Pb^{2+}$ releases $15.03\ eV$ when it is reduced to $Pb^+$. The combination of $Ga^{3+}$ to $Ga^{4+}$ and $Pb^{2+}$ to $Pb^+$, then, has a net energy change of $48.97\ eV$.

$$48.97\ eV + Ga^{3+} + Pb^{2+} + H_2\left[2c' = \sqrt{2}a_0\right] \rightarrow Ga^{4+} + Pb^+ + H_2\left[2c' = \frac{\sqrt{2}a_0}{2}\right] + 94.9\ eV \quad (5.144)$$

$$Ga^{4+} + Pb^+ \rightarrow Ga^{3+} + Pb^{2+} + 48.97\ eV \quad (5.145)$$

And, the overall reaction is:

$$H_2\left[2c' = \sqrt{2}a_0\right] \rightarrow H_2\left[2c' = \frac{\sqrt{2}a_0}{2}\right] + 94.9\ eV \quad (5.146)$$

The rate of an electronic transition of a molecule is a function of the change in internuclear distance during the transition. Transitions between electronic states that have equivalent internuclear distances at some point during their vibrational cycles have much greater rates than transitions that require the energy level of the electrons to change as well as the internuclear distance to change simultaneously. As shown in Figure 5.5, the transition from the $n = 1$ state to the $n = 1/2$ state of molecular hydrogen is not favored for this reason. A more likely transition pathway is a vibrational excitation of molecular hydrogen ($n = 1$) that breaks the bond, followed by a transition reaction of each of the hydrogen atoms via a $27.2\ eV$ energy hole catalyst

as given in the Hydrino Theory—BlackLight Process section, followed by reaction of the two hydrino atoms ( $n = 1/2$ ) to form a dihydrino molecule ( $n = 1/2$ ).

## REFERENCES


1. K. Akhtar, J. Scharer, R. L. Mills, Substantial Doppler broadening of atomic-hydrogen lines in DC and capacitively coupled RF plasmas**,** J. Phys. D, Applied Physics, Vol. 42, (2009), 42 135207 (2009) doi:10.1088/0022-3727/42/13/135207.
2. R. Mills, K. Akhtar, "Tests of Features of Field-Acceleration Models for the Extraordinary Selective H Balmer $\alpha$ Broadening in Certain Hydrogen Mixed Plasmas," Int. J. Hydrogen Energy, Vol. 34, (2009), pp. 6465-6477.
3. R. L. Mills, B. Dhandapani, K. Akhtar, "Excessive Balmer $\alpha$ Line Broadening of Water-Vapor Capacitively-Coupled RF Discharge Plasmas," International Journal of Hydrogen Energy, Vol. 33, (2008), pp. 802-815.
4. R. Mills, P. Ray, B. Dhandapani, "Evidence of an Energy Transfer Reaction Between Atomic Hydrogen and Argon II or Helium II as the Source of Excessively Hot H Atoms in RF Plasmas," Journal of Plasma Physics, (2006), Vol. 72, Issue 4, pp. 469-484.
5. J. Phillips, C-K Chen, K. Akhtar, B. Dhandapani, R. Mills, "Evidence of Catalytic Production of Hot Hydrogen in RF Generated Hydrogen/Argon Plasmas," Int. J. Hydrogen Energy, Vol. 32(14), (2007), 3010-3025.
6. R. L. Mills, P. C. Ray, R. M. Mayo, M. Nansteel, B. Dhandapani, J. Phillips, "Spectroscopic Study of Unique Line Broadening and Inversion in Low Pressure Microwave Generated Water Plasmas," J. Plasma Physics, Vol. 71, Part 6, (2005), pp. 877-888.
7. R. L. Mills, K. Akhtar, "Fast H in Hydrogen Mixed Gas Microwave Plasmas when an Atomic Hydrogen Supporting Surface Was Present," Int. J. Hydrogen Energy, 35 (2010), pp. 2546-2555, doi:10.1016/j.ijhydene.2009.12.148.
8. R. Mills, Y. Lu, R. Frazer, "Power Determination and Hydrino Product Characterization of Ultra-low Field Ignition of Hydrated Silver Shots", Chinese Journal of Physics, Vol. 56, (2018), pp. 1667-1717.
9. R. Mills, J. Lotoski, Y. Lu, "Mechanism of soft X-ray continuum radiation from low-energy pinch discharges of hydrogen and ultra-low field ignition of solid fuels", Plasma Science and Technology, Vol. 19, (2017), pp. 1-28.
10. R. Mills J. Lotoski, "$H_2O$-based solid fuel power source based on the catalysis of H by HOH catalyst", Int'l J. Hydrogen Energy, Vol. 40, (2015), 25-37.
11. R. Mills, J. Lotoski, J. Kong, G. Chu, J. He, J. Trevey, "High-Power-Density Catalyst Induced Hydrino Transition (CIHT) Electrochemical Cell." Int. J. Hydrogen Energy, 39 (2014), pp. 14512–14530 DOI: 10.1016/j.ijhydene.2014.06.153.
12. R. Mills, "Hydrino States of Hydrogen", https://brilliantlightpower.com/pdf/Hydrino_States_of_Hydrogen.pdf, submitted for publication.
13. R. L. Mills, R. Booker, Y. Lu, "Soft X-ray Continuum Radiation from Low-Energy Pinch Discharges of Hydrogen," J. Plasma Physics, Vol. 79, (2013), pp 489-507; doi:10.1017/S0022377812001109.
14. K. R. Lykke, K. K. Murray, W. C. Lineberger, "Threshold photodetachment of $H^-$," Phys. Rev. A, Vol. 43, No. 11, (1991), pp. 6104-6107.
15. D. R. Lide, *CRC Handbook of Chemistry and Physics*, 86th Edition, CRC Press, Taylor & Francis, Boca Raton, (2005-6), pp. 10-202 to 10-204.
16. K. K. Baldridge, J. S. Siegel, "Correlation of empirical $\delta$(TMS) and absolute NMR chemical shifts predicted by ab initio computations," J. Phys. Chem. A, Vol. 103, (1999), pp. 4038-4042.
17. J. Mason, Editor, *Multinuclear NMR*, Plenum Press, New York, (1987), Chp. 3.
18. C. Suarez, E. J. Nicholas, M. R. Bowman, "Gas-phase dynamic NMR study of the internal rotation in N-trifluoroacetlypyrrolidine," J. Phys. Chem. A, Vol. 107, (2003), pp. 3024-3029.
19. C. Suarez, "Gas-phase NMR spectroscopy," The Chemical Educator, Vol. 3, No. 2, (1998).
20. H. Beutler, Z. Physical Chem., "Die dissoziationswarme des wasserstoffmolekuls $H_2$, aus einem neuen ultravioletten resonanzbandenzug bestimmt," Vol. 27B, (1934), pp. 287-302.
21. G. Herzberg, L. L. Howe, "The Lyman bands of molecular hydrogen," Can. J. Phys., Vol. 37, (1959), pp. 636-659.
22. P. W. Atkins, *Physical Chemistry*, Second Edition, W. H. Freeman, San Francisco, (1982), p. 589.
23. N. V. Sidgwick, *The Chemical Elements and Their Compounds*, Volume I, Oxford, Clarendon Press, (1950), p.1
24. A. Beiser, *Concepts of Modern Physics*, Fourth Edition, McGraw-Hill Book Company, New York, (1978), pp. 153-155.
25. M. D. Lamb, *Luminescence Spectroscopy*, Academic Press, London, (1978), p. 68.
26. P. Kurunczi, H. Shah, and K. Becker, "Excimer formation in high-pressure microhollow cathode discharge plasmas in helium initiated by low-energy electron collisions," Int. J. Mass Spectrosc., Vol. 205, (2001), pp. 277-283.
27. P. F. Kurunczi, K. H. Becker, "Microhollow Cathode Discharge Plasma: Novel Source of Monochromatic Vacuum Ultraviolet Radiation," Proc. Hakone VII, Int. Symp. High Pressure, Low Temperature Plasma Chemistry, Greifswald, Germany, Sept. 10 - 13, (2000), Vol. 2, p. 491.
28. P. Kurunczi, H. Shah, and K. Becker, "Hydrogen Lyman-$\alpha$ and Lyman-$\beta$ emissions from high-pressure microhollow cathode discharges in $Ne-H_2$ mixtures," J. Phys. B: At. Mol. Opt. Phys., Vol. 32, (1999), L651-L658.
29. J. Wieser, D. E. Murnick, A. Ulrich, H. A Higgins, A. Liddle, W. L. Brown, "Vacuum ultraviolet rare gas excimer light source," Rev. Sci. Instrum., Vol. 68, No. 3, (1997), pp. 1360-1364.

30. A. Ulrich, J. Wieser, D. E. Murnick, "Excimer Formation Using Low Energy Electron Beam Excitation," Second International Conference on Atomic and Molecular Pulsed Lasers, Proceedings of SPIE, Vol. 3403, (1998), pp. 300-307.
31. D. R. Lide, *CRC Handbook of Chemistry and Physics*, 86th Edition, CRC Press, Taylor & Francis, Boca Raton, (2005-6), pp. 9-54 to 9-59.
32. R. Mills, "Spectroscopic Identification of a Novel Catalytic Reaction of Atomic Hydrogen and the Hydride Ion Product," Int. J. Hydrogen Energy, Vol. 26, No. 10, (2001), pp. 1041-1058.
33. B. J. Thompson, *Handbook of Nonlinear Optics*, Marcel Dekker, Inc., New York, (1996), pp. 497-548.
34. Y. R Shen, *The Principles of Nonlinear Optics*, John Wiley & Sons, New York, (1984), pp. 203-210.
35. B. de Beauvoir, F. Nez, L. Julien, B. Cagnac, F. Biraben, D. Touahri, L. Hilico, O. Acef, A. Clairon, and J. J. Zondy, Physical Review Letters, Vol. 78, No. 3, (1997), pp. 440-443.
36. E. Bulbul, M. Markevitch, A. Foster, R. K. Smith, M. Loewenstein, S. W. Randall, "Detection of an unidentified emission line in the stacked X-Ray spectrum of galaxy clusters," The Astrophysical Journal, Volume 789, Number 1, (2014).
37. A. Boyarsky, O. Ruchayskiy, D. Iakubovskyi, J. Franse, "An unidentified line in X-ray spectra of the Andromeda galaxy and Perseus galaxy cluster," (2014),arXiv:1402.4119 [astro-ph.CO].
38. Nico Cappelluti, Esra Bulbul, Adam Foster, Priyamvada Natarajan, Megan C. Urry, Mark W. Bautz, Francesca Civano, Eric Miller, Randall K. Smith, "Searching for the 3.5 keV Line in the Deep Fields with Chandra: The 10 ms Observations," The Astrophysical Journal, Vol. 854 (2), (2018), p. 179 DOI: 10.3847/1538-4357/aaaa68.
39. F. A. Cotton, "Chemical applications of Group Theory," 2nd Edition, Wiley Interscience, (1963), pp. 280-283.
40. F. Wilkinson, "Intramolecular Electronic Energy Transfer Between Organic Molecules," *Luminescence in Chemistry*, Edited by E. J. Bowen, D. Van Nostrand Co. Ltd., London, (1968), Chapter 8, pp. 154-182.
41. H. Morawetz, Science, 240, (1988), pp. 172-176.
42. O. Schnepp, Levy, M., J. Am. Chem. Soc., 84, (1962), pp. 172-177.
43. F. Wilkinson, *Luminescence in Chemistry*, Edited by E. J. Bowen, D. Van Nostrand Co. Ltd., London, (1968), pp. 155-182.
44. Th. Förster, *Comparative Effects of Radiation*, Report of a Conference held at the University of Puerto Rico, San Juan, February 15-19, (1960), sponsored by the National Academy of Sciences; National Research Council, Edited by Milton Burton, J. S. Kirby-Smith, and John L. Magee, John Wiley & Sons, Inc., New York pp. 300-325.
45. F. Bueche, *Introduction to Physics for Scientists and Engineers*, McGraw-Hill, (1975), pp. 352-353.
46. J. D. Jackson, *Classical Electrodynamics*, Second Edition, John Wiley & Sons, New York, (1975), pp. 739-747.
47. J. D. Jackson, *Classical Electrodynamics*, Second Edition, John Wiley & Sons, New York, (1975), pp. 758-760.
48. F. J. Bueche, *Introduction to Physics for Scientists and Engineers*, McGraw-Hill Book Company, New York, (1986), pp. 261-265.
49. I. Levine, *Physical Chemistry*, McGraw-Hill Book Company, New York, (1978), pp. 420-421.
50. F. J. Bueche, *Introduction to Physics for Scientists and Engineers*, McGraw-Hill Book Company, New York, (1986), pp. 261-265.
51. http://en.wikipedia.org/wiki/Nuclear_fusion.
52. L. I. Ponomarev, "Muon catalyzed fusion," Contemporary Physics, Vol. 31, No. 4, (1990), pp. 219-245.
53. J. Zmeskal, P. Kammel, A. Scrinzi, W. H. Breunlich, M. Cargnelli, J. Marton, N. Nagele, J. Werner, W. Bertl, and C. Petitjean, "Muon-catalyzed dd fusion between 25 and 150 K: experiment," Phys. Rev. A, Vol. 42, (1990), pp. 1165-1177.
54. R. Mills, Y. Lu, R. Frazer, "Power Determination and Hydrino Product Characterization of Ultra-low Field Ignition of Hydrated Silver Shots", Chinese Journal of Physics, Vol. 56, (2018), pp. 1667-1717.
55. R. Mills J. Lotoski, "$H_2O$-based solid fuel power source based on the catalysis of H by HOH catalyst", Int'l J. Hydrogen Energy, Vol. 40, (2015), 25-37.
56. https://brilliantlightpower.com/pdf/Spectroscopy_Nansteel_Report_040219.pdf.
57. https://www.brilliantlightpower.com/wp-content/uploads/pdf/Free-Air-TNT-Analysis.pdf.
58. R. Mills, "Hydrino States of Hydrogen", https://brilliantlightpower.com/pdf/Hydrino_States_of_Hydrogen.pdf, submitted for publication.
59. https://brilliantlightpower.com/.
60. T. Yamashita, Y. Kino, K. Okutsu, et al, "Roles of resonant muonic molecule in new kinetics model and muon catalyzed fusion in compressed gas", Sci Rep 12, 6393 (2022). https://doi.org/10.1038/s41598-022-09487-0.
61. J. D. Jackson, "Catalysis of Nuclear Reactions between hydrogen isotopes by μ−-Mesons". Physical Review. (1957), 106 (2): 330. Bibcode:1957PhRv..106..330J. doi:10.1103/PhysRev.106.330.
62. https://www.science.org/content/article/fusion-power-may-run-fuel-even-gets-started#:~:text=According%20to%20Kovari's%20study%2C%20D%2DD,%242%20billion%20per%20kilogram%20produced.
63. A. C. Vincent, P. Martin, J. M. Cline, "Interacting dark matter contribution to the Galactic 511 keV gamma ray emission: constraining the morphology with INTEGRAL/SPI observations", https://arxiv.org/pdf/1201.0997.
64. G. De Cesare, "Searching for the 511 keV annihilation line from galactic compact objects with the IBIS gamma ray telescope", A&A 531, A56 (2011) DOI: 10.1051/0004-6361/201116516, https://www.aanda.org/articles/aa/pdf/2011/07/aa16516-11.pdf.
65. J. Knodlseder, et al., "The all-sky distribution of 511 keV electron-positron annihilation emission", Astronomy & Astrophysics manuscript no. 2063, November 7, 2018, https://arxiv.org/pdf/astro-ph/0506026.

66. J. Knodlseder, et al., "The all-sky distribution of 511 keV electron-positron annihilation emission", astro-ph/0506026, Masaki Mori, ICRR Group Internal Seminar, June 20, 2005,https://www.icrr.u-tokyo.ac.jp/~morim/Presentations/INTEGRAL511keV.pdf.
67. N. Prantzos, C. Boehm, A. M. Bykov, et al., "The 511 keV emission from positron annihilation in the Galaxy", (2010), https://arxiv.org/abs/1009.4620.
68. N. Prantzos, C. Boehm, A. M. Bykov, et al., "The 511 keV emission from positron annihilation in the Galaxy", Reviews of Modern Physics, Vol. 83, July (2011), pp. 1001–1056.
69. R. Yang, E. Kafexhiu1, F. Aharonian, "Exploring the shape of the γ-ray spectrum around the "$\pi^0$-bump", A&A, Volume 615, July (2018), A108, https://doi.org/10.1051/0004-6361/201730908, https://www.aanda.org/articles/aa/pdf/2018/07/aa30908-17.pdf.
70. https://en.wikipedia.org/wiki/Milky_Way.
71. National Aeronautics and Space Administration, Goddard Space Flight Center, Fermi Gamma-ray Space Telescope, "Overview of GRB spectral analysis", https://fermi.gsfc.nasa.gov/ssc/data/analysis/documentation/Cicerone/Cicerone_GRBs/Overview_GRB_Spec_Anal.html.
72. R. Ramaty, R. J. Murphy, C. D. Dermer, "On the origin of the pion-decay radiation in the 1982 June 3 solar flare", The Astrophysical Journal, 316:L41-L44,1987 May 1. https://articles.adsabs.harvard.edu/cgi-bin/nph-iarticle_query?1987ApJ...316L..41R&defaultprint=YES&filetype=.pdf.
73. J. R. Dwyer, D. M. Smith, et al., "Positron clouds within thunderstorms", Journal of Plasma Physics, Volume 81 , Issue 4 , August (2015), 475810405, DOI: https://doi.org/10.1017/S0022377815000549.
74. F. Fuschino, M. Marisaldi, "AGILE and TGFs Latest results & activities", 11th AGILE Science workshop, "Gamma-rays and Galactic Cosmic Rays", May 16-17, 2013, ASI Headquarters, Via del Politecnico, Rome.
75. G. H. Share, R. J. Murphy, et al., "Characteristics of sustained >100 MeV γ ray emission associated with solar flares", February 28, (2022), https://arxiv.org/pdf/1711.01511.
76. N. Wolchover, "The Sun Is Stranger Than Astrophysicists Imagined", Quanta Magazine, May 1, 2019, https://www.quantamagazine.org/gamma-ray-data-reveal-surprises-about-the-sun-20190501/.
77. Costa, S., Ferroni, S., Gracco, V.G. et al., "Photoneutron production from the proton at high energy", Nuovo Cimento A (1965-1970) Vol. 45, (1966), pp. 696–705, https://doi.org/10.1007/BF02721135.
78. J. N. Bahcall, "Solving the mystery of the missing neutrinos", **The Nobel Prize**, https://www.nobelprize.org/prizes/themes/solving-the-mystery-of-the-missing-neutrinos/#:~:text=Combining%20the%20SNO%20and%20the%20Super%2DKamiokande%20measurements%2C,as%20the%20number%20of%20just%20electron%20neutrinos.&text=Only%20the%20water%20detectors%20(Kamiokande%2C%20Super%2DKamiokande%2C%20and,of%20the%20solar%20neutrinos%20that%20are%20observed.
79. R. Diehl, "Cosmic Gamma-Ray Spectroscopy", July 17, 2013, https://arxiv.org/pdf/1307.4198.
80. A. M. Ritchey , S. R. Federman, and D. L. Lambert, "Abundances and Depletions of Neutron-capture Elements in the Interstellar Medium", The Astrophysical Journal Supplement Series, 236:36 (40pp), 2018 June, DOI 10.3847/1538-4365/aab71e, https://iopscience.iop.org/article/10.3847/1538-4365/aab71e/pdf.
81. D. J. Mullan, J. L. Linsky, "Nonprimordial deuterium in interstellar medium", The Astrophysical Journal, Vol. 511, No. 1, (1999), pp. 502-512, DOI 10.1086/306650, https://iopscience.iop.org/article/10.1086/306650/pdf.
82. A. M. Ritchey , S. R. Federman, and D. L. Lambert, "Abundances and Depletions of Neutron-capture Elements in the Interstellar Medium", The Astrophysical Journal Supplement Series, 236:36 (40pp), 2018 June, DOI 10.3847/1538-4365/aab71e, https://iopscience.iop.org/article/10.3847/1538-4365/aab71e/pdf.
83. D. J. Mullan, J. L. Linsky, "Nonprimordial deuterium in interstellar medium", The Astrophysical Journal, Vol. 511, No. 1, (1999), pp. 502-512, DOI 10.1086/306650, https://iopscience.iop.org/article/10.1086/306650/pdf.
84. E. A. G. Armour, "Muon catalyzed fusion", Symposium on Atomic & Molecular Physics, pp. 211-226; https://ntrs.nasa.gov/api/citations/20080040752/downloads/20080040752.pdf.
85. D. A. Fynan, Y. Seo, G. Kim, S. Barros, M. Jin Kim, "Photoneutron production in heavy water reactor fuel lattice from accelerator-driven bremsstrahlung", Annals of Nuclear Energy, Vol. 155, June, 1, (2021), p. 108141 https://doi.org/10.1016/j.anucene.2021.108141.
86. R. L. Mills and S. Kneizys, "Excess heat by the electrolysis of aqueous potassium carbonate and the implications for cold fusion", Fusion Technol. Vol. 20, (1991), p. 6.
87. S. E. Jones, "Anomalous neutron emission from metal-deuterium system", (1990), (RAL--90-022). Davies, J.D. (Ed.). United Kingdom, https://inis.iaea.org/Search/searchsinglerecord.aspx?recordsFor=SingleRecord&RN=21081049
88. P. J. Smith, R. C. Hendricks, B. M. Steinetz, "Electrolytic co-deposition neutron production evaluation," (NASA report No. E-19924), (2021).
89. J. D. Kraus, J. M. Cork, "Radioactive Isotopes of Palladium and Silver from Palladium", Phys. Rev. 52, 15 October, (1937), p. 763, DOI: https://doi.org/10.1103/PhysRev.52.763.
90. https://en.wikipedia.org/wiki/Isotopes_of_palladium.
91. N. Petersen, "Measuring Neutron Absorption Cross Sections of Natural Platinum via Neutron Activation Analysis", A thesis submitted to Oregon State University, Department of Physics, Corvallis, Oregon, June 11, 2012; https://ir.library.oregonstate.edu/downloads/4m90dx05b

92. Gadly, T., Phapale, S., Gamre, S. et al. Experimental and theoretical validation for transmutation of palladium at electrochemical interfaces, Sci Rep 14, 21270 (2024). https://doi.org/10.1038/s41598-024-70597-y.
93. R. G. S. Pala, K. P. Rajeev, A. Kumar, R. Nehra, "Low Energy Nuclear Reactions via Electrolysis", 2024 ANS Annual Conference, June 16–19, 2024, https://dev.ans.org/meetings/ac2024/session/view-2545; https://www.ans.org/meetings/ac2024/session/view-2545/#paper_7627.
94. E. L. Alpen, **Radiation Biophysics**, Second Edition (1998), Chapter 5 - Energy Transfer Processes, pp. 78-103.
95. P. Mosler-Boss, S. Szpak, F. E. Gordan, L. P. G. Forsley, "Triple tracks in CR-39 as the result of Pd-D co-deposition: evidence of energetic neutrons", Naturwissenschaften, (2009) Jan;96(1):135-42. doi: 10.1007/s00114-008-0449-x.
96. P. A. Mosier-Boss, L. P. Forsley, "Chapter 2 - Review of Pd/D co-deposition", Cold Fusion Advances in Condensed Matter Nuclear Science, (2022), pp. 17-36, https://www.sciencedirect.com/science/article/abs/pii/B9780128159446000026.
97. P. A. Mosier-Boss, S. Szpak, F. E. Gordon, L. P. G. Forsley, "Use of CR-39 in Pd/D codeposition experiments," European Physical Journal Applied Physics, Vol. 40, (2007), pp. 293–303.
98. C. Gotzmer, L. F. DeChiaro, K. Conley, M. Litz, M. Millett, J. Ewing, L. P. Forsley, et al. "Li–Pd–Rh- D2O electrochemistry experiments at elevated voltage," APL Energy 1, no. 3, (2023); https://doi.org/10.1063/5.0153487.
99. S. Leray, "Nuclear reaction at high energy," CEA/Saclay, DAPNIA/SPhN, Gif-surYvette Cedex, France, Workshop on Nuclear data for Science and Technology: Accelerator Driven Waste Incineration, Trieste, 10-21 September 2001, LNS0212005,https://www.osti.gov/etdeweb/servlets/purl/20909666.
100. A. Kumar, P. Jain, K. P. Rajeev, R. G. Pala, "Upper Bound in the Fusion Products and Transmutation Enhancement in Alloys", Journal of Condensed Matter Nuclear Science 36 (1), 327-335 (20202), https://jcmns.scholasticahq.com/article/72607-upper-bound-in-the-fusion-products-and-transmutation-enhancement-in-alloys.
101. T. Markmaitree, R. Ren, L. L. Shaw, "Enhancement of lithium amide to lithium imide transition via mechanical activation", J. Phys. Chem. B., Vol. 110, No. 41, pp. 20710-20718.
102. W. R. Hagen, R. L. Mills, "Electron Paramagnetic Resonance Proof for the Existence of Molecular Hydrino", Int. J. Hydrogen Energy, Vol. 47, No. 56, (2022), pp. 23751-23761; https://www.sciencedirect.com/science/article/pii/S0360319922022406.
103. W. R. Hagen, R. L. Mills, "General EPR pattern from molecular hydrino produced in various reactors", (2024), https://chemrxiv.org/doi/full/10.26434/chemrxiv.15002560/v1; https://brilliantlightpower.com//pdf/General_EPR_pattern_from_molecular_hydrino_produced_in_various_reactors.pdf.
104. S. B. Borzakov, "Singlet Deuteron, Dineutron and Neutral Nuclei", FLNP JINR, Dubna, Russia, (Julu, (2023), DOI: 10.48550/arXiv.2307.12719.
105. A. Deltuva, R. Lazauskas, "Tetraneutron resonance in the presence of a dineutron", Phys. Rev. C 100, 044002 – Published 30 October, 2019, https://doi.org/10.1103/PhysRevC.100.044002.
106. Briefing on Low-Energy Nuclear Reactions (LENR) Research, A scientific survey of the international literature in response to the FY16, NDAA (report on HR4909, 4 May 2016), Office of the ASD(R&E) I Research, https://www.esd.whs.mil/Portals/54/Documents/FOID/Reading%20Room/Science_and_Technology/16-F-1333_%20DOC_02_LENR_Briefing.pdf.
107. M. H. Miles, P. Hagelstein, "Consistency of helium production with the excess power in the palladium-D2O electrochemical system", Journal of Electroanalytical Chemistry, Vol. 977, (2025), pp. 118786, DOI:10.1016/j.jelechem.2024.118786.
108. Fusion Physics, Edited by M. Kikuchi, K. Lackner, M. Q. Tran, IAEA International Atomic Energy Agency, p. 22, https://nucleus.iaea.org/sites/fusionportal/SiteCollectionDocuments/Fusion%20Book.pdf.

# Chapter 6

## STABILITY OF ATOMS AND HYDRINOS

The central field of the proton corresponds to integer one charge. Excited states comprise an electron with a trapped photon. In all energy states of hydrogen, the photon has an electric field that superposes with the field of the proton. In the $n=1$ state, the sum is one, and the sum is zero in the ionized state. In an excited state, the sum is a fraction of one (i.e. between zero and one). Derivations from first principles given in the Excited States of the One-Electron Atom section demonstrate that each "allowed" fraction corresponding to an excited state is $\frac{1}{\text{integer}}$. Following the derivation given in the Excited States of the One-Electron Atom (Quantization) section, the relationship between the electric field equation and the "trapped photon" source charge-density function is given by Maxwell's equation in two-dimensions.

$$\mathbf{n} \bullet \left( \mathbf{E}_1 - \mathbf{E}_2 \right) = \frac{\sigma}{\varepsilon_0} \tag{6.1}$$

where $\mathbf{n}$ is the radial normal unit vector, $\mathbf{E}_1 = 0$ ($\mathbf{E}_1$ is the electric field outside of the atomic orbital), $\mathbf{E}_2$ is given by the total electric field at $r_n = n a_H$, and $\sigma$ is the surface charge-density. The electric field of an excited state is fractional; therefore, the source charge function is fractional. It is well known that fractional charge is not "allowed." The reason given in the Instability of Excited States section is that fractional charge typically corresponds to a radiative current-density function. The excited states of the hydrogen atom are examples. They are radiative; consequently, they are not stable. Thus, an excited electron decays to the first nonradiative state corresponding to an integer field, $n=1$ (i.e. a field of integer one times the central field of the proton). Specifically, the superposition of $\sigma_{photon}$ (Eq. (2.23)) and $\sigma_{electron}$ (Eq. (2.24)) is equivalent to the sum of a radial electric dipole represented by a doublet function and a radial electric monopole represented by a delta function given in Eq. (2.25). Due to the radial doublet, excited states are radiative since spacetime harmonics of $\frac{\omega_n}{c} = k$ or $\frac{\omega_n}{c}\sqrt{\frac{\varepsilon}{\varepsilon_0}} = k$ do exist for which the spacetime Fourier transform of the current density function is nonzero.

Equally valid from first principles are electronic states where the magnitude of the sum of the electric field of the photon and the proton central field are an integer greater than one times the central field of the proton. These states are nonradiative. A catalyst can effect a transition between these states as described in the Hydrino Theory—BlackLight Process section.

The condition for radiation by a moving charge is derived from Maxwell's equations. To radiate, the spacetime Fourier transform of the current-density function must possess components synchronous with waves traveling at the speed of light [1]. Alternatively,

> *For non-radiative states, the current-density function must not possess spacetime Fourier components that are synchronous with waves traveling at the speed of light.*

As given in the One-Electron Atom section, the relationship between the radius and the wavelength of the electron is:

$$v_n = \lambda_n f_n \tag{6.2}$$

$$v_n = 2\pi r_n f_n = \lambda_n f_n \tag{6.3}$$

$$2\pi r_n = \lambda_n \tag{6.4}$$

Consider the wave vector of the sinc function of Eq. (38) of Appendix I, the Spacetime Fourier Transform of the Electron Function. When the velocity is $c$ corresponding to a potentially emitted photon

$$\mathbf{s}_n \bullet \mathbf{v}_n = \mathbf{s}_n \bullet \mathbf{c} = \omega_n \tag{6.5}$$

the relativistically corrected wavelength (Eq. (1.280)) is given by:

$$\mathbf{r}_n = \lambda_n \tag{6.6}$$

Substitution of Eq. (6.6) into the sinc function results in the vanishing of the entire Fourier transform of the current-density function. Thus, spacetime harmonics of $\frac{\omega_n}{c} = k$ or $\frac{\omega_n}{c}\sqrt{\frac{\varepsilon}{\varepsilon_0}} = k$ do not exist for which the Fourier transform of the current-density function is nonzero.

In the case of below "ground" (fractional quantum number) energy states, the sum of the source current corresponding to the photon and the electron current results in a radial Dirac delta function as shown in the Stability of Atoms and Hydrinos section. Whereas, in the case of above "ground" or excited (integer quantum number) energy states, the sum of the source current corresponding to the photon and the electron current results in a radial doublet function which has Fourier components of $\frac{\omega_n}{c} = k$. Thus, excited states are radiative as shown in the Instability of Excited States section.

## STABILITY OF "GROUND" AND HYDRINO STATES

For the below "ground" (fractional quantum number) energy states of the hydrogen atom, $\sigma_{photon}$, the two-dimensional surface charge due to the "trapped photon" at the electron atomic orbital, is given by Eqs. (5.27) and (2.11).

$$\sigma_{photon} = \frac{e}{4\pi(r_n)^2}\left[Y_0^0(\theta,\phi) - \frac{1}{n}\left[Y_0^0(\theta,\phi) + \mathrm{Re}\left\{Y_\ell^m(\theta,\phi)e^{im\omega_n t}\right\}\right]\right]\delta(r-r_n) \quad n = 1, \frac{1}{2}, \frac{1}{3}, \frac{1}{4}, \ldots \tag{6.7}$$

And, $\sigma_{electron}$, the two-dimensional surface charge of the electron atomic orbital is:

$$\sigma_{electron} = \frac{-e}{4\pi(r_n)^2}\left[Y_0^0(\theta,\phi) + \mathrm{Re}\left\{Y_\ell^m(\theta,\phi)e^{im\omega_n t}\right\}\right]\delta(r-r_n) \tag{6.8}$$

The superposition of $\sigma_{photon}$ (Eq. (6.7)) and $\sigma_{electron}$, (Eq. (6.8)) where the spherical harmonic functions satisfy the conditions given in the Bound Electron "Atomic Orbital"section is a radial electric monopole represented by a delta function.

$$\sigma_{photon} + \sigma_{electron} = \frac{-e}{4\pi(r_n)^2}\left[\frac{1}{n}Y_0^0(\theta,\phi) + \left(1+\frac{1}{n}\right)\mathrm{Re}\left\{Y_\ell^m(\theta,\phi)e^{im\omega_n t}\right\}\right]\delta(r-r_n) \quad n = 1, \frac{1}{2}, \frac{1}{3}, \frac{1}{4}, \ldots \tag{6.9}$$

In the case of lower-energy states or hydrino states, the superposition given by Eq. (6.9) involves integer charge only. Whereas, in the case of excited states, the superposition given by Eq. (2.25) involves the sum of a delta function with a fractional charge (radial monopole term) and two delta functions of charge plus one and minus one which is a doublet function (radial dipole term). As given in the Spacetime Fourier Transform of the Electron Function section, the radial delta function does not possess spacetime Fourier components synchronous with waves traveling at the speed of light. Thus, the below "ground" (fractional quantum number) energy states of the hydrogen atom are stable. The "ground" ($n = 1$ quantum number) energy state is just the first of the nonradiative states of the hydrogen atom; thus, it is the state to which excited states decay based on the nature of photon and corresponding electron source current of excited as opposed to the hydrino states as given in the Excited States of the One-Electron Atom (Quantization) section and Hydrino Theory—BlackLight Process section, respectively. The stability is also shown using the Poynting power theorem applied to the electric and magnetic fields from the electron source current as shown in Appendix I.

## NEW "GROUND" STATE

Once a hydrino atom is formed by a catalyst, further catalytic transitions $n = \frac{1}{2} \to \frac{1}{3}$, $\frac{1}{3} \to \frac{1}{4}$, $\frac{1}{4} \to \frac{1}{5}$, and so on may occur to an extent limited to the lowest energy state possible whose formation results in the exhaustion of the total potential energy in the electric field of the proton, thereafter the hydrino atom undergoes proton and electron decay emitted as gamma rays. Using the radius of the proton (Eq. (37.1)) and the potential energy equation (Eq. (1.292)), the total potential energy in the electric field between the electron and the proton of a hydrogen atom given by Eq.(5.116) is

$$V = \frac{e^2}{4\pi\varepsilon_0 r} = \frac{e^2}{4\pi\varepsilon_0 1.30\ X\ 10^{-15} m} = 1.77\ X\ 10^{-13} J\ =\ 1.11X10^6 eV \tag{6.10}$$

Further transitions to lower energy states corresponding to higher quantum numbers p are not possible in the limit that the total energy in the electric field of the proton has been released as ionization energy and relativistic kinetic energy, the sum of which is given by Eq. (5.112). Using relativistic potential energy of a hydrino atom $H(1/p)$ of a given state p given by Eq. (5.112), the maximum value of p and the minimum radius are determined by equating Eq. (5.112) to Eq. (5.116):

$$\frac{(\alpha p)^2 m_{e0} c^2}{\sqrt{1-(\alpha p)^2}} = 1.77\ X\ 10^{-13} J\ =\ 1.11X10^6 eV \tag{6.11}$$

The lowest energy state of the hydrogen atom comprises the limiting ground state having a p quantum number p = 126 corresponding to a minimum radius of 1.651 X $10^{-13}$, 2/3 the size of the muonic hydrogen atom. Using Eq. (5.115), the energy for the cascade of a hydrogen atom to the final state of H(1/126) results in an energy release of $2\times10^5$ eV.

The universe predominately comprises dark matter whose identity is hydrino atoms which ultimately decay to gamma rays. Competing with the annihilation cycle of H atoms is a production cycle of the formation of blackholes that reach a critical mass density, the Planck mass density, and decay as gamma ray bursts as the predominant source of cosmic rays that seed the universe with protons and electrons to form H atoms. The H atom decay and production cycle drives the spacetime expansion-contraction cycle of the universe wherein the recycling of matter and energy in the universe occurs during the oscillatory cycle wherein matter converts to energy primarily by hydrogen atom decay wherein the proton and electron are annihilated to gamma rays via a hydrino pathway, and energy to matter conversion occurs by hydrogen atom production during gamma ray bursts (See H Electronic Decay to Proton Decay Driving Subsequent Nuclear Reactions section and the H Atom Decay and Production Cycle Drive the Spacetime Expansion-Contraction Cycle of the Universe section). The emission of the high energy gamma rays in the presence of hydrogen results in photoneutron production which may undergo neutron capture and beta decay of the resulting nucleus. The predicted decaying dark matter signatures of power and 511 keV gamma [2-7], neutral pion [8-9], and neutron capture emission [8, 10] match those of hydrogen atom decay from the high-p-state hydrino inventory comprising the dark matter. The characteristics, composition, and high energetics of cosmic rays in the absence of neutrino emission overturn long-held theory but match the signatures of H atom production [11]. The rates of production and annihilation of matter and energy match those required to complete the cycle over the period of oscillation of the universe [12-13].

## SPIN-NUCLEAR AND ORBITAL-NUCLEAR COUPLING OF HYDRINOS

The "trapped photon" given by Eq. (5.27) is a "standing electromagnetic wave" which actually is a circulating wave that propagates along each great circle current loop of the atomic orbital. The time-function factor, $k(t)$, for the "standing wave" is identical to the time-function factor of the atomic orbital in order to satisfy the boundary (phase) condition at the atomic orbital surface. Thus, the angular frequency of the "trapped photon" has to be identical to the angular frequency of the electron atomic orbital, $\omega_n$. Furthermore, the phase condition requires that the angular functions of the "trapped photon" have to be identical to the spherical harmonic angular functions of the electron atomic orbital.

Photons obey Maxwell's equations. At the two-dimensional surface of the atomic orbital containing a "trapped photon," the relationship between the photon's electric field and its two-dimensional charge density at the atomic orbital is:

$$\mathbf{n}\bullet\left(\mathbf{E}_1-\mathbf{E}_2\right)=\frac{\sigma}{\varepsilon_0} \tag{6.12}$$

Thus, the photon's electric field acts as surface charge. According to Eq. (6.12), the "photon standing wave" in the electron atomic orbital resonator cavity gives rise to a two-dimensional surface charge at the atomic orbital two-dimensional surface. The surface charge is given by Eq. (6.12) for a central field strength equal in magnitude to that of a central charge $pe$. This surface charge possesses the same angular velocity as the atomic orbital; thus, it is a current with a corresponding magnetic field. The rotational parameters of the surface current of the "photon standing wave" are given in the Rotational Parameters of the Electron (Angular Momentum, Rotational Energy, Moment of Inertia) section. The solution to Legendre's equation given by Eq. (1.66) is the maximum term of a series of solutions corresponding to the $m$ and $\ell$ values [14-15]. From Eq. (1.72), $\mathbf{L}$, the amplitude of the orbital angular momentum along the z-axis is

$$\mathbf{L}=\pm\hbar\sqrt{\frac{\ell}{\ell+1}}\mathbf{i}_\mathbf{z} \tag{6.13}$$

Therefore, from Eq. (2.65), the corresponding magnetic moment is:

$$\mu=\pm\frac{e\hbar}{2m_e}\sqrt{\frac{\ell}{\ell+1}}\mathbf{i}_\mathbf{z}=\pm\mu_B\sqrt{\frac{\ell}{\ell+1}}\mathbf{i}_\mathbf{z} \tag{6.14}$$

where $\mu_B$ is the Bohr magneton. The magnetic moment gives rise to a magnetic field at the nucleus, which superimposes that due to spin. Thus, from Eqs. (2.215) and (6.14), the central force after the derivations in the Spin-Nuclear Coupling (Hyperfine Structure) section is:

$$\mathbf{F}_{mag}=\pm e\alpha c\frac{\mu_0}{r^3}\ \mu_P\sqrt{\frac{3}{4}}\left(\frac{1}{2}+\sqrt{\frac{\ell}{\ell+1}}\right) \tag{6.15}$$

where the plus corresponds to antiparallel alignment of the magnetic moments of the electron and proton, and the minus corresponds to parallel alignment. The outward centrifugal force (Eq. (1.241)) on the electron is balanced by the electric force (Eq. (1.242)) and the magnetic force given by Eq. (6.15)

$$\frac{m_e v^2}{r}=\frac{pe^2}{4\pi\varepsilon_0 r^2}-\frac{\hbar^2}{m_P r^3}\pm pe\alpha c\frac{\mu_0}{r^3}\ \mu_P\sqrt{\frac{3}{4}}\left(\frac{1}{2}+\sqrt{\frac{\ell}{\ell+1}}\right) \tag{6.16}$$

where the central field of the hydrino atom has a magnitude that is equivalent to $p$ times that of the "ground" state ($n=p=1$) hydrogen atom and $m_P$ is the mass of the proton. Using Eq. (1.35),

$$\frac{\hbar^2}{m_e r^3} = \frac{pe^2}{4\pi\varepsilon_0 r^2} - \frac{\hbar^2}{m_P r^3} \pm pe\alpha c \frac{\mu_0}{r^3}\ \mu_P \sqrt{\frac{3}{4}}\left(\frac{1}{2} + \sqrt{\frac{\ell}{\ell+1}}\right) \tag{6.17}$$

$$r = \frac{a_H}{p} \pm \frac{4\pi\alpha\ \mu_P}{ec}\sqrt{\frac{3}{4}}\left(\frac{1}{2} + \sqrt{\frac{\ell}{\ell+1}}\right) \tag{6.18}$$

where $a_H$ is the radius of the hydrogen atom and the plus corresponds to parallel alignment of the magnetic moments of the electron and proton, and the minus corresponds to antiparallel alignment.

## ENERGY CALCULATIONS

The magnetic energy $\Delta E_{magdipole}$ to flip the orientation of the proton's magnetic moment, $\mu_P$, from parallel to antiparallel to the direction of the magnetic flux $\mathbf{B}_s$ due to electron spin and the magnetic flux $\mathbf{B}_o$ due to the orbital angular momentum of the electron (180° rotation of the magnet moment vector) given by Eqs. (1.168), (2.222), (2.210), and (6.14) is:

$$\Delta E_{magdipole} = -\frac{p\mu_0 e\hbar}{m_e}\mu_P\sqrt{\frac{3}{4}}\left(\frac{1}{2} + \sqrt{\frac{\ell}{\ell+1}}\right)\left(\frac{1}{r_+^3} + \frac{1}{r_-^3}\right) = -2p\mu_0\mu_B\mu_P\sqrt{\frac{3}{4}}\left(\frac{1}{2} + \sqrt{\frac{\ell}{\ell+1}}\right)\left(\frac{1}{r_+^3} + \frac{1}{r_-^3}\right) \tag{6.19}$$

where the Bohr magneton, $\mu_B$, is given by Eq. (1.131), the radius of the hydrino atom is $\frac{a_H}{p}$, and the central field of the hydrino atom has a magnitude that is equivalent to $p$ times that of the "ground" state ($n = p = 1$) hydrogen atom.

The change in the electric energy of the electron due to the slight shift of the radius of the electron due to spin-nuclear and orbital-nuclear interactions is given by the difference between the electric energies associated with the two possible orientations of the magnetic moment of the electron with respect to the magnetic moment of the proton, parallel versus antiparallel. The electric energy is given by the substitution of the corresponding radius given by Eq. (6.18) into Eq. (1.264) where $Z = p$. The change in electric energy for the flip from antiparallel to parallel alignment, $\Delta E_{ele}^{S/N\ O/N}$, is:

$$\Delta E_{ele}^{S/N\ O/N} = \frac{-pe^2}{8\pi\varepsilon_0}\left[\frac{1}{r_+} - \frac{1}{r_-}\right] \tag{6.20}$$

In addition, the interaction of the magnetic moments of the electron and proton increases the magnetic energy of the electron given by Eq. (2.224). The change in the magnetic energy of the electron $\Delta E_{mag}^{S/N\ O/N}$ due to the slight shift of the radius of the electron due to spin-nuclear and orbital-nuclear interactions is:

$$\begin{aligned}\Delta E_{mag}^{S/N\ O/N} &= -\left(1 + \left(\frac{2}{3}\right)^2 + \alpha\left(\cos\frac{\pi}{3}\right)^2\right)\frac{\pi\mu_0 e^2\hbar^2}{m_e^2}\left(\frac{1}{r_+^3} - \frac{1}{r_-^3}\right) \\ &= -\left(1 + \left(\frac{2}{3}\right)^2 + \frac{\alpha}{4}\right)4\pi\mu_0\mu_B^2\left(\frac{1}{r_+^3} - \frac{1}{r_-^3}\right)\end{aligned} \tag{6.21}$$

The orbital rotational energy arises from a spin function (spin angular momentum) modulated by a spherical harmonic angular function (orbital angular momentum). The amplitude of the orbital rotational energy $E_{rotational\ \text{orbital}}$ is:

$$E_{rotational\ orbital} = \frac{\hbar^2}{2m_e r_n^2}\left[\frac{\ell}{\ell+1}\right] \tag{6.22}$$

However, the time-averaged mechanical angular momentum and rotational energy associated with the traveling charge-density wave on the atomic orbital is zero:

$$\left\langle L_{z\ orbital}\right\rangle = 0 \tag{6.23}$$

$$\left\langle E_{rotational\ orbital}\right\rangle = 0 \tag{6.24}$$

Thus, a term corresponding to Eq. (6.22) was not added to Eq. (6.21). Only the coupling of the dynamic angular momentum to the radiative reaction need be considered as given in Eqs. (6.15) and (6.19).

The total energy of the transition from antiparallel to parallel alignment due to spin-nuclear and orbital-nuclear interactions, $\Delta E_{total}^{S/N\ O/N}$, is given as the sum of Eqs. (6.19-6.21):

$$\Delta E_{total}^{S/N\ O/N} = \Delta E_{magdipole} + \Delta E_{ele}^{S/N\ O/N} + \Delta E_{mag}^{S/N\ O/N} \tag{6.25}$$

$$\begin{aligned}\Delta E_{total}^{S/N\ O/N} &= -2p\mu_0\mu_B\mu_P\sqrt{\frac{3}{4}}\left(\frac{1}{2} + \sqrt{\frac{\ell}{\ell+1}}\right)\left(\frac{1}{r_+^3} + \frac{1}{r_-^3}\right) \\ &\quad -\frac{pe^2}{8\pi\varepsilon_0}\left[\frac{1}{r_+} - \frac{1}{r_-}\right] - \left(1 + \left(\frac{2}{3}\right)^2 + \frac{\alpha}{4}\right)4\pi\mu_0\mu_B^2\left(\frac{1}{r_+^3} - \frac{1}{r_-^3}\right)\end{aligned} \tag{6.26}$$

For the case that $\ell = 0$, the hydrino hyperfine structure radius and energy $\Delta E_{total}^{S/N}$ given by Eqs. (2.221) and (2.225) respectively,

are the same as those of ordinary hydrogen with $p = 1$ in Eqs. (6.18) and (6.27):

$$\Delta E_{total}^{S/N} = -p\mu_0\mu_B\mu_P\sqrt{\frac{3}{4}}\left(\frac{1}{r_+^3}+\frac{1}{r_-^3}\right)-\frac{pe^2}{8\pi\varepsilon_0}\left[\frac{1}{r_+}-\frac{1}{r_-}\right]-\left(1+\left(\frac{2}{3}\right)^2+\frac{\alpha}{4}\right)4\pi\mu_0\mu_B^2\left(\frac{1}{r_+^3}-\frac{1}{r_-^3}\right) \tag{6.27}$$

The frequency, $f$, can be determined from the energy using the Planck relationship, Eq. (2.148).

$$f = \frac{-\Delta E_{total}^{\text{S/N O/N}}}{h} \tag{6.28}$$

From Eqs. (6.18), (6.26), (6.27), and the Planck relationship, Eq. (2.148), the energy, the wavelength, and the frequency corresponding to the spin-nuclear and orbital-nuclear coupling energy of the hydrino atom with the lower energy state quantum numbers $p$ and $\ell$ and with the radius $\frac{a_H}{p}$ are given in Table 6.1.

**Table 6.1.** The spin-nuclear and orbital-nuclear coupling energies of the hydrino atom with the lower energy state quantum numbers $p$ and $\ell$ and with the radius $\frac{a_H}{p}$.

| $p$ | $\ell$ | Energy ($J\ X\ 10^{-23}$) | Wavelength ($cm$) | Wave Number ($cm^{-1}$) | Frequency ($GHz$) |
|---|---|---|---|---|---|
| 1 | 0 | 0.094117 | 21.106 | 0.047380 | 1.4204 |
| 2 | 0 | 2.2736 | 0.87369 | 1.1446 | 34.314 |
| 2 | 1 | 5.4890 | 0.36189 | 2.7633 | 82.840 |
| 3 | 0 | 12.806 | 0.15512 | 6.4466 | 193.27 |
| 3 | 1 | 30.916 | 0.064253 | 15.564 | 466.58 |
| 3 | 2 | 33.718 | 0.058914 | 16.974 | 508.87 |
| 4 | 0 | 42.520 | 0.046718 | 21.405 | 641.71 |
| 4 | 1 | 102.65 | 0.019351 | 51.677 | 1549.2 |
| 4 | 2 | 111.96 | 0.017743 | 56.360 | 1689.6 |
| 4 | 3 | 116.17 | 0.017100 | 58.480 | 1753.2 |
| 5 | 0 | 106.81 | 0.018598 | 53.769 | 1611.9 |
| 5 | 1 | 257.86 | 0.0077036 | 129.81 | 3891.6 |
| 5 | 2 | 281.23 | 0.0070635 | 141.57 | 4244.2 |
| 5 | 3 | 291.81 | 0.0068074 | 146.90 | 4403.9 |
| 5 | 4 | 297.87 | 0.0066688 | 149.95 | 4495.5 |

## A COEFFICIENT

An estimate of the transition probability for magnetic multipoles is given by Eq. (16.105) of Jackson [16]. For a magnetic dipole $\ell = 1$, and Eq. (16.105) of Jackson is:

$$\frac{1}{\tau_M} \cong \left(\frac{g}{mc}\right)^2\left(\frac{\hbar e^2}{c}\right)\frac{\pi}{4}k^2\omega \tag{6.29}$$

where $\tau_M$ is the mean life of the magnetic multipole. Substitution of:

$$k = \frac{\omega}{c} \tag{6.30}$$

into Eq. (6.29) gives

$$\frac{1}{\tau_M} \cong \left(\frac{g}{mc}\right)^2\left(\frac{\hbar e^2}{c}\right)\frac{\pi}{4}\frac{\omega^3}{c^2} \tag{6.31}$$

From Eq. (6.31), the transition probability is proportional to the frequency cubed. The experimental A coefficient for hydrogen $H(n=1)$ [17] is

$$A = 2.87\ X\ 10^{-15}\ \text{sec}^{-1} \tag{6.32}$$

The frequencies for the spin/nuclear hyperfine transition of hydrogen $H(n=1)$ and hydrino $H(n=1/2)$ are given in Table 6.1. The A coefficient for hydrino $H(n=1/2)$ is given by Eq. (6.31) and Eq. (6.32) and the frequencies of Table 6.1.

$$A_{H(n=1/2)} = A_{H(n=1)}\left(\frac{\omega_{H(n=1/2)}}{\omega_{H(n=1)}}\right)^3 = 2.87\ X\ 10^{-15}\ \left(\frac{34.31}{1.420}\right)^3\ \text{sec}^{-1} = 4.05\ X\ 10^{-11}\ \text{sec}^{-1} \tag{6.33}$$

## INTENSITY OF SPIN-NUCLEAR AND ORBITAL-NUCLEAR COUPLING TRANSITIONS OF HYDRINOS

The intensity, $I$, of spin-nuclear and orbital-nuclear coupling transitions of hydrinos can be calculated from the column density of hydrino atoms, $N(H)$, and the A coefficient, $A_{ul}$. The column density is given by the product of the number of hydrino atoms per unit volume, $n_H$, and the path length, $\ell$, which is calculated in steradians from its integral.

$$I = \frac{1}{4\pi} A_{ul} N(H) = \frac{1}{4\pi} A_{ul} n_H \ell \tag{6.34}$$

wherein $A_{ul}$ is given by Eq. (6.33). The number of hydrino atoms per unit volume, $n_H$, can be estimated from the experimental results of the integrated continuum emission for a selected transition from a celestial source. The number of electronic transitions per atom per second, $k_1$ (Eq. (5.105)), estimated to be equivalent to the number of photons per atom per second ( $A_{ul}$ (Eq. (6.34)) for the hydrino transition). Equating intensities of integrated photon flux (Eq. (6.34)) and the rate of the disproportionation reaction, $r_{m,m',p}$ Eq. (5.106), gives:

$$I = \frac{1}{4\pi} A_{ul} N(H) = \frac{1}{\sqrt{2}} n_H \left(\frac{a_H}{p}\right)^2 \sqrt{\frac{3kT}{m_H}} N(H) \tag{6.35}$$

where $N(H) = n_H \ell$ is the column density and $g_{m,p} = 1$ (the result is equivalent to Förster's theory for the efficiencies of dipole-dipole resonant energy transfers). $N(H)$, the column density of hydrino atoms, $H\left(\frac{a_H}{p}\right)$, can be calculated along the selected sight-line and substituted into Eq. (6.34) to give the intensity of the spin-nuclear and orbital-nuclear coupling transitions of hydrinos as a function of the path length, $\ell$, which is calculated in steradians from its integral.

## REFERENCES


1. H. A. Haus, "On the radiation from point charges," Am. J. Phys., 54, (1986), pp. 1126-1129.
2. A. C. Vincent, P. Martin, J. M. Cline, "Interacting dark matter contribution to the Galactic 511 keV gamma ray emission: constraining the morphology with INTEGRAL/SPI observations", https://arxiv.org/pdf/1201.0997.
3. G. De Cesare, "Searching for the 511 keV annihilation line from galactic compact objects with the IBIS gamma ray telescope", A&A 531, A56 (2011) DOI: 10.1051/0004-6361/201116516, https://www.aanda.org/articles/aa/pdf/2011/07/aa16516-11.pdf.
4. J. Knodlseder, et al., "The all-sky distribution of 511 keV electron-positron annihilation emission", Astronomy & Astrophysics manuscript no. 2063, November 7, 2018, https://arxiv.org/pdf/astro-ph/0506026.
5. J. Knodlseder, et al., "The all-sky distribution of 511 keV electron-positron annihilation emission", astro-ph/0506026, Masaki Mori, ICRR Group Internal Seminar, June 20, 2005,https://www.icrr.u-tokyo.ac.jp/~morim/Presentations/INTEGRAL511keV.pdf.
6. N. Prantzos, C. Boehm, A. M. Bykov, et al., "The 511 keV emission from positron annihilation in the Galaxy", (2010), https://arxiv.org/abs/1009.4620.
7. N. Prantzos, C. Boehm, A. M. Bykov, et al., "The 511 keV emission from positron annihilation in the Galaxy", Reviews of Modern Physics, Vol. 83, July (2011), pp. 1001–1056.
8. R. Yang, E. Kafexhiu1, F. Aharonian, "Exploring the shape of the γ-ray spectrum around the "$\pi^0$-bump", A&A, Volume 615, July (2018), A108, https://doi.org/10.1051/0004-6361/201730908, https://www.aanda.org/articles/aa/pdf/2018/07/aa30908-17.pdf.
9. National Aeronautics and Space Administration, Goddard Space Flight Center, Fermi Gamma-ray Space Telescope, "Overview of GRB spectral analysis", https://fermi.gsfc.nasa.gov/ssc/data/analysis/documentation/Cicerone/Cicerone_GRBs/Overview_GRB_Spec_Anal.html.
10. R. Ramaty, R. J. Murphy, C. D. Dermer, "On the origin of the pion-decay radiation in the 1982 June 3 solar flare", The Astrophysical Journal, 316:L41-L44,1987 May 1. https://articles.adsabs.harvard.edu/cgi-bin/nph-iarticle_query?1987ApJ...316L..41R&defaultprint=YES&filetype=.pdf.
11. IceCube Collaboration. "An absence of neutrinos associated with cosmic-ray acceleration in γ-ray bursts", Nature. Vol. 484, (2012), pp. 351–354, https://doi.org/10.1038/nature11068.
12. G. Ghisellini, G. Ghirlanda, "Proton–synchrotron as the radiation mechanism of the prompt emission of gamma-ray bursts?", A&A, Vol. 636, April (2020), A82, https://doi.org/10.1051/0004-6361/201937244, https://www.aanda.org/articles/aa/full_html/2020/04/aa37244-19/aa37244-19.html.
13. D. Kazanas, D. C. Ellison, "Proton acceleration in γ-ray bursts", Advances in Space Research, Vol. 6, Issue 4, (1986), pp. 81-84, ISSN 0273-1177, https://doi.org/10.1016/0273-1177(86)90243-7, https://www.sciencedirect.com/science/article/abs/pii/0273117786902437.
14. D. A. McQuarrie, *Quantum Chemistry*, University Science Books, Mill Valley, CA, (1983), pp. 206-221.
15. L. Pauling, E. Wilson, *Introduction to Quantum Mechanics with Applications to Chemistry*, McGraw-Hill Book Company, New York, (1935), pp. 118-121.

16. J. D. Jackson, *Classical Electrodynamics*, Second Edition, John Wiley & Sons, New York, (1975), pp. 758-760.
17. C. W. Allen, *Astrophysical Quantities*, 3rd Edition, (1973), University of London, The Athlone Press, p. 79.

# Chapter 7

# TWO-ELECTRON ATOMS

As is the case for one-electron atoms shown in the corresponding section, two-electron atoms can also be solved exactly. Two-electron atoms comprise two indistinguishable electrons bound to a nucleus of $+Z$. Each electron experiences a centrifugal force, and the balancing centripetal force (on each electron) is produced by the electric force between the electron and the nucleus and the magnetic force between the two electrons causing the electrons to pair.

## DETERMINATION OF ATOMIC ORBITAL RADII

As shown in the One-Electron Atom section, bound electrons are described by a charge-density (mass-density) function, which is the product of a radial delta function ( $f(r)=\delta(r-r_n)$ ), two angular functions (spherical harmonic functions), and a time harmonic function. Thus, an electron is a two-dimensional spherical current-density surface that can exist in a bound state at only specified distances from the nucleus. More explicitly, the uniform current-density function $Y_0^0(\theta,\phi)$ (Eqs. (1.27-1.29)) called the electron atomic orbital (shown in Figure 1.22) that gives rise to the spin of the electron is generated from two current-vector fields (CVFs). Each CVF comprises a continuum of correlated *orthogonal great circle current-density elements (one dimensional "current loops")*. The current pattern comprising each CVF is generated over a half-sphere surface by a set of rotations of two orthogonal great circle current loops that serve as basis elements about each of the $\left(-\mathbf{i}_x,\mathbf{i}_y,0\mathbf{i}_z\right)$ and $\left(-\frac{1}{\sqrt{2}}\mathbf{i}_x,\frac{1}{\sqrt{2}}\mathbf{i}_y,\mathbf{i}_z\right)$-axis; the span being $\pi$ radians. Then, the two CVFs are convoluted, and the result is normalized to exactly generate the *continuous* uniform electron current density function $Y_0^0(\theta,\phi)$ covering a spherical shell and having the three angular momentum components of $\mathbf{L}_{xy}=+/-\frac{\hbar}{4}$ and $\mathbf{L}_z=\frac{\hbar}{2}$ (Figure 1.23)[1].

Each one-electron atomic orbital is a static two-dimensional spherical shell of moving negative charge ( $\text{total charge}=-e$ ) of zero thickness at a distance $r_n$ from the nucleus ( $\text{charge}=+Ze$ ). It is well known that the field of a spherical shell of charge is zero inside the shell and that of a point charge at the origin outside the shell [1] (See Figure 1.32). Thus, for a nucleus of charge $Z$, the force balance equation for the electron atomic orbital is obtained by equating the forces on the mass and charge densities. The centrifugal force of each electron is given by[2]

$$\mathbf{F}_{centrifugal}=\frac{m_e}{4\pi r_n^{\,2}}\frac{\mathbf{v}_n^{\,2}}{r_n} \tag{7.1}$$

where $r_n$ is the radius of electron $n$ which has velocity $\mathbf{v}_n$. In order to be nonradiative, the velocity for every point on the atomic orbital is given by Eq. (1.35).

$$\mathbf{v}_n=\frac{\hbar}{m_e r_n} \tag{7.2}$$

Helium can be formed by the binding of two electrons simultaneously to $He^{2+}$. It can also be formed by the binding of an electron to $He^{+}$. The same boundary condition, that helium has no spin, applies in both cases. The forces must be consistent with the binding of both electrons at the same radius such that their currents corresponding to spin are identical mirror images

[1] $+/-$ designates both the positive and negative vector directions along an axis in the xy-plane.

[2] In this section, $n=1$ *or* $2$ for electron one and electron two, respectively, not to be confused with the previous use of $n$ as the principal quantum number.

and consequently identically cancel. This implies that the forces at balance are equivalent for the two electrons. As an approach to the helium solution using these constraints, now consider electron 1 initially at $r = r_1 = \frac{a_0}{Z}$ (the radius of the one-electron atom of charge $Z$ given in the One-Electron Atom section where $a_0 = \frac{4\pi\varepsilon_0\hbar^2}{e^2 m_e}$ and the spin-nuclear interaction corresponding to the electron reduced mass (Eq. (1.255)) is not used here since the electrons have no field at the nucleus upon pairing) and electron 2 initially at $r_n = \infty$. Each electron can be treated as $-e$ charge at the nucleus with $\mathbf{E} = \frac{-e}{4\pi\varepsilon_0 r^2}$ for $r > r_n$ and $\mathbf{E} = 0$ for $r < r_n$ where $r_n$ is the radius of the electron atomic orbital. The centripetal force is the electric force, $\mathbf{F}_{ele}$, between the electron and the nucleus. Thus, the electric force between electron 2 and the nucleus is:

$$\mathbf{F}_{ele(electron\ 2)} = \frac{(Z-1)e^2}{4\pi\varepsilon_0 r_2^2} \tag{7.3}$$

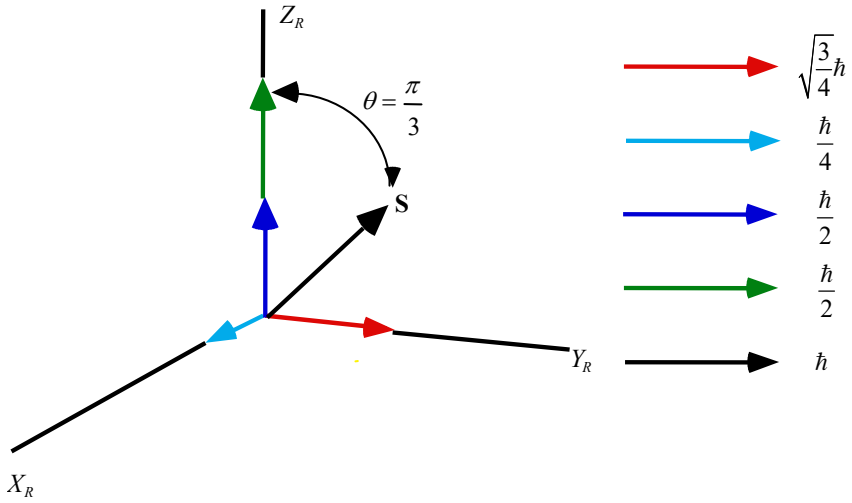
where $\varepsilon_0$ is the permittivity of free-space. The second centripetal force, $\mathbf{F}_{mag}$, on the electron 2 (initially at infinity) from electron 1 (at $r_1$) is the magnetic force. Each infinitesimal point (mass or charge-density element) of each atomic orbital moves on a great circle, and each point has the charge density $\frac{e}{4\pi r_n^2}$. Due to the relative motion of the charge-density elements of each electron, a radiation reaction force arises between the two electrons. This force given in Sections 6.6, 12.10, and 17.3 of Jackson [2] achieves the condition that the sum of the mechanical momentum and electromagnetic momentum is conserved[3]. The magnetic central force is derived from the Lorentz force that is relativistically corrected.

The magnetic force is derived by first determining the interaction of the two electrons due to the field of the outer electron 2 acting on the magnetic moments of electron 1 and vice versa. Insight to the behavior is given by considering the physics of a single bound electron in an externally applied uniform magnetic field. As shown in the Resonant Precession of the Spin-1/2-Current-Density Function Gives Rise to the Bohr Magneton section, the angular momentum of the atomic orbital in the magnetic field of an external applied field $B\mathbf{i}_z$ comprises the static $\frac{\hbar}{2}$ projection on the z-axis (Eq. (1.128)) and the $\frac{\hbar}{4}$ vector component in the xy-plane (Eq. (1.127)) that precesses about the z-axis at the Larmor frequency, $\omega_L$. A resonant excitation of the Larmor precession frequency gives rise to a trapped photon with $\hbar$ of angular momentum along the precessing $\mathbf{S}$-axis. As shown in Box 1.1, the photon standing wave is phase-matched to a spherical harmonic source current, a spherical harmonic dipole $Y_\ell^m(\theta,\phi) = \sin\theta$ with respect to the $\mathbf{S}$-axis. The dipole spins about the $\mathbf{S}$-axis at the angular velocity given by Eq. (1.36).

In the coordinate system rotating at the Larmor frequency (denoted by the axes labeled $X_R$, $Y_R$, and $Z_R$ in Figure 7.1), the $X_R$-component of magnitude $\frac{\hbar}{4}$ and $\mathbf{S}$ of magnitude $\hbar$ are stationary. The $\frac{\hbar}{4}$ angular momentum along $X_R$ with a corresponding magnetic moment of $\frac{\mu_B}{4}$ (Eq. (28) of Box 1.1) causes $\mathbf{S}$ to rotate in the $Y_R\,Z_R$-plane to an angle of $\theta = \frac{\pi}{3}$ such that the torques due to the $Z_R$-component of $\frac{\hbar}{2}$ and the orthogonal $X_R$-component of $\frac{\hbar}{4}$ are balanced. Then the $Z_R$-component due to $\mathbf{S}$ is $\pm\hbar\cos\frac{\pi}{3} = \pm\frac{\hbar}{2}$, and the $Y_R$-component of $\mathbf{S}$ is $\pm\hbar\sin\frac{\pi}{3} = \pm\sqrt{\frac{3}{4}}\hbar$.

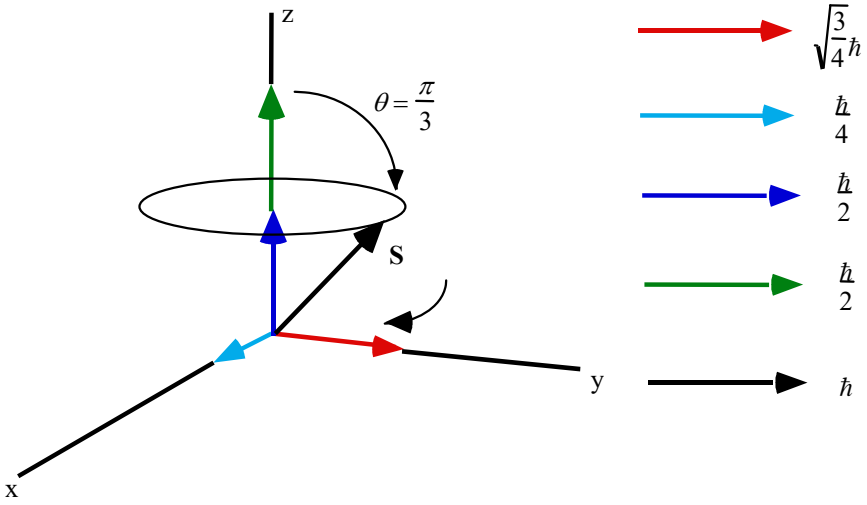
[3] The angular momentum of the two electrons cancels with pairing, and the conserved angular momentum is carried with the $\hbar$ of angular momentum of the photon corresponding to the radiation reaction force and energy. The energy of the Coulombic field is also conserved with the emission of photons of quantized energy wherein the radial acceleration during binding gives rise to the radiation as given in the Excited States of the One-Electron Atom (Quantization) section.

**Figure 7.1.** The angular momentum components of the atomic orbital and $\mathbf{S}$ in the rotating coordinate system $X_R$, $Y_R$, and $Z_R$ that precesses at the Larmor frequency about $Z_R$ such that the vectors are stationary.




As shown in Figure 7.2, $\mathbf{S}$ forms a cone in time in the nonrotating laboratory frame with an angular momentum of $\hbar$ that is the source of the known magnetic moment of a Bohr magneton (Eq. (2.65)) as shown in the Magnetic Parameters of the Electron (Bohr Magneton) section. The projection of this angular momentum onto the z-axis of $\frac{\hbar}{2}$ adds to the z-axis component before the magnetic field was applied to give a total of $\hbar$. Thus, in the absence of a resonant precession, the z-component of the angular momentum is $\frac{\hbar}{2}$, but the excitation of the precessing $\mathbf{S}$ component gives $\hbar$—twice the angular momentum on the z-axis.

**Figure 7.2.** The angular momentum components of the atomic orbital and $\mathbf{S}$ in the stationary coordinate system. $\mathbf{S}$ and the components in the xy-plane precess at the Larmor frequency about the z-axis.




In summary, since the vector $\mathbf{S}$ that precesses about the z-axis at an angle of $\theta = \frac{\pi}{3}$ and an angle of $\phi = \frac{\pi}{2}$ with respect to $\mathbf{L}_{xy}$ given by Eq. (1.127) and has a magnitude of $\hbar$, the $\mathbf{S}$ projections in the $X_R$ $Y_R$-plane and along the $Z_R$-axis (Eqs. (1.129-1.130)) are

$$\mathbf{S}_{\perp} = \hbar \sin\frac{\pi}{3} = \pm\sqrt{\frac{3}{4}}\hbar\ \mathbf{i}_{Y_R} \tag{7.4}$$

$$\mathbf{S}_{\parallel} = \pm\hbar\cos\frac{\pi}{3} = \pm\frac{\hbar}{2}\ \mathbf{i}_{Z_R} \tag{7.5}$$

The plus or minus sign of Eqs. (7.4) and (7.5) corresponds to the two possible vector orientations.

Consider the case that the external field is due to electron 2 on the moments of electron 1 and vice versa. In the limit, the magnetic moments of electrons 1 and 2 will cancel as they spin pair to form an energy minimum. In this case, the radii will be equal (i.e. $r_1 = r_2$). Cases other than the bound case correspond to excited states, which are solved for helium in the Excited States of Helium section. These states correspond to the atom having trapped photons. The central magnetic force to determine the bound state with $r_1 = r_2$ is derived by first determining the magnetic moments and fields of the interacting electrons from the corresponding angular momenta due to the trapped photons.

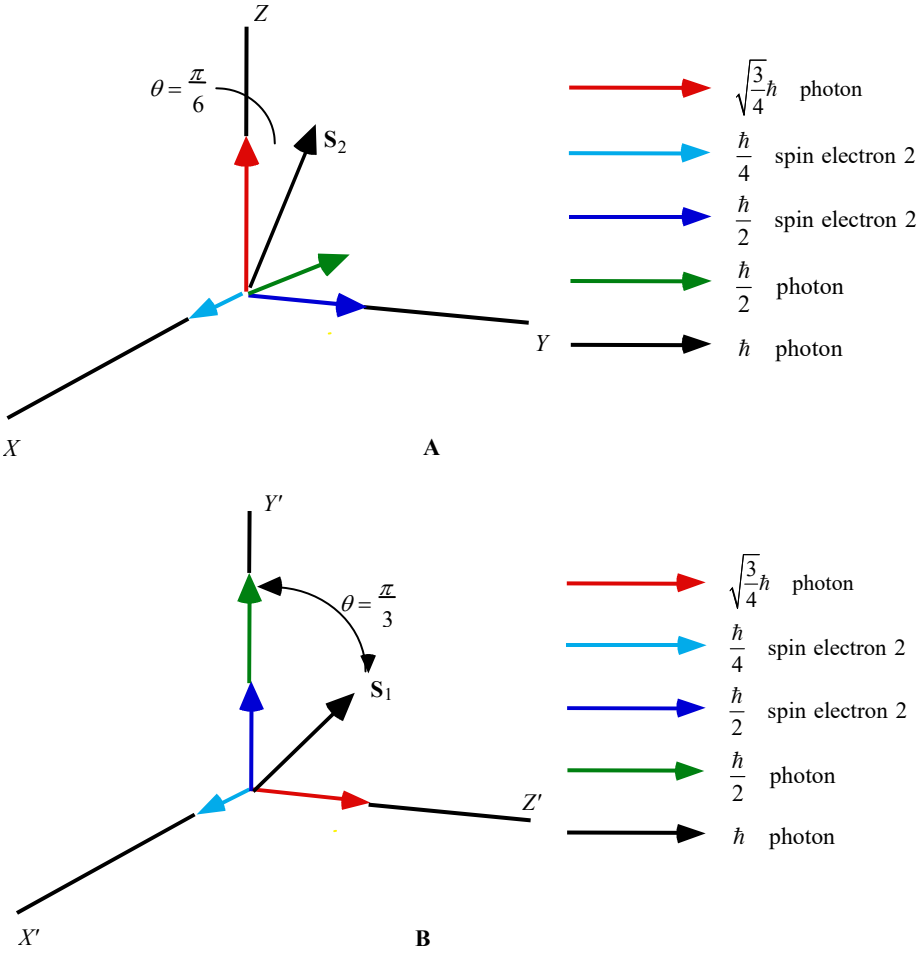
Unlike the external-applied-field case, each of the two interacting electrons have two orthogonal components of angular momentum. Each has $\frac{\hbar}{2}$ along the principal-axis (Eq. (1.128)) and $\frac{\hbar}{4}$ along an axis in the transverse-plane (Eq. (1.127)). For each electron, torque balance is also achieved when a photon standing wave is phase-matched to a spherical harmonic source current, a spherical harmonic dipole $Y_\ell^m(\theta,\phi) = \sin\theta$ with respect to the $\mathbf{S}$-axis. The dipole spins about the $\mathbf{S}$-axis at the angular velocity given by Eq. (1.36) as in the external-applied-field case, but the orientations are as shown in Figures 7.3A and 7.3B rather than that shown in Figures 7.1 and 7.2.

In the stationary coordinate system of electron 2 (denoted by the axes labeled $X$, $Y$, and $Z$ in Figure 7.3A), the $\frac{\hbar}{4}$ of intrinsic angular momentum is along $X$, the $\frac{\hbar}{2}$ of intrinsic angular momentum is along $Y$, and the photon angular momentum vector $\mathbf{S}_2$ of magnitude $\hbar$ is in the $XZ$-plane at an angle of $\theta = \frac{\pi}{6}$ relative to the $Z$-axis. The $Z$-axis projection of $\mathbf{S}_2$ is $\sqrt{\frac{3}{4}}\hbar$, and the $X$-axis projection of $\mathbf{S}_2$ is $-\frac{\hbar}{2}$.

In the stationary coordinate system of electron 1 (denoted by the axes labeled $X'$, $Y'$, and $Z'$ in Figure 7.3B), the $\frac{\hbar}{4}$ of intrinsic angular momentum is along $X'$, the $\frac{\hbar}{2}$ of intrinsic angular momentum is along $Y'$, and the photon angular momentum vector $\mathbf{S}_1$ of magnitude $\hbar$ is in the $Y'Z'$-plane at an angle of $\theta = \frac{\pi}{3}$ relative to the $Y'$-axis. The $Z'$-axis projection of $\mathbf{S}_1$ is $\sqrt{\frac{3}{4}}\hbar$, and the $Y'$-axis projection of $\mathbf{S}_1$ is $\frac{\hbar}{2}$.

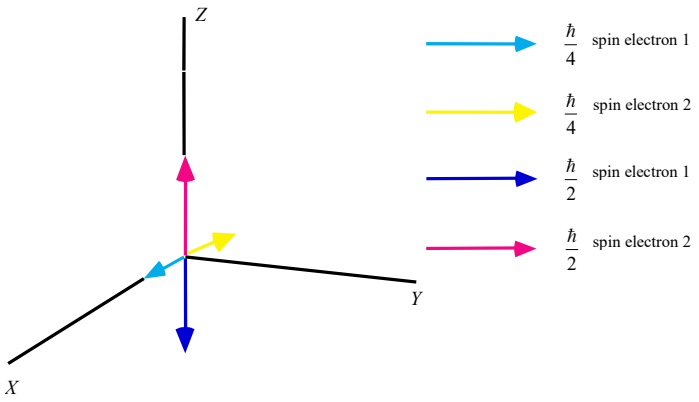
The torques from the corresponding magnetic moments given by Eq. (2.65) are balanced in the absence of Larmor precession for the angular momentum projections of electron 2 shown in Figure 7.3A relative to those of electron 1 shown in Figure 7.3B. The photonic $-\frac{\hbar}{2}$ $X$-axis projection of $\mathbf{S}_2$ with a corresponding magnetic moment of $-\frac{\mu_B}{2}$ cancels the superposition of the $\frac{\hbar}{4}$ of intrinsic angular momentum of electrons 1 and 2 along $X'$ and $X$, respectively, each with a corresponding magnetic moment of $\frac{\mu_B}{4}$ (Eq. (2.65)). The $\frac{\hbar}{2}$ of intrinsic angular momentum of electron 2 along $Y$ gives rise to a magnetic field corresponding to $\frac{\mu_B}{2}$ in the direction of the $\sqrt{\frac{3}{4}}\hbar$ $Z'$-axis projection of $\mathbf{S}_1$ of electron 1. The $\frac{\hbar}{2}$ of intrinsic angular momentum of electron 1 along $Y'$ and the $Y'$-axis projection of $\mathbf{S}_1$ of $\frac{\hbar}{2}$ gives rise to a magnetic field corresponding to $\mu_B$ in the direction of the $\sqrt{\frac{3}{4}}\hbar$ $Z$-axis projection of $\mathbf{S}_2$ of electron 2.

**Figure 7.3.** The relative angular momentum components of electron 1 and electron 2 to determine the magnetic interactions and the central magnetic force. (A) The atomic orbital and $\mathbf{s}_2$ of electron 2 in the stationary coordinate system $X,Y,Z$ that is designated the unprimed spherical coordinate system relative to the $Z$-axis as shown. The photon angular momentum vector $\mathbf{s}_2$ of magnitude $\hbar$ is in the $XZ$-plane at an angle of $\theta = \frac{\pi}{6}$ relative to the $Z$-axis. (B) The angular momentum components of the atomic orbital and $\mathbf{s}_1$ of electron 1 in the stationary coordinate system $X',Y',Z'$ that is designated the primed spherical coordinate system relative to the $Z'$-axis as shown. The photon angular momentum vector $\mathbf{s}_1$ of magnitude $\hbar$ is in the $Y'Z'$-plane at an angle of $\theta = \frac{\pi}{3}$ relative to the $Y'$-axis.




When the electrons pair, the photon is emitted as the corresponding excited state decays and the orientation of the magnetic moments of electron 1 relative to those of electron 2 rotate as shown in Figure 7.4 compared to Figures 7.3A and 7.3B. In the paired orientation, the angular momenta and the corresponding magnetic fields identically cancel.

**Figure 7.4.** The angular momentum components of the superimposed atomic orbitals of electron 1 and 2 in the stationary coordinate system *X,Y,Z* when binding occurs and the magnetic moments cancel.




The magnetic central force is due to the interaction of the magnetic field of the electron 2 and the current dipole of the photon at the radius of electron 1 and vice versa. Considering the angular momentum vectors given in Figures 7.3A and 7.3B, the magnetostatic magnetic flux of electron 2 and electron 1 corresponding to $\frac{\mu_B}{2}$ and $\mu_B$, respectively, follow from Eqs. (1.132) and (1.133) and after McQuarrie [3]:

$$\mathbf{B} = \frac{\mu_0 e\hbar}{2m_e r_2^3}(\mathbf{i}_{r'}\cos\theta - \mathbf{i}_{\theta'}\sin\theta) \tag{7.6}$$

$$\mathbf{B} = \frac{\mu_0 e\hbar}{2m_e r^3}(\mathbf{i}_r 2\cos\theta + \mathbf{i}_\theta \sin\theta) \tag{7.7}$$

where $\mu_0$ is the permeability of free-space ($4\pi\ X\ 10^{-7}\ N/A^2$) and the coordinates of the magnetic field due to electron 2 acting on the magnetic moments of electron 1 is designated as the primed system and the magnetic field of electron 1 acting on the magnetic moments of electron 2 is designated as the unprimed system. It follows from Eq. (1.131), the relationship for the Bohr magneton, and relationship between the magnetic dipole field and the magnetic moment $\mathbf{m}$ [4] that Eqs. (1.132) and (1.137) are the equations for the magnetic field due to a magnetic moment of one half a Bohr magneton, $\mathbf{m} = \frac{\mu_B}{2}\mathbf{i}_\mathbf{z}$ and one Bohr magneton, $\mathbf{m} = \mu_B \mathbf{i}_\mathbf{z}$, respectively, where $\mathbf{i}_\mathbf{z} = \mathbf{i}_\mathbf{r}\cos\theta - \mathbf{i}_\theta \sin\theta$. In each case, the spherical harmonic dipole $Y_\ell^m(\theta,\phi) = \sin\theta$ spins about the **S**-axis at the angular velocity given by Eq. (1.36). Thus, angular velocity $\hat{\omega}$ and linear velocity $\mathbf{v}$ projections onto each $Z(Z')$-axis are:

$$\hat{\omega} = \frac{\hbar}{m_e r_1^2}\sqrt{\frac{3}{4}}\mathbf{i}_{Z,Z'} \tag{7.8}$$

$$\mathbf{v} = \frac{\hbar}{m_e r_1}\sqrt{\frac{3}{4}}\sin\theta\mathbf{i}_{\phi,\phi'} \tag{7.9}$$

The Lorentz force density at each point moving at velocity $\mathbf{v}$ given by Eq. (7.9) is

$$\mathbf{F}_{mag} = \frac{e}{4\pi r_2^2}\mathbf{v}\times\mathbf{B} \tag{7.10}$$

Substitution of Eq. (7.9) and Eqs. (7.6-7.7) into Eq. (7.10) while maintaining the designation of the coordinates of the magnetic field of electron 2 acting on the magnetic moments of electron 1 as the primed system and the coordinates of the magnetic field of electron 1 acting on the magnetic moments of electron 2 as the unprimed system gives:

$$\mathbf{F}_{mag} = -\frac{e}{4\pi r_2^2}\left(\begin{array}{l}\frac{\hbar}{m_e r_1}\sqrt{\frac{3}{4}}\sin\theta\mathbf{i}_{\phi'}\times\frac{\mu_0 e\hbar}{2m_e r_2^3}(\mathbf{i}_{r'}\cos\theta - \mathbf{i}_{\theta'}\sin\theta) \\ +\frac{\hbar}{m_e r_2}\sqrt{\frac{3}{4}}\sin\theta\mathbf{i}_\phi\times\frac{\mu_0 e\hbar}{2m_e r_2^3}(\mathbf{i}_r 2\cos\theta + \mathbf{i}_\theta\sin\theta)\end{array}\right) \tag{7.11}$$

As shown in Eqs. (7.16-7.24), the relativistic form of Eq. (7.11) results in the equivalence of the velocity at the two radii; thus, $r_1$ may be substituted for $r_2$ in the velocity factor of the second term to give:

$$\begin{aligned}\mathbf{F}_{mag} &= -\frac{1}{4\pi r_2^{\,2}}\frac{\mu_0 e^2\hbar^2}{2r_1 m_e^2 r_2^3}\sqrt{\frac{3}{4}}\begin{pmatrix}\sin\theta\mathbf{i}_{\phi'}\times\left(\mathbf{i}_{r'}\cos\theta-\mathbf{i}_{\theta'}\sin\theta\right)\\+\sin\theta\mathbf{i}_{\phi}\times\left(\mathbf{i}_{r}2\cos\theta+\mathbf{i}_{\theta}\sin\theta\right)\end{pmatrix}\\ &= -\frac{1}{4\pi r_2^{\,2}}\frac{\mu_0 e^2\hbar^2}{2r_1 m_e^2 r_2^3}\sqrt{\frac{3}{4}}\begin{pmatrix}-\sin\theta\cos\theta\mathbf{i}_{\theta'}+\sin^2\theta\mathbf{i}_{r'}\\+2\sin\theta\cos\theta\mathbf{i}_{\theta}+\sin^2\theta\mathbf{i}_{r}\end{pmatrix}\end{aligned} \tag{7.12}$$

The $\mathbf{i}_{r'}$ unit vector is transformed to $\mathbf{i}_r$ by substituting $\theta$ with $\theta+\frac{\pi}{2}$ in the second term of Eq. (7.12):

$$\begin{aligned}\mathbf{F}_{mag} &= -\frac{1}{4\pi r_2^{\,2}}\frac{\mu_0 e^2\hbar^2}{2r_1 m_e^2 r_2^3}\sqrt{\frac{3}{4}}\begin{pmatrix}-\sin\theta\cos\theta\mathbf{i}_{\theta'}+\sin^2\left(\theta+\frac{\pi}{2}\right)\mathbf{i}_{r'}\\+2\sin\theta\cos\theta\mathbf{i}_{\theta}+\sin^2\theta\mathbf{i}_{r}\end{pmatrix}\\ &= -\frac{1}{4\pi r_2^{\,2}}\frac{\mu_0 e^2\hbar^2}{2r_1 m_e^2 r_2^3}\sqrt{\frac{3}{4}}\begin{pmatrix}-\sin\theta\cos\theta\mathbf{i}_{\theta'}+\left(\sin^2\theta+\cos^2\theta\right)\mathbf{i}_{r}\\+2\sin\theta\cos\theta\mathbf{i}_{\theta}\end{pmatrix}\\ &= -\frac{1}{4\pi r_2^{\,2}}\frac{\mu_0 e^2\hbar^2}{2r_1 m_e^2 r_2^3}\sqrt{\frac{3}{4}}\left(-\sin\theta\cos\theta\mathbf{i}_{\theta'}+2\sin\theta\cos\theta\mathbf{i}_{\theta}+\mathbf{i}_{r}\right)\\ &= -\frac{1}{4\pi r_2^{\,2}}\frac{\mu_0 e^2\hbar^2}{2r_1 m_e^2 r_2^3}\sqrt{\frac{3}{4}}\left(-\frac{1}{2}\sin 2\theta\mathbf{i}_{\theta'}+\sin 2\theta\mathbf{i}_{\theta}+\mathbf{i}_{r}\right)\end{aligned} \tag{7.13}$$

The $F_{mag}\mathbf{i}_{\theta}$ and $F_{mag}\mathbf{i}_{\theta'}$ average to zero over the surface for $0\le\theta\le\pi$. The relativistic correction given *infra.* is based on quantized-angular-momentum conservation with the emission of a photon. The relativistic correction for the lightlike frame causes the circumferential distances on the surface to dilate to the radial dimension alone as given *infra.* and in the Special Relativistic Correction to the Ionization Energies section. This causes the angular force to vanish since it averages to zero such that only the radial force remains. Since there is no net angular force on the electron, only the resultant radial force need be considered:

$$\mathbf{F}_{mag} = -\frac{1}{4\pi r_2^{\,2}}\frac{\mu_0 e^2\hbar^2}{2r_1 m_e^2 r_2^3}\sqrt{\frac{3}{4}}\mathbf{i}_{r} \tag{7.14}$$

Eq. (7.14) may be written in the form

$$\mathbf{F}_{mag} = -\frac{1}{4\pi r_2^{\,2}}\left[\frac{e^2\mu_0}{2m_e r_1}\right]\frac{\hbar^2}{m_e r_2^{\,3}}\sqrt{s(s+1)}\mathbf{i}_{r} \tag{7.15}$$

where $s=1/2$ and $\sqrt{s(s+1)}=\sqrt{\frac{3}{4}}$ is the historical designation of the spin-angular momentum magnitude factor.

Furthermore, the term in brackets can be expressed in terms of the fine structure constant $\alpha$. The radius of the electron atomic orbital in the $v=c$ frame[4] is $\lambda\!\!\!^{-}_{C}$, where $v=c$ corresponds to the magnetic field front propagation velocity which is the same in all inertial frames, independent of the electron velocity as shown by the velocity addition formula of special relativity [5]. From Eq. (1.35) and Eqs. (1.179-1.180)

$$\frac{e^2\mu_0}{2m_e r_1} = 2\pi\alpha\frac{v}{c} \tag{7.16}$$

where $v=c$. Based on the relativistic invariance of the electron's magnetic moment of a Bohr magneton $\mu_B$ given by Eq. (1.131) as well as its invariant angular momentum of $\hbar$, it can be shown that the relativistic correction to Eq. (7.15) is $\frac{1}{Z}$ times the reciprocal of Eq. (7.16). As shown previously in the One-Electron Atom—Determination of Atomic Orbital Radii section, the radius term in the brackets of Eq. (7.15) is relativistically corrected due to invariance of charge under Gauss' Integral Law [6]. The radius of the electron relative to the $v=c$ frame, $r_\alpha^*$, is relativistically corrected as follows. The wave equation relationship is:

$$v = \lambda\frac{\omega}{2\pi} \tag{7.17}$$

[4] For the radiation-reaction force, v in Eq. (7.10) is not the electron velocity relative to the laboratory frame.

It can be demonstrated that the velocity of the electron atomic orbital satisfies the relationship for the velocity of a wave by substitution of Eqs. (1.15) and (1.36) into Eq. (7.17), which gives Eq. (1.35). The result of the substitution into Eq. (7.17) of $c$ for $v_n$, $\lambda_n$ given by Eq. (2.2):

$$2\pi(nr_1) = 2\pi r_n = n\lambda_1 = \lambda_n \tag{7.18}$$

with $r_1$ given by Eq. (1.260):

$$r_1 = \frac{a_0}{Z} \tag{7.19}$$

for $\lambda$, and of $\omega_n$ given by Eq. (1.36)

$$\omega_n = \frac{\hbar}{m_e r_n^2} \tag{7.20}$$

for $\omega$ is

$$c = 2\pi \frac{\gamma^* a_0}{Z} \frac{\hbar}{m_e \left[\frac{\gamma^* a_0}{Z}\right]^2 2\pi} \tag{7.21}$$

$$\gamma^* = \frac{Z\hbar}{m_e c a_0} = \frac{Z\sqrt{\varepsilon_0\mu_0}\hbar}{m_e} \frac{e^2 m_e}{4\pi\varepsilon_0\hbar^2} = Z\frac{1}{4\pi}\sqrt{\frac{\mu_0}{\varepsilon_0}}\frac{e^2}{\hbar} = \alpha Z \tag{7.22}$$

where $\gamma^*$ is the relativistic factor corresponding to the radius, $c$ is given by Eq. (1.178), and $\alpha$ is given by Eq. (2.123). It follows from Eq. (7.22) that the radius $r_1$ of Eq. (7.15) must be corrected by the factor $(\alpha Z)^{-1}$.

Due to relativistic invariance of $\frac{e}{m_e}$ corresponding to the invariance of $\mu_B$, the correction of the electron mass of the bracketed term of Eq. (7.15) is $2\pi$ as given in the One-Electron Atom—Determination of Atomic Orbital Radii section (Eq. (1.273)). By correcting the radius and the mass, the relativistic correction $\gamma'$ due to the light speed electrodynamic central force is

$$\gamma' = \left(2\pi\alpha Z\frac{v}{c}\right)^{-1} \tag{7.23}$$

where $v = c$ [5]. Thus, $\frac{1}{Z}$ is substituted for the term in brackets in Eq. (7.15). Thus, Eq. (7.15) becomes:

$$\mathbf{F}_{mag} = -\frac{1}{4\pi r_2^2}\frac{1}{Z}\frac{\hbar^2}{m_e r_2^3}\sqrt{s(s+1)}\mathbf{i}_r \tag{7.24}$$

The radiation-reaction force between the two electrons that achieves the condition that the sum of the mechanical momentum and electromagnetic momentum is conserved can also be derived from the relativistically invariant relationship between momentum and energy. As shown in the Excited States of the One-Electron Atom (Quantization) section and the Excited States of Helium section, in general, for a macroscopic multipole with a single $m$ value, a comparison of Eq. (2.62) and Eq. (2.55) shows that the relationship between the angular momentum $M_z$, energy $U$, and angular frequency $\omega$ is given by Eq. (2.63):

$$\frac{dM_z}{dr} = \frac{m}{\omega}\frac{dU}{dr} \tag{7.25}$$

independent of $r$ where $m$ is an integer. Furthermore, the ratio of the square of the angular momentum, $M^2$, to the square of the energy, $U^2$, for a pure ($\ell$, $m$) multipole follows from Eq. (2.55) and Eqs. (2.60-2.62) as given by Eq. (2.64):

$$\frac{M^2}{U^2} = \frac{m^2}{\omega^2} \tag{7.26}$$

From Jackson [7], the quantum mechanical interpretation is that the radiation from such a multipole of order ($\ell$, $m$) carries off $m\hbar$ units of the z component of angular momentum per photon of energy $\hbar\omega$. However, the photon and the electron can each possess only $\hbar$ of angular momentum which requires that Eqs. (7.25-7.26) correspond to a state of the radiation field containing $m$ photons. Then, the magnetic energy due to the interaction of the magnetic moment of each electron and the magnetic field of the opposite member of the pair is quantized in terms of the magnetic field as well as the magnetic moment as opposed to being a continuous function of magnetic flux $B$ in the case of the energy due to an applied field. In the applied-field case, the energy $\Delta E_{mag}$ of interaction of a magnetic moment **m** and flux **B** is given by Eq. (1.168)

[5] The same relativistic correction is obtained by consideration of the kinetic and vector potential components of the angular momentum in the light-like frame as shown in Box 1.1.

$$\Delta E_{mag} = \mathbf{m} \cdot \mathbf{B} = mB\cos\theta \tag{7.27}$$

In the case of the interaction of the magnetic moments of two electrons of two-electron atoms, Eq. (7.27) does not apply due to the result of Eq. (7.26).

The quantized energy for an electron $\Delta E_{mag}^{spin}$ to switch from parallel to antiparallel to an applied field $\mathbf{B}$ is given by Eq. (1.168)

$$\Delta E_{mag}^{spin} = 2\mu_{\mathbf{B}}\, \mathbf{i_z} \cdot \mathbf{B} = 2\mu_B B\cos\theta = 2\mu_B B = 2\hbar\omega_L \tag{7.28}$$

where $\omega_L$ is the Larmor frequency given by Eq. (2) of Box 1.1. In the case of the interaction between the two electrons, the frequency must satisfy Eq. (7.26). From Eq. (7.8), the angular velocity $\hat{\omega}_L$ is:

$$\hat{\omega}_L = \frac{\hbar}{m_e r_2^2}\sqrt{\frac{3}{4}}\mathbf{i}_Z \tag{7.29}$$

Energy is conserved between the electric and magnetic energies of the helium atom as shown by Eq. (7.42). Since charge is relativistically invariant under Gauss' Integral Law, the relationships between the parameters of Eqs. (7.25) and (7.26) due to quantization of angular momentum $\hbar$ and energy $\hbar\omega$ requires the normalization of the energy $U$ by the central field $Z$ such that the magnetic-force dependence on the nuclear charge is the reciprocal of that of the electric force. Then, the radial electric field has a magnitude proportional to $Z$ and the magnetic interaction has a magnitude of $\frac{1}{Z}$ such that the corresponding magnetic energy $U$ is decreased by the factor of $\frac{1}{Z^2}$ corresponding to the electric energy given by Eqs. (1.263-1.264). Using Eqs. (7.26) and (7.29) with $m = 2$ for the magnetic dipole interaction and the invariance of charge gives

$$\Delta E_{mag}^{spin} = \frac{\hbar\omega_L}{2Z} = \frac{\hbar^2}{2Zm_e r_2^2}\sqrt{\frac{3}{4}} \tag{7.30}$$

The corresponding magnetic force is given as the gradient of the energy:

$$\mathbf{F}_{mag} = \frac{1}{4\pi r_2^2}\nabla\left(\Delta E_{mag}^{spin}\right) = \frac{1}{4\pi r_2^2}\frac{\delta\Delta E_{mag}^{spin}}{\delta r_2}\mathbf{i}_r = -\frac{1}{4\pi r_2^2}\frac{\hbar^2}{Zm_e r_2^3}\sqrt{\frac{3}{4}}\mathbf{i}_r \tag{7.31}$$

The outward centrifugal force on electron 2 (Eqs. (7.1-7.2)) is balanced by the electric force (Eq. (7.3)) and the magnetic force (on electron 2) (Eqs. (7.24) and (7.31)):

$$\frac{m_e}{4\pi r_2^2}\frac{v_2^2}{r_2} = \frac{e}{4\pi r_2^2}\frac{(Z-1)e}{4\pi\varepsilon_0 r_2^2} + \frac{1}{4\pi r_2^2}\frac{\hbar^2}{Zm_e r_2^3}\sqrt{s(s+1)} \tag{7.32}$$

From Eq. (1.35) and Eq. (7.2)

$$v_2^2 = \frac{\hbar^2}{m_e^2 r_2^2} \tag{7.33}$$

Then,

$$\frac{m_e v_2^2}{r_2} = \frac{\hbar^2}{m_e r_2^3} = \frac{(Z-1)e^2}{4\pi\varepsilon_0 r_2^2} + \frac{1}{Z}\frac{\hbar^2}{m_e r_2^3}\sqrt{s(s+1)} \tag{7.34}$$

Solving for $r_2$,

$$r_2 = r_1 = a_0\left(\frac{1}{Z-1} - \frac{\sqrt{s(s+1)}}{Z(Z-1)}\right);\ s = \frac{1}{2} \tag{7.35}$$

That is, the final radius of electron 2, $r_2$, is given by Eq. (7.35); this is also the final radius of electron 1. The energies and radii of several two-electron atoms are given in Table 7.1.

(Since the density factor always cancels, it will not be used in subsequent force balance equations).

## ENERGY CALCULATIONS

The electric work to bring electron 2 to $r_2 = r_1$ is given by the integral of the electric force from infinity to $r_1$,

$$work(electric, electron2) = \frac{(Z-1)e^2}{8\pi\varepsilon_0 r_1} \tag{7.36}$$

And, the electric energy is the negative of the electric work,

$$E(electric) = \frac{-(Z-1)e^2}{8\pi\varepsilon_0 r_1} \tag{7.37}$$

The potential energy of each electron at $r = r_1$, is given as:

$$V = \frac{-(Z-1)e^2}{4\pi\varepsilon_0 r_1} \tag{7.38}$$

The kinetic energy is $\frac{1}{2}m_e v^2$, where $v$ is given by Eq. (1.35).

$$T = \frac{1}{2}\frac{\hbar^2}{m_e r_1^2} \tag{7.39}$$

The magnetic work is the integral of the magnetic force from infinity to $r_1$,

$$work(magnetic, electron2) = -\frac{1}{2}\frac{1}{Z}\frac{\hbar^2}{m_e r_1^2}\sqrt{s(s+1)} \tag{7.40}$$

## CONSERVATION OF ENERGY

Energy is conserved. Thus, the potential energy (electron 2 at $r_1$) with the nucleus plus the magnetic work (electron 2 going from infinity to $r_1$) must equal the sum of the negative of the electric work (electron 2 going from infinity to $r_1$) and the kinetic energy (electron 2 at $r_1$). This is shown below with Eq. (7.41) and Eq. (7.42).

$$V(electron\ 2\ at\ r_1) = \frac{-(Z-1)e^2}{8\pi\varepsilon_0 r_1} + \frac{1}{2}\frac{1}{Z}\frac{\hbar^2}{m_e r_1^2}\sqrt{s(s+1)} - \frac{1}{2}\frac{\hbar^2}{m_e r_1^2} \tag{7.41}$$

and using $r_1$ from Eq. (7.35),

$$V(electron\ 2\ at\ r_1) = -\frac{(Z-1)e^2}{4\pi\varepsilon_0 r_1} \tag{7.42}$$

This is also the potential energy of electron 1 where their potential energies are indistinguishable when $r_1 = r_2$, but once one is excited they are distinguishable [6].

---

[6] The decrease in the central force of electron 1 from that corresponding to $Z$ to that corresponding to $Z-1$ as given by Eq. (7.42) allows the potential energies of the two electrons to match upon pairing. This is possible according to Maxwell's equations by the relationship between the two-dimensional surface charge density of each binding electron and the field:

$$\mathbf{n} \bullet \left( \mathbf{E}_1 - \mathbf{E}_2 \right) = \frac{\sigma}{\varepsilon_0} \tag{1}$$

Whenever there is a potential energy difference in any perfect conductor, current will flow to redistribute the charge and, thus, the field lines, until an equipotential is achieved. This is true even in the case of the two-dimensional layer of charge of paired electrons. However, in this case, the orientation of the field lines changes since current flow in the radial direction is not possible. Reverse-directed field lines partially cancel the central field of the nucleus at the shell such that the equipotential condition is met for the shell.

In the case of helium for example, the two spin-paired electrons comprise a single two-dimensional shell (zero thickness) at radius $0.566987a_0$. They satisfy Maxwell's source charge equation (Eq. (1)) and Gauss' law (Eq. (33.6)) while achieving a minimum energy, equipotential surface with one half of the combined field lines directed radial inward and one half directed radial outward from the surface of the shell. The inward-directed lines are cancelled by those of the $+2e$ charged nucleus. The result is that each electron of the superposition of the two comprising the shell of $-2e$ total charge experiences a central field of $+e$. The minimum energy is achieved by spin pairing with a significant reduction in the radius of the initial electron 2 due to the spin pairing force (Eq. (7.24)) in Eq. (7.34) relative to the pure Lorentz force (Eq. (7.15)). Using $r_1 = 0.5a_0$ from Eq. (1.260) as a first-order approximation of the multibody unpaired-electron problem, the corresponding radius without spin pairing is $0.999a_0$. Using Eq. (7.37), the corresponding binding energy of electron 2 is $13.61\ eV$ compared to the case with spin pairing of $24.58750\ eV$. Thus, spin pairing lowers the total energy of the system of interacting electrons by $10.98\ eV$ even though the electrons become indistinguishable upon pairing.

As a consequence of the spin-pairing interaction and associated stabilization, it is not possible to assign an independent energy to any single electron of $He$. Rather, the total system must be considered. Only for a one-electron atom is the electron's energy equal to the total energy. Specifically, the electrons of $He$ in the ground state are paired in the same shell and are indistinguishable. That does not mean that the ionization of $He$ to $He^{2+}$ is twice $24.58750\ eV$. Both electrons cannot be ionized from the position $r_1 = r_2 = 0.566987a_0$ to a continuum level without becoming unpaired since paired free electrons at the same position is energetically unobtainable. In excited states, the electrons are distinguishable; yet, dependent in terms of their positions and energies. With photon absorption, one electron moves to a greater radius and the other moves closer to the nucleus. It is a sequential quantized process as shown in the Excited States of Helium section. In the limit, the total energy of the photon required for one of the initially indistinguishable electrons to be ionized with the other moving to the radius of $0.5a_0$ is $24.58750\ eV$ (Eqs. (7.44-7.46)). The corresponding $He^+$ ion has an ionization energy of $54.423\ eV$ (Eqs. (1.260) and (1.264))). Thus, the total binding energy of $He$ in the ground state is $24.58750\ eV + 54.423\ eV$.

An energy balance can be assigned to the two electrons. From Eq. (1.264), the binding energy of $He^+$ is

$$E_B\left(He^+\right) = 54.423\ eV \tag{2}$$

The spin pairing of the two electrons with the binding of an electron 2 to $He^+$ with an electron 1 causes an energy change corresponding to the central field at electron 1 to decrease by an integer such that both electrons are bound with the same force and are equivalent. The binding or ionization energy change given by Eq. (1.264) is

$$\Delta E_B = -\Delta \frac{Ze^2}{8\pi\varepsilon_0 r_1} = -\frac{e^2}{8\pi\varepsilon_0 a_0}\left(\frac{2}{0.5} - \frac{1}{0.566987}\right) = -30.42654\ eV \tag{3}$$

where the radius of $He^+$ (Eq. (1.260)) is $0.5a_0$ and the radius of $He$ is $0.566987a_0$ (Eq. (7.35)). From Eq. (7.45), the electric energy of either of the equivalent electrons at $r_1 = r_2 = 0.566987a_0$ is

$$E(electric) = -\frac{e^2}{8\pi\varepsilon_0 0.566987a_0} = -23.996467\ eV \tag{4}$$

With the contribution of the magnetic energy (Eqs. (7.44) and (7.46))), the binding energy of **either** of the equivalent electrons of helium (Eqs. (7.44-7.46)) is

$$E_B\left(He\right) = 24.58741\ eV \tag{5}$$

With the ionization of either electron 1 or electron 2, the central field of the unionized electron, say electron 1, increases by one. The electric and magnetic fields are conservative, and the energy $E_B\left(e_1\right)$ of the unionized electron is given by the negative of the sum of Eqs. (3) and (4):

$$E_B\left(e_1\right) = -\left(\Delta E_B + E(electric)\right) = -\left(-30.42654\ eV - 23.996467\ eV\right) = 54.423\ eV \tag{6}$$

which matches Eq. (2). Thus, the total ionization energy of helium $E_{BT}\left(He\right)$ given by the sum of the first and second ionization energies is

$$E_{BT}\left(He\right) = IP_1 + IP_2 = 54.423\ eV + 24.58741\ eV = 79.011\ eV \tag{7}$$

where $IP$ is the ionization potential.

The central field lines of the nucleus of two-electron atoms end equally on each electron. Thus, the difference in energy of electron 1 before and after pairing given by Eq. (3) can be considered the energy of pairing that is conserved upon unpairing of the electrons such that the binding energy is increased by the negative of Eq. (3). In general, the matched potential of the binding electrons is that which achieves a minimum energy of the atom, ion, molecular ion, or molecule and obeys Maxwell's source charge equation (Eq. (1)) and Gauss' law (Eq. (33.6)) for the total charge and total fields across the shell comprised of two or more electrons bound by at least one of spin- and orbital- interactions. Further examples of the application of the equal potential condition for the binding of multi-electrons per shell are the cases of the hydride ion, three- through twenty-electron atoms, and molecules given in the corresponding sections.

## IONIZATION ENERGIES

During ionization, power must be conserved. Power flow is governed by the Poynting power theorem,

$$\nabla \bullet (\mathbf{E} \times \mathbf{H}) = -\frac{\partial}{\partial t}\left[\frac{1}{2}\mu_0 \mathbf{H} \bullet \mathbf{H}\right] - \frac{\partial}{\partial t}\left[\frac{1}{2}\varepsilon_0 \mathbf{E} \bullet \mathbf{E}\right] - \mathbf{J} \bullet \mathbf{E} \tag{7.43}$$

Energy is superposable; thus, the calculation of the ionization energy is determined as a sum of the electric and magnetic contributions. Energy must be supplied to overcome the electric force of the nucleus, and this energy contribution is the negative of the electric work given by Eq. (7.37). Additionally, the electrons are initially spin-paired at $r_1 = r_2 = 0.566987a_0$ producing no magnetic fields; whereas, following ionization, the electrons possess magnetic fields and corresponding energies. For helium, the contribution to the ionization energy is given as the energy stored in the magnetic fields of the two electrons at the initial radius where they become spin-unpaired. Part of this energy and the corresponding relativistic term corresponds to the precession of the outer electron about the z-axis due to the spin angular momentum of the inner electron. These terms are the same as those of the corresponding terms of the hyperfine structure interval of muonium as given in the Muonium Hyperfine Structure Interval section. Thus, for helium, which has no electric field beyond $r_1$ the ionization energy is given by the general formula:

$$Ionization\ Energy(He) = -E(electric) + E(magnetic)\left(1 - \frac{1}{2}\left(\left(\frac{2}{3}\cos\frac{\pi}{3}\right)^2 + \alpha\right)\right) \tag{7.44}$$

where,

$$E(electric) = -\frac{(Z-1)e^2}{8\pi\varepsilon_0 r_1} \tag{7.45}$$

$$E(magnetic) = \frac{2\pi\mu_0 e^2\hbar^2}{m_e^2 r_1^3} = \frac{8\pi\mu_0\mu_B^2}{r_1^3} \tag{7.46}$$

Eq. (7.46) is derived for each of the two electrons as Eq. (1.161) of the Magnetic Parameters of the Electron (Bohr Magneton) section with the radius given by Eq. (7.35). By substituting the radius given by Eq. (7.35) into Eq. (1.35), the velocity $v$ is given by:

$$v = \frac{\hbar}{\frac{4\pi\varepsilon_0\hbar^2}{e^2}\left(\frac{1}{Z-1} - \frac{\sqrt{\frac{3}{4}}}{Z(Z-1)}\right)} = \frac{\alpha c(Z-1)}{\left(1 - \frac{\sqrt{\frac{3}{4}}}{Z}\right)} \tag{7.47}$$

with $Z > 1$ where Eqs. (1.204) and (1.208) were used. For increasing *Z*, the velocity becomes a significant fraction of the speed of light; thus, special relativistic corrections were included in the calculation of the ionization energies of two-electron atoms given in Table 7.1. The relativistic corrections follow from those given in the Special Relativistic Correction to the Ionization Energies section wherein the nuclear-electron magnetic interactions as well as the electron-electron interactions of two-electron atoms must be included to be precise.

For a nuclear charge $Z$ greater than two, a central electric field equal to that of an elementary charge quanta of $Z-2$ exists outside of the atomic orbital of the unionized atom. During ionization, the energy contribution of the expansion of the atomic orbital of the ionized electron (electron 2) from $r_1$ to infinity in the presence of the electric fields present inside and outside of the atomic orbital is calculated as the $\mathbf{J} \bullet \mathbf{E}$ term of the Poynting theorem. This energy contribution can be determined by designing an energy cycle and considering the individual contributions of each electron (electron 1 and electron 2) in going from the initial unionized to the final ionized state. Consider two paired atomic orbitals. Expansion of an atomic orbital in the presence of an electric field which is positive in the outward radial direction requires energy, and contraction of an atomic orbital in this field releases energy. Thus, the contribution of the $\mathbf{J} \bullet \mathbf{E}$ term to ionization is the difference in the energy required to expand one atomic orbital (electron 2) from $r_1$ to infinity and to contract one atomic orbital (electron 1) from infinity to $r_1$. The energy contribution for the expanding atomic orbital follows the derivation of Eq. (1.225) of the Electron g Factor section as follows (the vector direction is taken to give a positive dissipated energy).

## DISSIPATED ENERGY

The $\mathbf{J} \bullet \mathbf{E}$ energy over time is derived from the central electric field from the nucleus against which electron 2 expands and the current of the expanding electron 2 wherein the latter is dependent on the magnetic field of the inner electron 1. The magnetic field of electron 1 gives rise to a Lorentz force on electron 2, and the dissipative current density of electron 2 depends on this force wherein the superconducting condition given by Eq. (1.187) is maintained with the electric field of electron 1. The magnitude of the magnetic flux at electron 2 due to electron 1 is given by that of the Bohr magneton at the origin that follows from McQuarrie [3]:

$$B = \frac{\mu_0 e\hbar}{2m_e r_2^3} \tag{7.48}$$

The magnetic force on electron 2 due to the magnetic field of electron 1 is the Lorentz force given by Eq. (1.183). Substitution of Eq. (1.35) for $\mathbf{v}$ and Eq. (7.48) for the magnetic flux into Eq. (1.183) gives

$$\mathbf{F}_{mag} = \frac{\mu_0 e^2\hbar^2}{2m_e^2 r_2^4}\mathbf{i}_r \tag{7.49}$$

Furthermore, the velocity of electron 1 is proportional to the nuclear charge as given by Eqs. (1.35) and (1.257). Thus, in order to maintain the superconducting condition given by Eq. (1.187), the magnetic force corresponding to $B$ must be given by

$$\mathbf{F}_{mag} = \frac{1}{Z}\frac{\mu_0 e^2\hbar^2}{2m_e^2 r_2^4}\mathbf{i}_r \tag{7.50}$$

The expansion of the atomic orbital of electron 2 produces a current. The current over time $\Delta t\mathbf{J}$ is:

$$\Delta t\mathbf{J} = \Delta t\sigma\ \mathbf{E}_f \tag{7.51}$$

where $\mathbf{J}$ is the current density, $\Delta t$ is the time interval, $\sigma$ is the conductivity, and $\mathbf{E}_f$ is the effective electric field defined as follows:

$$\mathbf{F} = q(\theta,\phi)\mathbf{E}_f \tag{7.52}$$

where $\mathbf{F}$ is the magnetic force given by Eq. (7.50), and $q(\theta,\phi)$ is the angular charge density given as follows:

$$q(\theta,\phi) = \frac{e}{4\pi} \tag{7.53}$$

The orbit expands in free space; thus, the relation for the conductivity is:

$$\Delta t\sigma = \varepsilon_0 \tag{7.54}$$

The electric field provided by the nucleus for the expanding atomic orbital is:

$$\mathbf{E} = \frac{(Z-2)e}{4\pi\varepsilon_0 r_2^2}\mathbf{i}_r \tag{7.55}$$

where $\varepsilon_0$ is the permittivity of free space ($8.854\ X\ 10^{-12}\ C^2 / N \cdot m^2$). Using Eqs. (7.50-7.55), the $\mathbf{J} \bullet \mathbf{E}$ energy density over time for the expansion of electron 2 with the contraction of electron 1 is:

$$\Delta t(\mathbf{J} \bullet \mathbf{E}) = \frac{(Z-2)}{Z}\frac{\mu_0 e^2\hbar^2}{2m_e^2 r_2^6} \tag{7.56}$$

The $\mathbf{J} \bullet \mathbf{E}$ energy over time is the volume integral of the energy density over time

$$[\Delta t(\mathbf{J} \bullet \mathbf{E})]_{energy\ external} = \int_0^{2\pi}\int_0^{\pi}\int_{\infty}^{r_1}\frac{(Z-2)}{Z}\frac{\mu_0 e^2\hbar^2}{2m_e^2 r_2^6} r^2 \sin\theta dr d\theta d\Phi \tag{7.57}$$

$$[\Delta t(\mathbf{J} \bullet \mathbf{E})]_{energy\ external} = \frac{(Z-2)}{Z}\frac{2\pi\mu_0 e^2\hbar^2}{3m_e^2 r_1^3} \tag{7.58}$$

The $\mathbf{J} \bullet \mathbf{E}$ energy over time involving the electric field external to the atomic orbital of electron 2 is $\frac{(Z-2)}{Z}$ times the magnetic energy stored in the space external to the atomic orbital as given by Eq. (1.170). The left and right sides of the Poynting theorem must balance. Given the form of the $\mathbf{J} \bullet \mathbf{E}$ energy over time involving the electric field external to the atomic orbital of electron 2 and given that the electric field inside of the atomic orbital is $Z-1$ times the electric field of a point charge, the $\mathbf{J} \bullet \mathbf{E}$ energy over time involving the electric field internal to the atomic orbital of electron 2 is $\frac{(Z-1)}{Z}$ times the magnetic energy stored inside of the atomic orbital as given by Eq. (1.159). This energy is

$$[\Delta t(\mathbf{J} \bullet \mathbf{E})]_{energy\ internal} = \frac{(Z-1)}{Z}\frac{4\pi\mu_0 e^2\hbar^2}{3m_e^2 r_1^3} \tag{7.59}$$

Thus, the total $\mathbf{J} \bullet \mathbf{E}$ energy over time of electron 2 is the sum of Eqs. (7.58) and (7.59).

The $\mathbf{J} \bullet \mathbf{E}$ energy over time of electron 1 during contraction from infinity to $r_1$ is negative, and the equations for the external and internal contributions are of the same form as Eqs. (7.58) and (7.59) where the appropriate effective charge is

substituted. The $\mathbf{J} \bullet \mathbf{E}$ energy over time involving the electric field external to the atomic orbital of electron 1 is

$$[\Delta t(\mathbf{J} \bullet \mathbf{E})]_{energy\ external} = \frac{(Z-1)}{Z} \frac{2\pi\mu_0 e^2 \hbar^2}{3m_e^2 r_1^3} \tag{7.60}$$

And, the $\mathbf{J} \bullet \mathbf{E}$ energy over time involving the electric field internal to the atomic orbital of electron 1 is:

$$[\Delta t(\mathbf{J} \bullet \mathbf{E})]_{\text{energy } internal} = \frac{Z}{Z} \frac{4\pi\mu_0 e^2 \hbar^2}{3m_e^3 r_1^3} \tag{7.61}$$

The difference, $\Delta$, between the $\mathbf{J} \bullet \mathbf{E}$ energy over time for expanding electron 2 from $r_1$ to infinity and contracting electron 1 from infinity to $r_1$ is $-\frac{1}{Z}$ times the stored magnetic energy given by Eq. (7.46).

$$\Delta = -\frac{1}{Z} \frac{2\pi\mu_0 e^2 \hbar^2}{m_e^2 r_1^3} \tag{7.62}$$

Thus, the ionization energies are given by

$$Ionization\ Energy = -Electric\ Energy - \frac{1}{Z} Magnetic\ Energy \tag{7.63}$$

The energies of several two-electron atoms are given in Table 7.1. The relativistic factor $\gamma^*$ involving the spin pairing between the two electrons is derived in the Special Relativistic Effect on the Electron Radius and the Relativistic Ionization Energies section.

**Table 7.1.** Relativistically corrected ionization energies for some two-electron atoms.

| 2 e Atom | Z | $r_1$ ($a_o$) [a] | Electric Energy [b] (eV) | Magnetic Energy [c] (eV) | Velocity (m/s) [d] | $\gamma^*$ [e] | Theoretical Ionization Energies [f] (eV) | Experimental Ionization Energies [g] (eV) | Relative Error [h] |
|---|---|---|---|---|---|---|---|---|---|
| $He$ | 2 | 0.566987 | 23.996467 | 0.590536 | 3.85845E+06 | 1.000021 | 24.58750 | 24.58741 | -0.000004 |
| $Li^{+}$ | 3 | 0.35566 | 76.509 | 2.543 | 6.15103E+06 | 1.00005 | 75.665 | 75.64018 | -0.0003 |
| $Be^{2+}$ | 4 | 0.26116 | 156.289 | 6.423 | 8.37668E+06 | 1.00010 | 154.699 | 153.89661 | -0.0052 |
| $B^{3+}$ | 5 | 0.20670 | 263.295 | 12.956 | 1.05840E+07 | 1.00016 | 260.746 | 259.37521 | -0.0053 |
| $C^{4+}$ | 6 | 0.17113 | 397.519 | 22.828 | 1.27836E+07 | 1.00024 | 393.809 | 392.087 | -0.0044 |
| $N^{5+}$ | 7 | 0.14605 | 558.958 | 36.728 | 1.49794E+07 | 1.00033 | 553.896 | 552.0718 | -0.0033 |
| $O^{6+}$ | 8 | 0.12739 | 747.610 | 55.340 | 1.71729E+07 | 1.00044 | 741.023 | 739.29 | -0.0023 |
| $F^{7+}$ | 9 | 0.11297 | 963.475 | 79.352 | 1.93649E+07 | 1.00057 | 955.211 | 953.9112 | -0.0014 |
| $Ne^{8+}$ | 10 | 0.10149 | 1206.551 | 109.451 | 2.15560E+07 | 1.00073 | 1196.483 | 1195.8286 | -0.0005 |
| $Na^{9+}$ | 11 | 0.09213 | 1476.840 | 146.322 | 2.37465E+07 | 1.00090 | 1464.871 | 1465.121 | 0.0002 |
| $Mg^{10+}$ | 12 | 0.08435 | 1774.341 | 190.652 | 2.59364E+07 | 1.00110 | 1760.411 | 1761.805 | 0.0008 |
| $Al^{11+}$ | 13 | 0.07778 | 2099.05 | 243.13 | 2.81260E+07 | 1.00133 | 2083.15 | 2085.98 | 0.0014 |
| $Si^{12+}$ | 14 | 0.07216 | 2450.98 | 304.44 | 3.03153E+07 | 1.00159 | 2433.13 | 2437.63 | 0.0018 |
| $P^{13+}$ | 15 | 0.06730 | 2830.11 | 375.26 | 3.25043E+07 | 1.00188 | 2810.42 | 2816.91 | 0.0023 |
| $S^{14+}$ | 16 | 0.06306 | 3236.46 | 456.30 | 3.46932E+07 | 1.00221 | 3215.09 | 3223.78 | 0.0027 |
| $Cl^{15+}$ | 17 | 0.05932 | 3670.02 | 548.22 | 3.68819E+07 | 1.00258 | 3647.22 | 3658.521 | 0.0031 |
| $Ar^{16+}$ | 18 | 0.05599 | 4130.79 | 651.72 | 3.90705E+07 | 1.00298 | 4106.91 | 4120.8857 | 0.0034 |
| $K^{17+}$ | 19 | 0.05302 | 4618.77 | 767.49 | 4.12590E+07 | 1.00344 | 4594.25 | 4610.8 | 0.0036 |
| $Ca^{18+}$ | 20 | 0.05035 | 5133.96 | 896.20 | 4.34475E+07 | 1.00394 | 5109.38 | 5128.8 | 0.0038 |
| $Sc^{19+}$ | 21 | 0.04794 | 5676.37 | 1038.56 | 4.56358E+07 | 1.00450 | 5652.43 | 5674.8 | 0.0039 |
| $Ti^{20+}$ | 22 | 0.04574 | 6245.98 | 1195.24 | 4.78241E+07 | 1.00511 | 6223.55 | 6249 | 0.0041 |
| $V^{21+}$ | 23 | 0.04374 | 6842.81 | 1366.92 | 5.00123E+07 | 1.00578 | 6822.93 | 6851.3 | 0.0041 |
| $Cr^{22+}$ | 24 | 0.04191 | 7466.85 | 1554.31 | 5.22005E+07 | 1.00652 | 7450.76 | 7481.7 | 0.0041 |
| $Mn^{23+}$ | 25 | 0.04022 | 8118.10 | 1758.08 | 5.43887E+07 | 1.00733 | 8107.25 | 8140.6 | 0.0041 |
| $Fe^{24+}$ | 26 | 0.03867 | 8796.56 | 1978.92 | 5.65768E+07 | 1.00821 | 8792.66 | 8828 | 0.0040 |
| $Co^{25+}$ | 27 | 0.03723 | 9502.23 | 2217.51 | 5.87649E+07 | 1.00917 | 9507.25 | 9544.1 | 0.0039 |
| $Ni^{26+}$ | 28 | 0.03589 | 10235.12 | 2474.55 | 6.09529E+07 | 1.01022 | 10251.33 | 10288.8 | 0.0036 |
| $Cu^{27+}$ | 29 | 0.03465 | 10995.21 | 2750.72 | 6.31409E+07 | 1.01136 | 11025.21 | 11062.38 | 0.0034 |

[a] From Eq. (7.35).

[b] From Eq. (7.45).

[c] From Eq. (7.46), except Eq. (7.44) for neutral $He$.

[d] From Eq. (7.47).

[e] From Eq. (1.281) with the velocity given by Eq. (7.47).

[f] From Eq. (7.44) for neutral atom helium, and ions from Eq. (7.63) with $E(electric)$ of Eq. (7.45) relativistically corrected by $\gamma^*$ according to Eq. (1.281).

[g] From theoretical calculations for ions $Ne^{8+}$ to $Cu^{27+}$ [8-9].

[h] (Experimental-theoretical)/experimental.

The agreement between the experimental and calculated values of Table 7.1 is within the experimental capability of the spectroscopic determinations at large Z, which relies on X-ray spectroscopy. In this case, the experimental capability is three to four significant figures, which is consistent with the last column. The helium atom isoelectronic series is given in Table 7.1 [8-9] to much higher precision than the capability of X-ray spectroscopy, but these values are based on theoretical and interpolation techniques rather than data alone. Ionization energies are difficult to determine since the cut-off of the Rydberg series of lines at the ionization energy is often not observed, and the ionization energy must be determined from theoretical calculations, interpolation of He isoelectronic and Rydberg series, as well as direct experimental data.

The theoretical values for low Z can be improved by calculating the spin-nuclear relativistic factor, which corresponds to the reduced mass for one-electron atoms given in the Determination of Atomic Orbital Radii section.

## HYDRIDE ION

The hydride ion comprises two indistinguishable electrons bound to a proton of $Z = +1$. Each electron experiences a centrifugal force, and the balancing centripetal force (on each electron) is produced by the electric force between the electron and the nucleus. In addition, a magnetic force exists between the two electrons causing the electrons to pair.

## DETERMINATION OF THE ATOMIC ORBITAL RADIUS, $R_N$

Consider the binding of a second electron to a hydrogen atom to form a hydride ion. The second electron experiences no central electric force because the electric field is zero outside of the radius of the first electron. However, the second electron experiences a magnetic force due to electron 1 causing it to pair with electron 1. Thus, electron 1 experiences the reaction force of electron 2 which acts as a centrifugal force. The force balance equation can be determined by equating the total forces acting on the two bound electrons taken together. The force balance equation for the paired electron atomic orbital is obtained by equating the forces on the mass and charge densities. The centrifugal force of both electrons is given by Eq. (7.1) and Eq. (7.2) where the mass is $2m_e$. Electric field lines end on charge. Since both electrons are paired at the same radius, the number of field lines ending on the charge density of electron 1 equals the number that end on the charge density of electron 2. The electric force is proportional to the number of field lines; thus, the centripetal electric force, $\mathbf{F}_{ele}$, between the electrons and the nucleus is

$$\mathbf{F}_{ele(electron\ 1,2)} = \frac{\frac{1}{2}e^2}{4\pi\varepsilon_0 r_n^2} \tag{7.64}$$

where $\varepsilon_0$ is the permittivity of free space. The outward magnetic force on the two paired electrons is given by the negative of Eq. (7.24) where the mass is $2m_e$. The outward centrifugal force and magnetic forces on electrons 1 and 2 are balanced by the electric force

$$\frac{\hbar^2}{2m_e r_2^3} = \frac{\frac{1}{2}e^2}{4\pi\varepsilon_0 r_2^2} - \frac{1}{Z}\frac{\hbar^2}{2m_e r_2^3}\sqrt{s(s+1)} \tag{7.65}$$

where $Z = 1$. Solving for $r_2$,

$$r_2 = r_1 = a_0\left(1+\sqrt{s\left(s+1\right)}\right);\ s = \frac{1}{2} \tag{7.66}$$

where $a_0$ is given by Eq. (1.256). That is, the final radius of electron 2, $r_2$, is given by Eq. (7.66); this is also the final radius of electron 1.

## IONIZATION ENERGY

Since the hydrogen atom is neutral, the ionization energy of the hydride ion is determined from the magnetic energy balance. During ionization, electron 2 is moved to infinity. By the selection rules for absorption of electromagnetic radiation dictated by conservation of angular momentum, absorption of a photon causes the spin axes of the antiparallel spin-paired electrons to become parallel. The unpairing energy, $E_{unpairing}(magnetic)$, is given by Eq. (7.46) and Eq. (7.66) multiplied by two because the magnetic energy is proportional to the square of the magnetic field as derived in Eqs. (1.154-1.161). The magnetic energy of electron 1 following ionization of the hydride ion, $E_{electron\ 1\ final}(magnetic)$, is given by Eq. (1.161) and Eq. (1.260).

In addition, a third ionization energy term arises from the interaction of the two electrons during ionization. A magnetic force exists on the electron to be ionized due to the spin-spin interaction. The energy to move electron 2 to a radius which is infinitesimally greater than that of electron 1 is zero. In this case, the only force acting on electron 2 is the magnetic force. Due to conservation of energy, the potential energy change to move electron 2 to infinity to ionize the hydride ion can be calculated from the magnetic force of Eq. (7.65). The magnetic work, $E_{magwork}$, is the negative integral of the magnetic force (the second term on the right side of Eq. (7.65)) from $r_2$ to infinity,

$$E_{magwork} = \int_{r_2}^{\infty} \frac{\hbar^2}{2m_e r^3}\sqrt{s(s+1)}dr \tag{7.67}$$

where $r_2$ is given by Eq. (7.66). The result of the integration is:

$$E_{magwork} = \frac{\hbar^2\sqrt{s(s+1)}}{4m_e a_0^2\left[1+\sqrt{s(s+1)}\right]^2} \tag{7.68}$$

where $s = \frac{1}{2}$. By moving electron 2 to infinity, electron 1 moves to the radius $r_1 = a_H$, and the corresponding magnetic energy, $E_{electron\ 1\ final}(magnetic)$, is given by Eq. (7.46). In the present case of an inverse squared central field corresponding to the reaction force on electron 1, the magnitude of the binding energy is one half the magnitude of the potential energy [10], which is equivalent to that of Eq. (7.68). Thus, the ionization energy is given by subtracting the two magnetic energy terms from one half the magnetic work (Eq. (7.68)) wherein $m_e$ is the electron reduced mass $\mu_e = \frac{m_e m_p}{\frac{m_e}{\sqrt{\frac{3}{4}}} + m_p}$ due to the electrodynamic magnetic

energy that arises from the force between the unpaired electrons and the nucleus which follows from Eqs. (1.253-1.255) and Eq. (7.67)[7]. The electrodynamic force goes to zero as the two electrons pair due to the cancellation of the electron currents and magnetic fields. Thus, the corresponding reduced mass only appears in the $E_{magwork}$ term and in the magnetic energy of the free hydrogen atom term, $E_{electron\ 1\ final}(magnetic)$. Thus, the ionization energy of the hydride ion is given by:

$$Ionization\ Energy = \frac{1}{2}E_{magwork} - E_{electron\ 1\ final}(magnetic) - E_{unpairing}(magnetic)$$

$$= \frac{\hbar^2\sqrt{s(s+1)}}{8\mu_e a_0^2\left[1+\sqrt{s(s+1)}\right]^2} - \frac{\pi\mu_0 e^2\hbar^2}{m_e^2}\left(\frac{1}{a_H^3} + \frac{2^2}{a_0^3\left[1+\sqrt{s(s+1)}\right]^3}\right) \tag{7.69}$$

**From Eq. (7.69), the calculated ionization energy of the hydride ion is 0.75418 eV.**

**The experimental value given by Lykke [11] is** $6082.99 \pm 0.15\ cm^{-1}$ **(0.75418 eV).**

Without deriving the details of the nuclear structure of the deuterium nucleus and its magnetic moment, the electrodynamic magnetic energy term of the deuterium hydride ion due to the corresponding force between the interacting electrons and the nucleus with two nucleons may be taken as twice that of hydrogen, which has only one nucleon. From Eqs. (1.253-1.255) and Eq. (7.68), the corresponding reduced electron mass in Eq. (7.69) is $\mu_e = \frac{m_e m_p}{\frac{2m_e}{\sqrt{\frac{3}{4}}} + m_p}$.

**From Eq. (7.69), the calculated ionization energy of the deuterium hydride ion is 0.75471 eV.**

**The experimental value given by Lykke [11] is** $6086.2 \pm 0.6\ cm^{-1}$ **(0.75457 eV).**

---

[7]The electrodynamic force between the unpaired electrons and the nucleus which follows from Eqs. (1.253-1.255) goes to zero as the two electrons pair due to the cancellation of the electron currents and magnetic fields. During ionization, the corresponding energy due to the unpaired electrons is given by

$$E_{electrodynamic\ magwork} = \frac{\hbar^2}{2m_p r_1^2}\sqrt{s(s+1)} - \int_{r_2}^{\infty}\frac{\hbar^2}{2m_p r^3}\sqrt{s(s+1)}dr \tag{1}$$

where the mass in Eq. (1.246) is $2m_e$. Eq. (7.67) with the inclusion of the electrodynamic energy given by Eq. (1) is

$$E_{magwork} = \int_{r_2}^{\infty}\frac{\hbar^2}{2r^3}\sqrt{s(s+1)}\left(\frac{1}{m_e} + \frac{1}{m_p\sqrt{s(s+1)}}\right)dr \tag{2}$$

Thus, Eq. (7.68) with the electrodynamic energy is given by

$$E_{magwork} = \frac{\hbar^2\sqrt{s(s+1)}}{4\mu_e a_0^2\left[1+\sqrt{s(s+1)}\right]^2} \tag{3}$$

where the reduced electron mass is

$$\mu_e = \frac{m_e m_p}{\frac{m_e}{\sqrt{\frac{3}{4}}} + m_p} \tag{4}$$

## HYDRINO HYDRIDE ION

The hydrino atom $H\left(1/2\right)$ can form a stable hydride ion. The central field is twice that of the hydrogen atom, and it follows from Eq. (7.65) that the radius of the hydrino hydride ion $H^-\left(n=1/2\right)$ is one half that of atomic hydrogen hydride, $H^-\left(n=1\right)$, given by Eq. (7.66).

$$r_2 = r_1 = \frac{a_0}{2}\left(1+\sqrt{s\left(s+1\right)}\right);\ s=\frac{1}{2} \tag{7.70}$$

The energy follows from Eq. (7.69) and Eq. (7.70) where due to the invariance of $e/m$ and $\hbar$ for lower-energy states as well as excited states as shown in the Spin-Orbit Coupling section, the relativistic correction to the binding of the electron to a hydrogen atom or hydrino atom is the energy stored in the magnetic field of the hydrogen atom.

$$\begin{aligned} Ionization\ Energy &= \frac{1}{2}E_{magwork} - E_{electron\ 1\ final}(magnetic) - E_{unpairing}(magnetic) \\ &= \frac{\hbar^2\sqrt{s(s+1)}}{8\mu_e a_0^2\left[\frac{1+\sqrt{s(s+1)}}{2}\right]^2} - \frac{\pi\mu_0 e^2\hbar^2}{m_e^2}\left(\frac{1}{a_H^3}+\frac{2^2}{a_0^3\left[\frac{1+\sqrt{s(s+1)}}{2}\right]^3}\right) \end{aligned} \tag{7.71}$$

From Eq. (7.71), the calculated ionization energy of the hydrino hydride ion $H^-\left(n=1/2\right)$ is $3.047\ eV$ which corresponds to a wavelength of $\lambda = 407\ nm$.

In general, the central field of hydrino atom $H\left(n=1/p\right);\ p=\text{integer}$ is $p$ times that of the hydrogen atom. Thus, the force balance equation is:

$$\frac{\hbar^2}{2m_e r_2^3} = \frac{\frac{p}{2}e^2}{4\pi\varepsilon_0 r_2^2} - \frac{1}{Z}\frac{\hbar^2}{2m_e r_2^3}\sqrt{s(s+1)} \tag{7.72}$$

where $Z=1$ because the field is zero for $r > r_1$. Solving for $r_2$,

$$r_2 = r_1 = \frac{a_0}{p}\left(1+\sqrt{s\left(s+1\right)}\right);\ s=\frac{1}{2} \tag{7.73}$$

From Eq. (7.73), the radius of the hydrino hydride ion $H^-\left(n=1/p\right);\ p=\text{integer}$ is $\frac{1}{p}$ that of atomic hydrogen hydride, $H^-\left(n=1\right)$, given by Eq. (7.66). The energy follows from Eq. (7.69) and Eq. (7.73).

$$\begin{aligned} Ionization\ Energy &= \frac{1}{2}E_{magwork} - E_{electron\ 1\ final}(magnetic) - E_{unpairing}(magnetic) \\ &= \frac{\hbar^2\sqrt{s(s+1)}}{8\mu_e a_0^2\left[\frac{1+\sqrt{s(s+1)}}{p}\right]^2} - \frac{\pi\mu_0 e^2\hbar^2}{m_e^2}\left(\frac{1}{a_H^3}+\frac{2^2}{a_0^3\left[\frac{1+\sqrt{s(s+1)}}{p}\right]^3}\right) \end{aligned} \tag{7.74}$$

From Eq. (7.74), the calculated ionization energy of the hydrino hydride ion $H^-\left(n=1/p\right)$ as a function of $p$ is given in Table 7.2.

**Table 7.2.** The ionization energy of the hydrino hydride ion $H^-\left(n=1/p\right)$ as a function of *p*.

| Hydride Ion | $r_1$ ($a_o$)[a] | Cal. Ionization Energy (eV)[b] | Cal. Wavelength (nm) |
|---|---|---|---|
| $H^-\left(n=1\right)$ | 1.8660 | 0.7542 | 1644 |
| $H^-\left(n=1/2\right)$ | 0.9330 | 3.047 | 406.9 |
| $H^-\left(n=1/3\right)$ | 0.6220 | 6.610 | 187.6 |
| $H^-\left(n=1/4\right)$ | 0.4665 | 11.23 | 110.4 |
| $H^-\left(n=1/5\right)$ | 0.3732 | 16.70 | 74.23 |
| $H^-\left(n=1/6\right)$ | 0.3110 | 22.81 | 54.35 |
| $H^-\left(n=1/7\right)$ | 0.2666 | 29.34 | 42.25 |
| $H^-\left(n=1/8\right)$ | 0.2333 | 36.09 | 34.46 |
| $H^-\left(n=1/9\right)$ | 0.2073 | 42.84 | 28.94 |
| $H^-\left(n=1/10\right)$ | 0.1866 | 49.38 | 25.11 |
| $H^-\left(n=1/11\right)$ | 0.1696 | 55.50 | 22.34 |
| $H^-\left(n=1/12\right)$ | 0.1555 | 60.98 | 20.33 |
| $H^-\left(n=1/13\right)$ | 0.1435 | 65.63 | 18.89 |
| $H^-\left(n=1/14\right)$ | 0.1333 | 69.22 | 17.91 |
| $H\ \left(n=1/15\right)$ | 0.1244 | 71.55 | 17.33 |
| $H^-\left(n=1/16\right)$ | 0.1166 | 72.40 | 17.12 |
| $H^-\left(n=1/17\right)$ | 0.1098 | 71.56 | 17.33 |
| $H^-\left(n=1/18\right)$ | 0.1037 | 68.83 | 18.01 |
| $H^-\left(n=1/19\right)$ | 0.0982 | 63.98 | 19.38 |
| $H^-\left(n=1/20\right)$ | 0.0933 | 56.81 | 21.82 |
| $H^-\left(n=1/21\right)$ | 0.0889 | 47.11 | 26.32 |
| $H^-\left(n=1/22\right)$ | 0.0848 | 34.66 | 35.76 |
| $H^-\left(n=1/23\right)$ | 0.0811 | 19.26 | 64.36 |
| $H^-\left(n=1/24\right)$ | 0.0778 | 0.6945 | 1785 |
| $H^-\left(n=1/25\right)$ | | not stable[c] | |

[a] from Eq. (7.73).
[b, c] from Eq. (7.74).

## HYDRINO HYDRIDE ION NUCLEAR MAGNETIC RESONANCE SHIFT

The proton gyromagnetic ratio, $\gamma_p/2\pi$, is

$$\gamma_P/2\pi = 42.57602\ MHz\ T^{-1} \tag{7.75}$$

The NMR frequency, $f$, is the product of the proton gyromagnetic ratio given by Eq. (7.75) and the magnetic flux, $\mathbf{B}$.

$$f = \gamma_P/2\pi\mathbf{B} = 42.57602\ MHz\ T^{-1}\mathbf{B} \tag{7.76}$$

A typical radio frequency (RF) is $400\ MHz$. According to Eq. (7.76) this corresponds to a flux of $9.39496\ T$ provided by a superconducting NMR magnet. With a constant magnetic field, the frequency is scanned to yield the spectrum where the frequency scan is typically achieved using a Fourier transform on the free induction decay signal following a radio frequency pulse. Historically, the radiofrequency was held constant, the applied magnetic field, $H_0$ ($H_0 = \frac{B}{\mu_0}$), was varied over a small range, and the frequency of energy absorption was recorded at the various values for $H_0$. By convention based on this historic mode of operation, the radiofrequency spectrum is converted into the corresponding applied magnetic field, $H_0$ ($H_0 = \frac{B}{\mu_0}$), of energy absorption and displayed as a function of increasing $H_0$. The protons that would absorb energy at a lower $H_0$ give rise

to a downfield absorption peak; whereas, the protons that would absorb energy at a higher $H_0$ give rise to an upfield absorption peak. The electrons of the compound of a sample influence the field at the nucleus such that it deviates slightly from the applied value. For the case that the chemical environment has no NMR effect, the value of $H_0$ at resonance with the radiofrequency held constant at $400\ MHz$ is

$$\frac{2\pi f}{\mu_0\gamma_P} = \frac{(2\pi)(400\ MHz)}{\mu_0 42.57602\ MHz\ T^{-1}} = H_0 \tag{7.77}$$

In the case that the chemical environment has a NMR effect, a different value of $H_0$ is required for resonance. This chemical shift is proportional to the electronic magnetic flux change at the nucleus due to the applied field that in the case of each hydrino hydride ion is a function of its radius.

The change in the magnetic moment, $\Delta\mathbf{m}$, of each electron of the hydride ion due to an applied magnetic flux $\mathbf{B}$ is [12]

$$\Delta\mathbf{m} = -\frac{e^2 r^2 \mathbf{B}}{4m_e} \tag{7.78}$$

The two electrons are spin-paired and the velocities are mirror opposites. Thus, the change in velocity of each electron treated individually (Eq. (10.3)) due to the applied field would be equal and opposite. However, as shown in the Three Electron Atom section, the two paired electrons may be treated as one with twice the mass where $m_e$ is replaced by $2m_e$ in Eq. (7.78). In this case, the paired electrons spin together about the applied field axis, the z-axis, to cause a reduction in the applied field according to Lenz's law. Then, the radius in Eq. (7.78) corresponds to the coordinate $\rho$ in cylindrical coordinates since it is perpendicular to the direction of the applied field along the z-axis. The integral over the entire flux linked by the hydride ion atomic orbital is given by

$$\Delta\mathbf{m} = -\frac{e^2\mathbf{B}}{8m_e}\frac{\int_{-r_1}^{r_1}\left(r_1^2 - z^2\right)dz}{2r_1} = -\frac{2}{3}\frac{e^2 r_1^2\mathbf{B}}{8m_e} \tag{7.79}$$

where $r_1$ is the radius of the hydride ion [13]. The change in magnetic flux $\Delta\mathbf{B}$ at the nucleus due to the change in magnetic moment, $\Delta\mathbf{m}$, given by Eq. (7.79) follows from Eq. (1.132).

$$\Delta\mathbf{B} = \mu_0\frac{\Delta m}{r_1^3}(\mathbf{i}_r\cos\theta - \mathbf{i}_\theta\sin\theta) \qquad \text{for } r < r_n \tag{7.80}$$

where $\mu_0$ is the permeability of vacuum. Substitution of Eq. (7.79) into Eq. (7.80) gives the absolute upfield chemical shift $\frac{\Delta B}{B}$ of $H^-(1/p)$ relative to a bare proton:

$$\frac{\Delta B_T}{B} = -\mu_0\frac{pe^2}{12m_e a_0\left(1+\sqrt{s(s+1)}\right)} = -p29.9\ ppm \tag{7.81}$$

where $p$ is an integer.

It follows from Eqs. (7.73) and (7.81) that the diamagnetic flux (flux opposite to the applied field) at the nucleus is inversely proportional to the radius, $r_1 = \frac{a_0}{p}\left(1+\sqrt{s(s+1)}\right)$. For resonance to occur, $\Delta H_0$, the change in applied field from that given by Eq. (7.77), must compensate by an equal and opposite amount as the field due to the electrons of the hydrino hydride ion. According to Eq. (7.73), the ratio of the radius of the hydrino hydride ion $H^-(1/p)$ to that of the ordinary hydride ion $H^-$ is the reciprocal of an integer $p$. It follows from Eqs. (7.75-7.81) that compared to a proton with no chemical shift, the ratio of $\Delta H_0$ for resonance of the proton of the hydrino hydride ion $H^-(1/p)$ to that of the ordinary hydride ion $H^-$ is a positive integer. That is, if only the size is considered, the absolute absorption peak of the hydrino hydride ion (i.e. relative to a proton with no shift) occurs at a value of $\Delta H_0$ that is a multiple of $p$ times the value that is resonant for $H^-$. However, the source current of the state must be considered in addition to the reduced radius.

As shown in the Stability of "Ground" and Hydrino States section, for the below "ground" (fractional quantum number) energy states of the hydrogen atom, $\sigma_{photon}$, the two-dimensional surface charge due to the "trapped photon" at the electron atomic orbital and phase-locked with the electron atomic orbital current, is given by Eqs. (6.7) and (6.8) wherein the principal quantum number of excited states is replaced by $n = \frac{1}{p}$.

$$\sigma_{photon} = \frac{e}{4\pi(r_n)^2}\left[Y_0^0(\theta,\phi) - \frac{1}{n}\left[Y_0^0(\theta,\phi) + \mathrm{Re}\left\{Y_\ell^m(\theta,\phi)e^{im\omega_n t}\right\}\right]\right]\delta(r-r_n)$$
$$n = \frac{1}{p};\ \ell = 0,1,2,...,p-1;\ m_\ell = -\ell,-\ell+1,...,0,...+\ell;\ m_s = \pm\frac{1}{2} \tag{7.82}$$

And, $\sigma_{electron}$ , the two-dimensional surface charge of the electron atomic orbital is

$$\sigma_{electron} = \frac{-e}{4\pi(r_n)^2}\left[Y_0^0(\theta,\phi) + \mathrm{Re}\left\{Y_\ell^m(\theta,\phi)e^{im\omega_n t}\right\}\right]\delta(r-r_n) \tag{7.83}$$

The superposition of $\sigma_{photon}$ (Eq. (7.82)) and $\sigma_{electron}$ , (Eq. (7.83)) where the spherical harmonic functions satisfy the conditions given in the Bound Electron "Atomic Orbital" section is:

$$\sigma_{photon} + \sigma_{electron} = \frac{-e}{4\pi(r_n)^2}\left[\frac{1}{n}Y_0^0(\theta,\phi) + \left(1+\frac{1}{n}\right)\mathrm{Re}\left\{Y_\ell^m(\theta,\phi)e^{im\omega_n t}\right\}\right]\delta(r-r_n) \tag{7.84}$$

The ratio of the total charge distributed over the surface at the radius of the hydride ion of the hydrino hydride ion $H^-(1/p)$ to that of the ordinary hydride ion $H^-$ is an integer $p$ , and the corresponding total source current of the hydrino hydride ion is equivalent to an integer $p$ times that of an electron. The "trapped photon" obeys the phase-matching condition given in Excited States of the One-Electron Atom (Quantization) section, and the source current of the state must be considered in addition to the reduced radius.

In the case that the photons and corresponding source current spin in opposite directions for the two electrons, the orbital magnetic moments cancel. However, as given in the Pair Production section, a photon having an energy equivalent to that of the mass energy of the electron may undergo particle production to form an electron. To maintain continuity, the photon surface current of a hydrino hydride state must behave as the charge equivalent to its energy during the interaction of the electrons and the phased locked photon-field surface current with the external magnetic field such that the photon component gives rise to a proportional diamagnetic effect as well. The photon diamagnetic component is given by Eqs. (29.10-29.11) as the charge equivalent to its energy that superimposes with the diamagnetism of the two electrons. The relativistic term after Eq. (29.10) and the central field magnitude term for the hydrino hydride state having principle quantum number $p$ are $\alpha^2$ and $p$ , respectively. The photon contribution to the change in flux $\Delta\mathbf{B}_{SR}$ for hydrino hydride $H^-(1/p)$ given by applying the corresponding relativistic factor of $\gamma_{SR} = \alpha^2$ to Eq. (7.80) is

$$\Delta\mathbf{B}_{SR} = -p\alpha^2\mu_0\frac{\Delta m}{r_n^3}(\mathbf{i}_r\cos\theta - \mathbf{i}_\theta\sin\theta) \qquad \text{for } r < r_n \tag{7.85}$$

Thus, using Eqs. (7.81) and (7.86), the upfield chemical shift $\frac{\Delta B_{SR}}{B}$ due to the photon contribution of the ion $H^-(1/p)$ corresponding to the lower-energy state with principal quantum energy state $p$ is given by:

$$\frac{\Delta B_{SR}}{B} = -p\alpha^2\mu_0\frac{pe^2}{12m_e a_0\left(1+\sqrt{s(s+1)}\right)} \tag{7.86}$$

The total shift $\frac{\Delta B_T}{B}$ for $H^-(1/p)$ is given by the sum of that of the two electrons given by Eq. (7.81) and that of the photon given by Eq. (7.86):

$$\frac{\Delta B_T}{B} = -\mu_0\frac{pe^2}{12m_e a_0\left(1+\sqrt{s(s+1)}\right)}\left(1+p\alpha^2\right) = -\left(p29.9 + p^2 1.59\ X\ 10^{-3}\right)ppm \tag{7.87}$$

where the first term applies to $H^-$ with $p=1$ and $p=\text{integer}>1$ for $H^-(1/p)$. The experimental absolute resonance shift of TMS is -31.5 ppm relative to the proton's gyromagnetic frequency [14-15]. Thus, the theoretical shift of $H^-(1/p)$ relative to TMS standard is given by the difference of Eq. (7.87) and -31.5 ppm.

## Hydrino Hydride Ion Hyperfine Lines

For the ordinary hydride ion $H^-$, a continuum is observed at shorter wavelengths of the ionization or binding energy referred to as the bound-free continuum. For typical conditions in the photosphere, Figure 4.5 of Stix [16] shows the continuous absorption coefficient $\kappa_C(\lambda)$ of the Sun. In the visible and infrared spectrum, the hydride ion $H^-$ is the dominant absorber. Its free-free continuum starts at $\lambda = 1.645\ \mu m$, corresponding to the ionization energy of $0.745\ eV$ for $H^-$ with strongly increasing absorption towards the far infrared. The ordinary hydride spectrum recorded on the Sun is representative of the hydride spectrum in a very hot plasma.

The reaction of a hydrogen atom with a second electron to form ordinary hydride ion comprising two paired electrons in a single shell releases continuum radiation to longer wavelengths with a cutoff of the binding energy of the second electron of the hydride ion as shown by Stix [16]. However, hydrino hydride ion and the corresponding emission of a hydrino atom binding a second electron are unique. Hydrino hydride ion comprises an unpaired electron which results the emission of the binding energy of the second electron being released with additional quantized units of energy based on linkage of flux increments of the fluxon or magnet flux quantum $\frac{h}{2e}$. Specifically, hydrino $H^-(1/p)$comprises (i) two electrons bound in a minimum energy, equipotential, spherical, two-dimensional current membrane wherein the electrons of $H^-(1/p)$ are unpaired in the same shell at the same position $r$ and (ii) a photon that increases the central field by an integer of the fundamental charge at the nucleus centered on the origin of the sphere. The interaction of the hydrino state photon electric field with each electron gives rise to a nonradiative radial monopole such that the state is stable. The combination of two electrons into a single atomic orbital (AO) while maintaining the radiationless integer photonic central field gives rise to the special case of a doublet AO state in hydrino hydride ion rather than a singlet state as in the case of ordinary hydride ion. The singlet state is nonmagnetic; whereas, the doublet state has a net magnetic moment of a Bohr magneton $\mu_B$.

Specifically, the basis element of the current of the atomic orbital is a great circle as shown in the Generation of the Atomic Orbital-CVFS section. As shown in the Equation of the Electric Field inside the Atomic Orbital section, (i) photons carry electric field and comprise closed field line loops, (ii) a hydrino atom comprises a trapped photon wherein the photon field-line loops each travel along a mated great circle current loop basis element in the same vector direction, (iii) the direction of each field line increases in the direction perpendicular to the propagation direction with relative motion as required by special relativity, and (iv) since the linear velocity of each point along a field line loop of a trapped photon is light speed $c$, the electric field direction relative to the laboratory frame is purely perpendicular to its mated current loop and it exists only at $\delta(r - r_n)$. The paired electrons of the $H^-$ atomic orbital comprise a singlet state having no net magnetic moment. However, the photon field lines of a hydrino hydride ion can only propagate in one direction to avoid cancellation and give rise to a central field to provide force balance between the centrifugal and central forces (Eq. (7.72)). This special case gives rise to a doublet state in hydrino hydride ion.

The hydrino hydride AO may be treated as a linear combination of the great circles that comprise the current density function of each electron as given in the Generation of the Orbitsphere-CVFS section. To meet the boundary conditions that the photon is matched in direction with the electron current and that the electron angular momentum is $\hbar$ are satisfied, one half of electron 1 and one half of electron 2 may be spin up and matched with the photon, and the other half of electron 1 may be spin up and the other half of electron 2 may be spin down such that one half of the currents are paired and one half of the currents are unpaired. Given the indivisibility of each electron and the condition that the AO comprises two identical electrons, the force of the photon is transferred to the totality of the electron AO comprising a linear combination of the two identical electrons to satisfy Eq. (7.72). The resulting angular momentum and magnetic moment of the unpaired current density are $\hbar$ and a Bohr magneton $\mu_B$, respectively. As given in the Electron g Factor section, flux is linked by an unpaired electron in quantized units of the fluxon or magnetic flux quantum $\frac{h}{2e}$.

Hydride ions formed by the reaction of hydrogen or hydrino atoms with free electrons with a kinetic energy distribution give rise to the bound-free emission band to shorter wavelengths than the ionization or binding energy due to the release of the electron kinetic energy and the hydride ion binding energy. As shown by Eq. (7.74) compared to Eq. (7.71), the energies for the formation of hydrino hydride ions are much greater, and with sufficient spectroscopic resolution, it may be possible to resolve the unique hyperfine structure in the corresponding bound-free band due to interactions of the free and bound electrons during the formation of hydrino hydride ion. The derivation of the hyperfine lines of the unique doublet state follows.

Consider a free electron binding to a hydrino atom to form a hydrino hydride ion. The total angular momentum of an electron is $\hbar$. During binding of the free electron, the bound electron produces a magnetic field at the free electron given by Eq. (1.133). Thus, for radial distances greater than the radius of the hydride ion, the magnetic field is equivalent to that of a magnetic dipole of a Bohr magneton at the origin. The energy of interaction of a magnetic dipole with the magnetic field of the bound electron $E_{ss}$, the spin-spin energy, is given by Eq. (1.227)—the product of the electron g factor given by Eq. (1.226), the magnetic moment of the free electron, a Bohr magneton given by Eq. (1.131), and the magnetic flux which follows from Eq. (1.133).

$$E_{ss} = g\mu_B\mu_0 H = g\mu_B B = g\frac{\mu_0}{r^3}\left(\frac{e\hbar}{2m_e}\right)^2 \tag{7.88}$$

where $\mu_0$ is the permeability of free space, $r$ is the radius of the hydride ion $H^-(1/p)$ given by Eq. (7.73), and $p$ is an integer. $E_{ss}$ for $H^-(1/2)$ is given by

$$E_{ss} = 0.011223\ eV \tag{7.89}$$

where the radius given by Eq. (7.73) for $p = 2$ is:

$$r_1 = 0.93301 a_0 \tag{7.90}$$

From Eqs. (7.74) and (7.73), the binding energy $E_B$ of $H^-(1/2)$ is:

$$E_B = 3.0471\ eV\ \ (4069.0\ \text{Å}) \tag{7. 91}$$

When a free electron binds to the hydrino atom $H(1/2)$ to form a hydride ion $H^-(1/2)$, a photon is emitted with a minimum energy equal to the binding energy ($E_B = 3.0471\ eV$). Any kinetic energy that the free electron possesses must increase the energy of the emitted photon. The interaction of the two electrons quantizes this emission by the same mechanism as that observed in the Stern Gerlach experiment—quantization of flux linkage. Superconducting Quantum Interference Devices (SQUIDs) or wire loops linked to SQUIDs also show quantization of flux and the corresponding energies as shown in the Schrödinger Fat Cats—Another Flawed Interpretation section.

In the Stern-Gerlach experiment, a magnetic field is applied along the z-axis called the spin axis. The superposition of the vector projection of the atomic orbital angular momentum on the z-axis is $\frac{\hbar}{2}$ with an orthogonal component of $\frac{\hbar}{4}$. Excitation of a resonant Larmor precession gives rise to $\hbar$ on an axis $\mathbf{S}$ that precesses about the spin axis at an angle of $\theta = \frac{\pi}{3}$. $\mathbf{S}$ rotates about the z-axis at the Larmor frequency. $\mathbf{S}_\perp$, the transverse projection ($Y_R$-axis of Figure 1.25), is $\pm\sqrt{\frac{3}{4}}\hbar$, and $\mathbf{S}_\parallel$, the projection onto the axis of the applied magnetic field (z-axis), is $\pm\frac{\hbar}{2}$. As shown in the Spin Angular Momentum of the Atomic Orbital $Y_0^0(\theta,\phi)$ section, the superposition of the $\frac{\hbar}{2}$ z-axis component of the atomic orbital angular momentum and the $\frac{\hbar}{2}$ z-axis component of $\mathbf{S}$ gives $\hbar$ corresponding to the observed electron magnetic moment of a Bohr magneton, $\mu_B$. As given in the Electron g Factor section, the electron links flux in units of the magnetic flux quantum $\Phi_0 = \frac{h}{2e}$ during a Stern-Gerlach transition, which conserves the angular momentum of the electron of $\hbar$. Due to the field of the bound electron, the free electron possessing kinetic energy will precess about the z-axis as it orbits the bound electron giving an additional component of angular momentum. A resonance exists when the transverse precessional angular momentum along the $Y_R$-axis of Figure 1.25 is an integer number of $\frac{\hbar}{\sqrt{s(s+1)}}$ such that its projection onto the $\mathbf{S}$-axis is $\hbar$. In order to conserve angular momentum of both electrons as the bound electron links an integer number of fluxons due to the free electron, the corresponding fluxon energy $E_\Phi$ due the free electron's $Y_R$-axis component of $j\frac{\hbar}{\sqrt{s(s+1)}}$ follows from Eq. (1.226) wherein the angular momentum corresponding to the Bohr magneton, $\hbar$, is replaced by $j\frac{\hbar}{\sqrt{s(s+1)}}$, and the magnetic flux density $B$ is given by the ratio of the flux to the area.

$$\begin{aligned} E_\Phi &= j(g-2)\frac{\mu_B}{\sqrt{s(s+1)}}B = j(g-2)\frac{\mu_B}{\sqrt{s(s+1)}}\left(\frac{j\Phi_0}{A}\right) = j^2(g-2)\frac{\mu_B}{\sqrt{s(s+1)}}B \\ &= j^2(g-2)\frac{\mu_B}{\sqrt{s(s+1)}}\frac{\mu_0}{r^3}\left(\frac{e\hbar}{2m_e}\right) \end{aligned} \tag{7.92}$$

where $j$ is an integer, $s = 1/2$, and $A$ is the area linked by the integer number of fluxons as given in the Electron g Factor section. The additional angular momentum due to the kinetic energy of the binding free electron is conserved in rotational energy of the resulting hydride ion. The flux linkage energy applies to each of the two electrons; thus, a factor of two in Eq. (7.92) is required. This is analogous to mutual induction. The electrons flip in opposite directions and conserve angular momentum by linking flux in integer units of the magnetic flux quantum, which corresponds to the term $(g-2)$. With the

radius given by Eq. (7.73), the fluxon energy $E_\Phi$ of $H^-(1/2)$ for both electrons is given by

$$E_\Phi = j^2 2(g-2)\frac{\mu_B}{\sqrt{s(s+1)}}\frac{\mu_0}{r^3}\left(\frac{e\hbar}{2m_e}\right) = j^2 3.00213\ X\ 10^{-5}\ eV \tag{7.93}$$

The energies of the hyperfine lines $E_{HF}$, are given by the sum of the binding energy (Eqs. (7.74) and (7.91)), the spin-spin energy (Eqs. (7.88) and (7.89)), and the fluxon energy (Eqs. (7.92) and (7.93)).

$$\begin{aligned} E_{HF} &= E_\Phi + E_{ss} + E_B = \left(j^2 3.00213\ X\ 10^{-5} + 0.011223 + 3.0471\right)\ eV \\ &= \left(j^2 3.00213\ X\ 10^{-5} + 3.0583\right)\ eV \end{aligned} \qquad (j \text{ is an integer}) \tag{7.94}$$

The observation of bound-free hyperfine peaks requires an electron-binding threshold with a large cross section. Ordinary hydride ion does not have a fine structure transition; thus, it shows only a hydride binding energy continuum [17]. The existence of fine structure transitions in $H(1/2)$ provides a mechanism to observe a peak corresponding to the formation of a free hydride ion by the binding of an electron. The predicted energy difference between the $1/2P_{1/2}$, $1/2S_{1/2}$ and $1/2P_{3/2}$ levels of the hydrogen atom, the fine structure splitting given by Eq. (2.194), is:

$$E_{s/o} = 8\alpha^5(2\pi)^2 m_e c^2\sqrt{\frac{3}{4}} = 2.8922\ X\ 10^{-3}\ eV \tag{7.95}$$

From Eq. (2.69) and the Spin-Nuclear Coupling section, the spin-orbit coupling is proportional to the applied flux due to spin and orbital angular momentum. With the requirement of the quantization of flux in integer units of the magnetic flux quantum during binding as shown in the Electron g Factor section, the corresponding emission is at a longer wavelength having an energy of the binding energy minus an integer times the fine structure energy. The peak due to the binding energy (Eqs. (7.91)) with excitation of the fine structure splitting (Eq. (7.95)) is given by:

$$E_{Bs/o} = E_B - E_{s/o} = 3.0471\ eV - 2.8922\ X\ 10^{-3}\ eV = 3.0442\ eV\ \ (\lambda_{air} = 4071.7\ \text{Å}) \tag{7.96}$$

The $1/2P_{3/2}$, $1/2P_{1/2}$, and $1/2S_{1/2}$ levels are also split by spin-nuclear and orbital-nuclear coupling. $1/2S_{1/2}$—$1/2P_{3/2}$ and $1/2P_{1/2}$—$1/2P_{3/2}$ transitions occur between hyperfine levels; thus, the transition energy is the sum of the fine structure and the corresponding hyperfine energy. The hyperfine splitting of $H(1/2)$ given in the Spin-Nuclear Coupling section are $1.4191\ X\ 10^{-4}\ eV$ and $3.426\ X\ 10^{-4}\ eV$ for $\ell = 0$ and $\ell = 1$, respectively. In addition to a continuum, the binding of an electron to $H(1/2)$ has a resonance emission with excitation of transitions between hyperfine levels of the fine structure levels.

The ionization of $Rb^+$ and an electron transfer between two $K^+$ ions (Eqs. (5.6-5.9)) provide a reaction with a net enthalpy of an integer multiple of the potential energy of atomic hydrogen, $27.2\ eV$. The corresponding Group I nitrates provide these reactants as volatilized ions directly or as atoms by undergoing decomposition or reduction to the corresponding metals that are ionized in a plasma. The presence of each of the reactants identified as providing an enthalpy of $27.2\ eV$ formed a low-applied temperature, extremely-low-voltage plasma in atomic hydrogen called a resonant transfer or rt-plasma having strong vacuum ultraviolet (VUV) emission [18-20]. The catalyst product of $Rb^+$ and two $K^+$, $H(1/2)$, was predicted to be a highly reactive intermediate which further reacts to form a hydrino hydride ion $H^-(1/2)$.

$H^-(1/2)$ ions form by the reaction of $H(1/2)$ atoms with free electrons that have a kinetic energy distribution. The release of the electron kinetic energies and the hydrino hydride ion binding energy gives rise to the bound-free emission band to shorter wavelengths than the ionization or binding energy of the corresponding hydride ion. Due to the requirement that flux is linked by $H(1/2)$ in integer units of the magnetic flux quantum, the energy is quantized, and the emission due to $H^-(1/2)$ formation comprises a series of hyperfine lines in the corresponding bound-free band. From the electron g factor and using the observed binding energy peak $E_B^*$, the bound-free hyperfine structure lines due to interactions of the free and bound electrons have predicted energies $E_{HF}$ given by the sum of the fluxon energy $E_\Phi$, the spin-spin energy $E_{ss}$, and the observed binding energy peak $E_B^*$:

$$\begin{aligned} E_{HF} &= E_\Phi + E_{ss} + E_B^* \\ &= j^2 2(g-2)\frac{\mu_B}{\sqrt{s(s+1)}}\frac{\mu_0}{r^3}\left(\frac{e\hbar}{2m_e}\right) + g\frac{\mu_0}{r^3}\left(\frac{e\hbar}{2m_e}\right)^2 + E_B^* \\ &= \left(j^2 3.00213\ X\ 10^{-5} + 0.011223 + 3.0451\right)\ eV \\ &= \left(j^2 3.00213\ X\ 10^{-5} + 3.0563\right)\ eV \end{aligned} \tag{7.97}$$

where j = integer. This is compared to $E_{HF} = \left( j^2 3.00213\, X\, 10^{-5} + 3.0583 \right) eV$ with the unperturbed $E_B$ given by Eqs. (7.73) and (7.74). The predicted spectrum is an inverse Rydberg-type series that converges at increasing wavelengths and terminates at 3.0563 eV, the hydride binding energy with the fine structure plus the spin-pairing energies. The high-resolution visible plasma emission spectra in the region of 4000 Å to 4060 Å shown in FIGURE 62 matched the predicted emission lines to 1 part in $10^5$.

Specifically, the predicted $3.0471\, eV$ binding energy of $H^- \left( 1/2 \right)$ was observed as a continuum threshold at 3.047 eV ($\lambda_{air} = 4068$ Å). The experimental $H^- \left( 1/2 \right)$ peak $E_B^*$ at 4070.6 Å (air wavelength) was used to calculate the peak positions of the bound-free hyperfine lines by substitution of the corresponding energy of 3.0451 eV into Eq. (7.97) for $E_B$ to give the bound-free hyperfine structure lines of $H^- \left( 1/2 \right)$. The high resolution visible plasma emission lines in the region of 3995 Å to 4060 Å, comprising an inverse Rydberg-type series from 3.0563 eV to 3.1012 eV matched the predicted hyperfine splitting emission energies $E_{HF}$ given by Eq. (7.97) for $j = 1$ to $j = 39$ with the series edge at 3996.3 Å up to 1 part in $10^5$ [18-20]. The flat intensity profile matches that of Josephson junctions such as ones of superconducting quantum interference devices (SQUIDs) that also link magnetic flux in quantized units of the magnetic flux quantum $\frac{h}{2e}$.

# REFERENCES


1. F. Bueche, *Introduction to Physics for Scientists and Engineers*, McGraw-Hill, (1975), pp. 352-353.
2. J. D. Jackson, *Classical Electrodynamics*, Second Edition, John Wiley & Sons, New York, (1975), pp. 236-240, 601-608, 786-790.
3. D. A. McQuarrie, *Quantum Chemistry*, University Science Books, Mill Valley, CA, (1983), pp. 238-241.
4. J. D. Jackson, *Classical Electrodynamics*, Second Edition, John Wiley & Sons, New York, (1975), p. 178.
5. E. M. Purcell, *Electricity and Magnetism*, McGraw-Hill, New York, (1985), Second Edition, pp. 451-458.
6. E. M. Purcell, *Electricity and Magnetism*, McGraw-Hill, New York, (1985), Second Edition, pp. 176-178.
7. J. D. Jackson, *Classical Electrodynamics*, Second Edition, John Wiley & Sons, New York, (1975), pp. 747-752.
8. C. E. Moore, "Ionization Potentials and Ionization Limits Derived from the Analyses of Optical Spectra," Nat. Stand. Ref. Data Ser.-Nat. Bur. Stand. (U.S.), No. 34, 1970.
9. R. C. Weast, CRC Handbook of Chemistry and Physics, 58 Edition, CRC Press, West Palm Beach, Florida, (1977), p. E-68.
10. G. R. Fowles, *Analytical Mechanics*, Third Edition, Holt, Rinehart, and Winston, New York, (1977), pp. 154-156.
11. K. R. Lykke, K. K. Murray, W. C. Lineberger, "Threshold photodetachment of $H^-$," Phys. Rev. A, Vol. 43, No. 11, (1991), pp. 6104-6107.
12. E. Purcell, *Electricity and Magnetism*, McGraw-Hill, New York, (1985), pp. 413-418.
13. G. R. Fowles, *Analytical Mechanics*, Third Edition, Holt, Rinehart, and Winston, New York, (1977), p. 195-196.
14. K. K. Baldridge, J. S. Siegel, "Correlation of empirical $\delta$(TMS) and absolute NMR chemical shifts predicted by ab initio computations," J. Phys. Chem. A, Vol. 103, (1999), pp. 4038-4042.
15. J. Mason, Editor, *Multinuclear NMR*, Plenum Press, New York, (1987), Chp. 3.
16. M. Stix, *The Sun*, Springer-Verlag, Berlin, (1991), p. 136
17. K. R. Lykke, K. K. Murray, W. C. Lineberger, "Threshold photodetachment of $H^-$," Phys. Rev. A, Vol. 43, No. 11, (1991), pp. 6104-6107.
18. R. L. Mills, P. Ray, "A Comprehensive Study of Spectra of the Bound-Free Hyperfine Levels of Novel Hydride Ion $H^-\left(1/2\right)$, Hydrogen, Nitrogen, and Air", Int. J. Hydrogen Energy, Vol. 28, No. 8, (2003), pp. 825-871.
19. R. Mills, W. Good, P. Jansson, J. He, "Stationary Inverted Lyman Populations and Free-Free and Bound-Free Emission of Lower-Energy State Hydride Ion formed by and Exothermic Catalytic Reaction of Atomic Hydrogen and Certain Group I Catalysts," Cent. Eur. J. Phys., Vol. 8, (2010), 7–16, doi: 10.2478/s11534-009-0052-6.
20. R. L. Mills, P. Ray, "Stationary Inverted Lyman Population and a Very Stable Novel Hydride Formed by a Catalytic Reaction of Atomic Hydrogen and Certain Catalysts," J. Opt. Mat., 27, (2004), 181–186.
21. R. L. Mills, P. C. Ray, R. M. Mayo, M. Nansteel, W. Good, P. Jansson, B. Dhandapani, J. He, "Hydrogen Plasmas Generated Using Certain Group I Catalysts Show Stationary Inverted Lyman Populations and Free-Free and Bound-Free Emission of Lower-Energy State Hydride," Res. J. Chem Env., Vol. 12(2), (2008), 42–72.

# Chapter 8

# CLASSICAL PHOTON AND ELECTRON SCATTERING

## CLASSICAL SCATTERING OF ELECTROMAGNETIC RADIATION

Light is an electromagnetic disturbance that is propagated by vector wave equations that are readily derived from Maxwell's equations. The Helmholtz wave equation results from Maxwell's equations. The Helmholtz equation is linear; thus, superposition of solutions is allowed. Huygens' principle is that a point source of light will give rise to a spherical wave emanating equally in all directions. Superposition of this particular solution of the Helmholtz equation permits the construction of a general solution. An arbitrary wave shape may be considered as a collection of point sources whose strength is given by the amplitude of the wave at that point. The field, at any point in space, is simply a sum of spherical waves. Applying Huygens' principle to a disturbance across a plane aperture gives the amplitude of the far field as the Fourier transform of the aperture distribution, i.e., apart from constant factors,

$$\psi(x,y) = \int\int A(\xi,\eta)\exp\left[\frac{-ik}{f}(\xi \mathrm{x} + \eta \mathrm{y})\right] d\xi d\eta \tag{8.1}$$

Here $A(\xi,\eta)$ describes the amplitude and phase distribution across the aperture and $\psi(x,y)$ describes the far field [1] where $f$ is the focal length.

## DELTA FUNCTION

In many diffraction and interference problems, it proves convenient to make use of the Dirac delta function. This function is defined by the following property: let $f(\xi)$ be any function (satisfying some very weak convergence conditions which need not concern us here) and let $\delta(\xi - \xi')$ be a delta function centered at the point $\xi'$; then:

$$\int_a^b f(\xi)\delta(\xi - \xi')d\xi = f(\xi') \qquad (a < \xi' < b);\ 0\ \textit{otherwise} \tag{8.2}$$

We note, therefore, that:

$$\int_{-\infty}^{\infty} \delta(\xi - \xi')d\xi = 1 \tag{8.3}$$

the Fourier transform of the delta function is given by:

$$\psi(x) = \int \delta(\xi - \xi')\exp\left[\frac{-ik\mathrm{x}\xi}{f}\right] d\xi \tag{8.4}$$

which by definition of the delta function becomes:

$$\psi(x) = \exp\left[\frac{-ik\mathrm{x}\xi'}{f}\right] \tag{8.5}$$

The amplitude is constant and the phase function $\left(\frac{-ik\mathrm{x}\xi'}{f}\right)$ depends on the origin.

## THE ARRAY THEOREM

A large number of interference problems involve the mixing of similar diffraction patterns. That is, they arise in the study of the combined diffraction patterns of an array of similar diffracting apertures. This entire class of interference effects can be described by a single equation, the array theorem. This unifying theorem is easily developed as follows: Let $\psi(\xi)$ represent the amplitude and phase distribution across one aperture centered in the diffraction plane, and let the total diffracting aperture consist of a collection of these elemental apertures at different locations $\xi_n$. We require first a method of representing such an array. The appropriate representation is obtained readily by means of the delta function. Thus, if an elemental aperture is positioned such that its center is at the point $\xi_n$, the appropriate distribution function is $\psi(\xi-\xi_n)$. The combining property of the delta function allows us to represent this distribution as follows:

$$\psi(\xi-\xi_n)=\int\psi(\xi-\alpha)\delta(\alpha-\xi_n)d\alpha \tag{8.6}$$

The integral in Eq. (8.6) is termed a "convolution" integral and plays an important role in Fourier analysis. Thus, if we wish to represent a large number $N$ of such apertures with different locations, we could write the total aperture distribution $\Psi(\xi)$ as a sum, i.e.,

$$\Psi(\xi)=\sum_{n=1}^{N}\psi(\xi-\xi_n) \tag{8.7}$$

Or in terms of the delta function we could write, combining the features of Eqs. (8.6) and (8.7),

$$\Psi(\xi)=\sum_{n=1}^{N}\int\psi(\xi-\alpha)\delta(\alpha-\xi_n)d\alpha \tag{8.8}$$

Eq. (8.8) may be put in a more compact form by introducing the notation

$$A(\alpha)=\sum_{n=1}^{N}\delta(\alpha-\xi_n) \tag{8.9}$$

thus, Eq. (8.8) becomes:

$$\Psi(\xi)=\int\psi(\xi-\alpha)A(\alpha)d\alpha \tag{8.10}$$

which is physically pleasing in the sense that $A(\alpha)$ characterizes the array itself. That is, $A(\alpha)$ describes the location of the apertures and $\psi(\xi)$ describes the distribution across a single aperture. We are in a position to calculate the far field or Fraunhofer diffraction pattern associated with the array. We have the theorem that the Fraunhofer pattern is the Fourier transform of the aperture distribution. Thus, the Fraunhofer pattern $\tilde{\Psi}(\mathrm{x})$ of the distribution $\Psi(\xi)$ is given by

$$\tilde{\Psi}(\mathrm{x})=\int\Psi(\xi)\exp\left(\frac{-2\pi i\xi\cdot\mathbf{x}}{\lambda \mathrm{f}}\right)d\xi \tag{8.11}$$

substituting from Eq. (8.10) gives:

$$\tilde{\Psi}(\mathrm{x})=\left[\iint\psi(\xi-\alpha)A(\alpha)d\alpha\right]\exp\left(\frac{-2\pi i\xi\cdot\mathbf{x}}{\lambda \mathrm{f}}\right)d\xi \tag{8.12}$$

A very important theorem of Fourier analysis states that the Fourier transform of a convolution is the product of the individual Fourier transforms [1]. Thus, Eq. (8.12) may be written as:

$$\tilde{\Psi}(\mathrm{x})=\tilde{\psi}(\mathrm{x})\tilde{A}(\mathrm{x}) \tag{8.13}$$

where $\tilde{\psi}(\mathrm{x})$ and $\tilde{A}(\mathrm{x})$ are the Fourier transforms of $\psi(\xi)$ and $A(\alpha)$. Eq. (8.13) is the array theorem and states that the diffraction pattern of an array of similar apertures is given by the product of the elemental pattern $\tilde{\psi}(\mathrm{x})$ and the pattern that would be obtained by a similar array of point sources, $\tilde{A}(\mathrm{x})$. Thus, the separation that first arose in Eq. (8.10) is retained. To analyze the complicated patterns that arise in interference problems of this sort, one may analyze separately the effects of the array and the effects of the individual apertures.

## APPLICATIONS OF THE ARRAY THEOREM

### TWO-SLIT INTERFERENCE (WAVE-PARTICLE DUALITY)

Photons superimpose such that in the far field, the emitted wave is a spherical wave where the total electric field is given by Eq. (4.23):

$$\mathbf{E}_{total}=E_0\frac{e^{-ikr}}{r} \tag{8.14}$$

which is shown by Bonham to be required in order to insure continuity of power flow for wavelets from a single source [2]. The Green Function, (Eq. (6.62) of Jackson [3]) is given as the solution of the wave equation (Eq. (6.58) of Jackson [3]). Thus, the superposition of photons gives the classical result. As $r$ goes to infinity, the spherical wave given by Eq. (8.14) or Eq. (4.23) becomes a plane wave. The double slit interference pattern is derived in Eqs. (8.15-8.23). From the equations of a photon given in the Equation of the Photon section, the wave-particle duality arises naturally. The energy is always given by Planck's equation as also shown in the Equation of the Photon section; yet, an interference pattern is observed when photons add over time or space.

Similarly, rather than a point, the electron is an extended particle which may impinge on a double slit one electron at a

time. As shown in the Electron in Free Space section, the ionized electron is a plane-lamina disc of charge (mass)-density given by Eqs. (3.7-3.8) and current (momentum)-density given by Eqs. (3.19) and (3.20) with a radius $\rho_0$ such that $2\pi\rho_0 = \lambda_0$ wherein $\lambda_0$ is the de Broglie wavelength. In the case that the electron de Broglie wavelength (Eq. (3.24)) and therefore the size of the electron is comparable to the slit size and/or separation, the resulting intensity pattern of electrons striking a detector beyond the slits is equivalent to a wave interference pattern. This result arises even though the electrons are not physically interacting with each other. Nothing is actually interfering. As in the case of the photon, the wave-particle duality nature of the electron arises classically.

The electron-slit interaction is mediated by photons, each of which have quantized angular momentum in units of $\hbar$. This angular momentum and the $\hbar$ of angular momentum of the electron is conserved during the interaction such that the de Broglie relationship holds as given in the Classical Physics of the de Broglie Relationship section. For photon diffraction, the $\hbar$ of angular momentum of the photon is conserved during an interaction directly. In each case, the pattern in the far-field is a map of the conserved momentum density of the particles incident on the slit or slits.

We use Eq. (8.13) to describe the simplest of interference experiments, Young's double-slit experiment in one dimension. The individual aperture will be described by

$$\Psi(\xi) = (C \quad |\xi| < a; \qquad 0 \quad |\xi| > a) = rec(\xi \,|\, a) \tag{8.15}$$

Here C is a constant representing the amplitude transmission of the apertures. This is essentially a one-dimensional problem and the diffraction integral may be written as

$$\tilde{\Psi}(\mathrm{x}) = \int \Psi(\xi) \exp\left(\frac{-ik\xi\cdot\mathbf{x}}{\mathrm{f}}\right) d\xi = C\int_{-a}^{a} \exp\left(\frac{-ik\xi\cdot\mathbf{x}}{\mathrm{f}}\right) d\xi \tag{8.16}$$

The integral in Eq. (8.16) is readily evaluated to give:

$$\tilde{\Psi}(\mathrm{x}) = \frac{-Cf}{ik\mathrm{x}}\left[\exp\left(\frac{-ika\mathrm{x}}{\mathrm{f}}\right) - \exp\left(\frac{+ika\mathrm{x}}{\mathrm{f}}\right)\right] = 2aC\frac{\sin\left(\frac{ka\mathrm{x}}{\mathrm{f}}\right)}{\left(\frac{ka\mathrm{x}}{\mathrm{f}}\right)} \tag{8.17}$$

The notation $\mathrm{sinc}\,\theta = \dfrac{\sin\theta}{\theta}$ is frequently used and in terms of this function $\tilde{\Psi}(\mathrm{x})$ may be written as:

$$\tilde{\Psi}(\mathrm{x}) = 2aC\ \mathrm{sinc}\left(\frac{ka\mathrm{x}}{\mathrm{f}}\right) \tag{8.18}$$

Thus, the result is that the elemental distribution in the Fraunhofer plane is Eq. (8.18). The array in this case is simply two delta functions; thus,

$$A(\xi) = \delta(\xi - b) + \delta(\xi + b) \tag{8.19}$$

The array pattern is, therefore,

$$\tilde{A}(\mathrm{x}) = \int\left[\delta(\xi - b) + \delta(\xi + b)\right]\exp\left(\frac{-2\pi i\xi\cdot\mathbf{x}}{\lambda\mathrm{f}}\right) d\xi \tag{8.20}$$

Eq. (8.20) is readily evaluated by using the combining property of the delta function, thus,

$$\tilde{A}(\mathrm{x}) = \exp\left(\frac{2\pi ib\mathrm{x}}{\lambda\mathrm{f}}\right) + \exp\left(\frac{-2\pi ib\mathrm{x}}{\lambda\mathrm{f}}\right) = 2\cos\left(\frac{2\pi b\mathrm{x}}{\lambda\mathrm{f}}\right) \tag{8.21}$$

Finally, the diffraction pattern of the array of two slits is:

$$\tilde{\Psi}(\mathrm{x}) = 4aC\ \mathrm{sinc}\left(\frac{2\pi a\mathrm{x}}{\lambda\mathrm{f}}\right)\cos\left(\frac{2\pi b\mathrm{x}}{\lambda\mathrm{f}}\right) \tag{8.22}$$

The intensity is

$$I(\mathrm{x}) = 16a^2C^2\mathrm{sinc}^2\left(\frac{2\pi a\mathrm{x}}{\lambda f}\right)\cos^2\left(\frac{2\pi b\mathrm{x}}{\lambda f}\right) \tag{8.23}$$

From Eq. (8.23), it is clear that the resulting pattern has the appearance of cosine-squared fringes of period $\lambda f / b$ with an envelope $\mathrm{sinc}^2\left(2\pi a\mathrm{x} / \lambda f\right)$.

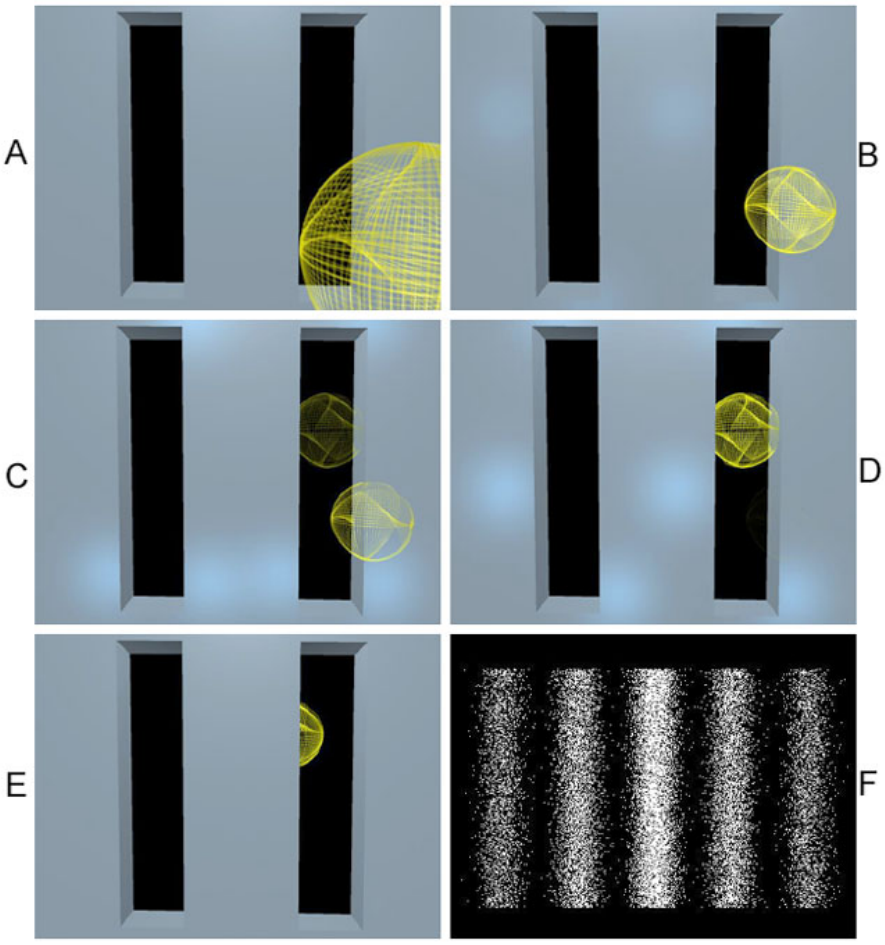
In the case of photon diffraction, the far field interference pattern given by Eqs. (8.22-8.23) is due to conservation of angular momentum of the photon interaction with the slits. The pattern is not due to constructive and destructive interference of photon electric fields. Photons cannot be created or destroyed by superimposing. If this were true, it would be possible to cool a room or to cloak an object by illumination. Constructive and destructive interference violates the first and second laws of thermodynamics[1]. The correct physics is based on conservation of the $\hbar$ of photon angular momentum and $\hbar\omega$ of photon energy.

The incident photons have a size comparable to their wavelength as given in the Equation of the Photon section. A

[1] Similarly, the constructive and destructive interference of probability waves makes no sense. Nor does negative probability or probability that is based on noncausality. The interference pattern is a map of the momentum density. This physical basis applies to photon and particle diffraction as given *infra.* wherein the particle, photon, and consequently the slit interaction is quantized in units of $\hbar$. The double-slit experiment is predicted by classical laws that dispel the belief that quantum weirdness must be invoked to explain the double-slit experiment.

diffraction pattern is observed when the slit dimensions are comparable to the photon wavelength. The physical basis of the mechanism is that each photon interacts with the slit apparatus to give rise to an electron or polarization current. Each photon is reemitted, and the regions of high and low intensity due to more or less photons impinging at locations of the detector are generated, as the number of photons diffracted grows large. The pattern is based on conservation of the momentum of the slit-source currents and re-emitted photon distribution. Here, in the case of each incident and diffracted photon, the transverse displacement is related to the change in the transverse component of the angular momentum of the photon. The corresponding pattern is representative of the aggregate momentum distribution of slit-apparatus current induced by many photon interactions. The same physics of momentum conservation in the electric and magnetic radiation fields determines the radiation pattern of a multipole source as given in the Excited States of the One-Electron Atom (Quantization) section. Photon diffraction is shown schematically in Figure 8.1.

**Figure 8.1.** (A) The incident photon is emitted from a source and travels to the slit apparatus in the distance. The photon's electric and magnetic fields are confined on its two-dimensional surface. (B) The photon contacts the double slit apparatus. (C) The photon's electric and magnetic fields give rise to electron or polarization currents at both slits (blue). As in the case with the application of a voltage to an object, there is an effect at a distance. The transition of the photon's fields from incident to transmitted is shown translucently. (D) The slit's currents cause reemission of a photon in the direction of the detector in the far field. (E) The transverse displacement of the reemitted photon conserves the angular momentum of the source current. The superposition of reemitted photons from the interaction of many incident photons over time forms a photon field characteristic of the slits as their source. The source is equivalent to a uniform-electric-field silhouette of the slits given by Eqs. (8.15) and (8.19). (F) In the far field, the distribution of photons corresponding to the intensity pattern is the Fourier transform of the slit pattern.




Eq. (8.22) also applies to two-slit diffraction of other particles as well as photons wherein the amplitude reflects the transverse momentum density of the particles. The proton and neutron as well as photons and electrons demonstrate interference patterns during diffraction. An example is the interference pattern for rubidium atoms given in the Wave-Particle Duality is Not Due to the Uncertainty Principle Section. Particle-particle interactions may be involved, and in other cases the interference pattern arises without fundamental-particle-particle interaction. In these cases, the pattern-generating interaction can be attributed to that between the particle and the diffraction apparatus with conservation of the angular momentum of the particle and any photons involved in mediating the interaction wherein even neutral particles such as neutrons comprise charged sub-

particles such as quarks and also possess magnetic moments that can give rise to induced electrodynamic currents and fields of a scatterer during interaction.

Conservation of the photon's angular momentum of $\hbar$ gives rise to the de Broglie relationship of the electron as given in the Classical Physics of the de Broglie Relationship section. This result also applies to other fundamental particles. Since all particle-slit interactions are mediated by photons, and the angular momentum change must be conserved in the far-field, the corresponding amplitude function that arises from the electron-aperture function is equivalent to that of a corresponding photon-front aperture function. Both amplitude functions are given by Eq. (8.22).

In Michelson interferometry, photons interact with the optical elements wherein the velocity is slower than free space. There is dispersion in velocity based on phase such that photons speed up and slow down relative to each other and are bunched to create a pattern of concentration or compression and rarefaction of photon spatial density over each period of the incident electromagnetic wave. The redistribution is observed as dark and light bands that repeat every photon wavelength based on the periodicity of the light wave comprising an ensemble of photons. The distribution pattern observed with diffracting electrons is equivalent to that for diffracting light. Note that Eq. (8.16) represents a plane wave. In the case of the Davison-Germer experiment, the intensity is given by Eq. (8.13) as the product of the Fourier transforms of the elemental pattern corresponding to a plane wave of wavelength $\lambda = h / p$ and the array pattern of the nickel crystal.

In general, the observed far-field position distribution is a picture of the particle transverse momentum distribution after the interaction. As shown in the Classical Wave Theory of Electron Scattering section, the phase of the amplitude of the angular-momentum-distribution function contains the term $(\mathbf{k}_i - \mathbf{k}_s)\cdot\mathbf{r}_t$, where $\mathbf{k}_i - \mathbf{k}_s$ is proportional to the momentum change of the incident particle upon scattering, since $\hbar\mathbf{k}_i$ is the initial momentum and $\hbar\mathbf{k}_s$ is the final momentum of the scattered particle such as an electron. The wavelength, $\lambda$, is the de Broglie wavelength associated with the momentum of the particle which is transferred through interactions corresponding to the wavenumber $k = \frac{2\pi}{\lambda}$. Since the two-slit aperture pattern is the convolution of the single-slit pattern with two delta functions, the intensity of the two-slit experiment is given as cosine squared fringes of the single-slit pattern as given by Eq. (8.23) wherein the extended particle interacts with both slits with conservation of momentum to give the modulation of the single-slit momentum pattern.

The energy is proportional to the square of the momentum. The conservation of power flow requires that the intensity distribution representing the number of particles incident on the detector at a given position is given by the amplitude of the momentum-distribution function squared.

During electron diffraction, the initially unpolarized electron becomes polarized to minimize the energy of interaction with the slit such that the angular momentum of the polarized free electron is parallel or antiparallel to the direction of propagation. If the forward momentum is unchanged, then the electron is detected at $\mathrm{x} = 0$ in the far field. However, the interaction with the slit can cause momentum transfer to the transverse direction that can be mediated by photons having $\hbar$ of angular momentum. Each photon provides a torque to change the direction of the angular momentum vector; concomitantly, the linear momentum is redirected to have a transverse component. The momentum transfer from the z-axis to the transverse or x-axis in the far field depends on the strength and the time duration of a photon-generated torque as given in the Stern-Gerlach Experiment subsection of the Free Electron section. The spatial distribution of the electron positions is determined by the conservation of momentum. With sufficient application of torque the angular momentum vector is reversed. The interaction of the free electron with the slit to reverse the angular momentum corresponds to a sign change of the amplitude, and periodic reversals of the angular momentum gives rise to maximum and minima of the amplitude. Since the magnitude of the angular momentum change depends on the strength and duration of the torque, which has a finite half-life, the amplitude decreases steeply as a function of transverse momentum.

## CLASSICAL WAVE THEORY OF ELECTRON SCATTERING

The following mathematical development of scattering is adapted from Bonham [4] with the exception that the CP model is a Fourier optics derivation for an exact elemental pattern, a plane wave, and an exact array pattern, an atomic orbital. In contrast, Bonham derives similar scattering equations for an incident plane wave via an averaged probability density function description of the electron, the Born model.

In scattering experiments in which Fraunhofer diffraction is the most important mode for scattering, measurements are made in momentum or reciprocal space. The data is then transformed in terms of real space, where the structure of the scatterer is expressed in terms of distances from its center of mass. There are, fortunately, well known mathematical techniques for making this transformation. If we are given a model of the scattering system, we can, in general, uniquely calculate the results to be expected in reciprocal space for scattering from the model. Unfortunately, the converse—deducing the nature of the scatterer uniquely by transforming the experimental results obtained in reciprocal space—is not always possible. But, as we will see, certain possibilities can be eliminated because they violate fundamental physical laws such as Special Relativity.

In classical optics, a diffraction pattern results whenever light is scattered by a slit system whose dimensions are small compared to the wavelength of light. In order to develop a mathematical model for diffraction scattering, let us represent the amplitude of an incident plane wave traveling from left to right as $e^{i(\mathbf{k}\cdot\mathbf{r}-\omega t)}$, where the absolute magnitude of the wave vector $\mathbf{k}$ is $|\mathbf{k}| = \frac{2\pi}{\lambda}$. The quantity $\lambda$ is the wavelength of the incident radiation and $\hbar\mathbf{k}$ is the momentum $\mathbf{p}$. The vector $\mathbf{r}$ represents the position in real space at which the amplitude is evaluated, and $\omega$ and $t$ are the angular frequency and time, respectively. A

plane wave traveling in the opposite direction is $e^{-i(\mathbf{k}\cdot\mathbf{r}+\omega t)}$ where the sign of $\mathbf{k}\cdot\mathbf{r}$ changes, but not the sign of $t$. That is, we may reflect a wave from a mirror and reverse its direction, but we cannot change the sign of the time since that would indicate a return to the past. The intensity of a classical wave is the square magnitude of the amplitude, and thus the intensity of a plane wave is constant in space and time. If a plane wave is reflected back on itself by a perfectly reflecting mirror, then the resultant amplitude is $e^{i(\mathbf{k}\cdot\mathbf{r}-\omega t)}+e^{-i(\mathbf{k}\cdot\mathbf{r}+\omega t)}=e^{-i\omega t}2\cos\mathbf{k}\cdot\mathbf{r}$, and the intensity is $I=4\cos^2\mathbf{k}\cdot\mathbf{r}e^{i\omega t}e^{-i\omega t}$ which is independent of time and given as $4\cos^2\mathbf{k}\cdot\mathbf{r}$ which clearly exhibits maxima and minima dictated by the wavelength of the radiation and the position in space at which intensity is measured.

In an experiment, we measure the intensity of scattered particles, which is related to plane waves in a simple fashion. To see this, consider a collimated plane-wave source, whose width is small compared to the scattering angle region where the scattering is to be investigated, incident upon a diffraction grating. If we integrate the incident intensity over a time interval $\Delta t$, we obtain a number proportional to the energy content of the incident wave. We may safely assume in most cases that the scattering power of the diffraction image does not change with time, so that a constant fraction of the incident radiation and hence constant energy will be transferred into the scattered wave. We further assume that the effect of the diffraction grating on the incident radiation occurs only in a region very close to the grating in comparison to its distance from the detection point. For elastic scattering (no energy transfer to the grating), once the scattered portion of the wave has left the field of influence of the scatterer, all parts of the scattered amplitude at the same radial distance from the scatterer must travel at the velocity of the incident wave. For simplicity, we neglect resonance effects, which can introduce significant time delays in the scattering process even if the waves are scattered elastically. The effects of resonance states on the scattering at high energies, is usually negligible and hence will not be discussed here. In the case of inelastic scattering, in which waves are scattered with various velocities, we can focus our attention successively on parts of the outgoing scattered radiation that have velocities falling within a certain narrow band, and the following argument will hold for each such velocity segment. The result of the integration of a constant-velocity segment of the scattered intensity over the volume element,

$$\int_R^{R+\Delta R} r^2 dr \int_0^{\pi} \sin\theta d\theta \int_0^{2\pi} d\Phi \tag{8.24}$$

is proportional to the energy content in that portion of the scattered wave, and the result must be independent of $R$. This restriction, which is a direct consequence of conservation of energy, then demands that the outgoing scattered waves have in polar coordinates the form:

$$\Psi_{sc}(R,\theta,\phi)=\frac{e^{ikR}}{R}f(\theta,\phi) \tag{8.25}$$

where the term $1/R$ is a dilution effect to guarantee energy on an ever-spreading wave.

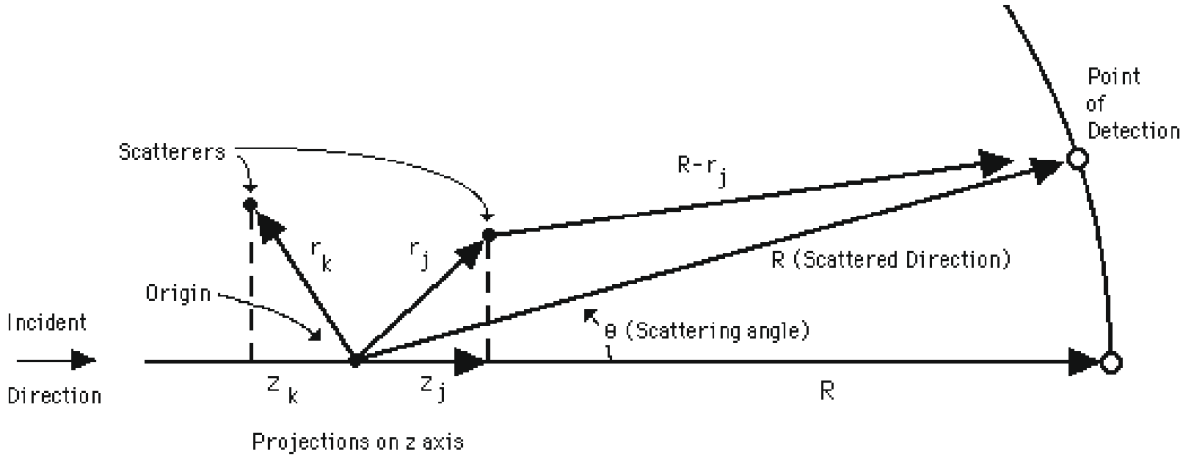
$\Psi_{sc}$ only describes the scattered amplitude after the scattered wave has left the field of influence of the scatterer and is thus an asymptotic form. The function $f(\theta,\varphi)$ is called the scattered amplitude and depends on the nature of the scatterer. The classical theory tells us that the scattered intensity is proportional to the square magnitude of the scattered amplitude; so, the intensity will be directly proportional to $\frac{|f(\theta,\varphi)|^2}{R^2}$.

Let us next consider the expression for the scattering of a plane wave by a number of disturbances in some fixed arrangement in space. Consider the scatterers comprising a nucleus and electrons; this would correspond to a plane wave scattered by an atom.

We shall choose the center of mass of the scatterer as our origin and shall for the most part consider dilute-gas electron scattering in the keV energy range, where the electron wavelength $\lambda$ lies in the range $0.03\ \text{Å}<\lambda<0.1\ \text{Å}$. The scattering experimental conditions are such that to a high degree of approximation, at least within 0.1% or better, we can consider the scattering as a single electron scattered by a single atom. Note also that no laboratory to center-of-mass coordinate system transformation is required because the ratio of the electron mass to the mass of the target will be on the order of $10^{-3}$ or smaller.

Let us consider an ensemble of scattering centers as shown in Figure 8.2.

**Figure 8.2.** An ensemble of scattering centers.




We may write the total scattered amplitude in the first approximation as a sum of amplitudes, each of which is produced by scattering from one of the single scattering centers. In this view, we generally neglect multiple scattering, the re-scattering of portions of the primary scattered amplitudes whenever they come in contact with other centers, except in the case of elastic scattering in the heavier atoms. Clearly a whole hierarchy of multiple-scattering processes may result. The incident wave may experience a primary scattering from one center, a portion of the scattered amplitude may re-scatter from a second center, and part of this amplitude may in turn be scattered by a third center (which can even be the first center), and so on.

An incident plane wave will obviously travel a distance along the incident direction before scattering from a particular center, depending on the instantaneous location of that center. To keep proper account of the exact amplitude and phase of the incident wave at the instant it scatters from a particular center, we select our origin, as mentioned previously, to lie at the center of mass. The phase of the scattered wave depends on the total distance traveled from the center of mass to the detector. We can now write the scattered amplitude as:

$$\Psi_{total} = \sum_{l=1}^{N} \left( \frac{\exp\left[ ik\left( z_l + \left|\mathbf{R} - \mathbf{r}_l\right| \right) \right]}{\left|\mathbf{R} - \mathbf{r}_l\right|} \right) f_l\left(\theta, \phi\right) \tag{8.26}$$

where $z_l + \left|\mathbf{R} - \mathbf{r}_l\right|$ is the distance traveled from a plane perpendicular to the incident direction and passing through the center of mass and $f_l\left(\theta, \phi\right)$ is the scattered amplitude characteristic of the $l-th$ scattering center. It should be clear at this point that the term $\left( \frac{\exp\left[ ik\left|\mathbf{R} - \mathbf{r}_l\right| \right]}{\left|\mathbf{R} - \mathbf{r}_l\right|} \right) f_l\left(\theta, \phi\right)$ is made up of a plane wave in the scattered direction with the dilution factor $\frac{1}{\left|\mathbf{R} - \mathbf{r}_l\right|}$ to account for energy conservation and with allowances made through $f_l\left(\theta, \phi\right)$ for any special influence that the scatterer may have on the scattering because of the detailed structure of the scatterer. The additional term $e^{ikz_1}$ enters whenever two or more scattering centers are encountered and accounts for the fact that the instantaneous location of our scattering centers may not coincide with planes of equal amplitude of the incident plane wave. That is, in a two-center case, the first particle may scatter a plane wave of amplitude +1 while at the same time a second scatterer may encounter an amplitude of -1. The amplitudes of the incident plane wave which the various particles encounter depend on their separation from each other along the z-axis and on the wavelength of the incident radiation. By adding to the phase, the projections of the various $\mathbf{r}_l$ vectors onto the incident direction, referenced to the same origin, this problem is automatically corrected. As long as our composite scatterer is on the order of atomic dimensions, the magnitude of $R$ will be enormously larger than either $\mathbf{z}_l$ or $\mathbf{r}_l$. This allows us to expand $\left|\mathbf{R} - \mathbf{r}_l\right|$ in a binomial expansion through first-order terms as $R - \left( \frac{\mathbf{R}}{\left|\mathbf{R}\right|} \cdot \mathbf{r}_l \right)$. In the denominator, the first-order correction term $R$ can be neglected but not in the phase.

To see this, suppose that $R$ is $\pi$ X $10^6$ and $\frac{\mathbf{R}}{\left|\mathbf{R}\right|} \cdot \mathbf{r}_l$ is $\pi/2$. Clearly $\pi/2$ would seem negligible compared to $\pi$ X $10^6$, but look what a difference the value of a sine or cosine function has if $\pi/2$ is retained or omitted from the sum of the two terms. The product $kz_l$ may be rewritten as $\mathbf{k_i} \cdot \mathbf{r}_l$, where the subscript i on $\mathbf{k}$ denotes the fact that $\mathbf{k}_i$ is a vector parallel to the incident

direction magnitude $k = \frac{2\pi}{\lambda}$. Similarly, since $\frac{\mathbf{R}}{|\mathbf{R}|}$ is a unit vector whose sense is essentially in the direction of the scattered electron, we may write $k\frac{\mathbf{R}}{|\mathbf{R}|}\cdot\mathbf{r}_l$ as $\mathbf{k}_s\cdot\mathbf{r}_l$ where $\mathbf{k}_s$ is a wave vector in the scattering direction. The phase of Eq. (8.26) now contains the term $(\mathbf{k}_i-\mathbf{k}_s)\cdot\mathbf{r}_l$, where $\mathbf{k}_i-\mathbf{k}_s$ must be proportional to the momentum change of the incident particle on scattering, since $\hbar\mathbf{k}_i$ is the initial momentum and $\hbar\mathbf{k}_s$ is the final momentum of the scattered electron. This vector difference is labeled by the symbol $\mathbf{s}$. The asymptotic total amplitude is now expressible as:

$$\Psi_{total} = \frac{e^{ikR}}{R}\sum_{l=1}^{N} e^{i\mathbf{s}\cdot\mathbf{r}_l} f_l(\theta,\phi) \tag{8.27}$$

## CLASSICAL WAVE THEORY APPLIED TO SCATTERING FROM ATOMS AND MOLECULES

Let us first apply Eq. (8.27) to scattering from atoms. We will consider the theoretical side of high-energy electron scattering and X-ray scattering from gaseous targets as well. In the X-ray case, the intensity for an X-ray scattered by an electron is found experimentally to be a constant, usually denoted by $I_{cl}$, which varies inversely as the square of the mass of the scatterer where $I_{cl}$ is the Thompson X-ray scattering constant. This means that X-rays are virtually un-scattered by the nucleus, since the ratio of electron to nuclear scattering will be greater than $\left[\frac{m_p}{m_e}\right]^2 \cong \left[\frac{1X\ 10^{-24}}{9X10^{-28}}\right]^2 \sim 10^6$, where $m_p$ is the proton rest mass and $m_e$ is the electron rest mass. The total amplitude for X-ray scattering by an atom can then be written as:

$$\Psi^{\mathrm{xr}}_{total} = \sqrt{I_{cl}}\ e^{i\eta_{cl}} e^{ikR}\sum_{l=1}^{N} e^{i\mathbf{s}\cdot\mathbf{r}_l} \tag{8.28}$$

where $\eta_{cl}$ is a phase factor introduced because of a possibility that the X-ray scattered amplitude may be complex. The intensity can be written as:

$$I^{xr}_{total} = I_{cl}(N + \sum_{l\neq k}^{N}\sum_{l\neq k}^{N} e^{i\mathbf{s}\cdot\mathbf{r}_{l\,k}}) \tag{8.29}$$

where $\mathbf{r}_{lk} = \mathbf{r}_l - \mathbf{r}_k$ is an inter-electron distance. Both expressions, Eqs. (8.28) and (8.29), correspond to a fixed arrangement of electrons in space. For electrons, the intensity of scattering by another charged particle proceeds according to the Rutherford experimental law $I = \frac{I_e Z^2}{s^4}$, where $Z$ is the charge of the scatterer and $I_e$ is a characteristic constant. Note that both $I_{cl}$ and $I_e$ include the $\frac{1}{R^2}$ dilution factor and depend on the incident X-ray or electron beam flux $I_0$ and on the number $N_0$ of target particles per cubic centimeter in the path of the incident beam as the product $I_0N_0$. We may take $f_l(\theta,\phi) = \sqrt{I_e}\left(\frac{Z}{s^2}\right)\exp[i\eta(Z)]$, where $\eta(Z)$ is again an unknown phase shift introduced because of the possibility that the amplitude may be complex. In the X-ray case for scattering by an atom, the intensity is independent of the phase $\eta_{cl}$, and we need not investigate it further. In electron scattering, this term is different for electrons and nuclei since they contain charges of opposite sign and usually different magnitude. The amplitude for this case is:

$$\Psi^{ed}_{total} = \sqrt{I_e}\left(\frac{e^{ikR}}{s^2}\right)\left[Ze^{(i\eta(Z)+i\mathbf{s}\cdot\mathbf{r}_n)} + \sum_{i=1}^{N} e^{(i\eta(-1)+i\mathbf{s}\cdot\mathbf{r}_i)}\right] \tag{8.30}$$

which for an atom simplifies further, since the nuclear position vector $\mathbf{r}_n$ is zero because the nucleus lies at the center of mass. The term $\eta(Z)$ is the nuclear phase and $\eta(-1)$ is the phase for scattering by an individual electron. The notation $-1$ signifies a unit negative charge on each electron as opposed to $+Z$ on the nucleus, where $Z$ is the atomic number. The intensity with $\mathbf{r}_n = 0$ becomes:

$$I^{ed}_{total} = \left(\frac{I_e}{s^4}\right)\{Z^2 + 2Z\sum_{i=1}^{N}\cos[\eta(Z)-\eta(-1)-\mathbf{s}\cdot\mathbf{r}_i] + N + \sum_{i\neq j}^{N}\sum_{i\neq j}^{N} e^{i\mathbf{s}\cdot\mathbf{r}_{i\,j}}\} \tag{8.31}$$

Note that the last two terms on the right in Eq. (8.31) are identical to those in Eq. (8.29).

According to Huygens' principle, the function $\sum_{i=1}^{N} e^{i\mathbf{s}\cdot\mathbf{r}_i}$ of Eq. (8.30) represents the sum over each spherical wave source arising from the scattering of an incident plane wave from each point of the electron function where the wavelength of the incident plane wave is given by the de Broglie equation $\lambda = h/p$. The sum is replaced by the integral over $\rho$ and $\phi$ of the single point element aperture distribution function. The single point element aperture distribution function, $a(\rho,\phi,z)$, for the

scattering of an incident plane wave by an atom is given by the convolution of a plane wave function with the electron atomic orbital function. The convolution is $a(\rho,\phi,z)=\pi(z)\otimes[\delta(r-r_0)]Y_\ell^m(\theta,\phi)$ where $a(\rho,\phi,z)$ is given in cylindrical coordinates, $\pi(z)$, the xy-plane wave is given in Cartesian coordinates with the propagation direction along the z-axis, and the atomic orbital function, $[\delta(r-r_0)]Y_\ell^m(\theta,\phi)$, is given in spherical coordinates. Using cylindrical coordinates,

$$\sum_{i=1}^{N} e^{i\mathbf{s}\cdot\mathbf{r}_i} = \int_0^\infty \int_0^{2\pi} \int_{-\infty}^{\infty} a(\rho,\phi,z) e^{-i[s\rho\cos(\phi-\Phi)+wz]} \rho^2 \rho d\rho d\phi dz \tag{8.32}$$

The general Fourier transform integral is given in reference [5].

For an aperture distribution with circular symmetry, $F(s)$, the Fourier transform of the aperture array distribution function, $A(z)$, is [5]:

$$\sum_{i=1}^{N} e^{i\mathbf{s}\cdot\mathbf{r}_i} = 2\pi \int_0^\infty \int_{-\infty}^{\infty} a(\rho,z) J_0(s\rho) e^{-iwz} \rho d\rho dz \tag{8.33}$$

$$= \int_0^\infty A(z) e^{-iwz} dz \tag{8.34}$$

$$= F(s) \tag{8.35}$$

The same derivation applies for the two-point term $\sum_{i\neq j}^{N}\sum_{i\neq j}^{N} e^{i\mathbf{s}\cdot\mathbf{r}_{ij}}$ of Eq. (8.31). The sum is replaced by the integral over $\rho$ and $\phi$ of the single point element autocorrelation function, $\mathsf{r}(\rho,\phi,z)$, of the single point element aperture distribution function. For circular symmetry [5] :

$$\mathsf{r}(\rho,\phi,z) = a(\rho,\phi,z)\otimes a(\rho,\phi,z) \tag{8.36}$$

and

$$\sum_{i\neq j}^{N}\sum_{i\neq j}^{N} e^{i\mathbf{s}\cdot\mathbf{r}_{ij}} = 2\pi \int_0^\infty \int_{-\infty}^{\infty} \mathsf{r}(\rho,z) J_0(s\rho) e^{-iwz} \rho d\rho dz \tag{8.37}$$

$$= \int_0^\infty R(z) e^{-iwz} dz \tag{8.38}$$

and

$$R(z) = A(z)A(z) \tag{8.39}$$

For closed shell atoms in single states such as rare gases, $Y(\theta,\phi)$, the spherical harmonic angular function of the electron function is a constant, and only two expressions are possible from all orders of averaging over all possible orientations in space. For the X-ray case the scattered intensities are:

$$I_1^{xr} = I_{cl}\left[\int_0^\infty A(z) e^{-iwz} dz\right]^2 = I_{cl} F(s)^2 \tag{8.40}$$

and

$$I_2^{xr} = I_{cl}\left[N + \int_0^\infty R(z) e^{-iwz} dz\right] \tag{8.41}$$

while for electrons, the scattered intensities are:

$$I_1^{ed} = \left[\frac{I_e}{s^4}\right]\{Z^{2+} 2Z\cos[\eta(Z)-\eta(-1)]F(s) + F(s)^2\} \tag{8.42}$$

and

$$I_2^{ed} = \left[\frac{I_e}{s^4}\right]\{Z^2 + 2Z\cos[\eta(Z)-\eta(-1)]F(s) + N + \int_0^\infty R(z) e^{-iwz} dz\} \tag{8.43}$$

where the subscript 1 denotes an amplitude derivation and 2 an intensity derivation. The aperture function of the nucleus is a delta function of magnitude $Z$, the nuclear charge. The Fourier transform is a constant of magnitude $Z$ as appears in Eqs. (8.42) and (8.43). Note that the Fourier convolution theorem proves the equivalence of Eq. (8.40) and Eq. (8.41) and the equivalence of Eq. (8.42) and Eq. (8.43).

The aperture array distribution function, $A(z)$, Eq. (8.34), corresponds to the electron radial distribution function of Bonham, and the aperture array autocorrelation function $R(z)$, Eq. (8.38), corresponds to the electron pair correlation function of Bonham [4].

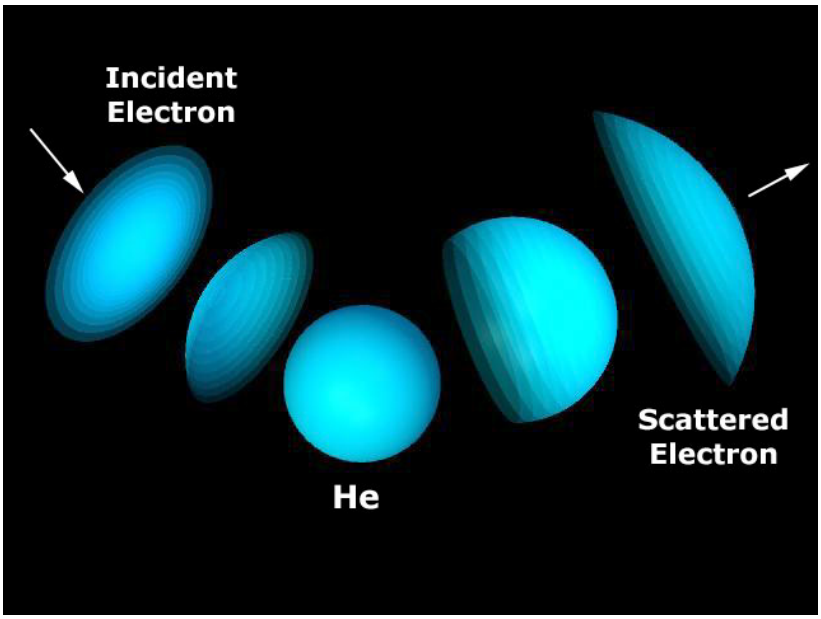
## ELECTRON SCATTERING EQUATION FOR THE HELIUM ATOM BASED ON THE ATOMIC ORBITAL MODEL

The closed form solution of all two electron atoms is given in the Two Electron Atom section. In the helium ground state, both electrons atomic orbitals are at a radius where:

$$r_1 = 0.567a_0 \tag{8.44}$$

The helium atom comprises a central nucleus of charge $+2e$ which is at the center of an infinitely thin spherical shell comprising two bound electrons of $-2e$. Thus, the helium atom is neutrally charged, and the electric field of the atom is zero for $r > 0.567a_0$. The Rutherford scattering equation for isolated charged particles does *not* apply. The appropriate scattering equation for helium in the ground state can be derived as a Fourier optics problem as given in the Classical Scattering of Electromagnetic Radiation section. The incident plane-wave free electron given in the Electron in Free Space section scatters from the helium atom by time-symmetrically deforming onto and from the surface of the helium atom as shown in Figure 8.3 such that the far field intensity pattern of many electrons is modeled by Huygens's Principle.

**Figure 8.3.** The time-symmetrical elastic scattering behavior of a free electron from a helium atom.




The aperture distribution function, $a(\rho,\phi,z)$, for the scattering of an incident plane wave by the He atom is given by the convolution of the plane wave function with the two electron atomic orbital Dirac delta function of $radius = 0.567a_0$ and charge/mass density of $\frac{2}{4\pi(0.567a_0)^2}$. For radial units in terms of $a_0$

$$a(\rho,\phi,z) = \pi(z) \otimes \frac{2}{4\pi(0.567a_0)^2}[\delta(r - 0.567a_0)] \tag{8.45}$$

where $a(\rho,\phi,z)$ is given in cylindrical coordinates, $\pi(z)$, the xy-plane wave is given in Cartesian coordinates with the propagation direction along the z-axis, and the He atom atomic orbital function, $\frac{2}{4\pi(0.567a_0)^2}[\delta(r - 0.567a_0)]$, is given in spherical coordinates.

$$a(\rho,\phi,z) = \frac{2}{4\pi(0.567a_0)^2}\sqrt{(0.567a_0)^2 - z^2}\,\delta(r - \sqrt{(0.567a_0)^2 - z^2}) \tag{8.46}$$

For circular symmetry [5],

$$F(s) = \frac{2}{4\pi(0.567a_0)^2} 2\pi \int_0^{\infty}\int_{-\infty}^{\infty} \sqrt{(0.567a_0)^2 - z^2}\,\delta(\rho - \sqrt{(0.567a_0)^2 - z^2}) J_0(s\rho) e^{-iwz} \rho d\rho dz \tag{8.47}$$

Eq. (8.47) may be expressed as:

$$F(s) = \frac{4\pi}{4\pi(0.567a_0)^2} \int_{-z_0}^{z_0} (z_0^2 - z^2) J_0(s\sqrt{z_0^2 - z^2}) e^{-iwz} dz \;\; ; \;\; z_0 = 0.567a_0 \tag{8.48}$$

Substitute $\frac{z}{z_0} = -\cos\theta$

$$F(s) = \frac{4\pi z_0^2}{4\pi z_0^2}\int_0^{\pi} \sin^3\theta J_0(sz_0\sin\theta)e^{iz_0 w\cos\theta}d\theta \tag{8.49}$$

Substitution of the recurrence relationship,

$$J_0(\mathrm{x}) = \frac{2J_1(\mathrm{x})}{\mathrm{x}} - J_2(\mathrm{x}) \;\; ; \;\; \mathrm{x} = \mathrm{s}z_0\sin\theta \tag{8.50}$$

into Eq. (8.49), and, using the general integral of Apelblat [6] :

$$\int_0^{\pi}(\sin\theta)^{\upsilon+1}J_{\upsilon}(b\sin\theta)e^{ia\cos\theta}d\theta = \left[\frac{2\pi}{a^2+b^2}\right]^{\frac{1}{2}}\left[\frac{b}{a^2+b^2}\right]^{\upsilon}J_{\upsilon+1/2}\left[(a^2+b^2)^{\frac{1}{2}}\right] \tag{8.51}$$

with $a = z_0 w$ and $b = z_0 s$ gives:

$$F(s) = \left[\frac{2\pi}{(z_0 w)^2+(z_0 s)^2}\right]^{\frac{1}{2}}$$

$$\left\{2\left[\frac{z_0 s}{(z_0 w)^2+(z_0 s)^2}\right]J_{3/2}\left[((z_0 w)^2+(z_0 s)^2)^{1/2}\right] - \left[\frac{z_0 s}{(z_0 w)^2+(z_0 s)^2}\right]^2 J_{5/2}\left[((z_0 w)^2+(z_0 s)^2)^{1/2}\right]\right\} \tag{8.52}$$

The magnitude of the single point element autocorrelation function, $|\mathrm{r}(\rho,\phi,z)|$, is given by the convolution of the magnitude of the single point element aperture distribution function, $a(\rho,\phi,z)$, with itself.

$$|\mathrm{r}(\rho,\phi,z)| = |a(\rho,\phi,z)| \otimes |a(\rho,\phi,z)| \tag{8.53}$$

The Fourier convolution theorem permits Eq. (8.53) to be determined by Fourier transformation.

$$|\mathrm{r}(\rho,\phi,z)| = \int_0^{\infty} e^{i\mathbf{w}\bullet\mathbf{z}}\left[\int_0^{\infty}\sqrt{\left(0.567a_0\right)^2 - z^2}\,e^{-i\mathbf{w}\bullet\mathbf{z}}dz\right]^2 dw \tag{8.54}$$

$$|\mathrm{r}(\rho,\phi,z)| = -e^{i\pi}\left\{\int_0^{\infty}\sin\left(\mathbf{w}\bullet\mathbf{z}\right)\left[\frac{J_1\left(0.567a_0 w\right)}{w}\right]^2 dw\right\} + C \tag{8.55}$$

where $C$ is an integration constant for which $R(\rho)$ equals zero at $r = 1.134a_o$

$$\left|\mathrm{r}(\rho,\phi,z)\right| = \left[\frac{1}{2} - \left(\frac{4z_0}{3\pi}\right)\left[\left(1+\frac{z^2}{4z_0^2}\right)E\left(\frac{z}{2z_0}\right) + \left(1-\frac{z^2}{4z_0^2}\right)K\left(\frac{z}{2z_0}\right)\right]\right] + C \tag{8.56}$$

$$0 < z \le 2z_0;\; z_0 = 0.567a_0$$

Eq. (8.56) was derived from a similar transform by Bateman [7]. The electron elastic scattering intensity is given by a constant times the square of the amplitude given by Eq. (8.52).

$$I_1^{ed} = I_e\left\{\begin{array}{l}\left[\dfrac{2\pi}{(z_0 w)^2+(z_0 s)^2}\right]^{\frac{1}{2}} \\ \left\{2\left[\dfrac{z_0 s}{(z_0 w)^2+(z_0 s)^2}\right]J_{3/2}\left[((z_0 w)^2+(z_0 s)^2)^{1/2}\right] - \left[\dfrac{z_o s}{(z_0 w)^2+(z_0 s)^2}\right]^2 J_{5/2}\left[((z_0 w)^2+(z_0 s)^2)^{1/2}\right]\right\}\end{array}\right\}^2 \tag{8.57}$$

$$s = \frac{4\pi}{\lambda}\sin\frac{\theta}{2};\; w = 0 \;(\textit{units of } \mathring{A}^{-1}) \tag{8.58}$$

## RESULTS

The magnitude of the single point element aperture distribution function, $a(\rho,\phi,z)$, convolved with the function $\delta(z-0.567a_0)$ is shown graphically in Figure 8.4 in units of $a_0$. The function was normalized to 2.

The magnitude of the single point element autocorrelation function, $\mathsf{r}(\rho,\phi,z)$, convolved with the function $\delta(z-1.134a_0)$ is shown graphically in Figure 8.5 in units of $a_0$. The function was normalized to 2 and the constant of $0.352183$ was added to meet the boundary condition for the convolution integral.

The experimental setup for the measuring the intensity of elastically scattered 500 eV electrons from an atomic beam of helium is shown in Figure 8.6.

The experimental results of Bromberg [8], the extrapolated experimental data of Hughes [8], the small angle data of Geiger [9], and the semi-experimental results of Lassettre [8] for the elastic differential cross section for the elastic scattering of electrons by helium atoms are shown graphically in Figure 8.7. The elastic differential cross section as a function of angle numerically calculated by Khare [8] using the first Born approximation and first-order exchange approximation also appear in Figure 8.7.

**Figure 8.4.** The magnitude of the single point element aperture distribution function, $a(\rho,\phi,z)$, convolved with the function $\delta(z-0.567a_0)$ in units of $a_0$.

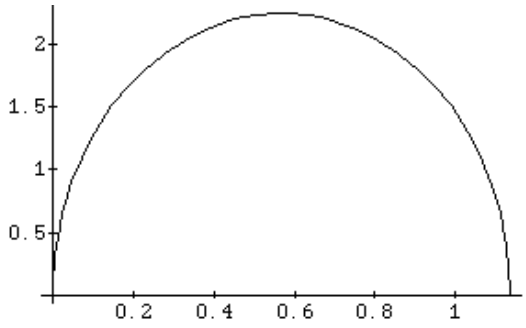



**Figure 8.5.** The magnitude of the single point element autocorrelation function, $\mathsf{r}(\rho,\phi,z)$, convolved with the function $\delta(z-1.134a_0)$ is shown graphically in units of $a_0$.

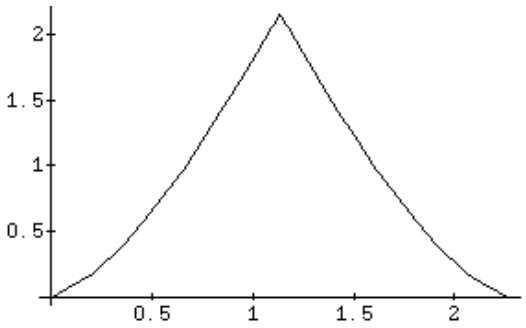



**Figure 8.6.** The incident electron and electron beams intersect and the scattered free electrons are detected in the far field.

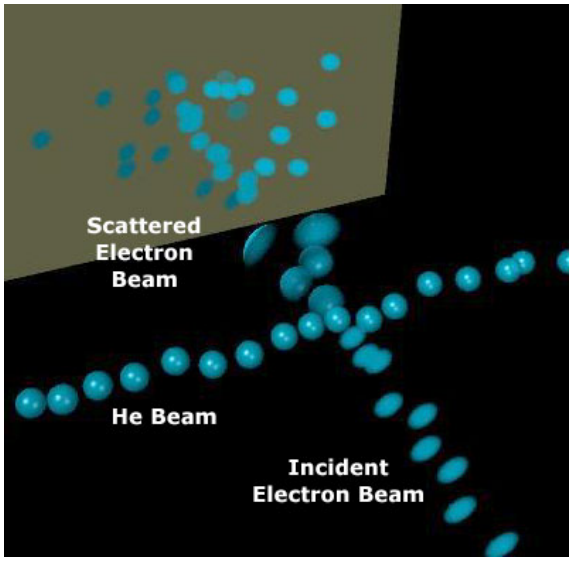
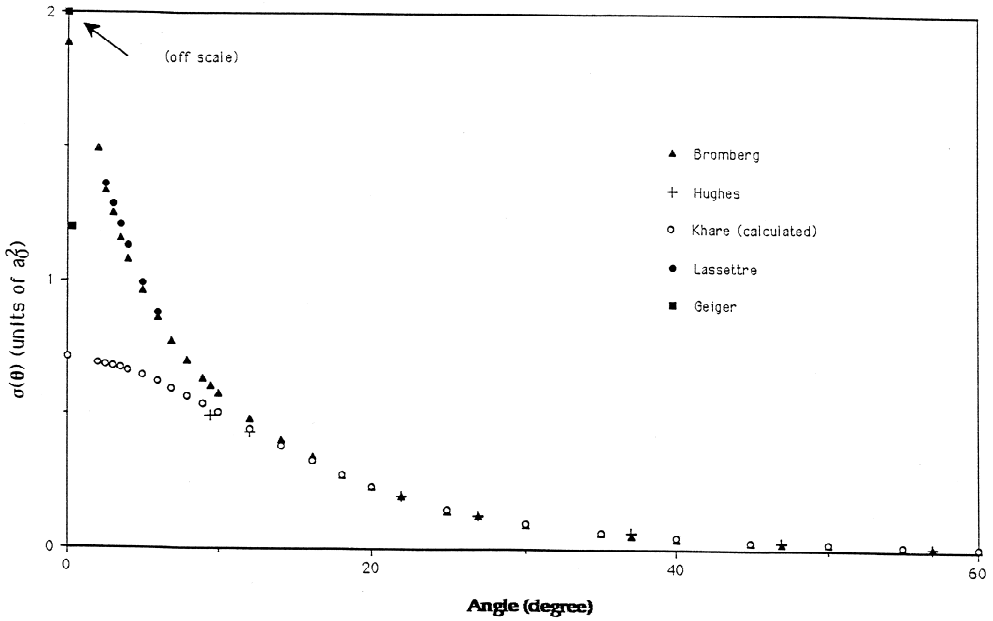
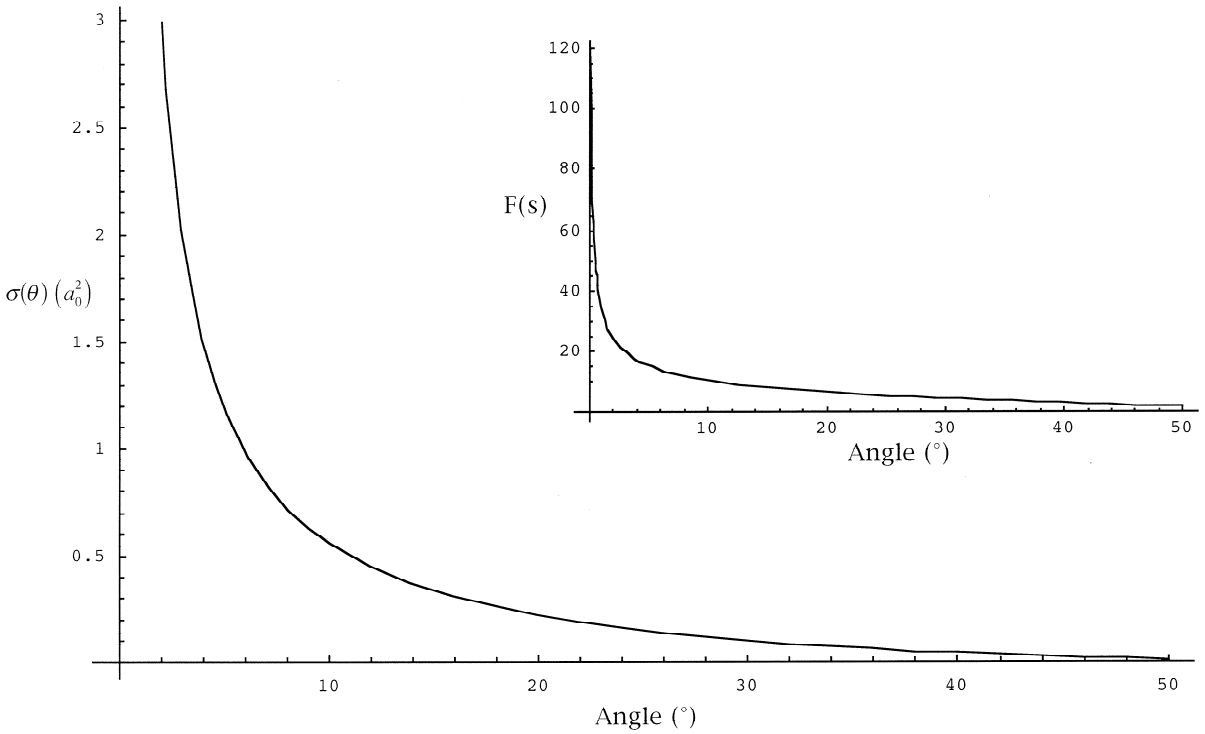


**Figure 8.7.** The experimental results of Bromberg [8], the extrapolated experimental data of Hughes [8], the small angle data of Geiger [9], and the semi-experimental results of Lassettre [8] for the elastic differential cross section for the elastic scattering of electrons by helium atoms and the elastic differential cross section as a function of angle numerically calculated by Khare [8] using the first Born approximation and first-order exchange approximation.




These results, which are based on a quantum mechanical model, are compared with experimentation [8, 9]. The closed-form function (Eqs. (8.57) and (8.58)) for the elastic differential cross section for the elastic scattering of electrons by helium atoms is shown graphically in Figure 8.8. The scattering amplitude function, $F(s)$ (Eq. (8.52)), is shown as an insert.

**Figure 8.8.** The closed form function (Eqs. (8.57) and (8.58)) for the elastic differential cross section for the elastic scattering of electrons by helium atoms. The scattering amplitude function, $F(s)$ (Eq. (8.52)), is shown as an insert.



## DISCUSSION

The magnitude of the single point element autocorrelation function, $\mathsf{r}(\rho,\phi,z)$, convolved with the function $\delta(z-1.134a_0)$ (Figure 8.5) and the electron pair correlation function, $P(r)$, of Bonham [10] are similar. According to Bonham [10], the electron radial distribution function, $D(r)$, calculated from properly correlated CI wave functions for He is similar in shape to the $P(r)$ function but its maximum occurs at a value of $r$ almost exactly half of that for $P(r)$. Thus, the function $D(r)$ is similar to the magnitude of the single point element aperture distribution function, $a(r,\theta,z)$, (Figure 8.4). $D(r)$ and $P(r)$ lead to a most probable structure for the He atom in which the electrons and the nucleus are collinear with the nucleus lying between the two electrons [4]. This is an average picture that is an ad hoc modification of the true model involving a three-point-body atom and a point-particle incident electron for which it is impossible to get neutral scattering, let alone the observed pattern shown in Figure 8.7. Furthermore, even with this unjustified modification, it is apparent from Figure 8.7 that the modified quantum mechanical calculations fail completely at predicting the experimental results at small scattering angles; whereas, Eq. (8.57) predicts the correct scattering intensity as a function of angle. Another problem for the quantum mechanical model is that the helium wave equation used to calculate the scattering is not the solution of the Schrödinger equation for the helium atom that gives the correct ionization energy. Since it involves three bodies, the exact solution is impossible to be obtained. Many solutions have been obtained with great effort using various perturbation and adjustable-parameter methods as given by McQuarrie [11]. Such solutions are very dubious in that they are non-unique, not based on physical laws, and are better classified as curve fitting techniques in that they use up to 1000 adjustable parameters to obtain the ionization energy [11].

In the far field, the solution of the Schrödinger equation for the amplitude of the scattered plane wave incident on a three dimensional static potential field $U(r)$ is identical to Eq. (8.26) only if one assumes a continuous distribution of individual scattering points and replaces the sum over $\ell$ in Eq. (8.26) with an integral over the scattering power $f_l$ of point $\ell$ replaced by the instantaneous value of the potential at the same point. This result is the basis of the failures of Schrödinger's interpretation that $\Psi(x)$ is the amplitude of the electron over three-dimensional space in some sense since the entire electron must correspond to each point $\ell$ and the superseding interpretation of Born that $\Psi(x)$ represents a probability function of a point electron. The Born interpretation can only be valid if the speed of the electron is equal to infinity. (The electron must be in all positions weighted by the probability density function during the time of the scattering event). The correct aperture function for the Born interpretation is a Dirac delta function, $\delta(r)$, having a Fourier transform of a constant divided by $\mathbf{s}^2$ which is equivalent to the case of the point nucleus (Rutherford Equation). The Born interpretation must be rejected because the electron velocity cannot exceed $c$ without violating special relativity.

Solutions to the Schrödinger equation involve the set of Laguerre functions, spherical Bessel functions, and Newmann functions. From the infinite set of solutions to real problems, a linear combination of functions and the amplitude and phases of these functions are sought which gives results that are consistent with scattering experiments. The Schrödinger equation is a statistical model representing an approximation to the actual nature of the bound electron. Statistical models are good at predicting averages as exemplified by the reasonable agreement between the calculated and experimental scattering results at large angles. However, in the limit of zero scattering angle, the results calculated via the Schrödinger equation are not in agreement with experimentation. In the limit, the "blurred" representation cannot be averaged, and only the exact description of the electron will yield scattering predictions which are consistent with the experimental results.

Also, a contradiction arises in the quantum mechanical scattering calculation. For hydrogen electron orbitals, the $n=\infty$ orbital is equivalent to an ionized electron. According to the quantum mechanical scattering model, the incident ionized electron is a plane wave. However, substitution of $n=\infty$ into the solution of the Schrödinger equation yields a radial function that has an infinite number of nodes and exists over all space. The hydrogen-like radial functions have $n-\ell-1$ nodes between $r=0$ and $r=\infty$. In fact, as $n\to\infty$ the Schrödinger equation becomes the equation of a linear harmonic oscillator [12]. The wavefunction shows sinusoidal behavior; thus, the wavefunction for the free electron can not be normalized and is infinite. In addition, the angular momentum of the free electron is infinite since it is given by $\ell(\ell+1)\hbar^2$ where $\ell\to\infty$. The results of the Davison-Germer experiment confirm that the ionized electron is a plane wave. In contrast, for the present atomic orbital model, as $n$ goes to infinity the electron is a plane wave with wavelength $\lambda=h/p$ as shown in the Electron in Free Space section.

Although there are parallels in the mathematical derivations wherein the Schwartz inequality is invoked, the physics of the Heisenberg Uncertainty Principle is quite distinct from the physics of the rise-time/band-width relationship of classical mechanics [13] as given in the Resonant Line Shape and Lamb Shift section. The Heisenberg Uncertainty Principle is derived from the probability model of the electron by applying the Schwartz inequality [14] to obtain the "indefiniteness" in the conjugate electron position and momentum in the absence of measurement; whereas, the physical rise-time/band-width relationship of classical mechanics is an energy conservation statement according to Parseval's Theorem. The Born model of the electron violates Special Relativity. The failure of the Born and Schrödinger model of the electron to provide a consistent representation of the states of the electron from a bound state to an ionized state to a scattered state also represents a failure of the dependent Heisenberg Uncertainty Principle.

In contrast, the Maxwellian, exact atomic orbital model provides a continuous representation of all states of the electron including the ionized state as a plane wave having the de Broglie wavelength as given in the Electron in Free Space section. Using the exact, unique solution of the helium atom given in the Two-Electron Atom section, in a closed-form solution, the Maxwellian model predicts the experimental results of the electron scattering from helium for all angles. The solution of the helium atom is further proven to be correct since it is used to solve up through twenty-electron atoms in the Three- Through

Twenty-Electron Atoms section and 100 excited-state energy levels in the Excited States of Helium section. In the former case, the physical approach was applied to multielectron atoms that were solved exactly disproving the deep-seated view that such exact solutions cannot exist according to quantum mechanics. The predictions from general solutions for one through twenty-electron atoms are in remarkable agreement with the experimental values known for 400 atoms and ions. In the latter case, the results given for any given $n$ and $\ell$ quantum number in the equations agree remarkably well—up to 6 significant figures where the data is obtainable to that accuracy. These consistent results and the failure of the true quantum mechanical model as well as the unphysical Born approximation disprove the nature of the electron as a point particle which further disproves the primary assumption of quantum mechanics. The results directly prove that the electron is an extended particle and specifically show, in the case of the helium atom, that the electron function comprises two paired, electron atomic orbitals at a radius given by Eq. (8.44) as derived in the Two-Electron Atom section. Furthermore, the deep-seated notion that probability waves are required to explain the nature of the double-slit experiment is dispelled by classical predictions using the correct nature of the electron considered next.

## PHYSICS OF CLASSICAL ELECTRON DIFFRACTION RESOLVES THE WAVE-PARTICLE DUALITY MYSTERY OF QUANTUM MECHANICS

The beginning of the Wave-Particle Duality section describes how early 20th century theoreticians proclaimed that light and atomic particles have a wave-particle duality that was unlike anything in our common everyday experience. The wave-particle duality is the central mystery of quantum mechanics—the one to which all others could ultimately be reduced. The current mental picture of the two-slit experiment is shown in Figures 42.1-42.4. The classical depiction of the two-slit-experiment shown in Figures 8.9-8.11 is very similar to the depiction of the quantum notion of the wave-particle duality shown in Figure 42.4. In fact, the mathematics of the quantum mechanical and classical pictures is essentially identical including the relationship between the transverse momentum and position given by Eqs. (8.60) and (8.61). However, what is very different is the physics. Consider the quantum conundrum due to the nature of the photon and electron being point particles. If each electron passes individually through one slit, with what does it "interfere?" Although each electron arrives at the target at a single place and a single time, it seems that each has passed through—or somehow felt the presence of both slits at once. Thus, the electron is understood in terms of a wave-particle duality as represented in Figure 42.4.

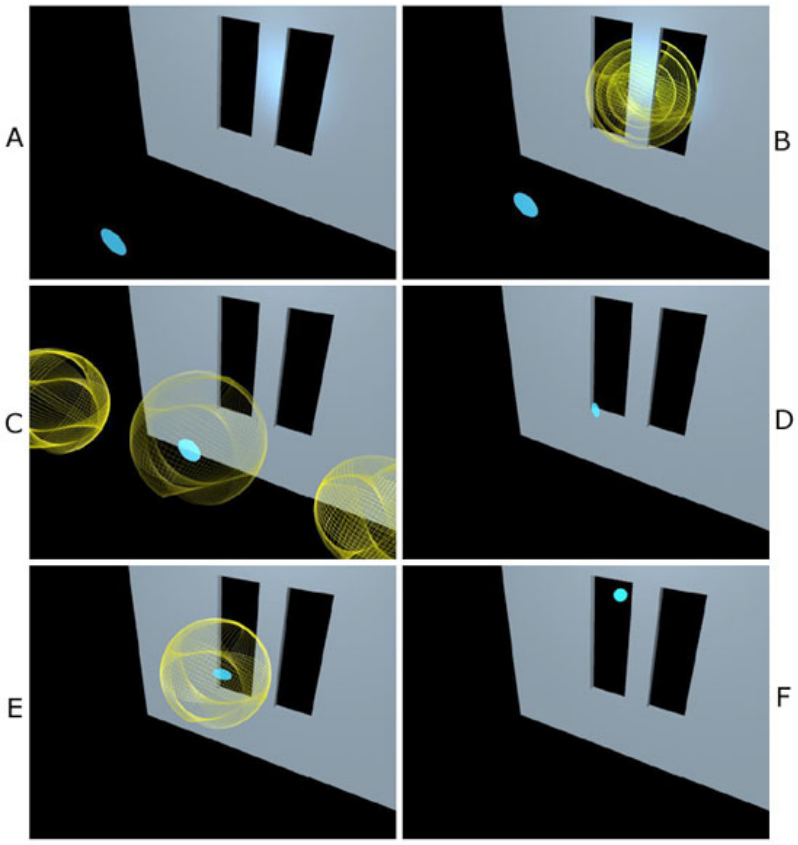
Here, the point electron or photon is everywhere at once—rather than being local to the slits of nanometer dimensions it exits as a probability wave of equal amplitude from positive to negative infinity, simultaneously! It is incident to and transmitted through both slits simultaneously, "guided" by the probability wave over all space with a phase that depends on the Heisenberg Uncertainty Principle:

$$\Delta x \Delta \mathbf{p} \geq \frac{\hbar}{2} \tag{8.59}$$

The phase contains the term $(\mathbf{k}_i - \mathbf{k}_s)\cdot\mathbf{r}_l$, where $\Delta p = \mathbf{k}_i - \mathbf{k}_s$ is interpreted as the contribution to the *uncertainty in the momentum of the incident particle on scattering*, since $\hbar\mathbf{k}_i$ is the initial momentum and $\hbar\mathbf{k}_s$ is the final momentum of the scattered particle such as an electron. In the classical picture, the phase also contains the term $(\mathbf{k}_i - \mathbf{k}_s)\cdot\mathbf{r}_l$, where $\mathbf{k}_i - \mathbf{k}_s$ is the *physical momentum change of the incident particle on scattering*, since $\hbar\mathbf{k}_i$ is the initial momentum and $\hbar\mathbf{k}_s$ is the final momentum of the scattered particle. In both cases, $\Delta x$ corresponds to the transverse displacement of the particle due to diffraction.

Furthermore, each electron only goes through one slit classically, but it is imprinted with the wave character of the photon that it creates across both slits due to its interaction with the slit. An electromagnetic wave exits. Quantum mechanics reproduces the mathematics that corresponds to this physical electromagnetic wave by invoking a nonsensical waving probability. Thus, it is stuck with the unfortunate result that the "wave-particle duality is unlike anything in our common everyday experience." Physics can now be reinstated over mysticism for this simple experiment based on an understanding of the physical nature of fundamental particles. An outline of the classical explanation of the observations made on the double-slit experiment is shown in Figures 8.9A-F, 8.10, and 8.11.

**Figure 8.9.** The electron-slit interaction is mediated by electron-induced radiation of photons from the split aperture that causes transverse electron displacements with the photon-momentum distribution imprinted onto that of the diffracting electrons such that the transverse momentum distribution in the far-field is a result of this interaction and is characteristic of the slit pattern. (A) The approaching charged electron interacts with both slits by inducing slit mirror currents (blue). (B) The slit's electron mirror currents that mediate its interaction with the approaching charged electron cause emission of photons. (C) The superposition of the photons forms a photon field characteristic of the slits as its source. (D) The electron angular momentum vector precesses about that of an absorbed photon from the slit photon field. (E) The photon is readmitted and the electron gained transverse momentum depending on the strength and duration of the electron's interaction with the photon field wherein the photon's angular momentum is conserved according to the change in the electron's de Broglie wavelength. (F) Rather than uncertainty in position and momentum according to the Uncertainty Principle: $\Delta x \Delta \mathbf{p} \geq \frac{\hbar}{2}$, $\Delta p$ is the physical momentum change of the incident electron and $\Delta x$ is the physical distance change from the incident direction such that the electron distribution in the far field is the Fourier transform of the slit pattern.



Consider a beam of electrons propagating in the z-axis direction. The electron is a plane-wave with momentum $k_z\hbar$ initially along the z-axis only. The $\hbar$ of angular momentum of the free electron is perpendicular to the plane lamina and is initially in a random orientation relative to the z-axis. To minimize the energy of interaction, the slit polarizes the electron such that its angular momentum becomes aligned parallel or antiparallel to the z-axis (Figure 8.9A). The slit is comprised of matter having electrons that can provide image charges due to the electric field of the incident electron (Figure 8.9A). The slit's electron-mirror currents that mediate its interaction with the approaching charged electron cause emission of photons (Figure 8.9B). When one interacts with the electron (Figure 8.9C), the electron angular-frequency change corresponding to the elctron-de-Broglie-wavelength change matches the frequency of the photon as given in the Classical Physics of the de Broglie Relationship section. The result of this interaction over time is the reorientation and transverse displacement of the electron's angular elastic diffraction, the energies are low, and the photons are large, encompassing and emanating from both slits. Each photon has a quantized angular momentum of $\hbar$. The $\hbar$ of angular momentum of the electron precesses about the $\hbar$ of angular momentum vector of the absorbed photon to cause a momentum transfer from the z-axis to the transverse axis. The photon is reemitted (Figure 8.9E), and the electron gained transverse momentum depending on the strength and duration of the electron's interaction with the photon field wherein the photon's angular momentum is conserved according to the change in the electron's de Broglie wavelength.

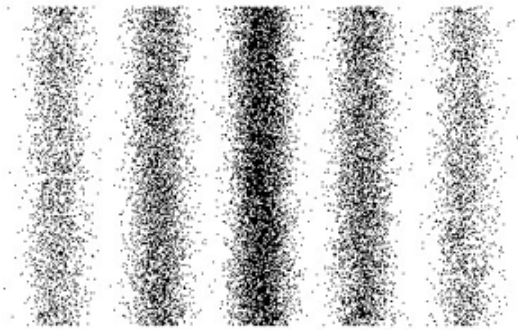
Over time, the electron beam statistically produces a uniform distribution across the slits. (Here, the statistics are deterministic and local/causal unlike the quantum mechanical case.) The photon pattern is also uniform across the slit. Since the electron and each photon that mediates the slit-electron interaction have quantized angular momentum in units of $\hbar$, the photon far-field pattern is imprinted on the electron beam pattern over time. The resulting transverse-momentum map is given by the Fourier transform of the two-slit aperture which arises classically from a consideration of conservation of power flow. The amplitude is periodically positive and negative corresponding to the cyclical reversal of the electron angular momentum as shown in Figure 8.10. The amplitude decreases from the center line due to the requirement of an increasing momentum transfer along the transverse axis from the center line with a decreasing probability for a long-duration photon-electron interaction or coupling with multiple photons to achieve increasing transverse momentum transfer.

**Figure 8.10.** The amplitude of the transverse electron momentum is a sinc function due to the decreasing probability of photon interactions causing a periodic reversal of the electron's angular momentum vector with an increasing transverse momentum transfer.



Since the number of electrons hitting a given position over time goes as the electron kinetic energy, the intensity pattern is given by the square of the amplitude. The predicted result shown in Figure 8.11 is the observed classical double slit interference pattern.

**Figure 8.11.** The classically predicted far-field electron distribution of the two-slit experiment matches that observed.



## EQUATIONS OF CLASSICAL DIFFRACTION

Consider the double-slit electron diffraction experiment shown in Figure 8.9. The interaction with the slit can cause momentum transfer to the transverse direction that can be mediated by photons having $\hbar$ of angular momentum. If the forward momentum is unchanged, then the electron is detected at $x = 0$ in the far field. However, momentum transfer from the z-axis to along the x-axis in the far field may occur depending on the strength and the time duration of a photon-generated torque as given in the Stern-Gerlach Experiment subsection of the Free Electron section. Also see Patz [15] and Slichter [16]. The spatial distribution of the electron position is determined by the conservation of momentum. Thus, the electron source at the aperture is analogous to an antenna, and the spatial electron-density pattern has as a parallel to the radiation pattern of the antenna as given by Kong [17]. If each point on the electron across a diffraction slit can act as a point source of a spherical wave according to Huygens' Principle, then the momentum pattern in the far field is given as the Fourier transform of the momentum-aperture function, and the electron density is given as the square of the amplitude of the Fourier transform.

Thus, the result of the double-slit experiment given by Eq. (8.23) can be interpreted as the positions of the electrons due to conservation of momentum following a semi-elastic interaction with the slit apparatus. The interaction is a time-dynamic equipotential and the forces statistically[2] cause the electrons over time to propagate as spherical waves from each point of a Laplacian surface according to Huygens' Principle. The incident pattern over time is determined by the superposition of the position and momenta of the incident individual electrons. The Fourier transform result given by Eq. (8.23) can be shown to arise by considering the diffraction of each electron individually.

The free electron is unpolarized, but the minimum energy constraint with slit-interrelations causes the polarization of the incident electrons. The angular momentum of the polarized electron may be parallel or antiparallel (negative direction) with respect to the z-axis. As shown in the Electron in Free Space section, there is a correspondence between the properties of the states of the free electron based on interactions with photons and those of bound-excited-state electrons. The time- and spherical harmonic current-density functions of bound and free-electron states comprise source currents for electromagnetic fields that are solutions of the wave equation as given in the Electron Source Current section. As shown in the Selection Rules section, multipole fields of an electron follow the same Maxwellian physics as that of a macroscopic radiating source. The radiation of a multipole of order $(\ell,\ m_\ell)$ carries $m\hbar$ units of the z component of angular momentum comprised of $\hbar$ per photon of energy $\hbar\omega$.

The distribution as a function of the position of the detector must conserve the angular momentum of the electron having an intrinsic angular momentum of $\hbar$ and an induced multipole of order $(\ell,\ m_\ell)$. The asymptotic electron-momentum total amplitude in the far field due to the scattering interactions of $N$ electrons with the slit mediated by photons with $\hbar$ of angular momentum follows from Eq. (8.27) given in the Classical Wave Theory of Electron Scattering section and Eq. (8.32) in the Classical Wave Theory Applied to Scattering from Atoms and Molecules section. Consider the assembly of $N$ coherently scattered electrons. The slit-electron interaction is an energy minimum or equipotential. The angular terms of Eq. (8.27) sum to unity. According to Huygens' principle, the function $\sum_{i=1}^{N} e^{i\mathbf{s}\cdot\mathbf{r}_i}$ of Eq. (8.32) represents the sum over each spherical wave source arising from the scattering of an incident plane wave from each point of the slit where the wavelength of the incident plane wave is given by the de Broglie equation $\lambda = h/p$. (The Green Function of Eqs. (8.25-8.27), is also given by Eq. (6.62) of Jackson [3] as the solution of the wave equation (Eq. (6.58) of Jackson [3]) as given in the Spherical Wave subsection of the Equation of the Photon section.) The sum is replaced by the integral over $\xi$ of the single point element aperture distribution function. For the case of a single slit, the aperture function is given by Eq. (8.15). Then, the amplitude of the scattering in the far field given by Eqs. (8.16) and (8.32) is:

$$\tilde{\Psi}(\mathrm{x}) = \sum_{i=1}^{N} e^{i\mathbf{s}\cdot\mathbf{r}_i} = \int \Psi(\xi) \exp\left(\frac{-ik\xi\cdot\mathbf{x}}{\mathrm{f}}\right) d\xi = C\int_{-a}^{a} \exp\left(\frac{-ik\xi\cdot\mathbf{x}}{\mathrm{f}}\right) d\xi \tag{8.60}$$

wherein the phase contains the term $(\mathbf{k}_i - \mathbf{k}_s)\cdot\mathbf{r}_l$, where $\mathbf{k}_i - \mathbf{k}_s$ is proportional to the momentum change of the incident particle on scattering, since $\hbar\mathbf{k}_i$ is the initial momentum and $\hbar\mathbf{k}_s$ is the final momentum of the scattered electron. This vector difference labeled by the symbol $\mathbf{s}$ is given by:

$$-i\mathbf{s}\cdot\mathbf{r}_i = \left(\frac{-ik\xi\cdot\mathbf{x}}{\mathrm{f}}\right) \tag{8.61}$$

The single-slit-momentum-amplitude pattern is then given by Eq. (8.22). The intensity of electrons is proportional to their kinetic energy which carry the electrons to the analyzer where it was shown by Bonham to be required in order to insure continuity of power flow for wavelets from a single source [4] and was used as the basis of Eqs. (8.27) and (8.32). The intensity pattern of electrons is then given as the square of the amplitude and, thus, the square of the momentum which is proportional to the electron energy. It follows that the single-slit pattern is given as the square of Eq. (8.18) and the double-slit pattern is given

[2] Here, the underlying physics is deterministic. Quantum mechanics postulates that the electron is a point-particle-probability wave wherein its sampling or measurement creates the statistics corresponding to a stochastic reality. In general, the theory of statistics is based on deterministic but unknown information. The concepts of quantum mechanics of an underlying distribution in a state of indeterminism as well as negative probability are nonsensical and are not a part of this classical result.

by Eq. (8.23).

The double-slit experiment may be modeled physically, and a computer simulation outlined in the Computer Simulation of Classical Electron Diffraction section is posted on the web [18]. The interaction of each incoming electron with the slit or slits causes a redistribution of the incident momentum that is shown visually as a corresponding trajectory from the aperture to the detector. The algorithm uses $N$ electrons that statistically form a uniform distribution at the aperture. To get the points of impact, the momentum-distribution pattern is calculated using Eq. (8.22) that arise from classical statistics. For diffraction at a single slit, the transverse-momentum-density map is given by:

$$2aC\sin\left(\mathbf{k}\cdot\mathbf{x}\right) \tag{8.62}$$

which is spatially diluted according to $\mathbf{k}\cdot\mathbf{x}$ and scaled according to the far field factor of $\frac{a}{f}$. The sine dependence of Eq. (8.62) is equivalent to that of the dot product of the plane lamina of the free electron with the z-axis. Each incident electron that is initially polarized by the slit interaction precesses due to the photon mediated, interaction-generated torque to reorient the plane lamina wherein the cross section of the interaction is proportional to this dot product. The sine dependence can easily be appreciated by considering that the interaction is concentrated at one end of the plane-lamina free electron when it is oriented perpendicularly to the slit; whereas, it is evenly distributed throughout the plane lamina when it is parallel to the slit.

The intensity of the one-slit pattern is then given as the square of the amplitude. Since the two-slit aperture pattern is the convolution of the single-slit pattern with two delta functions, the intensity of the two-slit experiment is given as cosine squared fringes of the single-slit pattern as given by Eq. (8.23) wherein the extended electron interacts with both slits with conservation of momentum to give the modulation of the single-slit momentum pattern. Thus, the superposition of electrons gives the classical result. The double-slit interference pattern associated with the wave-particle duality arises naturally whether electrons add over time or space.

CP predicts that the angular momentum of electrons or photons periodically reverses direction as a function of the transverse distance in the far field of the one-, two- or n-slit diffraction experiment. The pattern is not due to constructive interference of electron- or photon-probability waves; rather it is a map of the transverse momentum. The intensity is given by the amplitude squared, since energy and, thus, the number of electrons or photons is proportional to the amplitude of the momentum squared. The amplitude varies from a maximum to a minimum at which point the angular momentum of the photon or electron reverses direction, then it goes to a maximum again over a periodic cycle. The amplitude decreases away from the longitudinal axis of the slit in the transverse direction since the probability of multiple reversals is low. The amplitude also decreases when there is a large change in the angular momentum that is redirected to a transverse momentum component corresponding to a large torque or a long interaction time.

This can be tested with electrons by polarizing a beam using a Stern-Gerlach analyzer before the slit to select only electrons polarized parallel or antiparallel to the z-axis (the propagation direction of the beam). These electrons are then analyzed in the far field with a second Stern-Gerlach-type analyzer, which determines the polarization as a function of position in the transverse plane or along a transverse axis. Alternate polarization as a function of transverse distance confirms this mechanism of the n-slit pattern.

Recently, it was shown that the induction of surface currents on a metal sheet parallel to the propagation direction of the electron beam of a double-slit experiment interfered with the pattern as expected [19-20]. Furthermore, the double slit experiment has been demonstrated on a macroscopic scale using droplets bouncing on a vertically vibrated bath [21]. Here the localized droplets are coupled to surface waves generated in the bath and random transverse deviations imposed by restrictions of two slits results in a double slit pattern over many flights of droplets to a detector analogous to the transverse deviations of localized electrons or photons during flight due to interactions with the slits and corresponding currents and electromagnetic waves described here. In other recent experiments, the classical mechanism of the double slit experiment has been directly confirmed for photons. The results of Kocsis et al. [22] are consistent with the interpretation that photons have a determined position and momentum, and with an appropriately sensitive measurement apparatus, the causal transverse momentum and position change imparted by close double slits over an ensemble of photons that individually travel through a slit of the pair can be determined wherein the far-field pattern of the superposition of the transverse displacements imparted by the slit interaction over the ensemble is an interference pattern. The old view of constructive and destructive interference of waves is disproved. Photons cannot be created or destroyed by constructive or destructive interference, respectively. The pattern is merely due to photon trajectories corresponding to conservation of momentum altered by photons propagating through close slits. The uncertainty principle as the mechanism of the double-slit interference pattern is similarly disproved by the experiments of Durr et al. [23] as shown in the Wave-Particle Duality is Not Due to the Uncertainty Principle section. Again, the appearance and cancellation of the interference pattern, which in this case involves $^{85}Rb$ atoms diffracted from standing light waves as the atomic states are manipulated, is predicted classically as a transverse position density pattern corresponding to the transverse momentum distribution caused by the interaction of the manipulated states in the atoms with the standing light waves.

# REFERENCES


1. G. O. Reynolds, J. B. DeVelis, G. B. Parrent, B. J. Thompson, *The New Physical Optics Notebook*, SPIE Optical Engineering Press, (1990).
2. R. A. Bonham, M. Fink, *High Energy Electron Scattering*, ACS Monograph, Van Nostrand Reinhold Company, New York, (1974), pp. 1-3.
3. J. D. Jackson, *Classical Electrodynamics,* Second Edition, John Wiley & Sons, New York, (1975), pp. 739-779.
4. R. A. Bonham, M. Fink, *High Energy Electron Scattering*, ACS Monograph, Van Nostrand Reinhold Company, New York, (1974).
5. R. N. Bracewell, *The Fourier Transform and Its Applications*, McGraw-Hill Book Company, New York, (1978), pp. 252-253.
6. A. Apelblat, *Table of Definite and Infinite Integrals*, Elsevier Scientific Publishing Company, Amsterdam, (1983).
7. H. Bateman, *Tables of Integral Transforms*, Vol. I, McGraw-Hill Book Company, New York, (1954).
8. P. J. Bromberg, "Absolute differential cross sections of elastically scattered electrons. I. He, $N_2$, and CO at 500 eV," The Journal of Chemical Physics, Vol. 50, No. 9, (1969), pp. 3906-3921.
9. J. Geiger, "Elastische und unelastische streuung von elektronen an gasen," Zeitschrift fur Physik, Vol. 175, (1963), pp. 530-542.
10. E. M. Peixoto, C. F. Bunge, R. A. Bonham, "Elastic and inelastic scattering by He and Ne atoms in their ground states," Physical Review, Vol. 181, (1969), pp. 322-328.
11. D. A. McQuarrie, *Quantum Chemistry*, University Science Books, Mill Valley, CA, (1983), p. 291.
12. H. Margenau, G. M. Murphy, *The Mathematics of Chemistry and Physics*, D. Van Nostrand Company, Inc., New York, (1943), pp. 363-367.
13. W. McC. Siebert, *Circuits, Signals, and Systems*, The MIT Press, Cambridge, Massachusetts, (1986), pp. 488-502.
14. D. A. McQuarrie, *Quantum Chemistry*, University Science Books, Mill Valley, CA, (1983), p. 139.
15. S. Patz, Cardiovasc Interven Radiol, (1986), 8:25, pp. 225-237.
16. C. P. Slichter, *Principles of Magnetic Resonance*, Harper & Row, New York, (1963), pp. 1-44.
17. L. C. Shi, J. A. Kong, *Applied Electromagnetism*, Brooks/Cole Engineering Division, Monterey, CA, (1983), pp. 170-209.
18. Mathematica modeling of R. Mills' theory by B. Holverstott in "Computer Simulation of Classical Electron Diffraction," posted at www.blacklightpower.com.
19. D. Castelvecchi, Science News, Vol. 171, (2007), p. 292.
20. P. Sonnentag, F. Hasselbach, "Measurement of decoherence of electron waves and visualization of the quantum-classical transition," Phys. Rev. Letts., Vol. 98, May 18, (2007), 200402-1-200402-4.
21. Y. Couder and E. Fort, "Single-particle diffraction and interference at a macroscopic scale," Phys. Rev. Letts., Vol. 97, (2006), pp. 154101-1-154101-4.
22. S. Kocsis, B. Braverman, S. Ravets, M. J. Stevens, R. P. Mirin, L. K. Shalm, A. M. Steinberg, "Observing the average trajectories of single photons in a two-slit interferometer," Science 332, (2011), 1170.
23. S. Durr, T. Nonn, G. Rempe, "Origin of quantum-mechanical complementarity probed by a 'which-way' experiment in an atom interferometer," Nature, September 3, (1998), Vol. 395, pp. 33-37.

# Chapter 9

## EXCITED STATES OF HELIUM

Bound electrons are described by a charge-density (mass-density) function that is the product of a radial delta function ( $f(r)=\delta(r-r_n)$ ), two angular functions (spherical harmonic functions), and a time harmonic function. Thus, a bound electron is a dynamic "bubble-like" charge and current-density function. The two-dimensional spherical surface can exist in a bound state at only specified distances from the nucleus. More explicitly, the uniform current-density function $Y_0^0(\theta,\phi)$ (Eqs. (1.27-1.29)) called the electron atomic orbital that gives rise to the spin of the electron is generated from two current-vector fields (CVFs). Each CVF comprises a continuum of correlated *orthogonal great circle current-density elements (one dimensional "current loops")*. The current pattern comprising each CVF is generated over a half-sphere surface by a set of rotations of two orthogonal great circle current loops that serve as basis elements about each of the $\left(-\mathbf{i}_x,\mathbf{i}_y,0\mathbf{i}_z\right)$ and $\left(-\frac{1}{\sqrt{2}}\mathbf{i}_x,\frac{1}{\sqrt{2}}\mathbf{i}_y,\mathbf{i}_z\right)$-axis; the span being $\pi$ radians. Then, the two CVFs are convoluted, and the result is normalized to exactly generate the *continuous* uniform electron current density function $Y_0^0(\theta,\phi)$ covering a spherical shell and having the three angular momentum components of $\mathbf{L}_{xy}=+/-\frac{\hbar}{4}$ and $\mathbf{L}_z=\frac{\hbar}{2}$ (Figure 1.23)[1].

The spin function of the electron corresponds to the nonradiative $n=1$, $\ell=0$ state which is well known as an s state or orbital. (See Figure 1.1 for the charge function and Figure 1.22 for the current function.) In cases of orbitals of excited states with the $\ell$ quantum number not equal to zero and which are not constant as given by Eq. (1.27), the constant spin function is modulated by a time and spherical harmonic function as given by Eq. (1.29) and shown in Figure 1.2. The modulation or traveling charge-density wave corresponds to an orbital angular momentum in addition to a spin angular momentum. These states are typically referred to as p, d, f, etc. orbitals.

Each atomic orbital is a spherical shell of negative charge ( total charge $=-e$ ) of zero thickness at a distance $r_n$ from the nucleus ( charge $=+Ze$ ). It is well known that the field of a spherical shell of charge is zero inside the shell and that of a point charge at the origin outside the shell [1] (See Figure 1.32). The field of each electron can be treated as that corresponding to a $-e$ charge at the origin with $\mathbf{E}=\frac{-e}{4\pi\varepsilon_0 r^2}$ for $r>r_n$ and $\mathbf{E}=0$ for $r<r_n$ where $r_n$ is the radius of the electron atomic orbital. Thus, as shown in the Two-Electron Atoms section, the central electric fields due to the helium nucleus are $\mathbf{E}=\frac{2e}{4\pi\varepsilon_0 r^2}$ and $\mathbf{E}=\frac{e}{4\pi\varepsilon_0 r^2}$ for $r<r_1$ and $r_1<r<r_2$, respectively. In the ground state of the helium atom, both electrons are at $r_1=r_2=0.567a_0$. When a photon is absorbed, one of the initially indistinguishable electrons called electron 1 moves to a smaller radius, and the other called electron 2 moves to a greater radius. In the limiting case of the absorption of an ionizing photon, electron 1 moves to the radius of the helium ion, $r_1=0.5a_0$, and electron 2 moves to a continuum radius, $r_2=\infty$. When a photon is absorbed by the ground state helium atom it generates an effective charge, $Z_{P-eff}$, within the second atomic orbital such that the electrons move in opposite radial directions while conserving energy and angular momentum. We can determine $Z_{P-eff}$ of the "trapped photon" electric field by requiring that the resonance condition is met for photons of discrete energy, frequency, and wavelength for electron excitation in an electromagnetic potential energy well.

[1] $+/-$ designates both the positive and negative vector directions along an axis in the xy-plane.

It is well known that resonator cavities can trap electromagnetic radiation of discrete resonant frequencies. The atomic orbital is a resonator cavity that traps single photons of discrete frequencies. Thus, photon absorption occurs as an excitation of a resonator mode. The free space photon also comprises a radial Dirac delta function, and the angular momentum of the photon given by $\mathbf{m} = \int \frac{1}{8\pi c} \mathrm{Re}\left[\mathbf{r} \times (\mathbf{E} \times \mathbf{B}^*)\right] dx^4 = \hbar$ in the Photon section is conserved [2] for the solutions for the resonant photons and excited state electron functions as shown for one-electron atoms in the Excited States of the One-Electron Atom (Quantization) section. The correspondence principle holds. That is the change in angular frequency of the electron is equal to the angular frequency of the resonant photon that excites the resonator cavity mode corresponding to the transition, and the energy is given by Planck's equation. It can be demonstrated that the resonance condition between these frequencies is to be satisfied in order to have a net change of the energy field [3].

In general, for a macroscopic multipole with a single $m$ value, a comparison of Eq. (2.62) and Eq. (2.55) shows that the relationship between the angular momentum $M_z$, energy $U$, and angular frequency $\omega$ is given by Eq. (2.63):

$$\frac{dM_z}{dr} = \frac{m}{\omega}\frac{dU}{dr} \tag{9.1}$$

independent of $r$ where $m$ is an integer. Furthermore, the ratio of the square of the angular momentum, $M^2$, to the square of the energy, $U^2$, for a pure ($\ell$, $m$) multipole follows from Eq. (2.55) and Eqs. (2.60-2.62) as given by Eq. (2.64):

$$\frac{M^2}{U^2} = \frac{m^2}{\omega^2} \tag{9.2}$$

From Jackson [4], the quantum mechanical interpretation is that the radiation from such a multipole of order ($\ell$, $m$) carries off $m\hbar$ units of the z component of angular momentum per photon of energy $\hbar\omega$. However, the photon and the electron can each possess only $\hbar$ of angular momentum which requires that Eqs. (9.1-9.2) correspond to a state of the radiation field containing $m$ photons.

As shown in the Excited States of the One-Electron Atom (Quantization) section during excitation the spin, orbital, or total angular momentum of the atomic orbital can change by zero or $\pm\ \hbar$. The selection rules for multipole transitions between quantum states arise from conservation of the photon's multipole moment and angular momentum of $\hbar$. In an excited state, the time-averaged mechanical angular momentum and rotational energy associated with the traveling charge-density wave on the atomic orbital is zero (Eqs. (1.76-1.77)), and the angular momentum of $\hbar$ of the photon that excites the electronic state is carried by the fields of the trapped photon. The amplitudes of the rotational energy, angular momentum, and moment of inertia that couple to external magnetic and electromagnetic fields are given by Eqs. (1.71), (1.72), and (1.73), respectively. Furthermore, the electron charge-density waves are nonradiative due to the angular motion as shown in the Appendix I: Nonradiation Condition. But, excited states are radiative due to a radial dipole that arises from the presence of the trapped photon as shown in the Instability of Excited States section corresponding to $m = 1$ in Eqs. (9.1-9.2).

Then, as shown in the Excited States of the One-Electron Atom (Quantization) section and the Electron Mechanics and the Corresponding Classical Wave Equation for the Derivation of the Rotational Parameters of the Electron section, the total number of multipoles, $N_{\ell,s}$, of an energy level corresponding to a principal quantum number $n$ where each multipole corresponds to an $\ell$ and $m_\ell$ quantum number is:

$$N_{\ell,s} = \sum_{\ell=0}^{n-1} \sum_{m_\ell=-\ell}^{+\ell} 1 = \sum_{\ell=0}^{n-1} 2\ell + 1 = \left(\ell + 1\right)^2 = \ell^2 + 2\ell + 1 = n^2 \tag{9.3}$$

Any given state may be due to a direct transition or due to the sum of transitions between all intermediate states wherein the multiplicity of possible multipoles increases with higher states. Then, the relationships between the parameters of Eqs. (9.1) and (9.2) due to transitions of quantized angular momentum $\hbar$, energy $\hbar\omega$, and radiative via a radial dipole are given by substitution of $m = 1$ and normalization of the energy $U$ by the total number of degenerate multipoles, $n^2$. This requires that the photon's electric field superposes that of the nucleus for $r_1 < r < r_2$ such that the radial electric field has a magnitude proportional to $e/n$ at the electron 2 where $n = 2, 3, 4, \ldots$ for excited states such that $U$ is decreased by the factor of $1/n^2$.

Energy is conserved between the electric and magnetic energies of the helium atom as shown by Eq. (7.42). The helium atom and the "trapped photon" corresponding to a transition to a resonant excited state have neutral charge and obey Maxwell's equations. Since charge is relativistically invariant, the energies in the electric and magnetic fields of the electrons of the helium atom must be conserved as photons are emitted or absorbed. The corresponding forces are determined from the requirement that the radial excited-state electric field has a magnitude proportional to $e/n$ at electron 2.

The "trapped photon" is a "standing electromagnetic wave" which actually is a traveling wave that propagates on the surface around the z-axis, and its source current is only at the atomic orbital. The time-function factor, $k(t)$, for the "standing wave" is identical to the time-function factor of the atomic orbital in order to satisfy the boundary (phase) condition at the atomic orbital surface. Thus, the angular frequency of the "trapped photon" has to be identical to the angular frequency of the electron atomic orbital, $\omega_n$, given by Eq. (1.36). Furthermore, the phase condition requires that the angular functions of the "trapped photon" have to be identical to the spherical harmonic angular functions of the electron atomic orbital. Combining $k(t)$ with the $\phi$-function factor of the spherical harmonic gives $e^{i(m\phi - \omega_n t)}$ for both the electron and the "trapped photon" function.

The photon "standing wave" in an excited electronic state is a solution of Laplace's equation in spherical coordinates

with source currents given by Eq. (2.11) "glued" to the electron and phase-locked to the electron current density wave that travel on the surface with a radial electric field. As given in the Excited States of the One-Electron Atom (Quantization) section, the photon field is purely radial since the field is traveling azimuthally at the speed of light even though the spherical harmonic function has a velocity less than light speed given by Eq. (1.35). The photon field does not change the nature of the electrostatic field of the nucleus or its energy except at the position of the electron. The photon "standing wave" function comprises a radial Dirac delta function that "samples" the Laplace equation solution only at the position infinitesimally inside of the electron current-density function and superimposes with the proton field to give a field of radial magnitude corresponding to a charge of $e/n$ where $n = 2,3,4,\ldots$.

The electric field of the nucleus for $r_1 < r < r_2$ is:

$$\mathbf{E}_{nucleus} = \frac{e}{4\pi\varepsilon_0 r^2} \tag{9.4}$$

From Eq. (2.15), the equation of the electric field of the "trapped photon" for $r = r_2$ where $r_2$ is the radius of electron 2, is:

$$\mathbf{E}_{r\,photon\;\;n,l,m|_{r=r_2}} = \frac{e}{4\pi\varepsilon_0 r_2^2}\left[-1+\frac{1}{n}\left[Y_0^0(\theta,\phi)+\mathrm{Re}\left\{Y_\ell^m(\theta,\phi)e^{im\omega_n t}\right\}\right]\right]\delta(r-r_n) \tag{9.5}$$

The total central field for $r = r_2$ is given by the sum of the electric field of the nucleus and the electric field of the "trapped photon."

$$\mathbf{E}_{total} = \mathbf{E}_{nucleus} + \mathbf{E}_{photon} \tag{9.6}$$

Substitution of Eqs. (9.4) and (9.5) into Eq. (9.6) gives for $r = r_2$,

$$\begin{aligned}\mathbf{E}_{r\,total} &= \frac{e}{4\pi\varepsilon_0 r^2}+\frac{e}{4\pi\varepsilon_0 r_2^2}\left[-1+\frac{1}{n}\left[Y_0^0(\theta,\phi)+\mathrm{Re}\left\{Y_\ell^m(\theta,\phi)e^{im\omega_n t}\right\}\right]\right]\delta(r-r_n)\\ &= \frac{1}{n}\frac{e}{4\pi\varepsilon_0 r_2^2}\left[Y_0^0(\theta,\phi)+\mathrm{Re}\left\{Y_\ell^m(\theta,\phi)e^{im\omega_n t}\right\}\right]\delta(r-r_n)\end{aligned} \tag{9.7}$$

For $r = r_2$ and $m = 0$, the total radial electric field is:

$$\mathbf{E}_{r\,total} = \frac{1}{n}\frac{e}{4\pi\varepsilon_0 r^2} \tag{9.8}$$

The result is equivalent to Eq. (2.17) of the Excited States of the One-Electron Atom (Quantization) section.

In contrast to shortcomings of quantum-mechanical equations, with classical physics (CP), all excited states of the helium atom can be exactly solved in closed form. The radii of electron 2 are determined from the force balance of the electric, magnetic, and centrifugal forces that corresponds to the minimum of energy of the system. The excited-state energies are then given by the electric energies at these radii. All singlet and triplet states with $\ell = 0$ or $\ell \neq 0$ are solved exactly except for small terms corresponding to the magnetostatic energies in the magnetic fields of excited-state electrons, spin-nuclear interactions, and the very small term due to spin-orbit coupling. Spin-nuclear interactions resulted in the use of $a_{He}$ calculated from Eq. (1.259) using the reduced electron mass (Eqs. (1.252-1.255)) rather than $a_0$ given by Eq. (1.255). Furthermore, a table of the spin-orbit energies was calculated for $\ell = 1$ to compare to the effect of different $\ell$ quantum numbers. For over 100 states, the agreement between the predicted and experimental results is remarkable.

## SINGLET EXCITED STATES WITH $\ell = 0$ $(1s^2 \rightarrow 1s^1(ns)^1)$

With $\ell = 0$, the electron source current in the excited state is a constant function given by Eq. (1.27) that spins as a globe about the z-axis:

$$\rho(r,\theta,\phi,t) = \frac{e}{8\pi r^2}[\delta(r-r_n)]\left[Y_0^0(\theta,\phi)+Y_\ell^m(\theta,\phi)\right] \tag{9.9}$$

As given in the Derivation of the Magnetic Field section in Chapter One and by Eq. (11.391), the current is a function of $\sin\theta$ which gives rise to a correction of 2/3 to the field given by Eq. (7.6) and, correspondingly, the magnetic force of two-electron atoms given by Eq. (7.24). The vector orientations of the electrons and the derivation of the magnetic force is given in Appendix VI. The balance between the centrifugal and electric and magnetic forces follows from Eq. (7.32):

$$\frac{m_e v^2}{r_2} = \frac{\hbar^2}{m_e r_2^3} = \frac{1}{n}\frac{e^2}{4\pi\varepsilon_0 r_2^2}+\frac{2}{3}\frac{1}{n}\frac{\hbar^2}{2m_e r_2^3}\sqrt{s(s+1)} \tag{9.10}$$

with the exceptions that the electric and magnetic forces are reduced by a factor of $\frac{1}{n}$ since the corresponding charge from Eq. (9.8) is $\frac{e}{n}$ and the magnetic force is further corrected by the factor of 2/3. With $s = \frac{1}{2}$,

$$r_2 = \left[n-\frac{\sqrt{\frac{3}{4}}}{3}\right]a_{He} \qquad n = 2,3,4,\ldots \tag{9.11}$$

The excited-state energy is the energy stored in the electric field, $E_{ele}$, given by Eqs. (1.263), (1.264), and (10.102) which is the energy of electron 2 relative to the ionized electron at rest having zero energy:

$$E_{ele} = -\frac{1}{n}\frac{e^2}{8\pi\varepsilon_0 r_2} \tag{9.12}$$

where $r_2$ is given by Eq. (9.11) and from Eq. (9.8), $Z = 1/n$ in Eq. (1.264). The energies of the various singlet excited states of helium with $\ell = 0$ appear in Table 9.1.

As shown in the Special Relativistic Correction to the Ionization Energies section the electron possesses an invariant charge-to-mass ratio ($\frac{e}{m_e}$) angular momentum of $\hbar$, and magnetic moment of a Bohr magneton ($\mu_B$). *This invariance feature provides for the stability of multielectron atoms* as shown in the Two-Electron Atoms section and the Three- Through Twenty-Electron Atoms section. This feature also permits *the existence of excited states wherein electrons magnetically interact*. The electron's motion corresponds to a current which gives rise to a magnetic field with a field strength that is inversely proportional to its radius cubed as given in Eq. (9.10) wherein the magnetic field is a relativistic effect of the electric field as shown by Jackson [5]. Since the forces on electron 2 due to the nucleus and electron 1 (Eq. (9.10)) are radial/central, invariant of $r_1$, and independent of $r_1$ with the condition that $r_1 < r_2$, $r_2$ can be determined without knowledge of $r_1$. But, once $r_2$ is determined, $r_1$ can be solved using the equal and opposite magnetic force of electron 2 on electron 1 and the central Coulombic force corresponding to the nuclear charge of $2e$. Using Eq. (9.10), the force balance between the centrifugal and electric and magnetic forces is

$$\frac{m_e v^2}{r_1} = \frac{\hbar^2}{m_e r_1^3} = \frac{2e^2}{4\pi\varepsilon_0 r_1^2} - \frac{1}{3n}\frac{\hbar^2}{m_e r_2^3}\sqrt{s(s+1)} \tag{9.13}$$

With $s = \frac{1}{2}$,

$$r_1^3 - \left(\frac{12n}{\sqrt{3}}r_2^3\right)r_1 + \frac{6n}{\sqrt{3}}r_2^3 = 0 \qquad n = 2,3,4,... \tag{9.14}$$

where $r_2$ is given by Eq. (9.11) and $r_1$ and $r_2$ are in units of $a_{He}$. To obtain the solution of cubic Eq. (9.14) [6], let

$$g = \frac{6n}{\sqrt{3}}r_2^3 \qquad n = 2,3,4,... \tag{9.15}$$

Then, Eq. (9.14) becomes:

$$r_1^3 - 2gr_1 + g = 0 \tag{9.16}$$

and the roots are:

$$r_{11} = A + B \tag{9.17}$$

$$r_{12} = -\frac{A+B}{2} + \frac{A-B}{2}i\sqrt{3} \tag{9.18}$$

$$r_{13} = -\frac{A+B}{2} - \frac{A-B}{2}i\sqrt{3} \tag{9.19}$$

where

$$A = \sqrt[3]{-\frac{g}{2} + \sqrt{\frac{g^2}{4} - \frac{8g^3}{27}}} = \sqrt[3]{\frac{g}{2}}\sqrt[3]{z} \tag{9.20}$$

and

$$B = \sqrt[3]{-\frac{g}{2} - \sqrt{\frac{g^2}{4} - \frac{8g^3}{27}}} = \sqrt[3]{\frac{g}{2}}\sqrt[3]{\bar{z}} \tag{9.21}$$

The complex number $z$ is defined by

$$z = -1 + i\sqrt{\frac{32}{27}g - 1} = re^{i\theta} = r\left(\cos\theta + i\sin\theta\right) \tag{9.22}$$

where the modulus, $r$, and argument, $\theta$, are

$$r = \sqrt{\frac{32}{27}g} \tag{9.23}$$

and

$$\theta = \frac{\pi}{2} + \sin^{-1}(1/r) \tag{9.24}$$

respectively. The cube roots are:

$$\sqrt[3]{z} = \sqrt[3]{r}e^{i\theta/3} = \sqrt[3]{r}\left(\cos\frac{\theta}{3} + i\sin\frac{\theta}{3}\right) \tag{9.25}$$

$$\sqrt[3]{\bar{z}} = \sqrt[3]{r}e^{-i\theta/3} = \sqrt[3]{r}\left(\cos\frac{\theta}{3} - i\sin\frac{\theta}{3}\right) \tag{9.26}$$

so,

$$A = \sqrt[3]{\frac{g}{2}r}\left(\cos\frac{\theta}{3} + i\sin\frac{\theta}{3}\right) \tag{9.27}$$

and

$$B = \sqrt[3]{\frac{g}{2}r}\left(\cos\frac{\theta}{3} - i\sin\frac{\theta}{3}\right) \tag{9.28}$$

The physical root $r_1$ is from the roots that are real and distinct:

$$r_{11} = 2\left(\frac{8}{27}\right)^{1/6}\sqrt{g}\cos\frac{\theta}{3}; r_{12} = -\left(\frac{8}{27}\right)^{1/6}\sqrt{g}\left(\cos\frac{\theta}{3} + \sqrt{3}\sin\frac{\theta}{3}\right); r_{13} = -\left(\frac{8}{27}\right)^{1/6}\sqrt{g}\left(\cos\frac{\theta}{3} - \sqrt{3}\sin\frac{\theta}{3}\right) \tag{9.29}$$

**Table 9.1.** Calculated and experimental energies of He I singlet excited states with $\ell = 0$ $(1s^2 \rightarrow 1s^1(ns)^1)$.

| $n$ | $r_1$ $(a_{He})$ [a] | $r_2$ $(a_{He})$ [b] | **Term Symbol** | $E_{ele}$ CP He I Energy Levels [c] $(eV)$ | NIST He I Energy Levels [d] $(eV)$ | Difference CP-NIST $(eV)$ | Relative Difference [e] (CP-NIST) |
|---|---|---|---|---|---|---|---|
| 2 | 0.501820 | 1.71132 | 1s2s $^1$S | -3.97465 | -3.97161 | -0.00304 | 0.00077 |
| 3 | 0.500302 | 2.71132 | 1s3s $^1$S | -1.67247 | -1.66707 | -0.00540 | 0.00324 |
| 4 | 0.500088 | 3.71132 | 1s4s $^1$S | -0.91637 | -0.91381 | -0.00256 | 0.00281 |
| 5 | 0.500035 | 4.71132 | 1s5s $^1$S | -0.57750 | -0.57617 | -0.00133 | 0.00230 |
| 6 | 0.500016 | 5.71132 | 1s6s $^1$S | -0.39698 | -0.39622 | -0.00076 | 0.00193 |
| 7 | 0.500009 | 6.71132 | 1s7s $^1$S | -0.28957 | -0.2891 | -0.00047 | 0.00163 |
| 8 | 0.500005 | 7.71132 | 1s8s $^1$S | -0.22052 | -0.2202 | -0.00032 | 0.00144 |
| 9 | 0.500003 | 8.71132 | 1s9s $^1$S | -0.17351 | -0.1733 | -0.00021 | 0.00124 |
| 10 | 0.500002 | 9.71132 | 1s10s $^1$S | -0.14008 | -0.13992 | -0.00016 | 0.00116 |
| 11 | 0.500001 | 10.71132 | 1s11s $^1$S | -0.11546 | -0.11534 | -0.00012 | 0.00103 |
| | | | | | **Avg.** | **-0.00144** | **0.00175** |

[a] Radius of the inner electron 1 from Eq. (9.29).
[b] Radius of the outer electron 2 from Eq. (9.11).
[c] Classical physics (CP) calculated energy levels given by the electric energy (Eq. (9.12)).
[d] Experimental NIST levels [7] with the ionization potential defined as zero.
[e] (Theoretical-Experimental)/Experimental.

## TRIPLET EXCITED STATES WITH $\ell = 0$ $(1s^2 \rightarrow 1s^1(ns)^1)$

For the $\ell = 0$ singlet state, the time-averaged spin angular momentum of electron 2 is zero as given in Appendix VI. A triplet state requires the further excitation to unpair the spin states of the two electrons. The angular momentum corresponding to the excited state is $\hbar$ and the angular momentum change corresponding to the spin-flip is also $\hbar$ as given in the Magnetic Parameters of the Electron (Bohr Magneton) section. Then, the triplet state comprises spin interaction terms between the two electrons plus a contribution from the unpairing photon. As shown in the Resonant Precession of the Spin-1/2-Current-Density Function Gives Rise to the Bohr Magneton section, the electron spin angular momentum gives rise to a trapped photon with $\hbar$ of angular momentum along an $\mathbf{S}$-axis. Then, the spin state of each of electron 1 and 2 comprises a photon standing wave that is phase-matched to a spherical harmonic source current, a spherical harmonic dipole $Y_\ell^m(\theta,\phi) = \sin\theta$ with respect to the $\mathbf{S}$-axis. The dipole spins about the $\mathbf{S}$-axis at the angular velocity given by Eq. (1.36) with $\hbar$ of angular momentum. To conserve angular momentum, electron 2 rotates in the opposite direction about $\mathbf{S}$, the axis of the photon angular momentum due to the spin, and this rotation corresponds to $-\frac{2}{3}\hbar$ of angular momentum relative to $\mathbf{S}$. The corresponding angular momentum components of electron 2 due to spin, unpairing, and rotation are:

$$\mathbf{S}_Z = \left(\sqrt{\frac{3}{4}}\hbar + \sqrt{\frac{3}{4}}\hbar - \frac{2}{3}\sqrt{\frac{3}{4}}\hbar\right)\mathbf{i}_Z = \frac{4}{3}\sqrt{\frac{3}{4}}\hbar\mathbf{i}_Z \tag{9.30a}$$

$$\mathbf{S}_Y = \left(\frac{\hbar}{2} + \frac{\hbar}{2} - \frac{2}{3}\frac{\hbar}{2}\right)\mathbf{i}_Y = \frac{4}{3}\frac{\hbar}{2}\mathbf{i}_Y \tag{9.30b}$$

The corresponding angular momentum components of electron 1 are $\hbar$ and $\sqrt{\frac{3}{4}}\hbar$, respectively. The magnetic interaction of each electron is equivalent to the magnetic field corresponding to a magnetic moment of $\mu_B$ interacting with an aligned magnetic momentum of $\frac{4}{3}\sqrt{\frac{3}{4}}\mu_B$. Since the triplet electron-electron interactions are twice those of the singlet case, the triplet magnetic force for electron 2 is twice that of the singlet states as shown in Appendix VI:

$$\frac{m_e v^2}{r_2} = \frac{\hbar^2}{m_e r_2^3} = \frac{1}{n}\frac{e^2}{4\pi\varepsilon_0 r_2^2} + 2\frac{2}{3}\frac{1}{n}\frac{\hbar^2}{2m_e r_2^3}\sqrt{s(s+1)} \tag{9.31}$$

With $s = \frac{1}{2}$,

$$r_2 = \left[n - \frac{2\sqrt{\frac{3}{4}}}{3}\right]a_{He} \qquad n = 2,3,4,... \tag{9.32}$$

The excited-state energy is the energy stored in the electric field, $E_{ele}$, given by Eq. (9.12) where $r_2$ is given by Eq. (9.32). The energies of the various triplet excited states of helium with $\ell = 0$ appear in Table 9.2.

Using $r_2$ (Eq. (9.32)), $r_1$ can be solved using the equal and opposite magnetic force of electron 2 on electron 1 and the central Coulombic force corresponding to the nuclear charge of $2e$. Using Eq. (9.31), the force balance between the centrifugal and electric and magnetic forces is:

$$\frac{m_e v^2}{r_1} = \frac{\hbar^2}{m_e r_1^3} = \frac{2e^2}{4\pi\varepsilon_0 r_1^2} - \frac{2}{3n}\frac{\hbar^2}{m_e r_2^3}\sqrt{s(s+1)} \tag{9.33}$$

With $s = \frac{1}{2}$,

$$r_1^3 - \left(\frac{6n}{\sqrt{3}}r_2^3\right)r_1 + \frac{3n}{\sqrt{3}}r_2^3 = 0 \qquad n = 2,3,4,... \tag{9.34}$$

where $r_2$ is given by Eq. (9.32) and $r_1$ and $r_2$ are in units of $a_{He}$. To obtain the solution of cubic Eq. (9.34), let

$$g = \frac{3n}{\sqrt{3}}r_2^3 \qquad n = 2,3,4,... \tag{9.35}$$

Then, Eq. (9.34) becomes:

$$r_1^3 - 2gr_1 + g = 0 \tag{9.36}$$

Using Eqs. (9.16-9.29), the physical root $r_1$ is from the roots that are real and distinct:

$$r_{11} = 2\left(\frac{8}{27}\right)^{1/6}\sqrt{g}\cos\frac{\theta}{3}; r_{12} = -\left(\frac{8}{27}\right)^{1/6}\sqrt{g}\left(\cos\frac{\theta}{3} + \sqrt{3}\sin\frac{\theta}{3}\right); r_{13} = -\left(\frac{8}{27}\right)^{1/6}\sqrt{g}\left(\cos\frac{\theta}{3} - \sqrt{3}\sin\frac{\theta}{3}\right) \tag{9.37}$$

**Table 9.2.** Calculated and experimental energies of He I triplet excited states with $\ell = 0$ $(1s^2 \rightarrow 1s^1(ns)^1)$.

| $n$ | $r_1$ $(a_{He})$ [a] | $r_2$ $(a_{He})$ [b] | **Term Symbol** | $E_{ele}$ CP He I Energy Levels [c] $(eV)$ | NIST He I Energy Levels [d] $(eV)$ | Difference CP-NIST $(eV)$ | Relative Difference [e] (CP-NIST) |
|---|---|---|---|---|---|---|---|
| 2 | 0.506514 | 1.42265 | 1s2s $^3$S | -4.78116 | -4.76777 | -0.01339 | 0.00281 |
| 3 | 0.500850 | 2.42265 | 1s3s $^3$S | -1.87176 | -1.86892 | -0.00284 | 0.00152 |
| 4 | 0.500225 | 3.42265 | 1s4s $^3$S | -0.99366 | -0.99342 | -0.00024 | 0.00024 |
| 5 | 0.500083 | 4.42265 | 1s5s $^3$S | -0.61519 | -0.61541 | 0.00022 | -0.00036 |
| 6 | 0.500038 | 5.42265 | 1s6s $^3$S | -0.41812 | -0.41838 | 0.00026 | -0.00063 |
| 7 | 0.500019 | 6.42265 | 1s7s $^3$S | -0.30259 | -0.30282 | 0.00023 | -0.00077 |
| 8 | 0.500011 | 7.42265 | 1s8s $^3$S | -0.22909 | -0.22928 | 0.00019 | -0.00081 |
| 9 | 0.500007 | 8.42265 | 1s9s $^3$S | -0.17946 | -0.17961 | 0.00015 | -0.00083 |
| 10 | 0.500004 | 9.42265 | 1s10s $^3$S | -0.14437 | -0.1445 | 0.00013 | -0.00087 |
| 11 | 0.500003 | 10.42265 | 1s11s $^3$S | -0.11866 | -0.11876 | 0.00010 | -0.00087 |
| | | | | | **Avg.** | **-0.00152** | **-0.00006** |

[a] Radius of the inner electron 1 from Eq. (9.37).
[b] Radius of the outer electron 2 from Eq. (9.32).
[c] Classical physics (CP) calculated energy levels given by the electric energy (Eq. (9.12)).
[d] Experimental NIST levels [7] with the ionization potential defined as zero.
[e] (Theoretical-Experimental)/Experimental.

## SINGLET EXCITED STATES WITH $\ell \neq 0$

With $\ell \neq 0$, the electron source current in the excited state is the sum of constant and time-dependent functions where the latter, given by Eq. (1.29), travels about the z-axis. The current due to the time dependent term of Eq. (1.29) corresponding to p, d, f, etc. orbitals is:

$$\begin{aligned}\mathbf{J} &= \frac{m\omega_n}{2\pi}\frac{e}{4\pi r_n^2}N[\delta(r-r_n)]\mathrm{Re}\left\{Y_\ell^m(\theta,\phi)\right\}\left[\mathbf{u}(t)\times\mathbf{r}\right] = \frac{m\omega_n}{2\pi}\frac{e}{4\pi r_n^2}N'[\delta(r-r_n)]\left(P_\ell^m(\cos\theta)\cos\left(m\phi+m\omega_n t\right)\right)\left[\mathbf{u}\times\mathbf{r}\right] \\ &= \frac{m\omega_n}{2\pi}\frac{e}{4\pi r_n^2}N'[\delta(r-r_n)]\left(P_\ell^m(\cos\theta)\cos\left(m\phi+m\omega_n t\right)\right)\sin\theta\hat{\phi}\end{aligned} \tag{9.38}$$

where to keep the form of the spherical harmonic as a traveling wave about the z-axis, $\omega_n' = m\omega_n$ and $N$ and $N'$ are normalization constants. The vectors are defined as:

$$\hat{\phi} = \frac{\hat{u}\times\hat{r}}{\left|\hat{u}\times\hat{r}\right|} = \frac{\hat{u}\times\hat{r}}{\sin\theta}; \qquad \hat{u} = \hat{z} = orbital\ axis \tag{9.39}$$

$$\hat{\theta} = \hat{\phi}\times\hat{r} \tag{9.40}$$

"^" denotes the unit vectors $\hat{u} \equiv \dfrac{\mathbf{u}}{|\mathbf{u}|}$, non-unit vectors are designated in bold, and the current function is normalized.

Jackson [8] gives the general multipole field solution to Maxwell's equations in a source-free region of empty space with the assumption of a time dependence $e^{i\omega_n t}$:

$$\begin{aligned}\mathbf{B} &= \sum_{\ell,m}\left[a_E(\ell,m)f_\ell(kr)\mathbf{X}_{\ell,m} - \frac{i}{k}a_M(\ell,m)\nabla\times g_\ell(kr)\mathbf{X}_{\ell,m}\right] \\ \mathbf{E} &= \sum_{\ell,m}\left[\frac{i}{k}a_E(\ell,m)\nabla\times f_\ell(kr)\mathbf{X}_{\ell,m} + a_M(\ell,m)g_\ell(kr)\mathbf{X}_{\ell,m}\right]\end{aligned} \tag{9.41}$$

where the cgs units used by Jackson are retained in this section. The radial functions $f_\ell(kr)$ and $g_\ell(kr)$ are of the form:

$$g_\ell(kr) = A_\ell^{(1)}h_\ell^{(1)} + A_\ell^{(2)}h_\ell^{(2)} \tag{9.42}$$

$\mathbf{X}_{\ell,m}$ is the vector spherical harmonic defined by:

$$\mathbf{X}_{\ell,m}(\theta,\phi) = \frac{1}{\sqrt{\ell(\ell+1)}}\mathbf{L}Y_{\ell,m}(\theta,\phi) \tag{9.43}$$

where

$$\mathbf{L}=\frac{1}{i}(\mathbf{r}\times\nabla) \tag{9.44}$$

The coefficients $a_E(\ell,m)$ and $a_M(\ell,m)$ of Eq. (9.41) specify the amounts of electric $(\ell,m)$ multipole and magnetic $(\ell,m)$ multipole fields, and are determined by sources and boundary conditions as are the relative proportions in Eq. (9.42). Jackson gives the result of the electric and magnetic coefficients from the sources as

$$a_E(\ell,m)=\frac{4\pi k^2}{i\sqrt{\ell(\ell+1)}}\int Y_\ell^{m*}\left\{\rho\frac{\delta}{\delta r}\left[rj_\ell(kr)\right]+\frac{ik}{c}(\mathbf{r}\cdot\mathbf{J})\,j_\ell(kr)-ik\nabla\cdot(r\times\boldsymbol{M})\,j_\ell(kr)\right\}d^3x \tag{9.45}$$

and

$$a_M(\ell,m)=\frac{-4\pi k^2}{\sqrt{\ell(\ell+1)}}\int j_\ell(kr)Y_\ell^{m*}\mathbf{L}\cdot\left(\frac{\mathbf{J}}{c}+\nabla\times\boldsymbol{M}\right)d^3x \tag{9.46}$$

respectively, where the distribution of charge $\rho(\mathbf{x},t)$, current $\mathbf{J}(\mathbf{x},t)$, and intrinsic magnetization $\boldsymbol{M}(\mathbf{x},t)$ are harmonically varying sources: $\rho(\mathbf{x})e^{-\omega_n t}$, $\mathbf{J}(\mathbf{x})e^{-\omega_n t}$, and $\boldsymbol{M}(\mathbf{x})e^{-\omega_n t}$. From Eq. (9.38), the charge and intrinsic magnetization terms are zero. Since the source dimensions are very small compared to a wavelength ($kr_{\max}<<1$), the small argument limit can be used to give the magnetic multipole coefficient $a_M(\ell,m)$ as:

$$a_M(\ell,m)=\frac{-4\pi k^{\ell+2}}{(2\ell+1)!!}\left(\frac{\ell+1}{\ell}\right)^{1/2}\left(M_{\ell,m}+M'_{\ell,m}\right)=\frac{-4\pi k^{\ell+2}}{\frac{(2\ell+1)!}{2^\ell\ell!}}\left(\frac{\ell+1}{\ell}\right)^{1/2}\left(M_{\ell,m}+M'_{\ell,m}\right) \tag{9.47}$$

where $(2\ell+1)!!=(2\ell+1)(2\ell-1)(2\ell-3)\cdots(5)\cdot(3)\cdot(1)=\frac{(2\ell+1)!}{2^\ell\ell!}$ and the magnetic multipole moments are:

$$M_{\ell,m}=-\frac{1}{\ell+1}\int r^\ell Y^*_{\ell,m}\nabla\cdot\left(\frac{\mathbf{r}\times\mathbf{J}}{c}\right)d^3x$$

$$M'_{\ell,m}=-\int r^\ell Y^*_{\ell,m}\nabla\cdot\boldsymbol{M}d^3x \tag{9.48}$$

From Eq. (1.140), the geometrical factor of the surface current-density function of the atomic orbital about the z-axis is $\left(\frac{2}{3}\right)^{-1}$. Using the geometrical factor, Eqs. (9.47-9.48), and Eqs. (24.101) and (24.102) of Jackson [9], the multipole coefficient $a_{Mag}(\ell,m)$ of the magnetic force of Eq. (7.24) is:

$$a_{Mag}(\ell,m)=\frac{\frac{3}{2}}{(2\ell+1)!!}\frac{1}{\ell+2}\left(\frac{\ell+1}{\ell}\right)^{1/2} \tag{9.49}$$

For singlet states with $\ell\neq0$, a minimum energy is achieved with conservation of the photon's angular momentum of $\hbar$ when the magnetic moments of the corresponding angular momenta relative to the electron velocity (and corresponding Lorentz forces given by Eq. (7.10)) superimpose negatively such that the spin component is radial ($\mathbf{i}_r$-direction) and the orbital component is central ($-\mathbf{i}_r$-direction). The amplitude of the orbital angular momentum $\mathbf{L}_{rotational\ orbital}$, given by Eq. (1.76) is:

$$\mathbf{L}=I\omega\mathbf{i}_z=\hbar\left[\frac{\ell(\ell+1)}{\ell^2+2\ell+1}\right]^{\frac{1}{2}}=\hbar\sqrt{\frac{\ell}{\ell+1}} \tag{9.50}$$

Thus, using Eqs. (7.24), (9.8), (9.49-9.50), and Eq. (36) of Appendix VI, the magnetic force between the two electrons is:

$$\mathbf{F}_{mag}=\frac{1}{n}\frac{\frac{3}{2}}{(2\ell+1)!!}\frac{1}{\ell+2}\left(\frac{\ell+1}{\ell}\right)^{1/2}\frac{1}{2}\frac{\hbar^2}{m_e r^3}\left(\sqrt{s(s+1)}-\sqrt{\frac{\ell}{\ell+1}}\right)\mathbf{i}_r \tag{9.51}$$

and the force balance equation from Eq. (7.32) which achieves the condition that the sum of the mechanical momentum and electromagnetic momentum is conserved as given in Sections 6.6, 12.10, and 17.3 of Jackson [10] is:

$$\frac{m_e v^2}{r_2}=\frac{\hbar^2}{m_e r_2^3}=\frac{1}{n}\frac{e^2}{4\pi\varepsilon_0 r_2^2}-\frac{1}{n}\frac{\frac{3}{2}}{(2\ell+1)!!}\left(\frac{\ell+1}{\ell}\right)^{1/2}\frac{1}{\ell+2}\frac{1}{2}\frac{\hbar^2}{m_e r^3}\left(\sqrt{s(s+1)}-\sqrt{\frac{\ell}{\ell+1}}\right) \tag{9.52}$$

with $s=\frac{1}{2}$,

$$r_2 = \left[ n + \frac{\frac{3}{4}}{(2\ell+1)!!}\frac{1}{\ell+2}\left(\frac{\ell+1}{\ell}\right)^{1/2}\left(\sqrt{\frac{3}{4}} - \sqrt{\frac{\ell}{\ell+1}}\right)\right] a_{He} \qquad n = 2,3,4,... \tag{9.53}$$

The excited-state energy is the energy stored in the electric field, $E_{ele}$, given by Eq. (9.12) where $r_2$ is given by Eq. (9.53). The energies of the various singlet excited states of helium with $\ell \neq 0$ appear in Table 9.3.

Using $r_2$ (Eq. (9.53)), $r_1$ can be solved using the equal and opposite magnetic force of electron 2 on electron 1 and the central Coulombic force corresponding to the nuclear charge of $2e$. Using Eq. (9.52), the force balance between the centrifugal and electric and magnetic forces is:

$$\frac{m_e v^2}{r_1} = \frac{\hbar^2}{m_e r_1^3} = \frac{2e^2}{4\pi\varepsilon_0 r_1^2} + \frac{1}{n}\frac{\frac{3}{2}}{(2\ell+1)!!}\left(\frac{\ell+1}{\ell}\right)^{1/2}\frac{1}{\ell+2}\frac{1}{2}\frac{\hbar^2}{m_e r_2^3}\left(\sqrt{s(s+1)} - \sqrt{\frac{\ell}{\ell+1}}\right) \tag{9.54}$$

with $s = \frac{1}{2}$,

$$\begin{aligned} &r_1^3 + \frac{n8r_1r_2^3}{3\left(\sqrt{\frac{3}{4}} - \sqrt{\frac{\ell}{\ell+1}}\right)}(2\ell+1)!!\left(\frac{\ell}{\ell+1}\right)^{1/2}(\ell+2) \\ &\quad - \frac{n4r_2^3}{3\left(\sqrt{\frac{3}{4}} - \sqrt{\frac{\ell}{\ell+1}}\right)}(2\ell+1)!!\left(\frac{\ell}{\ell+1}\right)^{1/2}(\ell+2) = 0 \\ &\quad n = 2,3,4,... \end{aligned} \tag{9.55}$$

where $r_2$ is given by Eq. (9.53) and $r_1$ and $r_2$ are in units of $a_{He}$. To obtain the solution of cubic Eq. (9.55), let

$$g = -\frac{n4r_2^3}{3\left(\sqrt{\frac{3}{4}} - \sqrt{\frac{\ell}{\ell+1}}\right)}(2\ell+1)!!\left(\frac{\ell}{\ell+1}\right)^{1/2}(\ell+2) \qquad n = 2,3,4,... \tag{9.56}$$

Then, Eq. (9.55) becomes:

$$r_1^3 - 2gr_1 + g = 0 \tag{9.57}$$

Three distinct cases arise depending on the value of $\ell$. For $\ell = 1$ or $\ell = 2$, $g$ of Eq. (9.56) is negative and $A$ and $B$ of Eqs. (9.20) and (9.21), respectively, are real:

$$A = \sqrt[3]{-\frac{g}{2}}\sqrt[3]{1 + \sqrt{1 - \frac{32}{27}g}} \tag{9.58}$$

and

$$B = -\sqrt[3]{-\frac{g}{2}}\sqrt[3]{\sqrt{1 - \frac{32}{27}g} - 1} \tag{9.59}$$

The only real root is:

$$r_1 = r_{11} = \sqrt[3]{-\frac{g}{2}}\left\{\sqrt[3]{1 + \sqrt{1 - \frac{32}{27}g}} - \sqrt[3]{\sqrt{1 - \frac{32}{27}g} - 1}\right\} \tag{9.60}$$

while $r_{12}$ and $r_{13}$ are complex conjugates. When $\ell = 3$ the magnetic force term (2nd term on RHS) of Eq. (9.52) is zero, and the force balance trivially gives:

$$r_1 = 0.5a_{He} \tag{9.61}$$

When $\ell = 4,5,6...$, $g$ (Eq. (9.56)) is positive; so, all three roots are real, but, the physical root is $r_{13}$. In this case, note that $n \geq 5$, $\ell \geq 4$; so, the factor $g$ of Eq. (9.56) is large ($> 10^8$). Expanding $r_{13}$ (Eq. (9.29)) for large values of $g$ gives:

$$r_1 = r_{13} = -\left(\frac{8}{27}\right)^{1/6}\sqrt{g}\left(\cos\frac{\theta}{3} - \sqrt{3}\sin\frac{\theta}{3}\right) = \frac{1}{2} + \frac{1}{16g} + O\left(g^{-3/2}\right) \approx \frac{1}{2} \tag{9.62}$$

**Table 9.3.** Calculated and experimental energies of He I singlet excited states with $\ell \neq 0$.

| $n$ | $\ell$ | $r_1$ $(a_{He})$ [a] | $r_2$ $(a_{He})$ [b] | **Term Symbol** | $E_{ele}$ CP He I Energy Levels [c] $(eV)$ | NIST He I Energy Levels [d] $(eV)$ | Difference CP-NIST $(eV)$ | Relative Difference [e] (CP-NIST) |
|---|---|---|---|---|---|---|---|---|
| 2 | 1 | 0.499929 | 2.01873 | 1s2p $^1P^0$ | -3.36941 | -3.36936 | -0.0000477 | 0.0000141 |
| 3 | 2 | 0.499999 | 3.00076 | 1s3d $^1D$ | -1.51116 | -1.51331 | 0.0021542 | -0.0014235 |
| 3 | 1 | 0.499986 | 3.01873 | 1s3p $^1P^0$ | -1.50216 | -1.50036 | -0.0017999 | 0.0011997 |
| 4 | 2 | 0.500000 | 4.00076 | 1s4d $^1D$ | -0.85008 | -0.85105 | 0.0009711 | -0.0011411 |
| 4 | 3 | 0.500000 | 4.00000 | 1s4f $^1F^0$ | -0.85024 | -0.85037 | 0.0001300 | -0.0001529 |
| 4 | 1 | 0.499995 | 4.01873 | 1s4p $^1P^0$ | -0.84628 | -0.84531 | -0.0009676 | 0.0011446 |
| 5 | 2 | 0.500000 | 5.00076 | 1s5d $^1D$ | -0.54407 | -0.54458 | 0.0005089 | -0.0009345 |
| 5 | 3 | 0.500000 | 5.00000 | 1s5f $^1F^0$ | -0.54415 | -0.54423 | 0.0000764 | -0.0001404 |
| 5 | 4 | 0.500000 | 5.00000 | 1s5g $^1G$ | -0.54415 | -0.54417 | 0.0000159 | -0.0000293 |
| 5 | 1 | 0.499998 | 5.01873 | 1s5p $^1P^0$ | -0.54212 | -0.54158 | -0.0005429 | 0.0010025 |
| 6 | 2 | 0.500000 | 6.00076 | 1s6d $^1D$ | -0.37784 | -0.37813 | 0.0002933 | -0.0007757 |
| 6 | 3 | 0.500000 | 6.00000 | 1s6f $^1F^0$ | -0.37788 | -0.37793 | 0.0000456 | -0.0001205 |
| 6 | 4 | 0.500000 | 6.00000 | 1s6g $^1G$ | -0.37788 | -0.37789 | 0.0000053 | -0.0000140 |
| 6 | 5 | 0.500000 | 6.00000 | 1s6h $^1H^0$ | -0.37788 | -0.37788 | -0.0000045 | 0.0000119 |
| 6 | 1 | 0.499999 | 6.01873 | 1s6p $^1P^0$ | -0.37671 | -0.37638 | -0.0003286 | 0.0008730 |
| 7 | 2 | 0.500000 | 7.00076 | 1s7d $^1D$ | -0.27760 | -0.27779 | 0.0001907 | -0.0006864 |
| 7 | 3 | 0.500000 | 7.00000 | 1s7f $^1F^0$ | -0.27763 | -0.27766 | 0.0000306 | -0.0001102 |
| 7 | 4 | 0.500000 | 7.00000 | 1s7g $^1G$ | -0.27763 | -0.27763 | 0.0000004 | -0.0000016 |
| 7 | 5 | 0.500000 | 7.00000 | 1s7h $^1H^0$ | -0.27763 | -0.27763 | 0.0000006 | -0.0000021 |
| 7 | 6 | 0.500000 | 7.00000 | 1s7i $^1I$ | -0.27763 | -0.27762 | -0.0000094 | 0.0000338 |
| 7 | 1 | 0.500000 | 7.01873 | 1s7p $^1P^0$ | -0.27689 | -0.27667 | -0.0002186 | 0.0007900 |
| | | | | | | **Avg.** | **0.0000240** | **-0.0000220** |

[a] Radius of the inner electron 1 from Eq. (9.60) for $\ell = 1$ or $\ell = 2$, Eq. (9.61) for $\ell = 3$, and Eq. (9.62) for $\ell = 4, 5, 6...$.

[b] Radius of the outer electron 2 from Eq. (9.53).

[c] Classical physics (CP) calculated energy levels given by the electric energy (Eq. (9.12)).

[d] Experimental NIST levels [7] with the ionization potential defined as zero.

[e] (Theoretical-Experimental)/Experimental.

## TRIPLET EXCITED STATES WITH $\ell \neq 0$

For triplet states with $\ell \neq 0$, a minimum energy is achieved with conservation of the photon's angular momentum of $\hbar$ when the magnetic moments of the corresponding angular momenta superimpose negatively such that the spin component is central and the orbital component is radial. Furthermore, as given for the triplet states with $\ell = 0$, the spin component in Eqs. (9.51) and (9.52) is doubled. Thus, the force balance equation derived in Appendix VI is given by:

$$\frac{m_e v^2}{r_2} = \frac{\hbar^2}{m_e r_2^3} = \frac{1}{n}\frac{e^2}{4\pi\varepsilon_0 r_2^2} + \frac{1}{n}\frac{\frac{3}{2}}{(2\ell+1)!!}\left(\frac{\ell+1}{\ell}\right)^{1/2}\frac{1}{\ell+2}\frac{1}{2}\frac{\hbar^2}{m_e r^3}\left(2\sqrt{s(s+1)} - \sqrt{\frac{\ell}{\ell+1}}\right) \tag{9.63}$$

With $s = \frac{1}{2}$,

$$r_2 = \left[n - \frac{\frac{3}{4}}{(2\ell+1)!!}\frac{1}{\ell+2}\left(\frac{\ell+1}{\ell}\right)^{1/2}\left(2\sqrt{\frac{3}{4}} - \sqrt{\frac{\ell}{\ell+1}}\right)\right] a_{He} \tag{9.64}$$

$$n = 2, 3, 4, ...$$

The excited-state energy is the energy stored in the electric field, $E_{ele}$, given by Eq. (9.12) where $r_2$ is given by Eq. (9.64). The energies of the various triplet excited states of helium with $\ell \neq 0$ appear in Table 9.4.

Using $r_2$ (Eq. (9.64)), $r_1$ can be solved using the equal and opposite magnetic force of electron 2 on electron 1 and the central Coulombic force corresponding to the nuclear charge of $2e$. Using Eq. (9.63), the force balance between the centrifugal and electric and magnetic forces is:

$$\frac{m_e v^2}{r_1} = \frac{\hbar^2}{m_e r_1^3} = \frac{2e^2}{4\pi\varepsilon_0 r_1^2} - \frac{1}{n}\frac{\frac{3}{2}}{(2\ell+1)!!}\left(\frac{\ell+1}{\ell}\right)^{1/2}\frac{1}{\ell+2}\frac{1}{2}\frac{\hbar^2}{m_e r_2^3}\left(2\sqrt{s(s+1)} - \sqrt{\frac{\ell}{\ell+1}}\right) \tag{9.65}$$

with $s = \frac{1}{2}$,

$$r_1^3 - \frac{n8r_1r_2^3}{3\left(\sqrt{\frac{3}{4}} - \sqrt{\frac{\ell}{\ell+1}}\right)}(2\ell+1)!!\left(\frac{\ell}{\ell+1}\right)^{1/2}(\ell+2) + \frac{n4r_2^3}{3\left(\sqrt{\frac{3}{4}} - \sqrt{\frac{\ell}{\ell+1}}\right)}(2\ell+1)!!\left(\frac{\ell}{\ell+1}\right)^{1/2}(\ell+2) = 0 \tag{9.66}$$

$$n = 2,3,4,...$$

where $r_2$ is given by Eq. (9.64) and $r_1$ and $r_2$ are in units of $a_{He}$. To obtain the solution of cubic Eq. (9.66), let:

$$g = \frac{n4r_2^3}{3\left(\sqrt{3} - \sqrt{\frac{\ell}{\ell+1}}\right)}(2\ell+1)!!\left(\frac{\ell}{\ell+1}\right)^{1/2}(\ell+2) \qquad n = 2,3,4,... \tag{9.67}$$

Then, Eq. (9.66) becomes:

$$r_1^3 - 2gr_1 + g = 0 \tag{9.68}$$

Using Eqs. (9.16-9.29), $g$ (Eq. (9.67)) is positive, and the physical root $r_1$ is from the roots that are real and distinct:

$$r_{11} = 2\left(\frac{8}{27}\right)^{1/6}\sqrt{g}\cos\frac{\theta}{3}; r_{12} = -\left(\frac{8}{27}\right)^{1/6}\sqrt{g}\left(\cos\frac{\theta}{3} + \sqrt{3}\sin\frac{\theta}{3}\right); r_{13} = -\left(\frac{8}{27}\right)^{1/6}\sqrt{g}\left(\cos\frac{\theta}{3} - \sqrt{3}\sin\frac{\theta}{3}\right) \tag{9.69}$$

**Table 9.4.** Calculated and experimental energies of He I triplet excited states with $\ell \neq 0$.

| $n$ | $\ell$ | $r_1$ ($a_{He}$) [a] | $r_2$ ($a_{He}$) [b] | **Term Symbol** | $E_{ele}$ CP He I Energy Levels [c] ($eV$) | NIST He I Energy Levels [d] ($eV$) | Difference CP-NIST ($eV$) | Relative Difference [e] (CP-NIST) |
|---|---|---|---|---|---|---|---|---|
| 2 | 1 | 0.500571 | 1.87921 | 1s2p $^3P^0_2$ | -3.61957 | -3.6233 | 0.0037349 | -0.0010308 |
| 2 | 1 | 0.500571 | 1.87921 | 1s2p $^3P^0_1$ | -3.61957 | -3.62329 | 0.0037249 | -0.0010280 |
| 2 | 1 | 0.500571 | 1.87921 | 1s2p $^3P^0_0$ | -3.61957 | -3.62317 | 0.0036049 | -0.0009949 |
| 3 | 1 | 0.500105 | 2.87921 | 1s3p $^3P^0_2$ | -1.57495 | -1.58031 | 0.0053590 | -0.0033911 |
| 3 | 1 | 0.500105 | 2.87921 | 1s3p $^3P^0_1$ | -1.57495 | -1.58031 | 0.0053590 | -0.0033911 |
| 3 | 1 | 0.500105 | 2.87921 | 1s3p $^3P^0_0$ | -1.57495 | -1.58027 | 0.0053190 | -0.0033659 |
| 3 | 2 | 0.500011 | 2.98598 | 1s3d $^3D_3$ | -1.51863 | -1.51373 | -0.0049031 | 0.0032391 |
| 3 | 2 | 0.500011 | 2.98598 | 1s3d $^3D_2$ | -1.51863 | -1.51373 | -0.0049031 | 0.0032391 |
| 3 | 2 | 0.500011 | 2.98598 | 1s3d $^3D_1$ | -1.51863 | -1.51373 | -0.0049031 | 0.0032391 |
| 4 | 1 | 0.500032 | 3.87921 | 1s4p $^3P^0_2$ | -0.87671 | -0.87949 | 0.0027752 | -0.0031555 |
| 4 | 1 | 0.500032 | 3.87921 | 1s4p $^3P^0_1$ | -0.87671 | -0.87949 | 0.0027752 | -0.0031555 |
| 4 | 1 | 0.500032 | 3.87921 | 1s4p $^3P^0_0$ | -0.87671 | -0.87948 | 0.0027652 | -0.0031442 |
| 4 | 2 | 0.500003 | 3.98598 | 1s4d $^3D_3$ | -0.85323 | -0.85129 | -0.0019398 | 0.0022787 |
| 4 | 2 | 0.500003 | 3.98598 | 1s4d $^3D_2$ | -0.85323 | -0.85129 | -0.0019398 | 0.0022787 |

| $n$ | $\ell$ | $r_1$ ($a_{He}$) [a] | $r_2$ ($a_{He}$) [b] | **Term Symbol** | $E_{ele}$ CP He I Energy Levels [c] ($eV$) | NIST He I Energy Levels [d] ($eV$) | Difference CP-NIST ($eV$) | Relative Difference [e] (CP-NIST) |
|---|---|---|---|---|---|---|---|---|
| 4 | 2 | 0.500003 | 3.98598 | $1s4d\ ^3D_1$ | -0.85323 | -0.85129 | -0.0019398 | 0.0022787 |
| 4 | 3 | 0.500000 | 3.99857 | $1s4f\ ^3F^0_3$ | -0.85054 | -0.85038 | -0.0001638 | 0.0001926 |
| 4 | 3 | 0.500000 | 3.99857 | $1s4f\ ^3F^0_4$ | -0.85054 | -0.85038 | -0.0001638 | 0.0001926 |
| 4 | 3 | 0.500000 | 3.99857 | $1s4f\ ^3F^0_2$ | -0.85054 | -0.85038 | -0.0001638 | 0.0001926 |
| 5 | 1 | 0.500013 | 4.87921 | $1s5p\ ^3P^0_2$ | -0.55762 | -0.55916 | 0.0015352 | -0.0027456 |
| 5 | 1 | 0.500013 | 4.87921 | $1s5p\ ^3P^0_1$ | -0.55762 | -0.55916 | 0.0015352 | -0.0027456 |
| 5 | 1 | 0.500013 | 4.87921 | $1s5p\ ^3P^0_0$ | -0.55762 | -0.55915 | 0.0015252 | -0.0027277 |
| 5 | 2 | 0.500001 | 4.98598 | $1s5d\ ^3D_3$ | -0.54568 | -0.54472 | -0.0009633 | 0.0017685 |
| 5 | 2 | 0.500001 | 4.98598 | $1s5d\ ^3D_2$ | -0.54568 | -0.54472 | -0.0009633 | 0.0017685 |
| 5 | 2 | 0.500001 | 4.98598 | $1s5d\ ^3D_1$ | -0.54568 | -0.54472 | -0.0009633 | 0.0017685 |
| 5 | 3 | 0.500000 | 4.99857 | $1s5f\ ^3F^0_3$ | -0.54431 | -0.54423 | -0.0000791 | 0.0001454 |
| 5 | 3 | 0.500000 | 4.99857 | $1s5f\ ^3F^0_4$ | -0.54431 | -0.54423 | -0.0000791 | 0.0001454 |
| 5 | 3 | 0.500000 | 4.99857 | $1s5f\ ^3F^0_2$ | -0.54431 | -0.54423 | -0.0000791 | 0.0001454 |
| 5 | 4 | 0.500000 | 4.99988 | $1s5g\ ^3G_4$ | -0.54417 | -0.54417 | 0.0000029 | -0.0000054 |
| 5 | 4 | 0.500000 | 4.99988 | $1s5g\ ^3G_5$ | -0.54417 | -0.54417 | 0.0000029 | -0.0000054 |
| 5 | 4 | 0.500000 | 4.99988 | $1s5g\ ^3G_3$ | -0.54417 | -0.54417 | 0.0000029 | -0.0000054 |
| 6 | 1 | 0.500006 | 5.87921 | $1s6p\ ^3P^0_2$ | -0.38565 | -0.38657 | 0.0009218 | -0.0023845 |
| 6 | 1 | 0.500006 | 5.87921 | $1s6p\ ^3P^0_1$ | -0.38565 | -0.38657 | 0.0009218 | -0.0023845 |
| 6 | 1 | 0.500006 | 5.87921 | $1s6p\ ^3P^0_0$ | -0.38565 | -0.38657 | 0.0009218 | -0.0023845 |
| 6 | 2 | 0.500001 | 5.98598 | $1s6d\ ^3D_3$ | -0.37877 | -0.37822 | -0.0005493 | 0.0014523 |
| 6 | 2 | 0.500001 | 5.98598 | $1s6d\ ^3D_2$ | -0.37877 | -0.37822 | -0.0005493 | 0.0014523 |
| 6 | 2 | 0.500001 | 5.98598 | $1s6d\ ^3D_1$ | -0.37877 | -0.37822 | -0.0005493 | 0.0014523 |
| 6 | 3 | 0.500000 | 5.99857 | $1s6f\ ^3F^0_3$ | -0.37797 | -0.37793 | -0.0000444 | 0.0001176 |
| 6 | 3 | 0.500000 | 5.99857 | $1s6f\ ^3F^0_4$ | -0.37797 | -0.37793 | -0.0000444 | 0.0001176 |
| 6 | 3 | 0.500000 | 5.99857 | $1s6f\ ^3F^0_2$ | -0.37797 | -0.37793 | -0.0000444 | 0.0001176 |
| 6 | 4 | 0.500000 | 5.99988 | $1s6g\ ^3G_4$ | -0.37789 | -0.37789 | -0.0000023 | 0.0000060 |
| 6 | 4 | 0.500000 | 5.99988 | $1s6g\ ^3G_5$ | -0.37789 | -0.37789 | -0.0000023 | 0.0000060 |
| 6 | 4 | 0.500000 | 5.99988 | $1s6g\ ^3G_3$ | -0.37789 | -0.37789 | -0.0000023 | 0.0000060 |
| 6 | 5 | 0.500000 | 5.99999 | $1s6h\ ^3H^0_4$ | -0.37789 | -0.37788 | -0.0000050 | 0.0000133 |
| 6 | 5 | 0.500000 | 5.99999 | $1s6h\ ^3H^0_5$ | -0.37789 | -0.37788 | -0.0000050 | 0.0000133 |
| 6 | 5 | 0.500000 | 5.99999 | $1s6h\ ^3H^0_6$ | -0.37789 | -0.37788 | -0.0000050 | 0.0000133 |
| 7 | 1 | 0.500003 | 6.87921 | $1s7p\ ^3P^0_2$ | -0.28250 | -0.28309 | 0.0005858 | -0.0020692 |
| 7 | 1 | 0.500003 | 6.87921 | $1s7p\ ^3P^0_1$ | -0.28250 | -0.28309 | 0.0005858 | -0.0020692 |
| 7 | 1 | 0.500003 | 6.87921 | $1s7p\ ^3P^0_0$ | -0.28250 | -0.28309 | 0.0005858 | -0.0020692 |
| 7 | 2 | 0.500000 | 6.98598 | $1s7d\ ^3D_3$ | -0.27819 | -0.27784 | -0.0003464 | 0.0012468 |
| 7 | 2 | 0.500000 | 6.98598 | $1s7d\ ^3D_2$ | -0.27819 | -0.27784 | -0.0003464 | 0.0012468 |
| 7 | 2 | 0.500000 | 6.98598 | $1s7d\ ^3D_1$ | -0.27819 | -0.27784 | -0.0003464 | 0.0012468 |
| 7 | 3 | 0.500000 | 6.99857 | $1s7f\ ^3F^0_3$ | -0.27769 | -0.27766 | -0.0000261 | 0.0000939 |
| 7 | 3 | 0.500000 | 6.99857 | $1s7f\ ^3F^0_4$ | -0.27769 | -0.27766 | -0.0000261 | 0.0000939 |
| 7 | 3 | 0.500000 | 6.99857 | $1s7f\ ^3F^0_2$ | -0.27769 | -0.27766 | -0.0000261 | 0.0000939 |

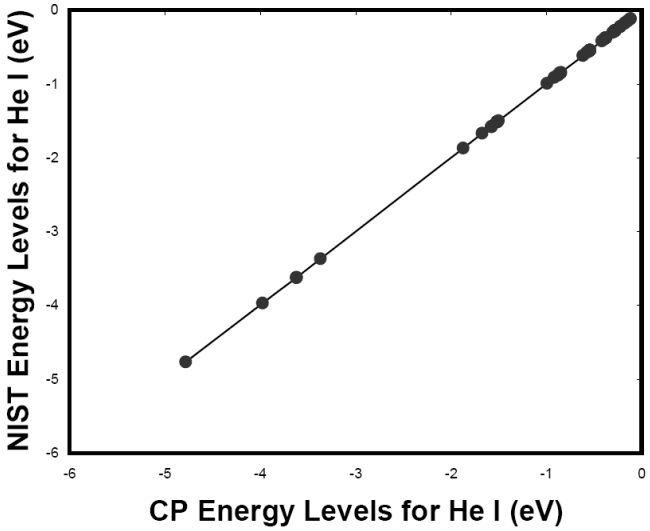
| $n$ | $\ell$ | $r_1$ ($a_{He}$) [a] | $r_2$ ($a_{He}$) [b] | **Term Symbol** | $E_{ele}$ CP He I Energy Levels [c] ($eV$) | NIST He I Energy Levels [d] ($eV$) | Difference CP-NIST ($eV$) | Relative Difference [e] (CP-NIST) |
|---|---|---|---|---|---|---|---|---|
| 7 | 4 | 0.500000 | 6.99988 | $1s7g\ ^3G_4$ | -0.27763 | -0.27763 | -0.0000043 | 0.0000155 |
| 7 | 4 | 0.500000 | 6.99988 | $1s7g\ ^3G_5$ | -0.27763 | -0.27763 | -0.0000043 | 0.0000155 |
| 7 | 4 | 0.500000 | 6.99988 | $1s7g\ ^3G_3$ | -0.27763 | -0.27763 | -0.0000043 | 0.0000155 |
| 7 | 5 | 0.500000 | 6.99999 | $1s7h\ ^3H^0_5$ | -0.27763 | -0.27763 | 0.0000002 | -0.0000009 |
| 7 | 5 | 0.500000 | 6.99999 | $1s7h\ ^3H^0_6$ | -0.27763 | -0.27763 | 0.0000002 | -0.0000009 |
| 7 | 5 | 0.500000 | 6.99999 | $1s7h\ ^3H^0_4$ | -0.27763 | -0.27763 | 0.0000002 | -0.0000009 |
| 7 | 6 | 0.500000 | 7.00000 | $1s7\ i^3I_5$ | -0.27763 | -0.27762 | -0.0000094 | 0.0000339 |
| 7 | 6 | 0.500000 | 7.00000 | $1s7i\ ^3I6$ | -0.27763 | -0.27762 | -0.0000094 | 0.0000339 |
| 7 | 6 | 0.500000 | 7.00000 | $1s7i\ ^3I_7$ | -0.27763 | -0.27762 | -0.0000094 | 0.0000339 |
| | | | | | | **Avg.** | **0.0002768** | **-0.0001975** |

[a] Radius of the inner electron 1 from Eq. (9.69).
[b] Radius of the outer electron 2 from Eq. (9.64).
[c] Classical physics (CP) calculated energy levels given by the electric energy (Eq. (9.12)).
[d] Experimental NIST levels [7] with the ionization potential defined as zero.
[e] (Theoretical-Experimental)/Experimental.

## ALL EXCITED HE I STATES

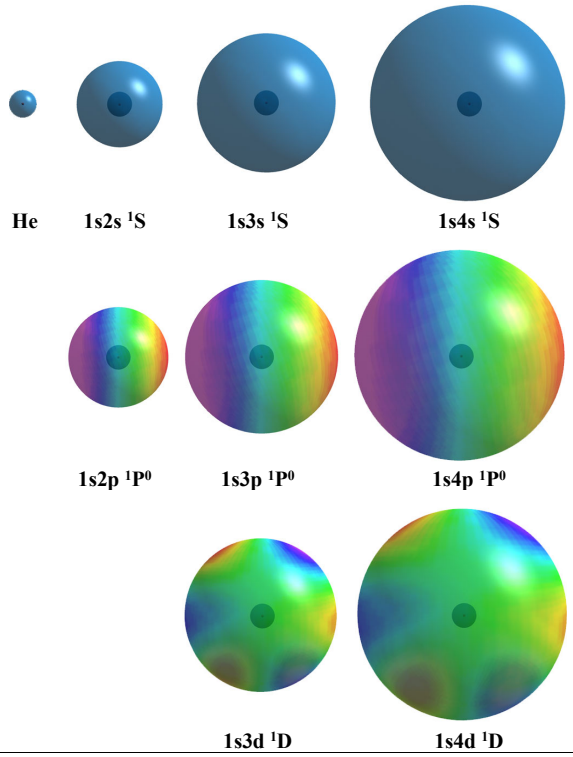
The combined energies of the various states of helium appear in Table 9.5. A plot of the predicted and experimental energies of levels assigned by NIST [7] appears in Figure 9.1.

**Figure 9.1.** A plot of the predicted and experimental energies of levels assigned by NIST [7].




For over 100 states, the r-squared value is 0.999994, and the typical average relative difference is about 5 significant figures, which is within the error of the experimental data. The agreement is remarkable. The color scale, translucent views of the charge densities of exemplary spherical harmonics that modulate the time-independent spin function are shown in Figure 9.2. For $\ell \neq 0$, the modulation functions propagate about the z-axis as spatially and temporally harmonic charge-density waves.

**Figure 9.2.** Exemplary color scale, translucent views of the charge-densities of the inner and outer electrons of helium excited states. The outer-electron orbital function modulates the time-constant (spin) function, (shown for t = 0; three-dimensional view). The inner electron is essentially that of $He^+$ (nuclei red, not to scale).




The hydrino states given in the Hydrino Theory—BlackLight Process section are strongly supported by the calculation of the helium excited states as well as the hydrogen excited states given in the Excited States of the One-Electron Atom (Quantization) section since the electron-photon model is the same in both the excited states and in the lower-energy states of hydrogen except that the photon provides a central field of magnitude $n$ in the hydrino case and $1/n$ in the excited-state case.

**Table 9.5.** Calculated and experimental energies of states of helium.

| $n$ | $\ell$ | $r_1$ ($a_{He}$) [a] | $r_2$ ($a_{He}$) [b] | Term Symbol | $E_{ele}$ CP He I Energy Levels [c] ($eV$) | NIST He I Energy Levels [d] ($eV$) | Difference CP-NIST ($eV$) | Relative Difference [e] (CP-NIST) |
|---|---|---|---|---|---|---|---|---|
| 1 | 0 | 0.56699 | 0.566987 | $1s^2\ ^1S$ | -24.58750 | -24.58741 | -0.000092 | 0.0000038 |
| 2 | 0 | 0.506514 | 1.42265 | $1s2s\ ^3S$ | -4.78116 | -4.76777 | -0.0133929 | 0.0028090 |
| 2 | 0 | 0.501820 | 1.71132 | $1s2s\ ^1S$ | -3.97465 | -3.97161 | -0.0030416 | 0.0007658 |
| 2 | 1 | 0.500571 | 1.87921 | $1s2p\ ^3P^0_2$ | -3.61957 | -3.6233 | 0.0037349 | -0.0010308 |
| 2 | 1 | 0.500571 | 1.87921 | $1s2p\ ^3P^0_1$ | -3.61957 | -3.62329 | 0.0037249 | -0.0010280 |
| 2 | 1 | 0.500571 | 1.87921 | $1s2p\ ^3P^0_0$ | -3.61957 | -3.62317 | 0.0036049 | -0.0009949 |
| 2 | 1 | 0.499929 | 2.01873 | $1s2p\ ^1P^0$ | -3.36941 | -3.36936 | -0.0000477 | 0.0000141 |
| 3 | 0 | 0.500850 | 2.42265 | $1s3s\ ^3S$ | -1.87176 | -1.86892 | -0.0028377 | 0.0015184 |
| 3 | 0 | 0.500302 | 2.71132 | $1s3s\ ^1S$ | -1.67247 | -1.66707 | -0.0054014 | 0.0032401 |
| 3 | 1 | 0.500105 | 2.87921 | $1s3p\ ^3P^0_2$ | -1.57495 | -1.58031 | 0.0053590 | -0.0033911 |
| 3 | 1 | 0.500105 | 2.87921 | $1s3p\ ^3P^0_1$ | -1.57495 | -1.58031 | 0.0053590 | -0.0033911 |
| 3 | 1 | 0.500105 | 2.87921 | $1s3p\ ^3P^0_0$ | -1.57495 | -1.58027 | 0.0053190 | -0.0033659 |
| 3 | 2 | 0.500011 | 2.98598 | $1s3d\ ^3D_3$ | -1.51863 | -1.51373 | -0.0049031 | 0.0032391 |
| 3 | 2 | 0.500011 | 2.98598 | $1s3d\ ^3D_2$ | -1.51863 | -1.51373 | -0.0049031 | 0.0032391 |
| 3 | 2 | 0.500011 | 2.98598 | $1s3d\ ^3D_1$ | -1.51863 | -1.51373 | -0.0049031 | 0.0032391 |
| 3 | 2 | 0.499999 | 3.00076 | $1s3d\ ^1D$ | -1.51116 | -1.51331 | 0.0021542 | -0.0014235 |
| 3 | 1 | 0.499986 | 3.01873 | $1s3p\ ^1P^0$ | -1.50216 | -1.50036 | -0.0017999 | 0.0011997 |
| 4 | 0 | 0.500225 | 3.42265 | $1s4s\ ^3S$ | -0.99366 | -0.99342 | -0.0002429 | 0.0002445 |
| 4 | 0 | 0.500088 | 3.71132 | $1s4s\ ^1S$ | -0.91637 | -0.91381 | -0.0025636 | 0.0028054 |

| $n$ | $\ell$ | $r_1$ ($a_{He}$) [a] | $r_2$ ($a_{He}$) [b] | **Term Symbol** | $E_{ele}$ CP He I EnergyLevels [c] ($eV$) | NIST He I Energy Levels [d] ($eV$) | Difference CP-NIST ($eV$) | Relative Difference [e] (CP-NIST) |
|---|---|---|---|---|---|---|---|---|
| 4 | 1 | 0.500032 | 3.87921 | $1s4p\ ^3P^0_2$ | -0.87671 | -0.87949 | 0.0027752 | -0.0031555 |
| 4 | 1 | 0.500032 | 3.87921 | $1s4p\ ^3P^0_1$ | -0.87671 | -0.87949 | 0.0027752 | -0.0031555 |
| 4 | 1 | 0.500032 | 3.87921 | $1s4p\ ^3P^0_0$ | -0.87671 | -0.87948 | 0.0027652 | -0.0031442 |
| 4 | 2 | 0.500003 | 3.98598 | $1s4d\ ^3D_3$ | -0.85323 | -0.85129 | -0.0019398 | 0.0022787 |
| 4 | 2 | 0.500003 | 3.98598 | $1s4d\ ^3D_2$ | -0.85323 | -0.85129 | -0.0019398 | 0.0022787 |
| 4 | 2 | 0.500003 | 3.98598 | $1s4d\ ^3D_1$ | -0.85323 | -0.85129 | -0.0019398 | 0.0022787 |
| 4 | 2 | 0.500000 | 4.00076 | $1s4d\ ^1D$ | -0.85008 | -0.85105 | 0.0009711 | -0.0011411 |
| 4 | 3 | 0.500000 | 3.99857 | $1s4f\ ^3F^0_3$ | -0.85054 | -0.85038 | -0.0001638 | 0.0001926 |
| 4 | 3 | 0.500000 | 3.99857 | $1s4f\ ^3F^0_4$ | -0.85054 | -0.85038 | -0.0001638 | 0.0001926 |
| 4 | 3 | 0.500000 | 3.99857 | $1s4f\ ^3F^0_2$ | -0.85054 | -0.85038 | -0.0001638 | 0.0001926 |
| 4 | 3 | 0.500000 | 4.00000 | $1s4f\ ^1F^0$ | -0.85024 | -0.85037 | 0.0001300 | -0.0001529 |
| 4 | 1 | 0.499995 | 4.01873 | $1s4p\ ^1P^0$ | -0.84628 | -0.84531 | -0.0009676 | 0.0011446 |
| 5 | 0 | 0.500083 | 4.42265 | $1s5s\ ^3S$ | -0.61519 | -0.61541 | 0.0002204 | -0.0003582 |
| 5 | 0 | 0.500035 | 4.71132 | $1s5s\ ^1S$ | -0.57750 | -0.57617 | -0.0013253 | 0.0023002 |
| 5 | 1 | 0.500013 | 4.87921 | $1s5p\ ^3P^0_2$ | -0.55762 | -0.55916 | 0.0015352 | -0.0027456 |
| 5 | 1 | 0.500013 | 4.87921 | $1s5p\ ^3P^0_1$ | -0.55762 | -0.55916 | 0.0015352 | -0.0027456 |
| 5 | 1 | 0.500013 | 4.87921 | $1s5p\ ^3P^0_0$ | -0.55762 | -0.55915 | 0.0015252 | -0.0027277 |
| 5 | 2 | 0.500001 | 4.98598 | $1s5d\ ^3D_3$ | -0.54568 | -0.54472 | -0.0009633 | 0.0017685 |
| 5 | 2 | 0.500001 | 4.98598 | $1s5d\ ^3D_2$ | -0.54568 | -0.54472 | -0.0009633 | 0.0017685 |
| 5 | 2 | 0.500001 | 4.98598 | $1s5d\ ^3D_1$ | -0.54568 | -0.54472 | -0.0009633 | 0.0017685 |
| 5 | 2 | 0.500000 | 5.00076 | $1s5d\ ^1D$ | -0.54407 | -0.54458 | 0.0005089 | -0.0009345 |
| 5 | 3 | 0.500000 | 4.99857 | $1s5f\ ^3F^0_3$ | -0.54431 | -0.54423 | -0.0000791 | 0.0001454 |
| 5 | 3 | 0.500000 | 4.99857 | $1s5f\ ^3F^0_4$ | -0.54431 | -0.54423 | -0.0000791 | 0.0001454 |
| 5 | 3 | 0.500000 | 4.99857 | $1s5f\ ^3F^0_2$ | -0.54431 | -0.54423 | -0.0000791 | 0.0001454 |
| 5 | 3 | 0.500000 | 5.00000 | $1s5f\ ^1F^0$ | -0.54415 | -0.54423 | 0.0000764 | -0.0001404 |
| 5 | 4 | 0.500000 | 4.99988 | $1s5g\ ^3G_4$ | -0.54417 | -0.54417 | 0.0000029 | -0.0000054 |
| 5 | 4 | 0.500000 | 4.99988 | $1s5g\ ^3G_5$ | -0.54417 | -0.54417 | 0.0000029 | -0.0000054 |
| 5 | 4 | 0.500000 | 4.99988 | $1s5g\ ^3G_3$ | -0.54417 | -0.54417 | 0.0000029 | -0.0000054 |
| 5 | 4 | 0.500000 | 5.00000 | $1s5g\ ^1G$ | -0.54415 | -0.54417 | 0.0000159 | -0.0000293 |
| 5 | 1 | 0.499998 | 5.01873 | $1s5p\ ^1P^0$ | -0.54212 | -0.54158 | -0.0005429 | 0.0010025 |
| 6 | 0 | 0.500038 | 5.42265 | $1s6s\ ^3S$ | -0.41812 | -0.41838 | 0.0002621 | -0.0006266 |
| 6 | 0 | 0.500016 | 5.71132 | $1s6s\ ^1S$ | -0.39698 | -0.39622 | -0.0007644 | 0.0019291 |
| 6 | 1 | 0.500006 | 5.87921 | $1s6p\ ^3P^0_2$ | -0.38565 | -0.38657 | 0.0009218 | -0.0023845 |
| 6 | 1 | 0.500006 | 5.87921 | $1s6p\ ^3P^0_1$ | -0.38565 | -0.38657 | 0.0009218 | -0.0023845 |
| 6 | 1 | 0.500006 | 5.87921 | $1s6p\ ^3P^0_0$ | -0.38565 | -0.38657 | 0.0009218 | -0.0023845 |
| 6 | 2 | 0.500001 | 5.98598 | $1s6d\ ^3D_3$ | -0.37877 | -0.37822 | -0.0005493 | 0.0014523 |
| 6 | 2 | 0.500001 | 5.98598 | $1s6d\ ^3D_2$ | -0.37877 | -0.37822 | -0.0005493 | 0.0014523 |
| 6 | 2 | 0.500001 | 5.98598 | $1s6d\ ^3D_1$ | -0.37877 | -0.37822 | -0.0005493 | 0.0014523 |
| 6 | 2 | 0.500000 | 6.00076 | $1s6d\ ^1D$ | -0.37784 | -0.37813 | 0.0002933 | -0.0007757 |
| 6 | 3 | 0.500000 | 5.99857 | $1s6f\ ^3F^0_3$ | -0.37797 | -0.37793 | -0.0000444 | 0.0001176 |
| 6 | 3 | 0.500000 | 5.99857 | $1s6f\ ^3F^0_4$ | -0.37797 | -0.37793 | -0.0000444 | 0.0001176 |

| $n$ | $\ell$ | $r_1$ ($a_{He}$) [a] | $r_2$ ($a_{He}$) [b] | **Term Symbol** | $E_{ele}$ CP He I EnergyLevels [c] ($eV$) | NIST He I Energy Levels [d] ($eV$) | Difference CP-NIST ($eV$) | Relative Difference [e] (CP-NIST) |
|---|---|---|---|---|---|---|---|---|
| 6 | 3 | 0.500000 | 5.99857 | $1s6f\ ^3F^0_2$ | -0.37797 | -0.37793 | -0.0000444 | 0.0001176 |
| 6 | 3 | 0.500000 | 6.00000 | $1s6f\ ^1F^0$ | -0.37788 | -0.37793 | 0.0000456 | -0.0001205 |
| 6 | 4 | 0.500000 | 5.99988 | $1s6g\ ^3G_4$ | -0.37789 | -0.37789 | -0.0000023 | 0.0000060 |
| 6 | 4 | 0.500000 | 5.99988 | $1s6g\ ^3G_5$ | -0.37789 | -0.37789 | -0.0000023 | 0.0000060 |
| 6 | 4 | 0.500000 | 5.99988 | $1s6g\ ^3G_3$ | -0.37789 | -0.37789 | -0.0000023 | 0.0000060 |
| 6 | 4 | 0.500000 | 6.00000 | $1s6g\ ^1G$ | -0.37788 | -0.37789 | 0.0000053 | -0.0000140 |
| 6 | 5 | 0.500000 | 5.99999 | $1s6h\ ^3H^0_4$ | -0.37789 | -0.37788 | -0.0000050 | 0.0000133 |
| 6 | 5 | 0.500000 | 5.99999 | $1s6h\ ^3H^0_5$ | -0.37789 | -0.37788 | -0.0000050 | 0.0000133 |
| 6 | 5 | 0.500000 | 5.99999 | $1s6h\ ^3H^0_6$ | -0.37789 | -0.37788 | -0.0000050 | 0.0000133 |
| 6 | 5 | 0.500000 | 6.00000 | $1s6h\ ^1H^0$ | -0.37788 | -0.37788 | -0.0000045 | 0.0000119 |
| 6 | 1 | 0.499999 | 6.01873 | $1s6p\ ^1P^0$ | -0.37671 | -0.37638 | -0.0003286 | 0.0008730 |
| 7 | 0 | 0.500019 | 6.42265 | $1s7s\ ^3S$ | -0.30259 | -0.30282 | 0.0002337 | -0.0007718 |
| 7 | 0 | 0.500009 | 6.71132 | $1s7s\ ^1S$ | -0.28957 | -0.2891 | -0.0004711 | 0.0016295 |
| 7 | 1 | 0.500003 | 6.87921 | $1s7p\ ^3P^0_2$ | -0.28250 | -0.28309 | 0.0005858 | -0.0020692 |
| 7 | 1 | 0.500003 | 6.87921 | $1s7p\ ^3P^0_1$ | -0.28250 | -0.28309 | 0.0005858 | -0.0020692 |
| 7 | 1 | 0.500003 | 6.87921 | $1s7p\ ^3P^0_0$ | -0.28250 | -0.28309 | 0.0005858 | -0.0020692 |
| 7 | 2 | 0.500000 | 6.98598 | $1s7d\ ^3D_3$ | -0.27819 | -0.27784 | -0.0003464 | 0.0012468 |
| 7 | 2 | 0.500000 | 6.98598 | $1s7d\ ^3D_2$ | -0.27819 | -0.27784 | -0.0003464 | 0.0012468 |
| 7 | 2 | 0.500000 | 6.98598 | $1s7d\ ^3D_1$ | -0.27819 | -0.27784 | -0.0003464 | 0.0012468 |
| 7 | 2 | 0.500000 | 7.00076 | $1s7d\ ^1D$ | -0.27760 | -0.27779 | 0.0001907 | -0.0006864 |
| 7 | 3 | 0.500000 | 6.99857 | $1s7f\ ^3F^0_3$ | -0.27769 | -0.27766 | -0.0000261 | 0.0000939 |
| 7 | 3 | 0.500000 | 6.99857 | $1s7f\ ^3F^0_4$ | -0.27769 | -0.27766 | -0.0000261 | 0.0000939 |
| 7 | 3 | 0.500000 | 6.99857 | $1s7f\ ^3F^0_2$ | -0.27769 | -0.27766 | -0.0000261 | 0.0000939 |
| 7 | 3 | 0.500000 | 7.00000 | $1s7f\ ^1F^0$ | -0.27763 | -0.27766 | 0.0000306 | -0.0001102 |
| 7 | 4 | 0.500000 | 6.99988 | $1s7g\ ^3G_4$ | -0.27763 | -0.27763 | -0.0000043 | 0.0000155 |
| 7 | 4 | 0.500000 | 6.99988 | $1s7g\ ^3G_5$ | -0.27763 | -0.27763 | -0.0000043 | 0.0000155 |
| 7 | 4 | 0.500000 | 6.99988 | $1s7g\ ^3G_3$ | -0.27763 | -0.27763 | -0.0000043 | 0.0000155 |
| 7 | 4 | 0.500000 | 7.00000 | $1s7g\ ^1G$ | -0.27763 | -0.27763 | 0.0000004 | -0.0000016 |
| 7 | 5 | 0.500000 | 6.99999 | $1s7h\ ^3H^0_5$ | -0.27763 | -0.27763 | 0.0000002 | -0.0000009 |
| 7 | 5 | 0.500000 | 6.99999 | $1s7h\ ^3H^0_6$ | -0.27763 | -0.27763 | 0.0000002 | -0.0000009 |
| 7 | 5 | 0.500000 | 6.99999 | $1s7h\ ^3H^0_4$ | -0.27763 | -0.27763 | 0.0000002 | -0.0000009 |
| 7 | 5 | 0.500000 | 7.00000 | $1s7h\ ^1H^0$ | -0.27763 | -0.27763 | 0.0000006 | -0.0000021 |
| 7 | 6 | 0.500000 | 7.00000 | $1s7\ i^3I_5$ | -0.27763 | -0.27762 | -0.0000094 | 0.0000339 |
| 7 | 6 | 0.500000 | 7.00000 | $1s7i\ ^3I_6$ | -0.27763 | -0.27762 | -0.0000094 | 0.0000339 |
| 7 | 6 | 0.500000 | 7.00000 | $1s7i\ ^3I_7$ | -0.27763 | -0.27762 | -0.0000094 | 0.0000339 |
| 7 | 6 | 0.500000 | 7.00000 | $1s7i\ ^1I$ | -0.27763 | -0.27762 | -0.0000094 | 0.0000338 |
| 7 | 1 | 0.500000 | 7.01873 | $1s7p\ ^1P^0$ | -0.27689 | -0.27667 | -0.0002186 | 0.0007900 |
| 8 | 0 | 0.500011 | 7.42265 | $1s8s\ ^3S$ | -0.22909 | -0.22928 | 0.0001866 | -0.0008139 |
| 8 | 0 | 0.500005 | 7.71132 | $1s8s\ ^1S$ | -0.22052 | -0.2202 | -0.0003172 | 0.0014407 |
| 9 | 0 | 0.500007 | 8.42265 | $1s9s\ ^3S$ | -0.17946 | -0.17961 | 0.0001489 | -0.0008291 |
| 9 | 0 | 0.500003 | 8.71132 | $1s9s\ ^1S$ | -0.17351 | -0.1733 | -0.0002141 | 0.0012355 |

| $n$ | $\ell$ | $r_1$ ($a_{He}$) [a] | $r_2$ ($a_{He}$) [b] | **Term Symbol** | $E_{ele}$ CP He I EnergyLevels [c] ($eV$) | NIST He I Energy Levels [d] ($eV$) | Difference CP-NIST ($eV$) | Relative Difference [e] (CP-NIST) |
|---|---|---|---|---|---|---|---|---|
| 10 | 0 | 0.500004 | 9.42265 | 1s10s $^3$S | -0.14437 | -0.1445 | 0.0001262 | -0.0008732 |
| 10 | 0 | 0.500002 | 9.71132 | 1s10s $^1$S | -0.14008 | -0.13992 | -0.0001622 | 0.0011594 |
| 11 | 0 | 0.500003 | 10.42265 | 1s11s $^3$S | -0.11866 | -0.11876 | 0.0001037 | -0.0008734 |
| 11 | 0 | 0.500001 | 10.71132 | 1s11s $^1$S | -0.11546 | -0.11534 | -0.0001184 | 0.0010268 |
| | | | | | | **Avg.** | **-0.000112** | **0.0000386** |

[a] Radius of the inner electron 1 of singlet excited states with $\ell = 0$ from Eq. (9.29); triplet excited states with $\ell = 0$ from Eq. (9.37); singlet excited states with $\ell \neq 0$ from Eq. (9.60) for $\ell = 1$ or $\ell = 2$ and Eq. (9.61) for $\ell = 3$, and Eq. (9.62) for $\ell = 4, 5, 6...$; triplet excited states with $\ell \neq 0$ from Eq. (9.69), and 1s$^2$ $^1$S from Eq. (7.35).

[b] Radius of the outer electron 2 of singlet excited states with $\ell = 0$ from Eq. (9.11); triplet excited states with $\ell = 0$ from Eq. (9.32); singlet excited states with $\ell \neq 0$ from Eq. (9.53); triplet excited states with $\ell \neq 0$ from Eq. (9.64), and 1s$^2$ $^1$S from Eq. (7.35).

[c] Classical physics (CP) calculated excited-state energy levels given by the electric energy (Eq. (9.12)) and the energy level of 1s$^2$ $^1$S is given by Eqs. (7.44-7.46).

[d] Experimental NIST levels [7] with the ionization potential defined as zero.

[e] (Theoretical-Experimental)/Experimental.

## SPIN-ORBIT COUPLING OF EXCITED STATES WITH $\ell \neq 0$

The energy of the $2P$ level is split by a relativistic interaction between the spin and orbital angular momentum as well as the corresponding radiation reaction force. The corresponding energy $\Delta E_{total}^{H\ FS}$ and frequency $\Delta f_{total}^{H\ FS}$ for the transition $^2P_{1/2} \rightarrow {}^2P_{3/2}$ is known as the hydrogen fine structure and is given by the sum of the spin-orbital coupling energy (Eq. (2.194)):

$$E_{s/o} = \frac{\alpha^5 (2\pi)^2}{8} m_e c^2 \sqrt{\frac{3}{4}} = 7.24043\ X\ 10^{-24}\ J \tag{9.70}$$

and the radiation reaction force that shifts the H radius from $r_0 = 2a_H$ to:

$$r = 2a_H - (2\pi\alpha)^3 \frac{\hbar}{6m_e c} \sqrt{\frac{3}{4}} = 1.99999990 a_H \tag{9.71}$$

given by Eqs. (2.198-2.199). The radiation reaction energy of the hydrogen fine structure $\Delta E_{RRtotal}^{H\ FS}$ is given as the sum of the electric and magnetic energy changes (Eqs. (2.200-2.202)):

$$\begin{aligned} \Delta E_{RRtotal}^{H\ FS} &= \frac{-0.5e^2}{8\pi\varepsilon_0}\left[\frac{1}{r_0} - \frac{1}{r_-}\right] + 4\pi\mu_0\mu_B^2\left(\frac{1}{r_0^3} - \frac{1}{r_-^3}\right) = 2.76347\ X\ 10^{-26}\ J - 1.74098\ X\ 10^{-28}\ J \\ &= 2.74606\ X\ 10^{-26}\ J \end{aligned} \tag{9.72}$$

Then, the total energy of the hydrogen fine structure $\Delta E_{total}^{H\ FS}$ is given by the sum (Eq. (2.204)):

$$\Delta E_{total}^{H\ FS} = E_{s/o} + \Delta E_{RRtotal}^{H\ FS} = 7.24043\ X\ 10^{-24}\ J + 2.74606\ X\ 10^{-26}\ J = 7.26789\ X\ 10^{-24}\ J \tag{9.73}$$

The fine structure energy expressed in terms of frequency (Eq. (2.205)) is

$$\Delta f_{total}^{H\ FS} = 10{,}968.46\ MHz \tag{9.74}$$

The experimental hydrogen fine structure (Eq. (2.206)) is:

$$\Delta f_{total}^{H\ FS}(\text{experimental}) = 10{,}969.05\ MHz \tag{9.75}$$

Given the large natural linewidth of the $2P$ state, the 0.005% relative difference is within the measurement error and propagated errors in the fundamental constants of the equations. Using $r_2$ given by Eq. (9.53), the spin-orbital energies were calculated for $\ell = 1$ using Eq. (9.70) to compare to the effect of different $\ell$ quantum numbers. There is agreement between the magnitude of the predicted results given in Table 9.6 and the experimental dependence on the $\ell$ quantum number as given in Table 9.5.

**Table 9.6.** Calculated spin-orbital energies of He I singlet excited states with $\ell = 1$ as a function of the radius of the outer electron.

| $n$ | $r_2$ $(a_{He})$ [a] | Term Symbol | $E_{s/o}$ spin-orbit coupling [b] $(eV)$ |
|---|---|---|---|
| 2 | 2.01873 | $1s2p\ ^1P^0$ | 0.0000439 |
| 3 | 3.01873 | $1s3p\ ^1P^0$ | 0.0000131 |
| 4 | 4.01873 | $1s4p\ ^1P^0$ | 0.0000056 |
| 5 | 5.01873 | $1s5p\ ^1P^0$ | 0.0000029 |
| 6 | 6.01873 | $1s6p\ ^1P^0$ | 0.0000017 |
| 7 | 7.01873 | $1s7p\ ^1P^0$ | 0.0000010 |

[a] Radius of the outer electron 2 from Eq. (9.53).

[b] The spin-orbit coupling energy of electron 2 from Eq. (9.70) using $r_2$ from Eq. (9.53).

# REFERENCES


1. F. Bueche, *Introduction to Physics for Scientists and Engineers*, McGraw-Hill, (1975), pp. 352-353.
2. J. D. Jackson, *Classical Electrodynamics*, Second Edition, John Wiley & Sons, New York, (1975), pp. 739-779.
3. M. Mizushima, *Quantum Mechanics of Atomic Spectra and Atomic Structure*, W.A. Benjamin, Inc., New York, (1970), p.17.
4. J. D. Jackson, *Classical Electrodynamics*, Second Edition, John Wiley & Sons, New York, (1975), pp. 747-752.
5. J. D. Jackson, *Classical Electrodynamics*, Second Edition, John Wiley & Sons, New York, (1975), pp. 503-561.
6. M. W. Nansteel, personal communication, cube root formulas using the method given in CRC Standard Mathematical Tables, 15th Ed., (1967), p.85, and also Abramowitz and Stegun, Handbook of Mathematical Functions, 9th printing, (1972), p.17, November, (2018).
7. NIST Atomic Spectra Database, www.physics.nist.gov/cgi-bin/AtData/display.ksh.
8. J. D. Jackson, *Classical Electrodynamics*, Second Edition, John Wiley & Sons, New York, (1975), pp. 739-779.
9. J. D. Jackson, *Classical Electrodynamics*, Second Edition, John Wiley & Sons, New York, (1975), p. 759.
10. J. D. Jackson, *Classical Electrodynamics*, Second Edition, John Wiley & Sons, New York, (1975), pp. 236-240, 601-608, 786-790.

# Chapter 10

# THREE- THROUGH TWENTY-ELECTRON ATOMS

Three- through twenty-electron atoms are solved in this section with supporting material on the magnetic forces given in the Two-Electron Atoms section and Appendix VI. The charge-density functions of one- through twenty-electron atoms and their corresponding positive ions are shown in Figures 10.1 and 10.2, respectively. The electrons of multielectron atoms and ions exist as concentric atomic orbitals ("bubble-like" charge-density functions) of discrete radii that are given by $r_n$ of the radial Dirac delta function, $\delta(r-r_n)$ as shown by the exemplary sectional view of the potassium atom in Figure 10.3.

## THREE-ELECTRON ATOMS

As is the case for one and two-electron atoms shown in the corresponding sections, three through ten-electron atoms can also be solved exactly using the results of the solutions of the preceding atoms. For example, three-electron atoms can be solved exactly using the results of the solutions of the one and two-electron atoms.

## THE LITHIUM ATOM

For $Li^+$, there are two spin-paired electrons in an atomic orbital with:

$$r_1 = r_2 = a_0\left[\frac{1}{2} - \frac{\sqrt{\frac{3}{4}}}{6}\right] \tag{10.1}$$

as given by Eq. (7.35) where $r_n$ is the radius of electron $n$ which has velocity $v_n$. The next electron is added to a new atomic orbital because of the repulsive diamagnetic force between the two spin-paired electrons and the spin-unpaired electron. This repulsive diamagnetic force is due to the interaction of the magnetic field of the outer spin-unpaired electron on the electron current of the two spin-paired electrons of the inner shell. The diamagnetic force on the outer electron is determined by first considering the central force on each electron of the inner shell due to the magnetic flux $B$ of the outer electron that follows from Purcell [1]:

$$\mathbf{F} = \frac{2m_e v_n \Delta v}{r}\mathbf{i}_\mathbf{r} \tag{10.2}$$

where $\mathbf{i}_\mathbf{r}$ is defined as the radial vector in the direction of the central electric field of the nucleus and

$$\frac{\Delta v}{r} = \frac{eB}{2m_e} \tag{10.3}$$

**Figure 10.1.** Charge-Density Functions Shown in Color Scale of One- Through Twenty-Electron Atoms. The electrons of multielectron atoms exist as concentric atomic orbitals (" bubble-like" charge-density functions) of discrete radii, which are given by $r_n$ of the radial Dirac delta function, $\delta(r - r_n)$. The electron configuration for one through twenty-electron atoms that achieves an energy minimum is: $1s < 2s < 2p < 3s < 3p < 4s$ wherein each s orbital is a constant current-density function which gives rise to spin, and the charge-density of each p orbital is a superposition of a constant and a spherical and time harmonic function. The corresponding charge-density wave on the surface gives rise to electron orbital angular momentum that superimposes the spin angular momentum. To achieve an energy minimum, electrons of an atom with the same principal and $\ell$ quantum numbers align parallel until each of the $m_\ell$ levels are occupied, and then pairing occurs until each of the $m_\ell$ levels contain paired electrons.

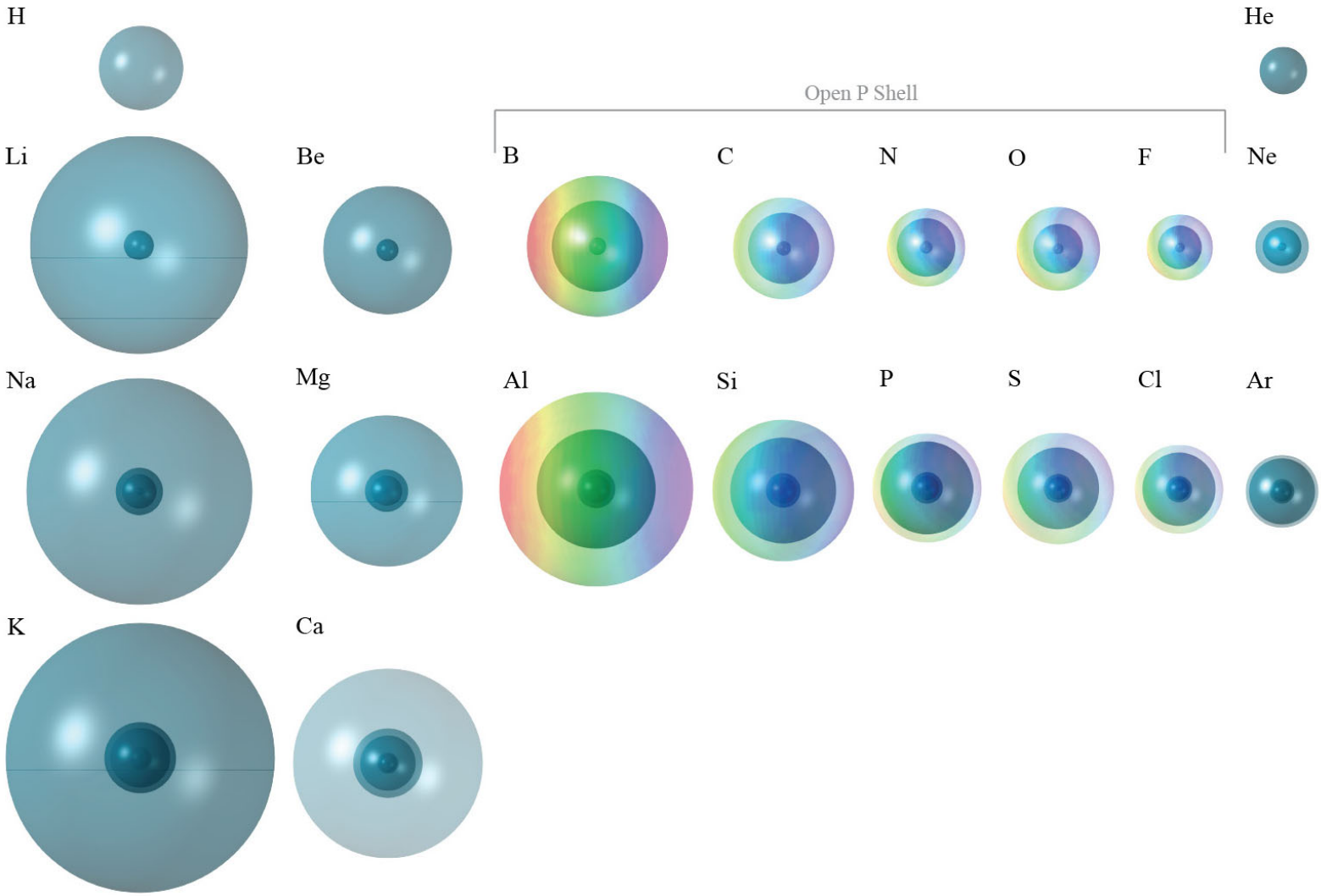


**Figure 10.2.** Charge-Density Functions Shown in Color Scale of One- Through Twenty-Electron-Plus-One Ions. The electrons of multielectron ions also exist as concentric atomic orbitals (" bubble-like" charge-density functions) of discrete radii which are given by $r_n$ of the radial Dirac delta function, $\delta(r - r_n)$, and the electron configuration follows the same principles as that for one through twenty-electron atoms: 1s < 2s < 2p < 3s < 3p < 4s wherein electrons of an ion with the same principal and $\ell$ quantum numbers align parallel until each of the $m_\ell$ levels are occupied, and then pairing occurs until each of the $m_\ell$ levels contain paired electrons.

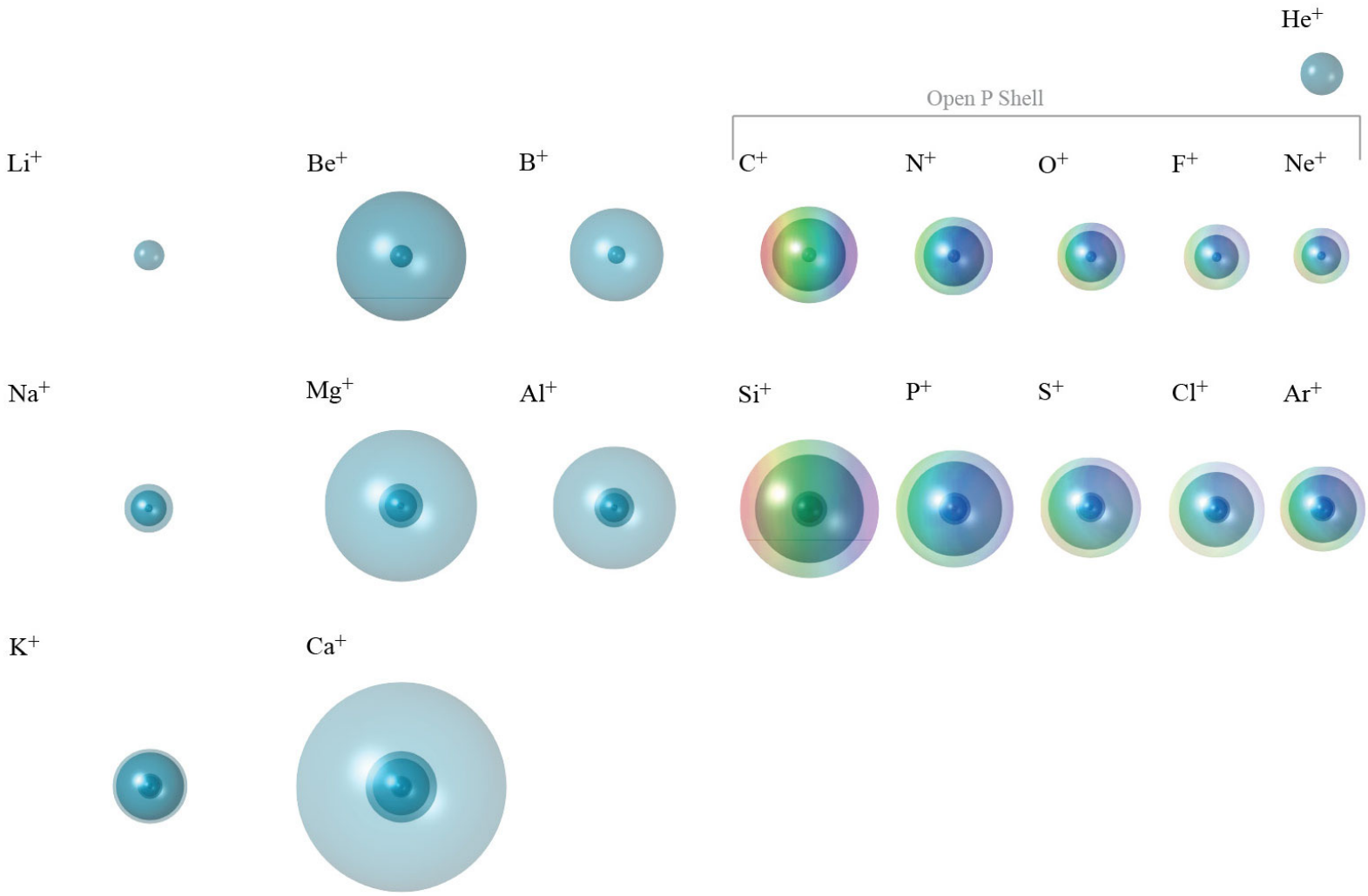
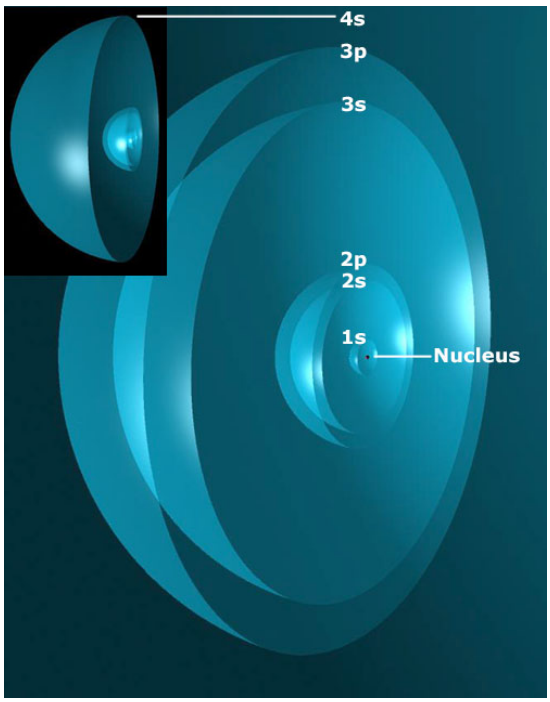


**Figure 10.3.** A sectional view of the potassium atom showing the radii of the paired 1s, paired 2s, three sets of paired 2p, paired 3s, and three sets of paired 3p inner electrons and the unpaired 4s outer electron.




The velocity $v_n$ is given by the boundary condition for no radiation as follows:

$$v_1 = \frac{\hbar}{m_e r_1} \tag{10.4}$$

where $r_1$ is the radius of the first atomic orbital; therefore, the force on each of the inner electrons is given as follows:

$$\mathbf{F} = \frac{\hbar e B}{m_e r_1}\mathbf{i}_\mathbf{r} \tag{10.5}$$

The change in magnetic moment, $\Delta m$, of each electron of the inner shell due to the magnetic flux $B$ of the outer electron is [1]:

$$\Delta m = -\frac{e^2 r_1^2 B}{4m_e} \tag{10.6}$$

The diamagnetic force on the outer electron due to the two inner shell electrons is in the opposite direction of the force given by Eq. (10.5), and this diamagnetic force on the outer electron is proportional to the sum of the changes in magnetic moments of the two inner electrons due to the magnetic flux $B$ of the outer electron. The two electrons are spin-paired and the velocities are mirror opposites. Thus, the change in velocity of each electron treated individually (Eq. (10.3)) due to the magnetic flux $B$ would be equal and opposite. However, the two paired electrons may be treated as one with twice the mass where $m_e$ is replaced by $2m_e$ in Eq. (10.6). In this case, the paired electrons spin together about the field axis to cause a reduction in the flux according to Lenz's law. It is then apparent that the force given by Eq. (10.5) is proportional to the flux $B$ of the outer electron; whereas, the total of the change in magnetic moments of the inner shell electrons given by Eq. (10.6) applied to the combination of the inner electrons is proportional to one eighth of the flux, $B$. Thus, the force on the outer electron due to the reaction of the inner shell to the flux of the outer electron is given as follows:

$$\mathbf{F}_{diamagnetic} = -\frac{\hbar}{8r_1}\frac{eB}{m_e}\mathbf{i}_\mathbf{r} \tag{10.7}$$

where $r_1$ is the radial distance of the first atomic orbital from the nucleus. The magnetic flux, $B$, is supplied by the constant field inside the atomic orbital of the outer electron at radius $r_3$ and is given by the product of $\mu_0$ times Eq. (1.152).

$$B = \frac{\mu_0 e\hbar}{m_e r_3^3} \tag{10.8}$$

The result of substitution of Eq. (10.8) into Eq. (10.7) is:

$$\mathbf{F}_{diamagnetic} = -\left[\frac{e^2\mu_0}{2m_e r_3}\right]\frac{\hbar^2}{4m_e r_1 r_3^2}\mathbf{i}_\mathbf{r} \tag{10.9}$$

The term in brackets can be expressed in terms of the fine structure constant, $\alpha$. From Eqs. (1.176-1.180)

$$\frac{e^2\mu_0}{2m_e r_3} = 2\pi\alpha\frac{v}{c} \tag{10.10}$$

It is demonstrated in the Two-Electron Atoms section that the relativistic correction to Eq. (10.9) is $\frac{1}{Z}$ times the reciprocal of Eq. (10.10). $Z$ for electron three is one; thus, one is substituted for the term in brackets in Eq. (10.9).

The force must be corrected for the $\sqrt{s(s+1)} = \sqrt{\frac{3}{4}}$ vector projection of the velocity onto the z-axis as given in the Two-Electron Atoms section and Appendix VI. Thus, Eq. (10.9) becomes:

$$\mathbf{F}_{diamagnetic} = -\frac{\hbar^2}{4m_e r_3^2 r_1}\sqrt{s(s+1)}\mathbf{i}_\mathbf{r} \tag{10.11}$$

## THE RADIUS OF THE OUTER ELECTRON OF THE LITHIUM ATOM

The radius for the outer electron is calculated by equating the outward centrifugal force to the sum of the electric and diamagnetic forces as follows:

$$\frac{m_e v_3^2}{r_3} = \frac{e^2}{4\pi\varepsilon_0 r_3^2} - \frac{\hbar^2}{4m_e r_3^2 r_1}\sqrt{s(s+1)} \tag{10.12}$$

With $v_3 = \frac{\hbar}{m_e r_3}$ (Eq. (1.35)), $r_1 = a_0\left[\frac{1}{2} - \frac{\sqrt{\frac{3}{4}}}{6}\right]$ (Eq. (7.35)), and $s = \frac{1}{2}$, we solve for $r_3$.

$$r_3 = \frac{a_0}{\left[1 - \frac{\sqrt{3/4}}{4\left(\frac{1}{2} - \frac{\sqrt{3/4}}{6}\right)}\right]} \tag{10.13}$$

$$r_3 = 2.5559\ a_0$$

## THE IONIZATION ENERGY OF LITHIUM

From Eq. (1.264), the magnitude of the energy stored in the electric field is:

$$\frac{e^2}{8\pi\varepsilon_0 r_3} = 5.318\ eV \tag{10.14}$$

The magnetic field of the outer electron changes the angular velocities of the inner electrons. However, the magnetic field of the outer electron provides a central Lorentz force that exactly balances the change in centrifugal force because of the change in angular velocity [1]. Thus, the electric energy of the inner atomic orbital is unchanged upon ionization. The magnetic field of the outer electron, however, also changes the magnetic moment, $m$, of each of the inner atomic orbital electrons. From Eq. (10.6), the change in magnetic moment, $\Delta m$, (per electron) is:

$$\Delta m = -\frac{e^2 r_1^2}{4m_e}B \tag{10.15}$$

where $B$ is the magnetic flux of the outer electron given by the product of $\mu_o$ times Eq. (1.152).

$$B = \frac{\mu_0 e\hbar}{m_e r_3^3} \tag{10.16}$$

Substitution of Eq. (10.16) and $2m_e$ for $m_e$ (because there are two electrons) into Eq. (10.15) gives:

$$\Delta m = -\left[\frac{e^2\mu_0}{2m_e r_3}\right]\frac{e\hbar r_1^2}{4m_e r_3^2} \tag{10.17}$$

Furthermore, we know from Eqs. (10.9) and (10.11) that the term in brackets is replaced by $\sqrt{s(s+1)}$.

$$\Delta m = -\frac{e\hbar r_1^2}{4m_e r_3^2}\sqrt{s(s+1)} \tag{10.18}$$

Substitution of Eq. (10.1) for $r_1$, Eq. (10.13) for $r_3$, and given that the magnetic moment of an electron is one Bohr magneton according to Eq. (1.131),

$$\mu_B = \frac{e\hbar}{2m_e} \tag{10.19}$$

the fractional change in magnetic moment of an inner shell electron, $\Delta m_f$, is given as follows:

$$\Delta m_f = \frac{\dfrac{e\hbar r_1^2\sqrt{s(s+1)}}{4m_e r_3^2}}{\dfrac{e\hbar}{2m_e}} \tag{10.20}$$

$$= \frac{1}{2}\frac{r_1^2}{r_3^2}\sqrt{s(s+1)} \tag{10.21}$$

With $r_1$ given by Eq. (10.1), $r_3$ given by Eq. (10.13), and $s = \frac{1}{2}$, the fractional change in magnetic moment of the two inner shell electrons is:

$$\Delta m_f = \frac{\left(a_0\left[\frac{1}{2} - \frac{\sqrt{\frac{3}{4}}}{6}\right]\right)^2\sqrt{\frac{3}{4}}}{\left(\frac{a_0}{1 - \frac{\sqrt{\frac{3}{4}}}{4\left(\frac{1}{2} - \frac{\sqrt{\frac{3}{4}}}{6}\right)}}\right)^2} \tag{10.22}$$

$$\Delta m_f = 0.016767$$

We add one (corresponding to $m_f$) to $\Delta m_f$ which is the fractional change in the magnetic moment. The energy stored in the magnetic field is proportional to the magnetic field strength squared as given by Eq. (1.144); thus, the sum is squared

$$(1.016767)^2 = 1.033815 \tag{10.23}$$

Thus, the change in magnetic energy of the inner atomic orbital is $3.382\ \%$, so that the corresponding energy $\Delta E_{mag}$ is

$$\Delta E_{mag} = (0.033815)(2.543\ eV) = 0.08599\ eV \tag{10.24}$$

where the magnetic energy of the inner electrons given in Table 7.1 is $2.543\ eV$. Then the ionization energy of the lithium atom is given by Eqs. (10.13-10.14) and (10.24):

$$E(ionization;\ Li) = \frac{(Z-2)e^2}{8\pi\varepsilon_0 r_3} + \Delta E_{mag} \tag{10.25}$$

$$= 5.3230\ eV + 0.08599\ eV = 5.4090\ eV$$

The experimental ionization energy of lithium is $5.392\ eV$ [2-3].

## THREE ELECTRON ATOMS WITH A NUCLEAR CHARGE Z>3

Three-electron atoms having $Z > 3$ possess an electric field of:

$$\mathbf{E} = \frac{(Z-3)e}{4\pi\varepsilon_0 r^2}\mathbf{i}_r \tag{10.26}$$

for $r > r_3$. For three-electron atoms having $Z > 3$, the diamagnetic force given by Eq. (10.11) is unchanged. However, for three-electron atoms having $Z > 3$, an electric field exists for $r > r_3$. This electric field gives rise to an additional diamagnetic force term which adds to Eq. (10.11). The additional diamagnetic force is derived as follows. The diamagnetic force repels the third (outer) electron, and the electric force attracts the third electron. Consider the reverse of ionization where the third electron is at infinity and the two spin-paired electrons are at $r_1 = r_2$ given by Eq. (7.35).

Power must be conserved as the net force of the diamagnetic and electric forces cause the third electron to move from infinity to its final radius. Power flow is given by the Poynting Power Theorem:

$$\nabla \bullet (\mathbf{E}\times\mathbf{H}) = -\frac{\partial}{\partial t}\left[\frac{1}{2}\mu_0\mathbf{H}\bullet\mathbf{H}\right] - \frac{\partial}{\partial t}\left[\frac{1}{2}\varepsilon_0\mathbf{E}\bullet\mathbf{E}\right] - \mathbf{J}\bullet\mathbf{E} \tag{10.27}$$

During binding, the radius of electron three decreases. The electric force where:

$$\mathbf{F}_{ele} = \frac{(Z-2)e^2}{4\pi\varepsilon_0 r_3^2}\mathbf{i}_r \tag{10.28}$$

increases the stored electric energy which corresponds to the power term, $-\frac{\partial}{\partial t}\left[\frac{1}{2}\varepsilon_0\mathbf{E}\bullet\mathbf{E}\right]$, of Eq. (10.27). The diamagnetic

force given by Eq. (10.7) changes the stored magnetic energy which corresponds to the power term, $-\frac{\partial}{\partial t}\left[\frac{1}{2}\mu_0 \mathbf{H} \bullet \mathbf{H}\right]$, of Eq. (10.27). An additional diamagnetic force arises when $Z-3>0$. This diamagnetic force corresponds to that given by Purcell [1] for a charge moving in a central field having an imposed magnetic field perpendicular to the plane of motion. The second diamagnetic force $\mathbf{F}_{diamagnetic\ 2}$ is given by

$$\mathbf{F}_{diamagnetic\ 2} = -2\frac{m_e \Delta v^2}{r_1}\mathbf{i}_\mathbf{r} \tag{10.29}$$

where $\Delta v$ is derived from Eq. (10.3). The result of substitution of $\Delta v$ into Eq. (10.29) is:

$$\mathbf{F}_{diamagnetic\ 2} = -\frac{2m_e}{r_1}\left[\frac{er_1 B}{2m_e}\right]^2 \mathbf{i}_\mathbf{r} \tag{10.30}$$

The magnetic flux, $B$, at electron three for $r < r_3$ is given by the product of $\mu_o$ times Eq. (1.152). The result of the substitution of the flux into Eq. (10.30) is:

$$\mathbf{F}_{diamagnetic\ 2} = -2\left[\frac{e^2\mu_0}{2m_e r_3}\right]^2 \frac{r_1\hbar^2}{m_e r_3^4}\mathbf{i}_\mathbf{r} \tag{10.31}$$

The term in brackets can be expressed in terms of the fine structure constant, $\alpha$. From Eqs. (1.176-1.181)

$$\frac{Z_1 e^2 \mu_0}{2m_e r_3} = 2\pi\alpha Z_1 \frac{v}{c} \tag{10.32}$$

It is demonstrated in the Two-Electron Atoms section that the relativistic correction to Eq. (10.31) is $\frac{1}{Z}$ times the reciprocal of Eq. (10.32). Consider the case wherein $Z_1$ of Eq. (10.32) is different from $Z = Z_2$ of Eq. (7.22) in order to maintain relativistic invariance of the electron angular momentum and magnetic moment. The relativistic correction to Eq. (10.31) can be considered the product of two corrections—a correction of electron three relative to electron one and two, and electron one and two relative to electron three. In the former case, $Z_1$ and $Z_2 = 1$ which corresponds to electron three. In the latter case, $Z_1 = Z-3$, and $Z_2 = Z-2$ which corresponds to $r_3^+$, infinitesimally greater than the radius of the outer atomic orbital and $r_3^-$, infinitesimally less than the radius of the outer atomic orbital, respectively, where $Z$ is the nuclear charge. Thus, $\frac{Z-3}{Z-2}$ is substituted for the term in brackets in Eq. (10.31). The force must be corrected for the $\sqrt{s(s+1)} = \sqrt{\frac{3}{4}}$ vector projection of the velocity onto the z-axis as given in the Two-Electron Atoms section and Appendix VI. Thus, Eq. (10.31) becomes:

$$\mathbf{F}_{diamagnetic\ 2} = -2\frac{(Z-3)r_1\hbar^2}{(Z-2)m_e r_3^4}\sqrt{s(s+1)}\mathbf{i}_\mathbf{r} \tag{10.33}$$

As given previously in the Two Electron section, this force corresponds to the dissipation term of Eq. (10.27), $\mathbf{J} \bullet \mathbf{E}$. The current $\mathbf{J}$ is proportional to the sum of one for the outer electron and two times two—the number of spin-paired electrons. For the inner electrons, the factor of two arises because they possess mutual inductance which doubles their contribution to $\mathbf{J}$. (Recall the general relationship that the current is equal to the flux divided by the inductance.) Thus, the second diamagnetic force is:

$$\mathbf{F}_{diamagnetic\ 2} = -2\left[\frac{Z-3}{Z-2}\right]\frac{(1+4)r_1\hbar^2}{m_e r_3^4}\sqrt{s(s+1)}\mathbf{i}_\mathbf{r};\quad s=\frac{1}{2} \tag{10.34}$$

$$\mathbf{F}_{diamagnetic\ 2} = -\left[\frac{Z-3}{Z-2}\right]\frac{r_1\hbar^2}{m_e r_3^4}10\sqrt{3/4}\mathbf{i}_\mathbf{r} \tag{10.35}$$

## THE RADIUS OF THE OUTER ELECTRON OF THREE-ELECTRON ATOMS WITH A NUCLEAR CHARGE Z>3

The radius of the outer electron is calculated by equating the outward centrifugal force to the sum of the electric and diamagnetic forces as follows:

$$\frac{m_e v_3^2}{r_3} = \frac{(Z-2)e^2}{4\pi\varepsilon_0 r_3^2} - \frac{\hbar^2}{4m_e r_3^2 r_1}\sqrt{s(s+1)} - \left[\frac{Z-3}{Z-2}\right]\frac{r_1\hbar^2}{r_3^4 m_e}10\sqrt{s(s+1)} \tag{10.36}$$

With $v_3 = \frac{\hbar}{m_e r_3}$ (Eq. (1.35)), $r_1 = a_0\left(\frac{1}{Z-1} - \frac{\sqrt{s(s+1)}}{Z(Z-1)}\right)$ (Eq. (7.35), and $s = \frac{1}{2}$, we solve for $r_3$ using the quadratic formula or reiteratively.

$$r_3 = \frac{\left[1+\left[\frac{Z-3}{Z-2}\right]\frac{r_1}{r_3}10\sqrt{\frac{3}{4}}\right]}{\left[\frac{(Z-2)}{a_0} - \frac{\sqrt{\frac{3}{4}}}{4r_1}\right]} \tag{10.37}$$

The quadratic equation corresponding to Eq. (10.37) is:

$$r_3^2 - \frac{r_3}{\left[\frac{(Z-2)}{a_0} - \frac{\sqrt{\frac{3}{4}}}{4r_1}\right]} - \frac{\left[\frac{Z-3}{Z-2}\right]r_1 10\sqrt{\frac{3}{4}}}{\left[\frac{(Z-2)}{a_0} - \frac{\sqrt{\frac{3}{4}}}{4r_1}\right]} = 0 \tag{10.38}$$

The solution of Eq. (10.38) using the quadratic formula is:

$$r_3 = \frac{\frac{a_0}{\left[(Z-2) - \frac{\sqrt{\frac{3}{4}}}{4r_1}\right]} \pm a_0\sqrt{\frac{1}{\left[(Z-2) - \frac{\sqrt{\frac{3}{4}}}{4r_1}\right]^2} + 4\frac{\left[\frac{Z-3}{Z-2}\right]r_1 10\sqrt{\frac{3}{4}}}{\left[(Z-2) - \frac{\sqrt{\frac{3}{4}}}{4r_1}\right]}}}{2}, \quad r_1 \text{ in units of } a_0 \tag{10.39}$$

$$r_3 = \frac{\frac{a_0}{\left[(Z-2) - \frac{\sqrt{3/4}}{4r_1}\right]}\left[1 \pm \sqrt{1+4\left[\frac{Z-3}{Z-2}\right]r_1 10\sqrt{\frac{3}{4}}\left[(Z-2) - \frac{\sqrt{\frac{3}{4}}}{4r_1}\right]}\right]}{2}, \quad r_1 \text{ in units of } a_0 \tag{10.40}$$

$$r_3 = \frac{\frac{a_o}{\left[(Z-2) - \frac{\sqrt{3/4}}{4r_1}\right]}\left[1 \pm \sqrt{1+4(Z-3)r_1 10\sqrt{\frac{3}{4}} - \left[\frac{Z-3}{Z-2}\right]\frac{30}{4}}\right]}{2}, \quad r_1 \text{ in units of } a_0 \tag{10.41}$$

$$r_3 = \frac{\frac{a_0}{\left[(Z-2) - \frac{\sqrt{3/4}}{4\left(\frac{1}{Z-1} - \frac{\sqrt{3/4}}{Z(Z-1)}\right)}\right]}\left[1 \pm \sqrt{1+4(Z-3)\left(\frac{1}{Z-1} - \frac{\sqrt{3/4}}{Z(Z-1)}\right)10\sqrt{\frac{3}{4}} - \left[\frac{Z-3}{Z-2}\right]\frac{30}{4}}\right]}{2} \tag{10.42}$$

The positive root of Eq. (10.42) must be taken in order that $r_3 > 0$.

## THE IONIZATION ENERGIES OF THREE-ELECTRON ATOMS WITH A NUCLEAR CHARGE Z>3

The energy stored in the electric field, $E(electric)$, is:

$$E(electric) = -\frac{(Z-2)e^2}{8\pi\varepsilon_0 r_3} \tag{10.43}$$

where $r_3$ is given by Eq. (10.42). The magnetic field of the outer electron changes the velocities of the inner electrons. However, the magnetic field of the outer electron provides a central Lorentz field which balances the change in centrifugal force because of the change in velocity. Thus, the electric energy of the inner atomic orbital is unchanged upon ionization. The change in the velocities of the inner electrons upon ionization gives rise to a change in kinetic energies of the inner electrons. The change in velocity, $\Delta v$, is given by Eq. (10.3)

$$\Delta v = \frac{er_1 B}{2m_e} \tag{10.44}$$

Substitution of the flux, $B$, given by the product of $\mu_0$ and Eq. (1.152), into Eq. (10.44) is:

$$\Delta v = \left[\frac{e^2\mu_0}{2m_e r_1}\right]\frac{r_1^2\hbar}{m_e r_3^3} \tag{10.45}$$

It is demonstrated in the One-Electron Atom section and the Two-Electrons Atom section (at Eq. (7.23)) that the relativistic correction to Eq. (10.45) is $\frac{1}{Z}$ times the reciprocal of the term in brackets. In this case, $Z$ corresponding to electron three is one; thus, one is substituted for the term in brackets in Eq. (10.45). Thus, Eq. (10.45) becomes,

$$\Delta v = \frac{r_1^2\hbar}{r_3^3 m_e} \tag{10.46}$$

wherein $r_1$ given by Eq. (7.35), and $r_3$ is given by Eq. (10.42). The change in kinetic energy, $\Delta E_T$, of the two inner shell electrons is given by:

$$\Delta E_T = 2\frac{1}{2}m_e\Delta v^2 \tag{10.47}$$

The ionization energy is the sum of the electric energy, Eq. (10.43), and the change in the kinetic energy, Eq. (10.47), of the inner electrons.

$$E(Ionization) = E(Electric) + E_T \tag{10.48}$$

The relativistic correction to Eq. (10.48) is given by (1) relativistically correcting the radius of the inner paired electrons $r_1$, (2) using the relativistically corrected $r_1$ to determine $r_3$ which is then relativistically corrected. The relativistically corrected $r_1$ is given by dividing the radius given Eq. (7.35) by $\gamma^*$ of Eq. (1.281)

$$r_2 = r_1 = \frac{r_1'}{\gamma^*} = \frac{a_0\left(\frac{1}{Z-1} - \frac{\sqrt{s(s+1)}}{Z(Z-1)}\right)}{2\pi}\Bigg/\frac{2\pi\sqrt{1-\left(\frac{v}{c}\right)^2}\sin\left[\frac{\pi}{2}\left(1-\left(\frac{v}{c}\right)^2\right)^{3/2}\right] + \cos\left[\frac{\pi}{2}\left(1-\left(\frac{v}{c}\right)^2\right)^{3/2}\right]}{2\pi}, \; s = \frac{1}{2} \tag{10.49}$$

where the velocity is given by Eq. (1.35) with the radius given by Eq. (7.35). Similarly, the relativistically corrected $r_3$ is given by dividing the radius given Eq. (10.41) by $\gamma^*$ of Eq. (1.281)

$$r_3 = \frac{r_3'}{\gamma^*} = \frac{\frac{a_0}{\left[(Z-2) - \frac{\sqrt{3/4}}{4r_1}\right]}\left[1+\sqrt{1+4(Z-3)r_1 10\sqrt{\frac{3}{4}} - \left[\frac{Z-3}{Z-2}\right]\frac{30}{4}}\right]}{\frac{2}{2\pi}}\Bigg/\frac{2\pi\sqrt{1-\left(\frac{v}{c}\right)^2}\sin\left[\frac{\pi}{2}\left(1-\left(\frac{v}{c}\right)^2\right)^{3/2}\right] + \cos\left[\frac{\pi}{2}\left(1-\left(\frac{v}{c}\right)^2\right)^{3/2}\right]}{2\pi}, \; r_1 \text{ in units of } a_0 \tag{10.50}$$

where $r_1$ is given by Eq. (10.49) and the velocity is given by Eq. (1.35) with the radius given by Eq. (10.42). The ionization energies are given by Eq. (10.48) wherein the relativistically corrected radii given by Eqs. (10.49-10.50) are used in the sum of the electric energy, Eq. (10.43), and the change in the kinetic energy, Eq. (10.47), of the inner electrons. The ionization energies for several three-electron atoms are given in Table 10.1.

**Table 10.1.** Ionization energies for some three-electron atoms.

| 3 e Atom | Z | $r_1$ $(a_0)$ [a] | $r_3$ $(a_0)$ [b] | Electric Energy [c] $(eV)$ | $\Delta v$ [d] (m/s) | $\Delta E_T$ [e] $(eV)$ | Theoretical Ionization Energies [f] $(eV)$ | Experimental Ionization Energies [g] $(eV)$ | Relative Error [h] |
|---|---|---|---|---|---|---|---|---|---|
| $Li$ | 3 | 0.35566 | 2.55606 | 5.3230 | 1.6571E+04 | 1.5613E-03 | 5.40390 | 5.39172 | -0.00226 |
| $Be^{+}$ | 4 | 0.26116 | 1.49849 | 18.1594 | 4.4346E+04 | 1.1181E-02 | 18.1706 | 18.21116 | 0.00223 |
| $B^{2+}$ | 5 | 0.20670 | 1.07873 | 37.8383 | 7.4460E+04 | 3.1523E-02 | 37.8701 | 37.93064 | 0.00160 |
| $C^{3+}$ | 6 | 0.17113 | 0.84603 | 64.3278 | 1.0580E+05 | 6.3646E-02 | 64.3921 | 64.4939 | 0.00158 |
| $N^{4+}$ | 7 | 0.14605 | 0.69697 | 97.6067 | 1.3782E+05 | 1.0800E-01 | 97.7160 | 97.8902 | 0.00178 |
| $O^{5+}$ | 8 | 0.12739 | 0.59299 | 137.6655 | 1.7026E+05 | 1.6483E-01 | 137.8330 | 138.1197 | 0.00208 |
| $F^{6+}$ | 9 | 0.11297 | 0.51621 | 184.5001 | 2.0298E+05 | 2.3425E-01 | 184.7390 | 185.186 | 0.00241 |
| $Ne^{7+}$ | 10 | 0.10149 | 0.45713 | 238.1085 | 2.3589E+05 | 3.1636E-01 | 238.4325 | 239.0989 | 0.00279 |
| $Na^{8+}$ | 11 | 0.09213 | 0.41024 | 298.4906 | 2.6894E+05 | 4.1123E-01 | 298.9137 | 299.864 | 0.00317 |
| $Mg^{9+}$ | 12 | 0.08435 | 0.37210 | 365.6469 | 3.0210E+05 | 5.1890E-01 | 366.1836 | 367.5 | 0.00358 |
| $Al^{10+}$ | 13 | 0.07778 | 0.34047 | 439.5790 | 3.3535E+05 | 6.3942E-01 | 440.2439 | 442 | 0.00397 |
| $Si^{11+}$ | 14 | 0.07216 | 0.31381 | 520.2888 | 3.6868E+05 | 7.7284E-01 | 521.0973 | 523.42 | 0.00444 |
| $P^{12+}$ | 15 | 0.06730 | 0.29102 | 607.7792 | 4.0208E+05 | 9.1919E-01 | 608.7469 | 611.74 | 0.00489 |
| $S^{13+}$ | 16 | 0.06306 | 0.27132 | 702.0535 | 4.3554E+05 | 1.0785E+00 | 703.1966 | 707.01 | 0.00539 |
| $Cl^{14+}$ | 17 | 0.05932 | 0.25412 | 803.1158 | 4.6905E+05 | 1.2509E+00 | 804.4511 | 809.4 | 0.00611 |
| $Ar^{15+}$ | 18 | 0.05599 | 0.23897 | 910.9708 | 5.0262E+05 | 1.4364E+00 | 912.5157 | 918.03 | 0.00601 |
| $K^{16+}$ | 19 | 0.05302 | 0.22552 | 1025.6241 | 5.3625E+05 | 1.6350E+00 | 1027.3967 | 1033.4 | 0.00581 |
| $Ca^{17+}$ | 20 | 0.05035 | 0.21350 | 1147.0819 | 5.6993E+05 | 1.8468E+00 | 1149.1010 | 1157.8 | 0.00751 |
| $Sc^{18+}$ | 21 | 0.04794 | 0.20270 | 1275.3516 | 6.0367E+05 | 2.0720E+00 | 1277.6367 | 1287.97 | 0.00802 |
| $Ti^{19+}$ | 22 | 0.04574 | 0.19293 | 1410.4414 | 6.3748E+05 | 2.3106E+00 | 1413.0129 | 1425.4 | 0.00869 |
| $V^{20+}$ | 23 | 0.04374 | 0.18406 | 1552.3606 | 6.7135E+05 | 2.5626E+00 | 1555.2398 | 1569.6 | 0.00915 |
| $Cr^{21+}$ | 24 | 0.04191 | 0.17596 | 1701.1197 | 7.0530E+05 | 2.8283E+00 | 1704.3288 | 1721.4 | 0.00992 |
| $Mn^{22+}$ | 25 | 0.04022 | 0.16854 | 1856.7301 | 7.3932E+05 | 3.1077E+00 | 1860.2926 | 1879.9 | 0.01043 |
| $Fe^{23+}$ | 26 | 0.03867 | 0.16172 | 2019.2050 | 7.7342E+05 | 3.4011E+00 | 2023.1451 | 2023 | -0.00007 |
| $Co^{24+}$ | 27 | 0.03723 | 0.15542 | 2188.5585 | 8.0762E+05 | 3.7084E+00 | 2192.9020 | 2219 | 0.01176 |
| $Ni^{25+}$ | 28 | 0.03589 | 0.14959 | 2364.8065 | 8.4191E+05 | 4.0300E+00 | 2369.5803 | 2399.2 | 0.01235 |
| $Cu^{26+}$ | 29 | 0.03465 | 0.14418 | 2547.9664 | 8.7630E+05 | 4.3661E+00 | 2553.1987 | 2587.5 | 0.01326 |

[a] Radius of the paired inner electrons of three-electron atoms from Eq. (10.49).

[b] Radius of the unpaired outer electron of three-electron atoms from Eq. (10.50).

[c] Electric energy of the outer electron of three-electron atoms from Eq. (10.43).

[d] Change in the velocity of the paired inner electrons due to the unpaired outer electron of three-electron atoms from Eq. (10.46).

[e] Change in the kinetic energy of the paired inner electrons due to the unpaired outer electron of three-electron atoms from Eq. (10.47).

[f] Calculated ionization energies of three-electron atoms from Eq. (10.48) for $Z > 3$ and Eq. (10.25) for *Li*.

[g] From theoretical calculations, interpolation of isoelectronic and spectral series, and experimental data [2-3].

[h] (Experimental-theoretical)/experimental.

The agreement between the experimental and calculated values of Table 10.1 is well within the experimental capability of the spectroscopic determinations including the values at large Z which relies on X-ray spectroscopy. In this case, the experimental capability is three to four significant figures, which is consistent with the last column. The lithium atom isoelectronic series is given in Table 10.1 [2-3] to much higher precision than the capability of X-ray spectroscopy, but these values are based on theoretical and interpolation techniques rather than data alone. Ionization energies are difficult to determine since the cut-off of the Rydberg series of lines at the ionization energy is often not observed, and the ionization energy must be determined from theoretical calculations, interpolation of Li isoelectronic and Rydberg series, as well as direct experimental data.

The ionization energies of four- through twenty-electron atoms are calculated next using the electric energy at the radius of the force balance between the outward centrifugal force and the sum of the Coulombic force and any magnetic forces to the order $r^{-3}$. The agreement between the experimental and calculated values is excellent, but could even be improved, especially for lower Z ions, by considering higher order magnetic terms involving the interaction between the outer electron and any lower-lying inner shell electrons.

## FOUR-ELECTRON ATOMS

Four-electron atoms can be solved exactly using the results of the solutions of one, two, and three-electron atoms.

## RADII OF THE OUTER ELECTRONS OF FOUR-ELECTRON ATOMS

For each three-electron atom having a central charge of $Z$ times that of the proton, there are two indistinguishable spin-paired electrons in an atomic orbital with radii $r_1$ and $r_2$ both given by Eq. (7.35):

$$r_1 = r_2 = a_0\left[\frac{1}{Z-1} - \frac{\sqrt{\frac{3}{4}}}{Z(Z-1)}\right] \tag{10.51}$$

and an unpaired electron with a radius $r_3$ given by Eq. (10.42). For $Z \geq 4$, the next electron which binds to form the corresponding four-electron atom becomes spin-paired with the outer electron such that they become indistinguishable with the same radius $r_3 = r_4$. The corresponding spin-pairing force $\mathbf{F}_{mag}$ is given by Eq. (7.24):

$$\mathbf{F}_{mag} = \frac{1}{Z}\frac{\hbar^2}{m_e r_4^3}\sqrt{s(s+1)}\mathbf{i}_\mathbf{r} \tag{10.52}$$

The central forces given by Eq. (10.36) and Eq. (10.52) act on the outer electron to cause it to bind wherein the electric force on the outer-most electron due to the nucleus and the inner three electrons is given by Eq. (10.28) with the appropriate charge and radius:

$$\mathbf{F}_{ele} = \frac{(Z-3)e^2}{4\pi\varepsilon_0 r_4^2}\mathbf{i}_\mathbf{r} \tag{10.53}$$

for $r > r_3$.

In addition to the paramagnetic spin-pairing force between the third electron initially at radius $r_3$, the pairing causes the diamagnetic interaction between the outer electrons and the inner electrons given by Eq. (10.11) to vanish, except for an electrodynamic effect for $Z > 4$ described in the Two-Electron Atoms section, since upon pairing the magnetic field of the outer electrons becomes zero. Therefore, the corresponding force $\mathbf{F}_{mag\ 2}$ is in the same direction as the spin-pairing force and is given by substitution of Eq. (7.6) with the radius $r_4$ into Eq. (10.5):

$$\mathbf{F}_{mag\ 2} = \frac{\hbar eB}{2m_e r_1} = \frac{\mu_0 e^2 \hbar^2}{2m_e^2 r_1 r_4^3}\mathbf{i}_\mathbf{r} \tag{10.54}$$

Then, from Eqs. (10.54) and (7.6-7.24), the paramagnetic force is given by:

$$\mathbf{F}_{mag\ 2} = \frac{1}{Z}\frac{\hbar^2}{m_e r_1 r_4^2}\sqrt{s(s+1)}\mathbf{i}_\mathbf{r} \tag{10.55}$$

The outward centrifugal force on electron 4 is balanced by the electric force and the magnetic forces (on electron 4). The radius of the outer electron is calculated by equating the outward centrifugal force to the sum of the electric (Eq. (10.53)), diamagnetic (Eqs. (10.11) and (10.35) for $r_4$), and paramagnetic (Eqs. (10.52) and (10.55)) forces as follows:

$$\frac{m_e v_4^2}{r_4} = \frac{(Z-3)e^2}{4\pi\varepsilon_0 r_4^2} - \frac{\hbar^2}{4m_e r_4^2 r_1}\sqrt{s(s+1)} + \frac{\hbar^2}{Zm_e r_4^2 r_1}\sqrt{s(s+1)} - \left[\frac{Z-3}{Z-2}\right]\frac{r_1\hbar^2}{r_4^4 m_e}10\sqrt{s(s+1)} + \frac{\hbar^2}{Zm_e r_4^3}\sqrt{s(s+1)} \tag{10.56}$$

Substitution of $v_4 = \dfrac{\hbar}{m_e r_4}$ (Eq. (1.35)) and $s = \dfrac{1}{2}$ into Eq. (10.56) gives:

$$\frac{\hbar^2}{m_e r_4^3} = \frac{(Z-3)e^2}{4\pi\varepsilon_0 r_4^2} - \frac{\hbar^2}{4m_e r_4^2 r_1}\sqrt{\frac{3}{4}} + \frac{\hbar^2}{Zm_e r_4^2 r_1}\sqrt{\frac{3}{4}} - \left[\frac{Z-3}{Z-2}\right]\frac{r_1\hbar^2}{r_4^4 m_e}10\sqrt{\frac{3}{4}} + \frac{\hbar^2}{Zm_e r_4^3}\sqrt{\frac{3}{4}} \tag{10.57}$$

$$\left(\frac{(Z-3)e^2}{4\pi\varepsilon_0} - \left(\frac{1}{4}-\frac{1}{Z}\right)\frac{\hbar^2}{m_e r_1}\sqrt{\frac{3}{4}}\right)\frac{1}{r_4^2} - \left[\frac{Z-3}{Z-2}\right]\frac{r_1\hbar^2}{r_4^4 m_e}10\sqrt{\frac{3}{4}} - \frac{\hbar^2}{m_e r_4^3}\left(1 - \frac{\sqrt{\frac{3}{4}}}{Z}\right) = 0 \tag{10.58}$$

The quadratic equation corresponding to Eq. (10.58) is

$$\left(\frac{(Z-3)e^2}{4\pi\varepsilon_0} - \left(\frac{1}{4}-\frac{1}{Z}\right)\frac{\hbar^2}{m_e r_1}\sqrt{\frac{3}{4}}\right)r_4^2 - \frac{\hbar^2}{m_e}\left(1 - \frac{\sqrt{\frac{3}{4}}}{Z}\right)r_4 - \left[\frac{Z-3}{Z-2}\right]\frac{r_1\hbar^2}{m_e}10\sqrt{\frac{3}{4}} = 0 \tag{10.59}$$

$$r_4^2-\frac{\dfrac{\hbar^2}{m_e}\left(1-\dfrac{\sqrt{\frac{3}{4}}}{Z}\right)}{\left(\dfrac{(Z-3)e^2}{4\pi\varepsilon_0}-\left(\dfrac{1}{4}-\dfrac{1}{Z}\right)\dfrac{\hbar^2}{m_e r_1}\sqrt{\frac{3}{4}}\right)}r_4-\frac{\left[\dfrac{Z-3}{Z-2}\right]\dfrac{r_1\hbar^2}{m_e}10\sqrt{\frac{3}{4}}}{\left(\dfrac{(Z-3)e^2}{4\pi\varepsilon_0}-\left(\dfrac{1}{4}-\dfrac{1}{Z}\right)\dfrac{\hbar^2}{m_e r_1}\sqrt{\frac{3}{4}}\right)}=0 \tag{10.60}$$

$$r_4^2-\frac{\left(1-\dfrac{\sqrt{\frac{3}{4}}}{Z}\right)}{\left(\dfrac{(Z-3)}{a_0}-\left(\dfrac{1}{4}-\dfrac{1}{Z}\right)\dfrac{\sqrt{\frac{3}{4}}}{r_1}\right)}r_4-\frac{\left[\dfrac{Z-3}{Z-2}\right]r_1 10\sqrt{\frac{3}{4}}}{\left(\dfrac{(Z-3)}{a_0}-\left(\dfrac{1}{4}-\dfrac{1}{Z}\right)\dfrac{\sqrt{\frac{3}{4}}}{r_1}\right)}=0 \tag{10.61}$$

The solution of Eq. (10.61) using the quadratic formula is:

$$r_4=r_3=\frac{\dfrac{a_0\left(1-\dfrac{\sqrt{\frac{3}{4}}}{Z}\right)}{\left((Z-3)-\left(\dfrac{1}{4}-\dfrac{1}{Z}\right)\dfrac{\sqrt{\frac{3}{4}}}{r_1}\right)}\pm a_0\sqrt{\dfrac{\left(1-\dfrac{\sqrt{\frac{3}{4}}}{Z}\right)^2}{\left((Z-3)-\left(\dfrac{1}{4}-\dfrac{1}{Z}\right)\dfrac{\sqrt{\frac{3}{4}}}{r_1}\right)^2}+4\dfrac{\left[\dfrac{Z-3}{Z-2}\right]r_1 10\sqrt{\frac{3}{4}}}{\left((Z-3)-\left(\dfrac{1}{4}-\dfrac{1}{Z}\right)\dfrac{\sqrt{\frac{3}{4}}}{r_1}\right)}}}{2},\ r_1\ in\ units\ of\ a_0 \tag{10.62}$$

where $r_1$ is given by Eq. (10.51) and also Eq. (7.35). The positive root of Eq. (10.62) must be taken in order that $r_4>0$. The final radius of electron 4, $r_4$, is given by Eq. (10.62); this is also the final radius of electron 3. The radii of several four-electron atoms are given in Table 10.2.

## ENERGIES OF THE BERYLLIUM ATOM

The energy stored in the electric field, $E(electric)$, is given by Eq. (10.43) with the appropriate charge and radius:

$$E(electric)=-\frac{(Z-3)e^2}{8\pi\varepsilon_0 r_4} \tag{10.63}$$

The ionization energy is given by the sum of the electric energy and the diamagnetic and paramagnetic energy terms. The magnetic energy, $E(magnetic)$, for an electron corresponding to a radius $r_n$ given by Eq. (7.46) is:

$$E(magnetic)=\frac{2\pi\mu_0 e^2\hbar^2}{m_e^2 r_n^3} \tag{10.64}$$

Since there is no source of dissipative power, $\mathbf{J}\bullet\mathbf{E}$ of Eq. (10.27), to compensate for any potential change in the magnetic moments, $\Delta m$, of the inner electrons due to the ionization of an outer electron of the beryllium atom, there is a diamagnetic energy term in the ionization energy for this atom that follows from the corresponding term for the lithium atom. This term is given by Eqs. (10.15-10.24) wherein $r_1$ is given by Eq. (10.51) with $Z=4$ and $r_3=r_4$ is given by Eq. (10.62). Thus, the change in magnetic energy of the inner atomic orbital is $5.144\ \%$, so that the corresponding energy $\Delta E_{mag}$ is:

$$\Delta E_{mag}=0.05144\ X\ 6.42291\ eV=0.33040\ eV \tag{10.65}$$

where the magnetic energy of the inner electrons is $6.42291\ eV$. In addition, there is a paramagnetic energy term $E(magnetic)$ corresponding to the ionization of a spin-paired electron from a neutral atom with a closed s-shell. The energy follows from that given for helium by Eqs. (7.44) and (7.46) wherein the electron radius for helium is replaced by the radius $r_4$ of Eq. (10.62). Then, the ionization energy of the beryllium atom is given by Eqs. (7.44), (7.46), (10.25), and (10.62-10.65):

$$E(ionization;\ Be)=\frac{(Z-3)e^2}{8\pi\varepsilon_0 r_4}+\frac{2\pi\mu_0 e^2\hbar^2}{m_e^2 r_4^3}+\Delta E_{mag}=8.9216\ eV+0.03226\ eV+0.33040\ eV=9.28430\ eV \tag{10.66}$$

The experimental ionization energy of beryllium is $9.32263\ eV$ [3].

## THE IONIZATION ENERGIES OF FOUR-ELECTRON ATOMS WITH A NUCLEAR CHARGE Z>4

The ionization energies for the four-electron atoms with $Z > 4$ are given by the sum of the electric energy, $E(electric)$, given by Eq. (10.63) and the magnetic energies. The paramagnetic energy term corresponding to the ionization of a spin-paired electron from an atom with an external electric field is given by Eqs. (7.46) and (7.63) wherein the electron radius for helium is replaced by the radius $r_4$ of Eq. (10.62):

$$Ionization\ Energy = -Electric\ Energy - \frac{1}{Z} Magnetic\ Energy \tag{10.67}$$

Once the outer electrons of four-electron atoms with $Z > 4$ become spin unpaired during ionization, the corresponding magnetic field changes the velocities of the inner electrons in the same manner as shown for the case of the outer electron of three-electron atoms with $Z > 3$. The magnetic effect is calculated for the remaining electron 3 at the radius $r_4$ corresponding to condition of the derivation of Eq. (10.67) that follows from Eqs. (7.46) and (7.63). Thus, change in velocity, $\Delta v$, in the four-electron-atom case is that of three-electron atoms given by Eq. (10.46) wherein the electron radius $r_3$ is replaced by the radius $r_4$ of Eq. (10.62).

Since the velocities of electrons one and two decrease during ionization in the case of four-electron atoms rather than increase as in the case of three-electron atoms, the corresponding kinetic energy decreases and the kinetic energy term given by Eq. (10.47) is the opposite sign in Eq. (10.48). Thus, the ionization energies of four-electron atoms with $Z > 4$ given by Eqs. (10.48) and (10.67) with the electric energy (Eq. (10.63)), the magnetic energy (Eq. (10.64)), and the change in the kinetic energy of the inner electrons (Eq. (10.47)) are

$$E(Ionization) = -Electric\ Energy - \frac{1}{Z} Magnetic\ Energy - E_T \tag{10.68}$$

The ionization energies for several four-electron atoms are given in Table 10.2. Since the radii, $r_4$, are greater than 10% of $a_0$ corresponding to a velocity of less than $1.5 \times 10^7\ m/s$, the relativistic corrections are negligible and are not included in Table 10.2.

**Table 10.2.** Ionization energies for some four-electron atoms.

| 4 e Atom | Z | $r_1$ $(a_0)$ [a] | $r_3$ $(a_0)$ [b] | Electric Energy [c] $(eV)$ | Magnetic Energy [d] $(eV)$ | $\Delta v$ [e] (m/s X $10^{-5}$) | $\Delta E_T$ [f] $(eV)$ | Theoretical Ionization Energies [g] $(eV)$ | Experimental Ionization Energies [h] $(eV)$ | Relative Error [i] |
|---|---|---|---|---|---|---|---|---|---|---|
| $Be$ | 4 | 0.26116 | 1.52503 | 8.9178 | 0.03226 | 0.4207 | 0.0101 | 9.28430 | 9.32263 | 0.0041 |
| $B^{+}$ | 5 | 0.20670 | 1.07930 | 25.2016 | 0.0910 | 0.7434 | 0.0314 | 25.1627 | 25.15484 | -0.0003 |
| $C^{2+}$ | 6 | 0.17113 | 0.84317 | 48.3886 | 0.1909 | 1.0688 | 0.0650 | 48.3125 | 47.8878 | -0.0089 |
| $N^{3+}$ | 7 | 0.14605 | 0.69385 | 78.4029 | 0.3425 | 1.3969 | 0.1109 | 78.2765 | 77.4735 | -0.0104 |
| $O^{4+}$ | 8 | 0.12739 | 0.59020 | 115.2148 | 0.5565 | 1.7269 | 0.1696 | 115.0249 | 113.899 | -0.0099 |
| $F^{5+}$ | 9 | 0.11297 | 0.51382 | 158.8102 | 0.8434 | 2.0582 | 0.2409 | 158.5434 | 157.1651 | -0.0088 |
| $Ne^{6+}$ | 10 | 0.10149 | 0.45511 | 209.1813 | 1.2138 | 2.3904 | 0.3249 | 208.8243 | 207.2759 | -0.0075 |
| $Na^{7+}$ | 11 | 0.09213 | 0.40853 | 266.3233 | 1.6781 | 2.7233 | 0.4217 | 265.8628 | 264.25 | -0.0061 |
| $Mg^{8+}$ | 12 | 0.08435 | 0.37065 | 330.2335 | 2.2469 | 3.0567 | 0.5312 | 329.6559 | 328.06 | -0.0049 |
| $Al^{9+}$ | 13 | 0.07778 | 0.33923 | 400.9097 | 2.9309 | 3.3905 | 0.6536 | 400.2017 | 398.75 | -0.0036 |
| $Si^{10+}$ | 14 | 0.07216 | 0.31274 | 478.3507 | 3.7404 | 3.7246 | 0.7888 | 477.4989 | 476.36 | -0.0024 |
| $P^{11+}$ | 15 | 0.06730 | 0.29010 | 562.5555 | 4.6861 | 4.0589 | 0.9367 | 561.5464 | 560.8 | -0.0013 |
| $S^{12+}$ | 16 | 0.06306 | 0.27053 | 653.5233 | 5.7784 | 4.3935 | 1.0975 | 652.3436 | 652.2 | -0.0002 |
| $Cl^{13+}$ | 17 | 0.05932 | 0.25344 | 751.2537 | 7.0280 | 4.7281 | 1.2710 | 749.8899 | 749.76 | -0.0002 |
| $Ar^{14+}$ | 18 | 0.05599 | 0.23839 | 855.7463 | 8.4454 | 5.0630 | 1.4574 | 854.1849 | 854.77 | 0.0007 |
| $K^{15+}$ | 19 | 0.05302 | 0.22503 | 967.0007 | 10.0410 | 5.3979 | 1.6566 | 965.2283 | 968 | 0.0029 |
| $Ca^{16+}$ | 20 | 0.05035 | 0.21308 | 1085.0167 | 11.8255 | 5.7329 | 1.8687 | 1083.0198 | 1087 | 0.0037 |
| $Sc^{17+}$ | 21 | 0.04794 | 0.20235 | 1209.7940 | 13.8094 | 6.0680 | 2.0935 | 1207.5592 | 1213 | 0.0045 |
| $Ti^{18+}$ | 22 | 0.04574 | 0.19264 | 1341.3326 | 16.0032 | 6.4032 | 2.3312 | 1338.8465 | 1346 | 0.0053 |
| $V^{19+}$ | 23 | 0.04374 | 0.18383 | 1479.6323 | 18.4174 | 6.7384 | 2.5817 | 1476.8813 | 1486 | 0.0061 |
| $Cr^{20+}$ | 24 | 0.04191 | 0.17579 | 1624.6929 | 21.0627 | 7.0737 | 2.8450 | 1621.6637 | 1634 | 0.0075 |
| $Mn^{21+}$ | 25 | 0.04022 | 0.16842 | 1776.5144 | 23.9495 | 7.4091 | 3.1211 | 1773.1935 | 1788 | 0.0083 |
| $Fe^{22+}$ | 26 | 0.03867 | 0.16165 | 1935.0968 | 27.0883 | 7.7444 | 3.4101 | 1931.4707 | 1950 | 0.0095 |
| $Co^{23+}$ | 27 | 0.03723 | 0.15540 | 2100.4398 | 30.4898 | 8.0798 | 3.7118 | 2096.4952 | 2119 | 0.0106 |
| $Ni^{24+}$ | 28 | 0.03589 | 0.14961 | 2272.5436 | 34.1644 | 8.4153 | 4.0264 | 2268.2669 | 2295 | 0.0116 |
| $Cu^{25+}$ | 29 | 0.03465 | 0.14424 | 2451.4080 | 38.1228 | 8.7508 | 4.3539 | 2446.7858 | 2478 | 0.0126 |

[a] Radius of the paired inner electrons of four-electron atoms from Eq. (10.51).

[b] Radius of the paired outer electrons of four-electron atoms from Eq. (10.62).

[c] Electric energy of the outer electrons of four-electron atoms from Eq. (10.63).

[d] Magnetic energy of the outer electrons of four-electron atoms upon unpairing from Eq. (7.46) and Eq. (10.64).

[e] Change in the velocity of the paired inner electrons due to the unpaired outer electron of four-electron atoms during ionization from Eq. (10.46).

[f] Change in the kinetic energy of the paired inner electrons due to the unpaired outer electron of four-electron atoms during ionization from Eq. (10.47).

[g] Calculated ionization energies of four-electron atoms from Eq. (10.68) for $Z > 4$ and Eq. (10.66) for *Be*.

[h] From theoretical calculations, interpolation of isoelectronic and spectral series, and experimental data [2-3].

[i] (Experimental-theoretical)/experimental.

The agreement between the experimental and calculated values of Table 10.2 is well within the experimental capability of the spectroscopic determinations including the values at large Z which relies on X-ray spectroscopy. In this case, the experimental capability is three to four significant figures which is consistent with the last column. The beryllium atom isoelectronic series is given in Table 10.2 [2-3] to much higher precision than the capability of X-ray spectroscopy, but these values are based on theoretical and interpolation techniques rather than data alone. Ionization energies are difficult to determine since the cut-off of the Rydberg series of lines at the ionization energy is often not observed, and the ionization energy must be determined from theoretical calculations, interpolation of Be isoelectronic and Rydberg series, as well as direct experimental data.

## 2P-ORBITAL ELECTRONS BASED ON AN ENERGY MINIMUM

For each four-electron atom having a central charge of $Z$ times that of the proton, there are two indistinguishable spin-paired electrons in an atomic orbital with radii $r_1$ and $r_2$ both given by Eq. (7.35) (Eq. (10.51)) and two indistinguishable spin-paired electrons in an atomic orbital with radii $r_3$ and $r_4$ both given by Eq. (10.62). For $Z \geq 5$, the next electron which binds to form the corresponding five-electron atom is attracted by the central Coulomb field and is repelled by diamagnetic force due to the spin-paired inner electrons such that it forms an unpaired atomic orbital at radius $r_5$.

The central Coulomb force, $\mathbf{F}_{ele}$, acts on the outer electron to cause it to bind wherein this electric force on the outer-most electron due to the nucleus and the inner four electrons is given by Eq. (10.28) with the appropriate charge and radius:

$$\mathbf{F}_{ele} = \frac{(Z-4)e^2}{4\pi\varepsilon_0 r_5^2}\mathbf{i}_\mathbf{r} \tag{10.69}$$

for $r > r_4$. The same form of force equation also applies to six through ten-electron atoms as well as five-electron atoms:

$$\mathbf{F}_{ele} = \frac{(Z-n)e^2}{4\pi\varepsilon_0 r_n^2}\mathbf{i}_\mathbf{r} \tag{10.70}$$

for $r > r_{n-1}$ where $n$ corresponds to the number of electrons of the atom and $Z$ is its atomic number. In each case, the magnetic field of the binding outer electron changes the angular velocities of the inner electrons. However, in each case, the magnetic field of the outer electron provides a central Lorentz force which exactly balances the change in centrifugal force because of the change in angular velocity [1]. The inner electrons remain at their initial radii, but cause a diamagnetic force according to Lenz's law.

The diamagnetic force, $\mathbf{F}_{diamagnetic}$, for the formation of an s orbital given by Eq. (10.11) with the appropriate radii is:

$$\mathbf{F}_{diamagnetic} = -\frac{\hbar^2}{4m_e r_n^2 r_3}\sqrt{s(s+1)}\mathbf{i}_\mathbf{r} \tag{10.71}$$

However, with the formation of a third shell, a nonuniform distribution of charge is possible that achieves an energy minimum. Minimum energy configurations are given by solutions to Laplace's Equation. The general form of the solution (Eq. (10.449)) is:

$$\Phi(r,\theta,\phi) = \sum_{\ell=0}^{\infty}\sum_{m=-\ell}^{\ell} B_{\ell,m} r^{-(\ell+1)} Y_\ell^m(\theta,\phi) \tag{10.72}$$

As shown in the Excited States of the One-Electron Atom (Quantization) section, this general solution in the form of a source matching the wave-equation gives the functions of the resonant photons of excited states. From Eqs. (2.15-2.16):

$$\mathbf{E}_{r\,photon\;\,n,l,m} = \frac{e(na_H)^\ell}{4\pi\varepsilon_0}\frac{1}{r^{(\ell+2)}}\left[-Y_0^0(\theta,\phi) + \frac{1}{n}\left[Y_0^0(\theta,\phi) + \mathrm{Re}\left\{Y_\ell^m(\theta,\phi)e^{im\omega_n t}\right\}\right]\right]\delta(r-r_n) \tag{10.73}$$

$n = 1, 2, 3, 4, \ldots$

$\ell = 1, 2, \ldots, n-1$

$m = -\ell, -\ell+1, \ldots, 0, \ldots, +\ell$

$\mathbf{E}_{rtotal}$ is the sum of the "trapped photon" and proton electric fields,

$$\mathbf{E}_{rtotal} = \frac{e}{4\pi\varepsilon_0 r^2} + \frac{e(na_H)^\ell}{4\pi\varepsilon_0}\frac{1}{r^{(\ell+2)}}\left[-Y_0^0(\theta,\phi) + \frac{1}{n}\left[Y_0^0(\theta,\phi) + \mathrm{Re}\left\{Y_\ell^m(\theta,\phi)e^{im\omega_n t}\right\}\right]\right]\delta(r-r_n) \tag{10.74}$$

As shown in the Bound Electron "Atomic Orbital" section and the Instability of Excited States section, the angular part of the charge-density functions are eigenfunctions of Eq. (1.59), match the angular functions of the inhomogeneous Helmholtz equation, and include the time-harmonic function factor (Eqs. (1.27-1.29)) that comprises the electron source current of the corresponding electromagnetic waves. The latter are solutions of the wave-equation (Eqs. (1.1)) and arise with a change in electron radius:

$\ell = \mathbf{0}$

$$\rho(r,\theta,\phi,t) = \frac{e}{8\pi r^2}[\delta(r-r_n)]\left[Y_0^0(\theta,\phi) + Y_\ell^m(\theta,\phi)\right] \tag{10.75}$$

$\ell \neq \mathbf{0}$

$$\rho(r,\theta,\phi,t) = \frac{e}{4\pi r^2}[\delta(r-r_n)]\left[Y_0^0(\theta,\phi) + \mathrm{Re}\left\{\pi\left(R_z(\omega_n t)\right)Y_\ell^m(\theta,\phi)\right\}\right] \tag{10.76}$$

$$\rho(r,\theta,\phi,t) = \frac{e}{4\pi r^2}[\delta(r-r_n)]\left[Y_0^0(\theta,\phi) + \mathrm{Re}\left\{Y_\ell^m(\theta,\phi)e^{im\omega_n t}\right\}\right] \tag{10.77}$$

where to keep the form of the spherical harmonic as a traveling wave about the z-axis $\pi(R_z)$ is the representation of the rotational matrix about the z-axis $R_z$ (Eq. (1.82)) in the space of functions $\pi\left(R_z(\omega_n t)\right)Y_\ell^m(\theta,\phi) = Y_\ell^m(\theta,\phi + m\omega_n t)$ and

$\mathrm{Re}\left\{Y_\ell^m(\theta,\phi)e^{im\omega_n t}\right\} = P_\ell^m(\cos\theta)\cos(m\phi + m\omega_n t)$. In the cases that $m \neq 0$, Eq. (10.77) is a traveling charge-density wave that moves on the surface of the atomic orbital about the z-axis with frequency $\omega_n$ and modulates the atomic orbital corresponding to $\ell = 0$ at $m\omega_n$. These functions comprise the well known s, p, d, f, etc. orbitals wherein the constant function $Y_0^0(\theta,\phi)$ corresponds to the spin function having spin angular momentum and the modulation function $\mathrm{Re}\left\{Y_\ell^m(\theta,\phi)e^{im\omega_n t}\right\}$ corresponds to the orbital function having orbital angular momentum as given in the Bound Electron "Atomic Orbital" section and the Rotational Parameters of the Electron (Angular Momentum, Rotational Energy, Moment of Inertia) section.

Similar to the phenomenon observed for spherical conductors [4-5], spherical harmonic charge-density waves may be induced in the inner electron atomic orbitals with the addition of one or more outer electrons, each having an orbital quantum number $\ell \neq 0$ as given by Eq. (10.77). With $Z > 5$, an energy minimum is achieved when the fifth through tenth electrons of each five through ten-electron atom fills a p orbital with the formation of orthogonal complementary charge-density waves in the inner shell electrons. To maintain the symmetry of the central charge and the energy minimum condition given by solutions to Laplace's equation (Eq. (10.72)), the charge-density waves on electron atomic orbitals at $r_1$ and $r_3$ complement those of the outer orbitals when the outer p orbitals are not all occupied by at least one electron, and the complementary charge-density waves are provided by electrons at $r_3$ when this condition is met. Since the angular harmonic charge-density waves are nonradiative as shown in Appendix I: Nonradiation Condition, the time-averaged central field is inverse $r$-squared even though the central field is modulated by the concentric charge-density waves. The modulated central field maintains the spherical harmonic orbitals that maintain the spherical-harmonic phase according to Eq. (10.72). For $\ell = 1$ and $m = \pm 1$, the spherical harmonics $Y_\ell^m(\theta,\phi)$ given by Eqs. (1.30-1.31) are:

$$Y_{1,x} = \sin\theta\cos\phi \tag{10.78}$$

$$Y_{1,y} = \sin\theta\sin\phi \tag{10.79}$$

wherein the $x$ and $y$ designation corresponds, respectively, to the historical $p_x$ and $p_y$ probability-density functions of quantum mechanics. The $p_x$ and $p_y$ charge-density waves rotate in the same direction such that their individual contributions to the diamagnetic force add, or they rotate in opposite directions such that their contributions cancel. In addition, for $\ell = 1$ and $m = 0$, the spherical harmonic $Y_\ell^m(\theta,\phi)$ is:

$$Y_{1,z} = \cos\theta \tag{10.80}$$

wherein the $z$ designation corresponds to the historical $p_z$ probability-density function of quantum mechanics.

As shown by Eq. (10.9), the diamagnetic force is dependent on the integral of the charge-density squared over the surface of the atomic orbital with the further constant of the invariance of charge under Gauss's integral law. The correction to the force due to a time and spatially-dependent spherical harmonic current-density wave is given by the normalization term for spherical harmonics given by Eq. (3.53) of Jackson [6] and Eq. (6-76) of McQuarrie [7]:

$$\frac{(\ell+|m|)!}{(2\ell+1)(\ell-|m|)!} \tag{10.81}$$

Since the spin function is constant and the orbital function is a traveling wave, only the latter contributes to the diamagnetic and paramagnetic-force contributions of an unpaired electron. Substitution of Eq. (10.81) into Eq. (10.11) gives the contribution of each orbital to the diamagnetic force, $\mathbf{F}_{diamagnetic}$, which is summed over the orbitals:

$$\mathbf{F}_{diamagnetic} = -\sum_m \frac{(\ell+|m|)!}{(2\ell+1)(\ell-|m|)!}\frac{\hbar^2}{4m_e r_n^2 r_3}\sqrt{s(s+1)}\mathbf{i}_\mathbf{r} \tag{10.82}$$

where the contributions from orbitals having $|m| = 1$ add positively or negatively.

For each five-electron atom having a central charge of $Z$ times that of the proton, there are two indistinguishable spin-paired electrons in an atomic orbital with radii $r_1$ and $r_2$ both given by Eq. (7.35) (Eq. (10.51)), two indistinguishable spin-paired electrons in an atomic orbital with radii $r_3$ and $r_4$ both given by Eq. (10.62), and an unpaired electron in an atomic orbital at $r_5$ given by Eq. (10.113). For $Z \geq 6$, the next electron which binds to form the corresponding six-electron atom is attracted by the central Coulomb field and is repelled by diamagnetic force due to the spin-paired inner electrons. A paramagnetic spin-pairing force to form a filled s orbital is also possible, but the force due to the spin-pairing of the electrons (Eq. (7.24) with the radius $r_6$) reduces the energy of the atom less than that due to the alternative forces on two unpaired p electrons in an atomic orbital at the same radius $r_6$.

In general, a nonuniform distribution of charge achieves an energy minimum with the formation of a third shell due to the dependence of the magnetic forces on the nuclear charge and orbital energy (Eqs. (10.52), (10.55), and (10.93)). The outer electrons of atoms and ions that are isoelectronic with the series boron through neon half-fill a 2p level with unpaired electrons at nitrogen, then fill the level with paired electrons at neon. *Thus, it is found that the purely postulated Hund's Rule and the Pauli Exclusion Principle of the assignment of unique quantum numbers to all electrons are not "weird spooky action" phenomena unique to quantum mechanics that require all electrons in the universe to have instantaneous communication and coordination*

*with no basis in physical laws such as Maxwell's equations. Rather they are phenomenological consequences of those laws.*

Each outer 2p electron contributes spin as well as orbital angular momentum. The former gives rise to spin pairing to another 2p electron when an energy minimum is achieved. The corresponding force, $\mathbf{F}_{mag\ 2}$, given by Eq. (10.52) is:

$$\mathbf{F}_{mag\ 2} = \frac{1}{Z}\frac{\hbar^2}{m_e r_n^2 r_3}\sqrt{s(s+1)}\mathbf{i}_\mathbf{r} \tag{10.83}$$

The orbital angular momenta of spin-paired electrons may add to double the spin-pairing force of each individual p electron such that the resultant force is four times that of Eq. (10.83) in agreement with the energy (and force) relationship of magnetic fields (Eq. (1.154)):

$$\mathbf{F}_{mag\ 2} = \frac{1}{Z}\frac{4\hbar^2}{m_e r_n^2 r_3}\sqrt{s(s+1)}\mathbf{i}_\mathbf{r} \tag{10.84}$$

Or, the orbital angular momenta of spin-paired electrons may add negatively to cancel such that $\mathbf{F}_{mag\ 2}$ due to the contribution from spin-pairing alone is equivalent to that given by Eq. (10.83).

The electron velocity given by Eq. (1.35) is:

$$v_n = \frac{\hbar}{m_e r_n} \tag{10.85}$$

The velocity (Eq. (1.35)) and angular frequency (Eq. (1.36)) are determined by the boundary conditions that the angular momentum density at each point on the surface is constant and the magnitude of the total angular momentum of the atomic orbital $\mathbf{L}$ must also be constant. The constant total is $\hbar$ given by the integral:

$$\mathbf{m} = \int \frac{1}{4\pi r^2}\left|\mathbf{r} \times m_e \mathbf{v}\right|\delta\left(r - r_n\right)dx^4 = m_e r_n \frac{\hbar}{m_e r_n} = \hbar \tag{10.86}$$

The integral of the magnitude of the angular momentum of the electron is $\hbar$ in any inertial frame and is ***relativistically invariant*** as a Lorentz scalar $\mathbf{L} = \hbar$. The vector projections of the atomic orbital spin angular momentum relative to the Cartesian coordinates are given in the Spin Angular Momentum of the Atomic Orbital $Y_0^0(\theta,\phi)$ with $\ell = 0$ section. The orbital and spin angular momentum of excited states is also quantized in units of $\hbar$ as shown in the Orbital and Spin Splitting section. The orbital moment of inertia, $I_{orbital}$, corresponding to orbital quantum number $\ell$ (Eq. (1.147)) is:

$$I_{orbital} = m_e r_n^{\ 2}\left[\frac{\ell(\ell+1)}{\ell^2 + 2\ell + 1}\right]^{\frac{1}{2}} = m_e r_n^{\ 2}\sqrt{\frac{\ell}{\ell+1}} \tag{10.87}$$

The spin and orbital angular momentum can superimpose positively or negatively:

$$L_{z\ total} = L_{z\ spin} + L_{z\ orbital} \tag{10.88}$$

Thus, the contribution of the orbital angular momentum to the paramagnetic force is also that given by Eq. (10.83).

$$\mathbf{F}_{mag\ 2} = \frac{1}{Z}\frac{\hbar^2}{m_e r_n^2 r_3}\sqrt{s(s+1)}\mathbf{i}_\mathbf{r} \tag{10.89}$$

And, the total force is given as the sum over the orbital and spin angular momenta that may add positively or negatively to achieve an energy minimum while maintaining the conservation of angular momentum.

The amplitude of the corresponding rotational energy, $E_{rotational\ \text{orbital}}$, given by Eq. (1.71) is:

$$E_{rotational\ \text{orbital}} = \frac{\hbar^2}{2m_e r_n^{\ 2}}\left[\frac{\ell(\ell+1)}{\ell^2 + 2\ell + 1}\right]^{\frac{1}{2}} = \frac{\hbar^2}{2m_e r_n^{\ 2}}\sqrt{\frac{\ell}{\ell+1}} \tag{10.90}$$

Since the orbital rotational energy arises from a spin function (spin angular momentum) modulated by a spherical harmonic angular function (orbital angular momentum), the time-averaged orbital rotational energy having an amplitude given by Eq. (1.71) (Eq. (10.90)) is zero:

$$\left\langle E_{rotational\ \text{orbital}} \right\rangle = 0 \tag{10.91}$$

However, the orbital energy is nonzero in the presence of a magnetic field.

N-electron atoms having $Z > n$ possess an electric field of:

$$\mathbf{E} = \frac{(Z-n)e}{4\pi\varepsilon_0 r^2}\mathbf{i}_\mathbf{r} \tag{10.92}$$

for $r > r_n$. Since there is a source of dissipative power, $\mathbf{J} \bullet \mathbf{E}$ of Eq. (10.27), the magnetic moments of the inner electrons may change due to the outer electron such that the energy of the n-electron atom is lowered. The diamagnetic force, $\mathbf{F}_{diamagnetic\ 2}$, due to a relativistic effect with an electric field for $r > r_n$ (Eq. (10.35)) is dependent on the amplitude of the orbital energy. Using the orbital energy with $\ell = 1$ (Eq. (10.90)), the energy $m_e \Delta v^2$ of Eq. (10.29) is reduced by the factor of $\left(1 - \frac{\sqrt{2}}{2}\right)$ due to the contribution of the charge-density wave of the inner electrons at $r_3$. Thus, $\mathbf{F}_{diamagnetic\ 2}$ is given by:

$$\mathbf{F}_{diamagnetic\ 2}=-\left[\frac{Z-n}{Z-(n-1)}\right]\left(1-\frac{\sqrt{2}}{2}\right)\frac{r_3\hbar^2}{m_e r_n^4}10\sqrt{s(s+1)}\mathbf{i}_{\mathbf{r}} \tag{10.93}$$

Using the forces given by Eqs. (10.70), (10.82-10.84), (10.89), (10.93), and the radii $r_3$ given by Eq. (10.62), the radii of the 2p electrons of all five through ten-electron atoms may be solved exactly. The electric energy given by Eq. (10.102) gives the corresponding exact ionization energies. $\mathbf{F}_{ele}$ and $\mathbf{F}_{diamagnetic\ 2}$ given by Eqs. (10.70) and (10.93), respectively, are of the same form for all atoms with the appropriate nuclear charges and atomic radii. $\mathbf{F}_{diamagnetic}$ given by Eq. (10.82) and $\mathbf{F}_{mag\ 2}$ given by Eqs. (10.83-10.84) and (10.89) are of the same form with the appropriate factors that depend on the minimum-energy electron configuration. The general equation and the summary of the parameters that determine the exact radii and ionization energies of all five through ten-electron atoms are given the General Equation For The Ionization Energies of Five Through Ten-Electron Atoms section and in Table 10.9.

## FIVE-ELECTRON ATOMS

Five-electron atoms can be solved exactly using the results of the solutions of one, two, three, and four-electron atoms.

## RADIUS AND IONIZATION ENERGY OF THE OUTER ELECTRON OF THE BORON ATOM

For each four-electron atom having a central charge of $Z$ times that of the proton, there are two indistinguishable spin-paired electrons in an atomic orbital with radii $r_1$ and $r_2$ both given by Eq. (7.35) (Eq. (10.51)) and two indistinguishable spin-paired electrons in an atomic orbital with radii $r_3$ and $r_4$ both given by Eq. (10.62). For $Z \geq 5$, the next electron which binds to form the corresponding five-electron atom is attracted by the central Coulomb field and is repelled by diamagnetic force due to the spin-paired inner electrons such that it forms an unpaired atomic orbital at radius $r_5$. The resulting electron configuration is $1s^2 2s^2 2p^1$, and the orbital arrangement is:

2p state

$$\begin{array}{ccc} \uparrow & & \\ \hline 1 & 0 & -1 \end{array} \tag{10.94}$$

corresponding to the ground state ${}^2P^0_{1/2}$.

The central Coulomb force acts on the outer electron to cause it to bind wherein this electric force on the outer-most electron due to the nucleus and the inner four electrons is given by Eq. (10.70) with the appropriate charge and radius:

$$\mathbf{F}_{ele}=\frac{(Z-4)e^2}{4\pi\varepsilon_0 r_5^2}\mathbf{i}_{\mathbf{r}} \tag{10.95}$$

for $r > r_4$.

The single p orbital of the boron atom produces a diamagnetic force equivalent to that of the formation of an s orbital due to the induction of complementary and spherically symmetrical charge-density waves on electron atomic orbitals at $r_1$ and $r_3$ in order to achieve a solution of Laplace's equation (Eq. (10.72)). The inner electrons remain at their initial radii, but cause a diamagnetic force according to Lenz's law that is two times that of Eqs. (10.11) and (10.71) since the two electrons at $r_1 = r_2$ act on the two electrons at $r_3 = r_4$ which in turn act of the outer electron. $\mathbf{F}_{diamagnetic}$ is also given by Eq. (10.82) with $\ell = 0$ and the appropriate radii when the contributions from the three orthogonal spherical harmonics are summed over including those induced:

$$\mathbf{F}_{diamagnetic}=-\frac{2\hbar^2}{4m_e r_5^2 r_3}\sqrt{s(s+1)}\mathbf{i}_{\mathbf{r}} \tag{10.96}$$

The charge induction forms complementary mirror charge-density waves which must have opposing angular momenta such that momentum is conserved. In this case, $\mathbf{F}_{mag\ 2}$ given by Eq. (10.89) is zero:

$$\mathbf{F}_{mag\ 2}=0 \tag{10.97}$$

The outward centrifugal force on electron 5 is balanced by the electric force and the magnetic force (on electron 5). The radius of the outer electron is calculated by equating the outward centrifugal force to the sum of the electric (Eq. (10.95)) and diamagnetic (Eq. (10.96)) forces as follows:

$$\frac{m_e v_5^2}{r_5}=\frac{(Z-4)e^2}{4\pi\varepsilon_0 r_5^2}-\frac{2\hbar^2}{4m_e r_5^2 r_3}\sqrt{s(s+1)} \tag{10.98}$$

Substitution of $v_5=\frac{\hbar}{m_e r_5}$ (Eq. (1.35)) and $s=\frac{1}{2}$ into Eq. (10.98) gives:

$$\frac{\hbar^2}{m_e r_5^3}=\frac{(Z-4)e^2}{4\pi\varepsilon_0 r_5^2}-\frac{\hbar^2}{2m_e r_5^2 r_3}\sqrt{\frac{3}{4}} \tag{10.99}$$

$$r_5 = \frac{a_0}{\left((Z-4)-\frac{\sqrt{\frac{3}{4}}}{2r_3}\right)},\ r_3 \textit{ in units of } a_0 \tag{10.100}$$

Substitution of $\frac{r_3}{a_0} = 1.07930$ (Eq. (10.62) with $Z = 5$) into Eq. (10.100) gives:

$$r_5 = 1.67000351 a_0 \tag{10.101}$$

In general, the energy stored in the electric field, $E(electric)$, is given by Eq. (10.43) with the appropriate charge and radius:

$$E(electric) = -\frac{(Z-(n-1))e^2}{8\pi\varepsilon_0 r_n} \tag{10.102}$$

where $n$ corresponds to the number of electrons of the atom and $Z$ is its atomic number. The ionization energy is given by the sum of the electric energy and the energy corresponding to the change in magnetic-moments of the inner shell electrons. Since there is no source of dissipative power, $\mathbf{J} \bullet \mathbf{E}$ of Eq. (10.27), to compensate for any potential change in the magnetic moments, $\Delta m$, of the inner electrons due to the ionization of the outer electron of the boron atom, there is a diamagnetic energy term in the ionization energy for this atom that follows from the corresponding term for the lithium atom. Since the diamagnetic force for the boron atom (Eq. (10.96)) is twice that of the corresponding force (Eq. (10.11)) of the lithium atom, this term is given by twice that of Eqs. (10.15-10.24), with $Z = 5$, $r_3$ given by Eq. (10.62), and $r_5$ given by Eq. (10.101). Thus, the change in magnetic energy of the inner atomic orbital at $r_3$ is 85.429321 %, so that the corresponding energy $\Delta E_{mag}$ is:

$$\Delta E_{mag} = 2\left(0.85429321\ X\ 0.09100214\ eV\right) = 0.15548501\ eV \tag{10.103}$$

where the magnetic energy of the inner electrons is $0.09100214\ eV$ (Eqs. (10.64) and (10.101)). Then, the ionization energy of the boron atom is given by Eqs. (10.101-10.102) and (10.103):

$$\begin{aligned} E(ionization;\ B) &= \frac{(Z-4)e^2}{8\pi\varepsilon_0 r_5} + \Delta E_{mag} \\ &= 8.147170901\ eV + 0.15548501\ eV = 8.30265592\ eV \end{aligned} \tag{10.104}$$

The experimental ionization energy of the boron atom is $8.29803\ eV$ [3].

## THE IONIZATION ENERGIES OF FIVE-ELECTRON ATOMS WITH A NUCLEAR CHARGE Z>5

Five-electron atoms having $Z > 5$ possess an external electric field given by Eq. (10.92). In this case, an energy minimum is achieved with conservation of momentum when the orbital angular momentum is such that $\mathbf{F}_{diamagnetic}$ is minimized while $\mathbf{F}_{mag\ 2}$ is maximized. From Eq. (10.82), the diamagnetic force, $\mathbf{F}_{diamagnetic}$, is given by the sum of the contributions from the $p_x$, $p_y$, and $p_z$ orbitals corresponding to $m$ = 1, -1, and 0, respectively:

$$\mathbf{F}_{diamagnetic} = -\left(\frac{2}{3}+\frac{2}{3}+\frac{1}{3}\right)\frac{\hbar^2}{4m_e r_5^2 r_3}\sqrt{s(s+1)}\mathbf{i}_\mathbf{r} = -\left(\frac{5}{3}\right)\frac{\hbar^2}{4m_e r_5^2 r_3}\sqrt{s(s+1)}\mathbf{i}_\mathbf{r} \tag{10.105}$$

With $Z > 5$, the charge induction forms complementary mirror charge-density waves such that the angular momenta do not cancel. From Eq. (10.89), $\mathbf{F}_{mag\ 2}$ corresponding to the orbital angular momentum of the single $p_x$ electron is

$$\mathbf{F}_{mag\ 2} = \frac{1}{Z}\frac{\hbar^2}{m_e r_5^2 r_3}\sqrt{s(s+1)}\mathbf{i}_\mathbf{r} \tag{10.106}$$

The second diamagnetic force, $\mathbf{F}_{diamagnetic\ 2}$, due to the binding of the p-orbital electron having an electric field outside of its radius is given by Eq. (10.93):

$$\mathbf{F}_{diamagnetic\ 2} = -\left[\frac{Z-5}{Z-4}\right]\left(1-\frac{\sqrt{2}}{2}\right)\frac{r_3\hbar^2}{m_e r_5^4}10\sqrt{s(s+1)}\mathbf{i}_\mathbf{r} \tag{10.107}$$

In the case that $Z > 5$, the radius of the outer electron is calculated by equating the outward centrifugal force to the sum of the electric (Eq. (10.95)) and diamagnetic (Eqs. (10.105) and (10.107)), and paramagnetic (Eq. (10.106)) forces as follows:

$$\frac{m_e v_5^2}{r_5} = \frac{(Z-4)e^2}{4\pi\varepsilon_0 r_5^2} - \frac{5\hbar^2}{12m_e r_5^2 r_3}\sqrt{s(s+1)} + \frac{\hbar^2}{Zm_e r_5^2 r_3}\sqrt{s(s+1)} - \left[\frac{Z-5}{Z-4}\right]\left(1-\frac{\sqrt{2}}{2}\right)\frac{r_3\hbar^2}{r_5^4 m_e}10\sqrt{s(s+1)} \tag{10.108}$$

Substitution of $v_5 = \frac{\hbar}{m_e r_5}$ (Eq. (1.35)) and $s = \frac{1}{2}$ into Eq. (10.108) gives:

$$\frac{\hbar^2}{m_e r_5^3}=\frac{(Z-4)e^2}{4\pi\varepsilon_0 r_5^2}-\frac{5\hbar^2}{12m_e r_5^2 r_3}\sqrt{\frac{3}{4}}+\frac{\hbar^2}{Zm_e r_5^2 r_3}\sqrt{\frac{3}{4}}-\left[\frac{Z-5}{Z-4}\right]\left(1-\frac{\sqrt{2}}{2}\right)\frac{r_3\hbar^2}{r_5^4 m_e}10\sqrt{\frac{3}{4}} \tag{10.109}$$

The quadratic equation corresponding to Eq. (10.109) is:

$$\left(\frac{(Z-4)e^2}{4\pi\varepsilon_0}-\left(\frac{5}{12}-\frac{1}{Z}\right)\frac{\hbar^2}{m_e r_3}\sqrt{\frac{3}{4}}\right)r_5^2-\frac{\hbar^2}{m_e}r_5-\left[\frac{Z-5}{Z-4}\right]\left(1-\frac{\sqrt{2}}{2}\right)\frac{r_3\hbar^2}{m_e}10\sqrt{\frac{3}{4}}=0 \tag{10.110}$$

$$r_5^2-\frac{\dfrac{\hbar^2}{m_e}}{\left(\dfrac{(Z-4)e^2}{4\pi\varepsilon_0}-\left(\dfrac{5}{12}-\dfrac{1}{Z}\right)\dfrac{\hbar^2}{m_e r_3}\sqrt{\dfrac{3}{4}}\right)}r_5-\frac{\dfrac{\hbar^2}{m_e}\left[\dfrac{Z-5}{Z-4}\right]\left(1-\dfrac{\sqrt{2}}{2}\right)r_3 10\sqrt{\dfrac{3}{4}}}{\left(\dfrac{(Z-4)e^2}{4\pi\varepsilon_0}-\left(\dfrac{5}{12}-\dfrac{1}{Z}\right)\dfrac{\hbar^2}{m_e r_3}\sqrt{\dfrac{3}{4}}\right)}=0 \tag{10.111}$$

The solution of Eq. (10.111) using the quadratic formula is:

$$r_5=\frac{\dfrac{\dfrac{\hbar^2}{m_e}}{\left(\dfrac{(Z-4)e^2}{4\pi\varepsilon_0}-\left(\dfrac{5}{12}-\dfrac{1}{Z}\right)\dfrac{\hbar^2}{m_e r_3}\sqrt{\dfrac{3}{4}}\right)}\pm\sqrt{\left(\dfrac{\dfrac{\hbar^2}{m_e}}{\left(\dfrac{(Z-4)e^2}{4\pi\varepsilon_0}-\left(\dfrac{5}{12}-\dfrac{1}{Z}\right)\dfrac{\hbar^2}{m_e r_3}\sqrt{\dfrac{3}{4}}\right)}\right)^2+4\dfrac{\dfrac{\hbar^2}{m_e}\left[\dfrac{Z-5}{Z-4}\right]\left(1-\dfrac{\sqrt{2}}{2}\right)r_3 10\sqrt{\dfrac{3}{4}}}{\left(\dfrac{(Z-4)e^2}{4\pi\varepsilon_0}-\left(\dfrac{5}{12}-\dfrac{1}{Z}\right)\dfrac{\hbar^2}{m_e r_3}\sqrt{\dfrac{3}{4}}\right)}}}{2} \tag{10.112}$$

$$r_5=\frac{\dfrac{a_0}{\left((Z-4)-\left(\dfrac{5}{24}-\dfrac{1}{2Z}\right)\dfrac{\sqrt{3}}{r_3}\right)}\pm a_0\sqrt{\left(\dfrac{1}{\left((Z-4)-\left(\dfrac{5}{24}-\dfrac{1}{2Z}\right)\dfrac{\sqrt{3}}{r_3}\right)}\right)^2+\dfrac{20\sqrt{3}\left(\left[\dfrac{Z-5}{Z-4}\right]\left(1-\dfrac{\sqrt{2}}{2}\right)r_3\right)}{\left((Z-4)-\left(\dfrac{5}{24}-\dfrac{1}{2Z}\right)\dfrac{\sqrt{3}}{r_3}\right)}}}{2},\ r_3\ \textit{in units of}\ a_0 \tag{10.113}$$

where $r_3$ is given by Eq. (10.62). The positive root of Eq. (10.113) must be taken in order that $r_5>0$. The radii of several five-electron atoms are given in Table 10.3.

The ionization energies for the five-electron atoms with $Z>5$ are given by the electric energy, $E(electric)$, (Eq. (10.102) with the radii, $r_5$, given by Eq. (10.113)):

$$E(Ionization)=-Electric\ Energy=\frac{(Z-4)e^2}{8\pi\varepsilon_0 r_5} \tag{10.114}$$

Since the relativistic corrections were small, the nonrelativistic ionization energies for experimentally measured five-electron atoms are given in Table 10.3.

**Table 10.3.** Ionization energies for some five-electron atoms.

| 5 e Atom | Z | $r_1$ $(a_o)$ [a] | $r_3$ $(a_o)$ [b] | $r_5$ $(a_o)$ [c] | Theoretical Ionization Energies [d] $(eV)$ | Experimental Ionization Energies [e] $(eV)$ | Relative Error [f] |
|---|---|---|---|---|---|---|---|
| $B$ | 5 | 0.20670 | 1.07930 | 1.67000 | 8.30266 | 8.29803 | -0.00056 |
| $C^{+}$ | 6 | 0.17113 | 0.84317 | 1.12092 | 24.2762 | 24.38332 | 0.0044 |
| $N^{2+}$ | 7 | 0.14605 | 0.69385 | 0.87858 | 46.4585 | 47.44924 | 0.0209 |
| $O^{3+}$ | 8 | 0.12739 | 0.59020 | 0.71784 | 75.8154 | 77.41353 | 0.0206 |
| $F^{4+}$ | 9 | 0.11297 | 0.51382 | 0.60636 | 112.1922 | 114.2428 | 0.0179 |
| $Ne^{5+}$ | 10 | 0.10149 | 0.45511 | 0.52486 | 155.5373 | 157.93 | 0.0152 |
| $Na^{6+}$ | 11 | 0.09213 | 0.40853 | 0.46272 | 205.8266 | 208.5 | 0.0128 |
| $Mg^{7+}$ | 12 | 0.08435 | 0.37065 | 0.41379 | 263.0469 | 265.96 | 0.0110 |
| $Al^{8+}$ | 13 | 0.07778 | 0.33923 | 0.37425 | 327.1901 | 330.13 | 0.0089 |
| $Si^{9+}$ | 14 | 0.07216 | 0.31274 | 0.34164 | 398.2509 | 401.37 | 0.0078 |
| $P^{10+}$ | 15 | 0.06730 | 0.29010 | 0.31427 | 476.2258 | 479.46 | 0.0067 |
| $S^{11+}$ | 16 | 0.06306 | 0.27053 | 0.29097 | 561.1123 | 564.44 | 0.0059 |
| $Cl^{12+}$ | 17 | 0.05932 | 0.25344 | 0.27090 | 652.9086 | 656.71 | 0.0058 |
| $Ar^{13+}$ | 18 | 0.05599 | 0.23839 | 0.25343 | 751.6132 | 755.74 | 0.0055 |
| $K^{14+}$ | 19 | 0.05302 | 0.22503 | 0.23808 | 857.2251 | 861.1 | 0.0045 |
| $Ca^{15+}$ | 20 | 0.05035 | 0.21308 | 0.22448 | 969.7435 | 974 | 0.0044 |
| $Sc^{16+}$ | 21 | 0.04794 | 0.20235 | 0.21236 | 1089.1678 | 1094 | 0.0044 |
| $Ti^{17+}$ | 22 | 0.04574 | 0.19264 | 0.20148 | 1215.4975 | 1221 | 0.0045 |
| $V^{18+}$ | 23 | 0.04374 | 0.18383 | 0.19167 | 1348.7321 | 1355 | 0.0046 |
| $Cr^{19+}$ | 24 | 0.04191 | 0.17579 | 0.18277 | 1488.8713 | 1496 | 0.0048 |
| $Mn^{20+}$ | 25 | 0.04022 | 0.16842 | 0.17466 | 1635.9148 | 1644 | 0.0049 |
| $Fe^{21+}$ | 26 | 0.03867 | 0.16165 | 0.16724 | 1789.8624 | 1799 | 0.0051 |
| $Co^{22+}$ | 27 | 0.03723 | 0.15540 | 0.16042 | 1950.7139 | 1962 | 0.0058 |
| $Ni^{23+}$ | 28 | 0.03589 | 0.14961 | 0.15414 | 2118.4690 | 2131 | 0.0059 |
| $Cu^{24+}$ | 29 | 0.03465 | 0.14424 | 0.14833 | 2293.1278 | 2308 | 0.0064 |

[a] Radius of the first set of paired inner electrons of five-electron atoms from Eq. (10.51).

[b] Radius of the second set of paired inner electrons of five-electron atoms from Eq. (10.62).

[c] Radius of the outer electron of five-electron atoms from Eq. (10.113) for $Z > 5$ and Eq. (10.101) for $B$.

[d] Calculated ionization energies of five-electron atoms given by the electric energy (Eq. (10.114)) for $Z > 5$ and Eq. (10.104) for $B$.

[e] From theoretical calculations, interpolation of isoelectronic and spectral series, and experimental data [2-3].

[f] (Experimental-theoretical)/experimental.

The agreement between the experimental and calculated values of Table 10.3 is well within the experimental capability of the spectroscopic determinations including the values at large Z which relies on X-ray spectroscopy. In this case, the experimental capability is three to four significant figures which is consistent with the last column. The boron atom isoelectronic series is given in Table 10.3 [2-3] to much higher precision than the capability of X-ray spectroscopy, but these values are based on theoretical and interpolation techniques rather than data alone. Ionization energies are difficult to determine since the cut-off of the Rydberg series of lines at the ionization energy is often not observed, and the ionization energy must be determined from theoretical calculations, interpolation of B isoelectronic and Rydberg series, as well as direct experimental data.

# SIX-ELECTRON ATOMS

Six-electron atoms can be solved exactly using the results of the solutions of one, two, three, four, and five-electron atoms.

## RADIUS AND IONIZATION ENERGY OF THE OUTER ELECTRON OF THE CARBON ATOM

For each five-electron atom having a central charge of $Z$ times that of the proton, there are two indistinguishable spin-paired electrons in an atomic orbital with radii $r_1$ and $r_2$ both given by Eq. (7.35) (Eq. (10.51)), two indistinguishable spin-paired electrons in an atomic orbital with radii $r_3$ and $r_4$ both given by Eq. (10.62), and an unpaired electron in an atomic orbital at $r_5$ given by Eq. (10.113). For $Z \geq 6$, the next electron which binds to form the corresponding six-electron atom is attracted by the central Coulomb field and is repelled by diamagnetic force due to the spin-paired inner electrons. A paramagnetic spin-pairing force to form a filled s orbital is also possible, but the force due to the spin-pairing of the electrons (Eq. (7.24) with the radius $r_6$) reduces the energy of the atom less than that due to the alternative forces on two unpaired p electrons in an atomic orbital at the same radius $r_6$. The resulting electron configuration is $1s^2 2s^2 2p^2$, and the orbital arrangement is:

2p state

$$\underset{1}{\uparrow} \quad \underset{0}{\uparrow} \quad \underset{-1}{__} \tag{10.115}$$

corresponding to the ground state ${}^3P_0$.

The central Coulomb force acts on the outer electron to cause it to bind wherein this electric force on the outer-most electron due to the nucleus and the inner five electrons is given by Eq. (10.70) with the appropriate charge and radius:

$$\mathbf{F}_{ele} = \frac{(Z-5)e^2}{4\pi\varepsilon_0 r_6^2}\mathbf{i}_\mathbf{r} \tag{10.116}$$

for $r > r_5$.

The two orthogonal electrons form charge-density waves such that the total angular momentum of the two outer electrons is conserved which determines the diamagnetic force according to Eq. (10.82). $\mathbf{F}_{diamagnetic}$ is:

$$\mathbf{F}_{diamagnetic} = -\left(\frac{2}{3}\right)\frac{\hbar^2}{4m_e r_6^2 r_3}\sqrt{s(s+1)}\mathbf{i}_\mathbf{r} \tag{10.117}$$

corresponding to $m = 1$.

The charge induction forms complementary mirror charge-density waves which must have opposing angular momenta such that momentum is conserved. In this case, $\mathbf{F}_{mag\ 2}$ given by Eq. (10.89) is zero:

$$\mathbf{F}_{mag\ 2} = 0 \tag{10.118}$$

The outward centrifugal force on electron 6 is balanced by the electric force and the magnetic forces (on electron 6). The radius of the outer electron is calculated by equating the outward centrifugal force to the sum of the electric (Eq. (10.116)) and diamagnetic (Eq. (10.117)) forces as follows:

$$\frac{m_e v_6^2}{r_6} = \frac{(Z-5)e^2}{4\pi\varepsilon_0 r_6^2} - \frac{\hbar^2}{6m_e r_6^2 r_3}\sqrt{s(s+1)} \tag{10.119}$$

Substitution of $v_6 = \frac{\hbar}{m_e r_6}$ (Eq. (1.35)) and $s = \frac{1}{2}$ into Eq. (10.119) gives:

$$\frac{\hbar^2}{m_e r_6^3} = \frac{(Z-5)e^2}{4\pi\varepsilon_0 r_6^2} - \frac{\hbar^2}{6m_e r_6^2 r_3}\sqrt{\frac{3}{4}} \tag{10.120}$$

$$r_6 = \frac{a_0}{\left((Z-5) - \frac{\sqrt{\frac{3}{4}}}{6r_3}\right)},\ r_3 \textit{ in units of } a_0 \tag{10.121}$$

Substitution of $\frac{r_3}{a_0} = 0.84317$ (Eq. (10.62) with $Z = 6$) into Eq. (10.121) gives:

$$r_6 = 1.20654 a_0 \tag{10.122}$$

The ionization energy of the carbon atom is given by the electric energy, $E(electric)$, (Eq. (10.102) with the radius, $r_6$, given by Eq. (10.122)):

$$E(ionization;\ C) = -Electric\ Energy = \frac{(Z-5)e^2}{8\pi\varepsilon_0 r_6} = 11.27671\ eV \tag{10.123}$$

where $r_6 = 1.20654 a_0$ (Eq. (10.122)) and $Z = 6$. The experimental ionization energy of the carbon atom is 11.2603 $eV$ [3].

## THE IONIZATION ENERGIES OF SIX-ELECTRON ATOMS WITH A NUCLEAR CHARGE Z>6

Six-electron atoms having $Z > 6$ possess an external electric field given by Eq. (10.92). In this case, an energy minimum is achieved with conservation of momentum when the orbital angular momentum is such that $\mathbf{F}_{diamagnetic}$ is minimized while $\mathbf{F}_{mag\ 2}$ is maximized. From Eq. (10.82), the diamagnetic force, $\mathbf{F}_{diamagnetic}$, is given by the sum of the contributions from the $p_x$, $p_y$, and $p_z$ orbitals corresponding to $m = 1,\ -1,$ and $0,$ respectively:

$$\mathbf{F}_{diamagnetic} = -\left(\frac{2}{3}+\frac{2}{3}+\frac{1}{3}\right)\frac{\hbar^2}{4m_e r_6^2 r_3}\sqrt{s(s+1)}\mathbf{i}_{\mathbf{r}} = -\left(\frac{5}{3}\right)\frac{\hbar^2}{4m_e r_6^2 r_3}\sqrt{s(s+1)}\mathbf{i}_{\mathbf{r}} \tag{10.124}$$

With $Z > 6$, the charge induction forms complementary mirror charge-density waves such that the angular momenta do not cancel. From Eq. (10.89), $\mathbf{F}_{mag\ 2}$ corresponding to the orbital angular momentum of the two p electrons in addition to complementary charge-density waves is:

$$\mathbf{F}_{mag\ 2} = 2\frac{1}{Z}\frac{2\hbar^2}{m_e r_6^2 r_3}\sqrt{s(s+1)}\mathbf{i}_{\mathbf{r}} = \frac{1}{Z}\frac{4\hbar^2}{m_e r_6^2 r_3}\sqrt{s(s+1)}\mathbf{i}_{\mathbf{r}} \tag{10.125}$$

The second diamagnetic force, $\mathbf{F}_{diamagnetic\ 2}$, due to the binding of the p-orbital electron having an electric field outside of its radius, is given by Eq. (10.93):

$$\mathbf{F}_{diamagnetic\ 2} = -\left[\frac{Z-6}{Z-5}\right]\left(1-\frac{\sqrt{2}}{2}\right)\frac{r_3\hbar^2}{m_e r_6^4}10\sqrt{s(s+1)}\mathbf{i}_{\mathbf{r}} \tag{10.126}$$

In the case that $Z > 6$, the radius of the outer electron is calculated by equating the outward centrifugal force to the sum of the electric (Eq. (10.116)), diamagnetic (Eqs. (10.124) and (10.126)), and paramagnetic (Eq. (10.125)) forces as follows:

$$\frac{m_e v_6^2}{r_6} = \frac{(Z-5)e^2}{4\pi\varepsilon_0 r_6^2} - \frac{5\hbar^2}{12m_e r_6^2 r_3}\sqrt{s(s+1)} + \frac{4\hbar^2}{Zm_e r_6^2 r_3}\sqrt{s(s+1)} - \left[\frac{Z-6}{Z-5}\right]\left(1-\frac{\sqrt{2}}{2}\right)\frac{r_3\hbar^2}{m_e r_6^4}10\sqrt{s(s+1)} \tag{10.127}$$

Substitution of $v_6 = \dfrac{\hbar}{m_e r_6}$ (Eq. (1.35)) and $s = \dfrac{1}{2}$ into Eq. (10.127) gives:

$$\frac{\hbar^2}{m_e r_6^3} = \frac{(Z-5)e^2}{4\pi\varepsilon_0 r_6^2} - \frac{5\hbar^2}{12m_e r_6^2 r_3}\sqrt{\frac{3}{4}} + \frac{4\hbar^2}{Zm_e r_6^2 r_3}\sqrt{\frac{3}{4}} - \left[\frac{Z-6}{Z-5}\right]\left(1-\frac{\sqrt{2}}{2}\right)\frac{r_3\hbar^2}{r_6^4 m_e}10\sqrt{\frac{3}{4}} \tag{10.128}$$

The quadratic equation corresponding to Eq. (10.128) is:

$$\left(\frac{(Z-5)e^2}{4\pi\varepsilon_0} - \left(\frac{5}{12}-\frac{4}{Z}\right)\frac{\hbar^2}{m_e r_3}\sqrt{\frac{3}{4}}\right)r_6^2 - \frac{\hbar^2}{m_e}r_6 - \left[\frac{Z-6}{Z-5}\right]\left(1-\frac{\sqrt{2}}{2}\right)\frac{r_3\hbar^2}{m_e}10\sqrt{\frac{3}{4}} = 0 \tag{10.129}$$

$$r_6^2 - \frac{\dfrac{\hbar^2}{m_e}}{\left(\dfrac{(Z-5)e^2}{4\pi\varepsilon_0} - \left(\dfrac{5}{12}-\dfrac{4}{Z}\right)\dfrac{\hbar^2}{m_e r_3}\sqrt{\dfrac{3}{4}}\right)}r_6 - \frac{\dfrac{\hbar^2}{m_e}\left[\dfrac{Z-6}{Z-5}\right]\left(1-\dfrac{\sqrt{2}}{2}\right)r_3 10\sqrt{\dfrac{3}{4}}}{\left(\dfrac{(Z-5)e^2}{4\pi\varepsilon_0} - \left(\dfrac{5}{12}-\dfrac{4}{Z}\right)\dfrac{\hbar^2}{m_e r_3}\sqrt{\dfrac{3}{4}}\right)} = 0 \tag{10.130}$$

The solution of Eq. (10.130) using the quadratic formula is:

$$r_6 = \frac{\dfrac{\dfrac{\hbar^2}{m_e}}{\left(\dfrac{(Z-5)e^2}{4\pi\varepsilon_0} - \left(\dfrac{5}{12}-\dfrac{4}{Z}\right)\dfrac{\hbar^2}{m_e r_3}\sqrt{\dfrac{3}{4}}\right)} \pm \sqrt{\left(\dfrac{\dfrac{\hbar^2}{m_e}}{\left(\dfrac{(Z-5)e^2}{4\pi\varepsilon_0} - \left(\dfrac{5}{12}-\dfrac{4}{Z}\right)\dfrac{\hbar^2}{m_e r_3}\sqrt{\dfrac{3}{4}}\right)}\right)^2 + 4\dfrac{\dfrac{\hbar^2}{m_e}\left[\dfrac{Z-6}{Z-5}\right]\left(1-\dfrac{\sqrt{2}}{2}\right)r_3 10\sqrt{\dfrac{3}{4}}}{\left(\dfrac{(Z-5)e^2}{4\pi\varepsilon_0} - \left(\dfrac{5}{12}-\dfrac{4}{Z}\right)\dfrac{\hbar^2}{m_e r_3}\sqrt{\dfrac{3}{4}}\right)}}}{2} \tag{10.131}$$

$$r_6 = \frac{\dfrac{a_0}{\left((Z-5)-\left(\dfrac{5}{24}-\dfrac{2}{Z}\right)\dfrac{\sqrt{3}}{r_3}\right)} \pm a_0\sqrt{\left(\dfrac{1}{\left((Z-5)-\left(\dfrac{5}{24}-\dfrac{2}{Z}\right)\dfrac{\sqrt{3}}{r_3}\right)}\right)^2 + \dfrac{20\sqrt{3}\left(\left[\dfrac{Z-6}{Z-5}\right]\left(1-\dfrac{\sqrt{2}}{2}\right)r_3\right)}{\left((Z-5)-\left(\dfrac{5}{24}-\dfrac{2}{Z}\right)\dfrac{\sqrt{3}}{r_3}\right)}}}{2}, r_3 \text{ in units of } a_0 \tag{10.132}$$

where $r_3$ is given by Eq. (10.62). The positive root of Eq. (10.132) must be taken in order that $r_6 > 0$. The final radius of electron 6, $r_6$, is given by Eq. (10.132); this is also the final radius of electron 5. The radii of several six-electron atoms are given in Table 10.4.

The ionization energies for the six-electron atoms with $Z > 6$ are given by the electric energy, $E(electric)$, (Eq. (10.102) with the radii $r_6$, given by Eq. (10.132)):

$$E(Ionization) = -Electric\ Energy = \frac{(Z-5)e^2}{8\pi\varepsilon_0 r_6} \tag{10.133}$$

Since the relativistic corrections were small, the nonrelativistic ionization energies for experimentally measured six-electron atoms are given in Table 10.4.

**Table 10.4.** Ionization energies for some six-electron atoms.

| 6 e Atom | Z | $r_1$ $(a_0)$ [a] | $r_3$ $(a_0)$ [b] | $r_6$ $(a_0)$ [c] | Theoretical Ionization Energies [d] $(eV)$ | Experimental Ionization Energies [e] $(eV)$ | Relative Error [f] |
|---|---|---|---|---|---|---|---|
| $C$ | 6 | 0.17113 | 0.84317 | 1.20654 | 11.27671 | 11.2603 | -0.0015 |
| $N^{+}$ | 7 | 0.14605 | 0.69385 | 0.90119 | 30.1950 | 29.6013 | -0.0201 |
| $O^{2+}$ | 8 | 0.12739 | 0.59020 | 0.74776 | 54.5863 | 54.9355 | 0.0064 |
| $F^{3+}$ | 9 | 0.11297 | 0.51382 | 0.63032 | 86.3423 | 87.1398 | 0.0092 |
| $Ne^{4+}$ | 10 | 0.10149 | 0.45511 | 0.54337 | 125.1986 | 126.21 | 0.0080 |
| $Na^{5+}$ | 11 | 0.09213 | 0.40853 | 0.47720 | 171.0695 | 172.18 | 0.0064 |
| $Mg^{6+}$ | 12 | 0.08435 | 0.37065 | 0.42534 | 223.9147 | 225.02 | 0.0049 |
| $Al^{7+}$ | 13 | 0.07778 | 0.33923 | 0.38365 | 283.7121 | 284.66 | 0.0033 |
| $Si^{8+}$ | 14 | 0.07216 | 0.31274 | 0.34942 | 350.4480 | 351.12 | 0.0019 |
| $P^{9+}$ | 15 | 0.06730 | 0.29010 | 0.32081 | 424.1135 | 424.4 | 0.0007 |
| $S^{10+}$ | 16 | 0.06306 | 0.27053 | 0.29654 | 504.7024 | 504.8 | 0.0002 |
| $Cl^{11+}$ | 17 | 0.05932 | 0.25344 | 0.27570 | 592.2103 | 591.99 | -0.0004 |
| $Ar^{12+}$ | 18 | 0.05599 | 0.23839 | 0.25760 | 686.6340 | 686.1 | -0.0008 |
| $K^{13+}$ | 19 | 0.05302 | 0.22503 | 0.24174 | 787.9710 | 786.6 | -0.0017 |
| $Ca^{14+}$ | 20 | 0.05035 | 0.21308 | 0.22772 | 896.2196 | 894.5 | -0.0019 |
| $Sc^{15+}$ | 21 | 0.04794 | 0.20235 | 0.21524 | 1011.3782 | 1009 | -0.0024 |
| $Ti^{16+}$ | 22 | 0.04574 | 0.19264 | 0.20407 | 1133.4456 | 1131 | -0.0022 |
| $V^{17+}$ | 23 | 0.04374 | 0.18383 | 0.19400 | 1262.4210 | 1260 | -0.0019 |
| $Cr^{18+}$ | 24 | 0.04191 | 0.17579 | 0.18487 | 1398.3036 | 1396 | -0.0017 |
| $Mn^{19+}$ | 25 | 0.04022 | 0.16842 | 0.17657 | 1541.0927 | 1539 | -0.0014 |
| $Fe^{20+}$ | 26 | 0.03867 | 0.16165 | 0.16899 | 1690.7878 | 1689 | -0.0011 |
| $Co^{21+}$ | 27 | 0.03723 | 0.15540 | 0.16203 | 1847.3885 | 1846 | -0.0008 |
| $Ni^{22+}$ | 28 | 0.03589 | 0.14961 | 0.15562 | 2010.8944 | 2011 | 0.0001 |
| $Cu^{23+}$ | 29 | 0.03465 | 0.14424 | 0.14970 | 2181.3053 | 2182 | 0.0003 |

[a] Radius of the first set of paired inner electrons of six-electron atoms from Eq. (10.51).

[b] Radius of the second set of paired inner electrons of six-electron atoms from Eq. (10.62).

[c] Radius of the two unpaired outer electrons of six-electron atoms from Eq. (10.132) for $Z > 6$ and Eq. (10.122) for $C$.

[d] Calculated ionization energies of six-electron atoms given by the electric energy (Eq. (10.133)).
[e] From theoretical calculations, interpolation of isoelectronic and spectral series, and experimental data [2-3].
[f] (Experimental-theoretical)/experimental.

The agreement between the experimental and calculated values of Table 10.4 is well within the experimental capability of the spectroscopic determinations including the values at large Z which relies on X-ray spectroscopy. In this case, the experimental capability is three to four significant figures which is consistent with the last column. The carbon atom isoelectronic series is given in Table 10.4 [2-3] to much higher precision than the capability of X-ray spectroscopy, but these values are based on theoretical and interpolation techniques rather than data alone. Ionization energies are difficult to determine since the cut-off of the Rydberg series of lines at the ionization energy is often not observed, and the ionization energy must be determined from theoretical calculations, interpolation of C isoelectronic and Rydberg series, as well as direct experimental data.

## SEVEN-ELECTRON ATOMS

Seven-electron atoms can be solved exactly using the results of the solutions of one, two, three, four, five, and six-electron atoms.

### RADIUS AND IONIZATION ENERGY OF THE OUTER ELECTRON OF THE NITROGEN ATOM

For each six-electron atom having a central charge of $Z$ times that of the proton, there are two indistinguishable spin-paired electrons in an atomic orbital with radii $r_1$ and $r_2$ both given by Eq. (7.35) (Eq. (10.51)), two indistinguishable spin-paired electrons in an atomic orbital with radii $r_3$ and $r_4$ both given by Eq. (10.62), and two unpaired electrons in an atomic orbital at $r_6$ given by Eq. (10.132). For $Z \geq 7$, the next electron which binds to form the corresponding seven-electron atom is attracted by the central Coulomb field and is repelled by diamagnetic force due to the spin-paired inner electrons. A paramagnetic spin-pairing force is also possible, but the force due to the spin-pairing of the electrons (Eq. (7.24) with the radius $r_7$) reduces the energy of the atom less than that due to the alternative forces on three unpaired p electrons in an atomic orbital at the same radius $r_7$. The resulting electron configuration is $1s^2 2s^2 2p^3$, and the orbital arrangement is:

2p state

$$\begin{array}{ccc} \uparrow & \uparrow & \uparrow \\ \underline{\quad} & \underline{\quad} & \underline{\quad} \\ 1 & 0 & -1 \end{array} \tag{10.134}$$

corresponding to the ground state ${}^4S^0_{3/2}$.

The central Coulomb force acts on the outer electron to cause it to bind wherein this electric force on the outer-most electron due to the nucleus and the inner six electrons is given by Eq. (10.70) with the appropriate charge and radius:

$$\mathbf{F}_{ele} = \frac{(Z-6)e^2}{4\pi\varepsilon_0 r_7^2}\mathbf{i}_\mathbf{r} \tag{10.135}$$

for $r > r_6$.

The energy is minimized with conservation of angular momentum when the angular momenta of the two orthogonal $p_x$ and $p_y$ electrons cancel such that the diamagnetic force (Eq. (10.82)), $\mathbf{F}_{diamagnetic}$, is:

$$\mathbf{F}_{diamagnetic} = -\left(\frac{1}{3}\right)\frac{\hbar^2}{4m_e r_7^2 r_3}\sqrt{s(s+1)}\mathbf{i}_\mathbf{r} \tag{10.136}$$

corresponding to $m = 0$.

From Eq. (10.89), $\mathbf{F}_{mag\ 2}$ corresponding to the orbital angular momentum of the $p_z$ electron is:

$$\mathbf{F}_{mag\ 2} = \frac{1}{Z}\frac{\hbar^2}{m_e r_7^2 r_3}\sqrt{s(s+1)}\mathbf{i}_\mathbf{r} \tag{10.137}$$

The outward centrifugal force on electron 7 is balanced by the electric force and the magnetic forces (on electron 7). The radius of the outer electron is calculated by equating the outward centrifugal force to the sum of the electric (Eq. (10.135)), diamagnetic (Eq. (10.136)), and paramagnetic (Eq. (10.137)) forces as follows:

$$\frac{m_e v_7^2}{r_7} = \frac{(Z-6)e^2}{4\pi\varepsilon_0 r_7^2} - \frac{\hbar^2}{12m_e r_7^2 r_3}\sqrt{s(s+1)} + \frac{\hbar^2}{Zm_e r_7^2 r_3}\sqrt{s(s+1)} \tag{10.138}$$

Substitution of $v_7 = \frac{\hbar}{m_e r_7}$ (Eq. (1.35)) and $s = \frac{1}{2}$ into Eq. (10.138) gives:

$$\frac{\hbar^2}{m_e r_7^3} = \frac{(Z-6)e^2}{4\pi\varepsilon_0 r_7^2} - \frac{\hbar^2}{12m_e r_7^2 r_3}\sqrt{\frac{3}{4}} + \frac{\hbar^2}{Zm_e r_7^2 r_3}\sqrt{\frac{3}{4}} \tag{10.139}$$

$$r_7 = \frac{\frac{\hbar^2}{m_e}}{\frac{(Z-6)e^2}{4\pi\varepsilon_0} - \frac{\hbar^2}{12m_e r_3}\sqrt{\frac{3}{4}} + \frac{\hbar^2}{Zm_e r_3}\sqrt{\frac{3}{4}}} \tag{10.140}$$

$$r_7 = \frac{a_0}{(Z-6) - \left(\frac{1}{12} - \frac{1}{Z}\right)\frac{\sqrt{\frac{3}{4}}}{r_3}},\ r_3 \text{ in units of } a_0 \tag{10.141}$$

Substitution of $\frac{r_3}{a_0} = 0.69385$ (Eq. (10.62) with $Z = 7$) into Eq. (10.141) gives:

$$r_7 = 0.93084 a_0 \tag{10.142}$$

The ionization energy of the nitrogen atom is given by the electric energy, $E(electric)$, (Eq. (10.102) with the radius, $r_7$, given by Eq. (10.142)):

$$E(ionization;\ N) = -Electric\ Energy = \frac{(Z-6)e^2}{8\pi\varepsilon_0 r_7} = 14.61664\ eV \tag{10.143}$$

where $r_7 = 0.93084 a_0$ (Eq. (10.142)) and $Z = 7$. The experimental ionization energy of the nitrogen atom is 14.53414 $eV$ [3].

## THE IONIZATION ENERGIES OF SEVEN-ELECTRON ATOMS WITH A NUCLEAR CHARGE Z>7

Seven-electron atoms having $Z > 7$ possess an external electric field given by Eq. (10.92). In this case, an energy minimum is achieved with conservation of momentum when the orbital angular momentum is such that $\mathbf{F}_{diamagnetic}$ is minimized while $\mathbf{F}_{mag\ 2}$ is maximized. From Eq. (10.82), the diamagnetic force, $\mathbf{F}_{diamagnetic}$, is given by the sum of the contributions from the $p_x$, $p_y$, and $p_z$ orbitals corresponding to $m$ = 1, -1, and 0, respectively:

$$\mathbf{F}_{diamagnetic} = -\left(\frac{2}{3} + \frac{2}{3} + \frac{1}{3}\right)\frac{\hbar^2}{4m_e r_7^2 r_3}\sqrt{s(s+1)}\mathbf{i}_\mathbf{r} = -\left(\frac{5}{3}\right)\frac{\hbar^2}{4m_e r_7^2 r_3}\sqrt{s(s+1)}\mathbf{i}_\mathbf{r} \tag{10.144}$$

With $Z > 6$, the charge induction forms complementary mirror charge-density waves such that the angular momenta do not cancel. From Eq. (10.89), $\mathbf{F}_{mag\ 2}$ corresponding to the orbital angular momentum of the three p electrons in addition complementary charge-density waves is

$$\mathbf{F}_{mag\ 2} = 2\frac{1}{Z}\frac{3\hbar^2}{m_e r_7^2 r_3}\sqrt{s(s+1)}\mathbf{i}_\mathbf{r} \tag{10.145}$$

The second diamagnetic force, $\mathbf{F}_{diamagnetic\ 2}$, due to the binding of the p-orbital electron having an electric field outside of its radius is given by Eq. (10.93):

$$\mathbf{F}_{diamagnetic\ 2} = -\left[\frac{Z-7}{Z-6}\right]\left(1 - \frac{\sqrt{2}}{2}\right)\frac{r_3\hbar^2}{m_e r_7^4}10\sqrt{s(s+1)}\mathbf{i}_\mathbf{r} \tag{10.146}$$

In the case that $Z > 7$, the radius of the outer electron is calculated by equating the outward centrifugal force to the sum of the electric (Eq. (10.135)), diamagnetic (Eqs. (10.10.144) and (10.146)), and paramagnetic (Eq. (10.145)) forces as follows:

$$\frac{m_e v_7^2}{r_7} = \frac{(Z-6)e^2}{4\pi\varepsilon_0 r_7^2} - \frac{5\hbar^2}{12m_e r_7^2 r_3}\sqrt{s(s+1)} + \frac{6\hbar^2}{Zm_e r_7^2 r_3}\sqrt{s(s+1)} - \left[\frac{Z-7}{Z-6}\right]\left(1 - \frac{\sqrt{2}}{2}\right)\frac{r_3\hbar^2}{m_e r_7^4}10\sqrt{s(s+1)} \tag{10.147}$$

Substitution of $v_7 = \frac{\hbar}{m_e r_7}$ (Eq. (1.35)) and $s = \frac{1}{2}$ into Eq. (10.147) gives:

$$\frac{\hbar^2}{m_e r_7^3} = \frac{(Z-6)e^2}{4\pi\varepsilon_0 r_7^2} - \frac{5\hbar^2}{12m_e r_7^2 r_3}\sqrt{\frac{3}{4}} + \frac{6\hbar^2}{Zm_e r_7^2 r_3}\sqrt{\frac{3}{4}} - \left[\frac{Z-7}{Z-6}\right]\left(1 - \frac{\sqrt{2}}{2}\right)\frac{r_3\hbar^2}{r_7^4 m_e}10\sqrt{\frac{3}{4}} \tag{10.148}$$

The quadratic equation corresponding to Eq. (10.148) is

$$\left(\frac{(Z-6)e^2}{4\pi\varepsilon_0} - \left(\frac{5}{12} - \frac{6}{Z}\right)\frac{\hbar^2}{m_e r_3}\sqrt{\frac{3}{4}}\right)r_7^2 - \frac{\hbar^2}{m_e}r_7 - \left[\frac{Z-7}{Z-6}\right]\left(1 - \frac{\sqrt{2}}{2}\right)\frac{r_3\hbar^2}{m_e}10\sqrt{\frac{3}{4}} = 0 \tag{10.149}$$

$$r_7^2 - \frac{\frac{\hbar^2}{m_e}}{\left(\frac{(Z-6)e^2}{4\pi\varepsilon_0} - \left(\frac{5}{12} - \frac{6}{Z}\right)\frac{\hbar^2}{m_e r_3}\sqrt{\frac{3}{4}}\right)}r_7 - \frac{\frac{\hbar^2}{m_e}\left[\frac{Z-7}{Z-6}\right]\left(1 - \frac{\sqrt{2}}{2}\right)r_3 10\sqrt{\frac{3}{4}}}{\left(\frac{(Z-6)e^2}{4\pi\varepsilon_0} - \left(\frac{5}{12} - \frac{6}{Z}\right)\frac{\hbar^2}{m_e r_3}\sqrt{\frac{3}{4}}\right)} = 0 \tag{10.150}$$

The solution of Eq. (10.150) using the quadratic formula is:

$$r_7 = \frac{\dfrac{\dfrac{\hbar^2}{m_e}}{\left(\dfrac{(Z-6)e^2}{4\pi\varepsilon_0} - \left(\dfrac{5}{12} - \dfrac{6}{Z}\right)\dfrac{\hbar^2}{m_e r_3}\sqrt{\dfrac{3}{4}}\right)} \pm \sqrt{\left(\dfrac{\dfrac{\hbar^2}{m_e}}{\left(\dfrac{(Z-6)e^2}{4\pi\varepsilon_0} - \left(\dfrac{5}{12} - \dfrac{6}{Z}\right)\dfrac{\hbar^2}{m_e r_3}\sqrt{\dfrac{3}{4}}\right)}\right)^2 + 4\dfrac{\dfrac{\hbar^2}{m_e}\left[\dfrac{Z-7}{Z-6}\right]\left(1-\dfrac{\sqrt{2}}{2}\right)r_3 10\sqrt{\dfrac{3}{4}}}{\left(\dfrac{(Z-6)e^2}{4\pi\varepsilon_0} - \left(\dfrac{5}{12} - \dfrac{6}{Z}\right)\dfrac{\hbar^2}{m_e r_3}\sqrt{\dfrac{3}{4}}\right)}}}{2} \tag{10.151}$$

$$r_7 = \frac{\dfrac{a_0}{\left((Z-6) - \left(\dfrac{5}{24} - \dfrac{3}{Z}\right)\dfrac{\sqrt{3}}{r_3}\right)} \pm a_0\sqrt{\left(\dfrac{1}{\left((Z-6) - \left(\dfrac{5}{24} - \dfrac{3}{Z}\right)\dfrac{\sqrt{3}}{r_3}\right)}\right)^2 + \dfrac{20\sqrt{3}\left(\left[\dfrac{Z-7}{Z-6}\right]\left(1-\dfrac{\sqrt{2}}{2}\right)r_3\right)}{\left((Z-6) - \left(\dfrac{5}{24} - \dfrac{3}{Z}\right)\dfrac{\sqrt{3}}{r_3}\right)}}}{2}, \; r_3 \text{ in units of } a_0 \tag{10.152}$$

where $r_3$ is given by Eq. (10.62). The positive root of Eq. (10.152) must be taken in order that $r_7 > 0$. The final radius of electron 7, $r_7$, is given by Eq. (10.152); this is also the final radius of electrons 5 and 6. The radii of several seven-electron atoms are given in Table 10.5.

The ionization energies for the seven-electron atoms with $Z > 7$ are given by the electric energy, $E(electric)$, (Eq. (10.102) with the radii, $r_7$, given by Eq. (10.152)):

$$E(Ionization) = -Electric\ Energy = \frac{(Z-6)e^2}{8\pi\varepsilon_0 r_7} \tag{10.153}$$

Since the relativistic corrections were small, the nonrelativistic ionization energies for experimentally measured seven-electron atoms are given in Table 10.5.

**Table 10.5.** Ionization energies for some seven-electron atoms.

| 7 e Atom | Z | $r_1$ $(a_0)$ [a] | $r_3$ $(a_0)$ [b] | $r_7$ $(a_0)$ [c] | Theoretical Ionization Energies [d] $(eV)$ | Experimental Ionization Energies [e] $(eV)$ | Relative Error [f] |
|---|---|---|---|---|---|---|---|
| $N$ | 7 | 0.14605 | 0.69385 | 0.93084 | 14.61664 | 14.53414 | -0.0057 |
| $O^{+}$ | 8 | 0.12739 | 0.59020 | 0.78489 | 34.6694 | 35.1173 | 0.0128 |
| $F^{2+}$ | 9 | 0.11297 | 0.51382 | 0.67084 | 60.8448 | 62.7084 | 0.0297 |
| $Ne^{3+}$ | 10 | 0.10149 | 0.45511 | 0.57574 | 94.5279 | 97.12 | 0.0267 |
| $Na^{4+}$ | 11 | 0.09213 | 0.40853 | 0.50250 | 135.3798 | 138.4 | 0.0218 |
| $Mg^{5+}$ | 12 | 0.08435 | 0.37065 | 0.44539 | 183.2888 | 186.76 | 0.0186 |
| $Al^{6+}$ | 13 | 0.07778 | 0.33923 | 0.39983 | 238.2017 | 241.76 | 0.0147 |
| $Si^{7+}$ | 14 | 0.07216 | 0.31274 | 0.36271 | 300.0883 | 303.54 | 0.0114 |
| $P^{8+}$ | 15 | 0.06730 | 0.29010 | 0.33191 | 368.9298 | 372.13 | 0.0086 |
| $S^{9+}$ | 16 | 0.06306 | 0.27053 | 0.30595 | 444.7137 | 447.5 | 0.0062 |
| $Cl^{10+}$ | 17 | 0.05932 | 0.25344 | 0.28376 | 527.4312 | 529.28 | 0.0035 |
| $Ar^{11+}$ | 18 | 0.05599 | 0.23839 | 0.26459 | 617.0761 | 618.26 | 0.0019 |
| $K^{12+}$ | 19 | 0.05302 | 0.22503 | 0.24785 | 713.6436 | 714.6 | 0.0013 |
| $Ca^{13+}$ | 20 | 0.05035 | 0.21308 | 0.23311 | 817.1303 | 817.6 | 0.0006 |
| $Sc^{14+}$ | 21 | 0.04794 | 0.20235 | 0.22003 | 927.5333 | 927.5 | 0.0000 |
| $Ti^{15+}$ | 22 | 0.04574 | 0.19264 | 0.20835 | 1044.8504 | 1044 | -0.0008 |
| $V^{16+}$ | 23 | 0.04374 | 0.18383 | 0.19785 | 1169.0800 | 1168 | -0.0009 |
| $Cr^{17+}$ | 24 | 0.04191 | 0.17579 | 0.18836 | 1300.2206 | 1299 | -0.0009 |
| $Mn^{18+}$ | 25 | 0.04022 | 0.16842 | 0.17974 | 1438.2710 | 1437 | -0.0009 |
| $Fe^{19+}$ | 26 | 0.03867 | 0.16165 | 0.17187 | 1583.2303 | 1582 | -0.0008 |
| $Co^{20+}$ | 27 | 0.03723 | 0.15540 | 0.16467 | 1735.0978 | 1735 | -0.0001 |
| $Ni^{21+}$ | 28 | 0.03589 | 0.14961 | 0.15805 | 1893.8726 | 1894 | 0.0001 |
| $Cu^{22+}$ | 29 | 0.03465 | 0.14424 | 0.15194 | 2059.5543 | 2060 | 0.0002 |

[a] Radius of the first set of paired inner electrons of seven-electron atoms from Eq. (10.51).

[b] Radius of the second set of paired inner electrons of seven-electron atoms from Eq. (10.62).

[c] Radius of the three unpaired paired outer electrons of seven-electron atoms from Eq. (10.152) for $Z > 7$ and Eq. (10.142) for $N$.

[d] Calculated ionization energies of seven-electron atoms given by the electric energy (Eq. (10.153)).

[e] From theoretical calculations, interpolation of isoelectronic and spectral series, and experimental data [2-3].

[f] (Experimental-theoretical)/experimental.

The agreement between the experimental and calculated values of Table 10.5 is well within the experimental capability of the spectroscopic determinations including the values at large Z which relies on X-ray spectroscopy. In this case, the experimental capability is three to four significant figures which is consistent with the last column. The nitrogen atom isoelectronic series is given in Table 10.5 [2-3] to much higher precision than the capability of X-ray spectroscopy, but these values are based on theoretical and interpolation techniques rather than data alone. Ionization energies are difficult to determine since the cut-off of the Rydberg series of lines at the ionization energy is often not observed, and the ionization energy must be determined from theoretical calculations, interpolation of N isoelectronic and Rydberg series, as well as direct experimental data.

## EIGHT-ELECTRON ATOMS

Eight-electron atoms can be solved exactly using the results of the solutions of one, two, three, four, five, six, and seven-electron atoms.

## RADIUS AND IONIZATION ENERGY OF THE OUTER ELECTRON OF THE OXYGEN ATOM

For each seven-electron atom having a central charge of $Z$ times that of the proton, there are two indistinguishable spin-paired electrons in an atomic orbital with radii $r_1$ and $r_2$ both given by Eq. (7.35) (Eq. (10.51)), two indistinguishable spin-paired electrons in an atomic orbital with radii $r_3$ and $r_4$ both given by Eq. (10.62), and three unpaired electrons in an atomic orbital at $r_7$ given by Eq. (10.152). For $Z \geq 8$, the next electron which binds to form the corresponding eight-electron atom is attracted by the central Coulomb field and is repelled by diamagnetic force due to the spin-paired inner electrons. A paramagnetic spin-pairing force that results in the formation of a filled s orbital is also possible, but the force due to the spin-pairing of the electrons (Eq. (7.24) with the radius $r_8$) reduces the energy of the atom less than that due to the alternative forces on two paired electrons in a $p_x$ orbital and two unpaired electrons in $p_y$ and $p_z$ orbitals of an atomic orbital at the same radius $r_8$. The resulting electron configuration is $1s^2 2s^2 2p^4$, and the orbital arrangement is:

| 2p state | | |
|---|---|---|
| $\uparrow\downarrow$ | $\uparrow$ | $\uparrow$ |
| 1 | 0 | -1 |

(10.154)

corresponding to the ground state ${}^3P_2$.

The central Coulomb force acts on the outer electron to cause it to bind wherein this electric force on the outer-most electron due to the nucleus and the inner seven electrons is given by Eq. (10.70) with the appropriate charge and radius:

$$\mathbf{F}_{ele} = \frac{(Z-7)e^2}{4\pi\varepsilon_0 r_8^2}\mathbf{i}_\mathbf{r} \tag{10.155}$$

for $r > r_7$.

The energy is minimized with conservation of angular momentum by the cancellation of the orbital angular momentum of a $p_x$ electron by that of the $p_y$ electron with the pairing of electron eight to fill the $p_x$ orbital. Then, the diamagnetic force is that of $N$ given by Eq. (10.136) corresponding to the $p_z$-orbital electron (Eq. (10.82) with $m = 0$) as the source of diamagnetism with an additional contribution from the uncanceled $p_x$ electron (Eq. (10.82) with $m = 1$). $\mathbf{F}_{diamagnetic}$ for the oxygen atom is:

$$\mathbf{F}_{diamagnetic} = -\left(\frac{1}{3}+\frac{2}{3}\right)\frac{\hbar^2}{4m_e r_8^2 r_3}\sqrt{s(s+1)}\mathbf{i}_\mathbf{r} = -\frac{\hbar^2}{4m_e r_8^2 r_3}\sqrt{s(s+1)}\mathbf{i}_\mathbf{r} \tag{10.156}$$

From Eqs. (10.83) and (10.89), $\mathbf{F}_{mag\ 2}$ is

$$\mathbf{F}_{mag\ 2} = (1+1)\frac{1}{Z}\frac{\hbar^2}{m_e r_8^2 r_3}\sqrt{s(s+1)}\mathbf{i}_\mathbf{r} = \frac{1}{Z}\frac{2\hbar^2}{m_e r_8^2 r_3}\sqrt{s(s+1)}\mathbf{i}_\mathbf{r} \tag{10.157}$$

corresponding to the spin-angular-momentum contribution alone of the $p_x$ electron and the orbital angular momentum of the $p_z$ electron, respectively.

The outward centrifugal force on electron 8 is balanced by the electric force and the magnetic forces (on electron 8). The radius of the outer electron is calculated by equating the outward centrifugal force to the sum of the electric (Eq. (10.155)), diamagnetic (Eq. (10.156)), and paramagnetic (Eq. (10.157)) forces as follows:

$$\frac{m_e v_8^2}{r_8} = \frac{(Z-7)e^2}{4\pi\varepsilon_0 r_8^2} - \frac{\hbar^2}{4m_e r_8^2 r_3}\sqrt{s(s+1)} + \frac{2\hbar^2}{Zm_e r_8^2 r_3}\sqrt{s(s+1)} \tag{10.158}$$

Substitution of $v_8 = \frac{\hbar}{m_e r_8}$ (Eq. (1.35)) and $s = \frac{1}{2}$ into Eq. (10.158) gives:

$$\frac{\hbar^2}{m_e r_8^3} = \frac{(Z-7)e^2}{4\pi\varepsilon_0 r_8^2} - \frac{\hbar^2}{4m_e r_8^2 r_3}\sqrt{\frac{3}{4}} + \frac{2\hbar^2}{Zm_e r_8^2 r_3}\sqrt{\frac{3}{4}} \tag{10.159}$$

$$r_8 = \frac{\frac{\hbar^2}{m_e}}{\frac{(Z-7)e^2}{4\pi\varepsilon_0} - \frac{\hbar^2}{4m_e r_3}\sqrt{\frac{3}{4}} + \frac{2\hbar^2}{Zm_e r_3}\sqrt{\frac{3}{4}}} \tag{10.160}$$

$$r_8 = \frac{a_0}{(Z-7)-\left(\frac{1}{4}-\frac{2}{Z}\right)\frac{\sqrt{\frac{3}{4}}}{r_3}},\ r_3 \text{ in units of } a_0 \tag{10.161}$$

Substitution of $\frac{r_3}{a_0} = 0.59020$ (Eq. (10.62) with $Z = 8$) into Eq. (10.161) gives:

$$r_8 = a_0 \tag{10.162}$$

The ionization energy of the oxygen atom is given by the negative of $E(electric)$ given by Eq. (10.102) with the appropriate charge and radius:

$$E(ionization;\ O) = -Electric\ Energy = \frac{(Z-7)e^2}{8\pi\varepsilon_0 r_8} = 13.60580\ eV \tag{10.163}$$

where $r_8 = a_0$ (Eq. (10.162)) and $Z = 8$. The experimental ionization energy of the oxygen atom is 13.6181 $eV$ [3].

## THE IONIZATION ENERGIES OF EIGHT-ELECTRON ATOMS WITH A NUCLEAR CHARGE Z>8

Eight-electron atoms having $Z > 8$ possess an external electric field given by Eq. (10.92). In this case, an energy minimum is achieved with conservation of momentum when the orbital angular momentum is such that $\mathbf{F}_{diamagnetic}$ is minimized while $\mathbf{F}_{mag\ 2}$ is maximized. From Eq. (10.82), the diamagnetic force, $\mathbf{F}_{diamagnetic}$, is given by the sum of the contributions from the $p_x$, $p_y$, and $p_z$ orbitals corresponding to $m$ = 1, -1, and 0, respectively:

$$\mathbf{F}_{diamagnetic} = -\left(\frac{2}{3}+\frac{2}{3}+\frac{1}{3}\right)\frac{\hbar^2}{4m_e r_8^2 r_3}\sqrt{s(s+1)}\mathbf{i}_\mathbf{r} = -\left(\frac{5}{3}\right)\frac{\hbar^2}{4m_e r_8^2 r_3}\sqrt{s(s+1)}\mathbf{i}_\mathbf{r} \tag{10.164}$$

The filled p orbitals with the maintenance of symmetry according to Eq. (10.72) requires that the diamagnetic force is only due to the electrons at $r_3$. From Eqs. (10.84) and (10.89), $\mathbf{F}_{mag\ 2}$ is:

$$\mathbf{F}_{mag\ 2} = (4+1+1)\frac{1}{Z}\frac{\hbar^2}{m_e r_8^2 r_3}\sqrt{s(s+1)}\mathbf{i}_\mathbf{r} = \frac{1}{Z}\frac{6\hbar^2}{m_e r_8^2 r_3}\sqrt{s(s+1)}\mathbf{i}_\mathbf{r} \tag{10.165}$$

corresponding to the spin and orbital angular momenta of the paired $p_x$ electrons and the orbital angular momentum of each of the $p_y$ and $p_z$ electrons, respectively.

The second diamagnetic force, $\mathbf{F}_{diamagnetic\ 2}$, due to the binding of the p-orbital electron having an electric field outside of its radius is given by Eq. (10.93).

$$\mathbf{F}_{diamagnetic\ 2} = -\left[\frac{Z-8}{Z-7}\right]\left(1-\frac{\sqrt{2}}{2}\right)\frac{r_3\hbar^2}{m_e r_8^4}10\sqrt{s(s+1)}\mathbf{i}_\mathbf{r} \tag{10.166}$$

In the case that $Z > 8$, the radius of the outer electron is calculated by equating the outward centrifugal force to the sum of the electric (Eq. (10.155)), diamagnetic (Eqs. (10.164) and (10.166)), and paramagnetic (Eq. (10.165)) forces as follows:

$$\frac{m_e v_8^2}{r_8} = \frac{(Z-7)e^2}{4\pi\varepsilon_0 r_8^2} - \frac{5\hbar^2}{12m_e r_8^2 r_3}\sqrt{s(s+1)} + \frac{6\hbar^2}{Zm_e r_8^2 r_3}\sqrt{s(s+1)} - \left[\frac{Z-8}{Z-7}\right]\left(1-\frac{\sqrt{2}}{2}\right)\frac{r_3\hbar^2}{m_e r_8^4}10\sqrt{s(s+1)} \tag{10.167}$$

Substitution of $v_8 = \frac{\hbar}{m_e r_8}$ (Eq. (1.35)) and $s = \frac{1}{2}$ into Eq. (10.167) gives:

$$\frac{\hbar^2}{m_e r_8^3} = \frac{(Z-7)e^2}{4\pi\varepsilon_0 r_8^2} - \frac{5\hbar^2}{12m_e r_8^2 r_3}\sqrt{\frac{3}{4}} + \frac{6\hbar^2}{Zm_e r_8^2 r_3}\sqrt{\frac{3}{4}} - \left[\frac{Z-8}{Z-7}\right]\left(1-\frac{\sqrt{2}}{2}\right)\frac{r_3\hbar^2}{r_8^4 m_e}10\sqrt{\frac{3}{4}} \tag{10.168}$$

The quadratic equation corresponding to Eq. (10.168) is

$$\left(\frac{(Z-7)e^2}{4\pi\varepsilon_0} - \left(\frac{5}{12}-\frac{6}{Z}\right)\frac{\hbar^2}{m_e r_3}\sqrt{\frac{3}{4}}\right)r_8^2 - \frac{\hbar^2}{m_e}r_8 - \left[\frac{Z-8}{Z-7}\right]\left(1-\frac{\sqrt{2}}{2}\right)\frac{r_3\hbar^2}{m_e}10\sqrt{\frac{3}{4}} = 0 \tag{10.169}$$

$$r_8^2 - \frac{\frac{\hbar^2}{m_e}}{\left(\frac{(Z-7)e^2}{4\pi\varepsilon_0} - \left(\frac{5}{12}-\frac{6}{Z}\right)\frac{\hbar^2}{m_e r_3}\sqrt{\frac{3}{4}}\right)}r_8 - \frac{\frac{\hbar^2}{m_e}\left[\frac{Z-8}{Z-7}\right]\left(1-\frac{\sqrt{2}}{2}\right)r_3 10\sqrt{\frac{3}{4}}}{\left(\frac{(Z-7)e^2}{4\pi\varepsilon_0} - \left(\frac{5}{12}-\frac{6}{Z}\right)\frac{\hbar^2}{m_e r_3}\sqrt{\frac{3}{4}}\right)} = 0 \tag{10.170}$$

The solution of Eq. (10.170) using the quadratic formula is:

$$r_8 = \frac{\dfrac{\dfrac{\hbar^2}{m_e}}{\left(\dfrac{(Z-7)e^2}{4\pi\varepsilon_0} - \left(\dfrac{5}{12} - \dfrac{6}{Z}\right)\dfrac{\hbar^2}{m_e r_3}\sqrt{\dfrac{3}{4}}\right)} \pm \sqrt{\left(\dfrac{\dfrac{\hbar^2}{m_e}}{\left(\dfrac{(Z-7)e^2}{4\pi\varepsilon_0} - \left(\dfrac{5}{12} - \dfrac{6}{Z}\right)\dfrac{\hbar^2}{m_e r_3}\sqrt{\dfrac{3}{4}}\right)}\right)^2 + 4\dfrac{\dfrac{\hbar^2}{m_e}\left[\dfrac{Z-8}{Z-7}\right]\left(1-\dfrac{\sqrt{2}}{2}\right)r_3 10\sqrt{\dfrac{3}{4}}}{\left(\dfrac{(Z-7)e^2}{4\pi\varepsilon_0} - \left(\dfrac{5}{12} - \dfrac{6}{Z}\right)\dfrac{\hbar^2}{m_e r_3}\sqrt{\dfrac{3}{4}}\right)}}}{2} \tag{10.171}$$

$$r_8 = \frac{\dfrac{a_0}{\left((Z-7) - \left(\dfrac{5}{24} - \dfrac{3}{Z}\right)\dfrac{\sqrt{3}}{r_3}\right)} \pm a_0\sqrt{\left(\dfrac{1}{\left((Z-7) - \left(\dfrac{5}{24} - \dfrac{3}{Z}\right)\dfrac{\sqrt{3}}{r_3}\right)}\right)^2 + \dfrac{20\sqrt{3}\left(\left[\dfrac{Z-8}{Z-7}\right]\left(1-\dfrac{\sqrt{2}}{2}\right)r_3\right)}{\left((Z-7) - \left(\dfrac{5}{24} - \dfrac{3}{Z}\right)\dfrac{\sqrt{3}}{r_3}\right)}}}{2}, \; r_3 \text{ in units of } a_0 \tag{10.172}$$

where $r_3$ is given by Eq. (10.62). The positive root of Eq. (10.172) must be taken in order that $r_8 > 0$. The final radius of electron 8, $r_8$, is given by Eq. (10.172); this is also the final radius of electrons 5, 6, and 7. The radii of several eight-electron atoms are given in Table 10.6.

The ionization energies for the eight-electron atoms with $Z > 8$ are given by the electric energy, $E(electric)$, (Eq. (10.102) with the radii, $r_8$, given by Eq. (10.172)):

$$E(Ionization) = -Electric\ Energy = \frac{(Z-7)e^2}{8\pi\varepsilon_0 r_8} \tag{10.173}$$

Since the relativistic corrections were small, the nonrelativistic ionization energies for experimentally measured eight-electron atoms are given in Table 10.6.

**Table 10.6.** Ionization energies for some eight-electron atoms.

| 8 e Atom | Z | $r_1$ $(a_0)$ [a] | $r_3$ $(a_0)$ [b] | $r_8$ $(a_0)$ [c] | Theoretical Ionization Energies [d] $(eV)$ | Experimental Ionization Energies [e] $(eV)$ | Relative Error [f] |
|---|---|---|---|---|---|---|---|
| $O$ | 8 | 0.12739 | 0.59020 | 1.00000 | 13.60580 | 13.6181 | 0.0009 |
| $F^{+}$ | 9 | 0.11297 | 0.51382 | 0.7649 | 35.5773 | 34.9708 | -0.0173 |
| $Ne^{2+}$ | 10 | 0.10149 | 0.45511 | 0.6514 | 62.6611 | 63.45 | 0.0124 |
| $Na^{3+}$ | 11 | 0.09213 | 0.40853 | 0.5592 | 97.3147 | 98.91 | 0.0161 |
| $Mg^{4+}$ | 12 | 0.08435 | 0.37065 | 0.4887 | 139.1911 | 141.27 | 0.0147 |
| $Al^{5+}$ | 13 | 0.07778 | 0.33923 | 0.4338 | 188.1652 | 190.49 | 0.0122 |
| $Si^{6+}$ | 14 | 0.07216 | 0.31274 | 0.3901 | 244.1735 | 246.5 | 0.0094 |
| $P^{7+}$ | 15 | 0.06730 | 0.29010 | 0.3543 | 307.1791 | 309.6 | 0.0078 |
| $S^{8+}$ | 16 | 0.06306 | 0.27053 | 0.3247 | 377.1579 | 379.55 | 0.0063 |
| $Cl^{9+}$ | 17 | 0.05932 | 0.25344 | 0.2996 | 454.0940 | 455.63 | 0.0034 |
| $Ar^{10+}$ | 18 | 0.05599 | 0.23839 | 0.2782 | 537.9756 | 538.96 | 0.0018 |
| $K^{11+}$ | 19 | 0.05302 | 0.22503 | 0.2597 | 628.7944 | 629.4 | 0.0010 |
| $Ca^{12+}$ | 20 | 0.05035 | 0.21308 | 0.2434 | 726.5442 | 726.6 | 0.0001 |
| $Sc^{13+}$ | 21 | 0.04794 | 0.20235 | 0.2292 | 831.2199 | 830.8 | -0.0005 |
| $Ti^{14+}$ | 22 | 0.04574 | 0.19264 | 0.2165 | 942.8179 | 941.9 | -0.0010 |
| $V^{15+}$ | 23 | 0.04374 | 0.18383 | 0.2051 | 1061.3351 | 1060 | -0.0013 |
| $Cr^{16+}$ | 24 | 0.04191 | 0.17579 | 0.1949 | 1186.7691 | 1185 | -0.0015 |
| $Mn^{17+}$ | 25 | 0.04022 | 0.16842 | 0.1857 | 1319.1179 | 1317 | -0.0016 |
| $Fe^{18+}$ | 26 | 0.03867 | 0.16165 | 0.1773 | 1458.3799 | 1456 | -0.0016 |
| $Co^{19+}$ | 27 | 0.03723 | 0.15540 | 0.1696 | 1604.5538 | 1603 | -0.0010 |
| $Ni^{20+}$ | 28 | 0.03589 | 0.14961 | 0.1626 | 1757.6383 | 1756 | -0.0009 |
| $Cu^{21+}$ | 29 | 0.03465 | 0.14424 | 0.1561 | 1917.6326 | 1916 | -0.0009 |

[a] Radius of the first set of paired inner electrons of eight-electron atoms from Eq. (10.51).

[b] Radius of the second set of paired inner electrons of eight-electron atoms from Eq. (10.62).

[c] Radius of the two paired and two unpaired outer electrons of eight-electron atoms from Eq. (10.172) for $Z > 8$ and Eq. (10.162) for $O$.

[d] Calculated ionization energies of eight-electron atoms given by the electric energy (Eq. (10.173)).

[e] From theoretical calculations, interpolation of isoelectronic and spectral series, and experimental data [2-3].

[f] (Experimental-theoretical)/experimental.

The agreement between the experimental and calculated values of Table 10.6 is well within the experimental capability of the spectroscopic determinations including the values at large Z that relies on X-ray spectroscopy. In this case, the experimental capability is three to four significant figures which is consistent with the last column. The oxygen atom isoelectronic series is given in Table 10.6 [2-3] to much higher precision than the capability of X-ray spectroscopy, but these values are based on theoretical and interpolation techniques rather than data alone. Ionization energies are difficult to determine since the cut-off of the Rydberg series of lines at the ionization energy is often not observed, and the ionization energy must be determined from theoretical calculations, interpolation of O isoelectronic and Rydberg series, as well as direct experimental data.

## NINE-ELECTRON ATOMS

Nine-electron atoms can be solved exactly using the results of the solutions of one, two, three, four, five, six, seven, and eight-electron atoms.

## RADIUS AND IONIZATION ENERGY OF THE OUTER ELECTRON OF THE FLUORINE ATOM

For each eight-electron atom having a central charge of $Z$ times that of the proton, there are two indistinguishable spin-paired electrons in an atomic orbital with radii $r_1$ and $r_2$ both given by Eq. (7.35) (Eq. (10.51)), two indistinguishable spin-paired electrons in an atomic orbital with radii $r_3$ and $r_4$ both given by Eq. (10.62), and two paired and unpaired electrons in an atomic orbital at $r_8$ given by Eq. (10.172). For $Z \geq 9$, the next electron which binds to form the corresponding nine-electron atom is attracted by the central Coulomb field and is repelled by diamagnetic force due to the spin-paired inner electrons. A paramagnetic spin-pairing force that results in the formation of a filled s orbital is also possible, but the force due to the spin-pairing of the electrons (Eq. (7.24) with the radius $r_9$) reduces the energy of the atom less than that due to the alternative forces on an unpaired electron in a $p_y$ orbital and two pairs of electrons of opposite spin in $p_x$ and $p_z$ orbitals of an atomic orbital at the same radius $r_9$. The resulting electron configuration is $1s^2 2s^2 2p^5$, and the orbital arrangement is:

2p state

$$\underset{1}{\uparrow\downarrow} \quad \underset{0}{\uparrow\downarrow} \quad \underset{-1}{\uparrow} \tag{10.174}$$

corresponding to the ground state ${}^2P^0_{3/2}$.

The central Coulomb force acts on the outer electron to cause it to bind wherein this electric force on the outer-most electron due to the nucleus and the inner eight electrons is given by Eq. (10.70) with the appropriate charge and radius:

$$\mathbf{F}_{ele} = \frac{(Z-8)e^2}{4\pi\varepsilon_0 r_9^2}\mathbf{i}_\mathbf{r} \tag{10.175}$$

for $r > r_8$.

The energy is minimized and the angular momentum is conserved with the pairing of electron nine to fill the $p_z$ orbital when the orbital angular momenta of each set of $p_x$ and $p_z$ spin-paired electrons adds negatively to cancel. Then, the diamagnetic force (Eq. (10.82)), $\mathbf{F}_{diamagnetic}$, is:

$$\mathbf{F}_{diamagnetic} = -\left(\frac{2}{3}\right)\frac{\hbar^2}{4m_e r_9^2 r_3}\sqrt{s(s+1)}\mathbf{i}_\mathbf{r} \tag{10.176}$$

corresponding to $m = -1$ for the unpaired $p_y$ electron.

From Eqs. (10.83) and (10.89), $\mathbf{F}_{mag\ 2}$ is:

$$\mathbf{F}_{mag\ 2} = (1+1+1)\frac{1}{Z}\frac{\hbar^2}{m_e r_9^2 r_3}\sqrt{s(s+1)}\mathbf{i}_\mathbf{r} = \frac{1}{Z}\frac{3\hbar^2}{m_e r_9^2 r_3}\sqrt{s(s+1)}\mathbf{i}_\mathbf{r} \tag{10.177}$$

corresponding to the spin-angular-momentum contribution alone from each of the $p_x$ and $p_z$ orbitals and the orbital-angular-momentum contribution of the $p_y$ electron, respectively.

The outward centrifugal force on electron 9 is balanced by the electric force and the magnetic forces (on electron 9). The radius of the outer electron is calculated by equating the outward centrifugal force to the sum of the electric (Eq. (10.175)), diamagnetic (Eq. (10.176)), and paramagnetic (Eq. (10.177)) forces as follows:

$$\frac{m_e v_9^2}{r_9} = \frac{(Z-8)e^2}{4\pi\varepsilon_0 r_9^2} - \frac{\hbar^2}{6m_e r_9^2 r_3}\sqrt{s(s+1)} + \frac{3\hbar^2}{Zm_e r_9^2 r_3}\sqrt{s(s+1)} \tag{10.178}$$

Substitution of $v_9 = \frac{\hbar}{m_e r_9}$ (Eq. (1.35)) and $s = \frac{1}{2}$ into Eq. (10.178) gives:

$$\frac{\hbar^2}{m_e r_9^3} = \frac{(Z-8)e^2}{4\pi\varepsilon_0 r_9^2} - \frac{\hbar^2}{6m_e r_9^2 r_3}\sqrt{\frac{3}{4}} + \frac{3\hbar^2}{Zm_e r_9^2 r_3}\sqrt{\frac{3}{4}} \tag{10.179}$$

$$r_9 = \frac{\frac{\hbar^2}{m_e}}{\frac{(Z-8)e^2}{4\pi\varepsilon_0} - \frac{\hbar^2}{6m_e r_3}\sqrt{\frac{3}{4}} + \frac{3\hbar^2}{Zm_e r_3}\sqrt{\frac{3}{4}}} \tag{10.180}$$

$$r_9 = \frac{a_0}{(Z-8)-\left(\frac{1}{6}-\frac{3}{Z}\right)\frac{\sqrt{\frac{3}{4}}}{r_3}},\ r_3 \text{ in units of } a_0 \tag{10.181}$$

Substitution of $\frac{r_3}{a_0} = 0.51382$ (Eq. (10.62) with $Z = 9$) into Eq. (10.181) gives:

$$r_9 = 0.78069 a_0 \tag{10.182}$$

The ionization energy of the fluorine atom is given by the negative of $E(electric)$ given by Eq. (10.102) with the appropriate charge and radius:

$$E(ionization;\ F) = -Electric\ Energy = \frac{(Z-8)e^2}{8\pi\varepsilon_0 r_9} = 17.42782\ eV \tag{10.183}$$

where $r_9 = 0.78069 a_0$ (Eq. (10.183)) and $Z = 9$. The experimental ionization energy of the fluorine atom is 17.42282 $eV$ [3].

## THE IONIZATION ENERGIES OF NINE-ELECTRON ATOMS WITH A NUCLEAR CHARGE Z>9

Nine-electron atoms having $Z > 9$ possess an external electric field given by Eq. (10.92). In this case, an energy minimum is achieved with conservation of momentum when the orbital angular momentum is such that $\mathbf{F}_{diamagnetic}$ is minimized while $\mathbf{F}_{mag\ 2}$ is maximized. From Eq. (10.82), the diamagnetic force, $\mathbf{F}_{diamagnetic}$, is given by the sum of the contributions from the $p_x$, $p_y$, and $p_z$ orbitals corresponding to $m = 1,\ -1$, and 0, respectively:

$$\mathbf{F}_{diamagnetic} = -\left(\frac{2}{3}+\frac{2}{3}+\frac{1}{3}\right)\frac{\hbar^2}{4m_e r_9^2 r_3}\sqrt{s(s+1)}\mathbf{i}_\mathbf{r} = -\left(\frac{5}{3}\right)\frac{\hbar^2}{4m_e r_9^2 r_3}\sqrt{s(s+1)}\mathbf{i}_\mathbf{r} \tag{10.184}$$

The filled p orbitals with the maintenance of symmetry according to Eq. (10.72) requires that the diamagnetic force is only due to the electrons at $r_3$. From Eqs. (10.84) and (10.89), $\mathbf{F}_{mag\ 2}$ is:

$$\mathbf{F}_{mag\ 2} = (4+4+1)\frac{1}{Z}\frac{\hbar^2}{m_e r_9^2 r_3}\sqrt{s(s+1)}\mathbf{i}_\mathbf{r} = \frac{1}{Z}\frac{9\hbar^2}{m_e r_9^2 r_3}\sqrt{s(s+1)}\mathbf{i}_\mathbf{r} \tag{10.185}$$

corresponding to the spin and orbital angular momenta of the paired $p_x$ and $p_z$ electrons and the orbital angular momentum of the unpaired $p_y$ electron, respectively.

The second diamagnetic force, $\mathbf{F}_{diamagnetic\ 2}$, due to the binding of the p-orbital electron having an electric field outside of its radius is given by Eq. (10.93):

$$\mathbf{F}_{diamagnetic\ 2} = -\left[\frac{Z-9}{Z-8}\right]\left(1-\frac{\sqrt{2}}{2}\right)\frac{r_3\hbar^2}{m_e r_9^4}10\sqrt{s(s+1)}\mathbf{i}_\mathbf{r} \tag{10.186}$$

In the case that $Z > 9$, the radius of the outer electron is calculated by equating the outward centrifugal force to the sum of the electric (Eq. (10.175)), diamagnetic (Eqs. (10.184) and (10.186)), and paramagnetic (Eq. (10.185)) forces as follows:

$$\frac{m_e v_9^2}{r_9} = \frac{(Z-8)e^2}{4\pi\varepsilon_0 r_9^2} - \frac{5\hbar^2}{12 m_e r_9^2 r_3}\sqrt{s(s+1)} + \frac{9\hbar^2}{Z m_e r_9^2 r_3}\sqrt{s(s+1)} - \left[\frac{Z-9}{Z-8}\right]\left(1-\frac{\sqrt{2}}{2}\right)\frac{r_3\hbar^2}{m_e r_9^4}10\sqrt{s(s+1)} \tag{10.187}$$

Substitution of $v_9 = \frac{\hbar}{m_e r_9}$ (Eq. (1.35)) and $s = \frac{1}{2}$ into Eq. (10.187) gives:

$$\frac{\hbar^2}{m_e r_9^3} = \frac{(Z-8)e^2}{4\pi\varepsilon_0 r_9^2} - \frac{5\hbar^2}{12 m_e r_9^2 r_3}\sqrt{\frac{3}{4}} + \frac{9\hbar^2}{Z m_e r_9^2 r_3}\sqrt{\frac{3}{4}} - \left[\frac{Z-9}{Z-8}\right]\left(1-\frac{\sqrt{2}}{2}\right)\frac{r_3\hbar^2}{r_9^4 m_e}10\sqrt{\frac{3}{4}} \tag{10.188}$$

The quadratic equation corresponding to Eq. (10.188) is

$$\left(\frac{(Z-8)e^2}{4\pi\varepsilon_0} - \left(\frac{5}{12}-\frac{9}{Z}\right)\frac{\hbar^2}{m_e r_3}\sqrt{\frac{3}{4}}\right)r_9^2 - \frac{\hbar^2}{m_e}r_9 - \left[\frac{Z-9}{Z-8}\right]\left(1-\frac{\sqrt{2}}{2}\right)\frac{r_3\hbar^2}{m_e}10\sqrt{\frac{3}{4}} = 0 \tag{10.189}$$

$$r_9^2 - \frac{\frac{\hbar^2}{m_e}}{\left(\frac{(Z-8)e^2}{4\pi\varepsilon_0} - \left(\frac{5}{12}-\frac{9}{Z}\right)\frac{\hbar^2}{m_e r_3}\sqrt{\frac{3}{4}}\right)}r_9 - \frac{\frac{\hbar^2}{m_e}\left[\frac{Z-9}{Z-8}\right]\left(1-\frac{\sqrt{2}}{2}\right)r_3 10\sqrt{\frac{3}{4}}}{\left(\frac{(Z-8)e^2}{4\pi\varepsilon_0} - \left(\frac{5}{12}-\frac{9}{Z}\right)\frac{\hbar^2}{m_e r_3}\sqrt{\frac{3}{4}}\right)} = 0 \tag{10.190}$$

The solution of Eq. (10.190) using the quadratic formula is:

$$r_9 = \frac{\dfrac{\dfrac{\hbar^2}{m_e}}{\left(\dfrac{(Z-8)e^2}{4\pi\varepsilon_0} - \left(\dfrac{5}{12} - \dfrac{9}{Z}\right)\dfrac{\hbar^2}{m_e r_3}\sqrt{\dfrac{3}{4}}\right)} \pm \sqrt{\left(\dfrac{\dfrac{\hbar^2}{m_e}}{\left(\dfrac{(Z-8)e^2}{4\pi\varepsilon_0} - \left(\dfrac{5}{12} - \dfrac{9}{Z}\right)\dfrac{\hbar^2}{m_e r_3}\sqrt{\dfrac{3}{4}}\right)}\right)^2 + 4\dfrac{\dfrac{\hbar^2}{m_e}\left[\dfrac{Z-9}{Z-8}\right]\left(1-\dfrac{\sqrt{2}}{2}\right)r_3 10\sqrt{\dfrac{3}{4}}}{\left(\dfrac{(Z-8)e^2}{4\pi\varepsilon_0} - \left(\dfrac{5}{12} - \dfrac{9}{Z}\right)\dfrac{\hbar^2}{m_e r_3}\sqrt{\dfrac{3}{4}}\right)}}}{2} \tag{10.191}$$

$$r_9 = \frac{\dfrac{a_0}{\left((Z-8) - \left(\dfrac{5}{24} - \dfrac{9}{2Z}\right)\dfrac{\sqrt{3}}{r_3}\right)} \pm a_0\sqrt{\left(\dfrac{1}{\left((Z-8) - \left(\dfrac{5}{24} - \dfrac{9}{2Z}\right)\dfrac{\sqrt{3}}{r_3}\right)}\right)^2 + \dfrac{20\sqrt{3}\left(\left[\dfrac{Z-9}{Z-8}\right]\left(1-\dfrac{\sqrt{2}}{2}\right)r_3\right)}{\left((Z-8) - \left(\dfrac{5}{24} - \dfrac{9}{2Z}\right)\dfrac{\sqrt{3}}{r_3}\right)}}}{2}, \; r_3 \text{ in units of } a_0 \tag{10.192}$$

where $r_3$ is given by Eq. (10.62). The positive root of Eq. (10.192) must be taken in order that $r_9 > 0$. The final radius of electron 9, $r_9$, is given by Eq. (10.192); this is also the final radius of electrons 5, 6,7, and 8. The radii of several nine-electron atoms are given in Table 10.7.

The ionization energies for the nine-electron atoms with $Z > 9$ are given by the electric energy, $E(electric)$, (Eq. (10.102) with the radii, $r_9$, given by Eq. (10.192)):

$$E(Ionization) = -Electric\ Energy = \frac{(Z-8)e^2}{8\pi\varepsilon_0 r_9} \tag{10.193}$$

Since the relativistic corrections were small, the nonrelativistic ionization energies for experimentally measured nine-electron atoms are given in Table 10.7.

**Table 10.7.** Ionization energies for some nine-electron atoms.

| 9 e Atom | Z | $r_1$ $(a_0)$ [a] | $r_3$ $(a_0)$ [b] | $r_9$ $(a_0)$ [c] | Theoretical Ionization Energies [d] (eV) | Experimental Ionization Energies [e] (eV) | Relative Error [f] |
|---|---|---|---|---|---|---|---|
| $F$ | 9 | 0.11297 | 0.51382 | 0.78069 | 17.42782 | 17.42282 | -0.0003 |
| $Ne^{+}$ | 10 | 0.10149 | 0.45511 | 0.64771 | 42.0121 | 40.96328 | -0.0256 |
| $Na^{2+}$ | 11 | 0.09213 | 0.40853 | 0.57282 | 71.2573 | 71.62 | 0.0051 |
| $Mg^{3+}$ | 12 | 0.08435 | 0.37065 | 0.50274 | 108.2522 | 109.2655 | 0.0093 |
| $Al^{4+}$ | 13 | 0.07778 | 0.33923 | 0.44595 | 152.5469 | 153.825 | 0.0083 |
| $Si^{5+}$ | 14 | 0.07216 | 0.31274 | 0.40020 | 203.9865 | 205.27 | 0.0063 |
| $P^{6+}$ | 15 | 0.06730 | 0.29010 | 0.36283 | 262.4940 | 263.57 | 0.0041 |
| $S^{7+}$ | 16 | 0.06306 | 0.27053 | 0.33182 | 328.0238 | 328.75 | 0.0022 |
| $Cl^{8+}$ | 17 | 0.05932 | 0.25344 | 0.30571 | 400.5466 | 400.06 | -0.0012 |
| $Ar^{9+}$ | 18 | 0.05599 | 0.23839 | 0.28343 | 480.0424 | 478.69 | -0.0028 |
| $K^{10+}$ | 19 | 0.05302 | 0.22503 | 0.26419 | 566.4968 | 564.7 | -0.0032 |
| $Ca^{11+}$ | 20 | 0.05035 | 0.21308 | 0.24742 | 659.8992 | 657.2 | -0.0041 |
| $Sc^{12+}$ | 21 | 0.04794 | 0.20235 | 0.23266 | 760.2415 | 756.7 | -0.0047 |
| $Ti^{13+}$ | 22 | 0.04574 | 0.19264 | 0.21957 | 867.5176 | 863.1 | -0.0051 |
| $V^{14+}$ | 23 | 0.04374 | 0.18383 | 0.20789 | 981.7224 | 976 | -0.0059 |
| $Cr^{15+}$ | 24 | 0.04191 | 0.17579 | 0.19739 | 1102.8523 | 1097 | -0.0053 |
| $Mn^{16+}$ | 25 | 0.04022 | 0.16842 | 0.18791 | 1230.9038 | 1224 | -0.0056 |
| $Fe^{17+}$ | 26 | 0.03867 | 0.16165 | 0.17930 | 1365.8746 | 1358 | -0.0058 |
| $Co^{18+}$ | 27 | 0.03723 | 0.15540 | 0.17145 | 1507.7624 | 1504.6 | -0.0021 |
| $Ni^{19+}$ | 28 | 0.03589 | 0.14961 | 0.16427 | 1656.5654 | 1648 | -0.0052 |
| $Cu^{20+}$ | 29 | 0.03465 | 0.14424 | 0.15766 | 1812.2821 | 1804 | -0.0046 |

[a] Radius of the first set of paired inner electrons of nine-electron atoms from Equation (10.51).

[b] Radius of the second set of paired inner electrons of nine-electron atoms from Equation (10.62).

[c] Radius of the one unpaired and two sets of paired outer electrons of nine-electron atoms from Eq. (10.192) for $Z > 9$ and Eq. (10.182) for $F$.

[d] Calculated ionization energies of nine-electron atoms given by the electric energy (Eq. (10.193)).

[e] From theoretical calculations, interpolation of isoelectronic and spectral series, and experimental data [2-3].

[f] (Experimental-theoretical)/experimental.

The agreement between the experimental and calculated values of Table 10.7 is well within the experimental capability of the spectroscopic determinations including the values at large Z which relies on X-ray spectroscopy. In this case, the experimental capability is three to four significant figures which is consistent with the last column. The fluorine atom isoelectronic series is given in Table 10.7 [2-3] to much higher precision than the capability of X-ray spectroscopy, but these values are based on theoretical and interpolation techniques rather than data alone. Ionization energies are difficult to determine since the cut-off of the Rydberg series of lines at the ionization energy is often not observed, and the ionization energy must be determined from theoretical calculations, interpolation of F isoelectronic and Rydberg series, as well as direct experimental data.

## TEN-ELECTRON ATOMS

Ten-electron atoms can be solved exactly using the results of the solutions of one, two, three, four, five, six, seven, eight, and nine-electron atoms.

## RADIUS AND IONIZATION ENERGY OF THE OUTER ELECTRON OF THE NEON ATOM

For each nine-electron atom having a central charge of $Z$ times that of the proton, there are two indistinguishable spin-paired electrons in an atomic orbital with radii $r_1$ and $r_2$ both given by Eq. (7.35) (Eq. (10.51)), two indistinguishable spin-paired electrons in an atomic orbital with radii $r_3$ and $r_4$ both given by Eq. (10.62), and two sets of paired and an unpaired electron in an atomic orbital at $r_9$ given by Eq. (10.192). For $Z \geq 10$, the next electron which binds to form the corresponding ten-electron atom is attracted by the central Coulomb field and is repelled by diamagnetic force due to the spin-paired inner electrons. A paramagnetic spin-pairing force that results in the formation of a filled s orbital is also possible, but the force due to the spin-pairing of the electrons (Eq. (7.24) with the radius $r_{10}$) reduces the energy of the atom less than that due to the alternative forces on three pairs of electrons of opposite spin in $p_x$, $p_y$, and $p_z$ orbitals of an atomic orbital at the same radius $r_{10}$. The resulting electron configuration is $1s^2 2s^2 2p^6$, and the orbital arrangement is:

2p state

$$\underset{1}{\underline{\uparrow\downarrow}} \quad \underset{0}{\underline{\uparrow\downarrow}} \quad \underset{-1}{\underline{\uparrow\downarrow}} \tag{10.194}$$

corresponding to the ground state ${}^1S_0$.

The central Coulomb force acts on the outer electron to cause it to bind wherein this electric force on the outer-most electron due to the nucleus and the inner nine electrons is given by Eq. (10.70) with the appropriate charge and radius:

$$\mathbf{F}_{ele} = \frac{(Z-9)e^2}{4\pi\varepsilon_0 r_{10}^2}\mathbf{i}_\mathbf{r} \tag{10.195}$$

for $r > r_9$.

The energy is minimized and the angular momentum is conserved with the pairing of electron ten to fill the $p_y$ orbital when the orbital angular momenta of each set of the $p_x$, $p_y$, and $p_z$ spin-paired electrons add negatively to cancel. Then, the diamagnetic force (Eq. (10.82)), $\mathbf{F}_{diamagnetic}$, is zero:

$$\mathbf{F}_{diamagnetic} = 0 \tag{10.196}$$

From Eq. (10.83), $\mathbf{F}_{mag\ 2}$ is

$$\mathbf{F}_{mag\ 2} = (1+1+1)\frac{1}{Z}\frac{\hbar^2}{m_e r_{10}^2 r_3}\sqrt{s(s+1)}\mathbf{i}_\mathbf{r} = \frac{1}{Z}\frac{3\hbar^2}{m_e r_{10}^2 r_3}\sqrt{s(s+1)}\mathbf{i}_\mathbf{r} \tag{10.197}$$

corresponding to the spin-angular-momentum contribution alone from each of the $p_x$, $p_y$, and $p_z$ orbitals.

The outward centrifugal force on electron 10 is balanced by the electric force and the magnetic forces (on electron 10). The radius of the outer electron is calculated by equating the outward centrifugal force to the sum of the electric (Eq. (10.195)), diamagnetic (Eq. (10.196)), and paramagnetic (Eq. (10.197)) forces as follows:

$$\frac{m_e v_{10}^2}{r_{10}} = \frac{(Z-9)e^2}{4\pi\varepsilon_0 r_{10}^2} + \frac{3\hbar^2}{Z m_e r_{10}^2 r_3}\sqrt{s(s+1)} \tag{10.198}$$

Substitution of $v_{10} = \dfrac{\hbar}{m_e r_{10}}$ (Eq. (1.35)) and $s = \dfrac{1}{2}$ into Eq. (10.198) gives:

$$\frac{\hbar^2}{m_e r_{10}^3} = \frac{(Z-9)e^2}{4\pi\varepsilon_0 r_{10}^2} + \frac{3\hbar^2}{Z m_e r_{10}^2 r_3}\sqrt{\frac{3}{4}} \tag{10.199}$$

$$r_{10} = \frac{\dfrac{\hbar^2}{m_e}}{\dfrac{(Z-9)e^2}{4\pi\varepsilon_0} + \dfrac{3\hbar^2}{Z m_e r_3}\sqrt{\dfrac{3}{4}}} \tag{10.200}$$

$$r_{10} = \frac{a_0}{(Z-9) + \dfrac{3}{Z}\dfrac{\sqrt{\dfrac{3}{4}}}{r_3}}, \; r_3 \textit{ in units of } a_0 \tag{10.201}$$

Substitution of $\frac{r_3}{a_0} = 0.45511$ (Eq. (10.62) with $Z = 10$) into Eq. (10.201) gives:

$$r_{10} = 0.63659 a_0 \tag{10.202}$$

The ionization energy of the neon atom is given by the negative of $E(electric)$ given by Eq. (10.102) with the appropriate charge and radius:

$$E(ionization;\ Ne) = -Electric\ Energy = \frac{(Z-9)e^2}{8\pi\varepsilon_0 r_{10}} = 21.37296\ eV \tag{10.203}$$

where $r_{10} = 0.63659 a_0$ (Eq. (10.202)) and $Z = 10$. The experimental ionization energy of the neon atom is $21.56454\ eV$ [3].

## THE IONIZATION ENERGIES OF TEN-ELECTRON ATOMS WITH A NUCLEAR CHARGE Z>10

Ten-electron atoms having $Z > 10$ possess an external electric field given by Eq. (10.92). In this case, an energy minimum is achieved with conservation of momentum when the orbital angular momentum is such that $\mathbf{F}_{diamagnetic}$ is minimized while $\mathbf{F}_{mag\ 2}$ is maximized. From Eq. (10.82), the diamagnetic force, $\mathbf{F}_{diamagnetic}$, is given by the sum of the contributions from the $p_x$, $p_y$, and $p_z$ orbitals corresponding to $m$ = 1, -1, and 0, respectively:

$$\mathbf{F}_{diamagnetic} = -\left(\frac{2}{3}+\frac{2}{3}+\frac{1}{3}\right)\frac{\hbar^2}{4m_e r_{10}^2 r_3}\sqrt{s(s+1)}\mathbf{i}_\mathbf{r} = -\left(\frac{5}{3}\right)\frac{\hbar^2}{4m_e r_{10}^2 r_3}\sqrt{s(s+1)}\mathbf{i}_\mathbf{r} \tag{10.204}$$

The filled p orbitals with the maintenance of symmetry according to Eq. (10.72) requires that the diamagnetic force is only due to the electrons at $r_3$. From Eq. (10.84), $\mathbf{F}_{mag\ 2}$ is

$$\mathbf{F}_{mag\ 2} = \left(4+4+4\right)\frac{1}{Z}\frac{\hbar^2}{m_e r_{10}^2 r_3}\sqrt{s(s+1)}\mathbf{i}_\mathbf{r} = \frac{1}{Z}\frac{12\hbar^2}{m_e r_{10}^2 r_3}\sqrt{s(s+1)}\mathbf{i}_\mathbf{r} \tag{10.205}$$

corresponding to the spin and orbital angular momenta of the paired $p_x$, $p_y$, and $p_z$ electrons.

The second diamagnetic force, $\mathbf{F}_{diamagnetic\ 2}$, due to the binding of the p-orbital electron having an electric field outside of its radius is given by Eq. (10.93):

$$\mathbf{F}_{diamagnetic\ 2} = -\left[\frac{Z-10}{Z-9}\right]\left(1-\frac{\sqrt{2}}{2}\right)\frac{r_3\hbar^2}{m_e r_{10}^4}10\sqrt{s(s+1)}\mathbf{i}_\mathbf{r} \tag{10.206}$$

In the case that $Z > 10$, the radius of the outer electron is calculated by equating the outward centrifugal force to the sum of the electric (Eq. (10.195)), diamagnetic (Eqs. (10.204) and (10.206)), and paramagnetic (Eq. (10.205)) forces as follows:

$$\frac{m_e v_{10}^2}{r_{10}} = \frac{(Z-9)e^2}{4\pi\varepsilon_0 r_{10}^2} - \frac{5\hbar^2}{12m_e r_{10}^2 r_3}\sqrt{s(s+1)} + \frac{12\hbar^2}{Zm_e r_{10}^2 r_3}\sqrt{s(s+1)} - \left[\frac{Z-10}{Z-9}\right]\left(1-\frac{\sqrt{2}}{2}\right)\frac{r_3\hbar^2}{m_e r_{10}^4}10\sqrt{s(s+1)} \tag{10.207}$$

Substitution of $v_{10} = \frac{\hbar}{m_e r_{10}}$ (Eq. (1.35)) and $s = \frac{1}{2}$ into Eq. (10.207) gives:

$$\frac{\hbar^2}{m_e r_{10}^3} = \frac{(Z-9)e^2}{4\pi\varepsilon_0 r_{10}^2} - \frac{5\hbar^2}{12m_e r_{10}^2 r_3}\sqrt{\frac{3}{4}} + \frac{12\hbar^2}{Zm_e r_{10}^2 r_3}\sqrt{\frac{3}{4}} - \left[\frac{Z-10}{Z-9}\right]\left(1-\frac{\sqrt{2}}{2}\right)\frac{r_3\hbar^2}{r_{10}^4 m_e}10\sqrt{\frac{3}{4}} \tag{10.208}$$

The quadratic equation corresponding to Eq. (10.208) is

$$\left(\frac{(Z-9)e^2}{4\pi\varepsilon_0} - \left(\frac{5}{12}-\frac{12}{Z}\right)\frac{\hbar^2}{m_e r_3}\sqrt{\frac{3}{4}}\right)r_{10}^2 - \frac{\hbar^2}{m_e}r_{10} - \left[\frac{Z-10}{Z-9}\right]\left(1-\frac{\sqrt{2}}{2}\right)\frac{r_3\hbar^2}{m_e}10\sqrt{\frac{3}{4}} = 0 \tag{10.209}$$

$$r_{10}^2 - \frac{\frac{\hbar^2}{m_e}}{\left(\frac{(Z-9)e^2}{4\pi\varepsilon_0} - \left(\frac{5}{12}-\frac{12}{Z}\right)\frac{\hbar^2}{m_e r_3}\sqrt{\frac{3}{4}}\right)}r_{10} - \frac{\frac{\hbar^2}{m_e}\left[\frac{Z-10}{Z-9}\right]\left(1-\frac{\sqrt{2}}{2}\right)r_3 10\sqrt{\frac{3}{4}}}{\left(\frac{(Z-9)e^2}{4\pi\varepsilon_0} - \left(\frac{5}{12}-\frac{12}{Z}\right)\frac{\hbar^2}{m_e r_3}\sqrt{\frac{3}{4}}\right)} = 0 \tag{10.210}$$

The solution of Eq. (10.210) using the quadratic formula is:

$$r_{10} = \frac{\dfrac{\dfrac{\hbar^2}{m_e}}{\left(\dfrac{(Z-9)e^2}{4\pi\varepsilon_0} - \left(\dfrac{5}{12} - \dfrac{12}{Z}\right)\dfrac{\hbar^2}{m_e r_3}\sqrt{\dfrac{3}{4}}\right)} \pm \sqrt{\left(\dfrac{\dfrac{\hbar^2}{m_e}}{\left(\dfrac{(Z-9)e^2}{4\pi\varepsilon_0} - \left(\dfrac{5}{12} - \dfrac{12}{Z}\right)\dfrac{\hbar^2}{m_e r_3}\sqrt{\dfrac{3}{4}}\right)}\right)^2 + 4\dfrac{\dfrac{\hbar^2}{m_e}\left[\dfrac{Z-10}{Z-9}\right]\left(1-\dfrac{\sqrt{2}}{2}\right)r_3 10\sqrt{\dfrac{3}{4}}}{\left(\dfrac{(Z-9)e^2}{4\pi\varepsilon_0} - \left(\dfrac{5}{12} - \dfrac{12}{Z}\right)\dfrac{\hbar^2}{m_e r_3}\sqrt{\dfrac{3}{4}}\right)}}}{2} \tag{10.211}$$

$$r_{10} = \frac{\dfrac{a_0}{\left((Z-9) - \left(\dfrac{5}{24} - \dfrac{6}{Z}\right)\dfrac{\sqrt{3}}{r_3}\right)} \pm a_0\sqrt{\left(\dfrac{1}{\left((Z-9) - \left(\dfrac{5}{24} - \dfrac{6}{Z}\right)\dfrac{\sqrt{3}}{r_3}\right)}\right)^2 + \dfrac{20\sqrt{3}\left(\left[\dfrac{Z-10}{Z-9}\right]\left(1-\dfrac{\sqrt{2}}{2}\right)r_3\right)}{\left((Z-9) - \left(\dfrac{5}{24} - \dfrac{6}{Z}\right)\dfrac{\sqrt{3}}{r_3}\right)}}}{2}, \; r_3 \text{ in units of } a_0 \tag{10.212}$$

where $r_3$ is given by Eq. (10.62). The positive root of Eq. (10.212) must be taken in order that $r_{10} > 0$. The final radius of electron 10, $r_{10}$, is given by Eq. (10.62); this is also the final radius of electrons 5, 6, 7, 8, and 9. The radii of several ten-electron atoms are given in Table 10.8.

The ionization energies for the ten-electron atoms with $Z > 10$ are given by the electric energy, $E(electric)$, (Eq. (10.102) with the radii, $r_{10}$, given by Eq. (10.212)):

$$E(Ionization) = -Electric\ Energy = \frac{(Z-9)e^2}{8\pi\varepsilon_0 r_{10}} \tag{10.213}$$

Since the relativistic corrections were small, the nonrelativistic ionization energies for experimentally measured ten-electron atoms are given in Table 10.8.

**Table 10.8.** Ionization energies for some ten-electron atoms.

| 10 e Atom | Z | $r_1$ $(a_0)$ [a] | $r_3$ $(a_0)$ [b] | $r_{10}$ $(a_0)$ [c] | Theoretical Ionization Energies [d] $(eV)$ | Experimental Ionization Energies [e] $(eV)$ | Relative Error [f] |
|---|---|---|---|---|---|---|---|
| $Ne$ | 10 | 0.10149 | 0.45511 | 0.63659 | 21.37296 | 21.56454 | 0.00888 |
| $Na^{+}$ | 11 | 0.09213 | 0.40853 | 0.560945 | 48.5103 | 47.2864 | -0.0259 |
| $Mg^{2+}$ | 12 | 0.08435 | 0.37065 | 0.510568 | 79.9451 | 80.1437 | 0.0025 |
| $Al^{3+}$ | 13 | 0.07778 | 0.33923 | 0.456203 | 119.2960 | 119.992 | 0.0058 |
| $Si^{4+}$ | 14 | 0.07216 | 0.31274 | 0.409776 | 166.0150 | 166.767 | 0.0045 |
| $P^{5+}$ | 15 | 0.06730 | 0.29010 | 0.371201 | 219.9211 | 220.421 | 0.0023 |
| $S^{6+}$ | 16 | 0.06306 | 0.27053 | 0.339025 | 280.9252 | 280.948 | 0.0001 |
| $Cl^{7+}$ | 17 | 0.05932 | 0.25344 | 0.311903 | 348.9750 | 348.28 | -0.0020 |
| $Ar^{8+}$ | 18 | 0.05599 | 0.23839 | 0.288778 | 424.0365 | 422.45 | -0.0038 |
| $K^{9+}$ | 19 | 0.05302 | 0.22503 | 0.268844 | 506.0861 | 503.8 | -0.0045 |
| $Ca^{10+}$ | 20 | 0.05035 | 0.21308 | 0.251491 | 595.1070 | 591.9 | -0.0054 |
| $Sc^{11+}$ | 21 | 0.04794 | 0.20235 | 0.236251 | 691.0866 | 687.36 | -0.0054 |
| $Ti^{12+}$ | 22 | 0.04574 | 0.19264 | 0.222761 | 794.0151 | 787.84 | -0.0078 |
| $V^{13+}$ | 23 | 0.04374 | 0.18383 | 0.210736 | 903.8853 | 896 | -0.0088 |
| $Cr^{14+}$ | 24 | 0.04191 | 0.17579 | 0.19995 | 1020.6910 | 1010.6 | -0.0100 |
| $Mn^{15+}$ | 25 | 0.04022 | 0.16842 | 0.19022 | 1144.4276 | 1134.7 | -0.0086 |
| $Fe^{16+}$ | 26 | 0.03867 | 0.16165 | 0.181398 | 1275.0911 | 1266 | -0.0072 |
| $Co^{17+}$ | 27 | 0.03723 | 0.15540 | 0.173362 | 1412.6783 | 1397.2 | -0.0111 |
| $Ni^{18+}$ | 28 | 0.03589 | 0.14961 | 0.166011 | 1557.1867 | 1541 | -0.0105 |
| $Cu^{19+}$ | 29 | 0.03465 | 0.14424 | 0.159261 | 1708.6139 | 1697 | -0.0068 |
| $Zn^{20+}$ | 30 | 0.03349 | 0.13925 | 0.153041 | 1866.9581 | 1856 | -0.0059 |

[a] Radius of the first set of paired inner electrons of ten-electron atoms from Equation (10.51).
[b] Radius of the second set of paired inner electrons of ten-electron atoms from Equation (10.62).
[c] Radius of three sets of paired outer electrons of ten-electron atoms from Eq. (10.212) for $Z > 10$ and Eq. (10.202) for *Ne*.
[d] Calculated ionization energies of ten-electron atoms given by the electric energy (Eq. (10.213)).
[e] From theoretical calculations, interpolation of isoelectronic and spectral series, and experimental data [2-3].
[f] (Experimental-theoretical)/experimental.

The agreement between the experimental and calculated values of Table 10.8 is well within the experimental capability of the spectroscopic determinations, including the values at large Z, which rely on X-ray spectroscopy. In this case, the experimental capability is three to four significant figures, which is consistent with the last column. The neon atom isoelectronic series is given in Table 10.8 [2-3] to much higher precision than the capability of X-ray spectroscopy, but these values are based on theoretical and interpolation techniques rather than data alone. Ionization energies are difficult to determine since the cut-off of the Rydberg series of lines at the ionization energy is often not observed, and the ionization energy must be determined from theoretical calculations, interpolation of Ne isoelectronic and Rydberg series, as well as direct experimental data.

## GENERAL EQUATION FOR THE IONIZATION ENERGIES OF FIVE THROUGH TEN-ELECTRON ATOMS

Using the forces given by Eqs. (10.70), (10.82-10.84), (10.89), (10.93), and the radii $r_3$ given by Eq. (10.62), the radii of the 2p electrons of all five through ten-electron atoms may be solved exactly. The electric energy given by Eq. (10.102) gives the corresponding exact ionization energies. A summary of the parameters of the equations that determine the exact radii and ionization energies of all five through ten-electron atoms is given in Table 10.9.

$\mathbf{F}_{ele}$ and $\mathbf{F}_{diamagnetic\ 2}$ given by Eqs. (10.70) and (10.93), respectively, are of the same form for all atoms with the appropriate nuclear charges and atomic radii. $\mathbf{F}_{diamagnetic}$ given by Eq. (10.82) and $\mathbf{F}_{mag\ 2}$ given by Eqs. (10.83-10.84) and (10.89) are of the same form with the appropriate factors that depend on the electron configuration wherein the electron configuration must be a minimum of energy.

For each n-electron atom having a central charge of $Z$ times that of the proton and an electron configuration $1s^2 2s^2 2p^{n-4}$, there are two indistinguishable spin-paired electrons in an atomic orbital with radii $r_1$ and $r_2$ both given by Eqs. (7.35) and (10.51):

$$r_1 = r_2 = a_0\left[\frac{1}{Z-1} - \frac{\sqrt{\frac{3}{4}}}{Z(Z-1)}\right] \tag{10.214}$$

two indistinguishable spin-paired electrons in an atomic orbital with radii $r_3$ and $r_4$ both given by Eq. (10.62):

$$r_4 = r_3 = \frac{\dfrac{a_0\left(1-\dfrac{\sqrt{\frac{3}{4}}}{Z}\right)}{\left((Z-3)-\left(\frac{1}{4}-\frac{1}{Z}\right)\frac{\sqrt{\frac{3}{4}}}{r_1}\right)} \pm a_o\sqrt{\dfrac{\left(1-\dfrac{\sqrt{\frac{3}{4}}}{Z}\right)^2}{\left((Z-3)-\left(\frac{1}{4}-\frac{1}{Z}\right)\frac{\sqrt{\frac{3}{4}}}{r_1}\right)^2} + 4\dfrac{\left[\frac{Z-3}{Z-2}\right]r_1 10\sqrt{\frac{3}{4}}}{\left((Z-3)-\left(\frac{1}{4}-\frac{1}{Z}\right)\frac{\sqrt{\frac{3}{4}}}{r_1}\right)}}}{2}, \quad r_1 \text{ in units of } a_o \tag{10.215}$$

where $r_1$ is given by Eq. (10.214), and $n-4$ electrons in an atomic orbital with radius $r_n$ given by:

$$r_n = \frac{\dfrac{a_0}{\left((Z-(n-1))-\left(\frac{A}{8}-\frac{B}{2Z}\right)\frac{\sqrt{3}}{r_3}\right)} \pm a_0\sqrt{\dfrac{\left(\dfrac{1}{\left((Z-(n-1))-\left(\frac{A}{8}-\frac{B}{2Z}\right)\frac{\sqrt{3}}{r_3}\right)}\right)^2 + \dfrac{20\sqrt{3}\left(\left[\frac{Z-n}{Z-(n-1)}\right]\left(1-\frac{\sqrt{2}}{2}\right)r_3\right)}{\left((Z-(n-1))-\left(\frac{A}{8}-\frac{B}{2Z}\right)\frac{\sqrt{3}}{r_3}\right)}}}{2}, \quad r_3 \text{ in units of } a_0 \tag{10.216}$$

where $r_3$ is given by Eq. (10.215), the parameter $A$ given in Table 10.9 corresponds to the diamagnetic force, $\mathbf{F}_{diamagnetic}$, (Eq. (10.82)), and the parameter $B$ given in Table 10.9 corresponds to the paramagnetic force, $\mathbf{F}_{mag\ 2}$ (Eqs. (10.83-10.84) and (10.89)). The positive root of Eq. (10.216) must be taken in order that $r_n > 0$. The radii of several n-electron atoms are given in Tables 10.3-10.8.

The ionization energy for the boron atom is given by Eq. (10.104). The ionization energies for the n-electron atoms are given by the negative of the electric energy, $E(electric)$, (Eq. (10.102) with the radii, $r_n$, given by Eq. (10.216)).

$$E(Ionization) = -Electric\ Energy = \frac{(Z-(n-1))e^2}{8\pi\varepsilon_0 r_n} \tag{10.217}$$

Since the relativistic corrections were small, the nonrelativistic ionization energies for experimentally measured n-electron atoms are given by Eqs. (10.217) and (10.216) in Tables 10.3-10.8.

**Table 10.9.** Summary of the parameters of five through ten-electron atoms.

| Atom Type | Electron Configuration | Ground State Term [a] | Orbital Arrangement of 2p Electrons (2p state) | Diamagnetic Force Factor $A$ [b] | Paramagnetic Force Factor $B$ [c] |
|---|---|---|---|---|---|
| Neutral 5 e Atom $B$ | $1s^2 2s^2 2p^1$ | $^2P^0_{1/2}$ | $\underline{\uparrow}\ \ \underline{\ \ }\ \ \underline{\ \ }$ <br> 1 0 -1 | 2 | 0 |
| Neutral 6 e Atom $C$ | $1s^2 2s^2 2p^2$ | $^3P_0$ | $\underline{\uparrow}\ \ \underline{\uparrow}\ \ \underline{\ \ }$ <br> 1 0 -1 | $\frac{2}{3}$ | 0 |
| Neutral 7 e Atom $N$ | $1s^2 2s^2 2p^3$ | $^4S^0_{3/2}$ | $\underline{\uparrow}\ \ \underline{\uparrow}\ \ \underline{\uparrow}$ <br> 1 0 -1 | $\frac{1}{3}$ | 1 |
| Neutral 8 e Atom $O$ | $1s^2 2s^2 2p^4$ | $^3P_2$ | $\underline{\uparrow\downarrow}\ \ \underline{\uparrow}\ \ \underline{\uparrow}$ <br> 1 0 -1 | 1 | 2 |
| Neutral 9 e Atom $F$ | $1s^2 2s^2 2p^5$ | $^2P^0_{3/2}$ | $\underline{\uparrow\downarrow}\ \ \underline{\uparrow\downarrow}\ \ \underline{\uparrow}$ <br> 1 0 -1 | $\frac{2}{3}$ | 3 |
| Neutral 10 e Atom $Ne$ | $1s^2 2s^2 2p^6$ | $^1S_0$ | $\underline{\uparrow\downarrow}\ \ \underline{\uparrow\downarrow}\ \ \underline{\uparrow\downarrow}$ <br> 1 0 -1 | 0 | 3 |
| 5 e Ion | $1s^2 2s^2 2p^1$ | $^2P^0_{1/2}$ | $\underline{\uparrow}\ \ \underline{\ \ }\ \ \underline{\ \ }$ <br> 1 0 -1 | $\frac{5}{3}$ | 1 |
| 6 e Ion | $1s^2 2s^2 2p^2$ | $^3P_0$ | $\underline{\uparrow}\ \ \underline{\uparrow}\ \ \underline{\ \ }$ <br> 1 0 -1 | $\frac{5}{3}$ | 4 |
| 7 e Ion | $1s^2 2s^2 2p^3$ | $^4S^0_{3/2}$ | $\underline{\uparrow}\ \ \underline{\uparrow}\ \ \underline{\uparrow}$ <br> 1 0 -1 | $\frac{5}{3}$ | 6 |
| 8 e Ion | $1s^2 2s^2 2p^4$ | $^3P_2$ | $\underline{\uparrow\downarrow}\ \ \underline{\uparrow}\ \ \underline{\uparrow}$ <br> 1 0 -1 | $\frac{5}{3}$ | 6 |
| 9 e Ion | $1s^2 2s^2 2p^5$ | $^2P^0_{3/2}$ | $\underline{\uparrow\downarrow}\ \ \underline{\uparrow\downarrow}\ \ \underline{\uparrow}$ <br> 1 0 -1 | $\frac{5}{3}$ | 9 |
| 10 e Ion | $1s^2 2s^2 2p^6$ | $^1S_0$ | $\underline{\uparrow\downarrow}\ \ \underline{\uparrow\downarrow}\ \ \underline{\uparrow\downarrow}$ <br> 1 0 -1 | $\frac{5}{3}$ | 12 |

[a] The theoretical ground state terms match those given by NIST [8].

[b] Eq. (10.82).

[c] Eqs. (10.83-10.84) and (10.89).

## ELEVEN-ELECTRON ATOMS

Eleven-electron atoms can be solved exactly using the results of the solutions of one, two, three, four, five, six, seven, eight, nine, and ten-electron atoms.

## RADIUS AND IONIZATION ENERGY OF THE OUTER ELECTRON OF THE SODIUM ATOM

For each ten-electron atom having a central charge of $Z$ times that of the proton, there are two indistinguishable spin-paired electrons in an atomic orbital with radii $r_1$ and $r_2$ both given by Eq. (7.35) (Eq. (10.51)), two indistinguishable spin-paired electrons in an atomic orbital with radii $r_3$ and $r_4$ both given by Eq. (10.62), and three sets of paired electrons in an atomic orbital at $r_{10}$ given by Eq. (10.212). For $Z \geq 11$, the next electron which binds to form the corresponding eleven-electron atom is attracted by the central Coulomb field and is repelled by diamagnetic forces due to the 3 sets of spin-paired inner electrons such that it forms an unpaired atomic orbital at radius $r_{11}$.

The central Coulomb force acts on the outer electron to cause it to bind wherein this electric force on the outer-most electron due to the nucleus and the inner ten electrons is given by Eq. (10.70) with the appropriate charge and radius:

$$\mathbf{F}_{ele} = \frac{(Z-10)e^2}{4\pi\varepsilon_0 r_{11}^2}\mathbf{i}_r \tag{10.218}$$

for $r > r_{10}$.

The spherically symmetrical closed 2p shell of eleven-electron atoms produces a diamagnetic force, $\mathbf{F}_{diamagnetic}$, that is equivalent to that of a closed s shell given by Eq. (10.11) with the appropriate radii. The inner electrons remain at their initial radii, but cause a diamagnetic force according to Lenz's law that is

$$\mathbf{F}_{diamagnetic} = -\frac{\hbar^2}{4m_e r_{11}^2 r_{10}}\sqrt{s(s+1)}\mathbf{i}_\mathbf{r} \tag{10.219}$$

In addition to the spin-spin interaction between electron pairs, the three sets of 2p electrons are orbitally paired. The single s orbital of the sodium atom produces a magnetic field at the position of the three sets of spin-paired 2p electrons. In order for the electrons to remain spin and orbitally paired, a corresponding diamagnetic force, $\mathbf{F}_{diamagnetic\ 3}$, on electron eleven from the three sets of spin-paired electrons is given by:

$$\mathbf{F}_{diamagnetic\ 3} = -8\left[\frac{e^2\mu_0}{2m_e r_{10}}\right]\frac{\hbar^2}{m_e r_{11}^{\ 3}}\mathbf{i}_\mathbf{r} \tag{10.220}$$

corresponding to the $p_x$ and $p_y$ electrons with no interaction from the orthogonal $p_z$ electrons (Eq. (10.84)). As demonstrated by Eqs. (7.15-7.23), the maintenance of the invariance of the electron's angular momentum of $\hbar$, mass to charge ratio, $\frac{e}{m_e}$, and corresponding magnetic moment of a Bohr magneton, $\mu_B$, requires that the term in brackets is be replaced by $\frac{1}{Z}$ corresponding to the relativistic correction given by Eq. (7.23). Thus, $\mathbf{F}_{diamagnetic\ 3}$ is given by:

$$\mathbf{F}_{diamagnetic\ 3} = -\frac{1}{Z}\frac{8\hbar^2}{m_e r_{11}^{\ 3}}\sqrt{s(s+1)}\mathbf{i}_\mathbf{r} \tag{10.221}$$

where the vector projection of the spin interaction of $\sqrt{s(s+1)} = \sqrt{\frac{3}{4}}$ is given in the Two-Electron Atoms section and Appendix VI.

The outward centrifugal force on electron 11 is balanced by the electric force and the magnetic forces (on electron 11). The radius of the outer electron is calculated by equating the outward centrifugal force to the sum of the electric (Eq. (10.218)) and diamagnetic (Eqs. (10.219) and (10.221)) forces as follows:

$$\frac{m_e v_{11}^2}{r_{11}} = \frac{(Z-10)e^2}{4\pi\varepsilon_0 r_{11}^2} - \frac{\hbar^2}{4m_e r_{11}^2 r_{10}}\sqrt{s(s+1)} - \frac{8\hbar^2}{Zm_e r_{11}^3}\sqrt{s(s+1)} \tag{10.222}$$

Substitution of $v_{11} = \frac{\hbar}{m_e r_{11}}$ (Eq. (1.35)) and $s = \frac{1}{2}$ into Eq. (10.222) gives:

$$\frac{\hbar^2}{m_e r_{11}^3} = \frac{(Z-10)e^2}{4\pi\varepsilon_0 r_{11}^2} - \frac{\hbar^2}{4m_e r_{11}^2 r_{10}}\sqrt{\frac{3}{4}} - \frac{8\hbar^2}{Zm_e r_{11}^3}\sqrt{\frac{3}{4}} \tag{10.223}$$

$$r_{11} = \frac{\frac{\hbar^2}{m_e}\left(1+\frac{8}{Z}\sqrt{\frac{3}{4}}\right)}{\frac{(Z-10)e^2}{4\pi\varepsilon_0} - \frac{\hbar^2}{4m_e r_{10}}\sqrt{\frac{3}{4}}} \tag{10.224}$$

$$r_{11} = \frac{a_0\left(1+\frac{8}{Z}\sqrt{\frac{3}{4}}\right)}{(Z-10) - \frac{\sqrt{\frac{3}{4}}}{4r_{10}}},\ r_{10}\ \textit{in units of}\ a_0 \tag{10.225}$$

Substitution of $\frac{r_{10}}{a_0} = 0.56094$ (Eq. (10.212) with $Z = 11$) into Eq. (10.225) gives:

$$r_{11} = 2.65432a_0 \tag{10.226}$$

The ionization energy of the sodium atom is given by the negative of $E(electric)$ given by Eq. (10.102) with the appropriate charge and radius:

$$E(ionization;\ Na) = -Electric\ Energy = \frac{(Z-10)e^2}{8\pi\varepsilon_0 r_{11}} = 5.12592\ eV \tag{10.227}$$

where $r_{11} = 2.65432a_0$ (Eq. (10.226)) and $Z = 11$. The experimental ionization energy of the sodium atom is $5.13908\ eV$ [3].

## THE IONIZATION ENERGIES OF ELEVEN-ELECTRON ATOMS WITH A NUCLEAR CHARGE Z>11

Eleven-electron atoms having $Z>11$ possess an external electric field given by Eq. (10.92). Since there is a source of dissipative power, $\mathbf{J}\bullet\mathbf{E}$ of Eq. (10.27), the magnetic moments of the inner electrons may change due to the outer electron such that the energy of the eleven-electron atom is lowered. The orbital angular momenta of the paired $p_x$ and $p_y$ electrons give rise to the paramagnetic force given by Eq. (10.89), which is also equivalent to that given by Eq. (10.55):

$$\mathbf{F}_{mag\ 2}=\frac{1}{Z}\frac{4\hbar^2}{m_e r_{11}^2 r_{10}}\sqrt{s(s+1)}\mathbf{i}_{\mathbf{r}} \tag{10.228}$$

The diamagnetic force, $\mathbf{F}_{diamagnetic\ 2}$, due to a relativistic effect with an electric field for $r>r_n$ (Eq. (10.35)) may be determined by considering the corresponding force due to the binding of a 2p electron. It was shown in the Five-Electron Atom section, that $\mathbf{F}_{diamagnetic\ 2}$ for five through ten-electron atoms, is dependent on the amplitude of the orbital energy. Using the orbital energy with $\ell=1$ (Eq. (10.90)), the energy $m_e\Delta v^2$ of Eq. (10.29) is reduced by the factor of $\left(1-\frac{\sqrt{2}}{2}\right)$ due to the contribution of the charge-density wave of the inner electrons at $r_3$. Thus, $\mathbf{F}_{diamagnetic\ 2}$ is given by Eq. (10.93). Conversely, the binding of a 3s electron increases the energy $m_e\Delta v^2$ of Eq. (10.29) by the factor of $\left(1+\frac{\sqrt{2}}{2}\right)$ such that $\mathbf{F}_{diamagnetic\ 2}$ becomes

$$\mathbf{F}_{diamagnetic\ 2}=-\left[\frac{Z-11}{Z-10}\right]\left(1+\frac{\sqrt{2}}{2}\right)\frac{r_{10}\hbar^2}{m_e r_{11}^4}10\sqrt{s(s+1)}\mathbf{i}_{\mathbf{r}} \tag{10.229}$$

In the case that $Z>11$, the radius of the outer electron is calculated by equating the outward centrifugal force to the sum of the electric (Eq. (10.218)), diamagnetic (Eq. (10.229)), and paramagnetic (Eq. (10.228)) forces as follows:

$$\frac{m_e v_{11}^2}{r_{11}}=\frac{(Z-10)e^2}{4\pi\varepsilon_0 r_{11}^2}-\frac{\hbar^2}{4m_e r_{11}^2 r_{10}}\sqrt{s(s+1)}+\frac{4\hbar^2}{Zm_e r_{11}^2 r_{10}}\sqrt{s(s+1)}$$
$$-\frac{8\hbar^2}{Zm_e r_{11}^3}\sqrt{s(s+1)}-\left[\frac{Z-11}{Z-10}\right]\left(1+\frac{\sqrt{2}}{2}\right)\frac{r_{10}\hbar^2}{m_e r_{11}^4}10\sqrt{s(s+1)} \tag{10.230}$$

Substitution of $v_{11}=\frac{\hbar}{m_e r_{11}}$ (Eq. (1.35)) and $s=\frac{1}{2}$ into Eq. (10.230) gives:

$$\frac{\hbar^2}{m_e r_{11}^3}=\frac{(Z-10)e^2}{4\pi\varepsilon_0 r_{11}^2}-\frac{\hbar^2}{4m_e r_{11}^2 r_{10}}\sqrt{\frac{3}{4}}+\frac{4\hbar^2}{Zm_e r_{11}^2 r_{10}}\sqrt{\frac{3}{4}}-\frac{8\hbar^2}{Zm_e r_{11}^3}\sqrt{\frac{3}{4}}-\left[\frac{Z-11}{Z-10}\right]\left(1+\frac{\sqrt{2}}{2}\right)\frac{r_{10}\hbar^2}{m_e r_{11}^4}10\sqrt{\frac{3}{4}} \tag{10.231}$$

The quadratic equation corresponding to Eq. (10.231) is

$$\left(\frac{(Z-10)e^2}{4\pi\varepsilon_0}-\left(\frac{1}{4}-\frac{4}{Z}\right)\frac{\hbar^2}{m_e r_{10}}\sqrt{\frac{3}{4}}\right)r_{11}^2-\frac{\hbar^2}{m_e}\left(1+\frac{8\sqrt{\frac{3}{4}}}{Z}\right)r_{11}-\left[\frac{Z-11}{Z-10}\right]\left(1+\frac{\sqrt{2}}{2}\right)\frac{r_{10}\hbar^2}{m_e}10\sqrt{\frac{3}{4}}=0 \tag{10.232}$$

$$r_{11}^2-\frac{\frac{\hbar^2}{m_e}\left(1+\frac{8\sqrt{\frac{3}{4}}}{Z}\right)}{\left(\frac{(Z-10)e^2}{4\pi\varepsilon_0}-\left(\frac{1}{4}-\frac{4}{Z}\right)\frac{\hbar^2}{m_e r_{10}}\sqrt{\frac{3}{4}}\right)}r_{11}-\frac{\left[\frac{Z-11}{Z-10}\right]\left(1+\frac{\sqrt{2}}{2}\right)\frac{r_{10}\hbar^2}{m_e}10\sqrt{\frac{3}{4}}}{\left(\frac{(Z-10)e^2}{4\pi\varepsilon_0}-\left(\frac{1}{4}-\frac{4}{Z}\right)\frac{\hbar^2}{m_e r_{10}}\sqrt{\frac{3}{4}}\right)}=0 \tag{10.233}$$

The solution of Eq. (10.233) using the quadratic formula is:

$$r_{11}=\frac{\dfrac{\dfrac{\hbar^2}{m_e}\left(1+\dfrac{8\sqrt{\dfrac{3}{4}}}{Z}\right)}{\left(\dfrac{(Z-10)e^2}{4\pi\varepsilon_0}-\left(\dfrac{1}{4}-\dfrac{4}{Z}\right)\dfrac{\hbar^2}{m_e r_{10}}\sqrt{\dfrac{3}{4}}\right)}\pm\sqrt{\left(\dfrac{\dfrac{\hbar^2}{m_e}\left(1+\dfrac{8\sqrt{\dfrac{3}{4}}}{Z}\right)}{\left(\dfrac{(Z-10)e^2}{4\pi\varepsilon_0}-\left(\dfrac{1}{4}-\dfrac{4}{Z}\right)\dfrac{\hbar^2}{m_e r_{10}}\sqrt{\dfrac{3}{4}}\right)}\right)^2+4\dfrac{\left[\dfrac{Z-11}{Z-10}\right]\left(1+\dfrac{\sqrt{2}}{2}\right)\dfrac{r_{10}\hbar^2}{m_e}10\sqrt{\dfrac{3}{4}}}{\left(\dfrac{(Z-10)e^2}{4\pi\varepsilon_0}-\left(\dfrac{1}{4}-\dfrac{4}{Z}\right)\dfrac{\hbar^2}{m_e r_{10}}\sqrt{\dfrac{3}{4}}\right)}}}{2} \tag{10.234}$$

$$r_{11}=\frac{\dfrac{a_0\left(1+\dfrac{4\sqrt{3}}{Z}\right)}{\left((Z-10)-\left(\dfrac{1}{8}-\dfrac{2}{Z}\right)\dfrac{\sqrt{3}}{r_{10}}\right)}\pm a_0\sqrt{\left(\dfrac{1+\dfrac{4\sqrt{3}}{Z}}{\left((Z-10)-\left(\dfrac{1}{8}-\dfrac{2}{Z}\right)\dfrac{\sqrt{3}}{r_{10}}\right)}\right)^2+\dfrac{20\sqrt{3}\left(\left[\dfrac{Z-11}{Z-10}\right]\left(1+\dfrac{\sqrt{2}}{2}\right)r_{10}\right)}{\left((Z-10)-\left(\dfrac{1}{8}-\dfrac{2}{Z}\right)\dfrac{\sqrt{3}}{r_{10}}\right)}}}{2},\ r_{10}\ \textit{in units of}\ a_0 \tag{10.235}$$

where $r_{10}$ is given by Eq. (10.212). The positive root of Eq. (10.235) must be taken in order that $r_{11}>0$. The radii of several eleven-electron atoms are given in Table 10.10.

The ionization energies for the eleven-electron atoms with $Z>11$ are given by the electric energy, $E(electric)$, (Eq. (10.102) with the radii, $r_{11}$, given by Eq. (10.235)):

$$E(Ionization)=-Electric\ Energy=\frac{(Z-10)e^2}{8\pi\varepsilon_0 r_{11}} \tag{10.236}$$

Since the relativistic corrections were small, the nonrelativistic ionization energies for experimentally measured eleven-electron atoms are given in Table 10.10.

**Table 10.10.** Ionization energies for some eleven-electron atoms.

| 11 e Atom | Z | $r_1$ $(a_o)$ [a] | $r_3$ $(a_o)$ [b] | $r_{10}$ $(a_o)$ [c] | $r_{11}$ $(a_o)$ [d] | Theoretical Ionization Energies [e] $(eV)$ | Experimental Ionization Energies [f] $(eV)$ | Relative Error [g] |
|---|---|---|---|---|---|---|---|---|
| $Na$ | 11 | 0.09213 | 0.40853 | 0.560945 | 2.65432 | 5.12592 | 5.13908 | 0.0026 |
| $Mg^{+}$ | 12 | 0.08435 | 0.37065 | 0.510568 | 1.74604 | 15.5848 | 15.03528 | -0.0365 |
| $Al^{2+}$ | 13 | 0.07778 | 0.33923 | 0.456203 | 1.47399 | 27.6918 | 28.44765 | 0.0266 |
| $Si^{3+}$ | 14 | 0.07216 | 0.31274 | 0.409776 | 1.25508 | 43.3624 | 45.14181 | 0.0394 |
| $P^{4+}$ | 15 | 0.06730 | 0.29010 | 0.371201 | 1.08969 | 62.4299 | 65.0251 | 0.0399 |
| $S^{5+}$ | 16 | 0.06306 | 0.27053 | 0.339025 | 0.96226 | 84.8362 | 88.0530 | 0.0365 |
| $Cl^{6+}$ | 17 | 0.05932 | 0.25344 | 0.311903 | 0.86151 | 110.5514 | 114.1958 | 0.0319 |
| $Ar^{7+}$ | 18 | 0.05599 | 0.23839 | 0.288778 | 0.77994 | 139.5577 | 143.460 | 0.0272 |
| $K^{8+}$ | 19 | 0.05302 | 0.22503 | 0.268844 | 0.71258 | 171.8433 | 175.8174 | 0.0226 |
| $Ca^{9+}$ | 20 | 0.05035 | 0.21308 | 0.251491 | 0.65602 | 207.3998 | 211.275 | 0.0183 |
| $Sc^{10+}$ | 21 | 0.04794 | 0.20235 | 0.236251 | 0.60784 | 246.2213 | 249.798 | 0.0143 |
| $Ti^{11+}$ | 22 | 0.04574 | 0.19264 | 0.222761 | 0.56631 | 288.3032 | 291.500 | 0.0110 |
| $V^{12+}$ | 23 | 0.04374 | 0.18383 | 0.210736 | 0.53014 | 333.6420 | 336.277 | 0.0078 |
| $Cr^{13+}$ | 24 | 0.04191 | 0.17579 | 0.19995 | 0.49834 | 382.2350 | 384.168 | 0.0050 |
| $Mn^{14+}$ | 25 | 0.04022 | 0.16842 | 0.19022 | 0.47016 | 434.0801 | 435.163 | 0.0025 |
| $Fe^{15+}$ | 26 | 0.03867 | 0.16165 | 0.181398 | 0.44502 | 489.1753 | 489.256 | 0.0002 |
| $Co^{16+}$ | 27 | 0.03723 | 0.15540 | 0.173362 | 0.42245 | 547.5194 | 546.58 | -0.0017 |
| $Ni^{17+}$ | 28 | 0.03589 | 0.14961 | 0.166011 | 0.40207 | 609.1111 | 607.06 | -0.0034 |
| $Cu^{18+}$ | 29 | 0.03465 | 0.14424 | 0.159261 | 0.38358 | 673.9495 | 670.588 | -0.0050 |
| $Zn^{19+}$ | 30 | 0.03349 | 0.13925 | 0.153041 | 0.36672 | 742.0336 | 738 | -0.0055 |

[a] Radius of the first set of paired inner electrons of eleven-electron atoms from Eq. (10.51).
[b] Radius of the second set of paired inner electrons of eleven-electron atoms from Eq. (10.62).
[c] Radius of three sets of paired inner electrons of eleven-electron atoms from Eq. (10.212).
[d] Radius of unpaired outer electron of eleven-electron atoms from Eq. (10.235) for $Z > 11$ and Eq. (10.226) for *Na*.
[e] Calculated ionization energies of eleven-electron atoms given by the electric energy (Eq. (10.236)).
[f] From theoretical calculations, interpolation of isoelectronic and spectral series, and experimental data [2-3].
[g] (Experimental-theoretical)/experimental.

The agreement between the experimental and calculated values of Table 10.10 is well within the experimental capability of the spectroscopic determinations including the values at large Z, which relies on X-ray spectroscopy. In this case, the experimental capability is three to four significant figures, which is consistent with the last column. The sodium atom isoelectronic series is given in Table 10.10 [2-3] to much higher precision than the capability of X-ray spectroscopy, but these values are based on theoretical and interpolation techniques rather than data alone. Ionization energies are difficult to determine since the cut-off of the Rydberg series of lines at the ionization energy is often not observed, and the ionization energy must be determined from theoretical calculations, interpolation of Na isoelectronic and Rydberg series, as well as direct experimental data.

# TWELVE-ELECTRON ATOMS

Twelve-electron atoms can be solved exactly using the results of the solutions of one, two, three, four, five, six, seven, eight, nine, ten, and eleven-electron atoms.

## RADIUS AND IONIZATION ENERGY OF THE OUTER ELECTRON OF THE MAGNESIUM ATOM

For each eleven-electron atom having a central charge of $Z$ times that of the proton, there are two indistinguishable spin-paired electrons in an atomic orbital with radii $r_1$ and $r_2$ both given by Eq. (7.35) (Eq. (10.51)), two indistinguishable spin-paired electrons in an atomic orbital with radii $r_3$ and $r_4$ both given by Eq. (10.62), three sets of paired electrons in an atomic orbital at $r_{10}$ given by Eq. (10.212), and an unpaired electron in an atomic orbital at $r_{11}$. For $Z \geq 12$, the next electron which binds to form the corresponding twelve-electron atom is attracted by the central Coulomb field and the spin-pairing force with the unpaired 3s inner electron and is repelled by diamagnetic forces due to the 3 sets of spin-paired inner electrons such that it forms an unpaired atomic orbital at radius $r_{12}$.

The central Coulomb force acts on the outer electron to cause it to bind wherein this electric force on the outer-most electron due to the nucleus and the inner eleven electrons is given by Eq. (10.70) with the appropriate charge and radius:

$$\mathbf{F}_{ele} = \frac{(Z-11)e^2}{4\pi\varepsilon_0 r_{12}^2}\mathbf{i}_\mathbf{r} \tag{10.237}$$

for $r > r_{11}$.

The outer electron which binds to form the corresponding twelve-electron atom becomes spin-paired with the unpaired inner electron such that they become indistinguishable with the same radius $r_{11} = r_{12}$ corresponding to a filled 3s shell. The corresponding spin-pairing force $\mathbf{F}_{mag}$ is given by Eq. (7.24).

$$\mathbf{F}_{mag} = \frac{1}{Z}\frac{\hbar^2}{m_e r_{12}^3}\sqrt{s(s+1)}\mathbf{i}_\mathbf{r} \tag{10.238}$$

The spherically symmetrical closed 2p shell of twelve-electron atoms produces a diamagnetic force, $\mathbf{F}_{diamagnetic}$, that is equivalent to that of a closed s shell given by Eq. (10.11) with the appropriate radii. The inner electrons remain at their initial radii, but cause a diamagnetic force according to Lenz's law that is:

$$\mathbf{F}_{diamagnetic} = -\frac{\hbar^2}{4m_e r_{12}^2 r_{10}}\sqrt{s(s+1)}\mathbf{i}_\mathbf{r} \tag{10.239}$$

In addition to the paramagnetic spin-pairing force between the eleventh electron initially at radius $r_{11}$, the pairing causes the diamagnetic interaction between the outer electrons and the inner electrons given by Eq. (10.11) to vanish, except for an electrodynamic effect for $Z > 12$ described in the Two-Electron Atoms section, since upon pairing the magnetic field of the outer electrons becomes zero. Using Eq. (10.55), $\mathbf{F}_{mag\ 2}$ due to the three 2p orbitals is given by:

$$\mathbf{F}_{mag\ 2} = \frac{3}{Z}\frac{\hbar^2}{m_e r_{10} r_{12}^2}\sqrt{s(s+1)}\mathbf{i}_\mathbf{r} \tag{10.240}$$

In addition to the spin-spin interactions between electron pairs, the three sets of 2p electrons are orbitally paired. The s electrons of the magnesium atom produce a magnetic field at the position of the three sets of spin-paired 2p electrons. In order for the electrons to remain spin and orbitally paired, the corresponding diamagnetic force, $\mathbf{F}_{diamagnetic\ 3}$ (Eq. (10.221)), on electron twelve from the three sets of spin-paired electrons is given by:

$$\mathbf{F}_{diamagnetic\ 3} = -\frac{1}{Z}\frac{12\hbar^2}{m_e r_{12}^3}\sqrt{s(s+1)}\mathbf{i}_\mathbf{r} \tag{10.241}$$

corresponding to the $p_x$, $p_y$, and $p_z$ electrons.

The outward centrifugal force on electron 12 is balanced by the electric force and the magnetic forces (on electron 12). The radius of the outer electron is calculated by equating the outward centrifugal force to the sum of the electric (Eq. (10.237)), diamagnetic (Eqs. (10.239) and (10.241)) and paramagnetic (Eqs. (10.238) and (10.240)) forces as follows:

$$\frac{m_e v_{12}^2}{r_{12}} = \frac{(Z-11)e^2}{4\pi\varepsilon_0 r_{12}^2} - \frac{\hbar^2}{4m_e r_{12}^2 r_{10}}\sqrt{s(s+1)} + \frac{3\hbar^2}{Zm_e r_{12}^2 r_{10}}\sqrt{s(s+1)} \tag{10.242}$$

$$-\frac{12\hbar^2}{Zm_e r_{12}^3}\sqrt{s(s+1)} + \frac{\hbar^2}{Zm_e r_{12}^3}\sqrt{s(s+1)}$$

Substitution of $v_{12} = \frac{\hbar}{m_e r_{12}}$ (Eq. (1.35)) and $s = \frac{1}{2}$ into Eq. (10.242) gives:

$$\frac{\hbar^2}{m_e r_{12}^3} = \frac{(Z-11)e^2}{4\pi\varepsilon_0 r_{12}^2} - \frac{\hbar^2}{4m_e r_{12}^2 r_{10}}\sqrt{\frac{3}{4}} + \frac{3\hbar^2}{Zm_e r_{12}^2 r_{10}}\sqrt{\frac{3}{4}} - \frac{12\hbar^2}{Zm_e r_{12}^3}\sqrt{\frac{3}{4}} + \frac{\hbar^2}{Zm_e r_{12}^3}\sqrt{\frac{3}{4}} \tag{10.243}$$

$$r_{12} = \frac{\frac{\hbar^2}{m_e}\left(1 + \frac{11\sqrt{\frac{3}{4}}}{Z}\right)}{\frac{(Z-11)e^2}{4\pi\varepsilon_0} - \left(\frac{1}{4} - \frac{3}{Z}\right)\frac{\hbar^2}{m_e r_{10}}\sqrt{\frac{3}{4}}} \tag{10.244}$$

$$r_{12} = \frac{a_0\left(1 + \frac{11\sqrt{\frac{3}{4}}}{Z}\right)}{(Z-11) - \left(\frac{1}{4} - \frac{3}{Z}\right)\frac{\sqrt{\frac{3}{4}}}{r_{10}}},\ r_{10}\ \textit{in units of}\ a_0 \tag{10.245}$$

Substitution of $\frac{r_{10}}{a_0} = 0.51057$ (Eq. (10.212) with $Z = 12$) into Eq. (10.245) gives:

$$r_{12} = 1.79386 a_0 \tag{10.246}$$

The ionization energy of the magnesium atom is given by the electric energy, $E(electric)$, (Eq. (10.102) with the radius, $r_{12}$, given by Eq. (10.246)).

$$E(ionization;\ Mg) = -Electric\ Energy = \frac{(Z-11)e^2}{8\pi\varepsilon_0 r_{12}} = 7.58467\ eV \tag{10.247}$$

where $r_{12} = 1.79386 a_0$ (Eq. (10.246)) and $Z = 12$. The experimental ionization energy of the magnesium atom is $7.64624\ eV$ [3].

## THE IONIZATION ENERGIES OF TWELVE-ELECTRON ATOMS WITH A NUCLEAR CHARGE Z>12

Twelve-electron atoms having $Z > 12$ possess an external electric field given by Eq. (10.92). Since there is a source of dissipative power, $\mathbf{J} \bullet \mathbf{E}$ of Eq. (10.27), the magnetic moments of the inner electrons may change due to the outer electron such that the energy of the twelve-electron atom is lowered with conservation of angular momentum. Of the possible forces based on Maxwell's equations, those that give rise to an energy minimum are used to calculate the atomic radii and energies. With this constraint, the only paramagnetic force is that given by Eq. (10.89) due to the spin angular momenta of the paired 2 $p_x$, $p_y$, and $p_z$ electrons interacting equivalently with each of the 3s electrons. This force, which is also equivalent to that given by Eq. (10.145), is:

$$\mathbf{F}_{mag\ 2} = 2\frac{1}{Z}\frac{3\hbar^2}{m_e r_{12}^2 r_{10}}\sqrt{s(s+1)}\mathbf{i}_{\mathbf{r}} \tag{10.248}$$

From Eq. (10.229), the diamagnetic force, $\mathbf{F}_{diamagnetic\ 2}$, due to a relativistic effect with an electric field for $r > r_{12}$ (Eq. (10.35)) is:

$$\mathbf{F}_{diamagnetic\ 2} = -\left[\frac{Z-12}{Z-11}\right]\left(1+\frac{\sqrt{2}}{2}\right)\frac{r_{10}\hbar^2}{m_e r_{12}^4}10\sqrt{s(s+1)}\mathbf{i}_{\mathbf{r}} \tag{10.249}$$

In the case that $Z > 12$, the radius of the outer electron is calculated by equating the outward centrifugal force to the sum of the electric (Eq. (10.237)), diamagnetic (Eq. (10.249)), and paramagnetic (Eq. (10.248)) forces as follows:

$$\frac{m_e v_{12}^2}{r_{12}} = \frac{(Z-11)e^2}{4\pi\varepsilon_0 r_{12}^2} - \frac{\hbar^2}{4m_e r_{12}^2 r_{10}}\sqrt{s(s+1)} + \frac{6\hbar^2}{Z m_e r_{12}^2 r_{10}}\sqrt{s(s+1)} - \left[\frac{Z-12}{Z-11}\right]\left(1+\frac{\sqrt{2}}{2}\right)\frac{r_{10}\hbar^2}{m_e r_{12}^4}10\sqrt{s(s+1)} \tag{10.250}$$

Substitution of $v_{12} = \frac{\hbar}{m_e r_{12}}$ (Eq. (1.35)) and $s = \frac{1}{2}$ into Eq. (10.250) gives:

$$\frac{\hbar^2}{m_e r_{12}^3} = \frac{(Z-11)e^2}{4\pi\varepsilon_0 r_{12}^2} - \frac{\hbar^2}{4m_e r_{12}^2 r_{10}}\sqrt{\frac{3}{4}} + \frac{6\hbar^2}{Z m_e r_{12}^2 r_{10}}\sqrt{\frac{3}{4}} - \left[\frac{Z-12}{Z-11}\right]\left(1+\frac{\sqrt{2}}{2}\right)\frac{r_{10}\hbar^2}{m_e r_{12}^4}10\sqrt{\frac{3}{4}} \tag{10.251}$$

The quadratic equation corresponding to Eq. (10.251) is

$$\left(\frac{(Z-11)e^2}{4\pi\varepsilon_0} - \left(\frac{1}{4}-\frac{6}{Z}\right)\frac{\hbar^2}{m_e r_{10}}\sqrt{\frac{3}{4}}\right)r_{12}^2 - \frac{\hbar^2}{m_e}r_{12} - \left[\frac{Z-12}{Z-11}\right]\left(1+\frac{\sqrt{2}}{2}\right)\frac{r_{10}\hbar^2}{m_e}10\sqrt{\frac{3}{4}} = 0 \tag{10.252}$$

$$r_{12}^2 - \frac{\frac{\hbar^2}{m_e}}{\left(\frac{(Z-11)e^2}{4\pi\varepsilon_0} - \left(\frac{1}{4}-\frac{6}{Z}\right)\frac{\hbar^2}{m_e r_{10}}\sqrt{\frac{3}{4}}\right)}r_{12} - \frac{\left[\frac{Z-12}{Z-11}\right]\left(1+\frac{\sqrt{2}}{2}\right)\frac{r_{10}\hbar^2}{m_e}10\sqrt{\frac{3}{4}}}{\left(\frac{(Z-11)e^2}{4\pi\varepsilon_0} - \left(\frac{1}{4}-\frac{6}{Z}\right)\frac{\hbar^2}{m_e r_{10}}\sqrt{\frac{3}{4}}\right)} = 0 \tag{10.253}$$

The solution of Eq. (10.253) using the quadratic formula is:

$$r_{12}=\frac{\dfrac{\dfrac{\hbar^2}{m_e}}{\left(\dfrac{(Z-11)e^2}{4\pi\varepsilon_0}-\left(\dfrac{1}{4}-\dfrac{6}{Z}\right)\dfrac{\hbar^2}{m_e r_{10}}\sqrt{\dfrac{3}{4}}\right)}\pm\sqrt{\left(\dfrac{\dfrac{\hbar^2}{m_e}}{\left(\dfrac{(Z-11)e^2}{4\pi\varepsilon_0}-\left(\dfrac{1}{4}-\dfrac{6}{Z}\right)\dfrac{\hbar^2}{m_e r_{10}}\sqrt{\dfrac{3}{4}}\right)}\right)^2+4\dfrac{\left[\dfrac{Z-12}{Z-11}\right]\left(1+\dfrac{\sqrt{2}}{2}\right)\dfrac{r_{10}\hbar^2}{m_e}10\sqrt{\dfrac{3}{4}}}{\left(\dfrac{(Z-11)e^2}{4\pi\varepsilon_0}-\left(\dfrac{1}{4}-\dfrac{6}{Z}\right)\dfrac{\hbar^2}{m_e r_{10}}\sqrt{\dfrac{3}{4}}\right)}}}{2} \tag{10.254}$$

$$r_{12}=\frac{\dfrac{a_0}{\left((Z-11)-\left(\dfrac{1}{8}-\dfrac{3}{Z}\right)\dfrac{\sqrt{3}}{r_{10}}\right)}\pm a_0\sqrt{\left(\dfrac{1}{\left((Z-11)-\left(\dfrac{1}{8}-\dfrac{3}{Z}\right)\dfrac{\sqrt{3}}{r_{10}}\right)}\right)^2+\dfrac{20\sqrt{3}\left(\left[\dfrac{Z-12}{Z-11}\right]\left(1+\dfrac{\sqrt{2}}{2}\right)r_{10}\right)}{\left((Z-11)-\left(\dfrac{1}{8}-\dfrac{3}{Z}\right)\dfrac{\sqrt{3}}{r_{10}}\right)}}}{2},\ r_{10}\ \textit{in units of}\ a_0 \tag{10.255}$$

where $r_{10}$ is given by Eq. (10.212). The positive root of Eq. (10.255) must be taken in order that $r_{12}>0$. The radii of several twelve-electron atoms are given in Table 10.11.

The ionization energies for the twelve-electron atoms with $Z>12$ are given by the electric energy, $E(electric)$, (Eq. (10.102) with the radii, $r_{12}$, given by Eq. (10.255)).

$$E(Ionization)=-Electric\ Energy=\frac{(Z-11)e^2}{8\pi\varepsilon_0 r_{12}} \tag{10.256}$$

Since the relativistic corrections were small, the nonrelativistic ionization energies for experimentally measured twelve-electron atoms are given in Table 10.11.

**Table 10.11.** Ionization energies for some twelve-electron atoms.

| 12 e Atom | Z | $r_1$ $(a_o)$ [a] | $r_3$ $(a_o)$ [b] | $r_{10}$ $(a_o)$ [c] | $r_{12}$ $(a_o)$ [d] | Theoretical Ionization Energies [e] $(eV)$ | Experimental Ionization Energies [f] $(eV)$ | Relative Error [g] |
|---|---|---|---|---|---|---|---|---|
| $Mg$ | 12 | 0.08435 | 0.37065 | 0.51057 | 1.79386 | 7.58467 | 7.64624 | 0.0081 |
| $Al^{+}$ | 13 | 0.07778 | 0.33923 | 0.45620 | 1.41133 | 19.2808 | 18.82856 | -0.0240 |
| $Si^{2+}$ | 14 | 0.07216 | 0.31274 | 0.40978 | 1.25155 | 32.6134 | 33.49302 | 0.0263 |
| $P^{3+}$ | 15 | 0.06730 | 0.29010 | 0.37120 | 1.09443 | 49.7274 | 51.4439 | 0.0334 |
| $S^{4+}$ | 16 | 0.06306 | 0.27053 | 0.33902 | 0.96729 | 70.3296 | 72.5945 | 0.0312 |
| $Cl^{5+}$ | 17 | 0.05932 | 0.25344 | 0.31190 | 0.86545 | 94.3266 | 97.03 | 0.0279 |
| $Ar^{6+}$ | 18 | 0.05599 | 0.23839 | 0.28878 | 0.78276 | 121.6724 | 124.323 | 0.0213 |
| $K^{7+}$ | 19 | 0.05302 | 0.22503 | 0.26884 | 0.71450 | 152.3396 | 154.88 | 0.0164 |
| $Ca^{8+}$ | 20 | 0.05035 | 0.21308 | 0.25149 | 0.65725 | 186.3102 | 188.54 | 0.0118 |
| $Sc^{9+}$ | 21 | 0.04794 | 0.20235 | 0.23625 | 0.60857 | 223.5713 | 225.18 | 0.0071 |
| $Ti^{10+}$ | 22 | 0.04574 | 0.19264 | 0.22276 | 0.56666 | 264.1138 | 265.07 | 0.0036 |
| $V^{11+}$ | 23 | 0.04374 | 0.18383 | 0.21074 | 0.53022 | 307.9304 | 308.1 | 0.0006 |
| $Cr^{12+}$ | 24 | 0.04191 | 0.17579 | 0.19995 | 0.49822 | 355.0157 | 354.8 | -0.0006 |
| $Mn^{13+}$ | 25 | 0.04022 | 0.16842 | 0.19022 | 0.46990 | 405.3653 | 403.0 | -0.0059 |
| $Fe^{14+}$ | 26 | 0.03867 | 0.16165 | 0.18140 | 0.44466 | 458.9758 | 457 | -0.0043 |
| $Co^{15+}$ | 27 | 0.03723 | 0.15540 | 0.17336 | 0.42201 | 515.8442 | 511.96 | -0.0076 |
| $Ni^{16+}$ | 28 | 0.03589 | 0.14961 | 0.16601 | 0.40158 | 575.9683 | 571.08 | -0.0086 |
| $Cu^{17+}$ | 29 | 0.03465 | 0.14424 | 0.15926 | 0.38305 | 639.3460 | 633 | -0.0100 |
| $Zn^{18+}$ | 30 | 0.03349 | 0.13925 | 0.15304 | 0.36617 | 705.9758 | 698 | -0.0114 |

[a] Radius of the first set of paired inner electrons of twelve-electron atoms from Eq. (10.51).

[b] Radius of the second set of paired inner electrons of twelve-electron atoms from Eq. (10.62).

[c] Radius of three sets of paired inner electrons of twelve-electron atoms from Eq. (10.212).

[d] Radius of paired outer electrons of twelve-electron atoms from Eq. (10.255) for $Z > 12$ and Eq. (10.246) for *Mg*.

[e] Calculated ionization energies of twelve-electron atoms given by the electric energy (Eq. (10.256)).

[f] From theoretical calculations, interpolation of isoelectronic and spectral series, and experimental data [2-3].

[g] (Experimental-theoretical)/experimental.

The agreement between the experimental and calculated values of Table 10.11 is well within the experimental capability of the spectroscopic determinations including the values at large Z which relies on X-ray spectroscopy. In this case, the experimental capability is three to four significant figures, which is consistent with the last column. The magnesium atom isoelectronic series is given in Table 10.11 [2-3] to much higher precision than the capability of X-ray spectroscopy, but these values are based on theoretical and interpolation techniques rather than data alone. Ionization energies are difficult to determine since the cut-off of the Rydberg series of lines at the ionization energy is often not observed, and the ionization energy must be determined from theoretical calculations, interpolation of Mg isoelectronic and Rydberg series, as well as direct experimental data.

## 3P-ORBITAL ELECTRONS BASED ON AN ENERGY MINIMUM

For each thirteen through eighteen-electron atom having a central charge of $Z$ times that of the proton, there are two indistinguishable spin-paired electrons in an atomic orbital with radii $r_1$ and $r_2$ both given by Eq. (7.35) (Eq. (10.51)), two indistinguishable spin-paired electrons in an atomic orbital with radii $r_3$ and $r_4$ both given by Eq. (10.62), three sets of paired electrons in an atomic orbital at $r_{10}$ given by Eq. (10.212), and two indistinguishable spin-paired electrons in an atomic orbital with radii $r_{11}$ and $r_{12}$ both given by Eq. (10.255). For $Z \geq 12$, the next electron which binds to form the corresponding n-electron atom $(13 \leq n \leq 18)$ is attracted by the central Coulomb field and is repelled by diamagnetic forces and attracted by paramagnetic forces due to the 3 sets of spin-paired inner 2p electrons and two spin-paired inner 3s electrons such that it forms an atomic orbital comprising all of the 3p electrons at radius $r_n$. The resulting electron configuration is $1s^2 2s^2 2p^6 3s^2 3p^{n-12}$.

The central Coulomb force, $\mathbf{F}_{ele}$, acts on the outer electron to cause it to bind wherein this electric force on the outer-most electron due to the nucleus and the inner $n-1$ electrons is given by Eq. (10.70).

$$\mathbf{F}_{ele} = \frac{(Z-(n-1))e^2}{4\pi\varepsilon_0 r_n^2}\mathbf{i}_r \tag{10.257}$$

for $r > r_{n-1}$ where $n$ corresponds to the number of electrons of the atom and $Z$ is its atomic number. In each case, the magnetic field of the binding outer electron changes the angular velocities of the inner electrons. However, in each case, the magnetic field of the outer electron provides a central Lorentz force which exactly balances the change in centrifugal force because of the change in angular velocity [1]. The inner electrons remain at their initial radii, but cause a diamagnetic force according to Lenz's law.

As shown in the 2P-Orbital Electrons Based on an Energy Minimum section the quantum numbers $\ell = 1 \quad m = \pm 1$ and $\ell = 1 \quad m = 0$ correspond to spherical harmonics solutions, $Y_\ell^m(\theta,\phi)$, of Laplace's equation designated the $2\,p_x$, $2\,p_y$, and $2\,p_z$ orbitals, respectively. Similarly, for $13 \le n \le 18$, the energy may be lowered by filling 3p orbitals in the same manner to achieve an energy minimum relative to other configurations and arrangements. In general, a nonuniform distribution of charge achieves an energy minimum with the formation of a fifth shell due to the dependence of the magnetic forces on the nuclear charge and orbital energy (Eqs. (10.70), (10.258-10.264), and (10.268)). The outer electrons of atoms and ions that are isoelectronic with the series aluminum through argon half-fill a 3p level with unpaired electrons at phosphorous, then fill the level with paired electrons at argon.

Similarly to the case of the 2p orbitals, spherical harmonic charge-density waves may be induced in the inner electron atomic orbitals with the addition of one or more outer electrons to the 3p orbitals. An energy minimum is achieved when the thirteenth through eighteenth electrons of each thirteen through eighteen-electron atom fills a 3p orbital with the formation of orthogonal complementary charge-density waves in the inner shell 2p and 3s electrons. To maintain the symmetry of the central charge and the energy minimum condition given by solutions to Laplace's equation (Eq. (10.72)), the charge-density waves on electron atomic orbitals at $r_{10}$ and $r_{12}$ complement those of the outer orbitals when the outer 3p orbitals are not all occupied by at least one electron, and the complementary charge-density waves are provided by electrons at $r_{12}$ when this condition is met. In the case of the 3p electrons, an exception to the trends in 2p orbital forces arises due to the interaction between the 2p, 3s, and 3p electrons due to magnetic fields independent of induced complementary charge-density waves. The spin and angular momenta of the 2p electrons give rise to corresponding magnetic fields that interact with the two 3s electrons. The filled 2p orbitals with the maintenance of symmetry according to Laplace's equation (Eq. (10.72)) requires that the 2p as well as the 3s electrons contribute forces to the 3p electrons due to the electrons at $r_{10}$ acting on the electrons at $r_{12}$ which complies with the reactive force, $\mathbf{F}_{diamagnetic\ 2}$, having the factor $\left(1+\frac{\sqrt{2}}{2}\right)$ and given by Eq. (10.229).

The total orbital contribution to the diamagnetic force, $\mathbf{F}_{diamagnetic}$, given by Eq. (10.82) is:

$$\mathbf{F}_{diamagnetic} = -\sum_m \frac{(\ell+|m|)!}{(2\ell+1)(\ell-|m|)!}\frac{\hbar^2}{4m_e r_n^2 r_{12}}\sqrt{s(s+1)}\mathbf{i}_\mathbf{r} \tag{10.258}$$

where the contributions from orbitals having $|m| = 1$ add positively or negatively. From Eq. (10.204), the diamagnetic force, $\mathbf{F}_{diamagnetic}$, contribution from the 2p electrons is given by the sum of the contributions from the $p_x$, $p_y$, and $p_z$ orbitals corresponding to $m$ = 1, -1, and 0, respectively:

$$\mathbf{F}_{diamagnetic} = -\left(\frac{2}{3}+\frac{2}{3}+\frac{1}{3}\right)\frac{\hbar^2}{4m_e r_n^2 r_{12}}\sqrt{s(s+1)}\mathbf{i}_\mathbf{r} = -\left(\frac{5}{3}\right)\frac{\hbar^2}{4m_e r_n^2 r_{12}}\sqrt{s(s+1)}\mathbf{i}_\mathbf{r} \tag{10.259}$$

where $r_{12}$ is given by Eq. (10.255). Due to the 2p-3s-3p interaction, the 3s electrons provide spin or orbital angular momentum in order conserve angular momentum of the interacting orbitals. In the case that an energy minimum is achieved with 3s orbital angular momentum, the diamagnetic force, $\mathbf{F}_{diamagnetic}$, contribution is given by Eqs. (10.82) and (10.258) where $m$ = 1, -1, or 0 corresponding to induced charge-density waves. The contribution from the 3s orbital is added to the contributions from the 3p and the 2p orbitals until the 3p orbitals are at least half filled. Then the diamagnetic force is only due to 3p and 3s electrons since the induced charge-density waves only involve the inner-most shell, the 3s orbital.

As given by Eq. (10.89), the contribution of the orbital angular momentum of an unpaired 3p electron to the paramagnetic force, $\mathbf{F}_{mag\ 2}$, is:

$$\mathbf{F}_{mag\ 2} = \frac{1}{Z}\frac{\hbar^2}{m_e r_n^2 r_{12}}\sqrt{s(s+1)}\mathbf{i}_\mathbf{r} \tag{10.260}$$

Each outer 3p electron contributes spin as well as orbital angular momentum. The former gives rise to spin pairing to another 3p electron when an energy minimum is achieved. In the case that the orbital angular momenta of paired 3p electrons cancel, the contribution to $\mathbf{F}_{mag\ 2}$ due to spin alone given by Eq. (10.83) is equivalent to that due to orbital angular momentum alone (Eq. (10.260)). Due to the 2p-3s-3p interaction, the 3s electrons can also provide a paramagnetic force, $\mathbf{F}_{mag\ 2}$, contribution given by Eqs. (10.82) and (10.260) due to spin angular momentum corresponding to induced charge-density waves.

N-electron atoms having $Z > n$ possess an electric field given by Eq. (10.92) for $r > r_n$. Since there is a source of dissipative power, $\mathbf{J} \bullet \mathbf{E}$ of Eq. (10.27), the magnetic moments of the inner electrons may change due to the outer electron such that the energy of the n-electron atom is lowered. $\mathbf{F}_{diamagnetic}$, is given by Eqs. (10.82) and (10.258). Due to the 2p-3s-3p interaction, the 2p level contributes to the forces even when the filling of the 3p level is half or greater, and the 3s electrons may

provide orbital angular momentum in order conserve angular momentum of the interacting orbitals. In the case that an energy minimum is achieved with 3s orbital angular momentum, the diamagnetic force, $\mathbf{F}_{diamagnetic}$, contribution is given by Eqs. (10.82) and (10.258) where $m$ = 1, -1, or 0 corresponding to induced charge-density waves. The contribution from the 3s orbital is added to the contributions from the 3p and the 2p orbitals.

Due to the 2p-3s-3p interaction with $Z > n$, $\mathbf{F}_{mag\ 2}$ has a contribution from the 2p, 3s, and 3p orbitals. The filled 2p orbitals with the maintenance of symmetry according to Eq. (10.72) requires that the diamagnetic force, $\mathbf{F}_{mag\ 2}$, contribution is:

$$\mathbf{F}_{mag\ 2} = \left(4+4+4\right)\frac{1}{Z}\frac{\hbar^2}{m_e r_n^2 r_{12}}\sqrt{s(s+1)}\mathbf{i}_{\mathbf{r}} = \frac{1}{Z}\frac{12\hbar^2}{m_e r_n^2 r_{12}}\sqrt{s(s+1)}\mathbf{i}_{\mathbf{r}} \tag{10.261}$$

corresponding to the spin and orbital angular momenta of the paired 2 $p_x$, $p_y$, and $p_z$ electrons (Eq. (10.205)). The 3s electrons can provide a $\mathbf{F}_{mag\ 2}$ contribution of:

$$\mathbf{F}_{mag\ 2} = \frac{1}{Z}\frac{4\hbar^2}{m_e r_n^2 r_{12}}\sqrt{s(s+1)}\mathbf{i}_{\mathbf{r}} \tag{10.262}$$

corresponding to coupling to the spin and induced orbital angular momentum wherein the orbitals interact such that this contribution superimposes negatively or positively to the contributions from the 2p and 3p orbitals. Each outer 3p electron contributes spin as well as orbital angular momentum. Each unpaired 3p electron can spin and orbitally pair with a 2p orbital. The corresponding force, $\mathbf{F}_{mag\ 2}$, contribution given by Eq. (10.84) is:

$$\mathbf{F}_{mag\ 2} = \frac{1}{Z}\frac{4\hbar^2}{m_e r_n^2 r_{12}}\sqrt{s(s+1)}\mathbf{i}_{\mathbf{r}} \tag{10.263}$$

The 3p electrons spin-pair upon further filling of the 3p orbital. Two spin-paired 3p electrons interacting with two spin-paired 2p orbital electrons double the corresponding force, $\mathbf{F}_{mag\ 2}$, contribution:

$$\mathbf{F}_{mag\ 2} = \frac{1}{Z}\frac{8\hbar^2}{m_e r_n^2 r_{12}}\sqrt{s(s+1)}\mathbf{i}_{\mathbf{r}} \tag{10.264}$$

The sum of the magnitude of the angular momentum of the electron is $\hbar$ in any inertial frame and is relativistically invariant. The vector projections of the atomic orbital spin angular momentum relative to the Cartesian coordinates are given in the Spin Angular Momentum of the Atomic Orbital $Y_0^0(\theta,\phi)$ with $\ell$ = 0 section. The magnitude of the z-axis projection of the spin angular momentum, $\left|L_z\right|$, the moment of inertia about the z-axis, $I_z$, and the rotational energy about the z-axis, $E_{rotational\ \ spin}$, given by Eqs. (1.51-1.55) are:

$$\left|L_z\right| = I\frac{\hbar}{m_e r^2} = \frac{\hbar}{2} \tag{10.265}$$

$$I_z = I_{spin} = \frac{m_e r_n^{\ 2}}{2} \tag{10.266}$$

$$E_{rotational} = E_{rotational\ \ spin} = \frac{1}{4}\left[\frac{\hbar^2}{2I_{spin}}\right] = \frac{1}{4}\left[\frac{\hbar^2}{m_e r_n^{\ 2}}\right] \tag{10.267}$$

N-electron atoms having $Z > n$ possess an electric field given by Eq. (10.92) for $r > r_n$. Since there is a source of dissipative power, $\mathbf{J} \bullet \mathbf{E}$ of Eq. (10.27), the magnetic moments of the inner electrons may change due to the outer electron such that the energy of the n-electron atom is lowered. As shown in the P-Orbital Electrons Based on an Energy Minimum section for $\mathbf{F}_{diamagnetic\ 2}$ given by Eq. (10.93), the corresponding diamagnetic force for 2p electrons, $\mathbf{F}_{diamagnetic\ 2}$, due to a relativistic effect with an electric field for $r > r_n$ (Eq. (10.35)) is dependent on the amplitude of the orbital energy. Using the orbital energy with $\ell = 1$ (Eq. (10.90)), the energy $m_e \Delta v^2$ of Eq. (10.29) is reduced by the factor of $\left(1-\frac{\sqrt{2}}{2}\right)$ due to the contribution of the charge-density wave of the inner electrons at $r_{12}$. In addition, the two 3s electrons contribute an energy factor based on Eq. (1.55) since the filled 2p orbitals with the maintenance of symmetry according to Eq. (10.72) requires that the diamagnetic force is due to the electrons at $r_{10}$ acting on the electrons at $r_{12}$ which complies with the reactive force, $\mathbf{F}_{diamagnetic\ 2}$, given by Eq. (10.229). Thus, $\mathbf{F}_{diamagnetic\ 2}$ for 3p electrons with $Z > n$ is given by:

$$\mathbf{F}_{diamagnetic\ 2} = -\left[\frac{Z-n}{Z-\left(n-1\right)}\right]\left(1-\frac{\sqrt{2}}{2}+\frac{1}{2}\right)\frac{r_{12}\hbar^2}{m_e r_n^4}10\sqrt{s(s+1)}\mathbf{i}_{\mathbf{r}} \tag{10.268}$$

The total diamagnetic and paramagnetic forces are given as the sum over the orbital and spin angular momenta that may add positively or negatively while maintaining the conservation of angular momentum. Of the possible forces based on Maxwell's equations, those which give rise to an energy minimum are used to calculated the atomic radii and energies. In general, an energy minimum is achieved by minimizing $\mathbf{F}_{diamagnetic}$ while maximizing $\mathbf{F}_{mag\ 2}$ with conservation of angular

momentum.

Using the forces given by Eqs. (10.257-10.264), (10.268), and the radii $r_{12}$ given by Eq. (10.255), the radii of the 3p electrons of all thirteen through eighteen-electron atoms may be solved exactly. The electric energy given by Eq. (10.102) gives the corresponding exact ionization energies. $\mathbf{F}_{ele}$ and $\mathbf{F}_{diamagnetic\ 2}$ given by Eqs. (10.257) and (10.268), respectively, are of the same form for all atoms with the appropriate nuclear charges and atomic radii. $\mathbf{F}_{diamagnetic}$ given by Eq. (10.258) and $\mathbf{F}_{mag\ 2}$ given by Eqs. (10.260-10.264) are of the same form with the appropriate factors that depend on the minimum-energy electron configuration. The general equation and the summary of the parameters that determine the exact radii and ionization energies of all thirteen through eighteen-electron atoms are given the General Equation For The Ionization Energies of Thirteen Through Eighteen-Electron Atoms section and in Table 10.18.

## THIRTEEN-ELECTRON ATOMS

Thirteen-electron atoms can be solved exactly using the results of the solutions of one, two, three, four, five, six, seven, eight, nine, ten, eleven, and twelve-electron atoms.

## RADIUS AND IONIZATION ENERGY OF THE OUTER ELECTRON OF THE ALUMINUM ATOM

For each twelve-electron atom having a central charge of $Z$ times that of the proton, there are two indistinguishable spin-paired electrons in an atomic orbital with radii $r_1$ and $r_2$ both given by Eq. (7.35) (Eq. (10.51)), two indistinguishable spin-paired electrons in an atomic orbital with radii $r_3$ and $r_4$ both given by Eq. (10.62), three sets of paired electrons in an atomic orbital at $r_{10}$ given by Eq. (10.212), and two indistinguishable spin-paired electrons in an atomic orbital with radii $r_{11}$ and $r_{12}$ both given by Eq. (10.255). For $Z \geq 13$, the next electron which binds to form the corresponding thirteen-electron atom is attracted by the central Coulomb field and is repelled by diamagnetic forces due to the 3 sets of spin-paired inner 2p electrons and two spin-paired inner 3s electrons such that it forms an unpaired atomic orbital at radius $r_{13}$. The resulting electron configuration is $1s^2 2s^2 2p^6 3s^2 3p^1$, and the orbital arrangement is:

3p state

$$\begin{array}{ccc} \uparrow & & \\ \hline 1 & 0 & -1 \end{array} \tag{10.269}$$

corresponding to the ground state ${}^2P^0_{1/2}$.

The central Coulomb force acts on the outer electron to cause it to bind wherein this electric force on the outer-most electron due to the nucleus and the inner twelve electrons is given by Eq. (10.70) with the appropriate charge and radius:

$$\mathbf{F}_{ele} = \frac{(Z-12)e^2}{4\pi\varepsilon_0 r_{13}^2}\mathbf{i}_{\mathbf{r}} \tag{10.270}$$

for $r > r_{12}$.

As in the case of the boron atom given in the Five-Electron Atom section, the single p orbital of the aluminum atom produces a diamagnetic force equivalent to that of the formation of an s orbital due to the induction of complementary and spherically symmetrical charge-density waves on electron atomic orbitals at $r_{10}$ and $r_{12}$ in order to achieve a solution of Laplace's equation (Eq. (10.72)). The inner electrons remain at their initial radii, but cause a diamagnetic force according to Lenz's law that is given by Eq. (10.96) with the appropriate radii. In addition, the contribution of the diamagnetic force, $\mathbf{F}_{diamagnetic}$, due to the 2p electrons is given by Eqs. (10.105) and (10.259) as the sum of the contributions from the $p_x$, $p_y$, and $p_z$ orbitals corresponding to $m$ = 1, -1, and 0, respectively. Thus, $\mathbf{F}_{diamagnetic}$ is given by:

$$\mathbf{F}_{diamagnetic} = -\left(2+\frac{2}{3}+\frac{2}{3}+\frac{1}{3}\right)\frac{\hbar^2}{4m_e r_{13}^2 r_{12}}\sqrt{s(s+1)}\mathbf{i}_{\mathbf{r}} = -\left(\frac{11}{3}\right)\frac{\hbar^2}{4m_e r_{13}^2 r_{12}}\sqrt{s(s+1)}\mathbf{i}_{\mathbf{r}} \tag{10.271}$$

The charge induction forms complementary mirror charge-density waves which must have opposing angular momenta such that momentum is conserved. In this case, $\mathbf{F}_{mag\ 2}$ given by Eq. (10.260) is zero:

$$\mathbf{F}_{mag\ 2} = 0 \tag{10.272}$$

The outward centrifugal force on electron 13 is balanced by the electric force and the magnetic force (on electron 13). The radius of the outer electron is calculated by equating the outward centrifugal force to the sum of the electric (Eq. (10.270)) and diamagnetic (Eq. (10.271)) forces as follows:

$$\frac{m_e v_{13}^2}{r_{13}} = \frac{(Z-12)e^2}{4\pi\varepsilon_o r_{13}^2} - \frac{\frac{11}{3}\hbar^2}{4m_e r_{13}^2 r_{12}}\sqrt{s(s+1)} \tag{10.273}$$

Substitution of $v_{13} = \frac{\hbar}{m_e r_{13}}$ (Eq. (1.35)) and $s = \frac{1}{2}$ into Eq. (10.273) gives:

$$\frac{\hbar^2}{m_e r_{13}^3} = \frac{(Z-12)e^2}{4\pi\varepsilon_0 r_{13}^2} - \frac{11\hbar^2}{12 m_e r_{13}^2 r_{12}}\sqrt{\frac{3}{4}} \tag{10.274}$$

$$r_{13} = \frac{a_0}{\left((Z-12) - \dfrac{11\sqrt{\dfrac{3}{4}}}{12 r_{12}}\right)},\ r_{12}\ in\ units\ of\ a_0 \tag{10.275}$$

Substitution of $\frac{r_{12}}{a_0} = 1.41133$ (Eq. (10.255) with $Z = 13$) into Eq. (10.275) gives:

$$r_{13} = 2.28565 a_0 \tag{10.276}$$

The energy stored in the electric field of the aluminum atom, $E(electric)$, is given by Eq. (10.102) with the appropriate with the radius, $r_{13}$, given by Eq. (10.276)):

$$E(electric;\ Al) = -\frac{(Z-12)e^2}{8\pi\varepsilon_0 r_{13}} = 5.95270\ eV \tag{10.277}$$

where $r_{13} = 2.28565 a_0$ (Eq. (10.276)) and $Z = 13$. The ionization energy is given by the sum of the electric energy and the energy corresponding to the change in magnetic-moments of the inner shell electrons. Since there is no source of dissipative power, $\mathbf{J} \bullet \mathbf{E}$ of Eq. (10.27), to compensate for any potential change in the magnetic moments, $\Delta m$, of the inner electrons due to the ionization of the outer electron of the aluminum atom, there is a diamagnetic energy term in the ionization energy for this atom that follows from the corresponding term for the lithium atom given by Eqs. (10.15-10.24), with $Z = 13$, $r_{12}$ given by Eq. (10.255), and $r_{13}$ given by Eq. (10.276). Thus, the change in magnetic energy of the inner atomic orbital at $r_{12}$ is 76.94147 %, so that the corresponding energy $\Delta E_{mag}$ is

$$\Delta E_{mag} = 0.7694147\ X\ 0.04069938\ eV = 0.0313147\ eV \tag{10.278}$$

where the magnetic energy of the inner electrons is $0.04069938\ eV$ (Eqs. (10.64) and (10.276)). Then, the ionization energy of the aluminum atom is given by Eqs. (10.276-10.278):

$$E(ionization;\ Al) = \frac{(Z-12)e^2}{8\pi\varepsilon_0 r_{13}} + \Delta E_{mag} = 5.95270\ eV + 0.031315\ eV = 5.98402\ eV \tag{10.279}$$

The experimental ionization energy of the boron atom is $5.98577\ eV$ [3].

## THE IONIZATION ENERGIES OF THIRTEEN-ELECTRON ATOMS WITH A NUCLEAR CHARGE Z>13

Thirteen-electron atoms having $Z > 13$ possess an external electric field given by Eq. (10.92). In this case, an energy minimum is achieved with conservation of momentum when the orbital angular momentum is such that $\mathbf{F}_{diamagnetic}$ is minimized while $\mathbf{F}_{mag\ 2}$ is maximized. From Eq. (10.258), the diamagnetic force, $\mathbf{F}_{diamagnetic}$, is given by the sum of the contributions from the 2 $p_x$, $p_y$, and $p_z$ orbitals corresponding to $m$ = 1, -1, and 0, respectively:

$$\mathbf{F}_{diamagnetic} = -\left(\frac{2}{3} + \frac{2}{3} + \frac{1}{3}\right)\frac{\hbar^2}{4 m_e r_{13}^2 r_{12}}\sqrt{s(s+1)}\mathbf{i}_{\mathbf{r}} = -\left(\frac{5}{3}\right)\frac{\hbar^2}{4 m_e r_{13}^2 r_{12}}\sqrt{s(s+1)}\mathbf{i}_{\mathbf{r}} \tag{10.280}$$

wherein the contribution due to the 3 $p_x$ ($m$ = 1) is canceled by the mirror charge-density wave with $m$ = -1 induced in the 3s orbital according to Eq. (10.258).

With $Z > 13$, the charge induction forms complementary mirror charge-density waves such that the angular momenta do not cancel. The filled 2p orbitals with the maintenance of symmetry according to Eq. (10.72) requires that the diamagnetic force is due to the electrons at $r_{10}$ acting on the electrons at $r_{12}$ which complies with the reactive force, $\mathbf{F}_{diamagnetic\ 2}$, given by Eq. (10.249). From Eq. (10.261), $\mathbf{F}_{mag\ 2}$ is:

$$\mathbf{F}_{mag\ 2} = (4+4+4)\frac{1}{Z}\frac{\hbar^2}{m_e r_{13}^2 r_{12}}\sqrt{s(s+1)}\mathbf{i}_{\mathbf{r}} = \frac{1}{Z}\frac{12\hbar^2}{m_e r_{13}^2 r_{12}}\sqrt{s(s+1)}\mathbf{i}_{\mathbf{r}} \tag{10.281}$$

corresponding to the spin and orbital angular momenta of the paired 2 $p_x$, $p_y$, and $p_z$ electrons wherein the contribution due to the 3 $p_x$ ($m$ = 1) is canceled by the mirror charge-density wave with $m = -1$ induced in the 3s orbital according to Eq. (10.262).

The diamagnetic force, $\mathbf{F}_{diamagnetic\ 2}$, due to the binding of the 3p-orbital electron having an electric field outside of its radius is given by Eq. (10.268):

$$\mathbf{F}_{diamagnetic\ 2} = -\left[\frac{Z-13}{Z-12}\right]\left(1 - \frac{\sqrt{2}}{2} + \frac{1}{2}\right)\frac{r_{12}\hbar^2}{m_e r_{13}^4}10\sqrt{s(s+1)}\mathbf{i}_{\mathbf{r}} \tag{10.282}$$

In the case that $Z > 13$, the radius of the outer electron is calculated by equating the outward centrifugal force to the sum

of the electric (Eq. (10.270)) and diamagnetic (Eqs. (10.280) and (10.282)), and paramagnetic (Eq. (10.281)) forces as follows:

$$\frac{m_e v_{13}^2}{r_{13}} = \frac{(Z-12)e^2}{4\pi\varepsilon_0 r_{13}^2} - \frac{5\hbar^2}{12 m_e r_{13}^2 r_{12}}\sqrt{s(s+1)} + \frac{12\hbar^2}{Z m_e r_{13}^2 r_{12}}\sqrt{s(s+1)}$$

$$-\left[\frac{Z-13}{Z-12}\right]\left(1-\frac{\sqrt{2}}{2}+\frac{1}{2}\right)\frac{r_{12}\hbar^2}{r_{13}^4 m_e}10\sqrt{s(s+1)} \tag{10.283}$$

Substitution of $v_{13} = \dfrac{\hbar}{m_e r_{13}}$ (Eq. (1.35)) and $s = \dfrac{1}{2}$ into Eq. (10.283) gives:

$$\frac{\hbar^2}{m_e r_{13}^3} = \frac{(Z-12)e^2}{4\pi\varepsilon_0 r_{13}^2} - \frac{5\hbar^2}{12 m_e r_{13}^2 r_{12}}\sqrt{\frac{3}{4}} + \frac{12\hbar^2}{Z m_e r_{13}^2 r_{12}}\sqrt{\frac{3}{4}} - \left[\frac{Z-13}{Z-12}\right]\left(1-\frac{\sqrt{2}}{2}+\frac{1}{2}\right)\frac{r_{12}\hbar^2}{r_{13}^4 m_e}10\sqrt{\frac{3}{4}} \tag{10.284}$$

The quadratic equation corresponding to Eq. (10.284) is:

$$\left(\frac{(Z-12)e^2}{4\pi\varepsilon_0} - \left(\frac{5}{12}-\frac{12}{Z}\right)\frac{\hbar^2}{m_e r_{12}}\sqrt{\frac{3}{4}}\right)r_{13}^2 - \frac{\hbar^2}{m_e}r_{13} - \left[\frac{Z-13}{Z-12}\right]\left(1-\frac{\sqrt{2}}{2}+\frac{1}{2}\right)\frac{r_{12}\hbar^2}{m_e}10\sqrt{\frac{3}{4}} = 0 \tag{10.285}$$

$$r_{13}^2 - \frac{\dfrac{\hbar^2}{m_e}}{\left(\dfrac{(Z-12)e^2}{4\pi\varepsilon_0} - \left(\dfrac{5}{12}-\dfrac{12}{Z}\right)\dfrac{\hbar^2}{m_e r_{12}}\sqrt{\dfrac{3}{4}}\right)}r_{13} - \frac{\left[\dfrac{Z-13}{Z-12}\right]\left(1-\dfrac{\sqrt{2}}{2}+\dfrac{1}{2}\right)\dfrac{r_{12}\hbar^2}{m_e}10\sqrt{\dfrac{3}{4}}}{\left(\dfrac{(Z-12)e^2}{4\pi\varepsilon_o} - \left(\dfrac{5}{12}-\dfrac{12}{Z}\right)\dfrac{\hbar^2}{m_e r_{12}}\sqrt{\dfrac{3}{4}}\right)} = 0 \tag{10.286}$$

The solution of Eq. (10.286) using the quadratic formula is:

$$r_{13} = \frac{\dfrac{\dfrac{\hbar^2}{m_e}}{\left(\dfrac{(Z-12)e^2}{4\pi\varepsilon_0} - \left(\dfrac{5}{12}-\dfrac{12}{Z}\right)\dfrac{\hbar^2}{m_e r_{12}}\sqrt{\dfrac{3}{4}}\right)} \pm \sqrt{\left(\dfrac{\dfrac{\hbar^2}{m_e}}{\left(\dfrac{(Z-12)e^2}{4\pi\varepsilon_0} - \left(\dfrac{5}{12}-\dfrac{12}{Z}\right)\dfrac{\hbar^2}{m_e r_{12}}\sqrt{\dfrac{3}{4}}\right)}\right)^2 + 4\dfrac{\dfrac{\hbar^2}{m_e}\left[\dfrac{Z-13}{Z-12}\right]\left(1-\dfrac{\sqrt{2}}{2}+\dfrac{1}{2}\right)r_{12}10\sqrt{\dfrac{3}{4}}}{\left(\dfrac{(Z-12)e^2}{4\pi\varepsilon_0} - \left(\dfrac{5}{12}-\dfrac{12}{Z}\right)\dfrac{\hbar^2}{m_e r_{12}}\sqrt{\dfrac{3}{4}}\right)}}}{2} \tag{10.287}$$

$$r_{13} = \frac{\dfrac{a_0}{\left((Z-12) - \left(\dfrac{5}{24}-\dfrac{6}{Z}\right)\dfrac{\sqrt{3}}{r_{12}}\right)} \pm a_0\sqrt{\left(\dfrac{1}{\left((Z-12) - \left(\dfrac{5}{24}-\dfrac{6}{Z}\right)\dfrac{\sqrt{3}}{r_{12}}\right)}\right)^2 + \dfrac{20\sqrt{3}\left(\left[\dfrac{Z-13}{Z-12}\right]\left(1-\dfrac{\sqrt{2}}{2}+\dfrac{1}{2}\right)r_{12}\right)}{\left((Z-12) - \left(\dfrac{5}{24}-\dfrac{6}{Z}\right)\dfrac{\sqrt{3}}{r_{12}}\right)}}}{2}, \; r_{12} \text{ in units of } a_0 \tag{10.288}$$

where $r_{12}$ is given by Eq. (10.255). The positive root of Eq. (10.288) must be taken in order that $r_{13} > 0$. The radii of several thirteen-electron atoms are given in Table 10.12.

The ionization energies for the thirteen-electron atoms with $Z > 13$ are given by the electric energy, $E(electric)$, (Eq. (10.102) with the radii, $r_{13}$, given by Eq. (10.288)).

$$E(Ionization) = -Electric\ Energy = \frac{(Z-12)e^2}{8\pi\varepsilon_0 r_{13}} \tag{10.289}$$

Since the relativistic corrections were small, the nonrelativistic ionization energies for experimentally measured thirteen-electron

atoms are given in Table 10.12.

**Table 10.12.** Ionization energies for some thirteen-electron atoms.

| 13 e Atom | Z | $r_1$ $(a_o)$ [a] | $r_3$ $(a_o)$ [b] | $r_{10}$ $(a_o)$ [c] | $r_{12}$ $(a_o)$ [d] | $r_{13}$ $(a_o)$ [e] | Theoretical Ionization Energies [f] (eV) | Experimental Ionization Energies [g] (eV) | Relative Error [h] |
|---|---|---|---|---|---|---|---|---|---|
| *Al* | 13 | 0.07778 | 0.33923 | 0.45620 | 1.41133 | 2.28565 | 5.98402 | 5.98577 | 0.0003 |
| $Si^{+}$ | 14 | 0.07216 | 0.31274 | 0.40978 | 1.25155 | 1.5995 | 17.0127 | 16.34585 | -0.0408 |
| $P^{2+}$ | 15 | 0.06730 | 0.29010 | 0.37120 | 1.09443 | 1.3922 | 29.3195 | 30.2027 | 0.0292 |
| $S^{3+}$ | 16 | 0.06306 | 0.27053 | 0.33902 | 0.96729 | 1.1991 | 45.3861 | 47.222 | 0.0389 |
| $Cl^{4+}$ | 17 | 0.05932 | 0.25344 | 0.31190 | 0.86545 | 1.0473 | 64.9574 | 67.8 | 0.0419 |
| $Ar^{5+}$ | 18 | 0.05599 | 0.23839 | 0.28878 | 0.78276 | 0.9282 | 87.9522 | 91.009 | 0.0336 |
| $K^{6+}$ | 19 | 0.05302 | 0.22503 | 0.26884 | 0.71450 | 0.8330 | 114.3301 | 117.56 | 0.0275 |
| $Ca^{7+}$ | 20 | 0.05035 | 0.21308 | 0.25149 | 0.65725 | 0.7555 | 144.0664 | 147.24 | 0.0216 |
| $Sc^{8+}$ | 21 | 0.04794 | 0.20235 | 0.23625 | 0.60857 | 0.6913 | 177.1443 | 180.03 | 0.0160 |
| $Ti^{9+}$ | 22 | 0.04574 | 0.19264 | 0.22276 | 0.56666 | 0.6371 | 213.5521 | 215.92 | 0.0110 |
| $V^{10+}$ | 23 | 0.04374 | 0.18383 | 0.21074 | 0.53022 | 0.5909 | 253.2806 | 255.7 | 0.0095 |
| $Cr^{11+}$ | 24 | 0.04191 | 0.17579 | 0.19995 | 0.49822 | 0.5510 | 296.3231 | 298.0 | 0.0056 |
| $Mn^{12+}$ | 25 | 0.04022 | 0.16842 | 0.19022 | 0.46990 | 0.5162 | 342.6741 | 343.6 | 0.0027 |
| $Fe^{13+}$ | 26 | 0.03867 | 0.16165 | 0.18140 | 0.44466 | 0.4855 | 392.3293 | 392.2 | -0.0003 |
| $Co^{14+}$ | 27 | 0.03723 | 0.15540 | 0.17336 | 0.42201 | 0.4583 | 445.2849 | 444 | -0.0029 |
| $Ni^{15+}$ | 28 | 0.03589 | 0.14961 | 0.16601 | 0.40158 | 0.4341 | 501.5382 | 499 | -0.0051 |
| $Cu^{16+}$ | 29 | 0.03465 | 0.14424 | 0.15926 | 0.38305 | 0.4122 | 561.0867 | 557 | -0.0073 |
| $Zn^{17+}$ | 30 | 0.03349 | 0.13925 | 0.15304 | 0.36617 | 0.3925 | 623.9282 | 619 | -0.0080 |

[a] Radius of the paired 1s inner electrons of thirteen-electron atoms from Eq. (10.51).

[b] Radius of the paired 2s inner electrons of thirteen-electron atoms from Eq. (10.62).

[c] Radius of the three sets of paired 2p inner electrons of thirteen-electron atoms from Eq. (10.212).

[d] Radius of the paired 3s inner electrons of thirteen-electron atoms from Eq. (10.255).

[e] Radius of the unpaired 3p outer electron of thirteen-electron atoms from Eq. (10.288) for $Z > 13$ and Eq. (10.276) for *Al*.

[f] Calculated ionization energies of thirteen-electron atoms given by the electric energy (Eq. (10.289)) for $Z > 13$ and Eq. (10.279) for *Al*.

[g] From theoretical calculations, interpolation of isoelectronic and spectral series, and experimental data [2-3].

[h] (Experimental-theoretical)/experimental.

The agreement between the experimental and calculated values of Table 10.12 is well within the experimental capability of the spectroscopic determinations including the values at large Z, which relies on X-ray spectroscopy. In this case, the experimental capability is three to four significant figures, which is consistent with the last column. The aluminum atom isoelectronic series is given in Table 10.12 [2-3] to much higher precision than the capability of X-ray spectroscopy, but these values are based on theoretical and interpolation techniques rather than data alone. Ionization energies are difficult to determine since the cut-off of the Rydberg series of lines at the ionization energy is often not observed, and the ionization energy must be determined from theoretical calculations, interpolation of Al isoelectronic and Rydberg series, as well as direct experimental data.

# FOURTEEN-ELECTRON ATOMS

Fourteen-electron atoms can be solved exactly using the results of the solutions of one, two, three, four, five, six, seven, eight, nine, ten, eleven, twelve, and thirteen-electron atoms.

## RADIUS AND IONIZATION ENERGY OF THE OUTER ELECTRON OF THE SILICON ATOM

For each thirteen-electron atom having a central charge of $Z$ times that of the proton, there are two indistinguishable spin-paired electrons in an atomic orbital with radii $r_1$ and $r_2$ both given by Eq. (7.35) (Eq. (10.51)), two indistinguishable spin-paired electrons in an atomic orbital with radii $r_3$ and $r_4$ both given by Eq. (10.62), three sets of paired electrons in an atomic orbital at $r_{10}$ given by Eq. (10.212), two indistinguishable spin-paired electrons in an atomic orbital with radii $r_{11}$ and $r_{12}$ both given by Eq. (10.255), and an unpaired electron in an atomic orbital with radius $r_{13}$ given by Eq. (10.288). For $Z \geq 14$, the next electron which binds to form the corresponding fourteen-electron atom is attracted by the central Coulomb field and is repelled by diamagnetic forces due to the 3 sets of spin-paired inner 2p electrons and two spin-paired inner 3s electrons. A paramagnetic spin-pairing force to form a filled s orbital is also possible, but the force due to the spin-pairing of the electrons (Eq. (7.24) with the radius $r_{14}$) reduces the energy of the atom less than that due to the alternative forces on two unpaired 3p electrons in an atomic orbital at the same radius $r_{14}$. The resulting electron configuration is $1s^2 2s^2 2p^6 3s^2 3p^2$, and the orbital arrangement is:

3p state

| ↑ | ↑ | |
|---|---|---|
| 1 | 0 | -1 |

(10.290)

corresponding to the ground state ${}^3P_0$.

The central Coulomb force acts on the outer electron to cause it to bind wherein this electric force on the outer-most electron due to the nucleus and the inner thirteen electrons is given by Eq. (10.70) with the appropriate charge and radius:

$$\mathbf{F}_{ele} = \frac{(Z-13)e^2}{4\pi\varepsilon_0 r_{14}^2}\mathbf{i}_\mathbf{r} \tag{10.291}$$

for $r > r_{13}$.

As in the case of the carbon atom given in the Six-Electron Atom section, the two orthogonal 3p electrons form charge-density waves such that the total angular momentum of the two outer electrons is conserved which determines the diamagnetic force according to Eq. (10.82) (Eq. (10.258)). The contribution is given by Eq. (10.117) corresponding to $m = 1$. In addition, the contribution of the diamagnetic force, $\mathbf{F}_{diamagnetic}$, due to the 2p electrons is given by Eq. (10.105) (Eq. (10.259)) as the sum of the contributions from the 2 $p_x$, $p_y$, and $p_z$ orbitals corresponding to $m$ = 1, -1, and 0, respectively. Thus, $\mathbf{F}_{diamagnetic}$ is given by:

$$\mathbf{F}_{diamagnetic} = -\left(\frac{2}{3}+\frac{2}{3}+\frac{2}{3}+\frac{1}{3}\right)\frac{\hbar^2}{4m_e r_{14}^2 r_{12}}\sqrt{s(s+1)}\mathbf{i}_\mathbf{r} = -\left(\frac{7}{3}\right)\frac{\hbar^2}{4m_e r_{14}^2 r_{12}}\sqrt{s(s+1)}\mathbf{i}_\mathbf{r} \tag{10.292}$$

The charge induction forms complementary mirror charge-density waves which must have opposing angular momenta such that momentum is conserved. In this case, $\mathbf{F}_{mag\ 2}$ given by Eq. (10.89) (Eq. (10.260)) is zero:

$$\mathbf{F}_{mag\ 2} = 0 \tag{10.293}$$

The outward centrifugal force on electron 14 is balanced by the electric force and the magnetic forces (on electron 14). The radius of the outer electron is calculated by equating the outward centrifugal force to the sum of the electric (Eq. (10.291)) and diamagnetic (Eq. (10.292)) forces as follows:

$$\frac{m_e v_{14}^2}{r_{14}} = \frac{(Z-13)e^2}{4\pi\varepsilon_0 r_{14}^2} - \frac{7\hbar^2}{12m_e r_{14}^2 r_{12}}\sqrt{s(s+1)} \tag{10.294}$$

Substitution of $v_{14} = \frac{\hbar}{m_e r_{14}}$ (Eq. (1.35)) and $s = \frac{1}{2}$ into Eq. (10.294) gives:

$$\frac{\hbar^2}{m_e r_{14}^3} = \frac{(Z-13)e^2}{4\pi\varepsilon_0 r_{14}^2} - \frac{7\hbar^2}{12m_e r_{14}^2 r_{12}}\sqrt{s(s+1)} \tag{10.295}$$

$$r_{14} = \frac{a_0}{\left((Z-13) - \frac{7\sqrt{\frac{3}{4}}}{12r_{12}}\right)},\ r_{12}\ \textit{in units of}\ a_0 \tag{10.296}$$

Substitution of $\frac{r_{12}}{a_0} = 1.25155$ (Eq. (10.255) with $Z = 14$) into Eq. (10.296) gives:

$$r_{14} = 1.67685 a_0 \tag{10.297}$$

The ionization energy of the silicon atom is given by the electric energy, $E(electric)$, (Eq. (10.102) with the radius, $r_{14}$, given by Eq. (10.297)):

$$E(ionization;\ Si) = -Electric\ Energy = \frac{(Z-13)e^2}{8\pi\varepsilon_0 r_{14}} = 8.11391\ eV \tag{10.298}$$

where $r_{14} = 1.67685a_0$ (Eq. (10.297)) and $Z = 14$. The experimental ionization energy of the silicon atom is $8.15169\ eV$ [3].

## THE IONIZATION ENERGIES OF FOURTEEN-ELECTRON ATOMS WITH A NUCLEAR CHARGE Z>14

Fourteen-electron atoms having $Z > 14$ possess an external electric field given by Eq. (10.92). In this case, an energy minimum is achieved with conservation of momentum when the orbital angular momentum is such that $\mathbf{F}_{diamagnetic}$ is minimized while $\mathbf{F}_{mag\ 2}$ is maximized. With a half-filled 3p shell, the diamagnetic force due to the orbital angular momenta of the 3p electrons cancels that of the 2p electrons. Thus, $\mathbf{F}_{diamagnetic}$ is minimized by the formation of a charge-density wave in the 3s orbital corresponding to $m = -1$ in Eq. (10.258) to form the equivalent of a half-filled 3p shell such that the contribution due to the 2p shell is canceled. From Eq. (10.258), the diamagnetic force, $\mathbf{F}_{diamagnetic}$, is given by the sum of the contributions from the 3 $p_x$ and $p_z$ orbitals corresponding to $m$ = 1 and 0, respectively, and the negative contribution due to the charge-density wave with $m$ = -1 induced in the 3s orbital according to Eq. (10.258):

$$\mathbf{F}_{diamagnetic} = -\left(\frac{2}{3}+\frac{1}{3}-\frac{2}{3}\right)\frac{\hbar^2}{4m_e r_{14}^2 r_{12}}\sqrt{s(s+1)}\mathbf{i}_\mathbf{r} = -\left(\frac{1}{3}\right)\frac{\hbar^2}{4m_e r_{14}^2 r_{12}}\sqrt{s(s+1)}\mathbf{i}_\mathbf{r} \tag{10.299}$$

From Eq. (10.261), $\mathbf{F}_{mag\ 2}$ corresponding to the spin and orbital angular momenta of the paired 2 $p_x$, $p_y$, and $p_z$ electrons is:

$$\mathbf{F}_{mag\ 2} = \left(4+4+4\right)\frac{1}{Z}\frac{\hbar^2}{m_e r_{14}^2 r_{12}}\sqrt{s(s+1)}\mathbf{i}_\mathbf{r} = \frac{1}{Z}\frac{12\hbar^2}{m_e r_{14}^2 r_{12}}\sqrt{s(s+1)}\mathbf{i}_\mathbf{r} \tag{10.300}$$

and the contribution from the 3p shell is

$$\mathbf{F}_{mag\ 2} = \left(4+4-4\right)\frac{1}{Z}\frac{\hbar^2}{m_e r_{14}^2 r_{12}}\sqrt{s(s+1)}\mathbf{i}_\mathbf{r} = \frac{1}{Z}\frac{4\hbar^2}{m_e r_{14}^2 r_{12}}\sqrt{s(s+1)}\mathbf{i}_\mathbf{r} \tag{10.301}$$

corresponding to the 3 $p_x$ and $p_z$ electrons wherein the contribution due to the 3 $p_x$ ($m$ = 1) electron is canceled by the mirror charge-density wave with $m = -1$ induced in the 3s orbital (Eq. (10.262)). Thus, the total of $\mathbf{F}_{mag\ 2}$ is

$$\mathbf{F}_{mag\ 2} = \frac{1}{Z}\frac{16\hbar^2}{m_e r_{14}^2 r_{12}}\sqrt{s(s+1)}\mathbf{i}_\mathbf{r} \tag{10.302}$$

The diamagnetic force, $\mathbf{F}_{diamagnetic\ 2}$, due to the binding of the 3p-orbital electron having an electric field outside of its radius is given by Eq. (10.268):

$$\mathbf{F}_{diamagnetic\ 2} = -\left[\frac{Z-14}{Z-13}\right]\left(1-\frac{\sqrt{2}}{2}+\frac{1}{2}\right)\frac{r_{12}\hbar^2}{m_e r_{14}^4}10\sqrt{s(s+1)}\mathbf{i}_\mathbf{r} \tag{10.303}$$

In the case that $Z > 14$, the radius of the outer electron is calculated by equating the outward centrifugal force to the sum of the electric (Eq. (10.291)), diamagnetic (Eqs. (10.299) and (10.303)), and paramagnetic (Eq. (10.302)) forces as follows:

$$\frac{m_e v_{14}^2}{r_{14}} = \frac{(Z-13)e^2}{4\pi\varepsilon_0 r_{14}^2} - \frac{\hbar^2}{12m_e r_{14}^2 r_{12}}\sqrt{s(s+1)} + \frac{16\hbar^2}{Zm_e r_{14}^2 r_{12}}\sqrt{s(s+1)} - \left[\frac{Z-14}{Z-13}\right]\left(1-\frac{\sqrt{2}}{2}+\frac{1}{2}\right)\frac{r_{12}\hbar^2}{m_e r_{14}^4}10\sqrt{s(s+1)} \tag{10.304}$$

Substitution of $v_{14} = \dfrac{\hbar}{m_e r_{14}}$ (Eq. (1.35)) and $s = \dfrac{1}{2}$ into Eq. (10.304) gives:

$$\frac{\hbar^2}{m_e r_{14}^3} = \frac{(Z-13)e^2}{4\pi\varepsilon_0 r_{14}^2} - \frac{\hbar^2}{12m_e r_{14}^2 r_{12}}\sqrt{\frac{3}{4}} + \frac{16\hbar^2}{Zm_e r_{14}^2 r_{12}}\sqrt{\frac{3}{4}} - \left[\frac{Z-14}{Z-13}\right]\left(1-\frac{\sqrt{2}}{2}+\frac{1}{2}\right)\frac{r_{12}\hbar^2}{m_e r_{14}^4}10\sqrt{\frac{3}{4}} \tag{10.305}$$

The quadratic equation corresponding to Eq. (10.305) is

$$\left(\frac{(Z-13)e^2}{4\pi\varepsilon_0} - \left(\frac{1}{12}-\frac{16}{Z}\right)\frac{\hbar^2}{m_e r_{12}}\sqrt{\frac{3}{4}}\right)r_{14}^2 - \frac{\hbar^2}{m_e}r_{14} - \left[\frac{Z-14}{Z-13}\right]\left(1-\frac{\sqrt{2}}{2}+\frac{1}{2}\right)\frac{r_{12}\hbar^2}{m_e}10\sqrt{\frac{3}{4}} = 0 \tag{10.306}$$

$$r_{14}^2 - \frac{\dfrac{\hbar^2}{m_e}}{\left(\dfrac{(Z-13)e^2}{4\pi\varepsilon_0} - \left(\dfrac{1}{12} - \dfrac{16}{Z}\right)\dfrac{\hbar^2}{m_e r_{12}}\sqrt{\dfrac{3}{4}}\right)} r_{14} - \frac{\dfrac{\hbar^2}{m_e}\left[\dfrac{Z-14}{Z-13}\right]\left(1 - \dfrac{\sqrt{2}}{2} + \dfrac{1}{2}\right) r_{12} 10\sqrt{\dfrac{3}{4}}}{\left(\dfrac{(Z-13)e^2}{4\pi\varepsilon_0} - \left(\dfrac{1}{12} - \dfrac{16}{Z}\right)\dfrac{\hbar^2}{m_e r_{12}}\sqrt{\dfrac{3}{4}}\right)} = 0 \tag{10.307}$$

The solution of Eq. (10.307) using the quadratic formula is:

$$r_{14} = \frac{\dfrac{\dfrac{\hbar^2}{m_e}}{\left(\dfrac{(Z-13)e^2}{4\pi\varepsilon_0} - \left(\dfrac{1}{12} - \dfrac{16}{Z}\right)\dfrac{\hbar^2}{m_e r_{12}}\sqrt{\dfrac{3}{4}}\right)} \pm \sqrt{\left(\dfrac{\dfrac{\hbar^2}{m_e}}{\left(\dfrac{(Z-13)e^2}{4\pi\varepsilon_0} - \left(\dfrac{1}{12} - \dfrac{16}{Z}\right)\dfrac{\hbar^2}{m_e r_{12}}\sqrt{\dfrac{3}{4}}\right)}\right)^2 + 4\dfrac{\dfrac{\hbar^2}{m_e}\left[\dfrac{Z-14}{Z-13}\right]\left(1 - \dfrac{\sqrt{2}}{2} + \dfrac{1}{2}\right) r_{12} 10\sqrt{\dfrac{3}{4}}}{\left(\dfrac{(Z-13)e^2}{4\pi\varepsilon_0} - \left(\dfrac{1}{12} - \dfrac{16}{Z}\right)\dfrac{\hbar^2}{m_e r_{12}}\sqrt{\dfrac{3}{4}}\right)}}}{2} \tag{10.308}$$

$$r_{14} = \frac{\dfrac{a_0}{\left((Z-13) - \left(\dfrac{1}{24} - \dfrac{8}{Z}\right)\dfrac{\sqrt{3}}{r_{12}}\right)} \pm a_0 \sqrt{\left(\dfrac{1}{\left((Z-13) - \left(\dfrac{1}{24} - \dfrac{8}{Z}\right)\dfrac{\sqrt{3}}{r_{12}}\right)}\right)^2 + \dfrac{20\sqrt{3}\left(\left[\dfrac{Z-14}{Z-13}\right]\left(1 - \dfrac{\sqrt{2}}{2} + \dfrac{1}{2}\right) r_{12}\right)}{\left((Z-13) - \left(\dfrac{1}{24} - \dfrac{8}{Z}\right)\dfrac{\sqrt{3}}{r_{12}}\right)}}}{2}, \; r_{12} \text{ in units of } a_0 \tag{10.309}$$

where $r_{12}$ is given by Eq. (10.255). The positive root of Eq. (10.309) must be taken in order that $r_{14} > 0$. The final radius of electron 14, $r_{14}$, is given by Eq. (10.309); this is also the final radius of electron 13. The radii of several fourteen-electron atoms are given in Table 10.13.

The ionization energies for the fourteen-electron atoms with $Z > 14$ are given by the electric energy, $E(electric)$, (Eq. (10.102) with the radii $r_{14}$, given by Eq. (10.309)).

$$E(Ionization) = -Electric\ Energy = \frac{(Z-13)e^2}{8\pi\varepsilon_0 r_{14}} \tag{10.310}$$

Since the relativistic corrections were small, the nonrelativistic ionization energies for experimentally measured fourteen-electron atoms are given in Table 10.13.

**Table 10.13.** Ionization energies for some fourteen-electron atoms.

| 14 e Atom | Z | $r_1$ $(a_o)$ [a] | $r_3$ $(a_o)$ [b] | $r_{10}$ $(a_o)$ [c] | $r_{12}$ $(a_o)$ [d] | $r_{14}$ $(a_o)$ [e] | Theoretical Ionization Energies [f] $(eV)$ | Experimental Ionization Energies [g] $(eV)$ | Relative Error [h] |
|---|---|---|---|---|---|---|---|---|---|
| $Si$ | 14 | 0.07216 | 0.31274 | 0.40978 | 1.25155 | 1.67685 | 8.11391 | 8.15169 | 0.0046 |
| $P^{+}$ | 15 | 0.06730 | 0.29010 | 0.37120 | 1.09443 | 1.35682 | 20.0555 | 19.7694 | -0.0145 |
| $S^{2+}$ | 16 | 0.06306 | 0.27053 | 0.33902 | 0.96729 | 1.21534 | 33.5852 | 34.790 | 0.0346 |
| $Cl^{3+}$ | 17 | 0.05932 | 0.25344 | 0.31190 | 0.86545 | 1.06623 | 51.0426 | 53.4652 | 0.0453 |
| $Ar^{4+}$ | 18 | 0.05599 | 0.23839 | 0.28878 | 0.78276 | 0.94341 | 72.1094 | 75.020 | 0.0388 |
| $K^{5+}$ | 19 | 0.05302 | 0.22503 | 0.26884 | 0.71450 | 0.84432 | 96.6876 | 99.4 | 0.0273 |
| $Ca^{6+}$ | 20 | 0.05035 | 0.21308 | 0.25149 | 0.65725 | 0.76358 | 124.7293 | 127.2 | 0.0194 |
| $Sc^{7+}$ | 21 | 0.04794 | 0.20235 | 0.23625 | 0.60857 | 0.69682 | 156.2056 | 158.1 | 0.0120 |
| $Ti^{8+}$ | 22 | 0.04574 | 0.19264 | 0.22276 | 0.56666 | 0.64078 | 191.0973 | 192.10 | 0.0052 |
| $V^{9+}$ | 23 | 0.04374 | 0.18383 | 0.21074 | 0.53022 | 0.59313 | 229.3905 | 230.5 | 0.0048 |
| $Cr^{10+}$ | 24 | 0.04191 | 0.17579 | 0.19995 | 0.49822 | 0.55211 | 271.0748 | 270.8 | -0.0010 |
| $Mn^{11+}$ | 25 | 0.04022 | 0.16842 | 0.19022 | 0.46990 | 0.51644 | 316.1422 | 314.4 | -0.0055 |
| $Fe^{12+}$ | 26 | 0.03867 | 0.16165 | 0.18140 | 0.44466 | 0.48514 | 364.5863 | 361 | -0.0099 |
| $Co^{13+}$ | 27 | 0.03723 | 0.15540 | 0.17336 | 0.42201 | 0.45745 | 416.4021 | 411 | -0.0131 |
| $Ni^{14+}$ | 28 | 0.03589 | 0.14961 | 0.16601 | 0.40158 | 0.43277 | 471.5854 | 464 | -0.0163 |
| $Cu^{15+}$ | 29 | 0.03465 | 0.14424 | 0.15926 | 0.38305 | 0.41064 | 530.1326 | 520 | -0.0195 |
| $Zn^{16+}$ | 30 | 0.03349 | 0.13925 | 0.15304 | 0.36617 | 0.39068 | 592.0410 | 579 | -0.0225 |

[a] Radius of the paired 1s inner electrons of fourteen-electron atoms from Eq. (10.51).

[b] Radius of the paired 2s inner electrons of fourteen-electron atoms from Eq. (10.62).

[c] Radius of the three sets of paired 2p inner electrons of fourteen-electron atoms from Eq. (10.212).

[d] Radius of the paired 3s inner electrons of fourteen-electron atoms from Eq. (10.255).

[e] Radius of the two unpaired 3p outer electrons of fourteen-electron atoms from Eq. (10.309) for $Z > 14$ and Eq. (10.297) for *Si*.

[f] Calculated ionization energies of fourteen-electron atoms given by the electric energy (Eq. (10.310)).

[g] From theoretical calculations, interpolation of isoelectronic and spectral series, and experimental data [2-3].

[h] (Experimental-theoretical)/experimental.

The agreement between the experimental and calculated values of Table 10.13 is well within the experimental capability of the spectroscopic determinations including the values at large Z which relies on X-ray spectroscopy. In this case, the experimental capability is three to four significant figures which is consistent with the last column. The silicon atom isoelectronic series is given in Table 10.13 [2-3] to much higher precision than the capability of X-ray spectroscopy, but these values are based on theoretical and interpolation techniques rather than data alone. Ionization energies are difficult to determine since the cut-off of the Rydberg series of lines at the ionization energy is often not observed, and the ionization energy must be determined from theoretical calculations, interpolation of Si isoelectronic and Rydberg series, as well as direct experimental data.

## FIFTEEN-ELECTRON ATOMS

Fifteen-electron atoms can be solved exactly using the results of the solutions of one, two, three, four, five, six, seven, eight, nine, ten, eleven, twelve, thirteen and fourteen-electron atoms.

## RADIUS AND IONIZATION ENERGY OF THE OUTER ELECTRON OF THE PHOSPHOROUS ATOM

For each fourteen-electron atom having a central charge of $Z$ times that of the proton, there are two indistinguishable spin-paired electrons in an atomic orbital with radii $r_1$ and $r_2$ both given by Eq. (7.35) (Eq. (10.51)), two indistinguishable spin-paired electrons in an atomic orbital with radii $r_3$ and $r_4$ both given by Eq. (10.62), three sets of paired electrons in an atomic orbital at $r_{10}$ given by Eq. (10.212), two indistinguishable spin-paired electrons in an atomic orbital with radii $r_{11}$ and $r_{12}$ both given by Eq. (10.255), and two unpaired electrons in an atomic orbital with radius $r_{14}$ given by Eq. (10.288). For $Z \geq 15$, the next electron which binds to form the corresponding fifteen-electron atom is attracted by the central Coulomb field and is repelled by diamagnetic forces due to the 3 sets of spin-paired inner 2p electrons and two spin-paired inner 3s electrons. A paramagnetic spin-pairing force to form a filled s orbital is also possible, but the force due to the spin-pairing of the electrons (Eq. (7.24) with the radius $r_{15}$) reduces the energy of the atom less than that due to the alternative forces on three unpaired 3p electrons in an atomic orbital at the same radius $r_{15}$. The resulting electron configuration is $1s^2 2s^2 2p^6 3s^2 3p^3$, and the orbital arrangement is

3p state

$$\underline{\uparrow}\quad\underline{\uparrow}\quad\underline{\uparrow} \tag{10.311}$$

1 0 -1

corresponding to the ground state ${}^4S^0_{3/2}$.

The central Coulomb force acts on the outer electron to cause it to bind wherein this electric force on the outer-most electron due to the nucleus and the inner fourteen electrons is given by Eq. (10.70) with the appropriate charge and radius:

$$\mathbf{F}_{ele} = \frac{(Z-14)e^2}{4\pi\varepsilon_0 r_{15}^2}\mathbf{i}_\mathbf{r} \tag{10.312}$$

for $r > r_{14}$.

The diamagnetic force, $\mathbf{F}_{diamagnetic}$, is only due to 3p and 3s electrons when the 3p shell is at least half filled since the induced charge-density waves only involve the inner-most shell, the 3s orbital. Thus, $\mathbf{F}_{diamagnetic}$, is given by Eq. (10.259) as the sum of the contributions from the 3 $p_x$, $p_y$, and $p_z$ orbitals corresponding to $m$ = 1, -1, and 0, respectively:

$$\mathbf{F}_{diamagnetic} = -\left(\frac{2}{3}+\frac{2}{3}+\frac{1}{3}\right)\frac{\hbar^2}{4m_e r_{15}^2 r_{12}}\sqrt{s(s+1)}\mathbf{i}_\mathbf{r} = -\left(\frac{5}{3}\right)\frac{\hbar^2}{4m_e r_{15}^2 r_{12}}\sqrt{s(s+1)}\mathbf{i}_\mathbf{r} \tag{10.313}$$

The energy is minimized with conservation of angular momentum when the spin angular momentum of the 3s orbital superimposes negatively with the orbital angular momentum of the 3p orbitals. From Eq. (10.260), $\mathbf{F}_{mag\ 2}$ corresponding to the orbital angular momentum of the 3 $p_x$, $p_y$, and $p_z$ orbitals minus the contribution from the 3s orbital is

$$\mathbf{F}_{mag\ 2} = (1+1+1-1)\frac{1}{Z}\frac{\hbar^2}{m_e r_{15}^2 r_{12}}\sqrt{s(s+1)}\mathbf{i}_\mathbf{r} = \frac{1}{Z}\frac{2\hbar^2}{m_e r_{15}^2 r_{12}}\sqrt{s(s+1)}\mathbf{i}_\mathbf{r} \tag{10.314}$$

The outward centrifugal force on electron 15 is balanced by the electric force and the magnetic forces (on electron 15). The radius of the outer electron is calculated by equating the outward centrifugal force to the sum of the electric (Eq. (10.312)), diamagnetic (Eq. (10.313)), and paramagnetic (Eq. (10.314)) forces as follows:

$$\frac{m_e v_{15}^2}{r_{15}} = \frac{(Z-14)e^2}{4\pi\varepsilon_0 r_{15}^2} - \frac{5\hbar^2}{12m_e r_{15}^2 r_{12}}\sqrt{s(s+1)} + \frac{2\hbar^2}{Zm_e r_{15}^2 r_{12}}\sqrt{s(s+1)} \tag{10.315}$$

Substitution of $v_{15} = \dfrac{\hbar}{m_e r_{15}}$ (Eq. (1.35)) and $s = \dfrac{1}{2}$ into Eq. (10.315) gives:

$$\frac{\hbar^2}{m_e r_{15}^3} = \frac{(Z-14)e^2}{4\pi\varepsilon_0 r_{15}^2} - \frac{5\hbar^2}{12m_e r_{15}^2 r_{12}}\sqrt{\frac{3}{4}} + \frac{2\hbar^2}{Zm_e r_{15}^2 r_{12}}\sqrt{\frac{3}{4}} \tag{10.316}$$

$$r_{15} = \frac{\dfrac{\hbar^2}{m_e}}{\dfrac{(Z-14)e^2}{4\pi\varepsilon_0} - \dfrac{5\hbar^2}{12m_e r_{12}}\sqrt{\dfrac{3}{4}} + \dfrac{2\hbar^2}{Zm_e r_{12}}\sqrt{\dfrac{3}{4}}} \tag{10.317}$$

$$r_{15} = \frac{a_0}{(Z-14) - \left(\dfrac{5}{12}-\dfrac{2}{Z}\right)\dfrac{\sqrt{\frac{3}{4}}}{r_{12}}},\ r_{12}\ in\ units\ of\ a_0 \tag{10.318}$$

Substitution of $\dfrac{r_{12}}{a_0} = 1.09443$ (Eq. (10.255) with $Z = 15$) into Eq. (10.318) gives:

$$r_{15} = 1.28900 a_0 \tag{10.319}$$

The ionization energy of the phosphorous atom is given by the electric energy, $E(electric)$, (Eq. (10.102) with the radius, $r_{15}$, given by Eq. (10.319)):

$$E(ionization;\ P) = -Electric\ Energy = \frac{(Z-14)e^2}{8\pi\varepsilon_0 r_{15}} = 10.5554\ eV \tag{10.320}$$

where $r_{15} = 1.28900 a_0$ (Eq. (10.319)) and $Z = 15$. The experimental ionization energy of the phosphorous atom is 10.48669 $eV$ [3].

## THE IONIZATION ENERGIES OF FIFTEEN-ELECTRON ATOMS WITH A NUCLEAR CHARGE Z>15

Fifteen-electron atoms having $Z>15$ possess an external electric field given by Eq. (10.92). In this case, an energy minimum is achieved with conservation of momentum when the orbital angular momentum is such that $\mathbf{F}_{diamagnetic}$ is minimized while $\mathbf{F}_{mag\ 2}$ is maximized. With a half-filled 3p shell, the diamagnetic force due to the orbital angular momenta of the 3p electrons cancels that of the 2p electrons. Thus, the diamagnetic force (Eq. (10.258)), $\mathbf{F}_{diamagnetic}$, is zero:

$$\mathbf{F}_{diamagnetic}=0 \tag{10.321}$$

From Eqs. (10.205) and (10.261), $\mathbf{F}_{mag\ 2}$ corresponding to the spin and orbital angular momenta of the paired 2 $p_x$, $p_y$, and $p_z$ electrons is:

$$\mathbf{F}_{mag\ 2}=\left(4+4+4\right)\frac{1}{Z}\frac{\hbar^2}{m_e r_{15}^2 r_{12}}\sqrt{s(s+1)}\mathbf{i}_{\mathbf{r}}=\frac{1}{Z}\frac{12\hbar^2}{m_e r_{15}^2 r_{12}}\sqrt{s(s+1)}\mathbf{i}_{\mathbf{r}} \tag{10.322}$$

and the contribution from the 3p level is:

$$\mathbf{F}_{mag\ 2}=\left(4+4+4\right)\frac{1}{Z}\frac{\hbar^2}{m_e r_{15}^2 r_{12}}\sqrt{s(s+1)}\mathbf{i}_{\mathbf{r}}=\frac{1}{Z}\frac{12\hbar^2}{m_e r_{15}^2 r_{12}}\sqrt{s(s+1)}\mathbf{i}_{\mathbf{r}} \tag{10.323}$$

corresponding to the 3 $p_x$, $p_y$, and $p_z$ electrons. Thus, the total of $\mathbf{F}_{mag\ 2}$ is:

$$\mathbf{F}_{mag\ 2}=\frac{1}{Z}\frac{24\hbar^2}{m_e r_{15}^2 r_{12}}\sqrt{s(s+1)}\mathbf{i}_{\mathbf{r}} \tag{10.324}$$

The diamagnetic force, $\mathbf{F}_{diamagnetic\ 2}$, due to the binding of the 3p-orbital electron having an electric field outside of its radius is given by Eq. (10.268):

$$\mathbf{F}_{diamagnetic\ 2}=-\left[\frac{Z-15}{Z-14}\right]\left(1-\frac{\sqrt{2}}{2}+\frac{1}{2}\right)\frac{r_{12}\hbar^2}{m_e r_{15}^4}10\sqrt{s(s+1)}\mathbf{i}_{\mathbf{r}} \tag{10.325}$$

In the case that $Z>15$, the radius of the outer electron is calculated by equating the outward centrifugal force to the sum of the electric (Eq. (10.312)), diamagnetic (Eqs. (10.321) and (10.325)), and paramagnetic (Eq. (10.324)) forces as follows:

$$\frac{m_e v_{15}^2}{r_{15}}=\frac{(Z-14)e^2}{4\pi\varepsilon_0 r_{15}^2}+\frac{24\hbar^2}{Zm_e r_{15}^2 r_{12}}\sqrt{s(s+1)}-\left[\frac{Z-15}{Z-14}\right]\left(1-\frac{\sqrt{2}}{2}+\frac{1}{2}\right)\frac{r_{12}\hbar^2}{m_e r_{15}^4}10\sqrt{s(s+1)} \tag{10.326}$$

Substitution of $v_{15}=\dfrac{\hbar}{m_e r_{15}}$ (Eq. (1.35)) and $s=\dfrac{1}{2}$ into Eq. (10.326) gives:

$$\frac{\hbar^2}{m_e r_{15}^3}=\frac{(Z-14)e^2}{4\pi\varepsilon_0 r_{15}^2}+\frac{24\hbar^2}{Zm_e r_{15}^2 r_{12}}\sqrt{\frac{3}{4}}-\left[\frac{Z-15}{Z-14}\right]\left(1-\frac{\sqrt{2}}{2}+\frac{1}{2}\right)\frac{r_{12}\hbar^2}{m_e r_{15}^4}10\sqrt{\frac{3}{4}} \tag{10.327}$$

The quadratic equation corresponding to Eq. (10.327) is:

$$\left(\frac{(Z-14)e^2}{4\pi\varepsilon_0}+\frac{24\hbar^2}{Zm_e r_{12}}\sqrt{\frac{3}{4}}\right)r_{15}^2-\frac{\hbar^2}{m_e}r_{15}-\left[\frac{Z-15}{Z-14}\right]\left(1-\frac{\sqrt{2}}{2}+\frac{1}{2}\right)\frac{r_{12}\hbar^2}{m_e}10\sqrt{\frac{3}{4}}=0 \tag{10.328}$$

$$r_{15}^2-\frac{\dfrac{\hbar^2}{m_e}}{\left(\dfrac{(Z-14)e^2}{4\pi\varepsilon_0}+\dfrac{24\hbar^2}{Zm_e r_{12}}\sqrt{\dfrac{3}{4}}\right)}r_{15}-\frac{\dfrac{\hbar^2}{m_e}\left[\dfrac{Z-15}{Z-14}\right]\left(1-\dfrac{\sqrt{2}}{2}+\dfrac{1}{2}\right)r_{12}10\sqrt{\dfrac{3}{4}}}{\left(\dfrac{(Z-14)e^2}{4\pi\varepsilon_0}-\dfrac{24\hbar^2}{Zm_e r_{12}}\sqrt{\dfrac{3}{4}}\right)}=0 \tag{10.329}$$

The solution of Eq. (10.329) using the quadratic formula is:

$$r_{15}=\frac{\dfrac{\dfrac{\hbar^2}{m_e}}{\left(\dfrac{(Z-14)e^2}{4\pi\varepsilon_0}+\dfrac{24\hbar^2}{Zm_e r_{12}}\sqrt{\dfrac{3}{4}}\right)}\pm\sqrt{\left(\dfrac{\dfrac{\hbar^2}{m_e}}{\left(\dfrac{(Z-14)e^2}{4\pi\varepsilon_0}+\dfrac{24\hbar^2}{Zm_e r_{12}}\sqrt{\dfrac{3}{4}}\right)}\right)^2+4\dfrac{\dfrac{\hbar^2}{m_e}\left[\dfrac{Z-15}{Z-14}\right]\left(1-\dfrac{\sqrt{2}}{2}+\dfrac{1}{2}\right)r_{12}10\sqrt{\dfrac{3}{4}}}{\left(\dfrac{(Z-14)e^2}{4\pi\varepsilon_0}+\dfrac{24\hbar^2}{Zm_e r_{12}}\sqrt{\dfrac{3}{4}}\right)}}}{2} \tag{10.330}$$

$$r_{15} = \frac{\dfrac{a_0}{\left((Z-14)+\dfrac{12\sqrt{3}}{Zr_{12}}\right)} \pm a_0\sqrt{\left(\dfrac{1}{\left((Z-14)+\dfrac{12\sqrt{3}}{Zr_{12}}\right)}\right)^2 + \dfrac{20\sqrt{3}\left(\left[\dfrac{Z-15}{Z-14}\right]\left(1-\dfrac{\sqrt{2}}{2}+\dfrac{1}{2}\right)r_{12}\right)}{\left((Z-14)+\dfrac{12\sqrt{3}}{Zr_{12}}\right)}}}{2}, \; r_{12} \; in \; units \; of \; a_0 \tag{10.331}$$

where $r_{12}$ is given by Eq. (10.255). The positive root of Eq. (10.331) must be taken in order that $r_{15} > 0$. The final radius of electron 15, $r_{15}$, is given by Eq. (10.331); this is also the final radius of electrons 13 and 14. The radii of several fifteen-electron atoms are given in Table 10.14.

The ionization energies for the fifteen-electron atoms with $Z > 15$ are given by the electric energy, $E(electric)$, (Eq. (10.102) with the radii $r_{15}$, given by Eq. (10.331)):

$$E(Ionization) = -Electric\ Energy = \frac{(Z-14)e^2}{8\pi\varepsilon_0 r_{15}} \tag{10.332}$$

Since the relativistic corrections were small, the nonrelativistic ionization energies for experimentally measured fifteen-electron atoms are given in Table 10.14.

**Table 10.14.** Ionization energies for some fifteen-electron atoms.

| 15 e Atom | Z | $r_1$ $(a_o)$ [a] | $r_3$ $(a_o)$ [b] | $r_{10}$ $(a_o)$ [c] | $r_{12}$ $(a_o)$ [d] | $r_{15}$ $(a_o)$ [e] | Theoretical Ionization Energies [f] $(eV)$ | Experimental Ionization Energies [g] $(eV)$ | Relative Error [h] |
|---|---|---|---|---|---|---|---|---|---|
| $P$ | 15 | 0.06730 | 0.29010 | 0.37120 | 1.09443 | 1.28900 | 10.55536 | 10.48669 | -0.0065 |
| $S^+$ | 16 | 0.06306 | 0.27053 | 0.33902 | 0.96729 | 1.15744 | 23.5102 | 23.3379 | -0.0074 |
| $Cl^{2+}$ | 17 | 0.05932 | 0.25344 | 0.31190 | 0.86545 | 1.06759 | 38.2331 | 39.61 | 0.0348 |
| $Ar^{3+}$ | 18 | 0.05599 | 0.23839 | 0.28878 | 0.78276 | 0.95423 | 57.0335 | 59.81 | 0.0464 |
| $K^{4+}$ | 19 | 0.05302 | 0.22503 | 0.26884 | 0.71450 | 0.85555 | 79.5147 | 82.66 | 0.0381 |
| $Ca^{5+}$ | 20 | 0.05035 | 0.21308 | 0.25149 | 0.65725 | 0.77337 | 105.5576 | 108.78 | 0.0296 |
| $Sc^{6+}$ | 21 | 0.04794 | 0.20235 | 0.23625 | 0.60857 | 0.70494 | 135.1046 | 138.0 | 0.0210 |
| $Ti^{7+}$ | 22 | 0.04574 | 0.19264 | 0.22276 | 0.56666 | 0.64743 | 168.1215 | 170.4 | 0.0134 |
| $V^{8+}$ | 23 | 0.04374 | 0.18383 | 0.21074 | 0.53022 | 0.59854 | 204.5855 | 205.8 | 0.0059 |
| $Cr^{9+}$ | 24 | 0.04191 | 0.17579 | 0.19995 | 0.49822 | 0.55652 | 244.4799 | 244.4 | -0.0003 |
| $Mn^{10+}$ | 25 | 0.04022 | 0.16842 | 0.19022 | 0.46990 | 0.52004 | 287.7926 | 286.0 | -0.0063 |
| $Fe^{11+}$ | 26 | 0.03867 | 0.16165 | 0.18140 | 0.44466 | 0.48808 | 334.5138 | 330.8 | -0.0112 |
| $Co^{12+}$ | 27 | 0.03723 | 0.15540 | 0.17336 | 0.42201 | 0.45985 | 384.6359 | 379 | -0.0149 |
| $Ni^{13+}$ | 28 | 0.03589 | 0.14961 | 0.16601 | 0.40158 | 0.43474 | 438.1529 | 430 | -0.0190 |
| $Cu^{14+}$ | 29 | 0.03465 | 0.14424 | 0.15926 | 0.38305 | 0.41225 | 495.0596 | 484 | -0.0229 |
| $Zn^{15+}$ | 30 | 0.03349 | 0.13925 | 0.15304 | 0.36617 | 0.39199 | 555.3519 | 542 | -0.0246 |

[a] Radius of the paired 1s inner electrons of fifteen-electron atoms from Eq. (10.51).

[b] Radius of the paired 2s inner electrons of fifteen-electron atoms from Eq. (10.62).

[c] Radius of the three sets of paired 2p inner electrons of fifteen-electron atoms from Eq. (10.212).

[d] Radius of the paired 3s inner electrons of fifteen-electron atoms from Eq. (10.255).

[e] Radius of the three unpaired 3p outer electrons of fifteen-electron atoms from Eq. (10.331) for $Z > 15$ and Eq. (10.319) for $P$.

[f] Calculated ionization energies of fifteen-electron atoms given by the electric energy (Eq. (10.332)).

[g] From theoretical calculations, interpolation of isoelectronic and spectral series, and experimental data [2-3].

[h] (Experimental-theoretical)/experimental.

The agreement between the experimental and calculated values of Table 10.14 is well within the experimental capability of the spectroscopic determinations including the values at large Z which relies on X-ray spectroscopy. In this case, the experimental capability is three to four significant figures which is consistent with the last column. The phosphorous atom isoelectronic series is given in Table 10.14 [2-3] to much higher precision than the capability of X-ray spectroscopy, but these values are based on theoretical and interpolation techniques rather than data alone. Ionization energies are difficult to determine since the cut-off of the Rydberg series of lines at the ionization energy is often not observed, and the ionization energy must be determined from theoretical calculations, interpolation of P isoelectronic and Rydberg series, as well as direct experimental data.

## SIXTEEN-ELECTRON ATOMS

Sixteen-electron atoms can be solved exactly using the results of the solutions of one, two, three, four, five, six, seven, eight, nine, ten, eleven, twelve, thirteen, fourteen, and fifteen-electron atoms.

## RADIUS AND IONIZATION ENERGY OF THE OUTER ELECTRON OF THE SULFUR ATOM

For each fifteen-electron atom having a central charge of $Z$ times that of the proton, there are two indistinguishable spin-paired electrons in an atomic orbital with radii $r_1$ and $r_2$ both given by Eq. (7.35) (Eq. (10.51)), two indistinguishable spin-paired electrons in an atomic orbital with radii $r_3$ and $r_4$ both given by Eq. (10.62), three sets of paired electrons in an atomic orbital at $r_{10}$ given by Eq. (10.212), two indistinguishable spin-paired electrons in an atomic orbital with radii $r_{11}$ and $r_{12}$ both given by Eq. (10.255), and three unpaired electrons in an atomic orbital with radius $r_{15}$ given by Eq. (10.331). For $Z \geq 16$, the next electron which binds to form the corresponding sixteen-electron atom is attracted by the central Coulomb field and is repelled by diamagnetic forces due to the 3 sets of spin-paired inner 2p electrons and two spin-paired inner 3s electrons. A paramagnetic spin-pairing force to form a filled s orbital is also possible, but the force due to the spin-pairing of the electrons (Eq. (7.24) with the radius $r_{16}$) reduces the energy of the atom less than that due to the alternative forces on a set of paired and two unpaired 3p electrons in an atomic orbital at the same radius $r_{16}$. The resulting electron configuration is $1s^2 2s^2 2p^6 3s^2 3p^4$, and the orbital arrangement is:

3p state

$$\underset{1}{\uparrow\downarrow} \quad \underset{0}{\uparrow} \quad \underset{-1}{\uparrow} \tag{10.333}$$

corresponding to the ground state ${}^3P_2$.

The central Coulomb force acts on the outer electron to cause it to bind wherein this electric force on the outer-most electron due to the nucleus and the inner fifteen electrons is given by Eq. (10.70) with the appropriate charge and radius:

$$\mathbf{F}_{ele} = \frac{(Z-15)e^2}{4\pi\varepsilon_0 r_{16}^2}\mathbf{i}_\mathbf{r} \tag{10.334}$$

for $r > r_{15}$.

The diamagnetic force, $\mathbf{F}_{diamagnetic}$, is only due to 3p and 3s electrons when the 3p shell is at least half filled since the induced charge-density waves only involve the inner-most shell, the 3s orbital. The energy is minimized with conservation of angular momentum when the induced orbital angular momentum of the 3s orbital superimposes positively with the orbital angular momenta of the other 3 $p_x$ and the 3 $p_z$-orbital electrons and the orbital angular momentum of one of the spin-paired 3 $p_x$ electrons is canceled by the 3 $p_y$ electron. Thus, $\mathbf{F}_{diamagnetic}$, is given by Eq. (10.258) as the sum of the contributions from the 3 $p_x$ and $p_z$ orbitals corresponding to $m$ = 1 and 0, respectively, and the induced contribution from the 3s orbital corresponding to $m$ = 0:

$$\mathbf{F}_{diamagnetic} = -\left(\frac{2}{3}+\frac{1}{3}+\frac{1}{3}\right)\frac{\hbar^2}{4m_e r_{16}^2 r_{12}}\sqrt{s(s+1)}\mathbf{i}_\mathbf{r} = -\left(\frac{4}{3}\right)\frac{\hbar^2}{4m_e r_{16}^2 r_{12}}\sqrt{s(s+1)}\mathbf{i}_\mathbf{r} \tag{10.335}$$

The energy is minimized with conservation of angular momentum when the spin angular momentum the 3s orbital superimposes negatively with the spin angular momentum of the 3 $p_x$ orbital-electron and the orbital angular momentum of the 3 $p_z$-orbital electron. From Eq. (10.260), $\mathbf{F}_{mag\ 2}$ corresponding to the orbital angular momentum of the 3 $p_x$, $p_y$, and $p_z$ orbitals minus the contribution from the 3s orbital is:

$$\mathbf{F}_{mag\ 2} = (1+1-1)\frac{1}{Z}\frac{\hbar^2}{m_e r_{16}^2 r_3}\sqrt{s(s+1)}\mathbf{i}_\mathbf{r} = \frac{1}{Z}\frac{\hbar^2}{m_e r_{16}^2 r_{12}}\sqrt{s(s+1)}\mathbf{i}_\mathbf{r} \tag{10.336}$$

The outward centrifugal force on electron 16 is balanced by the electric force and the magnetic forces (on electron 16). The radius of the outer electron is calculated by equating the outward centrifugal force to the sum of the electric (Eq. (10.334)), diamagnetic (Eq. (10.335)), and paramagnetic (Eq. (10.336)) forces as follows:

$$\frac{m_e v_{16}^2}{r_{16}} = \frac{(Z-15)e^2}{4\pi\varepsilon_0 r_{16}^2} - \frac{4\hbar^2}{12 m_e r_{16}^2 r_{12}}\sqrt{s(s+1)} + \frac{\hbar^2}{Z m_e r_{16}^2 r_{12}}\sqrt{s(s+1)} \tag{10.337}$$

Substitution of $v_{16} = \frac{\hbar}{m_e r_{16}}$ (Eq. (1.35)) and $s = \frac{1}{2}$ into Eq. (10.337) gives:

$$\frac{\hbar^2}{m_e r_{16}^3} = \frac{(Z-15)e^2}{4\pi\varepsilon_0 r_{16}^2} - \frac{4\hbar^2}{12 m_e r_{16}^2 r_{12}}\sqrt{\frac{3}{4}} + \frac{\hbar^2}{Z m_e r_{16}^2 r_{12}}\sqrt{\frac{3}{4}} \tag{10.338}$$

$$r_{16} = \frac{\frac{\hbar^2}{m_e}}{\frac{(Z-15)e^2}{4\pi\varepsilon_0} - \frac{4\hbar^2}{12 m_e r_{12}}\sqrt{\frac{3}{4}} + \frac{\hbar^2}{Z m_e r_{12}}\sqrt{\frac{3}{4}}} \tag{10.339}$$

$$r_{16} = \frac{a_0}{(Z-15) - \left(\frac{4}{12} - \frac{1}{Z}\right)\frac{\sqrt{\frac{3}{4}}}{r_{12}}},\ r_{12}\ in\ units\ of\ a_0 \tag{10.340}$$

Substitution of $\frac{r_{12}}{a_0} = 0.96729$ (Eq. (10.255) with $Z = 16$) into Eq. (10.340) gives:

$$r_{16} = 1.32010 a_0 \tag{10.341}$$

The ionization energy of the sulfur atom is given by the electric energy, $E(electric)$, (Eq. (10.102) with the radius, $r_{16}$, given by Eq. (10.341)).

$$E(ionization;\ S) = -Electric\ Energy = \frac{(Z-15)e^2}{8\pi\varepsilon_0 r_{16}} = 10.30666\ eV \tag{10.342}$$

where $r_{16} = 1.32010 a_0$ (Eq. (10.341)) and $Z = 16$. The experimental ionization energy of the sulfur atom is $10.36001\ eV$ [3].

## THE IONIZATION ENERGIES OF SIXTEEN-ELECTRON ATOMS WITH A NUCLEAR CHARGE Z>16

Sixteen-electron atoms having $Z > 16$ possess an external electric field given by Eq. (10.92). In this case, an energy minimum is achieved with conservation of momentum when the orbital angular momentum is such that $\mathbf{F}_{diamagnetic}$ is minimized while $\mathbf{F}_{mag\ 2}$ is maximized. With a half-filled 3p shell, the diamagnetic force due to the orbital angular momenta of the 3p electrons cancels that of the 2p electrons. Thus, $\mathbf{F}_{diamagnetic}$ is minimized by the formation of a charge-density wave in the 3s orbital corresponding to $m = 1$ in Eq. (10.258) that cancels the orbital angular momentum of one of the $3\,p_x$ electrons to form the equivalent of a half-filled 3p shell. Then, the contribution due to the 2p level is canceled. From Eq. (10.82), the diamagnetic force, $\mathbf{F}_{diamagnetic}$, is given by the sum of the contributions from the $3\,p_y$ and $p_z$ orbitals corresponding to $m = -1$, and $0$, respectively, and the negative contribution due to the charge-density wave with $m = 1$ induced in the 3s orbital (Eq. (10.258)).

$$\mathbf{F}_{diamagnetic} = -\left(\frac{2}{3} + \frac{1}{3} - \frac{2}{3}\right)\frac{\hbar^2}{4 m_e r_{16}^2 r_{12}}\sqrt{s(s+1)}\mathbf{i}_{\mathbf{r}} = -\left(\frac{1}{3}\right)\frac{\hbar^2}{4 m_e r_{16}^2 r_{12}}\sqrt{s(s+1)}\mathbf{i}_{\mathbf{r}} \tag{10.343}$$

From Eq. (10.261), $\mathbf{F}_{mag\ 2}$ corresponding to the spin and orbital angular momenta of the paired $2\,p_x$, $p_y$, and $p_z$ electrons is

$$\mathbf{F}_{mag\ 2} = (4+4+4)\frac{1}{Z}\frac{\hbar^2}{m_e r_{16}^2 r_{12}}\sqrt{s(s+1)}\mathbf{i}_{\mathbf{r}} = \frac{1}{Z}\frac{12\hbar^2}{m_e r_{16}^2 r_{12}}\sqrt{s(s+1)}\mathbf{i}_{\mathbf{r}} \tag{10.344}$$

and the contribution from the 3p level is:

$$\mathbf{F}_{mag\ 2} = (8+4+4-4)\frac{1}{Z}\frac{\hbar^2}{m_e r_{16}^2 r_{12}}\sqrt{s(s+1)}\mathbf{i}_{\mathbf{r}} = \frac{1}{Z}\frac{12\hbar^2}{m_e r_{16}^2 r_{12}}\sqrt{s(s+1)}\mathbf{i}_{\mathbf{r}} \tag{10.345}$$

corresponding to the $3\,p_x$ (Eq. (10.264)) and $p_z$ (Eq. (10.263)) electrons wherein the contribution due to the $3\,p_x$ ($m = 1$) electron is canceled by the mirror charge-density wave with $m = 1$ induced in the 3s orbital (Eq. (10.262)). Thus, the total of $\mathbf{F}_{mag\ 2}$ is

$$\mathbf{F}_{mag\ 2} = \frac{1}{Z}\frac{24\hbar^2}{m_e r_{16}^2 r_{12}}\sqrt{s(s+1)}\mathbf{i}_{\mathbf{r}} \tag{10.346}$$

The diamagnetic force, $\mathbf{F}_{diamagnetic\ 2}$, due to the binding of the 3p-orbital electron having an electric field outside of its radius is given by Eq. (10.268):

$$\mathbf{F}_{diamagnetic\ 2} = -\left[\frac{Z-16}{Z-15}\right]\left(1-\frac{\sqrt{2}}{2}+\frac{1}{2}\right)\frac{r_{12}\hbar^2}{m_e r_{16}^4}10\sqrt{s(s+1)}\mathbf{i}_\mathbf{r} \tag{10.347}$$

In the case that $Z>16$, the radius of the outer electron is calculated by equating the outward centrifugal force to the sum of the electric (Eq. (10.334)), diamagnetic (Eqs. (10.343) and (10.347)), and paramagnetic (Eq. (10.346)) forces as follows:

$$\frac{m_e v_{16}^2}{r_{16}} = \frac{(Z-15)e^2}{4\pi\varepsilon_0 r_{16}^2} - \frac{\hbar^2}{12 m_e r_{16}^2 r_{12}}\sqrt{s(s+1)} + \frac{24\hbar^2}{Z m_e r_{16}^2 r_{12}}\sqrt{s(s+1)} \tag{10.348}$$

$$-\left[\frac{Z-16}{Z-15}\right]\left(1-\frac{\sqrt{2}}{2}+\frac{1}{2}\right)\frac{r_{12}\hbar^2}{m_e r_{16}^4}10\sqrt{s(s+1)}$$

Substitution of $v_{16} = \dfrac{\hbar}{m_e r_{16}}$ (Eq. (1.35)) and $s=\dfrac{1}{2}$ into Eq. (10.348) gives:

$$\frac{\hbar^2}{m_e r_{16}^3} = \frac{(Z-15)e^2}{4\pi\varepsilon_0 r_{16}^2} - \frac{\hbar^2}{12 m_e r_{16}^2 r_{12}}\sqrt{\frac{3}{4}} + \frac{24\hbar^2}{Z m_e r_{16}^2 r_{12}}\sqrt{\frac{3}{4}} - \left[\frac{Z-16}{Z-15}\right]\left(1-\frac{\sqrt{2}}{2}+\frac{1}{2}\right)\frac{r_{12}\hbar^2}{m_e r_{16}^4}10\sqrt{\frac{3}{4}} \tag{10.349}$$

The quadratic equation corresponding to Eq. (10.349) is

$$\left(\frac{(Z-15)e^2}{4\pi\varepsilon_0} - \left(\frac{1}{12}-\frac{24}{Z}\right)\frac{\hbar^2}{m_e r_{12}}\sqrt{\frac{3}{4}}\right)r_{16}^2 - \frac{\hbar^2}{m_e}r_{16} - \left[\frac{Z-16}{Z-15}\right]\left(1-\frac{\sqrt{2}}{2}+\frac{1}{2}\right)\frac{r_{12}\hbar^2}{m_e}10\sqrt{\frac{3}{4}} = 0 \tag{10.350}$$

$$r_{16}^2 - \frac{\dfrac{\hbar^2}{m_e}}{\left(\dfrac{(Z-15)e^2}{4\pi\varepsilon_0} - \left(\dfrac{1}{12}-\dfrac{24}{Z}\right)\dfrac{\hbar^2}{m_e r_{12}}\sqrt{\dfrac{3}{4}}\right)}r_{16} - \frac{\dfrac{\hbar^2}{m_e}\left[\dfrac{Z-16}{Z-15}\right]\left(1-\dfrac{\sqrt{2}}{2}+\dfrac{1}{2}\right)r_{12}10\sqrt{\dfrac{3}{4}}}{\left(\dfrac{(Z-15)e^2}{4\pi\varepsilon_0} - \left(\dfrac{1}{12}-\dfrac{24}{Z}\right)\dfrac{\hbar^2}{m_e r_{12}}\sqrt{\dfrac{3}{4}}\right)} = 0 \tag{10.351}$$

The solution of Eq. (10.351) using the quadratic formula is:

$$r_{16} = \frac{\dfrac{\dfrac{\hbar^2}{m_e}}{\left(\dfrac{(Z-15)e^2}{4\pi\varepsilon_0} - \left(\dfrac{1}{12}-\dfrac{24}{Z}\right)\dfrac{\hbar^2}{m_e r_{12}}\sqrt{\dfrac{3}{4}}\right)} \pm \sqrt{\left(\dfrac{\dfrac{\hbar^2}{m_e}}{\left(\dfrac{(Z-15)e^2}{4\pi\varepsilon_0} - \left(\dfrac{1}{12}-\dfrac{24}{Z}\right)\dfrac{\hbar^2}{m_e r_{12}}\sqrt{\dfrac{3}{4}}\right)}\right)^2 + 4\dfrac{\dfrac{\hbar^2}{m_e}\left[\dfrac{Z-16}{Z-15}\right]\left(1-\dfrac{\sqrt{2}}{2}+\dfrac{1}{2}\right)r_{12}10\sqrt{\dfrac{3}{4}}}{\left(\dfrac{(Z-15)e^2}{4\pi\varepsilon_0} - \left(\dfrac{1}{12}-\dfrac{24}{Z}\right)\dfrac{\hbar^2}{m_e r_{12}}\sqrt{\dfrac{3}{4}}\right)}}}{2} \tag{10.352}$$

$$r_{16} = \frac{\dfrac{a_0}{\left((Z-15) - \left(\dfrac{1}{24}-\dfrac{12}{Z}\right)\dfrac{\sqrt{3}}{r_{12}}\right)} \pm a_0\sqrt{\left(\dfrac{1}{\left((Z-15) - \left(\dfrac{1}{24}-\dfrac{12}{Z}\right)\dfrac{\sqrt{3}}{r_{12}}\right)}\right)^2 + \dfrac{20\sqrt{3}\left(\left[\dfrac{Z-16}{Z-15}\right]\left(1-\dfrac{\sqrt{2}}{2}+\dfrac{1}{2}\right)r_{12}\right)}{\left((Z-15) - \left(\dfrac{1}{24}-\dfrac{12}{Z}\right)\dfrac{\sqrt{3}}{r_{12}}\right)}}}{2}, \quad r_{12}\ \textit{in units of}\ a_0 \tag{10.353}$$

where $r_{12}$ is given by Eq. (10.255). The positive root of Eq. (10.353) must be taken in order that $r_{16}>0$. The final radius of electron 16, $r_{16}$, is given by Eq. (10.353); this is also the final radius of electrons 13, 14, and 15. The radii of several sixteen-electron atoms are given in Table 10.15.

The ionization energies for the sixteen-electron atoms with $Z>16$ are given by the electric energy, $E(electric)$, (Eq. (10.102) with the radii $r_{16}$, given by Eq. (10.353)).

$$E(Ionization) = -Electric\ Energy = \frac{(Z-15)e^2}{8\pi\varepsilon_0 r_{16}} \tag{10.354}$$

Since the relativistic corrections were small, the nonrelativistic ionization energies for experimentally measured sixteen-electron atoms are given in Table 10.15.

**Table 10.15.** Ionization energies for some sixteen-electron atoms.

| 16 e Atom | Z | $r_1$ $(a_o)$ [a] | $r_3$ $(a_o)$ [b] | $r_{10}$ $(a_o)$ [c] | $r_{12}$ $(a_o)$ [d] | $r_{16}$ $(a_o)$ [e] | Theoretical Ionization Energies [f] $(eV)$ | Experimental Ionization Energies [g] $(eV)$ | Relative Error [h] |
|---|---|---|---|---|---|---|---|---|---|
| $S$ | 16 | 0.06306 | 0.27053 | 0.33902 | 0.96729 | 1.32010 | 10.30666 | 10.36001 | 0.0051 |
| $Cl^+$ | 17 | 0.05932 | 0.25344 | 0.31190 | 0.86545 | 1.10676 | 24.5868 | 23.814 | -0.0324 |
| $Ar^{2+}$ | 18 | 0.05599 | 0.23839 | 0.28878 | 0.78276 | 1.02543 | 39.8051 | 40.74 | 0.0229 |
| $K^{3+}$ | 19 | 0.05302 | 0.22503 | 0.26884 | 0.71450 | 0.92041 | 59.1294 | 60.91 | 0.0292 |
| $Ca^{4+}$ | 20 | 0.05035 | 0.21308 | 0.25149 | 0.65725 | 0.82819 | 82.1422 | 84.50 | 0.0279 |
| $Sc^{5+}$ | 21 | 0.04794 | 0.20235 | 0.23625 | 0.60857 | 0.75090 | 108.7161 | 110.68 | 0.0177 |
| $Ti^{6+}$ | 22 | 0.04574 | 0.19264 | 0.22276 | 0.56666 | 0.68622 | 138.7896 | 140.8 | 0.0143 |
| $V^{7+}$ | 23 | 0.04374 | 0.18383 | 0.21074 | 0.53022 | 0.63163 | 172.3256 | 173.4 | 0.0062 |
| $Cr^{8+}$ | 24 | 0.04191 | 0.17579 | 0.19995 | 0.49822 | 0.58506 | 209.2996 | 209.3 | 0.0000 |
| $Mn^{9+}$ | 25 | 0.04022 | 0.16842 | 0.19022 | 0.46990 | 0.54490 | 249.6938 | 248.3 | -0.0056 |
| $Fe^{10+}$ | 26 | 0.03867 | 0.16165 | 0.18140 | 0.44466 | 0.50994 | 293.4952 | 290.2 | -0.0114 |
| $Co^{11+}$ | 27 | 0.03723 | 0.15540 | 0.17336 | 0.42201 | 0.47923 | 340.6933 | 336 | -0.0140 |
| $Ni^{12+}$ | 28 | 0.03589 | 0.14961 | 0.16601 | 0.40158 | 0.45204 | 391.2802 | 384 | -0.0190 |
| $Cu^{13+}$ | 29 | 0.03465 | 0.14424 | 0.15926 | 0.38305 | 0.42781 | 445.2492 | 435 | -0.0236 |
| $Zn^{14+}$ | 30 | 0.03349 | 0.13925 | 0.15304 | 0.36617 | 0.40607 | 502.5950 | 490 | -0.0257 |

[a] Radius of the paired 1s inner electrons of sixteen-electron atoms from Eq. (10.51).

[b] Radius of the paired 2s inner electrons of sixteen-electron atoms from Eq. (10.62).

[c] Radius of the three sets of paired 2p inner electrons of sixteen-electron atoms from Eq. (10.212).

[d] Radius of the paired 3s inner electrons of sixteen-electron atoms from Eq. (10.255).

[e] Radius of the two paired and two unpaired 3p outer electrons of sixteen-electron atoms from Eq. (10.353) for $Z > 16$ and Eq. (10.341) for *S*.

[f] Calculated ionization energies of sixteen-electron atoms given by the electric energy (Eq. (10.354)).

[g] From theoretical calculations, interpolation of isoelectronic and spectral series, and experimental data [2-3].

[h] (Experimental-theoretical)/experimental.

The agreement between the experimental and calculated values of Table 10.15 is well within the experimental capability of the spectroscopic determinations including the values at large Z which relies on X-ray spectroscopy. In this case, the experimental capability is three to four significant figures which is consistent with the last column. The sulfur atom isoelectronic series is given in Table 10.15 [2-3] to much higher precision than the capability of X-ray spectroscopy, but these values are based on theoretical and interpolation techniques rather than data alone. Ionization energies are difficult to determine since the cut-off of the Rydberg series of lines at the ionization energy is often not observed, and the ionization energy must be determined from theoretical calculations, interpolation of S isoelectronic and Rydberg series, as well as direct experimental data.

## SEVENTEEN-ELECTRON ATOMS

Seventeen-electron atoms can be solved exactly using the results of the solutions of one, two, three, four, five, six, seven, eight, nine, ten, eleven, twelve, thirteen, fourteen, fifteen, and sixteen-electron atoms.

## RADIUS AND IONIZATION ENERGY OF THE OUTER ELECTRON OF THE CHLORINE ATOM

For each sixteen-electron atom having a central charge of $Z$ times that of the proton, there are two indistinguishable spin-paired electrons in an atomic orbital with radii $r_1$ and $r_2$ both given by Eq. (7.35) (Eq. (10.51)), two indistinguishable spin-paired electrons in an atomic orbital with radii $r_3$ and $r_4$ both given by Eq. (10.62), three sets of paired electrons in an atomic orbital at $r_{10}$ given by Eq. (10.212), two indistinguishable spin-paired electrons in an atomic orbital with radii $r_{11}$ and $r_{12}$ both given by Eq. (10.255), and two paired and two unpaired electrons in an atomic orbital with radius $r_{16}$ given by Eq. (10.353). For $Z \geq 17$, the next electron which binds to form the corresponding seventeen-electron atom is attracted by the central Coulomb field and is repelled by diamagnetic forces due to the 3 sets of spin-paired inner 2p electrons and two spin-paired inner 3s electrons. A paramagnetic spin-pairing force to form a filled s orbital is also possible, but the force due to the spin-pairing of the electrons

(Eq. (7.24) with the radius $r_{17}$) reduces the energy of the atom less than that due to the alternative forces on two sets of paired electrons and an unpaired 3p electron in an atomic orbital at the same radius $r_{17}$. The resulting electron configuration is $1s^2 2s^2 2p^6 3s^2 3p^5$, and the orbital arrangement is:

3p state

$$\underset{1}{\uparrow\downarrow} \quad \underset{0}{\uparrow\downarrow} \quad \underset{-1}{\uparrow} \tag{10.355}$$

corresponding to the ground state ${}^2P^0_{3/2}$.

The central Coulomb force acts on the outer electron to cause it to bind wherein this electric force on the outer-most electron due to the nucleus and the inner sixteen electrons is given by Eq. (10.70) with the appropriate charge and radius:

$$\mathbf{F}_{ele} = \frac{(Z-16)e^2}{4\pi\varepsilon_0 r_{17}^2}\mathbf{i}_\mathbf{r} \tag{10.356}$$

for $r > r_{16}$.

The diamagnetic force, $\mathbf{F}_{diamagnetic}$, is only due to 3p and 3s electrons when the 3p shell is at least half filled since the induced charge-density waves only involve the inner-most shell, the 3s orbital. Thus, $\mathbf{F}_{diamagnetic}$, is given by Eq. (10.258) as the contribution from the 3 $p_y$ orbital corresponding to $m = -1$ with the cancellation of the orbital angular momenta of the spin-paired 3 $p_x$ and $p_z$ electrons:

$$\mathbf{F}_{diamagnetic} = -\left(\frac{2}{3}\right)\frac{\hbar^2}{4m_e r_{17}^2 r_{12}}\sqrt{s(s+1)}\mathbf{i}_\mathbf{r} \tag{10.357}$$

The energy is minimized with conservation of angular momentum when the spin angular momentum of the 3s orbital superimposes negatively with the angular momenta of the 3p orbitals. From Eq. (10.260), $\mathbf{F}_{mag\ 2}$ corresponding to the sum of the spin angular momenta of the 3 $p_x$ and 3 $p_z$ orbitals and the orbital angular momentum of the 3 $p_y$ orbital, minus the contribution from the 3s orbital is:

$$\mathbf{F}_{mag\ 2} = (1+1+1-1)\frac{1}{Z}\frac{\hbar^2}{m_e r_{17}^2 r_{12}}\sqrt{s(s+1)}\mathbf{i}_\mathbf{r} = \frac{1}{Z}\frac{2\hbar^2}{m_e r_{17}^2 r_{12}}\sqrt{s(s+1)}\mathbf{i}_\mathbf{r} \tag{10.358}$$

The outward centrifugal force on electron 17 is balanced by the electric force and the magnetic forces (on electron 17). The radius of the outer electron is calculated by equating the outward centrifugal force to the sum of the electric (Eq. (10.356)), diamagnetic (Eq. (10.357)), and paramagnetic (Eq. (10.358)) forces as follows:

$$\frac{m_e v_{17}^2}{r_{17}} = \frac{(Z-16)e^2}{4\pi\varepsilon_0 r_{17}^2} - \frac{2\hbar^2}{12m_e r_{17}^2 r_{12}}\sqrt{s(s+1)} + \frac{2\hbar^2}{Zm_e r_{17}^2 r_{12}}\sqrt{s(s+1)} \tag{10.359}$$

Substitution of $v_{17} = \dfrac{\hbar}{m_e r_{17}}$ (Eq. (1.35)) and $s = \dfrac{1}{2}$ into Eq. (10.359) gives:

$$\frac{\hbar^2}{m_e r_{17}^3} = \frac{(Z-16)e^2}{4\pi\varepsilon_0 r_{17}^2} - \frac{2\hbar^2}{12m_e r_{17}^2 r_{12}}\sqrt{\frac{3}{4}} + \frac{2\hbar^2}{Zm_e r_{17}^2 r_{12}}\sqrt{\frac{3}{4}} \tag{10.360}$$

$$r_{17} = \frac{\dfrac{\hbar^2}{m_e}}{\dfrac{(Z-16)e^2}{4\pi\varepsilon_0} - \dfrac{2\hbar^2}{12m_e r_{12}}\sqrt{\dfrac{3}{4}} + \dfrac{2\hbar^2}{Zm_e r_{12}}\sqrt{\dfrac{3}{4}}} \tag{10.361}$$

$$r_{17} = \frac{a_0}{(Z-16) - \left(\dfrac{2}{12} - \dfrac{2}{Z}\right)\dfrac{\sqrt{\dfrac{3}{4}}}{r_{12}}},\ r_{12}\ in\ units\ of\ a_0 \tag{10.362}$$

Substitution of $\dfrac{r_{12}}{a_0} = 0.86545$ (Eq. (10.255) with $Z = 17$) into Eq. (10.362) gives:

$$r_{17} = 1.05158 a_0 \tag{10.363}$$

The ionization energy of the chlorine atom is given by the electric energy, $E(electric)$, (Eq. (10.102) with the radius, $r_{17}$, given by Eq. (10.363)):

$$E(ionization;\ Cl) = -Electric\ Energy = \frac{(Z-16)e^2}{8\pi\varepsilon_0 r_{17}} = 12.93841\ eV \tag{10.364}$$

where $r_{17} = 1.05158 a_0$ (Eq. (10.363)) and $Z = 17$. The experimental ionization energy of the chlorine atom is 12.96764 $eV$ [3].

## THE IONIZATION ENERGIES OF SEVENTEEN-ELECTRON ATOMS WITH A NUCLEAR CHARGE Z>17

Seventeen-electron atoms having $Z > 17$ possess an external electric field given by Eq. (10.92). In this case, an energy minimum is achieved with conservation of momentum when the orbital angular momentum is such that $\mathbf{F}_{diamagnetic}$ is minimized while $\mathbf{F}_{mag\ 2}$ is maximized. With a filled 3p shell, the diamagnetic force due to the orbital angular momenta of the 3p electrons cancels that of the 2p electrons. Thus, $\mathbf{F}_{diamagnetic}$ is minimized by the formation of a charge-density wave in the 3s orbital corresponding to two electrons with $m$ = -1 in Eq. (10.258) to form the equivalent of a filled 3p level such that the contribution due to the 2p level is canceled. From Eq. (10.82), the diamagnetic force, $\mathbf{F}_{diamagnetic}$, is given by the contribution due to the charge-density wave with $m$ = -1 induced in the 3s orbital according to Eq. (10.258).

$$\mathbf{F}_{diamagnetic} = -\left(\frac{2}{3}\right)\frac{\hbar^2}{4m_e r_{17}^2 r_{12}}\sqrt{s(s+1)}\mathbf{i}_{\mathbf{r}} \tag{10.365}$$

From Eqs. (10.205) and (10.261), $\mathbf{F}_{mag\ 2}$ corresponding to the spin and orbital angular momenta of the paired 2 $p_x$, $p_y$, and $p_z$ electrons is

$$\mathbf{F}_{mag\ 2} = (4+4+4)\frac{1}{Z}\frac{\hbar^2}{m_e r_{17}^2 r_{12}}\sqrt{s(s+1)}\mathbf{i}_{\mathbf{r}} = \frac{1}{Z}\frac{12\hbar^2}{m_e r_{17}^2 r_{12}}\sqrt{s(s+1)}\mathbf{i}_{\mathbf{r}} \tag{10.366}$$

and the contribution from the paired 3 $p_x$, $p_y$, and $p_z$ electrons given by Eq. (10.264) is

$$\mathbf{F}_{mag\ 2} = (8+8+8)\frac{1}{Z}\frac{\hbar^2}{m_e r_{17}^2 r_{12}}\sqrt{s(s+1)}\mathbf{i}_{\mathbf{r}} = \frac{1}{Z}\frac{24\hbar^2}{m_e r_{17}^2 r_{12}}\sqrt{s(s+1)}\mathbf{i}_{\mathbf{r}} \tag{10.367}$$

wherein the contribution due to the charge-density wave with $m$ = -1 induced in the 3s orbital (Eq. (10.262)) provides the equivalent of a filled 3 $p_y$ orbital and adds a negative contribution of:

$$\mathbf{F}_{mag\ 2} = -\frac{1}{Z}\frac{4\hbar^2}{m_e r_{17}^2 r_{12}}\sqrt{s(s+1)}\mathbf{i}_{\mathbf{r}} \tag{10.368}$$

Thus, the total of $\mathbf{F}_{mag\ 2}$ is:

$$\mathbf{F}_{mag\ 2} = \frac{1}{Z}\frac{32\hbar^2}{m_e r_{17}^2 r_{12}}\sqrt{s(s+1)}\mathbf{i}_{\mathbf{r}} \tag{10.369}$$

The diamagnetic force, $\mathbf{F}_{diamagnetic\ 2}$, due to the binding of the 3p-orbital electron having an electric field outside of its radius is given by Eq. (10.268):

$$\mathbf{F}_{diamagnetic\ 2} = -\left[\frac{Z-17}{Z-16}\right]\left(1-\frac{\sqrt{2}}{2}+\frac{1}{2}\right)\frac{r_{12}\hbar^2}{m_e r_{17}^4}10\sqrt{s(s+1)}\mathbf{i}_{\mathbf{r}} \tag{10.370}$$

In the case that $Z > 17$, the radius of the outer electron is calculated by equating the outward centrifugal force to the sum of the electric (Eq. (10.356)), diamagnetic (Eqs. (10.365) and (10.370)), and paramagnetic (Eq. (10.369)) forces as follows:

$$\frac{m_e v_{17}^2}{r_{17}} = \frac{(Z-16)e^2}{4\pi\varepsilon_0 r_{17}^2} - \frac{2\hbar^2}{12m_e r_{17}^2 r_{12}}\sqrt{s(s+1)} + \frac{32\hbar^2}{Zm_e r_{17}^2 r_{12}}\sqrt{s(s+1)} - \left[\frac{Z-17}{Z-16}\right]\left(1-\frac{\sqrt{2}}{2}+\frac{1}{2}\right)\frac{r_{12}\hbar^2}{m_e r_{17}^4}10\sqrt{s(s+1)} \tag{10.371}$$

Substitution of $v_{17} = \dfrac{\hbar}{m_e r_{17}}$ (Eq. (1.35)) and $s = \dfrac{1}{2}$ into Eq. (10.371) gives:

$$\frac{\hbar^2}{m_e r_{17}^3} = \frac{(Z-16)e^2}{4\pi\varepsilon_0 r_{17}^2} - \frac{2\hbar^2}{12m_e r_{17}^2 r_{12}}\sqrt{\frac{3}{4}} + \frac{32\hbar^2}{Zm_e r_{17}^2 r_{12}}\sqrt{\frac{3}{4}} - \left[\frac{Z-17}{Z-16}\right]\left(1-\frac{\sqrt{2}}{2}+\frac{1}{2}\right)\frac{r_{12}\hbar^2}{m_e r_{17}^4}10\sqrt{\frac{3}{4}} \tag{10.372}$$

The quadratic equation corresponding to Eq. (10.372) is

$$\left(\frac{(Z-16)e^2}{4\pi\varepsilon_0} - \left(\frac{2}{12}-\frac{32}{Z}\right)\frac{\hbar^2}{m_e r_{12}}\sqrt{\frac{3}{4}}\right)r_{17}^2 - \frac{\hbar^2}{m_e}r_{17} - \left[\frac{Z-17}{Z-16}\right]\left(1-\frac{\sqrt{2}}{2}+\frac{1}{2}\right)\frac{r_{12}\hbar^2}{m_e}10\sqrt{\frac{3}{4}} = 0 \tag{10.373}$$

$$r_{17}^2 - \frac{\dfrac{\hbar^2}{m_e}}{\left(\dfrac{(Z-16)e^2}{4\pi\varepsilon_0} - \left(\dfrac{2}{12}-\dfrac{32}{Z}\right)\dfrac{\hbar^2}{m_e r_{12}}\sqrt{\dfrac{3}{4}}\right)}r_{17} - \frac{\dfrac{\hbar^2}{m_e}\left[\dfrac{Z-17}{Z-16}\right]\left(1-\dfrac{\sqrt{2}}{2}+\dfrac{1}{2}\right)r_{12}10\sqrt{\dfrac{3}{4}}}{\left(\dfrac{(Z-16)e^2}{4\pi\varepsilon_0} - \left(\dfrac{2}{12}-\dfrac{32}{Z}\right)\dfrac{\hbar^2}{m_e r_{12}}\sqrt{\dfrac{3}{4}}\right)} = 0 \tag{10.374}$$

The solution of Eq. (10.374) using the quadratic formula is:

$$r_{17}=\frac{\dfrac{\dfrac{\hbar^2}{m_e}}{\left(\dfrac{(Z-16)e^2}{4\pi\varepsilon_0}-\left(\dfrac{2}{12}-\dfrac{32}{Z}\right)\dfrac{\hbar^2}{m_e r_{12}}\sqrt{\dfrac{3}{4}}\right)}\pm\sqrt{\left(\dfrac{\dfrac{\hbar^2}{m_e}}{\left(\dfrac{(Z-16)e^2}{4\pi\varepsilon_0}-\left(\dfrac{2}{12}-\dfrac{32}{Z}\right)\dfrac{\hbar^2}{m_e r_{12}}\sqrt{\dfrac{3}{4}}\right)}\right)^2+4\dfrac{\dfrac{\hbar^2}{m_e}\left\lfloor\dfrac{Z-17}{Z-16}\right\rfloor\left(1-\dfrac{\sqrt{2}}{2}+\dfrac{1}{2}\right)r_{12}10\sqrt{\dfrac{3}{4}}}{\left(\dfrac{(Z-16)e^2}{4\pi\varepsilon_0}-\left(\dfrac{2}{12}-\dfrac{32}{Z}\right)\dfrac{\hbar^2}{m_e r_{12}}\sqrt{\dfrac{3}{4}}\right)}}}{2} \tag{10.375}$$

$$r_{17}=\frac{\dfrac{a_0}{\left((Z-16)-\left(\dfrac{1}{12}-\dfrac{16}{Z}\right)\dfrac{\sqrt{3}}{r_{12}}\right)}\pm a_0\sqrt{\left(\dfrac{1}{\left((Z-16)-\left(\dfrac{1}{12}-\dfrac{16}{Z}\right)\dfrac{\sqrt{3}}{r_{12}}\right)}\right)^2+\dfrac{20\sqrt{3}\left(\left\lfloor\dfrac{Z-17}{Z-16}\right\rfloor\left(1-\dfrac{\sqrt{2}}{2}+\dfrac{1}{2}\right)r_{12}\right)}{\left((Z-16)-\left(\dfrac{1}{12}-\dfrac{16}{Z}\right)\dfrac{\sqrt{3}}{r_{12}}\right)}}}{2},\ r_{12}\ \textit{in units of}\ a_0 \tag{10.376}$$

where $r_{12}$ is given by Eq. (10.255). The positive root of Eq. (10.376) must be taken in order that $r_{17}>0$. The final radius of electron 17, $r_{17}$, is given by Eq. (10.376); this is also the final radius of electrons 13, 14, 15, and 16. The radii of several seventeen-electron atoms are given in Table 10.16.

The ionization energies for the seventeen-electron atoms with $Z>17$ are given by the electric energy, $E(electric)$, (Eq. (10.102) with the radii $r_{17}$, given by Eq. (10.376)).

$$E(Ionization)=-Electric\ Energy=\frac{(Z-16)e^2}{8\pi\varepsilon_0 r_{17}} \tag{10.377}$$

Since the relativistic corrections were small, the nonrelativistic ionization energies for experimentally measured seventeen-electron atoms are given in Table 10.16.

**Table 10.16.** Ionization energies for some seventeen-electron atoms.

| 17 e Atom | Z | $r_1$ $(a_o)$ [a] | $r_3$ $(a_o)$ [b] | $r_{10}$ $(a_o)$ [c] | $r_{12}$ $(a_o)$ [d] | $r_{17}$ $(a_o)$ [e] | Theoretical Ionization Energies [f] (eV) | Experimental Ionization Energies [g] (eV) | Relative Error [h] |
|---|---|---|---|---|---|---|---|---|---|
| $Cl$ | 17 | 0.05932 | 0.25344 | 0.31190 | 0.86545 | 1.05158 | 12.93841 | 12.96764 | 0.0023 |
| $Ar^+$ | 18 | 0.05599 | 0.23839 | 0.28878 | 0.78276 | 0.98541 | 27.6146 | 27.62967 | 0.0005 |
| $K^{2+}$ | 19 | 0.05302 | 0.22503 | 0.26884 | 0.71450 | 0.93190 | 43.8001 | 45.806 | 0.0438 |
| $Ca^{3+}$ | 20 | 0.05035 | 0.21308 | 0.25149 | 0.65725 | 0.84781 | 64.1927 | 67.27 | 0.0457 |
| $Sc^{4+}$ | 21 | 0.04794 | 0.20235 | 0.23625 | 0.60857 | 0.77036 | 88.3080 | 91.65 | 0.0365 |
| $Ti^{5+}$ | 22 | 0.04574 | 0.19264 | 0.22276 | 0.56666 | 0.70374 | 116.0008 | 119.53 | 0.0295 |
| $V^{6+}$ | 23 | 0.04374 | 0.18383 | 0.21074 | 0.53022 | 0.64701 | 147.2011 | 150.6 | 0.0226 |
| $Cr^{7+}$ | 24 | 0.04191 | 0.17579 | 0.19995 | 0.49822 | 0.59849 | 181.8674 | 184.7 | 0.0153 |
| $Mn^{8+}$ | 25 | 0.04022 | 0.16842 | 0.19022 | 0.46990 | 0.55667 | 219.9718 | 221.8 | 0.0082 |
| $Fe^{9+}$ | 26 | 0.03867 | 0.16165 | 0.18140 | 0.44466 | 0.52031 | 261.4942 | 262.1 | 0.0023 |
| $Co^{10+}$ | 27 | 0.03723 | 0.15540 | 0.17336 | 0.42201 | 0.48843 | 306.4195 | 305 | -0.0047 |
| $Ni^{11+}$ | 28 | 0.03589 | 0.14961 | 0.16601 | 0.40158 | 0.46026 | 354.7360 | 352 | -0.0078 |
| $Cu^{12+}$ | 29 | 0.03465 | 0.14424 | 0.15926 | 0.38305 | 0.43519 | 406.4345 | 401 | -0.0136 |
| $Zn^{13+}$ | 30 | 0.03349 | 0.13925 | 0.15304 | 0.36617 | 0.41274 | 461.5074 | 454 | -0.0165 |

[a] Radius of the paired 1s inner electrons of seventeen-electron atoms from Eq. (10.51).

[b] Radius of the paired 2s inner electrons of seventeen-electron atoms from Eq. (10.62).

[c] Radius of the three sets of paired 2p inner electrons of seventeen-electron atoms from Eq. (10.212).

[d] Radius of the paired 3s inner electrons of seventeen-electron atoms from Eq. (10.255).

[e] Radius of the two sets of paired and an unpaired 3p outer electron of seventeen-electron atoms from Eq. (10.376) for $Z > 17$ and Eq. (10.363) for *Cl*.

[f] Calculated ionization energies of seventeen-electron atoms given by the electric energy (Eq. (10.377)).

[g] From theoretical calculations, interpolation of isoelectronic and spectral series, and experimental data [2-3].

[h] (Experimental-theoretical)/experimental.

The agreement between the experimental and calculated values of Table 10.16 is well within the experimental capability of the spectroscopic determinations including the values at large Z which relies on X-ray spectroscopy. In this case, the experimental capability is about two to four significant figures which is consistent with the last column. Ionization energies are difficult to determine since the cut-off of the Rydberg series of lines at the ionization energy is often not observed. Thus, the chlorine atom isoelectronic series given in Table 10.16 [2-3] relies on theoretical calculations and interpolation of the Cl isoelectronic and Rydberg series as well as direct experimental data to extend the precision beyond the capability of X-ray spectroscopy. But, no assurances can be given that these techniques are correct, and they may not improve the results. The error given in the last column is very reasonable given the quality of the data.

## EIGHTEEN-ELECTRON ATOMS

Eighteen-electron atoms can be solved exactly using the results of the solutions of one, two, three, four, five, six, seven, eight, nine, ten, eleven, twelve, thirteen, fourteen, fifteen, sixteen, and seventeen-electron atoms.

## RADIUS AND IONIZATION ENERGY OF THE OUTER ELECTRON OF THE ARGON ATOM

For each seventeen-electron atom having a central charge of $Z$ times that of the proton, there are two indistinguishable spin-paired electrons in an atomic orbital with radii $r_1$ and $r_2$ both given by Eq. (7.35) (Eq. (10.51)), two indistinguishable spin-paired electrons in an atomic orbital with radii $r_3$ and $r_4$ both given by Eq. (10.62), three sets of paired electrons in an atomic orbital at $r_{10}$ given by Eq. (10.212), two indistinguishable spin-paired electrons in an atomic orbital with radii $r_{11}$ and $r_{12}$ both given by Eq. (10.255), and two sets of paired and an unpaired electron in an atomic orbital with radius $r_{17}$ given by Eq. (10.376). For $Z \geq 18$, the next electron which binds to form the corresponding eighteen-electron atom is attracted by the central Coulomb field and is repelled by diamagnetic forces due to the 3 sets of spin-paired inner 2p electrons and two spin-paired inner 3s electrons. A paramagnetic spin-pairing force to form a filled s orbital is also possible, but the force due to the spin-pairing of the electrons (Eq. (7.24) with the radius $r_{18}$) reduces the energy of the atom less than that due to the alternative forces on three sets of paired 3p electrons in an atomic orbital at the same radius $r_{18}$. The resulting electron configuration is $1s^2 2s^2 2p^6 3s^2 3p^6$, and the orbital arrangement is:

3p state

$$\underset{1}{\underline{\uparrow\ \downarrow}}\quad \underset{0}{\underline{\uparrow\ \downarrow}}\quad \underset{-1}{\underline{\uparrow\ \downarrow}} \tag{10.378}$$

corresponding to the ground state ${}^1S_0$.

The central Coulomb force acts on the outer electron to cause it to bind wherein this electric force on the outer-most electron due to the nucleus and the inner seventeen electrons is given by Eq. (10.70) with the appropriate charge and radius:

$$\mathbf{F}_{ele} = \frac{(Z-17)e^2}{4\pi\varepsilon_0 r_{18}^2}\mathbf{i}_\mathbf{r} \tag{10.379}$$

for $r > r_{17}$.

As in the case on the neon atom, the energy of the argon atom is minimized and the angular momentum is conserved with the pairing of electron eighteen to fill the 3 $p_y$ orbital when the orbital angular momenta of each set of the 3 $p_x$, $p_y$, and $p_z$ spin-paired electrons adds negatively to cancel. Then, the diamagnetic force (Eq. (10.258)), $\mathbf{F}_{diamagnetic}$, is given by the induced orbital angular momentum of the 3s orbital alone which conserves angular momentum.

$$\mathbf{F}_{diamagnetic} = -\left(\frac{1}{3}\right)\frac{\hbar^2}{4m_e r_{18}^2 r_{12}}\sqrt{s(s+1)}\mathbf{i}_\mathbf{r} \tag{10.380}$$

From Eq. (10.260), $\mathbf{F}_{mag\ 2}$ is:

$$\mathbf{F}_{mag\ 2} = (1+1+1+1)\frac{1}{Z}\frac{\hbar^2}{m_e r_{18}^2 r_{12}}\sqrt{s(s+1)}\mathbf{i}_\mathbf{r} = \frac{1}{Z}\frac{4\hbar^2}{m_e r_{18}^2 r_{12}}\sqrt{s(s+1)}\mathbf{i}_\mathbf{r} \tag{10.381}$$

corresponding to the spin-angular-momentum contribution alone from each of the 3 $p_x$, $p_y$, and $p_z$ orbitals and the spin angular momentum of the 3s orbital.

The outward centrifugal force on electron 18 is balanced by the electric force and the magnetic forces (on electron 18). The radius of the outer electron is calculated by equating the outward centrifugal force to the sum of the electric (Eq. (10.379)), diamagnetic (Eq. (10.380)), and paramagnetic (Eq. (10.381)) forces as follows:

$$\frac{m_e v_{18}^2}{r_{18}} = \frac{(Z-17)e^2}{4\pi\varepsilon_0 r_{18}^2} - \frac{\hbar^2}{12m_e r_{18}^2 r_{12}}\sqrt{s(s+1)} + \frac{4\hbar^2}{Zm_e r_{18}^2 r_{12}}\sqrt{s(s+1)} \tag{10.382}$$

Substitution of $v_{18} = \dfrac{\hbar}{m_e r_{18}}$ (Eq. (1.35)) and $s = \dfrac{1}{2}$ into Eq. (10.382) gives:

$$\frac{\hbar^2}{m_e r_{18}^3} = \frac{(Z-17)e^2}{4\pi\varepsilon_0 r_{18}^2} - \frac{\hbar^2}{12m_e r_{18}^2 r_{12}}\sqrt{\frac{3}{4}} + \frac{4\hbar^2}{Zm_e r_{18}^2 r_{12}}\sqrt{\frac{3}{4}} \tag{10.383}$$

$$r_{18} = \frac{\dfrac{\hbar^2}{m_e}}{\dfrac{(Z-17)e^2}{4\pi\varepsilon_0} - \dfrac{\hbar^2}{12m_e r_{12}}\sqrt{\dfrac{3}{4}} + \dfrac{4\hbar^2}{Zm_e r_{12}}\sqrt{\dfrac{3}{4}}} \tag{10.384}$$

$$r_{18} = \frac{a_0}{(Z-17) - \left(\dfrac{1}{12} - \dfrac{4}{Z}\right)\dfrac{\sqrt{\frac{3}{4}}}{r_{12}}},\ r_{12}\ in\ units\ of\ a_0 \tag{10.385}$$

Substitution of $\dfrac{r_{12}}{a_0} = 0.78276$ (Eq. (10.255) with $Z = 18$) into Eq. (10.385) gives:

$$r_{18} = 0.86680 a_0 \tag{10.386}$$

The ionization energy of the argon atom is given by the electric energy, $E(electric)$, (Eq. (10.102) with the radius, $r_{18}$, given by Eq. (10.386)).

$$E(ionization;\ Ar) = -Electric\ Energy = \frac{(Z-17)e^2}{8\pi\varepsilon_0 r_{18}} = 15.69651\ eV \tag{10.387}$$

where $r_{18} = 0.86680 a_0$ (Eq. (10.386)) and $Z = 18$. The experimental ionization energy of the argon atom is 15.75962 $eV$ [3].

## THE IONIZATION ENERGIES OF EIGHTEEN-ELECTRON ATOMS WITH A NUCLEAR CHARGE Z>18

Eighteen-electron atoms having $Z>18$ possess an external electric field given by Eq. (10.92). In this case, an energy minimum is achieved with conservation of momentum when the orbital angular momentum is such that $\mathbf{F}_{diamagnetic}$ is minimized while $\mathbf{F}_{mag\ 2}$ is maximized. With a filled 3p shell, the diamagnetic force due to the orbital angular momenta of the 3p electrons cancels that of the 2p electrons. Thus, the diamagnetic force (Eq. (10.258)), $\mathbf{F}_{diamagnetic}$, is zero:

$$\mathbf{F}_{diamagnetic}=0 \tag{10.388}$$

From Eqs. (10.205) and (10.261), $\mathbf{F}_{mag\ 2}$ corresponding to the spin and orbital angular momenta of the paired 2 $p_x$, $p_y$, and $p_z$ electrons is:

$$\mathbf{F}_{mag\ 2}=\left(4+4+4\right)\frac{1}{Z}\frac{\hbar^2}{m_e r_{18}^2 r_{12}}\sqrt{s(s+1)}\mathbf{i}_{\mathbf{r}}=\frac{1}{Z}\frac{12\hbar^2}{m_e r_{18}^2 r_{12}}\sqrt{s(s+1)}\mathbf{i}_{\mathbf{r}} \tag{10.389}$$

the contribution from the 3p level (Eq. (10.264)) is:

$$\mathbf{F}_{mag\ 2}=\left(8+8+8\right)\frac{1}{Z}\frac{\hbar^2}{m_e r_{18}^2 r_{12}}\sqrt{s(s+1)}\mathbf{i}_{\mathbf{r}}=\frac{1}{Z}\frac{24\hbar^2}{m_e r_{18}^2 r_{12}}\sqrt{s(s+1)}\mathbf{i}_{\mathbf{r}} \tag{10.390}$$

and the contribution due to the spin and induced orbital angular momentum of the 3s orbital that achieves conservation of angular momentum given by Eq. (10.262) is:

$$\mathbf{F}_{mag\ 2}=\frac{1}{Z}\frac{4\hbar^2}{m_e r_{18}^2 r_{12}}\sqrt{s(s+1)}\mathbf{i}_{\mathbf{r}} \tag{10.391}$$

Thus, the total of $\mathbf{F}_{mag\ 2}$ is

$$\mathbf{F}_{mag\ 2}=\frac{1}{Z}\frac{40\hbar^2}{m_e r_{18}^2 r_{12}}\sqrt{s(s+1)}\mathbf{i}_{\mathbf{r}} \tag{10.392}$$

The diamagnetic force, $\mathbf{F}_{diamagnetic\ 2}$, due to the binding of the 3p-orbital electron having an electric field outside of its radius is given by Eq. (10.268).

$$\mathbf{F}_{diamagnetic\ 2}=-\left[\frac{Z-18}{Z-17}\right]\left(1-\frac{\sqrt{2}}{2}+\frac{1}{2}\right)\frac{r_{12}\hbar^2}{m_e r_{18}^4}10\sqrt{s(s+1)}\mathbf{i}_{\mathbf{r}} \tag{10.393}$$

In the case that $Z>18$, the radius of the outer electron is calculated by equating the outward centrifugal force to the sum of the electric (Eq. (10.379)), diamagnetic (Eqs. (10.388) and (10.393)), and paramagnetic (Eq. (10.392)) forces as follows:

$$\frac{m_e v_{18}^2}{r_{18}}=\frac{(Z-17)e^2}{4\pi\varepsilon_0 r_{18}^2}+\frac{40\hbar^2}{Zm_e r_{18}^2 r_{12}}\sqrt{s(s+1)}-\left[\frac{Z-18}{Z-17}\right]\left(1-\frac{\sqrt{2}}{2}+\frac{1}{2}\right)\frac{r_{12}\hbar^2}{m_e r_{18}^4}10\sqrt{s(s+1)} \tag{10.394}$$

Substitution of $v_{18}=\dfrac{\hbar}{m_e r_{18}}$ (Eq. (1.35)) and $s=\dfrac{1}{2}$ into Eq. (10.394) gives:

$$\frac{\hbar^2}{m_e r_{18}^3}=\frac{(Z-17)e^2}{4\pi\varepsilon_0 r_{18}^2}+\frac{40\hbar^2}{Zm_e r_{18}^2 r_{12}}\sqrt{\frac{3}{4}}-\left[\frac{Z-18}{Z-17}\right]\left(1-\frac{\sqrt{2}}{2}+\frac{1}{2}\right)\frac{r_{12}\hbar^2}{m_e r_{18}^4}10\sqrt{\frac{3}{4}} \tag{10.395}$$

The quadratic equation corresponding to Eq. (10.395) is:

$$\left(\frac{(Z-17)e^2}{4\pi\varepsilon_0}+\frac{40\hbar^2}{Zm_e r_{12}}\sqrt{\frac{3}{4}}\right)r_{18}^2-\frac{\hbar^2}{m_e}r_{18}-\left[\frac{Z-18}{Z-17}\right]\left(1-\frac{\sqrt{2}}{2}+\frac{1}{2}\right)\frac{r_{12}\hbar^2}{m_e}10\sqrt{\frac{3}{4}}=0 \tag{10.396}$$

$$r_{18}^2-\frac{\dfrac{\hbar^2}{m_e}}{\left(\dfrac{(Z-17)e^2}{4\pi\varepsilon_0}+\dfrac{40\hbar^2}{Zm_e r_{12}}\sqrt{\dfrac{3}{4}}\right)}r_{18}-\frac{\dfrac{\hbar^2}{m_e}\left[\dfrac{Z-18}{Z-17}\right]\left(1-\dfrac{\sqrt{2}}{2}+\dfrac{1}{2}\right)r_{12}10\sqrt{\dfrac{3}{4}}}{\left(\dfrac{(Z-17)e^2}{4\pi\varepsilon_0}+\dfrac{40\hbar^2}{Zm_e r_{12}}\sqrt{\dfrac{3}{4}}\right)}=0 \tag{10.397}$$

The solution of Eq. (10.397) using the quadratic formula is:

$$r_{18}=\frac{\dfrac{\dfrac{\hbar^2}{m_e}}{\left(\dfrac{(Z-17)e^2}{4\pi\varepsilon_0}+\dfrac{40\hbar^2}{Zm_e r_{12}}\sqrt{\dfrac{3}{4}}\right)}\pm\sqrt{\left(\dfrac{\dfrac{\hbar^2}{m_e}}{\left(\dfrac{(Z-17)e^2}{4\pi\varepsilon_0}+\dfrac{40\hbar^2}{Zm_e r_{12}}\sqrt{\dfrac{3}{4}}\right)}\right)^2+4\dfrac{\dfrac{\hbar^2}{m_e}\left[\dfrac{Z-18}{Z-17}\right]\left(1-\dfrac{\sqrt{2}}{2}+\dfrac{1}{2}\right)r_{12}10\sqrt{\dfrac{3}{4}}}{\left(\dfrac{(Z-17)e^2}{4\pi\varepsilon_0}+\dfrac{40\hbar^2}{Zm_e r_{12}}\sqrt{\dfrac{3}{4}}\right)}}}{2} \tag{10.398}$$

$$r_{18}=\frac{\dfrac{a_0}{\left((Z-17)+\dfrac{20\sqrt{3}}{Zr_{12}}\right)}\pm a_0\sqrt{\left(\dfrac{1}{\left((Z-17)+\dfrac{20\sqrt{3}}{Zr_{12}}\right)}\right)^2+\dfrac{20\sqrt{3}\left(\left[\dfrac{Z-18}{Z-17}\right]\left(1-\dfrac{\sqrt{2}}{2}+\dfrac{1}{2}\right)r_{12}\right)}{\left((Z-17)+\dfrac{20\sqrt{3}}{Zr_{12}}\right)}}}{2},\ r_{12}\ \textit{in units of}\ a_0 \tag{10.399}$$

where $r_{12}$ is given by Eq. (10.255). The positive root of Eq. (10.399) must be taken in order that $r_{18}>0$. The final radius of electron 18, $r_{18}$, is given by Eq. (10.399); this is also the final radius of electrons 13, 14, 15, 16, and 17. The radii of several eighteen-electron atoms are given in Table 10.17.

The ionization energies for the eighteen-electron atoms with $Z>18$ are given by the electric energy, $E(electric)$, (Eq. (10.102) with the radii $r_{18}$, given by Eq. (10.399)).

$$E(Ionization)=-Electric\ Energy=\frac{(Z-17)e^2}{8\pi\varepsilon_0 r_{18}} \tag{10.400}$$

Since the relativistic corrections were small, the nonrelativistic ionization energies for experimentally measured eighteen-electron atoms are given in Table 10.17.

**Table 10.17.** Ionization energies for some eighteen-electron atoms.

| 18 e Atom | Z | $r_1$ $(a_o)$ [a] | $r_3$ $(a_o)$ [b] | $r_{10}$ $(a_o)$ [c] | $r_{12}$ $(a_o)$ [d] | $r_{18}$ $(a_o)$ [e] | Theoretical Ionization Energies [f] (eV) | Experimental Ionization Energies [g] (eV) | Relative Error [h] |
|---|---|---|---|---|---|---|---|---|---|
| $Ar$ | 18 | 0.05599 | 0.23839 | 0.28878 | 0.78276 | 0.86680 | 15.69651 | 15.75962 | 0.0040 |
| $K^+$ | 19 | 0.05302 | 0.22503 | 0.26884 | 0.71450 | 0.85215 | 31.9330 | 31.63 | -0.0096 |
| $Ca^{2+}$ | 20 | 0.05035 | 0.21308 | 0.25149 | 0.65725 | 0.82478 | 49.4886 | 50.9131 | 0.0280 |
| $Sc^{3+}$ | 21 | 0.04794 | 0.20235 | 0.23625 | 0.60857 | 0.76196 | 71.4251 | 73.4894 | 0.0281 |
| $Ti^{4+}$ | 22 | 0.04574 | 0.19264 | 0.22276 | 0.56666 | 0.70013 | 97.1660 | 99.30 | 0.0215 |
| $V^{5+}$ | 23 | 0.04374 | 0.18383 | 0.21074 | 0.53022 | 0.64511 | 126.5449 | 128.13 | 0.0124 |
| $Cr^{6+}$ | 24 | 0.04191 | 0.17579 | 0.19995 | 0.49822 | 0.59718 | 159.4836 | 160.18 | 0.0043 |
| $Mn^{7+}$ | 25 | 0.04022 | 0.16842 | 0.19022 | 0.46990 | 0.55552 | 195.9359 | 194.5 | -0.0074 |
| $Fe^{8+}$ | 26 | 0.03867 | 0.16165 | 0.18140 | 0.44466 | 0.51915 | 235.8711 | 233.6 | -0.0097 |
| $Co^{9+}$ | 27 | 0.03723 | 0.15540 | 0.17336 | 0.42201 | 0.48720 | 279.2670 | 275.4 | -0.0140 |
| $Ni^{10+}$ | 28 | 0.03589 | 0.14961 | 0.16601 | 0.40158 | 0.45894 | 326.1070 | 321.0 | -0.0159 |
| $Cu^{11+}$ | 29 | 0.03465 | 0.14424 | 0.15926 | 0.38305 | 0.43379 | 376.3783 | 369 | -0.0200 |
| $Zn^{12+}$ | 30 | 0.03349 | 0.13925 | 0.15304 | 0.36617 | 0.41127 | 430.0704 | 419.7 | -0.0247 |

[a] Radius of the paired 1s inner electrons of eighteen-electron atoms from Eq. (10.51).

[b] Radius of the paired 2s inner electrons of eighteen-electron atoms from Eq. (10.62).

[c] Radius of the three sets of paired 2p inner electrons of eighteen-electron atoms from Eq. (10.212).

[d] Radius of the paired 3s inner electrons of eighteen-electron atoms from Eq. (10.255).

[e] Radius of the three sets of paired 3p outer electrons of eighteen-electron atoms from Eq. (10.399) for $Z > 18$ and Eq. (10.386) for $Ar$.

[f] Calculated ionization energies of eighteen-electron atoms given by the electric energy (Eq. (10.400)).

[g] From theoretical calculations, interpolation of isoelectronic and spectral series, and experimental data [2-3].

[h] (Experimental-theoretical)/experimental.

The agreement between the experimental and calculated values of Table 10.17 is well within the experimental capability of the spectroscopic determinations including the values at large Z which relies on X-ray spectroscopy. In this case, the experimental capability is about two to four significant figures which is consistent with the last column. Ionization energies are difficult to determine since the cut-off of the Rydberg series of lines at the ionization energy is often not observed. Thus, the argon atom isoelectronic series given in Table 10.17 [2-3] relies on theoretical calculations and interpolation of the Ar isoelectronic and Rydberg series as well as direct experimental data to extend the precision beyond the capability of X-ray spectroscopy. But, no assurances can be given that these techniques are correct, and they may not improve the results. The error given in the last column is very reasonable given the quality of the data.

## GENERAL EQUATION FOR THE IONIZATION ENERGIES OF THIRTEEN THROUGH EIGHTEEN-ELECTRON ATOMS

Using the forces given by Eqs. (10.257-10.264), (10.268), and the radii $r_{12}$ given by Eq. (10.255), the radii of the 3p electrons of all thirteen through eighteen-electron atoms may be solved exactly. The electric energy given by Eq. (10.102) gives the corresponding exact ionization energies. A summary of the parameters of the equations that determine the exact radii and ionization energies of all thirteen through eighteen-electron atoms is given in Table 10.18.

$\mathbf{F}_{ele}$ and $\mathbf{F}_{diamagnetic\ 2}$ given by Eqs. (10.257) and (10.268), respectively, are of the same form for all atoms with the appropriate nuclear charges and atomic radii. $\mathbf{F}_{diamagnetic}$ given by Eq. (10.258) and $\mathbf{F}_{mag\ 2}$ given by Eqs. (10.259-10.264) are of the same form with the appropriate factors that depend on the electron configuration wherein the electron configuration must be a minimum of energy.

For each n-electron atom having a central charge of $Z$ times that of the proton and an electron configuration $1s^2 2s^2 2p^6 3s^2 3p^{n-12}$, there are two indistinguishable spin-paired electrons in an atomic orbital with radii $r_1$ and $r_2$ both given by Eq. (7.35) and (10.51).

$$r_1 = r_2 = a_0 \left[ \frac{1}{Z-1} - \frac{\sqrt{\frac{3}{4}}}{Z(Z-1)} \right] \tag{10.401}$$

two indistinguishable spin-paired electrons in an atomic orbital with radii $r_3$ and $r_4$ both given by Eq. (10.62):

$$r_4 = r_3 = \frac{\dfrac{a_0\left(1-\dfrac{\sqrt{\frac{3}{4}}}{Z}\right)}{\left((Z-3)-\left(\frac{1}{4}-\frac{1}{Z}\right)\frac{\sqrt{\frac{3}{4}}}{r_1}\right)} \pm a_0\sqrt{\dfrac{\left(1-\dfrac{\sqrt{\frac{3}{4}}}{Z}\right)^2}{\left((Z-3)-\left(\frac{1}{4}-\frac{1}{Z}\right)\frac{\sqrt{\frac{3}{4}}}{r_1}\right)^2}+4\dfrac{\left[\frac{Z-3}{Z-2}\right]r_1 10\sqrt{\frac{3}{4}}}{\left((Z-3)-\left(\frac{1}{4}-\frac{1}{Z}\right)\frac{\sqrt{\frac{3}{4}}}{r_1}\right)}}}{2} \qquad (10.402)$$

$r_1$ *in units of* $a_0$

where $r_1$ is given by Eqs. (10.51) and (10.401), three sets of paired indistinguishable electrons in an atomic orbital with radius $r_{10}$ given by Eq. (10.212).

$$r_{10} = \frac{\dfrac{a_0}{\left((Z-9)-\left(\frac{5}{24}-\frac{6}{Z}\right)\frac{\sqrt{3}}{r_3}\right)} \pm a_0\sqrt{\dfrac{\left(\frac{1}{\left((Z-9)-\left(\frac{5}{24}-\frac{6}{Z}\right)\frac{\sqrt{3}}{r_3}\right)}\right)^2}{+\dfrac{20\sqrt{3}\left(\left[\frac{Z-10}{Z-9}\right]\left(1-\frac{\sqrt{2}}{2}\right)r_3\right)}{\left((Z-9)-\left(\frac{5}{24}-\frac{6}{Z}\right)\frac{\sqrt{3}}{r_3}\right)}}}{2}, \; r_3 \text{ in units of } a_0 \qquad (10.403)$$

where $r_3$ is given by Eqs. (10.62) and (10.402), two indistinguishable spin-paired electrons in an atomic orbital with radius $r_{12}$ given by Eq. (10.255).

$$r_{12} = \frac{\dfrac{a_0}{\left((Z-11)-\left(\frac{1}{8}-\frac{3}{Z}\right)\frac{\sqrt{3}}{r_{10}}\right)} \pm a_0\sqrt{\dfrac{\left(\frac{1}{\left((Z-11)-\left(\frac{1}{8}-\frac{3}{Z}\right)\frac{\sqrt{3}}{r_{10}}\right)}\right)^2}{+\dfrac{20\sqrt{3}\left(\left[\frac{Z-12}{Z-11}\right]\left(1+\frac{\sqrt{2}}{2}\right)r_{10}\right)}{\left((Z-11)-\left(\frac{1}{8}-\frac{3}{Z}\right)\frac{\sqrt{3}}{r_{10}}\right)}}}{2}, \; r_{10} \text{ in units of } a_0 \qquad (10.404)$$

where $r_{10}$ is given by Eq. (10.212), and $n-12$ electrons in a 3p atomic orbital with radius $r_n$ given by:

$$r_n = \frac{\dfrac{a_0}{\left((Z-(n-1))-\left(\frac{A}{8}-\frac{B}{2Z}\right)\frac{\sqrt{3}}{r_{12}}\right)} \pm a_0\sqrt{\dfrac{\left(\frac{1}{\left((Z-(n-1))-\left(\frac{A}{8}-\frac{B}{2Z}\right)\frac{\sqrt{3}}{r_{12}}\right)}\right)^2}{+\dfrac{20\sqrt{3}\left(\left[\frac{Z-n}{Z-(n-1)}\right]\left(1-\frac{\sqrt{2}}{2}+\frac{1}{2}\right)r_{12}\right)}{\left((Z-(n-1))-\left(\frac{A}{8}-\frac{B}{2Z}\right)\frac{\sqrt{3}}{r_{12}}\right)}}}{2}, \; r_{12} \text{ in units of } a_0 \qquad (10.405)$$

where $r_{12}$ is given by Eqs. (10.255) and (10.404), the parameter $A$ given in Table 10.18 corresponds to the diamagnetic force, $\mathbf{F}_{diamagnetic}$, (Eq. (10.258)), and the parameter $B$ given in Table 10.18 corresponds to the paramagnetic force, $\mathbf{F}_{mag\,2}$ (Eqs. (10.260-10.264)). The positive root of Eq. (10.405) must be taken in order that $r_n > 0$. The radii of several n-electron 3p atoms are given in Tables 10.10-10.17.

The ionization energy for the aluminum atom is given by Eq. (10.227). The ionization energies for the n-electron 3p atoms are given by the negative of the electric energy, $E(electric)$, (Eq. (10.102) with the radii, $r_n$, given by Eq. (10.405)):

$$E(Ionization) = -Electric\ Energy = \frac{(Z-(n-1))e^2}{8\pi\varepsilon_0 r_n} \tag{10.406}$$

Since the relativistic corrections were small, the nonrelativistic ionization energies for experimentally measured n-electron 3p atoms are given by Eqs. (10.405) and (10.406) in Tables 10.10-10.17.

**Table 10.18.** Summary of the parameters of thirteen through eighteen-electron atoms.

| Atom Type | Electron Configuration | Ground State Term [a] | Orbital Arrangement of 3p Electrons (3p state) | Diamagnetic Force Factor $A$ [b] | Paramagnetic Force Factor $B$ [c] |
|---|---|---|---|---|---|
| Neutral 13 e Atom *Al* | $1s^2 2s^2 2p^6 3s^2 3p^1$ | $^2P^0_{1/2}$ | $\underline{\uparrow}$ $\underline{\quad}$ $\underline{\quad}$ <br> 1 0 -1 | $\frac{11}{3}$ | 0 |
| Neutral 14 e Atom *Si* | $1s^2 2s^2 2p^6 3s^2 3p^2$ | $^3P_0$ | $\underline{\uparrow}$ $\underline{\uparrow}$ $\underline{\quad}$ <br> 1 0 -1 | $\frac{7}{3}$ | 0 |
| Neutral 15 e Atom *P* | $1s^2 2s^2 2p^6 3s^2 3p^3$ | $^4S^0_{3/2}$ | $\underline{\uparrow}$ $\underline{\uparrow}$ $\underline{\uparrow}$ <br> 1 0 -1 | $\frac{5}{3}$ | 2 |
| Neutral 16 e Atom *S* | $1s^2 2s^2 2p^6 3s^2 3p^4$ | $^3P_2$ | $\underline{\uparrow\downarrow}$ $\underline{\uparrow}$ $\underline{\uparrow}$ <br> 1 0 -1 | $\frac{4}{3}$ | 1 |
| Neutral 17 e Atom *Cl* | $1s^2 2s^2 2p^6 3s^2 3p^5$ | $^2P^0_{3/2}$ | $\underline{\uparrow\downarrow}$ $\underline{\uparrow\downarrow}$ $\underline{\uparrow}$ <br> 1 0 -1 | $\frac{2}{3}$ | 2 |
| Neutral 18 e Atom *Ar* | $1s^2 2s^2 2p^6 3s^2 3p^6$ | $^1S_0$ | $\underline{\uparrow\downarrow}$ $\underline{\uparrow\downarrow}$ $\underline{\uparrow\downarrow}$ <br> 1 0 -1 | $\frac{1}{3}$ | 4 |
| 13 e Ion | $1s^2 2s^2 2p^6 3s^2 3p^1$ | $^2P^0_{1/2}$ | $\underline{\uparrow}$ $\underline{\quad}$ $\underline{\quad}$ <br> 1 0 -1 | $\frac{5}{3}$ | 12 |
| 14 e Ion | $1s^2 2s^2 2p^6 3s^2 3p^2$ | $^3P_0$ | $\underline{\uparrow}$ $\underline{\uparrow}$ $\underline{\quad}$ <br> 1 0 -1 | $\frac{1}{3}$ | 16 |
| 15 e Ion | $1s^2 2s^2 2p^6 3s^2 3p^3$ | $^4S^0_{3/2}$ | $\underline{\uparrow}$ $\underline{\uparrow}$ $\underline{\uparrow}$ <br> 1 0 -1 | 0 | 24 |
| 16 e Ion | $1s^2 2s^2 2p^6 3s^2 3p^4$ | $^3P_2$ | $\underline{\uparrow\downarrow}$ $\underline{\uparrow}$ $\underline{\uparrow}$ <br> 1 0 -1 | $\frac{1}{3}$ | 24 |
| 17 e Ion | $1s^2 2s^2 2p^6 3s^2 3p^5$ | $^2P^0_{3/2}$ | $\underline{\uparrow\downarrow}$ $\underline{\uparrow\downarrow}$ $\underline{\uparrow}$ <br> 1 0 -1 | $\frac{2}{3}$ | 32 |
| 18 e Ion | $1s^2 2s^2 2p^6 3s^2 3p^6$ | $^1S_0$ | $\underline{\uparrow\downarrow}$ $\underline{\uparrow\downarrow}$ $\underline{\uparrow\downarrow}$ <br> 1 0 -1 | 0 | 40 |

[a] The theoretical ground state terms match those given by NIST [8].
[b] Eq. (10.258).
[c] Eqs. (10.260-10.264).

## NINETEEN-ELECTRON ATOMS

Nineteen-electron atoms can be solved exactly using the results of the solutions of one, two, three, four, five, six, seven, eight, nine, ten, eleven, twelve, thirteen, fourteen, fifteen, sixteen, seventeen, and eighteen-electron atoms.

## RADIUS AND IONIZATION ENERGY OF THE OUTER ELECTRON OF THE POTASSIUM ATOM

For each eighteen-electron atom having a central charge of $Z$ times that of the proton, there are two indistinguishable spin-paired electrons in an atomic orbital with radii $r_1$ and $r_2$ both given by Eq. (7.35) (Eq. (10.51)), two indistinguishable spin-paired electrons in an atomic orbital with radii $r_3$ and $r_4$ both given by Eq. (10.62), three sets of paired electrons in an atomic orbital at $r_{10}$ given by Eq. (10.212), two indistinguishable spin-paired electrons in an atomic orbital with radii $r_{11}$ and $r_{12}$ both given by Eq. (10.255), and three sets of paired electrons in an atomic orbital with radius $r_{18}$ given by Eq. (10.399). For $Z \geq 19$, the next electron which binds to form the corresponding nineteen-electron atom is attracted by the central Coulomb field and is repelled by diamagnetic forces due to the 3 sets of spin-paired inner 3p electrons such that it forms an unpaired atomic orbital at radius $r_{19}$.

The central Coulomb force acts on the outer electron to cause it to bind wherein this electric force on the outer-most electron due to the nucleus and the inner eighteen electrons is given by Eq. (10.70) with the appropriate charge and radius:

$$\mathbf{F}_{ele} = \frac{(Z-18)e^2}{4\pi\varepsilon_0 r_{19}^2}\mathbf{i}_\mathbf{r} \tag{10.407}$$

for $r > r_{18}$.

The spherically symmetrical closed 3p shell of nineteen-electron atoms produces a diamagnetic force, $\mathbf{F}_{diamagnetic}$, that is equivalent to that of a closed s shell given by Eq. (10.11) with the appropriate radii except that the force is doubled due to the interaction of the 4s and 3p electrons as given by Eq. (10.96). The inner electrons remain at their initial radii, but cause a diamagnetic force according to Lenz's law that is:

$$\mathbf{F}_{diamagnetic} = -\frac{2\hbar^2}{4m_e r_{19}^2 r_{18}}\sqrt{s(s+1)}\mathbf{i}_\mathbf{r} \tag{10.408}$$

In addition to the spin-spin interaction between electron pairs, the three sets of 3p electrons are orbitally paired. As in the case of the sodium atom with the corresponding radii, the single 4s orbital of the potassium atom produces a magnetic field at the position of the three sets of spin-paired 3p electrons. In order for the electrons to remain spin and orbitally paired, a corresponding diamagnetic force, $\mathbf{F}_{diamagnetic\ 3}$, on electron nineteen from the three sets of spin-paired electrons that follows from the deviation given in the Eleven-Electron Atom section (Eq. (10.221)) is:

$$\mathbf{F}_{diamagnetic\ 3} = -\frac{1}{Z}\frac{12\hbar^2}{m_e r_{19}^3}\sqrt{s(s+1)}\mathbf{i}_\mathbf{r} \tag{10.409}$$

corresponding to the 3 $p_x$, $p_y$, and $p_z$ electrons.

The outward centrifugal force on electron 19 is balanced by the electric force and the magnetic forces (on electron 19). The radius of the outer electron is calculated by equating the outward centrifugal force to the sum of the electric (Eq. (10.407)) and diamagnetic (Eqs. (10.408) and (10.409)) forces as follows:

$$\frac{m_e v_{19}^2}{r_{19}} = \frac{(Z-18)e^2}{4\pi\varepsilon_0 r_{19}^2} - \frac{2\hbar^2}{4m_e r_{19}^2 r_{18}}\sqrt{s(s+1)} - \frac{12\hbar^2}{Zm_e r_{19}^3}\sqrt{s(s+1)} \tag{10.410}$$

Substitution of $v_{19} = \frac{\hbar}{m_e r_{19}}$ (Eq. (1.35)) and $s = \frac{1}{2}$ into Eq. (10.410) gives:

$$\frac{\hbar^2}{m_e r_{19}^3} = \frac{(Z-18)e^2}{4\pi\varepsilon_0 r_{19}^2} - \frac{2\hbar^2}{4m_e r_{19}^2 r_{18}}\sqrt{\frac{3}{4}} - \frac{12\hbar^2}{Zm_e r_{19}^3}\sqrt{\frac{3}{4}} \tag{10.411}$$

$$r_{19} = \frac{\frac{\hbar^2}{m_e}\left(1+\frac{12}{Z}\sqrt{\frac{3}{4}}\right)}{\frac{(Z-18)e^2}{4\pi\varepsilon_0} - \frac{\hbar^2}{2m_e r_{18}}\sqrt{\frac{3}{4}}} \tag{10.412}$$

$$r_{19} = \frac{a_0\left(1+\frac{12}{Z}\sqrt{\frac{3}{4}}\right)}{(Z-18) - \frac{\sqrt{\frac{3}{4}}}{2r_{18}}},\ r_{18}\ \textit{in units of}\ a_0 \tag{10.413}$$

Substitution of $\frac{r_{18}}{a_0} = 0.85215$ (Eq. (10.399) with $Z = 19$) into Eq. (10.413) gives:

$$r_{19} = 3.14515 a_0 \tag{10.414}$$

The ionization energy of the potassium atom is given by the electric energy, $E(electric)$, (Eq. (10.102) with the radius, $r_{19}$, given by Eq. (10.414)).

$$E(ionization;\ K) = -Electric\ Energy = \frac{(Z-18)e^2}{8\pi\varepsilon_0 r_{19}} = 4.32596\ eV \tag{10.415}$$

where $r_{19} = 3.14515 a_0$ (Eq. (10.414)) and $Z = 19$. The experimental ionization energy of the potassium atom is $4.34066\ eV$ [3].

## THE IONIZATION ENERGIES OF NINETEEN-ELECTRON ATOMS WITH A NUCLEAR CHARGE Z>19

Nineteen-electron atoms having $Z > 19$ possess an external electric field given by Eq. (10.92). Since there is a source of dissipative power, $\mathbf{J} \bullet \mathbf{E}$ of Eq. (10.27), the magnetic moments of the inner electrons may change due to the outer electron such that the energy of the nineteen-electron atom is lowered. The spherically symmetrical closed 3p shell of nineteen-electron atoms produces a diamagnetic force, $\mathbf{F}_{diamagnetic}$, that is equivalent to that of a closed s shell given by Eq. (10.11) with the appropriate radii except that the force is tripled due to the interaction of the 2p, 3s, and 3p electrons as discussed in the 3P-Orbital Electrons Based on an Energy Minimum section. The inner electrons remain at their initial radii, but cause a diamagnetic force according to Lenz's law that is:

$$\mathbf{F}_{diamagnetic} = -\frac{3\hbar^2}{4 m_e r_{19}^2 r_{18}} \sqrt{s(s+1)}\,\mathbf{i}_{\mathbf{r}} \tag{10.416}$$

In addition to the spin-spin interaction between electron pairs, the six sets of 2p and 3p electrons are orbitally paired. As in given in the Eleven-Electron Atom section, the single 4s orbital of each nineteen-electron atoms having $Z > 19$ produces a magnetic field at the position of the six sets of spin-paired 2p and 3p electrons. In order for the electrons to remain spin and orbitally paired, a corresponding diamagnetic force, $\mathbf{F}_{diamagnetic\ 3}$, on electron nineteen from the six sets of spin-paired electrons that follows from the deviation given in the Eleven-Electron Atom section (Eq. (10.221)) is:

$$\mathbf{F}_{diamagnetic\ 3} = -\frac{1}{Z}\frac{24\hbar^2}{m_e r_{19}^{\ 3}} \sqrt{s(s+1)}\,\mathbf{i}_{\mathbf{r}} \tag{10.417}$$

corresponding to the 2 and 3 $p_x$, $p_y$, and $p_z$ electrons.

As shown in the P-Orbital Electrons Based on an Energy Minimum section for $\mathbf{F}_{diamagnetic\ 2}$ given by Eq. (10.93), the corresponding diamagnetic force for 2p electrons due to a relativistic effect with an electric field for $r > r_n$ (Eq. (10.35)) is dependent on the amplitude of the orbital energy. Using the orbital energy with $\ell = 1$ (Eq. (10.90)), the energy $m_e \Delta v^2$ of Eq. (10.29) is reduced by the factor of $\left(1 - \frac{\sqrt{2}}{2}\right)$ due to the contribution of the charge-density wave of the inner electrons at $r_3$. In addition, it was shown in the 3P-Orbital Electrons Based on an Energy Minimum section that the two 3s electrons contribute an energy factor based on Eq. (1.55) since the filled 2p orbitals with the maintenance of symmetry according to Eq. (10.72) requires that the diamagnetic force is due to the electrons at $r_{10}$ acting on the electrons at $r_{12}$ which complies with the reactive force, $\mathbf{F}_{diamagnetic\ 2}$, given by Eq. (10.229). Thus, $\mathbf{F}_{diamagnetic\ 2}$ for the factor from 3p electrons with $Z > n$ is reduced by the factor of $\left(1 - \frac{\sqrt{2}}{2} + \frac{1}{2}\right)$. Similarly, the factor for 4s electrons due to the inner 2p, 3s, and 3p electrons is cumulative. Thus, $\mathbf{F}_{diamagnetic\ 2}$ for 4s electrons with $Z > n$ is:

$$\mathbf{F}_{diamagnetic\ 2} = -\left[\frac{Z-n}{Z-(n-1)}\right]\left(1 - \frac{\sqrt{2}}{2} + \frac{1}{2} - \frac{\sqrt{2}}{2} + \frac{1}{2}\right)\frac{r_{18}\hbar^2}{m_e r_n^4} 10\sqrt{s(s+1)}\,\mathbf{i}_{\mathbf{r}} \tag{10.418}$$

For $n = 19$, $\mathbf{F}_{diamagnetic\ 2}$ is

$$\mathbf{F}_{diamagnetic\ 2} = -\left[\frac{Z-19}{Z-18}\right]\left(1 - \frac{\sqrt{2}}{2} + \frac{1}{2} - \frac{\sqrt{2}}{2} + \frac{1}{2}\right)\frac{r_{18}\hbar^2}{m_e r_{19}^4} 10\sqrt{s(s+1)}\,\mathbf{i}_{\mathbf{r}} \tag{10.419}$$

In the case that $Z > 19$, the radius of the outer electron is calculated by equating the outward centrifugal force to the sum of the electric (Eq. (10.407)) and diamagnetic (Eqs. (10.416), (10.417), and (10.419)) forces as follows:

$$\frac{m_e v_{19}^2}{r_{19}} = \frac{(Z-18)e^2}{4\pi\varepsilon_0 r_{19}^2} - \frac{3\hbar^2}{4m_e r_{19}^2 r_{18}}\sqrt{s(s+1)} - \frac{24\hbar^2}{Zm_e r_{19}^3}\sqrt{s(s+1)}$$

$$-\left[\frac{Z-19}{Z-18}\right]\left(1-\frac{\sqrt{2}}{2}+\frac{1}{2}-\frac{\sqrt{2}}{2}+\frac{1}{2}\right)\frac{r_{18}\hbar^2}{m_e r_{19}^4}10\sqrt{s(s+1)} \tag{10.420}$$

Substitution of $v_{19} = \dfrac{\hbar}{m_e r_{19}}$ (Eq. (1.35)) and $s = \dfrac{1}{2}$ into Eq. (10.420) gives:

$$\frac{\hbar^2}{m_e r_{19}^3} = \frac{(Z-18)e^2}{4\pi\varepsilon_0 r_{19}^2} - \frac{3\hbar^2}{4m_e r_{19}^2 r_{18}}\sqrt{\frac{3}{4}} - \frac{24\hbar^2}{Zm_e r_{19}^3}\sqrt{\frac{3}{4}} - \left[\frac{Z-19}{Z-18}\right]\left(1-\frac{\sqrt{2}}{2}+\frac{1}{2}-\frac{\sqrt{2}}{2}+\frac{1}{2}\right)\frac{r_{18}\hbar^2}{m_e r_{19}^4}10\sqrt{\frac{3}{4}} \tag{10.421}$$

The quadratic equation corresponding to Eq. (10.421) is

$$\left(\frac{(Z-18)e^2}{4\pi\varepsilon_0} - \frac{3\hbar^2}{4m_e r_{18}}\sqrt{\frac{3}{4}}\right)r_{19}^2 - \frac{\hbar^2}{m_e}\left(1+\frac{24\sqrt{\frac{3}{4}}}{Z}\right)r_{19} - \left[\frac{Z-19}{Z-18}\right]\left(1-\frac{\sqrt{2}}{2}+\frac{1}{2}-\frac{\sqrt{2}}{2}+\frac{1}{2}\right)\frac{r_{18}\hbar^2}{m_e}10\sqrt{\frac{3}{4}} = 0 \tag{10.422}$$

$$r_{19}^2 - \frac{\dfrac{\hbar^2}{m_e}\left(1+\dfrac{24\sqrt{\frac{3}{4}}}{Z}\right)}{\left(\dfrac{(Z-18)e^2}{4\pi\varepsilon_0} - \dfrac{3\hbar^2}{4m_e r_{18}}\sqrt{\frac{3}{4}}\right)}r_{19} - \frac{\left[\dfrac{Z-19}{Z-18}\right]\left(1-\dfrac{\sqrt{2}}{2}+\dfrac{1}{2}-\dfrac{\sqrt{2}}{2}+\dfrac{1}{2}\right)\dfrac{r_{18}\hbar^2}{m_e}10\sqrt{\frac{3}{4}}}{\left(\dfrac{(Z-18)e^2}{4\pi\varepsilon_0} - \dfrac{3\hbar^2}{4m_e r_{18}}\sqrt{\frac{3}{4}}\right)} = 0 \tag{10.423}$$

The solution of Eq. (10.423) using the quadratic formula is:

$$r_{19} = \frac{\dfrac{\dfrac{\hbar^2}{m_e}\left(1+\dfrac{24\sqrt{\frac{3}{4}}}{Z}\right)}{\left(\dfrac{(Z-18)e^2}{4\pi\varepsilon_0} - \dfrac{3\hbar^2}{4m_e r_{18}}\sqrt{\frac{3}{4}}\right)} \pm \sqrt{\left(\dfrac{\dfrac{\hbar^2}{m_e}\left(1+\dfrac{24\sqrt{\frac{3}{4}}}{Z}\right)}{\left(\dfrac{(Z-18)e^2}{4\pi\varepsilon_0} - \dfrac{3\hbar^2}{4m_e r_{18}}\sqrt{\frac{3}{4}}\right)}\right)^2 + 4\dfrac{\left[\dfrac{Z-19}{Z-18}\right]\left(1-\dfrac{\sqrt{2}}{2}+\dfrac{1}{2}-\dfrac{\sqrt{2}}{2}+\dfrac{1}{2}\right)\dfrac{r_{18}\hbar^2}{m_e}10\sqrt{\frac{3}{4}}}{\left(\dfrac{(Z-18)e^2}{4\pi\varepsilon_0} - \dfrac{3\hbar^2}{4m_e r_{18}}\sqrt{\frac{3}{4}}\right)}}}{2} \tag{10.424}$$

$$r_{19} = \frac{\dfrac{a_0\left(1+\dfrac{12\sqrt{3}}{Z}\right)}{\left((Z-18)-\dfrac{3\sqrt{3}}{8r_{18}}\right)} \pm a_0\sqrt{\left(\dfrac{1+\dfrac{12\sqrt{3}}{Z}}{\left((Z-18)-\dfrac{3\sqrt{3}}{8r_{18}}\right)}\right)^2 + \dfrac{20\sqrt{3}\left(\left[\dfrac{Z-19}{Z-18}\right]\left(1-\dfrac{\sqrt{2}}{2}+\dfrac{1}{2}-\dfrac{\sqrt{2}}{2}+\dfrac{1}{2}\right)r_{18}\right)}{\left((Z-18)-\dfrac{3\sqrt{3}}{8r_{18}}\right)}}}{2}, \; r_{18} \text{ in units of } a_0 \tag{10.425}$$

where $r_{18}$ is given by Eq. (10.399). The positive root of Eq. (10.425) must be taken in order that $r_{19} > 0$. The radii of several nineteen-electron atoms are given in Table 10.19.

The ionization energies for the nineteen-electron atoms with $Z > 19$ are given by the electric energy, $E(electric)$, (Eq. (10.102) with the radii $r_{19}$, given by Eq. (10.425)):

$$E(Ionization) = -Electric\ Energy = \frac{(Z-18)e^2}{8\pi\varepsilon_0 r_{19}} \tag{10.426}$$

Since the relativistic corrections were small, the nonrelativistic ionization energies for experimentally measured nineteen-electron atoms are given in Table 10.19.

**Table 10.19.** Ionization energies for some nineteen-electron atoms.

| 19 e Atom | Z | $r_1$ $(a_o)$ [a] | $r_3$ $(a_o)$ [b] | $r_{10}$ $(a_o)$ [c] | $r_{12}$ $(a_o)$ [d] | $r_{18}$ $(a_o)$ [e] | $r_{19}$ $(a_o)$ [f] | Theoretical Ionization Energies [g] $(eV)$ | Experimental Ionization Energies [h] $(eV)$ | Relative Error [i] |
|---|---|---|---|---|---|---|---|---|---|---|
| $K$ | 19 | 0.05302 | 0.22503 | 0.26884 | 0.71450 | 0.85215 | 3.14515 | 4.32596 | 4.34066 | 0.0034 |
| $Ca^{+}$ | 20 | 0.05035 | 0.21308 | 0.25149 | 0.65725 | 0.82478 | 2.40060 | 11.3354 | 11.87172 | 0.0452 |
| $Sc^{2+}$ | 21 | 0.04794 | 0.20235 | 0.23625 | 0.60857 | 0.76196 | 1.65261 | 24.6988 | 24.75666 | 0.0023 |
| $Ti^{3+}$ | 22 | 0.04574 | 0.19264 | 0.22276 | 0.56666 | 0.70013 | 1.29998 | 41.8647 | 43.2672 | 0.0324 |
| $V^{4+}$ | 23 | 0.04374 | 0.18383 | 0.21074 | 0.53022 | 0.64511 | 1.08245 | 62.8474 | 65.2817 | 0.0373 |
| $Cr^{5+}$ | 24 | 0.04191 | 0.17579 | 0.19995 | 0.49822 | 0.59718 | 0.93156 | 87.6329 | 90.6349 | 0.0331 |
| $Mn^{6+}$ | 25 | 0.04022 | 0.16842 | 0.19022 | 0.46990 | 0.55552 | 0.81957 | 116.2076 | 119.203 | 0.0251 |
| $Fe^{7+}$ | 26 | 0.03867 | 0.16165 | 0.18140 | 0.44466 | 0.51915 | 0.73267 | 148.5612 | 151.06 | 0.0165 |
| $Co^{8+}$ | 27 | 0.03723 | 0.15540 | 0.17336 | 0.42201 | 0.48720 | 0.66303 | 184.6863 | 186.13 | 0.0078 |
| $Ni^{9+}$ | 28 | 0.03589 | 0.14961 | 0.16601 | 0.40158 | 0.45894 | 0.60584 | 224.5772 | 224.6 | 0.0001 |
| $Cu^{10+}$ | 29 | 0.03465 | 0.14424 | 0.15926 | 0.38305 | 0.43379 | 0.55797 | 268.2300 | 265.3 | -0.0110 |
| $Zn^{11+}$ | 30 | 0.03349 | 0.13925 | 0.15304 | 0.36617 | 0.41127 | 0.51726 | 315.6418 | 310.8 | -0.0156 |

[a] Radius of the paired 1s inner electrons of nineteen-electron atoms from Eq. (10.51).

[b] Radius of the paired 2s inner electrons of nineteen-electron atoms from Eq. (10.62).

[c] Radius of the three sets of paired 2p inner electrons of nineteen-electron atoms from Eq. (10.212).

[d] Radius of the paired 3s inner electrons of nineteen-electron atoms from Eq. (10.255).

[e] Radius of the three sets of paired 3p inner electrons of nineteen-electron atoms from Eq. (10.399).

[f] Radius of the unpaired 4s outer electron of nineteen-electron atoms from Eq. (10.425) for $Z > 19$ and Eq. (10.414) for $K$.

[g] Calculated ionization energies of nineteen-electron atoms given by the electric energy (Eq. (10.426)).

[h] From theoretical calculations, interpolation of isoelectronic and spectral series, and experimental data [2-3].

[i] (Experimental-theoretical)/experimental.

The agreement between the experimental and calculated values of Table 10.19 is well within the experimental capability of the spectroscopic determinations including the values at large Z which relies on X-ray spectroscopy. In this case, the experimental capability is about three to four significant figures which is consistent with the last column. Ionization energies are difficult to determine since the cut-off of the Rydberg series of lines at the ionization energy is often not observed. Thus, the potassium atom isoelectronic series given in Table 10.19 [2-3] relies on theoretical calculations and interpolation of the K isoelectronic and Rydberg series as well as direct experimental data to extend the precision beyond the capability of X-ray spectroscopy. But, no assurances can be given that these techniques are correct, and they may not improve the results. The error given in the last column is very reasonable given the quality of the data.

## TWENTY-ELECTRON ATOMS

Twenty-electron atoms can be solved exactly using the results of the solutions of one, two, three, four, five, six, seven, eight, nine, ten, eleven, twelve, thirteen, fourteen, fifteen, sixteen, seventeen, eighteen, and nineteen-electron atoms.

## RADIUS AND IONIZATION ENERGY OF THE OUTER ELECTRON OF THE CALCIUM ATOM

For each nineteen-electron atom having a central charge of $Z$ times that of the proton, there are two indistinguishable spin-paired electrons in an atomic orbital with radii $r_1$ and $r_2$ both given by Eq. (7.35) (Eq. (10.51)), two indistinguishable spin-paired electrons in an atomic orbital with radii $r_3$ and $r_4$ both given by Eq. (10.62), three sets of paired electrons in an atomic orbital at $r_{10}$ given by Eq. (10.212), two indistinguishable spin-paired electrons in an atomic orbital with radii $r_{11}$ and $r_{12}$ both given by Eq. (10.255), three sets of paired electrons in an atomic orbital with radius $r_{18}$ given by Eq. (10.399), and an unpaired electron in an atomic orbital with radius $r_{19}$ given by Eq. (10.425). For $Z \geq 20$, the next electron which binds to form the corresponding twenty-electron atom is attracted by the central Coulomb field and the spin-pairing force with the unpaired 4s inner electron and is repelled by diamagnetic forces due to the 3 sets of spin-paired inner 3p electrons such that it forms an unpaired atomic orbital at radius $r_{20}$.

The central Coulomb force acts on the outer electron to cause it to bind wherein this electric force on the outer-most electron due to the nucleus and the inner nineteen electrons is given by Eq. (10.70) with the appropriate charge and radius:

$$\mathbf{F}_{ele} = \frac{(Z-19)e^2}{4\pi\varepsilon_0 r_{20}^2}\mathbf{i}_\mathbf{r} \tag{10.427}$$

for $r > r_{19}$.

The forces for the calcium atom follow from those of the magnesium atom given in the Twelve-Electron Atom section. The outer electron which binds to form the corresponding twenty-electron atom becomes spin-paired with the unpaired inner electron such that they become indistinguishable with the same radius $r_{19} = r_{20}$ corresponding to a filled 4s shell. The corresponding spin-pairing force $\mathbf{F}_{mag}$ is given by Eqs. (7.24) and (10.239).

$$\mathbf{F}_{mag} = \frac{1}{Z}\frac{\hbar^2}{m_e r_{20}^3}\sqrt{s(s+1)}\mathbf{i}_\mathbf{r} \tag{10.428}$$

The spherically symmetrical closed 3p shell of twenty-electron atoms produces a diamagnetic force, $\mathbf{F}_{diamagnetic}$, that is equivalent to that of a closed s shell given by Eq. (10.11) with the appropriate radii. The inner electrons remain at their initial radii, but cause a diamagnetic force according to Lenz's law that is

$$\mathbf{F}_{diamagnetic} = -\frac{\hbar^2}{4m_e r_{20}^2 r_{18}}\sqrt{s(s+1)}\mathbf{i}_\mathbf{r} \tag{10.429}$$

In addition to the paramagnetic spin-pairing force between the nineteenth electron initially at radius $r_{19}$, the pairing causes the diamagnetic interaction between the outer electrons and the inner electrons given by Eq. (10.11) to vanish, except for an electrodynamic effect for $Z > 20$ described in the Two-Electron Atoms section, since upon pairing the magnetic field of the outer electrons becomes zero. Using Eqs. (10.55) and (10.240), $\mathbf{F}_{mag\ 2}$ due to the three 3p orbitals is given by:

$$\mathbf{F}_{mag\ 2} = \frac{3}{Z}\frac{\hbar^2}{m_e r_{20} r_{18}^2}\sqrt{s(s+1)}\mathbf{i}_\mathbf{r} \tag{10.430}$$

In addition to the spin-spin interactions between electron pairs, the three sets of 2p and 3p electrons are orbitally paired. The 4s electrons of the calcium atom produce a magnetic field at the position of the six sets of spin-paired 2p and 3p electrons which interact as described in the P-Orbital Electrons Based on an Energy Minimum section. In order for the electrons to remain spin and orbitally paired, the corresponding diamagnetic force, $\mathbf{F}_{diamagnetic\ 3}$, on electron twenty from the six sets of spin-paired electrons that follows from the deviation given in the Eleven-Electron Atom section (Eq. (10.221)) is:

$$\mathbf{F}_{diamagnetic\ 3} = -\frac{1}{Z}\frac{24\hbar^2}{m_e r_{20}^{\ 3}}\sqrt{s(s+1)}\mathbf{i}_\mathbf{r} \tag{10.431}$$

corresponding to the 2 and 3 $p_x$, $p_y$, and $p_z$ electrons.

The outward centrifugal force on electron 20 is balanced by the electric force and the magnetic forces (on electron 20). The radius of the outer electron is calculated by equating the outward centrifugal force to the sum of the electric (Eq. (10.427)), diamagnetic (Eq. (10.428-10.429) and (10.431)), and paramagnetic (Eq. (10.430)) forces as follows:

$$\frac{m_e v_{20}^2}{r_{20}} = \frac{(Z-19)e^2}{4\pi\varepsilon_0 r_{20}^2} - \frac{\hbar^2}{4m_e r_{20}^2 r_{18}}\sqrt{s(s+1)} + \frac{3\hbar^2}{Zm_e r_{20}^2 r_{18}}\sqrt{s(s+1)} - \frac{24\hbar^2}{Zm_e r_{20}^3}\sqrt{s(s+1)} + \frac{\hbar^2}{Zm_e r_{20}^3}\sqrt{s(s+1)} \tag{10.432}$$

Substitution of $v_{20} = \frac{\hbar}{m_e r_{20}}$ (Eq. (1.35)) and $s = \frac{1}{2}$ into Eq. (10.432) gives:

$$\frac{\hbar^2}{m_e r_{20}^3} = \frac{(Z-19)e^2}{4\pi\varepsilon_0 r_{20}^2} - \frac{\hbar^2}{4m_e r_{20}^2 r_{18}}\sqrt{\frac{3}{4}} + \frac{3\hbar^2}{Zm_e r_{20}^2 r_{18}}\sqrt{\frac{3}{4}} - \frac{24\hbar^2}{Zm_e r_{20}^3}\sqrt{\frac{3}{4}} + \frac{\hbar^2}{Zm_e r_{20}^3}\sqrt{\frac{3}{4}} \tag{10.433}$$

$$r_{20} = \frac{\frac{\hbar^2}{m_e}\left(1 + \frac{23\sqrt{\frac{3}{4}}}{Z}\right)}{\frac{(Z-19)e^2}{4\pi\varepsilon_0} - \left(\frac{1}{4} - \frac{3}{Z}\right)\frac{\hbar^2}{m_e r_{18}}\sqrt{\frac{3}{4}}} \tag{10.434}$$

$$r_{20}=\frac{a_0\left(1+\frac{23\sqrt{\frac{3}{4}}}{Z}\right)}{(Z-19)-\left(\frac{1}{4}-\frac{3}{Z}\right)\frac{\sqrt{\frac{3}{4}}}{r_{18}}},\ r_{18}\ in\ units\ of\ a_0 \tag{10.435}$$

Substitution of $\frac{r_{18}}{a_0}=0.82478$ (Eq. (10.399) with $Z=20$) into Eq. (10.435) gives:

$$r_{20}=2.23009a_0 \tag{10.436}$$

The ionization energy of the calcium atom is given by the electric energy, $E(electric)$, (Eq. (10.102) with the radius, $r_{20}$, given by Eq. (10.435)).

$$E(ionization;\ Ca)=-Electric\ Energy=\frac{(Z-19)e^2}{8\pi\varepsilon_0 r_{20}}=6.10101\ eV \tag{10.437}$$

where $r_{20}=2.23009a_0$ (Eq. (10.435)) and $Z=20$. The experimental ionization energy of the calcium atom is $6.11316\ eV$ [3].

## THE IONIZATION ENERGIES OF TWENTY-ELECTRON ATOMS WITH A NUCLEAR CHARGE Z>20

Nineteen-electron atoms having $Z>20$ possess an external electric field given by Eq. (10.92). Since there is a source of dissipative power, $\mathbf{J}\bullet\mathbf{E}$ of Eq. (10.27), the magnetic moments of the inner electrons may change due to the outer electron such that the energy of the nineteen-electron atom is lowered. The spherically symmetrical closed 3p shell of twenty-electron atoms produces a diamagnetic force, $\mathbf{F}_{diamagnetic}$, that is equivalent to that of a closed s shell given by Eq. (10.11) with the appropriate radii except that the force is doubled (Eq. (10.96)) due to the interaction of the 2p, 3s, and 3p electrons as discussed in the 3P-Orbital Electrons Based on an Energy Minimum section with the cancellation of the contribution of the 3s orbital by the 4s orbital. The inner electrons remain at their initial radii, but cause a diamagnetic force according to Lenz's law that is:

$$\mathbf{F}_{diamagnetic}=-\frac{2\hbar^2}{4m_e r_{20}^2 r_{18}}\sqrt{s(s+1)}\mathbf{i}_\mathbf{r} \tag{10.438}$$

In addition to the spin-spin interaction between electron pairs, the six sets of 2p and 3p electrons are orbitally paired. As in given in the Eleven-Electron Atom section, the single 4s orbital of each twenty-electron atoms having $Z>20$ produces a magnetic field at the position of the six sets of spin-paired 2p and 3p electrons. In order for the electrons to remain spin and orbitally paired, the corresponding diamagnetic force, $\mathbf{F}_{diamagnetic\ 3}$, on electron twenty from the six sets of spin-paired electrons given by Eq. (10.221) is:

$$\mathbf{F}_{diamagnetic\ 3}=-\frac{1}{Z}\frac{24\hbar^2}{m_e r_{20}^{\ 3}}\sqrt{s(s+1)}\mathbf{i}_\mathbf{r} \tag{10.439}$$

corresponding to the 2 and 3 $p_x$, $p_y$, and $p_z$ electrons.

From Eq. (10.418), the diamagnetic force, $\mathbf{F}_{diamagnetic\ 2}$, due to a relativistic effect with an electric field for $r>r_{20}$ (Eq. (10.35)) is:

$$\mathbf{F}_{diamagnetic\ 2}=-\left[\frac{Z-20}{Z-19}\right]\left(1-\frac{\sqrt{2}}{2}+\frac{1}{2}-\frac{\sqrt{2}}{2}+\frac{1}{2}\right)\frac{r_{18}\hbar^2}{m_e r_{20}^4}10\sqrt{s(s+1)}\mathbf{i}_\mathbf{r} \tag{10.440}$$

In the case that $Z>20$, the radius of the outer electron is calculated by equating the outward centrifugal force to the sum of the electric (Eq. (10.427)) and diamagnetic (Eqs. (10.438-10.440)) forces as follows:

$$\frac{m_e v_{20}^2}{r_{20}}=\frac{(Z-19)e^2}{4\pi\varepsilon_0 r_{20}^2}-\frac{2\hbar^2}{4m_e r_{20}^2 r_{18}}\sqrt{s(s+1)}-\frac{24\hbar^2}{Zm_e r_{20}^3}\sqrt{s(s+1)}$$
$$-\left[\frac{Z-20}{Z-19}\right]\left(1-\frac{\sqrt{2}}{2}+\frac{1}{2}-\frac{\sqrt{2}}{2}+\frac{1}{2}\right)\frac{r_{18}\hbar^2}{m_e r_{20}^4}10\sqrt{s(s+1)} \tag{10.441}$$

Substitution of $v_{20}=\frac{\hbar}{m_e r_{20}}$ (Eq. (1.35)) and $s=\frac{1}{2}$ into Eq. (10.441) gives:

$$\frac{\hbar^2}{m_e r_{20}^3}=\frac{(Z-19)e^2}{4\pi\varepsilon_0 r_{20}^2}-\frac{2\hbar^2}{4m_e r_{20}^2 r_{18}}\sqrt{\frac{3}{4}}-\frac{24\hbar^2}{Zm_e r_{20}^3}\sqrt{\frac{3}{4}}$$
$$-\left[\frac{Z-20}{Z-19}\right]\left(1-\frac{\sqrt{2}}{2}+\frac{1}{2}-\frac{\sqrt{2}}{2}+\frac{1}{2}\right)\frac{r_{18}\hbar^2}{m_e r_{20}^4}10\sqrt{\frac{3}{4}} \tag{10.442}$$

The quadratic equation corresponding to Eq. (10.442) is:

$$r_{20}^2-\frac{\dfrac{\hbar^2}{m_e}\left(1+\dfrac{24\sqrt{\frac{3}{4}}}{Z}\right)}{\left(\dfrac{(Z-19)e^2}{4\pi\varepsilon_0}-\dfrac{2\hbar^2}{4m_e r_{18}}\sqrt{\frac{3}{4}}\right)}r_{20}-\frac{\left[\dfrac{Z-20}{Z-19}\right]\left(1-\dfrac{\sqrt{2}}{2}+\dfrac{1}{2}-\dfrac{\sqrt{2}}{2}+\dfrac{1}{2}\right)\dfrac{r_{18}\hbar^2}{m_e}10\sqrt{\frac{3}{4}}}{\left(\dfrac{(Z-19)e^2}{4\pi\varepsilon_0}-\dfrac{2\hbar^2}{4m_e r_{18}}\sqrt{\frac{3}{4}}\right)}=0 \tag{10.443}$$

The solution of Eq. (10.443) using the quadratic formula is:

$$r_{20}=\frac{\dfrac{\dfrac{\hbar^2}{m_e}\left(1+\dfrac{24\sqrt{\frac{3}{4}}}{Z}\right)}{\left(\dfrac{(Z-19)e^2}{4\pi\varepsilon_0}-\dfrac{2\hbar^2}{4m_e r_{18}}\sqrt{\frac{3}{4}}\right)}\pm\sqrt{\left(\dfrac{\dfrac{\hbar^2}{m_e}\left(1+\dfrac{24\sqrt{\frac{3}{4}}}{Z}\right)}{\left(\dfrac{(Z-19)e^2}{4\pi\varepsilon_0}-\dfrac{2\hbar^2}{4m_e r_{18}}\sqrt{\frac{3}{4}}\right)}\right)^2+4\dfrac{\left[\dfrac{Z-20}{Z-19}\right]\left(1-\dfrac{\sqrt{2}}{2}+\dfrac{1}{2}-\dfrac{\sqrt{2}}{2}+\dfrac{1}{2}\right)\dfrac{r_{18}\hbar^2}{m_e}10\sqrt{\frac{3}{4}}}{\left(\dfrac{(Z-19)e^2}{4\pi\varepsilon_0}-\dfrac{2\hbar^2}{4m_e r_{18}}\sqrt{\frac{3}{4}}\right)}}}{2} \tag{10.444}$$

$$r_{20}=\frac{\dfrac{a_0\left(1+\dfrac{12\sqrt{3}}{Z}\right)}{\left((Z-19)-\dfrac{\sqrt{3}}{4r_{18}}\right)}\pm a_0\sqrt{\left(\dfrac{1+\dfrac{12\sqrt{3}}{Z}}{\left((Z-19)-\dfrac{\sqrt{3}}{4r_{18}}\right)}\right)^2+\dfrac{20\sqrt{3}\left(\left[\dfrac{Z-20}{Z-19}\right]\left(1-\dfrac{\sqrt{2}}{2}+\dfrac{1}{2}-\dfrac{\sqrt{2}}{2}+\dfrac{1}{2}\right)r_{18}\right)}{\left((Z-19)-\dfrac{\sqrt{3}}{4r_{18}}\right)}}}{2},\ r_{18}\ \textit{in units of}\ a_0 \tag{10.445}$$

where $r_{18}$ is given by Eq. (10.399). The positive root of Eq. (10.445) must be taken in order that $r_{20}>0$. The final radius of electron 20, $r_{20}$, is given by Eq. (10.445); this is also the final radius of electron 19. The radii of several twenty-electron atoms are given in Table 10.20. The general equation for the ionization energies of atoms having an outer s-shell is given in the General Equation for the Ionization Energies of Atoms Having an Outer S-Shell section.

The ionization energies for the twenty-electron atoms with $Z>20$ are given by the electric energy, $E(electric)$, (Eq. (10.102) with the radii $r_{20}$, given by Eq. (10.445)).

$$E(Ionization)=-Electric\ Energy=\frac{(Z-19)e^2}{8\pi\varepsilon_0 r_{20}} \tag{10.446}$$

Since the relativistic corrections were small, the nonrelativistic ionization energies for experimentally measured twenty-electron atoms are given in Table 10.20.

**Table 10.20.** Ionization energies for some twenty-electron atoms.

| 20 e Atom | Z | $r_1$ $(a_o)$ [a] | $r_3$ $(a_o)$ [b] | $r_{10}$ $(a_o)$ [c] | $r_{12}$ $(a_o)$ [d] | $r_{18}$ $(a_o)$ [e] | $r_{20}$ $(a_o)$ [f] | Theoretical Ionization Energies [g] $(eV)$ | Experimental Ionization Energies [h] $(eV)$ | Relative Error [i] |
|---|---|---|---|---|---|---|---|---|---|---|
| $Ca$ | 20 | 0.05035 | 0.21308 | 0.25149 | 0.65725 | 0.82478 | 2.23009 | 6.10101 | 6.11316 | 0.0020 |
| $Sc^{+}$ | 21 | 0.04794 | 0.20235 | 0.23625 | 0.60857 | 0.76196 | 2.04869 | 13.2824 | 12.79967 | -0.0377 |
| $Ti^{2+}$ | 22 | 0.04574 | 0.19264 | 0.22276 | 0.56666 | 0.70013 | 1.48579 | 27.4719 | 27.4917 | 0.0007 |
| $V^{3+}$ | 23 | 0.04374 | 0.18383 | 0.21074 | 0.53022 | 0.64511 | 1.19100 | 45.6956 | 46.709 | 0.0217 |
| $Cr^{4+}$ | 24 | 0.04191 | 0.17579 | 0.19995 | 0.49822 | 0.59718 | 1.00220 | 67.8794 | 69.46 | 0.0228 |
| $Mn^{5+}$ | 25 | 0.04022 | 0.16842 | 0.19022 | 0.46990 | 0.55552 | 0.86867 | 93.9766 | 95.6 | 0.0170 |
| $Fe^{6+}$ | 26 | 0.03867 | 0.16165 | 0.18140 | 0.44466 | 0.51915 | 0.76834 | 123.9571 | 124.98 | 0.0082 |
| $Co^{7+}$ | 27 | 0.03723 | 0.15540 | 0.17336 | 0.42201 | 0.48720 | 0.68977 | 157.8012 | 157.8 | 0.0000 |
| $Ni^{8+}$ | 28 | 0.03589 | 0.14961 | 0.16601 | 0.40158 | 0.45894 | 0.62637 | 195.4954 | 193 | -0.0129 |
| $Cu^{9+}$ | 29 | 0.03465 | 0.14424 | 0.15926 | 0.38305 | 0.43379 | 0.57401 | 237.0301 | 232 | -0.0217 |
| $Zn^{10+}$ | 30 | 0.03349 | 0.13925 | 0.15304 | 0.36617 | 0.41127 | 0.52997 | 282.3982 | 274 | -0.0307 |

[a] Radius of the paired 1s inner electrons of twenty-electron atoms from Eq. (10.51).

[b] Radius of the paired 2s inner electrons of twenty-electron atoms from Eq. (10.62).

[c] Radius of the three sets of paired 2p inner electrons of twenty-electron atoms from Eq. (10.212)).

[d] Radius of the paired 3s inner electrons of twenty-electron atoms from Eq. (10.255)).

[e] Radius of the three sets of paired 3p inner electrons of twenty-electron atoms from Eq. (10.399).

[f] Radius of the paired 4s outer electrons of twenty-electron atoms from Eq. (10.445) for $Z > 20$ and Eq. (10.436) for *Ca*.

[g] Calculated ionization energies of twenty-electron atoms given by the electric energy (Eq. (10.446)).

[h] From theoretical calculations, interpolation of isoelectronic and spectral series, and experimental data [2-3].

[i] (Experimental-theoretical)/experimental.

The agreement between the experimental and calculated values of Table 10.20 is well within the experimental capability of the spectroscopic determinations including the values at large Z which relies on X-ray spectroscopy. In this case, the experimental capability is about three to four significant figures which are consistent with the last column. Ionization energies are difficult to determine since the cut-off of the Rydberg series of lines at the ionization energy is often not observed. Thus, the calcium atom isoelectronic series given in Table 10.20 [2-3] relies on theoretical calculations and interpolation of the Ca isoelectronic and Rydberg series as well as direct experimental data to extend the precision beyond the capability of X-ray spectroscopy. But, no assurances can be given that these techniques are correct, and they may not improve the results. The error given in the last column is very reasonable given the quality of the data.

## GENERAL EQUATION FOR THE IONIZATION ENERGIES OF ATOMS HAVING AN OUTER S-SHELL

The derivation of the radii and energies of the 1s, 2s, 3s, and 4s electrons is given in the One-Electron Atoms, the Two-Electron Atoms, the Three-Electron Atoms, the Four-Electron Atoms, the Eleven-Electron Atoms, the Twelve-Electron Atoms, the Nineteen-Electron Atoms, and the Twenty-Electron Atoms sections. Similarly, to Eqs. (10.216) and (10.405), the general equation for the radii of s electrons is given by

$$r_n = \frac{\dfrac{a_0\left(1+(C-D)\dfrac{\sqrt{3}}{2Z}\right)}{(Z-(n-1))-\left(\dfrac{A}{8}-\dfrac{B}{2Z}\right)\dfrac{\sqrt{3}}{r_m}} \pm a_0\sqrt{\left(\dfrac{\left(1+(C-D)\dfrac{\sqrt{3}}{2Z}\right)}{(Z-(n-1))-\left(\dfrac{A}{8}-\dfrac{B}{2Z}\right)\dfrac{\sqrt{3}}{r_m}}\right)^2 + \dfrac{20\sqrt{3}\left(\left[\dfrac{Z-n}{Z-(n-1)}\right]Er_m\right)}{(Z-(n-1))-\left(\dfrac{A}{8}-\dfrac{B}{2Z}\right)\dfrac{\sqrt{3}}{r_m}}}}{2} \qquad (10.447)$$

$r_m$ *in units of* $a_0$

where $Z$ is the nuclear charge, $n$ is the number of electrons, $r_m$ is the radius of the preceding filled shell, the parameter $A$ given

in Table 10.21 corresponds to the diamagnetic force, $\mathbf{F}_{diamagnetic}$, (Eq. (10.11)), the parameter $B$ given in Table 10.21 corresponds to the paramagnetic force, $\mathbf{F}_{mag\ 2}$ (Eq. (10.55)), the parameter $C$ given in Table 10.21 corresponds to the diamagnetic force, $\mathbf{F}_{diamagnetic\ 3}$, (Eq. (10.221)), the parameter $D$ given in Table 10.21 corresponds to the paramagnetic force, $\mathbf{F}_{mag}$, (Eq. (7.24)), and the parameter $E$ given in Table 10.21 corresponds to the diamagnetic force, $\mathbf{F}_{diamagnetic\ 2}$, (Eqs. (10.35), (10.229), and (10.418)). The positive root of Eq. (10.447) must be taken in order that $r_n > 0$. The radii of several n-electron atoms having an outer s shell are given in Tables 1.3, 1.5, 7.1, 10.1, 10.2, 10.10, 10.11, 10.19, and 10.20.

The ionization energy for atoms having an outer s-shell are given by the negative of the electric energy, $E(electric)$, (Eq. (10.102) with the radii, $r_n$, given by Eq. (10.447)).

$$E(Ionization) = -Electric\ Energy = \frac{(Z-(n-1))e^2}{8\pi\varepsilon_0 r_n} \tag{10.448}$$

except that minor corrections due to the magnetic energy must be included in cases wherein the s electron does not couple to p electrons as given in Eqs. (7.44), (7.63), (10.25), (10.48), (10.66), and (10.68). Since the relativistic corrections were small except for one, two, and three-electron atoms, the nonrelativistic ionization energies for experimentally measured n-electron, s-filling atoms are given in most cases by Eqs. (10.447) and (10.448). The ionization energies of several n-electron atoms having an outer s shell are given in Tables 1.3, 1.5, 7.1, 10.1, 10.2, 10.10, 10.11, 10.19, and 10.20.

**Table 10.21.** Summary of the parameters of atoms filling the 1s, 2s, 3s, and 4s orbitals.

| Atom Type | Electron Configuration | Ground State Term [a] | Orbital Arrangement of s Electrons (s state) | Diamag. Force Factor $A$ [b] | Paramag. Force Factor $B$ [c] | Diamag. Force Factor $C$ [d] | Paramag. Force Factor $D$ [e] | Diamag. Force Factor $E$ [f] |
|---|---|---|---|---|---|---|---|---|
| Neutral 1 e Atom *H* | $1s^1$ | $^2S_{1/2}$ | $\underline{\uparrow}$ 1s | 0 | 0 | 0 | 0 | 0 |
| Neutral 2 e Atom *He* | $1s^2$ | $^1S_0$ | $\underline{\uparrow\downarrow}$ 1s | 0 | 0 | 0 | 1 | 0 |
| Neutral 3 e Atom *Li* | $2s^1$ | $^2S_{1/2}$ | $\underline{\uparrow}$ 2s | 1 | 0 | 0 | 0 | 0 |
| Neutral 11 e Atom *Na* | $1s^2 2s^2 2p^6 3s^1$ | $^2S_{1/2}$ | $\underline{\uparrow}$ 3s | 1 | 0 | 8 | 0 | 0 |
| Neutral 12 e Atom *Mg* | $1s^2 2s^2 2p^6 3s^2$ | $^1S_0$ | $\underline{\uparrow\downarrow}$ 3s | 1 | 3 | 12 | 1 | 0 |
| Neutral 19 e Atom *K* | $1s^2 2s^2 2p^6 3s^2 3p^6 4s^1$ | $^2S_{1/2}$ | $\underline{\uparrow}$ 4s | 2 | 0 | 12 | 0 | 0 |
| Neutral 20 e Atom *Ca* | $1s^2 2s^2 2p^6 3s^2 3p^6 4s^2$ | $^1S_0$ | $\underline{\uparrow\downarrow}$ 4s | 1 | 3 | 24 | 1 | 0 |
| 1 e Ion | $1s^1$ | $^2S_{1/2}$ | $\underline{\uparrow}$ 1s | 0 | 0 | 0 | 0 | 0 |
| 2 e Ion | $1s^2$ | $^1S_0$ | $\underline{\uparrow\downarrow}$ 1s | 0 | 0 | 0 | 1 | 0 |

| Atom Type | Electron Configuration | Ground State Term [a] | Orbital Arrangement of s Electrons (s state) | Diamag. Force Factor $A$ [b] | Paramag. Force Factor $B$ [c] | Diamag. Force Factor $C$ [d] | Paramag. Force Factor $D$ [e] | Diamag. Force Factor $E$ [f] |
|---|---|---|---|---|---|---|---|---|
| 3 e Ion | $2s^1$ | ${}^2S_{1/2}$ | $\underline{\uparrow}$ 2s | 1 | 0 | 0 | 0 | 1 |
| 4 e Ion | $2s^2$ | ${}^1S_0$ | $\underline{\uparrow\downarrow}$ 2s | 1 | 0 | 0 | 1 | 1 |
| 11 e Ion | $1s^2 2s^2 2p^6 3s^1$ | ${}^2S_{1/2}$ | $\underline{\uparrow}$ 3s | 1 | 4 | 8 | 0 | $1+\frac{\sqrt{2}}{2}$ |
| 12 e Ion | $1s^2 2s^2 2p^6 3s^2$ | ${}^1S_0$ | $\underline{\uparrow\downarrow}$ 3s | 1 | 6 | 0 | 0 | $1+\frac{\sqrt{2}}{2}$ |
| 19 e Ion | $1s^2 2s^2 2p^6 3s^2 3p^6 4s^1$ | ${}^2S_{1/2}$ | $\underline{\uparrow}$ 4s | 3 | 0 | 24 | 0 | $2-\sqrt{2}$ |
| 20 e Ion | $1s^2 2s^2 2p^6 3s^2 3p^6 4s^2$ | ${}^1S_0$ | $\underline{\uparrow\downarrow}$ 4s | 2 | 0 | 24 | 0 | $2-\sqrt{2}$ |

[a] The theoretical ground state terms match those given by NIST [8].
[b] Eq. (10.11).
[c] Eq. (10.55).
[d] Eq. (10.221).
[e] Eq. (7.24).
[f] Eqs. (10.35), (10.229), and (10.418).

The physical approach was applied to multielectron atoms that were solved exactly disproving the deep-seated view that such exact solutions cannot exist according to quantum mechanics. The predictions of the ionization energies for one through twenty-electron atoms are in remarkable agreement with the experimental values known for 400 atoms and ions. The trends of the radii also generally agree with those published [9], but the radii cannot be taken as the contact radii based on nuclear separation in molecules and solids. If the outer most electron of the negative ion was at the location of that of the positive ion, then the potential energies would be the same. Since the ionization energies of positive ions are much greater than the electron affinities of negative ions, the positive ions must have smaller radii. Furthermore the size taken as the contact distance can not be correct since the electron-electron repulsion energies would be dominant.

## THE ELECTRON CONFIGURATION OF ATOMS

The electrons of multielectron atoms all exist as atomic orbitals of discrete radii which are given by $r_n$ of the radial Dirac delta function, $\delta(r-r_n)$. These electron atomic orbitals may be paired or unpaired depending on the force balance that applies to each electron. Ultimately, the electron configuration must be a minimum of energy. Minimum energy configurations are given by solutions to Laplace's Equation. The general form of the solution is:

$$\Phi(r,\theta,\phi)=\sum_{\ell=0}^{\infty}\sum_{m=-\ell}^{\ell}B_{\ell,m}r^{-(\ell+1)}Y_{\ell}^{m}(\theta,\phi) \tag{10.449}$$

As demonstrated previously, this general solution gives the functions of the resonant photons. As shown in the One-Electron Atom section, the Two-Electron Atom section, and the Three- Through Twenty-Electron Atoms section, the electron configuration of an atom essentially parallels that of the excited modes of the helium atom: $1s<2s<2p<3s<3p<4s<3d<4p<5s<4d$. (See Excited States of Helium section.)

In general, electrons of an atom with the same principal and $\ell$ quantum numbers align parallel until each of the $m_\ell$ levels are occupied, and then pairing occurs until each of the $m_\ell$ levels contain paired electrons. Exceptions occur due to the relative importance of spin and orbital interactions and paramagnetic, diamagnetic, and electric forces for a given atom or ion.

The predictions of the ionization energies of one through twenty-electron atoms using Maxwell's equations are given in the One-Electron Atom section, the Two-Electron Atom section, and the Three- Through Twenty-Electron Atoms section. The agreement between the experimental ionization energies and the classical predictions based on concentric dynamical atomic orbitals ("bubble-like" charge-density functions) wherein the charge-density waves on the surface are time and spherically harmonic is remarkable. The classical shell model of atomic electrons is also being confirmed by studying electron dynamics using coherent short-pulse laser excitation [10-12].

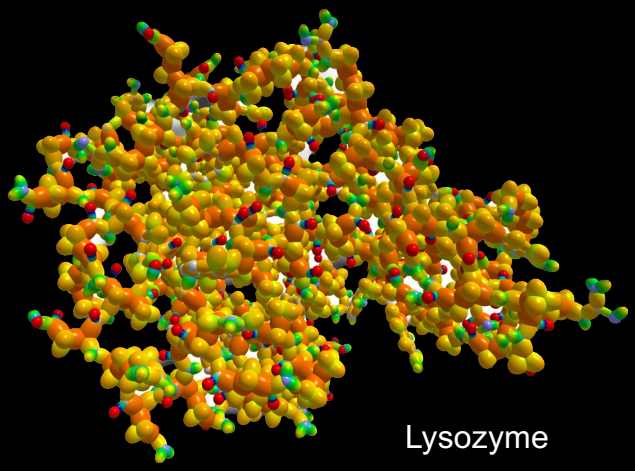
## REFERENCES


1. E. Purcell, *Electricity and Magnetism*, McGraw-Hill, New York, (1965), pp. 370-389.
2. C. E. Moore, "Ionization Potentials and Ionization Limits Derived from the Analyses of Optical Spectra," Nat. Stand. Ref. Data Ser.-Nat. Bur. Stand. (U.S.), No. 34, 1970.
3. R. C. Weast, CRC Handbook of Chemistry and Physics, 58th Edition, CRC Press, West Palm Beach, Florida, (1977), p. E-68.
4. A. O. Wistrom, A. V. M. Khachatourian, "Coulomb motor by rotation of spherical conductors via the electrostatic force," Applied Physics Letters, Volume 80, No. 15, (2002), pp. 2800-2802.
5. A. V. M. Khachatourian, A. O. Wistrom, "A sum rule for associated Legendre polynomials with spherical triangles," Journal of Mathematical Physics, Vol. 44(2), (2003), pp. 849-852.
6. J. D. Jackson, *Classical Electrodynamics*, Second Edition, John Wiley & Sons, New York, (1975), p. 99.
7. D. A. McQuarrie, *Quantum Chemistry*, University Science Books, Mill Valley, CA, (1983), p. 215.
8. NIST Atomic Spectra Database, www.physics.nist.gov/cgi-bin/AtData/display.ksh.
9. M. Karplus, R. N. Porter, *Atoms and Molecules an Introduction for Students of Physical Chemistry*, The Benjamin/Cummings Publishing Company, Menlo Park, California, (1970), pp. 202-207.
10. S. N. Pisharody, R. R. Jones, "Probing two electron dynamics of an atom," Science, Vol. 303, (2004), pp. 813-815.
11. C. R. Stroud, "Pas de deux for atomic electrons," Science, Vol. 303, (2004), pp. 778-779.
12. H. Maeda, D. V. L. Norum, T. F. Gallagher, "Microwave manipulation of an atomic electron in a classical orbit," Science, Vol. 307, (2005), pp. 1757-1760.

Dr. Mills has replaced the field generally known as Quantum Mechanics which postulates that classical physical laws do not apply at the atomic scale by deriving a new atomic theory of from those first principles, which unifies Maxwell's Equations, Newton's Laws, and General and Special Relativity. The central feature is that physical laws hold over all scales, from the scale of subatomic particles to that of the cosmos.

Quantum Mechanics has remained mysterious to all who have encountered it. Schrödinger postulated a boundary condition $\Psi \rightarrow 0$ as $r \rightarrow \infty$ of a wavelike positional probability for a singularity that is everywhere at once until measurement. The result was a purely algorithmic mathematical model of the hydrogen atom. In contrast, Mills solved the exact structure of matter and energy and related phenomena from known classical physics, (e.g. Maxwell's Equations wherein under special conditions, an extended distribution of charge may accelerate without radiating energy). This leads to a physical model of subatomic particles, atoms, and molecules. The closed-form solutions containing fundamental constants only agree with experimental observations demonstrating that the fundamental quantum mechanical postulate, "classical physical laws do not apply to the atomic scale", was erroneous.

From two basic equations, the key building blocks of organic chemistry have been solved, allowing the true physical structure and parameters of an infinite number of organic molecules up to infinite length and complexity to be obtained. These equations were also applied to bulk forms of matter, such as the allotropes of carbon, the solid bond of silicon and the semiconductor bond; as well as fundamental forms of matter such as the ionic bond and the metallic bond; and major fields of chemistry such as that of silicon, tin, aluminum, boron, and coordinate compounds.



Lysozyme

Further, the Schwarzschild Metric is derived by applying Maxwell's Equations to electromagnetic and gravitational fields at particle production. This modifies General Relativity to include the conservation of spacetime and gives the origin of gravity, the families and masses of fundamental particles, the acceleration of the expansion of the universe (predicted by Dr. Mills in 1995 and since confirmed experimentally), and overturns the Big Bang model of the origin of the universe.

"Mills' theory explains the answers to some very old scientific questions, such as 'what happens to a photon upon absorption' and some very modern ones, such as 'what is dark matter.' ...Lastly, Mills has made an extremely important contribution to the philosophy of science. He has reestablished cause and effect as the basic principle of science." - **Dr. John J. Farrell**, former Chair of the Dept. of Chemistry, Franklin & Marshall College

"Mills' ingenious way of thinking creates in different physical areas astonishing results with fascinating mathematical simplicity and harmony. And his theory is strongly supported by the fact that nearly all these results are in comfortable accordance with experimental findings, sometimes with breathtaking accuracy." - **Dr Günther Landvogt,** Retired Scientist, Philips Research Lab

"Dr. Mills has apparently completed Einstein's quest for a unified field theory… without largesse from the US Government, and without the benediction of the US scientific priesthood." - **Shelby T. Brewer**, former Assistant Secretary of Energy, former CEO of ABB Combustion Engineering, MS/Ph.D. MIT - Nuclear Engineering.

"Mills proposes such a basic approach to quantum theory that it deserves considerably more attention from the general scientific community than it has received so far. The new theory appears to be a realization of Einstein's vision and a fitting closure of the "Quantum Century" that started in 1900..." - **Dr. Reinhart Engelmann**, Professor of Electrical Engineering, Oregon Graduate Institute of Science and Technology

**Dr. Randell Mills** holds a Doctor of Medicine degree from Harvard, a BA degree in Chemistry from Franklin and Marshall College, and studied Electrical Engineering at MIT. He is President, Chairman and CEO of Brilliant Light Power, Inc.